Title
Seismic Performance of Buildings Subjected to Soil Liquefaction

Author
Zupan, Joshua David

Publication Date
2014

Peer reviewed|Thesis/dissertation

Seismic Performance of Buildings Subjected to Soil Liquefaction

By

Joshua David Zupan

A thesis submitted in partial satisfaction of the

requirements for the degree of

Doctor of Philosophy

in

Engineering – Civil and Environmental Engineering

in the

Graduate Division

of the

University of California, Berkeley

Committee in charge:

Professor Jonathan D. Bray, Chair
Professor Nicholas Sitar
Professor Misko Cubrinovski
Professor Douglas S. Dreger

Spring 2014

Seismic Performance of Buildings Subjected to Soil Liquefaction

by
Joshua David Zupan

Abstract

Seismic Performance of Buildings Subjected to Soil Liquefaction

by

Joshua David Zupan

Doctor of Philosophy in Engineering – Civil and Environmental Engineering

University of California, Berkeley

Professor Jonathan D. Bray, Chair

There have been numerous examples of damage to buildings due to the effects of soil liquefaction or cyclic softening in recent significant earthquake events. Of these examples, shallow-founded buildings on level ground atop shallow liquefiable soils have often been impacted by partial or complete bearing failures, loss of foundation soils due to eroded sediment ejecta, and vertical settlements that have been exacerbated by soil-structure-interaction (SSI). While significant progress has been made in recent years towards understanding these deformation mechanisms, there is still no widely-accepted simplified method by which engineering practitioners can reliably estimate the settlement of buildings due to liquefaction or cyclic softening. Rollins and Seed (1990) pointed out that the liquefaction potential below a building was often evaluated by treating the soil as if it were in the free-field. Two decades later, Bray and Dashti (2010) found that liquefaction-induced building settlements are still often estimated using empirical procedures developed to calculate post-liquefaction, one-dimensional, consolidation settlements in the free-field (e.g., Tokimatsu and Seed, 1987; Ishihara and Yoshimine, 1992). These free-field procedures do not capture important shear-induced and localized volumetric-induced building deformation mechanisms. Therefore, these procedures can significantly underestimate building settlements. Improvements are required to advance the state-of-the-art in liquefaction engineering.

The primary objective of this research effort is to advance the understanding of the seismic performance of buildings subjected to soil liquefaction or cyclic softening. This objective is achieved through the performance of a geotechnical centrifuge experiment and through the documentation and interpretation of a number of field performance case histories. Well-documented field and physical model case history data are essential to advancing the profession's understanding of the effects of liquefaction or cyclic softening on building performance. The field and laboratory studies are also critical to the development and calibration of simplified empirical procedures and advanced analytical procedures. Therefore, while the primary objective of the work presented herein is to advance the understanding of liquefaction-induced building settlements, an additional significant objective is to provide high quality and well-interpreted field and physical model case history data that can be used to develop, evaluate, and calibrate analytical procedures and design methods.

A sophisticated geotechnical centrifuge model of shallow-founded model structures atop shallow liquefiable soils was designed, constructed, and subjected to several realistic earthquake motions of varying intensity and duration as part of this work. This experiment was designed to build on previous centrifuge experiments described by Hausler (2002) and Dashti (2009). There were many design similarities between this model and the models described by Dashti (2009), and the findings were generally consistent. However, an additional key objective of this model was to evaluate the effects of building adjacency on the observed performance of the model structures. It was found that placing a baseline model structure next to an identical model structure did not significantly impact the building settlement of either building during the test. Placing the baseline model structure next to a taller, heavier shallow-founded model structure illustrated that it is erroneous to always expect a heavier shallow-founded structure to settle more than a lighter shallow-founded structure when subjected to shallow liquefaction. For some ground motions, less cyclic softening occurred under the heavier structure, so it settled less than the adjacent lighter baseline structure. The seismic demand on the building's foundation soils is directly related to the ground motion and both the building's weight and its dynamic response. In addition, the adjacent model buildings generally tilted and displaced laterally away from one another. These observations suggest that the physical presence of the adjacent building kinematically constrained ground movements under the structures on the sides nearest the adjacent buildings relative to the ground movements that occurred under the sides away from the adjacent building. Also, the confining stresses under the sides of closely-spaced adjacent buildings are lower under the side away from the neighboring building than the side closest to the neighboring building. Consequently, with all other things equal, one would expect a lower liquefaction resistance in the foundation soils on the sides away from the adjacent building, and therefore, relatively more cyclically-induced deformation to occur on that side during shaking

Building performance evaluations of select buildings in Christchurch, New Zealand during the 2010-2011 Canterbury earthquake sequence were also performed. Many multi-story buildings were heavily damaged by liquefaction-induced ground movements during the 22 February 2011 M_w 6.2 Christchurch earthquake, but not by other significant earthquakes. Conventional CPT-based liquefaction triggering evaluations were generally conservative for these field case histories, and this conservatism led to post-liquefaction free-field ground settlement estimates that were generally similar for the 4 September 2010 M_w 7.1 Darfield, 13 June 2011 M_w 6.0, and 22 February 2011 M_w 6.2 Christchurch earthquakes. Variability in the shallow subsurface conditions over relatively short distances was sometimes a critical factor in the seismic performance of the ground and buildings. Ground loss due to eroded sediment ejecta was found to be an important foundation settlement mechanism in several cases of shallow-founded buildings with shallow liquefiable foundation soils. In addition, two shallow-founded, tall buildings settled and tilted due to relatively deeper liquefaction or cyclic softening during the Christchurch event. Though these tall structures were founded at least 3 m above materials that were judged to have liquefied, the liquefied materials were well within the depth range with a significant vertical strain influence using the settlement approach developed by Schmertmann (1978) for rigid footings on sand. Therefore, cyclically-induced deformation of these materials due to increased pore water pressures likely led to the observed building settlements and tilts.

In summary, there are important physical constraints caused by building adjacency that can affect the seismic performance of buildings subjected to soil liquefaction or cyclic softening.

The performance of a building is also significantly affected by the earthquake motion, the ground beneath its foundation, and its dynamic response, including SSI effects such as superstructure rocking. Consequently, the combined effects of all these factors are difficult to judge a priori. Additional studies are warranted to develop insights and improved methods.

TABLE OF CONTENTS

ACKNOWLEDGEMENTS

This material is based upon work supported by the U.S. National Science Foundation (NSF) under Grant Nos. CMMI-0830331, CMMI-0825734, and CMMI-1137977 and the U.S. Geological Survey (USGS) through G12AP20034. Any opinions, findings, and conclusions or recommendations expressed in this material are those of the authors and do not necessarily reflect the views of the NSF or USGS.

I've been very fortunate to have had the opportunity to work with many incredible people over the past three and a half years, and I would like to thank them for the moral and technical support that they have provided during this journey. I will do my best to do this over the next several paragraphs, though it will certainly not be enough.

Ben Mason and Nick Trombetta taught me how to successfully build a geotechnical centrifuge model. More importantly, they demonstrated how to successfully lead a team of people through a challenging project and keep things fun. Hamilton Puangnak and Daniel Paez spent countless hours at the 'fuge during the construction and testing of Test-5. They deserve thanks for somehow putting up with me on a daily basis. Bruce Kutter, Tara Hutchinson, Gregg Fiegel, Chandrakanth Bolisetti, Jackee Allmond, Mark Stringer, Dan Wilson, Ray Gerhard, Chad Justice, Anatoliy Ganchenko, Peter Rojas, and Lars Pederson also deserve thanks for their guidance and assistance. In addition, my interactions with other students, from UC Davis and elsewhere, made my time at the 'fuge much more enjoyable than it otherwise would have been.

My work in New Zealand would have been far more difficult and far less enjoyable were it not for Merrick Taylor and Misko Cubrinovski. Merrick spent a number of hours assisting with the coordination of our subsurface investigations, particularly during the initial phase when procedural things were new to us. He also showed me around the South Island and introduced me to a number of really good people. Kelly Robinson helped coordinate and supervise the Phase II CPTs. Simona Giorgini shared valuable post-earthquake reconnaissance information. Iain Haycock, Nathan Barnes, Richard Wise and Mike Pickworth of McMillan Drilling Services and John Cresswell and Simon Faulkner of Fugro BTW were instrumental in our subsurface investigations. Ian McCahon of Geotech Consulting Ltd., Mike Jacka and Kirsti Murahidy of Tonkin & Taylor, Greg Martin and Neil Charters of Geoscience Consulting (NZ) Ltd., and Glenyss Whitnall of Shipleys Audiovisual shared useful information pertaining to several of the buildings that were evaluated as part of this work.

I want to acknowledge and thank my colleagues on the fourth floor of Davis Hall for their friendship and support. I couldn't have lucked out with better officemates than Tonguc Deger and Roozbeh Geraili Mikola. I am fortunate to have had a chance to get to know many of these current and former GeoBears, and many will be lifelong friends.

I would like to thank Profs. Nicholas Sitar, Misko Cubrinovski, and Douglas Dreger for reviewing this work and providing thoughtful comments.

My adviser, Prof. Jon Bray, provided clear direction and counsel throughout my career as a Ph.D. student. I have learned quite a bit from working with Jon, and the work presented herein would obviously not have been possible without his leadership. I am thankful for the opportunity he provided when we discussed the potential pursuit of a Ph.D. in 2010, and I am thankful for all

of the support he has provided since then. I have enjoyed working with Jon over the past several years, and I am a better engineer because of him.

I would like to thank my mother, Donna Zupan, for her unconditional love and for always believing in me. The person I am today is largely a reflection of the values she instilled in me growing up. I would also like to thank Jessica and Mark Beare, Valerie and Gus Walbolt, and Gary, Christine, and Ryan Zupan for their support. Gert Donovan deserves special thanks for demonstrating what toughness is. Often times when I feel like complaining about something, I wonder what Gert would do, and that usually sets me straight.

Lastly, and most importantly, I want to thank my wife, Sam. The decision to pursue a Ph.D. was very much a joint decision, and Sam has never wavered in her support of this endeavor. She is by far the most optimistic and naturally-loving person that I know (her mom is a close second), and she wakes up almost every day with a smile on her face. I have no idea what I did to deserve such a good mate. I guess even the somewhat-pessimistic luck out sometimes…

CHAPTER 1: INTRODUCTION

1.1 Overview

There have been numerous examples of damage to buildings due to the effects of soil liquefaction or cyclic softening in recent significant earthquake events. Of these examples, shallow-founded buildings on level ground atop shallow liquefiable soils have often been impacted by partial or complete bearing failures, loss of foundation soils due to eroded sediment ejecta, and vertical settlements that have been exacerbated by soil-structure-interaction (SSI). In the Central Business District (CBD) of Christchurch, New Zealand, for example, approximately 1500 of the 4000 buildings, including most of the city's high-rise buildings, have been or are expected to be demolished due to damage sustained during the 2010-2011 Canterbury earthquake sequence. Many of these buildings were heavily damaged by liquefaction-induced ground movements during the February 22, 2011 M_w 6.2 Christchurch earthquake. The primary objective of the work presented herein is to advance the understanding of the seismic performance of buildings subjected to soil liquefaction or cyclic softening by fully documenting and interpreting field performance case histories of select buildings within and near the CBD of Christchurch, New Zealand during the Canterbury earthquakes, as well as complex physical model case histories of simplified, shallow-founded, model structures atop shallow liquefiable soils subjected to several realistic earthquake motions of varying intensity and duration.

This work builds upon recent, important experimental investigations conducted by University of California, Berkeley Ph.D. researchers Hausler (2002), Sancio (2003), Dashti (2009), and Mason (2011). In a study of ground failure and building performance in Adapazari, Turkey during the August 17, 1999 M_w 7.4 Kocaeli earthquake, Sancio (2003) observed numerous cases of building damage caused by settlement, tilt, and horizontal movements due to cyclic softening of shallow Holocene silts of low to medium plasticity. These field performance case histories provided motivation for a series of geotechnical centrifuge experiments performed by Dashti (2009) in which the performance of simplified shallow-founded model structures atop a layered soil profile was studied in detail. The Dashti (2009) centrifuge experiments followed a series of centrifuge tests performed by Hausler (2002) which showed how unimproved and improved ground affected building settlement in a deep deposit of liquefiable sand. Based on these studies, and following other important work (e.g., Yoshimi and Tokimatsu 1977, Tokimatsu et al. 1994, Liu and Dobry 1997, and Adalier and Elgamal 2005), Dashti et al. (2010a) and Bray and Dashti (2010) identified key liquefaction-induced building displacement mechanisms, and these displacement mechanisms have been used as a basis to interpret the field and physical model performance case histories presented herein.

While significant progress has been made in recent years towards understanding the mechanisms of liquefaction-induced building settlements on level ground, there is still no widely-accepted simplified method by which engineering practitioners can reliably estimate the settlement of buildings due to liquefaction or cyclic softening. Rollins and Seed (1990) pointed out that, at that time, the liquefaction potential below a building was often evaluated by treating the soil as if it were in the free-field. The same can be said today. Bray and Dashti (2010) observe that liquefaction-induced building settlements are still often estimated using empirical

procedures developed to calculate post-liquefaction, one-dimensional, consolidation settlements in the free-field (e.g., Tokimatsu and Seed, 1987; Ishihara and Yoshimine, 1992). These free-field procedures do not capture important shear-induced and localized volumetric-induced building deformation mechanisms and can, therefore, significantly underestimate building settlements. Improvements to these procedures are required to advance the state-of-the-art in liquefaction engineering. Well-documented field and physical model case history data are essential to the development and calibration of empirical procedures. Therefore, while the primary objective of the work presented herein is to advance the understanding of building settlements due to liquefaction or cyclic softening, an additional significant objective is to provide high quality and well-interpreted field and physical model case history data that will supplement and enhance existing similar data.

1.2 Organization

There are two primary components of the work presented herein: 1) geotechnical centrifuge modeling of soil liquefaction effects on structures; and 2) evaluation of the performance of select buildings in Christchurch, New Zealand during the 2010 – 2011 Canterbury earthquakes. After this introductory chapter, Chapter 2 provides a brief review of literature relevant to the performance of buildings subjected to soil liquefaction. Dashti (2009) recently performed an in-depth literature review with a similar focus, so in this thesis, the literature review of Chapter 2 is focused primarily on research published since 2009. Following a brief overview of relevant principles of centrifuge modeling, Chapter 3 describes the rationale behind the design of the experiment performed as part of this work, results from the most significant simulated earthquake events, and a discussion of key observations. Chapter 4 begins with overviews of the Canterbury earthquake sequence, geology of Christchurch, regional and site-specific subsurface characterization efforts following the Christchurch earthquake, and CPT data processing procedures. These sections of Chapter 4 are followed by detailed site and building performance evaluations at selected locations within and near the CBD of Christchurch during the Canterbury earthquake sequence. Chapter 4 closes with a summary of key findings from the site and building performance evaluations. Chapter 5 summarizes the key findings from the work performed as part of this thesis and provides suggestions for future research.

CHAPTER 2: LITERATURE REVIEW

2.1 Introduction

Dashti (2009) recently performed an in-depth literature review with a similar focus, and the interested reader should consult this source for a detailed discussion of relevant literature up to that time. Following a brief summary of key findings from the literature review presented by Dashti (2009) in this section, Section 2.2 provides several examples of the effects of liquefaction on buildings during recent significant earthquakes. Section 2.3 provides a brief review of the state-of-the-practice methods for evaluating liquefaction triggering potential and post-liquefaction volumetric reconsolidation settlements in the free-field, followed by a summary of recent advances in the understanding of settlement mechanisms due to liquefaction or cyclic softening. Lastly, two recent simplified methods relevant to the evaluation of the settlement of shallow-founded buildings due to liquefaction or cyclic softening are summarized.

Key findings from the literature review presented by Dashti (2009)

- Partial and complete bearing failures of buildings on liquefied ground were observed in Niigata, Japan following the 1964 M_w 7.6 Niigata, Japan earthquake and in Dagupan City, Philippines following the 1990 M_w 7.7 Luzon, Philippines earthquake. Most of the buildings were two- to four-story, shallow-founded structures that were supported on relatively thick and uniform deposits of clean sand. Buildings with wider foundations generally settled less, with everything else being equal (Yoshimi and Tokimatsu, 1977; Adachi et al., 1992). These general trends are illustrated in Figure 2.1.1 (Liu and Dobry, 1997).

- Based on data from the 1964 Niigata, Japan earthquake, Ishii and Tokimatsu (1988) proposed that if the ratio of the width of the foundation to the thickness of the liquefiable layer is less than about 3, then structures will settle more than the free-field.

- Buildings in Adapazari, Turkey punched into the ground, tilted, and underwent horizontal movements during the 1999 M_w 7.4 Kocaeli earthquake due to liquefaction or cyclic softening of shallow and relatively thin layers of silts of low to medium plasticity (Sancio, 2003). Many buildings were three- to six-story RC frame structures with RC mat foundations at depths of about 1.5 m. The groundwater depth was typically 1 – 2 m. Based on a ground motion recording approximately 4 km from the city center, the PGA in Adapazari during this event was likely 0.35 – 0.45 g. Ground failure was systematically observed near structures and less so away from buildings. Building settlements were found to be directly proportional to the building's contact pressure, and its ratio of height to width (i.e., H/B) affected the amount of building tilt.

- Yoshimi and Tokimatsu (1977) performed a series of 1g shaking table tests consisting of rigid model structures on saturated Toyoura Sand, ranging from 30% to 70% relative density, that were subjected to horizontal shaking. Excess pore water pressure ratios under the center of the structure were smaller than away from the structure and

the excess pore water pressure ratio ($r_u = \Delta u/\sigma'_{v0}$) decreased as the weight of the structure increased. Settlement of the model structure increased when r_u reached 0.6, and the settlement decreased as the footing width increased for a given thickness of liquefiable soil.

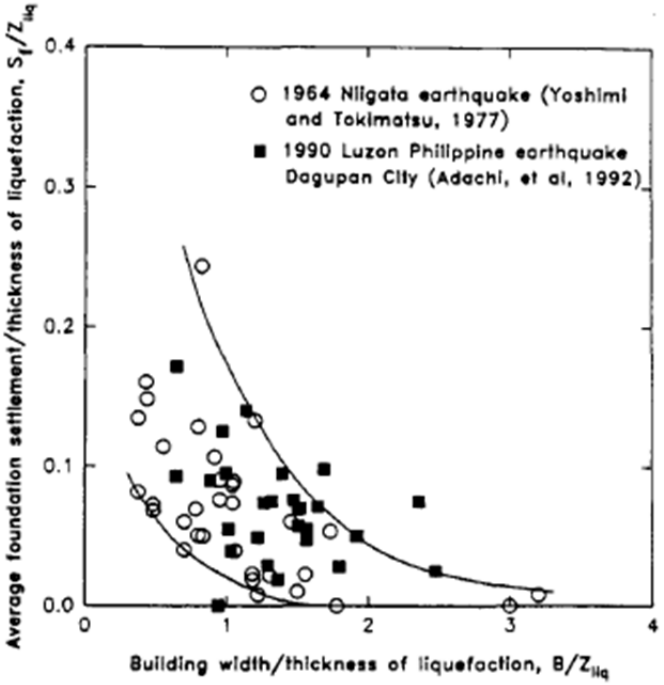

Figure 2.1.1. Normalized foundation settlement versus normalized building width for reinforced concrete buildings in the 1964 Niigata, Japan earthquake and 1990 Luzon, Philippines earthquake (from Liu and Dobry, 1997).

- Whitman and Lambe (1982) and Liu and Dobry (1997) performed geotechnical centrifuge experiments to study the response of rigid, circular footings subjected to soil liquefaction or cyclic softening. Dashti (2009) provides additional details regarding these experiments. Similar to previous studies, excess pore water pressure ratios were smaller beneath the model structures ($r_u < 1.0$) than at locations away from the structures, where $r_u \approx 1.0$ was often observed. Building settlements mainly occurred during shaking. Liu and Dobry (1997) observed that increasing the relative density of the foundation soil decreased structural settlements.

- Hausler (2002) performed a series of six dynamic geotechnical centrifuge experiments to study the effects of ground improvement on the seismic performance of an embedded, shallow-founded model structure subjected to soil liquefaction using realistic, simulated earthquake motions from the 1995 M_w 6.9 Kobe, Japan earthquake. Five key mechanisms were identified that explained the observed ground and structural settlements during these experiments: 1) lateral spreading and high vertical strain of the unimproved, but not liquefied soil under the improved zone or structure when the adjacent free-field soil liquefies; 2) rapid settlement due to loss of strength in the soil below the structure or improved zone when that soil liquefies; 3) rapid settlement due to dynamic compaction in the soil below the structure or improved zone

without full liquefaction of that soil; 4) permanent dilation resulting in negative (expansive) volumetric strains; and 5) long-term settlement due to post-liquefaction dissipation of excess pore water pressure in the soils below the structure or improved zone. The contribution of post-liquefaction reconsolidation settlement to the overall structural settlement was generally minor relative to other mechanisms. Other key findings from this experimental investigation have been presented recently by Sitar and Hausler (2012).

2.2 Field Case Histories

Examples of buildings subjected to soil liquefaction or cyclic softening have been observed in several recent significant earthquake events. These events include the February 27, 2010 M_w 8.8 Maule, Chile earthquake; the March 11, 2011 M_w 9.0 Tohoku, Japan earthquake; and the 2010 – 2011 Canterbury earthquakes affecting Christchurch, New Zealand and the surrounding suburbs and rural areas.

2010 M_w 8.8 Maule, Chile Earthquake

The seismic performance of several modern buildings subjected to soil liquefaction or cyclic softening during the February 27, 2010 M_w 8.8 Maule, Chile earthquake was documented by researchers from the Geotechnical Extreme Events Reconnaissance Association (Bray and Frost, 2010), henceforth GEER, and subsequently summarized by Bray et al. (2012).

These buildings included a modern hospital facility, opened in 2008, in the city of Curanilahue, Chile. The facility consisted of 10 structurally isolated wings with heights ranging from one to six stories (Figure 2.2.1), with the taller wings among the tallest buildings in the city. The buildings primarily resisted lateral forces with concrete shear walls that were sometimes coupled with deep spandrel beams. Gravity loads were carried by interior concrete columns that supported girder-supported floor slabs. The foundation system consisted of shallow, isolated footings and strip footings beneath walls that were interconnected with grade beams. Evidence of liquefaction was observed adjacent to the structures throughout the hospital site. Given the lack of observed liquefaction in other areas and at nearby sites with smaller buildings, this case history appears to illustrate the exacerbating effect of structural inertial loads on the cyclic shear stresses imposed on a building's foundation soils. Relative building movements were documented and are shown in Figure 2.2.2. Wing 1C was the tallest wing, and it settled the most. It settled 11 cm relative to 1A, 9.5 cm relative to 1B, and 1 cm relative to 1D. While structural and nonstructural damage was observed throughout the hospital site, the extent of structural damage was limited due to the isolation gaps provided between adjoining wings. However, there was some damage in areas where the isolation gap closed due to differential building movements and resulted in contact between adjoining wings.

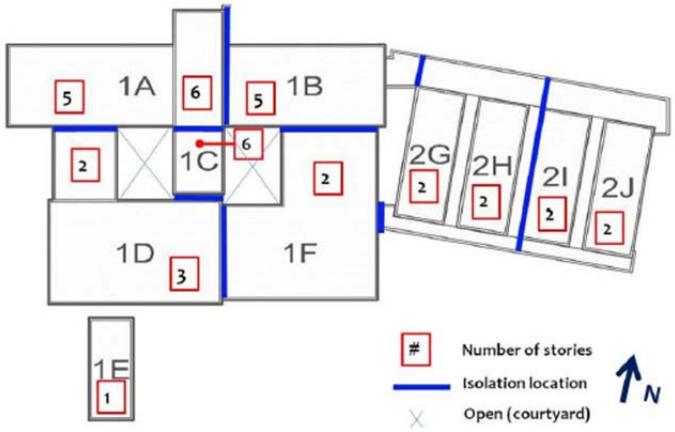

Figure 2.2.1. Plan view showing layout of structurally isolated hospital wings with isolation locations. The number of stories of each wing is indicated (from Bray and Frost, 2010).

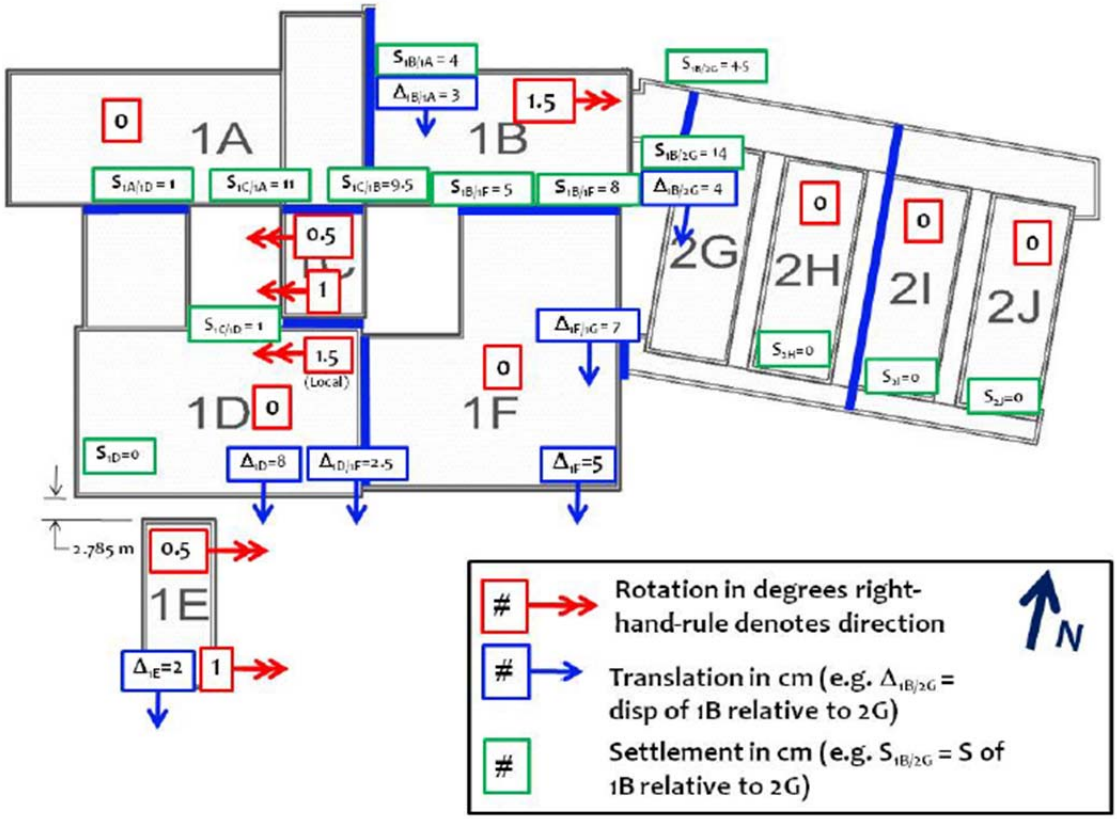

Figure 2.2.2. Relative movements of Curanilahue hospital building (from Bray and Frost, 2010).

An additional field performance case history consisting of a group of four eight-story condominium buildings in Concepcion, Chile was documented by Bray and Frost (2010). This

case history was also summarized by Bray et al. (2012). The buildings had identical floor plans and structural details and appeared to be founded on shallow spread footings with interconnected grade beams. Three of the four buildings were damaged due to liquefaction-induced ground movements and strong shaking. One building was tilted due to approximately 30 cm of differential settlement across its footprint, and this building suffered the most severe structural damage. Sandy fill was placed across the site to raise the ground level prior to construction, and evidence of liquefaction of this material was observed throughout the property. There was no evidence of liquefaction in the street that surrounded the site or at an adjacent property with one- to two-story residences.

2011 M_w 9.0 Tohoku, Japan Earthquake

Liquefaction-induced damage to the built environment in the Kanto Plain region, which includes the Tokyo Bay and Tone River areas, following the 2011 M_w 9.0 Tohoku, Japan earthquake was observed by GEER researchers (Ashford et al., 2011). Light residential and light commercial structures often settled and tilted significantly (Fig. 2.2.3). However, there was often little damage, if any, to the superstructures of buildings supported on mat foundations. Localized settlement depressions were observed around buildings, in addition to broader uneven ground settlements.

Figure 2.2.3. Settlement and tilting of residences in Kamisu City (N35.917, E140.642). Photographs from GEER Association Report No. GEER-025a (Ashford et al., 2011).

A detailed study of liquefaction-induced building damage in Urayasu City was performed by Tokimatsu and Katsumata (2012). Urayasu City consists of three towns, two of which were built on reclaimed land after 1964 using sand excavated from Tokyo Bay as the fill material (i.e., Naka-Machi and Shin-Machi; see Fig. 2.2.4). Fill materials typically extended to depths of about 4 – 8 m below the sea level, and ground surface elevations varied from about 2 m above sea level to greater than 9 m above sea level in several areas. Liquefaction-induced damage was not observed north of the pre-1964 coastline (Fig. 2.2.4), but was commonly observed, to varying degrees, in reclaimed areas. An extensive survey consisting of tilt angle measurements and 3-D laser scanning was performed and led to the following findings: 1) in areas affected by liquefaction, settlements up to 60 cm were observed and settlements and tilts of buildings and foundations were pervasive. Settlement of ground around pile-supported buildings damaged utilities (Fig. 2.2.5); 2) even when foundations settled and tilted, few superstructures atop rigid

foundation systems were damaged; 3) RC houses and houses with RC flooring on the first floor tended to have large settlements, likely because of higher contact pressure; 4) buildings facing each other across a street tended to tilt away from one another, whereas buildings close to one another tended to tilt towards one another. This latter observation was attributed to the combined loads of adjacent buildings causing higher settlements on the shared side; 5) several pile foundations were damaged, and this was likely caused by permanent lateral ground displacement; and 6) in many of the reclaimed areas unaffected by liquefaction, ground improvement of some kind had been performed.

The buildings shown in Fig. 2.2.5b illustrate differential settlements between the 'free-field' ground, a pile-supported building, and a three-story, shallow-founded structure. In this case, the surrounding ground settled approximately 40 cm relative to the pile-supported building, and the three-story, shallow-founded building settled approximately 30 cm relative to the surrounding ground. This is clear case of a shallow-founded building punching into the ground and experiencing more liquefaction-induced settlement than the liquefaction-induced 1-D volumetric reconsolidation settlements of the surrounding level ground.

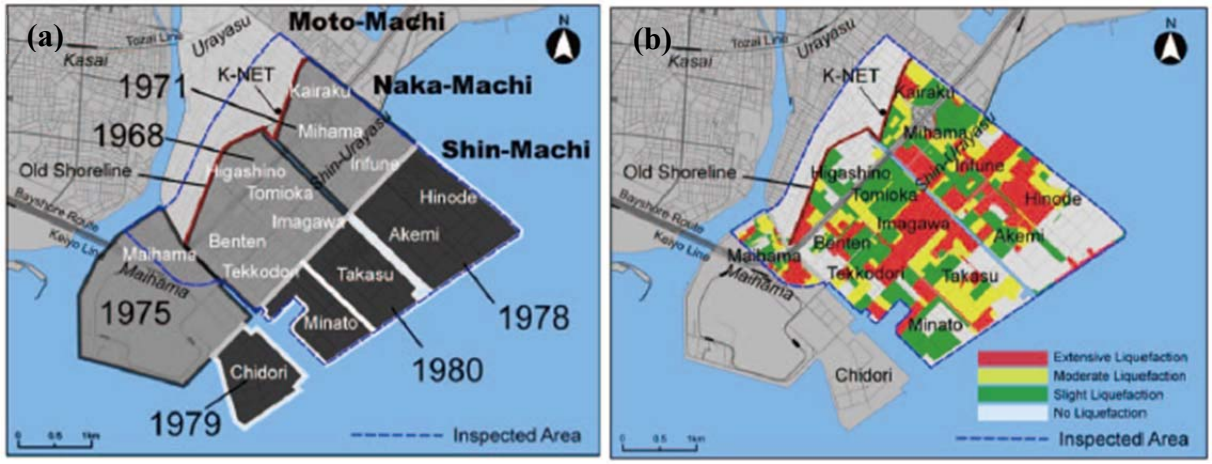

Figure 2.2.4. Maps of Urayasu City showing (a) the years of reclamation work and (b) liquefaction severity from field mapping following the M_w 9.0 Tohoku, Japan earthquake (from Tokimatsu and Katsumata, 2012). Note that the coastline prior to 1964 is indicated in red.

Figure 2.2.5. Examples of (a) large building settlement and tilt and (b) a pile-supported building (left) adjacent to a shallow-founded building (right) that has punched into the ground (from Tokimatsu and Katsumata, 2012).

2010 - 2011 Canterbury earthquake sequence affecting Christchurch, New Zealand and its surrounding suburban and rural areas

The 2010 – 2011 Canterbury earthquake sequence included seven earthquake events with $M_w \geq 5.5$ between September 4, 2010 and December 23, 2011. Of these events, the September 4, 2010 M_w 7.1 Darfield earthquake, February 22, 2011 M_w 6.2 Christchurch earthquake and June 13, 2011 M_w 6.0 earthquake were the largest and caused significant liquefaction in Christchurch, New Zealand and the surrounding suburbs and rural areas. Many buildings in the Central Business District (CBD) of Christchurch, New Zealand were significantly damaged during the Christchurch earthquake, and detailed evaluations of a number of buildings affected by soil liquefaction or cyclic softening are presented in Chapter 4 of this thesis. Cubrinovski et al. (2011a,b, and c) and Bray et al. (2014) provide additional detail about soil liquefaction effects in the CBD during the Canterbury earthquake sequence.

GEER researchers (Green et al., 2010) observed significant damage to houses, light commercial buildings, and school and church buildings due to ground failure following the Darfield earthquake. Buildings settled, tilted, and were subjected to lateral ground movements causing structural components to separate (Fig. 2.2.6). Lateral movements and settlements due to lateral spreading and liquefaction damaged many buildings in Kaiapoi in the vicinity of Kaiapoi River and in the Dallington area in the vicinity of the Avon River. Similar types of liquefaction- and lateral spread-induced damage were observed in the Bexley and Brooklands residential areas.

Figure 2.2.6. Example of residence in Kaiapoi subjected to liquefaction-induced ground movement during the September 4, 2010 M_w 7.1 Darfield earthquake. Note the liquefaction-induced sediment ejecta around the perimeter of the foundation. This house experienced approximately 40 cm of settlement along the north side (from Green et al., 2010).

2.3 Advances in Understanding

Most state-of-the-practice liquefaction triggering assessments consist of applying the simplified cyclic shear stress-based approach first proposed by Seed and Idriss (1971) and later summarized by Youd et al. (2001) wherein the seismic demand is expressed by the cyclic stress ratio (CSR) as follows:

$$[2.3.1] \qquad \text{CSR} = 0.65 * \frac{a_{max}}{g} * \frac{\sigma_v}{\sigma'_v} * r_d$$

where a_{max} = peak horizontal acceleration at the ground surface generated by the earthquake; g = acceleration of gravity; σ_v and σ'_v are the total and effective vertical overburden stresses, respectively; and r_d = stress reduction coefficient that accounts for flexibility of the soil profile. The liquefaction triggering assessment is then performed by estimating the soil's cyclic resistance (CRR), and this is commonly done using correlations with in-situ tests such as the cone penetration test (CPT) or standard penetration test (SPT). The factor of safety against liquefaction triggering is then calculated as the ratio of the resistance to the demand (i.e., FS_l = CRR/CSR). Alternatively, some procedures estimate the probability of liquefaction triggering based on the CSR and CRR. A thorough review of liquefaction triggering procedures is beyond the scope of this thesis and much more information about these procedures can be found in Seed and Idriss (1971), Robertson and Wride (1998), Youd et al. (2001), Seed et al. (2003), Cetin et al. (2004), Moss et al. (2006), and Idriss and Boulanger (2008).

Liquefaction-induced settlements are then commonly estimated using procedures that were developed to estimate post-liquefaction, one-dimensional consolidation settlement in the free-field (Bray and Dashti, 2010). More details about these procedures can be found in Tokimatsu and Seed (1987), Ishihara and Yoshimine (1992), Zhang et al. (2002), Seed et al. (2003), Idriss and Boulanger (2008), and Cetin et al. (2009). Although this approach is commonly applied to estimate liquefaction-induced building settlements, Dashti et al. (2010b), among others, argues that this neglects the importance of other settlement mechanisms that could damage the structure and its surrounding utilities. These other settlement mechanisms are described in more detail below.

Seed et al. (2003) summarized mechanisms causing total and differential liquefaction-induced vertical displacements as follows:

- Figure 2.3.1(a) illustrates ground loss due to cyclic densification of non-saturated soils or volumetric reconsolidation of liquefied or partially liquefied soils as pore water pressures dissipate. The overall magnitude of settlement caused by this mechanism can be estimated using the procedures of Tokimatsu and Seed (1987) and Ishihara and Yoshimine (1992), among others. However, these methods do not reliably predict the magnitude and distribution of locally differential settlements. An improved procedure, based on the work of Wu (2002) was subsequently presented by Seed et al. (2003).

- Figure 2.3.1(b) illustrates ground loss due to erosion of soil particles by water escaping through cracks and fissures as excess pore water pressures dissipate. This is usually localized, and can, therefore, lead to differential settlements. Seed et al. (2003) describes this mechanism as “essentially impossible” to predict.

- Figures 2.3.1(c) through (f) illustrate modes of settlement due to deviatoric ground movements. These mechanisms include rotational slope stability failures, distributed shearing leading to slumping, lateral spread-induced lateral and vertical displacements, and localized lateral movements causing settlement and heave.

- Figure 2.3.1(g) illustrates liquefaction-induced loss of strength and stiffness causing a complete bearing failure. This occurs when the overall bearing capacity, evaluated with post-liquefaction strengths, is insufficient for static equilibrium under gravity loads.

- Figure 2.3.1(h) illustrates partial bearing failure of limited “punching” settlements. These are the result of cyclic softening and the corresponding deformations required to generate enough dilational re-stiffening to arrest movements. This mechanism is associated with cases in which the post-liquefaction strengths are sufficient to prevent full bearing failure, and it can occur at isolated footings or with mat foundations.

- Figure 2.3.1(i) illustrates the mechanism by which cyclic vertical structural loads can be increased due to inertial rocking. This SSI mechanism can exacerbate punching settlements.

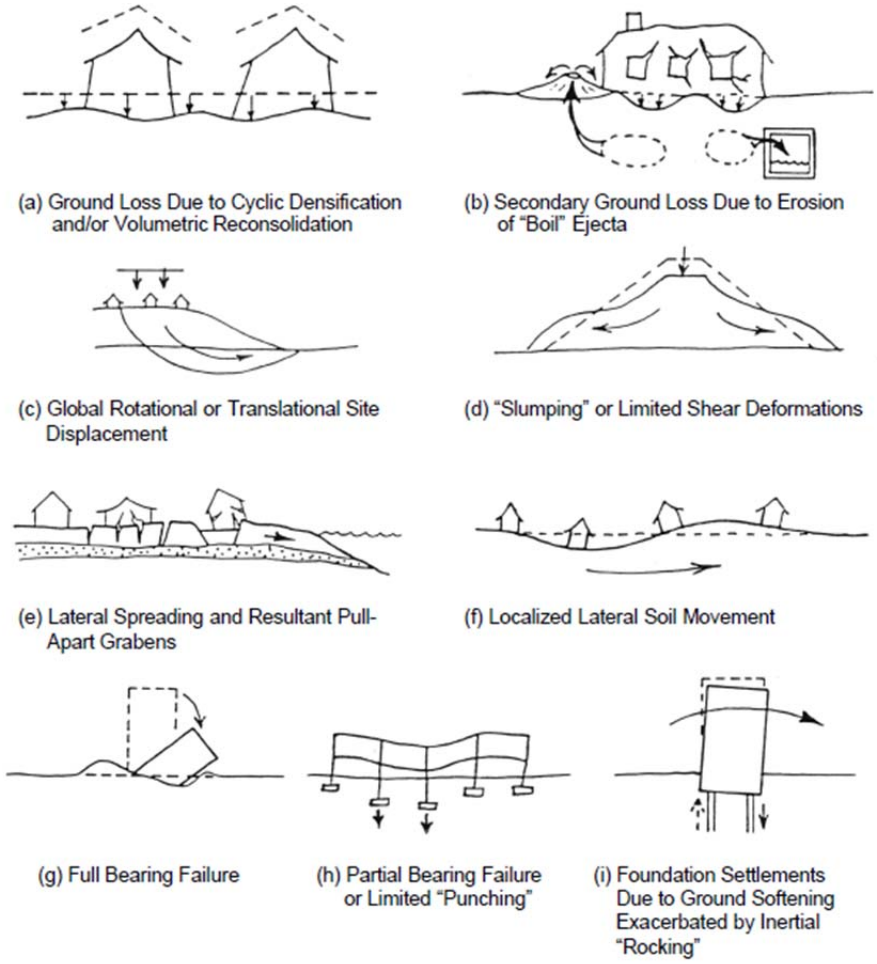

Figure 2.3.1. Schematic illustration of liquefaction-induced vertical displacement mechanisms (from Seed et al., 2003).

Based on the previous work of Dashti (2009) and Dashti et al. (2010a,b) in which a series of centrifuge experiments were performed to develop insight regarding the seismic response of structures subjected to liquefaction or cyclic softening, Bray and Dashti (2010) summarized five primary building displacement mechanisms. These mechanisms were grouped into volumetric-induced displacement mechanisms and deviatoric-induced displacement mechanisms as follows:

Volumetric-induced displacement mechanisms

- Localized volumetric strains during partially drained cyclic loading controlled by 3-D transient hydraulic gradients ($\varepsilon_{p\text{-}DR}$) (Fig. 2.3.2a);

- Downward displacement due to sedimentation or solidification after liquefaction or soil structure breakdown ($\varepsilon_{p\text{-}SED}$); and

- Consolidation-induced volumetric strains as excess pore water pressures dissipate and the soil's effective stress increases ($\varepsilon_{p\text{-}CON}$).

Deviatoric-induced displacement mechanisms

- Partial bearing failure under the static load of structures due to strength loss in the foundation soil resulting in punching settlements or tilting of the structure ($\varepsilon_{q\text{-}BC}$) (Fig. 2.3.2b); and

- Cumulative ratcheting foundation displacement due to SSI-induced cyclic loading near the edges of the foundation ($\varepsilon_{q\text{-}SSI}$) (Fig. 2.3.2c).

Dashti (2010a) provides a detailed discussion describing the effects of varying parameters including PGA, liquefiable layer relative density, liquefiable layer thickness, foundation width, static shear stress ratio, structure height to width ratio, building weight, and 3-D drainage on the settlement mechanisms described above. Additional key findings from this series of geotechnical centrifuge experiments were as follows:

- Building settlements are not proportional to the thickness of the liquefiable layer, and normalizing building settlements by the thickness of the liquefiable layer is misleading and should be avoided.

- Buildings started to settle after one significant ground motion cycle and then settled in an approximately linear manner during shaking. Settlement rates slowed significantly after shaking ceased, and this indicated that volumetric strains due to reconsolidation were relatively less important to the observed building settlements than deviatoric-induced movements, sedimentation, and localized volumetric strains due to partial drainage.

- An increase in relative density of the liquefiable layer of soil increases its resistance to excess pore water pressure generation and cyclic softening leading to smaller settlements due to the $\varepsilon_{q\text{-}BC}$ mechanism. However, the greater stiffness amplifies the dynamic demand imposed on the structures, and this can possibly amplify settlements due to $\varepsilon_{q\text{-}SSI}$.

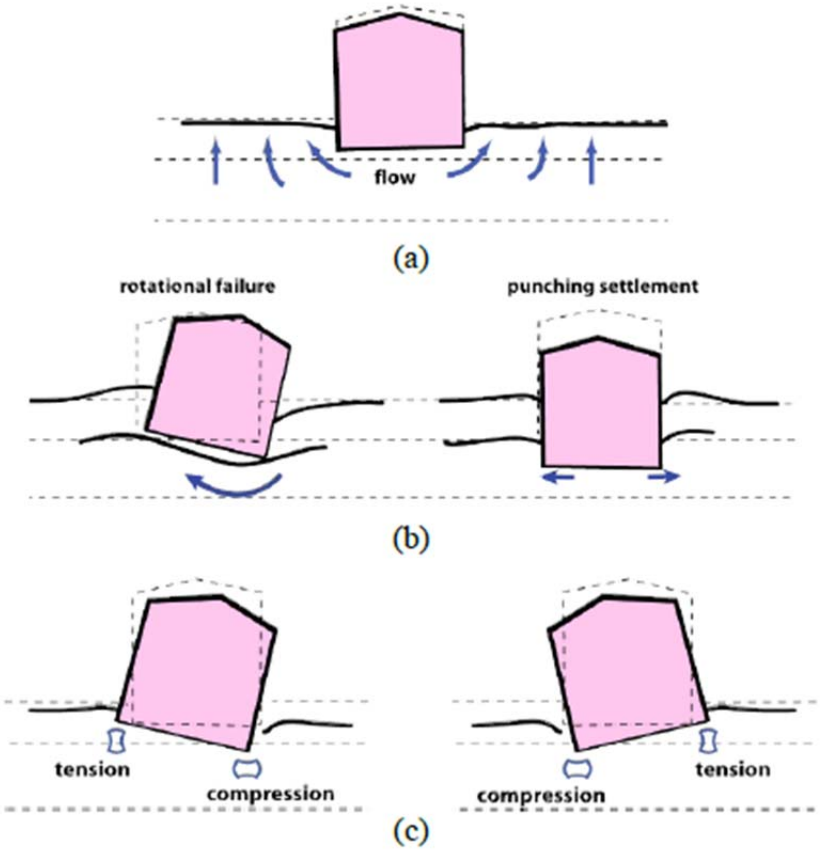

Figure 2.3.2. Liquefaction-induced displacement mechanisms: (a) volumetric strains caused by water flow in response to transient gradients; (b) partial bearing failure due to cyclic softening; and (c) SSI-induced building ratcheting during earthquake loading (from Bray and Dashti, 2010).

- The initiation, rate, and amount of liquefaction-induced building settlement are related to the rate of ground shaking intensity. The rate of ground shaking intensity was found to be captured by the shaking intensity rate (SIR), defined as $I_{a5\text{-}75}/D_{5\text{-}75}$ where $I_{a5\text{-}75}$ is the change in Arias intensity from 5 to 75% of its total value and $D_{5\text{-}75}$ is its corresponding duration.

Karamitros et al. (2013) performed 2-D fully coupled nonlinear effective stress finite difference analyses consisting of a shallow strip foundation over a non-liquefiable clay crust underlain by a 16 m-thick liquefiable sand layer with D_r = 50%. The average bearing pressure of the strip footing, as well as the undrained shear strength and thickness of the clay crust were varied as part of parametric analyses. Several key findings were as follows:

- The presence of a non-liquefiable crust above the liquefiable sand was found to be beneficial to the seismic performance of the strip footings. Settlements decreased as the thickness of the crust increased, and less post-shaking bearing capacity degradation occurred as the thickness and undrained shear strength of the crust increased.

- Foundation-induced deviatoric stresses prevented the excess pore pressure ratio ($r_u = \Delta u/\sigma'_{v0}$) from reaching unity in the foundation soils beneath the footing, whereas $r_u \approx 1.0$ was observed in the free-field.

- The pore water pressure beneath the footing reached its peak value during the early stages of loading and then decreased until it was slightly less than the pore water pressure in the free-field. Based on a comparison of results from undrained and drained numerical analyses, the primary cause of the decrease in excess pore pressures beneath the footing during shaking was argued to be due to shear-induced dilation caused by footing settlement. Permanent deviatoric strains in the soil beneath the strip footing were also found to be sufficient to cause dilation and, therefore, produce negative pore water pressures that outweighed the tendency for pore water pressure generation during cyclic loading. Transient flow due to 3-D hydraulic gradients also contributed, but not as much.

- The vertical footing velocity was nearly constant during shaking. This agrees with previous centrifuge experiments that showed seismic settlement accumulation is approximately linear with time (e.g., Dashti et al., 2010a).

- Foundation settlements occur during shaking as a result of shear deformations in the foundation soil. These settlements can't be predicted using procedures developed for free-field settlements.

Based on the understanding of settlement mechanisms at that time, Seed et al. (2003) provided a preview of a simplified method to estimate liquefaction-induced settlements of shallow-founded structures that was being developed at that time. The approach consisted of first evaluating the potential of a complete bearing failure utilizing post-liquefaction strengths. If the building was safe against a complete bearing failure, settlements should be estimated as a summation of volumetric settlements and deviatoric settlements. Volumetric settlements are primarily the result of post-liquefaction volumetric reconsolidation (i.e., Fig. 2.3.1(a)) and deviatoric settlements result from cyclic loading in combination with static shear stresses due to foundation loads (i.e., Figs. 2.3.1(g) through (i)). Volumetric settlements are then estimated using the existing procedures described previously, in combination with the SSI-exacerbated CSR, in place of the traditional CSR as would be calculated based on Equation 2.3.1, and appropriate K_σ correction. Deviatoric settlements would then be calculated as a function of the SSI-exacerbated CSR, the shear strain potential index (SPI) based on the work of Wu (2002), the initial static shear stress ratio, $\alpha = \tau/\sigma'_v$, and a factor denoted as $K_{\alpha\varepsilon}$ which accounts for accumulation of shear strains in the driving direction. At the time of the Seed et al. (2003) publication, this simplified method was still being refined.

Cetin et al. (2012) presented a simplified method for calculating the SSI-exacerbated CSR (i.e., CSR_{SSEI}). This procedure was based on static and dynamic three-dimensional (3-D) finite difference-based total stress analyses of structures with shallow mat foundations (i.e., 0.3 m to 0.5 m thick) atop four homogeneous soil profiles to calculate cyclic shear stresses that account for deviations from the free-field shear wave vertical propagation pattern (i.e., kinematic soil-structure-interaction) and the transfer of inertial forces from the overlying structure to the foundation soils (i.e., inertial soil-structure-interaction). Four recorded earthquake motions were utilized in this modeling. A schematic illustration of the soil, structure, and earthquake motions

that made up these combinations is provided in Figure 2.3.3. Case histories of liquefaction-induced foundation failures were also modeled. The calculation steps for the procedure are illustrated in the flow chart in Figure 2.3.4.

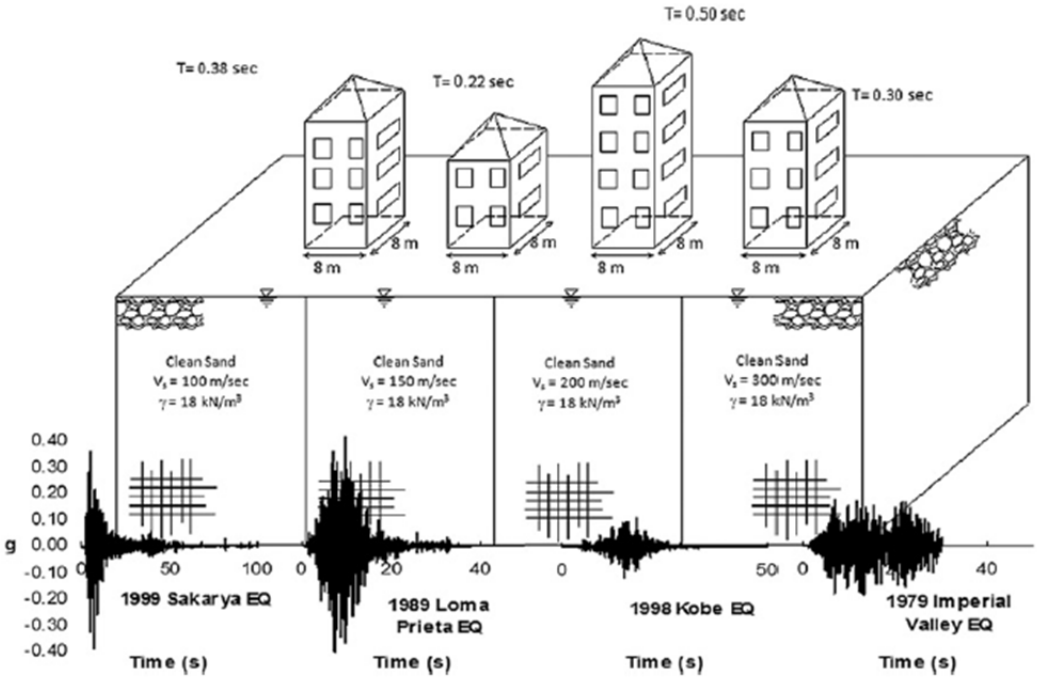

Figure 2.3.3. Schematic summary of soil profiles, structures, and earthquake motions modeled by Cetin et al. (2012) (from Cetin et al., 2012).

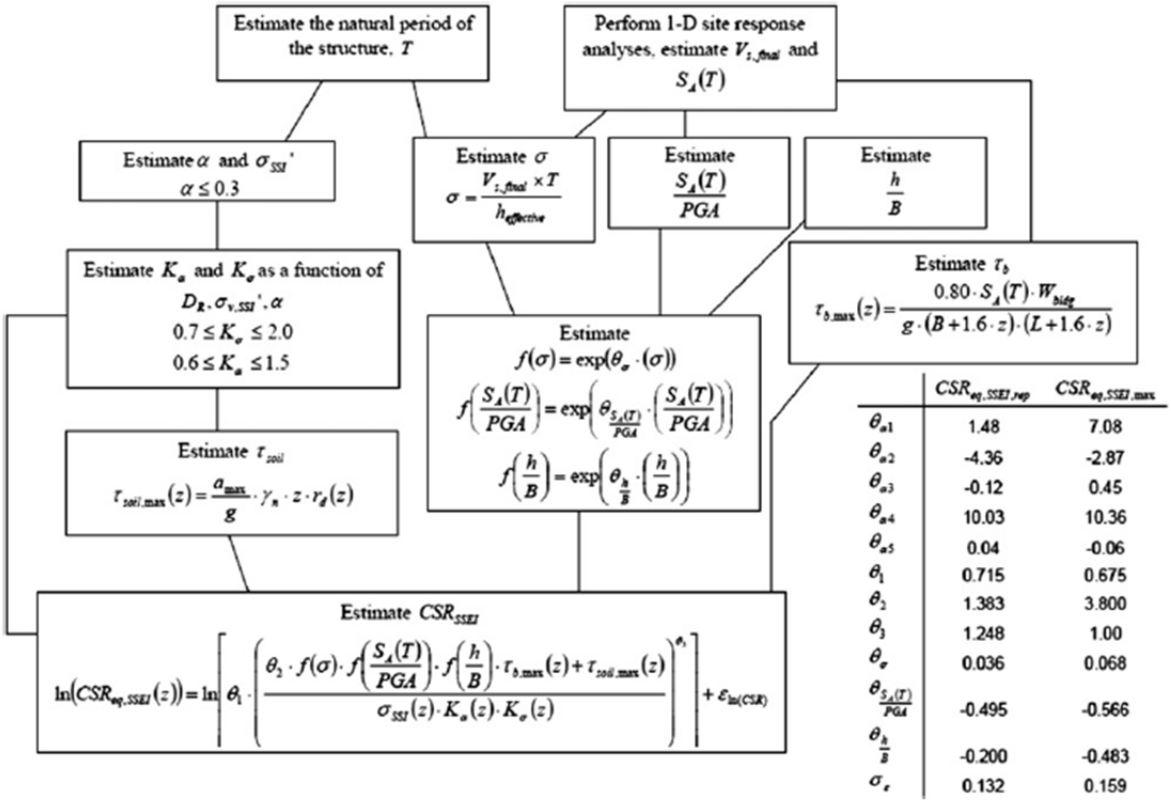

Figure 2.3.4. Calculation steps to estimate CSR_{SSEI} (from Cetin et al., 2012).

Following the general approach described by Seed et al. (2003), and utilizing the CSR_{SSEI} calculated in accordance with Cetin et al. (2012), Unutmaz and Cetin (2012) presented a simplified method to estimate the cyclically-induced settlement and tilting potential of mat foundations. This method was statistically calibrated using case histories primarily consisting of the performance of three- to six-story relatively rigid structures with no basement during the 1999 Kocaeli and Duzce, Turkey earthquakes. The foundation soil profiles at these case history sites consisted primarily of silty soils, sand-silt mixtures, and silt-clay mixtures. Using the maximum cyclic shear strain and post-cyclic volumetric strain relationships developed by Cetin et al. (2009) for sandy soils, and the maximum cyclic shear strain and post-cyclic volumetric strain relationships recommended by Bilge (2010) for silty and clayey soils, volumetric and deviatoric displacement potential indices were estimated. The displacement indices were then calibrated with the observed foundation settlements from the aforementioned case history data set using the method of maximum likelihood. Figure 2.3.5 illustrates the predicted settlements and tilts against the observed data. The data points generally fall within 1:2 and 2:1 lines. Additional field performance case history data from recent significant earthquakes, such as the data presented in Chapter 4, will provide an opportunity to validate or refine these and similar procedures so that they may be adopted to a wider range of conditions.

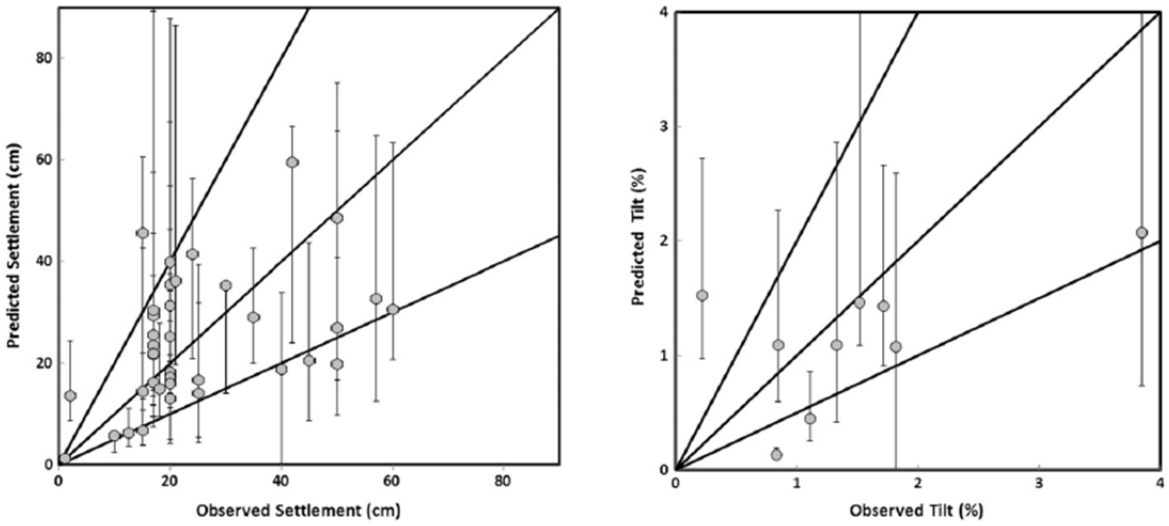

Figure 2.3.5. Predicted settlements and tilts using the procedure presented by Unutmaz and Cetin (2012) versus observed data (from Unutmaz and Cetin, 2012).

CHAPTER 3: GEOTECHNICAL CENTRIFUGE MODELING OF SOIL LIQUEFACTION EFFECTS ON STRUCTURES

3.1 Principles of Centrifuge Modeling

Introduction

The centrifuge experiments described herein were performed using the large centrifuge at the Network for Earthquake Engineering Simulation (NEES) equipment site facility at the University of California, Davis (NEES@UCD). This centrifuge has a radius of 9.1 m, as measured to the bucket floor, a bucket area of 4 m^2, and a maximum payload mass of 4,500 kg. A hydraulic, single-direction, shaking table is mounted on the bucket and was used to apply realistic simulated earthquake motions to the base of the physical model containers. Additional details about the large centrifuge at the NEES@UCD equipment site are available on their website (http://nees.ucdavis.edu) and are provided by Kutter et al. (1994) and Kutter (1995).

Hausler (2002), Dashti (2009), and Mason (2011), among others, have recently provided detailed discussions regarding the principles supporting proper physical modeling of geotechnical phenomena using the centrifuge. In their discussions, the advantages and limitations of this modeling technique are described, and important scaling factors are presented. The interested reader should consult these sources for in depth discussions of these issues. Several of the most important principles and advantages of centrifuge modeling are summarized below:

- The strength and stiffness properties of soil are stress-dependent, and this dependency is non-linear. Physical modeling using the centrifuge allows researchers to generate stresses at model scale that are equivalent to stresses in a much larger prototype. Consequently, soil strength and stiffness can be modeled reasonably well using the geotechnical centrifuge.

- Because strength and stiffness can be modeled reasonably well, geotechnical engineering problems that are governed or strongly influenced by these properties (e.g., liquefaction-induced building settlements) can be modeled reasonably well.

- Centrifuge models are constructed in a controlled laboratory environment. This enables the researcher to control, as much as possible, the placement of the soil and instrumentation. In addition, the construction process can be fully documented. Consequently, centrifuge models are repeatable and series of experiments that build on one another can be planned and executed. For example, Dashti (2009) performed a series of four centrifuge experiments to investigate the mechanisms of liquefaction-induced building settlements. While the thickness of the liquefiable layer and the relative density of the liquefiable sand were varied in these tests, the remaining components of the models were constructed in the same way, and therefore, results between tests could be compared and relevant insights could be gained. This concept of building on previous experiments was also employed in the Seismic Performance

Assessment in Dense Urban Environments project, described by Mason (2011) and summarized in Section 3.2 herein.

- A wide range of instrumentation types are available to measure important quantities. These instruments include accelerometers, pore water pressure transducers, linear potentiometers, and high-speed and analog cameras.

- Realistic simulated earthquake motions can be applied to the physical model while the model is spinning to model earthquake events. This is an important advantage of centrifuge modeling and allows researchers to model reasonably earthquake events at a low cost and in a controlled, well-instrumented, environment.

As with any type of physical modeling, there are limitations to centrifuge modeling. Thorough summaries of these limitations are provided in the previously-mentioned references, and some of the limitations relevant to the work summarized herein are provided below:

- The centrifuge creates a radial gravitational field (g-field) that is proportional to the distance from the axis of rotation. Consequently, gravitational accelerations within the physical model during a centrifuge experiment vary with depth within the model. The depth at which the desired g-field is achieved can be selected by the researcher. As reported by Mason (2011), however, this limitation is relatively minor for the NEES@UCD centrifuge, due to the long (i.e., approximately 9.1 m) centrifuge arm. For the experiments described herein, the difference between the centrifugal acceleration at the soil surface and the base of the soil profile was about 3 g.

- The radial g-field also acts across the transverse direction of the model container. Therefore, if the soil surface is parallel to the base of the model container, the g-field will be non-uniform across the surface in the transverse direction. In order to have a uniform g-field at the surface, the soil surface should be curved in accordance with the radius from the axis of rotation, with the soil surface higher along the longitudinal model boundaries than at the center of the model.

- The model container can lead to undesired boundary effects. The side walls of a flexible container can deflect outward when the model is spinning and lead to a reduction in horizontal stress and provide room for the soil to expand. Container walls can provide additional support to model structures if the model structures are placed close to them. Friction between the container walls and the soil changes the total stresses and may reduce vertical deformations along these boundaries. The base of the model container is rigid compared to the overlying soil and this creates an unrealistic impedance contrast. Lastly, the base of the model container provides a no fluid flow boundary condition.

- Measurement errors are amplified in accordance with the scaling laws described below.

Scaling Laws

Kutter (1995) states the motivation for the development of applicable scaling laws for centrifuge modeling:

> *The basic objective of using a centrifuge is to establish in a reduced scale model identical strength, stiffness and stress as that which exists in a much larger prototype. In other words, we require the scale factor for stress, $\sigma^* = 1$. The scale factor for length, L*, is determined by the size of the prototype and the size of the available centrifuge containers.* (p. 934).

The centrifuge scale factor, N, is defined as the ratio of the prototype-scale length to the model-scale length, $N = L_{prototype} / L_{model} = 1 / L^*$. With the stress scaling factor, σ^*, equal to unity and assuming that the densities of the materials used in the model are the same as the prototype (i.e., $\rho^* = 1$), Kutter (1995) showed that the gravitational acceleration must be increased by the same factor that the lengths have been reduced. Hence, the gravitational acceleration must be increased by N times the acceleration of gravity at prototype scale. Mason (2011) goes through a similar process to derive N. With these fundamental scaling factors between model scale and prototype scale established, other scaling relationships can be derived, some of which are provided in Table 3.1.1. Similar tables are found in Hausler (2002), Dashti (2009), and Mason (2011).

Table 3.1.1. Summary of Key Centrifuge Modeling Scale Factors

Parameter	Prototype Dimension / Model Dimension
Length, L	N/1
Area, A	$N^2/1$
Volume, V	$N^3/1$
Mass, m	$N^3/1$
Density, ρ	1/1
Force, F	$N^2/1$
Stress, σ	1/1
Strain, ε	1/1
Acceleration, gravity	1/N
Acceleration, dynamic	1/N
Time, dynamic	N/1
Frequency, dynamic	1/N
Time, diffusion	$N^2/1$
Energy, E	$N^3/1$

Of key importance in modeling soil liquefaction-related phenomena using the centrifuge is the difference between the scaling factors for dynamic time and diffusion time. Kutter (1995) discusses this time scale factor conflict and argues that this is only a serious problem when the time scales for diffusion and dynamics are of the same order of magnitude. For example, saturated clay under an applied load is unlikely to consolidate significantly during a simulated earthquake. However, excess pore water pressure dissipation in a liquefied soil during and after shaking can occur on the same order of magnitude in time as the dynamic loading. Consequently, researchers studying liquefaction-related phenomena using the centrifuge have often attempted to reduce the influence of this time scale factor conflict by using a viscous pore fluid, as opposed to water, or by using finer-grained soil to reduce the permeability. Stewart et al. (1998) provide guidance regarding the use of hydroxypropyl methylcellulose mixed with water as a viscous pore fluid. While this approach is commonly used, Hausler (2002) indicates that it has been shown that the use of viscous pore fluid can increase the damping of the soil when it is deformed, and that the shear modulus degradation curve is slightly reduced for the case of a soil with viscous pore fluid. Dashti (2009) pointed out that model saturation time increases and there are challenges with workability as the pore fluid viscosity increases. With these considerations in mind, Hausler (2002) used a pore fluid with N/4 times the viscosity of water and Dashti (2009) used a pore fluid with 22 (+/- 2) times the viscosity of water, with a scale factor N = 55. The centrifuge experiment summarized herein used a kinematic viscosity of approximately 21 – 22 times that of water with a centrifuge scale factor N = 55 to be consistent with the similar experiments performed by Dashti (2009).

3.2 Description of Seismic Performance Assessment in Dense Urban Environments Test-5

General

Much of Section 3.2 has been taken from the data report written for Test-5 of the Seismic Performance Assessment in Dense Urban Environments testing series (i.e., Zupan et. al., 2013). The data report, along with raw and processed data files for each simulated ground motion, can be found online through the NEEShub project warehouse at www.nees.org.

Seismic Performance Assessment in Dense Urban Environments

The objective of the project entitled “Seismic Performance Assessment in Dense Urban Environments”, also referred to as the NEESR “Shaking of a City Block” project, is to evaluate the interaction between adjacent structures, as would be present in a dense urban environment during earthquakes through the use of physical and analytical modeling. Just as superstructures interact with their supporting foundations and the foundations interact with the surrounding soil through soil-foundation-structure interaction (SFSI or SSI), adjacent building foundations interact with one another, through the soil, through a process called structure-soil-structure interaction (SSSI). SSSI is not well understood due, in large part, to a lack of well-instrumented field case histories. Consequently, a primary goal of the project was to develop a better understanding of the SSSI phenomenon by means of generating and studying well-instrumented and well-documented model case histories. To this end, the project consisted of a series of six progressive centrifuge experiments using the large geotechnical centrifuge at the NEES@UCD

equipment site facility. Mason (2011) provides a thorough description of the project. The first three experiments (i.e., Test-1, Test-2, and Test-3) are described and interpreted by Mason (2011), the fourth experiment is described and interpreted by Trombetta (2013), the fifth experiment is discussed herein, and the sixth experiment is described by Hayden et al. (2013).

Previous Tests in the Project Series

As described above, the focus of this chapter is on the fifth centrifuge test in a sequence of six tests designed with a primary goal of developing an understanding of SSSI in dense urban environments. The experiment described herein was preceded by HBM02 (Test-1), HBM03 (Test-2), HBM04 (Test-3), and NWT01 (Test-4). These previous experiments were all performed using a uniform subsurface profile consisting of dry, dense Nevada Sand. Data reports for all experiments in the testing series (i.e., Mason et al., 2010a, 2010b, 2010c; Trombetta et al., 2011; Zupan et. al., 2013; and Hayden et al., 2013) are available online through the NEEShub project warehouse at www.nees.org, and additional detail is presented by Mason et al. (2013), Trombetta et al. (2013a), Trombetta et al. (2013b), and Trombetta et al. (2013c). All experiments in this testing series were performed at the previously described NEES@UC Davis equipment site facility.

Test-1 focused on evaluating the effects of SSI on isolated inelastic frame structures subjected to simulated earthquake ground motions. The experiment consisted of a single-story model scale inelastic frame (three-story prototype) with shallow spread footings and a three-story model scale inelastic frame (nine-story prototype) with a one-story-deep basement, positioned far enough from each other to avoid SSSI during large earthquakes. Test-2 consisted of the same two structures positioned directly adjacent to each other to study the changes in the responses of each structure as a result of structural adjacency.

Test-3 consisted of an isolated inelastic frame structure on shallowly-embedded spread footings and a configuration consisting of the same type of frame structure adjacent to an elastic shear wall structure. As in Test-1 and Test-2, the inelastic frame structures were one-story at model scale but intended to represent three-story prototypes. The adjacent structures were aligned in the direction of applied shaking. The relative locations of the structures during Test-3 are illustrated in Figure 3.2.1 (Trombetta et al., 2013b). Both types of structures used during this experiment were designed to have a first, flexible base mode approximately equivalent to the estimated site period to achieve maximum energy transfer from both the soil to the structure and from the structure back into the soil during strong shaking. More detail regarding the design considerations for the structures used in Test-3 is provided in Mason et al. (2010c). Comparison of the response of the isolated frame structure to the non-isolated frame during Test-3 provided a basis for identifying in-plane SSSI (iSSSI or, alternatively, end-to-end rocking) effects and the resulting changes in structural response.

Test-4 was a natural progression from Test-3 and consisted of the same types of inelastic frame and elastic shear wall structures utilized in Test-3. Like Test-3, two sub-configurations were studied in Test-4: (1) an inelastic frame structure placed adjacent to an elastic shear wall structure with the alignment perpendicular to the direction of applied shaking, and (2) an inelastic frame structure with an adjacent elastic shear wall structure aligned in the direction of applied shaking and an elastic shear wall structure aligned in the direction perpendicular to the direction of applied shaking. The Test-4 configuration is illustrated in Figure 3.2.2 (Trombetta et al., 2013b). A comparison of the data obtained from the northern sub-configurations during Test-

3 and Test-4 enabled the identification of anti-plane SSSI (aSSSI or, alternatively, side-to-side rocking) effects. The response of the inelastic frame structure in the southern sub-configuration of Test-4 was hypothesized to contain both iSSSI and aSSSI effects.

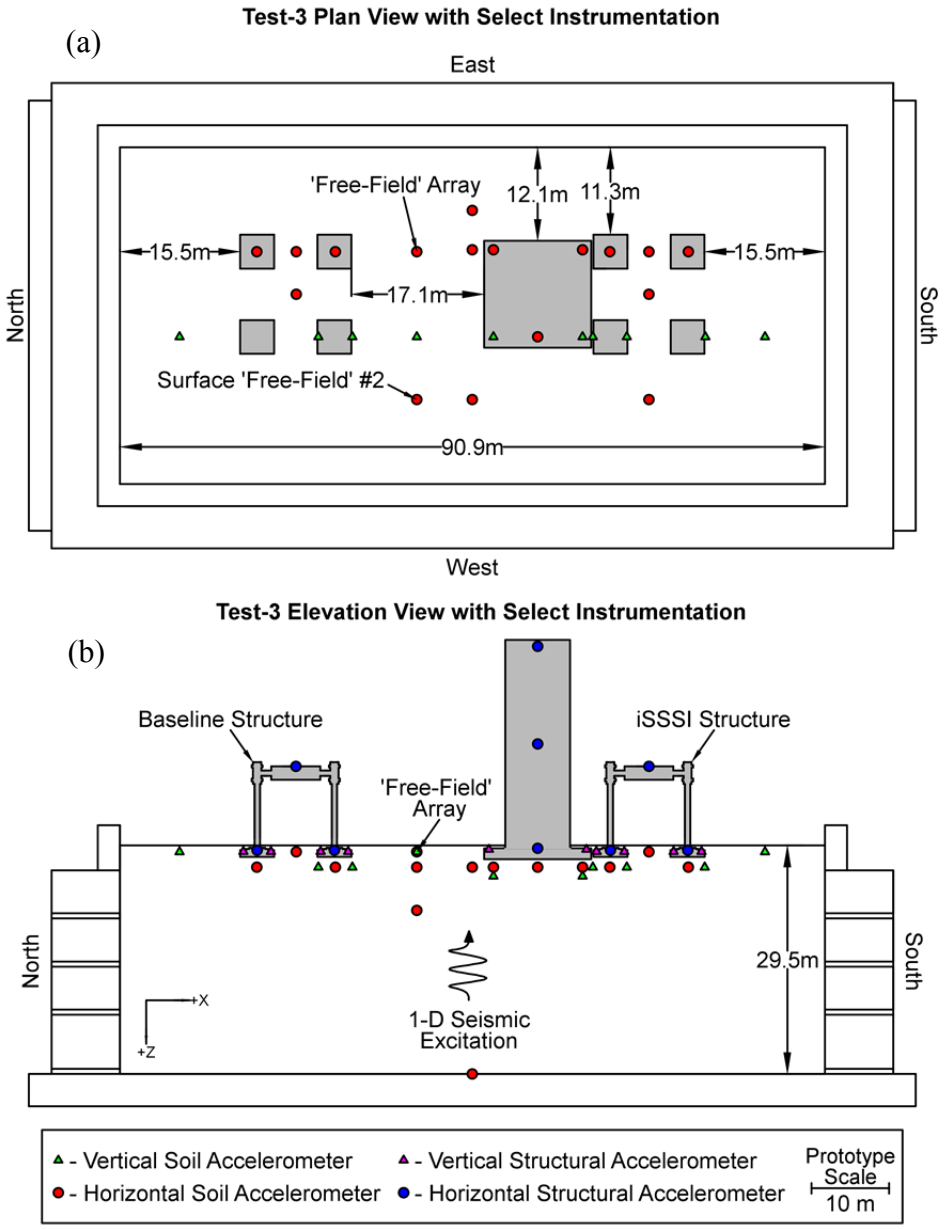

Figure 3.2.1. (a) Plan view and (b) elevation view from west of Test-3 configuration from Trombetta et al. (2013b). Indicated dimensions are prototype scale.

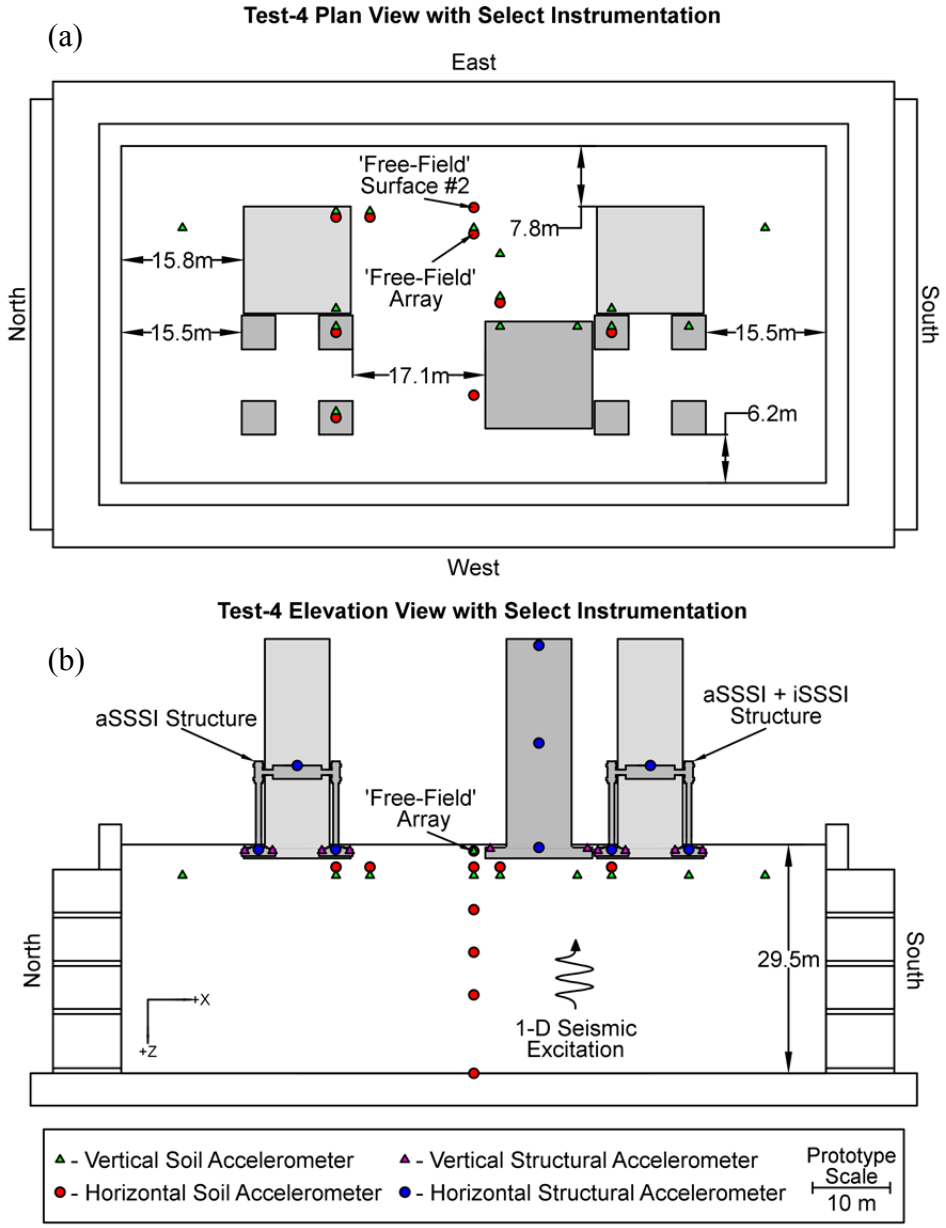

Figure 3.2.2. (a) Plan view and (b) elevation view from west of Test-4 configuration from Trombetta et al. (2013b). Indicated dimensions are prototype scale.

Test-1 through Test-4 were performed with a uniform soil profile consisting of dry Nevada Sand air-pluviated to a relative density of approximately 80%. As described by Mason (2011), the prototype site for this research project was located in downtown Los Angeles, CA (N34.082, W118.224) and the uniform soil profile of dry, dense, Nevada Sand was a reasonable model of the deep, dense, sandy soil deposits that are common in Los Angeles. An added benefit of this soil profile was that a large number of simulated intense earthquake ground motions could be applied, in sequence, without the added complexity of ground failure. Consequently, a large amount of data was collected during each experiment using a comprehensive suite of earthquake ground motions.

Test-5 Purpose and Configuration

As discussed previously, the 1964 Niigata Earthquake (Niigata, Japan), 1990 Luzon Earthquake (Dagupan City, Philippines), 1999 Kocaeli Earthquake (Adapazari, Turkey), and the 2010-2011 Canterbury earthquake sequence on the south island of New Zealand have provided many examples of damage to buildings due to seismically-induced soil liquefaction. Field observations following these important events have motivated earthquake engineering researchers to perform detailed studies of the seismic performance of isolated, rigid, shallow foundations sited atop soils with high liquefaction potential using physical modeling, and several physical models have been tested using the large geotechnical centrifuge at the NEES@UCD facility (e.g., Hausler, 2002; and Dashti, 2009).

Although previous centrifuge experiments have proven to be successful in identifying the underlying mechanisms of liquefaction-induced building displacements, they have thus far been limited to the study of isolated buildings. In accordance with the goals of the Seismic Performance Assessment in Dense Urban Environments project, a comparative approach was employed during Test-5 to explore the effects of building adjacency on the response of structures subjected to realistic earthquake ground motions sited atop shallow soils with high liquefaction potential. Consequently, the soil profile constructed for Test-5 contained a loose to medium-dense layer of Nevada Sand and the soil profile was saturated with viscous pore fluid. Model structures previously used by Dashti (2009) and Allmond and Kutter (2012) were used so that the results from this experiment could be compared with results of recent, similar, experiments studying isolated structures.

The Test-5 configuration is illustrated in Figure 3.2.3 (prototype scale units) and included a layered soil profile with 1.9 m of dense Monterey Sand underlain by 4.5 m of loose to medium-dense Nevada Sand underlain by dense Nevada Sand. The layer of loose to medium-dense Nevada Sand, air-pluviated at approximately 50% relative density, was designed to liquefy when subjected to intense shaking. The model container was divided into four quadrants. The northwest quadrant contained an isolated single degree of freedom (SDOF) model structure intended to represent a 2-story prototype building on a rigid mat foundation. This model building type will be referred to from this point forward as an 'A' building as it was originally designated as building type 'A' in the previous work of Dashti (2009). The purpose of the northwest quadrant was to establish the response of an 'A' building in relative isolation. This was the control case upon which the responses of the other 'A' buildings were to be compared. The northeast quadrant consisted of two 'A' buildings located adjacent to one another and separated by approximately 0.165 m. The objective with the northeast quadrant was to study the response of adjacent identical buildings. The southwest quadrant consisted of an 'A' building and a larger SDOF model structure with a shallow, rigid, foundation, referred to from this point forward as a 'J' building. The 'J' building was originally used in work performed by Allmond and Kutter (2012) and is intended to represent a prototype column supporting a superstructure. Allmond and Kutter (2012) employed six identical 'J' buildings to represent a prototype bridge. The objective of the southwest quadrant was to study the response of an 'A' building located adjacent to a much larger, yet still relatively simple building, on a shallow foundation. The southeast quadrant consisted of an 'A' building located adjacent to a 'J' building founded on piles.

From this point forward, the buildings will be referred to using a convention consisting of the building type followed by the adjacent building type as a subscript. In summary, the isolated ‘A’ building in the northwest quadrant will be referred to as A, the northern ‘A’ building in the

northeast quadrant will be referred to as $A_{A\text{-}N}$, the southern 'A' building in the northeast quadrant will be referred to as $A_{A\text{-}S}$, the 'A' building in the southwest quadrant will be referred to as A_J, the 'J' building in the southwest quadrant will be referred to as J_A, the 'A' building in the southeast quadrant will be referred to as $A_{J\text{-}pile}$, and the 'J' building in the southeast quadrant will be referred to as J-$pile_A$. The building names are indicated on Figure 3.2.3 for reference.

A total of 61 ICP accelerometers, 18 MEMS accelerometers, 26 pore water pressure transducers (PPTs), and 32 linear potentiometers (LPs) were incorporated into the Test-5 plan. The locations of these instruments are illustrated in Figures 3.2.4 – 3.2.6 and additional detail regarding the characteristics of the instruments used for this test is provided below. The coordinates of all instruments, available through NEEShub (www.nees.org), are relative to an origin at the northwest corner of the top of the top ring of the model container.

The centrifugal acceleration used for this test was approximately 55 times the acceleration of gravity at the designated effective radius (i.e., 55 g), corresponding to the center of the loose to medium-dense Nevada Sand layer. This centrifugal acceleration is consistent with previous tests in the project testing series, and also consistent with the centrifugal accelerations used by Dashti (2009) and Allmond and Kutter (2012). Simulated earthquake ground motions were applied at the base of the model container in the north-south direction. In total, Test-5 consisted of 11 shaking events. These events included 6 step waves and 5 ground motions. The step waves were used to level the bucket of the centrifuge, warm up the shaking table, and allow the research team to check instrumentation.

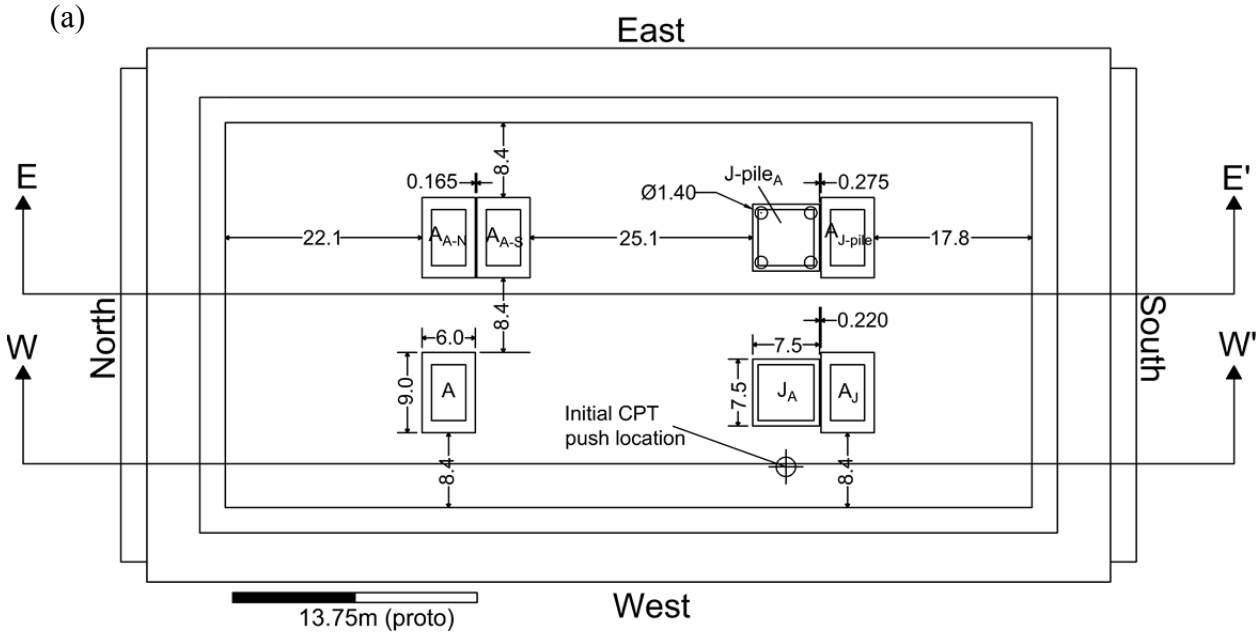

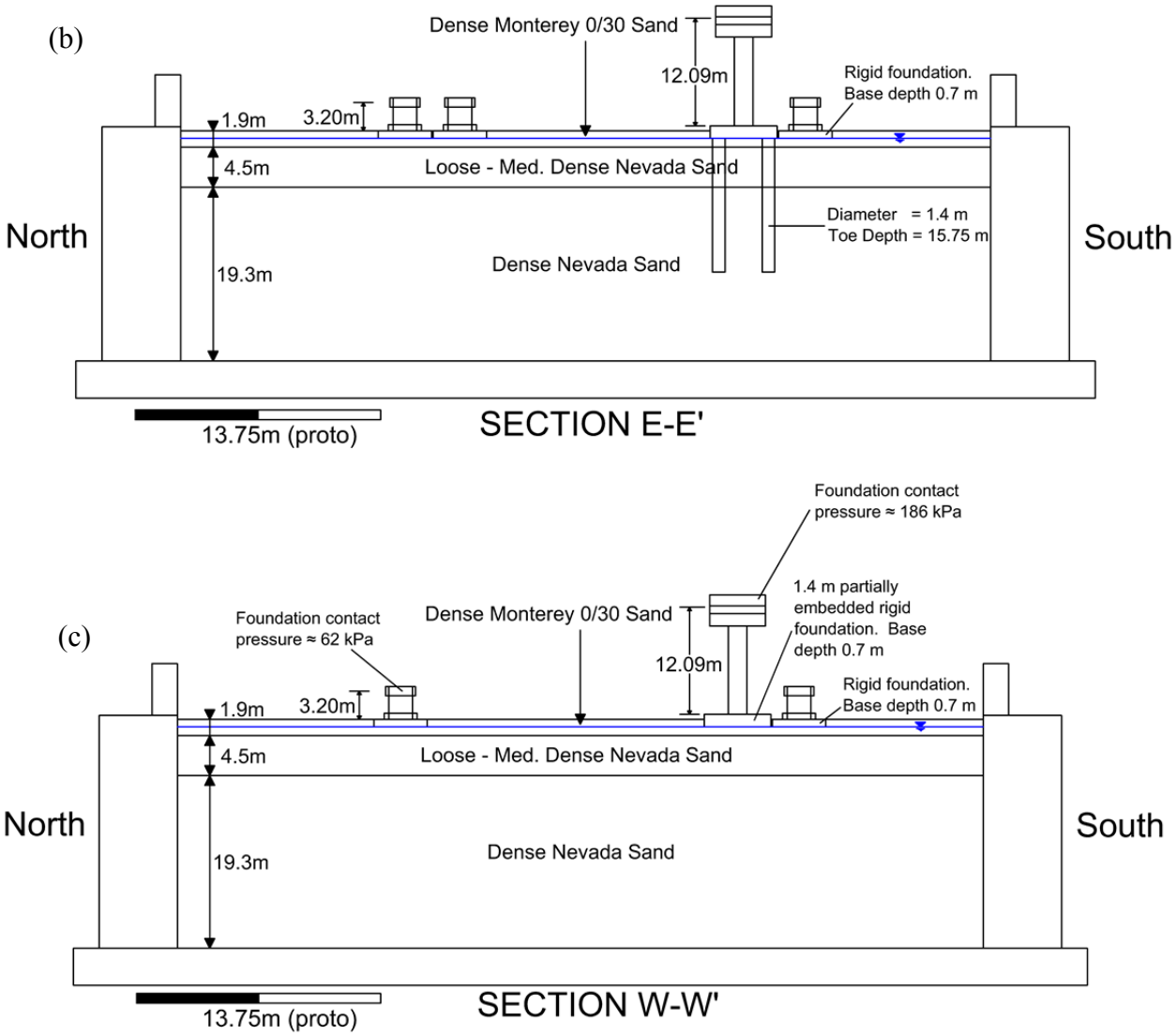

Figure 3.2.3. (a) Plan view, (b) elevation view along E-E', and (c) elevation view along W-W' of the Test-5 configuration. Indicated dimensions are prototype scale. As will be described subsequently, the groundwater depth, indicated by the blue line in this figure, was approximately 0.37 m during the PRI_small event, 0.50 m during the PRI_mod event and 0.87 m during the TCU_mod and PRI_large events, respectively.

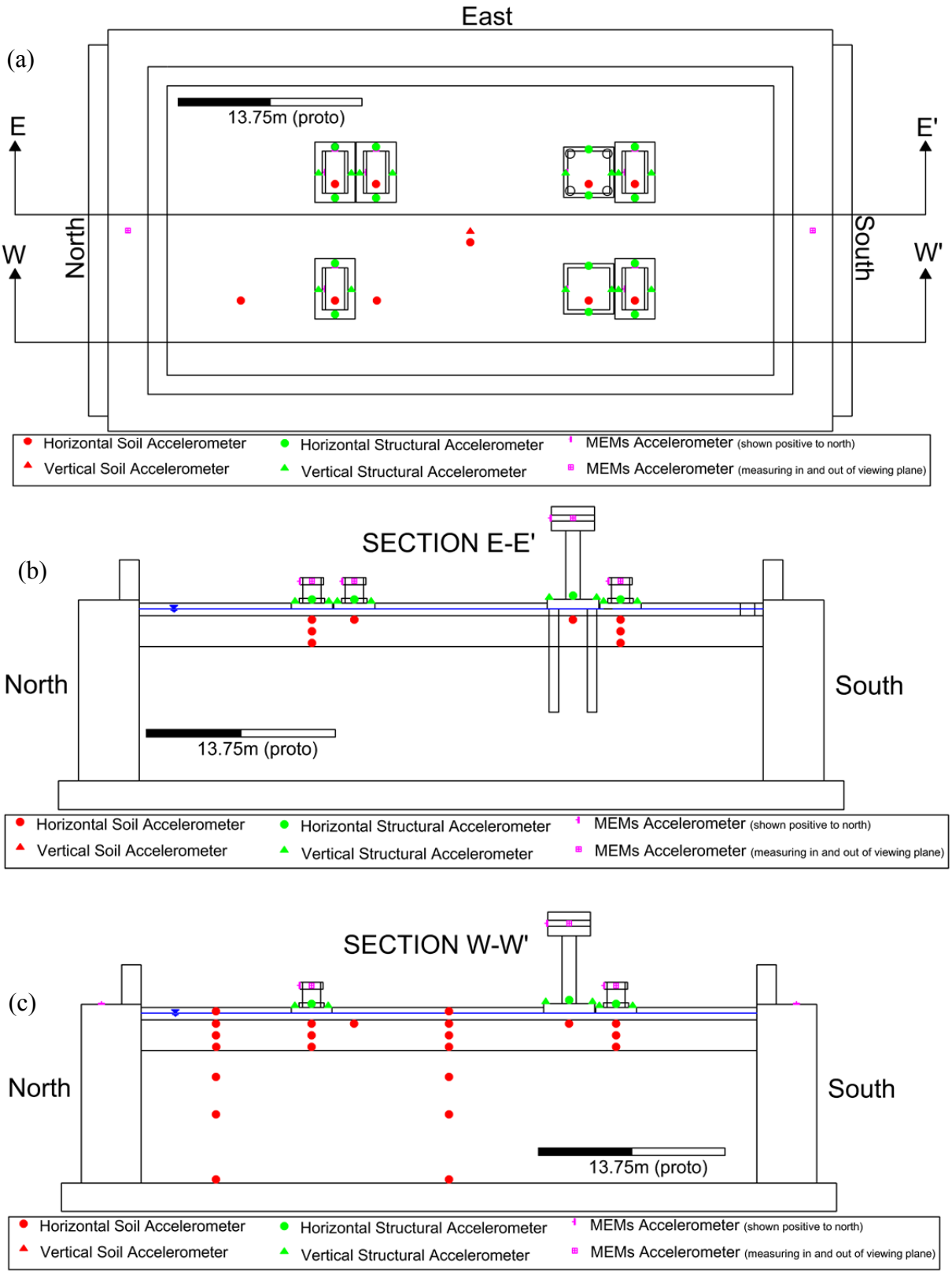

Figure 3.2.4. (a) Plan view, (b) elevation view along E-E', and (c) elevation view along W-W' showing the Test-5 accelerometer locations.

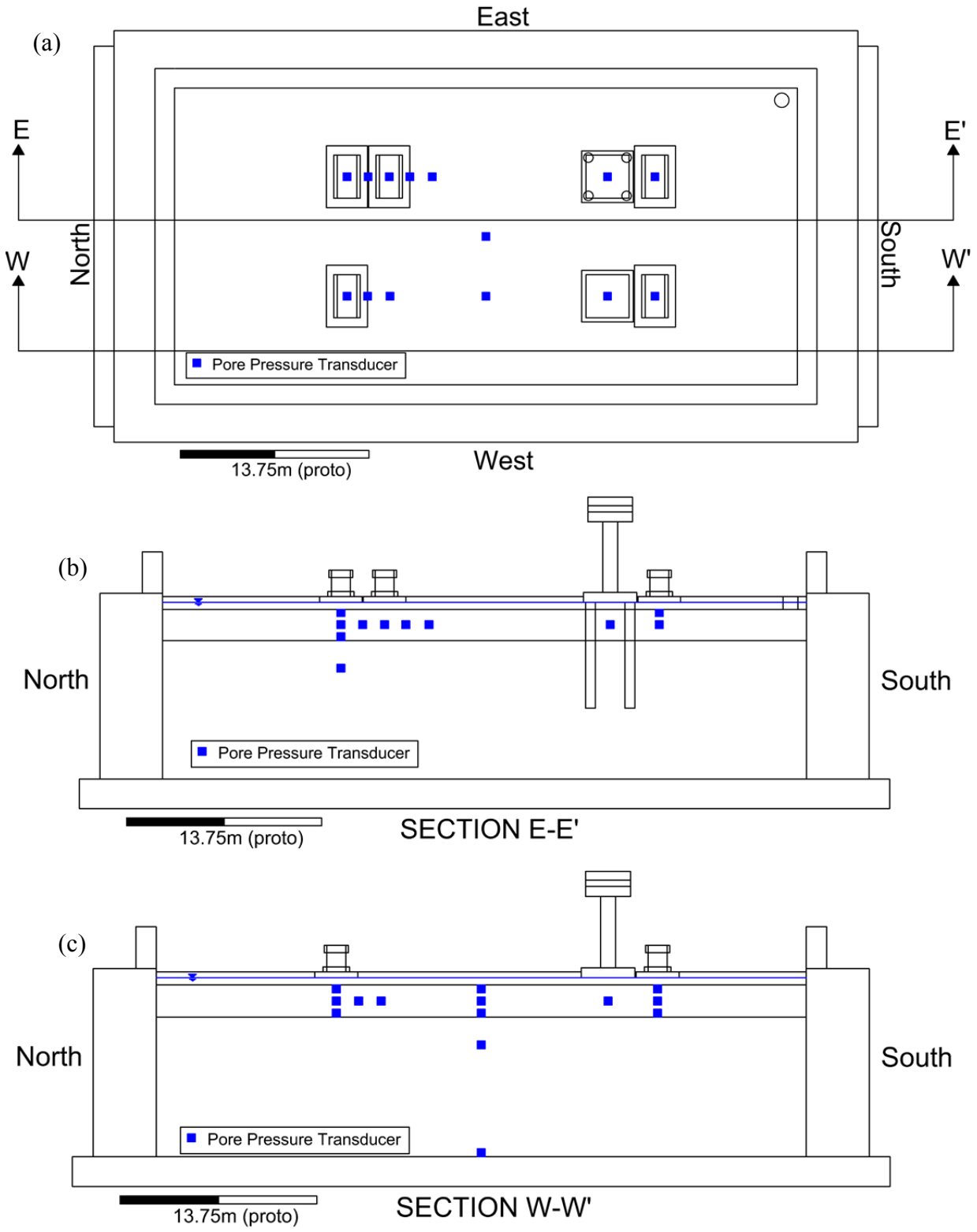

Figure 3.2.5. (a) Plan view, (b) elevation view along E-E', and (c) elevation view along W-W' showing the Test-5 PPT locations.

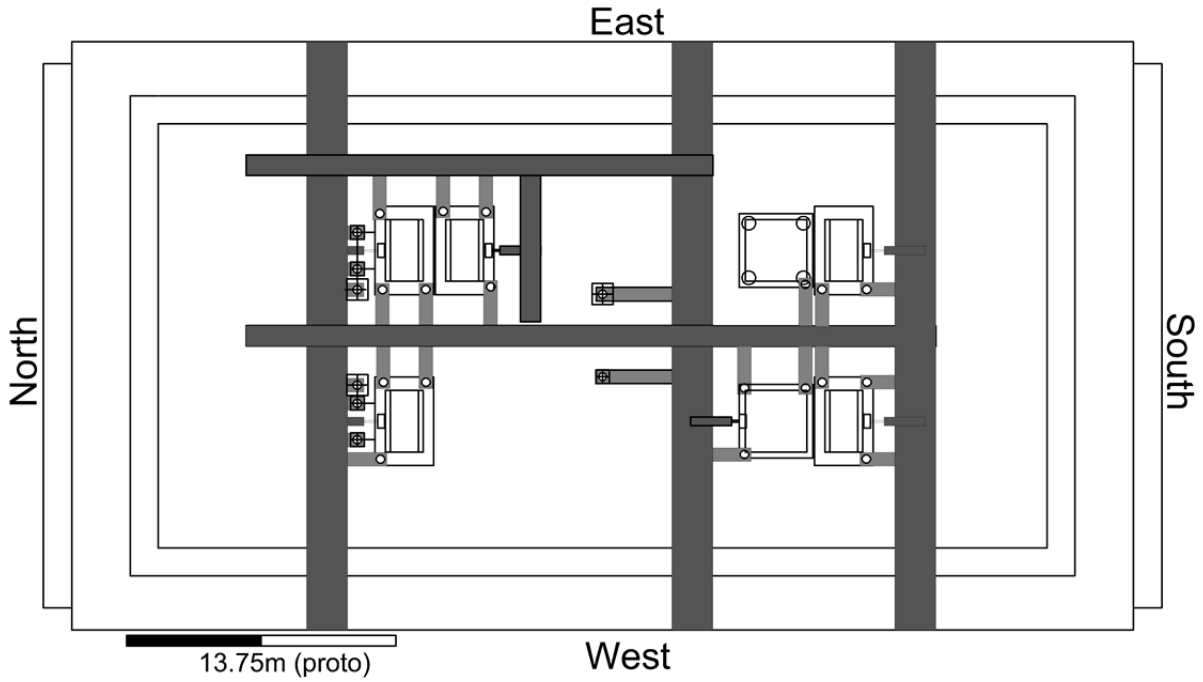

Figure 3.2.6. Test-5 LP location plan.

Soil and Pore Fluid Properties

As illustrated in Figure 3.2.3, the subsurface profile for Test-5 consisted of 1.9 m of dense Monterey 0/30 Sand at the surface, underlain by 4.5 m of loose to medium-dense Nevada Sand, underlain by 19.3 m of dense Nevada Sand. The model was saturated using a solution of hydroxypropyl methylcellulose (HPMC) and water with a target kinematic viscosity of approximately twenty times the kinematic viscosity of water. The initial concentration of HPMC was based on recommendations provided by Stewart et al. (1998). The concentration was then adjusted, as necessary, following regular fluid viscosity tests using an Ubbelohde-type viscometer. The target pore fluid table (referred to from this point forward as the groundwater table (GWT)), indicated on Figure 3.2.3, was at the base of the foundations of the model structures, at a depth of approximately 0.7 m below the soil surface. The achieved GWT depth, based on pore water pressure transducer data collected just prior to the application of the simulated earthquake motions, was approximately 0.37 m during the PRI_small event, 0.57 m during the PRI_mod event, and 0.87 m during the TCU_mod and PRI_large events, respectively.

Nevada Sand is a mined, non-processed, material. Consequently, the engineering properties of Nevada Sand are not constant and will change with each batch delivered to the NEES@UCD facility. The batch of Nevada Sand used during Test-5 was tested by Cooper Testing Labs in August 2010 to evaluate representative characteristics of the material. The laboratory tests consisted of a particle size distribution, determination of the minimum and maximum index unit weight (ASTM D4254 and ASTM D4253), and the determination of the specific gravity of the material (ASTM D854). Testing indicated that 6.7% of the particle size distribution sample passed the No. 200 sieve and the fines were non-plastic. Consequently, this

sample is classified SP-SM using the USCS methodology. Key results from the laboratory tests are summarized in Table 3.2.1.

As described by Wu (2002), Monterey 0/30 Sand is a type of commercially available washed and sieved beach sand. It can be classified as uniform, medium-grained, sub-rounded, clean sand composed primarily of white to tan quartz grains with a smaller amount of darker feldspar and mica grains (Wu, 2002; Kammerer, 2002). The average grain size, D_{50}, is typically on the order of 0.35 mm to 0.45 mm and the coefficient of uniformity, C_u, has been reported by previous researchers (e.g., Kammerer, 2002) to be between 1.2 and 1.3. Dashti (2009) provided a summary of the specific gravities, minimum and maximum void ratios, and minimum and maximum unit weights reported by previous researchers, and that summary has been reproduced here as Table 3.2.2. The target parameters for the Monterey 0/30 Sand reported in Table 3.2.2 were employed during the testing series described by Dashti (2009) and for Test-5.

Table 3.2.1. Important properties of Test-5 Nevada Sand

Quantity	**Value**
Supplier	Pyro Minerals, 2510 Wood Street Oakland, CA 94607
USCS Classification	SP-SM
Gradation	Poor
Specific Gravity	2.66
D_{30}	0.11 mm
D_{60}	0.16 mm
Coefficient of Uniformity	2.07
$\gamma_{d,max}$ (kN/m^3)	17.2
$\gamma_{d,min}$ (kN/m^3)	14.7

Table 3.2.2. Important properties of Monterey 0/30 Sand (modified from Dashti, 2009)

Source	Method	G_s	e_{min}	e_{max}	$\gamma_{d,min}$ (kN/m^3)	$\gamma_{d,max}$ (kN/m^3)
Wu (1999)	Dry Tipping	2.64	0.541	0.855	13.96	16.81
Nova-Roessing (1998)	Modified Japanese	-	0.530	0.830	14.15	16.93
Target	-	2.64	0.536	0.843	14.06	16.86

Model Structures

As described previously, two types of model structures were used during Test-5: 'A' buildings and 'J' buildings. Details regarding the design of the 'A' buildings are available in Dashti (2009) and details regarding the design of the 'J' buildings are available in Allmond and Kutter (2012). Construction drawings for these model structures are available online through NEEShub.

It is worth noting that there were a couple of minor modifications made to the Test-5 'J' buildings relative to the buildings previously utilized by Allmond and Kutter (2012). Firstly, the columns were welded to a column baseplate that could be bolted to the foundation. This modification allowed for the foundations to be installed during the model construction phase in the model preparation shop while the columns and structural lumped masses (referred to from this point forward as lumped masses or lumped mass) could be connected to the foundations following model saturation. This was necessary because the columns and lumped masses of the 'J' structures would not fit underneath the lid used to seal the model during saturation. Secondly, the foundation of the 'J' building in the southeast quadrant was connected to four 2.54 cm-diameter (model scale) aluminum piles. The piles were solid aluminum but they were counter-bored at the top with an inner diameter of 2 cm to a depth of 1.27 cm. The centers of the piles were then threaded to accept 1/4" - 20 thread rod for an additional 4.45 cm. Once sand was pluviated to the top of the piles during model construction the connection between the piles and foundation then consisted of the following steps:

1. 1/4" thread rod was installed in each pile and tightened with a lock washer and hex nut;
2. A second hex nut was then spun down the thread rod and glued into place leaving approximately 1/4" length of thread rod exposed between nuts;
3. Heat shrink tubing was then placed over the thread rod assembly to the top of the top hex nut and shrunk into place;
4. Sand was pluviated around and between the piles to the top of the pile connection assembly;
5. Holes were then drilled through the 'J' building foundation at the appropriate locations and the foundation was placed over the thread rod and on to washers placed on top of the hex nuts; and
6. The assembly was then tightened from the top.

The resulting connection was intended to minimize moment transfer between the piles and the superstructure.

Other important details of the model structures, including as-built measurements, are provided by Zupan et al. (2013). It is worth noting here that the model 'A' structures had an average foundation contact pressure of approximately 62 kPa and the J_A building had an average foundation contact pressure of approximately 186 kPa. Hayden et al. (2013) measured the fixed-base fundamental period of the 'A' and 'J' buildings to be 0.32 s and 0.85 s, respectively. In addition, the surface of the footings of all model structures were covered in Monterey 0/30 Sand along the base and the sides. To do this, the smooth aluminum footings were roughened with a wire brush and then coated with epoxy adhesive. Monterey 0/30 Sand was then spread over the epoxy and allowed to set. Similarly, the model piles surfaces were covered with Nevada Sand.

Model Construction

The following steps provide a general outline of model construction:

1. Prior to model construction, Nevada Sand was obtained from the stockpile at the NEES@UCD facility and dried in a large oven to make sure that there was no moisture in the soil during pluviation. Monterey 0/30 Sand was also dried in the large oven prior to placement in the model container. In addition to drying the soil, an attempt was made to mix the Nevada Sand as much as practical as it was obtained from the stockpile to maximize uniformity during placement.
2. The instrumentation was prepared for installation: ICP accelerometers were checked to make sure they were functioning properly and then waterproofed using a coat of primer followed by one to three coats of synthetic rubber (Plasti Dip). Calibration values for the linear potentiometers (LPs) and pore water pressure transducers (PPTs) were determined by following calibration procedures under the guidance of NEES@UCD staff (Figure 3.2.7). PPTs were dried prior to installation in the model.

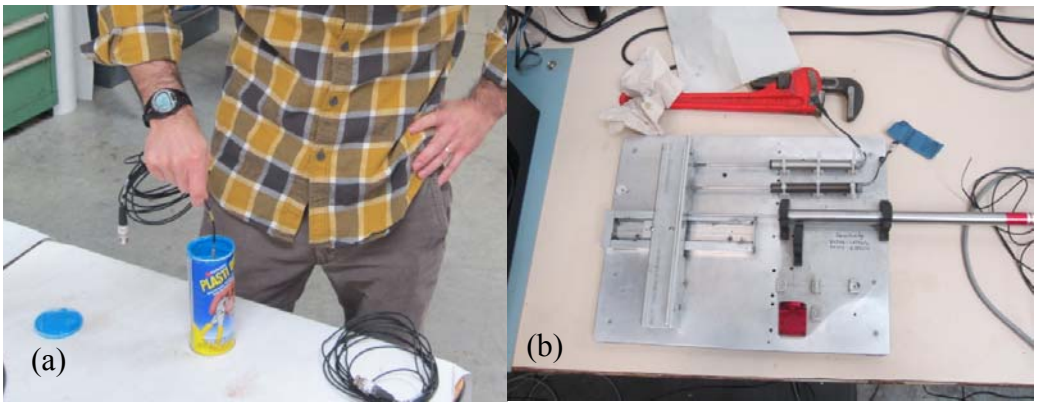

Figure 3.2.7. (a) Waterproofing ICP accelerometer with synthetic rubber. (b) View of the LP calibration station. (c) View of the PPT calibration station.

3. The model structures were prepared for installation. This included cleaning all parts, applying Monterey Sand around the base and the sides of the 'A' building and 'J' building footings, assembling the model structures, and installing the LP mounts (Figure 3.2.8). Model piles were coated in Nevada Sand. The masses of the model structure were wrapped in checkered contact paper to reduce light reflection and improve high speed and analog camera photo quality.

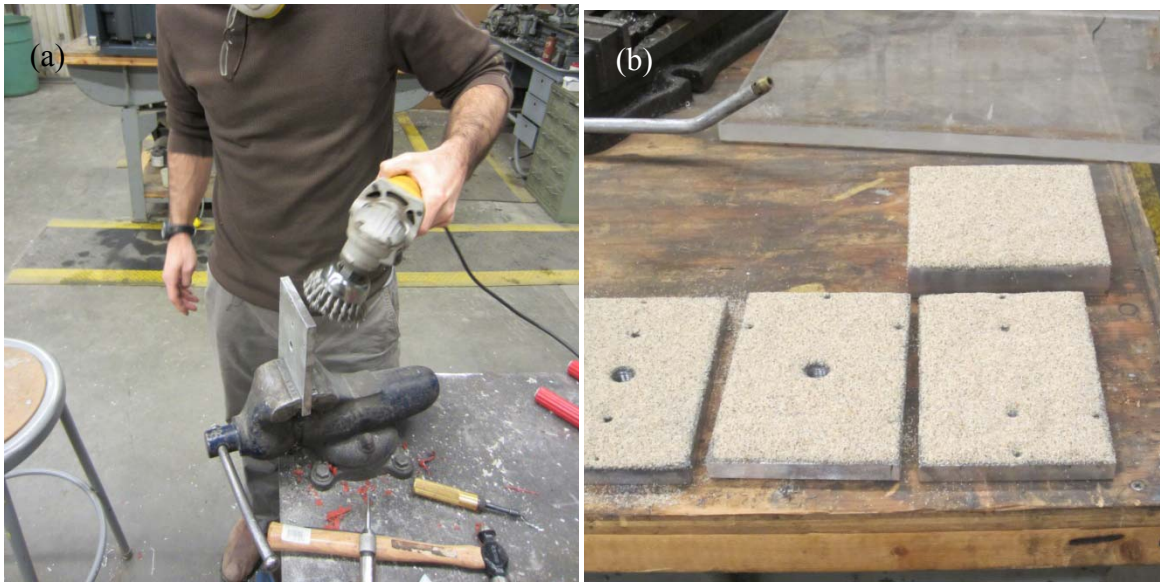

Figure 3.2.8. (a) Base and sides of foundation elements were roughened. (b) A thin layer of Monterey Sand was coated on the base and sides of the foundation elements using epoxy adhesive.

4. The model container (FSB 2.1) was obtained and cleaned. This container has approximate internal model scale dimensions of 1650 mm (length) by 790 mm (width) by 580 mm (depth). The coordinates used to identify the locations of instrumentation and the model structures are relative to an origin at the northwest corner of the inside of the model container with the x-axis measured in the north-south direction (positive to the south), the y-axis measured in the east-west direction (positive to the east) and the z-axis measured vertically (positive downward). This coordinate system is consistent with the coordinate system used in previous NCB experiments.
5. Subsurface saturation system components were installed. Twelve rectangular porous stones were installed at the base of the model container (six were installed at the north end and six at the south end). Each of the porous stones was connected to two plastic tubes. The larger of the two plastic tubes was sized such that it would connect to the saturation troughs during saturation and thus provided a conduit for pore fluid so that the model could be saturated from the bottom up. The smaller of the two plastic tubes was routed along the sides of the model container to above the future soil surface and was intended to provide a means for air bubbles to escape during saturation. Figure 3.2.9 is a photograph showing a plan view of the subsurface saturation system components.

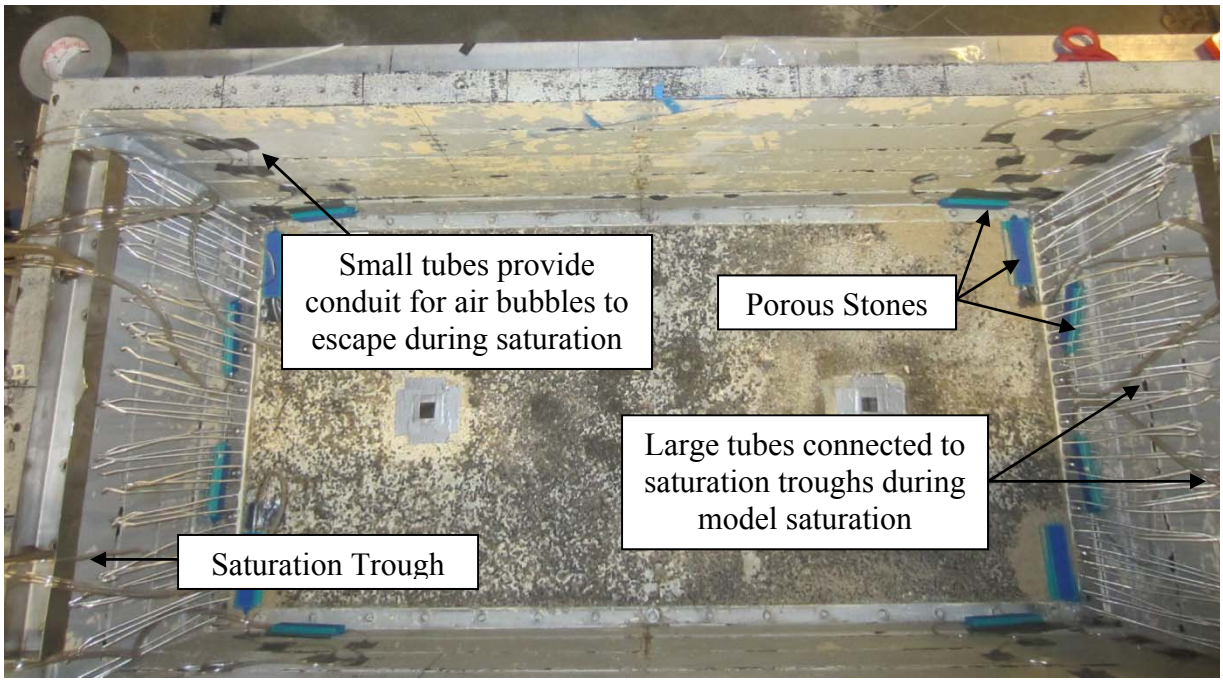

Figure 3.2.9. Plan view photograph of the subsurface components of the model saturation system. Saturation troughs are also shown for reference.

6. Instrumentation was installed on the base of the container (Figure 3.2.10). ICP accelerometers were seated in modeling clay and PPTs were seated on a thin layer of Nevada Sand. Instrumentation cables were routed up the interior side walls of the model container and secured using duct tape.

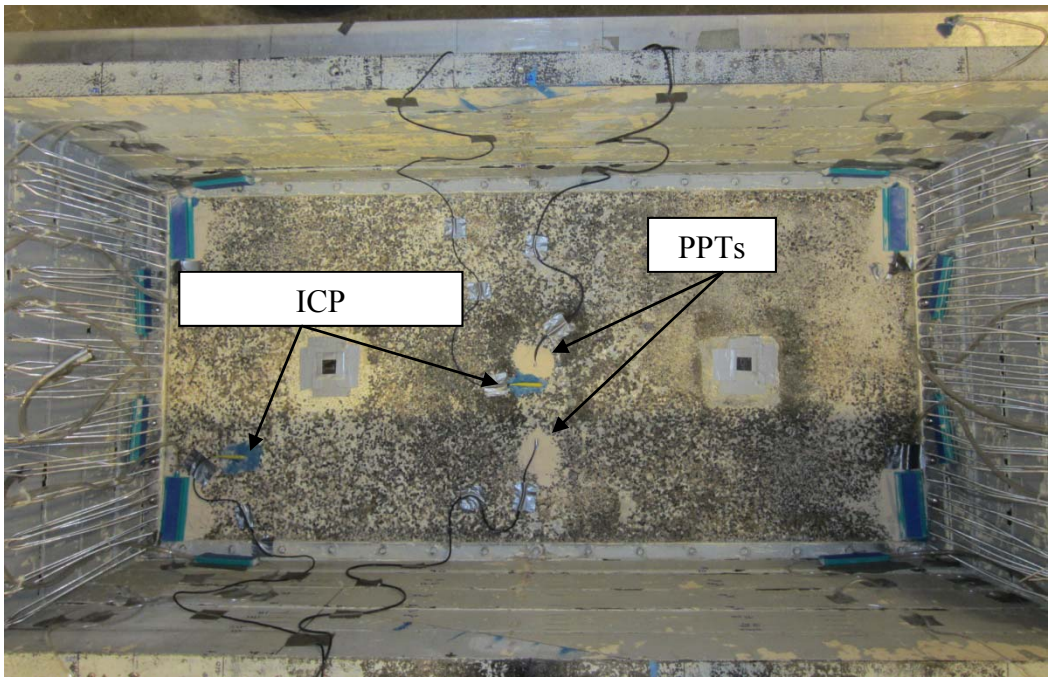

Figure 3.2.10. Plan view photograph of the base instrumentation

7. The container weight was measured.
8. Nevada Sand and Monterey 0/30 Sand were pluviated in lifts of varying thickness (Figure 3.2.11). Lift thicknesses were controlled by the instrumentation location plan and the structural location plan. All sand was placed by dry pluviation into the model container. Three pluviators were used to place the respective layers of dense Nevada Sand, loose to medium-dense Nevada Sand, and dense Monterey Sand. Each of the three pluviators was calibrated to place material at the desired dry density using a calibration chamber of known volume. The calibration process consisted of adjusting the drop height and flow rate of the sand until the correct weight of sand was measured for the known volume of the calibration chamber.

Figure 3.2.11. (a) Calibration of large pluviator. (b) Placing dense Nevada Sand using large pluviator. (c) Calibrating the pluviator for loose to medium-dense Nevada Sand. (d) Placing loose to medium-dense Nevada Sand. (e) Placing dense Monterey Sand.

9. Each lift of dense Nevada Sand was also vibrated using an electric vibratory plate, as shown in Figure 3.2.12. While the objective was to make the dense Nevada Sand as dense as possible, care was also taken to apply an equal amount of vibration to each lift of dense Nevada Sand to minimize variability in the density within and between each lift.

Figure 3.2.12. Vibration of dense Nevada Sand

10. After each lift was pluviated, the surface of the soil was groomed to the desired elevation using a vacuum cleaner (Figure 3.2.13). The vacuum cleaner filter was blown out with compressed air before it was used each time. Additionally, the hoses were kept clear of sand during the grooming process. These steps were necessary to ensure a constant suction height during grooming so that a correct final elevation could be achieved. After the lifts were finished to the correct elevation, the weight of the model was measured to get an estimate of the average relative density of the lift. Model weight measurements were performed until the model weight exceeded the capacity of the crane.

Figure 3.2.13. Vacuum soil lift to desired elevation.

11. The desired location of each instrument was marked on the surface of each lift and the instruments were carefully placed. Instrumentation cables were routed along the side walls of the model container and secured with duct tape.
12. When the surface of the soil was finished at a depth corresponding to approximately 50 mm above the toe depth of the piles, the piles were installed at the appropriate locations by driving the piles into the dense Nevada Sand using a rubber mallet (Figure 3.2.14).

The piles were then checked with a bullseye bubble level and a small carpenter's level to ensure they were plumb.

Figure 3.2.14. Installation of model piles.

13. When the top of the dense Nevada Sand layer was reached, a very thin layer of blue sand was spread over the surface to act as a marker during excavation following the test (Figure 3.2.15). An additional thin layer of blue sand was placed at the top of the loose-medium dense Nevada Sand layer.

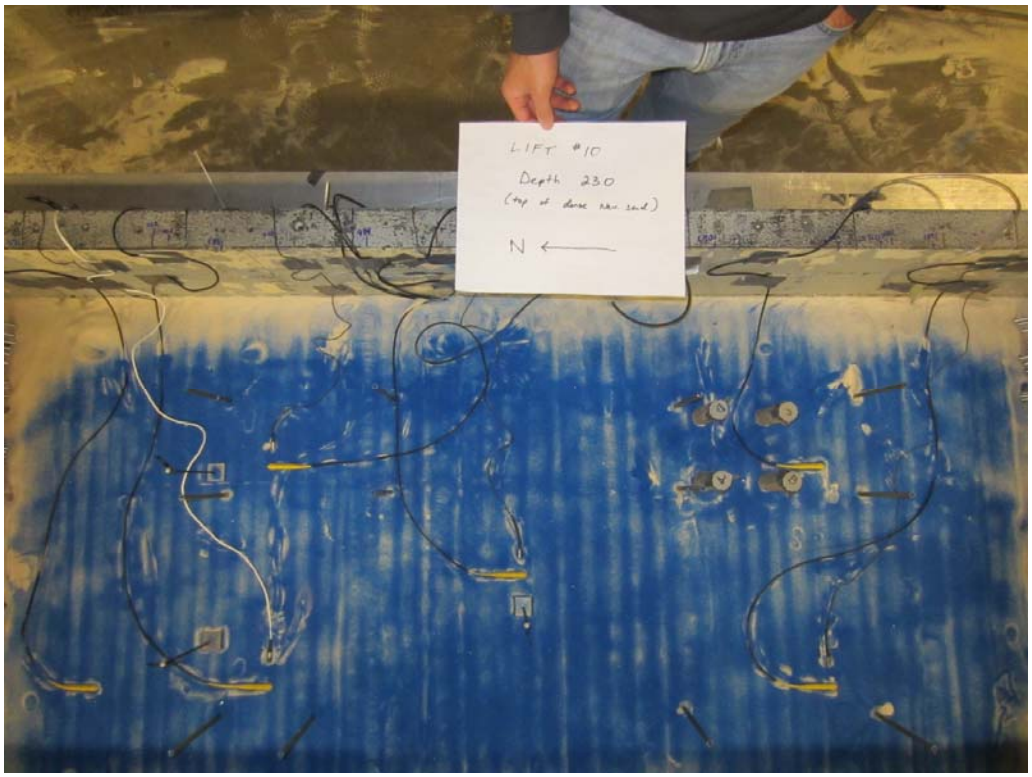

Figure 3.2.15. Thin layer of colored sand at top of dense Nevada Sand layer.

14. The soil surface was brought to an elevation just above the elevation of the base of the model structure foundations. At this point the foundation for the pile supported 'J' model structure was connected to the previously installed piles. Thread rod was threaded into the tops of the exposed piles. The tips of the thread rod were coated using a paint pen and the footing of the 'J' model structure was pressed lightly over the thread rods to mark the as-built pile locations. Four holes were then drilled through the 'J' model structure footing and the piles were connected to the footing using a hex nut and washers.
15. Given that the model structures were located off of the center line of the model container in the east-west direction, it was important to account for the radial g-field produced by the centrifuge when placing the model structures. Accordingly, the soil surface was sloped such that the model structures were placed with an initial tilt of approximately 1 degree towards the center of the container. The center of the model structures were placed at the design footing base depth. After placing the structures, the soil surface was curved up between the center of the container and the eastern and western container sides so that the gravitational field would be approximately normal to the surface along the transverse direction of the container.
16. The displacement rack was constructed on the model container in the model preparation shop with the structures in place. It was designed to be as stiff as possible to minimize both static deflections due to increased self-weight and dynamic deflections during strong shaking. Linear potentiometers (LPs) were mounted in holders and the holders were attached to the displacement rack using standard hardware. The tips of the LPs were either positioned to directly measure the displacement of a location, or placed on stiff flags added to the structures at locations where direct measurement of displacement was difficult or not possible to access. The displacement rack and the 'J' structure columns and masses were removed from the model after the displacement rack was constructed.
17. The model was transported from the model preparation shop to the centrifuge and mounted on the centrifuge arm.
18. The model was saturated with the HPMC and water pore fluid solution described previously. Saturation consisted of covering and sealing the model with an air tight lid, applying a vacuum to remove air from the pores, slowly releasing the vacuum and filling the pore space with carbon dioxide, and then re-applying the vacuum (Figure 3.2.16). While the model was under vacuum, the de-aired pore fluid solution was dripped into the saturation troughs and, through the large tubes connected to the saturation troughs, into the soil. Valves were used to control the flow rate of de-aired pore fluid into the saturation troughs.

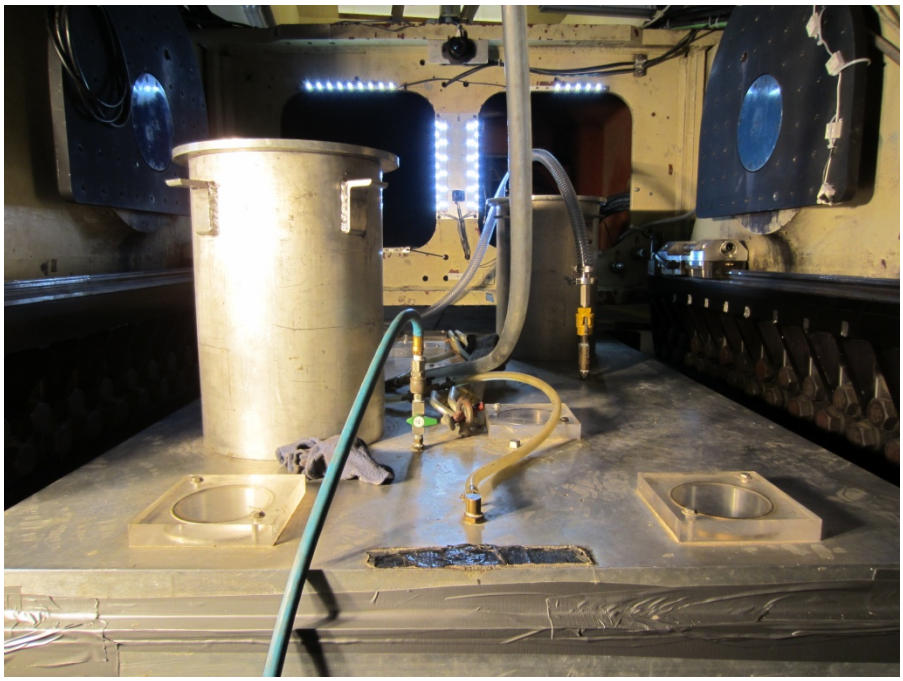

Figure 3.2.16. Saturation Set-up

19. After approximately 95 hours of model saturation, the model had taken approximately 60% of the theoretical required amount of pore fluid. At this point the pore fluid was allowed to overflow the metal saturation troughs and drip through several sponges into narrow saturation trenches on the soil surface to speed up the rate of progress (Figure 3.2.17). The idea with this procedure was to allow for the pore fluid to fill the soil pore space from both the bottom of the container (i.e., through the tubes connected to the saturation troughs) and through the surface of the container along the northern and southern edges of the container. Care was taken so as to not overflow the surface trenches. Pore fluid was introduced into the model up to the point where it was ponded across the surface of the entire model. The vacuum pressure was then released and the saturation lid was removed.

Figure 3.2.17. Sponges underneath saturation trough.

20. The columns and masses of the 'J' structures were bolted to their foundations.
21. The displacement gauge rack was installed and all instrumentation wiring was routed to the north end of the model container along the sides of the container or through the two longitudinal channel pipes that made up part of the displacement rack (Figure 3.2.18).
22. Instrumentation cables were plugged into the appropriate channels and signals were checked on the DAQ.
23. High-speed cameras, analog cameras, and LED lights were placed and connected.
24. After the final inspection, the model was ready for spin-up.

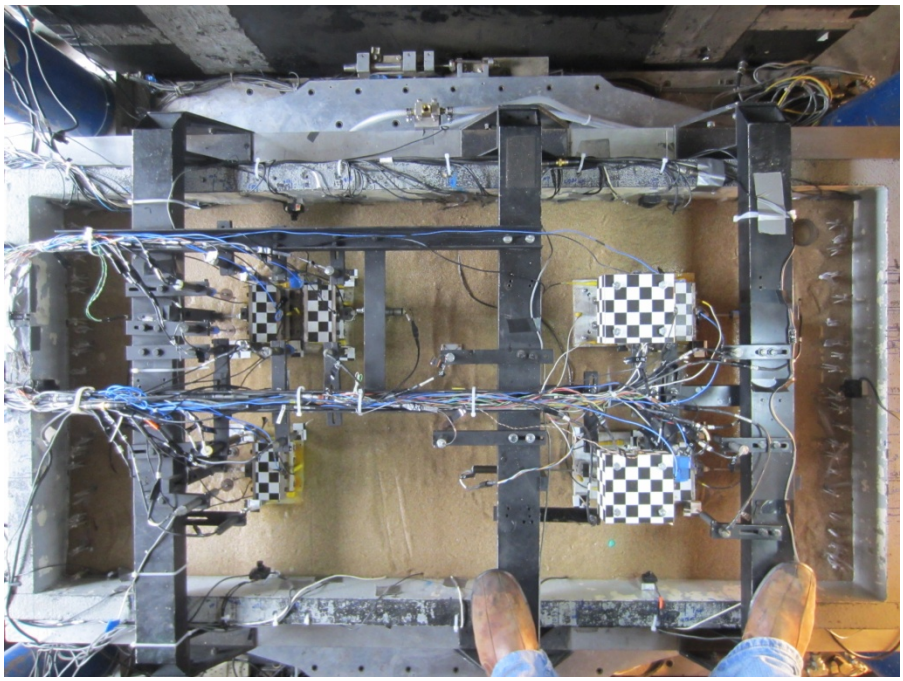

Figure 3.2.18. Plan view of model with displacement rack following saturation.

As-Built Model

The positions of the model structures and the thickness of the soil layers were typically within 2 mm of the design model geometry. Consequently, the plan dimensions indicated on Figure 3.2.3 can be considered as-built dimensions. Assuming negligible lateral displacements during the step waves, the building separation distances at prototype scale were 16.5 cm, 22.0 cm, and 27.5 cm for the NE, SW, and SE quadrants, respectively, prior to the first applied ground motion (i.e., the first PRI_small motion).

As described above, the thicknesses of each pluviation lift were controlled by the instrumentation layout plan and the structural layout plan. Estimates of the achieved relative density of most lifts were obtained by weighing the model before and after each lift and taking nine measurements spaced evenly on the surface to estimate the achieved lift thickness. For thinner layers, measurement error had a greater effect on the reported relative densities. In addition to the container weight measurements during pluviation, a pre-shake CPT was performed to assess the initial soil conditions and the CPT-based relative density correlations developed by Kulhawy and Mayne (1990), Salgado et al. (1997) and Jamiolkowski et al. (2001) were employed to provide an alternative means to estimate the relative density. The best estimates of the as-built relative density for each layer are indicated in Table 3.2.3. These estimates include consideration of pre-pluviation calibration, measurements taken during pluviation, and the CPT-based relative density correlations. Container weights could only be measured until the capacity of the crane in the model preparation shop was reached.

Twenty-seven viscosity tests of the pore fluid were performed just prior to and during model saturation using an Ubbelohde type viscometer. While there was some variability in the test results due to fluid temperature fluctuations, the average of the 27 tests suggests the pore fluid had a kinematic viscosity of approximately 21.6 times that of water with a sample standard deviation of 3.8.

Based on the kinematic viscosity and the approximate hydraulic conductivity of the loose to medium dense Nevada Sand, theoretical calculations were performed to estimate the average excess pore water pressure dissipation as a function of time (Fig. 3.2.19). These calculations were performed in accordance with 1-D consolidation theory and assume double drainage. The approximate hydraulic conductivity was taken as 1.7 x 10^{-3} cm/s based on a falling head test of an earlier batch of Nevada Sand at approximately 50% relative density (Hausler, 2002).

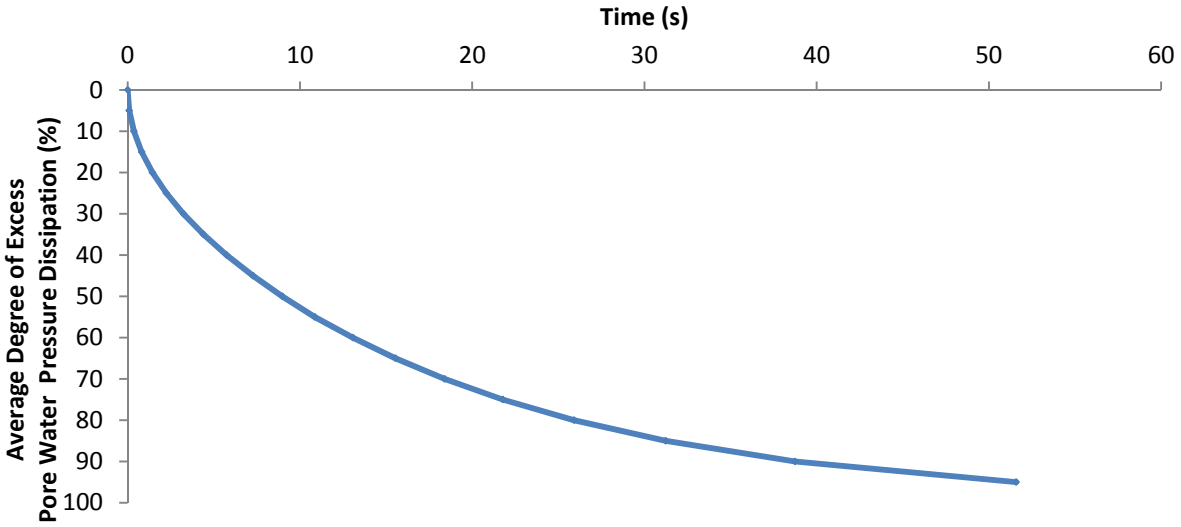

Figure 3.2.19. Average degree of excess pore water pressure dissipation as a function of time based on 1-D consolidation theory.

As described previously, the best estimated GWT depths, based upon the mean hydrostatic pore water pressure from the functional PPTs, were approximately 0.37 m during the PRI_small event, 0.50 m during the PRI_mod event, and 0.87 m during the TCU_mod and PRI_large ground motions.

Instrumentation locations are indicated on Figures 3.2.4 – 3.2.6 and the coordinates of the soils instrumentation, relative to the origin at the northwest corner of the top of the top ring of the model container, are provided on the sensor sheets available through NEEShub.

Table 3.2.3. As-built layer thicknesses and relative densities

Layer Description	Layer Thickness (m)	D_r (%)
Dense Nevada Sand	19.3	90 +/- 5
Loose to Medium-Dense Nevada Sand	4.5	50 +/- 5
Dense Monterey Sand	1.9	85

Instrumentation and Measurements

Four instrument types were used for this test: integrated circuit piezoelectric (ICP) accelerometers, micro-electro-mechanical system (MEMS) accelerometers, pore water pressure transducers (PPTs), and linear potentiometers (LP). As mentioned previously, a total of 61 ICP accelerometers, 18 MEMS, 26 PPTs, and 32 LPs were incorporated into the test plan. The cone penetration test (CPT) was performed using a system consisting of two load cells (LC) and one LP. Instrumentation tables are available through NEEShub and summarize the instrumentation used for each spin.

The ICP and MEMS accelerometers had ranges of ±100 g. Linear potentiometers were used with strokes of 1 in (25 mm), 2 in (50 mm), 3 in (75 mm), and 4 in (100 mm). The PPTs had ranges of 50 psi (345 kPa), 100 psi (689 kPa), or 200 psi (1379 kPa). Each instrument has either a factory-calibrated (ICP and MEMS accelerometers) or equipment site-calibrated (LPs and PPTs) sensitivity factor, which is included in the available instrumentation tables.

Four high-speed cameras were used during this test. The high-speed cameras record a maximum duration of 20 sec at a rate of 210 frames per second. Herein, the high speed cameras will be referred to as HS1 through HS4. HS1 was elevated above the top of the model container within the southern half of the model and viewed north to capture the adjacent 'A' buildings in the northeast quadrant, HS2 was located on the CPT rack guide rails above the southwest corner of the model and viewed northeast to capture the southwest quadrant, HS3 was located on the CPT rack guide rails above the model at the northwest corner and viewed east to capture the isolated 'A' building in the northwest quadrant, and HS4 was located on the CPT rack guide rails above the southeast corner of the model and viewed northwest to capture the 'A' building adjacent to the 'J' building on piles. High-speed captures recorded during the simulated ground motions have been converted to prototype speed (1/*N* of the captured rate) and are available through NEEShub. Analog cameras, capable of capturing video at 20 frames per second, were also utilized to capture images of important locations before and after each ground motion. Table 3.2.4 contains information about the analog cameras and their locations. More information about the camera specifications is provided at the NEES@UCD website (http://nees.ucdavis.edu/). The raw analog camera files recorded during the simulated ground motions have also been uploaded to NEEShub.

Table 3.2.4. Analog camera placements and their purposes.

Camera Channel	View	Purpose
2	Profile of northeast quadrant from east wall.	Monitor building response.
3	Profile of northwest quadrant from west wall.	Monitor building response
6	Profile of north quadrants from north wall.	Monitor building response.
9	Observation well at southeast corner from disp. rack.	Monitor groundwater level.
11	Plan view of centrifuge bucket from arm.	Monitor bucket.
13	Southeast quadrant from east wall.	Monitor building response.
14	Southwest quadrant from west wall.	Monitor building response.
15	Bucket level on north side.	Monitor bucket.
16	Bucket level on south side.	Monitor bucket.

Simulated earthquake motions

Simulated earthquake motions were applied to the base of the model container in the north-south direction when the model was spinning at approximately 76 RPM (corresponding to approximately 55 g at the effective radius). The motion sequence, summarized below in the *Centrifuge Test Chronology* section, generally followed the sequence applied during the fourth experiment performed by Dashti (2009). Consequently, key characteristics of the applied motions have been detailed recently by Dashti (2009) and Dashti et al. (2010b). The following is a brief summary of these more detailed descriptions:

- The PRI events were modified, scaled versions of the north-south component of the ground motion recorded at a depth of 83 m in the Kobe Port Island down-hole array during the 1995 M_w 6.9 Kobe, Japan earthquake. This simulated earthquake motion was

also used in the work described by Hausler (2002). Dashti et al. (2010b) reported a significant duration, D_{5-95}, of approximately 8 s for this motion.

- Different scaling factors were applied to the input PRI motion to generate different applied motion intensities. The "PRI_small" event achieved maximum horizontal accelerations of 0.04 g and 0.05 g, respectively at the base of the model container; the "PRI_mod" event achieved a maximum horizontal acceleration of 0.23 g at the base of the model container; and the "PRI_large" event achieved a maximum horizontal acceleration of 0.51 g at the base of the model container. Consequently, PRI_small was used to evaluate the performance of the instrumentation and study the response of the model with limited pore water pressure generation; whereas, PRI_mod and PRI_large were used to study the response of the model when the medium dense sand layer liquefied soil in the free-field (i.e., the excess pore water pressure ratio, r_u, defined as the excess pore pressure, Δu, divided by the initial vertical effective stress, σ'_v, was approximately unity).

- The TCU_mod event was a modified version of the fault-normal component of the ground motion recorded at the TCU078 station during the 1999 M_w 7.6 Chi-Chi, Taiwan earthquake. The peak horizontal acceleration at the base of the model during this event was 0.18 g. Dashti et al. (2010b) reported a significant duration of approximately 28 s for this event and noted that it had a slower rate of energy buildup relative to the PRI motion. Consequently, the TCU_mod event provided a nice complement to the PRI_mod event in that the model response could be studied for motions with similar maximum base accelerations but different significant durations and rates of energy buildup.
  Key time histories and pseudo-acceleration response spectra are provided in Section 3.3.

Centrifuge Test Chronology

The centrifuge was spun once on 03/15/2012 and twice on 03/19/2012. As described previously, the desired g-level (N) during both spins was 55 g at the center of the layer of loose to medium-dense Nevada Sand, corresponding to an effective radius of approximately 8.53 m. One cone penetration test (CPT) was performed on 03/15/2012, prior to application of the simulated earthquake ground motions. Two step waves and one simulated earthquake ground motion were performed on 03/15/2012 and four step waves and four simulated earthquake ground motions were performed on 03/19/2012. Step waves were used primarily to warm-up the centrifuge shaking table and check critical instrumentation. Table 3.2.5 contains the testing schedule used for Test-5. Table 3.2.6 contains a list of the data and instrumentation files for Test-5. The instrumentation and raw data files are available through NEEShub.

Table 3.2.5. Test-5 Testing Sequence.

Spin ID	Date	ID	Input File	Frequency (Hz)	Amp. Factor
I	3/15/2012	CPT1	N/A	N/A	N/A
		SW1	Step.txt	4000	0.9
		SW2	Step.txt	4000	0.9
		PRI_small	Kobe0807.txt	2750	0.5
II	3/19/2012	SW3	Step.txt	4000	0.9
		SW4	Step.txt	4000	0.9
III	3/19/2012	SW5	Step.txt	4000	0.9
		SW6	Step.txt	4000	0.9
		PRI_small	Kobe0807.txt	2750	0.5
		PRI_mod	Kobe0807.txt	2750	1.7
		TCU_mod	Kobe0807.txt	2750	0.36
		PRI_large	Kobe0807.txt	2750	5.1

Table 3.2.6. Data and instrumentation files for Test-5.

Spin ID	Instrumentation File	Motion	NEEShub Trial-Repetition	NEEShub Raw Data File
I	03152012_Instrumentation_Matlab.xls	CPT1	I-1	cpt1.txt
		SW1	I-2	sw1.txt
		SW2	I-3	sw2.txt
		PRI_small	I-4	pri_small.txt
II	03192012_Instrumentation_Matlab.xls	SW3	II-1	sw3.txt
		SW4	II-2	sw4.txt
III	03192012_Instrumentation_Matlab.xls	SW5	III-1	sw5.txt
		SW6	III-2	sw6.txt
		PRI_small	III-3	pri_small.txt
		PRI_mod	III-4	pri_mod.txt
		TCU_mod	III-5	tcu_mod.txt
		PRI_large	III-6	pri_large.txt

Data Processing

Data were collected during shaking events from all instruments at a sampling frequency of 4096 Hz (model scale) utilizing a user interface coded in LabView. The raw data was converted to engineering units by employing appropriate sensitivity factors. For the ICP and MEMS accelerometers, these sensitivity factors are determined and specified by the manufacturer. For the PPTs and LPs, these were determined by the research team through calibration processes performed at the NEES@UCD facility. As described previously, the sign conventions established for this project follow a global coordinate system where south, east, and down (into the soil) are positive and north, west, and up are negative. Coordinates are defined relative to an origin at the top of the top ring in the northwest corner of the container. Once voltages are converted to engineering units using the sensitivity factors, the measurements must then be multiplied by a direction vector (either +1 or -1) to account for the orientation of the

instrument. For sensors where the measurements are expected to be small, a gain value greater than 1 is used to boost the recorded signal. The gain value must then be divided out of the raw voltage values before the engineering unit data is finalized. In addition, accelerometers and LPs were further processed to remove the initial voltage offsets. This was accomplished by subtracting the mean of the first 100 samples of each record. Trombetta et al. (2011) describes the logic behind this in detail. For reference, the instrumentation lists available through NEEShub include the sensitivity factors for each sensor, as well as direction vectors and gain values.

Known Limitations with Test-5

Several of the PPT connectors were exposed to pore fluid while the model was under vacuum during model saturation. This was recognized during model saturation and the research team, with assistance from the NEES@UCD staff, attempted to minimize this exposure as much as possible. Despite these efforts, many of the PPTs were found to be not functioning properly when their signals were checked after model saturation. Significant effort was put into troubleshooting and attempting to repair the PPTs with bad signals, but some were unable to be repaired and did not function properly during Test-5.

After connecting the 'J' model building superstructures after saturation it was observed that the 'J' building in the southwest quadrant was tilted approximately 2.5 degrees to the east. To account for the radial gravitational field, the model structures were intended to be tilted just over 1 degree towards the center of the model container. To correct for this excessive tilt of the southwest 'J' building, a structural shim was designed and installed between the column baseplate and the foundation. The shim was 7.6 cm by 7.6 cm and 0.25 cm thick on the east side and 0.45 cm thick on the west side. An oppositely tapered shim was installed on top of the column baseplate so that the hardware used to connect the assembly could be tightened properly. Details of the shim have been uploaded to NEEShub.

Due to a channel configuration error, the CPT tip displacement data were not recorded during the CPT push. The CPT data presented herein has been processed assuming a constant push rate of 2 cm per second.

Instruments that did not appear to functioning properly were tracked during each of the spins. A summary of instruments that appeared to be not functioning or had questionable or noisy signals during Spin III is provided in Table 3.2.7.

Table 3.2.7. Non-working and/or questionable sensors during Test-5 Spin III.

Channel	Instrument Name	Motions with Issues
PCB1-12	SA_FF1_154	pri_large
PCB1-13	SA_FF1_192	pri_large
PCB1-14	SAV_FF1_Sfc	pri_small,
PCB2-4	SA_NW_2_154	pri_large
PCB2-6	SA_SE_1_154	pri_small, pri_mod, tcu_mod
PCB2-8	SA_FF2_154	pri_large
PCB2-13	A_NE_1_E_x	pri_small,
PCB3-6	A_SE_2_S_z	pri_large
PCB4-2	A_NW_S_z	pri_large
PCB4-10	SA_FF2_B	pri_large
PCB4-11	SA_SE_2_154	pri_large
ProgB1-0	PPT_NW_1_229	pri_large
ProgB1-1	PPT_NE_S_192	pri_small, tcu_mod, pri_large
ProgB1-2	PPT_NE_1_229	pri_small, tcu_mod, pri_large
ProgB1-3	PPT_FF1_229	pri_small, pri_mod, tcu_mod, pri_large
ProgB1-5	PPT_SW_2_154	pri_small, pri_mod, tcu_mod, pri_large
ProgB1-7	PPT_NE_2_S_192	tcu_mod, pri_large
ProgB2-0	PPT_SW_2_229	pri_small, pri_mod, tcu_mod, pri_large
ProgB2-5	PPT_SE_2_154	pri_mod, tcu_mod

ProgB2-6	PPT_NE_C_192	pri_small, pri_mod, tcu_mod, pri_large
ProgB3-0	PPT_FF1_Base	pri_small, pri_mod, tcu_mod
ProgA1-0	PPT_FF2_Base	tcu_mod
ProgA1-1	PPT_NW_C_192	pri_small, pri_mod, tcu_mod, pri_large
ProgA1-2	PPT_NW_2_192	pri_small, tcu_mod
ProgA1-3	PPT_SW_2_192	pri_small,
ProgA1-4	PPT_SW_1_192	pri_mod, tcu_mod, pri_large
ProgA1-5	PPT_NW_1_192	pri_small, pri_mod, tcu_mod, pri_large
ProgA2-2	PPT_NE_2_C_192	pri_small, pri_mod, tcu_mod, pri_large
ProgA4-1	A_SE_1_roof_y	pri_small, tcu_mod
ProgA4-3	A_SW_1_roof_y	tcu_mod, pri_large
PT1-2	D_NE_2_S_x	pri_mod, pri_large
PT3-4	D_NW_1_N_x	pri_large
PT3-6	D_soil_e_sfc	tcu_mod
Iso1-1	D_NE_1_N_x	tcu_mod
Iso2-4	D_SW_1_SWC_z	tcu_mod

3.3 Test-5 Results

Introduction

The key results from Test-5 are presented in this section. Following a brief presentation of results from the pre-shake cone penetration test (CPT), the results from the PRI_mod, TCU_mod, and PRI_large motions are presented. This section presents the most interesting

results. The data from each instrument collected during all events are provided by Zupan et al. (2013).

CPT Results

As described in Section 3.2, a pre-shake CPT was performed with the model at approximately 55 g at the location illustrated on Figure 3.2.3. The in-flight CPT device was mounted on a rack over the model container and positioned at the desired location by sliding the rack along guide rails that have been installed on the centrifuge bucket. This CPT device had a model-scale cone tip diameter of 6 mm. A photograph of the CPT device set up is presented in Figure 3.3.1.

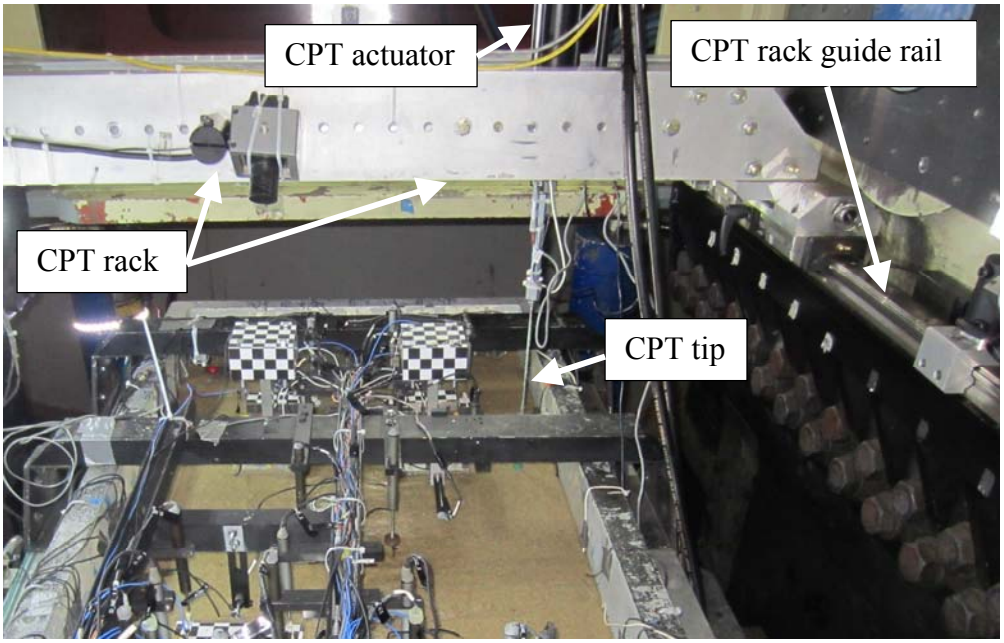

Figure 3.3.1. In-flight CPT device set up.

The raw cone tip resistance profile is presented in Figure 3.3.2. Several CPT-based relative density correlations (i.e., Kulhawy and Mayne, 1990; Salgado et al., 1997; and Jamiolkowski et al., 2001) were employed to estimate the relative density of the sand. These relative density profiles are also presented in Figure 3.3.2. As was discussed in Section 3.2, cone tip displacement rate data were not collected during the push due to a channel configuration error. Consequently, all CPT data presented herein has been processed assuming a constant push rate of 2 cm per second.

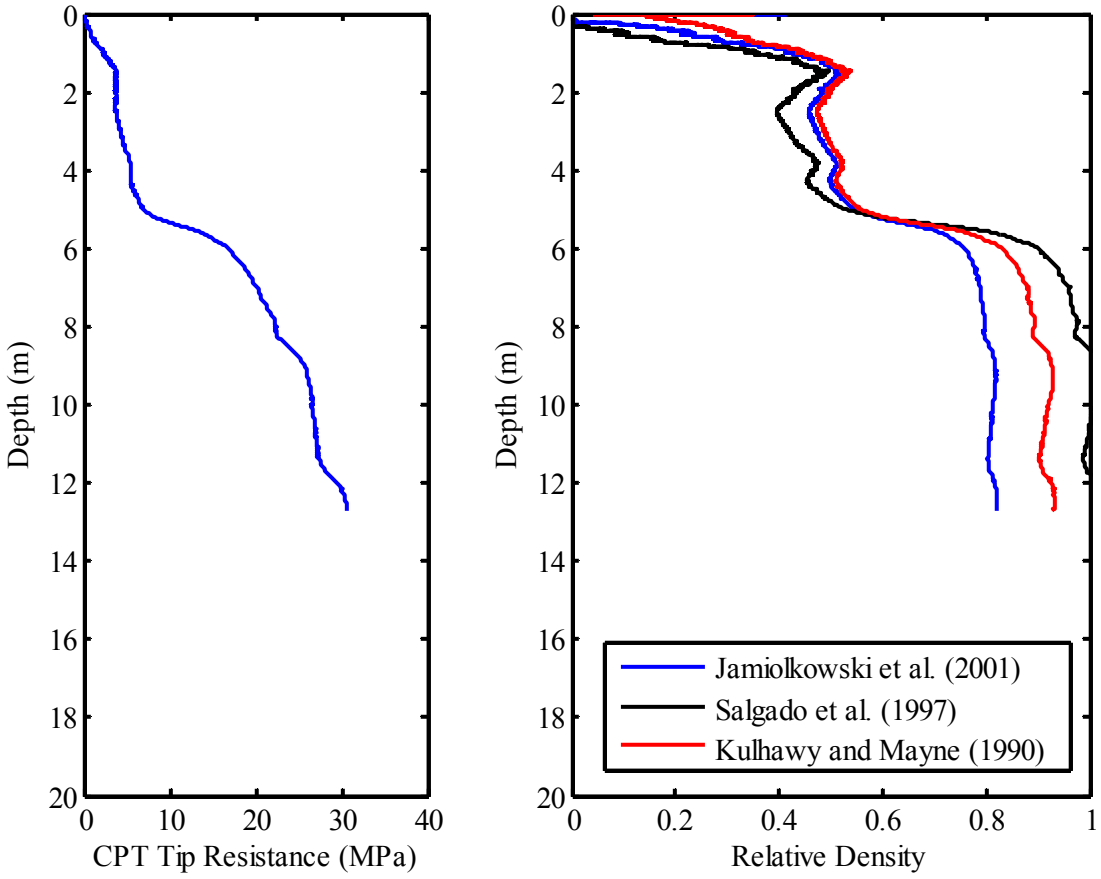

Figure 3.3.2. (a) Raw CPT tip resistance profile and (b) the relative density profiles as correlated from CPT tip resistance using formulas suggested by Kulhawy and Mayne (1990), Salgado et al. (1997), and Jamiolkowski et al. (2001).

Based on the profiles presented in Figure 3.3.2, along with the measured lift weights during model construction, best estimates of the representative relative density of each soil layer were developed (Table 3.2.3). While there are some minor differences between the relative density correlations presented in Figure 3.3.2, the correlations are generally consistent, particularly within the loose to medium-dense Nevada Sand layer, and they show the expected trend. Importantly, based on this correlation, the relative density of the loose to medium-dense Nevada Sand layer appears to be between 45% and 55% with a reasonable representative value of about 50%.

PRI_mod

PRI_mod was the first motion to generate significant excess pore water pressures. As will be seen below, $r_u \approx 1$ at the center of the loose to medium-dense Nevada Sand layer in the free-field during this event. Significant building settlements were observed. Following a discussion of the free-field response for context, key building response plots will be presented and interpreted. Just prior to the PRI_mod event the prototype building separation distances were 17 cm, 24 cm,

and 28 cm for the $A_{A\text{-}N}$ – $A_{A\text{-}S}$, A_J – J_A, and $A_{J\text{-}pile}$ – J-pile$_A$ building pairs, respectively. Additionally, based on an average of hydrostatic pore water pressures measured by 11 PPTs just prior to the PRI_mod motion, the groundwater table was approximately 0.5 m below the ground surface during this event.

Free-Field Response

As described previously, the PRI_mod event was a scaled version of the of the north-south, fault-normal component of the ground motion recorded at a depth of 83 m in the Kobe Port Island down-hole array during the 1995 M_w 6.9 Kobe, Japan earthquake. Free-field acceleration-time histories at the base, the top of the loose to medium-dense Nevada Sand layer, and just beneath the soil surface are presented in Figure 3.3.3. From this figure it can be observed that the free-field motion was amplified significantly between the base of the model container and the surface of the model. Large amplitude spikes, commonly associated with dilation-induced shear-strain hardening during cyclic loading, are observed at the top of the liquefiable layer and the soil surface. The PGA for this event was 0.57 g and the maximum base acceleration was 0.23 g.

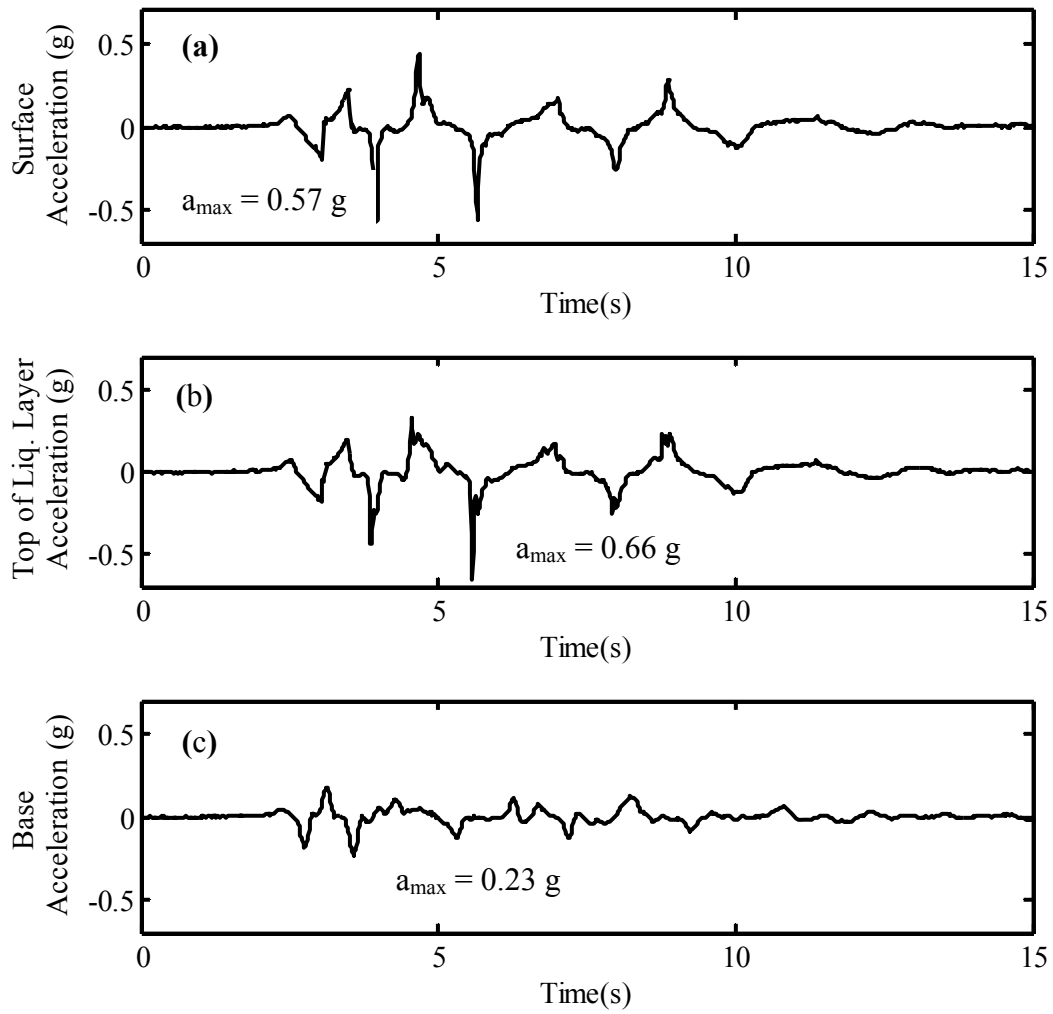

Figure 3.3.3. Free-field acceleration-time histories at (a) the soil surface, (b) the top of the loose to medium-dense Nevada Sand, and (c) the base of the model container during the PRI_mod motion.

The free-field settlement-time history at the surface and the excess pore water pressure-time history at the center of the liquefiable layer in the free-field are provided in Fig. 3.3.4. Free-field acceleration-time histories at the surface and the base are also provided for reference. The same plots, zoomed-in to focus on the during-shaking portions of the records, are provided in Fig. 3.3.5. It is observed that excess pore water pressures are generated rapidly during shaking and approach $r_u \approx 1.0$ (indicated with the blue horizontal line) before shaking is completed. Free-field surface settlements initiate during strong shaking, at nearly the same time excess pore water pressures begin to increase significantly, and continue until well after shaking is completed. These settlements would appear to be suggestive of partial drainage occurring during strong shaking. The final free-field soil surface settlement was measured to be 5.8 cm for this event.

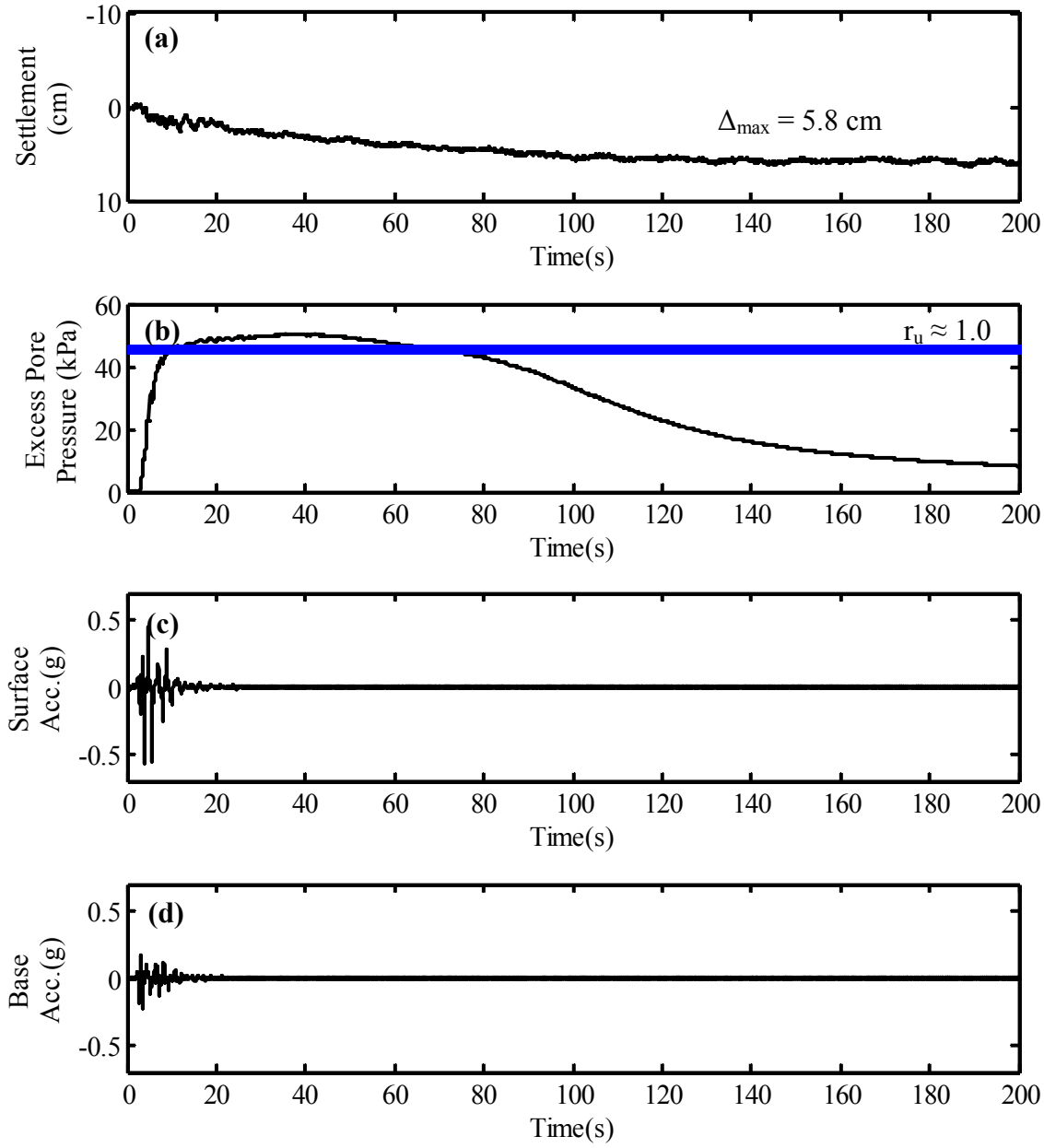

Figure 3.3.4. The free-field (a) settlement-time history at the soil surface, (b) excess pore water pressure-time history in the middle of the loose to medium-dense Nevada Sand layer, (c) the acceleration-time history at the surface, and (d) the acceleration-time history at the base of the model container.

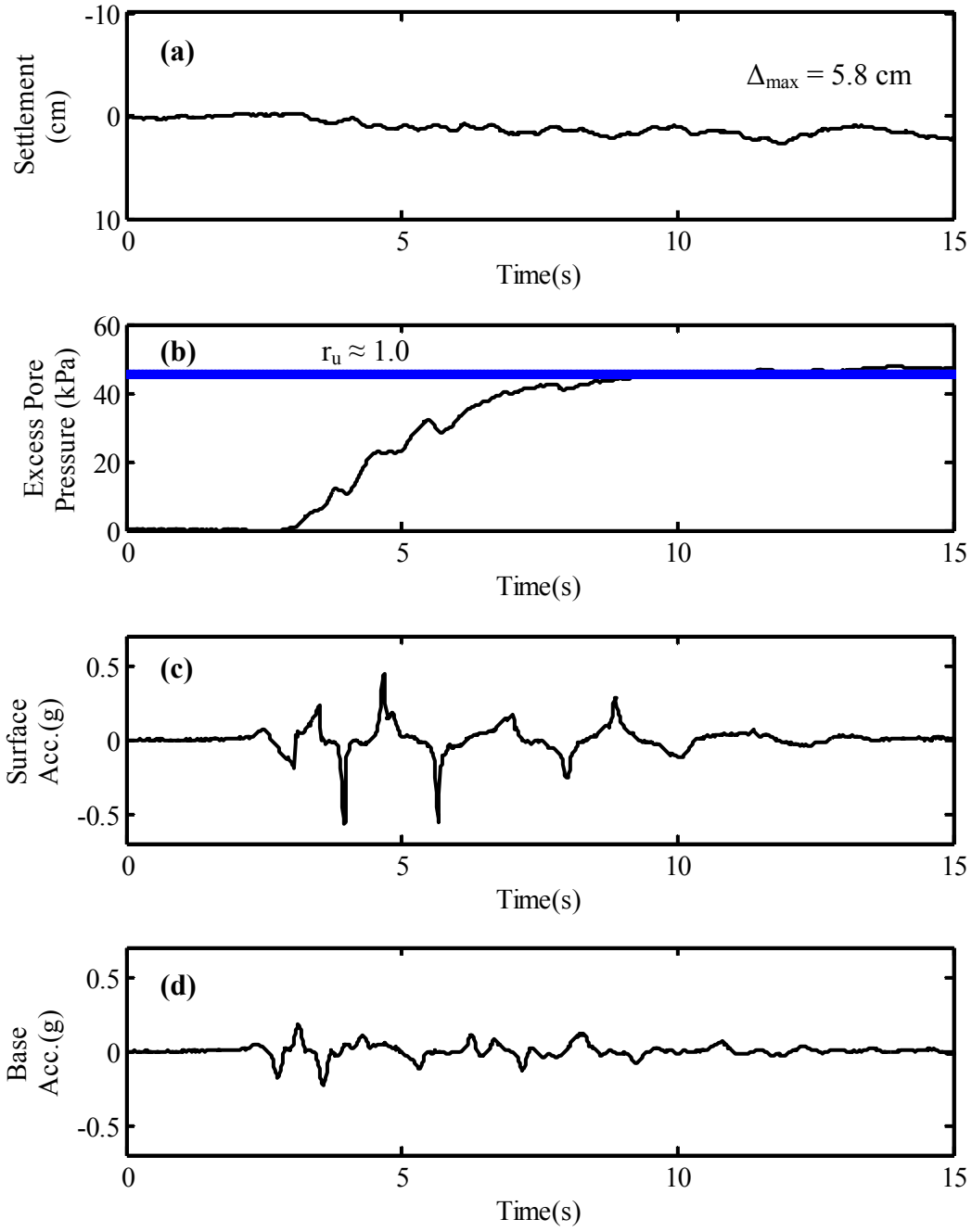

Figure 3.3.5. The zoomed-in free-field (a) settlement-time history at the soil surface, (b) excess pore water pressure-time history in the middle of the loose to medium-dense Nevada Sand layer, (c) the acceleration-time history at the surface, and (d) the acceleration-time history at the base of the model container.

Response Near Structures

Building settlement-time histories are presented in Figure 3.3.6, along with the free-field surface settlement and free-field surface acceleration-time history for reference. Several things are readily apparent from this figure: (1) similar to the free-field soil settlements, building settlements initiate at the onset of strong shaking; (2) the buildings settle much more than the free-field soil; (3) A, $A_{A\text{-}N}$, and $A_{A\text{-}S}$ settle at the same rate and about the same amount; (4) The 'A' buildings with 'J' neighbors settle less than the other 'A' buildings. Of these, $A_{J\text{-}pile}$ settles approximately 5 cm more than A_J; (5) J_A settles only slightly more than A_J, but it settles less than the 'A' buildings without 'J' neighbors; and (6) J-$pile_A$ settles by far the least amount among the buildings, as would be expected, and slightly less than the free-field surface (about 3 cm vs. 6 cm).

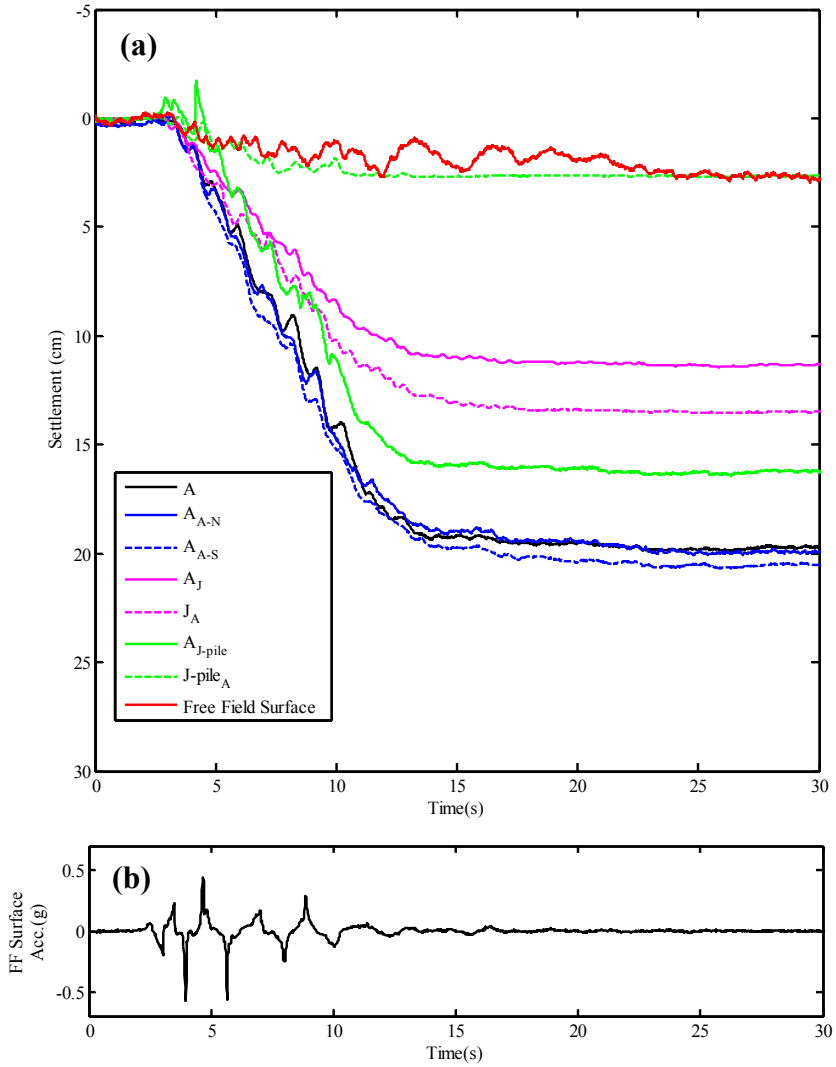

Figure 3.3.6. (a) Settlement-time histories at the centers of the A, $A_{A\text{-}N}$, $A_{A\text{-}S}$, A_J, and J_A buildings. Average settlement of the $A_{J\text{-}pile}$ building, and the settlement of the southwest corner of the J-pile building. Free-field surface settlements are shown for reference. (b) Free-field surface acceleration-time history.

Permanent settlements, measured at each LP location following the PRI_mod motion, are presented in Fig. 3.3.7. This figure also includes calculated settlements at building corners where there were no LPs, when possible (based on available data). Measured building settlements are indicated in black, calculated building settlements are indicated in blue, measured horizontal displacements are indicated in red (positive towards the south), and measured soil settlements are indicated in green. Several observations, in addition to those made above, can be made with reference to Fig. 3.3.7: (1) soil settlements measured adjacent to the buildings in the northern half of the container are much larger than the soil settlements measured in the free-field; (2) based on the settlement measured by a linear potentiometer connected to a settlement plate installed at the top of the liquefiable layer, more settlement is observed at the top of the liquefiable layer than at the soil surface in the northwest quadrant. The most reasonable explanation for this would seem to be that the dense Monterey 0/30 Sand layer has dilated; (3) $A_{A\text{-}N}$ and $A_{A\text{-}S}$ have moved horizontally away from each other and settled such that they are tilted slightly towards each other. $A_{A\text{-}N}$ tilted a very small amount to the west and $A_{A\text{-}S}$ tilted a small amount to the east; (4) A_J and J_A moved horizontally away from each other and both buildings settled such that they were tilted slightly to the south and to the west; and (5) $A_{J\text{-}pile}$ moved horizontally away from J-pile$_A$ and settled such that it was tilted away from J-pile$_A$.

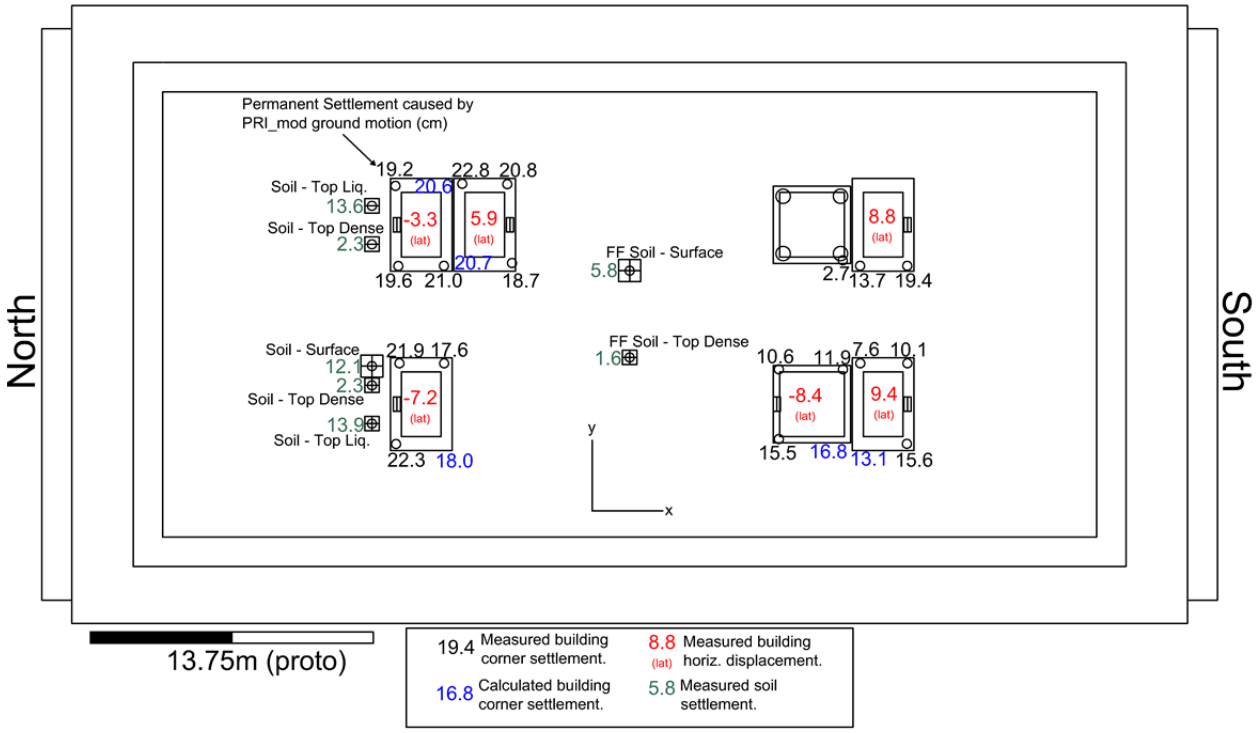

Figure 3.3.7. Permanent settlements following the PRI_mod motion. Black numbers represent settlement at a building corner, blue numbers indicate calculated settlement at a building corner, red numbers indicate horizontal building displacement in the north-south direction (positive toward south), and green numbers indicate soil settlements. All settlements are provided in prototype cm.

Excess pore water pressure-time histories beneath the center of the 'A' buildings are presented in Figure 3.3.8. Unfortunately, the PPT in the center of the liquefiable layer beneath

the isolated 'A' building did not function properly. Therefore, the excess pore water pressure-time history for the PPT at the top of the liquefiable layer is presented for this building (Fig. 3.3.8a). The remaining plots in this figure correspond to the center of the liquefiable layer. The excess pore water pressure corresponding to $r_u \approx 1.0$ has been indicated for each of the PPTs beneath buildings. From these plots it is clear that excess pore water pressures beneath the buildings increased rapidly at the onset of strong shaking and reached their peak values around t = 15 s. Beneath buildings $A_{A\text{-}N}$ and $A_{J\text{-}pile}$, these peak excess pore water pressures were clearly greater than the excess pore water pressure in the free-field at the same elevation. Consequently, at this time, pore water would have flowed from beneath the center of the buildings towards the free-field at these locations. However, dissipation of excess pore water pressures beneath the buildings occurred much faster than the free-field and at approximately t = 20 s the direction of flow would have reversed until hydrostatic conditions were reached. In addition, rapid changes in pore water pressures during strong shaking led to high transient hydraulic gradients that would have caused the direction of pore water flow to change. The conditions beneath A_J appear to have been different than $A_{A\text{-}N}$ in that less excess pore water pressure was generated beneath this building and the excess pore water pressures were not sustained above the corresponding excess pore water pressures in the free-field for a significant amount of time. However, rapid changes in pore water pressure beneath this building during strong shaking did cause transient pore water pressures to exceed the corresponding free-field pore water pressures several times. This is evident in the comparison plot presented in Figure 3.3.9 which compares the excess pore water pressure-time histories at the center of the liquefiable layer beneath $A_{A\text{-}N}$, A_J, and the free-field. It is also clear from this figure that the maximum excess pore water pressure beneath A_J is on the order of 60% of the maximum excess pore water pressure beneath $A_{A\text{-}N}$. This would appear to at least partially explain the difference in settlement between these two buildings (i.e., 12 cm for A_J vs. 20 cm for $A_{A\text{-}N}$). Elasticity calculations suggest that the vertical effective stress at the center of the liquefiable layer beneath Building A_J was approximately 10% higher than the corresponding vertical effective stress beneath Building $A_{A\text{-}N}$. In addition, the foundation-level acceleration intensities were slightly lower for Building A_J than Building $A_{A\text{-}N}$ (Fig. 3.3.10). While there could be additional factors involved, including the influence of the dynamic response of Building J_A, these two factors would have reduced the cyclic stress ratio beneath A_J relative to $A_{A\text{-}N,}$ and this could partially explain the observation of lower excess pore water pressures beneath A_J during this event.

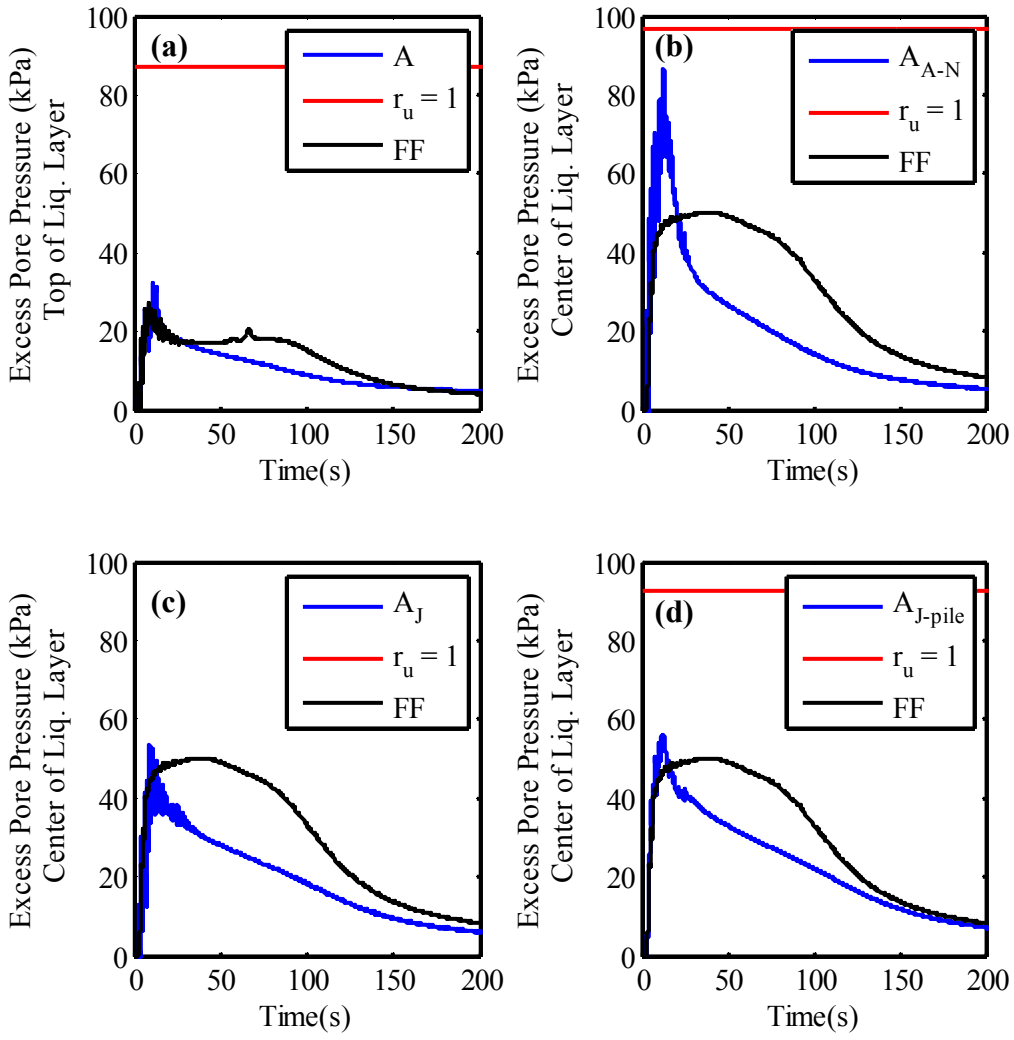

Figure 3.3.8. Excess pore water pressure-time histories at (a) the top of the liquefiable layer beneath the center of A, (b) the center of the liquefiable layer beneath the center of A_{A-N}, (c) the center of the liquefiable layer beneath A_J, and (d) the center of the liquefiable layer beneath A_{J-pile}. Corresponding $r_u \approx 1.0$ lines are indicated, along with the free-field excess pore water pressure-time history at the same elevation (i.e., top or center of liquefiable layer) for reference. Note that the $r_u \approx 1.0$ line for the A_J building corresponds to approximately 105 kPa.

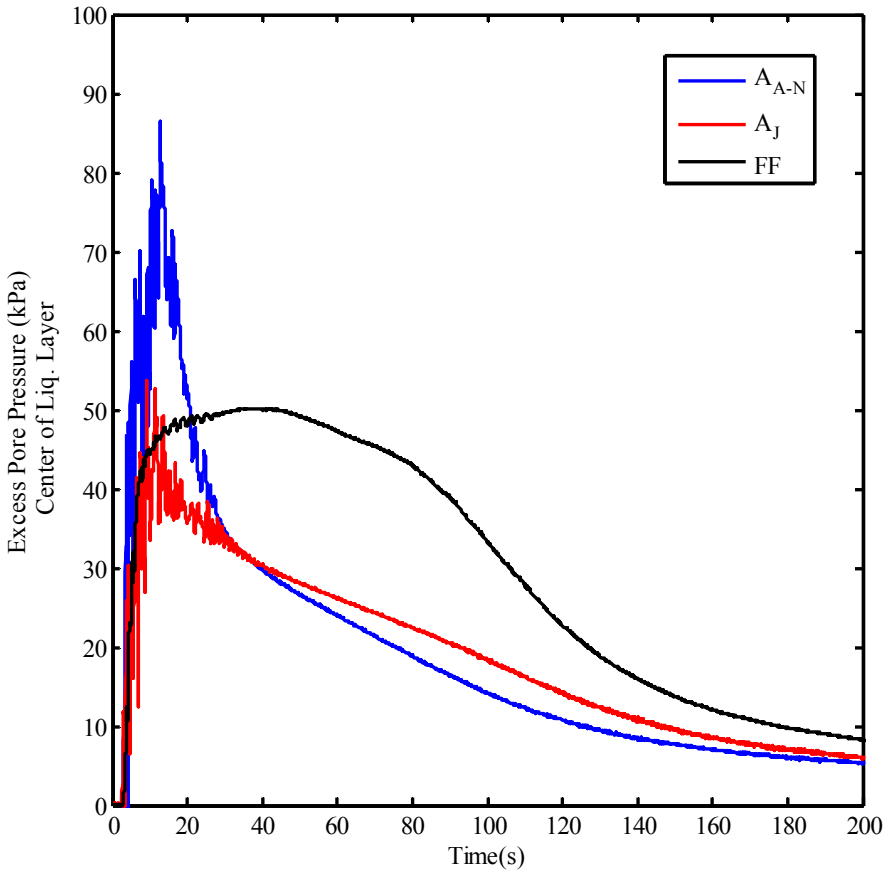

Figure 3.3.9. Excess pore water pressure-time histories at the center of the liquefiable layer beneath the center of $A_{A\text{-}N}$, the center of A_J, and the free-field.

As described previously, the average degree of excess pore water pressure dissipation was calculated as a function of time assuming double drainage with 1-D consolidation theory (Fig. 3.2.19). Based on these theoretical calculations, significant pore water pressure dissipation (drainage) occurred beneath the buildings during strong shaking. However, the experimental measurements during strong shaking indicate that excess pore water pressures were being generated as well during this time. The generation and dissipation of excess pore water pressures during strong shaking is complex as noted by Dashti et al. (2010a,b). Thus, the resulting amount of consolidation settlement that occurs during strong shaking is difficult to estimate. Dashti et al. (2010a) classify building settlement that occurs due to localized volumetric compression due to high transient hydraulic gradients generated during strong shaking as a separate mechanism and reserve the term of consolidation settlement for those cases when the effective stress is being transferred back to the soil skeleton.

Foundation-level and lumped mass-level acceleration-time histories are compared in Figures 3.3.10 and 3.3.11, respectively. The top three plots of each figure compare the acceleration-time histories for the buildings with neighbors to the acceleration-time history of the isolated building. At both foundation-level and lumped mass-level, the acceleration-time histories recorded at building A and building $A_{A\text{-}N}$ appear to be nearly identical. The

acceleration-time histories at the foundation level of A and $A_{J\text{-}pile}$ are similar but the foundation-level trace recorded at building A appears to envelope the trace recorded at building $A_{J\text{-}pile}$ (i.e., the peaks are slightly higher at building A). Additionally, the lumped mass-level traces are noticeably different. The differences are even more noticeable between buildings A and A_J. At the foundation level, particularly after the first cycle of motion, the acceleration amplitudes are typically lower for the A_J building than the A building. The lumped mass-level acceleration-time histories are clearly different with some of the larger peaks missing and some of the smaller peaks amplified at the A_J building.

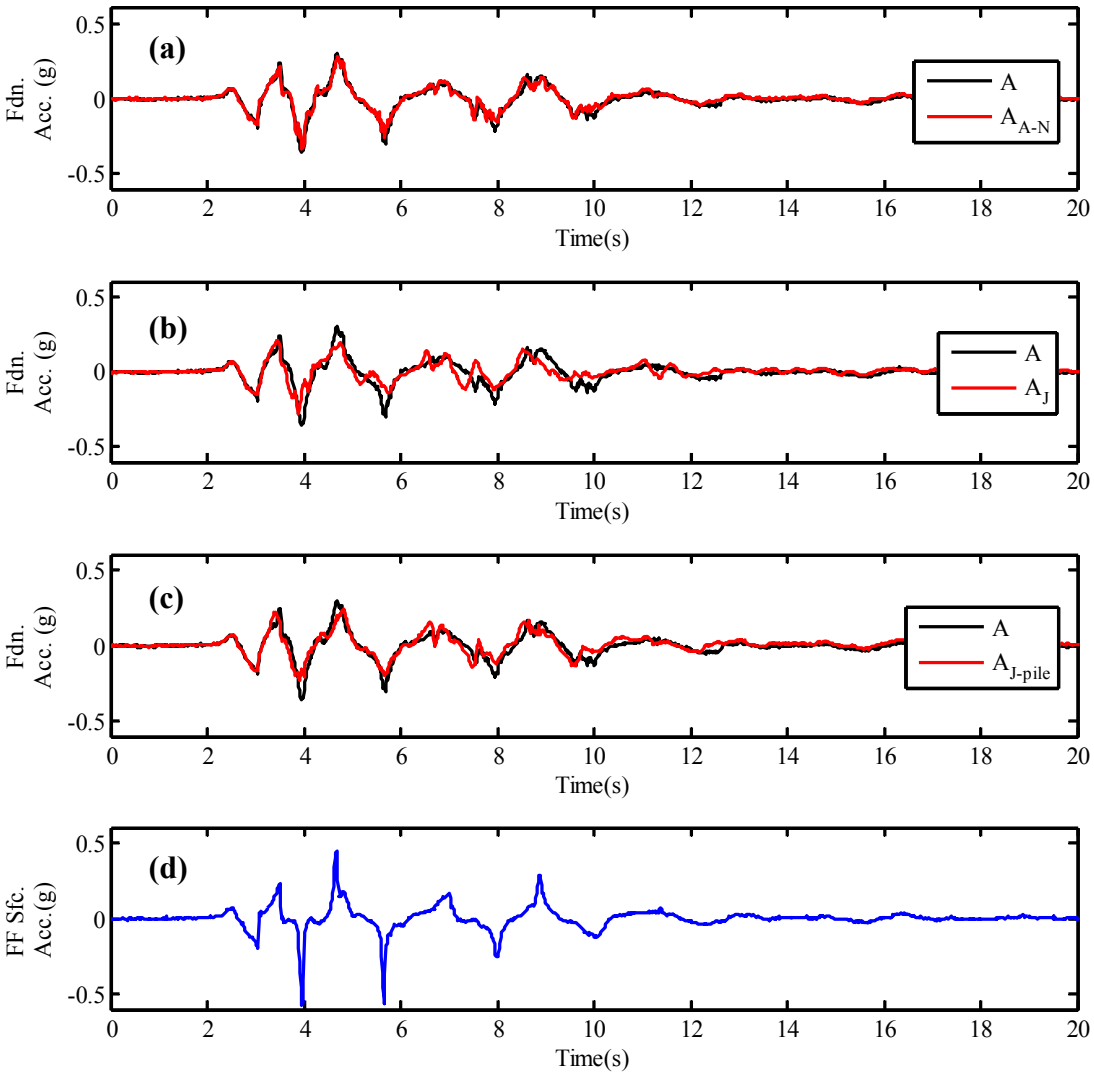

Figure 3.3.10. Foundation level acceleration-time histories at (a) $A_{A\text{-}N}$, (b) A_J, and (c) $A_{J\text{-}pile}$. The foundation level acceleration-time history of A is shown on each plot for the purposes of comparison. (d) Free-field surface acceleration-time history.

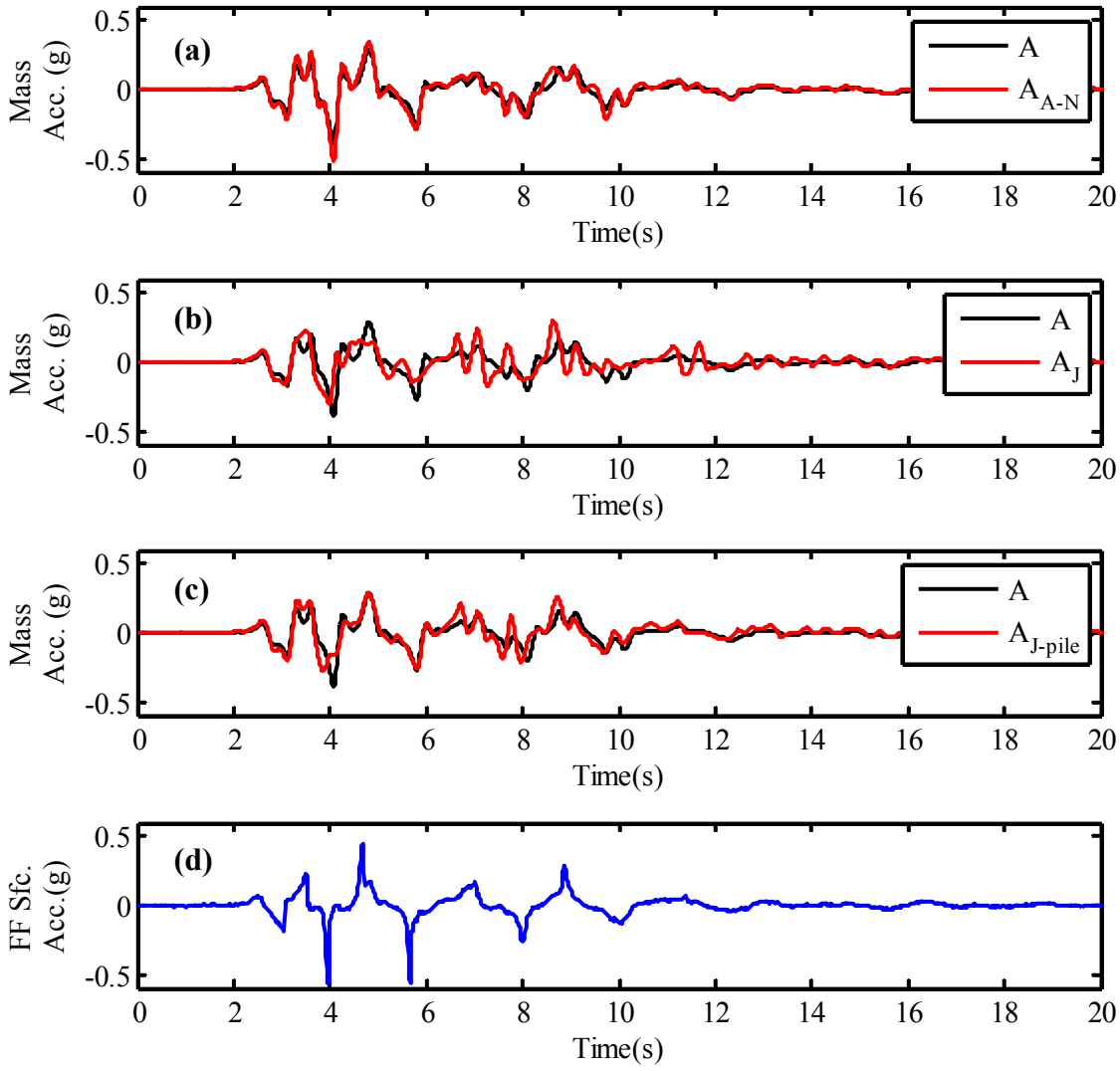

Figure 3.3.11. Lumped mass-level acceleration-time histories at (a) $A_{A\text{-}N}$, (b) A_J, and (c) $A_{J\text{-}pile}$. The lumped mass-level acceleration-time history of A is shown on each plot for the purposes of comparison. (d) Free-field surface acceleration-time history.

Pseudo-acceleration response spectra (5 % damped) at the foundation and lumped mass levels were calculated and plotted for A, $A_{A\text{-}N}$, A_J, and $A_{J\text{-}pile}$. These plots are presented in Fig. 3.3.12. In addition, spectral ratio plots (i.e., $S_{a,\ lumped\ mass}$ / $S_{a,\ foundation}$) for the 'A' buildings are shown in Fig. 3.3.13. The 'A' buildings show distinct peaks around T = 1 s and T = 2 s at both the foundation and lumped mass levels. In addition, peaks around the fundamental periods of the buildings (i.e., $T_n \approx 0.3$ s) are present in the lumped mass level spectra for A and $A_{A\text{-}N}$. The primary peaks around the fundamental periods are shifted slightly to the right for $A_{J\text{-}pile}$ and A_J and occur at approximately 0.35 s and 0.40 s, respectively. Secondary peaks at the lumped mass level are also clearly present at A and $A_{A\text{-}N}$ around T = 0.5 s, but they are not as clear at A_J and

$A_{J\text{-pile}}$. The peaks in the spectral ratio plots are 1.47 at T = 0.34 s, 2.44 at T = 0.32 s, 2.80 at T = 0.41 s, and 3.19 at T = 0.35 s for A, $A_{A\text{-}N}$, A_J, and $A_{J\text{-pile}}$, respectively. Therefore, the general trend is that the 'A' buildings with neighbors experienced more spectral amplification between the lumped mass and the base than the isolated 'A' building. In addition, this peak amplification was higher and occurred at a longer period for the A_J than $A_{A\text{-}N}$.

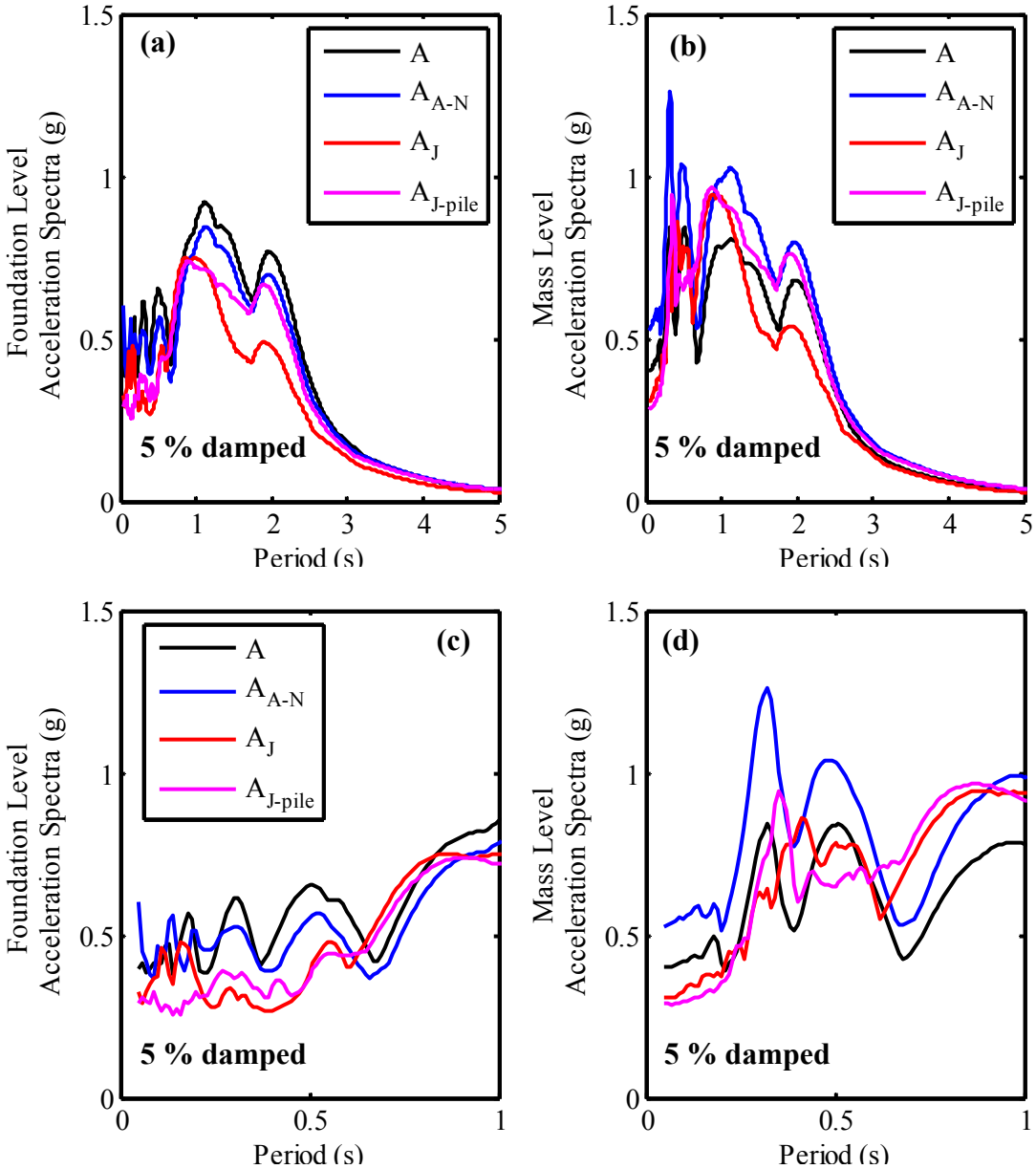

Figure 3.3.12. 5% damped pseudo-acceleration response spectra at (a) the foundation level and (b) the lumped mass level for A, $A_{A\text{-}N}$, A_J, and $A_{J\text{-pile}}$. Identical plot as (a) and (b), zoomed-in between T = 0 and T = 1 s, are presented in (c) and (d).

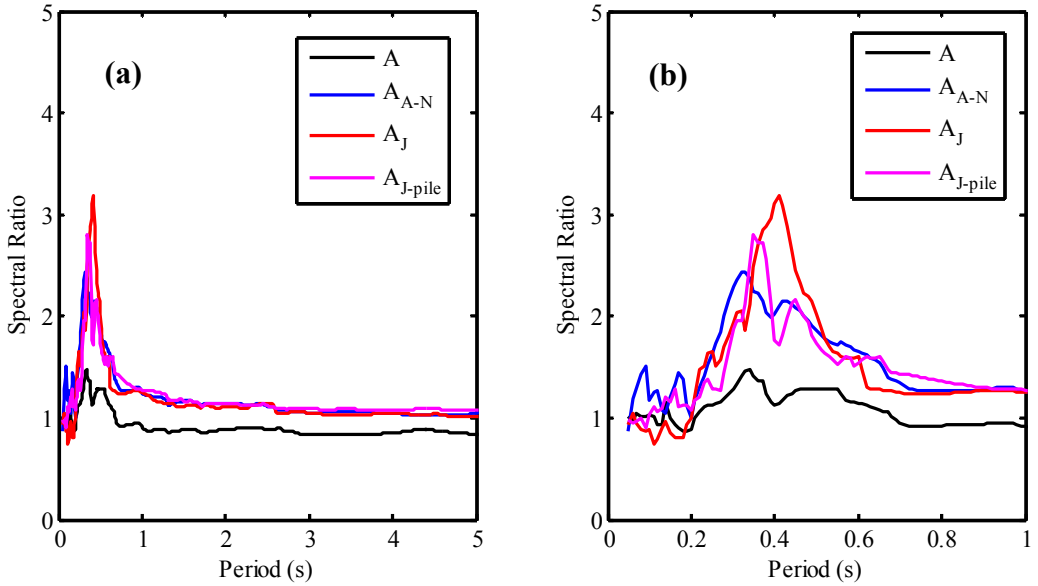

Figure 3.3.13. (a) Spectral ratios (i.e., $S_{a,\ lumped\ mass}$ / $S_{a,\ foundation}$) for A, $A_{A\text{-}N}$, A_J, and $A_{J\text{-}pile}$. (b) Identical plot as (a) zoomed-in between T = 0 and T = 1 s.

In summary, the A_J building settled less, generated less excess pore water pressure, and had different foundation-level and lumped mass-level accelerations than buildings A and $A_{A\text{-}N}$ during the PRI_mod event. In addition, there was more spectral amplification in building A_J than in building $A_{A\text{-}N}$, and this peak amplification occurred at a slightly longer period (T = 0.41 s vs. T = 0.32 s). Because the subsurface conditions and base motions were identical for buildings A, $A_{A\text{-}N}$, and A_J, the differences in the observed performance of the A_J building would seem to be primarily attributed to the presence of the much larger J_A building.

TCU_mod

Similar to the PRI_mod event, the TCU_mod event also caused full liquefaction (i.e., $r_u \approx 1.0$) of the free-field loose to medium-dense Nevada Sand. Significant building settlements were again observed. Just prior to the TCU_mod event the prototype building separation distances were 26 cm, 42 cm, and 37 cm for the $A_{A\text{-}N}$ – $A_{A\text{-}S}$, A_J – J_A, and $A_{J\text{-}pile}$ – $J\text{-}pile_A$ building pairs, respectively. Additionally, based on an average of hydrostatic pore water pressures measured by 11 PPTs just prior to the TCU_mod motion, the groundwater table was approximately 0.9 m below the ground surface during this event.

Free-Field Response

As described previously, the TCU_mod event was a modified version of the fault-normal component of the ground motion recorded at the TCU078 station during the 1999 M_w 7.6 Chi-Chi, Taiwan earthquake. Due primarily to its larger magnitude, the significant duration of the TCU_mod motion was much longer than for the PRI events (i.e., $D_{5\text{-}95} \approx 28$ s vs. 8 s). Free-field acceleration-time histories at the base, the top of the loose to medium-dense Nevada Sand layer, and just beneath the soil surface are presented in Figure 3.3.14. The free-field motion was clearly amplified between the base of the model container and the surface of the model. In addition, the

high frequency content of the surface motion appears to have been reduced relative to the base motion, particularly after the significant acceleration cycle at t ≈ 7.5 s. This is presumably a consequence of liquefaction. At least two large amplitude dilation spikes are observed at the top of the liquefiable layer and the soil surface. The surface PGA for this event was 0.38 g and the maximum acceleration at the base of the model container was 0.18 g.

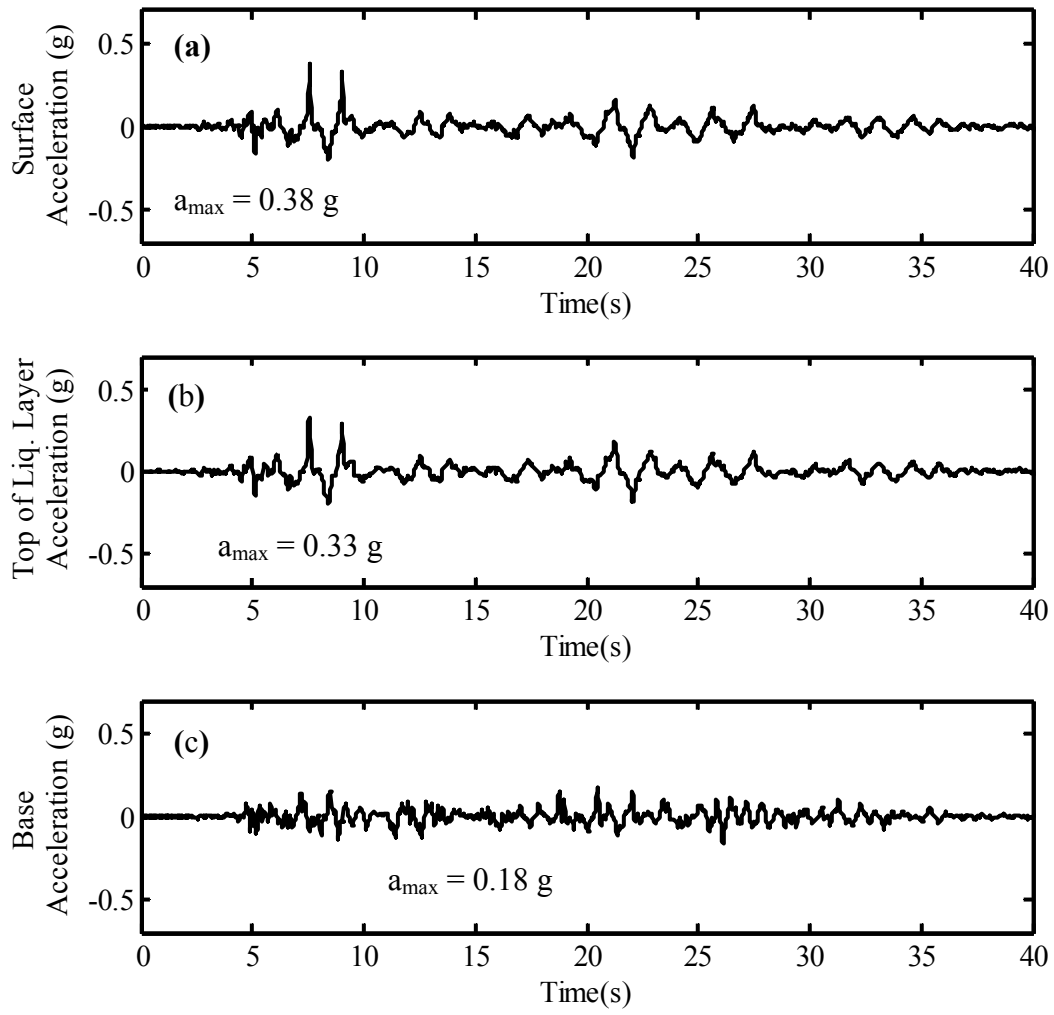

Figure 3.3.14. Free-field acceleration-time histories at (a) the soil surface, (b) the top of the loose to medium-dense Nevada Sand, and (c) the base of the model container during the TCU_mod motion.

The free-field settlement-time history at the surface and the excess pore water pressure-time history at the center of the liquefiable layer in the free-field are provided in Fig. 3.3.15. Free-field acceleration-time histories at the surface and the base are also provided for reference. The same plots, zoomed-in to focus on the during-shaking portions of the records, are provided in Fig. 3.3.16. It is observed that excess pore water pressures are generated rapidly during strong

shaking and approach $r_u \approx 1.0$ (indicated with the blue horizontal line) well before shaking is completed. Free-field surface settlements initiate during strong shaking, at nearly the same time excess pore water pressures begin to increase significantly, and continue until well after shaking is completed. These settlements would appear to be suggestive of partial drainage occurring during strong shaking. The final free-field soil surface settlement was measured to be 4.8 cm for this event.

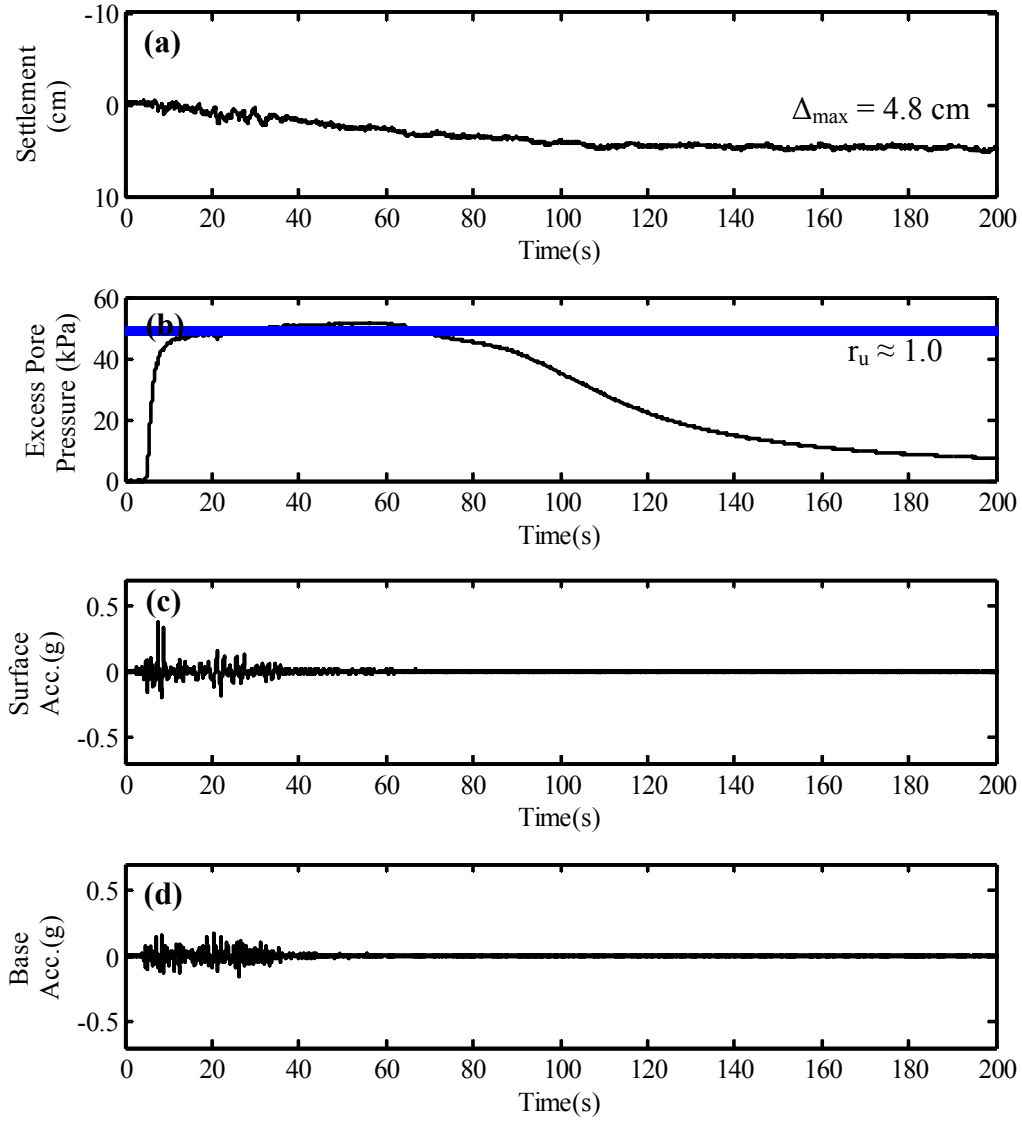

Figure 3.3.15. The free-field (a) settlement-time history at the soil surface, (b) excess pore water pressure-time history in the middle of the loose to medium-dense Nevada Sand layer, (c) the acceleration-time history at the surface, and (d) the acceleration-time history at the base of the model container.

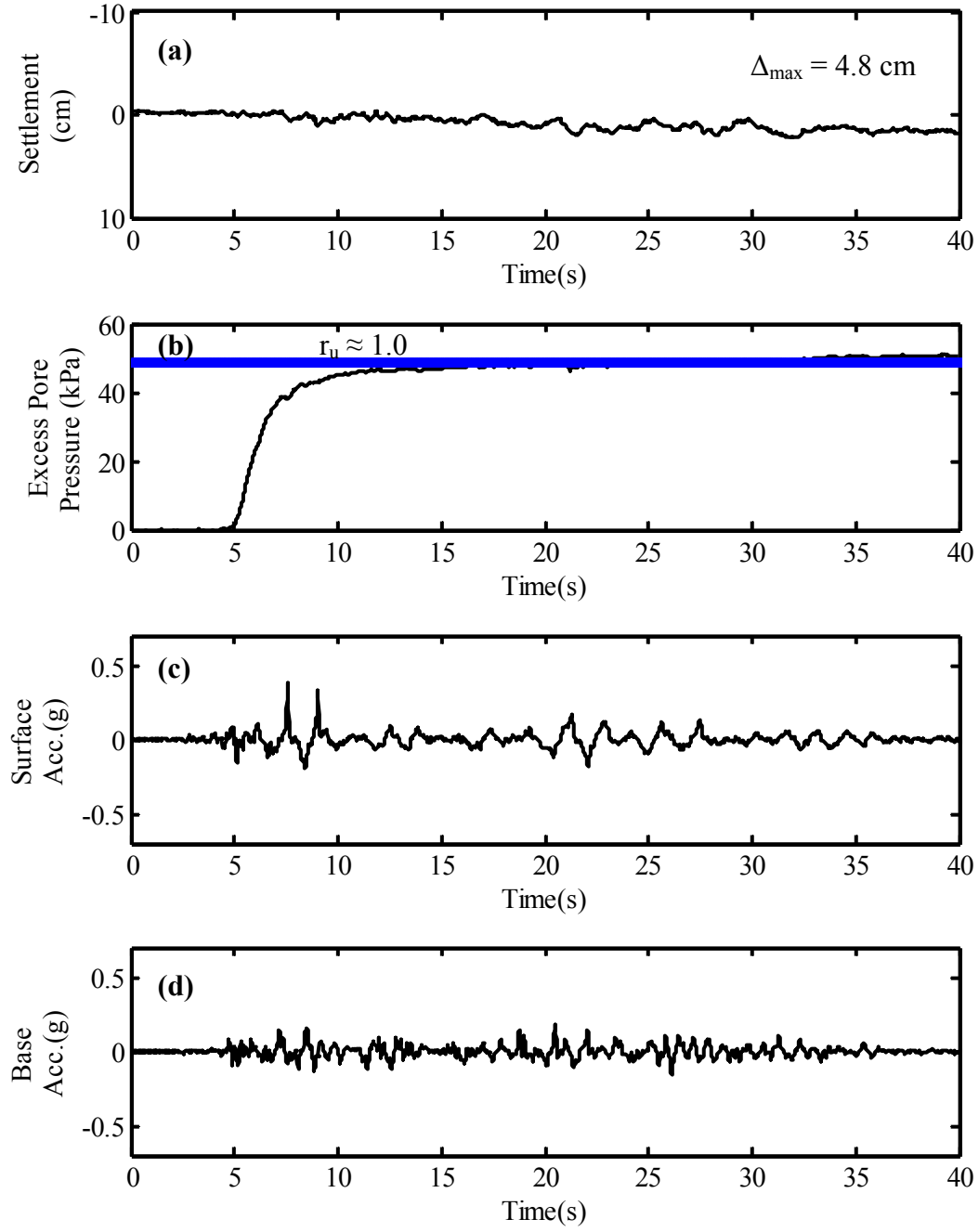

Figure 3.3.16. The zoomed-in free-field (a) settlement-time history at the soil surface, (b) excess pore water pressure-time history in the middle of the loose to medium-dense Nevada Sand layer, (c) the acceleration-time history at the surface, and (d) the acceleration-time history at the base of the model container.

Response Near Structures

Building settlement-time histories are presented in Figure 3.3.17, along with the free-field surface settlement and free-field surface acceleration-time history for reference. Several observations can be made from this figure: (1) similar to the free-field soil settlements, building settlements initiate shortly after the onset of strong shaking; (2) the shallow-founded buildings settle much more than the free-field soil; (3) again, $A_{A\text{-}N}$ and $A_{A\text{-}S}$ settle at the same rate and about the same amount; however, they settle slightly less than A; (4) $A_{J\text{-}pile}$ settles the most (approx. 18 cm) of any building and A_J settles the least (approx. 10 cm) among 'A' buildings during this event; (5) J_A settles less than A_J (7 cm vs. 10 cm), but settles more than J-$pile_A$, as expected; and (6) J-$pile_A$ settles by far the least amount among the buildings, as would be expected, and less than the free-field surface (about 0.5 cm vs. 5 cm). Observations (1), (2), and (6) are generally consistent with the observations made for the PRI_mod event. During PRI_mod, the settlements of buildings A, $A_{A\text{-}N,}$ and $A_{A\text{-}S}$ were within 1 cm; during TCU_mod, the settlements of these buildings are within about 2.5 cm. Consequently, the 'A' buildings without larger neighbors settle approximately the same amount during these two events. Unlike PRI_mod when $A_{J\text{-}pile}$ settled less than A, $A_{A\text{-}N,}$ and $A_{A\text{-}S}$, it settled the most of all the 'A' buildings during TCU_mod. Also, while building A_J settled the least of all 'A' buildings during both PRI_mod and TCU_mod, it settled slightly more (approx. 3 cm) than J_A during TCU_mod and slightly less than J_A (approx.. 2 cm) during PRI_mod. A discussion of these key observations is presented in Section 3.4.

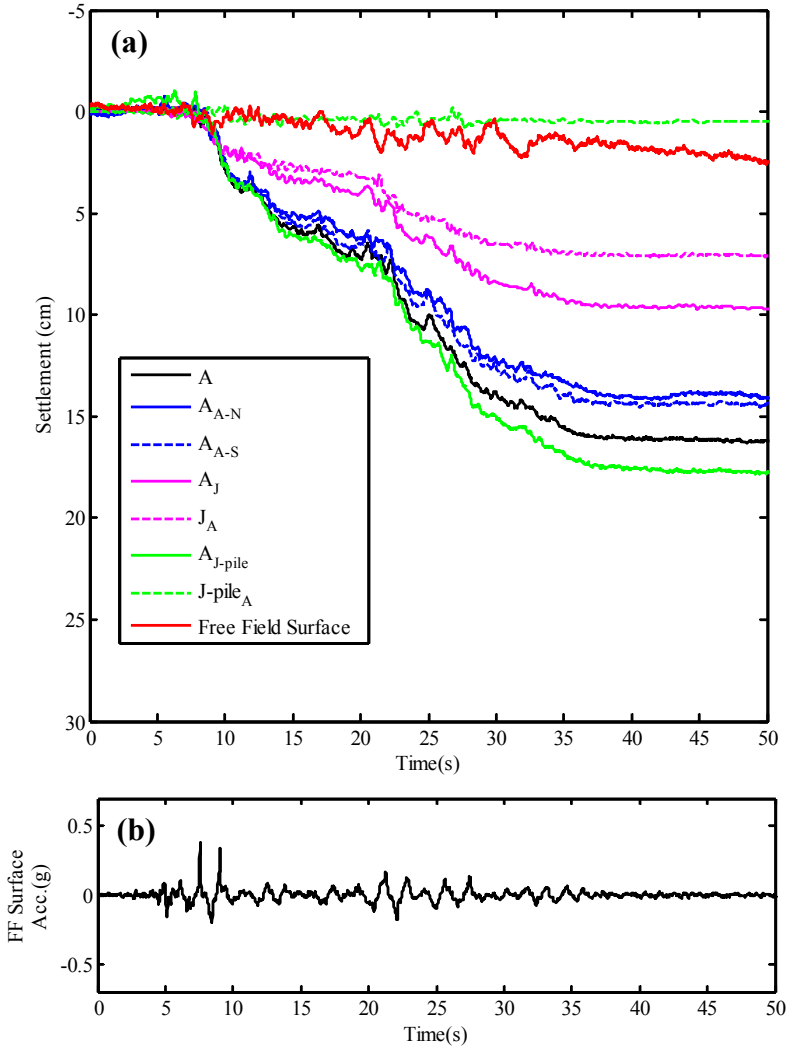

Figure 3.3.17. (a) Settlement-time histories at the centers of the A, $A_{A\text{-}N}$, $A_{A\text{-}S}$, A_J, and J_A buildings. Average settlement of the $A_{J\text{-}pile}$ building, and the settlement of the southwest corner of the J-pile building. Free-field surface settlements are shown for reference. (b) Free-field surface acceleration-time history.

Permanent settlements, measured at each LP location following the TCU_mod motion, are presented in Fig. 3.3.18. This figure also includes calculated settlements at building corners where there were no LPs, when possible (based on available data). Measured building settlements are indicated in black, calculated building settlements are indicated in blue, measured horizontal displacements are indicated in red (positive towards the south), and measured soil settlements are indicated in green. Several observations, in addition to those made above, can be made with reference to Fig. 3.3.18: (1) soil settlements measured adjacent to the buildings in the northern half of the container are much larger than the soil settlements measured in the free-field and slightly less than the adjacent building settlements; (2) more settlement is observed at the top of the liquefiable layer than at the soil surface in the northwest quadrant. Again, this appears to be best explained by dilation of the Monterey 0/30 Sand; (3) $A_{A\text{-}N}$ and $A_{A\text{-}S}$ both displaced

horizontally to the south and settled such that they are tilted away from each other. $A_{A\text{-}N}$ again tilted a very small amount to the west and $A_{A\text{-}S}$ tilted a small amount to the east; (4) A_J moved horizontally away from J_A and settled such that it was tilted away from J_A. J_A did not move much horizontally and settled such that it was tilted slightly away from A_J. Both J_A and A_J tilted slightly to the west; and (5) $A_{J\text{-}pile}$ moved horizontally away from J-$pile_A$ and settled such that it was tilted away from J-$pile_A$.

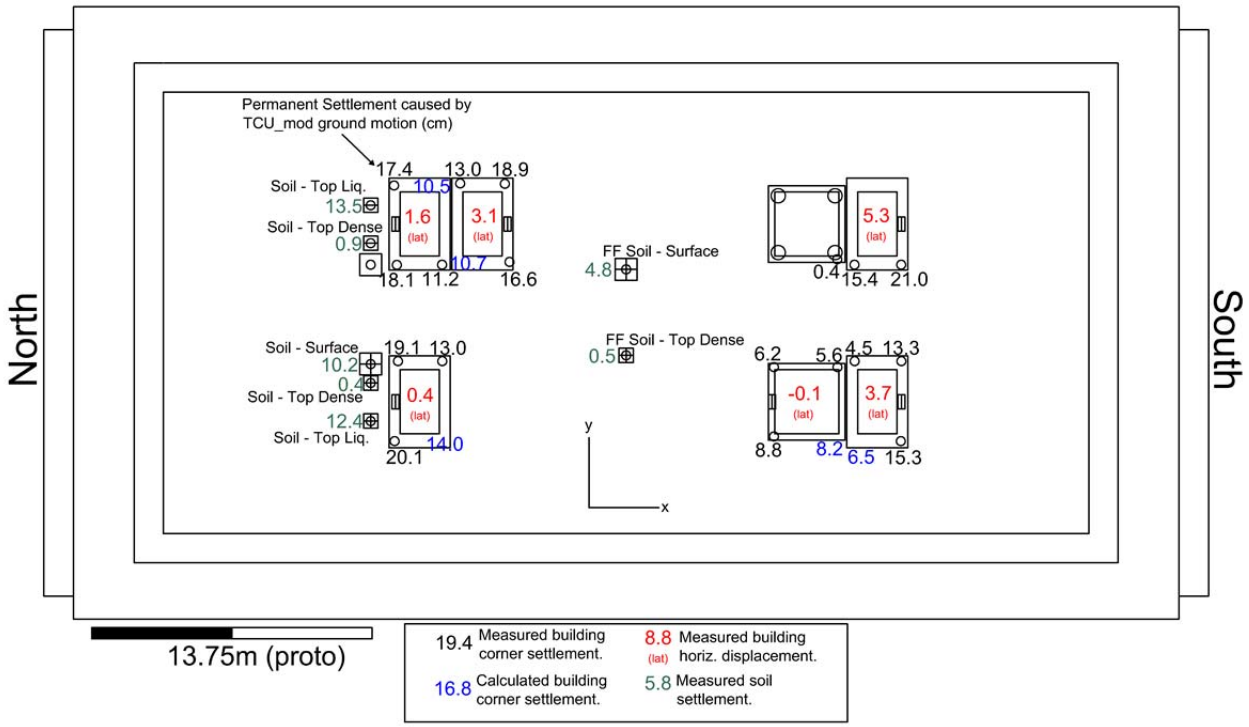

Figure 3.3.18. Permanent settlements following the TCU_mod motion. Black numbers represent settlement at a building corner, blue numbers indicate calculated settlement at a building corner, red numbers indicate horizontal building displacement in the north-south direction (positive toward south), and green numbers indicate soil settlements. All settlements are provided in prototype cm.

Excess pore water pressure-time histories beneath the center of the 'A' buildings are presented in Figure 3.3.19. As described previously, the PPT in the center of the liquefiable layer beneath the isolated 'A' building did not function properly so the excess pore water pressure-time history for the PPT at the top of the liquefiable layer is presented for this building (Fig. 3.3.19a). The remaining plots in this figure correspond to the center of the liquefiable layer. The excess pore water pressure corresponding to $r_u \approx 1.0$ has been indicated for each of the PPTs beneath buildings. From these plots it is clear that excess pore water pressures beneath the buildings increased rapidly at the onset of strong shaking and reached initial peak values around t = 10 - 15 s. Pore water pressures then dissipate briefly before increasing again and peaking a second time around t = 25 s. The periods of rapid pore water pressure generation between $t \approx 5 - 15$ s and $t \approx 20 - 25$ s correspond to the periods of most rapid settlement (Fig. 3.3.17). Beneath buildings $A_{A\text{-}N}$ and A, excess pore water pressures were often greater than the excess pore water pressure in the free-field at the same elevation. Under these conditions, pore water would have flowed from beneath the center of the buildings towards the free-field. As was the case following

the PRI_mod event, the excess pore water pressures beneath the buildings dissipated faster than the excess pore water pressures in the free-field. Consequently, the direction of flow would have reversed at the center of the liquefiable layer under $A_{A\text{-}N}$ around $t \approx 37$ s until hydrostatic conditions were reached.

Though the peak excess pore water pressure beneath building A_J was not sustained above the corresponding free-field pore water pressure for a substantial amount of time, excess pore water pressures beneath A_J, similar to excess pore water pressures beneath buildings $A_{A\text{-}N}$, A, and, to a lesser extent, $A_{J\text{-}pile}$, changed rapidly during shaking and briefly exceeded the corresponding free-field excess pore water pressures several times. This would have caused transient hydraulic gradients at these locations and led to rapid changes in pore water flow direction.

The plot shown in Figure 3.3.20 compares the excess pore water pressure-time histories at the center of the liquefiable layer beneath $A_{A\text{-}N}$, A_J, $A_{J\text{-}pile}$, and the free-field. The excess pore water pressure beneath A_J was typically on the order of one-half of the excess pore water pressure beneath $A_{A\text{-}N}$ and the excess pore water pressure beneath $A_{J\text{-}pile}$ was typically on the order of two-thirds times the excess pore water pressure beneath $A_{A\text{-}N}$.

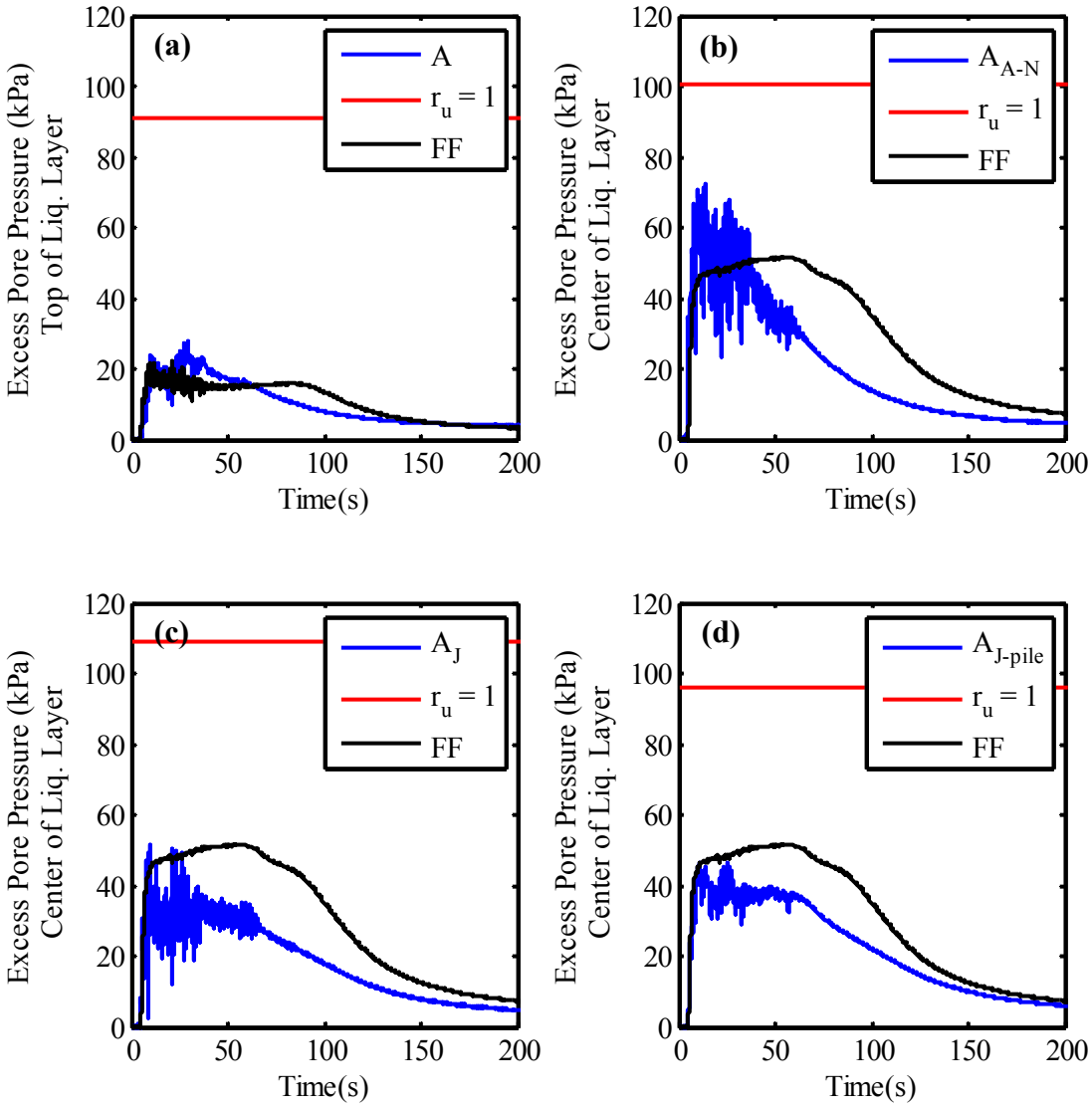

Figure 3.3.19. Excess pore water pressure-time histories at (a) the top of the liquefiable layer beneath the center of A, (b) the center of the liquefiable layer beneath the center of A_{A-N}, (c) the center of the liquefiable layer beneath A_J, and (d) the center of the liquefiable layer beneath A_{J-pile}. Corresponding $r_u \approx 1.0$ lines are indicated, along with the free-field excess pore water pressure-time history at the same elevation (i.e., top or center of liquefiable layer) for reference.

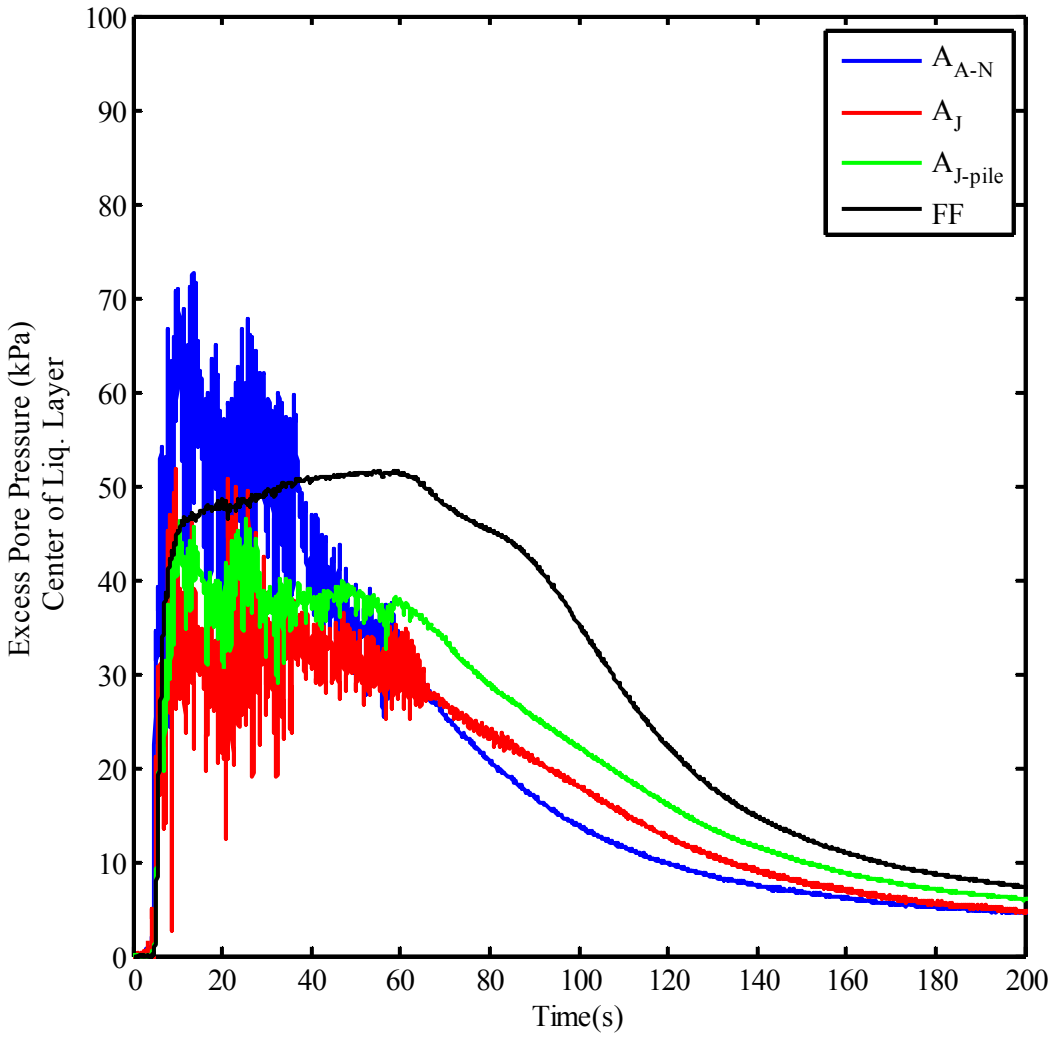

Figure 3.3.20. Excess pore water pressure-time histories at the center of the liquefiable layer beneath the center of $A_{A\text{-}N}$, the center of A_J, the center of $A_{J\text{-}pile}$, and the free-field.

Foundation-level and lumped mass-level acceleration-time histories are presented in Figures 3.3.21 and 3.3.22, respectively. The top three plots of each figure compare the acceleration-time histories for the buildings with neighbors to the acceleration-time history of the isolated building. At both foundation-level and lumped mass-level, the acceleration-time histories recorded at buildings A, $A_{A\text{-}N}$, and $A_{J\text{-}pile}$ appear to be similar, though there does appear to be a few spikes in the lumped mass recordings from $A_{A\text{-}N}$ and $A_{J\text{-}pile}$ that are not present in the recording from A. As was observed for the PRI_mod event, the acceleration-time histories from A and A_J were noticeably different. At both the foundation and lumped mass levels, there appears to be more high frequency content at A_J than at A. Also, in general, the lumped mass shaking amplitudes are higher for A_J than for A.

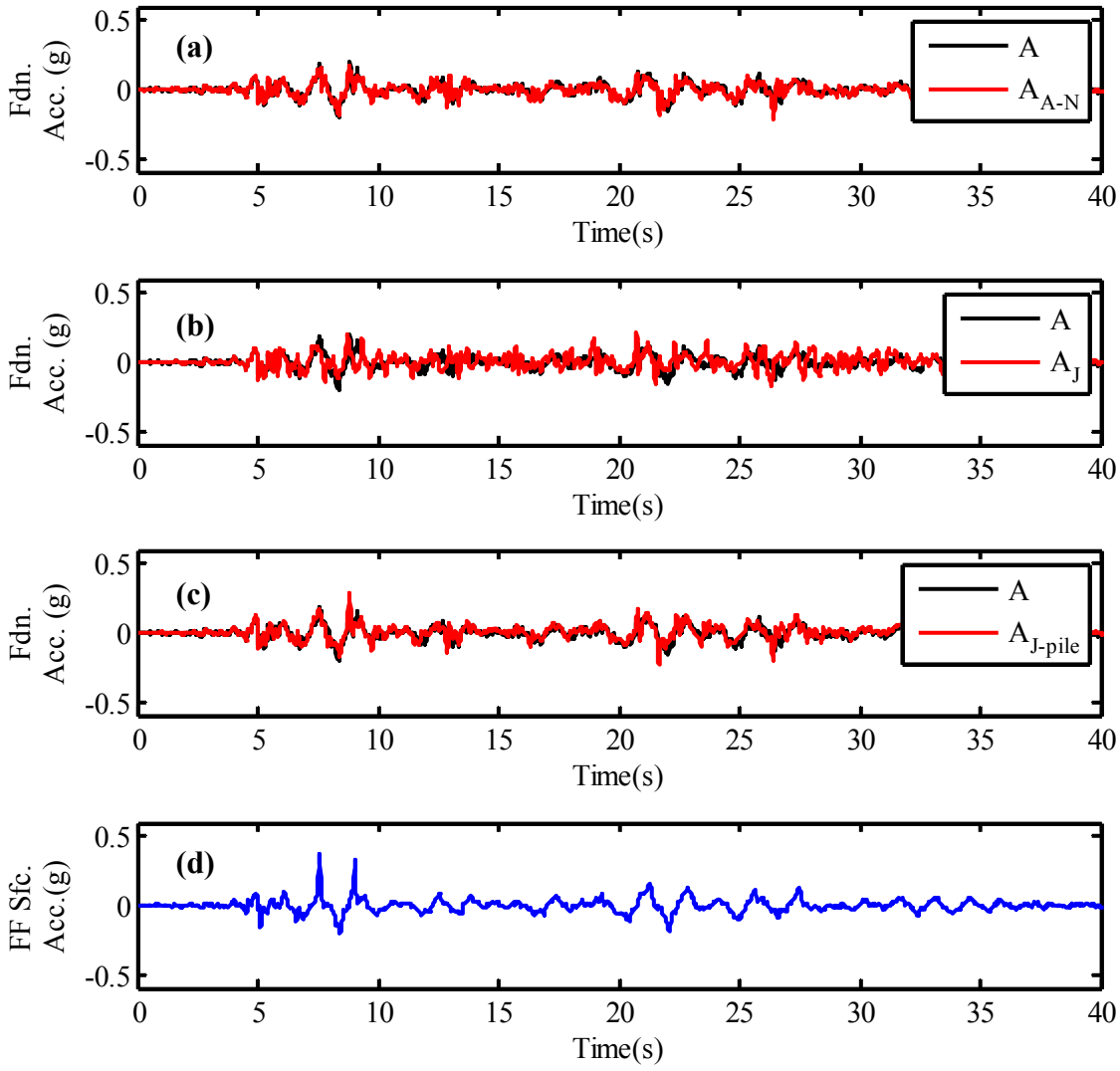

Figure 3.3.21. Foundation level acceleration-time histories at (a) $A_{A\text{-}N}$, (b) A_J, and (c) $A_{J\text{-}pile}$. The foundation level acceleration-time history of A is shown on each plot for the purposes of comparison. (d) Free-field surface acceleration-time history.

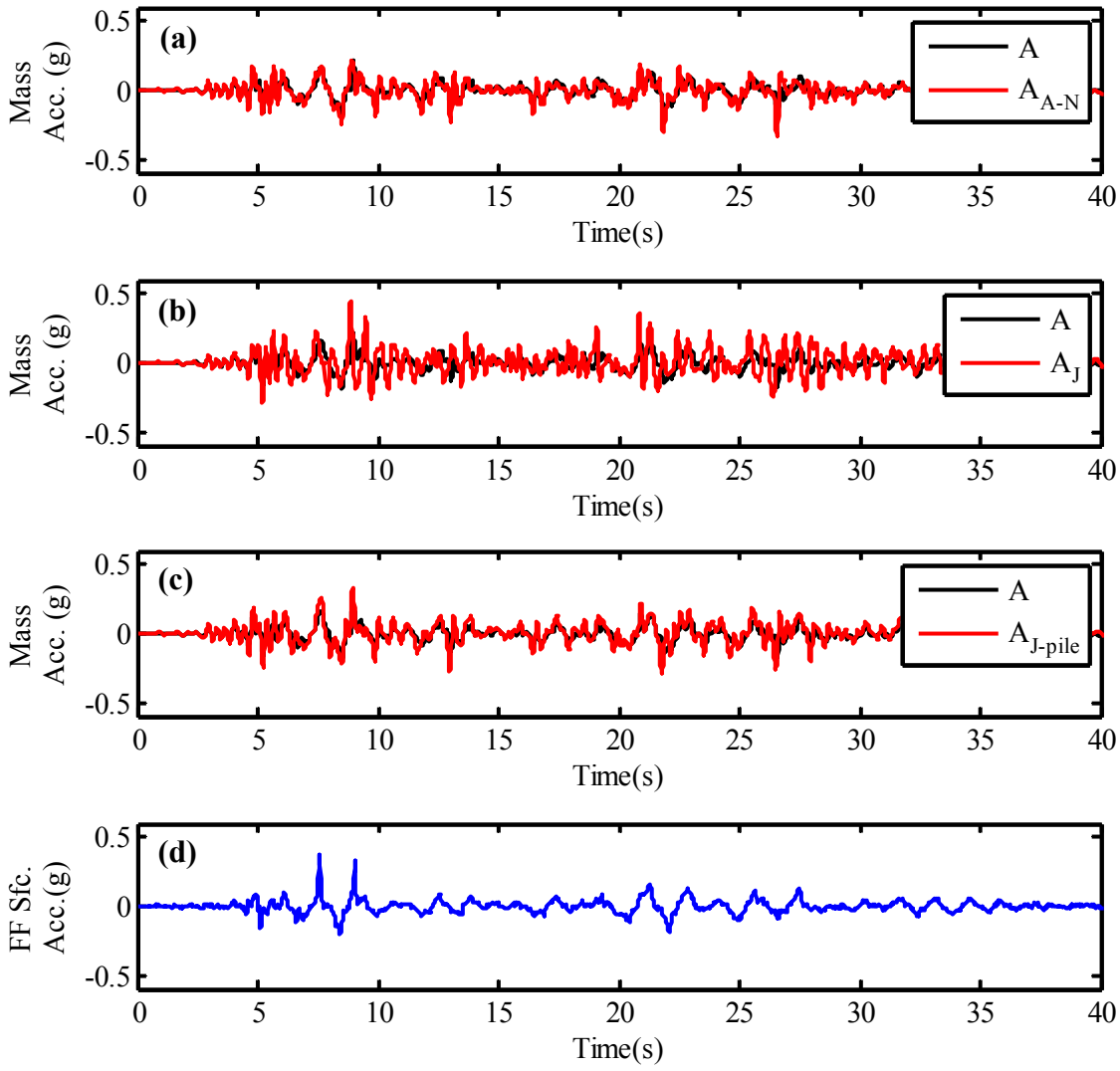

Figure 3.3.22. Lumped mass-level acceleration-time histories at (a) $A_{A\text{-}N}$, (b) A_J, and (c) $A_{J\text{-}pile}$. The lumped mass-level acceleration-time history of A is shown on each plot for the purposes of comparison. (d) Free-field surface acceleration-time history.

Pseudo-acceleration response spectra (5 % damped) at the foundation and lumped mass levels were calculated and plotted for A, $A_{A\text{-}N}$, A_J, and $A_{J\text{-}pile}$ (Fig. 3.3.23). In a general sense, these plots have the same shape with two primary peaks at T ≈ 0.25 – 0.3 s and T ≈ 1.35 – 1.5 s. Third peaks are present in the 'A' buildings with 'J' neighbors at T ≈ 0.65 s. In fact, this third peak is the dominant feature in the A_J spectral plots. It is also readily apparent that the peak around T ≈ 1.35 – 1.5 s is suppressed for A_J relative to the other buildings.

Spectral ratio plots (i.e., $S_{a,\ lumped\ mass}$ / $S_{a,\ foundation}$) for the 'A' buildings are shown in Fig. 3.3.24. Clearly, A_J experienced the most spectral amplification, with spectral ratios greater than two between T ≈ 0.3 s and T ≈ 0.7 s.

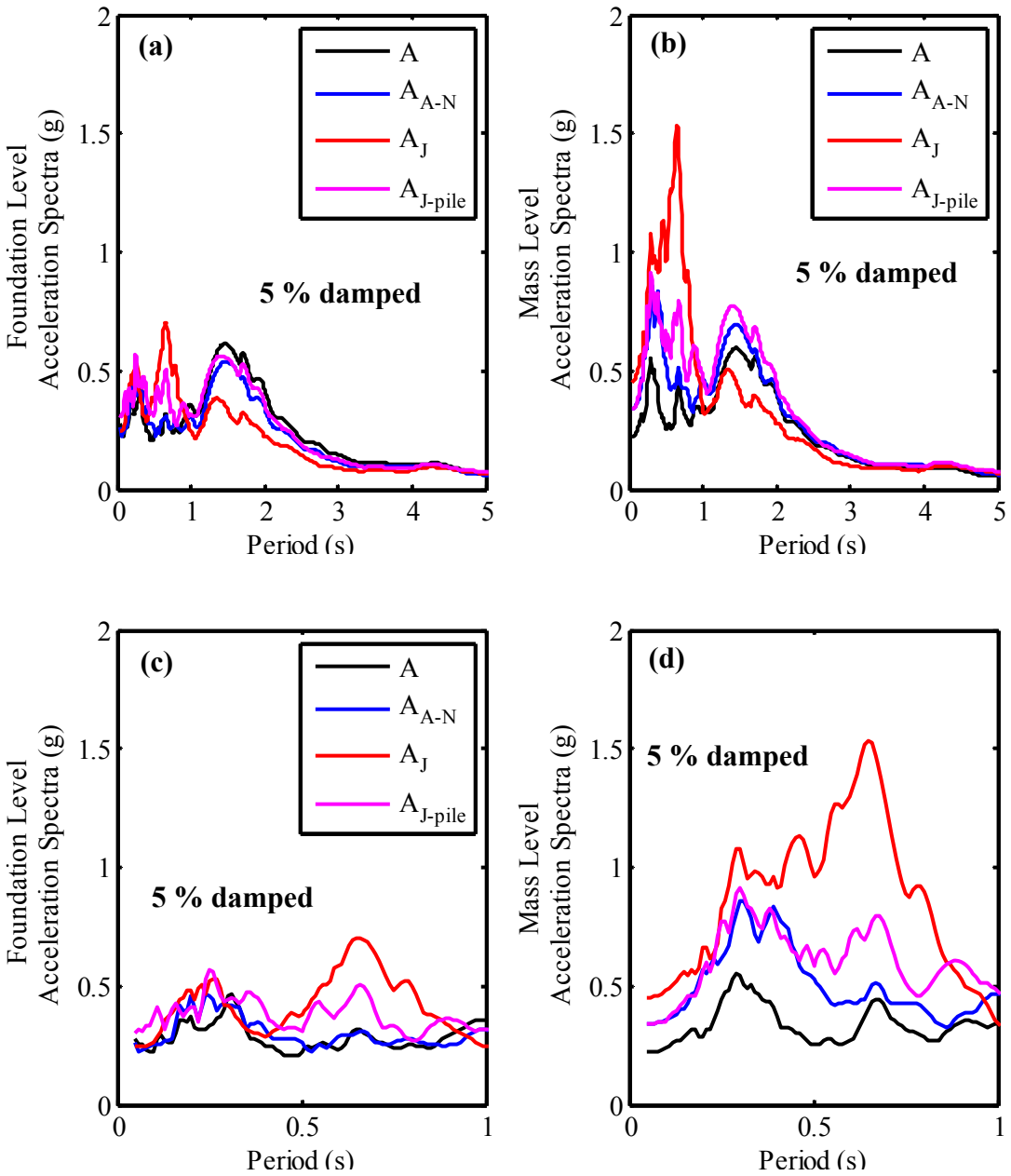

Figure 3.3.23. 5% damped pseudo-acceleration response spectra at (a) the foundation level and (b) the lumped mass level for A, $A_{A\text{-}N}$, A_J, and $A_{J\text{-}pile}$. Identical plot as (a) and (b), zoomed-in between T = 0 and T = 1 s, are presented in (c) and (d).

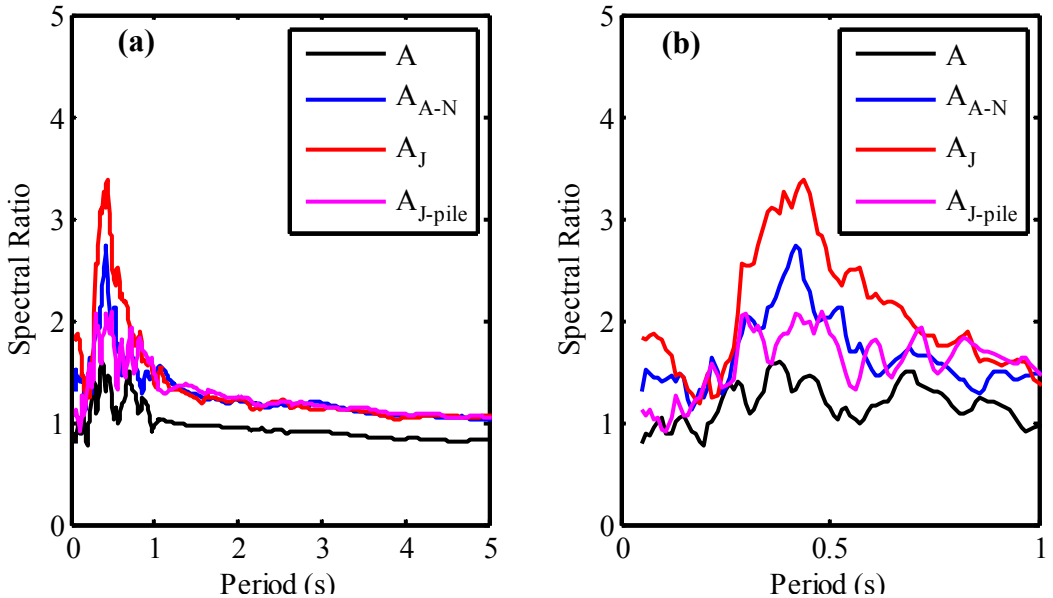

Figure 3.3.24. (a) Spectral ratios (i.e., $S_{a,\ lumped\ mass}$ / $S_{a,\ foundation}$) for A, $A_{A\text{-}N}$, A_J, and $A_{J\text{-}pile}$. (b) Identical plot as (a) zoomed-in between T = 0 and T = 1 s.

PRI_large

Full liquefaction (i.e., $r_u \approx 1.0$) of the free-field loose to medium-dense Nevada Sand was observed during the PRI_large motion. Significant building settlements were once again observed. Just prior to the PRI_large event the prototype building separation distances were 27.5 cm, 46 cm, and 42 cm for the $A_{A\text{-}N}$ – $A_{A\text{-}S}$, A_J – J_A, and $A_{J\text{-}pile}$ – J-$pile_A$ building pairs, respectively. Additionally, based on an average of hydrostatic pore water pressures measured by 11 PPTs just prior to the PRI_large motion, the groundwater table was approximately 0.87 m below the ground surface during this event.

Free-Field Response

Free-field acceleration-time histories at the base of the model container and just beneath the soil surface are presented in Figure 3.3.25. The free-field motion was clearly amplified between the base of the model container and the surface of the model. In addition, the high frequency content of the surface motion was reduced relative to the base motion. Again, this is presumably a consequence of liquefaction. Ten large amplitude dilation spikes were observed at the soil surface and the surface PGA for this event was 1.28 g. The base PGA was 0.51 g.

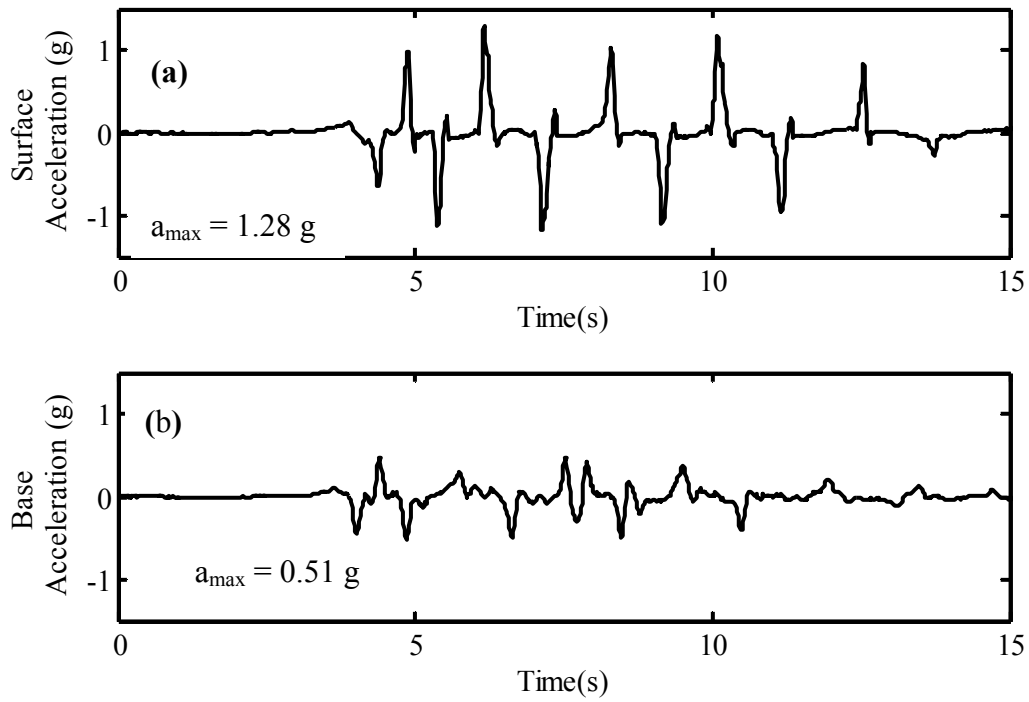

Figure 3.3.25. Free-field acceleration-time histories at (a) the soil surface and (b) the base of the model container during the PRI_large motion.

The free-field settlement-time history at the surface and the excess pore water pressure-time history at the center of the liquefiable layer in the free-field are provided in Fig. 3.3.26. Free-field acceleration-time histories at the surface and the base are also provided for reference. The same plots, zoomed-in to focus on the during-shaking portions of the records, are provided in Fig. 3.3.27. Excess pore water pressures are generated rapidly during strong shaking and approach $r_u \approx 1.0$ (indicated with the blue horizontal line) towards the end of the event. Free-field surface settlements initiate during strong shaking, at nearly the same time excess pore water pressures begin to increase significantly. Settlements occur at a higher rate during strong shaking and then continue at a slower rate until well after shaking is completed. The final free-field soil surface settlement was measured to be 7.0 cm for this event.

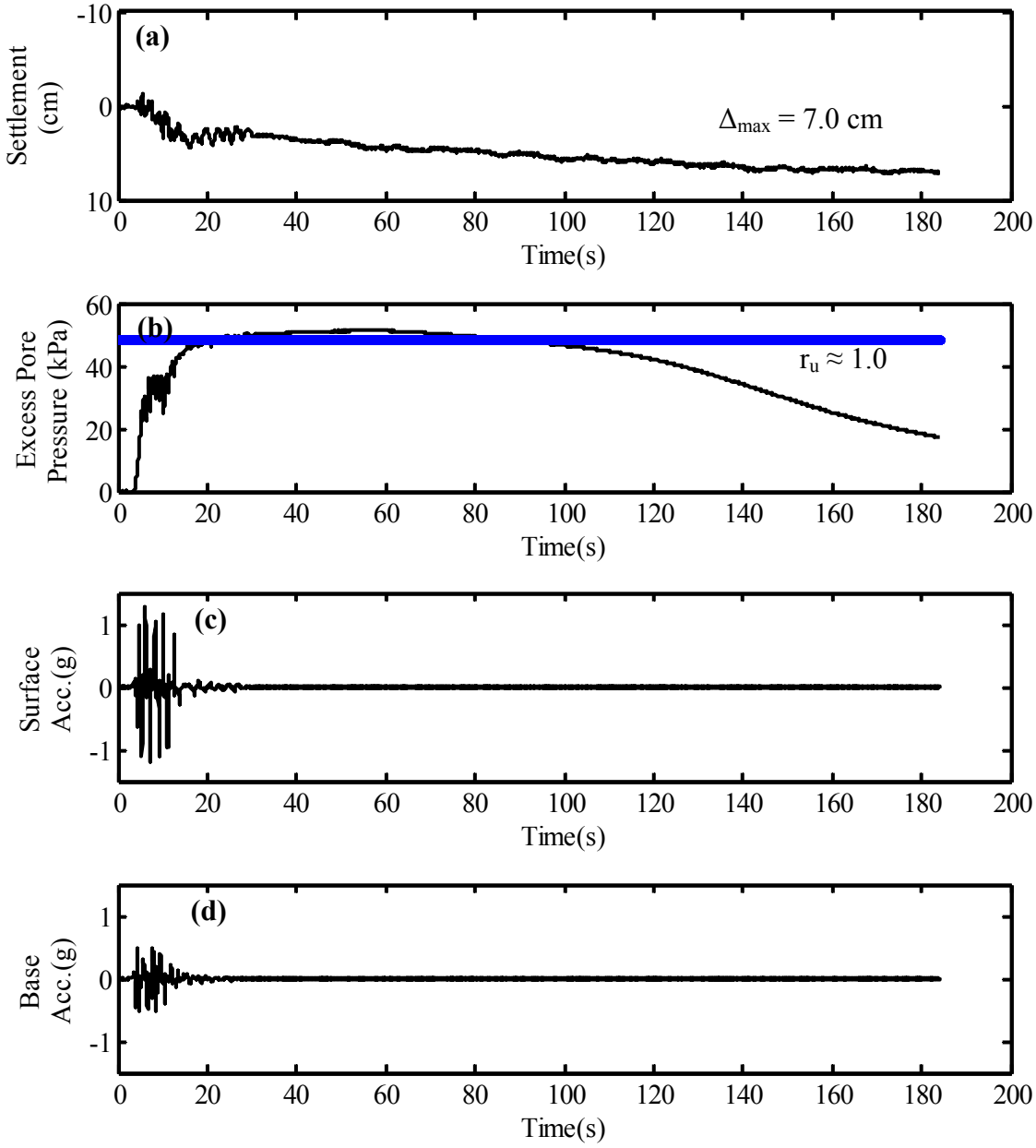

Figure 3.3.26. The free-field (a) settlement-time history at the soil surface, (b) excess pore water pressure-time history in the middle of the loose to medium-dense Nevada Sand layer, (c) the acceleration-time history at the surface, and (d) the acceleration-time history at the base of the model container.

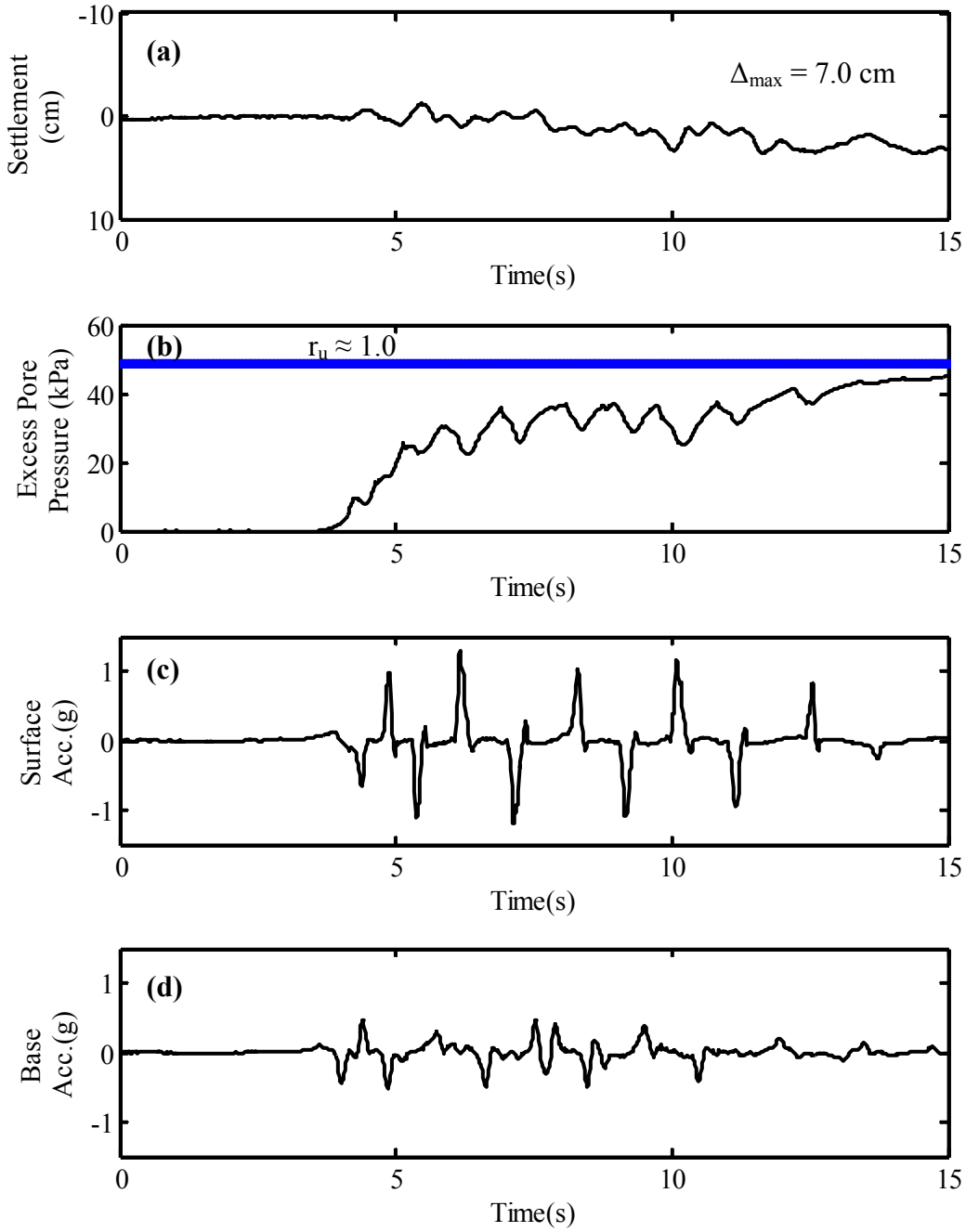

Figure 3.3.27. The zoomed-in free-field (a) settlement-time history at the soil surface, (b) excess pore water pressure-time history in the middle of the loose to medium-dense Nevada Sand layer, (c) the acceleration-time history at the surface, and (d) the acceleration-time history at the base of the model container.

Response Near Structures

Building settlement-time histories are presented in Figure 3.3.28, along with the free-field surface settlement and free-field surface acceleration-time history for reference. Several observations can be made from this figure: (1) similar to the free-field soil settlements, building settlements initiate shortly after the onset of strong shaking; (2) the shallow-founded buildings settle much more than the free-field soil; (3) Again, $A_{A\text{-}N}$ and $A_{A\text{-}S}$ settle at the same rate and about the same amount. However, as was observed during TCU_mod, they settle slightly less than A; (4) $A_{J\text{-}pile}$ settles the most (approx. 31.5 cm) of any building and A_J settles the least (approx. 19 cm) among 'A' buildings during this event; (5) J_A settles more than A_J (28 cm vs. 19 cm), but settles more than J-pile$_A$, as expected; and (6) J-pile$_A$ settles by far the least amount among the buildings, as would be expected, and about the same as the final free-field surface settlement (about 7.5 cm vs. 7 cm), though the mechanisms of free-field settlement and the settlement of J-pile$_A$ are different, as will be discussed in Section 3.4. The trends in the observations listed above are generally consistent with the trends observed for the PRI_mod motion. The A, $A_{A\text{-}N}$, and $A_{A\text{-}S}$ building settlements were all within about 3 cm. While this is slightly higher than the difference between the settlements of these buildings during PRI_mod and TCU_mod, it is still very small. Therefore, these three buildings settled about the same amount during the three significant events described herein. As was observed in both PRI_mod and TCU_mod, building A_J settled the least amount of the 'A' buildings during PRI_large. Similar to PRI_mod, building J_A settled more than building A_J during PRI_large. Also, as was observed with the TCU_mod motion, the $A_{J\text{-}pile}$ settled the most of all buildings during PRI_large. Additional discussion of key observations is provided in Section 3.4.

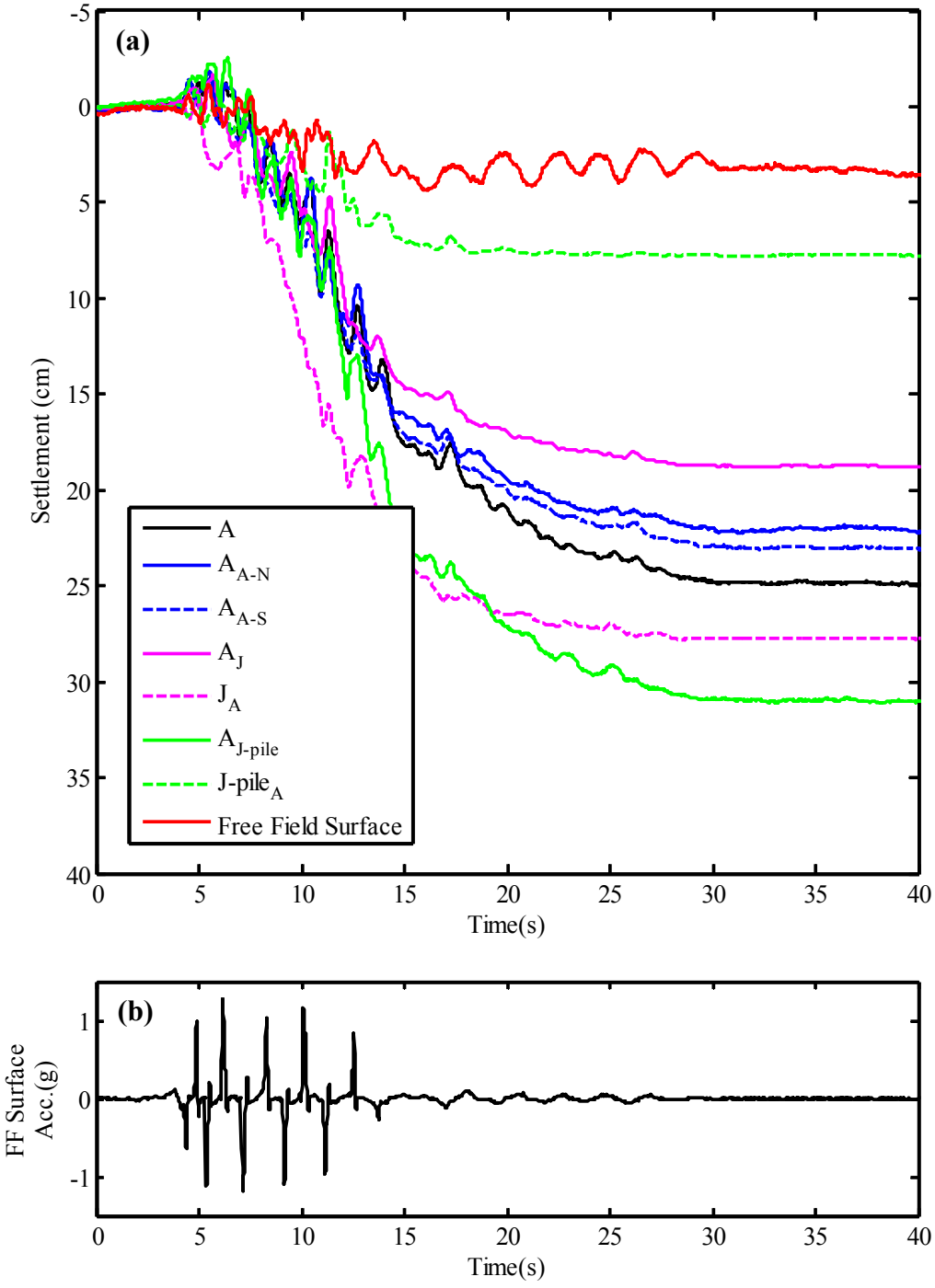

Figure 3.3.28. (a) Settlement-time histories at the centers of the A, $A_{A\text{-}N}$, $A_{A\text{-}S}$, A_J, and J_A buildings. Average settlement of the $A_{J\text{-}pile}$ building, and the settlement of the southwest corner of the J-pile building. Free-field surface settlements are shown for reference. (b) Free-field surface acceleration-time history.

Permanent settlements, measured at each LP location following the PRI_large motion, are presented in Fig. 3.3.29. This figure also includes calculated settlements at building corners where there were no LPs, when possible (based on available data). Measured building settlements are indicated in black, calculated building settlements are indicated in blue, measured horizontal displacements are indicated in red (positive towards the south), and measured soil settlements are indicated in green. Several observations, in addition to those made above, can be made with reference to Fig. 3.3.29: (1) the soil settlement measured adjacent to building A in the northwest quadrant of the container was larger than the soil settlement measured in the free-field and less than the adjacent building settlement; (2) $A_{A\text{-}N}$ and $A_{A\text{-}S}$ displaced horizontally away from each other and settled such that they are tilted away from each other. $A_{A\text{-}N}$ also tilted to the west and $A_{A\text{-}S}$ tilted a small amount to the east; (3) A_J moved horizontally away from J_A and settled such that it was tilted away from J_A. J_A did not move much horizontally and settled such that it was tilted toward A_J. Both J_A and A_J tilted slightly to the west with J_A tilting relatively more in this direction than A_J; and (4) $A_{J\text{-pile}}$ moved horizontally away from J-pile$_A$ and settled such that it was tilted away from J-pile$_A$.

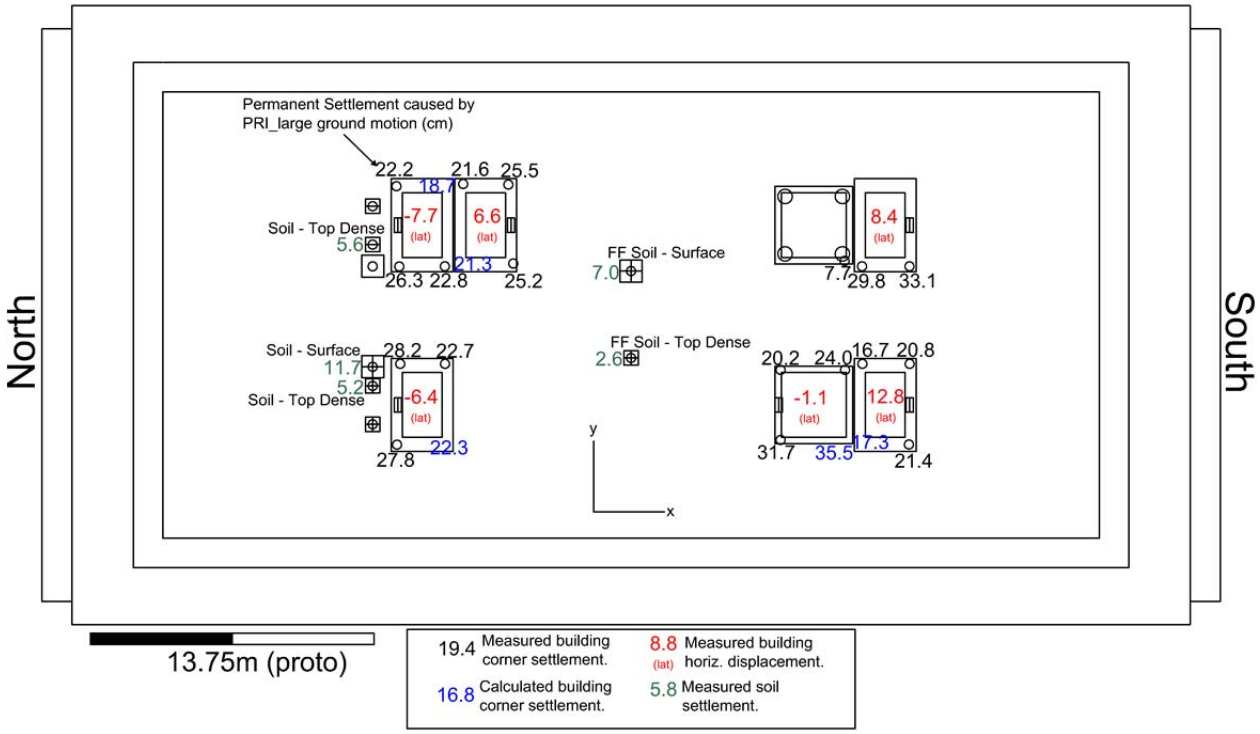

Figure 3.3.29. Permanent settlements following the PRI_large motion. Black numbers represent settlement at a building corner, blue numbers indicate calculated settlement at a building corner, red numbers indicate horizontal building displacement in the north-south direction (positive toward south), and green numbers indicate soil settlements. All settlements are provided in prototype cm.

Excess pore water pressure-time histories beneath the center of the 'A' buildings are presented in Figure 3.3.30. As described previously, the PPT in the center of the liquefiable layer beneath the isolated 'A' building did not function properly. Therefore, the excess pore water pressure-time history for the PPT at the top of the liquefiable layer is presented for this building

(Fig. 3.3.30a). The remaining plots in this figure correspond to the center of the liquefiable layer. The excess pore water pressure corresponding to $r_u \approx 1.0$ has been indicated for each of the PPTs beneath buildings. From these plots it is clear that excess pore water pressures beneath the buildings increased rapidly at the onset of strong shaking and reached their peak values around t = 15 s at the top of the liquefiable layer beneath Building A and the center of the liquefiable layer beneath Building A_J, and around t = 25 – 30 s at the center of the liquefiable layer beneath buildings $A_{A\text{-}N}$ and $A_{J\text{-}pile}$. In contrast to the PRI_mod event when excess pore water pressures beneath buildings $A_{A\text{-}N}$ and $A_{J\text{-}pile}$ exceeded free-field excess pore water pressures at the same depth for a significant amount of time and the excess pore water pressure beneath buildings A and A_J exceeded corresponding free-field excess pore water pressures only several times during strong shaking, it is clear that during the PRI_large event excess pore water pressures beneath all 'A' buildings exceeded the excess pore water pressure at the same depth in the free-field for a significant amount of time. Consequently, pore water would have flowed from beneath the center of the buildings towards the free-field at these locations during these time periods. Again, it is observed that the excess pore water pressures beneath the buildings dissipate at a faster rate than the corresponding excess pore water pressures in the free-field. However, the excess pore water pressures beneath buildings $A_{A\text{-}N}$ and $A_{J\text{-}pile}$ remain greater than the free-field longer than what was observed during the PRI_mod event and the direction of flow is not reversed under these buildings until t = 30 – 35 s (as opposed to t ≈ 20 s during the PRI_mod event). The direction of flow beneath Building A_J likely transitioned around t = 25 – 30 s. The plot shown in Figure 3.3.31 compares the excess pore water pressure-time histories at the center of the liquefiable layer beneath buildings $A_{A\text{-}N}$, A_J, $A_{J\text{-}pile}$, and the free-field. While the maximum excess pore water pressures for these 'A' buildings are approximately equal, it is clear that the excess pore water pressures are sustained at a higher level for a longer duration under buildings $A_{J\text{-}pile}$ and $A_{A\text{-}N}$ than Building A_J. This is suggestive of higher transient hydraulic gradients in the vicinity of Building A_J and might partially explain the relatively larger settlements observed at buildings $A_{J\text{-}pile}$ and $A_{A\text{-}N}$. Please note that the plots provided in Figures 3.3.30 and 3.3.31 were smoothed for clarity by averaging the data over a range consisting of the nearest 100 data points. This corresponds to average data points from samples collected over a 1.3 second interval (prototype).

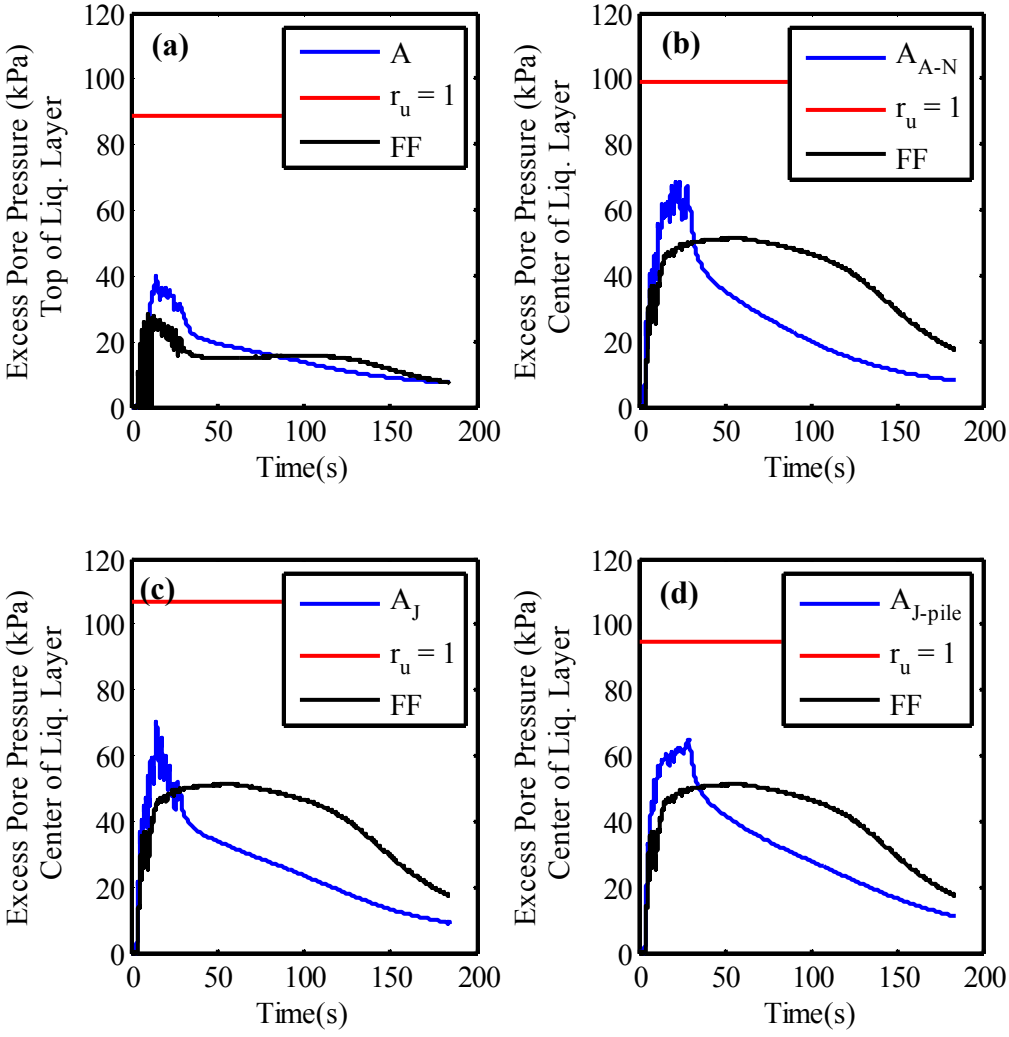

Figure 3.3.30. Excess pore water pressure-time histories at (a) the top of the liquefiable layer beneath the center of A, (b) the center of the liquefiable layer beneath the center of A_{A-N}, (c) the center of the liquefiable layer beneath A_J, and (d) the center of the liquefiable layer beneath A_{J-pile}. Corresponding $r_u \approx 1.0$ lines are indicated, along with the free-field excess pore water pressure-time history at the same elevation (i.e., top or center of liquefiable layer) for reference.

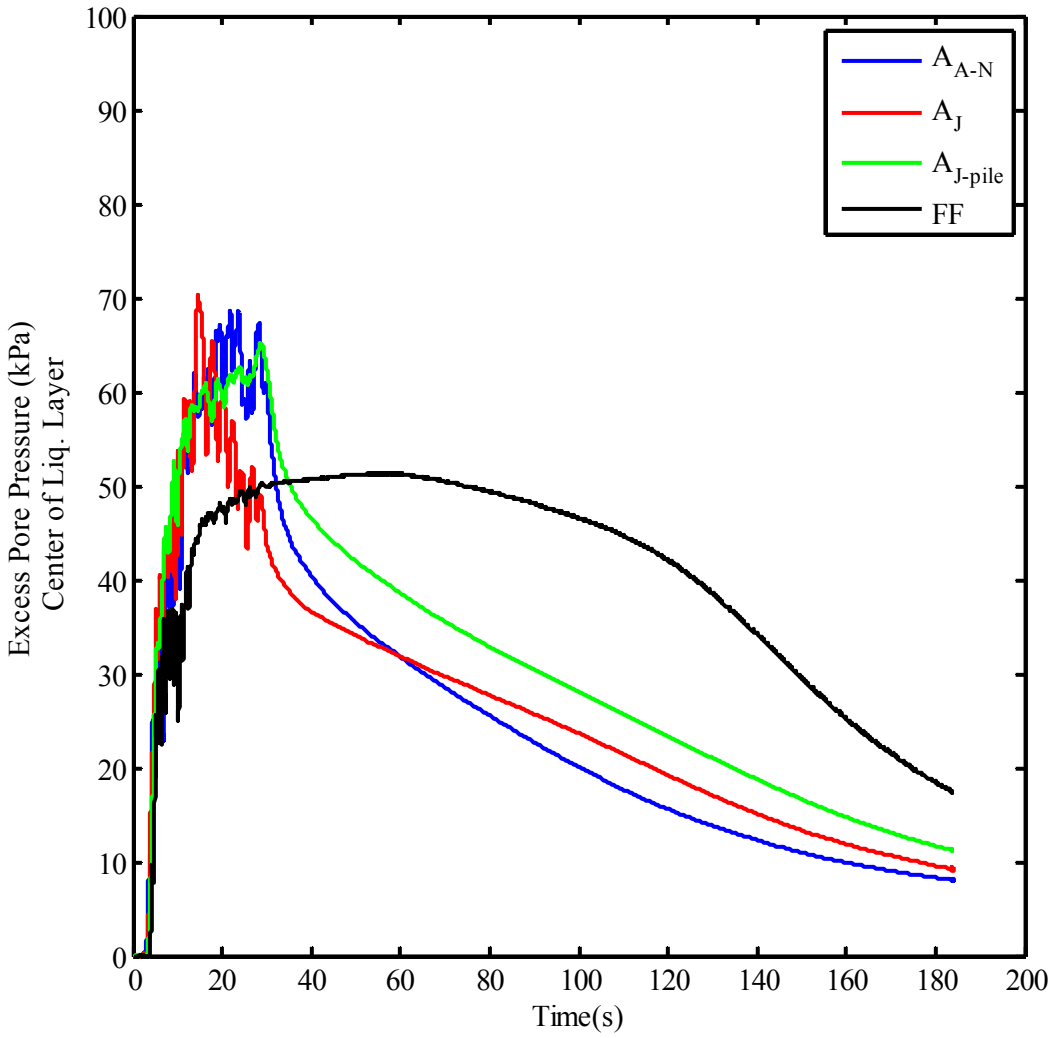

Figure 3.3.31. Excess pore water pressure-time histories at the center of the liquefiable layer beneath the center of $A_{A\text{-}N}$, the center of A_J, the center of $A_{J\text{-}pile}$, and the free-field.

Foundation-level and lumped mass-level acceleration-time histories are presented in Figures 3.3.32 and 3.3.33, respectively. The top three plots of each figure compare the acceleration-time histories for the 'A' buildings with neighbors to the acceleration-time history of the isolated 'A' building. At both foundation-level and lumped mass-level, the acceleration-time histories recorded at buildings A, $A_{A\text{-}N}$, and $A_{J\text{-}pile}$ appear to be very similar, with only minor differences. However, both foundation-level and lumped mass-level recordings at building A appear to envelope the traces recorded at building A_J (i.e., the peaks are slightly higher at building A).

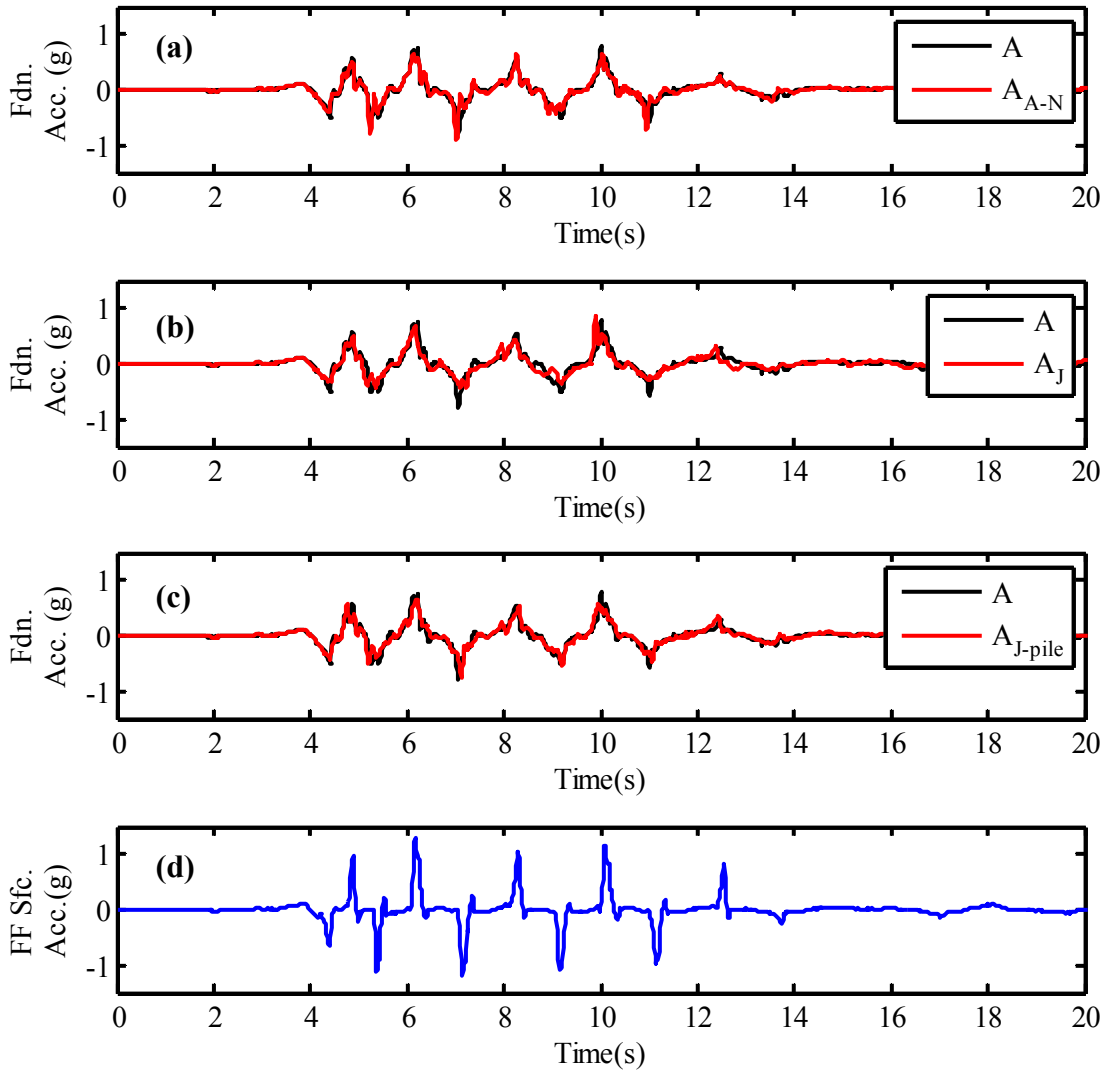

Figure 3.3.32. Foundation-level acceleration-time histories at (a) $A_{A\text{-}N}$, (b) A_J, and (c) $A_{J\text{-}pile}$. The foundation level acceleration-time history of A is shown on each plot for the purposes of comparison. (d) Free-field surface acceleration-time history.

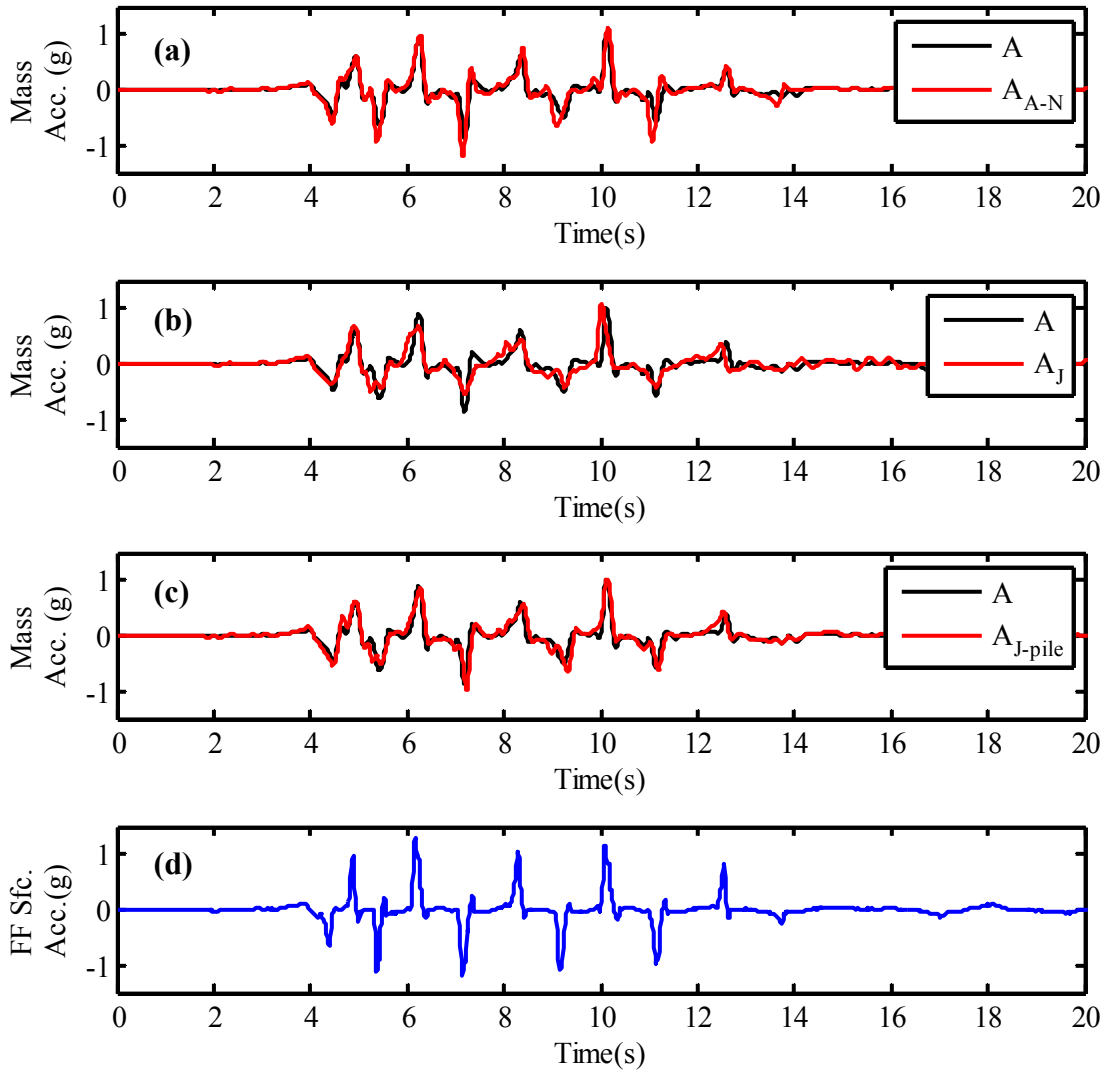

Figure 3.3.33. Lumped mass-level acceleration-time histories at (a) $A_{A\text{-}N}$, (b) A_J, and (c) $A_{J\text{-}pile}$. The lumped mass-level acceleration-time history of A is shown on each plot for the purposes of comparison. (d) Free-field surface acceleration-time history.

Pseudo-acceleration response spectra (5 % damped) at the foundation and lumped mass levels were calculated and plotted for A, $A_{A\text{-}N}$, A_J, and $A_{J\text{-}pile}$. These plots are presented in Fig. 3.3.34. In addition, spectral ratio plots (i.e., $S_{a,\ lumped\ mass}$ / $S_{a,\ foundation}$) for the 'A' buildings are shown in Fig. 3.3.35. The 'A' buildings show distinct peaks around T = 1.1 – 1.2 s and T = 1.7 – 1.85 s at both the foundation and lumped mass levels. In addition, peaks around the fundamental periods of the buildings (i.e., $T_n \approx 0.3$ s) are present in the lumped mass level spectra for A, $A_{A\text{-}N}$, $A_{J\text{-}pile}$, and, to a lesser extent, A_J. Additional peaks at the lumped mass level are also clearly present around T = 0.6 – 0.7 s, and this peak is most prominent at $A_{A\text{-}N}$. The peaks in the spectral

ratio plots generally occur around T = 0.3 – 0.4 s with maximum ratios of approximately 2.45, 2.3, 1.9, and 1.7 for $A_{J\text{-pile}}$, $A_{A\text{-}N}$, A, and A_J, respectively.

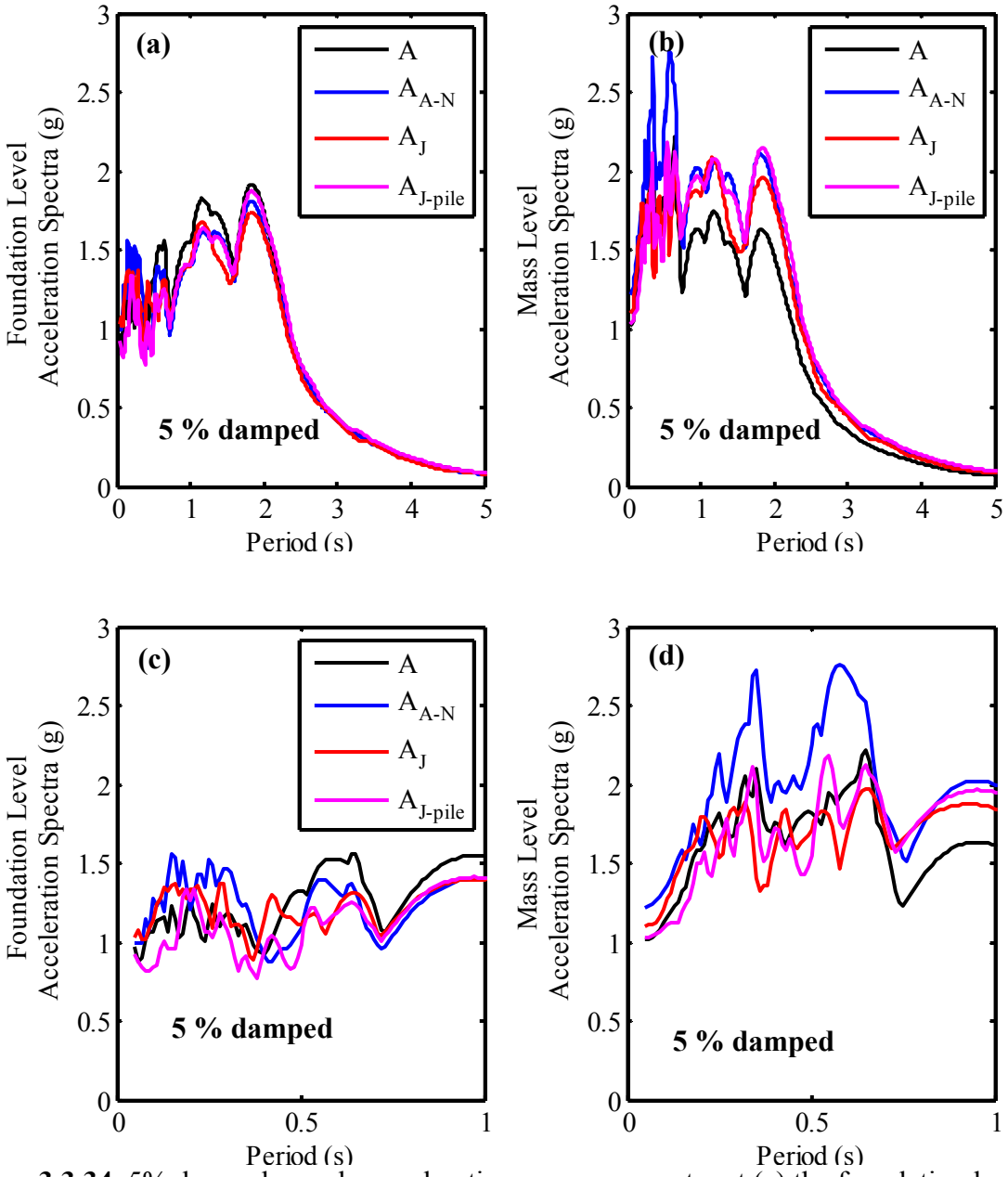

Figure 3.3.34. 5% damped pseudo-acceleration response spectra at (a) the foundation level and (b) the lumped mass level for A, $A_{A\text{-}N}$, A_J, and $A_{J\text{-pile}}$. Identical plot as (a) and (b), zoomed-in between T = 0 and T = 1 s, are presented in (c) and (d).

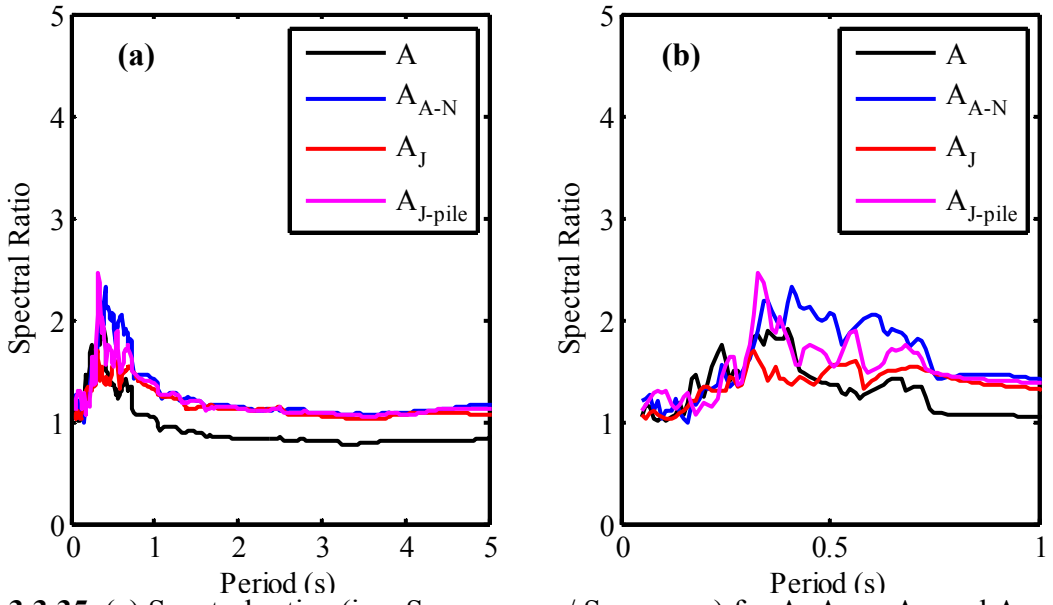

Figure 3.3.35. (a) Spectral ratios (i.e., $S_{a,\ lumped\ mass}$ / $S_{a,\ foundation}$) for A, $A_{A\text{-}N}$, A_J, and $A_{J\text{-}pile}$. (b) Identical plot as (a) zoomed-in between T = 0 and T = 1 s.

3.4 Discussion of Key Observations

The physical model designed and constructed as part of Test-5 was subjected to 11 shaking events. Six of the shaking events were step waves and five events were simulated earthquake motions. Two of the five simulated earthquake motions were low-intensity implementations of the PRI ground motion (i.e., PRI_small), during which negligible excess pore water pressures were generated in the loose to medium-dense Nevada Sand layer. The remaining three simulated earthquake motions (i.e., PRI_mod, TCU_mod, and PRI_large) led to significant excess pore water pressures in the loose to medium-dense Nevada Sand, and liquefaction (i.e., $r_u \approx 1.0$) was achieved in the loose to medium-dense Nevada Sand in the free-field area during these events. Significant free-field soil and building settlements were observed. The results from these three events were presented in detail in Section 3.3. Key aspects of the model and key observations of the experimental results are discussed in this section as follows:

- The in-flight CPT, performed prior to the shaking events, confirmed relative densities of the loose to medium-dense layer of Nevada sand and the dense layer of Nevada Sand to be approximately 50% and 90%, respectively.

- The groundwater table was at a depth of approximately 0.5 m during the PRI_mod event and 0.9 m during the TCU_mod and PRI_large events. The bases of the shallow foundations were approximately 0.7 m below the ground surface, and the top of the loose to medium-dense Nevada Sand layer was at a depth of approximately 1.9 m.

- Excess pore water pressure ratios of approximately 1.0 were achieved in the free-field at the center of the loose to medium-dense Nevada Sand layer during the PRI_mod, TCU_mod, and PRI_large events. Excess pore water pressures were negligible during the PRI_small and step wave events.

- Given that the simulated earthquake motions were applied in sequence, the loose to medium-dense Nevada Sand layer was denser prior to the application of the TCU_mod motion than it was prior to the PRI_mod motion. Similarly, the layer was denser prior to the PRI_large motion than it was prior to the TCU_mod motion. Using the measured settlements of the liquefiable layer in the free-field and the theory of 1-D compression, the relative density of the free-field liquefiable layer of Nevada Sand was approximately 55% prior to the application of TCU_mod and just over 60% prior to the application of PRI_large. Qualitative evidence of the increase in relative density is provided through a comparison of figures 3.3.5b and 3.3.27b. Despite the increase in ground motion intensity during PRI_large, there appears to be a slightly higher resistance to excess pore water pressure generation due to the relatively more dilative behavior during this event.

- Free-field settlements initiated during strong shaking at about the same time significant excess pore water pressures were generated. This is suggestive of partial drainage occurring during shaking. Free-field settlements occurred at slightly higher rates during shaking than after shaking was completed, and this was most evident during the PRI_large event (Fig. 3.3.26). Free-field settlements for all events continued well after the completion of shaking as excess pore water pressures dissipated.

- The ground adjacent to the model structures settled more than the ground in the free-field and the shallow-founded structures settled more than the adjacent ground settled.

- While excess pore water pressure ratios in the free-field reached 1.0, maximum excess pore water pressure ratios beneath the buildings were typically on the order of 0.4 – 0.8 during the three significant shaking events.

- Nearly all of the shallow-founded building settlements occurred during and just after strong shaking and these building settlements were significantly greater than the free-field ground settlements. Both of these observations are consistent with the presence of the shear-induced building settlement mechanisms of SSI-induced ratcheting (i.e., $\varepsilon_{q\text{-}SSI}$) and partial bearing capacity failure (i.e., $\varepsilon_{q\text{-}BC}$) as described by Dashti et al. (2010a).

- Significant transient hydraulic gradients were present during strong shaking that caused pore water to flow from beneath the center of the buildings towards the free-field at some locations and from the free-field towards the buildings at other locations at other times. For example, Figure 3.3.8 illustrated that the excess pore water pressures in the center of the liquefiable layer beneath buildings $A_{A\text{-}N}$ and $A_{J\text{-}pile}$ were greater than the free-field excess pore water pressures at approximately the same depth for a period of time during and just after shaking. However, the excess pore water pressures beneath the buildings did dissipate faster than the free-field pore water pressures so the direction of flow reversed for these cases.

- Figures 3.3.9 and 3.3.20 illustrated that the maximum excess pore water pressure beneath Building A_J was just over 60% of the maximum excess pore water pressure beneath Building $A_{A\text{-}N}$ at the same elevation during PRI_mod and approximately 70% during TCU_mod, respectively. This would appear to partially explain the differences in settlement between these two buildings during these events (i.e., 12 cm and 10 cm for A_J vs. 20 cm and 14 cm for $A_{A\text{-}N}$, respectively; Table 3.4.1). As described previously, elasticity calculations suggest that the vertical effective stress at the center of the liquefiable layer beneath Building A_J was approximately 10% higher than the corresponding vertical effective stress beneath Building $A_{A\text{-}N}$. In addition, the foundation-level acceleration intensities were slightly lower for Building A_J than Building $A_{A\text{-}N}$ (Fig. 3.3.10) during PRI_mod. While there could be additional factors involved, including the influence of the dynamic response of Building J_A, these two factors would have reduced the cyclic stress ratio beneath A_J relative to $A_{A\text{-}N}$, and this could partially explain the observation of lower excess pore water pressures beneath A_J during these events. On the other hand, the maximum excess pore water pressures beneath these buildings were about the same during PRI_large, as illustrated in Fig. 3.3.31, and Building $A_{A\text{-}N}$ settled approximately 4 cm more than Building A_J during this event. This suggests that the differences in building settlement cannot be completely explained by the differences in maximum excess pore water pressure and other factors, such as additional kinematic restraint caused by the presence and settlement of the larger adjacent J_A building, were likely important.

- Permanent building settlements for each building following PRI_mod, TCU_mod, and PRI_large are presented in Table 3.4.1. In general, buildings A, $A_{A\text{-}N}$, and $A_{A\text{-}S}$ settled approximately the same amount during each significant shaking event. Consequently, placing an 'A' building next to another 'A' building did not significantly impact the building settlement of either building during Test-5. The $A_{J\text{-}pile}$ building settled slightly less than these three 'A' buildings during PRI_mod, but slightly more than the other 'A' buildings during the other two motions. The additional vibration induced by strong shaking of the adjacent piles may have produced additional settlement of Building $A_{J\text{-}pile}$. The A_J building generally settled the least, but then the J_A building also settled less than the shorter, lighter A buildings during this experiment. It is not entirely clear why the heavier J_A building settled less than the lighter A, $A_{A\text{-}N}$, and $A_{A\text{-}S}$ buildings in some of the shaking events. However, it follows that if J_A settled less than these A buildings then the adjacent A_J building also settled less than these other 'A' buildings. A potential explanation for why the J_A building settled less than the A buildings for some of the shaking events is discussed in the next bullet.

Table 3.4.1. Permanent center-of-foundation or average building settlements. Center-of-foundation settlements are provided for A, $A_{A\text{-}N}$, $A_{A\text{-}S}$, A_J, and J_A. The average building settlement of $A_{J\text{-}pile}$, and the settlement of J-$pile_A$ at the southwest corner are presented.

Building ID	Building Settlement (cm)		
	PRI_mod	TCU_mod	PRI_large
A	20	17	25
$A_{A\text{-}N}$	20	14	23
$A_{A\text{-}S}$	21	15	23
A_J	12	10	19
$A_{J\text{-}pile}$	17	18	32
J_A	14	7	28
J-$pile_A$	3	0	8

- SSI numerical analyses of buildings with shallow foundations atop shallow liquefiable soils have shown that, while cyclic shear stresses increase beneath buildings due to the building's dynamic response, the CSR (i.e., τ/σ'_v) beneath the building can be decreased due to higher confining stresses (Travasarou et al., 2006). Consequently, the CSR demand on the building's foundation soils is directly related to the building's dynamic response, as well as the weight of the building. During Test-5, the J_A building settled slightly more than the A_J building during PRI_mod, slightly less than the A_J building during TCU_mod, and significantly more than the A_J building (and more than the other A buildings except for $A_{J\text{-}pile}$) during the PRI_large event. These observations provide further evidence that ground motion and the SSI response of the building are important considerations. One possible explanation for these observations is that the beneficial effect of the higher confining stress beneath Building J_A outweighed the increased cyclic shear stresses during the TCU_mod event, but was overcome by increased cyclic shear stresses during the more intense shaking of the PRI_large event. These observations also indicate that it would be erroneous to always expect a heavier shallow-founded structure to settle more than a lighter shallow-founded structure when subjected to shallow liquefaction.

- To put Test-5 in context, it is helpful to compare the observed free-field and isolated 'A' building settlements to the settlements reported by Dashti (2009). These settlements are summarized in Tables 3.4.2 and 3.4.3. The description for each test (i.e., T4.5 – 50) corresponds to the thickness and relative density of the liquefiable layer for that test. For example, T4.5 – 50 corresponds to a prototype thickness of 4.5 m for the liquefiable layer at an initial relative density of approximately 50%. Comparisons are discussed in the next two bullets.

Table 3.4.2. Comparison of free-field settlements during Test-5, SHD01, SHD02, SHD03 and SHD 04. Details regarding the SHD testing series are provided by Dashti (2009). The description for each test (i.e., T4.5 – 50) corresponds to the thickness and relative density of the liquefiable layer for that test. PRI_large was applied successively during SHD04 because the achieved motions were lower than anticipated during the initial attempt. Therefore, two settlements are reported for this event with the first settlement corresponding to an input motion with a peak base acceleration of 0.38 g and the second corresponding to a peak base acceleration of 0.66 g.

Test ID	**Free-Field Settlement (cm)**		
	PRI_mod	**TCU_mod**	**PRI_large**
Test-5 (T4.5-50)	6	5	7
SHD01 (T6-30)	-*	-	24
SHD02 (T3-30)	18	-	29
SHD03 (T3-50-SILT)	8	-	17
SHD04 (T3-50)	11	8	15, 14

*The soil for this event was likely overconsolidated (Dashti 2009).

Table 3.4.3. Comparison of permanent settlements for the isolated 'A' building during Test-5, SHD01, SHD02, SHD03 and SHD 04. Details regarding the SHD testing series are provided by Dashti (2009). The description for each test (i.e., T4.5 – 50) corresponds to the thickness and relative density of the liquefiable layer for that test. PRI_large was applied successively during SHD04 because the achieved motions were lower than anticipated during the initial attempt. Therefore, two settlements are reported for this event with the first settlement corresponding to an input motion with a peak base acceleration of 0.38 g and the second corresponding to a peak base acceleration of 0.66 g.

Test ID	**Isolated 'A' Building Settlement (cm)**		
	PRI_mod	**TCU_mod**	**PRI_large**
Test-5 (T4.5-50)	20	17	25
SHD01 (T6-30)	-*	-	59
SHD02 (T3-30)	28	-	50
SHD03 (T3-50-SILT)	12	-	42
SHD04 (T3-50)	11	3	20, 17

*The soil for this event was likely overconsolidated (Dashti 2009).

- Examining Table 3.4.2, the observed free-field settlements during Test-5 (i.e., T4.5-50) were lower than would have been anticipated relative to SHD03 (T3-50-SILT) and SHD04 (T3-50). Because free-field settlements should be governed by volumetric strains, one would expect T4.5–50 to have slightly larger free-field settlements than T3–50 because the liquefiable layer is thicker in T4.5-50. However, free-field settlements measured during T4.5-50 were lower than the corresponding settlements during T3-50-SILT and T3-50. Part of this difference can likely be attributed to curving the surface of the soil in attempt to match the radial g-field during T4.5-50. By curving the surface of the soil before spinning, the soil surface responds as if it is level when spinning in the radial g-field produced in the centrifuge. This was not done for Tests SHD01 – SHD04, so when these models were spun up, the level soil surfaces in these tests responded as if they were curved with high ground along the longitudinal (N-S) centerline of the container. Using a constant volume assumption, it can be shown that approximately 17 cm (prototype) of total settlement along the longitudinal centerline of the model container should occur as the shape of the soil surface transitions from curved to flat under the radial g-field. While it is unclear how quickly this process occurs (i.e., all at once or distributed over several simulated earthquake events), it is clear that not curving the soil surface for centrifuge experiments involving liquefaction will lead to a systematic bias towards higher observed settlements at the center of the model container and lower observed settlements near the eastern and western edges. The reported free-field settlement for SHD04, above, was measured along the longitudinal centerline. Consequently, it is not surprising that the measured free-field settlements are slightly high relative to the measured settlements observed during T4.5-50.

- Examining Table 3.4.3, the isolated 'A' building during T4.5-50 settled significantly more than the isolated 'A' buildings during T3-50-SILT and T3-50 for the PRI_mod motion, significantly more than T3-50 for the TCU_mod motion, and slightly more than the measured settlements during T3-50 for the PRI_large motion. If T4.5-50, T3-50-SILT, and T3-50 had loose to medium-dense Nevada Sand layers that were pluviated exactly the same way to identical initial relative densities, and the input ground motions were exactly the same, one would expect the settlements for these three tests to be nearly the same. This was not the case and that suggests that there are differences between these tests that should be accounted for. For example, while the same pluviation techniques were employed during model construction for all three tests, and the same command motions were applied, the achieved peak acceleration for the PRI_mod event at the base of the model container during T4.5-50 was 0.23 g versus 0.17 g and 0.15 g for T3-50-SILT and T3-50, respectively. Consequently, the Test-5 (i.e., T4.5-50) model was subjected to more intense shaking for the PRI_mod event than T3-50-SILT and T3-50 and this could partially explain the larger settlements observed during this test for that event. However, as previously discussed, the soil surface was not curved during T3-50-SILT and T3-50, but it was curved during T4.5-50. Not curving the soil surface should have caused higher settlements of the buildings that were along the longitudinal centerline of the model during T3-50-SILT and T3-50, so this would have likely partially counteracted the more intense achieved motion during T4.5-50. As also discussed previously, the motion sequence for T3-50-SILT did not include the TCU_mod motion. Therefore, one would expect less densification to have occurred during T3-50-SILT than for T4.5-50 and T3-50 prior to the PRI_large event, with all else being equal. This could potentially explain the higher settlement observed during T3-50-SILT, relative to T4.5-50 and T3-50. All things considered, the building settlements measured during Test-5 appear to be reasonable when compared to existing data.

- The $A_{A\text{-}N}$ and $A_{A\text{-}S}$ buildings displaced laterally away from each other during PRI_mod, TCU_mod, and PRI_large in the amounts of 9 cm, 5 cm, and 14 cm, respectively. While the buildings tilted toward each other a small amount during PRI_mod, they tilted away from each other during TCU_mod and PRI_large.

- The separation distance between buildings A_J and J_A increased by approximately 17 cm, 4 cm, and 14 cm during the PRI_mod, TCU_mod, and PRI_large events, respectively. During the PRI_mod event the buildings displaced about the same amount and during the subsequent two events, A_J accounted for nearly all of the lateral displacement.

- The A_J building tilted away from the J_A building during each event. The J_A building tilted towards Building A_J during PRI_mod and PRI_large, but slightly away from Building A_J during TCU_mod.

- The $A_{J\text{-}pile}$ building displaced laterally away from Building J-pile$_A$ during each event (9 cm, 5 cm, and 8 cm during PRI_mod, TCU_mod, and PRI_large, respectively). The Building $A_{J\text{-}pile}$ also settled such that it was tilted away from the J-pile$_A$ building during each event.

- These general trends appear to suggest that the physical presence of the adjacent building, particularly when it was of equal or greater size, kinematically constrained ground movements under the structures on the sides nearest the adjacent buildings relative to the ground movements that occurred under the sides away from the adjacent building. This caused relatively more settlement on the sides away from the adjacent buildings and, therefore, a corresponding tendency for the buildings to tilt away from each other. The photograph shown in Figure 3.4.2, taken just prior to model excavation, illustrates the tendency for the smaller 'A' buildings to tilt away from their larger neighbors. The $A_{J\text{-pile}}$ – J-pile$_A$ building pair is shown in the foreground with the A_J – J_A building pair in the background.

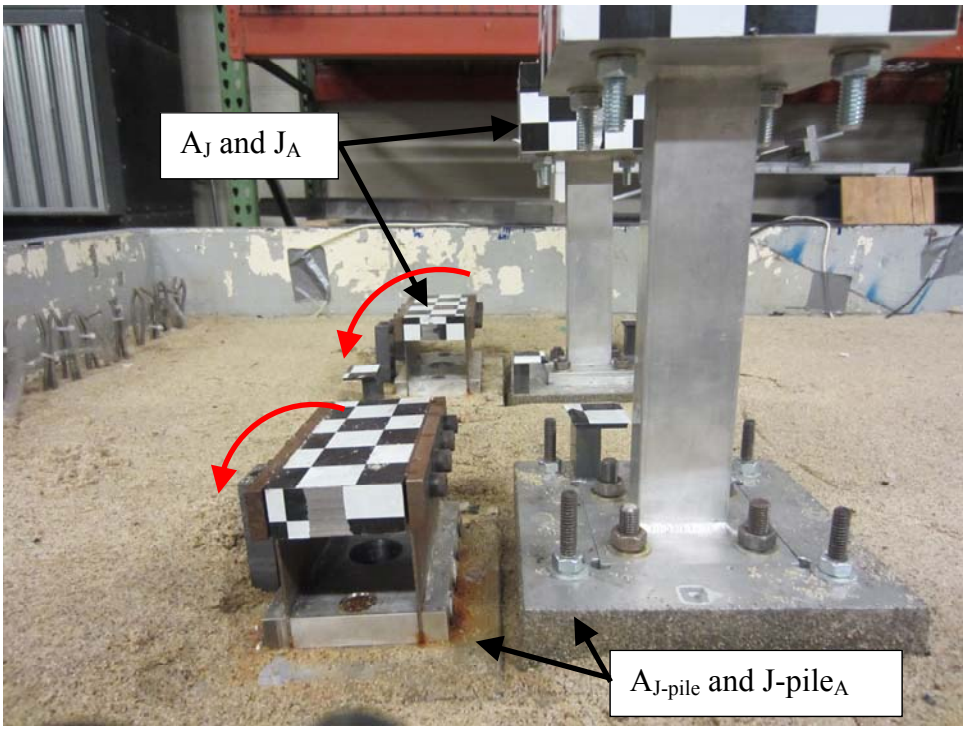

Figure 3.4.2. Photograph of the A_J – J_A and $A_{J\text{-pile}}$ – J-pile$_A$ building pairs just prior to model excavation. Tilt direction of the 'A' buildings is indicated in red.

- Ground being pushed to the side as adjacent buildings settle could also potentially explain the tendency for buildings to move horizontally away from one another during these events. That is, as the adjacent buildings settle, lateral ground displacements under the side of the building closest to the adjacent building would be opposed by ground displacements from under the adjacent building and the buildings would effectively push one another away.

- In addition, the confining stresses under the sides of closely-spaced adjacent buildings are lower under the side away from the neighboring building than the side closest to the neighboring building. Consequently, with all other things equal, one would expect a lower liquefaction resistance in the foundation soils on the sides away from the adjacent building and, therefore, relatively more cyclic softening to occur on that side during

shaking. As horizontal inertial forces are transferred from the superstructure to the foundation soils during shaking, this additional cyclic softening on the side away from the adjacent buildings would lead to a tendency for the buildings to incrementally move apart laterally.

- Building J-pile$_A$ settled significantly less than the J$_A$ building, as expected, during all events. It settled less than the free-field surface during PRI_mod and TCU_mod and about the same as the free-field ground surface during PRI_large. However, while the free-field ground settlement was caused by the volumetric settlement mechanisms described by Dashti et al. (2010a), the settlement of Building J-pile$_A$ was likely caused by: 1) cyclic softening of the dense Nevada Sand layer due to excess pore water pressure generation; and 2) loss of side friction due to excess pore water pressure generation and subsequent cyclic softening of the medium dense Nevada Sand. As described in Section 3.2, the piles were driven into the soil during model construction when the surrounding ground was approximately 50 mm (model scale) above the design pile toe depth. Sand was then dry pluviated around the piles for the remainder of the model construction. Consequently, a portion of the structural load was likely transferred from the pile cap to the piles and the resistance was transferred from side friction along the piles to end bearing due to cyclic softening and corresponding reduction of side friction within the loose to medium dense Nevada Sand during the simulated earthquake events. Excess pore water pressures within the dense Nevada Sand would have also reduced the side friction in this layer. This load transfer mechanism would have required a compatible amount of settlement to develop the required additional end bearing resistance. Excess pore water pressures in the free-field within the dense Nevada Sand layer at a depth of 10.2 m are provided in Table 3.4.4. It is clear that significant excess pore water pressures were generated in the dense Nevada Sand layer during each of the three events under consideration, and particularly during the PRI_large event. Therefore, the settlements of the J-pile$_A$ building during this test are not surprising.

Table 3.4.4. Maximum free-field excess pore water pressures, $\Delta u_{,max}$ (kPa), in the dense Nevada Sand layer at a depth of approximately 10.2 m below the ground surface during PRI_mod, TCU_mod, and PRI_large. Corresponding r_u values and the settlements of the J-pile$_A$ building are provided for reference.

Event ID	$\Delta u_{,max}$ (kPa)	r_u	Settlement of J-pile$_A$ (cm)
PRI_mod	58	0.53	3
TCU_mod	52	0.46	0
PRI_large	91	0.82	8

- Foundation-level and lumped mass-level acceleration-time histories differed for buildings A and A$_J$ during PRI_mod, TCU_mod, and PRI_large. After the first cycle of motion the acceleration amplitudes were typically slightly lower for the A$_J$ building than the A building. Though the details varied with each ground motion, the lumped mass-level

acceleration-time histories were also clearly different with some of the larger peaks missing and some of the smaller peaks amplified at the A_J building. The foundation-level acceleration-time histories were more similar for the A and $A_{A\text{-}N}$ buildings, and only minor differences were typically observed in the lumped mass-level acceleration-time histories. This suggests that the large J_A building influenced the shaking characteristics of the A_J building more significantly than $A_{A\text{-}S}$ influenced the shaking characteristics of $A_{A\text{-}N}$. This is in line with intuition and likely due to vibrations of the J_A building interacting with the shared foundation soils of the A_J building through SSSI, in addition to the kinematic restraint caused by the presence and settlement of the J_A building. While the impact of this on the liquefaction-induced settlement mechanisms is complex and not always clear, the generally lower foundation-level accelerations observed at Building A_J would likely reduce the impact of the SSI-induced ratcheting mechanism (i.e., $\varepsilon_{q\text{-}SSI}$), and this could be one of the reasons Building A_J typically settled less than the other 'A' buildings.

- Foundation-level spectral accelerations for the A_J building are typically the lowest or among the lowest of all the 'A' buildings at periods greater than $T \approx 1$ s during each of the three events under consideration (e.g., Figs. 3.3.12, 3.3.23, and 3.3.34), though the spectral values for all 'A' buildings were generally more similar during the PRI_large event. The $T > 1$ s foundation-level spectral accelerations at the A and $A_{A\text{-}N}$ buildings were generally similar during all events. This is consistent with the observations and previous discussion regarding the foundation-level acceleration-time histories and suggests that the large J_A building influenced the shaking characteristics of the A_J building more significantly than Building $A_{A\text{-}S}$ influenced the shaking characteristics of Building $A_{A\text{-}N}$. More specifically, the influence of the J_A building appears to have suppressed the $T > 1$ s spectral acceleration amplitudes relative to the other 'A' buildings. Again, while the impact of this on the liquefaction-induced settlement mechanisms was likely complex, one might expect the lower $T > 1$ s foundation level spectral amplitudes to reduce settlements of the A_J building due to $\varepsilon_{q\text{-}SSI}$, relative to the other 'A' buildings.

- Foundation-level spectral accelerations at $T < 1$ s were also generally similar for the A and $A_{A\text{-}N}$ buildings during all events, and all buildings had generally similar foundation-level spectral accelerations during the PRI_large event. However, during TCU_mod, foundation-level spectral accelerations at $T < 1$ s were generally higher for the A_J and $A_{J\text{-}pile}$ buildings. Pronounced peaks of 0.7 g and 0.5 g at $T \approx 0.65$ s were observed for the A_J and $A_{J\text{-}pile}$ buildings, respectively, during this event. Despite these relatively higher $T < 1$ s spectral accelerations at A_J and $A_{J\text{-}pile}$ buildings during this event, the A_J building settled approximately 5 – 10 cm less than the other 'A' buildings and the $A_{J\text{-}pile}$ building settled about the same as the A building and slightly more than the $A_{A\text{-}N}$ and $A_{A\text{-}S}$ buildings. With all else being equal, and given that the $T > 1$ s foundation-level spectral accelerations were generally similar for buildings A, $A_{A\text{-}N}$, and $A_{J\text{-}pile}$ during TCU_mod, it appears that the relatively higher $T < 1$ s spectral accelerations could have caused only a minor increase in the $A_{J\text{-}pile}$ building settlement. It also appears that the relatively high $T < 1$ s foundation-level spectral accelerations of the A_J building were offset by the relatively low $T > 1$ s foundation-level accelerations and perhaps other factors during this event.

- Spectral ratios ($S_{a,\ lumped\ mass}$ / $S_{a,\ foundation}$) for the buildings with adjacent buildings were typically higher than the isolated 'A' building at all periods, except at T < 0.2 s during PRI_mod and T < 0.5 s during PRI_large. This would appear to suggest that more shaking energy was typically transmitted through the model structures with adjacent model structures. By comparing results from Test-1 and Test-2 (described previously in Section 3.2), Mason (2011) observed that the presence of a deeply-embedded basement restrained the shallow footings of an adjacent building such that the footings next to the basement displaced and rotated less during strong shaking than the footings on the free side (i.e., away from the basement). This caused higher seismically-induced column moments above the restrained footings, relative to the free footings. Though the structures and structural layout of Test-2 are different than in this test and more extreme in that there were isolated footings up against a deep basement, the observation that more shaking energy was generally transmitted through the buildings with adjacent buildings could be due to similar effects wherein the adjacent buildings provided a kinematic restraint. Although the effect of this on the liquefaction-induced building settlement mechanisms is not entirely clear, it could potentially have an adverse effect on the structural components of the seismic force resisting system. A focused series of experiments with additional instrumentation would likely be required to confirm this hypothesis.

CHAPTER 4: EVALUATION OF THE PERFORMANCE OF SELECT BUILDINGS IN CHRISTCHURCH, NEW ZEALAND DURING THE 2010-2011 CANTERBURY EARTHQUAKES

4.1 Introduction

Background

The significant seismic events of the Canterbury earthquake sequence on the South Island of New Zealand between 4 September 2010 and 23 December 2011 provide a unique opportunity to study the performance of engineered structures during intense earthquake ground shaking. Approximately fifty earthquakes with magnitude greater than or equal to five occurred during this period (GNS Science, 2013). Of the fifty, seven were of moment magnitude (M_w) greater than or equal to 5.5, and three were of M_w greater than or equal to 6.0. The largest of the Canterbury earthquake sequence events, in terms of M_w, was the 4 September 2010 M_w 7.1 earthquake. This event is typically referred to as the Darfield earthquake, given the proximity of the epicenter to the town of Darfield, located in the Canterbury plains roughly 40 km west of the central business district (CBD) of Christchurch. The most damaging event, in terms of loss of life and economic damage, however, was the 22 February 2011 M_w 6.2 earthquake, which is referred to as the Christchurch earthquake. The Christchurch earthquake resulted in the loss of 185 lives and left many others with serious injuries. The majority of the lives lost were due to the collapse of two multi-story office buildings within the CBD: the Canterbury Television building (115 casualties) and the Pyne Gould Corporation building (18 casualties). Forty-two of the remaining 52 casualties were due to the collapse or partial collapse of unreinforced masonry structures within or very close to the CBD (Canterbury Earthquakes Royal Commission, 2011). In addition to the loss of human life, the city of Christchurch was devastated by the earthquake. Nearly half of the buildings inspected within the CBD were marked as restricted access because of potential safety issues. Parts of the CBD were cordoned off for over two years after the Christchurch earthquake. Over 1500 of the 4000 buildings within the CBD have been or are expected to be demolished. Most of the city's high-rise buildings have been demolished.

With a population of approximately 377,000 as of 30 June 2010 and 366,000 as of 30 June 2013 (Christchurch City Council, 2013), Christchurch is now the third largest city, by population, in New Zealand, behind Auckland and Wellington. It is located on the east coast of the South Island of New Zealand near the south end of Pegasus Bay (Figure 4.1.1). The total urban area of Christchurch covers approximately 450 km^2, over which there are approximately 150,000 residential dwellings, most of which are single story wood framed structures (Cubrinovski et al., 2011a). The CBD of Christchurch is on the order of 6 km^2 and is bounded by the four avenues: Bealey Avenue on the north, Deans Avenue on the west, Moorhouse Avenue on the south, and Fitzgerald Avenue on the east (Figure 4.1.2). Building types within the CBD include a mix of multi-story commercial and residential structures, single-story commercial and residential structures, and industrial buildings. There are also many historic masonry buildings from the 19th and early 20th centuries (Cubrinovski et al., 2011a).

The primary focus of this study is documentation of the performance of modern commercial and residential structures in the CBD during the events of the Canterbury earthquake sequence. Particular emphasis is placed on a subsurface characterization effort that primarily employed the cone penetration test (CPT) to characterize the foundation soils at each location and provide data upon which liquefaction triggering, simplified bearing capacity, and post-liquefaction volumetric reconsolidation settlement analyses could be performed.

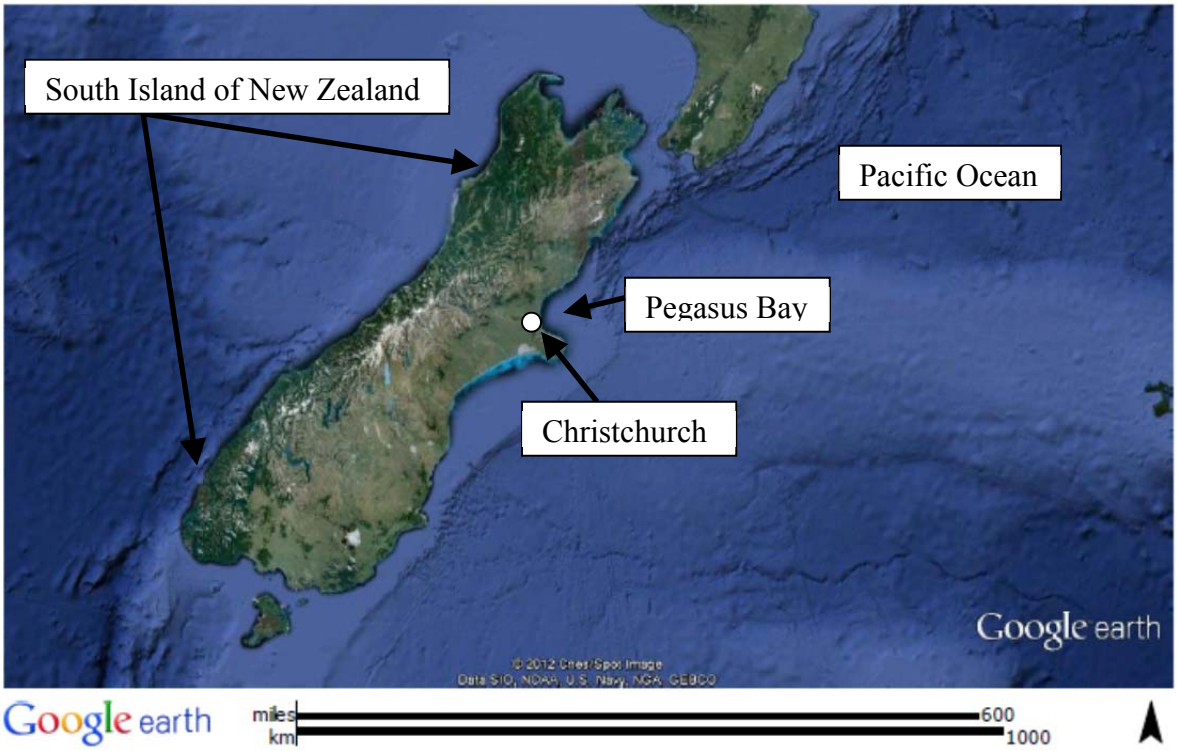

Figure 4.1.1. Christchurch location map.

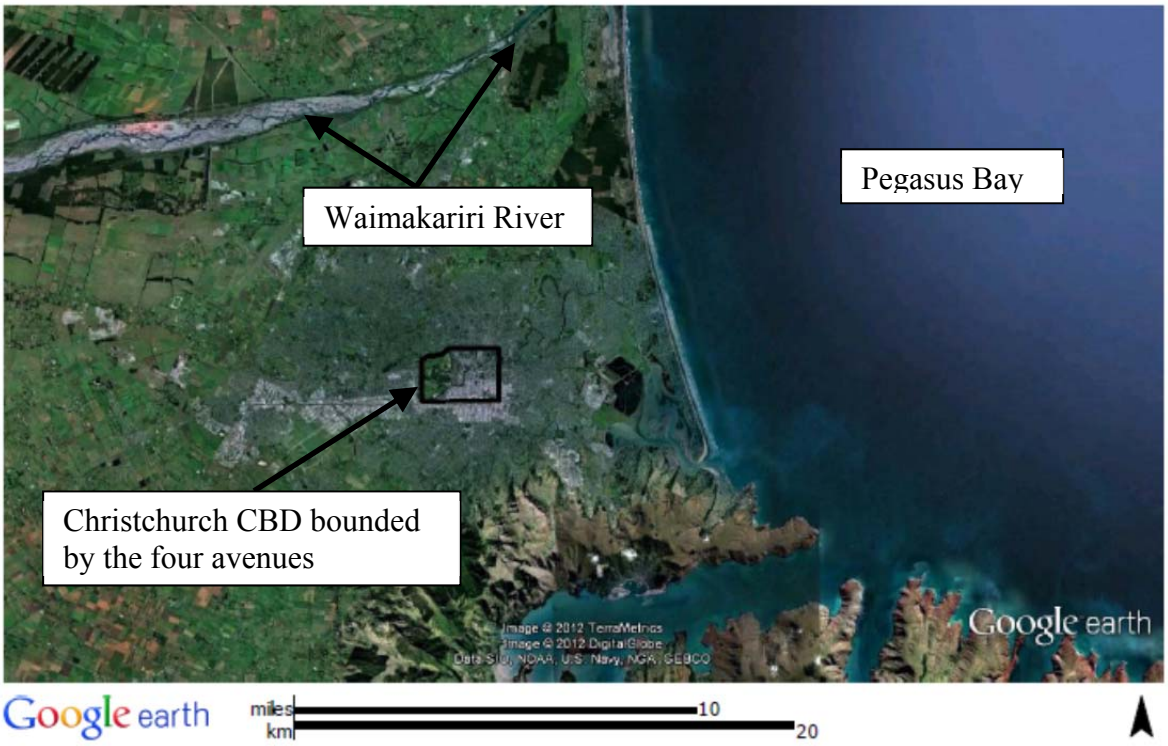

Figure 4.1.2. Christchurch CBD location map.

Please note that Deans Avenue, shown in Figure 4.1.2 as the western boundary of the CBD, is located on the west side of Hagley Park. Some researchers consider Rolleston Avenue, located east of Hagley Park and of a roughly parallel orientation with Deans Avenue, to be the western boundary of the CBD.

Important Seismic Events and the Associated Ground Motions Recorded During the Canterbury Earthquake Sequence

As discussed previously, there were seven earthquake events between 4 September 2010 and 23 December 2011 with M_w greater than or equal to 5.5. These events, along with additional important events on 26 December 2010, 16 April 2011 and 13 June 2011, are summarized in Table 4.1.1.

Table 4.1.1. Select Canterbury earthquake sequence events between 4 September 2010 and 23 December 2011.

Date	NZ Local Time	M_w	Epicentral Latitude	Epicentral Longitude	Hypocentral Depth (km)
4 SEP 10	04:35:46	7.1	-43.5382	172.1635	11.0
26 DEC 10	10:30:15	4.7	-43.5544	172.6615	5.0
22 FEB 11	12:51:42	6.2	-43.5644	172.6915	6.0
22 FEB 11	13:04:19	5.5	-43.5892	172.6605	5.9
22 FEB 11	14:50:29	5.6	-43.5904	172.6336	6.6
16 APR 11	17:49:23	5.0	-43.6134	172.7886	9.0
13 JUN 11	13:01:00	5.3	-43.5684	172.7531	8.9
13 JUN 11	14:20:50	6.0	-43.5638	172.7431	6.9
23 DEC 11	13:58:36	5.8	-43.4862	172.7957	9.6
23 DEC 11	15:18:02	5.9	-43.53	172.7428	6.8

Please note that the moment magnitudes, epicentral coordinates, and hypocentral depths indicated in Table 4.1.1 are based on values reported by GNS through the GeoNet database and values reported in available literature (i.e., Holden, 2011; Beavan et al., 2011; Sibson et al., 2011; and Bannister et al.; 2011). Moment magnitudes reported by the USGS are 0.1 units lower for the 4 SEP 10 event, the 22 FEB 11 event at 12:51:42 local time, and the 13 JUN 11 event at 14:20:50 local time. The USGS and GNS reported moment magnitudes agree for the remaining events.

The epicenters and modeled fault planes of several key events in the Canterbury Earthquake sequence are illustrated in Figure 4.1.3 (Beavan et al., 2012). The epicenters of the events described in Table 4.1.1, with the exception of the 4 SEP 10 Darfield event, are shown relative to the CBD in Figure 4.1.4.

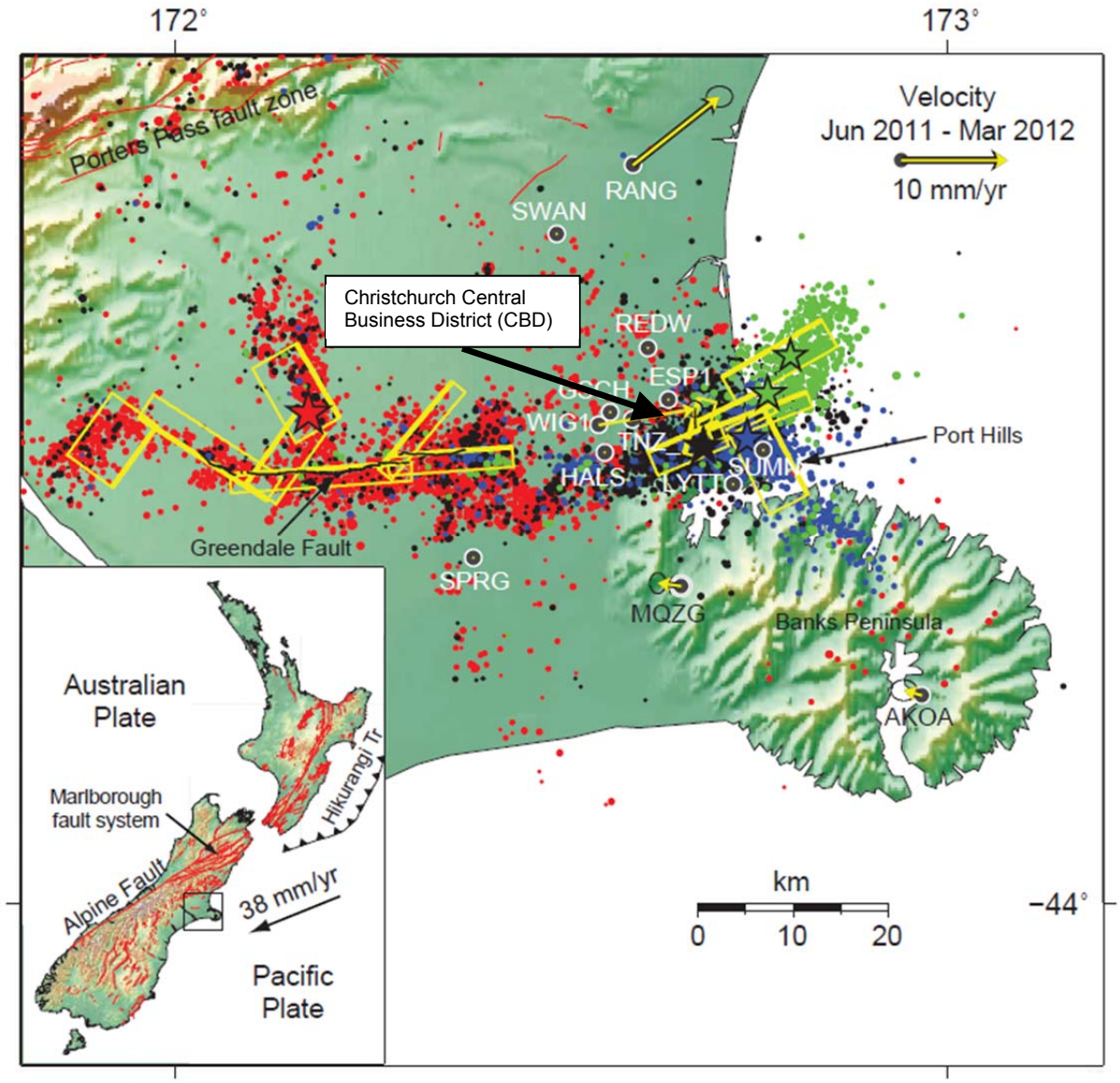

Figure 4.1.3. Epicenters and modeled fault planes of several key events in the Canterbury Earthquake sequence. Red, black, blue, and green stars show the epicenters of the 4 SEP 10 (M_w 7.1), 22 FEB 11 (M_w 6.2), 13 JUN 11 (M_w 6.0), and 23 DEC 11 (combined M_w 5.8 and M_w 5.9) events. Colored dots are the aftershocks following the mainshock with the corresponding color. Yellow rectangles show the outline of the fault planes inferred from geodetic data for the main shocks. The thick yellow lines correspond to the top edge of each rupture plane (from Beavan et al., 2012). The approximate location of the Christchurch Central Business District has been superimposed on this figure for reference.

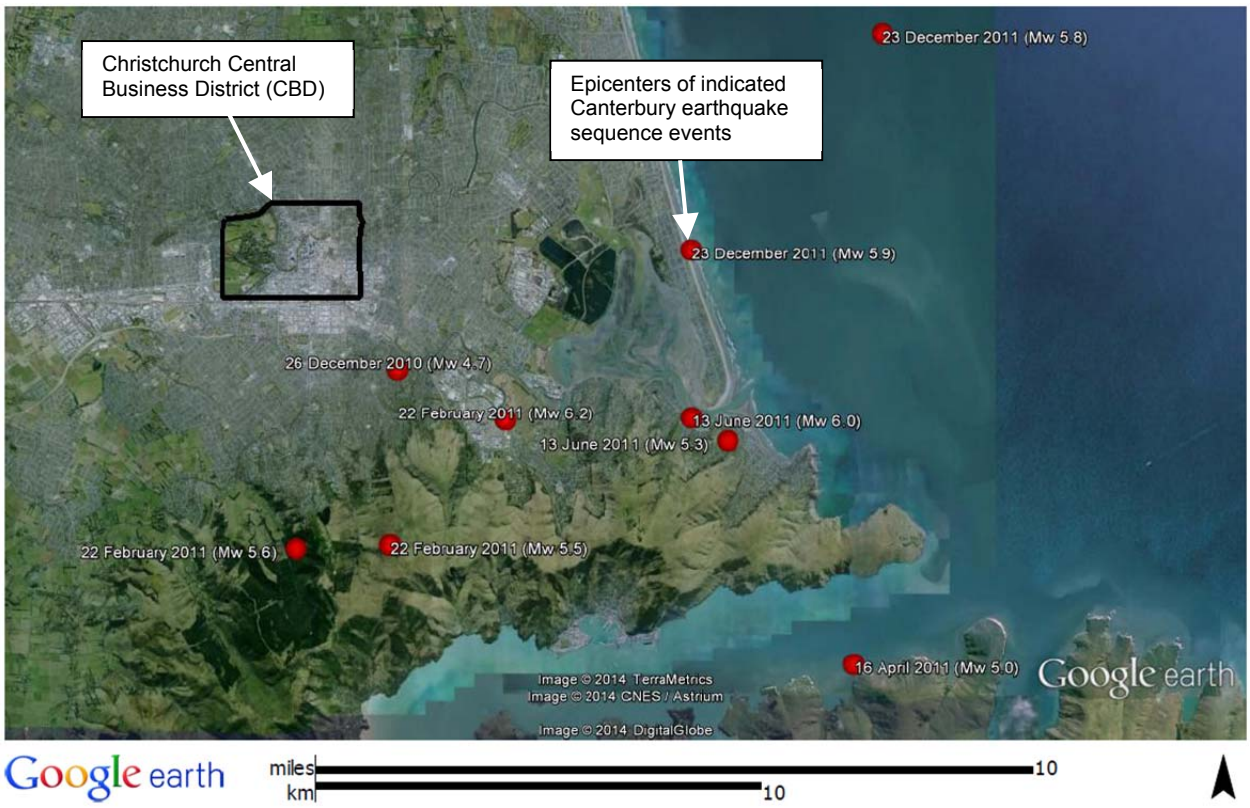

Figure 4.1.4. Epicenters of Canterbury earthquake sequence events relative to the CBD.

The events of the Canterbury earthquake sequence were well recorded by an array of strong motion instruments operated by GNS. These instruments consisted of instruments on the national network (i.e., New Zealand National Hazard Monitoring Network) and the regional network (i.e., CanNet). Following the 4 SEP 10 Darfield earthquake, 13 additional strong motion instruments were deployed in the Canterbury region. Consequently, at the time of the 22 FEB 11 event, there were 14 strong motion instruments within 20 km of the epicenter operated by GNS (Holden, 2011). There were four strong ground motion recording stations (SMS) within the CBD during the nine Canterbury earthquake sequence events under study. The locations of these stations are summarized in Table 4.1.2 and illustrated in Figure 4.1.5.

Table 4.1.2. Ground motion station locations within the CBD.

Station ID	**Latitude***	**Longitude**
CBGS	-43.529348	172.619917
CCCC	-43.538108	172.647556
CHHC	-43.535760	172.627483
REHS	-43.521927	172.635150

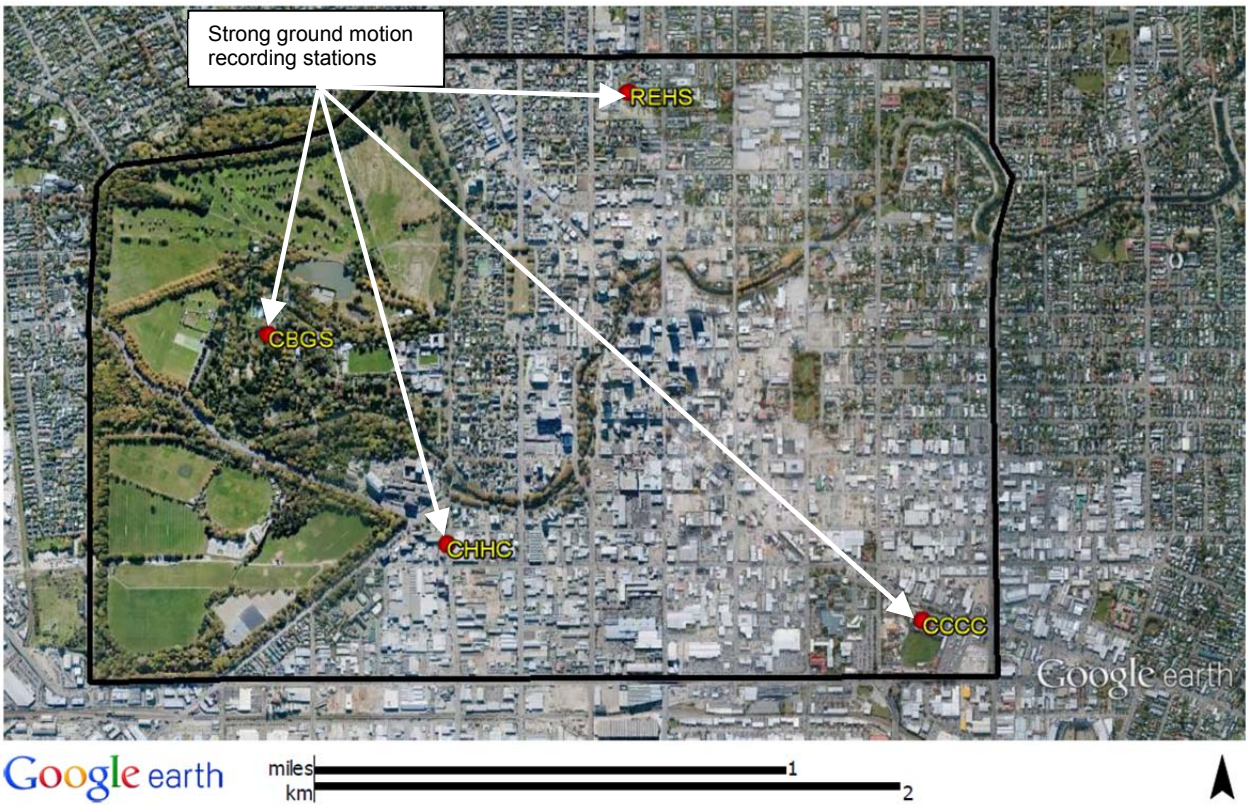

Figure 4.1.5. Strong ground motion recording stations within CBD.

Processed strong ground motion data from the four stations described above was obtained from GNS through the GeoNet database (ftp.geonet.org.nz/strong/processed/Proc). The band-pass filter transition bands applied by GNS for each event are summarized in Table 4.1.3.

Table 4.1.3. Summary of GNS band-pass filter transition bands applied for each event.

Date	NZ Local Time	M_w	High-Pass Transition Band (Hz)	Low-Pass Transition Band (Hz)
4 SEP 10	04:35:46	7.1	0.01 - 0.10	24.5 - 25.5
26 DEC 10	10:30:15	4.7	0.10 - 0.25	24.5 - 25.5
22 FEB 11	12:51:42	6.2	0.05 - 0.10	24.5 - 25.5
22 FEB 11	13:04:19	5.5	0.10 - 0.25	24.5 - 25.5
22 FEB 11	14:50:29	5.6	0.10 - 0.25	24.5 - 25.5
16 APR 11	17:49:23	5.0	0.10 – 0.25	24.5 – 25.5
13 JUN 11	13:01:00	5.3	0.10 - 0.25	24.5 - 25.5
13 JUN 11	14:20:50	6.0	0.10 - 0.20	24.5 - 25.5
23 DEC 11	13:58:36	5.8	0.10 - 0.25	24.5 - 25.5

23 DEC 11	15:18:02	5.9	0.10 - 0.25	24.5 - 25.5

A summary of the peak, geometric mean (geo-mean), horizontal ground accelerations recorded at each station for each of the events under study is provided in Table 4.1.4. Table 4.1.5 provides a summary of the peak, geo-mean, horizontal ground velocities.

Table 4.1.4. Summary of geo-mean peak ground accelerations for each of the events under study.

Event	**Geometric Mean PGA (g)**			
	CBGS	**CCCC**	**CHHC**	**REHS**
4 SEP 10, Mw 7.1	0.17	0.21	0.18	0.25
26 DEC 10, Mw 4.7	0.25	0.22	0.16	0.24
22 FEB 11, Mw 6.2	0.48	0.42	0.35	0.51
22 FEB 11, Mw 5.5	-	0.14	0.17	-
22 FEB 11, Mw 5.6	-	0.09	0.09	-
16 APR 11, Mw 5.0	0.07	-	0.15	0.10
13 JUN 11, Mw 5.3	0.18	-	0.20	0.18
13 JUN 11, Mw 6.0	0.16	-	0.21	0.29
23 DEC 11, Mw 5.8	0.16	0.14	0.18	0.21
23 DEC 11, Mw 5.9	0.20	0.18	0.21	0.30

Table 4.1.5. Summary of geo-mean peak ground velocities for each event.

Event	Geometric Mean PGV (cm/s)			
	CBGS	**CCCC**	**CHHC**	**REHS**
4 SEP 10, Mw 7.1	35.7	44.4	37.8	40.6
26 DEC 10, Mw 4.7	14.4	17.8	13.1	14.7
22 FEB 11, Mw 6.2	51.4	61.4	59.2	64.0
22 FEB 11, Mw 5.5	-	13.6	18.8	-
22 FEB 11, Mw 5.6	-	12.5	16.0	-
16 APR 11, Mw 5.0	4.9	-	9.4	9.4
13 JUN 11, Mw 5.3	10.6	-	15.6	17.4
13 JUN 11, Mw 6.0	27.7	-	33.6	38.9
23 DEC 11, Mw 5.8	16.0	18.6	17.5	23.4
23 DEC 11, Mw 5.9	26.8	23.6	24.7	42.9

The 10 events considered most important for the purposes of this study were clearly significant in terms of the ground motion intensity parameters summarized in Tables 4.1.4 and 4.1.5. While the M_w 6.2 Christchurch earthquake was not the largest magnitude event, it led to the most intense ground shaking in the CBD. In fact, the peak geo-mean horizontal ground accelerations in the Christchurch earthquake were on the order of twice those recorded during the larger, but more distant, M_w 7.1 Darfield event. The PGAs recorded in the CBD during the Darfield event were similar to those recorded during the 26 DEC 10 M_w 4.8, 13 JUN 11 M_w 6.0, and 23 DEC 11 M_w 5.9 events. The PGA values of the dozens of other M_w 5^+ events are lower than those recorded during these events.

The acceleration-time histories recorded at the REHS SMS for these four events are shown in Fig. 4.1.6a. The differing intensities and durations of these events are readily apparent. The characteristics of the ground motions recorded in the CBD are described further through 5% damped elastic acceleration response spectra and Arias intensity-time histories in Figs. 4.1.6b and 4.1.6c. The intensity and shaking intensity rate (SIR), as defined by Dashti et al., 2010b, of the ground motions of the Christchurch event indicate clearly why it was most damaging. The distinguishing feature of the Darfield event relative to the other earthquakes is its longer significant duration ($D_{5\text{-}95}$) of 30 s or so.

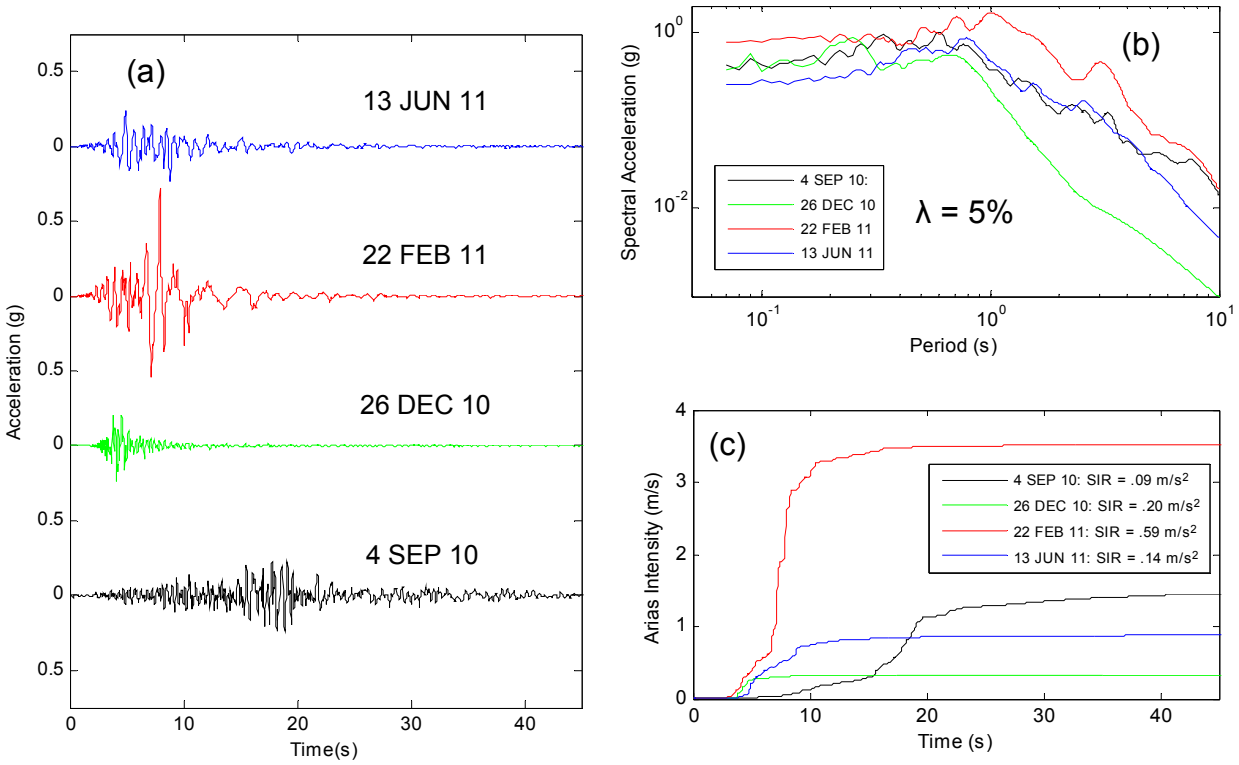

Figure 4.1.6. (a) Recorded acceleration-time histories, (b) 5% damped pseudo-acceleration response spectra, and (c) Arias intensity-time histories at REHS SMS at azimuth 092.

More details regarding the ground motions recorded during the Darfield and Christchurch earthquakes can be found in Bradley and Cubrinovski (2011), Cubrinovski et al. (2011a and 2011b), O'Rourke and Milashuk (2011), Bradley (2012), and Bradley and Hughes (2012).

Directivity in the Canterbury earthquake sequence

Directivity is a phenomenon associated with an earthquake when the direction of slip along the fault coincides with the direction of propagation of the rupture front and the velocity of the rupture front is very close to the shear wave velocity of the rock structure through which radiated shear waves propagate. These conditions allow for the radiated shear waves to coalesce in the direction of the propagating rupture front and to spread out in the direction opposite the rupture front. A site located along the direction of the propagating rupture front will observe most of the seismic radiation to arrive at nearly the same time as a single pulse of motion. A site located in the opposite direction of the rupture front will observe the motion to be more spread out in time and with relatively lower intensity. Ground motions recorded at sites that have experienced forward directivity typically exhibit increased spectral accelerations at periods greater than 0.6 s, and typically experience higher ground motion intensities in the fault normal direction than in the fault parallel direction (Somerville et al., 1997). Forward directivity effects are typically most noticeable along the direction of the rupture front at distances of less than 15 km from the fault.

As discussed by Bradley (2012), forward directivity effects were significant during the 4 SEP 10 Darfield earthquake and ground motion characteristics associated with forward directivity were observed at the four strong ground motion recording stations within the CBD (i.e., CBGS, CCCC, CHHC, and REHS). Forward directivity effects were not generally significant during the 22 FEB 11 event due to the misalignment between the fault slip direction and the inferred direction of rupture propagation, as well as the smaller magnitude of this event. Bradley (2012) provides a comprehensive discussion of forward directivity effects observed during the 4 SEP 10 and 22 FEB 11 events.

Site Response at Ground Motion Recording Stations

Smyrou et al. (2011) and Bradley and Cubrinovski (2011) observe that many of the ground motion recordings from the 22 FEB 11 event display characteristics of ground motions recorded on liquefied soils. These characteristics include the presence of large amplitude acceleration "spikes" associated with cyclic mobility, a reduction in the high-frequency content after strong shaking commenced, and long period spectral amplification. Figure 4.1.7 illustrates the recorded acceleration histories along azimuth 271 at station CBGS during the 4 SEP 10 and 22 FEB 11 earthquakes. Qualitative evidence of soil liquefaction is observed in the acceleration-time history during the Christchurch event but not during the Darfield event.

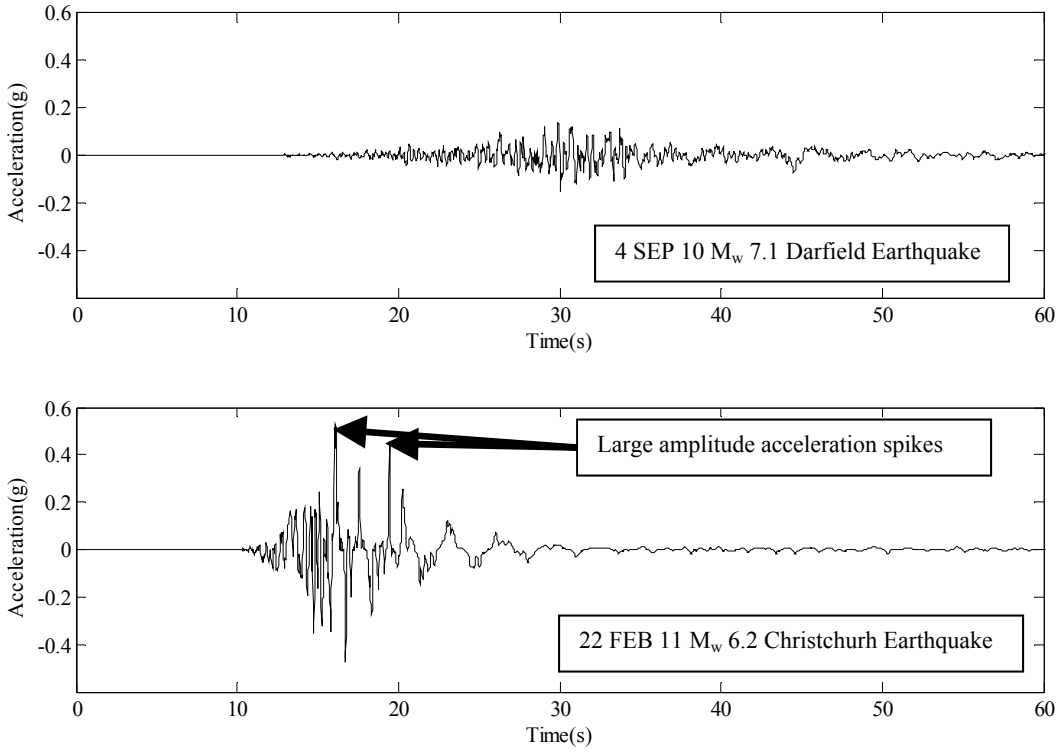

Figure 4.1.7. Acceleration-time histories recorded at station CBGS along azimuth 271 during the 4 SEP 10 and 22 FEB 11 events. Qualitative evidence of soil liquefaction is observed during the 22 FEB 11 event but not during the 4 SEP 10 event.

It is important to understand the site response of the ground motion recording station locations if the ground motion records are to be used in future site specific design analyses and in the development of future ground motion predictive relationships. Studies of SMS sites in Christchurch, Kaiapoi, and Lyttelton have been performed by Wotherspoon et al. (2013), and these investigations typically included CPTs, boreholes with SPTs, and shear wave velocity measurements.

Geology of Christchurch

There are three geological formations of primary interest in foundation engineering within the CBD of Christchurch: the Yaldhurst Member of the Springston Formation, the Christchurch Formation, and the Riccarton Gravels. The Yaldhurst Member of the Springston Formation was deposited during the last 3000 years and is the shallowest of the three formations. It consists of three lithologic units (Brown and Weeber, 1992):

1) Overbank alluvial silt and sandy silt;
2) Peat deposits formed in marshland; and
3) Gravels deposited in old flood channels of the Waimakariri River.

The Christchurch Formation underlies the Yaldhurst Member of the Springston Formation and consists of beach, estuarine, lagoon, dune, and coastal swamp deposits composed of gravel, sand, silt, clay, shells, and peat. Like the Yaldhurst Member of the Springston Formation, the Christchurch formation is geologically young. Brown and Weeber (1992) describe the age of the Christchurch formation as post-glacial and likely less than approximately 9000 years old at the present day coast and less than approximately 6500 years old near the maximum inland extent of the post-glacial marine transgression. Based on the presence of shells observed in samples and cuttings from exploratory boreholes, Tonkin & Taylor (2011) indicate that the marine transgression following the last glaciation extended across the entire central city. Depth to the top of the Christchurch Formation is variable, but typically on the order of 7 meters to 10 meters beneath the ground surface.

The Riccarton Gravels are beneath the Christchurch formation and consist of well-graded brown or blue-gray gravels up to cobble size (100 mm). This formation is identified as the uppermost confined gravel aquifer in coastal northern Canterbury and is typically about 18 to 30 meters below the surface within the CBD. Brown and Weeber (1992) indicate the thickness of the Riccarton Gravels from several meters to up to 20 meters thick. Recent investigations by Tonkin & Taylor (2011) have proven the thickness of the Riccarton Gravels up to 10.5 meters within the CBD. The formation was deposited during the last glaciation and is between 14,000 and 70,000 years old.

Brown and Weeber (1992) and Tonkin & Taylor (2011) provide more detail regarding the geologic formations mentioned above, and the geologic conditions of Christchurch in general.

Regional Investigations and Subsurface Characterization Efforts

The Geotechnical Extreme Events Reconnaissance Association (GEER), through funding from the National Science Foundation (NSF), sent teams of researchers from the United States to the Canterbury region following the 4 SEP 10 and the 22 FEB 11 earthquakes to survey the damage and document important aspects of these events related to geotechnical earthquake engineering. Following both events, the US-based GEER team members worked in close coordination with researchers from the University of Canterbury and the University of Auckland. Consequently, the overall GEER teams consisted of a contingent of researchers from the United States and a contingent of researchers from New Zealand. The findings and observations of the GEER teams have been published in reports available through the GEER website at http://geerassociation.org (Green et al., 2010 and Cubrinovski et al., 2011b) and these findings and observations form the basis for the study presented herein.

Following the 22 FEB 11 event, Tonkin & Taylor Inc. was commissioned by the Christchurch City Council (CCC) to perform a regional characterization of subsurface conditions within the CBD. This characterization effort included 48 boreholes, 151 CPTs, 45km of geophysical surveys, installation of piezometers and regular monitoring of groundwater levels at each borehole location, and laboratory testing of collected soil samples. Most of the field work was carried out between June and October 2011 with a smaller amount of work performed in October and November 2011. Groundwater monitoring continued through October 2012. The findings of this investigation were published in a Geological Interpretive Report (Tonkin & Taylor, 2011), and this report was made available to the public through the CCC. In addition to the publicly available Geological Interpretive Report, Tonkin & Taylor has made all of the data collected for the purposes of their regional subsurface characterization effort publicly available through the Canterbury Geotechnical Database (https://canterburygeotechnicaldatabase.projectorbit.com/).

It has been well documented by others (Cubrinovski et al., 2011a; Tonkin & Taylor, 2011) that the groundwater table within the CBD of Christchurch is generally within 1-3 meters of the ground surface. Tonkin & Taylor (2011) also point out that the groundwater table fluctuates seasonally. To refine the groundwater table depths and seasonal fluctuation, Tonkin & Taylor installed standpipes or groundwater level loggers in each of the 48 boreholes performed in the CBD as part of their regional ground characterization effort. The standpipes and loggers were generally installed to depths of 8-10 meters below the ground surface to characterize groundwater conditions in the near surface soils. Standpipes were monitored and data loggers were downloaded on a monthly basis. Tonkin & Taylor (2011) summarizes the data collected up to December 2011. Based on their monitoring efforts and data supplied by Environment Canterbury (ECan), Tonkin & Taylor developed regional groundwater elevation and groundwater depth models that represent the best estimate of groundwater conditions during the 4 SEP 10, 22 FEB 11, 13 JUN 11, and 23 DEC 11 events (Canterbury Geotechnical Database, 2013). These models were made publicly available as Google Earth .kmz files through the CGD and have been used throughout this study.

Site Specific Subsurface Characterization Efforts

Twenty-two sites within the CBD were identified for further study by the GEER team during damage surveys performed in late February and March 2011. An additional site, outside of but very close to the southeast corner of the CBD, was identified for further study in July 2011. The selected sites contained single- and multi-story buildings on shallow and deep foundations and were selected because they displayed unique engineering performance characteristics. An effort was made to include buildings that performed well, in addition to buildings that were severely damaged during the 22 February Christchurch earthquake. Two of the 23 sites selected for further study did not contain buildings. Instead, these two sites were selected due to their proximity to interesting ground deformation patterns.

For the purposes of this work, geographical areas within the CBD were delineated into five zones (Zone 1, Zone 2, Zone 4, Zone 5, and Zone 8). An additional zone was delineated to include the building site just southeast of the CBD (Zone 9). The boundaries for each of the zones are presented in Figure 4.1.8. The building sites within each zone were further classified into tiers to distinguish between quality and quantity of data for each site. Tier 1 sites are sites with post-earthquake performance observations and/or measurements, foundation details are known with confidence, and detailed high quality subsurface investigations have been performed. Detailed case histories of the Tier 1 sites are the focus of the remainder of this chapter. Tier 2 sites typically lack one or more of the characteristics associated with Tier 1 sites.

Forty-seven targeted cone penetration tests (CPTs) were planned and performed by UC Berkeley (UCB), in coordination with the University of Canterbury (UC), in the CBD in late July and early August 2011, 18 CPTs were performed in February 2012, five CPTs were performed in October 2012, and 37 CPTs were performed in March and April 2013. Figures 4.1.9 through 4.1.14 illustrate the locations of the CPTs performed, by zone, as well as the building sites of interest in this study. Table 4.1.6 summarizes the buildings of interest in this study.

Table 4.1.6. Summary of buildings of interest by zone. Latitudes and longitudes were estimated using Google Earth.

Zone	Building Address	Building Name	Latitude	Longitude	Site Tier
1	144 Kilmore Street	PILE-6	43.52683	172.63863	1
1	151 Kilmore Street	FTG-7	43.52626	172.63839	1
1	155 Kilmore Street	FTG-4	43.52633	172.63871	1
1	227 Cambridge Terrace	EY	43.52731	172.63823	2
1	233 Cambridge Terrace	PGC	43.52743	172.63878	2
2	90 Armagh Street	VT	43.52896	172.63524	1
2	100 Armagh Street	VSA	43.52894	172.63552	1
2	119 Armagh Street	PWC	43.52850	172.63788	1
2	210 Oxford Terrace	OT	43.52784	172.63728	2
4	199 Armagh Street	CTUC	43.52855	172.64247	1
4	Armagh St. and Madras St. parking lot		43.52842	172.64317	1
4	234-238 Armagh Street		43.52891	172.64222	2
4	240 Armagh Street	AM	43.52893	172.64247	2
4	271 Madras Street	HC	43.52920	172.64237	2
5	86-100 Kilmore Street	TH	43.52693	172.63514	1
5	87-89 Kilmore Street	SCH	43.52626	172.63466	1
5	95 Kilmore Street	CC	43.52599	172.63559	2
8	155 Peterborough Street		43.52532	172.63914	2
8	193 Peterborough Street	SA	43.52524	172.64190	1
8	329 Madras Street	SND	43.52496	172.64234	2
8	239 Salisbury Street	SSD	43.52390	172.64425	2
8	243 Salisbury Street	SSC	43.52390	172.64442	2
9	48 Lismore Street	LS-I and LS-II	43.54400	172.65293	1

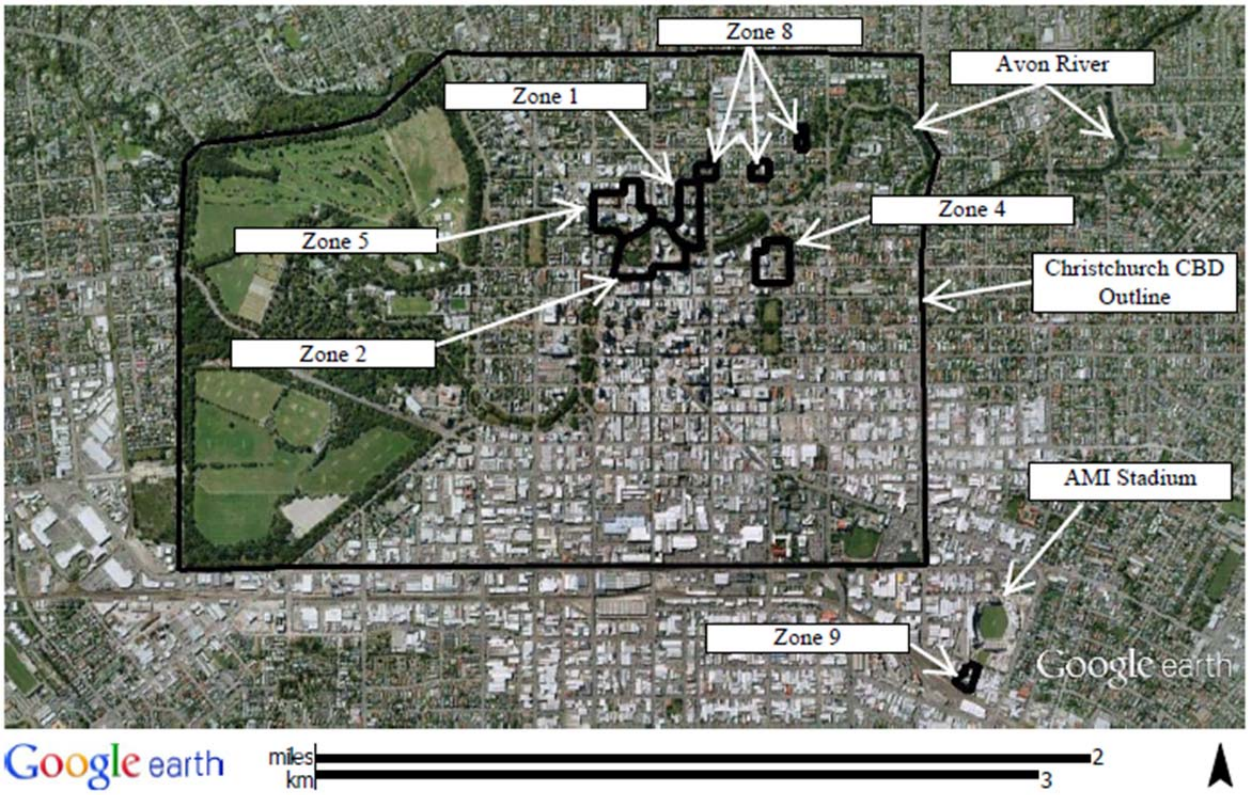

Figure 4.1.8. Study zone delineations.

Figure 4.1.9. Zone 1 overview with structures of interest indicated. CPT locations are indicated in red. University of Canterbury borehole location indicated in blue.

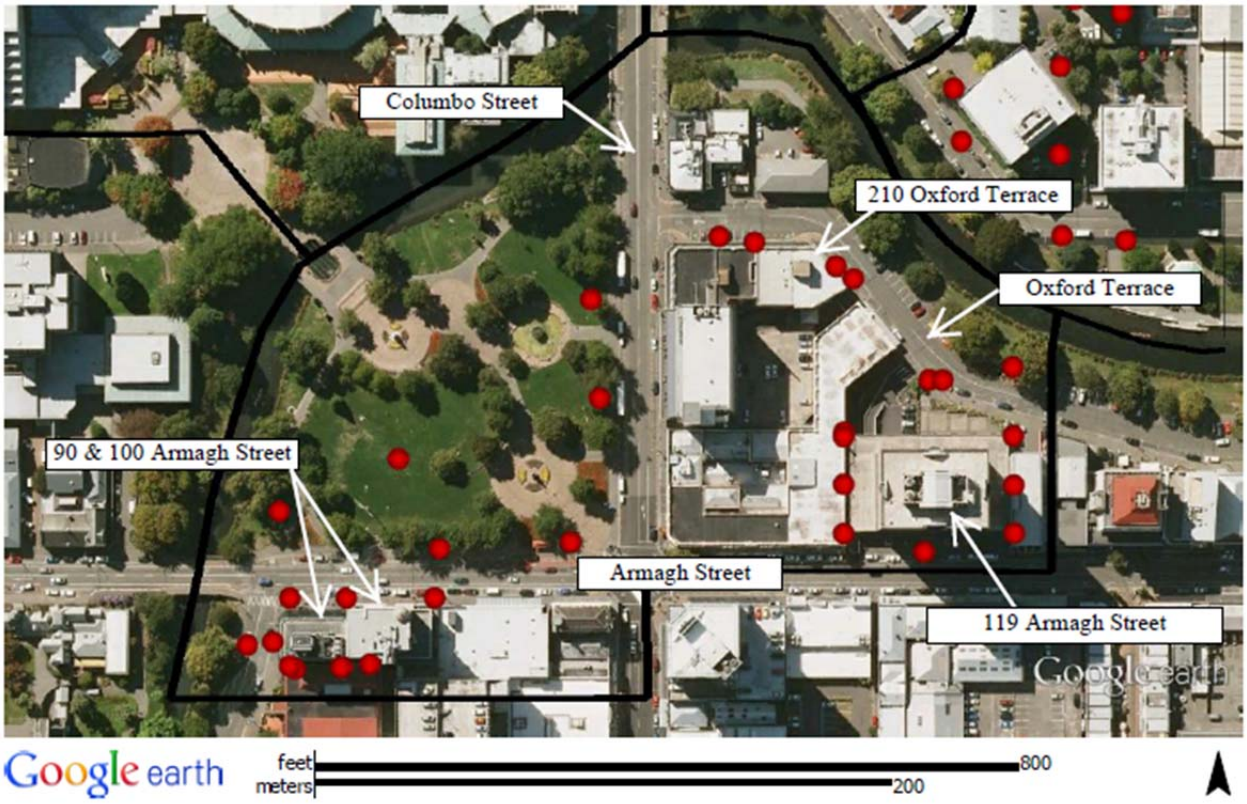

Figure 4.1.10. Zone 2 overview with structures of interest indicated. CPT locations are indicated in red.

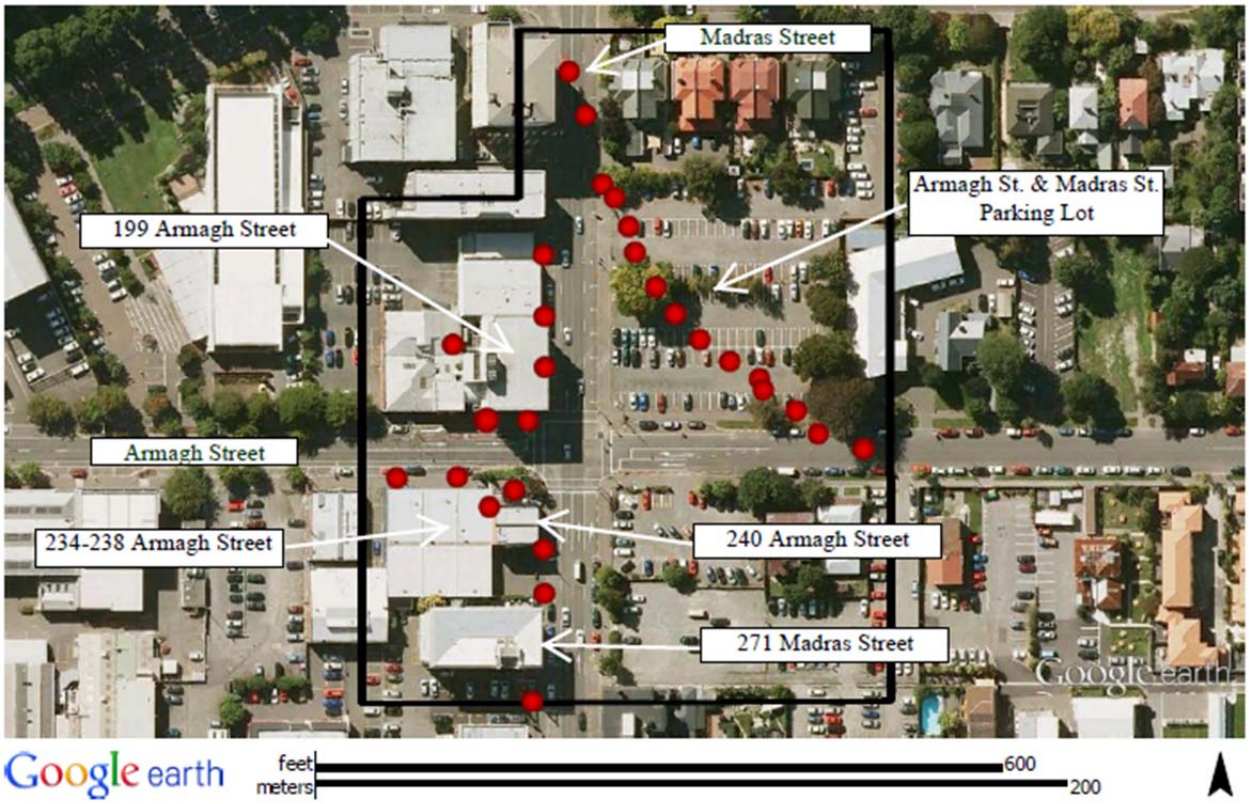

Figure 4.1.11. Zone 4 overview with structures of interest indicated. CPT locations are indicated in red.

Figure 4.1.12. Zone 5 overview with structures of interest indicated. CPT locations are indicated in red.

Figure 4.1.13. Zone 8 overview with structures of interest indicated. CPT locations are indicated in red.

Figure 4.1.14. Zone 9 overview with structures of interest indicated. CPT locations are indicated in red.

A parallel site investigation program carried out by UC consisted of exploratory boreholes at two sites within the CBD. One site was located near the southeast corner of 151 Kilmore Street and consisted of two closely spaced boreholes. In one borehole, continuous direct push samples were collected for soil identification purposes and index testing. In the other borehole, lightly disturbed samples were collected using a 'gel-push' technique for advanced laboratory testing. A similar set of two boreholes were performed at the second investigation site which was in the vicinity of 240 Armagh Street. Taylor et al. (2012) provides more detail regarding the gel-push sampling procedure.

In addition to the site investigations performed by UCB and the UC, researchers from the University of Arkansas and Virginia Tech performed geophysical investigations, consisting of SASW and MASW tests, at many of the locations described in 4.1.6 and illustrated in Figures 4.1.9 through 4.1.15. Data from these investigations are presented in a separate report by Cox et al. (2012).

Overview of CPT Equipment and Procedures

Eighty-four of the 107 CPTs performed for this study were performed by McMillan Drilling Services (henceforth McMillan) of Southbridge, Canterbury, New Zealand, and the remaining 23 CPTs were performed by Fugro Geotechnical NZ (henceforth Fugro) of Christchurch, New Zealand. The CPTs were generally performed in accordance with the procedures described in ASTM D5778-07. This included pushing a 10 cm^2 or 15 cm^2 cone penetrometer into the ground at a rate of approximately 2 cm/s and measuring the resistance at the tip and along the sleeve of the probe, the push rate, and inclination at every 1 or 2 cm depth increment during the test. Figures 4.1.15 through 4.1.17 are photographs of the CPT trucks used by McMillan and Fugro for this work.

Figure 4.1.15. McMillan Drilling Services 14 Tonne CPT Truck

Figure 4.1.16. McMillan Drilling Services 22 Tonne CPT Truck

Figure 4.1.17. Fugro Geotechnical NZ 20 tonne CPT Truck.

Two types of tests were performed, a standard CPT and a CPT with pore pressure measurements (CPTu). All of the Fugro tests were CPTu tests and some of the McMillan tests were CPTu tests. McMillan tests were performed using cone penetrometers manufactured by A.P. van den Berg of Herenveen, Friesland, The Netherlands (Icone ELCI-10), and Fugro tests were performed using cone penetrometers manufactured by Fugro Engineers B.V. Table 4.1.7 summarizes details of the cone penetrometers used in this study.

Table 4.1.7. Summary of cone penetrometers used in this study.

Cone Penetrometer Manufacturer and Type	Cone Base Cross Sectional Area (cm^2)	Pore Pressure Filter Element Location	Cone Penetrometer Serial Number	Dates Used
A.P. van den Berg - Icone ELCI-10	10	u2	71017	July/August, 2011 March, 2013
A.P. van den Berg - Icone ELCI-10	10	N/A	110542	July/August, 2011
A.P. van den Berg - Icone ELCI-10	10	N/A	070210	February, 2012 March, 2013
A.P. van den Berg - Icone ELCI-10	10	N/A	080238	October, 2012 March, 2013
Fugro Engineers B.V.	15	u2	1701-2522	April, 2013
Fugro Engineers B.V.	15	u2	1701-2517	April, 2013
Fugro Engineers B.V.	15	u2	1701-2524	April, 2013

The filter element for CPTu tests was located in the standard shoulder position just above the base of the cone. This is typically described in the literature as the u2 position and is the most common position for filter elements in modern electric cone penetrometers. McMillan filter elements consisted of greased stainless steel and the pore pressure fluid was silicone oil. Fugro filter elements were made of HDPE and the pore pressure fluid was glycerol. The filter elements were replaced prior to each CPTu. The pore pressure fluid ports were also flushed prior to each CPTu. Figure 4.1.18 illustrates a filter element prior to installation by McMillan on the penetrometer. Figure 4.1.19 shows the Fugro filter element installation and final assembly prior to push.

Figure 4.1.18. Stainless steel filter element being removed from silicone oil bath prior to installation.

Figure 4.1.19. (a) Fugro filter element installation and (b) final assembly prior to CPTu.

Shallow Gravels in the CBD

It was observed during the initial phase of CPTs performed in July and August 2011 that shallow layers of gravelly sand, sandy gravel, and/or gravel were present throughout much of Zone 2 and in the southern portions of Zone 1 and Zone 5. These layers were difficult to penetrate using the 10 cm^2 A.P. van den Berg cone with the McMillan 14 tonne CPT truck, and shallow refusal was often encountered in these areas. Consequently, subsequent investigations were planned and performed throughout these areas in October 2012 and March and April 2013.

During the investigations performed in October 2012 and March 2013, McMillan provided a larger CPT truck with a self-weight of approximately 22 tonnes. This truck also had the capability of 'pre-collaring' through denser and/or gravelly materials. The pre-collaring system was a steel dual tube system consisting of threaded steel outer casing with a nominal outer diameter of 6.99 cm and steel inner rods with a nominal outer diameter of 3.18 cm. At the base of the inner rod string was a conical steel tip that was designed to fit through the outer casing shoe. The dual tube assembly was then driven using a hydraulic hammer and direct push. Several photographs of the casing assembly are provided in Figure 4.1.20. CPTs that incorporated pre-collaring were performed in the following way:

1) The cone was advanced per ASTM D5778-07 until refusal was encountered;
2) If it was desired to advance the test to a greater depth, the CPT rods and probe were extracted from the hole;
3) Casing was then advanced using a hydraulic hammer in combination with direct push until the hydraulic ram gauge pressure was judged to be low enough to resume the CPT;
4) The inner casing rods were extracted leaving only the outer casing rods in the hole;
5) The CPT probe and rod string was re-installed into the hole to the depth of the bottom of casing; and
6) The CPT was resumed.

If necessary, this procedure was repeated. Ultimately, the McMillan pre-collaring system generally had success in penetrating the dense and/or gravelly soils of the type that caused refusal during tests in July and August 2011 and February 2012.

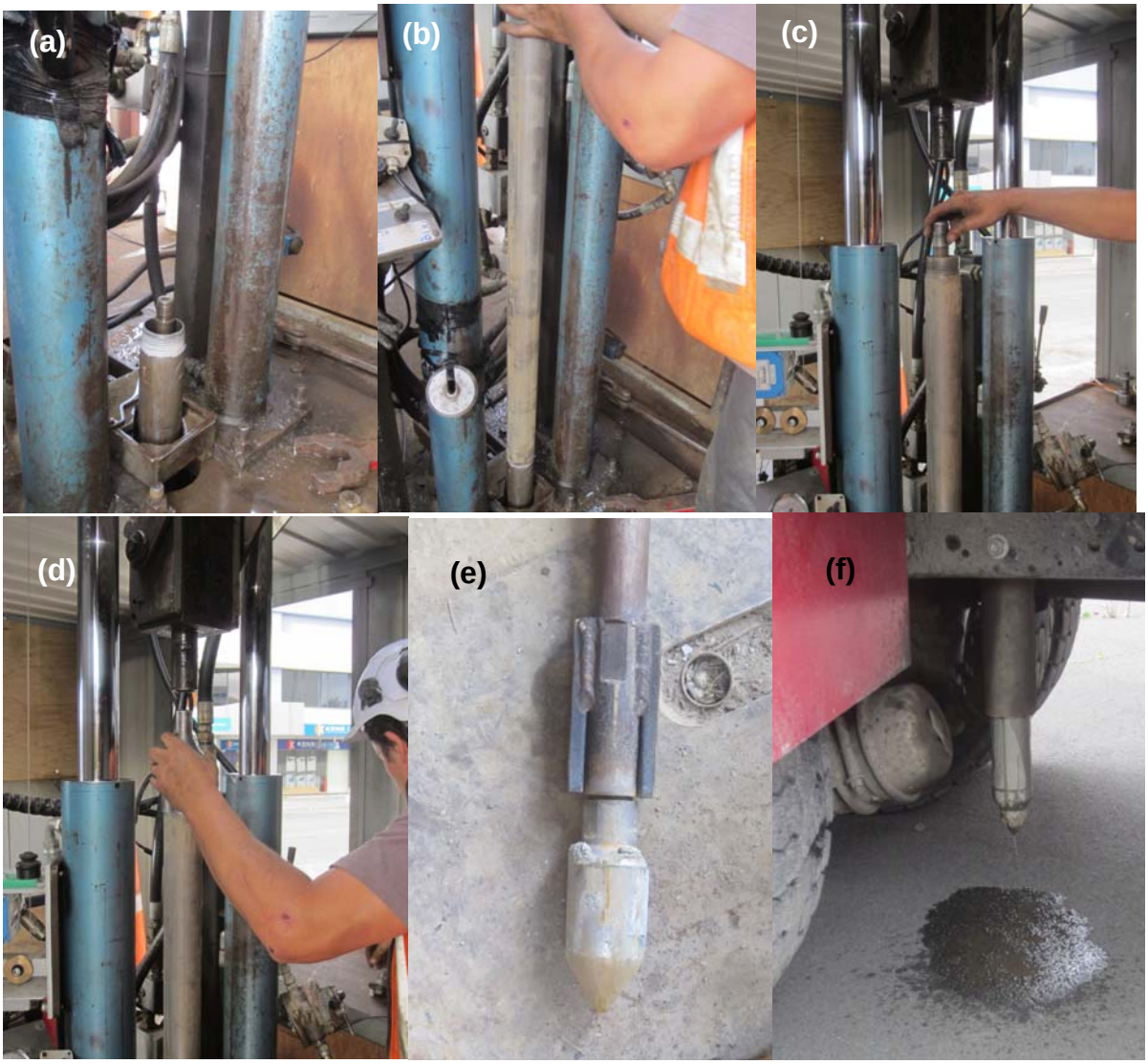

Figure 4.1.20. (a) View of dual tube casing system. (b) Connecting additional casing rods. (c) View of casing rods prior to driving cap placement. (d) View of casing rods following driving cap placement. (e) View of inner rod tip. (f) View of tip of casing assembly through the CPT truck sleeve prior to shallow driving.

The tests performed in April 2013 by Fugro were performed with a robust 15 cm^2 cone manufactured by Fugro Engineers B.V. using a 20 tonne CPT truck. The Fugro Engineers B.V. cone could be pushed through materials with uncorrected tip resistances greater than 80 MPa. In general, the CPTs performed by Fugro were also successful in penetrating through areas with layers of dense and/or gravelly materials.

Overview of CPT Data Processing

CPT data files, in Microsoft Excel format, were obtained from McMillan and Fugro for the CPTs performed for this study. These raw data files have been made publicly available through the CGD. When processing CPT data, it is important to make sure that the indicated measurements of tip resistance and sleeve friction are aligned such that they correspond to the same depth within the soil profile (i.e., equal depth format). The data files provided by Fugro were corrected for tip-sleeve offset, but the data files provided by McMillan were not. Accordingly, the offset between the tip of the cone and the approximate center of the friction sleeve was measured and this correction distance was applied to the McMillan CPT data to align the tip resistance and sleeve friction measurements. This has the effect of making the last 10 cm of data unusable, unless only tip resistance is required.

After ensuring all data was corrected for tip-sleeve offset, the data files were saved in .csv format and read into the computer software program Matlab for further processing and analyses. A Matlab script file was developed for each CPT.

When possible, it is preferred to correct the measured tip resistances to account for pore fluid pressures acting on both sides of the cone tip. This unequal end area effect occurs at the tip of most modern electric cone penetrometers and arises due to pore pressures acting in such a way as to reduce the measured tip resistance. Figure 4.1.21, taken from ASTM D5778-07, illustrates this issue.

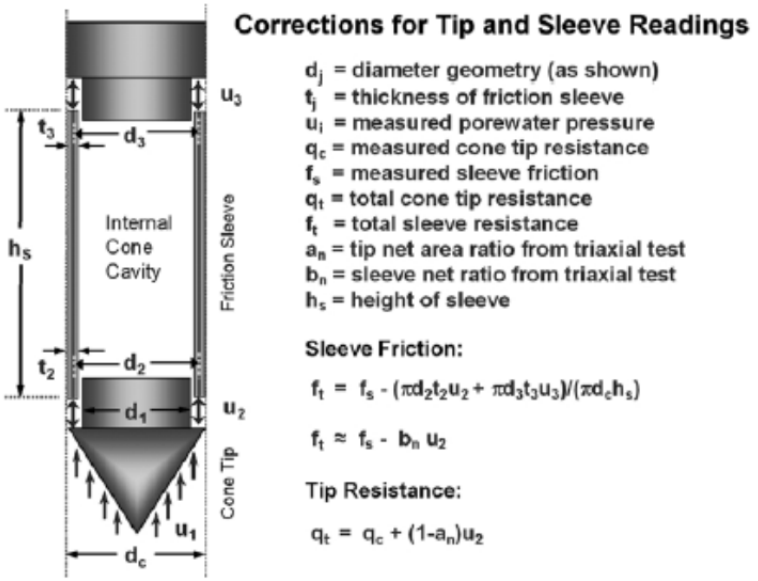

Figure 4.1.21. Diagram illustrating unequal area effects and necessary corrections (from ASTM D5778-07, 2007)

In this study no corrections have been made for unequal end areas of the friction sleeve. The net area ratio is typically very small (e.g., the net area ratio of the friction sleeve for Fugro Engineers B.V. cone 1701-2522 was reported as 0.01392). In addition, while there could theoretically be a difference between the pore fluid pressures at the u3 and u2 locations, pore pressures at the u3 location were not measured in this study and it is likely that the difference in

these pressures is very minor. ASTM D5778-07 notes that it is common to ignore the correction to the sleeve friction data.

As described in Figure 4.1.21, the corrected cone tip resistance is a function of the measured cone tip resistance, q_c, the tip net area ratio, a_n, and the measured pore fluid pressure at the u2 location, u_2. This relationship is given by equation 4.1.1:

$$[4.1.1] \qquad q_t = q_c + (1 - a_n) * u_2$$

The tip net area ratios, a_n, were reported to be 0.75 for the A.P. van den Berg cones and 0.58 for the Fugro Engineers B.V. cones. As discussed previously, some tests were performed without pore pressure measurements so no correction to the measured tip resistances was applied for these tests. While this correction is procedurally important in the correct processing of CPT data, and the effects can be important in materials which develop very high excess pore water pressures during testing, the pore water pressure corrections during this study were very minor. Therefore, it was determined that performing some CPTs without pore water pressure measurements would not impact the subsequent CPT-based analyses described below.

After applying the necessary corrections described above, the CPT data processing generally followed the procedures and recommendations provided by Robertson (2009). This processing consisted of normalizing the cone tip resistance and sleeve friction using estimates of the in-situ vertical total and effective stresses. In order to calculate these stresses, the CPT based unit weight correlation developed by Robertson and Cabal (2010) was implemented. This correlation is given by equation 4.1.2 and requires only the corrected cone tip resistance and the measured sleeve friction. Figure 4.1.22 illustrates the relationship described by equation 4.1.2.

$$[4.1.2] \qquad \frac{\gamma}{\gamma_w} = 0.27 * \left[\log\left(R_f\right)\right] + 0.36 * \left[\log\left(\frac{q_t}{p_a}\right)\right] + 1.236$$

where:

γ = unit weight of soil
γ_w = unit weight of water
q_t = corrected CPT tip resistance
R_f = CPT friction ratio, $f_s/q_t*100\%$
p_a = atmospheric pressure in the same units as q_t

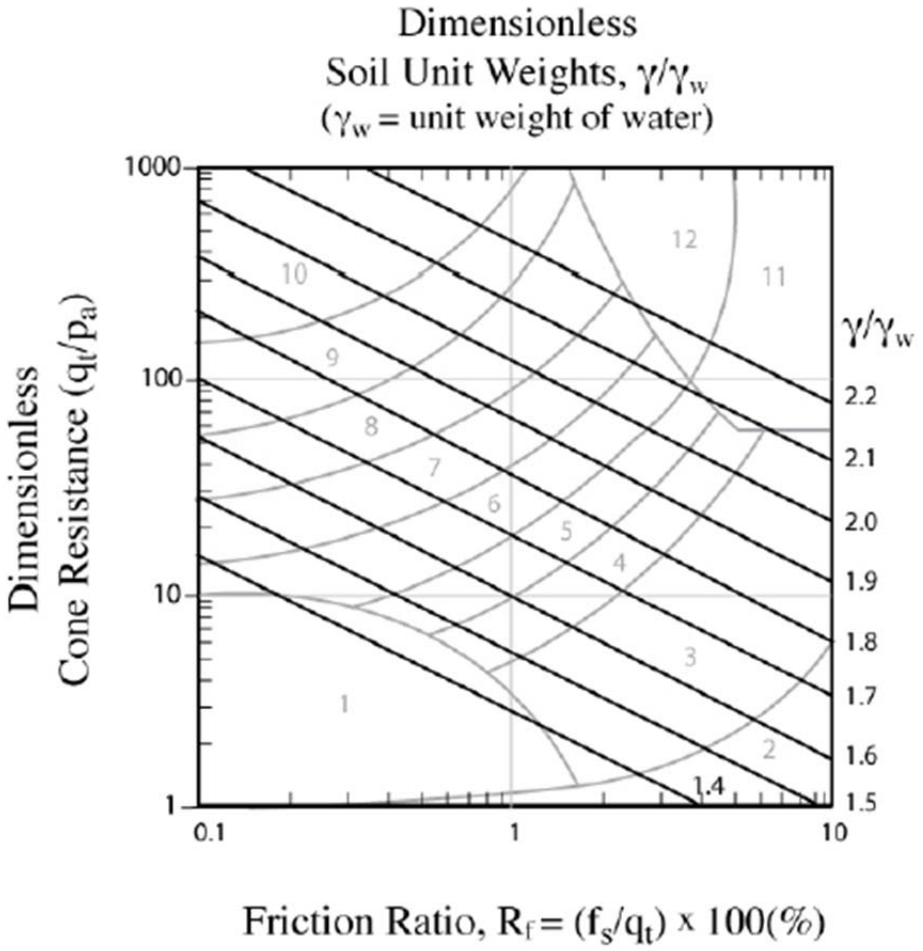

Figure 4.1.22. Relationship between specific gravity and corrected cone tip resistance and friction ratio (from Robertson and Cabal, 2010)

With the unit weights calculated using 4.1.2, the in-situ vertical total and effective stresses could be estimated (given an estimated groundwater table depth). The normalized sleeve friction, F_r, normalized tip resistance, Q_{tn}, and normalized soil behavior type (SBT) index, I_c, profiles could then be calculated in accordance with the procedures and recommendations of Robertson (2009).

Robertson (2009) describes the normalized SBT indices as the radii of concentric circles used to approximate the boundaries between different soil behavior types on the normalized soil behavior type chart. This concept is illustrated in Figure 4.1.23 from Robertson and Cabal (2010). Table 4.1.8, reproduced from Robertson and Cabal (2010), provides a brief description of soil behavior type ranges.

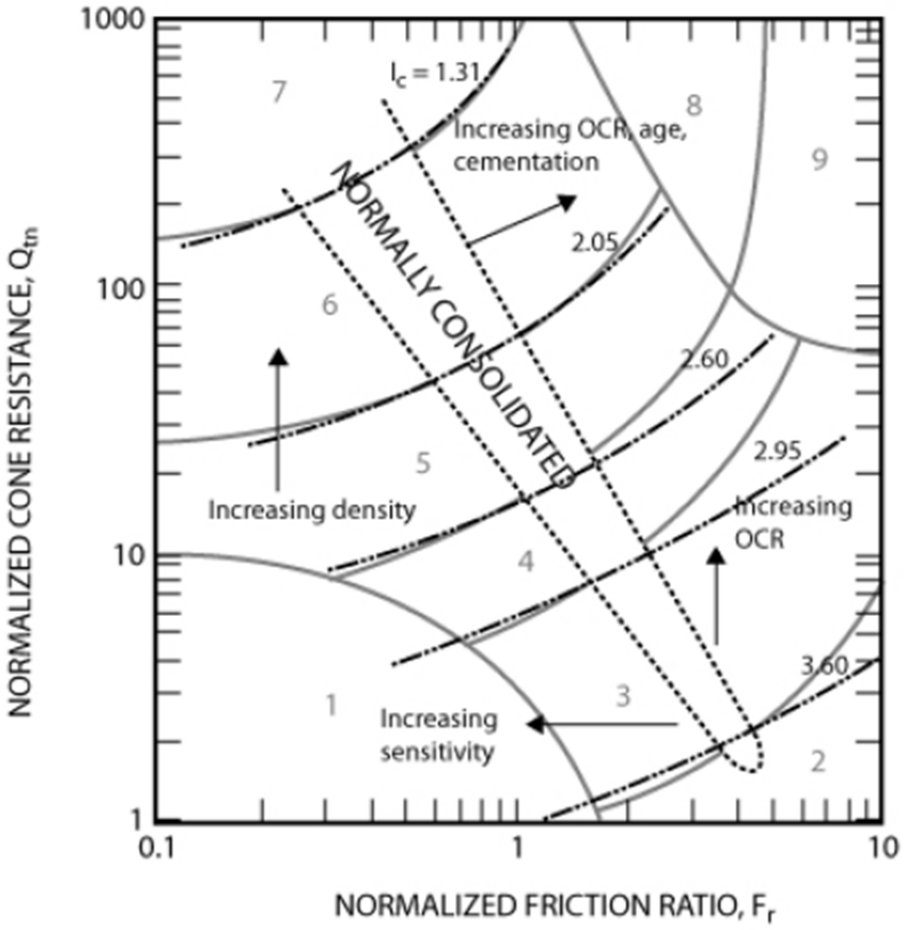

Figure 4.1.23. Normalized CPT soil behavior type (SBT) chart (from Robertson and Cabal, 2010)

Table 4.1.8. SBT and Ic descriptions (reproduced from Robertson and Cabal (2010)).

Zone	Soil Behavior Type	Ic
1	Sensitive, fine grained	N/A
2	Organic soils - clay	>3.6
3	Clays - silty clay to clay	2.95 - 3.6
4	Silt mixtures - clayey silt to silty clay	2.6 - 2.95
5	Sand mixtures - silty sand to sandy silt	2.05 - 2.6
6	Sands - clean sand to silty sand	1.31 - 2.05
7	Gravelly sand to dense sand	< 1.31
8	Very dense sand to clayey sand*	N/A
9	Very stiff, fine grained*	N/A

*Heavily overconsolidated or cemented

CPT-Based Liquefaction Triggering and Post-liquefaction Volumetric Strain Analyses

Based on the measured CPT data, along with the best estimate of the depth to the groundwater table from the T&T groundwater models, the liquefaction triggering potential of the soils encountered at each CPT location were evaluated using three state of the practice, CPT-based, liquefaction triggering correlations: the Robertson and Wride (1998), henceforth RW98, correlation using the magnitude scaling factor (MSF) of Idriss and Boulanger (2008) and K_σ recommendations presented in Youd et al. (2001), the Moss et al. (2006), henceforth MS06, correlation, and the Idriss and Boulanger (2008), henceforth IB08, correlation. While the procedures and recommendations provided by Robertson (2009) were followed to normalize the measured CPT data and calculate the normalized I_c profiles for the purposes of a general evaluation of the soil profile, the procedures and recommendations provided by the authors of the three liquefaction triggering correlations listed above have been followed carefully for the purposes of using each of these correlations. For example, the CPT tip resistance normalization procedure described by MS06 has been applied for purposes of the MS06 liquefaction triggering correlation. Several additional assumptions and procedural details related to these analyses are worth mentioning and are provided below:

1) Soil unit weights for stress calculations were estimated using the correlation developed by Robertson and Cabal (2010).
2) The overburden stress correction factors, C_q, were capped at 2.0 for the RW98 correlation, and were capped at 1.7 for the MS06 and IB08 correlations.
3) After applying overburden stress corrections, soils with I_c greater than 2.6 were assumed to be non-liquefiable, unless otherwise noted. These soils were assigned a FS = 5 against liquefaction triggering and a probability of liquefaction (P_L) = 0.
4) RW98 recommends using K_c = 1.0 when $1.64 < I_c < 2.36$ *and* F < 0.5%. This recommendation has been implemented.
5) K_σ corrections were not applied in the MS06 correlation. K_σ corrections were applied in the RW98 and IB08 correlations. The K_σ correction applied in the RW98 correlation was based on the recommendations provided in Youd et al. (2001) and required an estimate of the relative density. To approximate the relative density of the soils for this purpose, equation 35 of Mayne (2007) was used. The K_σ corrections applied in the IB08 correlation were capped at a maximum value of 1.1 in accordance with their recommendations.
6) R_f was bounded between 0.5% and 5% for the purposes of the fines content correction in the MS06 correlation. The fines content correction, Δq_{c1N}, in the IB08 correlation required an estimate of the fines content, FC. To estimate the FC for this purpose, equation 6 of RW98 was used unless site-specific FC data was available.
7) The MSF for the RW98 and IB08 correlations were capped at 1.8 in accordance with the recommendations by IB08.

8) No K_α factors have been applied in these analyses.
9) R_d calculations were performed as follows: equation 3 of Youd et al. (2001) was employed for the RW98 correlation, equations 8 and 9 of MS06 were used for the MS06 correlation, and equations 22 through 24 of IB08 were used for that correlation.
10) A_{max} estimates were based on the conditional PGA contours developed by Bradley and Hughes (2012). Calculations were performed using the median and +/- one standard deviation estimates of the PGA in order to calculate a reasonable range of results incorporating the uncertainty in the PGA at each location.

The simplified standard-of-practice CPT-based procedure developed by Zhang et al. (2002), henceforth ZR02, was applied to estimate level ground surface settlements due to liquefaction at the locations of each of the CPTs. This procedure was developed based on the work of Ishihara and Yoshimine (1992) and is considered to be applicable to sands and silty sands. Figure 4.1.24 illustrates the ZR02 relationship between clean sand equivalent, normalized, tip resistance and volumetric strain. The integration of volumetric strains throughout the soil profile provides an estimate of the vertical settlement for level ground sites. The ZR02 procedure was developed to estimate vertical settlements at level-ground, free-field sites due to post-liquefaction volumetric strains, but the procedure is often employed in engineering practice to get a sense of the seismic performance of soils beneath buildings. This procedure does not account for important liquefaction-induced building settlement mechanisms for shallow-founded buildings atop shallow liquefiable soils such as partial or complete bearing capacity failure, SSI-induced ratcheting, and ground loss dued to sediment ejecta. Nevertheless, as this procedure and similar free-field, level ground settlement procedures are often employed in engineering practice as part of analyses to estimate liquefaction-induced building settlements, ZR02 calculations are performed and presented herein to assess the validity of the insights gained in performing these analyses for that application.

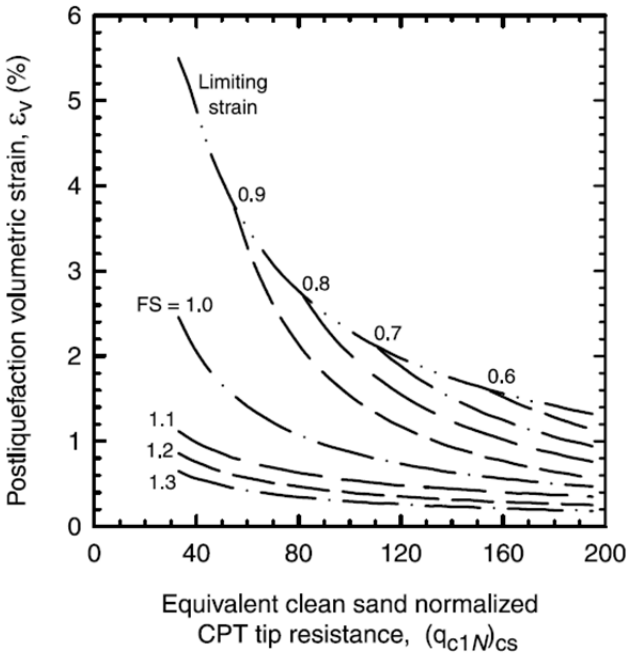

Figure 4.1.24. Relationship between volumetric strain and clean sand equivalent, normalized, CPT tip resistance (from Zhang et al. 2002)

The ZR02 procedure requires both the clean sand equivalent, normalized, CPT tip resistance $(q_{c1N})_{cs,}$ as well as a factor of safety against liquefaction triggering (FS_l). These parameters were calculated in accordance with the RW98 and IB08 correlations in this study. Consequently, the settlement calculations presented herein are referred to as ZR02-RW98 and ZR02-IB08, respectively. ZR02 provide equations to calculate the volumetric strains for discrete FS values and this required binning the FS for the purposes of these calculations. Interpolation was used to estimate the volumetric strains for $1.3 < FS < 2.0$ as there were no equations provided for this range.

It should be noted that the M_w 6.0 earthquake on 13 JUN 11 was preceded by an M_w 5.3 event a short distance away (Fig. 4.1.4) that occurred 80 minutes prior to the M_w 6.0 event (Table 4.1.1). There is a possibility that excess pore water pressures generated during the M_w 5.3 event had not fully dissipated by the time of the M_w 6.0 event. This has not been accounted for in the analyses pertaining to the M_w 6.0 event that are presented herein.

4.2 Investigation of Soil Variability at the Armagh Street and Madras Street Parking Lot

Introduction

The parking lot at the northeast corner of the intersection of Armagh Street and Madras Street, within the Zone 4 study area, is located along the southern boundary of an area within the CBD where researchers from the University of Canterbury observed moderate to severe

liquefaction following the 22 FEB 11 earthquake. This principal zone of liquefaction within the CBD was detailed by Cubrinovski et al. (2011a). In their description, Cubrinovski et al. (2011a) observed that, while it was possible to identify this principal zone of liquefaction within the CBD following the Christchurch earthquake, the intensity of liquefaction within this zone was very much non-uniform in space:

> *Even though the map shown in Figure 4 distinguishes the zone most significantly affected by liquefaction, the severity of liquefaction within this zone was not uniform. The manifestation of liquefaction was primarily of moderate intensity with relatively extensive areas and volumes of sediment ejecta (Figure 5). There were also areas of low manifestation or only traces of liquefaction, but also pockets of severe liquefaction with very pronounced ground distortion, fissures, large settlements, and substantial lateral ground movements. This non-uniformity in liquefaction manifestation reflects the complex and highly variable soil conditions even within the CBD principal liquefaction zone. (p. 897)*

Slightly modified versions of Figures 4 and 5 from Cubrinovski et al. (2011a) are reproduced here as Figures 4.2.1 and 4.2.2. The location of the Armagh Street and Madras Street parking lot has been added to Figure 4.2.1 for reference.

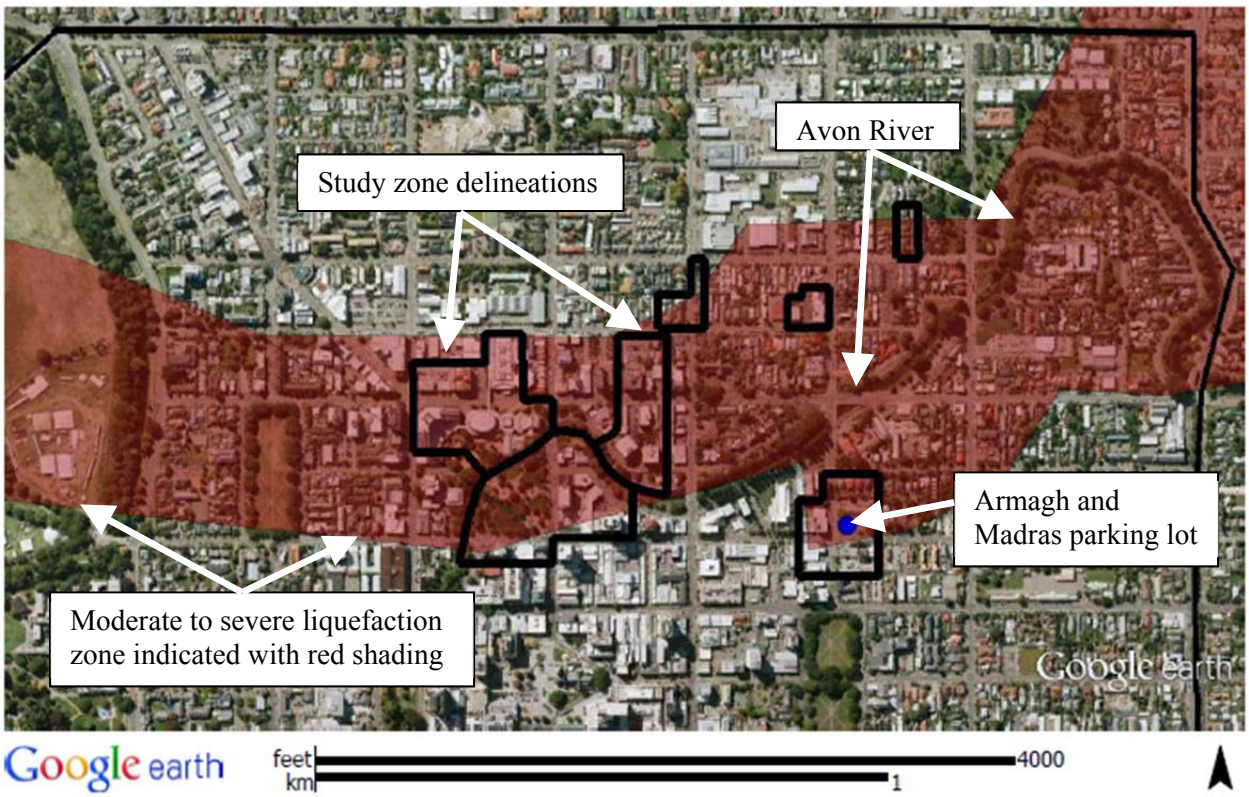

Figure 4.2.1. Modified version of Figure 4 from Cubrinovski et al. (2011a). Satellite photograph showing the moderate to severe liquefaction zone within the CBD (shaded in red), the study zone delineations, and the location of the Armagh and Madras parking lot.

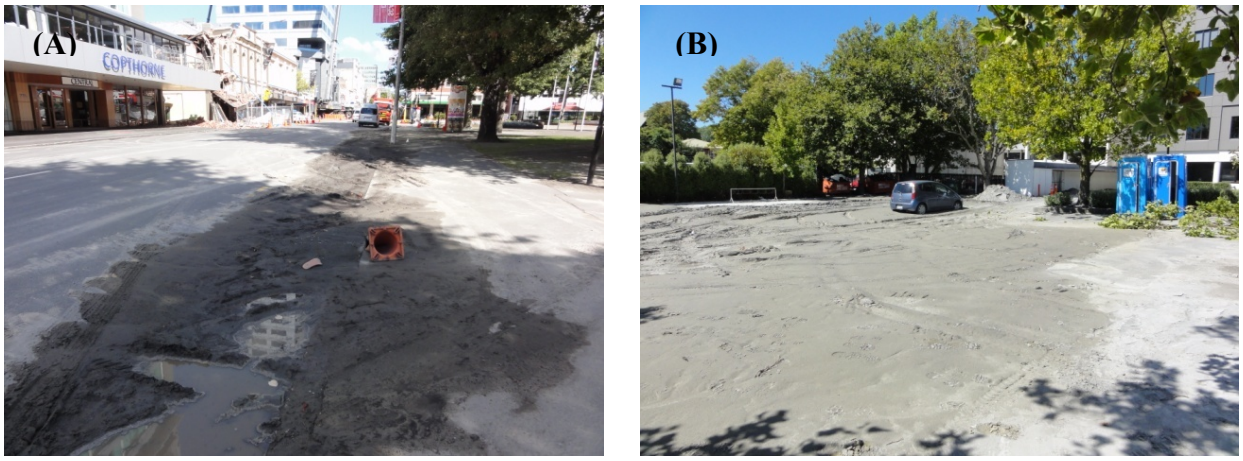

Figure 4.2.2. Reproduced Figure 5 from Cubrinovski et al. (2011a). Representative areas of: (A) moderate liquefaction [7 MAR 11; S43.52791 E172.63653], and (B) severe liquefaction within the CBD principal liquefaction zone [4 MAR 11; S43.52604 E172.63839]

Cubrinovski et al. (2011a) further describe how the variability in liquefaction severity over relatively short distances was observed in the vicinity of the Armagh and Madras parking lot:

> *At this location, the liquefaction was manifested by a well-defined, narrow zone of surface cracks, fissures, and depression of the ground surface about 50 m wide, as well as water and sand ejecta (Figure 10). This zone stretches from the Avon River to the north toward the buildings affected by this liquefaction feature, shown in the background of Figure 10 to the south. Traces of liquefaction were evident further to the south of these buildings.*

The buildings affected by this liquefaction feature, as mentioned above, include 199 Armagh Street (Section 4.3) as well as 240 Armagh Street. A slightly modified version of Figure 10 from Cubrinovski et al. (2011a) is presented as Figure 4.2.3.

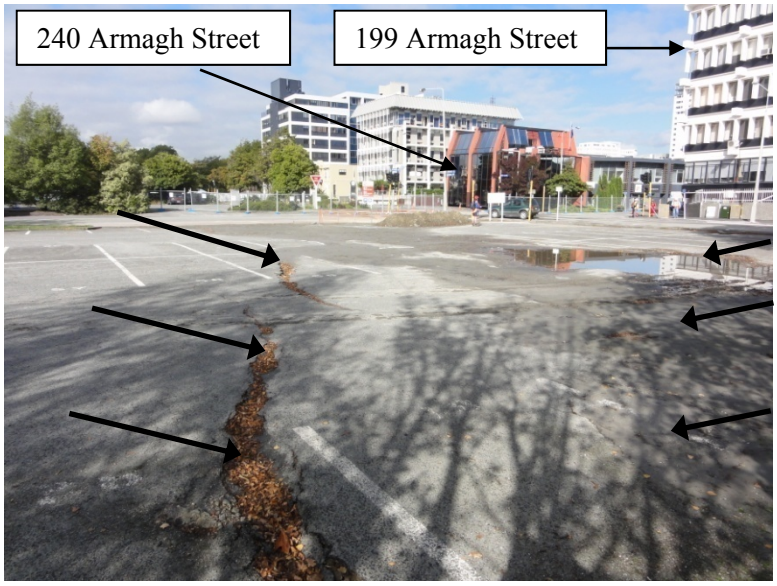

Figure 4.2.3. Reproduced from Cubrinovski et al. (2011a). Relatively narrow liquefaction-induced feature that traverses parking lot that is northeast of the intersection of Madras and Armagh streets [24 MAR 11; S43.52842 E172.64308]

The observation of the narrow liquefaction-induced feature illustrated in Figure 4.2.3, as well as the differential settlement observed at 199 Armagh Street and the horizontal movement observed at 240 Armagh Street, served as motivation for the study of soil variability at the Armagh and Madras parking lot described in this section.

Site Characterization

As described previously, Tonkin & Taylor Inc. produced regional scale cross sections along many of the prominent streets within the CBD as part of their regional subsurface characterization effort. Of these cross sections, geologic cross sections GXS-CBD-11 (along Armagh Street) and GXS-CBD-4 (along Madras Street) are relevant to the study of the ground conditions at the Armagh and Madras parking lot. Figure 4.2.4 illustrates the locations of GXS-CBD-11 and GXS-CBD-4 relative to the Armagh and Madras parking lot. Figures 4.2.5 and 4.2.6 illustrate the relevant portions of these Tonkin & Taylor cross sections, respectively. The location of the Armagh and Madras parking lot has been added to both sections for reference.

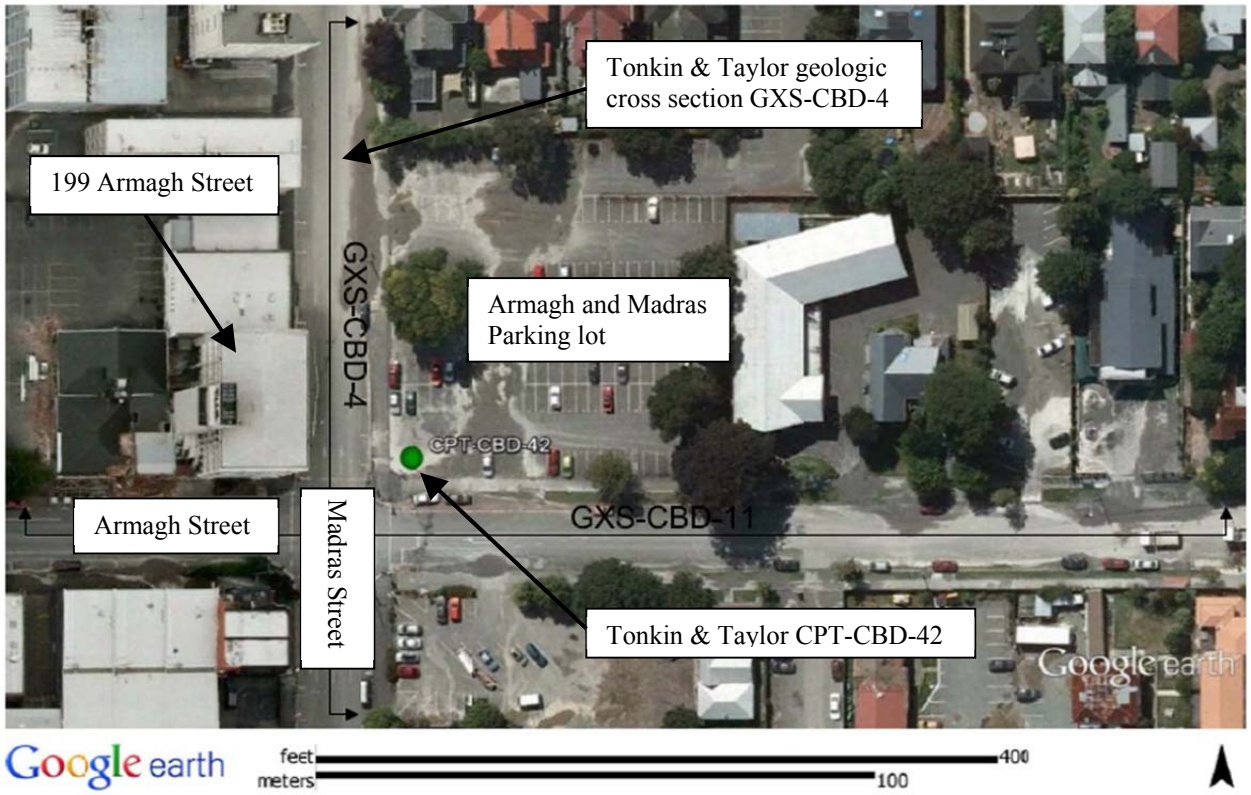

Figure 4.2.4. Locations of Tonkin & Taylor geologic cross sections GXS-CBD-11 and GXS-CBD-4 relative to the Armagh and Madras parking lot. Aerial photograph was taken 24 February 2011 by New Zealand Aerial Mapping (Canterbury Geotechnical Database, 2012a).

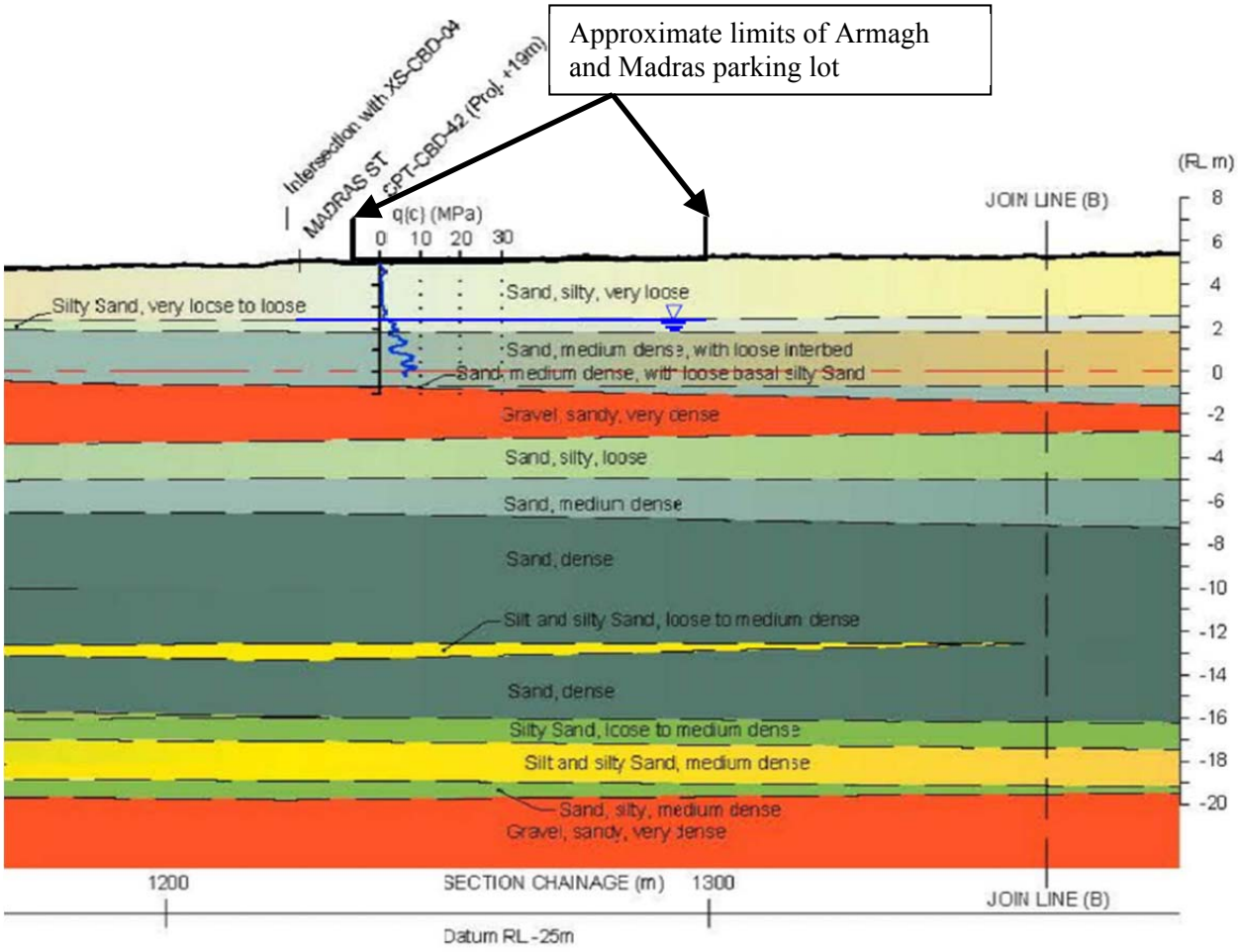

Figure 4.2.5. Portion of Tonkin & Taylor geologic cross section GXS-CBD-11, along Armagh Street (Tonkin & Taylor, 2011). The limits of the Armagh and Madras parking lot have been projected on the cross section for reference.

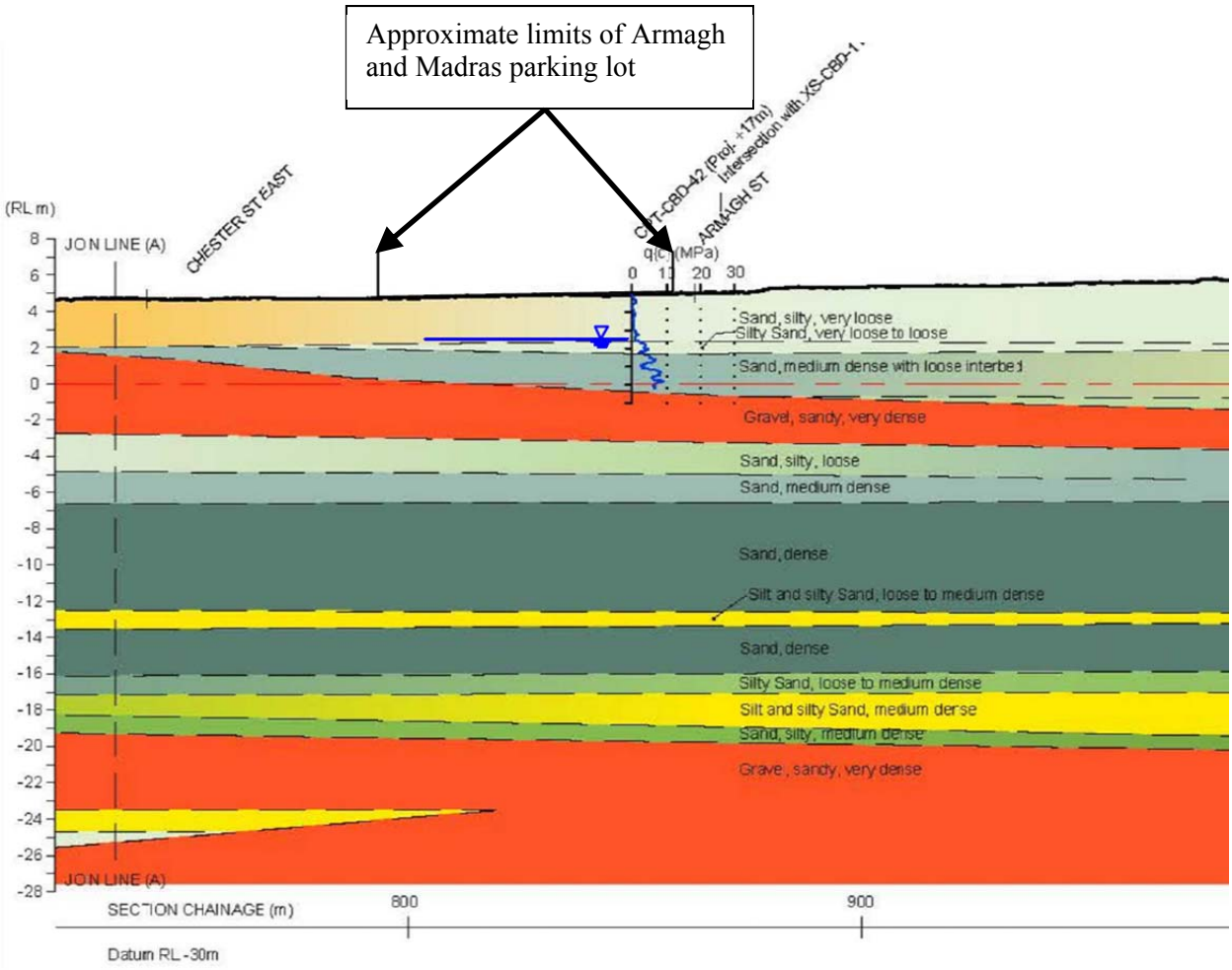

Figure 4.2.6. Portion of Tonkin & Taylor geologic cross section GXS-CBD-4, along Madras Street (Tonkin & Taylor, 2011). The limits of the Armagh and Madras parking lot have been projected on the cross section for reference.

Based on the regional interpretation by T&T shown in figures 4.2.5 and 4.2.6, the subsurface profile at the Armagh and Madras parking lot should consist of 3 – 4 meters of loose to very loose sands and silty sands underlain by approximately 1.5 to 2.5 meters of medium dense sand with interbedded loose deposits. These materials should be underlain by 2 to 3 meters of very dense sandy gravels. The subsurface profile should then consist of loose to dense sands and silty sands until the dense Riccarton Gravels are encountered at a depth of approximately 25 meters.

While the T&T cross sections are informative in the regional sense, they are constrained locally by a single CPT (CPT CBD-42) at the southwest corner of the parking lot. In order to obtain better resolution of the subsurface conditions in this area, 15 CPTs were performed at a spacing of about 10 m. Details of the CPTs are provided in Table 4.2.1 and the locations are indicated in Figure 4.2.7. Figures 4.2.8 and 4.2.9 illustrate the corrected tip resistance, q_t, the I_c-based layering, and the materials that likely liquefied during the 22 FEB 11 earthquake along cross sections A-A' and B-B', respectively.

Table 4.2.1. Summary of CPTs performed in parking lot adjacent to the CTUC Building.

Test ID	Test Type	Surface Elevation† (m)	Refusal Depth (m)
Z4-1	CPTu	5.2	19.11
Z4-8	CPTu	5.0	15.12
Z4-9	CPTu	4.9	5.53
Z4-14	CPT	n/a	6.88
Z4-15	CPT	n/a	6.56
Z4-16	CPT	n/a	2.82
Z4-17	CPT	n/a	3.03
Z4-18	CPT	n/a	6.54
Z4-19	CPT	n/a	5.70
Z4-20	CPT	n/a	5.33
Z4-22	CPT	n/a	3.55
Z4-23	CPT	n/a	3.10
Z4-24	CPT	n/a	13.40
Z4-25	CPT	n/a	9.28
Z4-26	CPT	n/a	18.95

†Indicated surface elevations are referenced from the Lyttelton Vertical Datum in meters above sea level and were provided by Tonkin & Taylor.

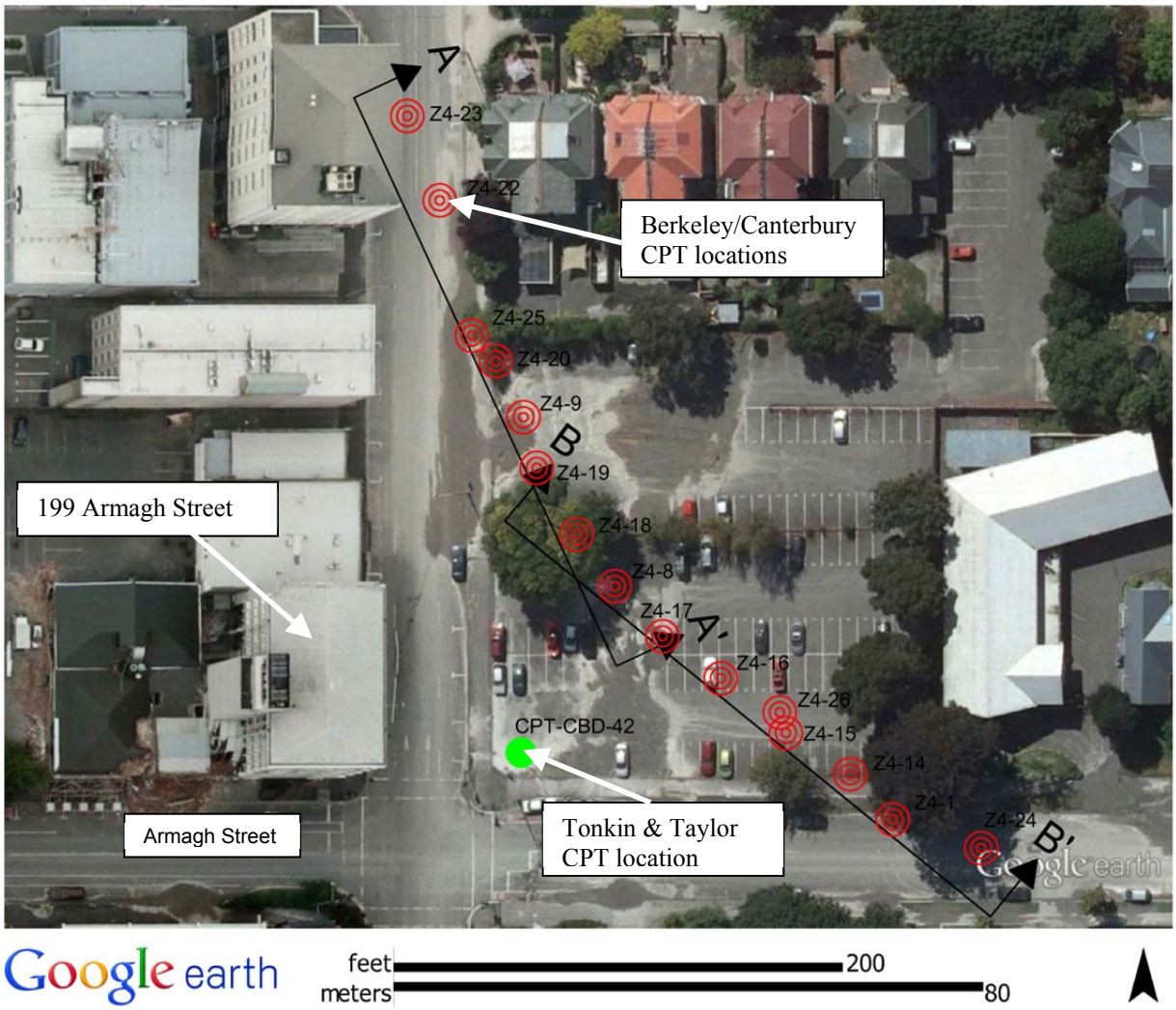

Figure 4.2.7. CPT location plan and orientation of engineering cross sections at the Armagh and Madras parking lot. Note the background aerial photograph was taken 24 February 2011 by New Zealand Aerial Mapping.

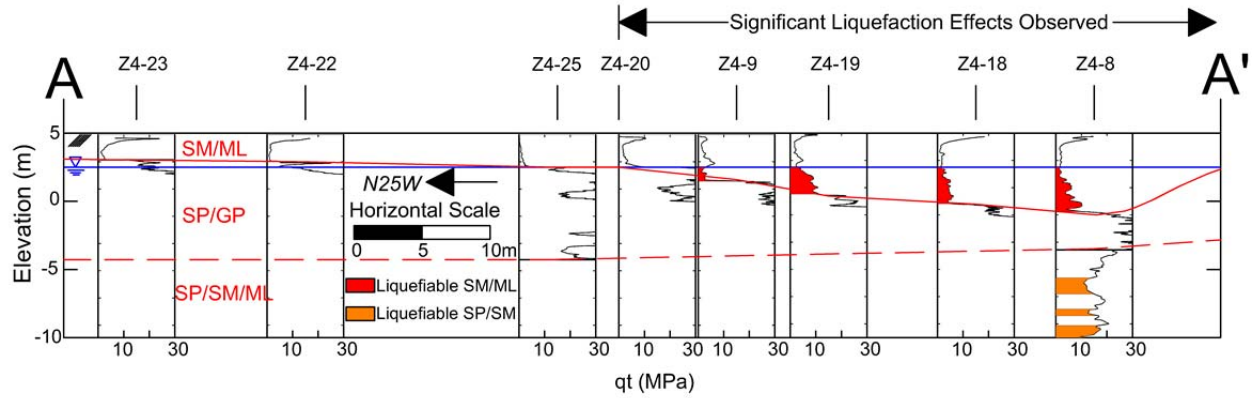

Figure 4.2.8. CPT tip resistance profiles at CPT locations within the Armagh Street and Madras Street parking lot as projected on cross section A-A'. The variability in the thickness of the shallow SM/ML layer is shown clearly between CPTs Z4-20 and Z4-8. Red and orange shading indicates materials with $FS_l < 1.0$ based on the RW98 procedure using PGA_{50} from Bradley and Hughes (2012) for the 22 FEB 11 earthquake.

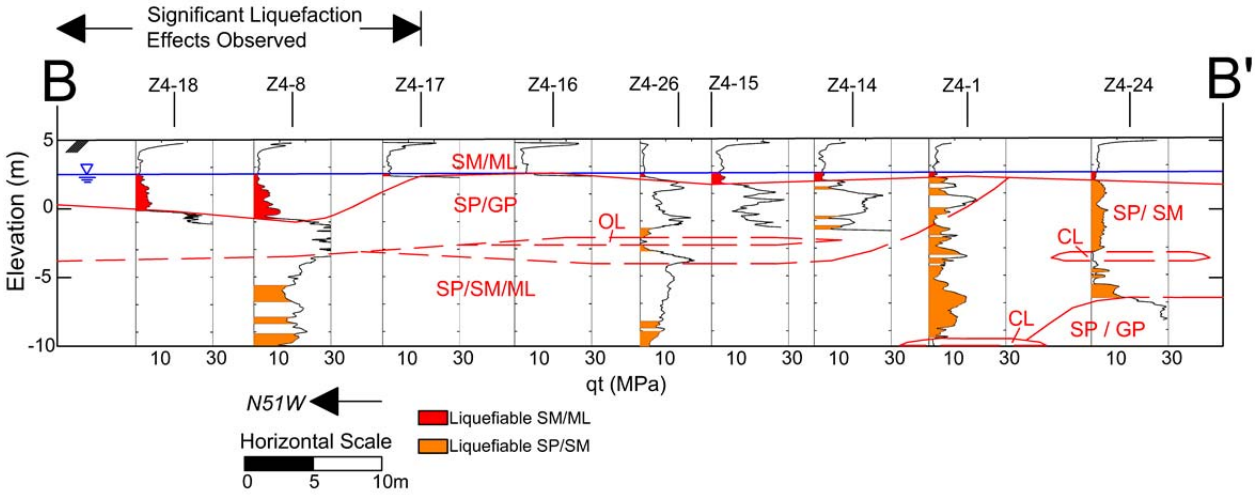

Figure 4.2.9. CPT tip resistance profiles at CPT locations within the Armagh Street and Madras Street parking lot as projected on cross section B-B'. The variability in the thickness of the shallow SM/ML layer is most pronounced between CPTs Z4-8 and Z4-17. Red and orange shading indicates materials with $FS_l < 1.0$ based on the RW98 procedure using PGA_{50} from Bradley and Hughes (2012) for the 22 FEB 11 earthquake.

As observed in Figures 4.2.8 and 4.2.9, the shallowest layer is composed of silty sand and sandy silt (SM/ML) with q_t generally less than 5 MPa and normalized soil behavior type indices, I_c, generally between 2.0 and 2.5. Samples from a nearby borehole indicated a fines content of about 50% for this layer. The next layer was a clean sand to gravelly sand (SP) with q_t greater than 20 MPa and often greater than 30 MPa and I_c between 1.0 and 1.5. Clean to silty sands and

sandy silts of varying penetration resistance, but typically with q_t greater than 10 MPa, followed the dense SP layer. Variable layer thicknesses are common throughout the site. While this is not surprising given the depositional environments of the Springston and Christchurch Formation sediments (Section 4.1), it reinforces the importance of performing site-specific investigations within the CBD as these variations would not be possible to detect with regional data only (e.g., Figs. 4.2.5 and 4.2.6).

Analyses and Observations

Based on the T&T groundwater models (Canterbury Geotechnical Database, 2013), the groundwater depth was likely 2.5 m below the ground surface during the 2010-2011 Canterbury earthquakes. The portion of the shallowest layer that was below the groundwater table should have liquefied based on the median PGA during the 22 FEB 11 event using any of the RW98, MS06, or IB08 liquefaction triggering procedures (e.g., Figs. 4.2.8 and 4.2.9). The resulting post-liquefaction vertical settlements using the ZR02-RW98 procedure within this layer decreased from a local maximum of about 10 cm in the middle of the significant liquefaction feature to zero over a total width of 45 m, which is consistent with the dimensions of the surficial depression in this area documented by Cubrinovski et al. (2011a). Consequently, the shallow liquefiable SM/ML layer, when it existed, was likely a critical layer in the observed liquefaction in Zone 4, and in other zones with similar stratigraphy. Its thickness below the water table could vary considerably over relatively short distances.

It is also notable that the settlement estimates at CPT Z4-14 are between 3 and 5 cm, depending upon the PGA value (i.e., PGA_{16}, PGA_{50}, or PGA_{84}, from Bradley and Hughes, 2012) while the settlement estimates at the adjacent CPT Z4-1 test location are between 20 and 30 cm. The approximate center to center distance between these locations is 8.5 meters. Without any further consideration, one would expect rather significant differential ground settlements over this distance. However, refusal was encountered at a depth of 6.88 meters at Z4-14 versus 19.11 meters at Z4-1 and much of the settlement at Z4-1 appears to be from materials at depths between 5 meters and 16.5 meters. Therefore, while the ZR02-RW98 analyses indicate that there would be a significant differential settlement between Z4-14 and Z4-1, it is likely that this is an artifact of performing these analyses over differing total depths because there were not drastic differential settlements observed at the ground surface in this area. For example, if only the shallowest 7 m are considered at CPT Z4-1, the ZR02-RW98 settlements are between 6 and 8 cm. Consequently, in subsequent analyses using the CPTs near buildings, a baseline depth will be selected to facilitate comparison between ZR02-RW98 settlements.

4.3 Engineering Performance of the CTUC Building

Introduction

The CTUC building, located at 199 Armagh Street in Christchurch, New Zealand (Lat -43.52855, Lon 172.64247), was a six-story, reinforced concrete (RC) frame structure, with a complex shallow foundation (Figures 4.3.1 and 4.3.2). The building was located only 20 m west of the Armagh and Madras parking lot discussed previously. Large differential settlements

during the 22 FEB 11 earthquake caused structural distortions and cracking (Cubrinovski et al. 2011a, Giorgini et al., 2011b) and the building was subsequently demolished. This section briefly describes relevant aspects of the structural design of the CTUC building, details the results of CPTs performed around the building footprint, and documents observations and measurements taken in July and August 2011, following the 22 FEB 11 and 13 JUN 11 events.

Figure 4.3.1. Photo of the CTUC building taken prior to Canterbury earthquake sequence (photo courtesy of L. Wotherspoon)

Figure 4.3.2. Photo of the CTUC building taken in July 2011, following several damaging earthquake events (photo courtesy of M. Taylor).

Structural Design

Based on its 1974 design drawings, the building frame was largely supported on shallow footings interconnected with tie beams (Figure 4.3.3). Six square footings were 2.44 by 2.44 m and were either 0.46 m or 0.61 m deep, and the two footings at the south end were 4.88 m by 0.91 m and 0.46 m deep. Each of these footings supported single rectangular RC columns that were spaced approximately 4.9 m and 9.1 m in the N-S and E-W directions, respectively. A larger footing on the west side of the building supported two rectangular RC columns in addition to the walls associated with the elevator and stair core, and strip footings supported core walls at the SW corner of the building and a block wall on its northern end. Adjacent footings were connected with RC tie beams that had cross sectional areas of either 0.74 m^2 or 0.12 m^2. Floors two through six were RC and were supported by RC beams 0.41 m wide by 0.61 m deep. Footing contact pressures for the effective seismic building weight were likely 100 – 200 kPa.

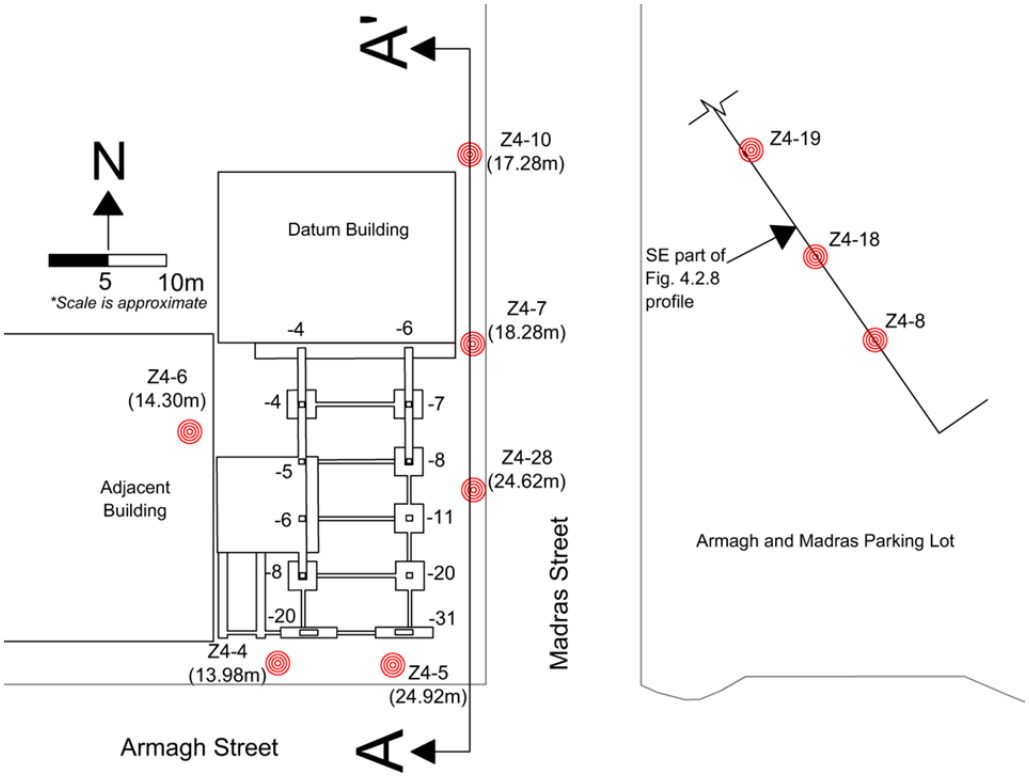

Figure 4.3.3. CTUC building site with its foundation system and CPT locations (with depths). Footing settlements at column locations relative to the datum building are provided in cm. The location of the subsurface profile in Figure 4.2.8 is shown for reference.

Site Characterization

Six CPTs were performed at the CTUC building site, in addition to the 15 CPTs performed at the nearby Armagh and Madras parking lot site that were used to develop the subsurface profiles shown previously in Figures 4.2.8 and 4.2.9. The locations of the CPTs at the CTUC building site are indicated on Figure 4.3.3 and details of these CPTs are provided in Table 4.3.1.

The generalized subsurface conditions along the east side of the CTUC building are depicted in Figure 4.3.4. The groundwater depth was estimated to be 2.5 m for the 4 SEP 10, 26 DEC 10, and 22 FEB 11 events, and 2.0 m for the 13 JUN 11 event based on the T&T groundwater models. The shallow SM/ML layer is similar to the upper unit described at the Armagh and Madras parking lot (Section 4.2) and had $q_t < 3$ MPa, $2 < I_c < 2.5$, and non-plastic FC $\approx$ 50%, which makes it likely to liquefy under strong ground shaking. It is noteworthy that this unit was observed at CPT Z4-5, which is at the SE corner of the building (Figure 4.3.3), to a depth of nearly 6 m; whereas it was not observed at CPT Z4-28 near the center of the east side of the building, CPT Z4-7 at the NE corner of the building, or below the groundwater table at CPT Z4-10.

Table 4.3.1. Summary of CPTs performed adjacent to the CTUC Building.

Test ID	Test Type	Surface Elevation† (m)	Refusal Depth (m)
Z4-4	CPTu	4.9	13.98
Z4-5	CPTu	4.9	24.92
Z4-6	CPTu	5.2	14.30
Z4-7	CPTu	4.8	18.28
Z4-10	CPTu	4.8*	17.28
Z4-28	CPTu	4.9	24.62

†Indicated surface elevations are referenced from the Lyttelton Vertical Datum in meters above sea level and were provided by Tonkin & Taylor.
*The elevation of CPT Z4-28 based on interpolation between Z4-7 and Z4-5.

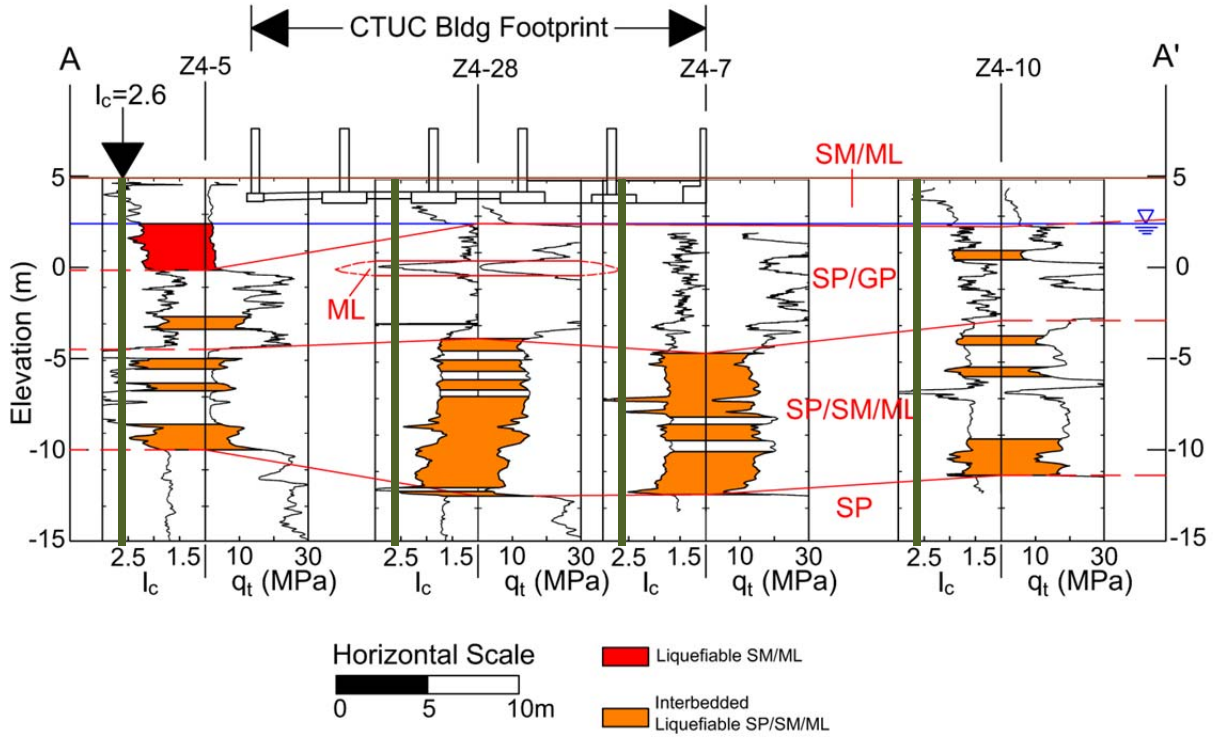

Figure 4.3.4. Subsurface conditions at the CTUC building site showing zones of materials with $FS_l < 1.0$ based on the RW98 procedure using PGA_{50} from Bradley and Hughes (2012) for the 22 FEB 11 earthquake.

Performance Observations and Analyses

While damage to the CTUC building was negligible during the 4 SEP 10 and 13 JUN 11 events, severe liquefaction of the foundation soils during the 22 FEB 11 earthquake induced significant total and differential settlements of the building, leading to structural distortions and cracking (Cubrinovski et al. 2011a). The building tilted to the east 0.4 – 0.5 degrees (Figure 4.3.5a). Differential settlement of the SE corner of the building produced most of the structural damage. Several of the exposed beams on the south side of the building were cracked near the beam-column connections (Figure 4.3.5b). Building settlement measurements were performed using the building located just to the north of the CTUC building as the datum, as it did not appear to displace relative to the surrounding ground. The settlement measurements are indicated on Figure 4.3.3. The building settled more on its south side than on its north side and more on its east side than its west side. Approximately 20 of the 25 cm of differential building settlement along the eastern side of the building was measured across its two southernmost spans (angular distortion ≈ 1/50). Thus, cracking of structural beams in this area is not surprising.

Figure 4.3.5. (a) South end of CTUC Building showing tilt to the east (taken July 2011) and (b) Close-up photograph of the SE corner of the building (taken March 2011).

Simplified liquefaction evaluations were performed utilizing the procedures described previously. From examining Figure 4.3.4, it is clear that while there are liquefiable soils at each of the CPT locations, the distinguishing difference between them is that CPT Z4-5 indicates that there are shallow liquefiable soils just beneath the building foundation whereas the liquefiable soils at CPTs Z4-28, Z4-7, and Z4-10 are located primarily at depths below 8 m. The dramatic change in the shallow soil conditions from the building's north end, which did not contain

shallow liquefiable soils, to its south end, which contained shallow liquefiable soils, led to the significant differential settlement over the southernmost spans of the building frame.

The calculated FS_l profiles for four events using the RW98 procedure with PGA_{50} from Bradley and Hughes (2012) are presented in Figure 4.3.6. Low FS_l values were calculated in the shallow SM/ML layer for the intense 22 FEB 11 earthquake, wherein severe liquefaction was observed at the site. However, FS_l values below one were also calculated for the 4 SEP 10 and 13 JUN 11 events. Although there were no reports of liquefaction at this location after these events, it is possible that a minor amount of liquefaction was unreported or that marginal liquefaction occurred and surface manifestations were not observed. Damage was not reported for these events, so if liquefaction did occur its effects were not significant. Liquefaction triggering procedures are deliberately conservative, so it is possible that liquefaction did not occur at this site although the calculated FS_l values were below one.

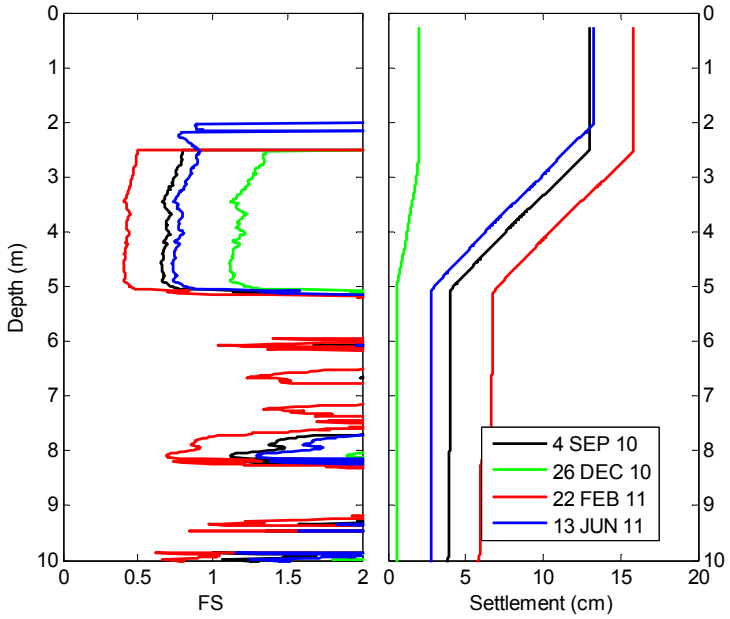

Figure 4.3.6. FS against liquefaction triggering and settlement due to post-liquefaction volumetric strain profiles at CPT Z4-5 using ZR02-RW98 and PGA_{50} from Bradley and Hughes (2012).

The post-liquefaction residual shear strength of the shallow SM/ML layer was estimated to be 6 kPa to 10 kPa using the Olson and Stark (2002) and IB08 procedures. The bottom of the SE footing adjacent to CPT Z4-5 was at a depth of about 1.3 m. The static bearing capacity of the foundation soils at this location can be estimated using procedures developed for a two-layer cohesive soil deposit (Naval Facilities Engineering Command, 1986). The FS against a bearing capacity failure is 2.1 to 2.3 at the location of the SE corner footing, which was judged to be most critical, using the residual shear strength of the shallow liquefiable SM/ML materials and an equivalent undrained shear strength of the SM/ML materials above the groundwater table. If the materials above the groundwater table lost strength due to the upward migration of liquefied

soil, then the FS is below one. The SE may have underwent a partial bearing capacity failure, but its differential settlement was largely the result of ground loss due to sediment ejecta and some contribution of other settlement mechanisms described by Bray and Dashti (2010), because bulging of the ground surface was not observed at this site.

Liquefaction-induced free-field level ground settlements at the locations of the CPTs were calculated based on the post-liquefaction volumetric strain ZR02-RW98 procedure discussed previously. The upper 17 m of the soil deposit was considered in these calculations and the results are summarized in Table 4.3.2. Calculated settlements due to post-liquefaction volumetric strains during the 22 FEB 11 earthquake range from 16 cm to 10 cm across the footprint of the CTUC building (i.e., CPTs Z4-5, Z4-28, and Z4-7). Hence, free-field vertical settlements due to post-liquefaction volumetric strains suggest a differential settlement of only about 6 cm across the building. However, the building actually settled differentially 25 cm more at its south end than at its north end for this event. The presence of the shallow loose SM/ML layer beneath the groundwater table, as depicted in CPT Z4-5 at the SE corner of the building, likely led to the significant differential settlement of the building across its two southernmost spans. Ground loss under the shallow foundations due to sediment ejecta and shear-induced mechanisms, such as SSI-ratcheting, likely contributed to larger settlements at the SE corner of the CTUC building. Liquefaction of soils below a depth of 8 m contributed significantly to the amount of calculated settlement, but their impact on the building performance appears to have been relatively minor. Thus, the equal weighting of post-liquefaction volumetric strains over all depths of the soil profile in the calculation of free-field vertical settlements can be misleading when this approach is used to evaluate the performance of buildings with shallow foundations.

Table 4.3.2. Calculated surface settlements at CPT locations near the CTUC Building. Settlements are due to post-liquefaction volumetric strains in the top 17 m and based on median PGA estimates.

CPT ID	Reconsolidation Settlement (cm)			
	4 SEP 10	26 DEC 10	22 FEB 11	13 JUN 11
Z4-5	13	2	16	13
Z4-7	2	0	10	1
Z4-10	2	0	7	1
Z4-28	10	3	16	9

Whereas the ZR02-RW98 procedure underestimated liquefaction-induced building settlement due to the 22 FEB 11 earthquake, it overestimated the observed settlement for the 4 SEP 10 and 13 JUN 11 earthquakes. Liquefaction triggering evaluation procedures are typically conservative. The calculation of $FS_l < 1.0$ for the 4 SEP 10 and 13 JUN 11 events leads to post-liquefaction settlements at CPT Z4-5 that are close to that calculated for the 22 FEB 11 event due to the sensitivity of the ZR02 procedure when the FS_l is near one. Severe liquefaction and significant damage were observed for the latter event, but not for the former events, so commonly used procedures are not able to discriminate between these events for this case. Post-liquefaction settlement estimates provide only a rough index of seismic performance. Engineering judgment is required in interpreting their results.

ZR02-RW98 analyses were performed using median, 16%, and 84% PGA estimates to capture the aleatory uncertainty in earthquake ground shaking at the CTUC building site. The resulting surface settlements at CPT Z4-5 ranged from 9 cm to 15 cm for the 4 SEP 10 earthquake, 14 cm to 17 cm for the 22 FEB 11 earthquake, and 3 cm to 16 cm for the 13 JUN 11 earthquake. The sensitivity of the surface settlement at CPT Z4-5 to the 16% PGA estimate during the 13 JUN 11 event is due to the resulting FS_l in the critical SM/ML layer being slightly greater than one for this seismic demand; as described previously, ZR02 settlement calculations are sensitive to minor changes in the FS_l when it is near one.

4.4 Engineering Performance of the SA Building

Introduction and Structural Design

The SA building, located at 193 Peterborough Street in Christchurch, New Zealand (S43.5252 E172.6419), was a two-story RC frame structure with concrete infilled walls, interior timber-framed walls, and timber flooring that was 15 m by 30 m in plan with two bays in the E-W direction and six bays in the N-S direction (Figure 4.4.1). The building was remodeled in 1997-98, during which time the two southernmost first floor bay frames were removed to create an exterior parking area and replaced with a more robust RC frame. In addition, several of the pre-existing frames were retrofitted with steel K-bracing. It appears that the original building was founded on a grid of shallow strip footings that were approximately 0.5 m wide and 0.6 m deep. The new shallow square footings within the southernmost two bays were either 1.5 m by 1.5 m or 3.3 m by 3.3 m and were 0.6 m thick. The footings were cast in place under the pre-existing foundation tie beams at a depth of approximately 1.4 m below the ground surface.

Figure 4.4.1. Photo of the SA building taken in March, 2011. Photo was taken from the NW and is viewing SE.

Site Characterization

Five CPTs were performed at the SA building site at the locations indicated on Figure 4.4.2. Details of the CPTs are provided in Table 4.4.1. The subsurface conditions along the length of the building (i.e., cross section A-A') are illustrated in Fig. 4.4.3. The site consists of a shallow SM/ML/SP layer to a depth of 1.5 – 2.5 m with $q_t < 5$ MPa and $2 < I_c < 2.5$ similar to the shallow SM/ML layer observed at the CTUC and Armagh-Madras sites, which is underlain predominantly by sands, gravelly sands, and sandy gravels (SP/GP) with significantly higher tip resistance until refusal was encountered. A layer of SM/ML/SP with $q_t \leq 10$ MPa was encountered between depths of 5.3 m and 9.1 m at CPT Z8-6. This layer was not observed at CPTs Z8-14 and Z8-15. The groundwater depth at the SA site was about 1.5 m throughout the Canterbury earthquake sequence (Canterbury Geotechnical Database, 2013).

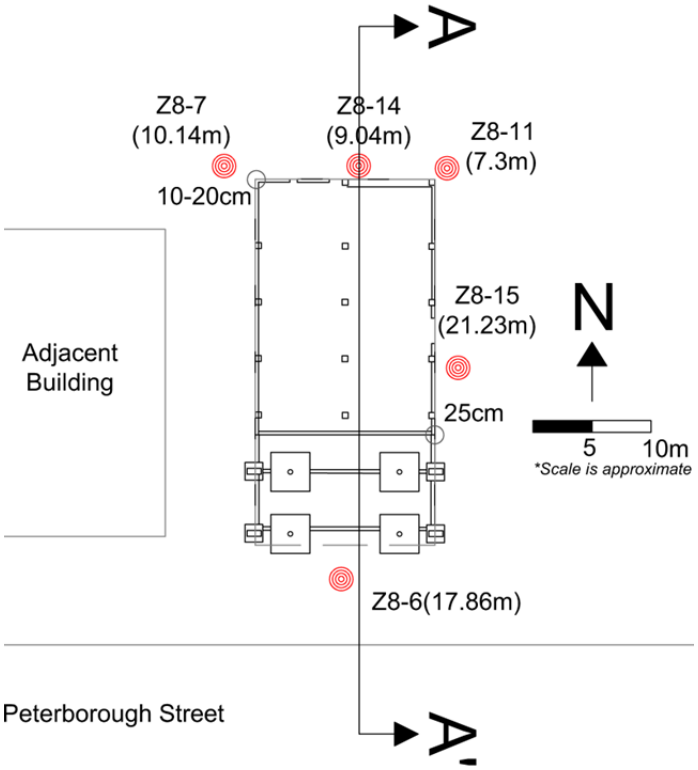

Figure 4.4.2. SA building site with its foundation system and CPT locations (with depths). Building settlements are relative to the surrounding ground and are provided in cm.

Table 4.4.1. Summary of CPTs performed adjacent to the SA building. Indicated surface elevations are referenced from the Lyttelton Vertical Datum in meters above sea level and were provided by Tonkin & Taylor for Z8-6, Z8-7, and Z8-11. Surface elevations for Z8-14 and Z8-15 are based on interpolation.

Test ID	Test Type	Surface Elevation (m)	Refusal Depth (m)
Z8-6	CPTu	4.4	17.86
Z8-7	CPTu	4.6	10.14
Z8-11	CPTu	4.5	7.30
Z8-14	CPTu	4.5	9.04
Z8-15	CPTu	4.4	21.23

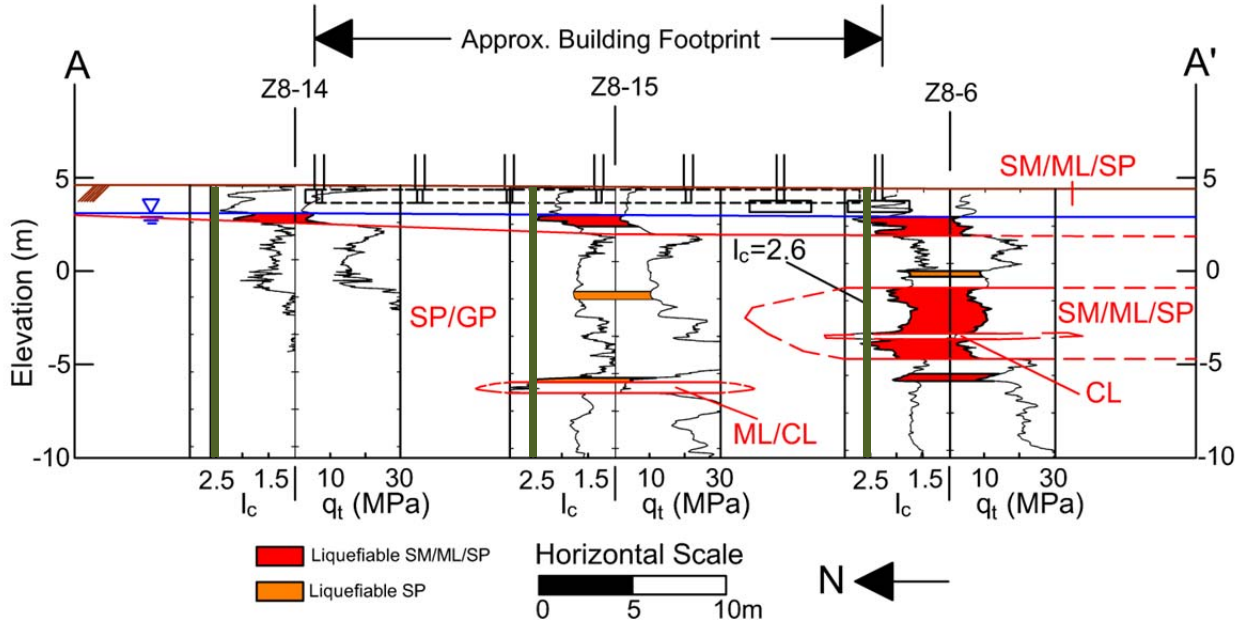

Figure 4.4.3. Subsurface conditions at the SA building site showing zones of materials with FS_l < 1.0 based on the RW98 procedure using PGA_{50} from Bradley and Hughes (2012) for the 22 FEB 11 earthquake.

Performance Observations and Analyses

Liquefaction occurred at the site during the Darfield earthquake (Ruamoko Solutions, 2010). While it was judged that there was no significant damage to the building's primary structural system from this event, there was sediment ejecta observed at the ground surface around the building perimeter and in the elevator shaft. Post-event inspections revealed ground cracks and surface depressions at the site, along with a "bulge" at the front of the building that they judged was likely caused by upward moving liquefied sediment that was trapped by an

overlying, well compacted, surface layer. Minor amounts of fresh sediment ejecta were also observed around the building perimeter following the 13 JUN 11 earthquake.

Liquefaction was far more severe and damaging during the Christchurch earthquake. Figure 4.4.4 illustrates severe ground cracking in the road south of the building and the extent of the ejected groundwater pond near the entrance of the building, which was reported to be 0.5 m deep, as well as the extent of liquefaction just north of the building. The building was surveyed by UCB-UC researchers in March 2011 and again in July 2011. During the March 2011 survey, Cubrinovski et al. (2011a) observed nearly continuous sediment ejecta around the perimeter of the building and evidence of its foundation displacing downward into the surrounding ground with the ground floor at the south entrance of the building uplifted and blistered. The building settled approximately 25 cm relative to the surrounding ground at its SE corner and approximately 10-20 cm at its NW corner. The locations of these settlements are indicated on Figure 4.4.2. Due to this damage, the building was demolished in 2012.

Figure 4.4.4. (a) Views of the south end and (b) north end of SA building taken approximately 2 hours after the Christchurch earthquake. (c) Photo of the east side of the building taken June 5th, 2011. (Photos courtesy of Shipleys Audiovisual Ltd.)

Zones of materials with $FS_l < 1.0$ using the median PGA during the Christchurch earthquake are indicated in Fig. 4.4.3. Consistent with previous evaluations, the critical liquefiable layer is the shallow SM/ML/SP unit when below the water table. The calculated FS_l profiles for all four events at CPT Z8-7 are presented in Fig. 4.4.5 using the median PGA estimates. As with CPT Z8-6, there is also a deeper layer of liquefiable SM/ML/SP at CPT Z8-7 (between depths of approximately 4 m and 6 m), and this deeper layer contributes significantly to the calculated ZR02-RW98 settlements (Fig. 4.4.5). The FS against bearing failure was calculated using the procedures described previously. It is likely that the FS against bearing capacity failure was near or below 1.0 at the southern end of the building due to the weakened state of the liquefied shallow SM/ML/SP materials. Consequently, a bearing capacity failure mechanism likely contributed to the observed foundation punching, though the effects of ground loss due to sediment ejecta were clearly evident and other displacement mechanisms noted in Bray and Dashti (2010) could have also occurred.

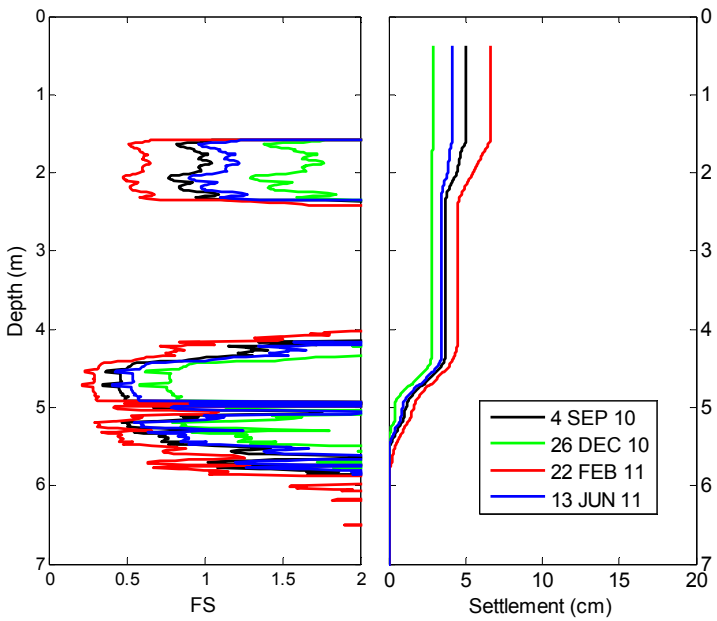

Figure 4.4.5. FS against liquefaction triggering and settlement due to post-liquefaction volumetric strain profiles at CPT Z8-7 using ZR02-RW98 and PGA_{50} estimates from Bradley and Hughes (2012).

The free-field, level ground settlement estimates due to post-liquefaction volumetric strains over the upper 10 m of the soil deposit using the ZR02-RW98 procedure are summarized in Table 4.4.2. Once again, the calculated settlements during the Christchurch earthquake are not much higher than those for the Darfield and June 2011 events. The settlements calculated at CPTs Z8-11, Z8-14, and Z8-15 are low for all events, because the deeper layers of liquefiable SM/ML/SP materials observed at CPTs Z8-6 and Z8-7 were not present. Significant amounts of sediment ejecta were observed in the vicinity of CPT Z8-11 after the Christchurch earthquake, and the building underwent a punching failure in this area. Whereas the only liquefiable materials in the upper 7.3 m at this location appear to be the 0.7 m-thick shallow SM/ML/SP materials, the observed sediment ejecta and building punching indicate that the effects of liquefaction of these materials were far more severe than what is suggested using post-liquefaction volumetric reconsolidation procedures intended for free-field applications. These procedures give equal emphasis to liquefaction-induced volumetric strains throughout the soil profile; when in fact, liquefaction-induced movements of shallow foundations are dominated by shallow soil layers that liquefy, especially if these soils are removed beneath the foundation through the development of sediment ejecta.

Table 4.4.2. Calculated surface settlements at CPT locations near the SA building. Settlements are due to post-liquefaction volumetric strains in the top 10 m and based on median PGA estimates.

CPT ID	Reconsolidation Settlement (cm)			
	4 SEP 10	26 DEC 10	22 FEB 11	13 JUN 11
Z8-6	5	1	9	3
Z8-7	5	3	7	4
Z8-11*	2	0	2	1
Z8-14*	0	0	1	0
Z8-15	2	0	3	1

* Refusal was encountered at depths of 7.3 m and 9.0 m for CPTs Z8-11 and Z8-14, respectively.

4.5 Engineering Performance of the PILE-6, FTG-7, and FTG-4 Buildings

Introduction and Structural Design

There were three multi-story buildings with different foundation types located close to each other in Zone 1. The buildings were located within an area marked as an old stream channel on the "Black Maps" (Cubrinovski et al. 2011a) and there was minor surficial evidence of liquefaction in this area following the 4 SEP 10 earthquake, severe and extensive liquefaction during the 22 FEB 11 earthquake, and moderate liquefaction during the 13 JUN 11 earthquake. Photographs of the buildings are shown in Fig. 4.5.1, and the site plan shown in Fig. 4.5.2 depicts the buildings and adjacent buildings with the locations of the CPTs and a soil boring.

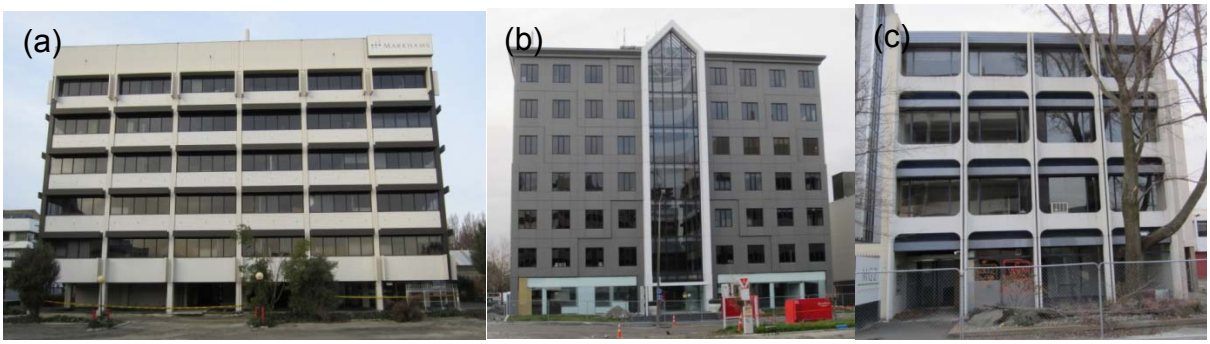

Figure 4.5.1. Zone 1 Building Group: (a) PILE-6 (S43.5268 E172.6386), (b) FTG-7 (S43.5263 E172.6384), and (c) FTG-4 buildings (S43.5263 E172.6387).

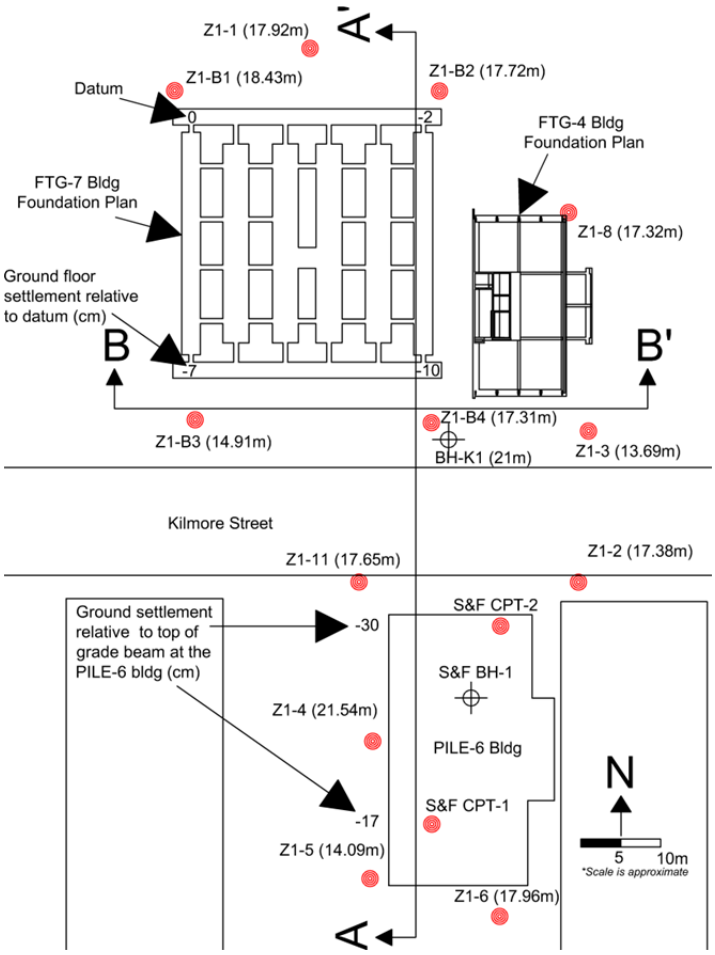

Figure 4.5.2. Zone 1 CPT locations, and shallow foundation plans for FTG-7 and FTG-4 buildings.

The "PILE-6" building, located at 144 Kilmore Street (S43.5268 E172.6386), was a six-story frame structure that was 18 m wide in the E-W direction and 34 m long in the N-S direction. Two CPTs and one borehole were performed in 1987 before the building was constructed (see Fig. 4.5.2; Soils & Foundations (1973) Ltd., 1987) and revealed very loose to loose sands, silty sands, and sandy silts to a depth of 12 m, with another loose layer under the northern part of the site between depths of 15 m and 17 m. The groundwater table was encountered at a depth of 2 m. The geotechnical consultant noted that much of the soil profile was liquefiable and recommended a mat foundation in combination with ground improvement or a pile foundation with toe depths of 12-14 m or 18 m, depending on local variations in the soil conditions. The constructed building's foundation consisted of 275 mm square piles interconnected with grade beams.

The "FTG-7" building, located at 151 Kilmore Street (S43.5263 E172.6384), was a

seven-story steel-framed structure (approved in 1987) that was 29 m wide in the E-W direction and 32 m long in the N-S direction and located across the street from the PILE-6 building. Its foundation consisted of shallow RC strip footings, between 2 m and 3.3 m wide and 0.6 m deep, interconnected with square RC tie beams that had a cross sectional area of 0.36 m^2 (Fig. 4.5.2). The base of the perimeter strip footings was 1.2 m deep, and the base of the interior strip footings was 0.7 m deep. The first floor perimeter wide-flange steel columns of the building were encased in concrete. The ground floor consisted of 10 cm-thick unreinforced concrete and floors two through seven consisted of 12 cm-thick RC over 0.75 mm galvanized steel decking. The exterior walls were composed of pre-cast RC wall panels.

The "FTG-4" building, located at 155 Kilmore Street (S43.5263 E172.6387), was a four-story RC framed structure (approved in 1972) that was 15 m wide in the E-W direction and 23 m long in the N-S direction and located adjacent to the FTG-7 building. Its foundation consisted of shallow RC strip footings interconnected with square RC tie beams with a cross-sectional area of 0.09 m^2. The strip footings were typically between 0.6 and 0.85 m wide and 0.35 and 0.6 m thick. In addition to the RC framing elements, the structure also contained parallel concrete block walls that extended from the floor to the roof (approximately 12.2 m), which were oriented in the N-S direction along the eastern and western edges of the building. Floor slabs consisted of 10 cm-thick concrete for the ground floor and 12 cm-thick RC for the upper floors.

Site Characterization

Twelve CPTs and one borehole were performed in the vicinity of these buildings (Fig. 4.5.2). The log of borehole K1, along with the profile of the adjacent CPT Z1-B4, is shown in Fig. 4.5.3. Figures 4.5.4 and 4.5.5 present the corrected cone tip resistance and soil behavior type index profiles based on the CPTs performed along cross sections A-A' and B-B', respectively. While there is some variability in the ground conditions, the shallow subsurface generally consists of two predominant units: a) silty sands and sandy silts with q_t generally less than 5 MPa and I_c generally between about 2.0 and 2.5, and b) sands and silty sands with q_t generally less than 10 MPa and I_c generally between about 1.5 and 2.0. The groundwater depth was about 2.0 m throughout the earthquake sequence (Canterbury Geotechnical Database, 2013).

Figure 4.5.3. Log of borehole K1 and adjacent CPTZ1-B4 profile.

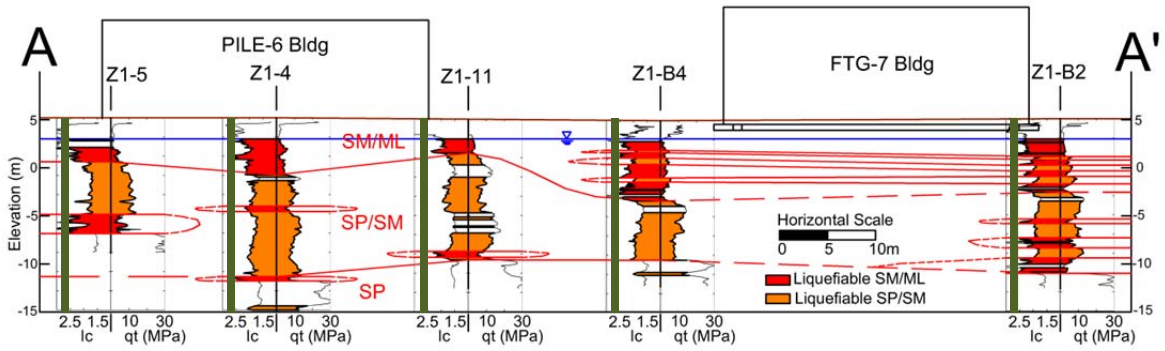

Figure 4.5.4. Subsurface conditions along section A-A' showing zones of materials with FS_l < 1.0 based on the RW98 procedure using PGA_{50} from Bradley and Hughes (2012) for the Christchurch earthquake.

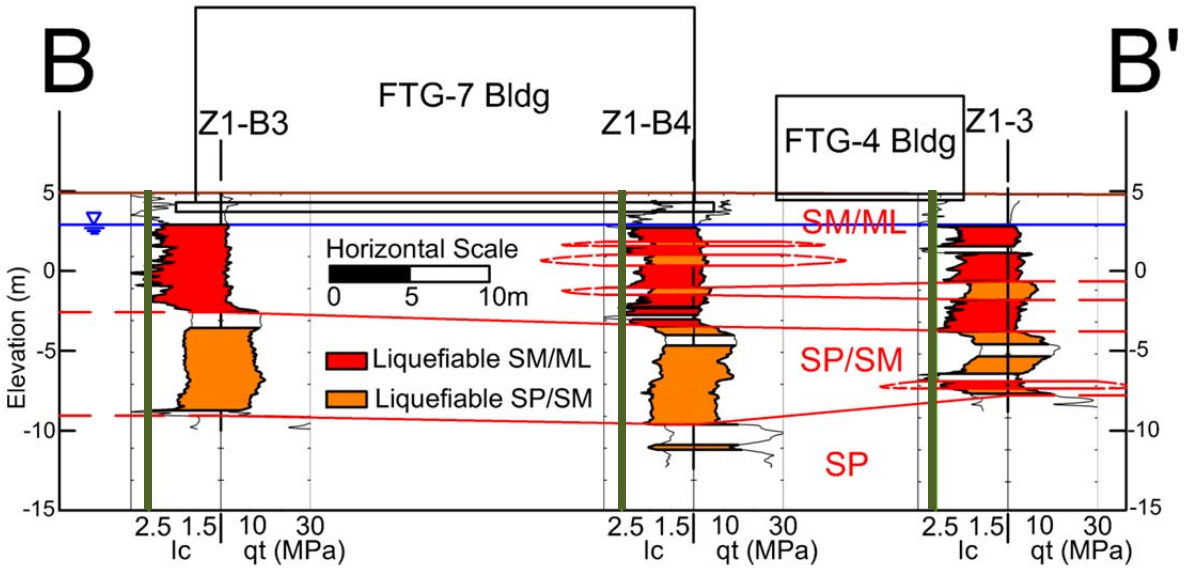

Figure 4.5.5. Subsurface conditions along section B-B' showing zones of materials with $FS_l < 1.0$ based on the RW98 procedure using PGA_{50} from Bradley and Hughes (2012) for the Christchurch earthquake.

Performance Observations and Analyses

Zones of materials with $FS_l < 1.0$ using the median PGA during the Christchurch earthquake are also indicated in Figs. 4.5.4 and 4.5.5. Significant liquefaction is calculated throughout much of the soil deposit for the Christchurch event. The FS against bearing failure was calculated using the procedures described previously, and the FS were estimated to be 1.4 for the southern strip footing of the FTG-7 building and 2.8 for the strip footing supporting the eastern block wall of the FTG-4 building. The free-field, level ground settlement estimates due to post-liquefaction volumetric strains over the upper 14 m of the soil deposit using the ZR02-RW98 procedure are summarized in Table 4.5.1. Significant settlements are estimated at most CPT locations as a result of the Darfield, Christchurch, and June 2011 events. Smaller, but non-zero, liquefaction-induced ground settlements are also calculated for the December 2010 event.

Table 4.5.1. Calculated surface settlements at some CPT locations in Zone 1. Settlements are due to post-liquefaction volumetric strains in the top 14 m and based on median PGA estimates.

CPT ID	Reconsolidation Settlement (cm)			
	4 SEP 10	26 DEC 10	22 FEB 11	13 JUN 11
Z1-B2	21	5	28	15
Z1-B3	17	6	24	14
Z1-B4	28	13	32	26
Z1-3	16	4	22	12
Z1-4	19	3	26	14
Z1-5	7	1	14	4
Z1-8	16	5	22	12
Z1-11	16	4	21	13

The ground settled approximately 30 cm and 17 cm relative to the north and south sides, respectively, of the PILE-6 building during the Christchurch earthquake (Cubrinovski et al. 2011a). Post-liquefaction volumetric reconsolidation settlements were calculated to be 21 cm, 26 cm, and 14 cm at the building's north end (CPT Z1-11), center (CPT Z1-4), and south end (CPT Z1-5), respectively, during the Christchurch earthquake using the ZR02-RW98 procedure. Assuming the pile-supported building did not settle significantly, ground settlements are underestimated slightly for the Christchurch earthquake. Conversely, ground settlements are overestimated for the Darfield earthquake. Despite the substantial ground settlements around the building, the first-story structural frame did not show significant damage.

The FTG-7 building, however, was damaged significantly during the Christchurch earthquake with evidence of damage to the structural columns at the ground level. A floor level survey performed in March 2011 indicated approximately 10 cm of settlement of the SE corner of the building relative to the datum at its NW corner (Eliot Sinclair and Partners Limited, 2011), and a subsequent building verticality survey (Beca Carter Hollings & Ferner Ltd., 2011a) confirmed the building was tilted to the S-SE. Relative settlements of the corners of the ground floor during this event are indicated on Fig. 4.5.2. As summarized by Beca Carter Hollings & Ferner Ltd. (2011a), additional floor level surveys were performed at the FTG-7 building following the 13 JUN 11 event. These surveys indicated an additional 3.5 cm of differential settlement of the SE corner relative to the NW corner. An additional survey following the 13 JUN 11 event was performed relative to city benchmarks. Total settlements relative to the city benchmarks at that time were estimated as 55 cm at the NW corner of the foundation and 70 cm at the SE corner. Based on regional tectonic models developed by GNS (Canterbury Geotechnical Database, 2012c), there had been approximately 10 – 15 cm of tectonic subsidence in the area of these buildings at the time of this survey, and it is unknown if these tectonic movements have been accounted for in the survey relative to city benchmarks. Consequently, there is a possibility that these surveyed settlements should be reduced 10 – 15 cm due to tectonic movements.

Post-liquefaction volumetric reconsolidation settlements from the Christchurch earthquake were calculated to be 25 cm at CPT Z1-B1, 28 cm at CPT Z1-B2, 24 cm at CPT Z1-B3, and 32 cm at CPT Z1-B4. Based on the observations of the settlement of the ground relative

to the PILE-6 building across the street, these estimates appear to be reasonable. However, the ground floor level survey indicated 7 cm of relative settlement of the SW corner (CPT Z1-B3) of the building to its NW corner (CPT Z1-B1). This differential settlement would not be estimated based on a direct comparison of the settlements calculated at CPT Z1-B1 and CPT Z1-B3.

The FTG-4 building was damaged significantly. A large amount of sediment ejecta was observed in the parking lot behind the building and in front of the building, as well as around and within the building footprint. The strip footings supporting the side block walls settled relatively more than the remainder of the building and the concrete slab on the ground floor was bowed up in the middle. Cracking was observed in several of the exposed concrete columns and in the concrete fascia on the north end of the building. The ground floor slab settled approximately 16 cm more at the building's NW corner than at its NE corner. Post-liquefaction volumetric reconsolidation settlements during the Christchurch earthquake were calculated to be 22 cm at both CPTs Z1-3 and Z1-8.

Thus, the three buildings in Zone 1 performed differently as a result of being located in an area of severe liquefaction during the Christchurch earthquake. The pile-supported building was comparatively less damaged than the two buildings that were supported on shallow foundations, though access to it was limited due to the significant settlement of the ground that surrounded it. The taller, but wider, FTG-7 building, underwent less differential settlement than the shorter and narrower FTG-4 building. The increased plan area of the FTG-7 building foundation may have also contributed to it undergoing less differential settlement than the FTG-4 building. Post-liquefaction estimates of ground settlement were reasonable for level ground settlement near the PILE-6 building, which likely did not settle significantly, for the Christchurch earthquake. However, settlements were overestimated for the other large earthquakes. Post-liquefaction volumetric strain-based methods do not capture the settlement of the buildings supported on shallow foundations, which also underwent shear-induced settlement and settlement due to ground loss from sediment ejecta. Moreover, post-liquefaction reconsolidation procedures should not be employed directly to estimate differential building settlement as is sometimes done in engineering practice.

4.6 Engineering Performance of the PWC Building

Introduction and Structural Design

The PWC building, located at 119 Armagh Street in Christchurch, New Zealand (Lat -43.52850, Lon 172.63788), was a 21-story, RC frame structure, with a one-story basement (Figure 4.6.1). Liquefaction-induced sediment ejecta was observed on both the north and south sides of the building following the Christchurch earthquake, and the tops of accessible structural columns were generally tilted slightly to the south. In addition, ground settlements of at least 30 cm were measured near the street on the north side of the building and areas of localized ground settlement of up to 10 - 15 cm were measured on the south side of the building. General ground settlements on the south side appeared to be less than approximately 10 cm. There was some lateral spreading of the ground north of the building toward the Avon River which could have contributed to the vertical ground displacements in this area. Prior to its demolition in 2012, the

PWC building was a landmark on the Christchuch skyline, as the third tallest building in the CBD; it was shorter than the Pacific Tower building and the Hotel Grand Chancellor.

Figure 4.6.1. Photo of the PWC Building Prior to the Canterbury Earthquake Sequence (from Colliers International New Zealand Ltd., 2009)

According to its 1988 design drawings, the PWC building consisted of a 21-story tower including a two-story podium atop a one-story basement with a RC mat foundation that transitioned in thickness from 0.4 m around the edges of the basement (podium slab), to 1.8 m underneath the perimeter of the tower, to 0.9 m underneath the center of the tower (Fig. 4.6.2). The basement footprint was approximately 55 m in the east-west direction and approximately 60 m in the north-south direction (including the irregular layout on the north end). The top of the basement mat was approximately 3.4 m below the ground surface at the south side of the building and approximately 2.4 m below the ground surface at the north side of the building. The tower was approximately 35 m in the east-west direction and 25 m in the north-south direction. Two elevator shafts were located in the center of the tower and the staircases were located just to the east of the easternmost elevator shaft.

Structural columns for the tower were typically cast-in-place RC columns with square or rectangular cross sections. The corner columns were 1.1 m by 1.1 m, perimeter columns were 0.8 m by 1.1 m, and interior columns were 0.7 m by 0.9 m or 0.7 m by 0.7 m. Column spacing was typically on the order of 6 m to 7 m. Beams were either pre-cast concrete with rectangular cross sections or steel I-beams. The dimensions of perimeter pre-cast concrete beams were usually 0.575 m by 1.1 m, 0.575 m by 0.975 m, or 0.8 m by 0.82 m. The dimensions of interior pre-cast concrete beams were typically 0.8 m by 0.7 m or 0.5 m by 0.585 m. While all of the perimeter

beams were pre-cast concrete, most of the interior beams were steel. Steel beam sections were either 530 UB 92, 530 UB 82, 460 UB 74, 410 UB 54, or 310 UB 46. Some of the interior beams within the first through third stories were pre-cast concrete whereas all interior beams within the fourth through the twenty-first stories were steel. Double Tee concrete flooring was utilized, typically with a 65 mm concrete topping.

Soils and Foundations Geotechnical Consulting Engineers performed the original geotechnical investigation prior to building construction in 1987. At that time, they estimated the average dead load transmitted through the mat foundation for bearing and settlement calculations as 11 kPa per story and the average reduced live load as 1.2 kPa per story. It appears that the basis for this assumption was known loadings for similar buildings in Christchurch. This would suggest an average load over the footprint of the mat foundation of approximately 255 kPa. Based on the self-weight of only the typical primary structural elements described above, it is likely that the average dead load over the footprint of the mat foundation under the tower was at least 140 kPa. Consequently, 255 kPa is a reasonable conservative estimate of the average foundation contact pressure of the PWC building tower structure during the Canterbury earthquakes.

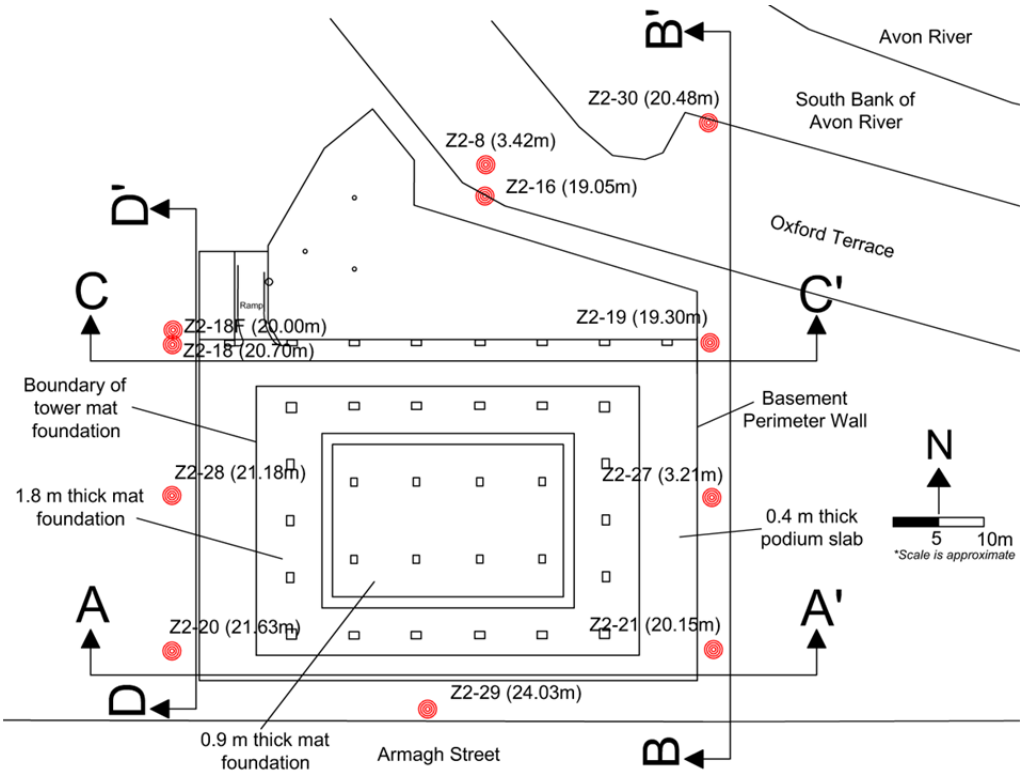

Figure 4.6.2. PWC Building site with foundation elements and CPT locations (with depths).

Site Characterization

Eight shallow hand-augered boreholes and seven deep cable-tool boreholes were performed by Soils and Foundations Geotechnical Consulting Engineers at the PWC building

site as part of the original geotechnical investigation prior to building construction in 1987 (Figure 4.6.3; Soils and Foundations Geotechnical Consulting Engineers, 1987). Based on a review of the boring logs, the subsurface profiles at the cable-tool borehole locations shown in Figure 4.6.3 generally consisted of loose silty fine to medium sand underlain by medium dense to dense sand, gravelly sand and/or sandy gravel underlain by sand, sandy silt and silt of varying density with occasional thin layers of fine grained materials to the Riccarton Gravels. Some relevant details from the cable tool boring logs are summarized in Table 4.6.1.

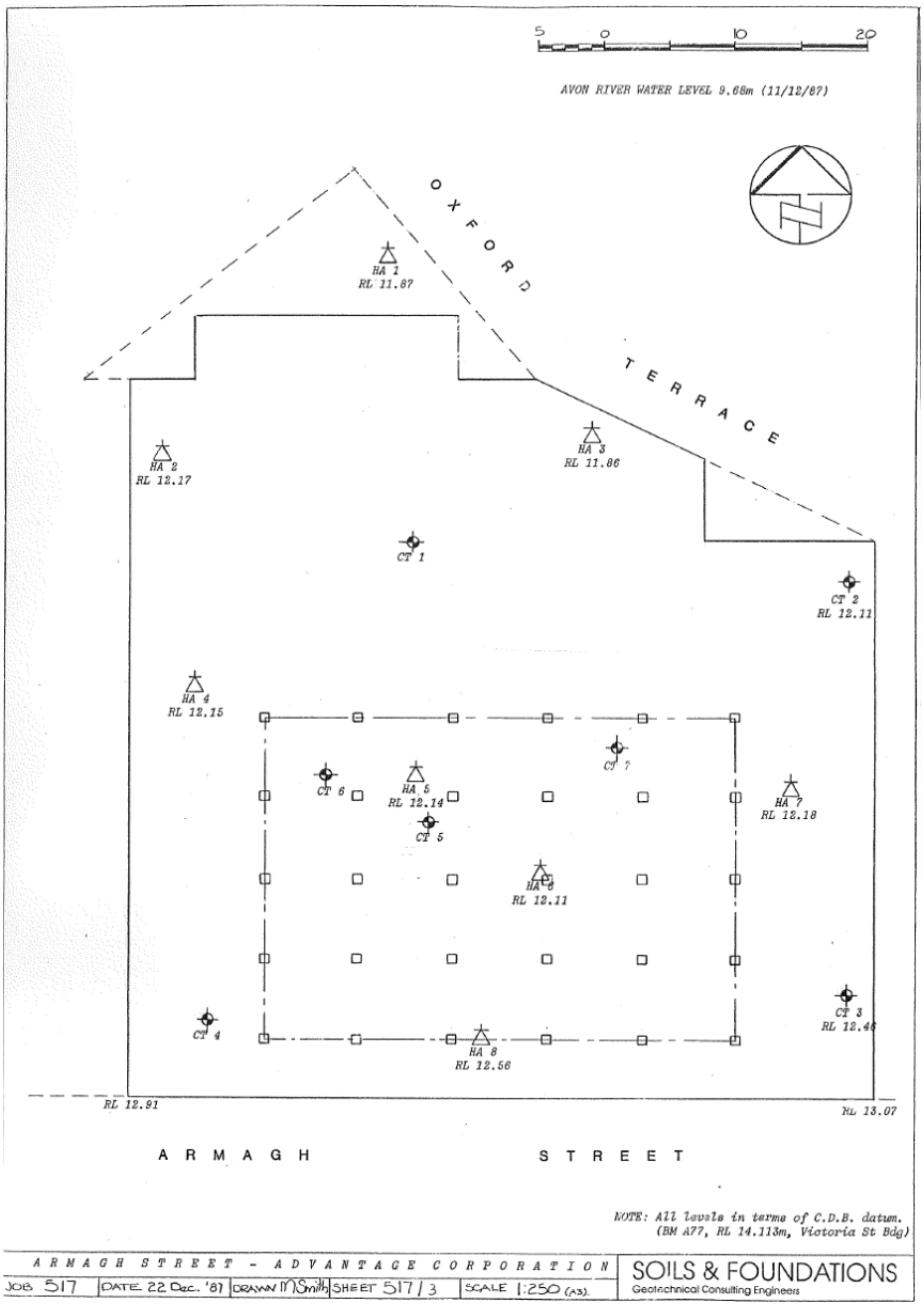

Figure 4.6.3. PWC Building Site Investigation Plan (from Soils and Foundations Geotechnical Consulting Engineers, 1987).

Table 4.6.1. Summary of Cable Tool Boreholes performed by Soils and Foundations Geotechnical Consulting Engineers (1987)

Borehole ID	Total Depth (m)	Depth to Gravel /Gravelly Sand (m)	Bottom of Gravel / Gravelly Sand (m)	Groundwater Depth (m)
CT1	23	2.25	9.75	2.1
CT2	21.25	2.75	9.75	2
CT3	25	2.75	12	2
CT4	17	3.75	12	2
CT5	17	2.75	10.5	2
CT6	17	2.0	10	Not Indicated
CT7	17	2.5	10	Not Indicated

As part of the current investigation, one CPT (Z2-8) was performed in July 2011, and ten additional CPTs were performed in March and April 2013. Of these eleven CPTs, six were performed by McMillan drilling services, mostly without pore pressure measurements, and five were performed by Fugro Geotechnical NZ, all with pore pressure measurements. The locations and corresponding depths of the CPTs are indicated on Figure 4.6.2 and summarized in Table 4.6.2. Please note that the PWC building was demolished in late 2012 but the basement was left in place. Consequently, the CPTs performed around the basement footprint in March and April of 2013 were all located a minimum distance of 2 m away from the basement walls to minimize the influence of the basement on the measured CPT resistance.

Table 4.6.2. Summary of CPTs performed adjacent to the PWC Building.

CPT ID	Testing Contractor	Test Type	Surface Elevation† (m)	Refusal Depth (m)
Z2-8	McMillan	CPTu	3.5	3.42
Z2-16	McMillan	CPT	3.6	19.05
Z2-18	McMillan	CPT	4.1	20.70
Z2-18F	Fugro	CPTu	3.9	20.00
Z2-19	McMillan	CPT	3.9	19.30
Z2-20	McMillan	CPT	4.4	21.63
Z2-21	McMillan	CPT	4.5	20.15
Z2-27	Fugro	CPTu	4.1	3.21
Z2-28	Fugro	CPTu	4.2	21.18

Z2-29	Fugro	CPTu	4.5	24.03
Z2-30	Fugro	CPTu	3.5	20.48

†Indicated surface elevations were estimated based on the digital elevation models available through the Canterbury Geotechnical Database (2012b) and a site survey using a ZIPLEVEL in April of 2013. Indicated elevations are relative to the Lyttelton Vertical Datum (meters above sea level).

The elevation of the groundwater table relative to the Lyttelton Vertical Datum was assumed to be approximately 2.5 m during the Canterbury earthquakes based on regional groundwater models developed by T&T (Canterbury Geotechnical Database, 2013). The Avon River is located just north of Oxford Terrace (approximately 15 – 20 m north of CPT Z2-30) and, as observed in Table 4.6.2, the ground surface elevations decrease slightly across the PWC building site from south to north. Consequently, the groundwater depth below the ground surface becomes slightly shallower from south to north. The assumed groundwater depths below the ground surface at each CPT location for subsequent analyses are summarized in Table 4.6.3.

Figures 4.6.4 through 4.6.7 provide the corrected tip resistance, q_t, and the normalized soil behavior type (SBT) index, I_c, profiles along cross sections A-A', B-B', C-C', and D-D' respectively.

Table 4.6.3. Summary of assumed groundwater depth below the ground surface at each CPT location.

Test ID	Assumed Groundwater Depth (m)
Z2-8	1.0
Z2-16	1.1
Z2-18	1.6
Z2-18F	1.4
Z2-19	1.4
Z2-20	1.9
Z2-21	2.0
Z2-27	1.6
Z2-28	1.7
Z2-29	2.0

Z2-30	1.0

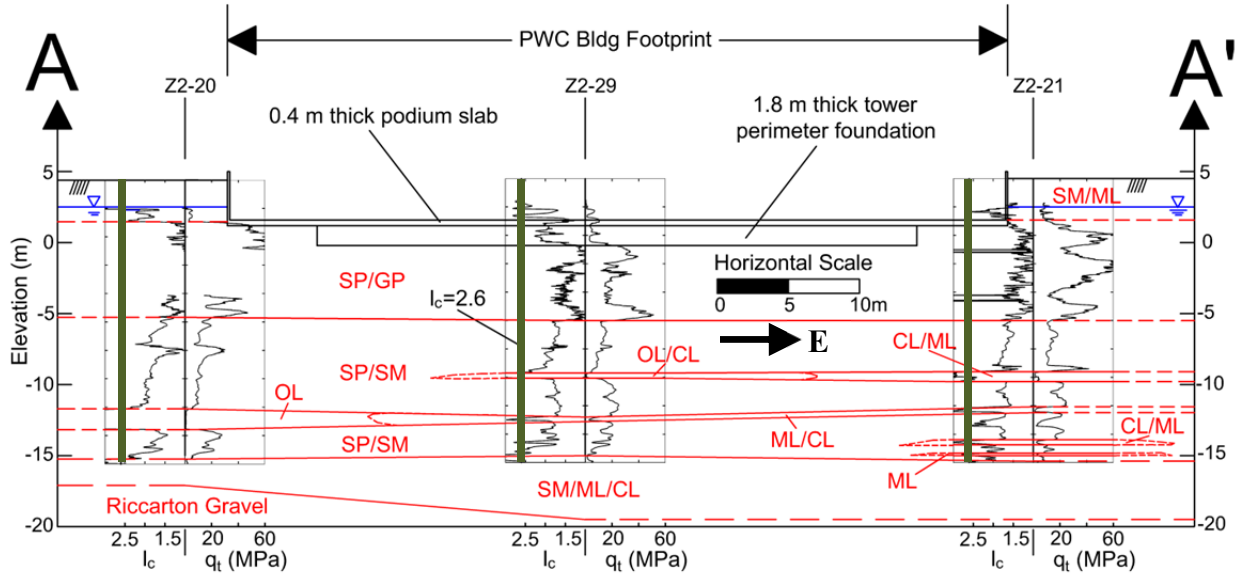

Figure 4.6.4. Subsurface profile with CPT tip resistance and normalized soil behavior type index profiles along cross section A-A'.

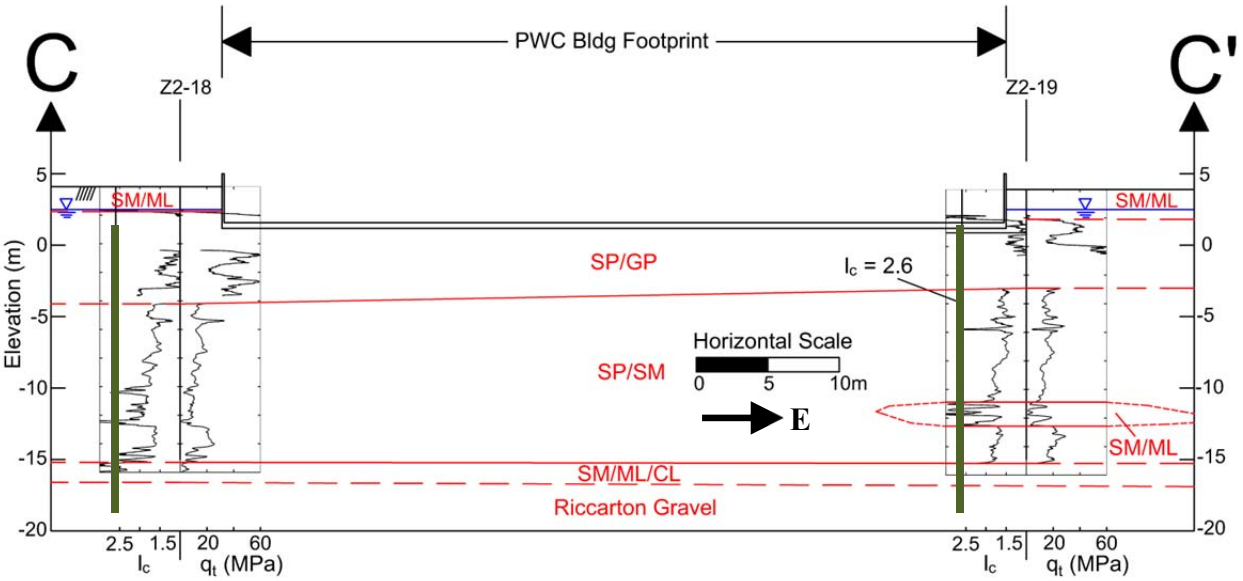

Figure 4.6.6. Subsurface profile with CPT tip resistance and normalized soil behavior type index profiles along cross section C-C'.

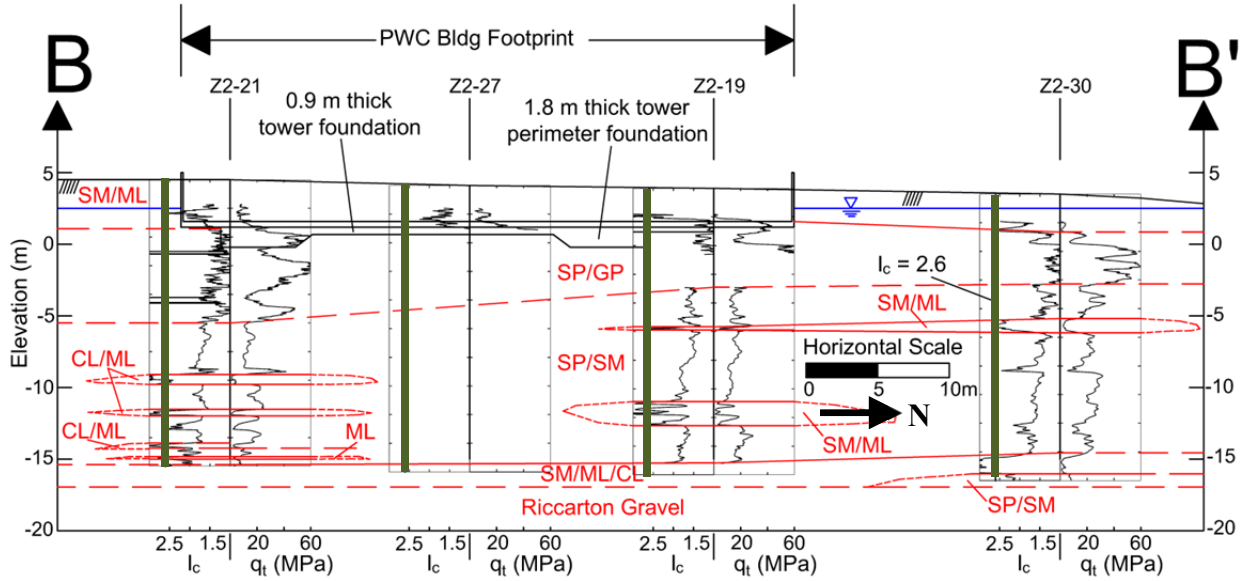

Figure 4.6.5. Subsurface profile with CPT tip resistance and normalized soil behavior type index profiles along cross section B-B'.

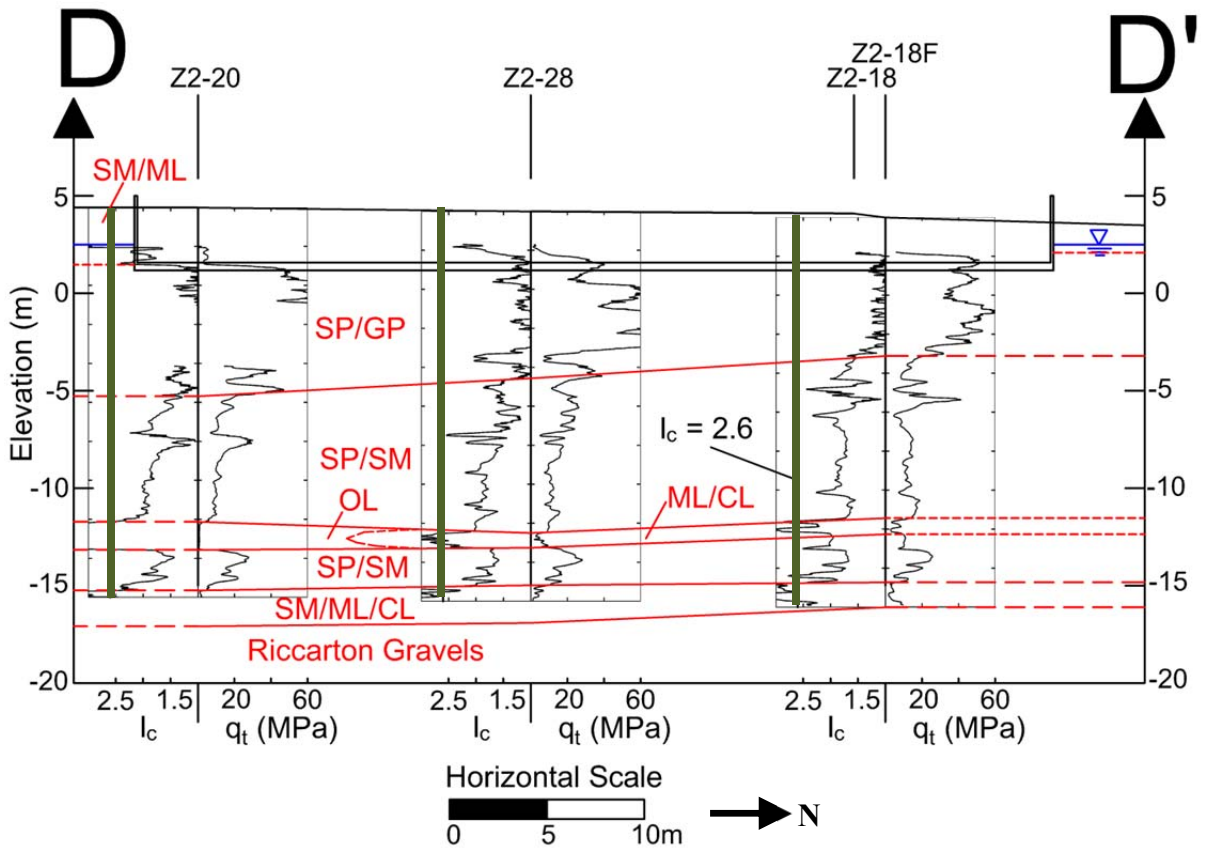

Figure 4.6.7. Subsurface profile with CPT tip resistance and normalized soil behavior type index profiles along cross section D-D'.

Figures 4.6.4 through 4.6.7 illustrate that there are five primary units in the subsurface profile beneath the PWC building:

1) Very loose to medium dense silty sand and sandy silt with q_t generally less than 10 MPa and $1.5 < I_c < 2.5$ to depths between 1.75 m and 4.5 m;
2) Dense to very dense sand, gravelly sand, and sandy gravel with q_t greater than 15 MPa and often greater than 40 MPa and $1.0 < I_c < 1.5$ to depths between 6.25 m and 10 m;
3) Medium dense to dense sand and silty sand with 10 MPa $< q_t <$ 20 MPa and $1.5 < I_c <$ 2.0 to depths between 18 m and 20 m. Thin layers of fine grained materials with $q_t < 5$ MPa and $I_c > 2.6$ are often present within the this unit;
4) Finer grained materials (SM/ML/CL) with relatively low CPT tip resistances (q_t typically less than 10 MPa) and I_c often greater than 2.6 to depths between 20 m and 24 m. This layer represents the oldest and deepest portion of the Christchurch Formation deposit and is common, with variable thickness, throughout the CBD just above the Riccarton Gravels; and
5) Riccarton Gravels. Additional detail regarding the Riccarton Gravels is provided in Section 4.1 and by Tonkin and Taylor (2011).

PWC building foundation elements have also been shown for reference on Figures 4.6.4 through 4.6.6, and it can be observed that the tower mat foundation is founded within the layer of dense sand and sandy gravel. The podium slab also appears to be founded within this unit.

Analyses and Observations

Simplified liquefaction triggering evaluations were performed utilizing the procedures described previously. The estimated PGA values at the PWC site for the 4 SEP 10, 26 DEC 10, 22 FEB 11 and 13 JUN 11 events are summarized in Table 4.6.4. The PGA during the 26 DEC 10 event is estimated as the median geo-mean PGA recorded at the four SMS within the CBD. The remaining PGAs reported above were estimated using the work of Bradley and Hughes (2012).

Table 4.6.4. PGA values at the PWC building site from Bradley and Hughes (2012) for RW98 and ZR02-RW98 analyses. The PGA during the 26 DEC 10 event is estimated as the median geo-mean PGA recorded at the four SMS within the CBD.

Event	M_w	PGA_{16} (g)	PGA_{50} (g)	PGA_{84} (g)
4 SEP 10	7.1	0.16	0.21	0.27
26 DEC 10	4.8	0.22		
22 FEB 11	6.2	0.34	0.45	0.59
13 JUN 11	6.0	0.18	0.24	0.32

Factor of safety against liquefaction triggering (FS_l) profiles, calculated in accordance with RW98 with the PGA_{50} during the 22 FEB 11 event, and liquefaction induced settlement profiles, calculated in accordance with ZR02-RW98 with the PGA_{16}, PGA_{50}, and PGA_{84} during the 22 FEB 11 event, are shown on Figures 4.6.8 through 4.6.11. It is clear from these figures that while liquefiable materials are present beneath the PWC building foundation throughout the building footprint, they are typically within the SP/SM layer at depths greater than 6.25 - 10 m below the ground surface. Consequently, the majority of liquefiable materials are at least 5 m below the base of the tower mat foundation. Ground surface settlements were calculated based on volumetric strains over the upper 20 m of the soil deposit and these calculations are presented in Table 4.6.5 for the 4 SEP 10, 26 DEC 10, 22 FEB 11, and 13 JUN 11 events. It is also worth noting that the shallow SM/ML layer, encountered at many of the CPT locations, also contains materials that should have liquefied in the 22 FEB 11 event. While this layer was not encountered beneath the podium slab or tower mat foundation and thus likely did not contribute to building foundation settlement, the cyclic softening of this unit could have potentially contributed to the tilt of the building observed following the 22 FEB 11 due to reduced support along basement walls.

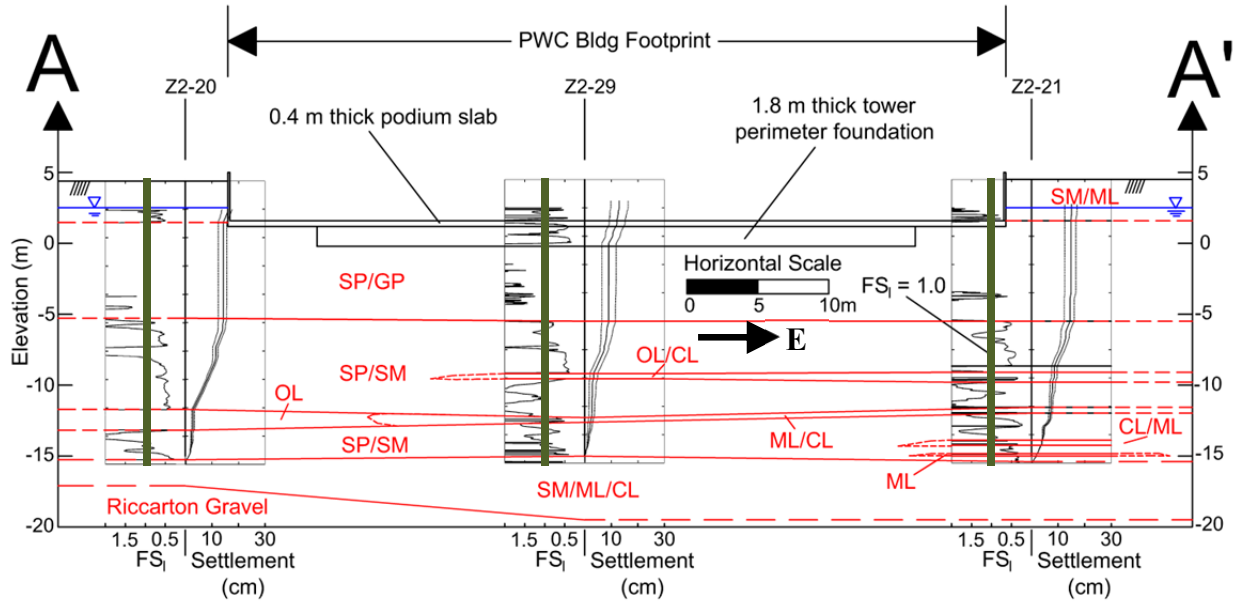

Figure 4.6.8. Factor of safety against liquefaction triggering (FS_l) profiles, calculated in accordance with RW98 for the PGA_{50} during the 22 FEB 11 event, and liquefaction induced settlement profiles, calculated in accordance with ZR02-RW98 for the PGA_{16}, PGA_{50}, and PGA_{84} during the 22 FEB 11 event, at CPT locations along cross section A-A'. Settlements are due to post-liquefaction volumetric strains in the top 20 m.

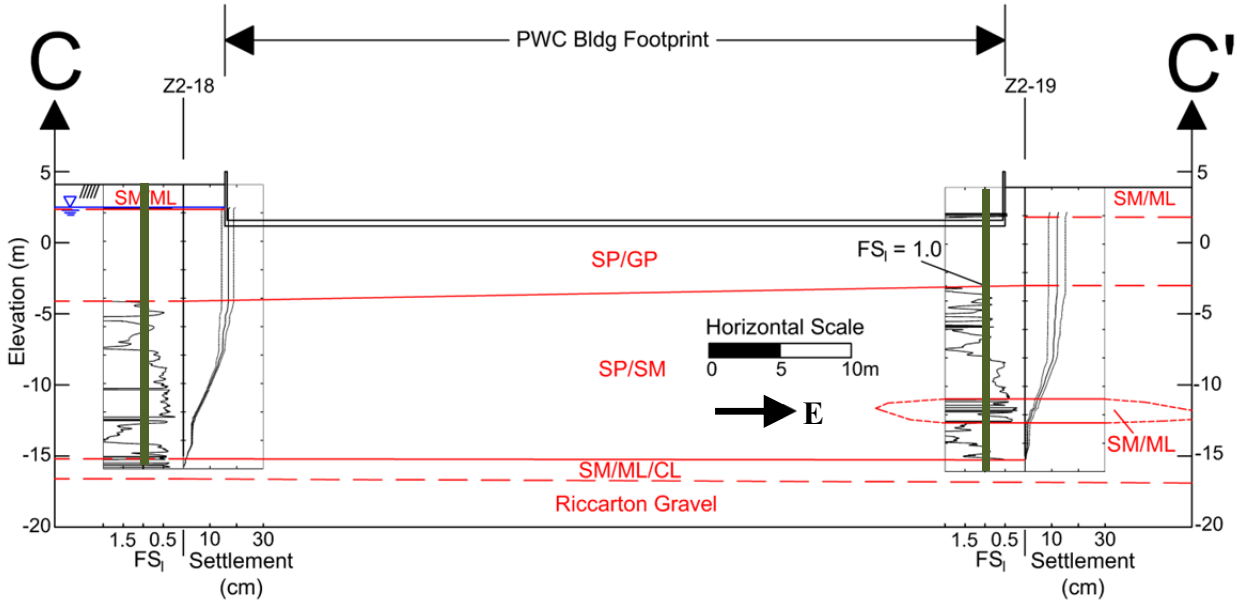

Figure 4.6.10. Factor of safety against liquefaction triggering (FS_l) profiles, calculated in accordance with RW98 for the PGA_{50} during the 22 FEB 11 event, and liquefaction induced settlement profiles, calculated in accordance with ZR02-RW98 for the PGA_{16}, PGA_{50}, and

PGA_{84} during the 22 FEB 11 event, at CPT locations along cross section C-C'. Settlements are due to post-liquefaction volumetric strains in the top 20 m.

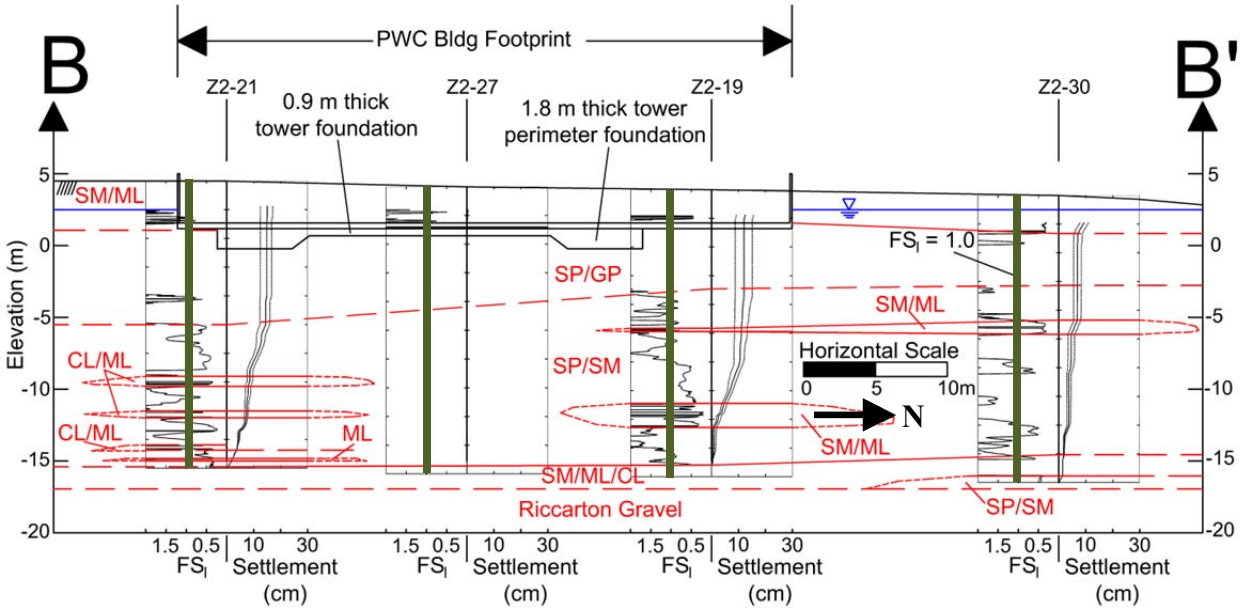

Figure 4.6.9. Factor of safety against liquefaction triggering (FS_l) profiles, calculated in accordance with RW98 for the PGA_{50} during the 22 FEB 11 event, and liquefaction induced settlement profiles, calculated in accordance with ZR02-RW98 for the PGA_{16}, PGA_{50}, and PGA_{84} during the 22 FEB 11 event, at CPT locations along cross section B-B'. Settlements are due to post-liquefaction volumetric strains in the top 20 m.

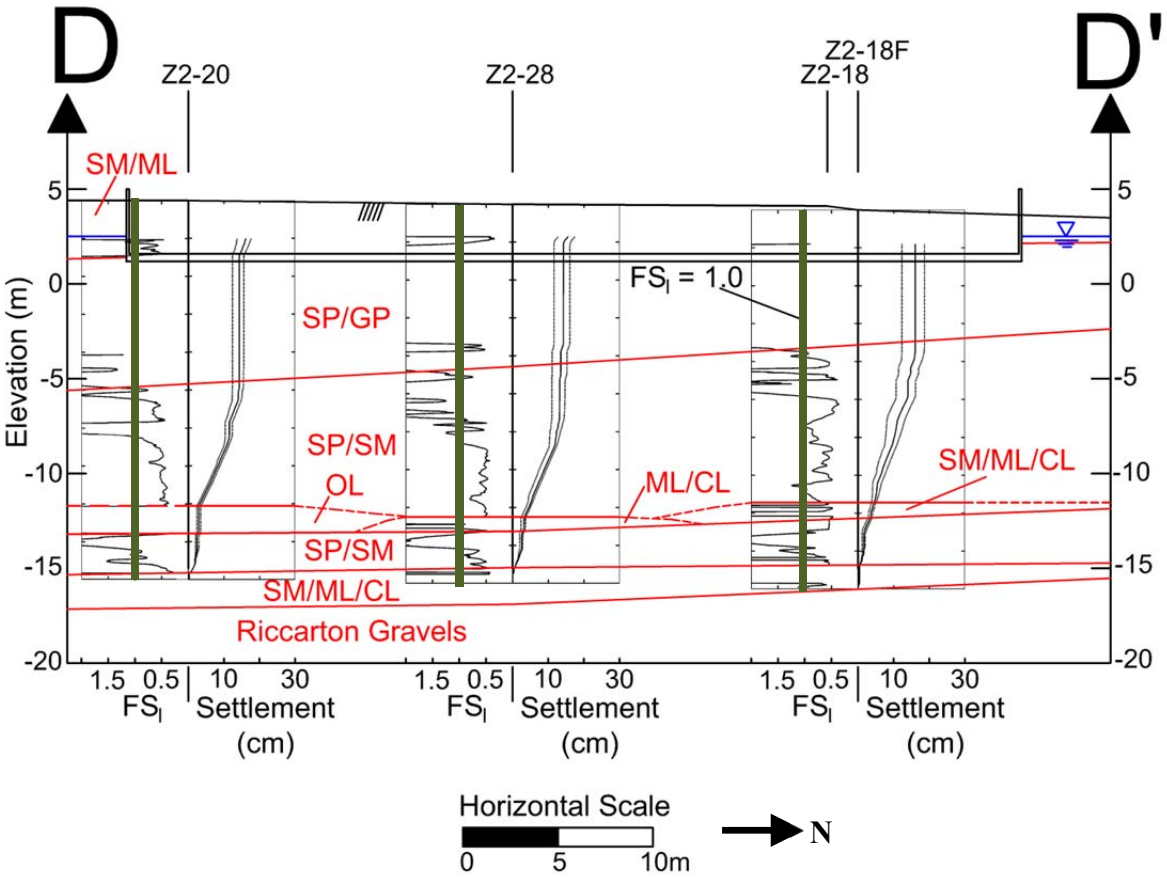

Figure 4.6.11. Factor of safety against liquefaction triggering (FS_l) profiles, calculated in accordance with RW98 for the PGA_{50} during the 22 FEB 11 event, and liquefaction induced settlement profiles, calculated in accordance with ZR02-RW98 for the PGA_{16}, PGA_{50}, and PGA_{84} during the 22 FEB 11 event, at CPT locations along cross section D-D'. Settlements are due to post-liquefaction volumetric strains in the top 20 m.

Table 4.6.5. Calculated ZR02-RW98 surface settlements at CPT locations near the PWC building for the PGA_{50} during the 4 SEP 10, 22 FEB 11, and 13 JUN 11 events. The PGA during the 26 DEC 10 event was estimated as the median geo-mean PGA recorded at the four SMS within the CBD. Settlements were calculated over the top 20 m at each location.

CPT ID	Reconsolidation Settlement at Surface (cm)			
	4 SEP 10	26 DEC 10	22 FEB 11	13 JUN 11
Z2-8	1	0	2	1
Z2-16	10	6	14	9
Z2-18	12	4	18	9
Z2-18F	8	1	16	4
Z2-19	7	3	13	5
Z2-20	10	3	16	7
Z2-21	10	5	15	8
Z2-27[†]	0	0	0	0
Z2-28	8	1	16	5
Z2-29	7	1	13	5
Z2-30	7	3	9	6

[†]Refusal was encountered at 3.21 m during CPT Z2-27

The performance of the PWC building site during the 22 FEB 11 Christchurch earthquake was evaluated by GEER, UCB and UC researchers in March 2011. A separate evaluation was performed by researchers from the UC around that time, and a field map developed during this separate evaluation is shown in Figure 4.6.12 (Giorgini et al., 2011a; and Giorgini, 2015). At that time, liquefaction-induced sediment ejecta were observed on both the north end and south end of the building site (Figure 4.6.13). Ground settlements of at least 30 cm were measured near the street on the north side of the building and areas of localized ground settlement of up to 10 - 15 cm were measured on the south side of the building. General ground settlements on the south side appeared to be less than approximately 10 cm. A long crack,

roughly parallel to the orientation of the Avon River was observed near the center of Oxford Terrace. To the southeast of this crack, settlement of the road and deformed pavement were observed. These observations are suggestive of lateral spreading along the bank of the Avon River, and this could have contributed to the vertical ground displacements in this area.

Water was observed in the exposed basement during the field testing performed in March and April 2013. Most of the water was ponded in the southern half of the basement which, assuming the basement was built level according to the design plans, would indicate differential settlement of the south end of the basement relative to the north end (Figure 4.6.14).

Accessible building columns between the first and second floors were surveyed with a digital level and tilt measurements were recorded during the March 2011 site evaluation. Twenty-four column tilt measurements in the north-south direction were recorded with a sample mean of 0.2 degrees to the south and a sample standard deviation of 0.15 degrees. Similarly, the sample mean and standard deviation of 24 column tilt measurements in the east-west direction was 0.1 degrees to the west, and 0.2 degrees, respectively. Locations of the tilt measurements are indicated on Figure 4.6.12.

A subsequent thorough structural evaluation of the PWC building was performed by researchers at the University of Canterbury in 2012, and some of their performance observations are summarized in Pampanin (2012):

> *A proper hierarchy of strength or capacity design protected the column from any inelastic mechanism. No noticeable cracking was evident even in the exterior-corner columns belonging to both direction frames and thus subject to a particularly high demand. Due to inelastic mechanisms developed in the structural elements at most floors, the post-earthquake building state was characterized by low to moderate residual interstorey drifts. Furthermore, permanent deformations in the soil-foundation-structures (consisting of shallow foundation) led to an overall leaning/tilting of the building. Repairing and strengthening options were considered, but found uneconomical when compared to the option of a controlled demolition and rebuild, partially or mostly covered by insurance.*

Several photographs of beam plastic hinges at the beam-column connections are also presented in Pampanin (2012). One of these photographs is shown below as Figure 4.6.15.

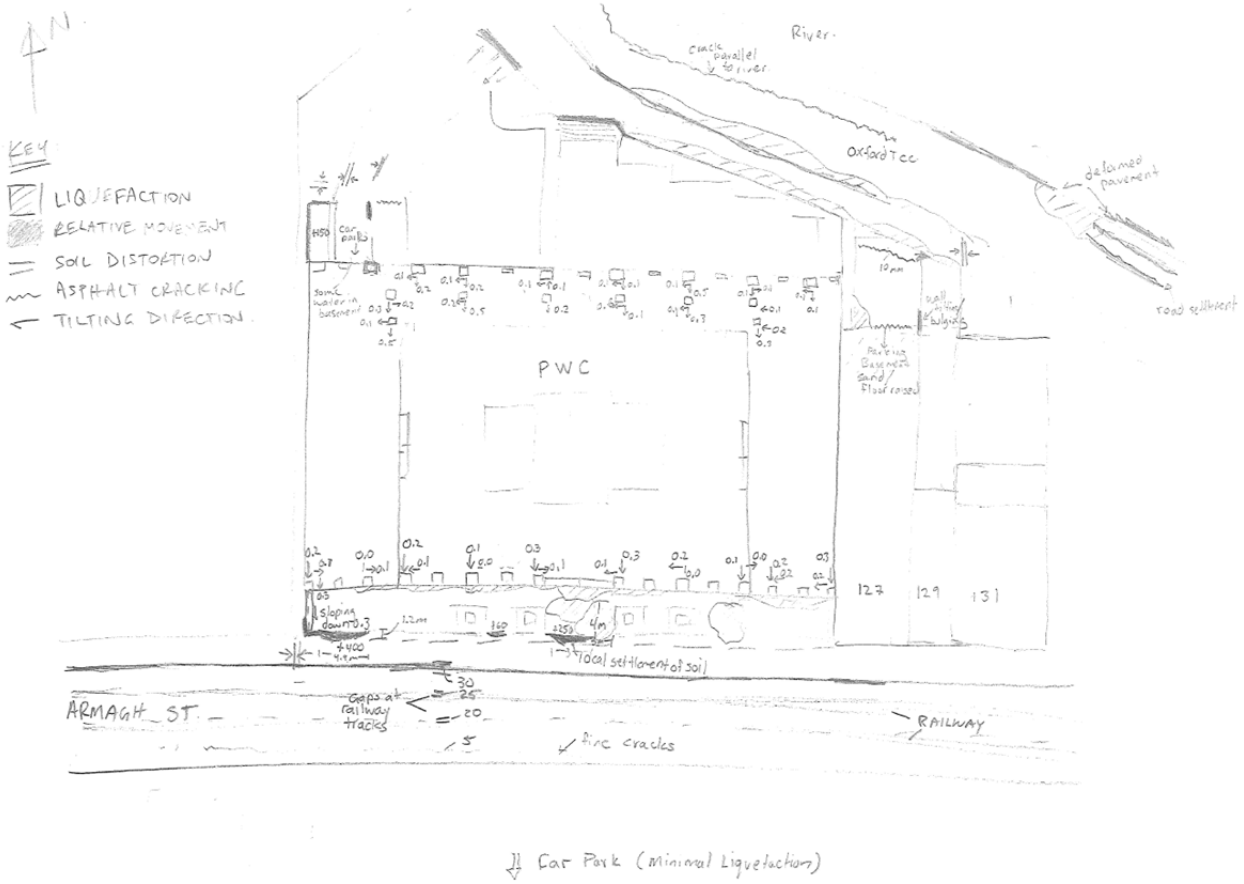

Figure 4.6.12. Field map developed during evaluation of PWC building site in March 2011 (from Giorgini et al., 2011a; and Giorgini, 2015).

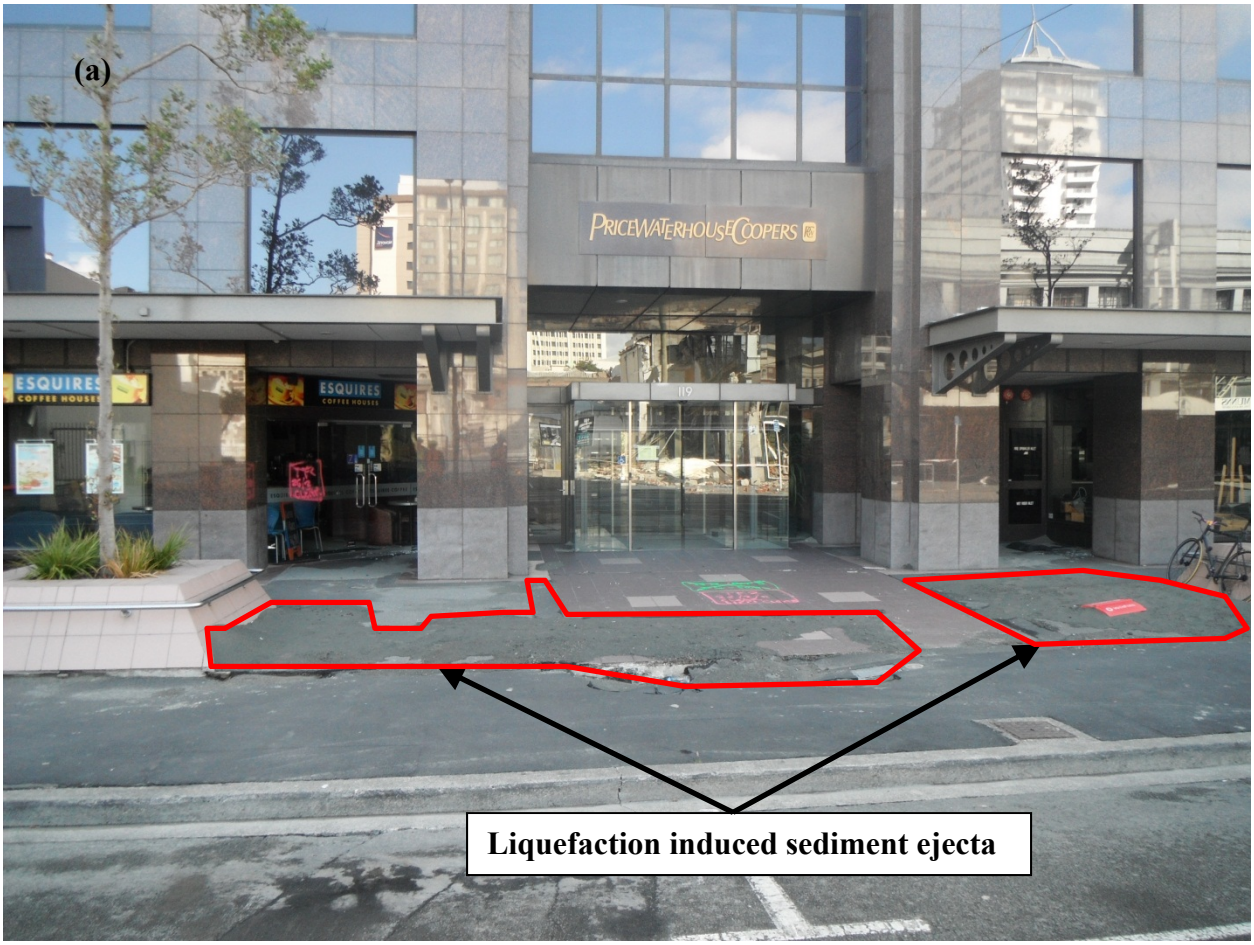
(a)
PRICEWATERHOUSECOOPERS
ESQUIRES
COFFEE HOUSES
Liquefaction induced sediment ejecta

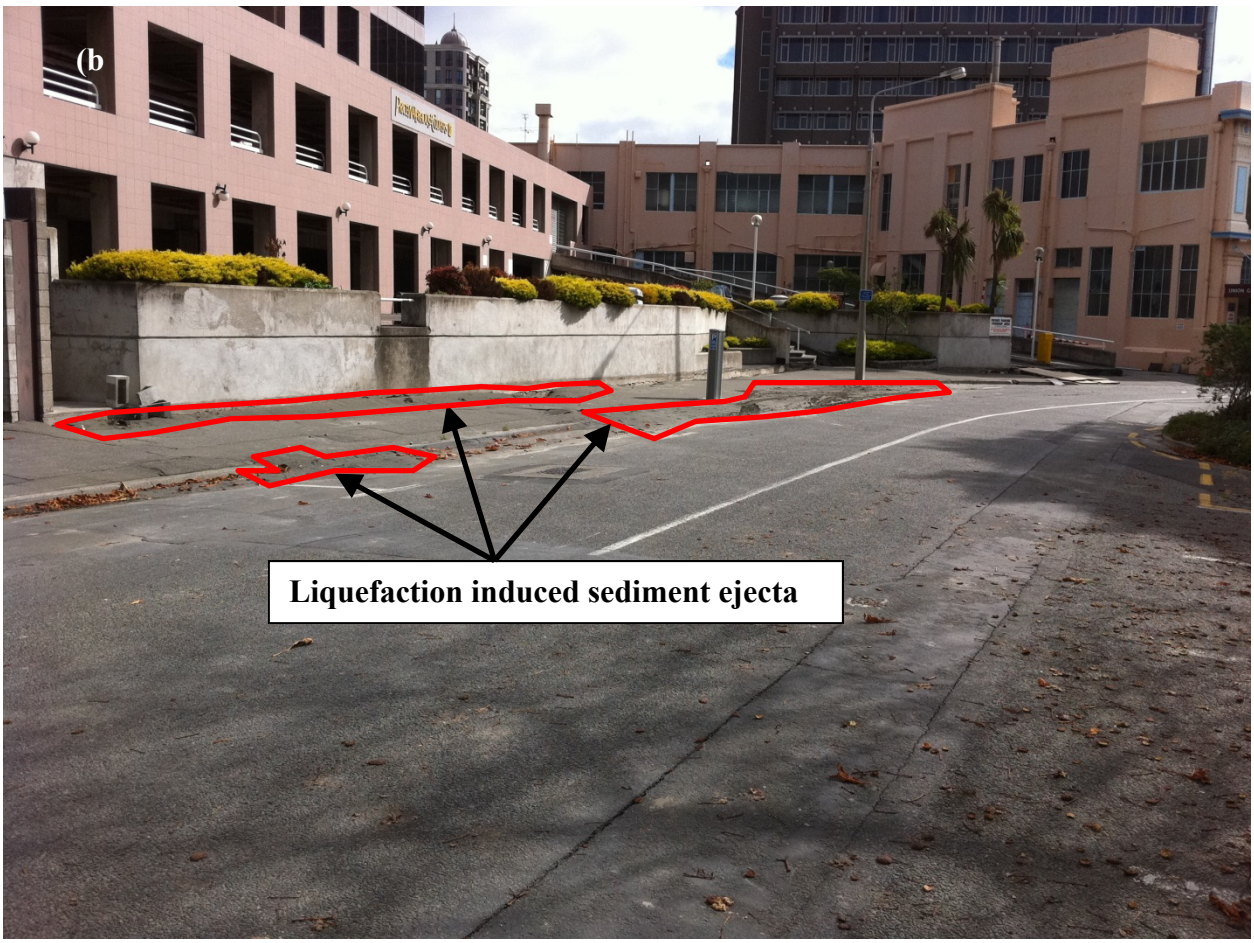

Figure 4.6.13. Photographs of (a) the south end and (b) the north end of the PWC building site taken in March 2011.

Figure 4.6.14. Photograph of the exposed basement of the PWC building from the north viewing south-southeast, taken in March 2013.

Figure 4.6.15. Photograph of beam plastic hinge (from Pampanin, 2012).

The PWC building was a 21-story reinforced concrete frame structure on a shallow foundation that was located above soils that liquefied during the 22 FEB 11 earthquake. Unlike the CTUC building, the SA building, and the FTG-7 and FTG-4 buildings, however, the PWC building foundation did not rest directly on liquefiable materials. Instead, the mat foundation was located on a layer of dense to very dense gravelly sand and sandy gravel. Liquefiable materials were located at least 3 m below the base of the foundation and often more than 5 m. However, this is well within the depth range with a significant vertical strain influence for a foundation with a width of 25 m and L/B = 1.4 (Schmertmann, 1978). Consequently, cyclic softening of these materials due to increased pore water pressures would have likely led to building settlements, despite the fact that the liquefiable materials were not directly beneath the building. In addition, cyclic softening due to increased pore water pressures during and immediately following the significant Canterbury earthquakes could have occurred in other materials beneath the PWC building, and this transient reduction in stiffness in materials that did not fully liquefy could have also contributed to the observed building settlement. Volumetric reconsolidation of the liquefiable materials beneath the building foundation would have also caused settlements. Additionally, lateral spreading toward the Avon River to the north of the building could have contributed to the observed vertical displacements of the ground in this area.

As described previously, the top of the PWC building tilted slightly to the south during the 22 FEB 11 event. Importantly, the basement mat foundation extends significantly to the north of the tower footprint (Figure 4.6.16). It is possible that the northern portion of the basement mat, therefore, acted as a cantilever that prevented the northern end of the PWC building tower from settling as much as the southern end, causing the building to tilt slightly to the south. Advanced SSI numerical models will likely be able to provide more insight into the complex performance

of the PWC building, and these analyses are underway by researchers at the University of California at Berkeley and the University of Canterbury.

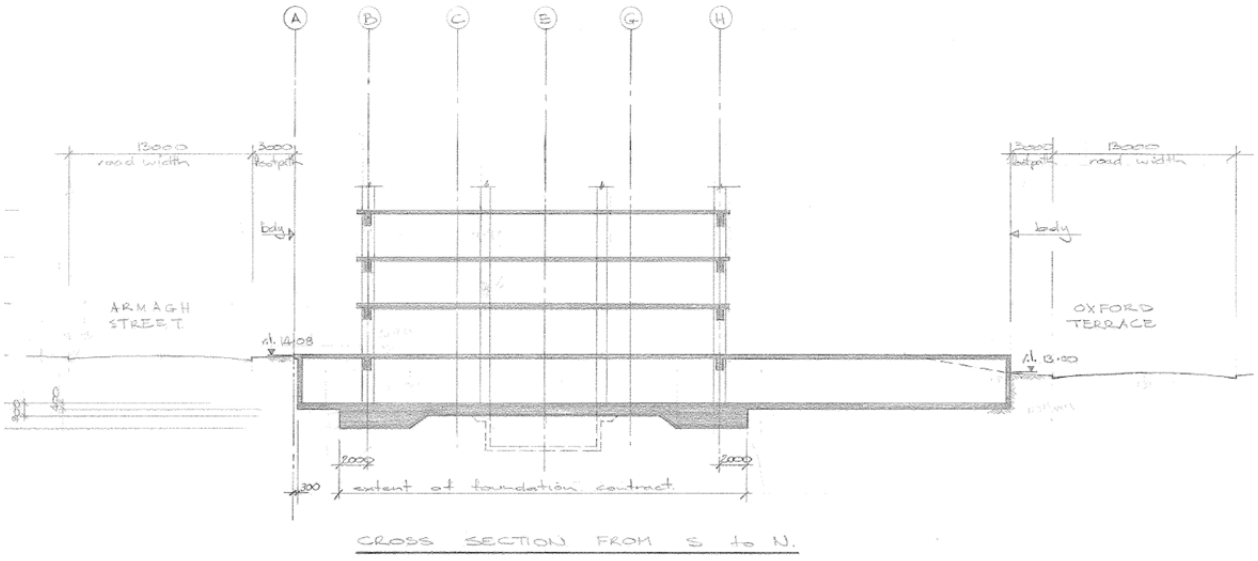

Figure 4.6.16. North-south cross section of the PWC building from the PWC building design drawings (Holmes Consulting Group et al., 1988).

4.7 Engineering Performance of the VT and VSA Buildings

Introduction

The VT building, which was located on the corner of Armagh Street and Oxford Terrace at 90 Armagh Street in Christchurch, New Zealand (Lat -43.52897, Lon 172.63523), was a 10-story, reinforced concrete frame structure, with a one-story basement (Figures 4.7.1, 4.7.2) atop a mat foundation that varied in thickness from 0.3 m to 0.9 m throughout the building footprint. Its neighboring building to the east, the VSA building, located at 100 Armagh Street, was a 14-story reinforced concrete building atop a complex foundation system consisting of a combination of piles with lengths of 6 m, 14 m, and 18 m and isolated shallow spread footings.

Liquefaction-induced sediment ejecta was observed on the inside edge of the sidewalk along the north and west sides of the VT building following the Christchurch earthquake, and the building had a residual tilt of its top toward the southeast. Localized asphalt cracking and settlements were observed along the sidewalk near where the sediment ejecta were observed. The VSA building settled differentially across the building footprint in the amount of approximately 22 cm at the NW corner and 16 cm at the NE corner, relative to the SE corner (Compusoft Engineering, 2012). This differential settlement caused the VSA building to tilt to the north-northwest following the 22 FEB 11 event. The relative tilt between the VSA and VT buildings in the north-south direction is apparent in Figure 4.7.1. Because the east wall of the VT building was located less than 40 cm from the west wall of the VSA building, it is possible that SSSI effects, in addition to SSI effects, played a role in the seismic response of both buildings. Contact

between the neighboring buildings near the top of the third floor (Figure 4.7.3) was observed following the 22 FEB 11 event, so it is possible that there was also interaction through pounding between the two buildings during this event.

Minor lateral spread-induced ground cracks (up to 10 cm wide) were observed along the nearby bank of the Avon River, located approximately 15 – 20 m west of the VT building. Several significant sand boils were located within and around Victoria Square Park, approximately 30 – 50 m to the north of the neighboring buildings.

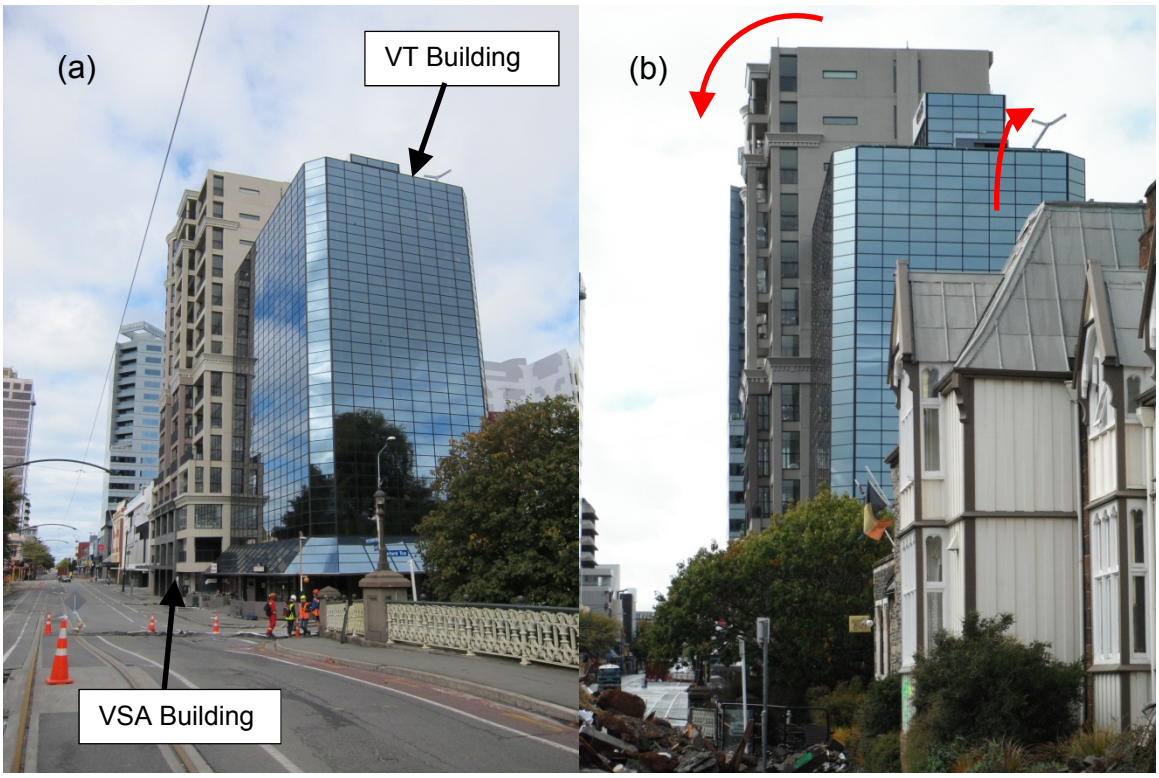

Figure 4.7.1. Photos of the VT building at 90 Armagh Street and the VSA building at 100 Armagh Street as viewed from the (a) northwest and (b) west taken in March 2011. Red arrows indicate the primary direction of tilt of the buildings (i.e., the VSA building top tilted to the north and the VT building top tilted to the southeast).

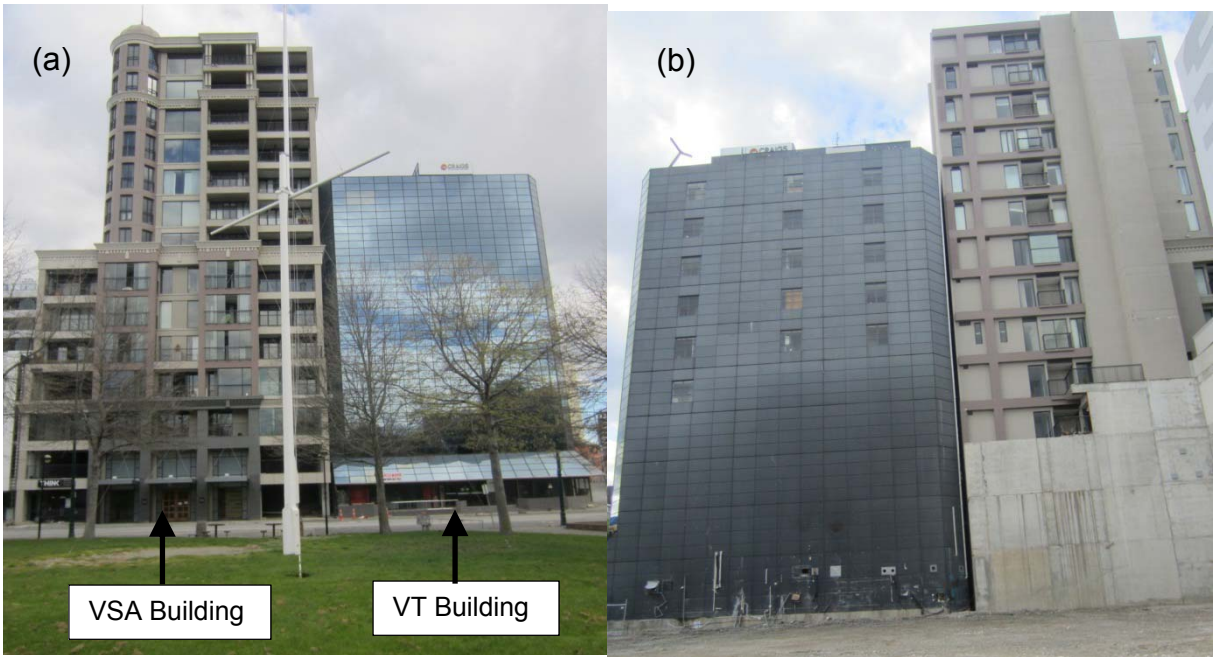

Figure 4.7.2. Photos of the VT and VSA buildings as viewed from the (a) north and (b) south taken in September 2012.

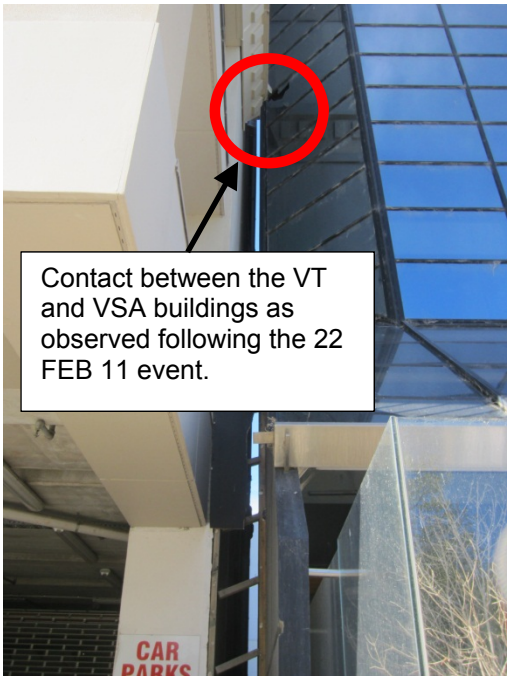

Figure 4.7.3. Contact between the VT and VSA buildings as observed following the 22 FEB 11 earthquake. The photograph was taken from the north near the NE corner of the VT building and NW corner of the VSA building.

Structural Design

Design drawings for the VT and VSA buildings were approved by CCC in 1986 and 2004, respectively. As illustrated in Figures 4.7.1 and 4.7.2, the VT building consisted of a 10-story RC frame structure atop a one-story basement with a RC mat foundation that varied in thickness from 0.3 m to 0.9 m throughout the building footprint. The basement footprint was approximately 23.8 m in the E-W direction and 18.8 m in the N-S direction (Figure 4.7.4). The top of the mat foundation was approximately 2.1 m below the adjacent sidewalk. The elevator shaft and stairs were slightly offset from the center of the building to the southwest. There were 18 structural columns for the VT building, 15 of which were located around the perimeter of the superstructure. The columns were either cast-in-place or pre-cast RC. Column dimensions were typically 0.55 m by 0.50 m for perimeter columns when below the ground floor, 0.90 m by 0.45 m for perimeter columns when above the ground floor, and 0.60 m by 0.40 m for the interior columns. Perimeter columns were typically spaced at 6 m OC in the E-W direction and at either 4.9 m or 2.75 m OC in the N-S direction. The three interior columns were spaced at 5.90 m and 6.05 m, respectively, in the E-W direction. RC beams varied in width between 0.45 m and 1.35 m and were typically 0.45 – 0.50 m deep. 0.25 m deep Double Tee concrete flooring was used, typically with a concrete topping of 65 mm. The roof consisted of 0.29 m deep Double Tee units, with a minimum topping of 65 mm. Using dead load and reduced live load estimates described by Soils and Foundations Geotechnical Consulting Engineers for similar buildings in Christchurch in the 1980s (as described in Section 4.6), it is likely that the average foundation contact pressure during the Canterbury earthquakes was on the order of 120 kPa for the VT building.

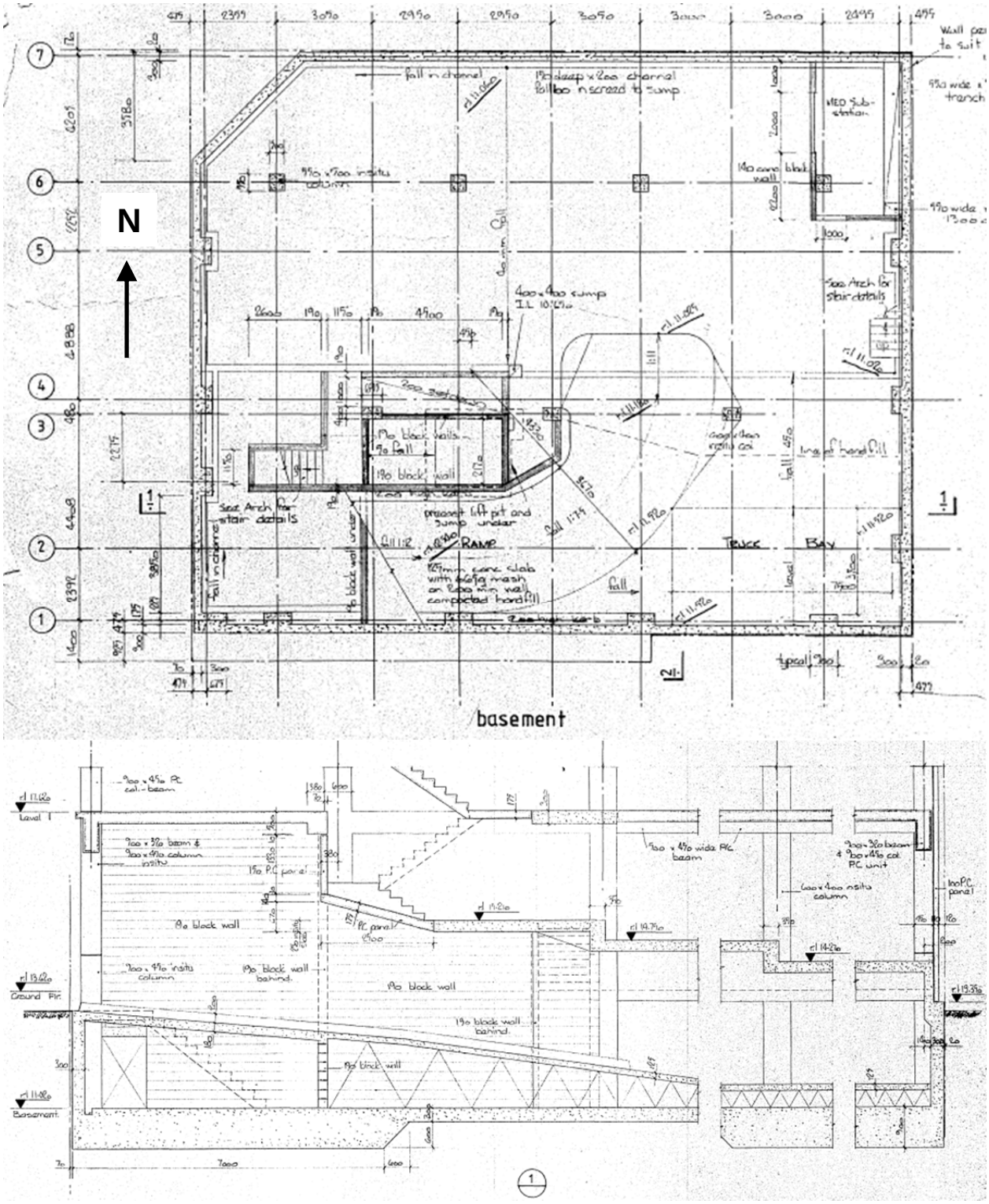

Figure 4.7.4. Basement plan and associated cross section 1-1' for the VT building (from structural design drawings; Holmes Wood Poole and Johnstone Ltd, 1986).

The VSA building was a 14-story RC structure (Figures 4.7.1 and 4.7.2) with a complex foundation system that consisted of 17 1.2 m-diameter RC piles around the southern, eastern and western edges of the building footprint and several shallow RC spread footings along the northern edge and within the building footprint (Figure 4.7.5). The building footprint area was approximately 595 m^2 (approximately 24.9 m north-south by 26.9 m east-west less the 5.0 m by 15.3 m area at the southwest corner). As illustrated on Figure 4.7.5, the lengths of the piles were either 6 m, 14 m, or 18 m. While 14 m long piles were located at the NE, SE, and SW corners of the building, only 6 m long piles appear to have been installed at the NW corner. The piles were connected at the surface by means of a 1.2 m wide by 1.2 m or 0.75 m deep grade beams. The grade beams were designed such that the piles along the southern and western sides of the buildings were structurally connected but the piles on eastern side, while connected to each other through an independent grade beam, were not connected to the remaining piles. As detailed in Figure 4.7.5, plan dimensions of the shallow spread footings varied and the depths of the base of the footings also varied from 0.6 m to 1.2 m.

The lateral force resisting and gravity systems of the VSA building consist of a combination of structural walls and frames. Compusoft Engineering (2012) summarized the lateral force resisting system as follows:

> - *At the lower levels of the structure there are structural walls on three sides of the structure and a moment resisting frame on the fourth (north) side of the building. These structural walls generally terminate at [the] fourth floor level to coincide with the change of floor plan that occurs at this height. The relative stiffnesses of the walls and frames at the lower levels indicate that the contribution of the north face moment resisting frame to lateral resistance would have been minor.*
> - *Full height walls surround the central lift core. Substantial columns exist at the corners of the lift core. These columns would function as boundary elements for the lift core walls.*
> - *Two additional walls exist on grids WG and WH that extend to the roof of the structure. The wall on gridline WH does not extend to ground level, and hence cannot be seen in Figure [4.7.5].*
> - *At the upper levels of the structure torsional resistance is provided by moment resisting frames around the perimeter of the structure. These frames would also contribute to the lateral resistance of the structure.*
>
> *Diaphragms in the Victoria Square Apartments building consist of structural toppings reinforced with conventional deformed (i.e., not mesh) reinforcement. The thickness of the topping varies between 75 mm and 150 mm. Reinforcement size and spacing varies depending on the location of the diaphragm, and additional "drag" bars are indicated on the drawings. The structural topping is supported by hollowcore planks spanning to beams or walls as discussed [below].*

Compusoft Engineering (2012) also note that the gravity load system is composed of the same elements that provide lateral force resistance. In addition:

The floor system of the Victoria Square Apartments building consists of precast concrete units with an in-situ topping. The type and size of precast unit and topping used varies through the structure depending on the span and usage of an area. The majority of the flooring consists of 200 mm and 300 mm deep hollowcore ("Dycore") planks topped with 75 mm to 150 mm of in-situ concrete. Smaller areas of the floors are constructed from solid precast planks ("Unispan"). Precast units generally span along the east-west axis to beams or walls.

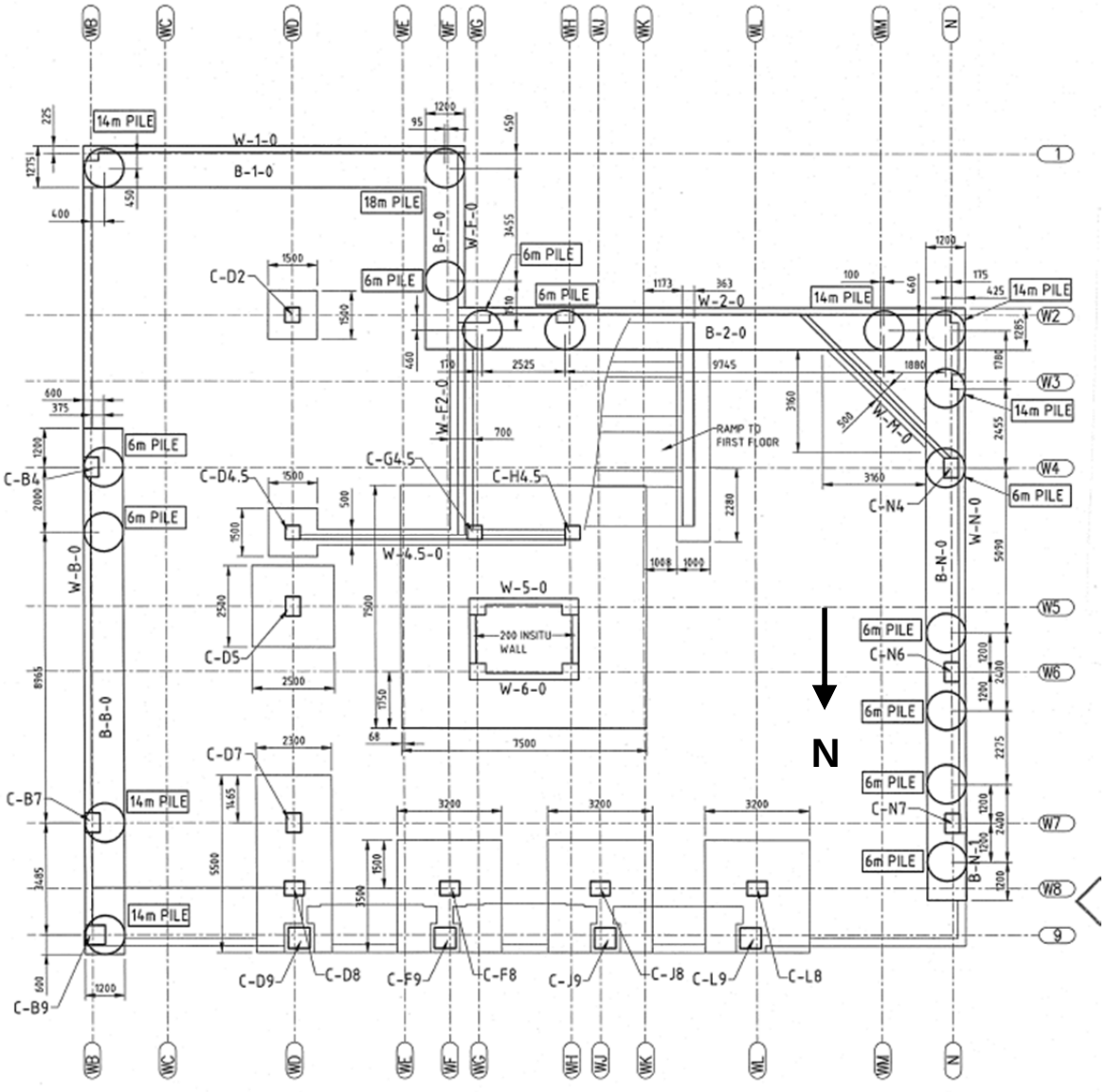

Figure 4.7.5. Foundation plan for the VSA building (from the structural design drawings; Connell Mott MacDonald, 2004). Note that north is oriented downward in this figure.

Site Characterization

Three CPTs (Z2-1, Z2-2, and Z2-9) were performed by the University of California at Berkeley, in coordination with the University of Canterbury in July 2011, and nine additional CPTs were performed in March and April 2013. Of these 12 CPTs, nine were performed by McMillan drilling services, mostly without pore pressure measurements, and three were performed by Fugro Geotechnical NZ, all with pore pressure measurements. The locations of the CPTs are indicated on Figure 4.7.6 and summarized in Table 4.7.1. Both the VT and VSA buildings were in place during the testing periods in July 2011 and March and April 2013. Consequently, the CPTs performed around the buildings were all located a minimum distance of 1.5 - 2 m away from known structural elements to minimize the influence of the buildings on the measured CPT resistance. Due to a minor layout error CPTs Z2-17 and Z2-24 were located slightly closer than was desired, at a distance of approximately 1.0 – 1.5 m. CPTs Z2-25 and Z2-25F were located approximately 1.8 m apart.

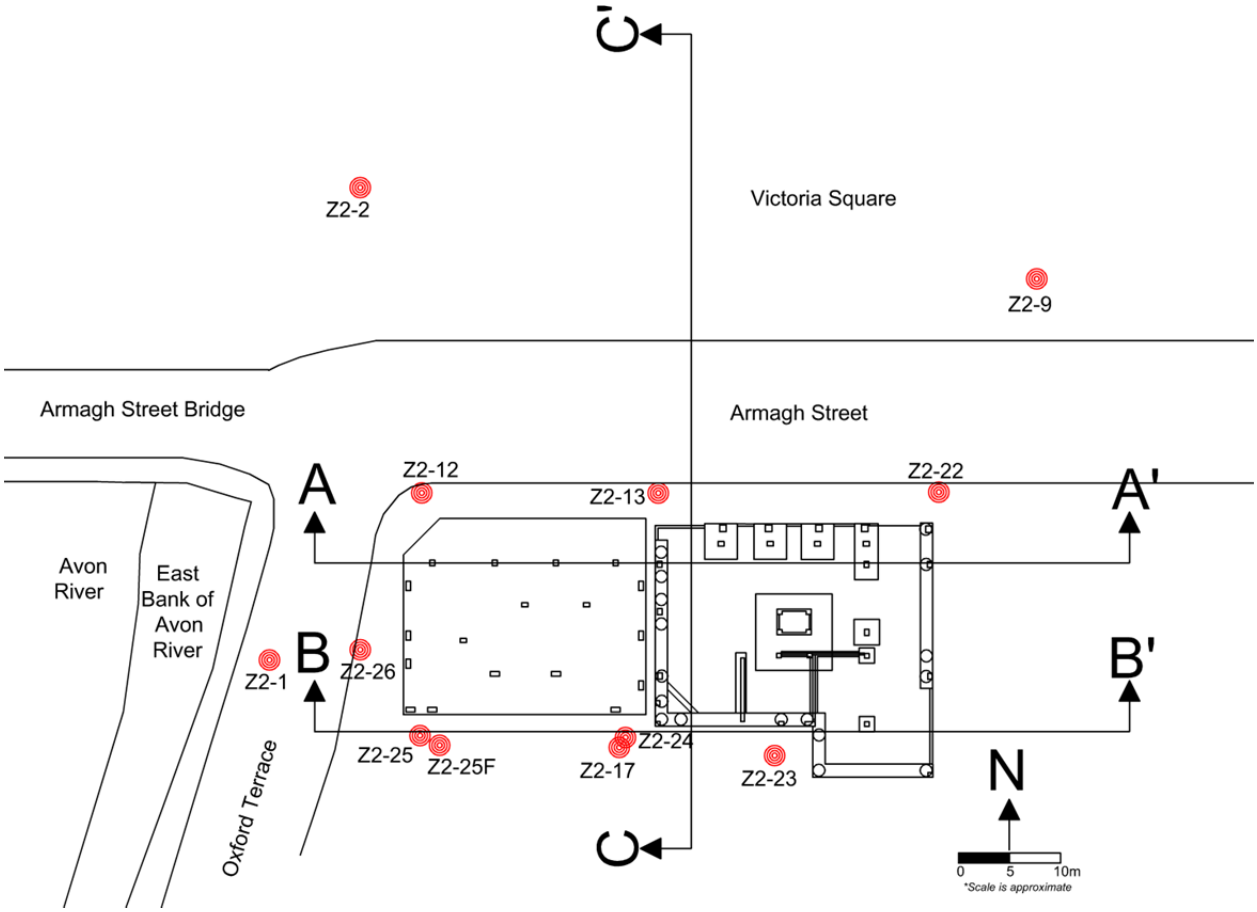

Figure 4.7.6. CPT location plan with VT and VSA building foundation elements shown for reference

Table 4.7.1. Summary of CPTs performed at the VT and VSA building sites.

CPT ID	Testing Contractor	Test Type	Surface Elevation† (m)	Refusal Depth (m)
Z2-1	McMillan	CPTu	4.0	9.86
Z2-2	McMillan	CPTu	3.5	2.43
Z2-9	McMillan	CPTu	4.1	2.09
Z2-12	McMillan	CPT	3.9	20.24
Z2-13	McMillan	CPT	3.7	20.45
Z2-17	McMillan	CPT	4.0	7.36
Z2-22	McMillan	CPT	4.0	13.53
Z2-23	McMillan	CPT	3.9	13.39
Z2-24	Fugro	CPTu	4.0	19.98
Z2-25	McMillan	CPT	3.8	20.48
Z2-25F	Fugro	CPTu	3.8	20.05
Z2-26	Fugro	CPTu	3.9	20.20

†Indicated surface elevations were estimated based on the digital elevation models available through the Canterbury Geotechnical Database (2012b) and a site survey using a ZIPLEVEL in April 2013. Indicated elevations are relative to the Lyttelton Vertical Datum (meters above sea level).

The elevation of the groundwater table relative to the Lyttelton Vertical Datum was assumed to be approximately 2.0 m above sea level during the Canterbury earthquakes based on regional groundwater models developed by T&T (Canterbury Geotechnical Database, 2013). Surface elevations at CPT locations were estimated based on the digital elevation models available through the CGD and a site survey performed with a ZIPLEVEL in April 2013. As can be observed from Table 4.7.1, surface elevations around the VT and VSA buildings were relatively uniform. The assumed groundwater depths below the ground surface at each CPT location for subsequent analyses are summarized in Table 4.7.2. By March 2013 demolition of the buildings south of the VT and VSA buildings had been completed and the surficial materials

in these lots were composed primarily of demolition debris. Based on shallow excavations performed at the CPT locations prior to testing, it appears as though the demolition debris extended to depths of up to approximately 2 m at the locations of Z2-17, Z2-23, Z2-24, Z2-25, and Z2-25F.

Table 4.7.2. Summary of Assumed Groundwater Table Depths at Each CPT Location

Test ID	Assumed Groundwater Depth (m)
Z2-1	2.0
Z2-12	1.9
Z2-13	1.7
Z2-17	2.0
Z2-22	2.0
Z2-23	1.9
Z2-24	2.0
Z2-25	1.8
Z2-25F	1.8
Z2-26	1.9

Figures 4.7.7 through 4.7.9 provide the corrected tip resistance, q_t, and the normalized soil behavior type (SBT) index, I_c, profiles along cross sections A-A', B-B', and C-C' respectively. The VSA building foundation is indicated on Figure 4.7.9 for reference. Figure 4.7.10 shows the q_t and I_c profiles projected on cross section C-C' with the VT building foundation indicated for reference.

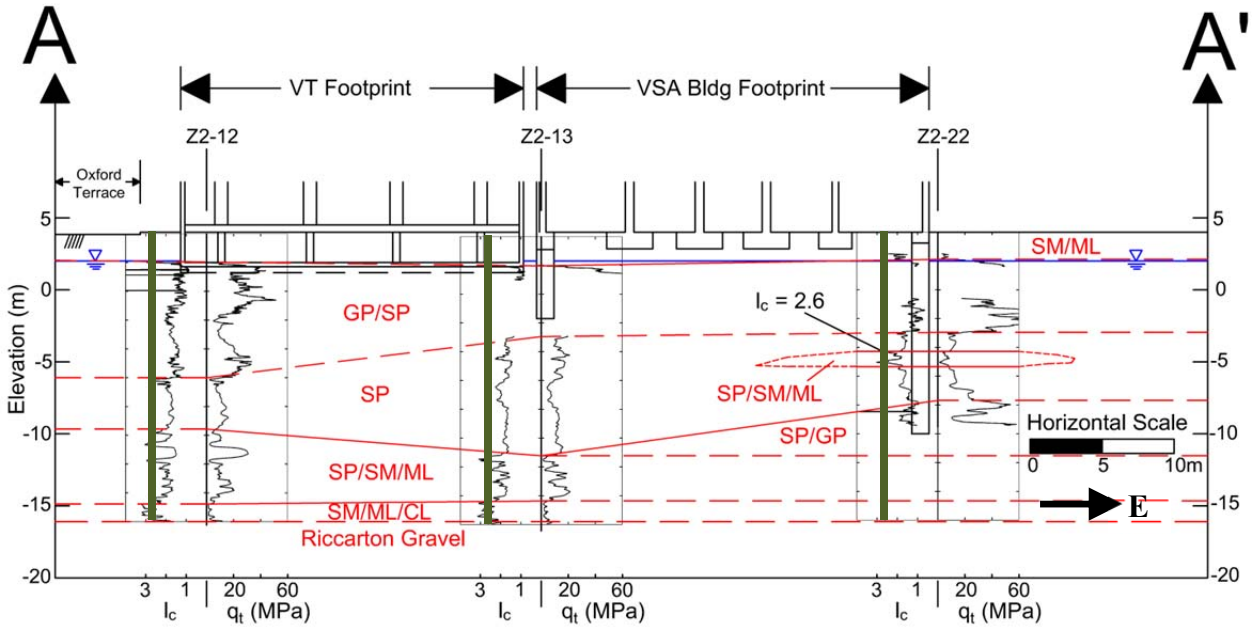

Figure 4.7.7. CPT tip resistance and normalized soil behavior type index profiles along cross section A-A'.

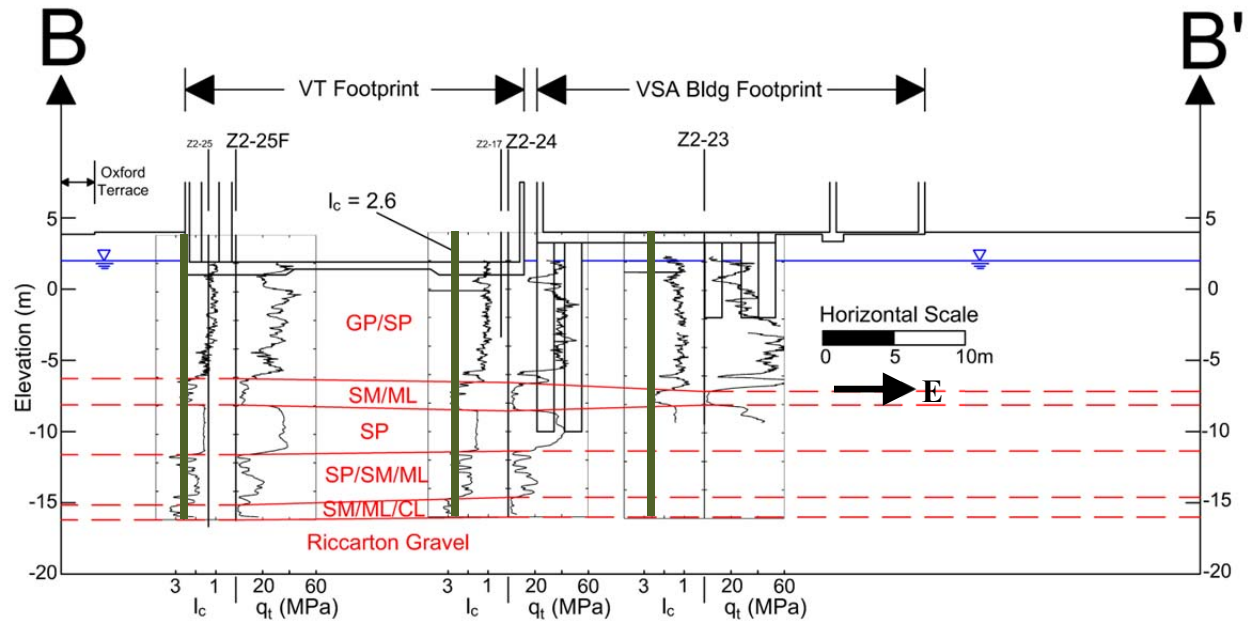

Figure 4.7.8. CPT tip resistance and normalized soil behavior type index profiles along cross section B-B'.

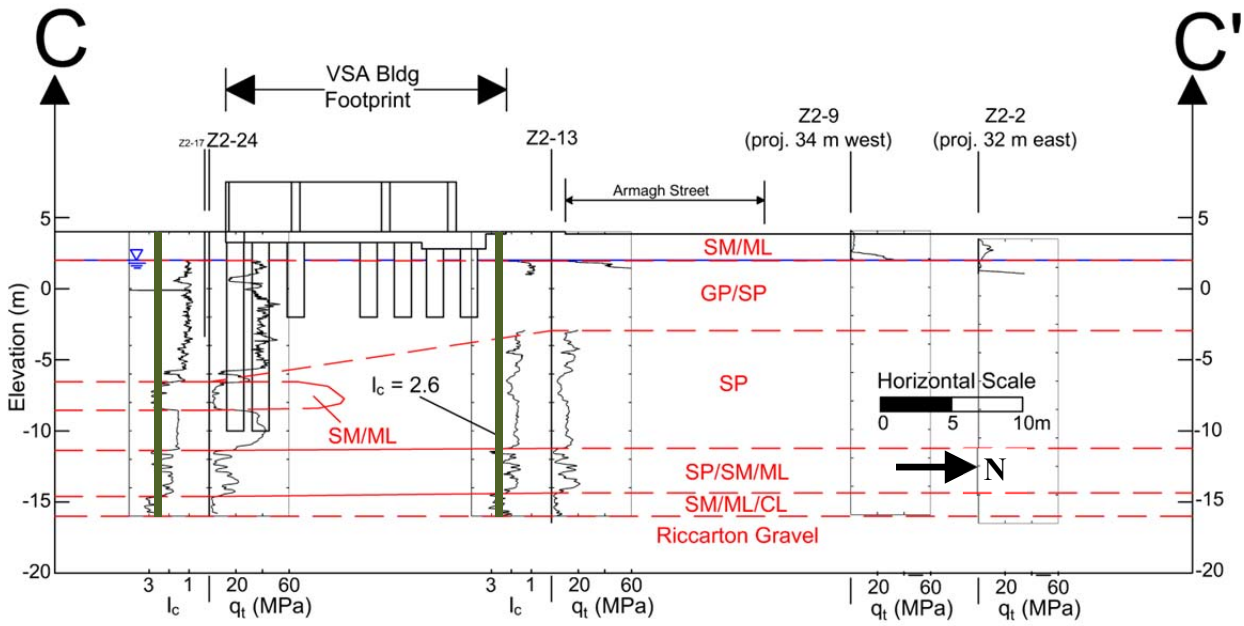

Figure 4.7.9. CPT tip resistance and normalized soil behavior type index profiles along cross section C-C' with VSA building foundation shown for reference.

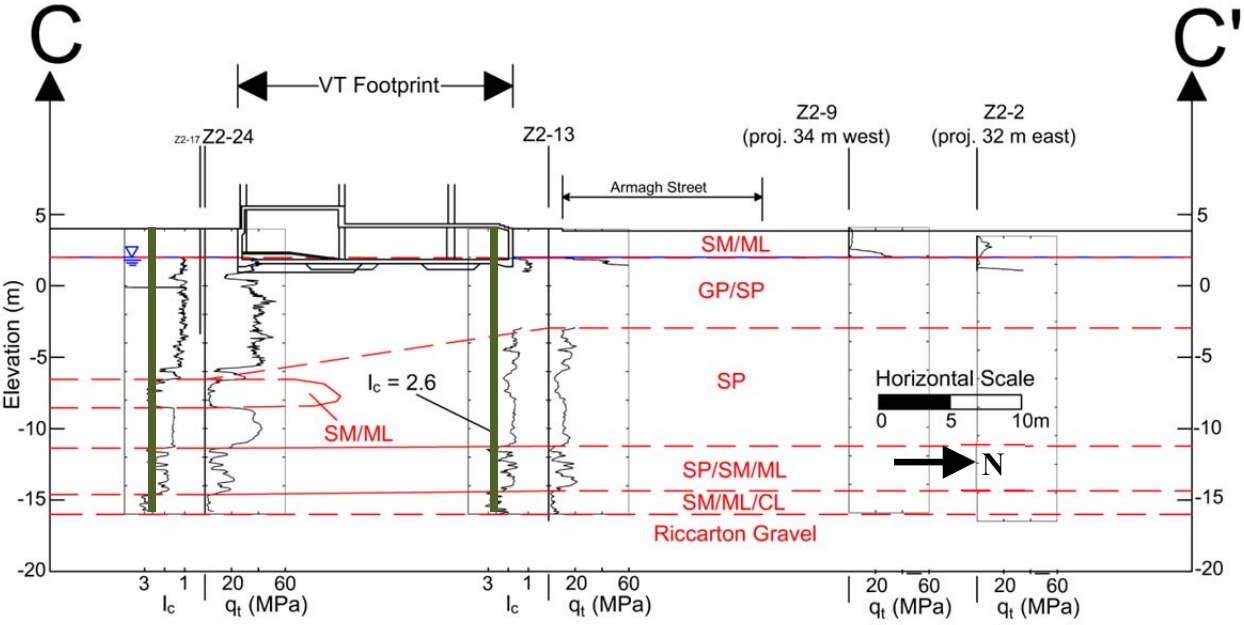

Figure 4.7.10. CPT tip resistance and normalized soil behavior type index profiles along cross section C-C' with VT building foundation shown for reference.

Figure 4.7.7 illustrates that the subsurface profile along the northern end of the site beneath the VT and VSA buildings generally consists of the following six units:

1) Very loose to medium dense silt and sandy silt with q_t generally less than 10 MPa and $1.5 < I_c < 2.5$ to depths typically less than about 2 m;
2) Medium dense to very dense sand, gravelly sand, and sandy gravel with q_t greater than 10 MPa and often greater than 40 MPa and $1.0 < I_c < 2.0$ to depths between about 7 m and 10 m;
3) Medium dense to dense sand with 5 MPa $< q_t <$ 20 MPa and $1.5 < I_c < 2.0$ to depths between 11.7 m and 15.2 m;
4) Interbedded SP/SM/ML with 0 MPa $< q_t <$ 20 MPa;
5) SM/ML/CL with q_t typically less than 10 MPa and I_c often greater than 2.6 to a depth of about 20 m; and
6) Riccarton Gravels. As discussed previously, more information regarding the characteristics of the Riccarton Gravels are provided in Section 4.1 and by Tonkin and Taylor (2011).

At CPT Z2-22, a layer of denser sand, gravelly sand, and/or sandy gravel was observed beneath the SP layer at a depth of about 11.7 m. This SP/GP layer had a tip resistance of 10 MPa to greater than 40 MPa and caused refusal at a depth of approximately 13.5 m.

The subsurface profile along the south end of the site, as illustrated in Figure 4.7.8, was relatively uniform and similar to the subsurface profile summarized above for the north end of the site with a few differences:

1) The layer of medium dense to very dense GP/SP was observed to depths of 10 - 11 m on the south end as opposed to 7 - 10 m on the north end.
2) Beneath the GP/SP layer there is a layer of loose to medium dense SM/ML with $q_t <$ 10 MPa and I_c often around 2.5 to 2.7 to depths of 12 – 12.5 m;
3) Beneath this SM/ML layer, there was a layer of very dense SP with $q_t >$ 30 Mpa to a depth of approximately 15.5 m. This layer was underlain by the interbedded SP/SM/ML described above and the remainder of the southern subsurface profile was similar to the profile described above for the northern portion of the site.

Key building foundation elements for the VT and VSA buildings have been shown on Figures 4.7.7 through 4.7.10. It is clear that the basement of the VT building is founded within the shallow gravel layer. Due to the complexity of the VSA building foundation system, some elements were founded within the shallow gravel layer and some were founded within deeper layers (e.g., the 14 and 18 m long piles located at the SW, SE, and NE corners).

Analyses and Observations

Simplified liquefaction triggering evaluations were performed utilizing the procedures described previously. The estimated PGA values at the VT and VSA building sites for the 4 SEP 10, 26 DEC 10, 22 FEB 11 and 13 JUN 11 events are summarized in Table 4.7.3. The PGA

during the 26 DEC 10 event is estimated as the median geo-mean PGA recorded at the four SMS within the CBD. The remaining PGAs were estimated using the work of Bradley and Hughes (2012).

Table 4.7.3. Summary of PGA values used in RW98 and ZR02-RW98 analyses.

Event	M_w	PGA_{16} (g)	PGA_{50} (g)	PGA_{84} (g)
4 SEP 10	7.1	0.16	0.21	0.27
26 DEC 10	4.8	0.22		
22 FEB 11	6.2	0.33	0.44	0.58
13 JUN 11	6.0	0.17	0.23	0.31

Factor of safety against liquefaction triggering (FS_l) profiles, calculated in accordance with RW98 with the PGA_{50} during the 22 FEB 11 event, and liquefaction induced settlement profiles, calculated in accordance with ZR02-RW98 with the PGA_{16}, PGA_{50}, and PGA_{84} during the 22 FEB 11 event, are shown on Figures 4.7.11 through 4.7.14. Settlements were calculated based on volumetric strains over the upper 20 m of the soil deposit. Table 4.7.4 summarizes the settlement at the surface for the 4 SEP 10, 26 DEC 10, 22 FEB 11, and 13 JUN 11 events.

These analyses suggest that much of the layers of sand and silty sand, located directly beneath the shallow gravels at CPTs Z2-12 (depths ≈ 10–19 m), Z2-13 (depths ≈ 7–19 m), and, to a lesser extent, at Z2-22 (depths ≈ 7–11m), had a FS_l less than 1.0 during the 22 FEB 11 event. Consequently, the ZR02-RW98 volumetric strains are largely concentrated in these layers, at depths greater than 10 m at Z2-12 and greater than 7 m at Z2-13 and Z2-22. Along the southern portion of the site there are liquefiable materials within the SM/ML layer beneath the GP/SP layer between depths of approximately 10–12.5 m and interbedded liquefiable materials in the layer of SP/SM/ML between depths of 15.5 and 19 m. The layer of SM/ML mainly consists of materials with I_c values around 2.6. As described in Section 4.1, the RW98 calculations assume materials with I_c greater than 2.6 to be non-liquefiable. However, the overall interpretation of the ZR02-RW98 analyses relative to the performance of these buildings was not sensitive to minor changes to this assumption (i.e., I_c cutoff at 2.7 or 2.8, as opposed to 2.6) for these dataA nearby exploratory borehole performed by Geotech Consulting Ltd. in 2002 indicate several materials between depths of 10.5 m and 13.5 m including plastic silts, peaty silts, peat, and fine to coarse sand. Consequently, while there is some uncertainty regarding the liquefaction potential of some of the materials located within this layer, it is likely that excess pore water pressures would have been generated and some degree of cyclic softening would have occurred. In general, however, the calculated ZR02-RW98 surface settlements along the southern portion of the site are lower than the northern portion of the site because the SP layer with 5 MPa < q_t < 20 MPa is not present in the southern portion of the site.

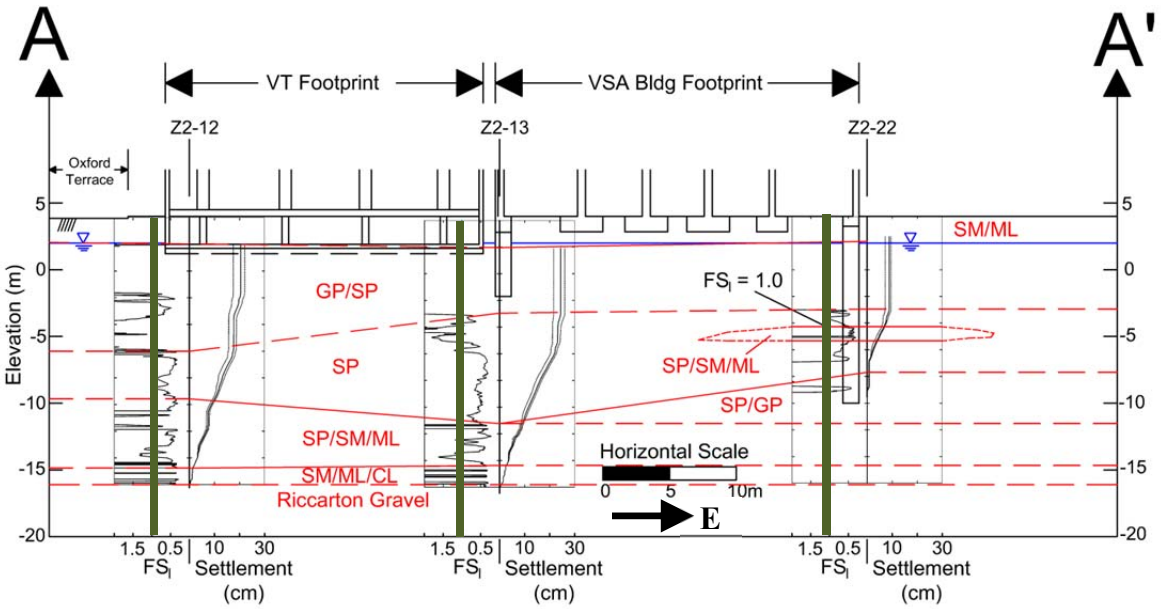

Figure 4.7.11. Factor of safety against liquefaction triggering (FS_l) profiles, calculated in accordance with RW98 for the PGA_{50} during the 22 FEB 11 event, and liquefaction induced settlement profiles, calculated in accordance with ZR02-RW98 for the PGA_{16}, PGA_{50}, and PGA_{84} during the 22 FEB 11 event, at CPT locations along cross section A-A'. Settlements are due to post-liquefaction volumetric strains in the top 20 m.

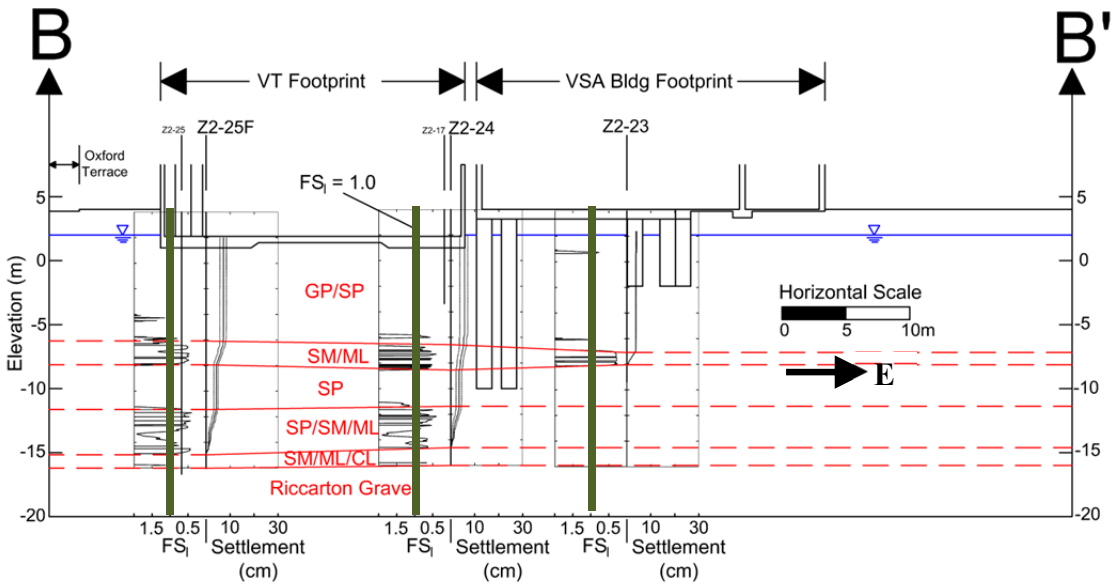

Figure 4.7.12. Factor of safety against liquefaction triggering (FS_l) profiles, calculated in accordance with RW98 for the PGA_{50} during the 22 FEB 11 event, and liquefaction induced settlement profiles, calculated in accordance with ZR02-RW98 for the PGA_{16}, PGA_{50}, and PGA_{84} during the 22 FEB 11 event, at CPT locations along cross section B-B'. Settlements are due to post-liquefaction volumetric strains in the top 20 m.

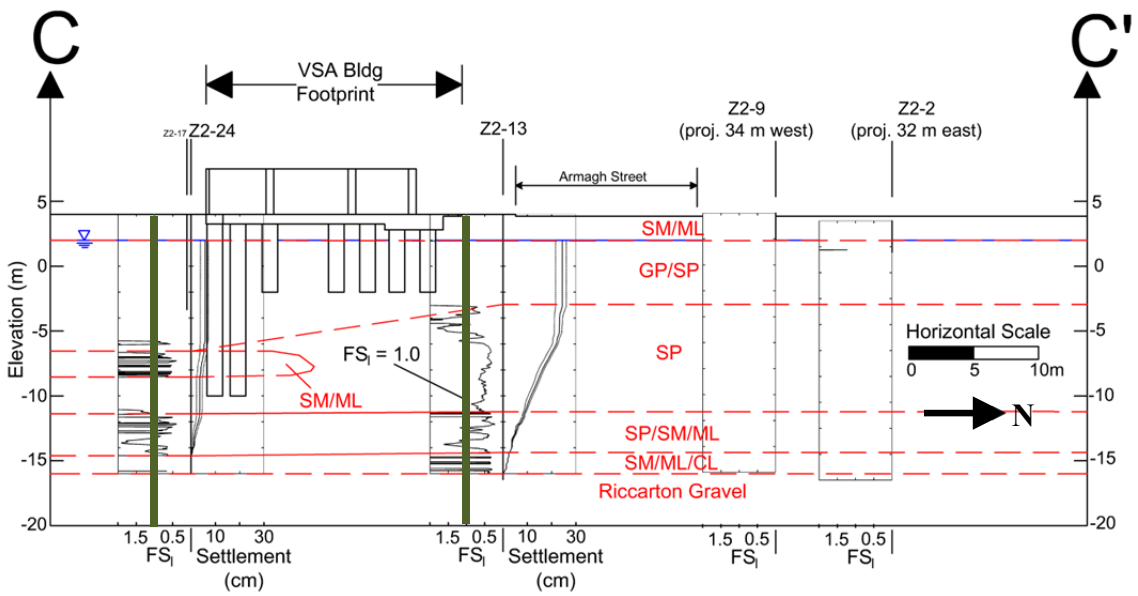

Figure 4.7.13. Factor of safety against liquefaction triggering (FS_l) profiles, calculated in accordance with RW98 for the PGA_{50} during the 22 FEB 11 event, and liquefaction induced settlement profiles, calculated in accordance with ZR02-RW98 for the PGA_{16}, PGA_{50}, and PGA_{84} during the 22 FEB 11 event, at CPT locations along cross section C-C' with the VSA building foundation shown for reference. Settlements are due to post-liquefaction volumetric strains in the top 20 m.

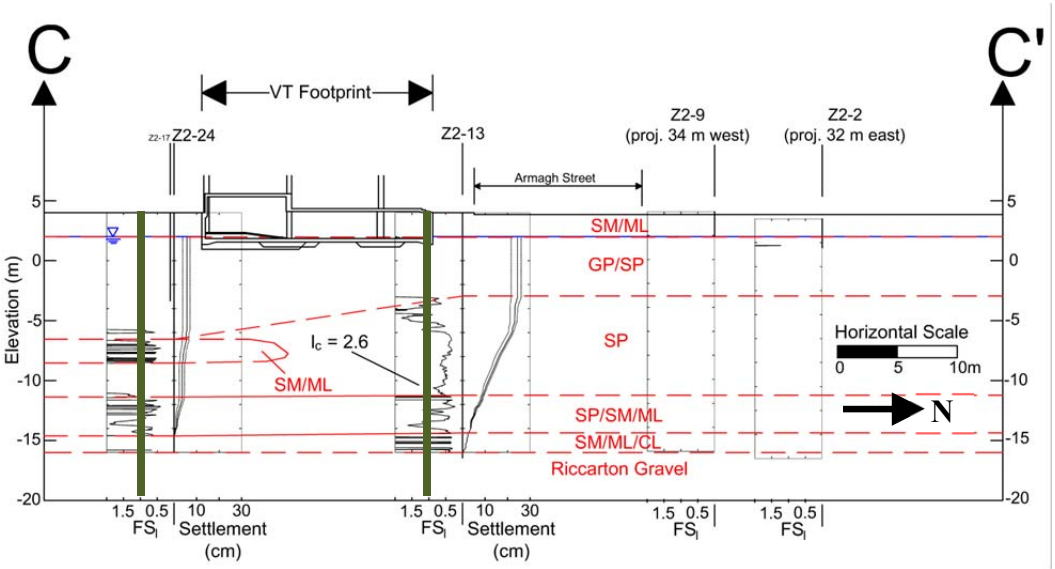

Figure 4.7.14. Factor of safety against liquefaction triggering (FS_l) profiles, calculated in accordance with RW98 for the PGA_{50} during the 22 FEB 11 event, and liquefaction induced settlement profiles, calculated in accordance with ZR02-RW98 for the PGA_{16}, PGA_{50}, and PGA_{84} during the 22 FEB 11 event, at CPT locations along cross section C-C' with the VT building foundation shown for reference. Settlements are due to post-liquefaction volumetric strains in the top 20 m.

Table 4.7.4. Calculated surface settlements at CPT locations near the VT and VSA buildings. Settlements are due to post-liquefaction volumetric strains in the top 20 m and based on median PGA estimates.

CPT ID	Reconsolidation Settlement at Surface (cm)			
	4 SEP 10	26 DEC 10	22 FEB 11	13 JUN 11
Z2-1	1	0	3	0
Z2-12	14	5	21	11
Z2-13	18	8	24	14
Z2-17	0	0	0	0
Z2-22	6	2	9	4
Z2-23	4	3	4	4
Z2-24	2	0	6	1
Z2-25	11	7	14	10
Z2-25F	4	1	7	2
Z2-26	3	1	8	2

The performance of the VT and VSA building sites during the 22 FEB 11 Christchurch earthquake was evaluated by GEER, UCB and UC researchers in March 2011. A separate evaluation was performed by researchers from the UC around that time, and a field map developed during this separate evaluation is shown in 4.7.13 (Giorgini et al., 2011a; and Giorgini, 2015). As described previously, liquefaction-induced sediment ejecta was observed on the inside edge of the sidewalk along the north and west sides of VT, and at the northeast corner. Localized asphalt cracking and settlements were observed along the sidewalk near where the sediment ejecta was observed. Further evidence of shallow liquefaction was provided by the presence of several large sand boils in nearby Victoria Park, approximately 30 – 50 m north of the building sites, as well as lateral spread-induced ground cracks up to 10 cm-wide observed along the bank of the Avon River, approximately 15 – 20 m west of VT. Tilt measurements performed at the ground floor of VT suggested a residual tilt of approximately 0.4 degrees south and 0.3 degrees east. A subsequent survey performed in October 2012 suggested a tilt of the first floor slab of approximately 0.4 - 0.5 degrees south and 0.3 – 0.4 degrees east. Water was

observed in the basement of VT following the 22 FEB 11 earthquake and again during the survey performed in October 2012. At the time of the October 2012 survey, the water was limited to the northern half of the basement because the basement access ramp was inclined downward from the south to the north and, therefore, the surface of the northern half of the basement was deeper.

Compusoft Engineering Limited was engaged by the Canterbury Earthquakes Royal Commission to study the seismic performance of the VSA building during the Canterbury earthquakes and they presented their findings in a report dated January 2012. According to this report, the VSA building settled differentially across the building footprint in the amount of 22 cm at the NW corner and 16 cm at the NE corner, relative to the SE corner during the 22 FEB 11 earthquake. This differential settlement caused the building to rotate rigidly to the northwest with a drift of approximately 0.8%. Despite this differential settlement and building rotation, damage to exposed structural elements was apparently minor and limited to minor cracking of concrete shear walls and spalling of concrete at stair landings.

The east wall of the VT building was located less than 40 cm from the west wall of the VSA building. Figures 4.7.1 through 4.7.3 illustrate the relative movement of VT and the VSA building observed following the 22 FEB 11 earthquake. The relative tilt between the VSA building and VT is apparent in Figure 4.7.1. As illustrated in Figure 4.7.3, contact between the two buildings was observed following the 22 FEB 11 earthquake. Additionally, the timber elements shown in Figure 4.7.3 suggested settlement of the VSA building relative to VT on the order of 14 cm. However, this relative settlement estimate carries some uncertainty due to the complex differential tilt between the two buildings.

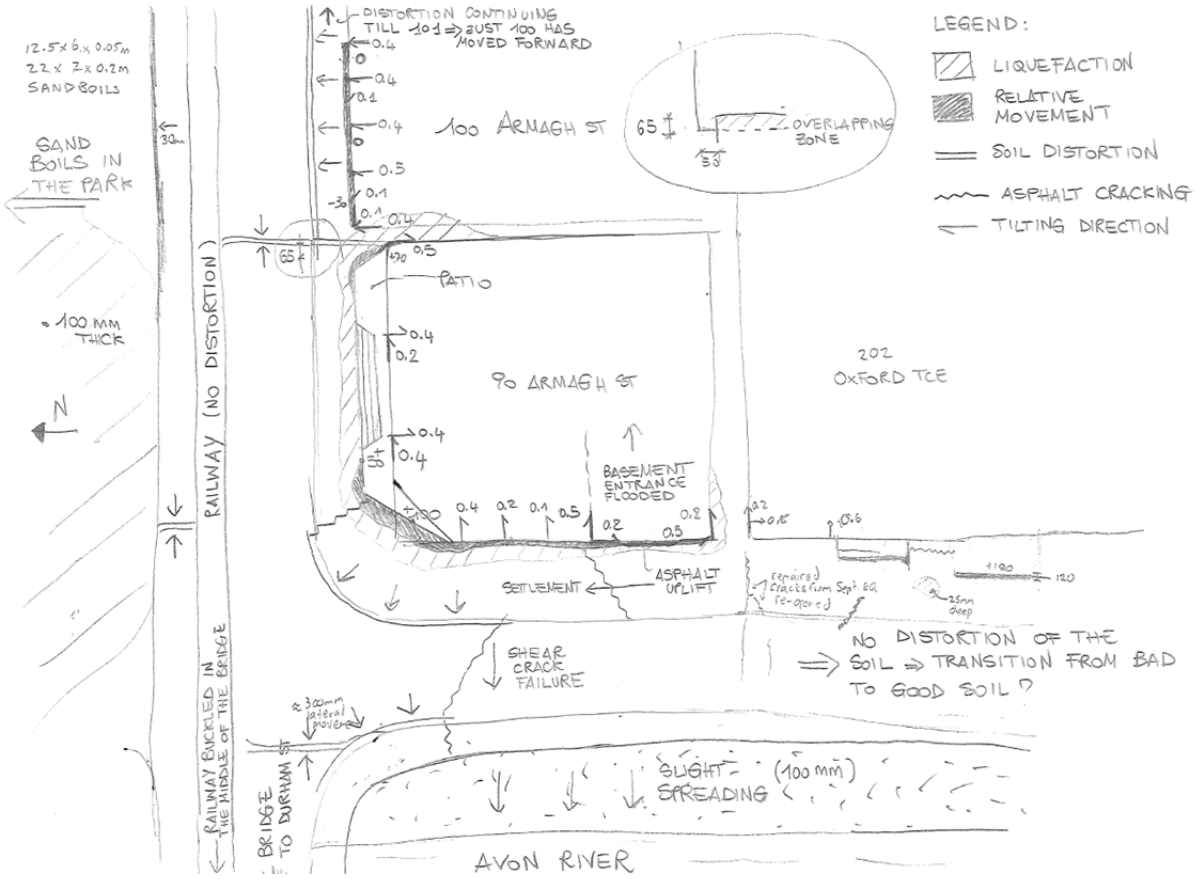

Figure 4.7.13. Field map developed during evaluation of PWC building site in March 2011 (from Giorgini et al., 2011a; and Giorgini, 2015).

As described by Cubrinovski et al. (2011a), the ground conditions near Victoria Square transition from the north where shallow and relatively thick liquefiable sand, silty sand, and sandy silt deposits predominate to the south where gravelly soils reach close to the ground surface. Near this transition the ground conditions can be quite complex. Based on the CPT data presented herein, the VT and VSA buildings appear to be located on the southern end of this transition. While there was clearly evidence of shallow liquefaction along the western and northern sides of the VT building, as well as to the north in Victoria Square, the shallow liquefiable deposits were not thick in the vicinity of the buildings and the soils encountered at the CPT locations at depths greater than or equal to 2 m generally consisted of gravel, sandy gravel, and gravelly sand. The VT basement mat foundation varied in thickness from 0.3 m to 0.9 m and was, therefore, at depths of approximately 2.4 – 3.0 m below the ground surface. The VSA building foundation system was complex and consisted of piles with lengths of 6 m, 14 m, and 18 m as well as several shallow spread footings with depths between 0.65 m and 1.2 m. Consequently, while VT was founded entirely on the shallow gravelly soils, the VSA building foundation system consisted of elements founded within and beneath the shallow gravelly soils.

As summarized in Table 4.7.5, larger ZR02-RW98 settlements are calculated for the northern end of the site than the southern end. Consequently, the 22 cm of differential settlement

between the north end of the VSA building and its south end can be explained by variable ground conditions in combination with the lack of deep piles at the NW corner of the building. This is perhaps best illustrated with Figure 4.7.12. The 6 cm of differential settlement between the NW corner of the building and the NE corner of the building appear to be explainable by the presence of 14 m piles at the NE corner (versus 6 m piles at the NW corner), in addition to slightly better ground conditions between CPTs Z2-13 and Z2-22.

The VT building was founded on a mat foundation within medium dense to very dense sand, gravelly sand, and sandy gravel that was underlain by materials at depths between approximately 7 m and 10 m that liquefied or cyclically softened due to excess pore pressure generation. Although the liquefiable materials were located at least 4 m below the base of the foundation, this is well within the depth range with a significant vertical strain influence for a foundation with a width of 19 m and L/B = 1.27 (Schmertmann, 1978). Consequently, cyclic softening of these materials due to increased pore water pressures would have likely led to building settlements. In addition, materials within the medium dense to very dense layer directly beneath the mat foundation could have cyclically softened due to increased pore water pressures during and immediately following the significant Canterbury earthquakes and this transient reduction in stiffness in materials that did not fully liquefy could have also contributed to the observed building settlement. Volumetric reconsolidation of the liquefiable materials beneath the building foundation would have also caused settlements. The tilt of the building to the south is likely best explained by a gravity load eccentricity due to the location of the elevator and stair core being offset slightly to the south from the center of the building (Fig. 4.7.4). The tilt of the VT building to the east is more difficult to explain based on the available information. However, it is possible that structural vibrations transmitted through the piles of the adjacent VSA building led to relatively higher excess pore water pressures in this area, and therefore, more significant cyclic softening, of the SM/ML materials on the east side of the building relative to the SM/ML materials on the west side of the building. As indicated on Fig. 4.7.5, the VSA building piles were mostly 14 m long in the vicinity of the southeast corner of the VT building. As with the PWC building, advanced SSI numerical models will likely be able to provide more insight into the complex performance of the VT and the VSA buildings, and these analyses are underway by researchers at the University of California at Berkeley and the University of Canterbury.

It should also be highlighted that the ZR02-RW98 settlement calculations presented in Table 4.7.5, yet again, suggest settlements higher than what were observed for the 4 SEP 10 and 13 JUN 11 events. Based on the Compusoft Engineering (2012) report, the 4 SEP 10 earthquake caused no structural damage and only minor cracking to non-structural components at the VSA building. The author is not aware of any reports of damage to VT following the 4 SEP 10 earthquake.

4.8 Engineering Performance of the SCH Building

Introduction and Structural Design

The SCH building, located at 87-89 Kilmore Street in Christchurch, New Zealand (Lat -43.52628, Lon 172.63470), was a seven-story, reinforced concrete frame structure (Figure 4.8.1) on a drilled shaft foundation. The building was located on the same street and approximately 270

m west of the FTG-7 building described previously. As described by Cubrinovski et al. (2011a), significant amounts of liquefaction induced sediment ejecta were observed in the area of this building following the Christchurch earthquake, but the building did not appear to punch into the ground or undergo significant differential settlement. Following the Christchurch earthquake, however, the building was vacated and several geotechnical studies were performed to assess its condition. The results of these studies have been summarized in reports by Geotech Consulting Ltd. (2012), Hushmand Associates, Inc. (2012), henceforth HAI, and KGA Geotechnical Investigations Ltd. (2012), henceforth KGA, and were made available for this work by the building owner.

Figure 4.8.1. Photo of the SCH Building from March 2011.

A plan view of the SCH building site is provided in Figure 4.8.2, along with key building foundation elements. Detailed summaries of the building design are provided by KGA (2012) and HAI (2012). The following is a brief summary based on these more detailed descriptions:

- Approval for construction was issued by Christchurch City Council in September 1995.
- The building was located on a flat lot and the building footprint was approximately 34 m in the east-west direction and 40 m in the north-south direction. The ground floor level was at or very near the ground surface level prior to construction.
- The building was a seven-story reinforced concrete frame with reinforced masonry perimeter wall cladding.

- Stairwells were located on both the east and west sides near the center of the building in the north-south direction. The elevator shaft was located just west of the eastern stairwell.
- The building foundation consisted of 75 reinforced concrete drilled shafts. The diameter of the drilled shafts was variable between 0.6 m and 0.9 m. The design toe depths were nominally 9 m, though it appears that the design intent was to penetrate a shallow layer of gravel that was expected between 6.5 and 7.5 m below the ground surface by 0.75 m.
- 34 of the 75 drilled shafts had enlarged bases over the bottom 1 m length of the shaft. These enlargements resulted in pile bases that ranged from 0.6 m to 1.7 m. The remaining shafts were straight sided shafts for the full depth.
- A Standard Penetration Test (SPT) was supposed to have been performed following excavation of each drilled shaft to assess the competency of the base materials. A minimum SPT blow count of 30 blows per foot was required.
- Perimeter drilled shafts were connected by a grade beam that was 1 m wide and 1.4 m deep. Six of the interior shafts were isolated with 1.8 m square pile caps that were 1.2 m deep.
- The ground floor slab was a 125 mm slab-on-grade, lightly reinforced with 663 mesh. The slab appears to have been connected to the pile caps in the middle of the building and also the pile caps around the perimeter of the building.

Based on additional information provided by KGA (2012), it appears that the drilled shafts were constructed without the use of dewatering measures. In addition, the as-built shafts were excavated deep enough to “reach” a gravel layer that was typically found at depths between 6 m and 7 m.

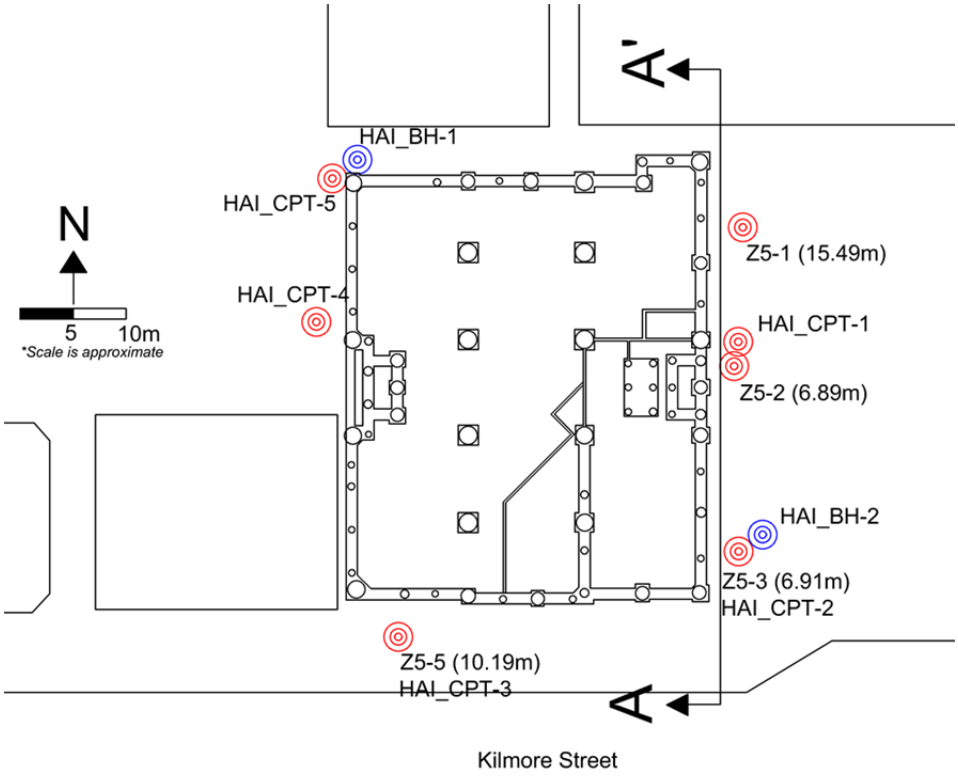

Figure 4.8.2. SCH Building site with foundation elements and CPT locations (with depths).

Site Characterization

Four CPTs were performed by UCB in July 2011, and five CPTs were performed by HAI in March and April 2012. HAI also performed two soil borings during their investigation. While the HAI geotechnical report has been made available to us, the CPT data collected by HAI was not made available and had not been uploaded to the CGD as of the time of this summary. Consequently, while the HAI results have been reviewed, the subsequent figures and analyses are based primarily on the results of the UC Berkeley CPTs.

The CPT data collected by UC Berkeley in July 2011 were made available to HAI prior to their field investigation. Between the completion of the UC Berkeley field investigations and the beginning of the HAI field investigation at this location, McMillan drilling services developed the pre-collaring system described in Section 4.1. HAI utilized this system to advance their CPTs to greater depths than were possible during the earlier UC Berkeley investigation. HAI_CPT-2 and HAI_CPT-3 appear to have been performed in the same locations as Z5-3 and Z5-5, respectively. HAI_CPT-1 appears to have been performed just north of Z5-2. The locations and corresponding depths of the CPTs and boreholes are indicated on Figure 4.8.2 and summarized in Table 4.8.1. All CPTs reported in Table 4.8.1 were performed by McMillan Drilling Services.

The HAI boreholes were performed by Pro-Drill using a “Mobile Drill Sonic 1000 drill rig”. SPTs were performed at 1.5 m intervals and consisted of using a 63.5 kg weight falling 760

mm. The number of blows to advance the SPT sampler over each 75 mm interval were recorded and are indicated on the HAI boring logs (HAI 2012). In their analyses, HAI assumed a hammer efficiency of 85%.

Table 4.8.1. Summary of CPTs performed adjacent to the PWC Building.

CPT/Borehole ID	Investigation	Test Type	Surface Elevation† (m)	Refusal Depth (m)
Z5-1	UC Berkeley	CPT	5.9	15.5
Z5-2	UC Berkeley	CPT	5.9	6.9
Z5-3	UC Berkeley	CPTu	5.9	6.9
Z5-5	UC Berkeley	CPT	5.7	10.2
HAI_CPT-1	HAI	CPT	n/a	21
HAI_CPT-2	HAI	CPT	5.9	21
HAI_CPT-3	HAI	CPT	5.7	15
HAI_CPT-4	HAI	CPTu	n/a	15
HAI_CPT-5	HAI	CPTu	n/a	16
HAI_BH-1	HAI	CPTu	n/a	30.5
HAI_BH-2	HAI	CPTu	n/a	25.9

†Indicated surface elevations were based on estimates provided by Tonkin and Taylor. Elevations are relative to the Lyttelton Vertical Datum (meters above sea level).

The groundwater table depth was assumed to be approximately 2.0 m below the ground surface during the 4 SEP 10, 26 DEC 10, and 22 FEB 11 events and 1.5 m below the ground surface during the 13 JUN 11 event based on regional groundwater models developed by T&T (Canterbury Geotechnical Database, 2013). Figure 4.8.3 provides the corrected tip resistance, q_t, and the normalized soil behavior type (SBT) index, I_c, profiles along cross section A-A' shown on Figure 4.8.2.

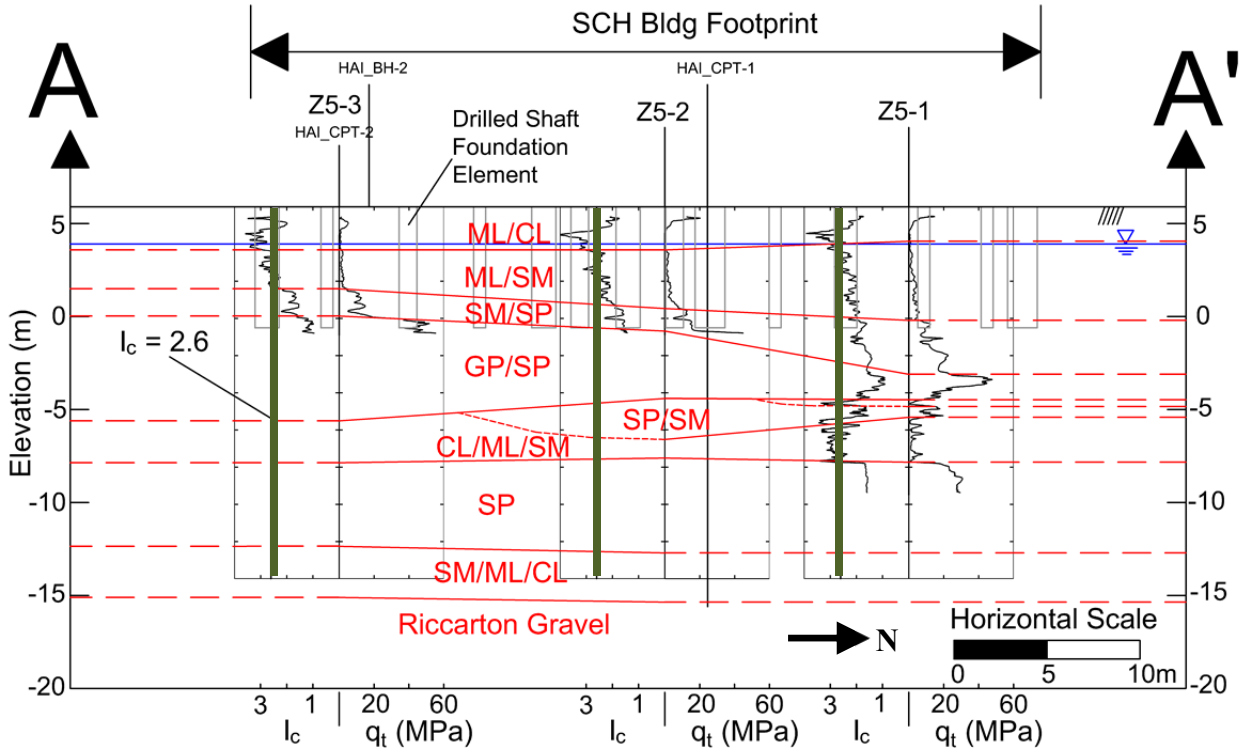

Figure 4.8.3. CPT tip resistance and normalized soil behavior type index profiles along cross section A-A'. Drilled shaft depths and diameters are approximate. Pile base enlargements are not shown. HAI_CPT-1 and HAI_CPT-2 provided additional subsurface information at the locations indicated and were considered during the development of the subsurface profile.

The SCH building drilled shafts are illustrated on Figure 4.8.3 for reference. As noted, the diameters and depths of the drilled shafts are approximate. Figure 4.8.3 illustrates that the shallow subsurface profile beneath the SCH building primarily consists of the following eight units:

1) Very loose and/or very soft to stiff ML/CL with q_t generally less than 2 MPa and $2.0 < I_c < 3.6$ to depths of around 2 m;
2) Very loose to medium dense SM/ML with $0 \text{ MPa} < q_t < 5 \text{ Mpa}$ and $2.0 < I_c < 3.0$ to depths between about 4 m and 6 m;
3) Medium dense to dense SM/SP with $10 \text{ MPa} < q_t < 20 \text{ MPa}$ and $1.5 < I_c < 2.0$ to depths between about 6 m and 9 m;
4) Dense to very dense GP/SP with q_t between 20 MPa and greater than 40 MPa and $1.0 < I_c < 2.0$ and typically less than 1.5 to depths between 9 m and 11.5 m.;
5) CL/ML/SM with $q_t < 10$ MPa and $2.0 < I_c < 3.0$ to depths of 13 m to 14 m;
6) Dense to very dense SP with $20 \text{ MPa} < q_t < 30 \text{ MPa}$ and $1.5 < I_c < 2.0$ to depths of 18 m to 19 m.
7) SM/ML/CL with $q_t < 15$ MPa and often less than 10 MPa to depths of 20 m to 21 m.
8) Riccarton Gravels. As discussed previously, more information regarding the characteristics of the Riccarton Gravels are provided in Section 4.1 and by Tonkin and Taylor (2011).

Although they are not shown, the CPT profiles for HAI_CPT-1 and HAI_CPT-2, and the borehole log for HAI_BH-2, were considered when developing the subsurface profile shown in Figure 4.8.3. It is unclear what depth the drilled shafts were extended to at the north end of the site as the GP/SP layer was not encountered until a depth of approximately 9.0 m at Z5-1.

Analyses and Observations

Simplified liquefaction triggering and free-field settlement evaluations were performed utilizing the RW98 and ZR02 procedures. The estimated PGA values at the SCH site for the 4 SEP 10, 26 DEC 10, 22 FEB 11 and 13 JUN 11 events are summarized in Table 4.8.2. The PGA during the 26 DEC 10 event is estimated as the median geo-mean PGA recorded at the four SMS within the CBD. The remaining PGAs reported above were estimated using the work of Bradley and Hughes (2012).

Table 4.8.2. PGA values for RW98 and ZR02-RW98 analyses

Event	M_w	PGA_{16} (g)	PGA_{50} (g)	PGA_{84} (g)
4 SEP 10	7.1	0.17	0.22	0.27
26 DEC 10	4.8	0.22		
22 FEB 11	6.2	0.35	0.45	0.58
13 JUN 11	6.0	0.18	0.24	0.30

Factor of safety against liquefaction triggering (FS_l) profiles, calculated in accordance with RW98 for the PGA_{50} during the 22 FEB 11 event, and liquefaction-induced settlement profiles, calculated in accordance with ZR02-RW98, at CPT locations along cross section A-A', are presented in Figure 4.8.4. Settlements are due to post-liquefaction volumetric strains in the top 6.5 m.

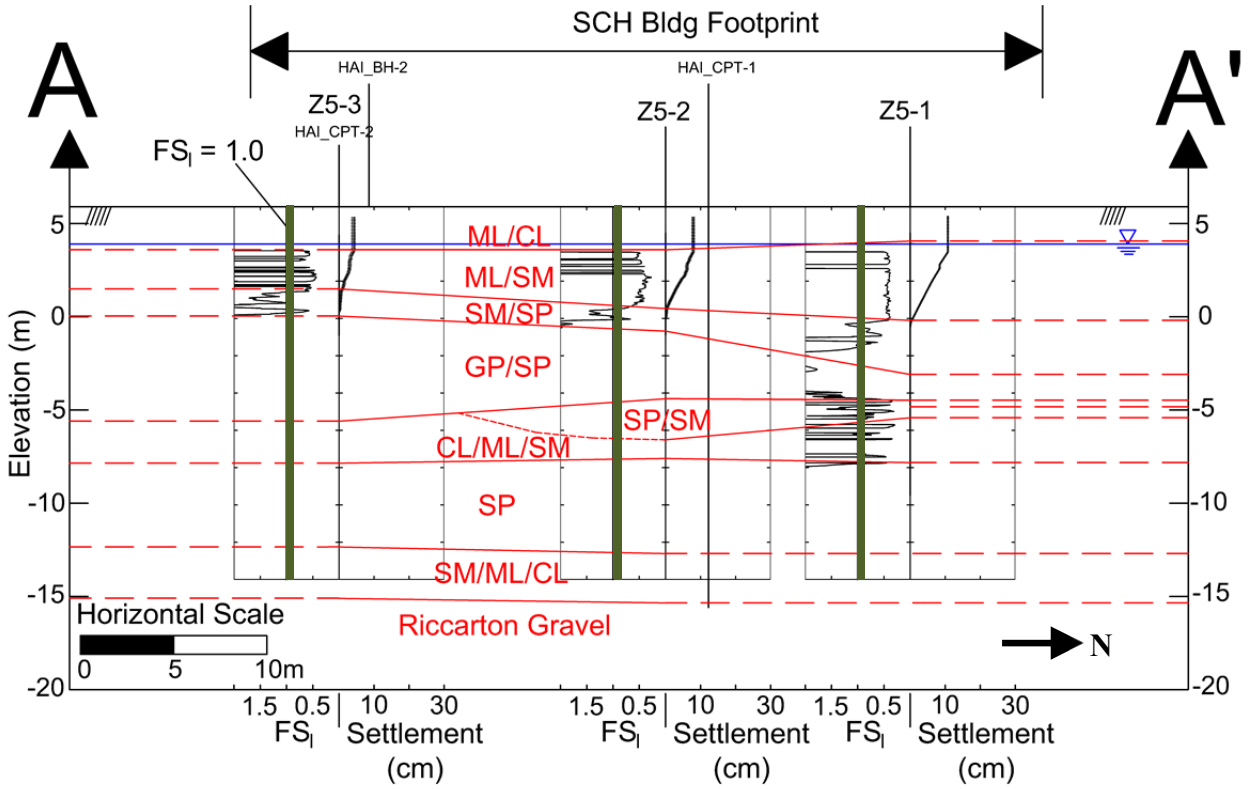

Figure 4.8.4. Factor of safety against liquefaction triggering (FS_l) profiles, calculated in accordance with RW98 for the PGA_{50} during the 22 FEB 11 event, and liquefaction-induced settlement profiles, calculated in accordance with ZR02-RW98, at CPT locations along cross section A-A'. Settlements are due to post-liquefaction volumetric strains in the top 6.5 m.

It is clear from this figure that much of the shallow ML/SM layer should have liquefied during the 22 FEB 11 event. As described previously, the RW98 liquefaction triggering correlation considers the soil non-liquefiable when $I_c > 2.6$. The soils within this layer have an I_c around 2.6 in many cases at this building site. As we would expect, the FS_l profile is erratic when this is the case and that is observed at CPT Z5-3. However, the overall interpretation of the ZR02-RW98 analyses relative to the observed performance of this building was not sensitive to minor changes to this assumption (i.e., I_c cutoff at 2.7 or 2.8, as opposed to 2.6) for these data. HAI performed a particle size analysis per ASTM D422 and Atterberg limits per ASTM D4318 on a sample collected from HAI_BH-2 at a depth of 3.0 m. Based on these tests, the soil was classified as a gray, non-plastic silt (ML) and the FC was determined to be 96.5%.

There are also liquefiable soils in the underlying SM/SP layer, though the FS_l values were generally higher than the shallower ML/SM materials. Similar laboratory tests were performed on a sample from HAI_BH-2 at a depth of 4.5 m and the soil was classified as a gray, silty sand (SM) with a FC = 26.6 %.

It is also observed from the profile at Z5-1 that there are deeper liquefiable deposits of SP/SM/ML beneath the GP/SP layer that was likely the founding stratum for the piles. The I_c within this layer varies around 2.6 at depths between approximately 11 m and 14 m.

Consequently, the FS_l profile is a little erratic within this unit. Corresponding layers of potentially liquefiable materials appear to have been encountered by HAI at HAI_CPT-1 and HAI_CPT-2 from approximately 10 m to 14 m (HAI, 2012).

Ground surface settlements were calculated based on volumetric strains over the upper 6.5 m of the soil deposit to facilitate direct comparison between CPTs Z5-1, Z5-2, Z5-3, and Z5-5. These calculations are presented in Table 4.8.3 for the 4 September 2010, 26 December 2010, 22 February 2011, and 13 June 2011 events.

Table 4.8.3. Calculated surface settlements at CPT locations near the SCH building. Settlements are due to post-liquefaction volumetric strains in the top 6.5 m and based on median PGA estimates.

CPT ID	Reconsolidation Settlement at Surface (cm)			
	4 SEP 10	26 DEC 10	22 FEB 11	13 JUN 11
Z5-1	10	3	11	10
Z5-2	7	2	8	6
Z5-3	3	0	4	2
Z5-5	6	1	8	6

It is clear from Table 4.8.3 that free-field settlements due to volumetric strains in the upper 6.5 m are estimated to be around 10 cm during the 22 FEB 11 event. The estimate is slightly lower at CPT Z5-3 due primarily to a thinner ML/SM layer and slightly higher I_c values within this layer. As has been the case for many of the CPT profiles evaluated for these four seismic events, the estimated free-field settlements are similar for the 4 SEP 10, 22 FEB 11, and 13 JUN 11 events while the observed settlements were significantly greater during the 22 FEB 11 event.

Assuming the drilled shafts were founded at depths of approximately 6.0 – 7.0 m, it is likely that increased pore pressures within the ML/SM and SM/SP layers and the resulting decreased effective stresses would have led to decreased side friction resistance. This loss of side friction resistance would have likely caused a portion of the structural load to be transferred to end bearing and resulted in the compatible amount of settlement required to develop the increased end bearing resistance. This load transfer process likely would have been complicated by a number of factors including vertical ground accelerations, superstructure rocking, and, importantly, liquefaction of soils beneath the bases of the drilled shafts.

To quantify the effect of liquefaction beneath the base of the drilled shafts, free-field settlements were calculated at CPT Z5-1 using the refusal depth (i.e., 15.5 m) as the settlement baseline depth. These calculations are summarized in Table 4.8.4.

Table 4.8.4. Calculated ZR02-RW98 settlements at CPT Z5-1

Event	Free-Field Settlement (cm) at CPT Z5-1		
	Baseline Depth = 6.5 m	**Baseline Depth = 15.5 m**	**Settlement Beneath Drilled Shafts**
4 SEP 10	10	13	3
26 DEC 10	3	4	1
22 FEB 11	11	15	4
13 JUN 11	10	12	2

As has been discussed previously, we don't expect to estimate building foundation settlement accurately using free-field methods based on the integration of post-liquefaction volumetric reconsolidation strains. The intent with Table 4.8.4 is not to do that. Rather, these methods are used to evaluate the insight that they might provide to these problems. In this case, we observe that there are minor, but non-zero, free-field settlements due to the materials beneath the base of the drilled shafts. Consequently, while these settlements are relatively small, they are not zero and, therefore, would likely have contributed to the settlement of the foundation shafts.

The SCH building was evaluated by GEER researchers following the 22 FEB 11 earthquake and their initial observations were summarized by Cubrinovski et al. (2011a). While significant amounts of liquefaction-induced sediment ejecta were found in the area, the building did not appear to have punched into the ground and differential settlements between adjacent columns were often negligible and rarely up to 3.5 cm.

Figure 4.8.5. Photos of the ground floor level of the SCH building. While significant sediment ejecta was observed, there was little differential settlement.

A post-earthquake floor level survey was performed by TM Consultants in January 2012. The results of this survey were included in the HAI geotechnical report (HAI, 2012). HAI

reported the maximum differential settlement was measured to be approximately 3 cm over a distance of 2.5 m. KGA reported a differential settlement of nearly 9 cm between the high point and the low point of the ground floor (the distance between the two points was not reported). A review of the floor level survey data appears to indicate that, in general, the center of the building settled slightly more than the perimeter of the building.

Similarly, differential settlements measured on level-two through level-seven were 11 cm, 12 cm, 12 cm, 12 cm, 10 cm, and 12 cm respectively. The building appeared to be plum and there was no verticality survey performed.

Consequently, there appears to have been a minor amount of differential settlement between the perimeter of the building and the interior of the building and the most likely explanation for this settlement is due to the load transfer mechanism described above and, possibly, liquefaction of soils at depths between approximately 10 m and 14 m. Despite these minor differential settlements, the SCH building performed well during the Canterbury earthquakes relative to many of its neighboring structures.

4.9 Engineering Performance of the CTH Building

Introduction and Structural Design

The CTH building was located at 86-100 Kilmore Street in Christchurch, New Zealand (Lat -43.52693, Lon 172.63514), approximately 30 m southeast of the SCH building described previously. Cubrinovski et al. (2011a) described the CTH building as follows:

> *The Christchurch Town Hall for Performing Arts, designed by Sir Miles Warren and Maurice Mahoney and opened in 1972, is located within the northwest quadrant of the CBD, with the meandering Avon River to its immediate south. It is a complex facility comprising a main auditorium (seating 2,500) with adjoining entrance lobby, ticketing, and café areas. Further extensions provide a second, smaller auditorium, the James Hay Theatre (seating 1,000), and a variety of function rooms and a restaurant. The structures are supported on shallow foundations except for the kitchen facility, which was added later. Air bridges connect the complex to the Crowne Plaza, a major hotel, and to the Christchurch Convention Centre (opened in 1997) to the north. Tiled paved steps lead from the southern side of the complex down to the river's edge, with fountains and views across to Victoria Park. (pp. 901-902)*

The CTH building site location plan is provided in Figure 4.9.1a and several views of the building complex are shown in Figure 4.9.2. The plan area of the building complex was approximately 6500 m^2 (Holmes Consulting Group, 2011). This section is focused on documenting the seismic performance of the auditorium. Therefore, the foundation plan for that portion of the CTH building site has been indicated on Figures 4.9.1a and 4.9.1b for reference.

Based on its 1968 structural design drawings, the auditorium footprint was approximately 63 m in the east-west direction and 47 m in the north-south direction and generally consisted of a basement, a ground floor, a gallery, and the roof. As shown in Figure 4.9.1b, the foundation system for the auditorium consisted of an outer ring of rectangular shallow RC spread footings

that were all 0.46 m thick and either 2.2 m by 3.2 m or 3.15 m by 3.2 m in plan and an inner ring of square shallow RC spread footings that were all 0.61 m thick and 3.65 m by 3.65 m in plan. The base depths of the outer ring of footings were 3.6 m, 2.7 m, or 1.9 m below the ground surface and the base depths of the inner ring of footings were 3.8 m or 2.9 m below the ground surface. The outer footings were connected by RC tie beams that were 0.46 m wide by 0.46 m deep and the inner footings were connected by RC tie beams that were 1.8 m wide and 0.61 m deep. 0.91 m wide by 0.46 m deep strip footings supported wall units around the outer ring at the northwest, northeast, southwest, and southeast corners. Several additional square RC spread footings were located within the inner ring and were 1.07 m by 1.07 m in plan and 0.46 m thick. The base depths of these footings were 3.6 m below the ground surface.

The thickness of the concrete basement slab was 0.20 m and the surface of the slab was 3.0 m below the ground surface. The ground floor slab was 0.10 - 0.13 m thick and the gallery flooring consisted of either 0.13 m thick slab concrete or precast double tee units. The ground flooring above the basement and the gallery flooring were supported by RC beams and RC columns of varying dimensions.

The roof was made up of mostly .075 – 0.10 m thick pre-cast concrete units that supported a .05 m thick lightweight concrete (6.3 – 7.9 kN/m^3) topping. The roof was supported by the outer ring and inner ring RC columns. Struts provided additional support between the outer column ring and inner column ring, and a series of north-south trending trusses provided additional support across the span of the inner column ring. Holmes Consulting Group (2011) estimated the natural period of the CTH building to be approximately 0.5 s in both the north-south and east-west directions.

The CTH building complex was significantly damaged during the 22 FEB 11 earthquake. Several studies were performed to assess its condition. The results of these studies have been made publicly available by the CCC. In particular, the Holmes Consulting Group, henceforth HCG, structural evaluation report (HCG, 2011) and the T&T post-earthquake and foundation repair assessment report (T&T, 2013) include important relevant information and have served as primary references for this work. Cubrinovski et al. (2011a) described the damage to the CTH building complex:

> *Differential settlements, caused by punching shear beneath the building's main internal columns that surround the auditorium and carry the largest dead loads to shallow foundations and a second ring of exterior columns [(Figure 4.9.2a)] that are connected to the inner ring via beams [(Figure 4.9.2b)], caused distortion to the structure. The cracked beam shown in [Figure 4.9.2b] underwent an angular distortion of 1/70 across its span. The seating for the auditorium has been tilted and dragged backward due to the settlement of the surrounding columns. Additionally, the floor of the auditorium is now domed due to differential uplift relative to the columns. The air bridge connecting the main auditorium to the Christchurch Convention Centre to the north (away from the river) has separated from the building. With no significant deformations of the ground as the obvious source of this lengthening between the two buildings, the explanation appears to be that distortions to the auditorium structure have pulled the outer walls in toward the building, creating this separation. The entire complex appears to have moved laterally toward the river (albeit by a barely perceptible amount on the northern side)*

with parts of the complex closest to the river undergoing increasingly larger movements [(Figure 4.9.2c)]. These sections have settled and moved laterally toward the river more than the remainder of the building, leading to significant structural deformations where the extension and original structures are joined. (p. 902)

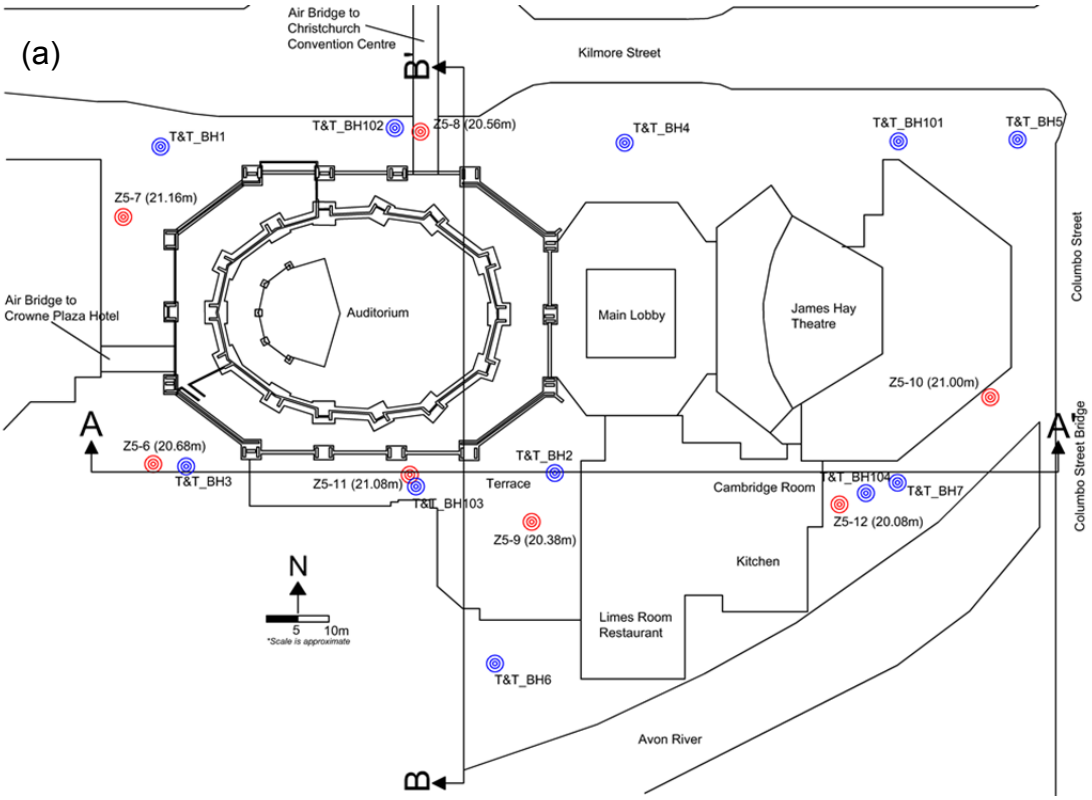

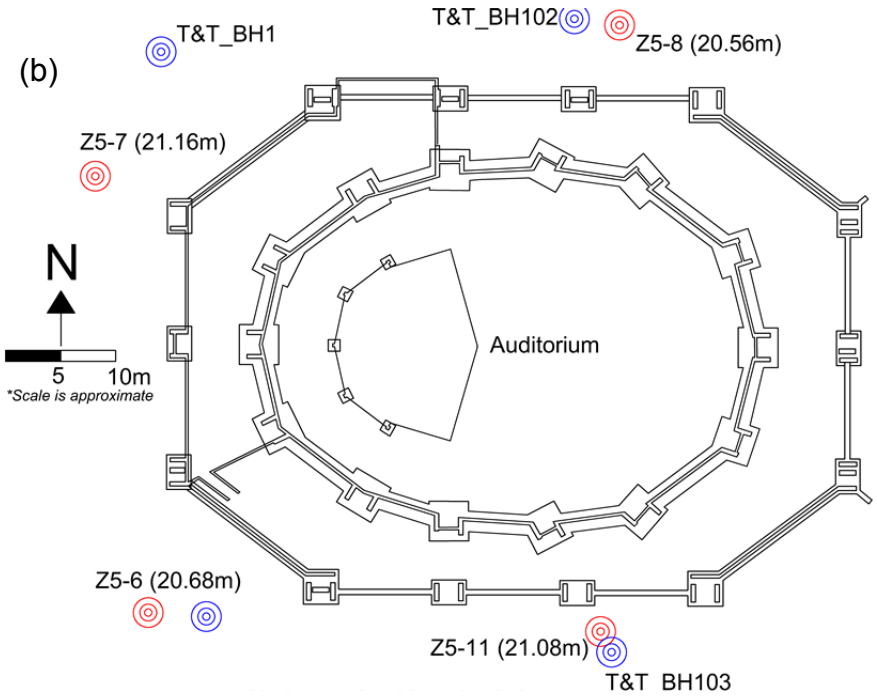

Figure 4.9.1. (a) Plan view of the CTH building site with CPT and borehole locations. (b) Zoomed-in view of the auditorium with the foundation plan shown for reference.

Figure 4.9.2. Photos of the (a) auditorium as viewed from the north, (b) the restaurant as viewed from the west, and (c) restaurant as viewed from Victoria Square Park to the south, Photos were taken March 2011.

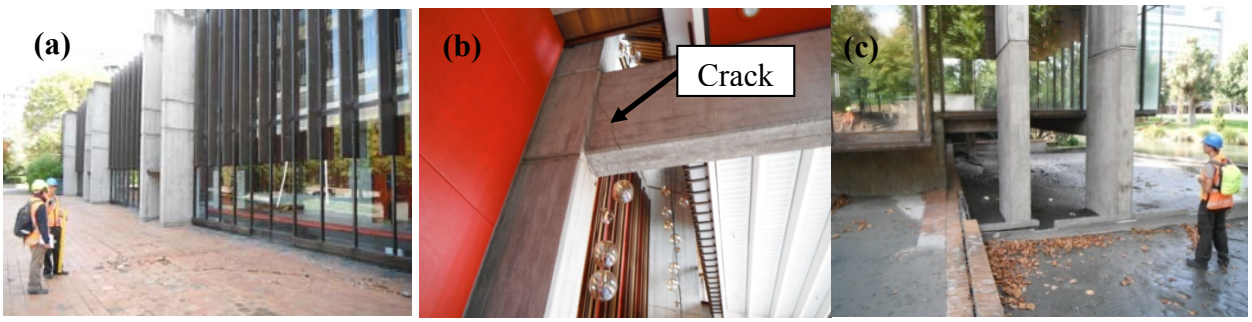

Figure 4.9.3. Modified version of Figure 13 from Cubrinovski et al. (2011a). Views of (a) the auditorium from the south, (b) a cracked beam that spanned between the interior ring of structural columns and the exterior ring of structural columns, and (c) the south end of the restaurant as viewed from the west.

Site Characterization

T&T performed subsurface investigations at the CTH building site during the periods of April - October 2011 and April 2013. The 2011 investigations consisted of eight CPTs to depths of approximately 8 m below the ground surface, seven boreholes (T&T_BH1 – T&T_BH7) to between 20 and 29 m below the ground surface, installation of four standpipe piezometers (T&T_BH2, BH4, BH6, and BH7), and installation of four inclinometers (T&T_BH2, BH4, BH6, and BH7) to monitor lateral movements towards the Avon River. The 2013 investigations consisted of four additional boreholes (T&T_BH101 – T&T_BH104). Vibrating wire piezometers were installed at T&T_BH102 and T&T_BH103 to monitor pore pressures within the Riccarton Formation at depths between 24 m and 27 m below the ground surface. The locations of the T&T boreholes are indicated on Figures 4.9.1a and 4.9.1b and more details regarding the T&T site investigations are provided by T&T (2013).

UC Berkeley performed seven CPTs across the CTH building site in April 2013. The CPTs were performed by Fugro Geotechnical NZ and included pore pressure measurements. The locations and corresponding depths of the CPTs are indicated on Figure 4.9.1 and summarized in Table 4.9.1.

Based on all of the subsurface investigations performed at the CTH building site, T&T (2013) developed a generalized soil profile. This profile has been reproduced in Table 4.9.2. As will be discussed herein, Layer 2 of Table 4.9.2 was of critical importance in the performance of the CTH building complex during the Canterbury earthquakes. T&T (2013) performed particle size analyses and Atterberg limits on collected samples from this layer and determined that the materials were primarily non-plastic silts with lesser amounts of non-plastic sandy silt and a minor amount of sand. Based on nine particle size analyses, the average fines content (reported by T&T as the percentage passing through the 63 μm sieve) of Layer 2 materials was 79%.

Table 4.9.1. Summary of UC Berkeley CPTs performed at the CTH building site.

CPT ID	Testing Contractor	Test Type	Surface Elevation† (m)	Refusal Depth (m)
Z5-6	Fugro	CPTu	5.4	20.68
Z5-7	Fugro	CPTu	5.5	19.05
Z5-8	Fugro	CPTu	5.4	20.70
Z5-9	Fugro	CPT_u	5.0	20.00
Z5-10	Fugro	CPTu	5.3	19.30
Z5-11	Fugro	CPTu	5.5	21.63
Z5-12	Fugro	CPTu	4.6	20.15

†Indicated surface elevations were estimated based on the digital elevation models available through the Canterbury Geotechnical Database (2012b) and a site survey using a ZIPLEVEL in April 2013. Indicated elevations are relative to the Lyttelton Vertical Datum (meters above sea level).

Table 4.9.2. Generalized soil profile at the CTH building site. Reproduced from Tonkin & Taylor (2013).

Layer	Depth to Top of Layer (m)	Depth to Bottom of Layer (m)	Material Description	Geological Formation	Typical SPT N	Typical q_c (MPa)
1	0	1.5	Fill	-	-	-
2	1.5	6	Non-plastic silt with minor sand and sandy silt.	Yaldhurst member, Springston	4 – 7	1 – 7
3	6	13	Interbedded sands, sandy gravel and gravels.	Yaldhurst member, Springston	15 – 50	5 – 30^+
4	13	14	Interbedded organic silts and peat.	Yaldhurst member, Springston	1 – 5	1 – 5
5	14	20	Silty sand and sand.	Christchurch	20 – 40	5 – 30^+
6	20	21	Silt (aquiclude).	Christchurch	5 – 20	1 – 5
7	21	29	Interbedded sands, sandy gravels and gravels.	Riccarton	$30 – 50^+$	N/A
8	29	31^+	Interbedded silt and peat.	Bromley	10 – 30	N/A

The standpipe piezometers installed by T&T in 2011 were designed to measure the groundwater head between 7 m and 15 m below the ground surface. These piezometers indicated groundwater table depths of approximately 1.5 m and 2.5 m below the ground surface. Consequently, a groundwater table depth of 1.5 m has been utilized in the analyses presented herein. Based on preliminary measurements, the vibrating wire piezometers, installed within the Riccarton Formation in 2013, indicate artesian pressures within this unit with a total head of approximately 0.5 to 1.0 m above the ground surface.

Figures 4.9.4 and 4.9.5 provide the corrected tip resistance, q_t, and the normalized soil behavior type (SBT) index, I_c, profiles from the UC Berkeley CPTs along cross sections A-A' and B-B' from Figure 4.9.1. The foundation elements of the auditorium are shown for reference. While the CPTs performed by UC Berkeley did not attempt to penetrate the Riccarton Formation, the CPT profiles presented on Figures 4.9.4 and 4.9.5 are generally consistent with the generalized soil profile developed by T&T above the Riccarton Formation. Fill materials typically were not encountered during the CPTs because the upper 1.5 m were vacuum excavated

(in order to avoid underground services) prior to performing the CPT. Also, the interbedded organic silts and peat materials described by T&T were not typically encountered at the UC Berkeley CPT locations. However, the shallow non-plastic silts, sandy silts, and silty sands were encountered across the CTH building site, and these materials were typically encountered to a depth of 4 – 6 m below the ground surface. As can be observed from Figures 4.9.4 and 4.9.5, the shallow foundation elements of the auditorium were founded within this layer. Consequently, this layer of shallow non-plastic silt, sandy silt, and silty sand, was critical to the observed performance of the CTH auditorium during the Canterbury earthquakes.

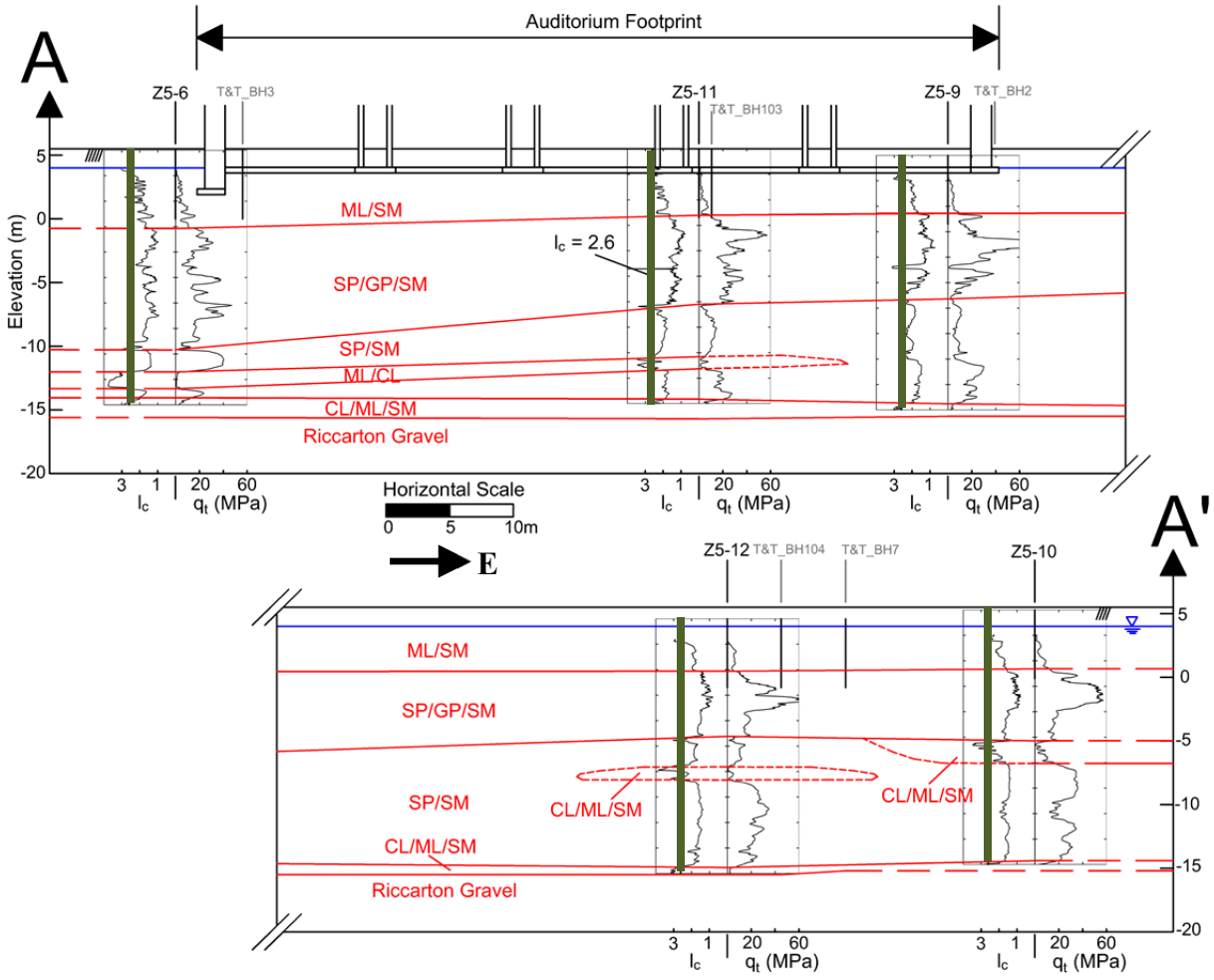

Figure 4.9.4. CPT tip resistance and normalized soil behavior type index profiles along cross section A-A'.

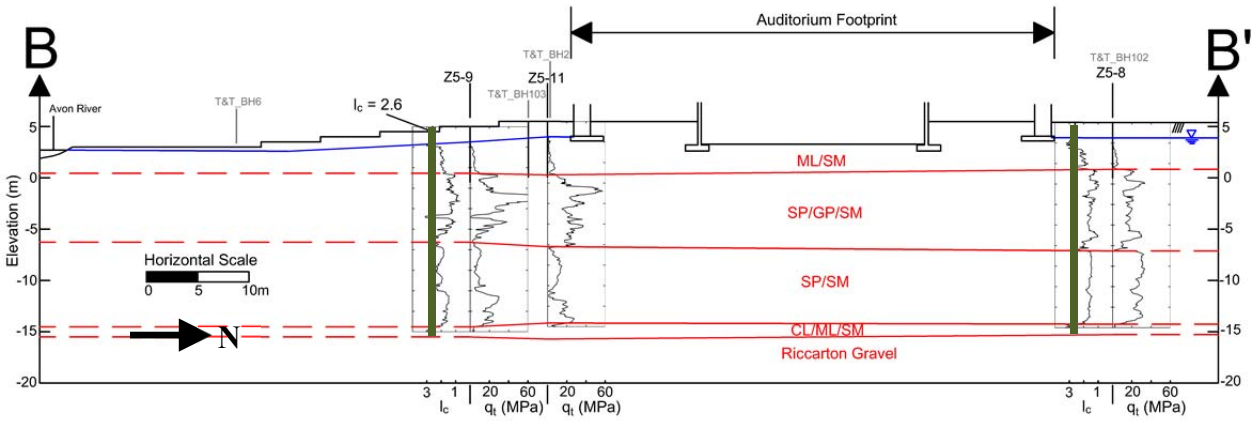

Figure 4.9.5. CPT tip resistance and normalized soil behavior type index profiles along cross section B-B'.

Analyses and Observations

The performance of the CTH building site during the 22 FEB 11 Christchurch earthquake was evaluated by GEER, UCB and UC researchers in March 2011. A separate evaluation was performed by researchers from the UC around that time, and a field map developed during this separate evaluation is shown in Figure 4.9.6 (Giorgini et al., 2011a; and Giorgini, 2015). As presented above, Cubrinovski et al. (2011a) summarized the most important observations during this survey. Several additional key observations around the auditorium are as follows:

- A small amount of liquefaction-induced sediment ejecta was observed on the north side of the auditorium.
- At the south side of the auditorium, column settlements relative to the floor slab varied from 2 cm to 14 cm and the concrete slab was cracked in this area.
- The location of the cracked beam spanning the walkway at the south end of the auditorium and shown in Figure 4.9.3b, likely caused by differential settlement of the inner column ring relative to the outer column ring, is indicated on Figure 4.9.6 and highlighted in Figure 4.9.6 as "Detail X".
- Non-uniform settlements and distortions of the paving blocks were observed on the terrace to the south of the auditorium. Liquefaction-induced sediment ejecta was observed in many areas south of the auditorium (Figure 4.9.7).

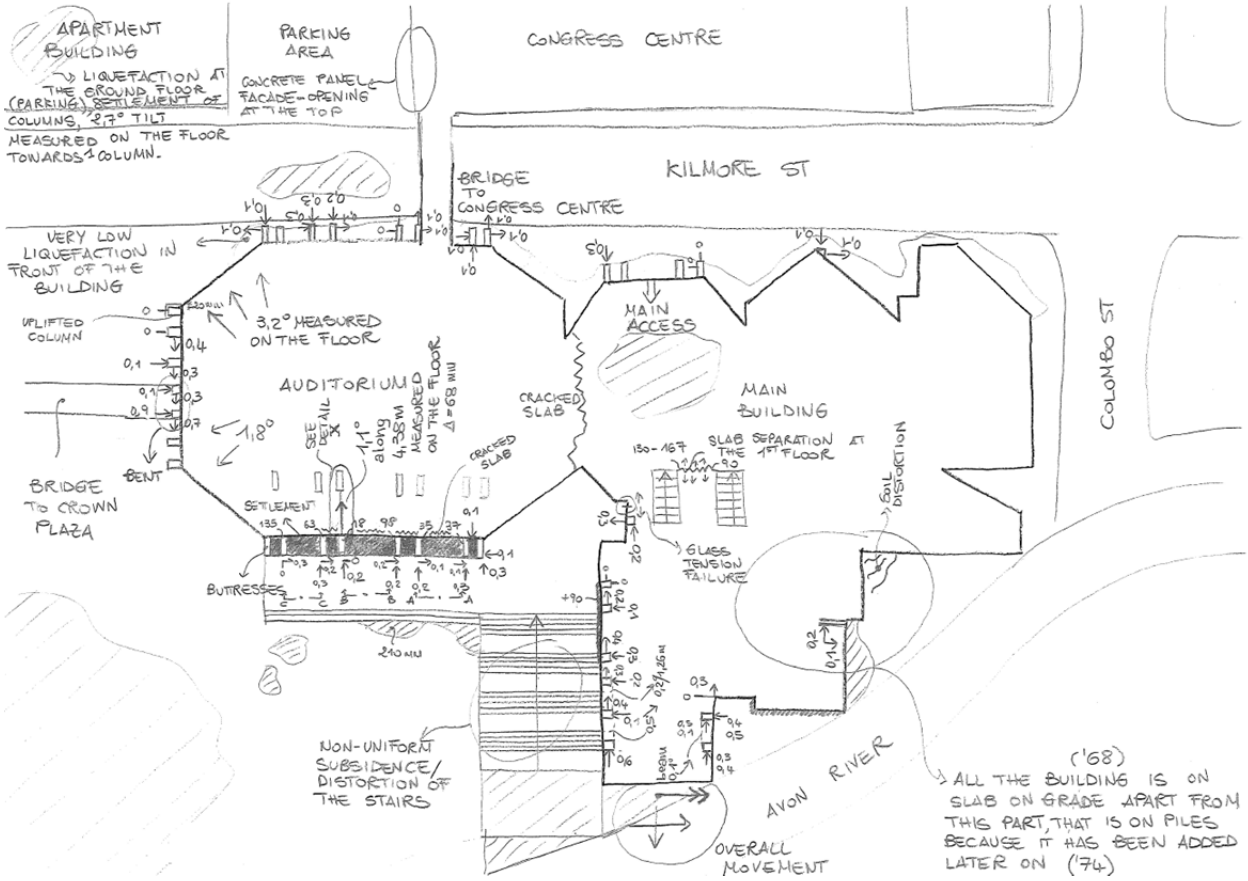
APARTMENT BUILDING
LIQUEFACTION AT THE GROUND FLOOR (PARKING) SETTLEMENT OF COLUMNS, 2,7° TILT MEASURED ON THE FLOOR TOWARDS 1 COLUMN.
PARKING AREA
CONCRETE PANEL FACADE - OPENING AT THE TOP
CONGRESS CENTRE
KILMORE ST
BRIDGE TO CONGRESS CENTRE
VERY LOW LIQUEFACTION IN FRONT OF THE BUILDING
UPLIFTED COLUMN
3,2° MEASURED ON THE FLOOR
AUDITORIUM
SEE DETAIL
1,1° along 4,35m MEASURED ON THE FLOOR Δ=68 mm
CRACKED SLAB
MAIN ACCESS
MAIN BUILDING
SLAB SEPARATION AT THE 1ST FLOOR
SOIL DISTORTION
COLOMBO ST
BRIDGE TO CROWN PLAZA
BENT
SETTLEMENT
BUTTRESSES
GLASS TENSION FAILURE
NON-UNIFORM SUBSIDENCE/ DISTORTION OF THE STAIRS
AVON RIVER
OVERALL MOVEMENT
('68)
ALL THE BUILDING IS ON SLAB ON GRADE APART FROM THIS PART, THAT IS ON PILES BECAUSE IT HAS BEEN ADDED LATER ON ('74)

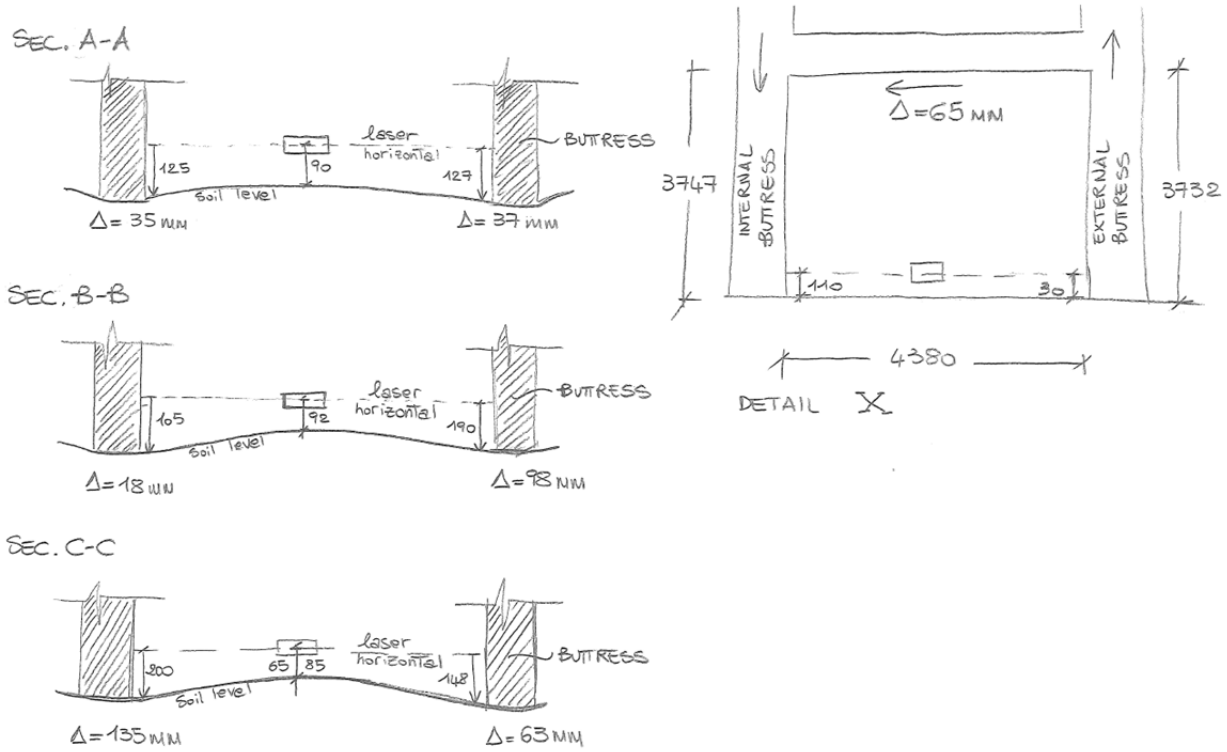

Figure 4.9.6. Field map developed during evaluation of the CTH building site in March 2011 (from Giorgini et al., 2011; and Giorgini, 2015).

Figure 4.9.7. Photographs from March 2011 showing (a) the non-uniform deformations of the terrace and terrace steps in the background and liquefaction-induced sediment ejecta in the foreground and (b) the proximity of the terrace steps to the Avon River.

T&T also performed geotechnical surveys of the CTH building site in March, June, and October 2011. Their findings are summarized in T&T (2013). Several key observations from the T&T survey are as follows:

- T&T references a level survey performed by Harrison Grierson Ltd. (HG) in April 2011. This survey indicated settlement of the building foundations of approximately 24 cm to 63 cm. Typically, foundation settlements were on the order of 30 – 50 cm.
- Based on T&T's discussions with the contractor engaged to perform emergency services for the CTH building site, approximately 70 m^3 of liquefaction-induced sediment ejecta was removed from the basement following the 22 FEB 11 event.
- Liquefaction also occurred at the site during the 13 JUN 11 event and additional sediment ejecta were observed in the basement.
- Evidence of lateral spreading along the north bank of the Avon River was observed. This evidence included ground cracking, slumping, cracks in pavement, and damage to the Limes Room and the James Hay Theatre (Figure 4.9.1). Lateral spread displacements were estimate by summing crack widths and were reported to be 35 cm within 20 m of the Avon River bank, 10 cm at the south side of the auditorium, 5 cm at the north side of the auditorium, and essentially zero at the north side of Kilmore Street. Much more detail, including a crack map, is provided by T&T (2013).
- Liquefaction-induced settlements led to differential settlement of the foundation elements and resulted in structural distress and a loss of serviceability.
- Additional damage to the Limes Room was observed following the 13 JUN 11 event. This was likely due to additional lateral spread displacements during this event.

Holmes Consulting Group performed a detailed structural review of the CTH building complex following the 22 FEB 11 earthquake, in addition to less-detailed structural assessments following the 4 SEP 10, 26 DEC 10, and 13 JUN 11 events. A detailed presentation of their findings is presented in HCG (2011). Several of their key observations pertaining to the auditorium are provided below:

- Liquefaction caused movement of the basement slab and resulted in intrusion of sediment ejecta into basement.
- Shallow foundations settled.
- Ground-level concrete flooring was cracked.
- Suspended timber flooring was sloped and/or uneven.
- Concrete block infill walls were damaged.
- Timber framed walls were damaged.
- RC beams were cracked with crack widths 0.2 – 2 mm.

A column verticality survey was performed by HG in April 2012 and made available online to the public by the CCC at the following URL:

http://www.ccc.govt.nz/cityleisure/projectstoimprovechristchurch/christchurchtownhall/index.aspx#jumplink15. Figure 4.9.8 summarizes these column tilt measurements. A few key observations from this survey are as follows:

- The columns on the west side of the outer ring of the auditorium were all tilted to the east and were mostly tilted to the south. The tilt of the western columns to the east (i.e., inward towards the interior columns) is consistent with observations that the interior columns settled more than exterior columns. The two southernmost columns on the west side were plumb in the north-south direction. On average, the tilts were 0.29 degrees to the east and 0.25 degrees to the south.
- The columns on the north side of the outer ring of the auditorium were all tilted to the south and to the east. The tilt to the south is also indicative of the interior columns settling relatively more than the exterior columns. On average, the columns were tilted 0.20 degrees to the east and 0.41 degrees to the south.
- The columns along the east side of the outer ring were tilted toward the auditorium centerline in the north-south direction and generally plumb in the east-west direction.
- The columns along the south side of the outer ring were tilted, on average, 0.17 degrees east. The amount of tilt in the east-west direction generally decreased from west to east across the auditorium. The north-south tilts did not appear to follow a coherent pattern.
- With the exception of five columns in and near the southeast quadrant of the auditorium that tilted to the north, all columns around the outer ring tilted to the south and to the east.
- The resultant tilt vectors for the inner ring of columns were all generally toward the south or southeast.

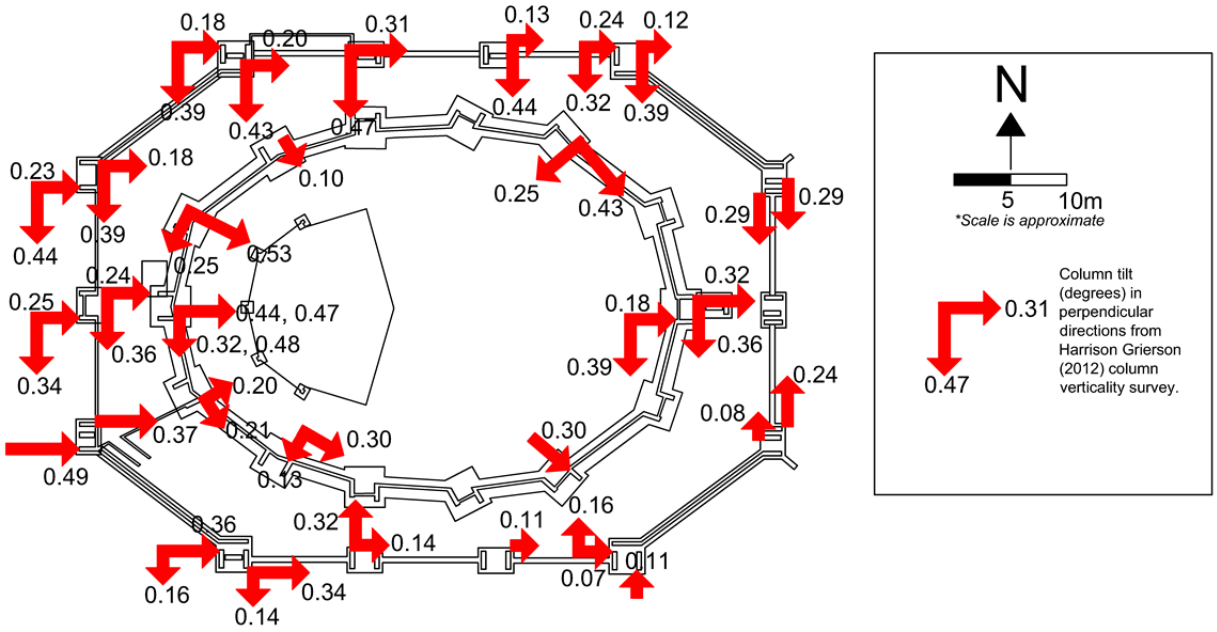

Figure 4.9.8. Auditorium column tilts (degrees) from April 2012 Harrison Grierson column verticality survey. Locations with just one tilt vector are plumb in the perpendicular direction.

Simplified liquefaction triggering evaluations were performed utilizing the procedures described previously. The estimated PGA values at the CTH building site for the 4 SEP 10, 26 DEC 10, 22 FEB 11 and 13 JUN 11 events are summarized in Table 4.9.3. The PGA during the 26 DEC 10 event is estimated as the median geo-mean PGA recorded at the four SMS within the CBD. The remaining PGAs were estimated using the work of Bradley and Hughes (2012).

Table 4.9.3. PGA values for RW98 and ZR02-RW98 analyses

Event	M_w	PGA_{16} (g)	PGA_{50} (g)	PGA_{84} (g)
4 SEP 10	7.1	0.17	0.22	0.27
26 DEC 10	4.8	0.22		
22 FEB 11	6.2	0.35	0.45	0.58
13 JUN 11	6.0	0.18	0.24	0.31

Factor of safety against liquefaction triggering (FS_l) profiles, calculated in accordance with RW98 for the median PGA during the 22 FEB 11 event, and liquefaction induced settlement profiles, calculated in accordance with ZR02-RW98 for the 22 FEB 11 event, are shown on Figures 4.9.9 and 4.9.10. The post-liquefaction residual shear strength ratio of the

shallow ML/SM layer (i.e., Layer 2 of Table 4.9.2) was estimated to be 0.07 to 0.10 using the Olson and Stark (2002) and IB08 procedures. The base of the exterior footings on the south side of the auditorium in the vicinity of CPT Z5-11 was at depths of 1.9 m below the ground surface. The static bearing capacity of the foundation soils at this location can be estimated using procedures developed for a two-layer cohesive soil deposit (Naval Facilities Engineering Command, 1986). The FS against a bearing capacity failure for a representative exterior footing on the south side of the building was estimated to be 0.8 to 1.0 using the residual shear strength of the shallow ML/SM materials and an equivalent undrained shear strength of the underlying medium dense to very dense SP/GP/SM. Consequently, typical foundation settlements of 30 – 50 cm, as reported by T&T, are not surprising. It should also be noted that the interior footings were more heavily loaded than the exterior footings and also founded within the shallow ML/SM layer. Therefore, similar calculations to evaluate the FS against a bearing capacity failure for a representative interior footing would yield a lower FS than that reported above for the exterior footing, and this is consistent with observations presented above by Cubrinovski et al. (2011a) that the interior footings settled more than the exterior footings.

Ground surface settlements were calculated based on volumetric strains over the upper 20 m of the soil deposit and these calculations are presented in Table 4.9.4 for the 4 SEP 10, 26 DEC 10, 22 FEB 11, and 13 JUN 11 events.

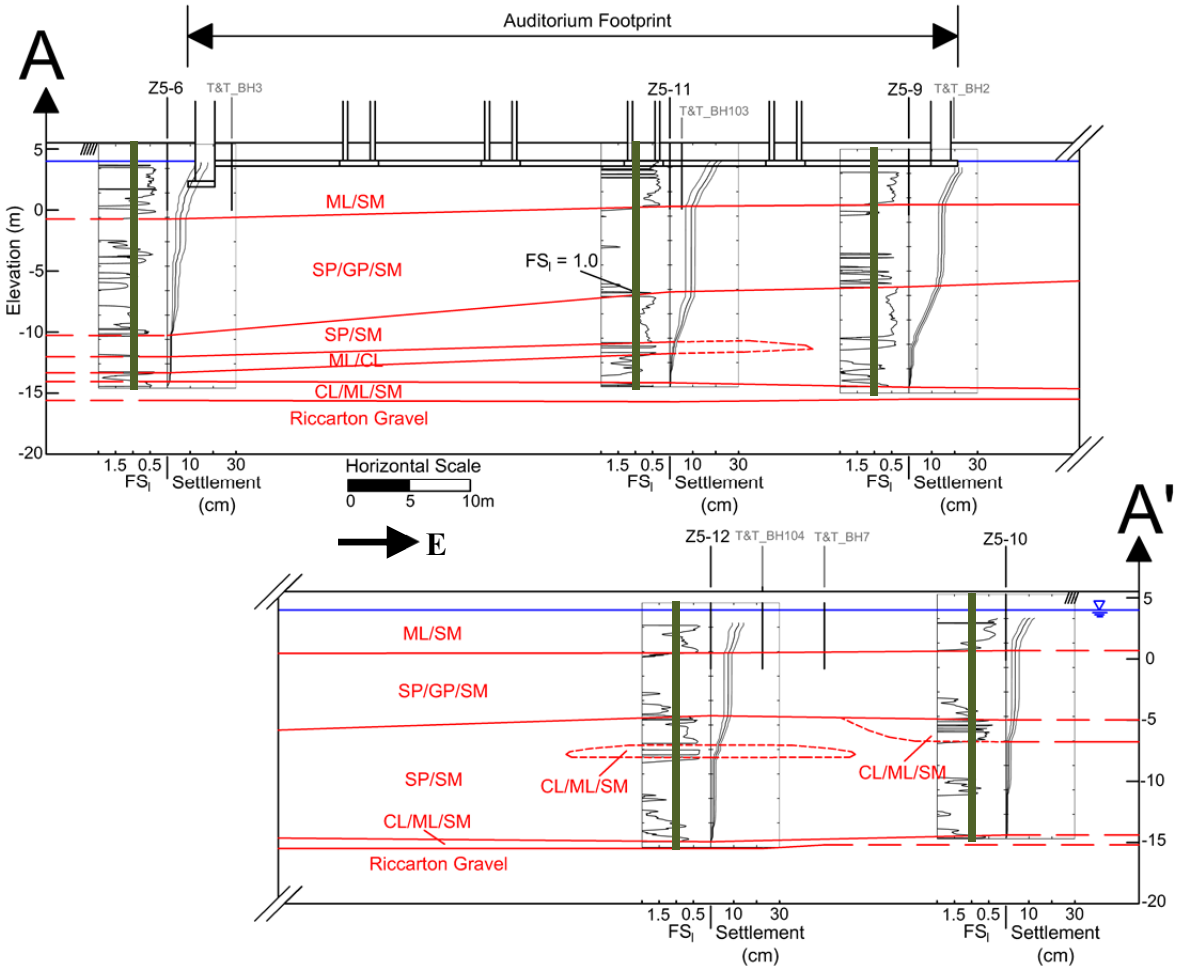

Figure 4.9.9. RW98 FS_l and ZR02-RW98 settlement profiles for the 22 FEB 11 event as projected on cross section A-A'. Settlements are due to post-liquefaction volumetric strains in the top 20 m and based on median PGA estimates.

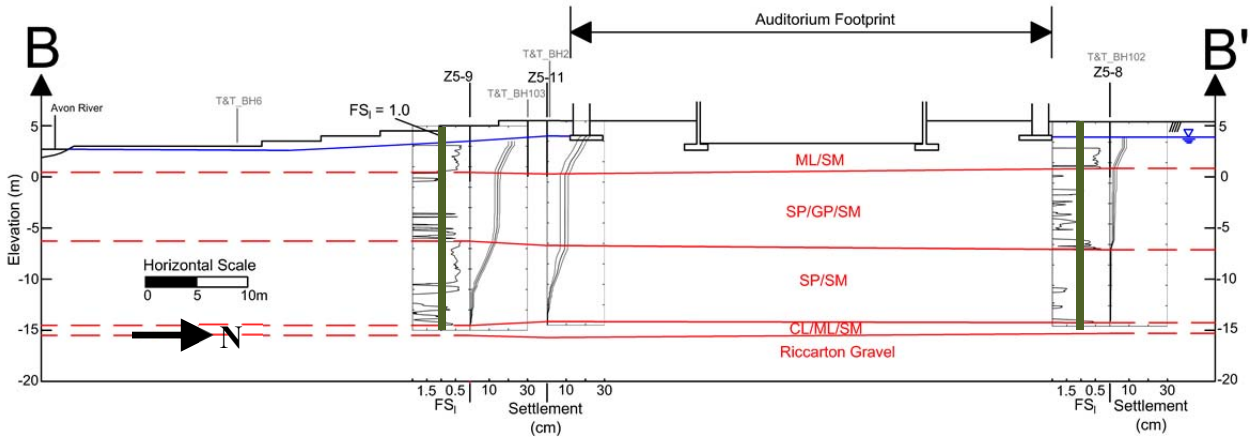

Figure 4.9.10. RW98 FS_l and ZR02-RW98 settlement profiles for the 22 FEB 11 event as projected on cross section B-B'. Settlements are due to post-liquefaction volumetric strains in the top 20 m and based on median PGA estimates.

Table 4.9.4. Calculated surface settlements at CPT locations in the CTH building site. Settlements are due to post-liquefaction volumetric strains in the top 20 m and based on median PGA estimates.

CPT ID	Reconsolidation Settlement at Surface (cm)			
	4 SEP 10	26 DEC 10	22 FEB 11	13 JUN 11
Z5-6	10	3	15	7
Z5-8	5	2	7	4
Z5-9	17	6	22	13
Z5-10	7	3	10	5
Z5-11	14	7	21	12
Z5-12	7	3	12	6

It is clear from Figures 4.9.9 and 4.9.10 that the shallow ML/SM materials had a calculated $FS_l \approx 0.5$ for the median PGA during the 22 FEB 11 event. As described previously, the auditorium foundation elements were founded within this layer. Consequently, it is not surprising that significant total and differential settlements were observed and it is also not surprising that great quantities of liquefaction-induced sediment ejecta were observed in the auditorium basement following the 22 FEB 11 event and, to a lesser extent, the 13 JUN 11 event.

As expected, the calculated free-field surface settlements during the 22 FEB 11 event presented in Table 4.9.4 underestimate the observed typical shallow foundation settlements reported by T&T (30 – 50 cm, as measured in April 2011 and described above). Given that the shallow foundation elements were supported within a layer that liquefied during this event, we would expect the shear-induced building settlement mechanisms to dominate. As described previously, the FS against a bearing capacity failure was likely on the order of 0.8 – 1.0 for the spread footings in the exterior ring using the post-liquefaction residual shear strengths of the ML/SM layer. The FS would be expected to be lower for spread footings in the interior ring. Consequently, partial bearing capacity failures, manifested through punching shearing settlements, likely occurred at footing locations throughout the auditorium footprint. Full rotational bearing capacity failures would have likely been restrained by the presence of tie beams holding the footings together. Also, given the amount of sediment ejecta in the basement following the 22 FEB 11 event reported by T&T, another very important contribution to the observed foundation settlements was the loss of foundation soils.

In addition to the shear- and volumetric-induced settlement mechanisms described by Bray and Dashti (2010), the auditorium was likely impacted by lateral spread-induced displacements, due to the proximity of the building to the Avon River (Figures 4.9.1, 4.9.2, 4.9.7). Using the CPT-based procedure described by Zhang et al. (2004), reasonable estimates of liquefaction-induced lateral displacements towards the Avon River at CPT Z5-8 and Z5-11 are 5 – 10 cm and 30 – 60 cm, respectively. As described previously, T&T measured the lateral displacements at the north and south sides of the auditorium to be approximately 5 cm and 10 cm, respectively, by summing crack widths. It is worth noting that summing crack widths typically provides a lower bound on actual displacement because lateral strains between cracks are not captured. Therefore, it is reasonable that the Zhang et al. (2004) estimates are higher than the T&T observations, though the calculated lateral displacement does appear to be overestimated for the south side of the auditorium. The topography used for these calculations was estimated. It is likely that the lateral displacements caused by spreading towards the Avon River also caused additional vertical settlement of the auditorium building. The magnitude of these additional settlements is tough to estimate but a commonly applied rule-of-thumb is 1:1 vertical displacement to horizontal displacement. Consequently, this rule-of-thumb would suggest an additional 10 cm of settlement at the south side of the auditorium and an additional 5 cm of settlement at the north side of the auditorium, in addition to the shear- and volumetric-induced settlements typical of a building with a shallow foundation on shallow liquefiable soils. It is, therefore, unlikely, that the lateral spread-induced settlements dominated the observed foundation settlements for this case. However, lateral displacement towards the Avon River to the south-southeast, in combination with the interior columns of the auditorium settling relatively more than the exterior columns, can explain the observed column tilts presented in Figure 4.9.8.

The free-field settlements reported in Table 4.9.4 show a trend similar to many of the building case histories described in this chapter. That is, though the calculated settlements are slightly higher for the 22 FEB 11 event, they are not significantly higher. The calculated free-field settlements are generally similar for the 4 SEP 10, 22 FEB 11, and 13 JUN 11 events, except for just a few CPTs with noticeably larger calculated settlement for the 22 FEB 11 event relative to the other events.. As described previously, liquefaction effects were far more severe

during the 22 FEB 11 event than for other events and this is not clearly described by the calculations summarized in Table 4.9.4.

4.10 Engineering Performance of the LS-I and LS-II Buildings

Introduction and Structural Design

The property located at 48 Lismore Street in Christchurch, New Zealand (Lat -43.54380, Lon 172.6530) was comprised of nine units, seven of which consisted of both office space and a warehouse with at least one shared wall (Unit Three – Unit Nine), one of which consisted of office space and a warehouse and was detached (Unit Two), and another detached building consisting of only office space (Unit One). The focus of this section is on the two detached buildings, Unit One and Unit Two, herein referred to as LS-I and LS-II, as they shared many common design characteristics but displayed different engineering performance characteristics following the 22 FEB 11 and 13 JUN 11 earthquakes (Figure 4.10.1).

Figure 4.10.1. Photos of the (a) LS-I and (b) LS-II buildings taken in July of 2011

Based on their 2007 design drawings, both the LS-I and LS-II buildings were two-story concrete panel buildings. The shallow foundation of LS-I consisted of 1.2 m wide by 0.65 m deep RC strip footings beneath the concrete panel walls with a 0.125 m thick concrete slab spanning between the wall footings. The shallow foundation of LS-II was nearly identical, with the exception being a 0.9 m wide by 1.5 m long by 2.25 m deep RC footing beneath a concrete encased steel column located at the center of the westernmost wall. The plan dimensions of the buildings were approximately 28 m by 18 m and 11 m by 18 m for LS-I and LS-II, respectively. The second floors of both buildings typically consisted of 7.5 cm of cast in place concrete atop permanent timber formwork. The floors were supported by precast concrete beams that connected to the panel walls with steel angles. Timber trusses supported 0.4 mm Zincalume Trimdeck roofing for both buildings. As described previously, the LS-II building consisted of both office space and an adjoining warehouse. The office space was divided into a first and

second floor and comprised approximately 60% of the floor plan on the east side of the building; the warehouse space was not divided into a first and second floor and comprised the west side of the building. The spaces were separated by a transverse concrete panel wall (see Fig. 4.10.2).

Site Characterization

The property located at 48 Lismore Street was located within Zone 9, southeast of the CBD (Figure 4.1.9). Geoscience Consulting (NZ) Limited, henceforth Geoscience Consulting, performed a site investigation that consisted of two boreholes, each to a depth of 20.9 m, and six CPTs to refusal or 20 m, whichever was shallower. Details regarding the Geoscience site investigation were summarized in a geotechnical investigation report dated 15 May 2012 (Geoscience Consulting (NZ) Ltd., 2012). Two additional CPTs to refusal were performed at the site by UC Berkeley in October 2012. Figure 4.10.2 illustrates the relative locations of the LS-I and LS-II buildings, along with the CPTs and boreholes performed at the site by Geoscience Consulting and UC Berkeley. Details of the CPTs are provided in Table 4.10.1.

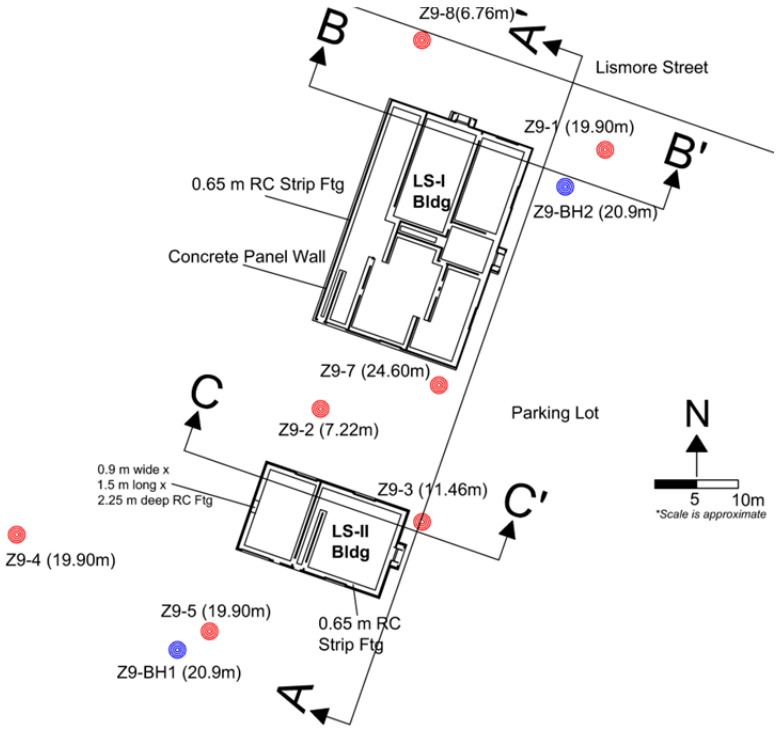

Figure 4.10.2. LS-I and LS-II site plan with CPT and Borehole locations and depths. Foundation elements are also indicated for reference. CPT Z9-6 (refusal depth of 0.4 m) is not shown.

Table 4.10.1. Summary of CPTs performed at the LS-I and LS-II building sites.

CPT ID	Testing Contractor	Investigation	Test Type	Refusal Depth (m)
Z9-1	McMillan	Geoscience Consulting	CPTu	19.90
Z9-2	McMillan	Geoscience Consulting	CPTu	7.22
Z9-3	McMillan	Geoscience Consulting	CPTu	11.46
Z9-4	McMillan	Geoscience Consulting	CPTu	19.90
Z9-5	McMillan	Geoscience Consulting	CPTu	19.90
Z9-6	McMillan	Geoscience Consulting	CPT	0.40
Z9-7	McMillan	UC Berkeley	CPT	24.60
Z9-8	McMillan	UC Berkeley	CPT	6.76

Based on the Geoscience Consulting and UCB investigations, along with the regional groundwater models developed by T&T (Canterbury Geotechnical Database, 2013), the groundwater depth was assumed to be approximately 1.5 m during the 4 SEP 10, 26 DEC 10, 22 FEB 11, and 13 JUN 11 events.

Figures 4.10.3 through 4.10.5 provide the q_t and I_c profiles along cross sections A-A', B-B', and C-C' respectively.

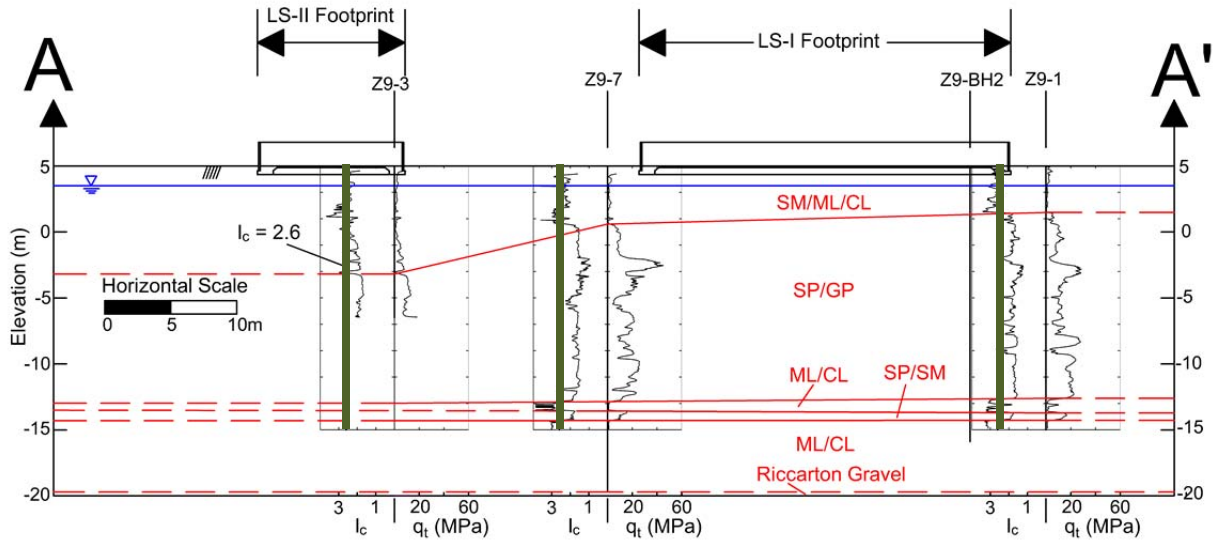

Figure 4.10.3. CPT tip resistance and normalized soil behavior type index profiles along cross section A-A'.

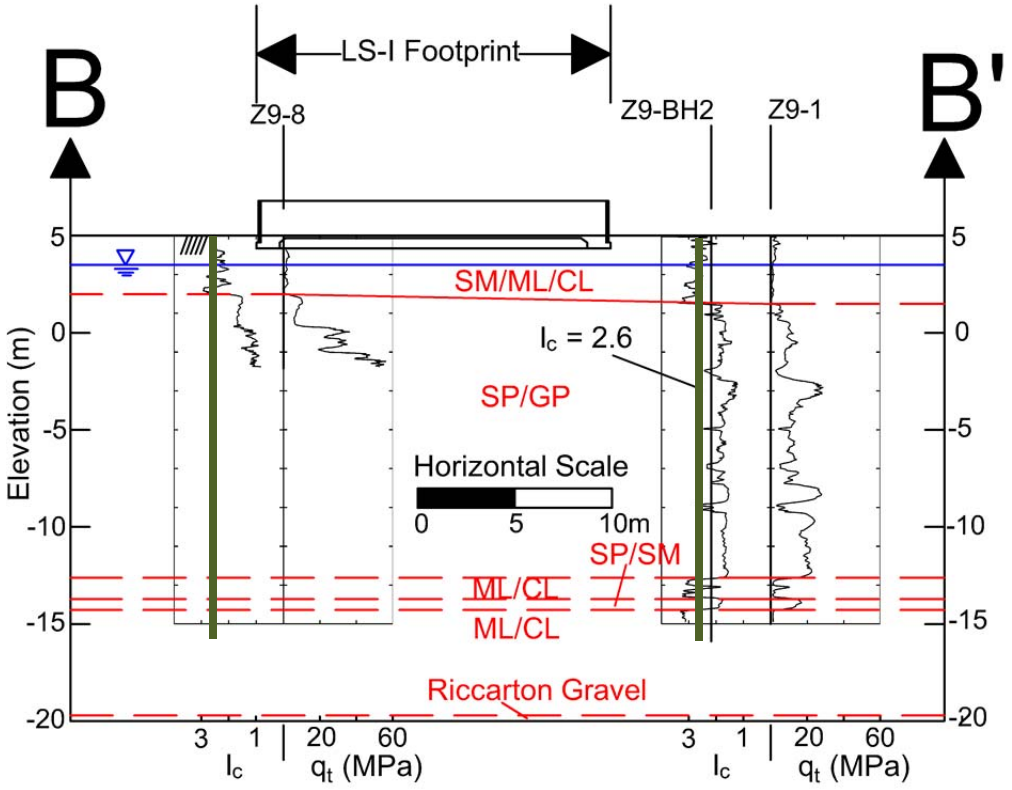

Figure 4.10.4. CPT tip resistance and normalized soil behavior type index profiles along cross section B-B'.

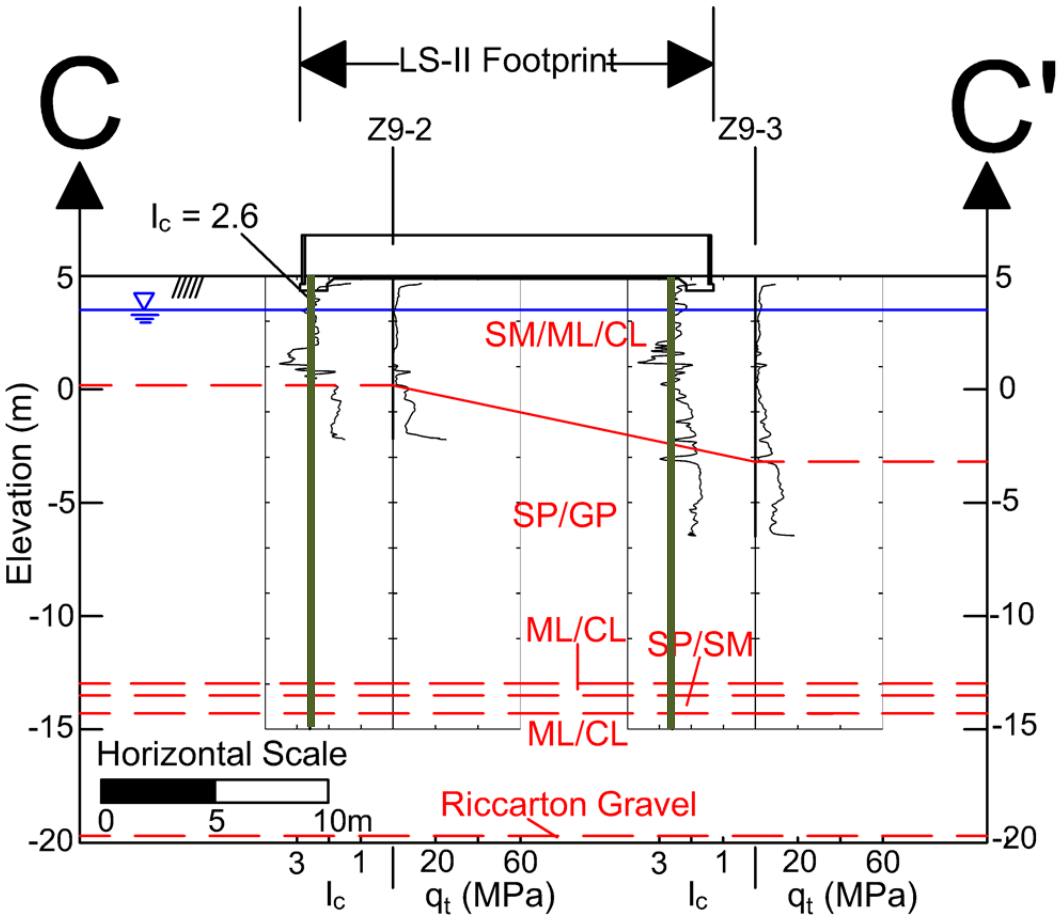

Figure 4.10.5. CPT tip resistance and normalized soil behavior type index profiles along cross section C-C'.

Figures 4.10.3 through 4.10.5 illustrate that the shallow subsurface profile beneath the LS-I and LS-II buildings primarily consists of the following six units:

1) Very loose to loose and/or very soft to stiff SM/ML/CL with q_t less than 5 MPa and typically less than 2 MPa and $2.0 < I_c < 3.0^+$ to depths between 3 m and just over 8 m;
2) Medium dense to very dense SP/GP with q_t greater than 5 MPa to greater than 40 MPa and $1.0 < I_c < 2.0$ to depths of 17.5 m to 18 m;
3) Loose to medium dense and very soft to stiff ML/CL with $q_t < 5$ MPa and $2.6 < I_c < 3$ to depths of 18.5 to 18.75 m;
4) Medium dense to dense SP/SM with 10 MPa $< q_t <$ 20 MPa and $I_c \approx 2$ to depths of about 19.25 m;
5) Loose to medium dense and very soft to stiff ML/CL with $q_t < 5$ MPa and $I_c \approx 3$ to depths of about 24.75 m;
6) Riccarton Gravels. As discussed previously, more information regarding the characteristics of the Riccarton Gravels are provided in Section 4.1 and by Tonkin and Taylor (2011).

It should be noted that the borehole logs provided by Geoscience Consulting typically describe the shallow (i.e., less than 5 m depth) fine grained materials as nonplastic silts or silts with moderate plasticity whereas the deeper (i.e., greater than depths of 17.5 m) fine grained materials are typically described as highly plastic silts. No clays were logged in either borehole. The plasticity descriptions appear to be based on the field identification procedures described by the New Zealand Geotechnical Society (New Zealand Geotechnical Society, 2005).

Building foundation elements have also been shown on Figures 4.10.3 through 4.10.5, and it can be observed that the shallow strip footings of both buildings are founded within the shallow silts, sandy silts, and silty sands described above.

Analyses and Observations

The estimated PGA values at the 48 Lismore Street site for the 4 SEP 10, 26 DEC 10, 22 FEB 11 and 13 JUN 11 events are summarized in Table 4.10.2. The PGA during the 26 DEC 10 event is estimated as the median geo-mean PGA recorded at the four SMS within the CBD. The remaining PGAs were estimated using the work of Bradley and Hughes (2012).

Table 4.10.2. PGA values for RW98 and ZR02-RW98 analyses.

Event	M_w	PGA_{16} (g)	PGA_{50} (g)	PGA_{84} (g)
4 SEP 10	7.1	0.17	0.23	0.31
26 DEC 10	4.8	0.22		
22 FEB 11	6.2	0.37	0.50	0.68
13 JUN 11	6.0	0.20	0.29	0.43

Factor of safety against liquefaction triggering (FS_l) profiles, calculated in accordance with RW98 for the PGA_{50} during the 22 FEB 11 event, and liquefaction-induced settlement profiles, calculated in accordance with ZR02-RW98 for the PGA_{16}, PGA_{50}, and PGA_{84} during the 22 FEB 11 event, are shown on Figures 4.10.6 through 4.10.8. Settlements were calculated based on volumetric strains over the upper 10 m of the soil deposit. Table 4.10.3 summarizes the settlement at the surface for the 4 SEP 10, 26 DEC 10, 22 FEB 11, and 13 JUN 11 events.

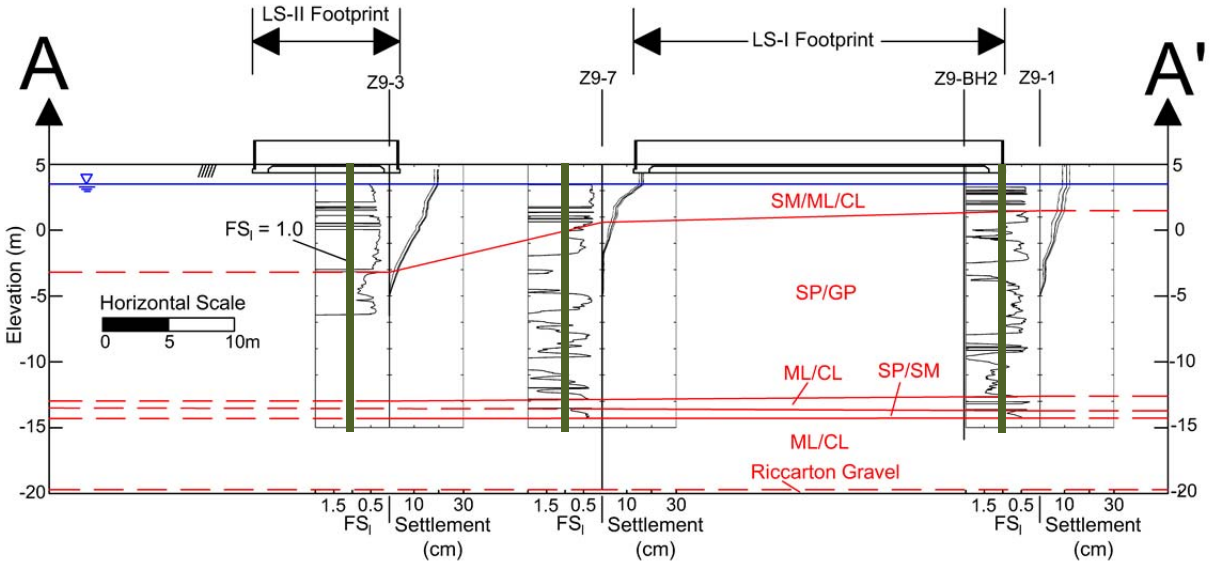

Figure 4.10.6. Factor of safety against liquefaction triggering (FS_l) profiles, calculated in accordance with RW98 for the PGA_{50} during the 22 FEB 11 event, and liquefaction-induced settlement profiles, calculated in accordance with ZR02-RW98 for the PGA_{16}, PGA_{50}, and PGA_{84} during the 22 FEB 11 event, at CPT locations along cross section C-C' with the LS-I and LS-II building foundations shown for reference. Settlements are due to post-liquefaction volumetric strains in the top 10 m.

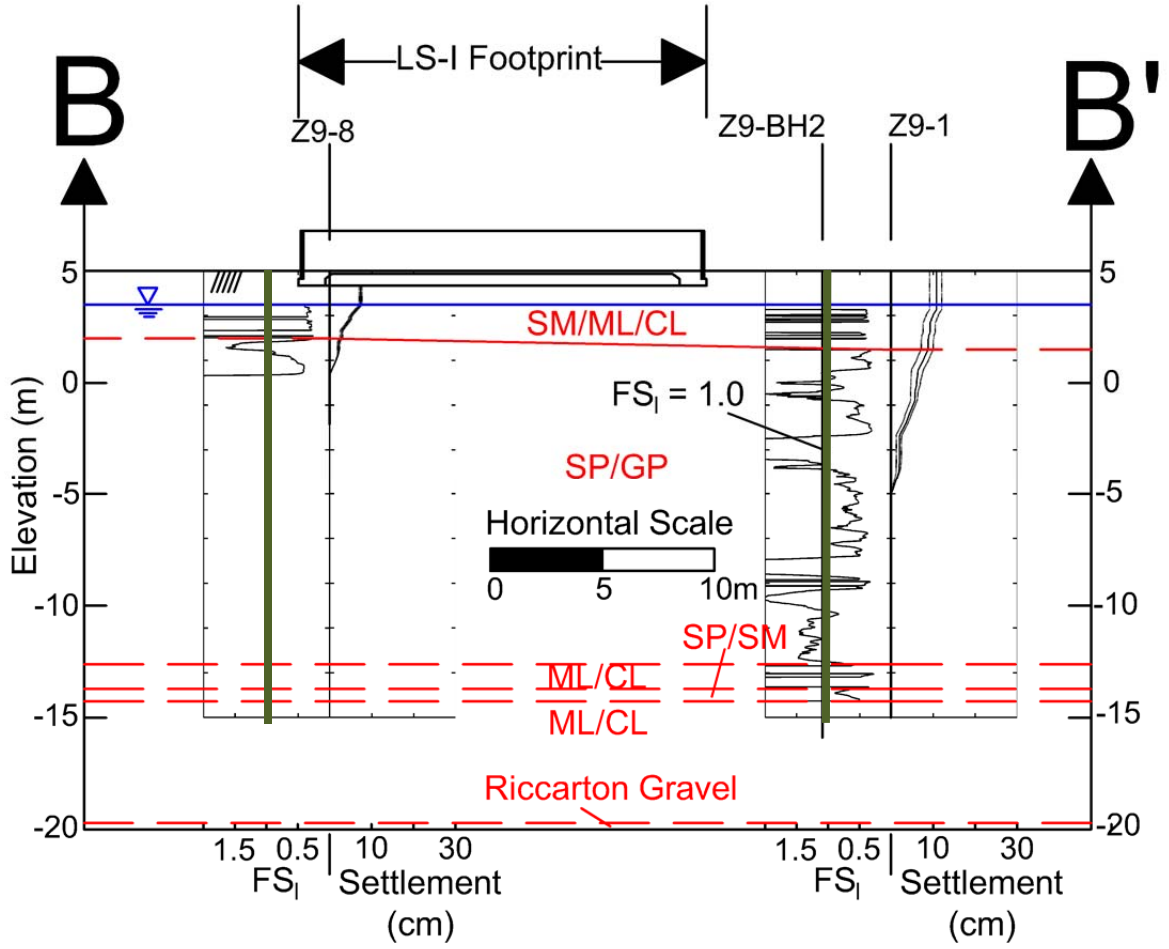

Figure 4.10.7. Factor of safety against liquefaction triggering (FS_l) profiles, calculated in accordance with RW98 for the PGA_{50} during the 22 FEB 11 event, and liquefaction-induced settlement profiles, calculated in accordance with ZR02-RW98 for the PGA_{16}, PGA_{50}, and PGA_{84} during the 22 FEB 11 event, at CPT locations along cross section C-C' with the LS-I building foundation shown for reference. Settlements are due to post-liquefaction volumetric strains in the top 10 m.

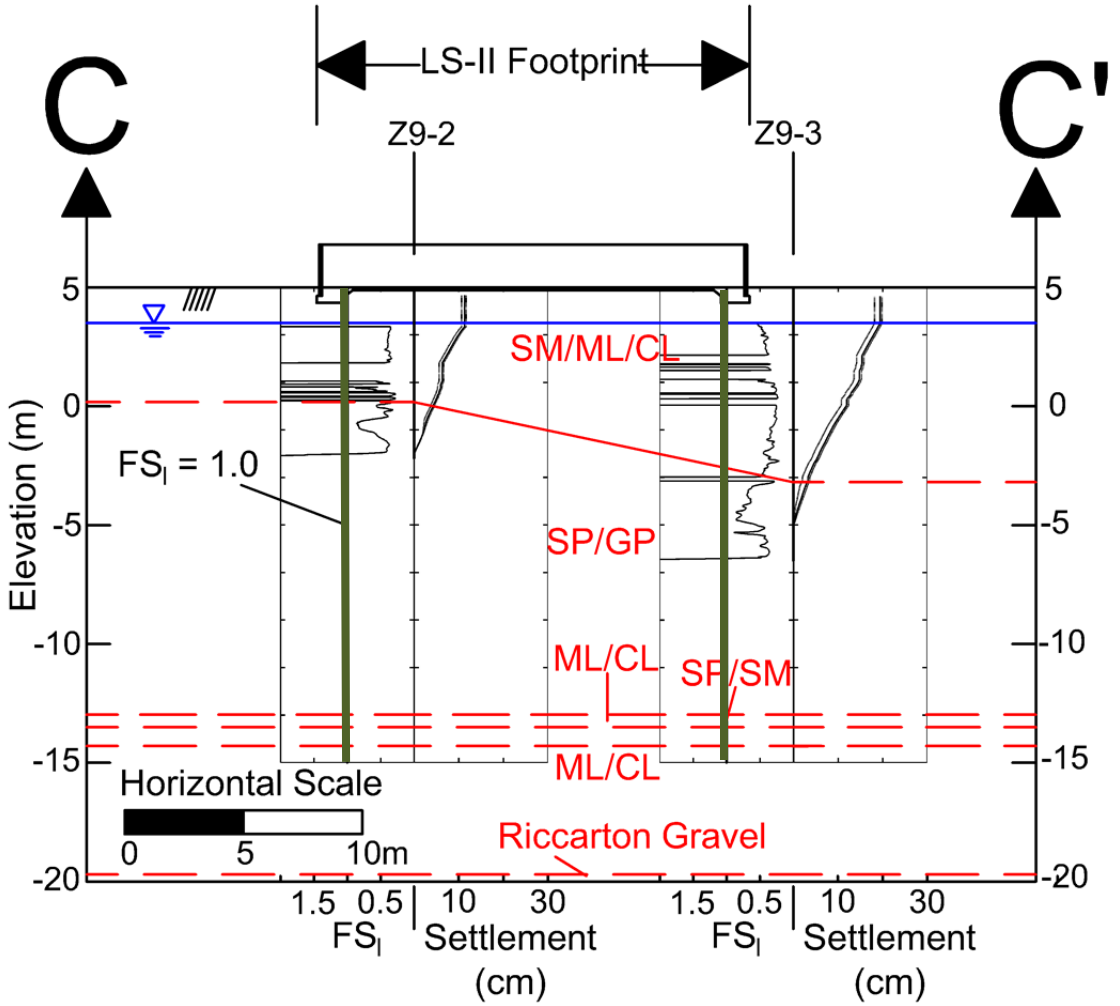

Figure 4.10.8. Factor of safety against liquefaction triggering (FS_l) profiles, calculated in accordance with RW98 for the PGA_{50} during the 22 FEB 11 event, and liquefaction-induced settlement profiles, calculated in accordance with ZR02-RW98 for the PGA_{16}, PGA_{50}, and PGA_{84} during the 22 FEB 11 event, at CPT locations along cross section C-C' with the LS-II building foundation shown for reference. Settlements are due to post-liquefaction volumetric strains in the top 10 m.

It is clear from Figures 4.10.6 through 4.10.8 that shallow liquefiable soils are present throughout the soil profile across the site. The ZR02-RW98 surface settlements for the median PGA estimates during the 4 SEP 10, 26 DEC 10, 22 FEB 11, and 13 JUN 11 events are summarized in Table 4.10.3.

Table 4.10.3. Calculated ZR02-RW98 surface settlements at CPT locations near the LS-I and LS-II buildings. Settlements are due to post-liquefaction volumetric strains in the top 10 m and based on median PGA estimates.

CPT ID	Reconsolidation Settlement at Surface (cm)			
	4 SEP 10	26 DEC 10	22 FEB 11	13 JUN 11
Z9-1	7	2	11	7
Z9-2	10	3	11	9
Z9-3	17	9	19	17
Z9-4	16	5	18	15
Z9-5	15	3	19	14
Z9-7	14	11	16	13
Z9-8	7	4	7	6

The ZR02-RW98 analyses summarized in Table 4.10.3 suggest that free field ground settlements should have been about the same for the 4 SEP 10, 22 FEB 11, and 13 JUN11 events while smaller, yet nonzero, settlements should have occurred during the 26 DEC 10 event. As has been discussed previously, simplified liquefaction triggering correlations are conservative and the ZR02 free-field settlement procedure is often relatively insensitive to changes in the FS_l when the FS_l is less than one. This is particularly true when $(q_{c1N})_{cs}$ is low. For example, for the materials between depths of 1.5 m and 4.3 m at CPT Z9-7 where $(q_{c1N})_{cs} < 60$, the same equation would be used to calculate volumetric strains for any FS_l below 0.9. This can be observed in Figure 4.1.25 as the 'limiting strain' curve. Consequently, the settlements for the large events of the Canterbury earthquakes are similar for this case. Refinements in these procedures will be required before ground performance, let alone building performance, can be predicted for the purposes of performance based design.

As described previously, the settlements presented in Table 4.10.3 were calculated based on volumetric strains over the upper 10 m of the soil deposit. As can be observed from Figures

4.10.6 through 4.10.8, there are liquefiable materials present at depths greater than 10 m at the locations of the deeper CPTs (i.e., Z9-1, Z9-4, Z9-5, and Z9-7). To better understand the potential contributions of the shallow versus the deep liquefiable soils, Table 4.10.4 presents settlements based on volumetric strains over the top 20 m, in addition to settlements based on volumetric strains over the top 5 m (i.e., approximately 4 times the width of the strip footings supporting the LS-I and LS-II buildings), for CPTs Z9-1, Z9-4, Z9-5, and Z9-7. The settlement at CPT Z9-3 with a baseline depth of 5 m is shown for reference. All settlements are based on the median PGA during the 22 FEB 11 event.

Table 4.10.4. Calculated ZR02-RW98 surface settlements at CPT locations near the LS-I and LS-II buildings. Settlements are due to post-liquefaction volumetric strains in the top 10 m and top 20 m and are based on median PGA estimates for the 22 FEB 11 earthquake.

CPT ID	**Reconsolidation Settlement at Surface (cm)**		
	Baseline Depth = 5 m	Baseline Depth = 20 m	Difference
Z9-1	5	20	15
Z9-4	8	36	28
Z9-5	8	34	26
Z9-7	13	25	12
Z9-3	8	N/A	N/A

Based on Table 4.10.4, the settlement due to deep liquefaction should have been greater at the south end of the site (i.e., south of LS-II) than the north end of the site. Unfortunately, there were no CPTs performed near the north side of LS-II that extended deep enough to estimate the deep liquefaction-induced settlement at this location. However, given that there should have been approximately 10 – 15 cm of deep liquefaction-induced settlement at Z9-7 and approximately 25 – 30 cm of deep liquefaction-induced settlement at CPTs Z9-4 and Z9-5, it appears more likely that differential deep liquefaction-induced settlements would have been present across the LS-II building footprint than at LS-I. While LS-II was more damaged than LS-I during the 22 FEB 11 event, the direction of observed differential settlement (i.e., to the north) is inconsistent with what would be expected given the calculated deep liquefaction-induced settlements in Table 4.10.4. This reinforces the fact that, while volumetric settlements due to liquefaction of deeper materials (i.e., greater than 4 times the width of the strip footings for this case) should contribute to the overall building settlement, the shear-induced building settlement mechanisms described previously govern the performance of shallow founded buildings atop shallow liquefiable soils.

A post-earthquake structural assessment was performed by Beca Carter Hollings and Ferner Ltd., henceforth referred to as Beca, on 14 April 2011. Beca also performed an external building verticality survey on 18-19 April 2011 and summarized their findings in a letter report dated 1 June 2011 (Beca Carter Hollings and Ferner Ltd., 2011b). The Beca report references a previous structural safety assessment of LS-I that was performed on 26 February 2011. At that time, a significant amount of sediment ejecta was observed around the building. However, their verticality survey indicated only minor horizontal movements (i.e., up to 30 mm) of the concrete wall panels at LS-I and visual inspection of key structural elements suggested no significant structural damage to the building.

The verticality survey performed at LS-II, on the other hand, suggested horizontal movements at the top of the concrete wall panels of up to 91 mm towards the north. The Beca verticality surveys are shown in Figure 4.10.9. While only hairline cracks were observed in the concrete wall panels, the concrete floor slab was uneven throughout the unit and sediment ejecta was observed in the interior of the unit. Partition walls were damaged and there were areas where ceiling tiles collapsed.

Geoscience visited the site on 10 June 2011 and observed undulations of the pavement throughout the parking area to the east of LS-I and LS-II and evidence of significant volumes of sediment ejecta. Buildings appeared to have settled both globally and differentially.

Researchers from UC Berkeley visited the site in late July 2011 and again in October 2012. During the July 2011 visit, significant sediment ejecta was observed around the perimeter of LS-II and, though to a lesser extent, LS-I (Figure 4.10.1). Several prominent pavement undulations in the parking area were also observed. While both buildings appeared to have settled relative to the surrounding ground, LS-II appeared to have settled more than LS-I. Measurements suggest that LS-I settled approximately 8 cm relative to the surrounding ground at the NE corner and the north side of LS-II settled approximately 12 cm more than the south side of LS-I. Tilt measurements were performed along the concrete panel walls of both buildings and were generally consistent with the Beca verticality surveys presented in Figure 4.10.9.

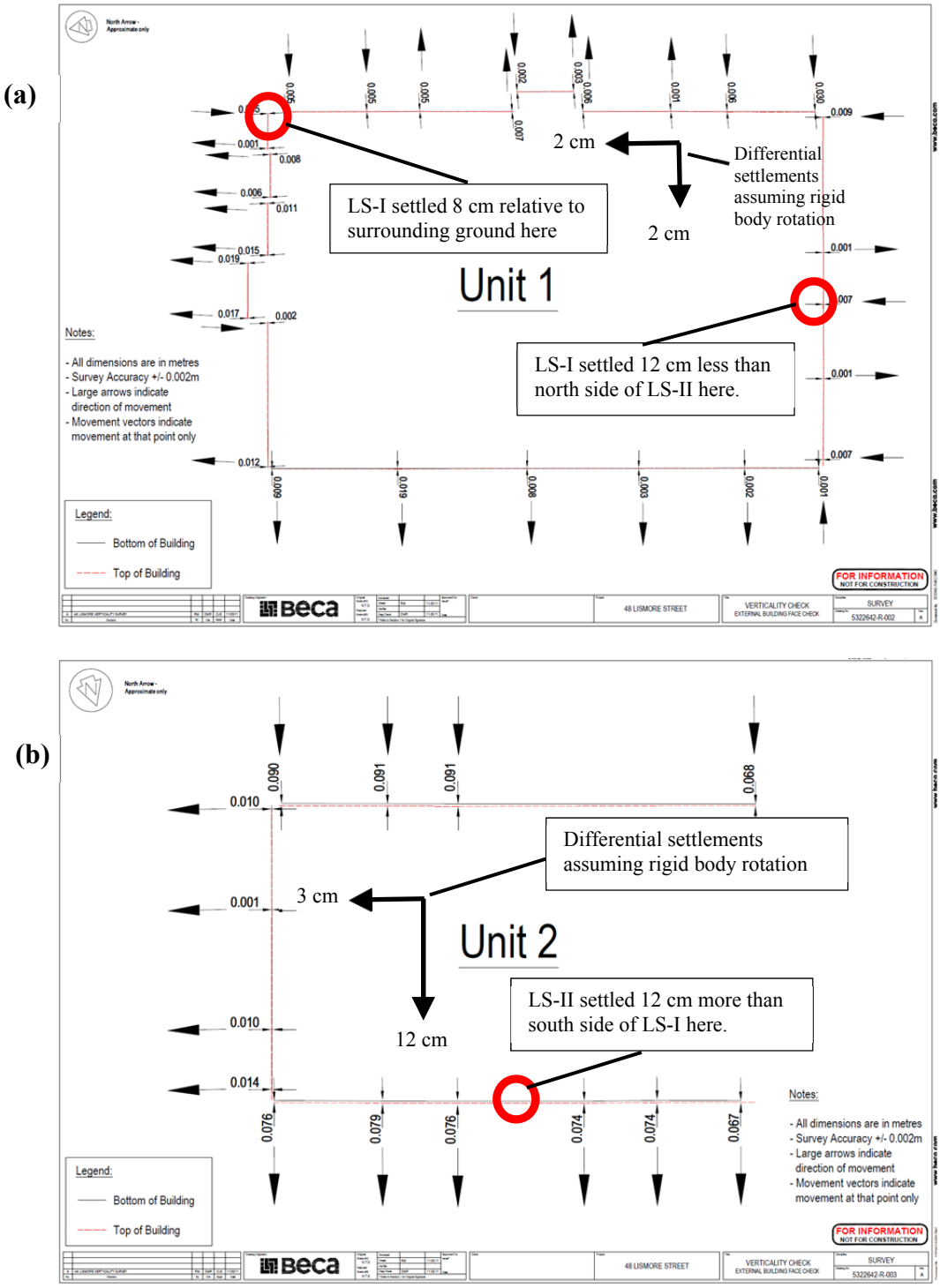

Figure 4.10.9. Building verticality surveys at (a) LS-I and (b) LS-II from April 2011 (Beca Carter Hollings and Ferner Ltd., 2011b). The orientation of the buildings is indicated relative to the respective north arrows.

Assuming that there was no relative rotation between the footings and the concrete panel walls, the verticality survey performed by Beca would seem to suggest approximately 12 cm of differential settlement of LS-II to the north and approximately 3 cm of differential settlement to the east. Similar calculations for LS-I suggest approximately 2 cm of differential settlement to the west and 2 cm to the north.

Though there are minor variations in the subsurface profile throughout the site, the likely critical layer with respect to the performance of the LS-I and LS-II buildings is the shallow liquefiable SM/ML. These materials, located immediately beneath the shallow strip footings that supported the building walls, appear to be present beneath the groundwater table throughout the site. Consequently, the shear induced building settlement mechanisms described by Dashti et al. (2010a) were important for this case.

The average post-liquefaction residual shear strength ratio (i.e., S_{ur}/σ'_{v0}) of the shallow SM/ML layer was estimated to be .06 using the Olson and Stark (2002) procedure. The bottom of the strip footings were at depths of 0.65 m. Using the procedures described previously for a two-layer subsurface profile consisting of cohesive materials, the FS against a bearing capacity failure was likely around 2.4 along the northern strip footing of LS-II and 2.6 in the vicinity of the western strip footing at LS-I. However, these safety factors would be lower if the SM/ML materials above the water table lost strength due to upward migration of liquefied soil. Given the amount of liquefaction-induced sediment ejecta around the perimeter of both buildings, it appears this was likely. Consequently, the LS-I and LS-II buildings were likely subjected to transient loss of strength and stiffness of the foundation soils beneath the strip footings supporting the concrete panel walls during the 22 FEB 11 earthquake, and punching settlements at footing locations are consistent with the significant deformations of the ground floor slab that were observed at LS-II. While this settlement mechanism could have contributed significantly to the observed settlement of the buildings relative to the surrounding ground, ground loss due to sediment ejecta was also clearly important.

As described previously, the LS-II building was more severely damaged than the LS-I building. Given that both buildings were founded on strip footings with the same geometry, it would seem that foundation width has not played a role in the relative performance of these buildings. However, the distribution of structural loads appears to be more even throughout the building footprint of the LS-I building (Fig. 4.10.2), whereas the loads appear to be concentrated around the perimeter of the LS-II building, with the exception being the two footings that cut across the building footprint near the center of the building in the transverse direction. One hypothesis, therefore, would be that the relatively more even distribution of structural loads has led to relatively more even foundation settlements at the LS-I building. This is consistent with the observation that the LS-II strip footings underwent punching settlement, thereby causing the ground floor slab to deform and appear to bulge in the center relative to the perimeter.

Differences in the SSI could have also played a significant role in the relative performance of the two buildings. As described previously, the second floor of the LS-II building was only present within the office portion of that building (i.e., the eastern 60% of the floor plan). The presence of a floor mass over the east side of the building but not the west side would have likely caused uneven superstructure inertial forces to be transferred to the building foundation, and this could have caused differential settlements due to non-uniform SSI-induced

ratcheting. As indicated on Figure 4.10.9 the horizontal movements of the top of the concrete panel walls in the north-south direction were slightly greater on the eastern side of LS-II than the western side.

4.11 Key Findings from Evaluations of Building Performance in Liquefied Ground in Christchurch

Christchurch, New Zealand experienced seven earthquake events with $M_w \geq 5.5$ between 4 September 2010 and 23 December 2011. Of these significant events, the 22 FEB 11 Christchurch earthquake was the most damaging. 185 lives were lost during this event. Over 1500 of the 4000 buildings within the CBD have been or are expected to be demolished due to damage. Most of the city's high rise buildings have been demolished. Parts of the CBD were cordoned off for over two years following the Christchurch earthquake.

Ground shaking in the CBD during the Canterbury earthquake sequence was well characterized through recordings at four SMS. Following the 4 SEP 10 and 22 FEB 11 events, GEER researchers, in close coordination with researchers from the University of Canterbury and the University of Auckland, performed damage surveys and documented their observations (Green et al., 2010 and Cubrinovski et al., 2011b). Modern commercial and residential buildings in the CBD were often significantly impacted by soil liquefaction during the Christchurch earthquake. Twenty-two sites within the CBD were identified for further study by the GEER team and an additional site, just outside of the CBD, was identified in July 2011 (Table 4.1.6). The selected sites contained single- and multi-story buildings on shallow and deep foundations that displayed unique performance characteristics. A total of 107 CPTs were performed at these sites during field investigations performed in July – August 2011, February 2012, October 2012, and March – April 2013. In addition to the site-specific investigations performed as part of this study, subsurface conditions within the CBD were evaluated on a regional level following the Christchurch earthquake (Tonkin and Taylor, 2011). Data collected during this regional investigation within the CBD, as well as additional investigations within and outside of the CBD, have been made available to the public through the CGD (https://canterburygeotechnicaldatabase.projectorbit.com). The CGD now contains data from over 15,000 CPTs, 3000 exploratory boreholes, 1000 shallow piezometers, and hundreds of geophysical surveys, and data continues to be added. Regional groundwater models were developed by T&T to estimate groundwater depths during the 4 SEP 10, 22 FEB 11, and 13 JUN 11 earthquake events (Canterbury Geotechnical Database, 2013). Additional data including aerial photographs, airborne LiDAR surveys, geological maps, topographical maps, residential zoning maps, historical maps, and much more are also available through the CGD. This chapter has focused on applying the immense amount of site-specific and public data to interpret the most interesting of the 23 sites. Key findings from these evaluations are summarized below:

- Many multi-story buildings in the CBD were heavily damaged by liquefaction-induced ground movements during the 22 FEB 11 Christchurch earthquake, but not by other significant earthquakes (e.g., 4 SEP 10 and 13 JUN 11). The peak geo-mean horizontal ground accelerations in the M_w 6.2 22 FEB 11 earthquake were on the order of twice those recorded during the larger, but more distant M_w 7.1 4 SEP 10 event. The PGAs during the 4 SEP 10 event were similar to those recorded during the 26 DEC 10 M_w 4.8, 13 JUN 11 M_w 6.0, and 23 DEC 11 M_w 5.9 events (Tables 4.1.4 and 4.1.5). The Arias intensity-time histories, as well as the SIR, also indicate clearly why the Christchurch event was the most damaging to buildings in the CBD (Fig. 4.1.6).

- CPT-based liquefaction triggering evaluations were generally conservative, and this conservatism led to post-liquefaction free-field ground settlement estimates that were generally similar for the 4 SEP 10, 22 FEB 11, and 13 JUN 11 events, whereas significant ground settlements and building damage in the CBD were only observed during the 22 FEB 11 event (e.g., Sections 4.3, 4.4, and 4.5).

- As described previously, ZR02-RW98 analyses were performed in the work presented herein to assess the validity of the insights gained in performing these analyses for the application of liquefaction-induced building settlements. Existing simplified free-field, level-ground liquefaction-induced settlement procedures (e.g., Zhang et al. 2002) do not capture the important shear-induced building deformation mechanisms described by Bray and Dashti (2010), nor do they capture settlement due to ground loss. Not surprisingly, therefore, building settlements were typically underestimated using the ZR02-RW98 analysis procedure for the 22 FEB 11 event (e.g., Sections 4.3, 4.4, and 4.9). In cases of shallow-founded buildings subjected to shallow liquefaction, free-field, level-ground liquefaction-induced settlement procedures are inappropriate for the estimation of building settlement. In addition to not capturing important building settlement mechanisms, these procedures give equal weighting to volumetric strains at all depths. Consequently, caution should be exercised when using these methods even as indices to expected building performance. Improved calibrated procedures that are specific to the settlement of shallow-founded buildings subjected to shallow liquefaction are needed.

- Because Christchurch was built on a historic floodplain of the Waimakiriri River, shallow subsurface conditions in the CBD are highly variable in space. At the Armagh Street and Madras Street parking lot (Section 4.2), for example, the shallow SM/ML layer was over 5 m thick at CPT Z4-8 but was only approximately 2.5 m thick at the adjacent CPT Z4-17, approximately 9.5 m away (Fig. 4.2.9). The groundwater table was at a depth of approximately 2.5 m during the 22 FEB 11 earthquake, and the portion of the SM/ML layer that was below the groundwater table should have liquefied during this event. The location of a surficial depression documented by Cubrinovski et al. (2011a) corresponded to the area where the shallow SM/ML extended beneath the water table, illustrating the importance of shallow subsurface variability on observed ground performance.

- Comparison of the ZR02-RW98 analyses performed for CPT Z4-14 and Z4-1, located approximately 8.5 apart, illustrated the importance of selecting a consistent baseline depth over which to calculate vertical strains. For example, CPT Z4-1 extended to a depth of 19.1 m, whereas CPT Z4-14 encountered refusal at approximately 6.9 m. Integration of vertical strains over the full depth of each CPT suggested free-field surface settlements of 3 – 5 cm at Z4-14 and 20 – 30 cm at Z4-1, depending upon the PGA level selected for the 22 FEB 11 event. However, drastic differential settlements were not observed at the ground surface in this area so the apparent difference is likely an artifact of performing these analyses over different baseline depths. Using a baseline depth of 7 m for CPT Z4-1, the corresponding ZR02-RW98 settlements are 6 – 8 cm.

- The CTUC building (Section 4.3), located approximately 20 m west of the Armagh – Madras parking lot, was also significantly affected by the variability in the thickness of the shallow liquefiable SM/ML layer. Figure 4.3.4 illustrated that the shallow liquefiable SM/ML layer was present to a depth of approximately 5 m at CPT Z4-5 (i.e., the south end of the building) whereas the layer was not present beneath the water table at other locations to the north of CPT Z4-5. This dramatic change in the shallow soil conditions from the building's north end, which did not contain shallow liquefiable soils, to its south end, which contained shallow liquefiable soils, led to the significant differential settlement over the southernmost spans of the building frame. Ground loss under the shallow foundations due to sediment ejecta and shear-induced mechanisms, such as SSI-ratcheting, likely contributed to the larger settlements at the southeast corner of the CTUC building. While liquefaction of soils below a depth of 8 m contributed significantly to the amount of calculated settlement, their impact on the building performance appears to have been relatively minor. Thus, the equal weighting of post-liquefaction volumetric strains over all depths of the soil profile in the calculation of free-field vertical settlements can be misleading when this approach is used to evaluate the performance of buildings with shallow foundations.

- Liquefaction occurred at the SA building site during the 4 SEP 10 earthquake. Although there was liquefaction-induced sediment ejecta observed at the ground surface around the building perimeter and in the elevator shaft, there was no significant damage to the building's primary structural system during this event. Liquefaction effects were far more severe during the 22 FEB 11 event, and the building settled approximately 25 cm relative to the surrounding ground at its southeast corner and approximately 10 – 20 cm at its northwest corner (Section 4.4). The critical layer in terms of the building performance was the shallow SM/ML/SP layer, located just beneath the building foundation, and the FS against a bearing capacity failure was estimated to be near or below 1.0 at the southern end of the building using the two-layer solution described previously with the post-liquefaction residual shear strengths of the SM/ML/SP layer. Consequently, a bearing capacity failure mechanism likely contributed to the observed foundation punching during the 22 FEB 11 event, though the effects of ground loss due to sediment ejecta were clearly evident and other displacement mechanisms noted in Bray and Dashti (2010) could have also occurred.

- The PILE-6 building was underlain by shallow and deep liquefiable soils (Fig. 4.5.4). Assuming this pile-supported building did not settle significantly during the Canterbury earthquakes, free-field ground settlements were slightly underestimated for the 22 FEB 11 event and overestimated for the 4 SEP 10 event using the ZR02-RW98 analysis procedure (Section 4.5). Despite substantial ground settlements around the building, the first-story structural frame of the PILE-6 building did not show significant damage. However, access to the building was impacted due to the settlement of the surrounding ground.

- The FTG-7 building, also atop shallow and deep liquefiable soils (Figs. 4.5.4 and 4.5.5), was damaged during the Christchurch earthquake. Structural columns were damaged at the ground level and a floor level survey performed in March 2011 indicated approximately 10 cm of settlement of the southeast corner of the building relative to the datum at its northwest corner. An additional 3.5 cm of differential settlement of the southeast corner relative to the northwest corner occurred during the 13 JUN 11 event. The adjacent FTG-4 building was significantly damaged and a large amount of sediment ejecta was observed in the parking lot behind the building and in front of the building, as well as around and within the building footprint. The strip footings supporting the side block walls settled relatively more than the remainder of the building and the concrete slab on the ground floor was bowed up in the middle. The ground floor slab settled approximately 16 cm more at the northwest corner than at its northeast corner. Consequently, the shorter and narrower FTG-4 building settled differentially more than the taller and wider FTG-7 building, and the differential settlements of the FTG-4 building occurred over a shorter distance.

- The PWC building (Section 4.6) was a 21-story RC frame structure with a one-story basement. Accessible building columns between the first and second floors were generally tilted with their tops to the south following the Christchurch earthquake, and water was observed in the southern half of the exposed basement during field testing in March and April 2013. The building was demolished in 2012. Although the liquefiable materials were at least 3 m below the base of the foundation and often more than 5 m, this is well within the depth range with a significant vertical strain influence for a foundation with a width of 25 m and L/B = 1.4 (Schmertmann, 1978). Consequently, cyclic softening of these materials due to increased pore water pressures would have likely led to building settlements, despite the fact that the liquefiable materials were not directly beneath the building. In addition, cyclic softening due to increased pore water pressures during and immediately following the significant Canterbury earthquakes could have occurred in other materials beneath the PWC building, and this transient reduction in stiffness in materials that did not fully liquefy could have also contributed to the observed building settlement. Volumetric reconsolidation of the liquefiable materials beneath the building foundation would have also caused settlements.

- As described previously, the top of the PWC building tilted slightly to the south during the 22 FEB 11 event. Importantly, the basement mat foundation extends significantly to the north of the tower footprint (Figure 4.6.16). It is possible that the northern portion of the basement mat, therefore, acted as a cantilever that prevented the northern end of the PWC building tower from settling as much as the southern end, causing the building to tilt slightly to the south.

- Shallow liquefiable materials were also present at the PWC site. While this layer was not encountered beneath the podium slab or tower mat foundation and thus likely did not contribute to building foundation settlement, the cyclic softening of this unit could have potentially contributed to the tilt of the building observed following the 22 FEB 11 due to reduced support along basement walls. Liquefaction-induced sediment ejecta was observed on the north and south ends of the building site. Ground settlements of at least 30 cm were measured near the street on the north side of the building and localized ground settlement of up to 10 – 15 cm were measured on the south side of the building. Evidence of lateral spreading towards the Avon River was observed along Oxford Terrace, just north of the northern end of the building site, and this could have contributed to the vertical ground displacements in this area.

- The VT building (Section 4.7) was a 10-story RC frame structure that was founded on a mat foundation within medium dense to very dense sand, gravelly sand, and sandy gravel that was underlain by materials at depths between approximately 7 m and 10 m that liquefied or cyclically softened due to excess pore pressure generation. This case is similar to the PWC building in that, although the liquefiable materials were located at least 4 m below the base of the foundation, this is well within the depth range with a significant vertical strain influence for a foundation with a width of 19 m and L/B = 1.27 (Schmertmann, 1978). Therefore, cyclic softening of these materials due to increased pore water pressures would have likely led to building settlements. In addition, materials within the medium dense to very dense layer directly beneath the mat foundation could have cyclically softened due to increased pore water pressures during and immediately following the significant Canterbury earthquakes and this transient reduction in stiffness in materials that did not fully liquefy could have also contributed to the observed building settlement. Volumetric reconsolidation of the liquefiable materials beneath the building foundation would have also caused settlements. The tilt of the building to the south is likely best explained by a gravity load eccentricity due to the location of the elevator and stair core being offset slightly to the south from the center of the building (Fig. 4.7.4). The tilt of the VT building to the east is more difficult to explain based on the available information. However, it is possible that structural vibrations transmitted through the piles of the adjacent VSA building led to relatively higher excess pore water pressures in this area, and therefore, more significant cyclic softening, of the SM/ML materials on the east side of the building relative to the SM/ML materials on the west side of the building.

- The VSA building (Section 4.7) was a 14-story RC building, located adjacent to the VT building, that underwent 22 cm of differential settlement in the north-south direction and

6 cm in the east-west direction. The building had a complex foundation system that consisted of 17 1.2 m-diameter RC piles around the southern, eastern and western edges of the building footprint and several shallow RC spread footings along the northern edge and within the building footprint. As illustrated on Figure 4.7.5, the lengths of the piles were either 6 m, 14 m, or 18 m. While 14 m long piles were located at the northeast, southeast, and southwest corners of the building, only 6 m long piles appear to have been installed at the northwest corner. This differential movement in the north-south direction was explained by variable ground conditions in combination with the lack of deep piles at the northwest corner of the building (Fig. 4.7.12). The 6 cm of differential settlement between the northwest corner of the building and the northeast corner of the building was explained by the presence of 14 m piles at the NE corner (versus 6 m piles at the NW corner), in addition to slightly better ground conditions between CPTs Z2-13 and Z2-22.

- The SCH building (Section 4.8) was a seven-story RC frame structure (Figure 4.8.1) on a drilled shaft foundation that performed well during the Canterbury earthquakes relative to many of its neighboring structures. Though a significant amount of sediment ejecta was observed around the building following the 22 FEB 11 event, the drilled shafts were extended to depths of 6 – 7 m, just beyond a shallow liquefiable layer of ML/SM that was typically present to depths of 4 – 6 m. Cubrinovski et al. (2011a) observed that the building did not appear to have punched into the ground, and differential settlements between adjacent columns were often negligible and rarely up to 3.5 cm. A subsequent floor level survey by TM Consultants in January 2012 indicated a maximum differential settlement of 3 cm over a distance of 2.5 m, and KGA (2012) indicated a maximum differential settlement of 9 cm at the ground floor. The small amount of movement observed was likely due to increased pore pressures within the shallow ML/SM layer, as well as an underlying medium dense to dense layer of SM/SP, reducing the effective stress and thereby decreasing the side friction resistance along the drilled shafts. This would have caused a portion of the structural load to be transferred to end bearing and resulted in the compatible amount of settlement required to develop the increased end bearing resistance. This load transfer process likely would have been complicated by a number of factors including vertical ground accelerations, superstructure rocking, and, importantly, liquefaction of soils beneath the bases of the drilled shafts (Table 4.8.4).

- The CTH building (Section 4.9) auditorium was founded on two rings of shallow RC spread footings, with the footings within each ring connected by tie beams. The components of the inner ring were larger and more heavily loaded than the corresponding outer ring components. Beams connected the building's main internal columns to the exterior columns, and Cubrinovski et al. (2011a) observed differential settlement of the inner footings relative to the outer footings. This caused many of the exterior columns to tilt inward (Figure 4.9.8). Similar to many of the other buildings studied in the CBD, the CTH building was underlain by a shallow liquefiable layer of ML/SM, and the auditorium foundation elements were founded within this layer. T&T (2013) reported typical foundation settlements of 30 – 50 cm and estimated approximately 70 m^3 liquefaction-induced sediment ejecta was removed from the auditorium basement

following the 22 FEB 11 Christchurch earthquake. The FS against a bearing capacity failure for a representative footing on the south side of the auditorium in the vicinity of CPT Z5-11 was estimated to be 0.8 – 1.0 using the procedure developed for a two-layer cohesive soil deposit (Naval Facilities Engineering Command, 1986) with the residual shear strength of the shallow ML/SM materials and an equivalent undrained shear strength of the underlying medium dense to very dense SP/GP/SM. Consequently, localized bearing capacity failures, along with ground loss due to sediment ejecta, were primarily responsible for the settlements observed for this case. Lateral movements and some settlement due to lateral spreading towards the nearby Avon River also likely occurred at this site, and this was discussed in Section 4.9.

- The LS-I and LS-II buildings (Section 4.10) were two-story concrete panel buildings. The shallow foundations of both buildings consisted of 1.2 m wide by 0.65 m deep RC strip footings that supported concrete panel walls. The plan dimensions of the buildings were approximately 28 m by 18 m and 11 m by 18 m for LS-I and LS-II, respectively. The shallow foundation soils at the site consisted of very loose to loose and/or very soft to stiff SM/ML/CL to depths between 3 m and just over 8 m, underlain by medium dense to very dense SP/GP to depths of 17.5 – 18 m. A significant portion of both layers should have liquefied based on the median PGA from Bradley and Hughes (2012) during the 22 FEB 11 Christchurch earthquake. Consequently, both buildings were subjected to shallow and deep liquefaction during this event. Though both buildings appeared to settle relative to the surrounding ground, LS-II appeared to settle more and was damaged more severely than LS-I. Transient reductions in stiffness and strength in the foundation materials appear to have caused localized punching shear settlements at footing locations. While the distribution of structural loads at the LS-I building appears to be more evenly distributed over the building footprint, the loads were concentrated around the perimeter of the LS-II building, with the exception of two footings that cut across the center of the LS-II building in the transverse direction. Therefore, it seems possible that the more spread out and severe punching shear failures at the footing locations of the LS-II building caused relatively more damage at this location. In addition, the eastern side of LS-II was divided into a first and second floor whereas the western side was utilized as warehouse space with a single floor. The presence of the second floor mass over the eastern side but not the western side likely caused uneven superstructure inertial forces to be transferred to the building foundation, and this could have caused differential settlements due to non-uniform SSI-induced ratcheting.

CHAPTER 5: CONCLUSIONS

5.1 Summary

Recent significant earthquakes have provided numerous examples of damage to buildings due to the effects of soil liquefaction and cyclic softening. Shallow-founded buildings on level ground atop shallow liquefiable soils have often been impacted by partial or complete bearing failures, loss of foundation soils due to eroded sediment ejecta, and vertical settlements that have been exacerbated by soil-structure-interaction (SSI). There is still no widely-accepted simplified method by which engineering practitioners can reliably estimate the settlement of buildings due to liquefaction or cyclic softening. Well-documented field and physical model case history data are essential to the development and calibration of empirical procedures. Therefore, the primary objectives of the work presented herein were to advance the understanding of building settlements due to liquefaction or cyclic softening, as well as provide high quality and well-interpreted field and physical model case history data that will supplement and enhance existing similar data.

5.2 Findings

A geotechnical centrifuge experiment that consisted of a physical model of simplified, shallow-founded model structures atop a layered, saturated soil profile consisting of 1.9 m (prototype scale) of Monterey 0/30 Sand at 85% relative density, underlain by 4.5 m of Nevada Sand at approximately 50% relative density, underlain by 19.3 m of Nevada Sand at 90% relative density was subjected to three realistic earthquake events that caused the loose to medium dense layer of Nevada Sand to liquefy (i.e., $r_u \approx 1.0$ in the free-field). Nearly 140 instruments, including ICP and MEMS accelerometers, PPTs, and LPs, measured the achieved motions, pore water pressures, and building and ground displacements within the model at various locations. Some of the most important findings from this experiment were as follows:

- Free-field settlements initiated during strong shaking at about the same time significant excess pore water pressures were generated. This is suggestive of partial drainage occurring during shaking. Free-field settlements occurred at slightly higher rates during shaking than after shaking was completed, and this was most evident during the PRI_large event. Free-field settlements for all events continued well after the completion of shaking as excess pore water pressures dissipated.

- The ground adjacent to the model structures settled more than the ground in the free-field and the shallow-founded structures settled more than the adjacent ground settled. The mat contact pressures for the ‘A’ buildings were 60 - 65 kPa, and the mat contact pressure for the shallow-founded ‘J’ building was about 185 kPa.

- While excess pore water pressure ratios in the free-field reached 1.0, maximum excess pore water pressure ratios beneath the buildings were typically on the order of 0.4 - 0.8 during the three significant shaking events.

- Nearly all of the shallow-founded building settlements occurred during and just after strong shaking and these building settlements were significantly greater than the free-field ground settlements. Both of these observations are consistent with the presence of the shear-induced building settlement mechanisms of SSI-induced ratcheting (i.e., $\varepsilon_{q\text{-}SSI}$) and partial bearing capacity failure (i.e., $\varepsilon_{q\text{-}BC}$) as described by Dashti et al. (2010a).

- Placing a model 'A' building next to another model 'A' building did not significantly impact the building settlement of either building during Test-5. This was illustrated by comparing the permanent building settlements for each building following PRI_mod, TCU_mod, and PRI_large shaking events.

- It is erroneous to always expect a heavier shallow-founded structure to settle more than a lighter shallow-founded structure when subjected to shallow liquefaction. SSI numerical analyses of buildings with shallow foundations atop shallow liquefiable soils have shown that, while cyclic shear stresses increase beneath buildings due to the building's dynamic response, the CSR beneath the building can be decreased due to higher confining stresses (e.g., Rollins and Seed, 1990; and Travasarou et al., 2006). Consequently, the CSR demand on the building's foundation soils is directly related to the building's dynamic response, as well as the weight of the building. During Test-5, the 'J_A' building settled slightly more than the 'A_J' building during the PRI_mod shake, slightly less than the 'A_J' building during the TCU_mod shake, and significantly more than the 'A_J' building (and more than the other 'A' buildings except for the '$A_{J\text{-}pile}$' building) during the PRI_large event. Therefore, it would appear that the higher confining stress beneath Building 'J_A' outweighed the increased cyclic shear stresses during the TCU_mod event, but was overcome by increased cyclic shear stresses during the more intense shaking of the PRI_large event.

- Curving the soil surface for centrifuge experiments involving liquefaction is important. By curving the surface of the soil before spinning, the soil surface responds as if it is level when spinning in the radial *g*-field produced in the centrifuge. This was not done for Tests SHD01 - SHD04, so when these models were spun up, the level soil surfaces in these tests responded as if they were curved with high ground along the longitudinal (N-S) centerline of the container. Using a constant volume assumption, it can be shown that approximately 17 cm (prototype) of total settlement along the longitudinal centerline of the model container should occur as the shape of the soil surface transitions from curved to flat under the radial *g*-field. While it is unclear how quickly this process occurs (i.e., all at once or distributed over several simulated earthquake events), it is clear that not curving the soil surface for centrifuge experiments involving liquefaction will lead to a systematic bias towards higher observed settlements at the center of the model container and lower observed settlements near the eastern and western edges. Consequently, it is

not surprising that the measured free-field settlements during SHD04, which were measured along the longitudinal centerline, are slightly high relative to the measured settlements observed during T4.5-50 (Table 3.4.2).

- The isolated 'A' building during T4.5-50 settled significantly more than the isolated 'A' buildings during T3-50-SILT and T3-50 for the PRI_mod motion, significantly more than T3-50 for the TCU_mod motion, and slightly more than the measured settlements during T3-50 for the PRI_large motion. While the same pluviation techniques were employed during model construction for all three tests, and the same command motions were applied, the achieved peak acceleration for the PRI_mod event at the base of the model container during T4.5-50 was 0.23 g versus 0.17 g and 0.15 g for T3-50-SILT and T3-50, respectively. Consequently, the T4.5-50 model was subjected to more intense shaking for the PRI_mod event than T3-50-SILT and T3-50 and this could partially explain the larger settlements observed during this test for that event. However, as previously discussed, the soil surface was not curved during T3-50-SILT and T3-50, but it was curved during T4.5-50. Not curving the soil surface should have caused higher settlements of the buildings that were along the longitudinal centerline of the model during T3-50-SILT and T3-50, so this would have likely partially counteracted the more intense achieved motion during T4.5-50. As discussed previously, the motion sequence for T3-50-SILT did not include the TCU_mod motion. Therefore, one would expect less densification to have occurred during T3-50-SILT (i.e., about 5% increase in relative density) than for T4.5-50 and T3-50 (i.e., about 10% increase in relative density) prior to the PRI_large event, with all else being equal. This could potentially explain the higher settlement observed during T3-50-SILT, relative to T4.5-50 and T3-50. All things considered, the building settlements measured during T4.5-50 appear to be reasonable when compared to existing data.

- The adjacent buildings during T4.5-50 generally tilted and displaced laterally away from one another. These observations suggest that the physical presence of the adjacent building, particularly when it was of equal or greater size, kinematically constrained ground movements under the structures on the sides nearest the adjacent buildings relative to the ground movements that occurred under the sides away from the adjacent building. This caused relatively more settlement on the sides away from the adjacent buildings, and therefore, a corresponding tendency for the buildings to tilt away from each other. Ground being pushed to the side as adjacent buildings settle could also potentially explain the tendency for buildings to move horizontally away from one another during these events. That is, as the adjacent buildings settle, lateral ground displacements under the side of the building closest to the adjacent building would be opposed by ground displacements from under the adjacent building and the buildings would effectively push one another away. The details of this mechanism are likely dependent on the foundation types of the adjacent buildings and further study is required to explore the mechanism that most significantly influences the performance of adjacent buildings supported on isolated spread footings or spread footings interconnected with tie beams. In addition, the confining stresses under the sides of closely-spaced adjacent buildings are lower under the side away from the neighboring building than the side

closest to the neighboring building. Consequently, with all other things equal, one would expect a lower liquefaction resistance in the foundation soils on the sides away from the adjacent building, and therefore, relatively more cyclic softening to occur on that side during shaking. As horizontal inertial forces are transferred from the superstructure to the foundation soils during shaking, this additional cyclic softening on the side away from the adjacent buildings would lead to a tendency for the buildings to incrementally move apart laterally.

- Building 'J-pile$_A$' settled significantly less than the 'J_A' building, as expected, during all events. It settled less than the free-field surface during PRI_mod and TCU_mod and about the same as the free-field ground surface during PRI_large. However, whereas the free-field ground settlement was caused by the volumetric settlement mechanisms described by Dashti et al. (2010a); the settlement of Building 'J-pile$_A$' was likely caused by: 1) cyclic softening of the dense Nevada Sand layer due to excess pore water pressure generation which reduced the side and tip resistance of the piles within this layer; and 2) loss of side friction due to excess pore water pressure generation and subsequent cyclic softening of the medium dense Nevada Sand which caused the load to transfer from the mat foundation and the upper part of the pile to its lower part. The latter mechanism would cause a portion of the structural load to transfer to end bearing and require a compatible amount of settlement to resist this additional load. Significant excess pore water pressures were generated in the dense Nevada Sand layer during each of the three events under consideration, and particularly during the PRI_large event. Consequently, the settlements of the 'J-pile$_A$' building during this test are not surprising.

Christchurch, New Zealand experienced seven earthquake events with $M_w \geq 5.5$ between 4 September 2010 and 23 December 2011. Of these significant events, the 22 FEB 11 Christchurch earthquake was the most damaging. Modern commercial and residential buildings in the CBD were often significantly impacted by soil liquefaction during the Christchurch earthquake. Twenty-two sites within the CBD were identified for further study by a team of researchers from GEER and an additional site, just outside of the CBD, was identified in July 2011. The selected sites contained single- and multi-story buildings on shallow and deep foundations that displayed unique performance characteristics. A total of 107 CPTs were performed at these sites during field investigations following the earthquakes. The most interesting of the 23 sites were investigated further in this study. Some of the key findings from these evaluations are summarized below:

- Many multi-story buildings in the CBD were heavily damaged by liquefaction-induced ground movements during the 22 FEB 11 Christchurch earthquake, but not by other significant earthquakes (e.g., 4 SEP 10 and 13 JUN 11). The peak geo-mean horizontal ground accelerations in the M_w 6.2 22 FEB 11 earthquake were on the order of twice those recorded during the larger, but more distant M_w 7.1 4 SEP 10 event. The PGAs during the 4 SEP 10 event were similar to those recorded during the 26 DEC 10 M_w 4.8, 13 JUN 11 M_w 6.0, and 23 DEC 11 M_w 5.9 events. The Arias intensity-time histories, as

well as the SIR, also indicate clearly why the Christchurch event was the most damaging to buildings in the CBD.

- Variability in shallow subsurface conditions over relatively short distances was sometimes a critical factor in the seismic performance of ground and buildings.

- CPT-based liquefaction triggering evaluations were generally conservative, and this conservatism led to post-liquefaction free-field ground settlement estimates that were generally similar for the 4 SEP 10, 22 FEB 11, and 13 JUN 11 events, whereas significant ground settlements and building damage in the CBD were only observed during the 22 FEB 11 event.

- Simplified liquefaction-induced ground settlement procedures (e.g., Zhang et al. 2002) do not capture the important shear-induced building deformation mechanisms described by Dashti et al. (2010a), nor do they capture settlement due to ground loss. Not surprisingly, therefore, building settlements were typically underestimated using the ZR02-RW98 analysis procedure for the 22 FEB 11 event.

- In addition to the shear-induced building settlement mechanisms described by Dashti et al. (2010a), ground loss under shallow foundations due to eroded sediment ejecta was often a significant factor in the seismic performance of the buildings evaluated as part of this study.

- As described previously, free-field, level-ground liquefaction-induced settlement procedures are inappropriate for the estimation of building settlement at sites with shallow liquefiable soils. Improved calibrated procedures that are specific to the settlement of shallow-founded buildings subjected to shallow liquefaction are needed. In addition to not capturing important building settlement mechanisms, free-field level ground procedures give equal weighting to volumetric strains at all depths. Consequently, caution should be exercised when using these methods even as indices to expected building performance. If free-field, level-ground methods are employed, it is important to select a consistent baseline depth over which to calculate vertical strains. The appropriate baseline depth should be a function of the foundation type and dimensions, such as the strain influence zone described by Schmertmann (1978).

- While liquefaction of soils below a depth of 8 m contributed significantly to the amount of calculated settlement at the CTUC building site, their impact on the building performance appears to have been relatively minor. Thus, the equal weighting of post-liquefaction volumetric strains over all depths of the soil profile in the calculation of free-field vertical settlements can be misleading when this approach is used to evaluate the performance of buildings with shallow foundations.

- The PILE-6 and SCH buildings both performed relatively well during the Canterbury earthquake sequence. The PILE-6 building was a six-story, pile-supported frame structure

underlain by shallow and deep liquefiable soils. Despite substantial ground settlements around the building, the first-story structural frame of the PILE-6 building did not appear to show significant damage. However, its structural performance was not fully documented due to restricted access by the GEER team. The SCH building was a seven-story RC frame structure on a drilled shaft foundation. Though a significant amount of sediment ejecta was observed around the building following the 22 FEB 11 event, the drilled shafts were extended to depths of 6 – 7 m, just beyond a shallow liquefiable layer of ML/SM that was typically present to depths of 4 – 6 m. Cubrinovski et al. (2011a) observed that the building did not appear to have punched into the ground, and differential settlements between adjacent columns were often negligible and rarely up to 3.5 cm. A subsequent floor level survey by TM Consultants in January 2012 indicated a maximum differential settlement of 3 cm over a distance of 2.5 m, and KGA (2012) indicated a maximum differential settlement of 9 cm at the ground floor.

- The PWC and VT buildings were 21-story and 10-story RC frame structures, respectively, that tilted during the Canterbury earthquakes. Liquefiable materials were at least 3 m below the base of the foundation and often more than 5 m at the PWC building site, and at least 4 m below the base of the foundation at the VT building site. However, the foundation widths of the buildings were 25 m (L/B = 1.4) and 19 m (L/B = 1.3) for the PWC and VT buildings, respectively, so the liquefiable materials were well within the depth range with a significant vertical strain influence using the settlement approach developed by Schmertmann (1978) for rigid footings on sand. Consequently, cyclic softening of these materials due to increased pore water pressures would have likely led to building settlements, despite the fact that the liquefiable materials were not directly beneath these buildings. In addition, cyclic softening due to increased pore water pressures during and immediately following the significant Canterbury earthquakes could have occurred in other materials beneath these buildings, and the transient reduction in stiffness in materials that did not fully liquefy could have also contributed to the observed building settlements. Volumetric reconsolidation of the liquefiable materials beneath the building foundations would have also caused settlements.

- The top of the PWC building tilted slightly to the south during the 22 FEB 11 event. Importantly, the basement mat foundation extends significantly to the north of the tower footprint. It is likely that the northern portion of the basement mat, therefore, acted as a cantilever that prevented the northern end of the PWC building tower from settling as much as the southern end, causing the building to tilt slightly to the south.

- The VSA building was a 14-story RC building, located adjacent to the VT building, that underwent 22 cm of differential settlement in the north-south direction and 6 cm in the east-west direction. The building had a complex foundation system that consisted of 17 1.2 m-diameter RC piles around the southern, eastern and western edges of the building footprint and several shallow RC spread footings along the northern edge and within the building footprint. The lengths of the piles were either 6 m, 14 m, or 18 m. Whereas 14 m long piles were located at the northeast, southeast, and southwest corners of the building;

only 6 m long piles appear to have been installed at the northwest corner. This differential movement in the north-south direction was explained by variable ground conditions in combination with the lack of deep piles at the northwest corner of the building. The 6 cm of differential settlement between the northwest corner of the building and the northeast corner of the building was explained by the presence of 14 m piles at the NE corner (versus 6 m piles at the NW corner), in addition to slightly better ground conditions between CPTs Z2-13 and Z2-22.

- The CTH building auditorium was founded on two rings of shallow RC spread footings, with the footings within each ring connected by tie beams. The components of the inner ring were larger and more heavily loaded than the corresponding outer ring components. Beams connected the building's main internal columns to the exterior columns, and Cubrinovski et al. (2011a) observed differential settlement of the inner footings relative to the outer footings. This caused many of the exterior columns to tilt inward. Similar to many of the other buildings studied in the CBD, the CTH building was underlain by a shallow liquefiable layer of ML/SM, and the auditorium foundation elements were founded within this layer. T&T (2013) reported typical foundation settlements of 30 - 50 cm and estimated approximately 70 m^3 liquefaction-induced sediment ejecta was removed from the auditorium basement following the 22 FEB 11 Christchurch earthquake. The FS against a bearing capacity failure for a representative footing on the south side of the auditorium in the vicinity of CPT Z5-11 was estimated to be slightly less than one using the procedure developed for a two-layer cohesive soil deposit with the residual shear strength of the shallow ML/SM materials and an equivalent undrained shear strength of the underlying medium dense to very dense SP/GP/SM. Consequently, localized bearing capacity failures, along with ground loss due to sediment ejecta, were primarily responsible for the settlements observed for this case. Lateral movements and some settlement due to lateral spreading towards the nearby Avon River also likely occurred at this site.

- The LS-I and LS-II buildings were two-story concrete panel buildings. The shallow foundations of both buildings consisted of 1.2 m wide by 0.65 m deep RC strip footings that supported concrete panel walls. The plan dimensions of the buildings were approximately 28 m by 18 m and 11 m by 18 m for LS-I and LS-II, respectively. The shallow foundation soils at the site consisted of very loose to loose or very soft to stiff SM/ML/CL to depths between 3 m and just over 8 m, underlain by medium dense to very dense SP/GP to depths of 17.5 – 18 m. A significant portion of both layers should have liquefied based on the median PGA from Bradley and Hughes (2012) during the 22 FEB 11 Christchurch earthquake. Consequently, both buildings were subjected to shallow and deep liquefaction during this event. Though both buildings appeared to settle relative to the surrounding ground, LS-II appeared to settle more and was damaged more severely than LS-I. Transient reductions in stiffness and strength in the foundation materials appear to have caused localized punching shear settlements at footing locations. Whereas the distribution of structural loads at the LS-I building appears to be more evenly distributed over the building footprint; the loads were concentrated around the perimeter

of the LS-II building, with the exception of two footings that cut across the center of the LS-II building in the transverse direction. Therefore, the more severe punching shear failures at the footing locations of the LS-II building caused relatively more damage at this location. In addition, the eastern side of LS-II was divided into a first and second floor whereas the western side was utilized as warehouse space with a single floor. The presence of the second floor mass over the eastern side but not the western side likely caused uneven superstructure inertial forces to be transferred to the building foundation, and this could have caused differential settlements due to non-uniform SSI-induced ratcheting.

5.3 Recommendations for Future Research

Although significant progress has been made towards understanding building displacements caused liquefaction or cyclic softening, there is much work that remains to be done. Of critical importance is the development of guidelines to evaluate liquefaction-induced building displacements that can be implemented in routine practice by engineering practitioners. As described previously, the liquefaction potential below a building is still often evaluated by treating the soil as if it were in the free-field. Liquefaction-induced building settlements are then often estimated using empirical procedures developed to calculate post-liquefaction, one-dimensional, consolidation settlements in the free-field (e.g., Tokimatsu and Seed, 1987; Ishihara and Yoshimine, 1992). Better alternatives to these procedures are necessary to advance the state-of-the-art in liquefaction engineering. This will be a challenging endeavor, but the significant amount of relevant data that has recently become available following the 2010 Maule, Chile and 2011 Tohoku, Japan earthquakes, in combination with the work presented herein and existing field and physical model case history data, provide a robust data set upon which new analytical procedures can be developed.

Well-calibrated SSI numerical models of the field and physical model case histories presented in Chapters 3 and 4 will enhance the interpretations of building performances presented in this thesis. Although it will be challenging to account for the effects liquefaction-induced sediment ejecta, important insights from these numerical analyses will be gained. During future post-earthquake reconnaissance investigations, the volume of liquefaction-induced sediment ejecta should be documented.

REFERENCES

Adachi, T., Iwai, S., Yasui, M., and Sato, Y. (1992). "Settlement and inclination of reinforced concrete buildings in Dagupan City due to liquefaction during the 1990 Philippine Earthquake." *Proc., 10th World Conf. on Earthquake Engineering,* International Association for Earthquake Engineering (IAEE), Madrid, Spain, 147 – 152.

Adalier, K., and Elgamal, A. (2005). "Liquefaction of Over-Consolidated Sand: A Centrifuge Investigation." *Journal of Earthquake Engineering*, 9(1), 127 – 150.

Allmond, J., and Kutter, B.L. (2012). "Centrifuge Testing of Rocking Foundations on Saturated and Submerged Sand: Centrifuge Data Report for JDA01." *Report Number: UCD/CGMDR-12/01*. Center for Geotechnical Modeling, Davis, CA.

Ashford, S.A., Boulanger, R.W., Donahue, J.L., and Stewart, J.P. (2011). "Geotechnical Quick Report on the Kanto Plain Region during the March 11, 2011, Off Pacific Coast of Tohoku Earthquake, Japan." *Technical report.* Retrieved from http://www.geerassociation.org/GEER_Post%20EQ%20Reports/Tohoku_Japan_2011/Quick%20Report_1_index.html.

ASTM Standard D854 (2006). "Standard Test Methods for Specific Gravity of Soil Solids by Water Pycnometer." ASTM International, West Conshohocken, PA, 2006. www.astm.org.

ASTM Standard D5778 (2007). "Standard Test Method for Electronic Friction Cone and Piezocone Penetration Testing." ASTM International, West Conshohocken, PA, 2007. DOI: 10.1520/D5778-07, www.astm.org.

ASTM Standard D4253 (2006). "Standard Test Methods for Maximum Index Density and Unit Weight of Soils Using a Vibratory Table." ASTM International, West Conshohocken, PA, 2006. DOI: 10.1520/D4253-00R06, www.astm.org.

ASTM Standard D4254 (2006). "Standard Test Methods for Minimum Index Density and Unit Weight of Soils and Calculation of Relative Density." ASTM International, West Conshohocken, PA, 2006. DOI: 10.1520/D4254-00R06, www.astm.org.

Bannister, S., Fry, B., Reyners, M., Ristau, J., and Zhang, H. (2011). "Fine-scale Relocation of Aftershocks of the 22 February M_w 6.2 Christchurch Earthquake Using Double-difference Tomography." *Seismological Research Letters,* 82(6), 839 – 845.

Beavan, J., Fielding, E., Motagh, M., Samsanov, S., and Donnelly, N. (2011). "Fault Location and Slip Distribution of the 22 February 2011 M_w 6.2 Christchurch, New Zealand Earthquake from Geodetic Data." *Seismological Research Letters,* 82(6), 789 – 799.

Beavan, J., Motagh, M., Fielding, E.J., Donnelly, N., and Collett, D. (2012). "Fault slip models of the 2010 – 2011 Canterbury, New Zealand, earthquakes from geodetic data and observations of postseismic ground deformation." *New Zealand Journal of Geology and Geophysics*, 55(3), 207 – 221.

Beca Carter Hollings & Ferner Ltd. (2011a). "Earthquake Damage Assessment – 151 Kilmore Street." *Technical report prepared for Westpark Estates 151 Ltd.*

Beca Carter Hollings & Ferner Ltd. (2011b). "48 Lismore Street, Christchurch – Earthquake Damage Assessment." *Technical report prepared for Skyway Body Corporate Services Ltd.*

Beca Carter Hollings & Ferner Ltd. (2011c). "Investigation into the Collapse of the Pyne Gould Corporation Building on 22nd February 2011." *Technical report prepared for the Department of Building and Housing.*

Bilge, H.T. (2010). "Cyclic Volumetric and Shear Strain Responses of Fine-Grained Soils." Ph.D. dissertation, Middle East Technical University, Ankara, Turkey.

Bradley, B.A. (2012). "Ground Motion and Seismicity Aspects of the 4 September 2010 Darfield and 22 February 2011 Christchurch Earthquakes." *Technical report prepared for the Canterbury Earthquakes Royal Commission*, 13 January 2012, Christchurh, New Zealand.

Bradley, B.A., and Cubrinovski, M. (2011). "Near-Source Ground Motions Observed in the 22 February 2011 Christchurch Earthquake." *Seismological Research Letters,* 82(6), 853 – 865.

Bradley, B.A., and Hughes, M. (2012). "Conditional Peak Ground Accelerations in the Canterbury Earthquakes for Conventional Liquefaction Assessment." *Technical Report Prepared for the Department of Building and Housing,* 22 pp.

Bray, J.D., and Dashti, S. (2010). "Liquefaction-Induced Movements of Buildings with Shallow Foundations." *Fifth International Conference on Recent Advances in Geotechnical Earthquake Engineering and Soil Dynamics*, May 24 – 29, San Diego, CA, Paper Number: OSP-2.

Bray, J.D., and Frost, D. [Eds.] (2010). "Geo-Engineering Reconnaissance of the February 27, 2010 Maule, Chile Earthquake." *Technical report.* Retrieved from http://www.geerassociation.org/GEER_Post%20EQ%20Reports/Maule_Chile_2010/Ver2_Maule_Chile_2010_index.html.

Bray, J.D., Rollins, K., Hutchinson, T., Verdugo, R., Ledezma, C., Mylonakis, G., Assimaki, A., Montalva, G., Arduino, P., Olson, S.M., Kayen, R., Hashash, Y.M.A., and Candia, G. (2012). "Effects of Ground Failure on Buildings, Ports, and Industrial Facilities." *Earthquake Spectra,* 28(S1), June 2012, S97 – S118.

Bray, J., Cubrinovski, M., Zupan, J., and Taylor, M. (2014). "Liquefaction Effects on Buildings in the Central Business District of Christchurch." *Earthquake Spectra*, In-Press.

Brown, L.J., and Weeber, J.H. (1992). *Geology of the Christchurch Urban Area*. Lower Hutt, New Zealand: Institute of Geological and Nuclear Sciences.

Canterbury Earthquakes Royal Commission (2011). "Interim Report, October 2011." *Technical report*, 11 October 2011, Wellington, New Zealand.

Canterbury Geotechnical Database (2012a). "Aerial Photography", Map Layer CGD0100 – 1 June 2012, retrieved 1 December 2012 from https://canterburygeotechnicaldatabase.projectorbit.com/.

Canterbury Geotechnical Database (2012b) "LiDAR and Digital Elevation Models", Map Layer CGD0500 - 23 July 2012, retrieved 1 December, 2012 from https://canterburygeotechnicaldatabase.projectorbit.com/.

Canterbury Geotechnical Database (2012c) "Vertical Ground Surface Movements", Map Layer CGD0600 - 23 July 2012, retrieved 1 December, 2012 from https://canterburygeotechnicaldatabase.projectorbit.com/.

Canterbury Geotechnical Database (2013). "Event Specific Groundwater Surface Elevations", Map Layer CGD0800 - 11 Feb 2013, retrieved 1 July, 2013 from https://canterburygeotechnicaldatabase.projectorbit.com/.

Cetin, K.O., Seed, R.B., Der Kiureghian, A., Tokimatsu, K., Harder, L.F., Kayen, R.E., and Moss, R.E.S. (2004). "Standard Penetration Test-Based Probabilistic and Deterministic Assessment of Seismic Soil Liquefaction Potential." *Journal of Geotechnical and Geoenvironmental Engineering.*, 130(12), 1314 – 1340.

Cetin, K.O., Bilge, H.T., Wu, J., Kammerer, A.M., and Seed, R.B. (2009). "Probabilistic Model for the Assessment of Cyclically Induced Reconsolidation (Volumetric) Settlements." *Journal of Geotechnical and Geoenvironmental Engineering.*, 135(3), 387 – 398.

Cetin, K.O., Unutmaz, B., and Jeremic, B. (2012). "Assessment of Seismic Soil Liquefaction Triggering Beneath Building Foundation Systems." *Soil Dynamics and Earthquake Engineering*, 43, 160 – 173.

Christchurch City Council (2013). Christchurch City population data. Retrieved from: http://www.ccc.govt.nz/cityleisure/statsfacts/statistics/population.aspx

Colliers International New Zealand Ltd. (2009). "South Island's largest office tower up for sale." *Online article published 11 September 2009*. Retrieved from http://www.colliers.co.nz/News/2009/September/South-Island-s-largest-office-tower-up-for-sale-300/.

Compusoft Engineering (2012). "Independent Earthquake Performance Assessment. Victoria Square Apartments. 100 Armagh Street, Christchurch." *Technical report prepared for the Canterbury Earthquakes Royal Commission*, January 2012.

Connell Mott MacDonald (2004). "Victoria Gardens West Tower Structural Drawings."

Cox, B., Wood, C., Deschenes, R., and Pearson, M. (2012). "University of Arkansas Preliminary CBD Data Report for: Surface Wave Testing in Christchurch, New Zealand Affected by the New Zealand Earthquakes." *Internal technical report*.

Cubrinovski, M., Bray, J.D., Taylor, M., Giorgini, S., Bradley, B., Wotherspoon, L., and Zupan, J. (2011a). "Soil Liquefaction Effects in the Central Business District during the February 2011 Christchurch Earthquake." *Seismological Research Letters*, 82(6), 893-904.

Cubrinovski, M., Green, R.A., and Wotherspoon, L. [Eds] (2011b). "Geotechnical Reconnaissance of the 2011 Christchurch Earthquake." *Technical Report*. Retrieved from http://geerassociation.org/GEER_Post%20EQ%20Reports/Christchurch_2011/Index_Christchurch_2011.html.

Cubrinovski, M., Bradley, B., Wotherspoon, L., Green, R., Bray, J., Wood, C., Pender, M., Allen, J., Bradshaw, A., Rix, G., Taylor, M., Robinson, K., Henderson, D., Giorgini, S., Ma, K., Winkley, A., Zupan, J., O'Rourke, T., DePascale, G. and Wells, D. (2011c). "Geotechnical Aspects of the 22 February 2011 Christchurch earthquake." *Bulletin of the New Zealand Society of Earthquake Engineering,* 44(4), 205-226.

Dashti, S. (2009). "Toward evaluating building performance on softened ground." Ph.D. dissertation, Univ. of California, Berkeley, Berkeley, CA.

Dashti, S., Bray, J.D., Pestana, J.M., Riemer, M.R., and Wilson, D. (2010a). "Mechanisms of seismically-induced settlement of buildings with shallow foundations on liquefiable soil." *J. Geotech. Geoenviron. Eng.,* 136(1), 151-164.

Dashti, S., Bray, J.D., Pestana, J.M., Riemer, M.R., and Wilson, D. (2010b). "Centrifuge testing to evaluate and mitigate liquefaction-induced building settlement mechanisms." *J. Geotech. Geoenviron. Eng.,* 136(7), 918-929.

Eliot Sinclair & Partners Limited (2011). "Ground Floor Levels – 4 March 2011."

Geoscience Consulting (NZ) Limited (2012). "Geotechnical Investigation. 48 Lismore Street, Waltham, Christcurch." *Technical report prepared for Skyway Body Corporate Services Ltd.*, 15 May 2012.

Geotech Consulting Ltd. (2012). "Preliminary Geotechnical Report. 87 Kilmore Street, Christchurch." *Technical report*, 7 February 2012.

Giorgini, S., Taylor, M., Cubrinovski, M., and Pampanin, S. (2011a). "Effects of soil-foundation-structure-interaction on the observed damage of multistory RC buildings in the 2011 Christchurch earthquake." *Internal technical report*. Department of Civil and Natural Resources Engineering, University of Canterbury, Christchurch, New Zealand.

Giorgini, S., Taylor, M., Cubrinovski, M., and Pampanin, S. (2011b). "Preliminary Observations of Multistorey RC Building Foundation Performance in Christchurch Following the 22nd February 2011 Earthquake." *New Zealand Concrete Industry Conference,* Energy Events Centre, Rotorua, New Zealand, August 2011.

Giorgini, S. (2015). "Towards Performance-Based Seismic Design and Assessment of Integrated Foundation-Structure Systems." Ph.D. dissertation, Department of Civil and Natural Resources Engineering, University of Canterbury, Christchurch, New Zealand. In preparation.

GNS Science (2013). Earthquake event data. Retrieved from: http://magma.geonet.org.nz/resources/quakesearch/

Green, R.A., and Cubrinovski, M. [Eds] (2010). "Geotechnical Reconnaissance of the 2010 Darfield (New Zealand) Earthquake." *Technical Report*. Retrieved from http://geerassociation.org/GEER_Post%20EQ%20Reports/Christchurch_2011/Index_Christchurch_2011.html.

Hausler, E.A. (2002). "Influence of ground improvement on settlement and liquefaction: A study based on field case history evidence and dynamic geotechnical centrifuge tests." Ph.D. dissertation, Univ. of California, Berkeley, CA.

Hayden, C.P., Allmond, J.A., Rawlings, I.A., Kutter, B.L., Bray, J.D., Hutchinson, T.C., Fiegel, G.L., Zupan, J.D., and Whittaker, A.S. (2013). "Seismic Performance Assessment in Dense Urban Environments: Centrifuge Data Report for Test-6." *Technical Report.* Center for Geotechnical Modeling, Davis, CA.

Holden, C. (2011). "Kinematic Source Model of the 22 February 2011 M_w 6.2 Christchurch Earthquake Using Strong Motion Data." *Seismological Research Letters*, 82(6), 783 – 788.

Holmes Consulting Group Limited (2011). "Detailed Structural Engineering Evaluation of the Christchurch Town Hall For Performing Arts." *Technical report prepared for Vbase Limited*, 8 August 2011.

Holmes Consulting Group, Wilkins & Davies Ltd., and Alun Wilkie Architects Ltd. (1988). "Price Waterhouse Centre Structural Drawings."

Holmes Wood Poole & Johnstone Ltd. (1986). "Victoria Tower Structural Drawings."

Hushmand Associates, Incorporated (2012). "Phase II Geotechnical Investigation. Liquefaction and Foundation Evaluation. Scenic Circle Hotel. 87-89 Kilmore Street, Christchurch, New Zealand." *Technical report prepared for Civil Concepts*, 2 July 2012.

Idriss, I.M., and Boulanger, R.S. (2008). *Soil Liquefaction During Earthquakes.* Earthquake Engineering Research Institute, EERIMNO-12, Oakland, CA.

Ishihara, K., and Yoshimine, M. (1992). "Evaluation of settlements in sand deposits following liquefaction during earthquakes." *J. Soils and Foundations*, 32(1), 173 – 188.

Ishii, Y., and Tokimatsu, K. (1988). "Simplified procedures for the evaluation of settlements of structures during earthquakes." *Proc., 9th World Conf. on Earthquake Engineering,* Tokyo-Kyoto, Japan, 95 - 100.

Jamiolkowski, M., LoPresti, D.C.F., and Manassero, M. (2001). "Evaluation of Relative Density and Shear Strength of Sands from Cone Penetration Test and Flat Dilatometer Test." *Soil Behavior and Soft Ground Construction* (GSP 119), American Society of Civil Engineers, Reston, Virginia, 201 – 238.

Kammerer, A., Pestana, J., and Seed, R. (2002). "Undrained Response of 0/30 Sand Under Multidirectional Cyclic Simple Shear Loading Conditions." *Geotechnical Engineering Research Report No. UCB/GT/02-01*, University of California, Berkeley, July, 2002.

Karamitros, D.K., Bouckovalas, G.D., Chaloulos, Y.K. (2013). "Insight into the Seismic Liquefaction Performance of Shallow Foundations." *Journal of Geotechnical and Geoenvironmental Engineering*, 139(4), 599 – 607.

KGA Geotechnical Investigations Ltd. (2012). "Geotechnical Assessment of Foundations. Scenic Circle Hotel. 87 Kilmore Street, Christchurch." *Technical report prepared for Civil Concepts*, 15 August 2012.

Kulhawy, F.H. and Mayne, P.H. (1990). *Manual on estimating soil properties for foundation design.* Electric Power Research Institute, August, 1990.

Kutter, B. L. (1995). "Recent advances in centrifuge modeling of seismic shaking." *Proc., 3rd Int. Conf. on Recent Advances in Geotechnical Earthquake Engineering and Soil Dynamics*, S. Prakash (Ed.). St. Louis, Vol. 2, 927–942.

Kutter, B. L., Idriss, I.M., Kohnke, T., Lakeland, J., Li, X.S., Sluis, W., Zeng, X., Tauscher, R.C., Goto, Y., and Kubodera, I. (1994). "Design of a Large earthquake Simulator at UC Davis." *Centrifuge 94: Proceedings of the International Centrifuge Conference 1994*, Leung, C.F., Lee, F.H., and Tan, T.S. (Eds.). Rotterdam, 169 – 175. A.A. Balkema.

Liu, L., and Dobry, R. (1997). "Seismic Response of Shallow Foundation on Liquefiable Sand." *Journal of Geotechnical and Geoenvironmental Engineering*, 123(6), 557 – 567.

Lunne, T., Robertson, P.K., and Powell, J.J.M. (1997). *Cone Penetration Testing in Geotechnical Practice.* New York, NY: Routledge.

Mason, H.B. (2011). "Seismic Performance Assessment in Dense Urban Environments." Ph.D. dissertation, University of California, Berkeley, CA.

Mason, H.B., Trombetta, N.W., Chen, Z., Choy, B.Y., Bolisetti, C., Bray, J.D., Hutchinson, T.C., Kutter, B.L., and Whittaker, A.S. (2010a). "Seismic Performance Assessment in Dense Urban Environments: Centrifuge data report for HBM02." *Report Number: UCD/CGMDR-01/11*. Center for Geotechnical Modeling, Davis, CA.

Mason, H.B., Trombetta, N.W., Chen, Z., Choy, B.Y., Bolisetti, C., Bray, J.D., Hutchinson, T.C., Kutter, B.L., and Whittaker, A.S. (2010b). "Seismic Performance Assessment in Dense Urban Environments: Centrifuge data report for HBM03." *Report Number: UCD/CGMDR-03/11*. Center for Geotechnical Modeling, Davis, CA.

Mason et al. (2010c). "Seismic Performance Assessment in Dense Urban Environments: Centrifuge data report for HBM04." *Report Number: UCD/CGMDR-02/11*. Center for Geotechnical Modeling, Davis, CA.

Mason, H. B., Trombetta, N. W., Chen, Z., Bray, J. D., Hutchinson, T. C., and Kutter, B. L. (2013). "Seismic soil–foundation–structure interaction observed in geotechnical centrifuge experiments." *Soil Dynamics and Earthquake Engineering*, 48, 162-174.

Mayne, P.W. (2007). "Cone Penetration Testing: A Synthesis of Highway Practice." *Technical Report*: *National Cooperative Highway Research Program Synthesis 368*. Transportation Research Board, Washington, D.C.

Moss, R.E.S., Seed, R.B., Kayen, R.E., Stewart, J.P., Der Kiureghian, A., and Cetin, K.O. (2006). "CPT-Based Probabilistic and Deterministic Assessment of In Situ Seismic Soil Liquefaction Potential." *Journal of Geotechnical and Geoenvironmental Engineering*, 132(8), 1032 – 1051.

Naval Facilities Engineering Command (1986). *Design Manual 7.02*. Alexandria, Virginia.

New Zealand Geotechnical Society (2005). *Field Description of Soil and Rock: Guideline for the Field Classification and Description of Soil and Rock for Engineering Purposes*. New Zealand Geotechnical Society, New Zealand.

Olson, S.M., and Stark, T.D. (2002). "Liquefied Strength Ratio from Liquefaction Flow Failure Case Histories." *Canadian Geotechnical Journal,* 39, 629 – 647.

O'Rourke, T., and Milashuk, S. (2011). "Spatial Distribution of Ground Motion During Earthquakes Affecting Christchurch, NZ." *Internal technical report,* 28 September 2011.

Pampanin, S. (2012). "Reality-Check and Renewed Challenges in Earthquake Engineering: Implementing Low-Damage Systems – From Theory to Practice." *Bulletin of the New Zealand Society for Earthquake Engineering*, 45(4), 137 – 160.

Robertson, P.K. (2009). "Interpretation of Cone Penetration Tests – A Unified Approach." *Canadian Geotechnical Journal*, 46, 1337 – 1355.

Robertson, P.K., and Cabal, K.L. (2010). *Guide to Cone Penetration Testing for Geotechnical Engineering, 4th Edition*. Gregg Drilling and Testing, April, 2010.

Robertson, P.K., and Cabal, K.L. (2010). "Estimating Soil Unit Weight from CPT." *2nd International Symposium on Cone Penetration Testing*, Huntington Beach, CA, May, 2010.

Robertson, P.K., and Wride, C.E. (1998). "Evaluating Cyclic Liquefaction Potential Using the Cone Penetration Test." *Canadian Geotechnical Journal*, 35, 442 – 459.

Rollins, K.M., and Seed, H.B. (1990). "Influence of Buildings on Potential Liquefaction Damage." *Journal of Geotechnical Engineering*, 116(2), 165 – 185.

Ruamoko Solutions (2010). "Earthquake Damage Inspection Report. Shipleys Audiovisual. 193 Peterborough Street, Christchurch." *Technical report prepared for Shipleys Audiovisual*, December 2010.

Salgado, R., Mitchell, J.K., and Jamiolkowski, M. (1997). "Cavity expansion and penetration resistance in sands." *Journal of Geotechnical and Geoenvironmental Engineering*, 123(4), 344 – 354.

Sancio, R.B. (2003). "Ground Failure and Building Performance in Adapazari, Turkey." Ph.D. dissertation, University of California, Berkeley, CA.

Schmertmann, J.H. (1978). "Guidelines for Cone Penetration Test: Performance and Design." *Technical report number: FHWA-TS-78-209*, U.S. Department of Transportation Federal Highway Administration, July 1978, Washington, D.C.

Seed, H.B., and Idriss, I.M. (1971). "Simplified Procedure for Evaluating Soil Liquefaction Potential." *Journal of the Soil Mechanics and Foundations Division*, 97(SM9), 1249 - 1273.

Seed, R.B., Cetin, K.O., Moss, R.E.S., Kammerer, A.M., Wu, J., Pestana, J.M., Riemer, M.F., Sancio, R.B., Bray, J.D., Kayen, R.E., and Faris, A. (2003). "Recent Advances in Soil Liquefaction Engineering: A Unified and Consistent Framework." *26th Annual ASCE Los Angeles Geotechnical Spring Seminar, Keynote Presentation*, H.M.S. Queen Mary, Long Beach, California, April 30, 2003.

Sibson, R., Ghisetti, F., and Ristau, J. (2011). "Stress Control of an Evolving Strike-Slip Fault System during the 2010 – 2011 Canterbury, New Zealand, Earthquake Sequence." *Seismological Research Letters*, 82(6), 824 – 832.

Sitar, N., and Hausler, E. (2012). "Influence of Ground Improvement on Liquefaction Induced Settlement: Observations from Case Histories and Centrifuge Experiments." *International Journal of Geo-Engineering*, 4(2), 5 – 15, June 2012.

Smyrou, E., Tasiopoulou, P., Bal, I.E., and Gazetas, G. (2011). "Ground Motions versus Geotechnical and Structural Damage in the February 2011 Christchurch Earthquake." *Seismological Research Letters*, 82(6), 882 - 892.

Soils & Foundations Geotechnical Consulting Engineers (1987). "Price Waterhouse Centre. Armagh Street." *Technical report.*

Soils & Foundations (1973) Ltd. (1987). "Subsurface Investigation Report. Proposed Development. 144 Kilmore Street, Christchurch." *Technical report prepared for Tyndall & Hanham Consulting Engineers*, 5 February 1987.

Somerville, P.G., Smith, N.F., Graves, R.W., and Abrahamson, N.A. (1997). "Modifications of empirical strong ground motion attenuation relations to include the amplitude and duration effects of rupture directivity." *Seismological Research Letters*, 68(1), 199 – 222.

Stewart, D.P., Chen, Y.R., and Kutter, B.L. (1998). "Experience with the use of methylcellulose as a viscous pore fluid in centrifuge models." *ASTM Geotechnical Testing Journal*, 21(4), 365-369.

Taylor, M.L., Cubrinovski, M., and Haycock, I. (2012). "Application of New 'Gel-Push' Sampling Procedure to Obtain High Quality Laboratory Test Data for Advanced Geotechnical Analyses." *New Zealand Society for Earthquake Engineering 2012 Annual Technical Conference Conference*, Paper Number: 123.

Tokimatsu, K. and Katsumata, K. (2012). "Liquefaction-Induced Damage to Buildings in Urayasu City During the 2011 Tohoku Pacific Earthquake." *Proceedings of the International Symposium on Engineering Lessons Learned from the 2011 Great East Japan Earthquake*, March 2012, Tokyo, Japan.

Tokimatsu, K., and Seed, H.B. (1987). "Evaluation of Settlement in Sands Due to Earthquake Shaking." *J. Geotech. Engrg.*, 113, 861 – 878.

Tokimatsu, K., Kojima, J., Kuwayama, A.A., and Midorikawa, S. (1994). "Liquefaction-Induced Damage to Buildings in 1990 Luzon Earthquake." *Journal of Geotechnical Engineering*, 120(2), 290 – 307.

Tonkin & Taylor Ltd. (2011). "Christchurch Central City Geological Interpretive Report." *Technical report prepared for the Christchurch City Council*, December 2011.

Tonkin & Taylor Ltd. (2013). "Christchurch Town Hall for Performing Arts Post Earthquake and Foundation Repair Assessment." *Technical report prepared for the Christchurch City Council*, June 2013.

Travasarou, T., Bray, J.D., and Sancio, R. (2006). “Soil-Structure Interaction Analyses of Building Responses During the 1999 Kocaeli Earthquake.” *Proceedings of the 8th U.S. National Conference on Earthquake Engineering*, April 18 – 22, 2006, San Franciscio, CA, Paper Number: 1877.

Trombetta, N.W. (2013). “Seismic Soil-Foundation-Structure Interaction in Urban Environments.” Ph.D. dissertation, University of California, San Diego, CA.

Trombetta, N. W., Zupan, J. D., Bolisetti, C., Puangnak, H., Jones, K. C., Tran, J. K., Bassal, B., Bray, J. D., Hutchinson, T. C., Fiegel, G. L., Kutter, B., and Whittaker, A. S. (2011). "Seismic peformance assessment in dense urban environments: Centrifuge Data Report for NWT01.” *Report Number: UCD/CGMDR-04/11*. Center for Geotechnical Modeling, Davis, CA.

Trombetta, N. W., Mason, H. B., Chen, Z., Hutchinson, T. C., Bray, J. D., and Kutter, B. L. (2013a). "Nonlinear dynamic foundation and frame structure response observed in geotechnical centrifuge experiments." *Soil Dynamics and Earthquake Engineering*, 50, 117-133.

Trombetta, N.W., Mason, H.B., Hutchinson, T.C., Zupan, J.D., Bray, J.D., and Kutter, B.L. (2013b). “Nonlinear soil-foundation-structure and structure-soil-structure interaction: centrifuge observations.” *ASCE Journal of Geotechnical and Geoenvironmental Engineering*, In-Press.

Trombetta, N.W., Mason, H.B., Hutchinson, T.C., Zupan, J.D., Bray, J.D., and Kutter, B.L. (2013c). “Nonlinear soil-foundation-structure and structure-soil-structure interaction: engineering demands.” *ASCE Journal of Structural Engineering*, In-Press.

Unutmaz, B., and Cetin, K.O. (2012). “Post-Cyclic Settlement and Tilting Potential of Mat Foundations.” *Soil Dynamics and Earthquake Engineering*, 43, 271 – 286.

Whitman, R.V., and Lambe, P.C. (1982). “Liquefaction: Consequences for a Structure.” *Soil Dynamics and Earthquake Engineering Conference*, Southamptom, England, 941 – 949.

Wotherspoon, L.M., Orense, R.P., Bradley, B.A., Cox, B.R., and Wood, C.M. (2013). "Soil Profile Characterisation of Christchurch Strong Motion Stations.” *New Zealand Society for Earthquake Engineering 2013 Annual Technical Conference Conference*.

Wu, J. (2002). "Liquefaction Triggering and Post Liquefaction Deformations of Monterey 0/30 Sand Under Uni-Directional Cyclic Simple Shear Loading." Ph.D. dissertation, University of California, Berkeley, CA.

Yoshimi, Y., and Tokimatsu, K. (1977). “Settlement of buildings on saturated sand during earthquakes.” *Soils and Foundations Journal*, 17(1), 23 – 38.

Youd, T.L., Idriss, I.M., Andrus, R.D., Arango, I., Castro, G., Christian, J.T., Dobry, R., Finn, W.D.L., Harder, L.F., Hynes, M.E., Ishihara, K., Koester, J.P., Liao, S.S.C., Marcuson, W.F., Martin, G.R., Mitchell, J.K., Moriwaki, Y., Power, M.S., Robertson, P.K., Seed, R.B., and Stokoe, K.H. (2001). “Liquefaction Resistance of Soils: Summary Report from the 1996 NCEER and 1998 NCEER/NSF Workshops on Evaluation of Liquefaction Resistance of Soils.” *Journal of Geotechnical and Geoenvironmental Engineering*, 127(10), 817 – 833.

Zhang, G., Robertson, P.K., and Brachman, R.W.I. (2002). “Estimating Liquefaction-Induced Ground Settlements from CPT for Level Ground.” *Canadian Geotechnical Journal*, 39, 1168 – 1180.

Zhang, G., Robertson, P.K., and Brachman, R.W.I. (2004). "Estimating Liquefaction-Induced Lateral Displacements Using the Standard Penetration Test or Cone Penetration Test." *Journal of Geotechnical and Geoenvironmental Engineering*, 130(8), 861 – 871.

Zupan, J.D., Trombetta, N.W., Puangnak, H., Paez, D., Bray, J.D., Kutter, B.L., Hutchinson, T.C., Fiegel, G.L., Bolisetti, C., and Whittaker, A.S. (2013). "Seismic Performance Assessment in Dense Urban Environments: Centrifuge Data Report for Test-5." *Technical Report.* Center for Geotechnical Modeling, Davis, CA.

APPENDIX A

PROCESSED CPT DATA


Z1-B1 (18.43m)
Z1-1 (17.92m)
Z1-B2 (17.72m)
Z1-8 (17.32m)
Z1-3 (17.69m)
BH K1
Z1-B4 (17.31m)
Z1-B3 (14.91m)
Z1-2 (17.38m)
Z1-14 (17.65m)
Z1-12 (16.82m)
Google earth
feet
meters
300
100
Google earth


Z1-12 (16.82m)
Z1-11 (17.65m)
Z1-2 (17.38m)
Z1-4 (21.54m)
Z1-6 (17.96m)
Z1-5 (14.09m)
Z1-10 (6.43m)
Z1-13 (21.82m)
Z1-9 (3.95m)
Z1-15 (20.81m)
Z1-14 (20.71m)
Z1-7 (3.93m)
Z2-7 (3.05m)
Google earth
feet
meters
500
100
Google earth


Z2-22 (13.53m)
Z2-13 (20.45m)
Z2-12 (20.24m)
Z2-26 (20.20m)
Z2-1 (9.86m)
Z2-25 (20.48m)
Z2-25F (20.05m)
Z2-24 (19.98m)
Z2-23 (13.39m)
Z2-17 (7.36 m)
Google earth
Google earth
feet
meters
100
50


Z2-1 (9.86m)
Z2-2 (2.53m)
Z2-3 (20.48m)
Z2-4 (3.46m)
Z2-5 (2.44m)
Z2-6 (5.43m)
Z2-7 (3.05m)
Z2-8 (3.42m)
Z2-9 (3.19m)
Z2-10 (2.41m)
Z2-11 (5.98m)
Z2-12 (20.24m)
Z2-13 (20.45m)
Z2-14 (19.78m)
Z2-15 (3.34m)
Z2-16 (19.05
Z2-17 (7.36 m)
Z2-18 (20.70m)
Z2-18F (20.00m)
Z2-19 (19.30 m)
Z2-20 (21.63m)
Z2-21
Z2-22 (13.58m)
Z2-23 (13.39m)
Z2-25 (20.20m)
Z2-26
Z2-27 (3.21m)
Z2-28 (21.18m)
Z2-29 (24.03m)
Google earth
feet
meters
600
200

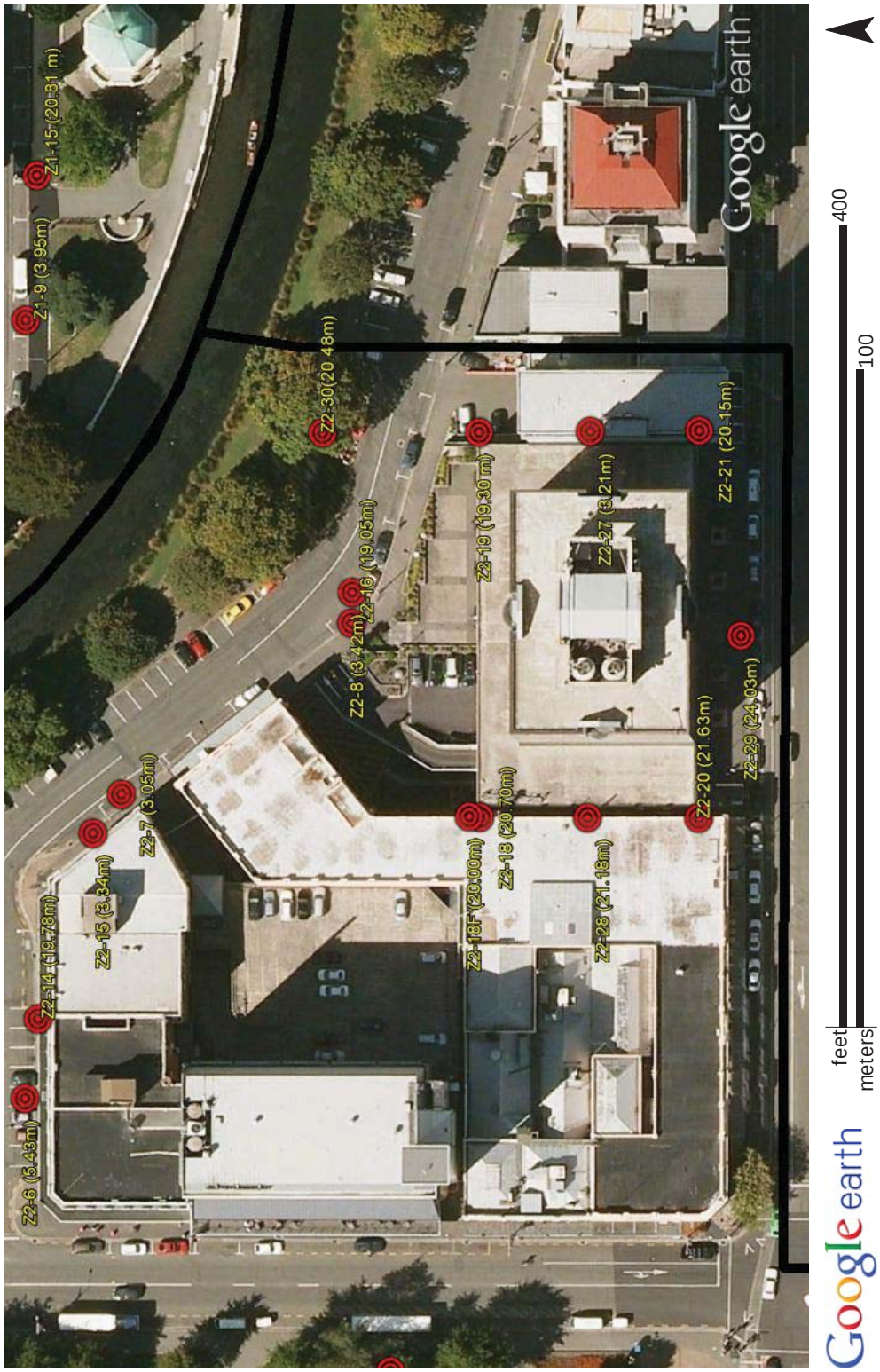
Z1-15 (20.81 m)
Z1-9 (3.95m)
Z2-30 (20.48m)
Z2-8 (3.42m)
Z2-16 (19.05m)
Z2-19 (19.30 m)
Z2-27 (3.21m)
Z2-21 (20.15m)
Z2-29 (24.03m)
Z2-20 (21.63m)
Z2-7 (3.05m)
Z2-15 (3.34m)
Z2-14 (19.78m)
Z2-18F (20.00m)
Z2-18 (20.70m)
Z2-28 (21.18m)
Z2-6 (5.43m)
Google earth
feet
meters
400
100
Google earth

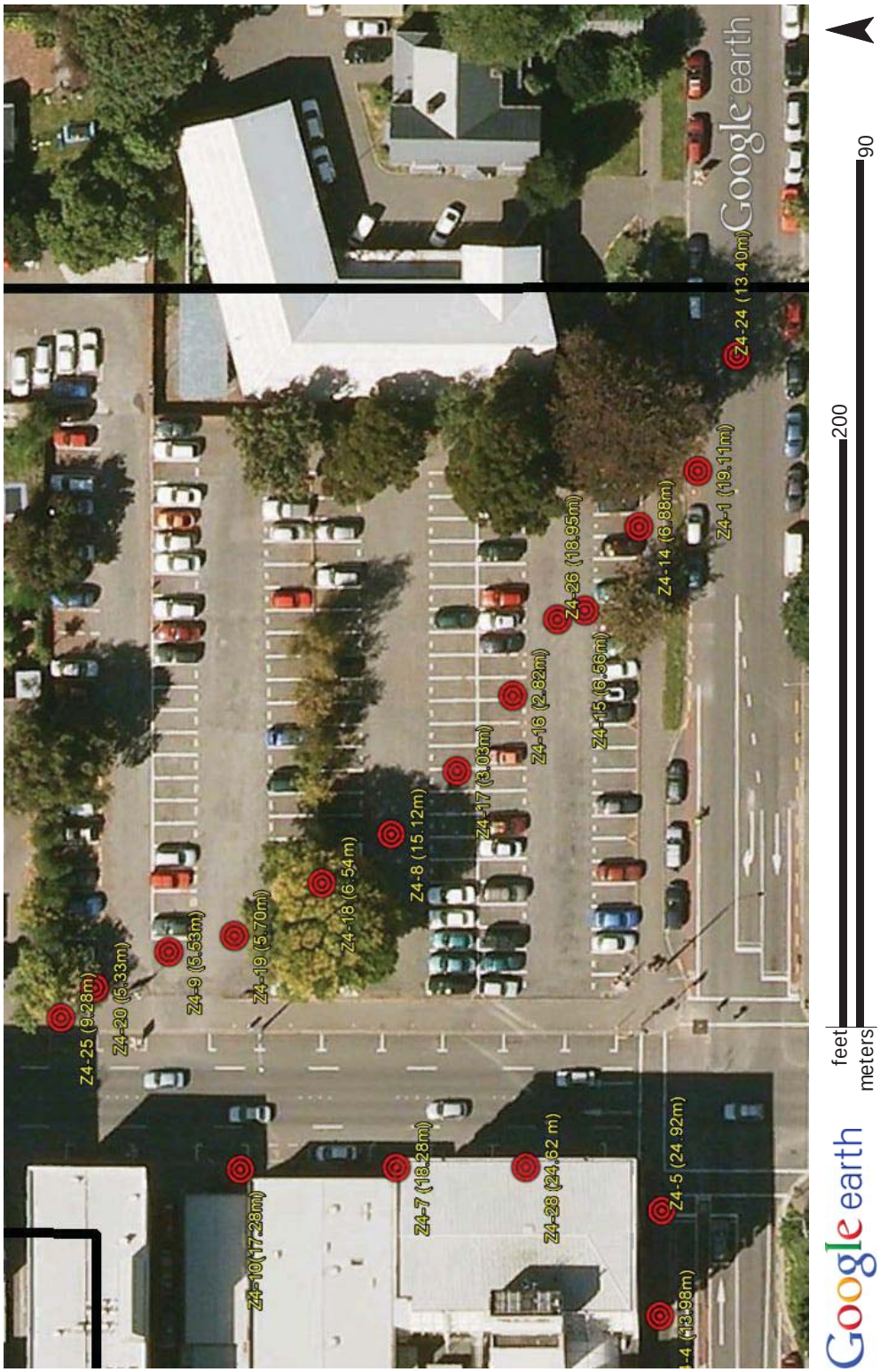
Z4-25 (9.28m)
Z4-20 (5.33m)
Z4-9 (5.53m)
Z4-19 (5.70m)
Z4-18 (6.54m)
Z4-8 (15.12m)
Z4-17 (3.03m)
Z4-16 (2.82m)
Z4-15 (6.56m)
Z4-26 (18.95m)
Z4-14 (6.88m)
Z4-1 (19.11m)
Z4-24 (13.40m)
Z4-10 (17.28m)
Z4-7 (18.28m)
Z4-28 (24.62 m)
Z4-5 (24.92m)
Google earth
feet
meters
200
90
Google earth


Z4-9 (5.53m)
Z4-19 (5.70m)
Z4-18 (6.54m)
Z4-8 (15.12m)
Z4-17 (3.05m)
Z4-16 (2.82m)
Z4-26 (18.95m)
Z4-15 (6.56m)
Z4-14 (6.88m)
Z4-1 (19.11m)
Z4-24 (13.40m)
Z4-10 (17.28m)
Z4-7 (18.28m)
Z4-28 (24.62 m)
Z4-5 (24.92m)
Z4-3 (13.49m)
Z4-27 (25.14m)
Z4-13 (17.71m)
Z4-6 (14.30m)
Z4-4 (13.98m)
Z4-12 (12.17m)
BH MA1
Z4-2 (14.14m)
Z4-11 (11.60m)
Google earth
feet
meters
400
100
Google earth


Z5-1 (15.49m)
Z5-2 (6.89m)
Z5-3 (6.91m)
Z5-5 (10.19m)
Z5-7 (21.16m)
Z5-8 (20.68m)
Z5-6 (20.80m)
Z5-11 (21.20m)
Z5-9 (20.50m)
Z5-10 (21.10m)
Z5-12 (20.19m)
Google earth
feet
meters
600
100
Google earth


Z8-1 (7.13m)
Z8-2 (13.98m)
Z8-3 (3.94m)
Z8-4 (20.64m)
Google earth
700
200
feet
meters
Google earth

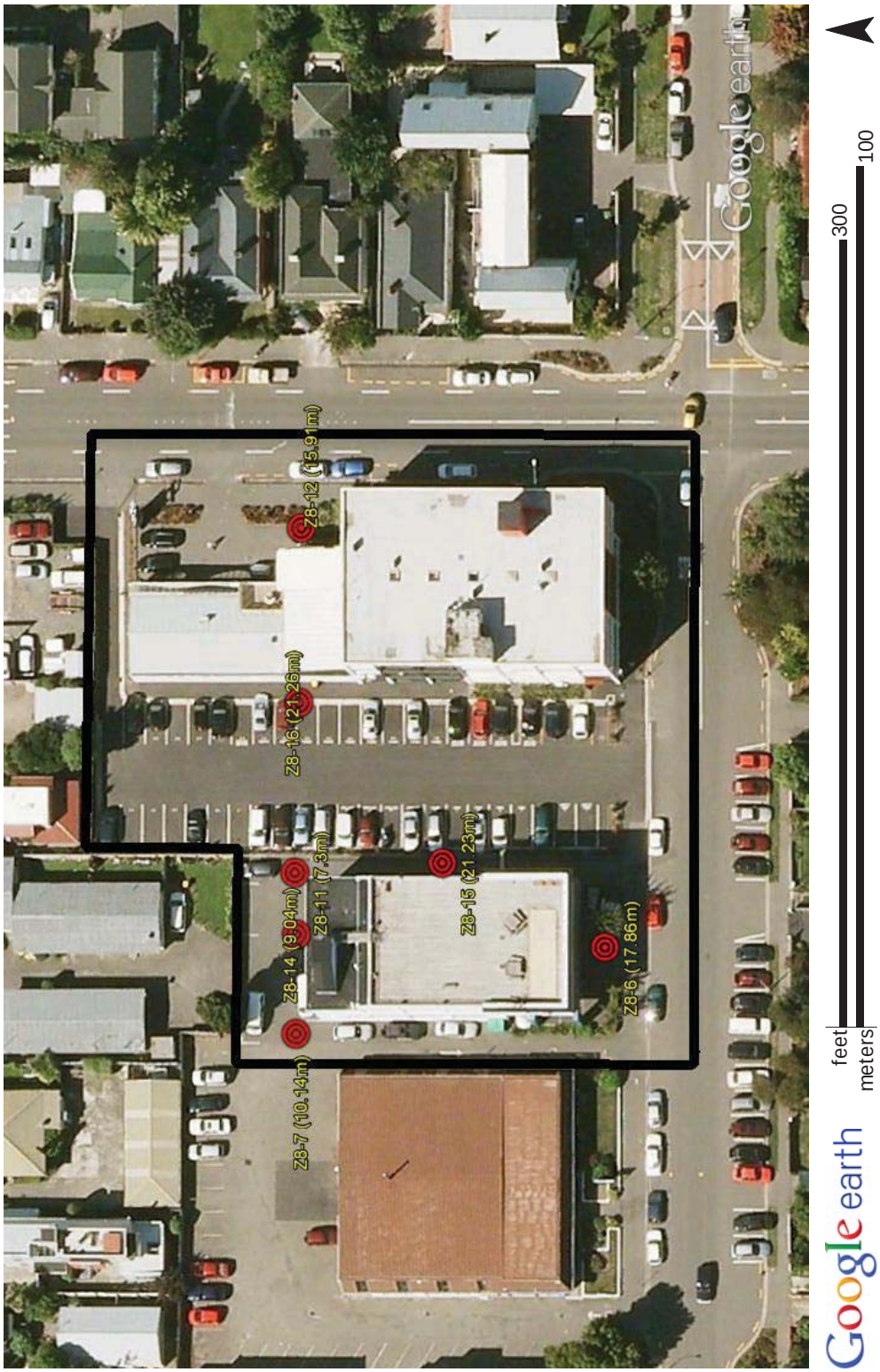
Z8-7 (10.14m)
Z8-14 (9.04m)
Z8-11 (7.3m)
Z8-16 (21.26m)
Z8-12 (15.91m)
Z8-15 (21.23m)
Z8-6 (17.86m)
Google earth
feet
meters
300
100
Google earth


Z8-18 (22.14 m)
Z8-17 (22.06 m)
Z8-10 (17.78m)
Z8-9 (17.68m)
Z8-8 (21.38m)
Z8-13 (16.67m)
Z8-7 (10.14 m)
Z8-14 (9.04
Z8-11 (7
Z8-15 (2
Z8-6 (17.86m
Google earth
feet
meters
800
200
Google earth

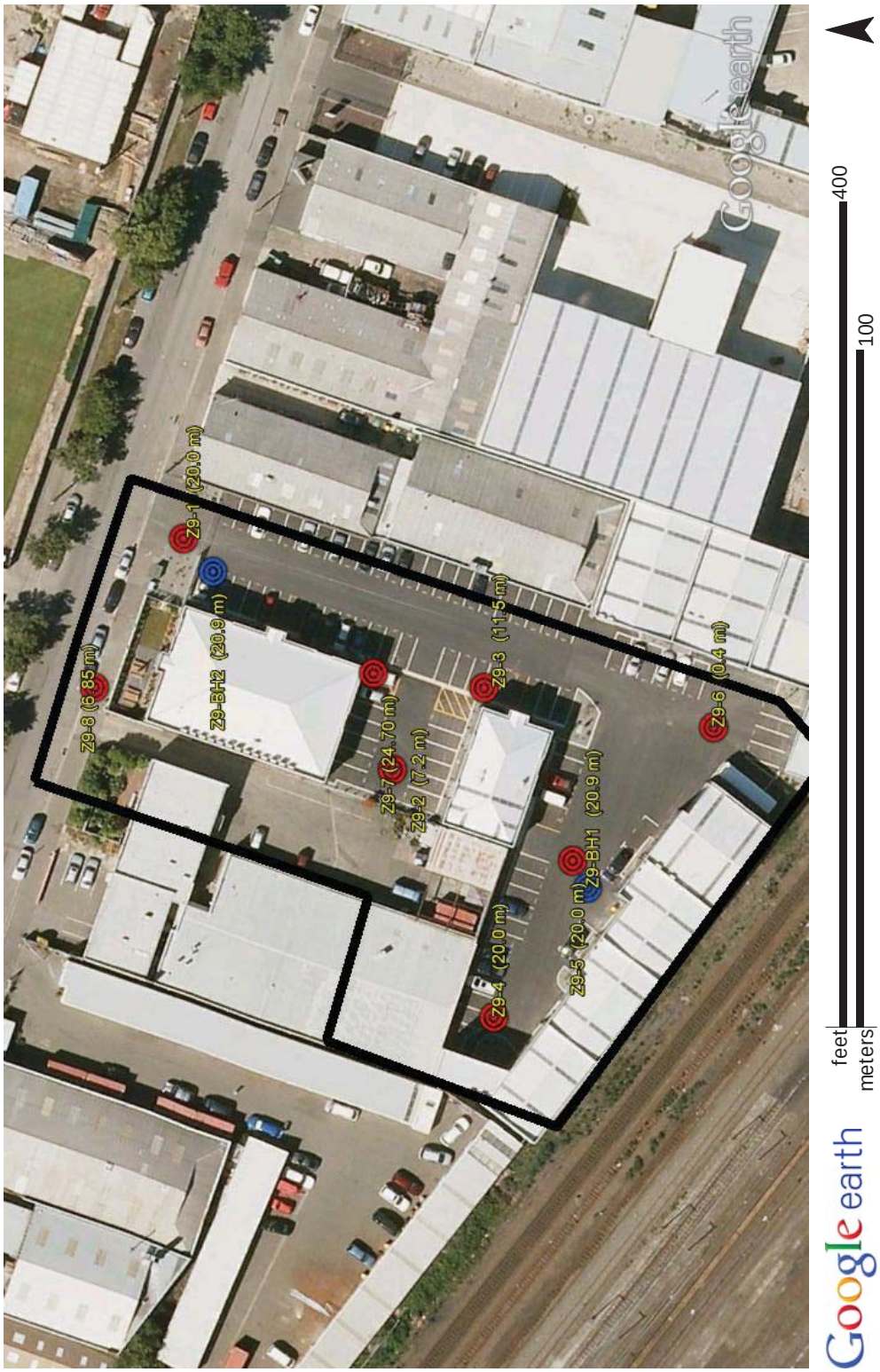
Z9-1 (20.0 m)
Z9-BH2 (20.9 m)
Z9-8 (6.85 m)
Z9-7 (24.70 m)
Z9-2 (7.2 m)
Z9-3 (11.5 m)
Z9-6 (0.4 m)
Z9-BH1 (20.9 m)
Z9-5 (20.0 m)
Z9-4 (20.0 m)
Google earth
feet
meters
400
100
Google earth

GeoLogismiki
Geotechnical Engineers
Merarhias 56
http://www.geologismiki.gr

CPT: Z1-B1
Total depth: 18.33 m
Surface Elevation: 0.00 m
Coords: X:0.00, Y:0.00
Cone Type: Uknown
Cone Operator: Uknown

Project:
Location:

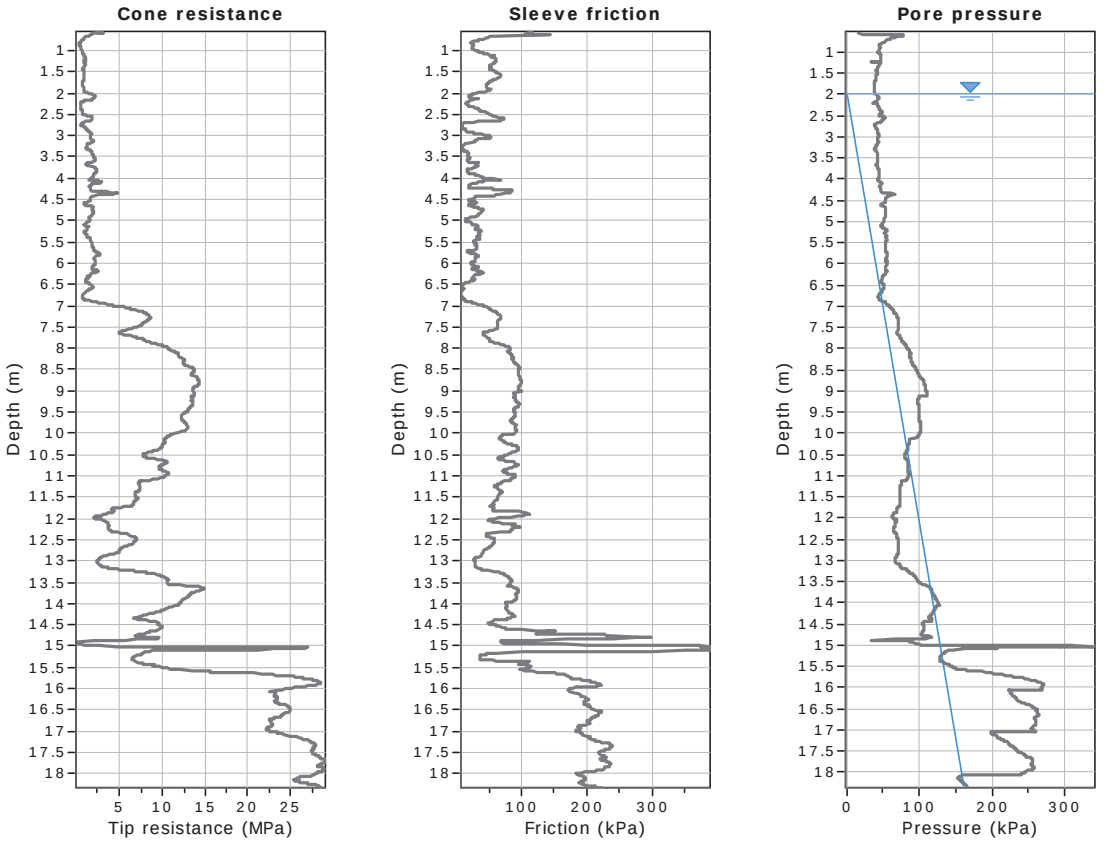

The plot below presents the cross correlation coeficient between the raw qc and fs values (as measured on the field). X axes presents the lag distance (one lag is the distance between two sucessive CPT measurements).

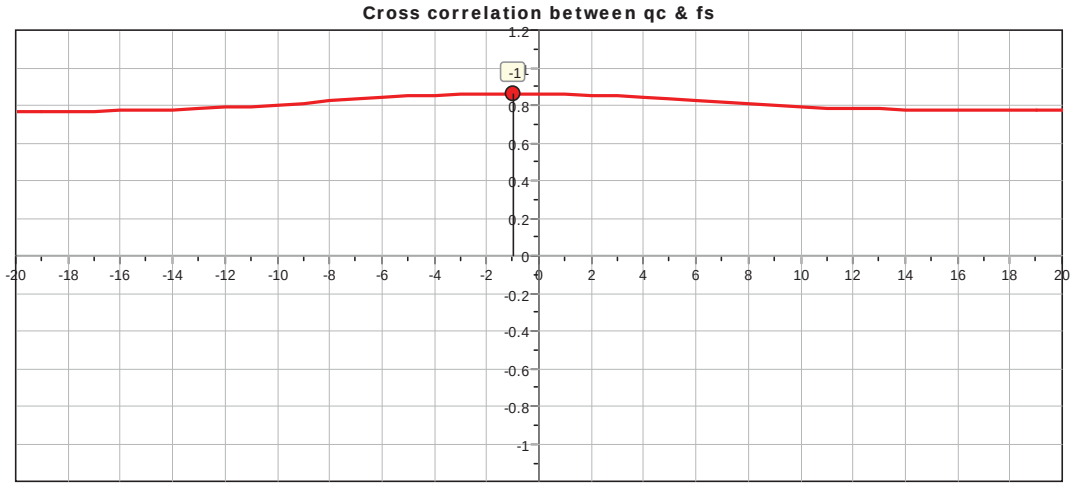

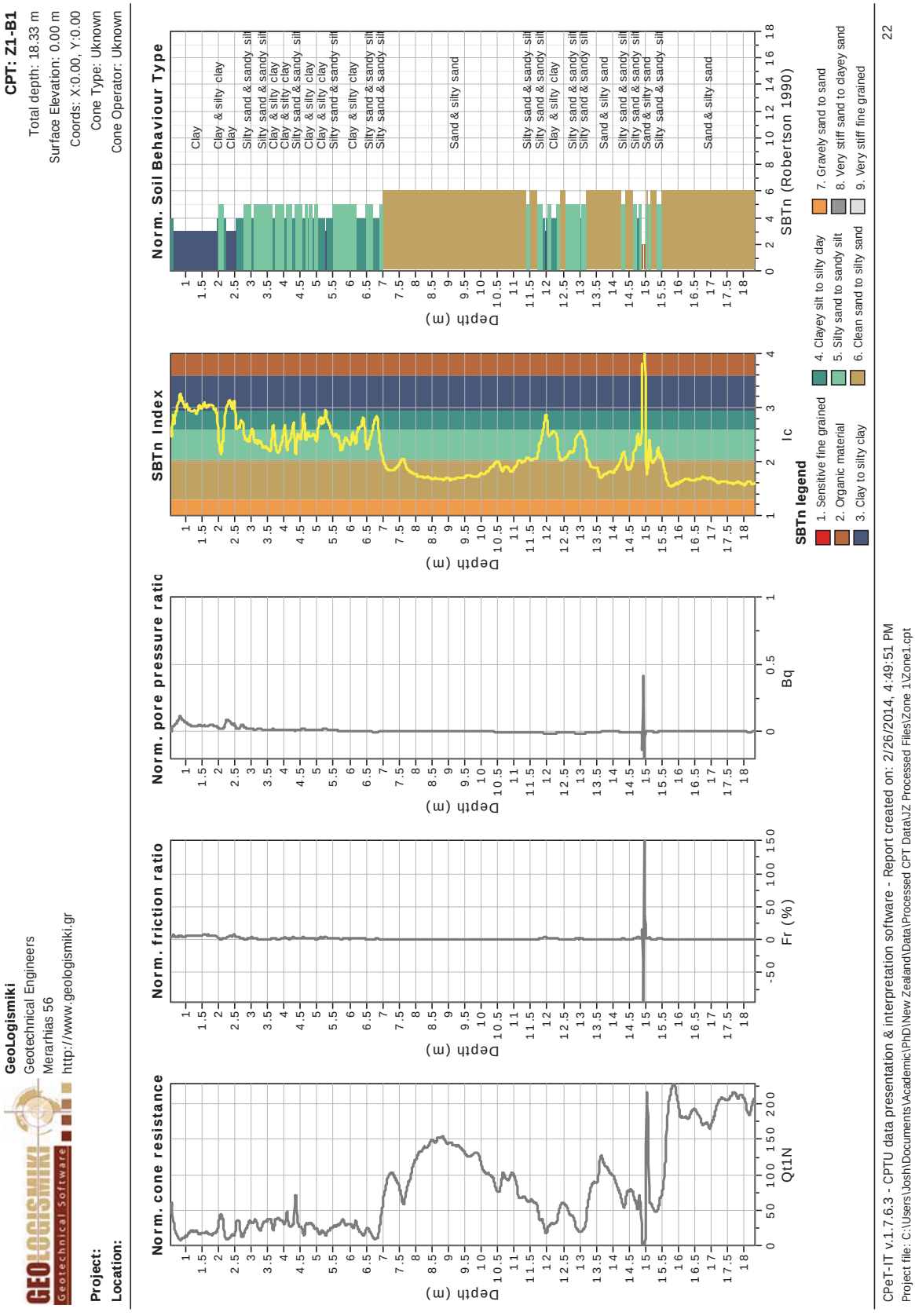
CPT: Z1-B1
Total depth: 18.33 m
Surface Elevation: 0.00 m
Coords: X:0.00, Y:0.00
Cone Type: Uknown
Cone Operator: Uknown
GeoLogismiki
Geotechnical Engineers
Merarhias 56
http://www.geologismiki.gr
Project:
Location:
Norm. cone resistance
Qt1N
Norm. friction ratio
Fr (%)
Norm. pore pressure ratio
Bq
SBTn Index
Ic
Norm. Soil Behaviour Type
SBTn (Robertson 1990)
Depth (m)
SBTn legend
1. Sensitive fine grained
2. Organic material
3. Clay to silty clay
4. Clayey silt to silty clay
5. Silty sand to sandy silt
6. Clean sand to silty sand
7. Gravely sand to sand
8. Very stiff sand to clayey sand
9. Very stiff fine grained
CPeT-IT v.1.7.6.3 - CPTU data presentation & interpretation software - Report created on: 2/26/2014, 4:49:51 PM
Project file: C:\Users\Josh\Documents\Academic\PhD\New Zealand\Data\Processed CPT Data\JZ Processed Files\Zone 1\Zone1.cpt
22

GeoLogismiki
Geotechnical Engineers
Merarhias 56
http://www.geologismiki.gr

CPT: Z1-B2
Total depth: 17.62 m
Surface Elevation: 0.00 m
Coords: X:0.00, Y:0.00
Cone Type: Uknown
Cone Operator: Uknown

Project:
Location:

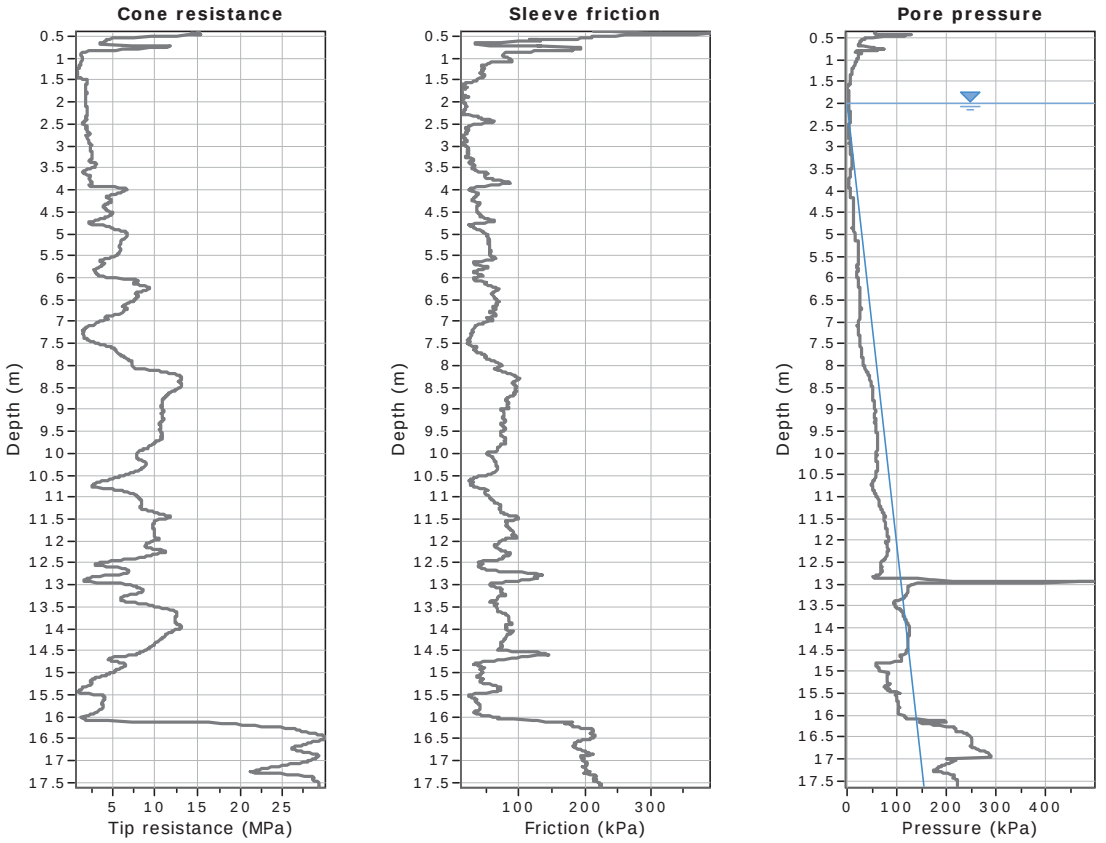

The plot below presents the cross correlation coeficient between the raw qc and fs values (as measured on the field). X axes presents the lag distance (one lag is the distance between two sucessive CPT measurements).

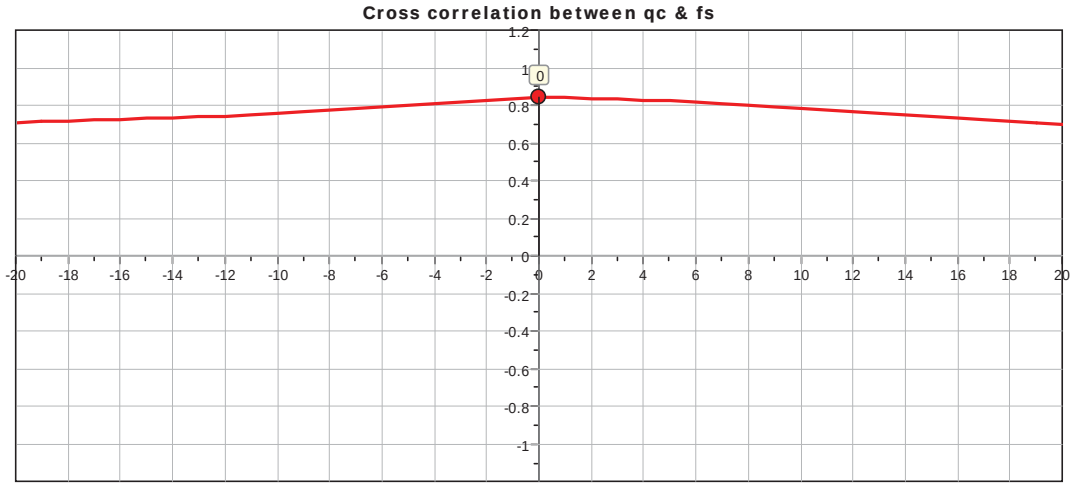

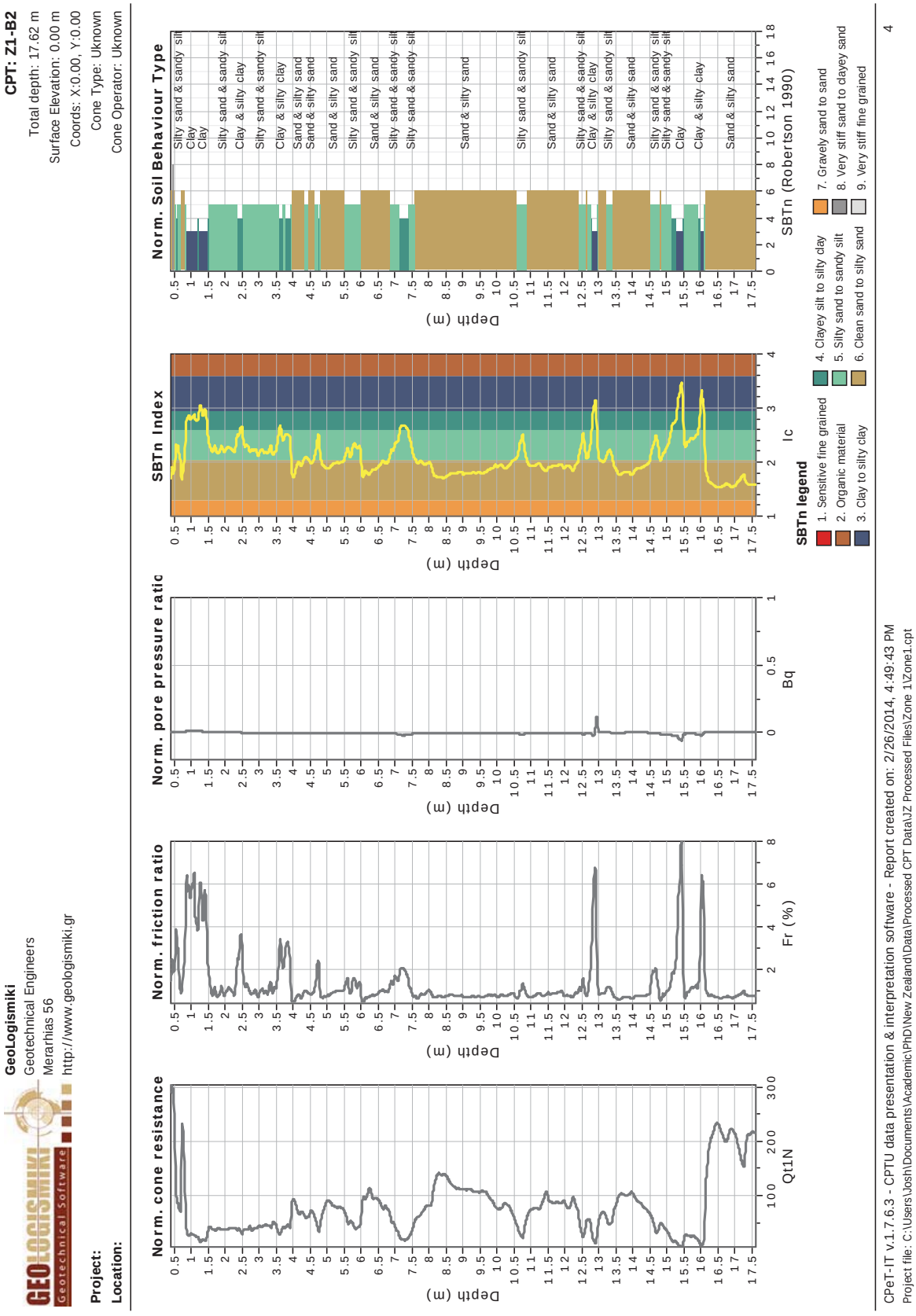
GeoLogismiki
Geotechnical Engineers
Merarchias 56
http://www.geologismiki.gr
Project:
Location:
CPT: Z1-B2
Total depth: 17.62 m
Surface Elevation: 0.00 m
Coords: X:0.00, Y:0.00
Cone Type: Uknown
Cone Operator: Uknown
Norm. cone resistance
Qt1N
Norm. friction ratio
Fr (%)
Norm. pore pressure ratio
Bq
SBTn Index
Ic
Norm. Soil Behaviour Type
SBTn (Robertson 1990)
Depth (m)
SBTn legend
1. Sensitive fine grained
2. Organic material
3. Clay to silty clay
4. Clayey silt to silty clay
5. Silty sand to sandy silt
6. Clean sand to silty sand
7. Gravely sand to sand
8. Very stiff sand to clayey sand
9. Very stiff fine grained
CPeT-IT v.1.7.6.3 - CPTU data presentation & interpretation software - Report created on: 2/26/2014, 4:49:43 PM
Project file: C:\Users\Josh\Documents\Academic\PhD\New Zealand\Data\Processed CPT Data\JZ Processed Files\Zone 1\Zone1.cpt
4

GeoLogismiki
Geotechnical Engineers
Merarhias 56
http://www.geologismiki.gr

CPT: Z1-B3
Total depth: 14.81 m
Surface Elevation: 0.00 m
Coords: X:0.00, Y:0.00
Cone Type: Uknown
Cone Operator: Uknown

Project:
Location:

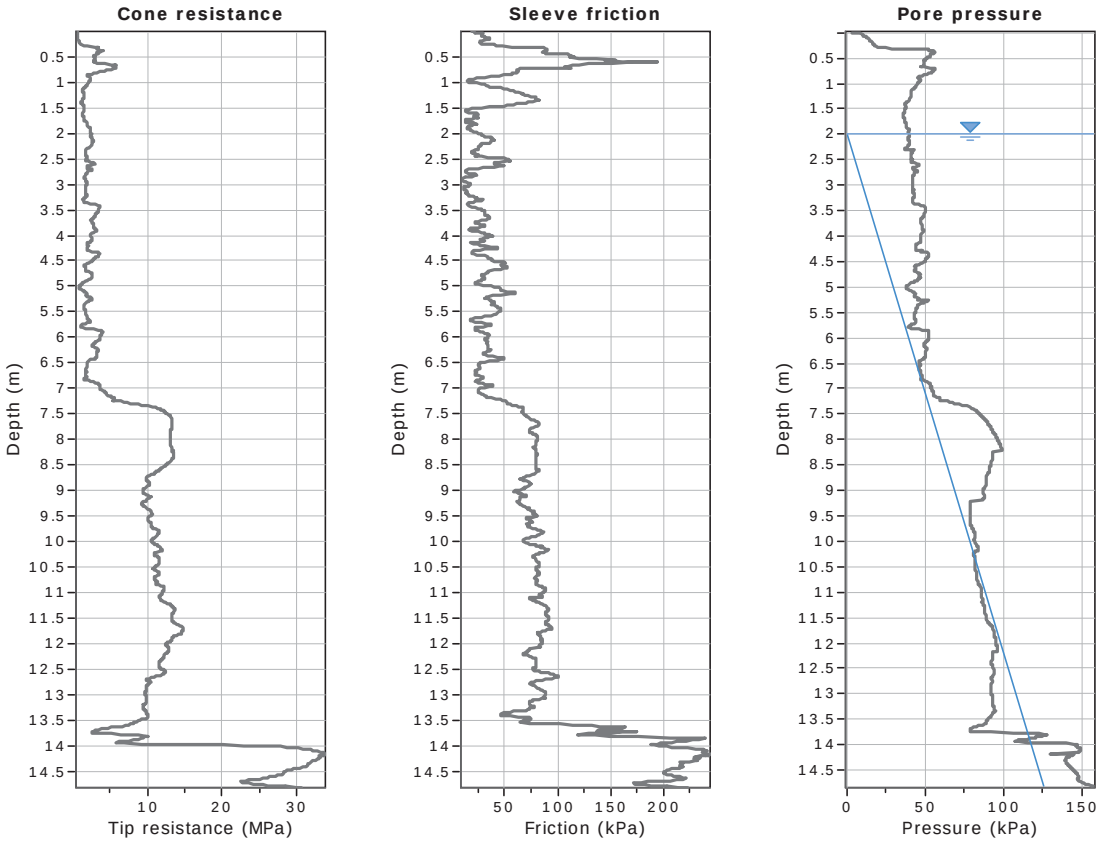

The plot below presents the cross correlation coeficient between the raw qc and fs values (as measured on the field). X axes presents the lag distance (one lag is the distance between two sucessive CPT measurements).

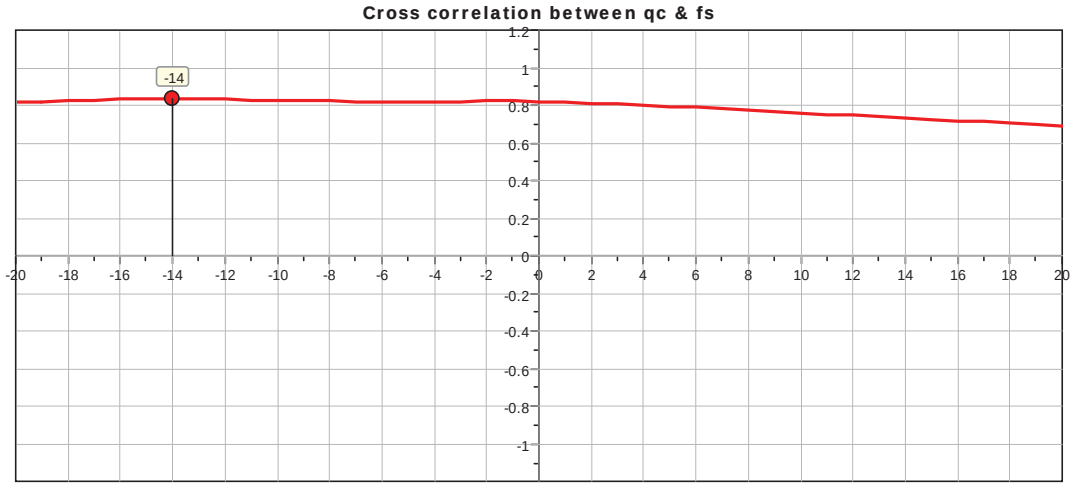

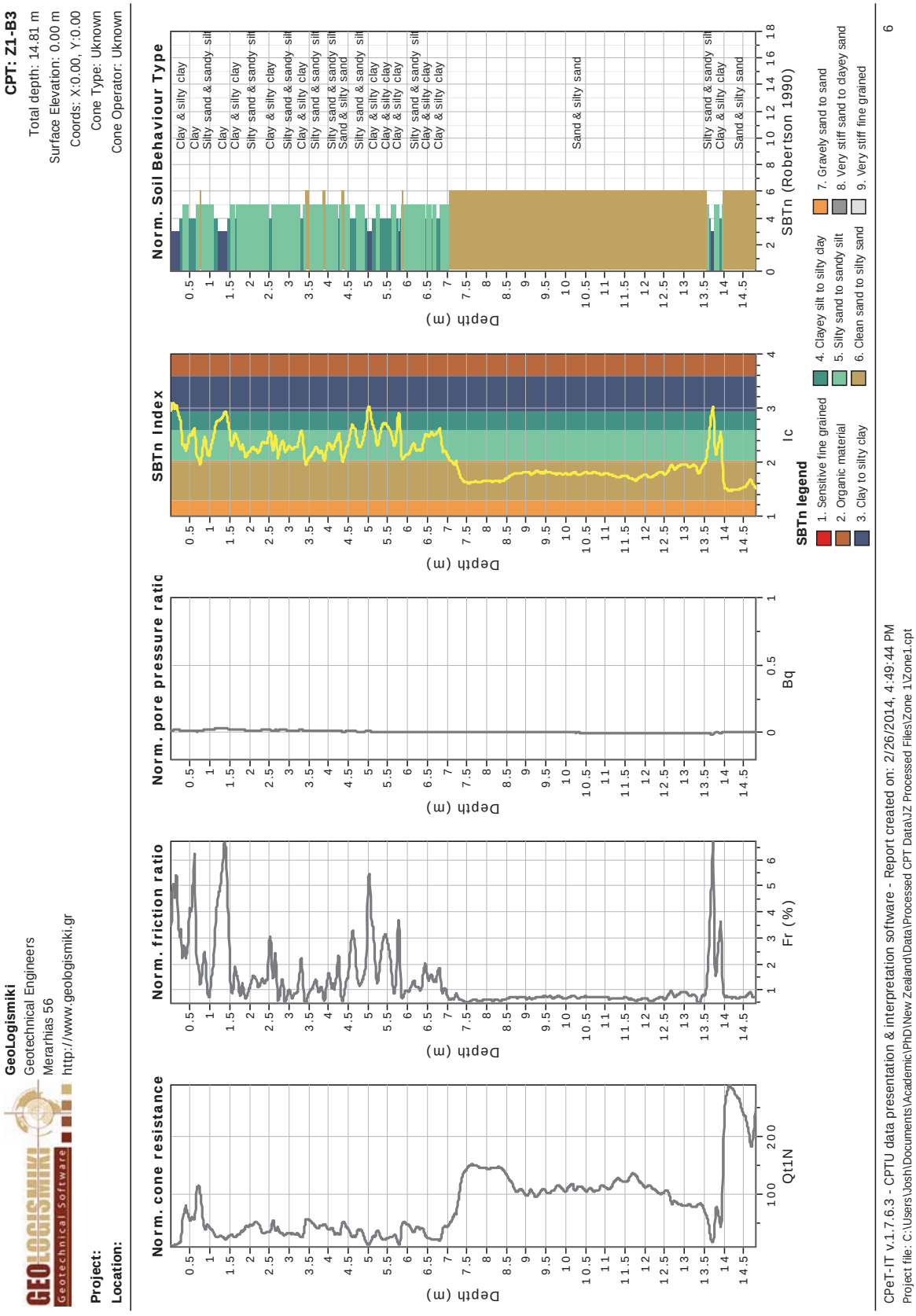
CPT: Z1-B3
Total depth: 14.81 m
Surface Elevation: 0.00 m
Coords: X:0.00, Y:0.00
Cone Type: Uknown
Cone Operator: Uknown
GeoLogismiki
Geotechnical Engineers
Merarhias 56
http://www.geologismiki.gr
Project:
Location:
Norm. cone resistance
Qt1N
Norm. friction ratio
Fr (%)
Norm. pore pressure ratio
Bq
SBTn Index
Ic
Norm. Soil Behaviour Type
SBTn (Robertson 1990)
Depth (m)
SBTn legend
1. Sensitive fine grained
2. Organic material
3. Clay to silty clay
4. Clayey silt to silty clay
5. Silty sand to sandy silt
6. Clean sand to silty sand
7. Gravely sand to sand
8. Very stiff sand to clayey sand
9. Very stiff fine grained
CPeT-IT v.1.7.6.3 - CPTU data presentation & interpretation software - Report created on: 2/26/2014, 4:49:44 PM
Project file: C:\Users\Josh\Documents\Academic\PhD\New Zealand\Data\Processed CPT Data\JZ Processed Files\Zone 1\Zone1.cpt
6

GeoLogismiki
Geotechnical Engineers
Merarhias 56
http://www.geologismiki.gr

CPT: Z1-B4
Total depth: 17.21 m
Surface Elevation: 0.00 m
Coords: X:0.00, Y:0.00
Cone Type: Uknown
Cone Operator: Uknown

Project:
Location:

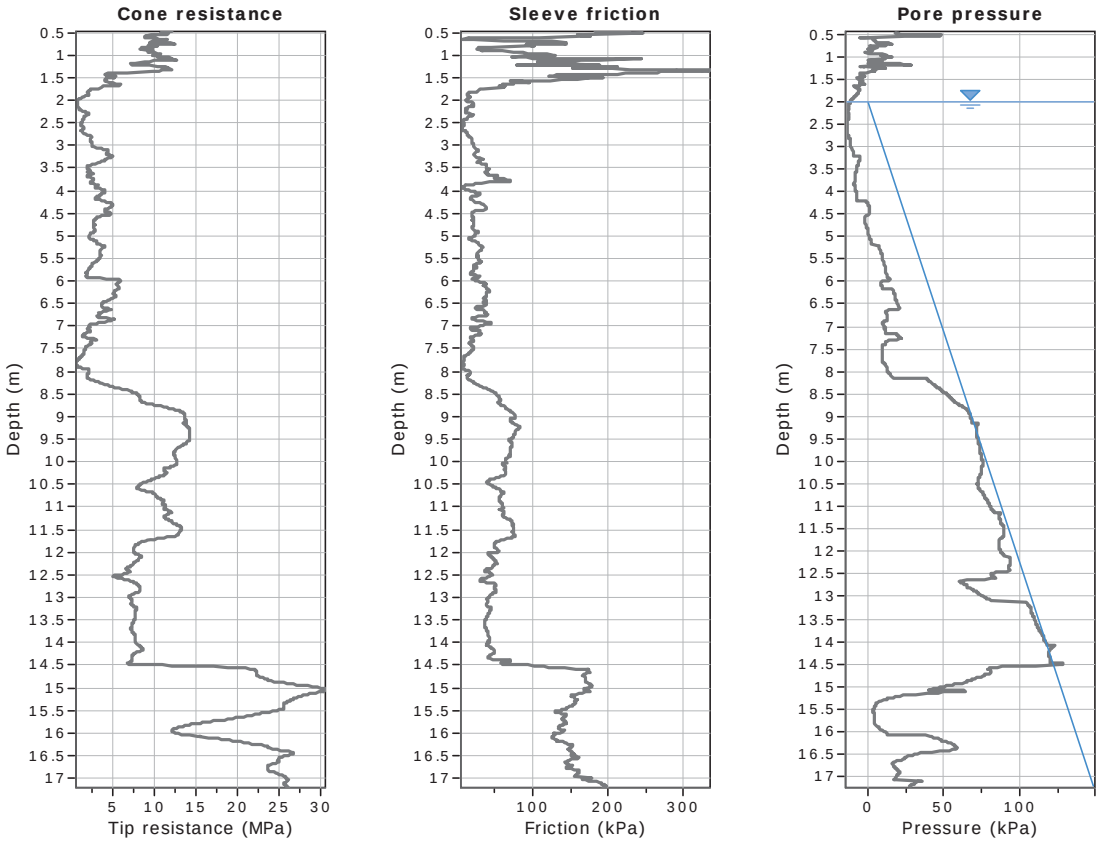

The plot below presents the cross correlation coeficient between the raw qc and fs values (as measured on the field). X axes presents the lag distance (one lag is the distance between two sucessive CPT measurements).

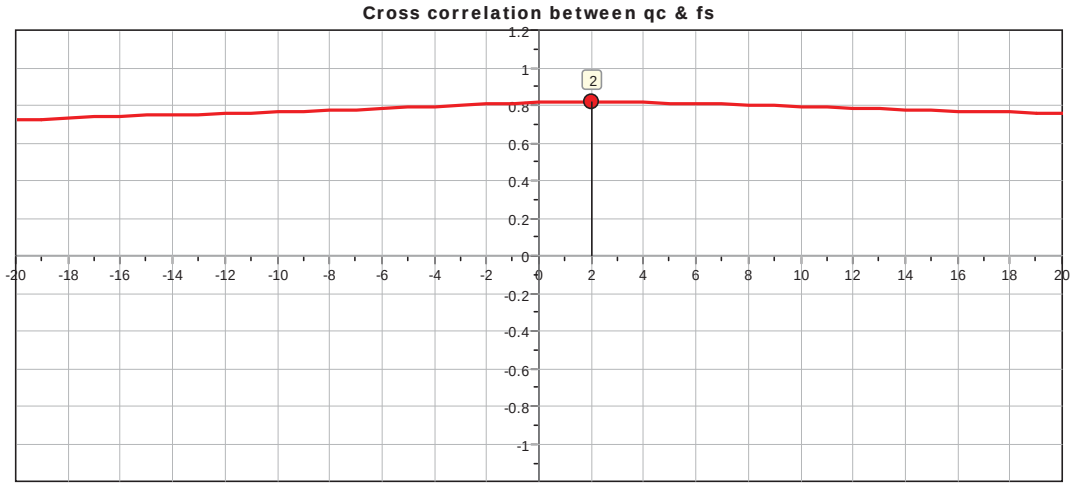

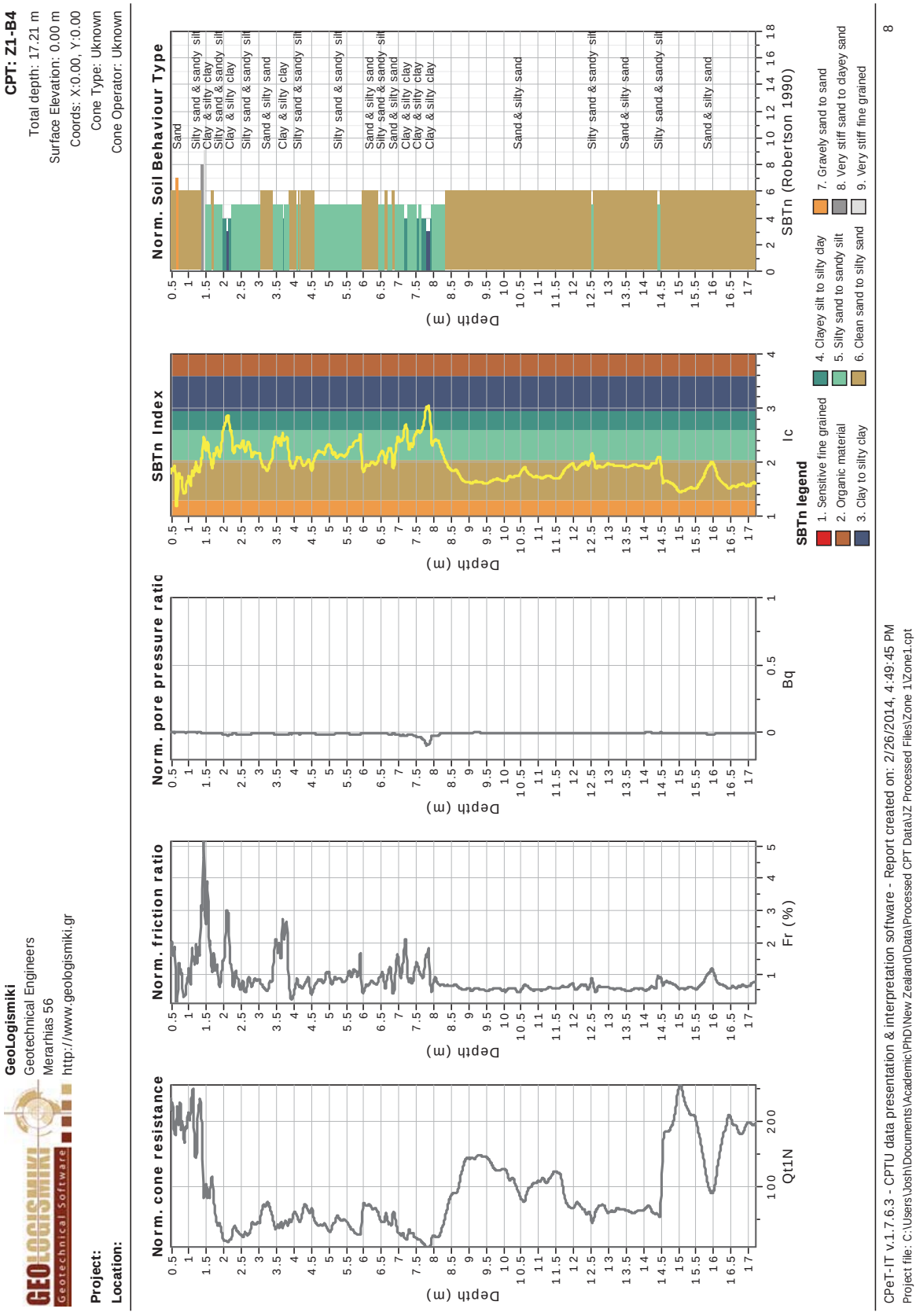
CPT: Z1-B4
Total depth: 17.21 m
Surface Elevation: 0.00 m
Coords: X:0.00, Y:0.00
Cone Type: Uknown
Cone Operator: Uknown
GeoLogismiki
Geotechnical Engineers
Merarhias 56
http://www.geologismiki.gr
Project:
Location:
Norm. cone resistance
Norm. friction ratio
Norm. pore pressure ratio
SBTn Index
Norm. Soil Behaviour Type
SBTn (Robertson 1990)
SBTn legend
1. Sensitive fine grained
2. Organic material
3. Clay to silty clay
4. Clayey silt to silty clay
5. Silty sand to sandy silt
6. Clean sand to silty sand
7. Gravely sand to sand
8. Very stiff sand to clayey sand
9. Very stiff fine grained
CPeT-IT v.1.7.6.3 - CPTU data presentation & interpretation software - Report created on: 2/26/2014, 4:49:45 PM
Project file: C:\Users\Josh\Documents\Academic\PhD\New Zealand\Data\Processed CPT Data\JZ Processed Files\Zone 1\Zone1.cpt
8

GeoLogismiki
Geotechnical Engineers
Merarhias 56
http://www.geologismiki.gr

CPT: Z1-1
Total depth: 17.82 m
Surface Elevation: 0.00 m
Coords: X:0.00, Y:0.00
Cone Type: Uknown
Cone Operator: Uknown

Project:
Location:

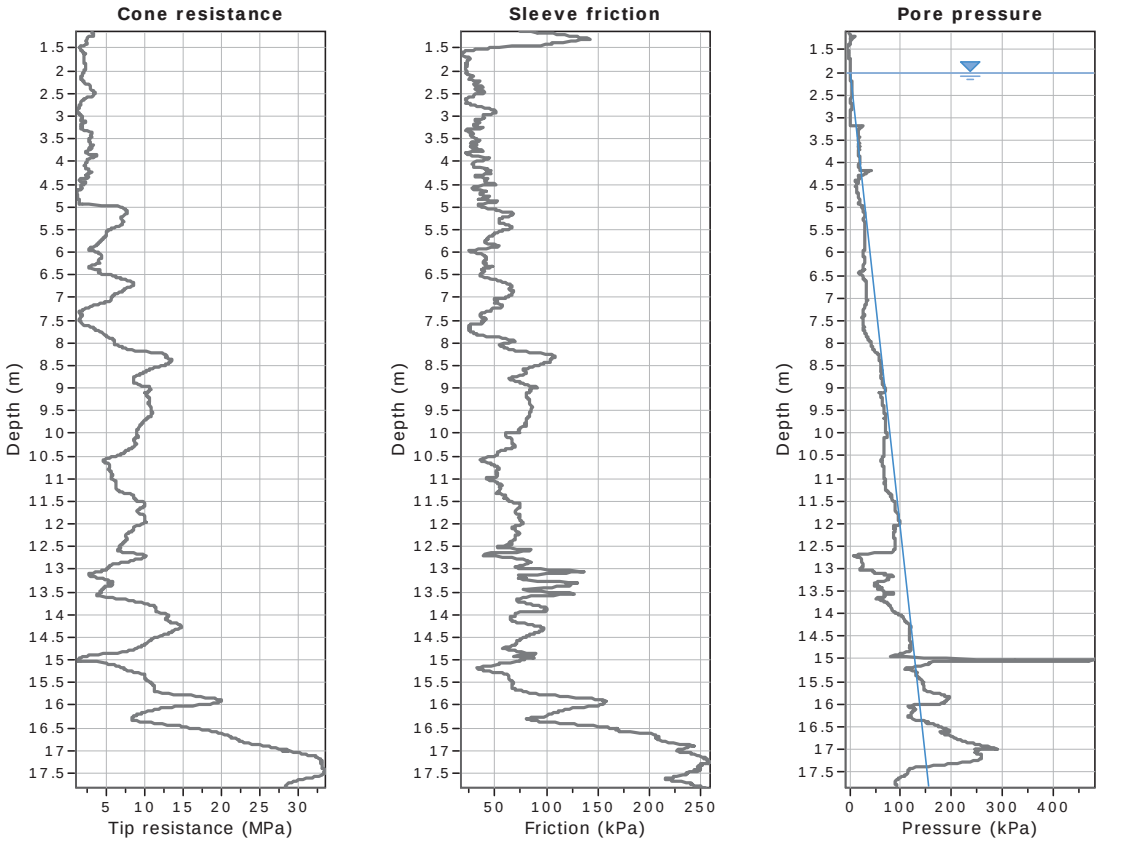

The plot below presents the cross correlation coeficient between the raw qc and fs values (as measured on the field). X axes presents the lag distance (one lag is the distance between two sucessive CPT measurements).

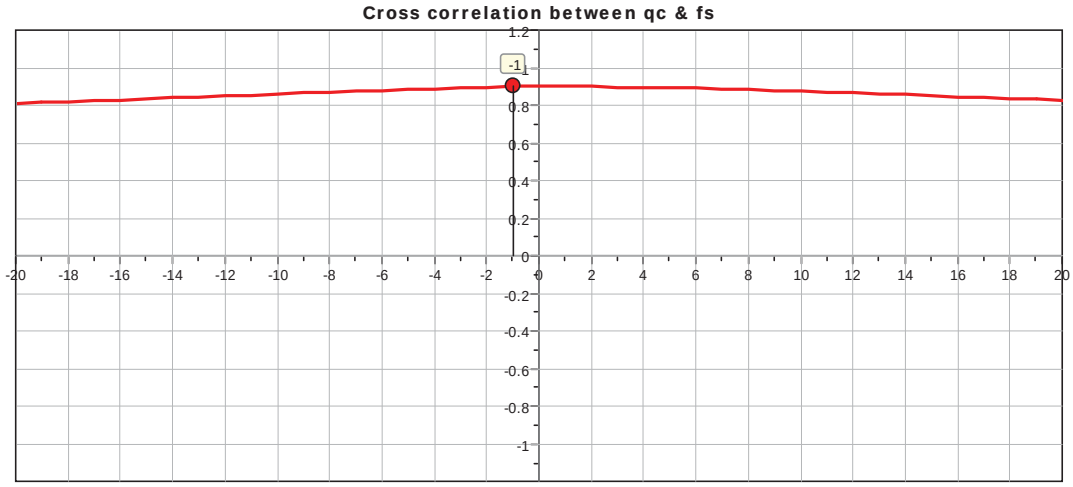

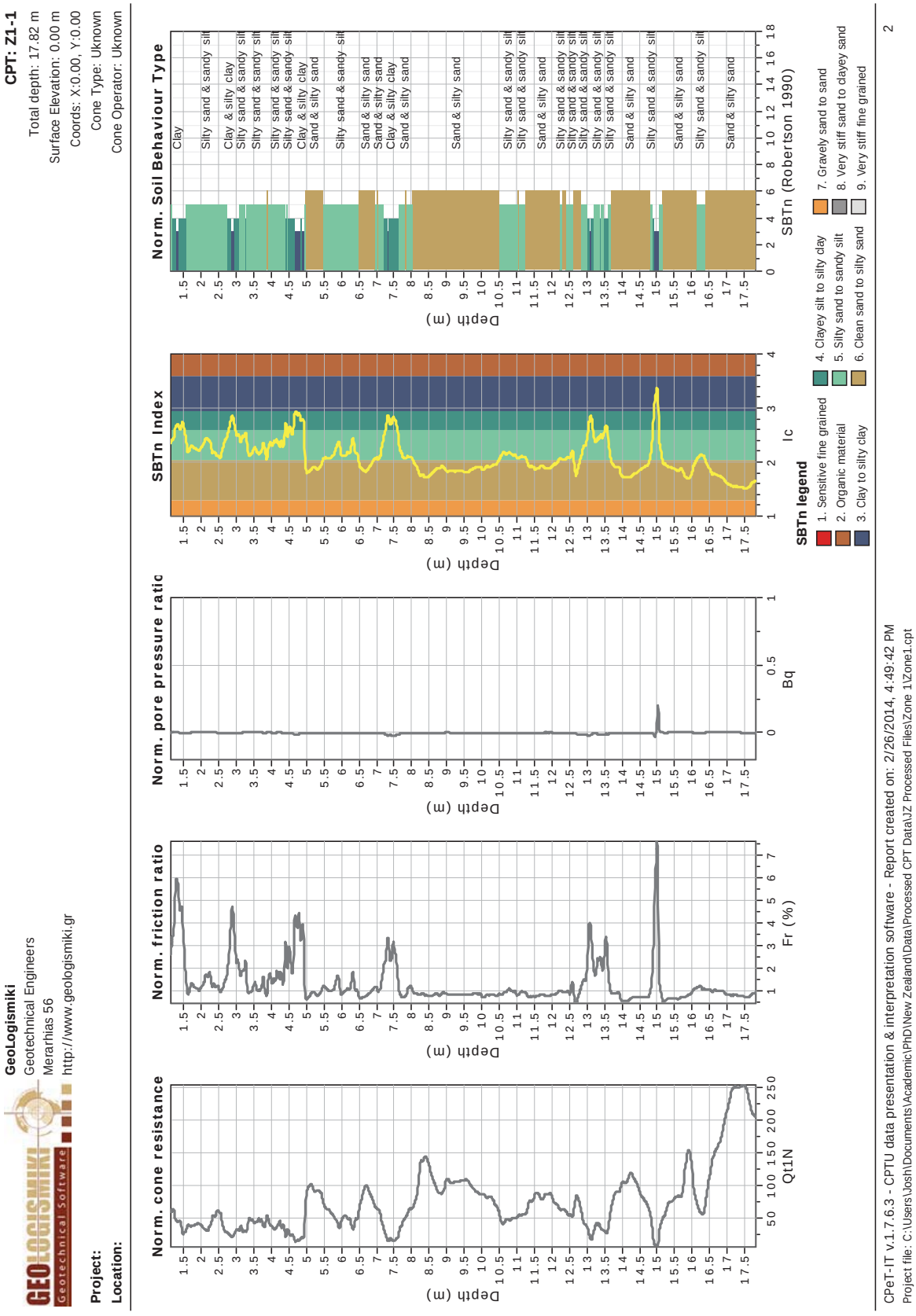
GeoLogismiki
Geotechnical Engineers
Merarhias 56
http://www.geologismiki.gr
Project:
Location:
CPT: Z1-1
Total depth: 17.82 m
Surface Elevation: 0.00 m
Coords: X:0.00, Y:0.00
Cone Type: Uknown
Cone Operator: Uknown
Norm. cone resistance
Qt1N
Norm. friction ratio
Fr (%)
Norm. pore pressure ratio
Bq
SBTn Index
Ic
Norm. Soil Behaviour Type
SBTn (Robertson 1990)
Depth (m)
SBTn legend
1. Sensitive fine grained
2. Organic material
3. Clay to silty clay
4. Clayey silt to silty clay
5. Silty sand to sandy silt
6. Clean sand to silty sand
7. Gravely sand to sand
8. Very stiff sand to clayey sand
9. Very stiff fine grained
CPeT-IT v.1.7.6.3 - CPTU data presentation & interpretation software - Report created on: 2/26/2014, 4:49:42 PM
Project file: C:\Users\Josh\Documents\Academic\PhD\New Zealand\Data\Processed CPT Data\JZ Processed Files\Zone 1\Zone1.cpt
2

GeoLogismiki
Geotechnical Engineers
Merarhias 56
http://www.geologismiki.gr

CPT: Z1-2
Total depth: 17.28 m
Surface Elevation: 0.00 m
Coords: X:0.00, Y:0.00
Cone Type: Uknown
Cone Operator: Uknown

Project:
Location:

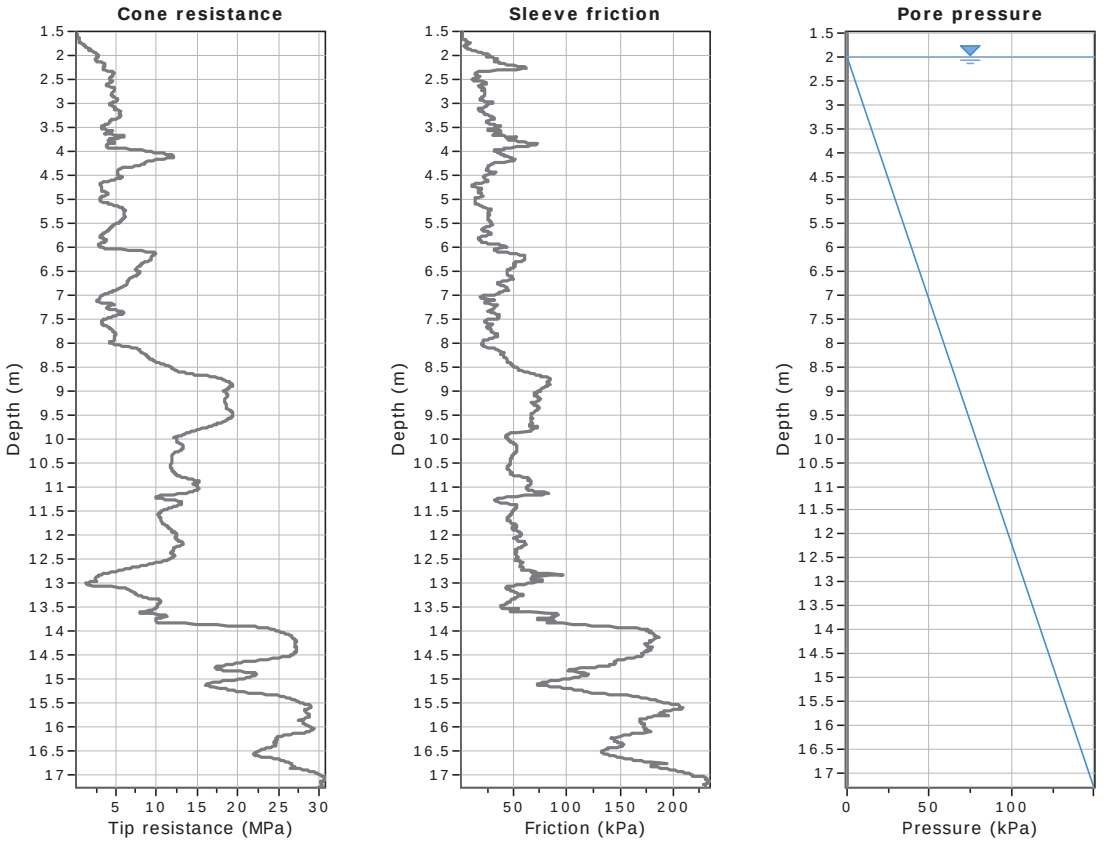

The plot below presents the cross correlation coeficient between the raw qc and fs values (as measured on the field). X axes presents the lag distance (one lag is the distance between two sucessive CPT measurements).

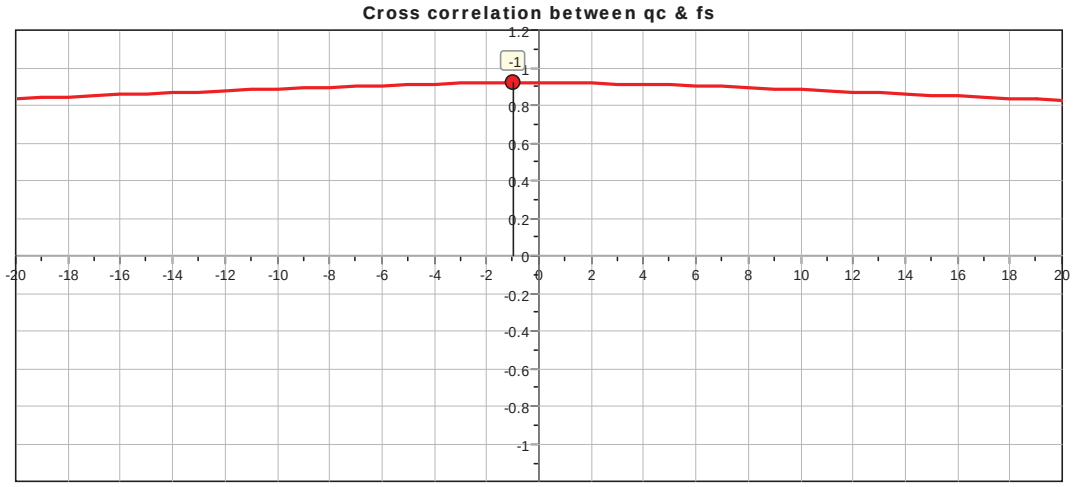

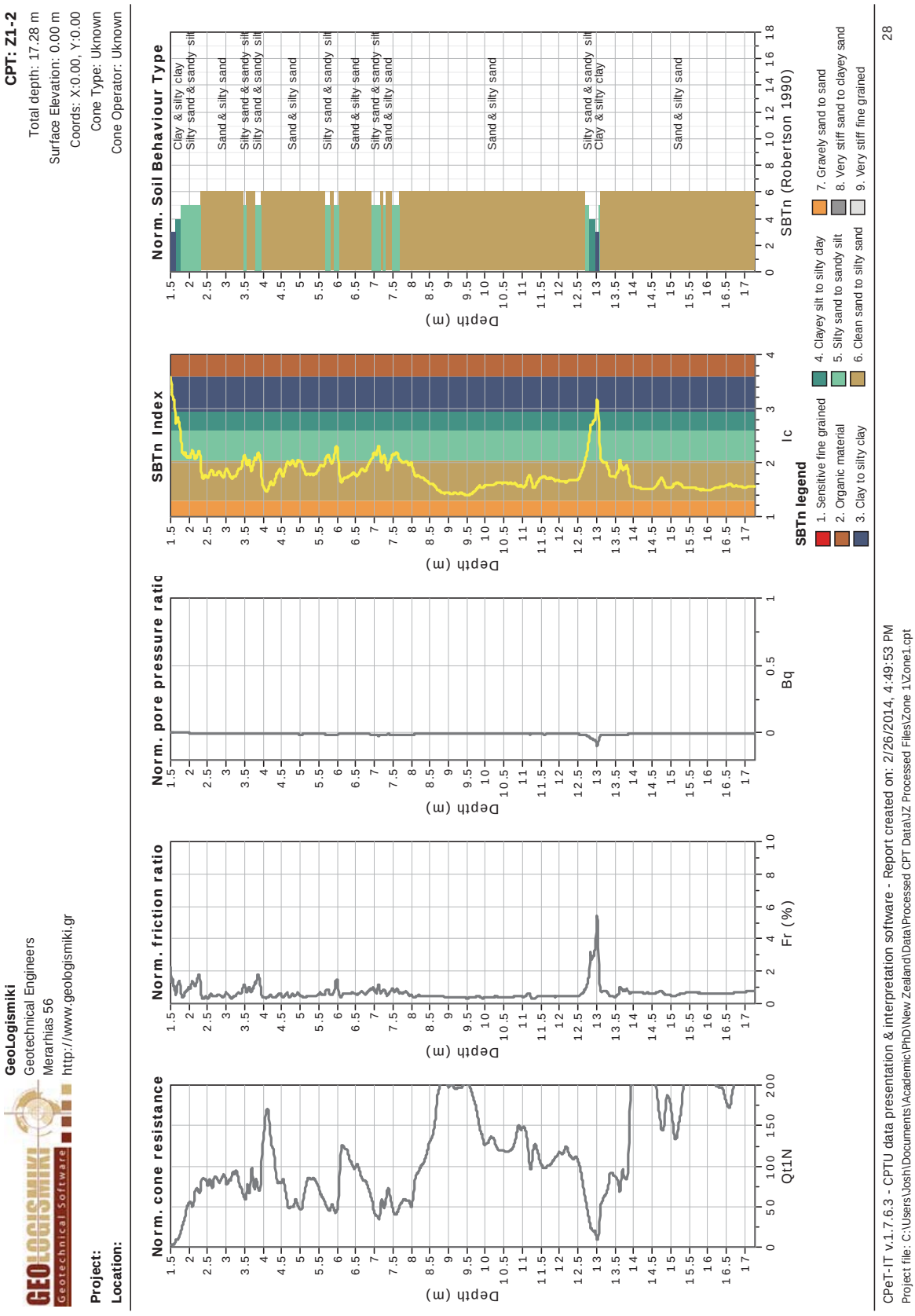
GeoLogismiki
Geotechnical Engineers
Merarhias 56
http://www.geologismiki.gr
Project:
Location:
CPT: Z1-2
Total depth: 17.28 m
Surface Elevation: 0.00 m
Coords: X:0.00, Y:0.00
Cone Type: Uknown
Cone Operator: Uknown
Norm. cone resistance
Qt1N
Norm. friction ratio
Fr (%)
Norm. pore pressure ratio
Bq
SBTn Index
Ic
Norm. Soil Behaviour Type
SBTn (Robertson 1990)
Depth (m)
SBTn legend
1. Sensitive fine grained
2. Organic material
3. Clay to silty clay
4. Clayey silt to silty clay
5. Silty sand to sandy silt
6. Clean sand to silty sand
7. Gravely sand to sand
8. Very stiff sand to clayey sand
9. Very stiff fine grained
CPeT-IT v.1.7.6.3 - CPTU data presentation & interpretation software - Report created on: 2/26/2014, 4:49:53 PM
Project file: C:\Users\Josh\Documents\Academic\PhD\New Zealand\Data\Processed CPT Data\JZ Processed Files\Zone 1\Zone1.cpt
28

GeoLogismiki
Geotechnical Engineers
Merarhias 56
http://www.geologismiki.gr

CPT: Z1-3
Total depth: 13.59 m
Surface Elevation: 0.00 m
Coords: X:0.00, Y:0.00
Cone Type: Uknown
Cone Operator: Uknown

Project:
Location:

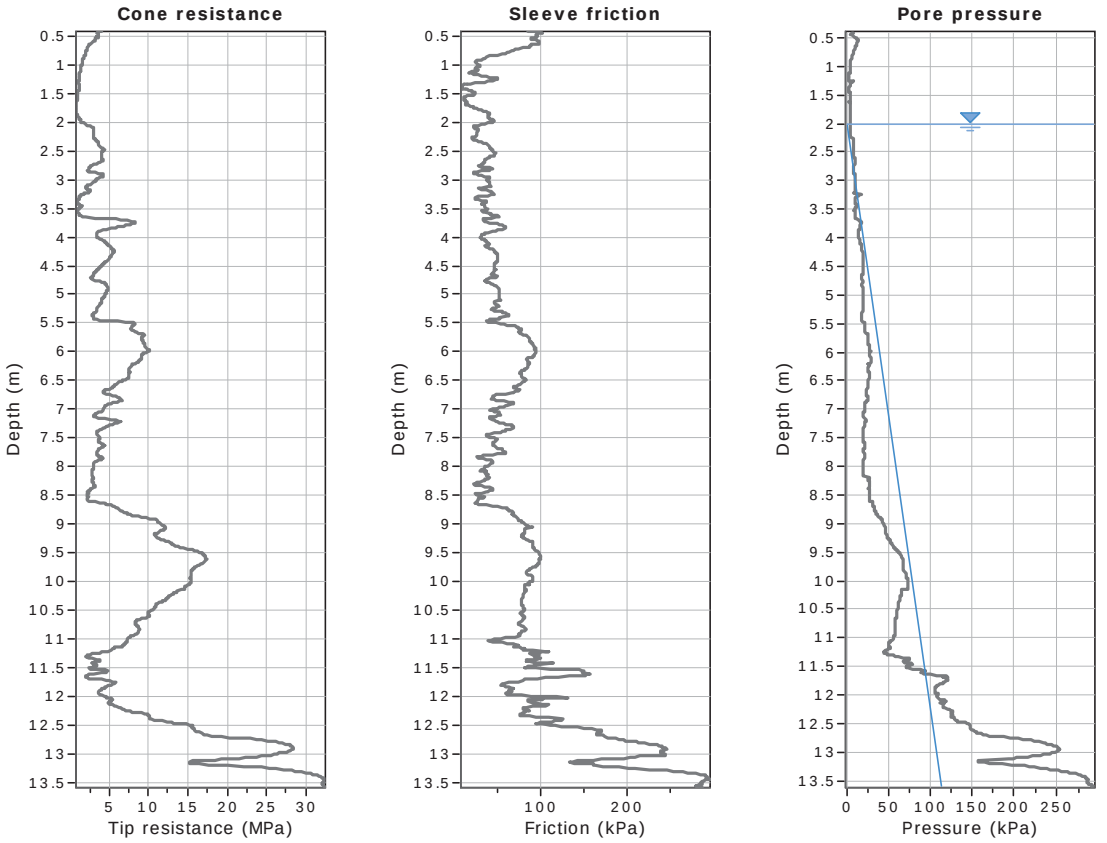

The plot below presents the cross correlation coeficient between the raw qc and fs values (as measured on the field). X axes presents the lag distance (one lag is the distance between two sucessive CPT measurements).

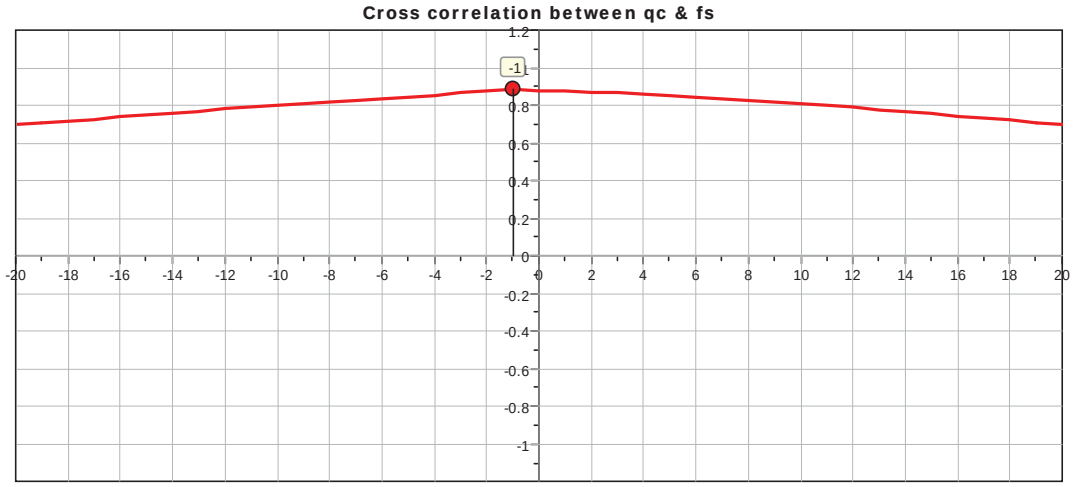

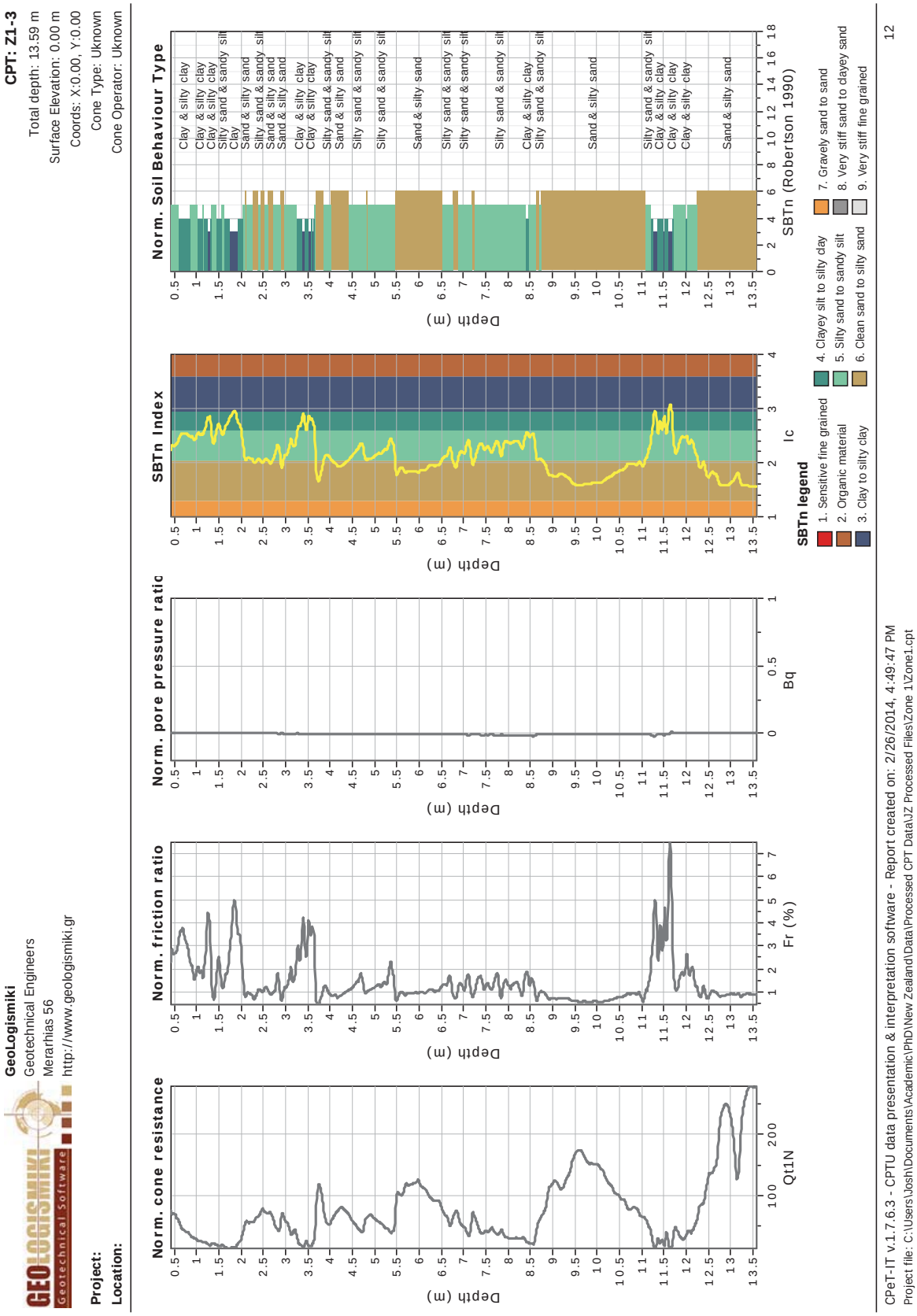
GeoLogismiki
Geotechnical Engineers
Merarhias 56
http://www.geologismiki.gr
Project:
Location:
CPT: Z1-3
Total depth: 13.59 m
Surface Elevation: 0.00 m
Coords: X:0.00, Y:0.00
Cone Type: Uknown
Cone Operator: Uknown
Norm. cone resistance
Qt1N
Norm. friction ratio
Fr (%)
Norm. pore pressure ratio
Bq
SBTn Index
Ic
Norm. Soil Behaviour Type
SBTn (Robertson 1990)
Depth (m)
SBTn legend
1. Sensitive fine grained
2. Organic material
3. Clay to silty clay
4. Clayey silt to silty clay
5. Silty sand to sandy silt
6. Clean sand to silty sand
7. Gravely sand to sand
8. Very stiff sand to clayey sand
9. Very stiff fine grained
CPeT-IT v.1.7.6.3 - CPTU data presentation & interpretation software - Report created on: 2/26/2014, 4:49:47 PM
Project file: C:\Users\Josh\Documents\Academic\PhD\New Zealand\Data\Processed CPT Data\JZ Processed Files\Zone 1\Zone1.cpt
12

GeoLogismiki
Geotechnical Engineers
Merarhias 56
http://www.geologismiki.gr

CPT: Z1-4
Total depth: 21.44 m
Surface Elevation: 0.00 m
Coords: X:0.00, Y:0.00
Cone Type: Uknown
Cone Operator: Uknown

Project:
Location:

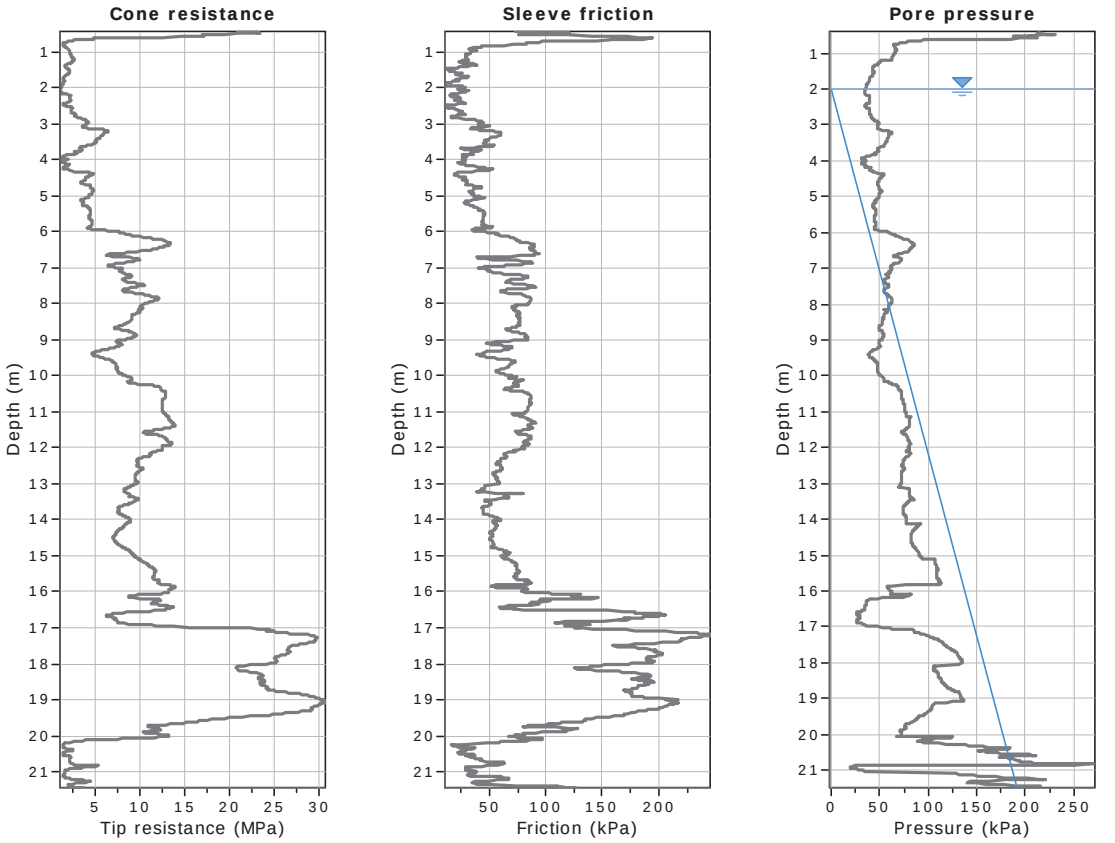

The plot below presents the cross correlation coeficient between the raw qc and fs values (as measured on the field). X axes presents the lag distance (one lag is the distance between two sucessive CPT measurements).

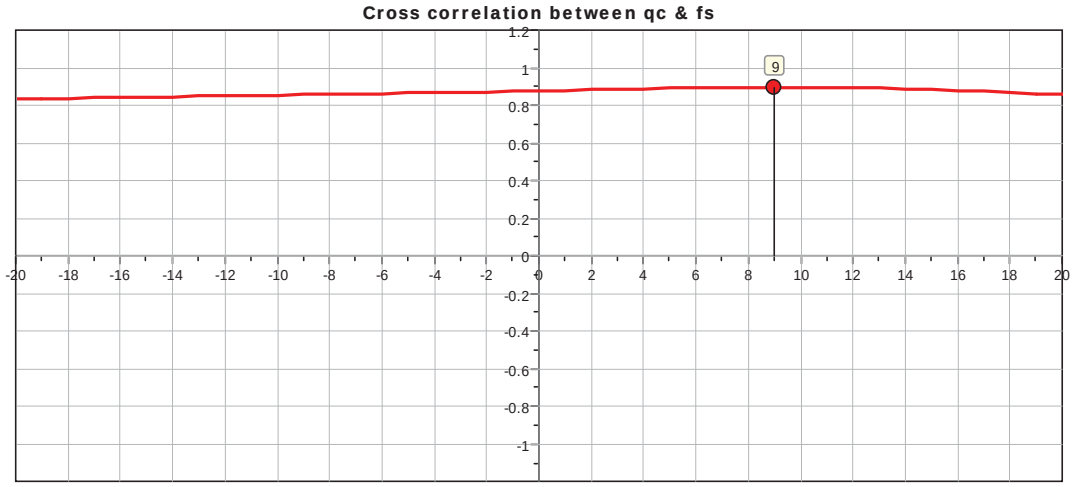

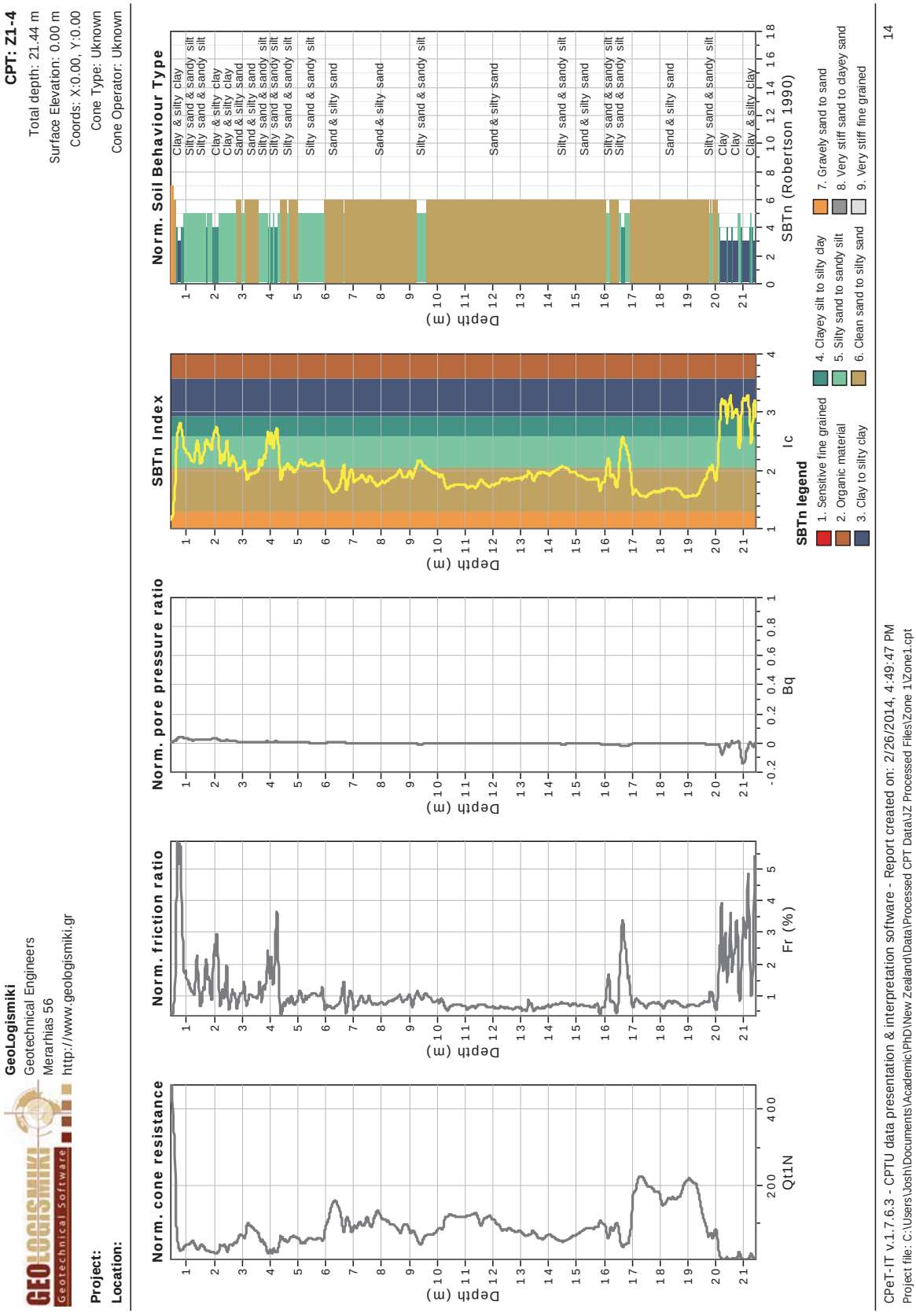
CPT: Z1-4
Total depth: 21.44 m
Surface Elevation: 0.00 m
Coords: X:0.00, Y:0.00
Cone Type: Uknown
Cone Operator: Uknown
GeoLogismiki
Geotechnical Engineers
Merarhias 56
http://www.geologismiki.gr
Project:
Location:
Norm. cone resistance
Qt1N
Norm. friction ratio
Fr (%)
Norm. pore pressure ratio
Bq
SBTn Index
Ic
Norm. Soil Behaviour Type
SBTn (Robertson 1990)
Depth (m)
SBTn legend
1. Sensitive fine grained
2. Organic material
3. Clay to silty clay
4. Clayey silt to silty clay
5. Silty sand to sandy silt
6. Clean sand to silty sand
7. Gravely sand to sand
8. Very stiff sand to clayey sand
9. Very stiff fine grained
CPeT-IT v.1.7.6.3 - CPTU data presentation & interpretation software - Report created on: 2/26/2014, 4:49:47 PM
Project file: C:\Users\Josh\Documents\Academic\PhD\New Zealand\Data\Processed CPT Data\JZ Processed Files\Zone 1\Zone1.cpt
14

GeoLogismiki
Geotechnical Engineers
Merarhias 56
http://www.geologismiki.gr

CPT: Z1-5
Total depth: 13.99 m
Surface Elevation: 0.00 m
Coords: X:0.00, Y:0.00
Cone Type: Uknown
Cone Operator: Uknown

Project:
Location:

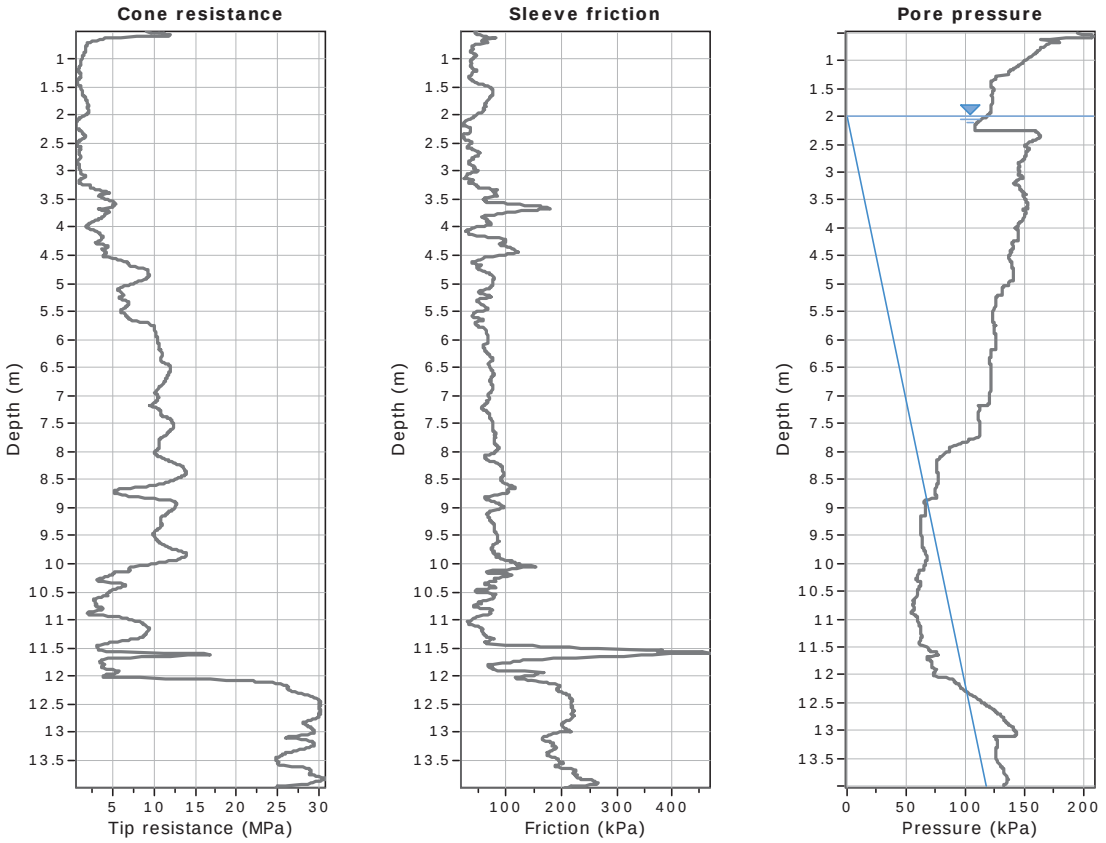

The plot below presents the cross correlation coeficient between the raw qc and fs values (as measured on the field). X axes presents the lag distance (one lag is the distance between two sucessive CPT measurements).

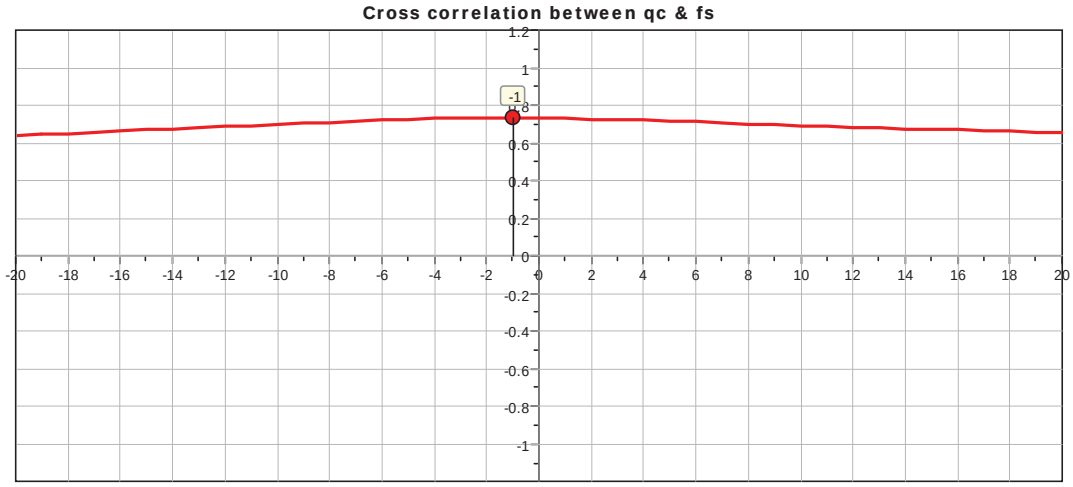

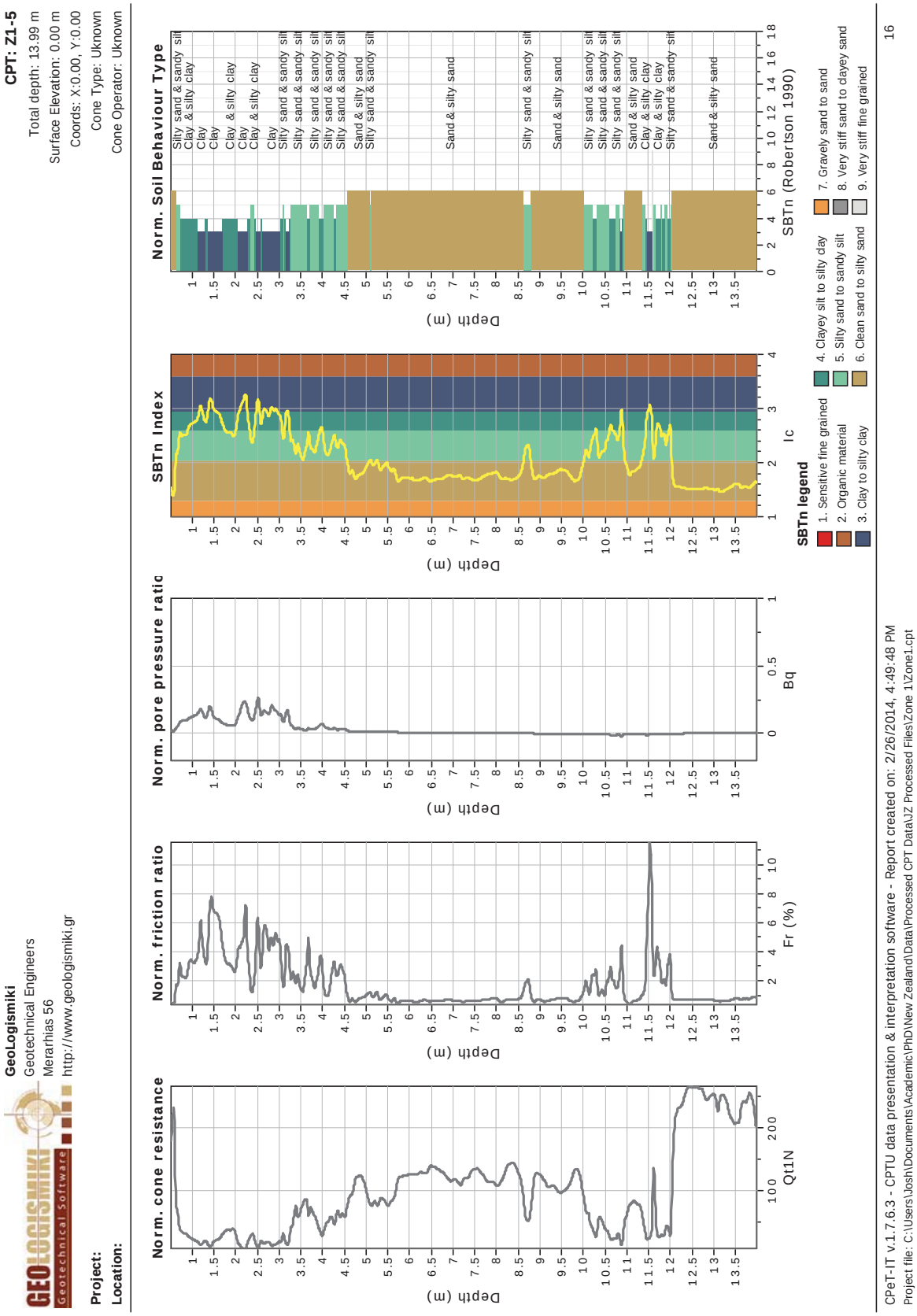
CPT: Z1-5
Total depth: 13.99 m
Surface Elevation: 0.00 m
Coords: X:0.00, Y:0.00
Cone Type: Uknown
Cone Operator: Uknown
GeoLogismiki
Geotechnical Engineers
Merarhias 56
http://www.geologismiki.gr
Project:
Location:
Norm. cone resistance
Norm. friction ratio
Norm. pore pressure ratio
SBTn Index
Norm. Soil Behaviour Type
Depth (m)
Qt1N
Fr (%)
Bq
Ic
SBTn (Robertson 1990)
SBTn legend
1. Sensitive fine grained
2. Organic material
3. Clay to silty clay
4. Clayey silt to silty clay
5. Silty sand to sandy silt
6. Clean sand to silty sand
7. Gravely sand to sand
8. Very stiff sand to clayey sand
9. Very stiff fine grained
CPeT-IT v.1.7.6.3 - CPTU data presentation & interpretation software - Report created on: 2/26/2014, 4:49:48 PM
Project file: C:\Users\Josh\Documents\Academic\PhD\New Zealand\Data\Processed CPT Data\JZ Processed Files\Zone 1\Zone1.cpt
16

GeoLogismiki
Geotechnical Engineers
Merarhias 56
http://www.geologismiki.gr

CPT: Z1-6
Total depth: 17.86 m
Surface Elevation: 0.00 m
Coords: X:0.00, Y:0.00
Cone Type: Uknown
Cone Operator: Uknown

Project:
Location:

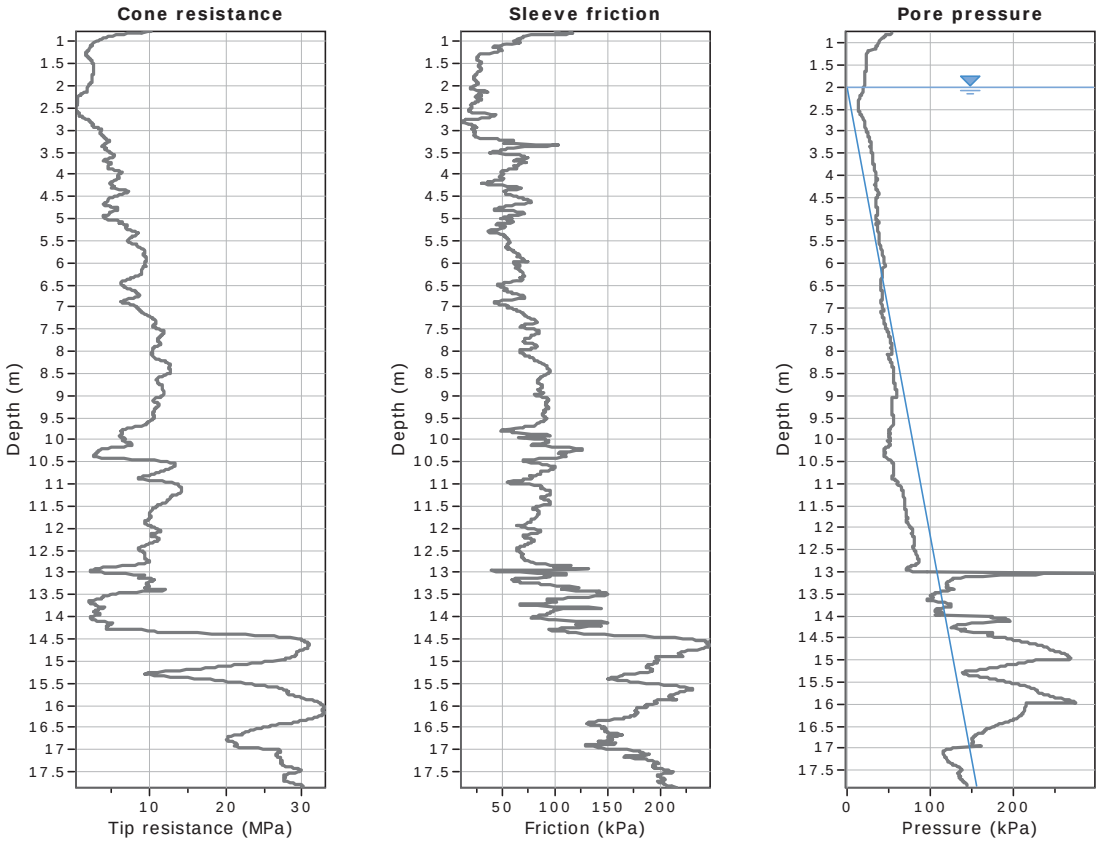

The plot below presents the cross correlation coeficient between the raw qc and fs values (as measured on the field). X axes presents the lag distance (one lag is the distance between two sucessive CPT measurements).

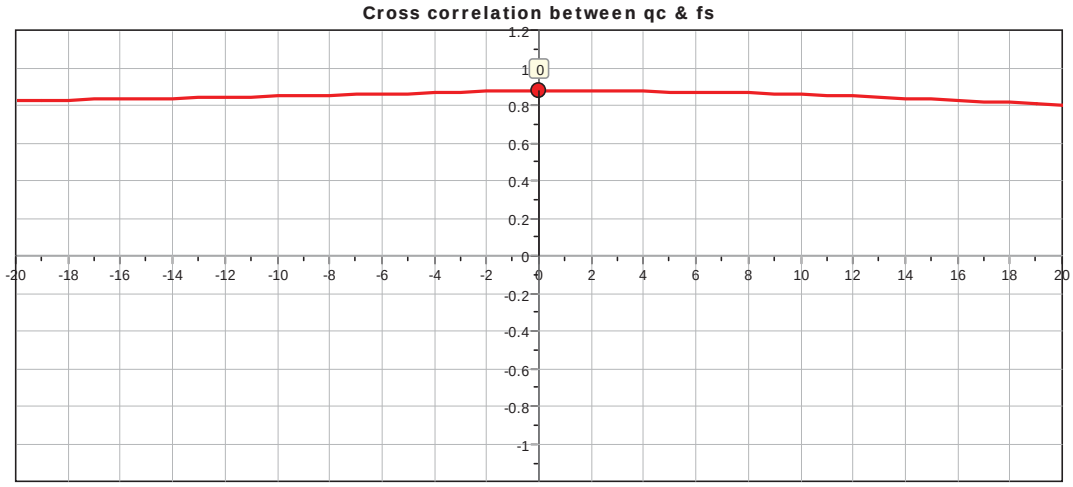

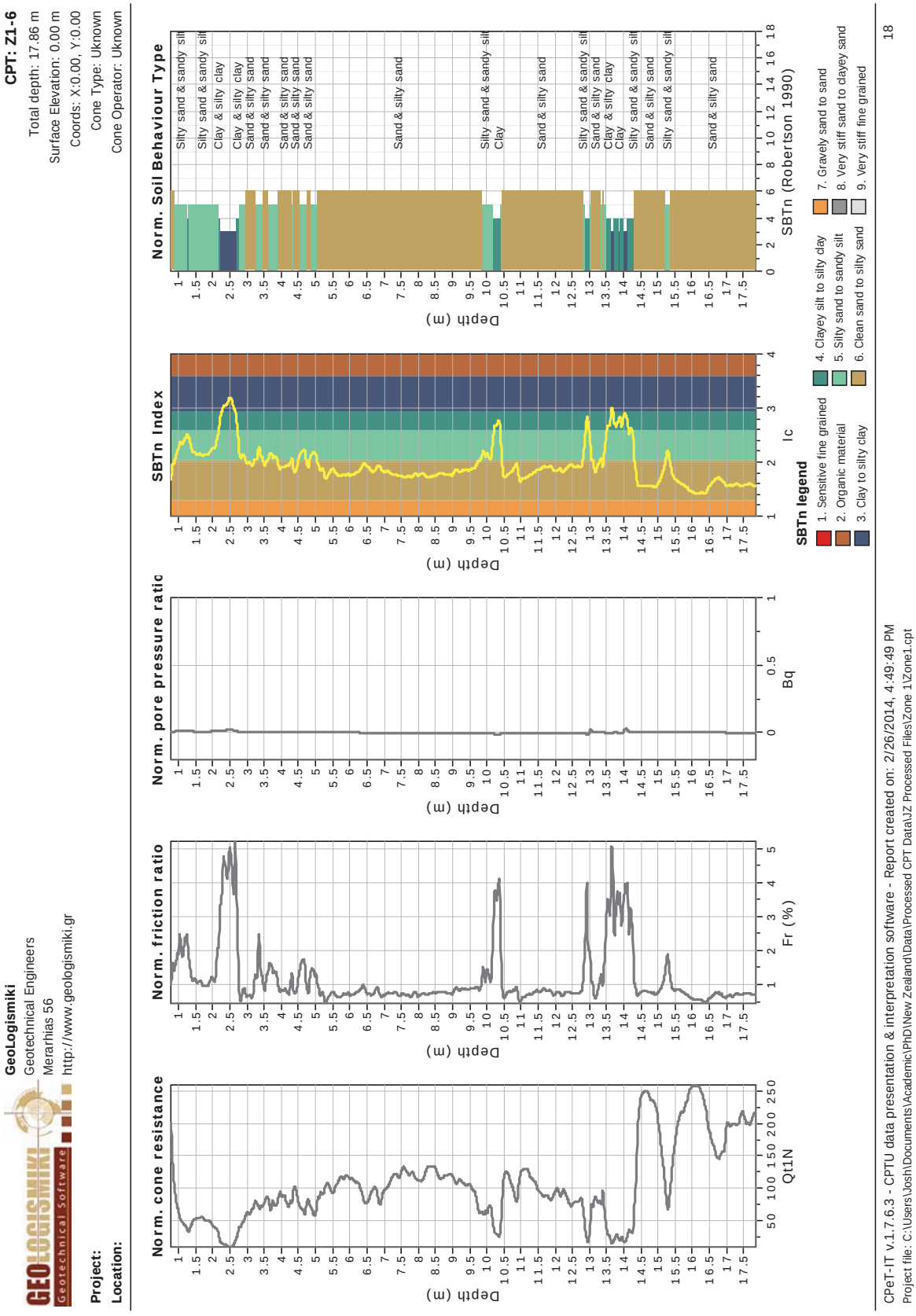
CPT: Z1-6
Total depth: 17.86 m
Surface Elevation: 0.00 m
Coords: X:0.00, Y:0.00
Cone Type: Uknown
Cone Operator: Uknown
GeoLogismiki
Geotechnical Engineers
Merarhias 56
http://www.geologismiki.gr
Project:
Location:
Norm. cone resistance
Qt1N
Norm. friction ratio
Fr (%)
Norm. pore pressure ratio
Bq
SBTn Index
Ic
Norm. Soil Behaviour Type
SBTn (Robertson 1990)
Depth (m)
SBTn legend
1. Sensitive fine grained
2. Organic material
3. Clay to silty clay
4. Clayey silt to silty clay
5. Silty sand to sandy silt
6. Clean sand to silty sand
7. Gravely sand to sand
8. Very stiff sand to clayey sand
9. Very stiff fine grained
CPeT-IT v.1.7.6.3 - CPTU data presentation & interpretation software - Report created on: 2/26/2014, 4:49:49 PM
Project file: C:\Users\Josh\Documents\Academic\PhD\New Zealand\Data\Processed CPT Data\JZ Processed Files\Zone 1\Zone1.cpt
18

GeoLogismiki
Geotechnical Engineers
Merarhias 56
http://www.geologismiki.gr

CPT: Z1-7
Total depth: 3.83 m
Surface Elevation: 0.00 m
Coords: X:0.00, Y:0.00
Cone Type: Uknown
Cone Operator: Uknown

Project:
Location:

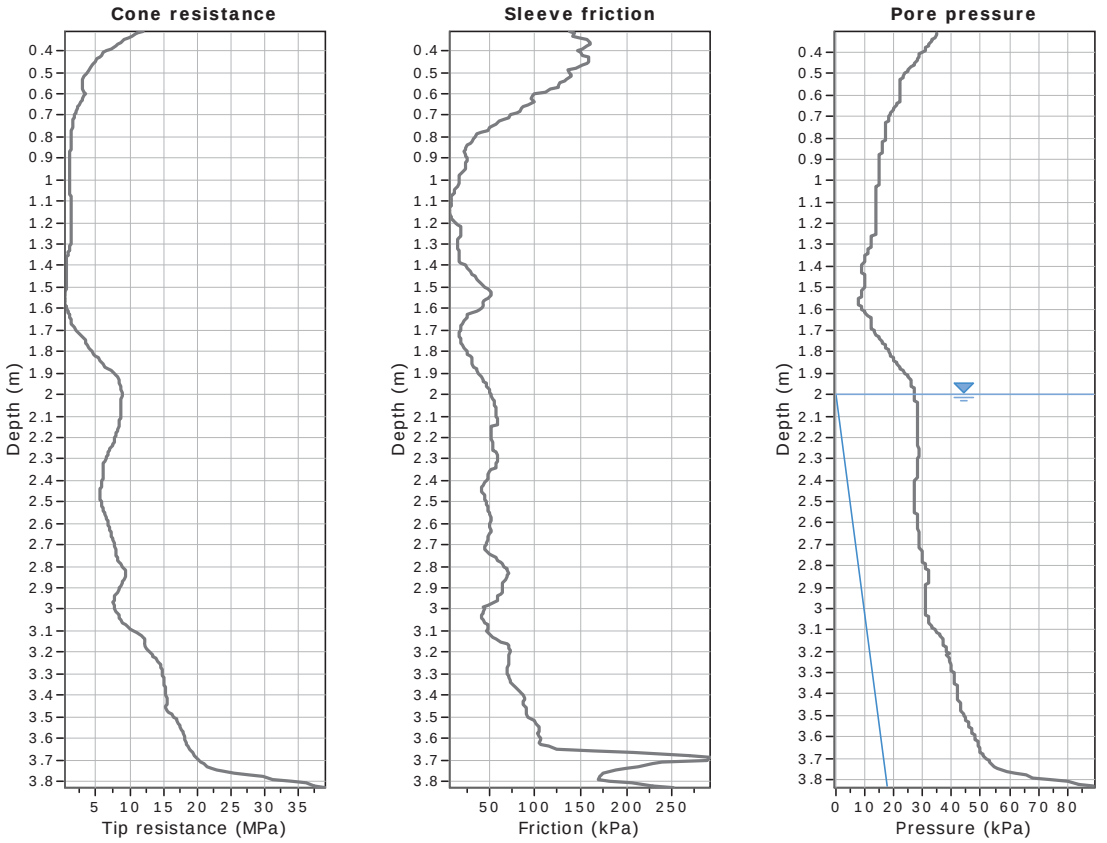

The plot below presents the cross correlation coeficient between the raw qc and fs values (as measured on the field). X axes presents the lag distance (one lag is the distance between two sucessive CPT measurements).

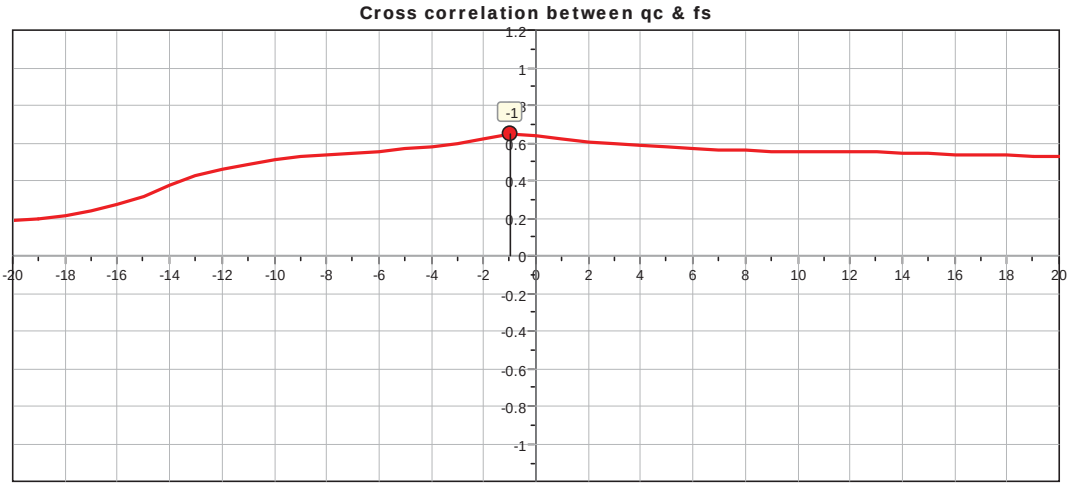

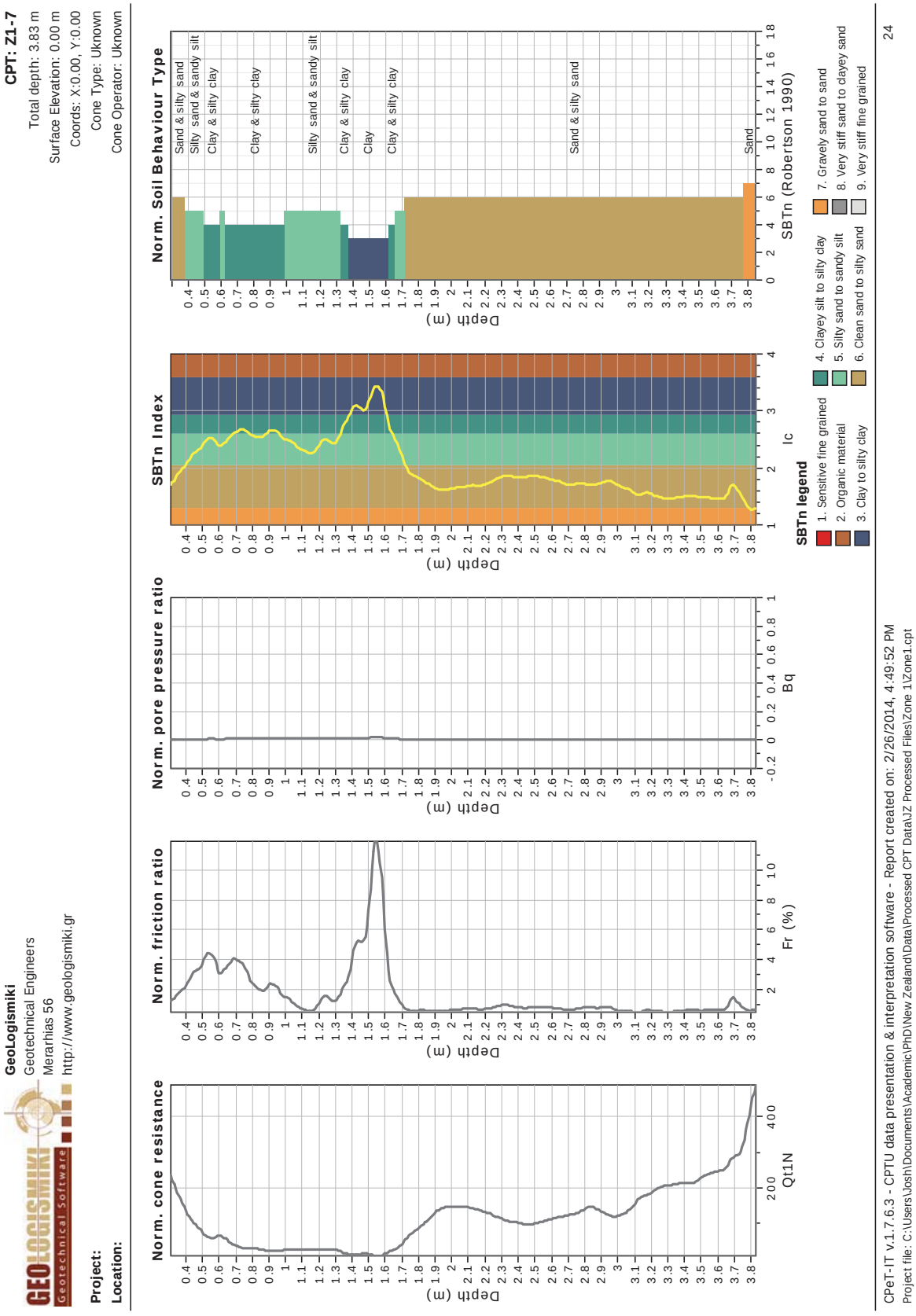
GeoLogismiki
Geotechnical Engineers
Merarchias 56
http://www.geologismiki.gr
Project:
Location:
CPT: Z1-7
Total depth: 3.83 m
Surface Elevation: 0.00 m
Coords: X:0.00, Y:0.00
Cone Type: Uknown
Cone Operator: Uknown
Norm. cone resistance
Qt1N
Norm. friction ratio
Fr (%)
Norm. pore pressure ratio
Bq
SBTn Index
Ic
Norm. Soil Behaviour Type
SBTn (Robertson 1990)
Sand & silty sand
Silty sand & sandy silt
Clay & silty clay
Clay & silty clay
Silty sand & sandy silt
Clay & silty clay
Clay
Clay & silty clay
Sand & silty sand
Sand
Depth (m)
SBTn legend
1. Sensitive fine grained
2. Organic material
3. Clay to silty clay
4. Clayey silt to silty clay
5. Silty sand to sandy silt
6. Clean sand to silty sand
7. Gravely sand to sand
8. Very stiff sand to clayey sand
9. Very stiff fine grained
CPeT-IT v.1.7.6.3 - CPTU data presentation & interpretation software - Report created on: 2/26/2014, 4:49:52 PM
Project file: C:\Users\Josh\Documents\Academic\PhD\New Zealand\Data\Processed CPT Data\JZ Processed Files\Zone 1\Zone1.cpt
24

GeoLogismiki
Geotechnical Engineers
Merarhias 56
http://www.geologismiki.gr

CPT: Z1-8
Total depth: 17.22 m
Surface Elevation: 0.00 m
Coords: X:0.00, Y:0.00
Cone Type: Uknown
Cone Operator: Uknown

Project:
Location:

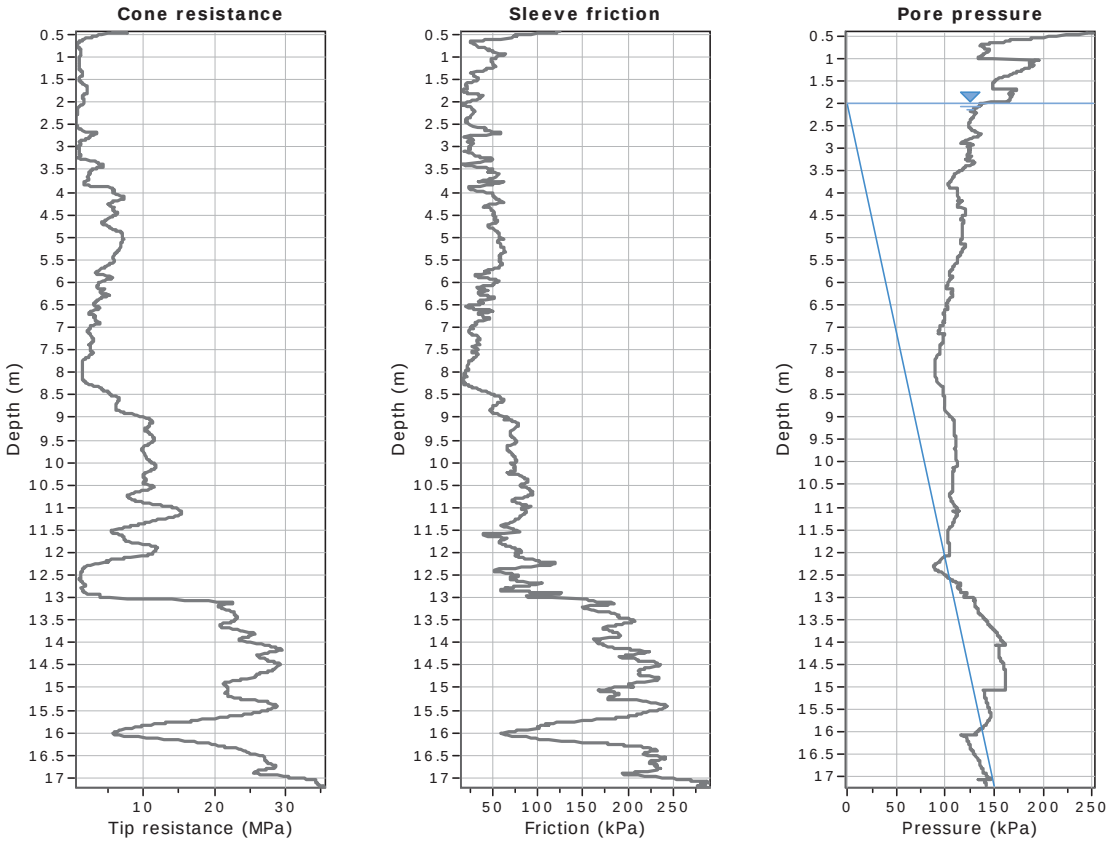

The plot below presents the cross correlation coeficient between the raw qc and fs values (as measured on the field). X axes presents the lag distance (one lag is the distance between two sucessive CPT measurements).

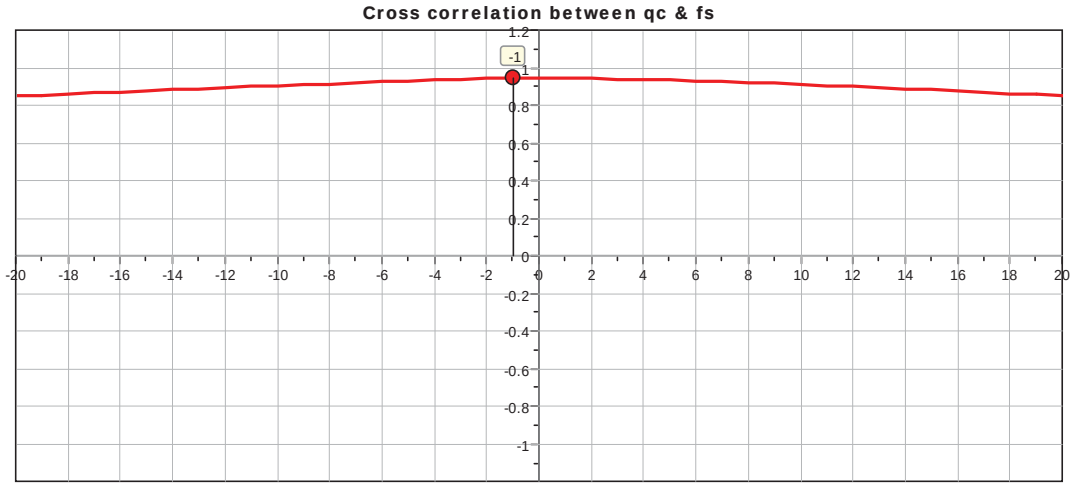

GeoLogismiki
Geotechnical Engineers
Merarhias 56
http://www.geologismiki.gr

CPT: Z1-8
Total depth: 17.22 m
Surface Elevation: 0.00 m
Coords: X:0.00, Y:0.00
Cone Type: Uknown
Cone Operator: Uknown

Project:
Location:

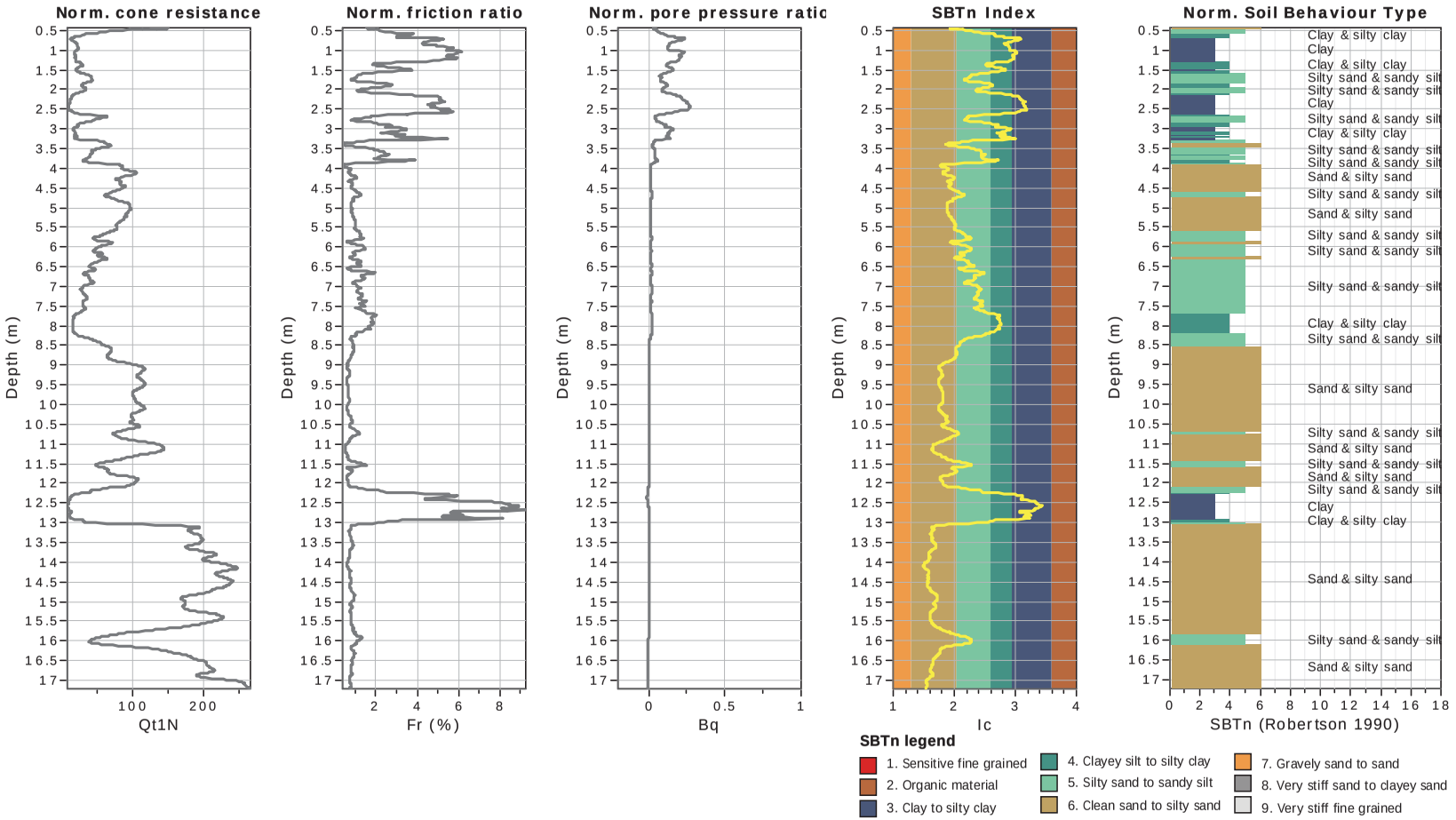

GeoLogismiki
Geotechnical Engineers
Merarhias 56
http://www.geologismiki.gr

CPT: Z1-9
Total depth: 3.85 m
Surface Elevation: 0.00 m
Coords: X:0.00, Y:0.00
Cone Type: Uknown
Cone Operator: Uknown

Project:
Location:

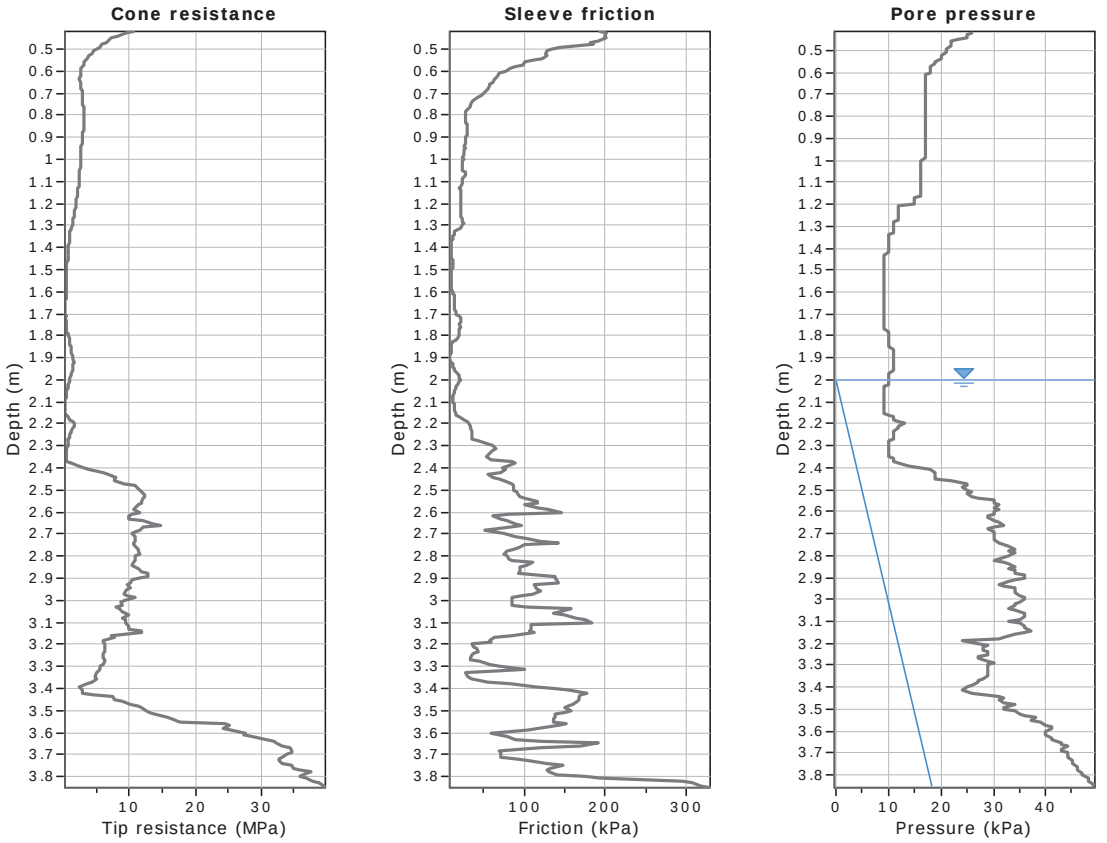

The plot below presents the cross correlation coeficient between the raw qc and fs values (as measured on the field). X axes presents the lag distance (one lag is the distance between two sucessive CPT measurements).

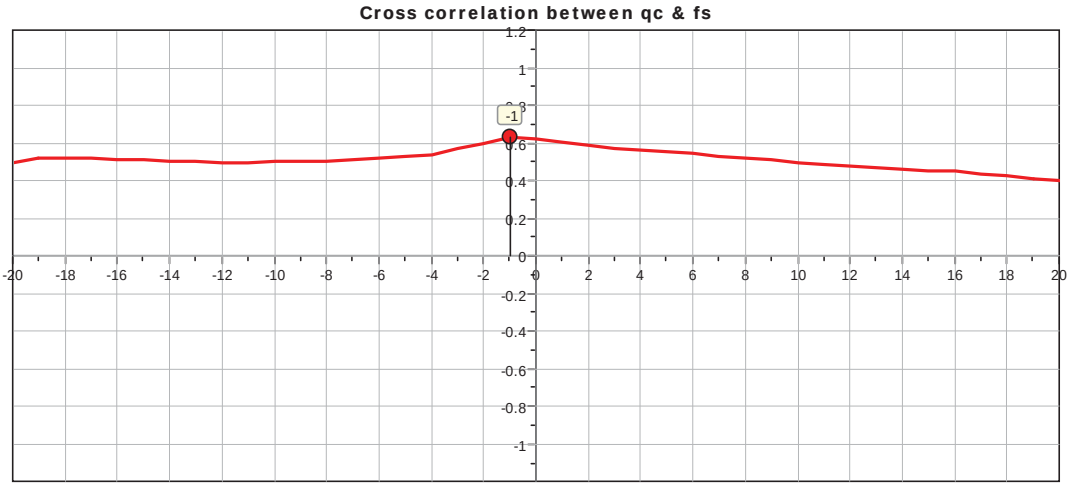

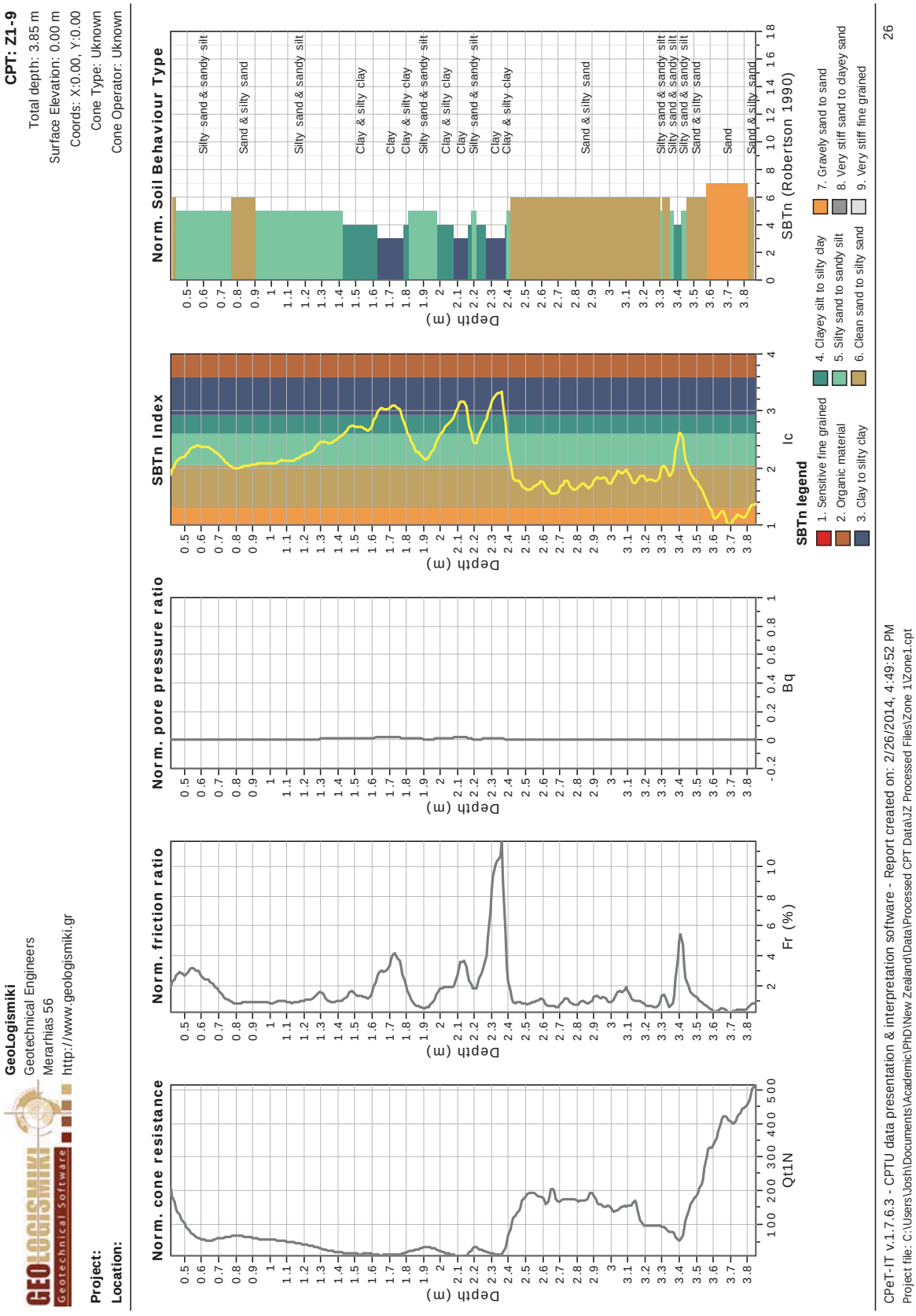
GeoLogismiki
Geotechnical Engineers
Merarhias 56
http://www.geologismiki.gr
Project:
Location:
CPT: Z1-9
Total depth: 3.85 m
Surface Elevation: 0.00 m
Coords: X:0.00, Y:0.00
Cone Type: Uknown
Cone Operator: Uknown
Norm. cone resistance
Qt1N
Norm. friction ratio
Fr (%)
Norm. pore pressure ratio
Bq
SBTn Index
Ic
Norm. Soil Behaviour Type
SBTn (Robertson 1990)
Depth (m)
SBTn legend
1. Sensitive fine grained
2. Organic material
3. Clay to silty clay
4. Clayey silt to silty clay
5. Silty sand to sandy silt
6. Clean sand to silty sand
7. Gravely sand to sand
8. Very stiff sand to clayey sand
9. Very stiff fine grained
CPeT-IT v.1.7.6.3 - CPTU data presentation & interpretation software - Report created on: 2/26/2014, 4:49:52 PM
Project file: C:\Users\Josh\Documents\Academic\PhD\New Zealand\Data\Processed CPT Data\JZ Processed Files\Zone 1\Zone1.cpt
26

GeoLogismiki
Geotechnical Engineers
Merarhias 56
http://www.geologismiki.gr

CPT: Z1-10
Total depth: 6.33 m
Surface Elevation: 0.00 m
Coords: X:0.00, Y:0.00
Cone Type: Uknown
Cone Operator: Uknown

Project:
Location:

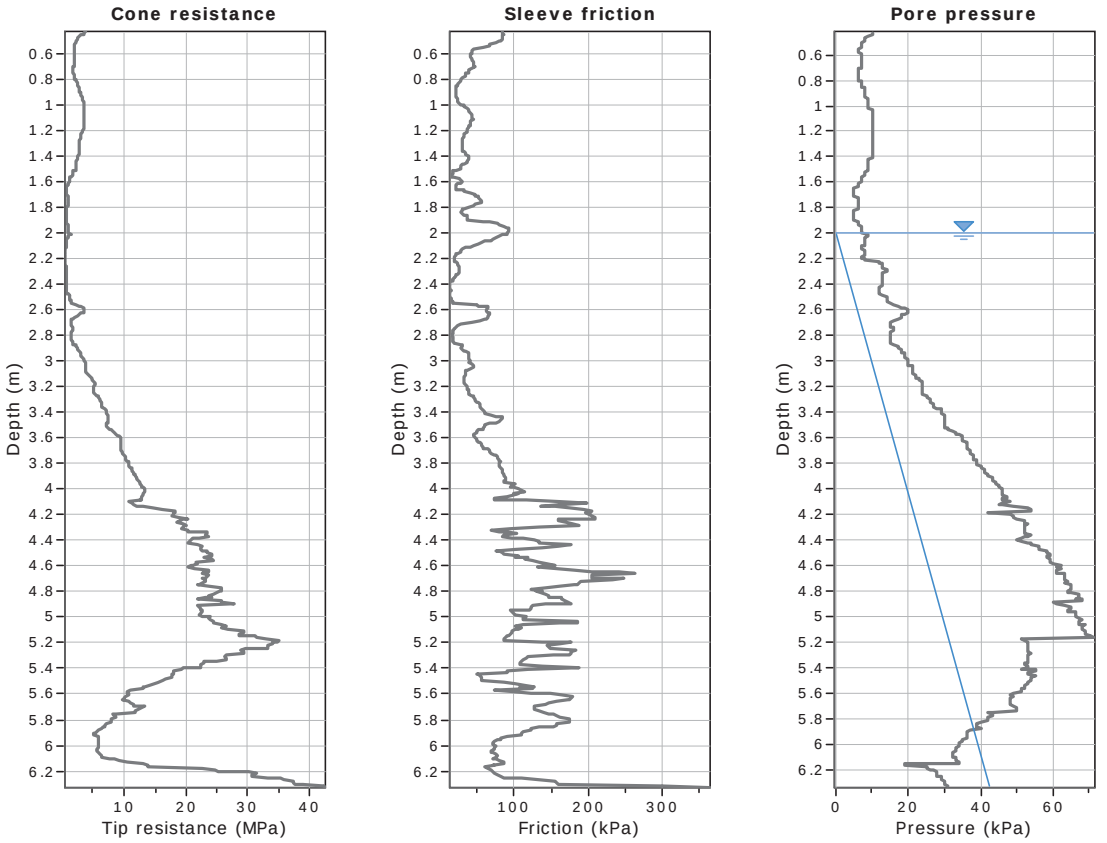

The plot below presents the cross correlation coeficient between the raw qc and fs values (as measured on the field). X axes presents the lag distance (one lag is the distance between two sucessive CPT measurements).

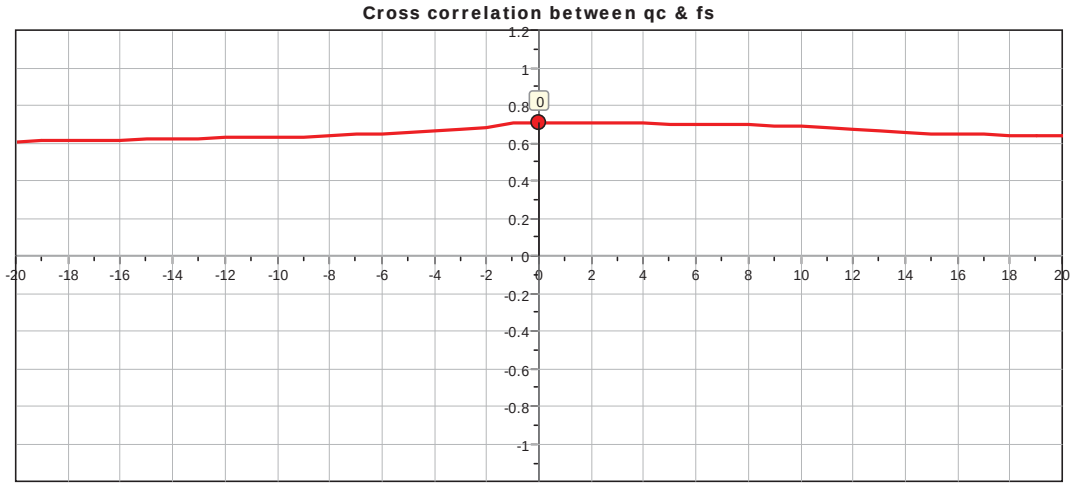

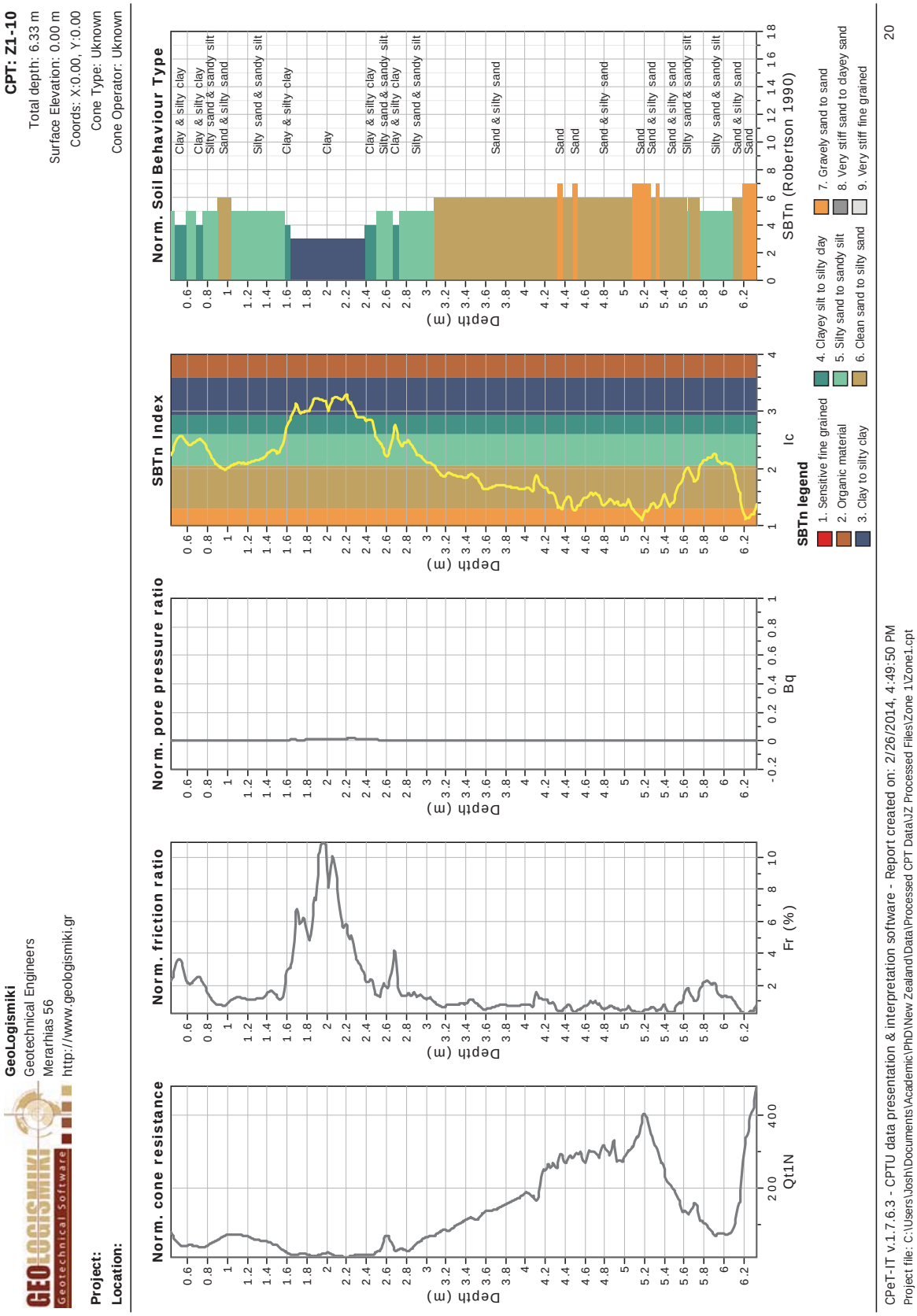
CPT: Z1-10
Total depth: 6.33 m
Surface Elevation: 0.00 m
Coords: X:0.00, Y:0.00
Cone Type: Uknown
Cone Operator: Uknown
GeoLogismiki
Geotechnical Engineers
Merarhias 56
http://www.geologismiki.gr
Project:
Location:
Norm. cone resistance
Qt1N
Norm. friction ratio
Fr (%)
Norm. pore pressure ratio
Bq
SBTn Index
Ic
Norm. Soil Behaviour Type
SBTn (Robertson 1990)
Depth (m)
SBTn legend
1. Sensitive fine grained
2. Organic material
3. Clay to silty clay
4. Clayey silt to silty clay
5. Silty sand to sandy silt
6. Clean sand to silty sand
7. Gravely sand to sand
8. Very stiff sand to clayey sand
9. Very stiff fine grained
CPeT-IT v.1.7.6.3 - CPTU data presentation & interpretation software - Report created on: 2/26/2014, 4:49:50 PM
Project file: C:\Users\Josh\Documents\Academic\PhD\New Zealand\Data\Processed CPT Data\JZ Processed Files\Zone 1\Zone1.cpt
20

GeoLogismiki
Geotechnical Engineers
Merarhias 56
http://www.geologismiki.gr

CPT: Z1-11
Total depth: 17.55 m
Surface Elevation: 0.00 m
Coords: X:0.00, Y:0.00
Cone Type: Uknown
Cone Operator: Uknown

Project:
Location:

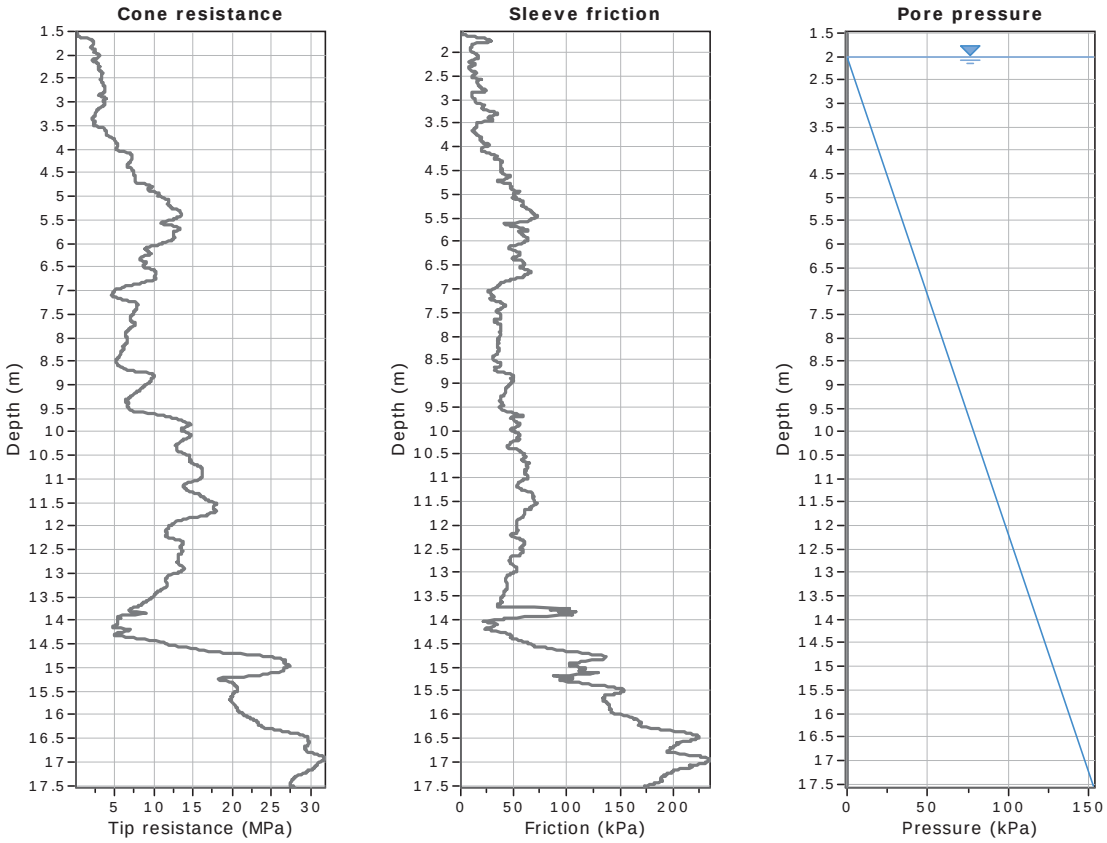

The plot below presents the cross correlation coeficient between the raw qc and fs values (as measured on the field). X axes presents the lag distance (one lag is the distance between two sucessive CPT measurements).

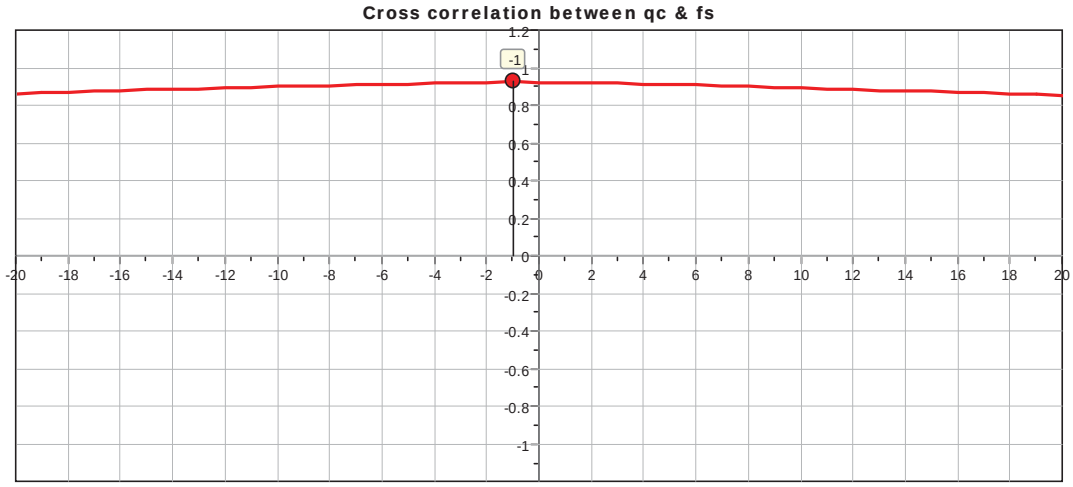

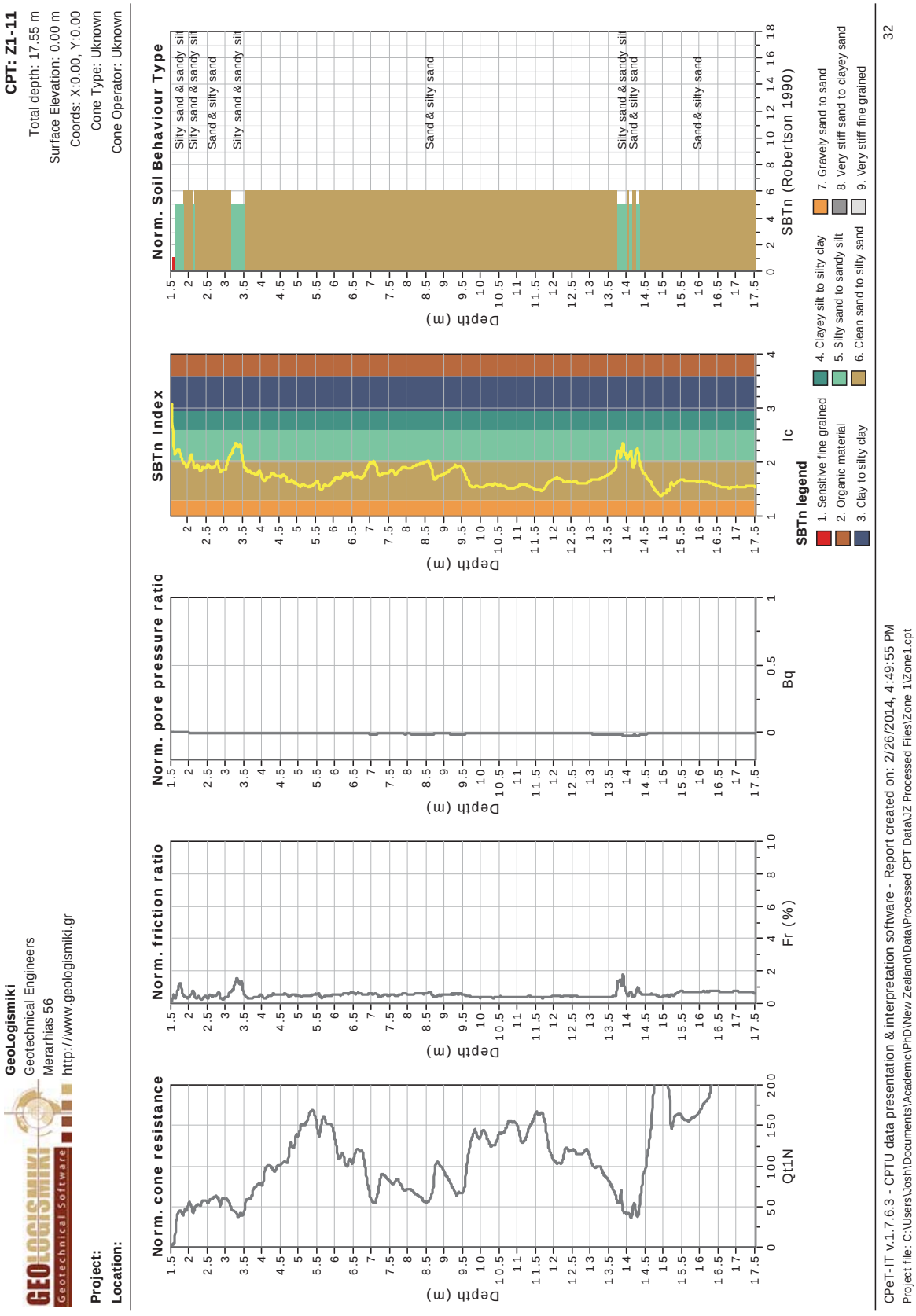
GeoLogismiki
Geotechnical Engineers
Merarchias 56
http://www.geologismiki.gr
Project:
Location:
CPT: Z1-11
Total depth: 17.55 m
Surface Elevation: 0.00 m
Coords: X:0.00, Y:0.00
Cone Type: Uknown
Cone Operator: Uknown
Norm. cone resistance
Qt1N
Norm. friction ratio
Fr (%)
Norm. pore pressure ratio
Bq
SBTn Index
Ic
Norm. Soil Behaviour Type
SBTn (Robertson 1990)
Depth (m)
SBTn legend
1. Sensitive fine grained
2. Organic material
3. Clay to silty clay
4. Clayey silt to silty clay
5. Silty sand to sandy silt
6. Clean sand to silty sand
7. Gravely sand to sand
8. Very stiff sand to clayey sand
9. Very stiff fine grained
Silty sand & sandy silt
Sand & silty sand
CPeT-IT v.1.7.6.3 - CPTU data presentation & interpretation software - Report created on: 2/26/2014, 4:49:55 PM
Project file: C:\Users\Josh\Documents\Academic\PhD\New Zealand\Data\Processed CPT Data\JZ Processed Files\Zone 1\Zone1.cpt
32

GeoLogismiki
Geotechnical Engineers
Merarhias 56
http://www.geologismiki.gr

CPT: Z1-12
Total depth: 16.72 m
Surface Elevation: 0.00 m
Coords: X:0.00, Y:0.00
Cone Type: Uknown
Cone Operator: Uknown

Project:
Location:

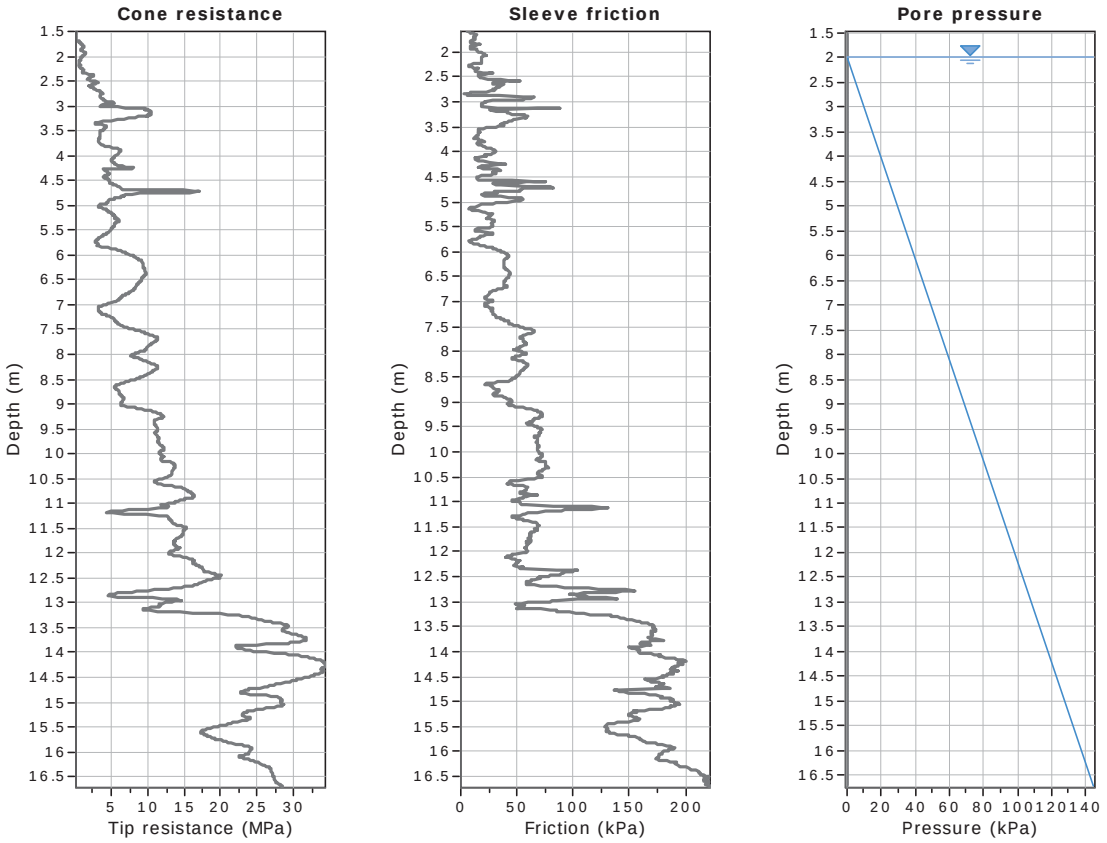

The plot below presents the cross correlation coeficient between the raw qc and fs values (as measured on the field). X axes presents the lag distance (one lag is the distance between two sucessive CPT measurements).

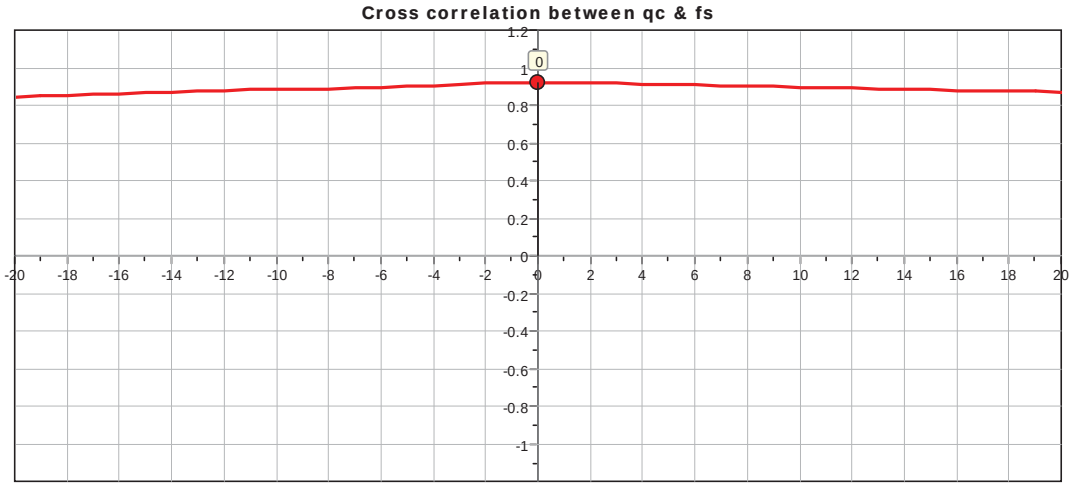

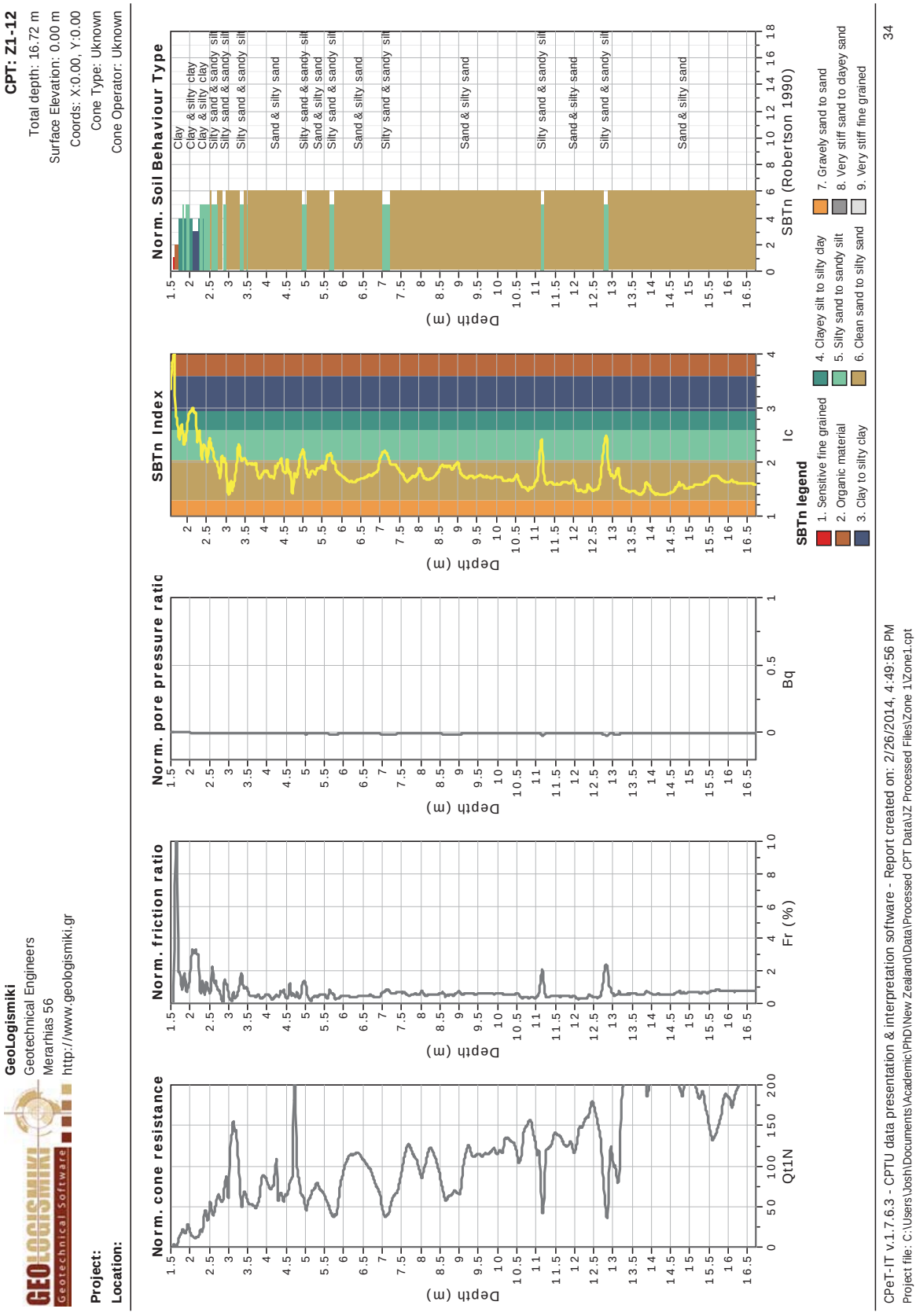
CPT: Z1-12
Total depth: 16.72 m
Surface Elevation: 0.00 m
Coords: X:0.00, Y:0.00
Cone Type: Uknown
Cone Operator: Uknown
GeoLogismiki
Geotechnical Engineers
Merarhias 56
http://www.geologismiki.gr
Project:
Location:
Norm. cone resistance
Norm. friction ratio
Norm. pore pressure ratio
SBTn Index
Norm. Soil Behaviour Type
Depth (m)
Qt1N
Fr (%)
Bq
Ic
SBTn (Robertson 1990)
Clay
Clay & silty clay
Silty sand & sandy silt
Sand & silty sand
SBTn legend
1. Sensitive fine grained
2. Organic material
3. Clay to silty clay
4. Clayey silt to silty clay
5. Silty sand to sandy silt
6. Clean sand to silty sand
7. Gravely sand to sand
8. Very stiff sand to clayey sand
9. Very stiff fine grained
CPeT-IT v.1.7.6.3 - CPTU data presentation & interpretation software - Report created on: 2/26/2014, 4:49:56 PM
Project file: C:\Users\Josh\Documents\Academic\PhD\New Zealand\Data\Processed CPT Data\JZ Processed Files\Zone 1\Zone1.cpt
34

GeoLogismiki
Geotechnical Engineers
Merarhias 56
http://www.geologismiki.gr

CPT: Z1-13-shallow
Total depth: 5.92 m
Surface Elevation: 0.00 m
Coords: X:0.00, Y:0.00
Cone Type: Uknown
Cone Operator: Uknown

Project:
Location:

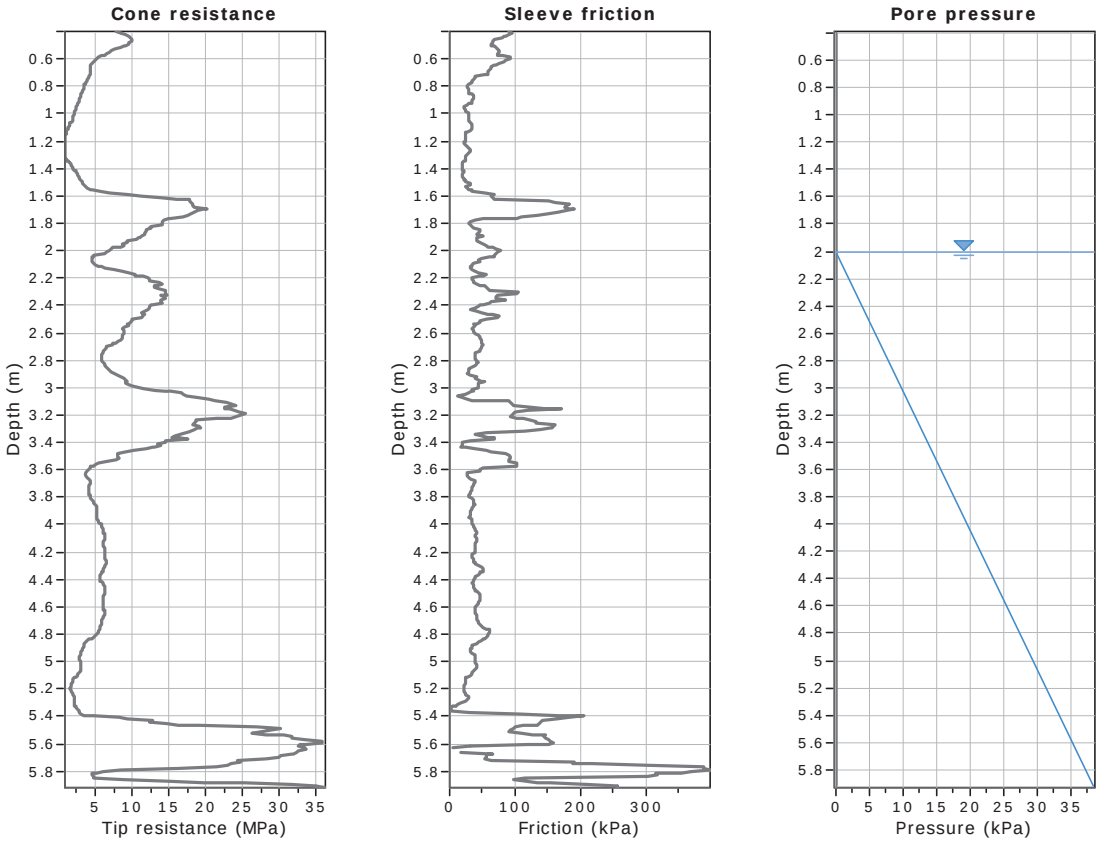

The plot below presents the cross correlation coeficient between the raw qc and fs values (as measured on the field). X axes presents the lag distance (one lag is the distance between two sucessive CPT measurements).

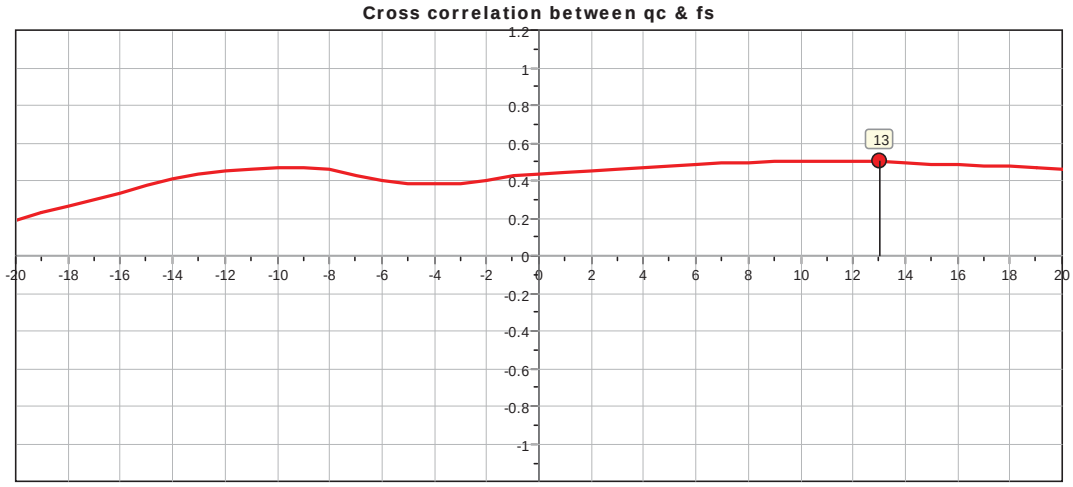

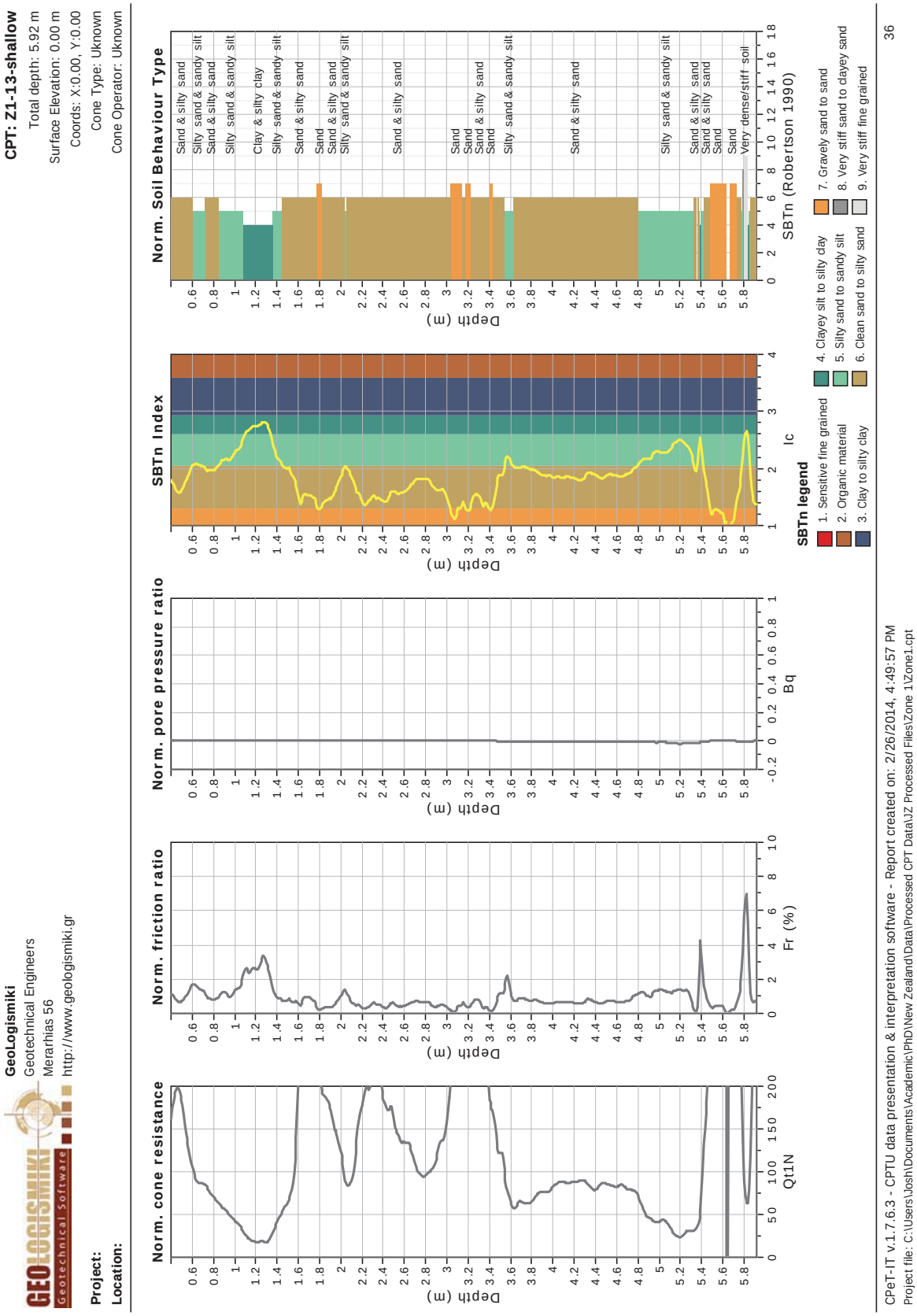
GeoLogismiki
Geotechnical Engineers
Merarhias 56
http://www.geologismiki.gr
Project:
Location:
CPT: Z1-13-shallow
Total depth: 5.92 m
Surface Elevation: 0.00 m
Coords: X:0.00, Y:0.00
Cone Type: Uknown
Cone Operator: Uknown
Norm. cone resistance
Qt1N
Norm. friction ratio
Fr (%)
Norm. pore pressure ratio
Bq
SBTn Index
Ic
Norm. Soil Behaviour Type
SBTn (Robertson 1990)
Depth (m)
SBTn legend
1. Sensitive fine grained
2. Organic material
3. Clay to silty clay
4. Clayey silt to silty clay
5. Silty sand to sandy silt
6. Clean sand to silty sand
7. Gravely sand to sand
8. Very stiff sand to clayey sand
9. Very stiff fine grained
CPeT-IT v.1.7.6.3 - CPTU data presentation & interpretation software - Report created on: 2/26/2014, 4:49:57 PM
Project file: C:\Users\Josh\Documents\Academic\PhD\New Zealand\Data\Processed CPT Data\JZ Processed Files\Zone 1\Zone1.cpt
36

GeoLogismiki
Geotechnical Engineers
Merarhias 56
http://www.geologismiki.gr

CPT: Z1-13-deep
Total depth: 21.52 m
Surface Elevation: 0.00 m
Coords: X:0.00, Y:0.00
Cone Type: Uknown
Cone Operator: Uknown

Project:
Location:

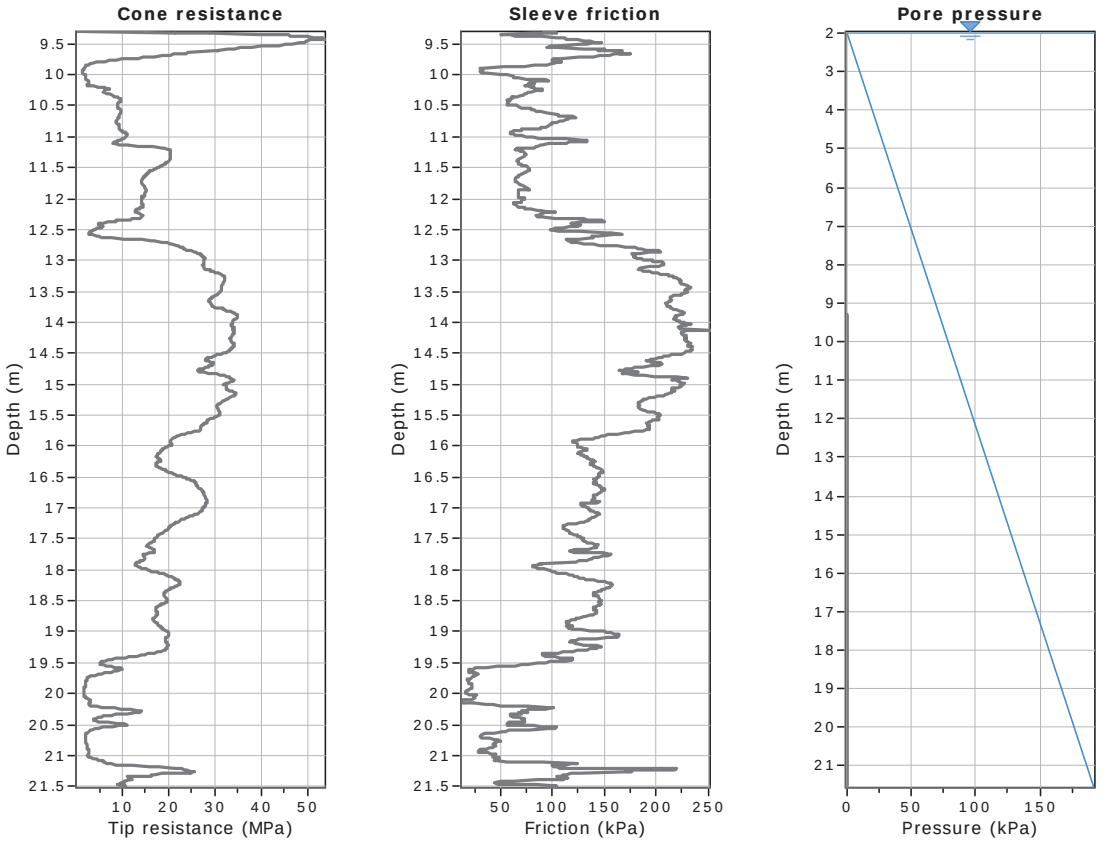

The plot below presents the cross correlation coeficient between the raw qc and fs values (as measured on the field). X axes presents the lag distance (one lag is the distance between two sucessive CPT measurements).

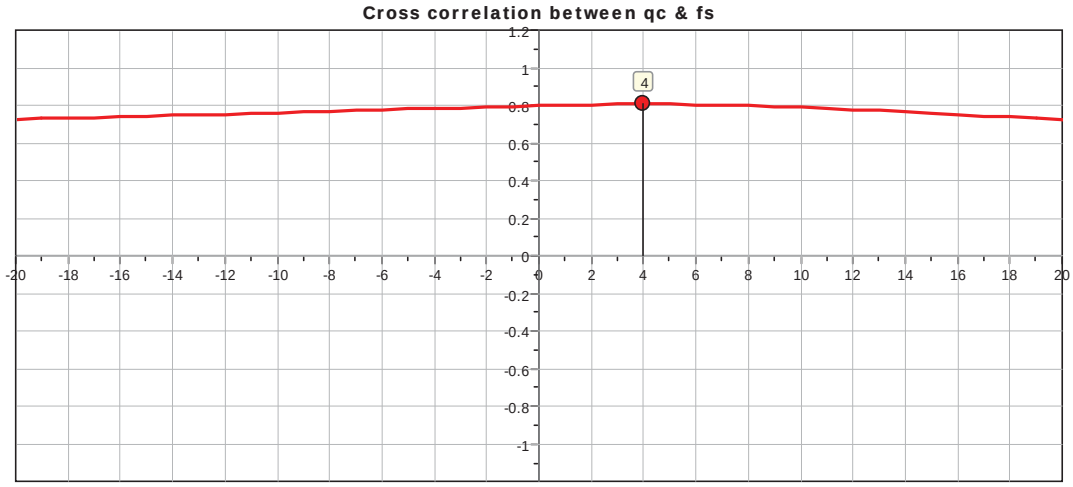

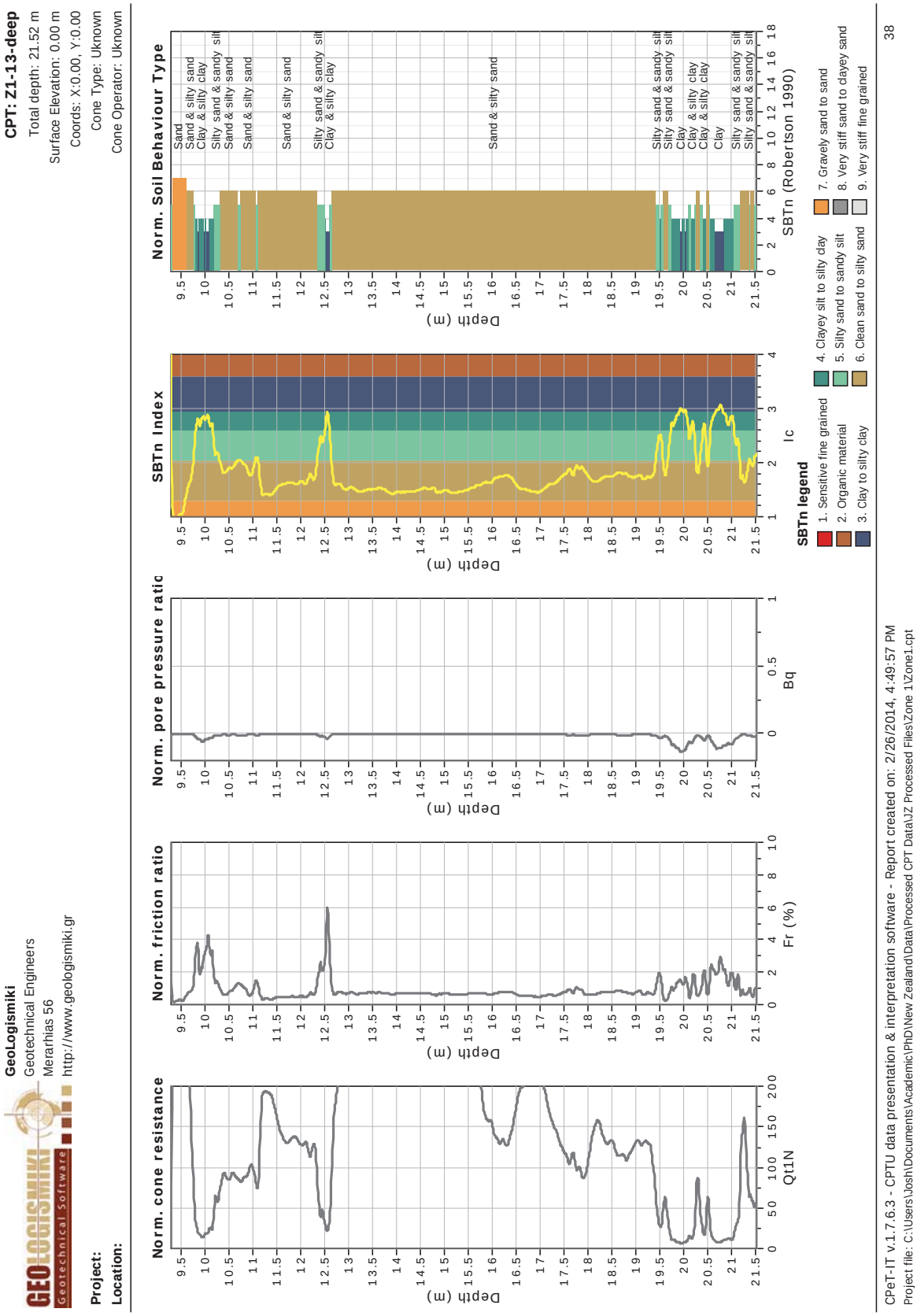
GeoLogismiki
Geotechnical Engineers
Merarhias 56
http://www.geologismiki.gr
Project:
Location:
CPT: Z1-13-deep
Total depth: 21.52 m
Surface Elevation: 0.00 m
Coords: X:0.00, Y:0.00
Cone Type: Uknown
Cone Operator: Uknown
Norm. cone resistance
Norm. friction ratio
Norm. pore pressure ratio
SBTn Index
Norm. Soil Behaviour Type
Depth (m)
Qt1N
Fr (%)
Bq
Ic
SBTn (Robertson 1990)
SBTn legend
1. Sensitive fine grained
2. Organic material
3. Clay to silty clay
4. Clayey silt to silty clay
5. Silty sand to sandy silt
6. Clean sand to silty sand
7. Gravely sand to sand
8. Very stiff sand to clayey sand
9. Very stiff fine grained
Sand
Sand & silty sand
Clay & silty clay
Silty sand & sandy silt
Sand & silty sand
Sand & silty sand
Silty sand & sandy silt
Clay & silty clay
Sand & silty sand
Silty sand & sandy silt
Silty sand & sandy silt
Clay
Clay & silty clay
Clay & silty clay
Clay
Silty sand & sandy silt
Silty sand & sandy silt
CPeT-IT v.1.7.6.3 - CPTU data presentation & interpretation software - Report created on: 2/26/2014, 4:49:57 PM
Project file: C:\Users\Josh\Documents\Academic\PhD\New Zealand\Data\Processed CPT Data\JZ Processed Files\Zone 1\Zone1.cpt
38

GeoLogismiki
Geotechnical Engineers
Merarhias 56
http://www.geologismiki.gr

CPT: Z1-14-shallow
Total depth: 6.99 m
Surface Elevation: 0.00 m
Coords: X:0.00, Y:0.00
Cone Type: Uknown
Cone Operator: Uknown

Project:
Location:

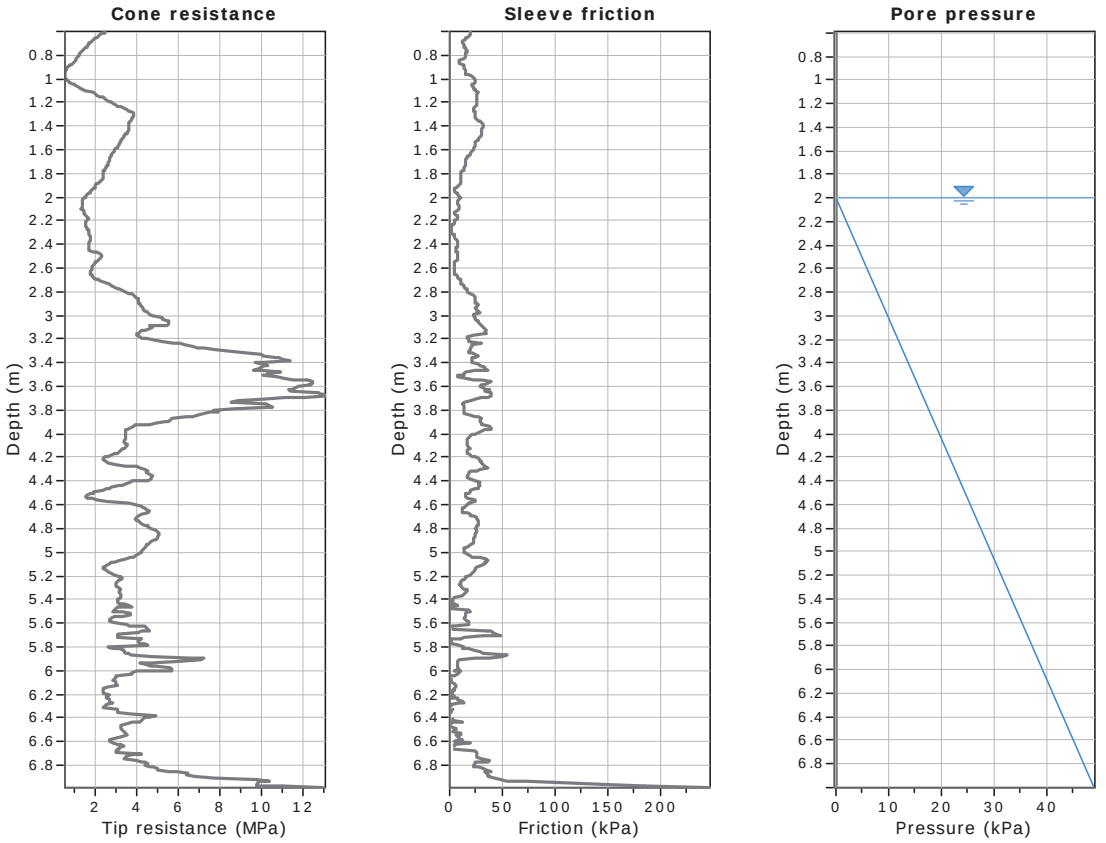

The plot below presents the cross correlation coeficient between the raw qc and fs values (as measured on the field). X axes presents the lag distance (one lag is the distance between two sucessive CPT measurements).

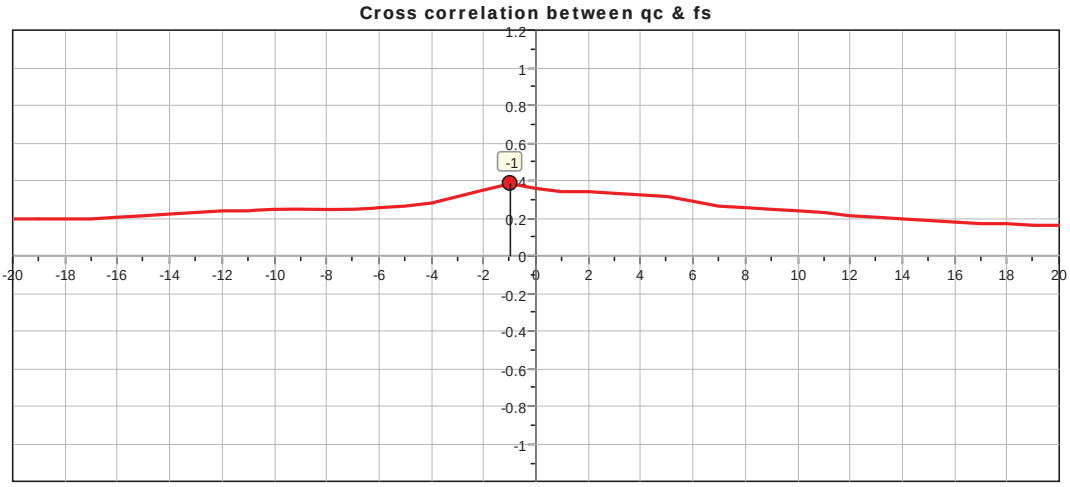

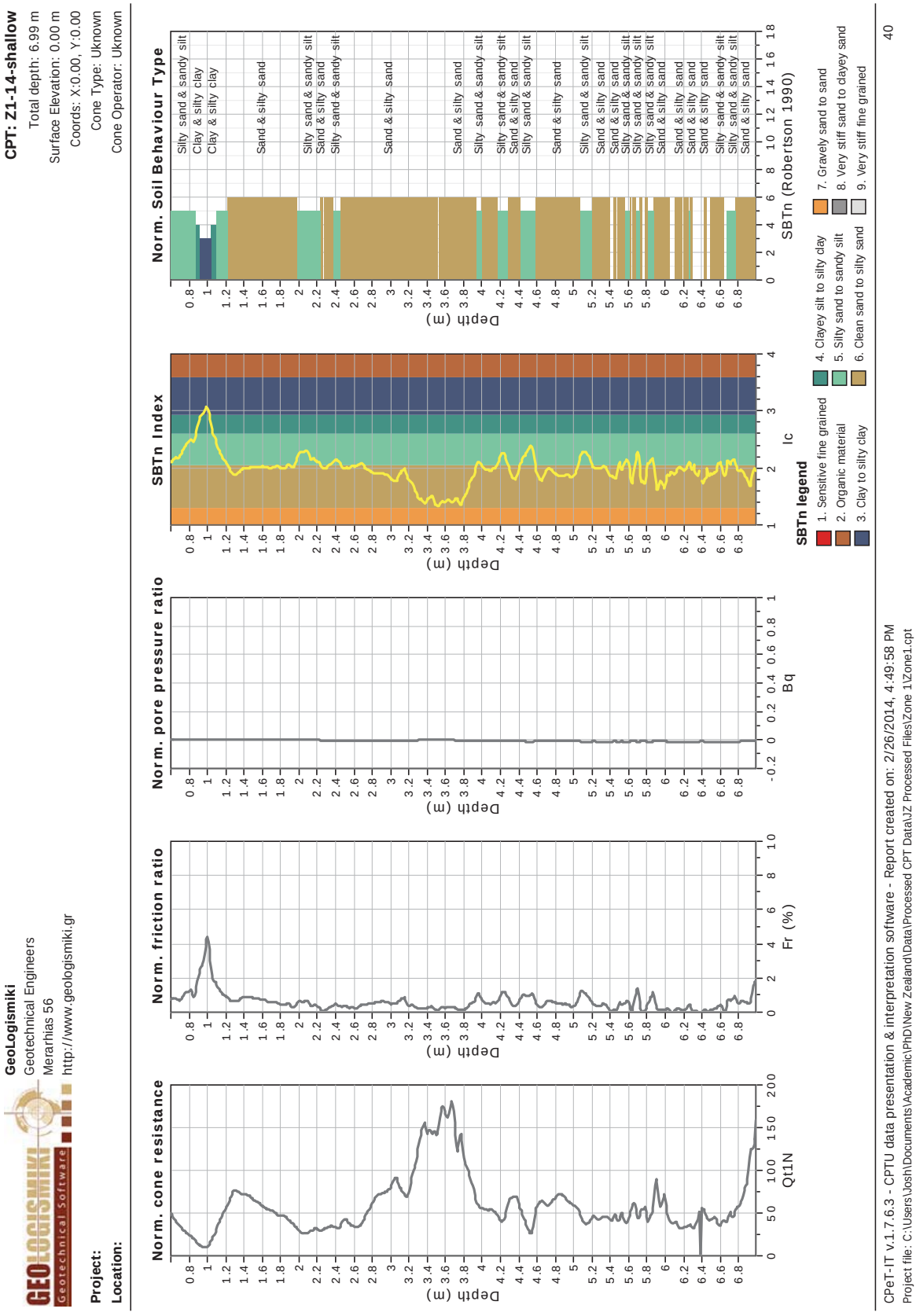
GeoLogismiki
Geotechnical Engineers
Merarhias 56
http://www.geologismiki.gr
Project:
Location:
CPT: Z1-14-shallow
Total depth: 6.99 m
Surface Elevation: 0.00 m
Coords: X:0.00, Y:0.00
Cone Type: Uknown
Cone Operator: Uknown
Norm. cone resistance
Qt1N
Norm. friction ratio
Fr (%)
Norm. pore pressure ratio
Bq
SBTn Index
Ic
Norm. Soil Behaviour Type
SBTn (Robertson 1990)
Depth (m)
SBTn legend
1. Sensitive fine grained
2. Organic material
3. Clay to silty clay
4. Clayey silt to silty clay
5. Silty sand to sandy silt
6. Clean sand to silty sand
7. Gravely sand to sand
8. Very stiff sand to clayey sand
9. Very stiff fine grained
CPeT-IT v.1.7.6.3 - CPTU data presentation & interpretation software - Report created on: 2/26/2014, 4:49:58 PM
Project file: C:\Users\Josh\Documents\Academic\PhD\New Zealand\Data\Processed CPT Data\JZ Processed Files\Zone 1\Zone1.cpt
40

GeoLogismiki
Geotechnical Engineers
Merarhias 56
http://www.geologismiki.gr

CPT: Z1-14-deep
Total depth: 20.61 m
Surface Elevation: 0.00 m
Coords: X:0.00, Y:0.00
Cone Type: Uknown
Cone Operator: Uknown

Project:
Location:

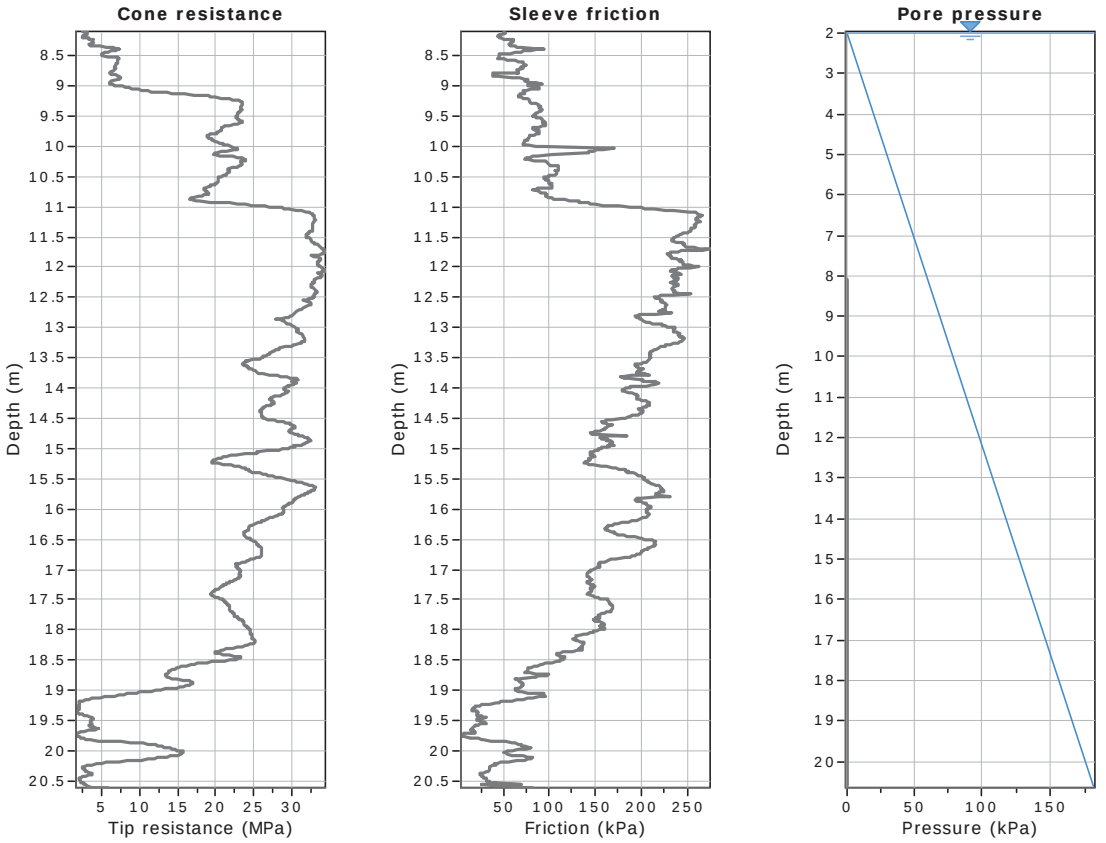

The plot below presents the cross correlation coeficient between the raw qc and fs values (as measured on the field). X axes presents the lag distance (one lag is the distance between two sucessive CPT measurements).

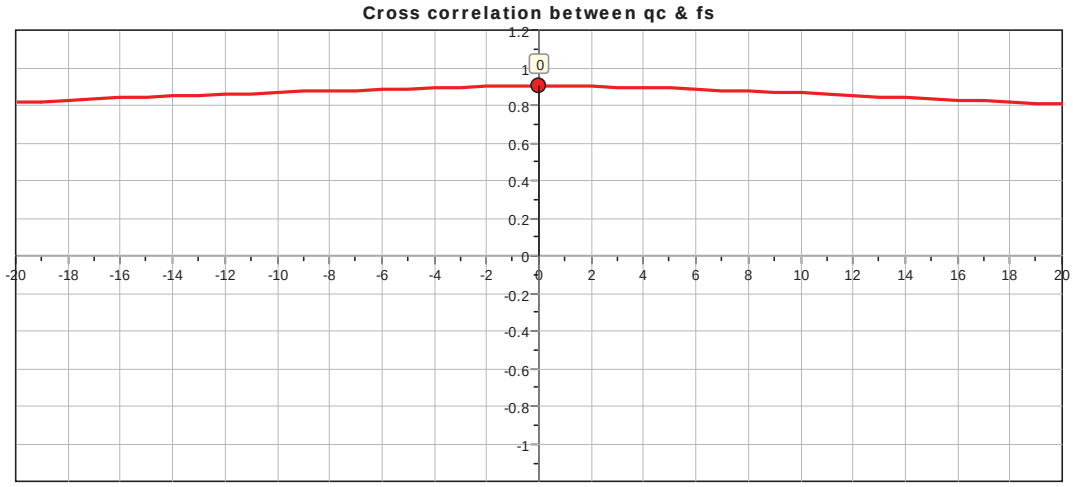

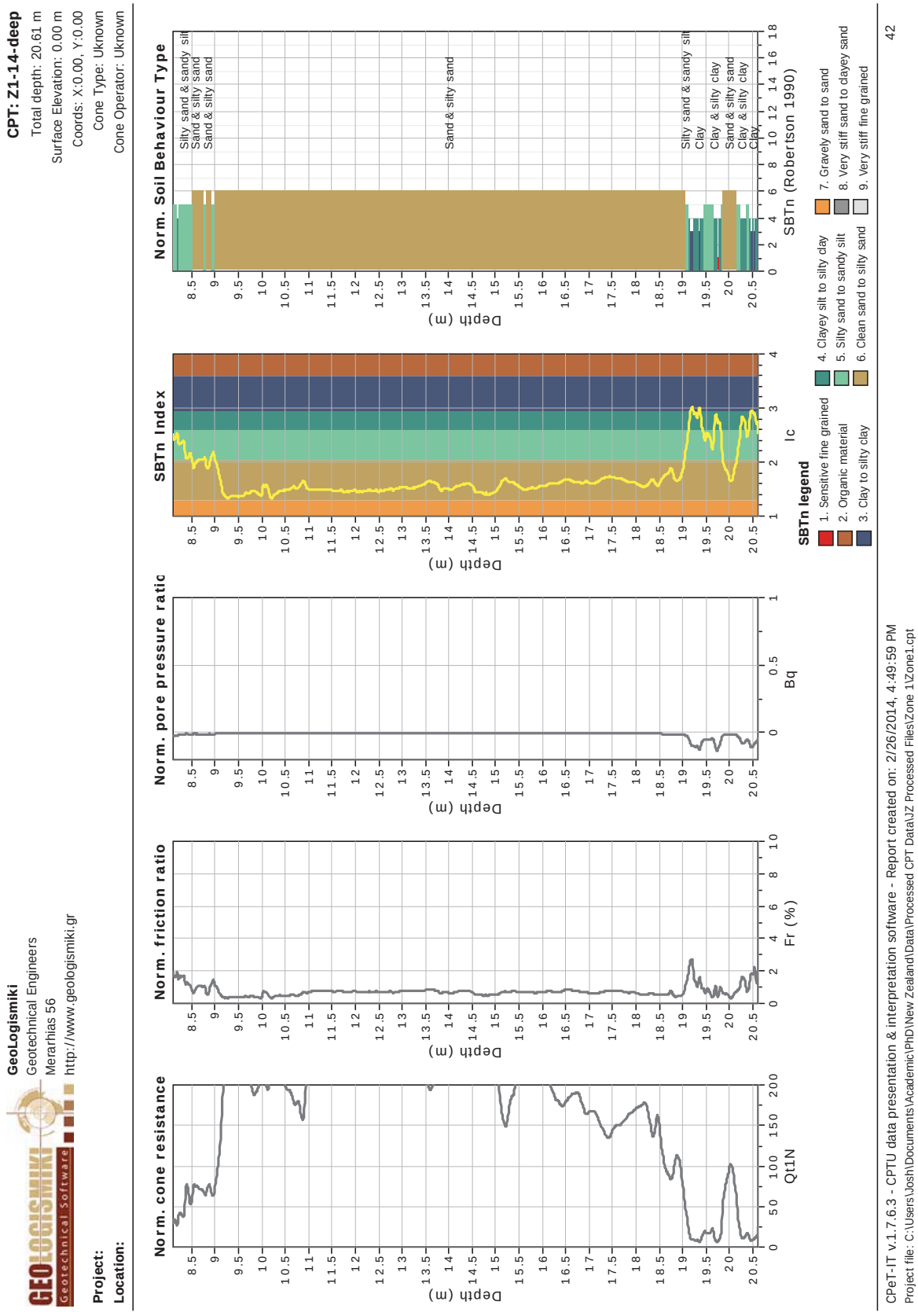
GeoLogismiki
Geotechnical Engineers
Merarchias 56
http://www.geologismiki.gr
Project:
Location:
CPT: Z1-14-deep
Total depth: 20.61 m
Surface Elevation: 0.00 m
Coords: X:0.00, Y:0.00
Cone Type: Uknown
Cone Operator: Uknown
Norm. cone resistance
Qt1N
Norm. friction ratio
Fr (%)
Norm. pore pressure ratio
Bq
SBTn Index
Ic
Norm. Soil Behaviour Type
SBTn (Robertson 1990)
Depth (m)
Silty sand & sandy silt
Sand & silty sand
Sand & silty sand
Sand & silty sand
Silty sand & sandy silt
Clay
Clay & silty clay
Sand & silty sand
Clay & silty clay
Clay
SBTn legend
1. Sensitive fine grained
2. Organic material
3. Clay to silty clay
4. Clayey silt to silty clay
5. Silty sand to sandy silt
6. Clean sand to silty sand
7. Gravely sand to sand
8. Very stiff sand to clayey sand
9. Very stiff fine grained
CPeT-IT v.1.7.6.3 - CPTU data presentation & interpretation software - Report created on: 2/26/2014, 4:49:59 PM
Project file: C:\Users\Josh\Documents\Academic\PhD\New Zealand\Data\Processed CPT Data\JZ Processed Files\Zone 1\Zone1.cpt
42

GeoLogismiki
Geotechnical Engineers
Merarhias 56
http://www.geologismiki.gr

CPT: Z1-15
Total depth: 20.70 m
Surface Elevation: 0.00 m
Coords: X:0.00, Y:0.00
Cone Type: Uknown
Cone Operator: Uknown

Project:
Location:

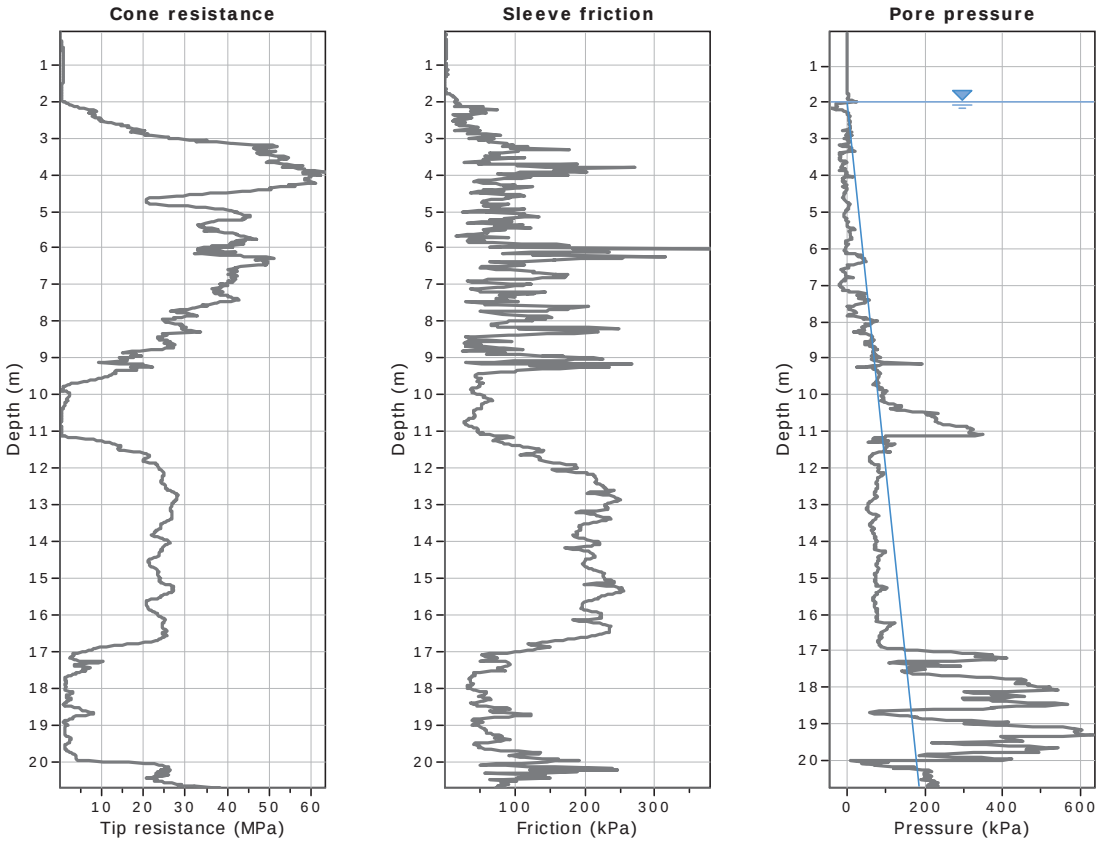

The plot below presents the cross correlation coeficient between the raw qc and fs values (as measured on the field). X axes presents the lag distance (one lag is the distance between two sucessive CPT measurements).

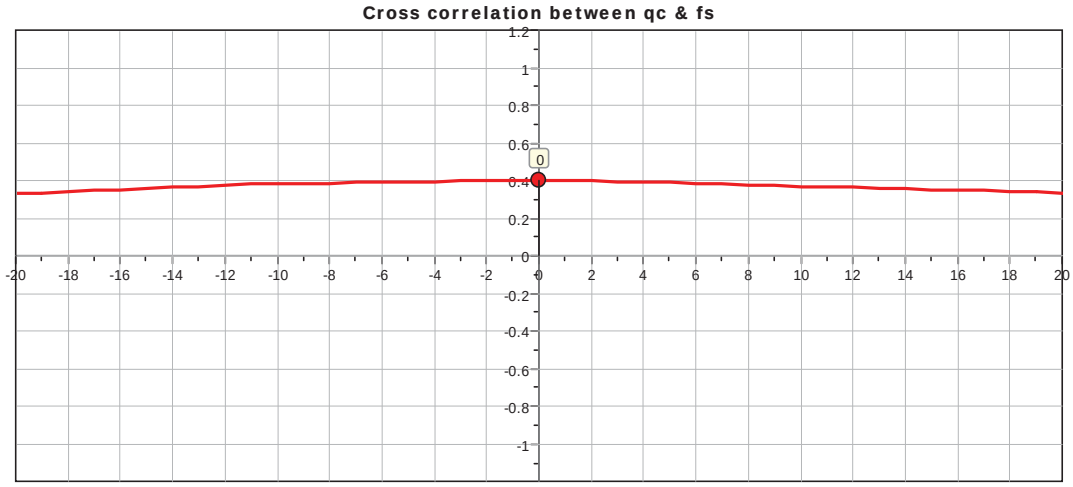

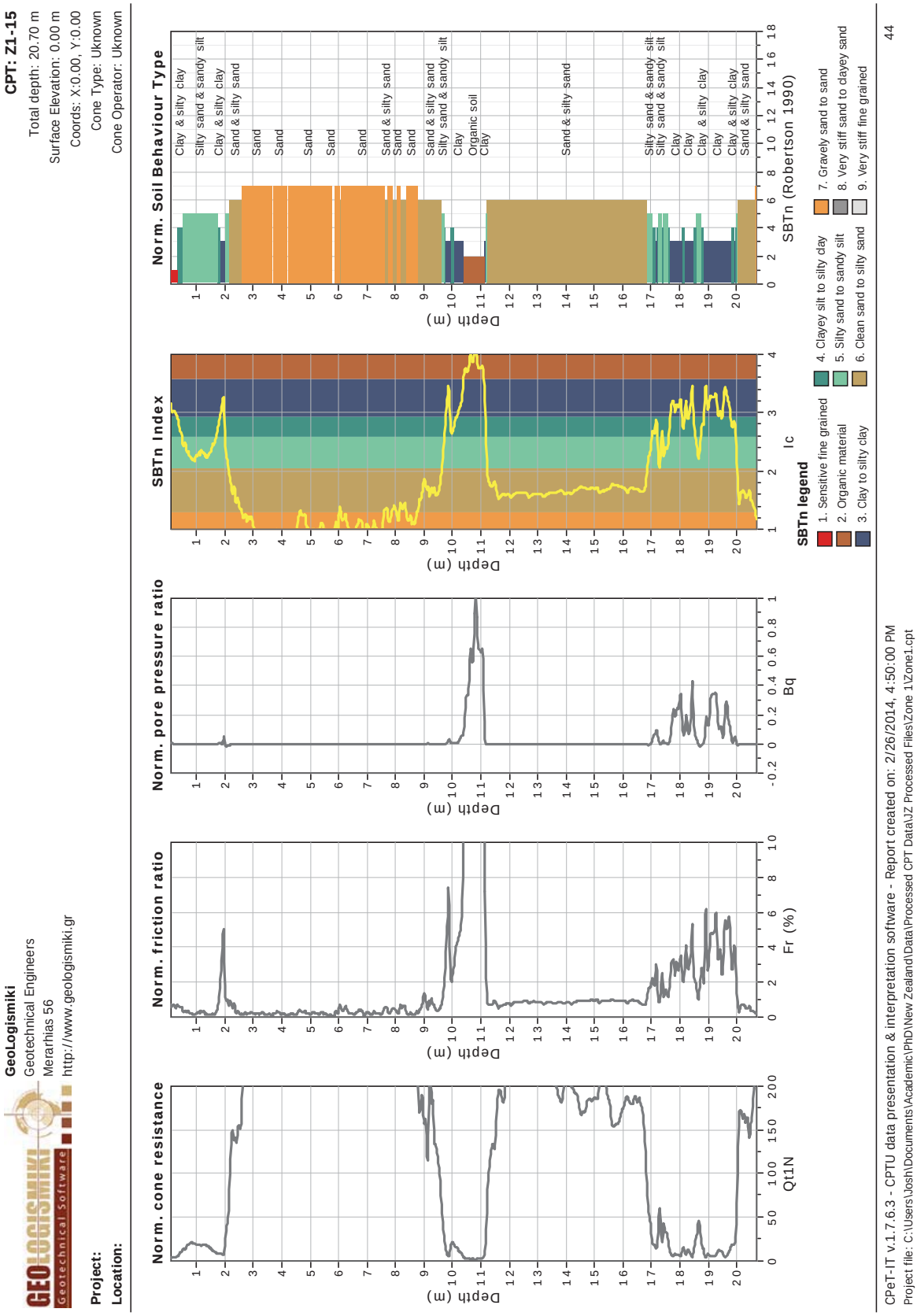
GeoLogismiki
Geotechnical Engineers
Merarhias 56
http://www.geologismiki.gr
Project:
Location:
CPT: Z1-15
Total depth: 20.70 m
Surface Elevation: 0.00 m
Coords: X:0.00, Y:0.00
Cone Type: Uknown
Cone Operator: Uknown
Norm. cone resistance
Qt1N
Norm. friction ratio
Fr (%)
Norm. pore pressure ratio
Bq
SBTn Index
Ic
Norm. Soil Behaviour Type
SBTn (Robertson 1990)
Depth (m)
SBTn legend
1. Sensitive fine grained
2. Organic material
3. Clay to silty clay
4. Clayey silt to silty clay
5. Silty sand to sandy silt
6. Clean sand to silty sand
7. Gravely sand to sand
8. Very stiff sand to clayey sand
9. Very stiff fine grained
CPeT-IT v.1.7.6.3 - CPTU data presentation & interpretation software - Report created on: 2/26/2014, 4:50:00 PM
Project file: C:\Users\Josh\Documents\Academic\PhD\New Zealand\Data\Processed CPT Data\JZ Processed Files\Zone 1\Zone1.cpt
44

GeoLogismiki
Geotechnical Engineers
Merarhias 56
http://www.geologismiki.gr

CPT: Z2-1
Total depth: 9.76 m
Surface Elevation: 0.00 m
Coords: X:0.00, Y:0.00
Cone Type: Uknown
Cone Operator: Uknown

Project: **Liquefaction and Its Effects on Buildings and Lifelines in the February 22, 2011 Christchurch Earthquake**
Location: **Christchurch CBD Zone 1**

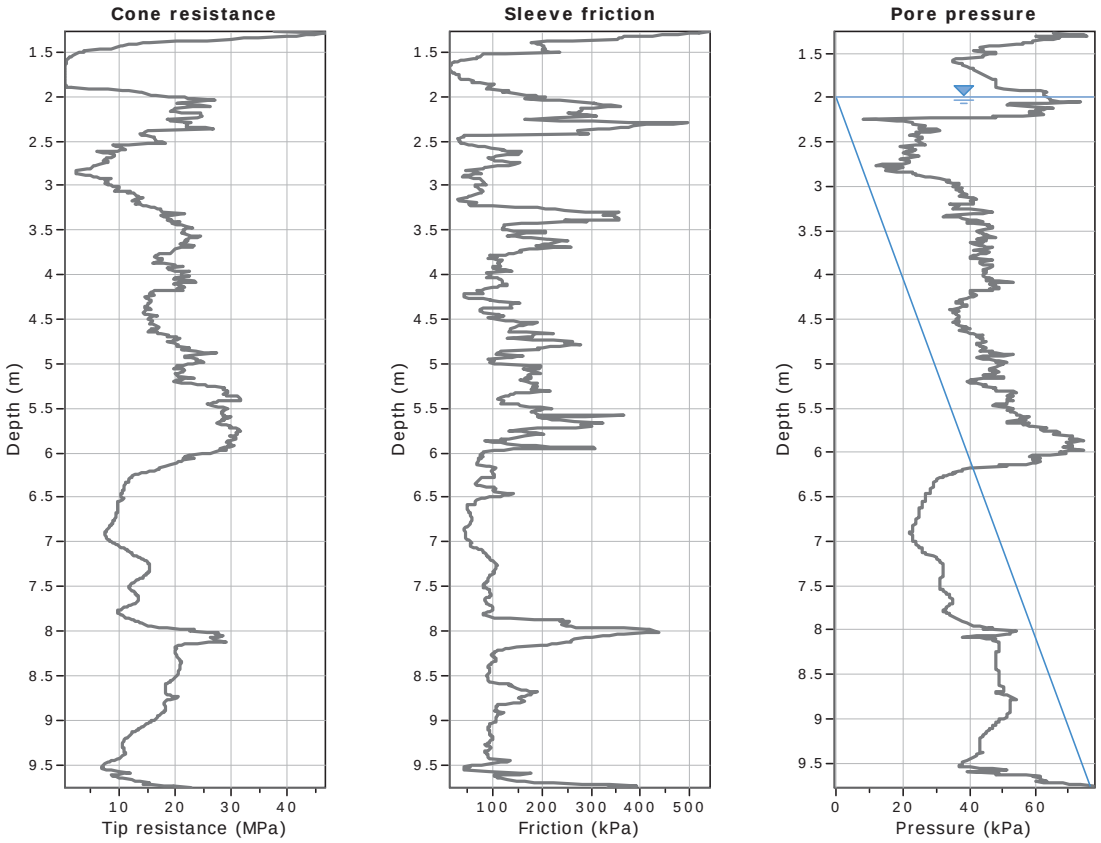

The plot below presents the cross correlation coeficient between the raw qc and fs values (as measured on the field). X axes presents the lag distance (one lag is the distance between two sucessive CPT measurements).

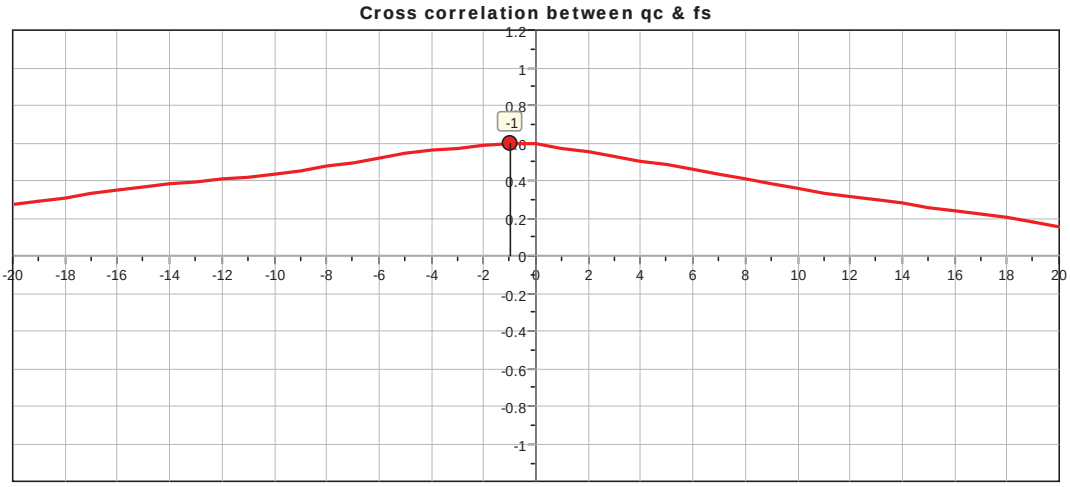

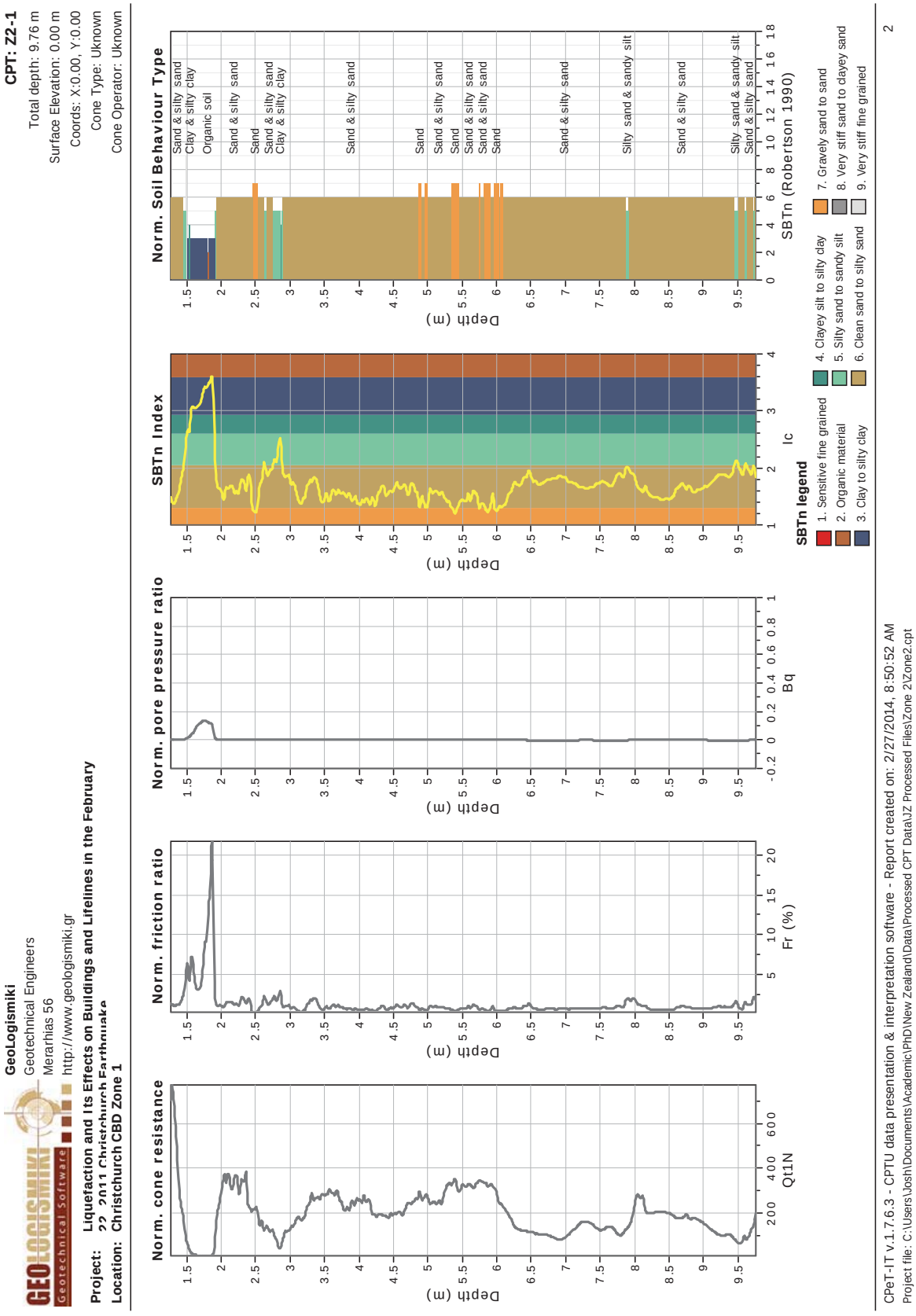
GeoLogismiki
Geotechnical Engineers
Merarhias 56
http://www.geologismiki.gr
Project: Liquefaction and Its Effects on Buildings and Lifelines in the February 22, 2011 Christchurch Earthquake
Location: Christchurch CBD Zone 1
CPT: Z2-1
Total depth: 9.76 m
Surface Elevation: 0.00 m
Coords: X:0.00, Y:0.00
Cone Type: Uknown
Cone Operator: Uknown
Norm. cone resistance
Norm. friction ratio
Norm. pore pressure ratio
SBTn Index
Norm. Soil Behaviour Type
Depth (m)
Qt1N
Fr (%)
Bq
Ic
SBTn (Robertson 1990)
Sand & silty sand
Clay & silty clay
Organic soil
Sand
Silty sand & sandy silt
SBTn legend
1. Sensitive fine grained
2. Organic material
3. Clay to silty clay
4. Clayey silt to silty clay
5. Silty sand to sandy silt
6. Clean sand to silty sand
7. Gravely sand to sand
8. Very stiff sand to clayey sand
9. Very stiff fine grained
CPeT-IT v.1.7.6.3 - CPTU data presentation & interpretation software - Report created on: 2/27/2014, 8:50:52 AM
Project file: C:\Users\Josh\Documents\Academic\PhD\New Zealand\Data\Processed CPT Data\JZ Processed Files\Zone 2\Zone2.cpt
2

GeoLogismiki
Geotechnical Engineers
Merarhias 56
http://www.geologismiki.gr

CPT: Z2-2
Total depth: 2.43 m
Surface Elevation: 0.00 m
Coords: X:0.00, Y:0.00
Cone Type: Uknown
Cone Operator: Uknown

Project: **Liquefaction and Its Effects on Buildings and Lifelines in the February 22, 2011 Christchurch Earthquake**
Location: **Christchurch CBD Zone 1**

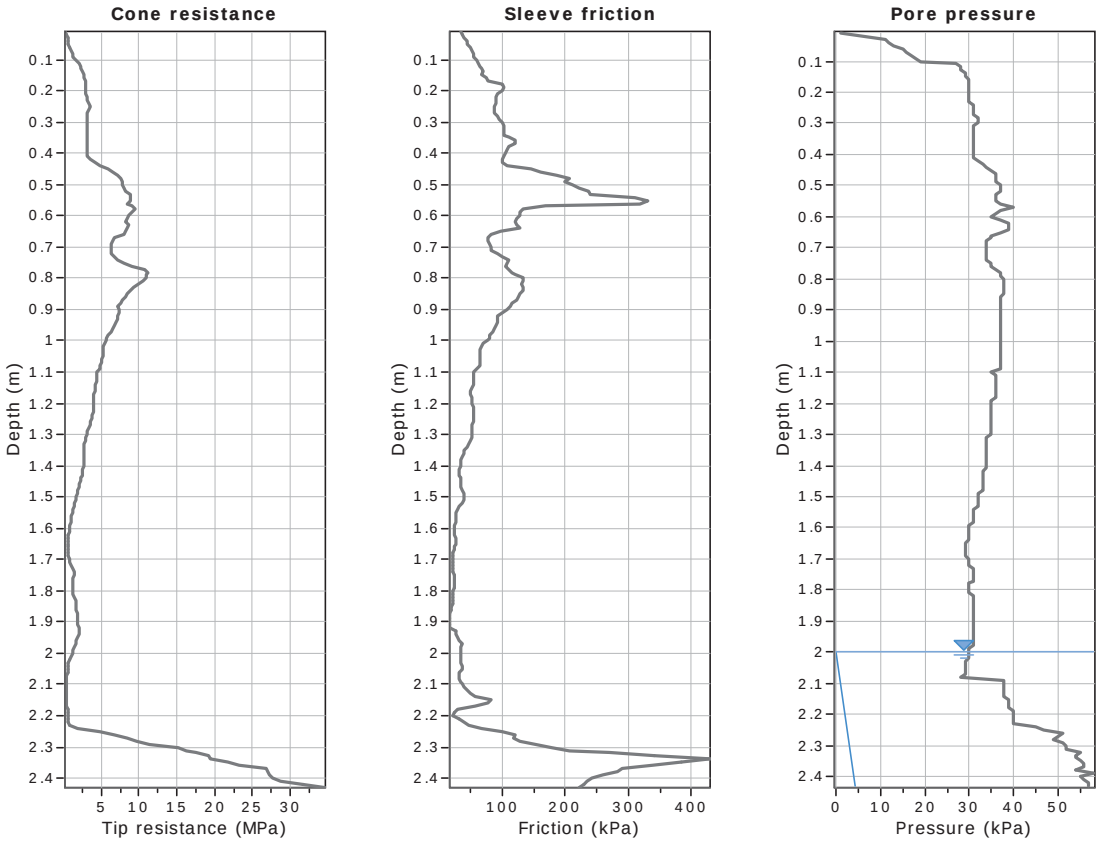

The plot below presents the cross correlation coeficient between the raw qc and fs values (as measured on the field). X axes presents the lag distance (one lag is the distance between two sucessive CPT measurements).

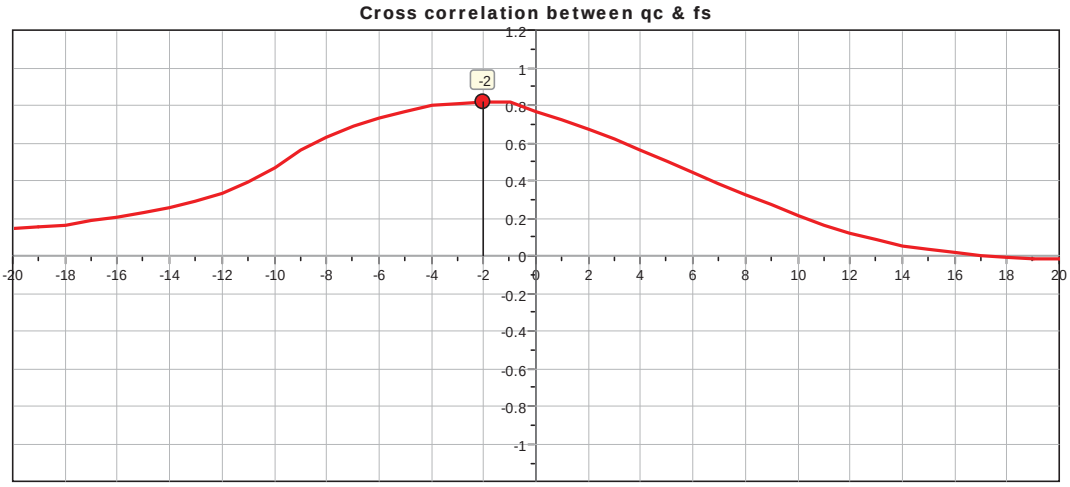

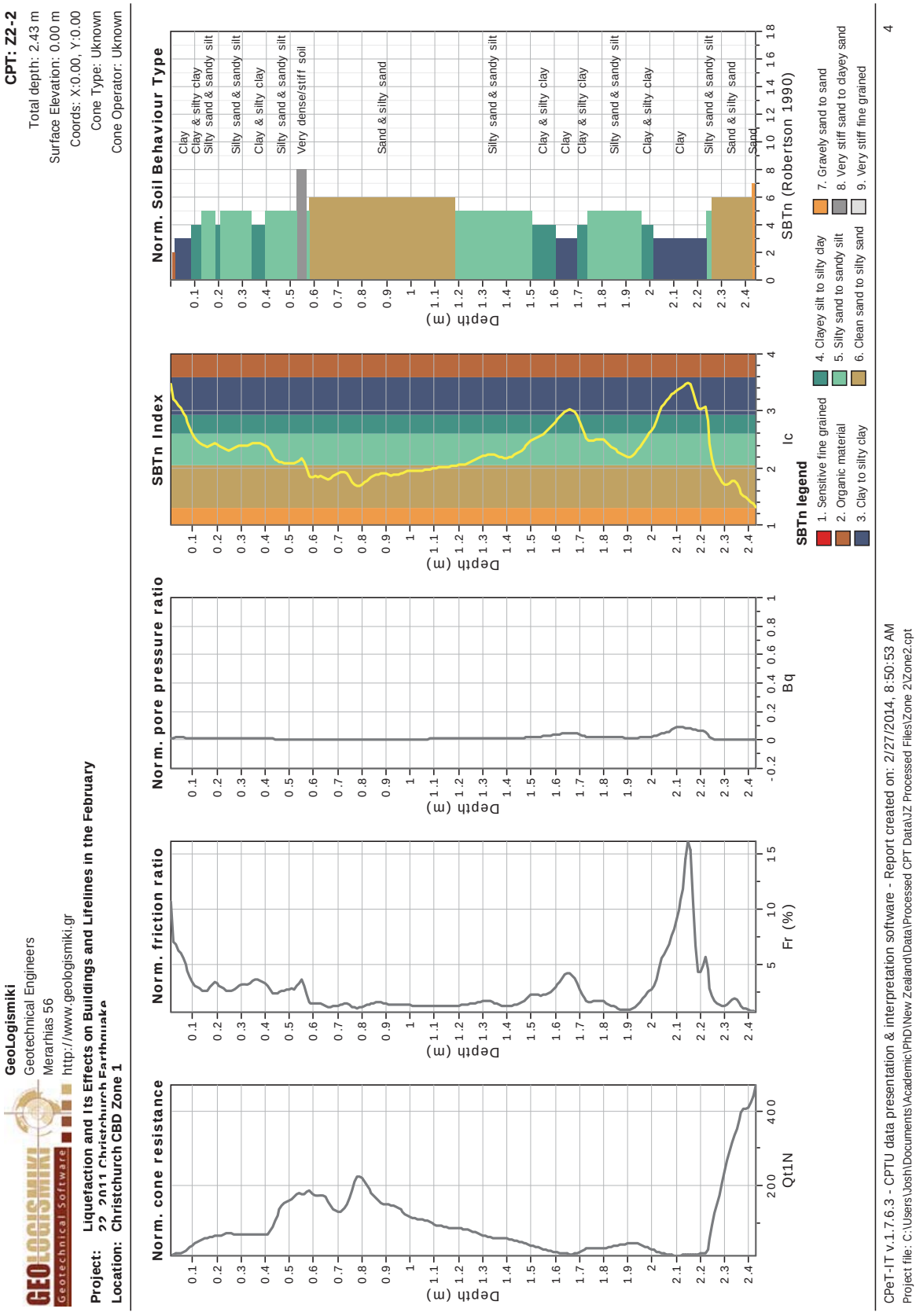
GeoLogismiki
Geotechnical Engineers
Merarhias 56
http://www.geologismiki.gr
Project: Liquefaction and Its Effects on Buildings and Lifelines in the February 22, 2011 Christchurch Earthquake
Location: Christchurch CBD Zone 1
CPT: Z2-2
Total depth: 2.43 m
Surface Elevation: 0.00 m
Coords: X:0.00, Y:0.00
Cone Type: Uknown
Cone Operator: Uknown
Norm. cone resistance
Norm. friction ratio
Norm. pore pressure ratio
SBTn Index
Norm. Soil Behaviour Type
Depth (m)
Qt1N
Fr (%)
Bq
Ic
SBTn (Robertson 1990)
Clay
Clay & silty clay
Silty sand & sandy silt
Clay & silty clay
Silty sand & sandy silt
Very dense/stiff soil
Sand & silty sand
Silty sand & sandy silt
Clay & silty clay
Clay
Clay & silty clay
Silty sand & sandy silt
Clay & silty clay
Clay
Silty sand & sandy silt
Sand & silty sand
Sand
SBTn legend
1. Sensitive fine grained
2. Organic material
3. Clay to silty clay
4. Clayey silt to silty clay
5. Silty sand to sandy silt
6. Clean sand to silty sand
7. Gravely sand to sand
8. Very stiff sand to clayey sand
9. Very stiff fine grained
CPeT-IT v.1.7.6.3 - CPTU data presentation & interpretation software - Report created on: 2/27/2014, 8:50:53 AM
Project file: C:\Users\Josh\Documents\Academic\PhD\New Zealand\Data\Processed CPT Data\JZ Processed Files\Zone 2\Zone2.cpt
4

GeoLogismiki
Geotechnical Engineers
Merarhias 56
http://www.geologismiki.gr

CPT: Z2-4
Total depth: 3.36 m
Surface Elevation: 0.00 m
Coords: X:0.00, Y:0.00
Cone Type: Uknown
Cone Operator: Uknown

Project: **Liquefaction and Its Effects on Buildings and Lifelines in the February 22, 2011 Christchurch Earthquake**
Location: **Christchurch CBD Zone 1**

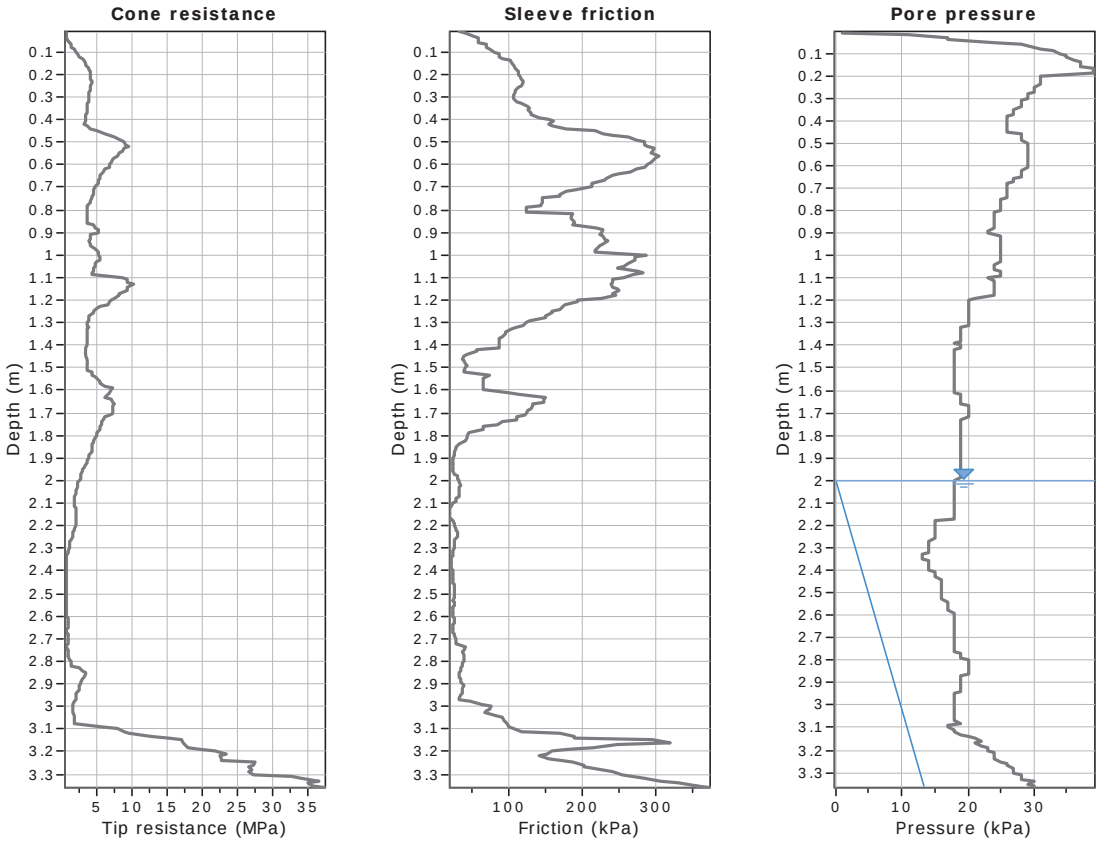

The plot below presents the cross correlation coeficient between the raw qc and fs values (as measured on the field). X axes presents the lag distance (one lag is the distance between two sucessive CPT measurements).

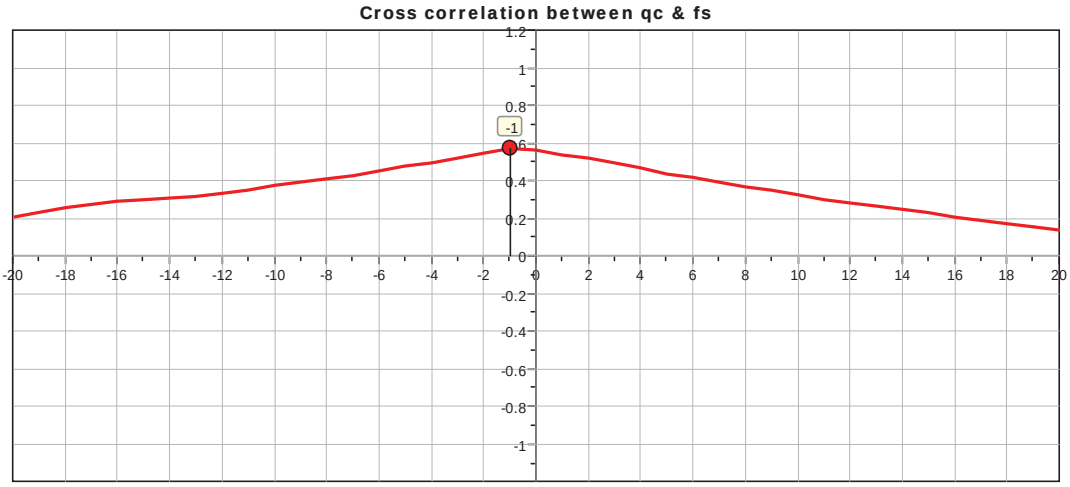

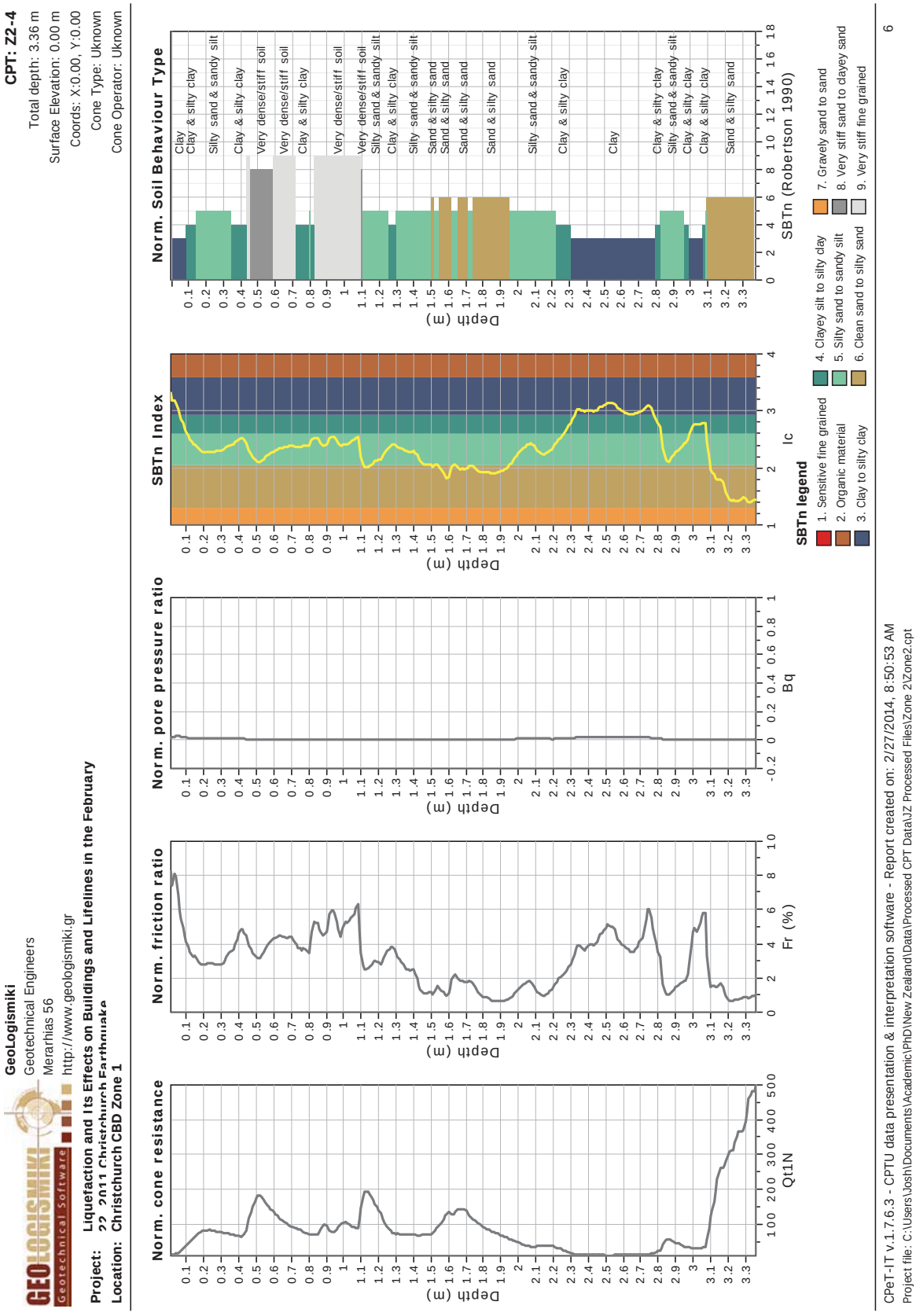
GeoLogismiki
Geotechnical Engineers
Merarchias 56
http://www.geologismiki.gr
Project: Liquefaction and Its Effects on Buildings and Lifelines in the February 22, 2011 Christchurch Earthquake
Location: Christchurch CBD Zone 1
CPT: Z2-4
Total depth: 3.36 m
Surface Elevation: 0.00 m
Coords: X:0.00, Y:0.00
Cone Type: Uknown
Cone Operator: Uknown
Norm. cone resistance
Norm. friction ratio
Norm. pore pressure ratio
SBTn Index
Norm. Soil Behaviour Type
Depth (m)
Qt1N
Fr (%)
Bq
Ic
SBTn (Robertson 1990)
SBTn legend
1. Sensitive fine grained
2. Organic material
3. Clay to silty clay
4. Clayey silt to silty clay
5. Silty sand to sandy silt
6. Clean sand to silty sand
7. Gravelly sand to sand
8. Very stiff sand to clayey sand
9. Very stiff fine grained
CPeT-IT v.1.7.6.3 - CPTU data presentation & interpretation software - Report created on: 2/27/2014, 8:50:53 AM
Project file: C:\Users\Josh\Documents\Academic\PhD\New Zealand\Data\Processed CPT Data\JZ Processed Files\Zone 2\Zone2.cpt
6

GeoLogismiki
Geotechnical Engineers
Merarhias 56
http://www.geologismiki.gr

CPT: Z2-5
Total depth: 2.34 m
Surface Elevation: 0.00 m
Coords: X:0.00, Y:0.00
Cone Type: Uknown
Cone Operator: Uknown

Project: **Liquefaction and Its Effects on Buildings and Lifelines in the February 22, 2011 Christchurch Earthquake**
Location: **Christchurch CBD Zone 1**

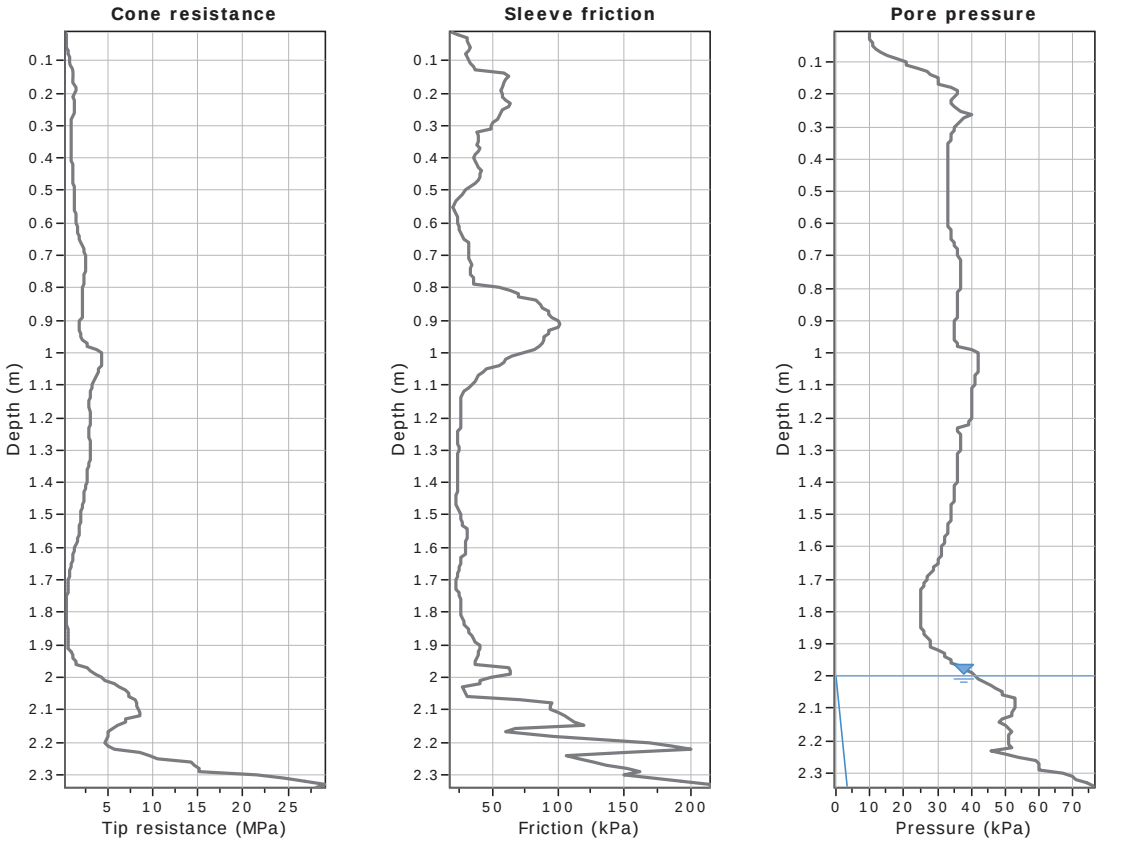

The plot below presents the cross correlation coeficient between the raw qc and fs values (as measured on the field). X axes presents the lag distance (one lag is the distance between two sucessive CPT measurements).

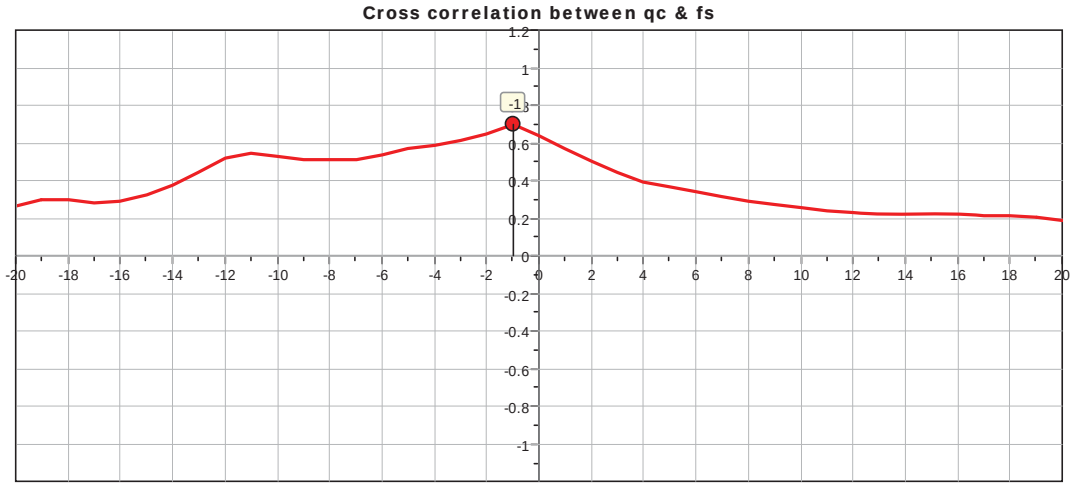

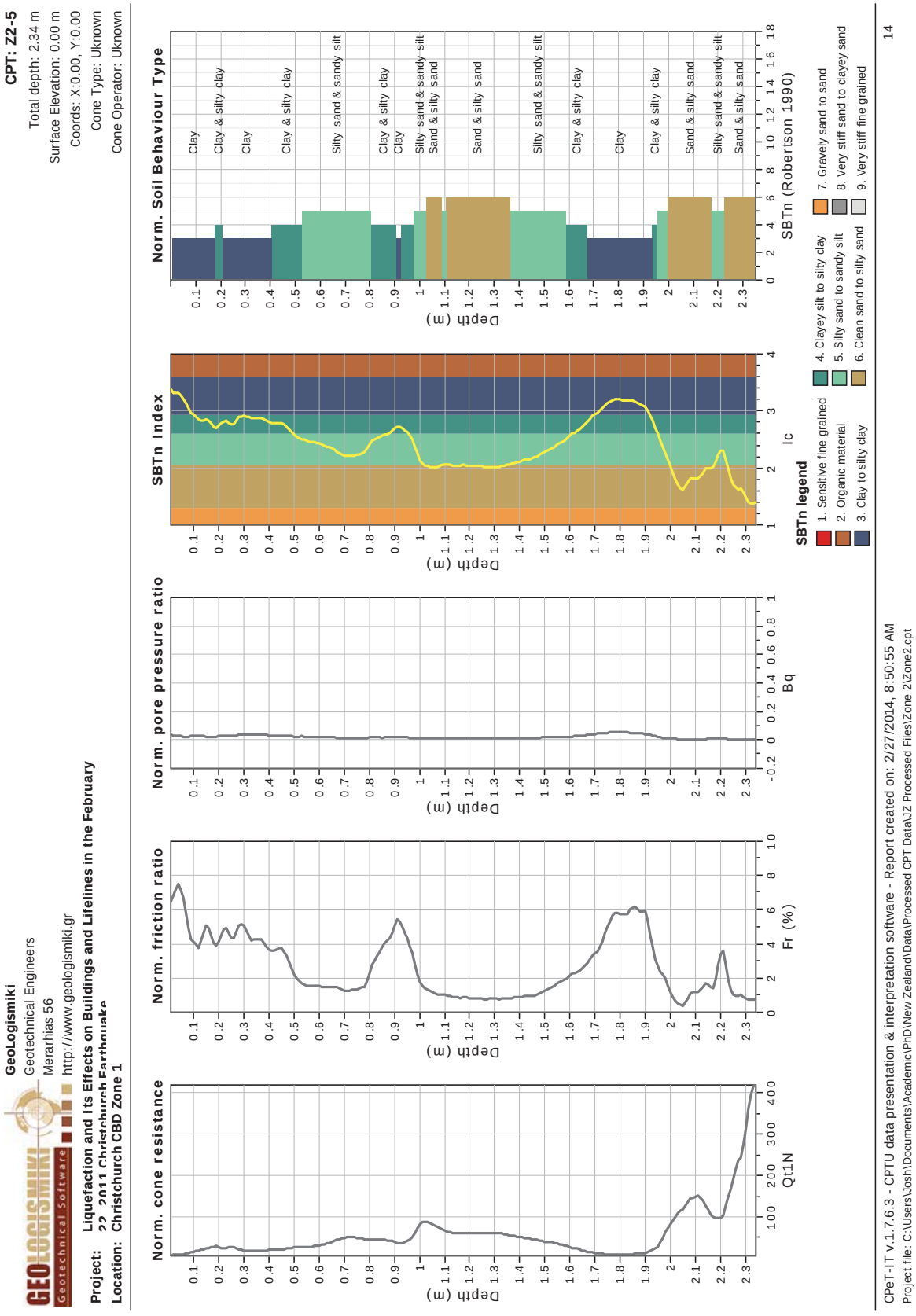
GeoLogismiki
Geotechnical Engineers
Merarchias 56
http://www.geologismiki.gr
Project: Liquefaction and Its Effects on Buildings and Lifelines in the February 22, 2011 Christchurch Earthquake
Location: Christchurch CBD Zone 1
CPT: Z2-5
Total depth: 2.34 m
Surface Elevation: 0.00 m
Coords: X:0.00, Y:0.00
Cone Type: Uknown
Cone Operator: Uknown
Norm. cone resistance
Qt1N
Norm. friction ratio
Fr (%)
Norm. pore pressure ratio
Bq
SBTn Index
Ic
Norm. Soil Behaviour Type
SBTn (Robertson 1990)
Depth (m)
SBTn legend
1. Sensitive fine grained
2. Organic material
3. Clay to silty clay
4. Clayey silt to silty clay
5. Silty sand to sandy silt
6. Clean sand to silty sand
7. Gravely sand to sand
8. Very stiff sand to clayey sand
9. Very stiff fine grained
CPeT-IT v.1.7.6.3 - CPTU data presentation & interpretation software - Report created on: 2/27/2014, 8:50:55 AM
Project file: C:\Users\Josh\Documents\Academic\PhD\New Zealand\Data\Processed CPT Data\JZ Processed Files\Zone 2\Zone2.cpt
14

GeoLogismiki
Geotechnical Engineers
Merarhias 56
http://www.geologismiki.gr

CPT: Z2-6
Total depth: 5.33 m
Surface Elevation: 0.00 m
Coords: X:0.00, Y:0.00
Cone Type: Uknown
Cone Operator: Uknown

Project: **Liquefaction and Its Effects on Buildings and Lifelines in the February 22, 2011 Christchurch Earthquake**
Location: **Christchurch CBD Zone 1**

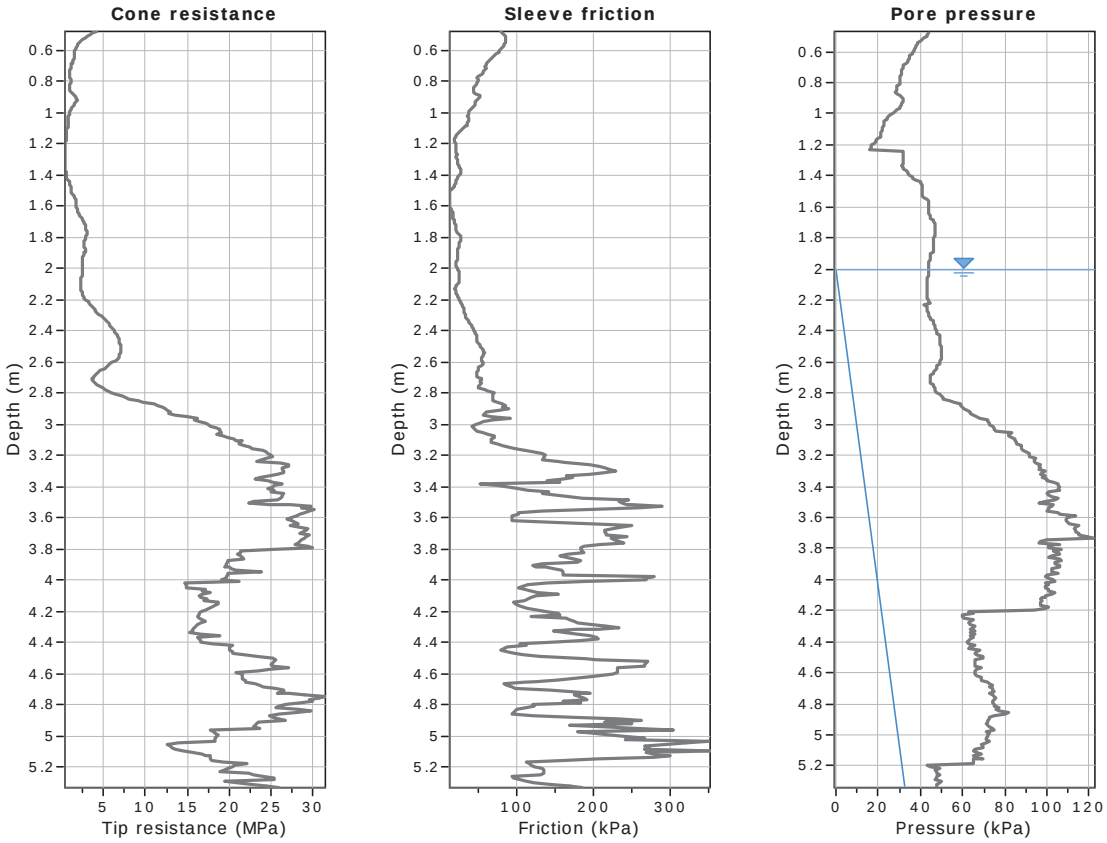

The plot below presents the cross correlation coeficient between the raw qc and fs values (as measured on the field). X axes presents the lag distance (one lag is the distance between two sucessive CPT measurements).

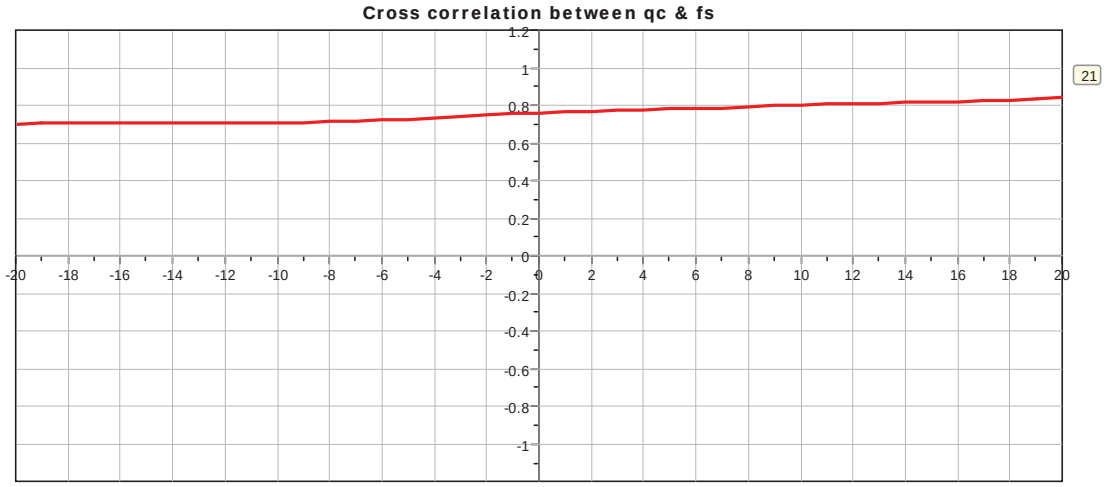

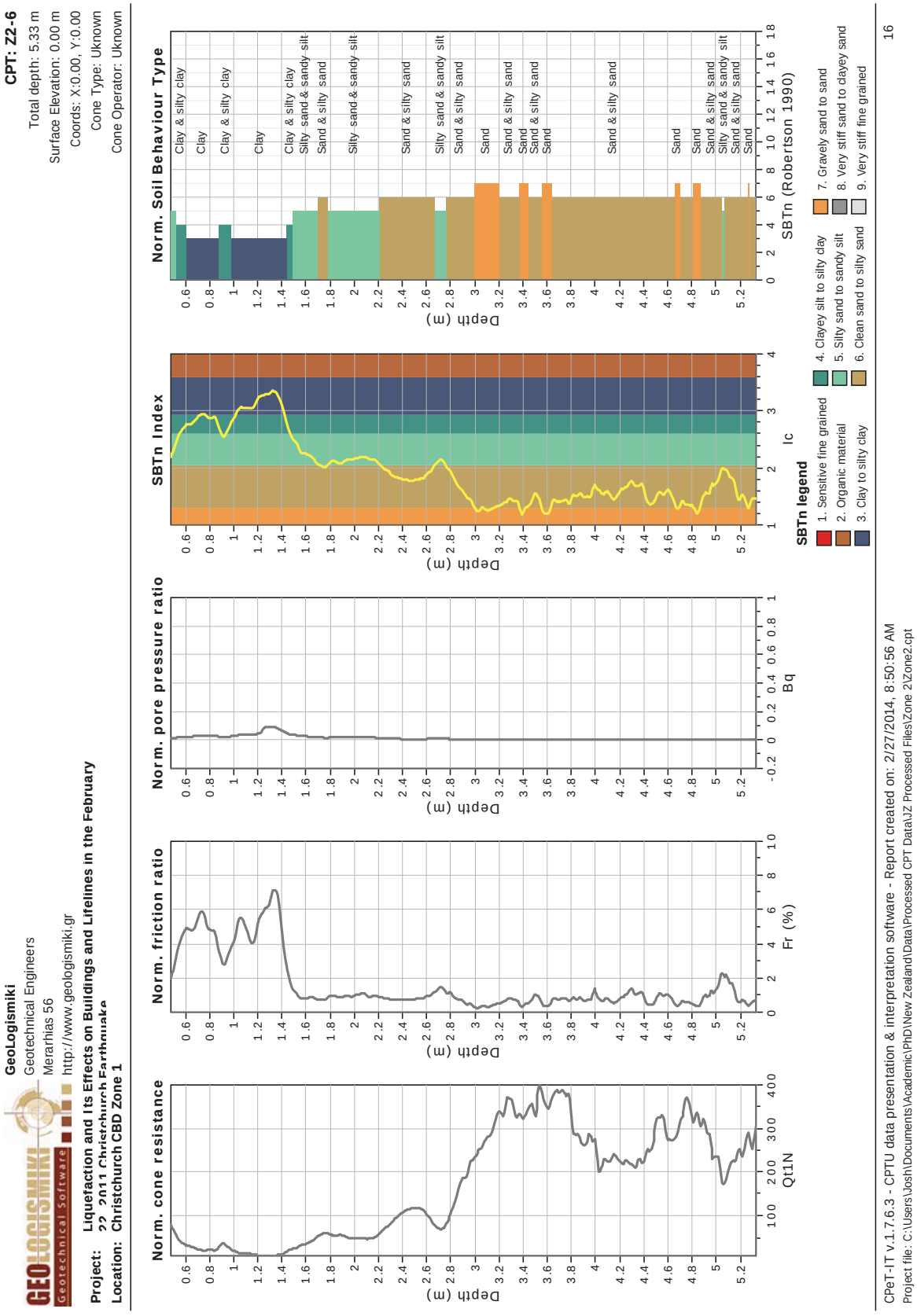
CPT: Z2-6
Total depth: 5.33 m
Surface Elevation: 0.00 m
Coords: X:0.00, Y:0.00
Cone Type: Uknown
Cone Operator: Uknown
GeoLogismiki
Geotechnical Engineers
Merarhias 56
http://www.geologismiki.gr
Project: Liquefaction and Its Effects on Buildings and Lifelines in the February 22 2011 Christchurch Earthquake
Location: Christchurch CBD Zone 1
Norm. cone resistance
Norm. friction ratio
Norm. pore pressure ratio
SBTn Index
Norm. Soil Behaviour Type
Depth (m)
Qt1N
Fr (%)
Bq
Ic
SBTn (Robertson 1990)
SBTn legend
1. Sensitive fine grained
2. Organic material
3. Clay to silty clay
4. Clayey silt to silty clay
5. Silty sand to sandy silt
6. Clean sand to silty sand
7. Gravely sand to sand
8. Very stiff sand to clayey sand
9. Very stiff fine grained
CPeT-IT v.1.7.6.3 - CPTU data presentation & interpretation software - Report created on: 2/27/2014, 8:50:56 AM
Project file: C:\Users\Josh\Documents\Academic\PhD\New Zealand\Data\Processed CPT Data\JZ Processed Files\Zone 2\Zone2.cpt
16

GeoLogismiki
Geotechnical Engineers
Merarhias 56
http://www.geologismiki.gr

CPT: Z2-7
Total depth: 2.95 m
Surface Elevation: 0.00 m
Coords: X:0.00, Y:0.00
Cone Type: Uknown
Cone Operator: Uknown

Project: **Liquefaction and Its Effects on Buildings and Lifelines in the February 22, 2011 Christchurch Earthquake**
Location: **Christchurch CBD Zone 1**

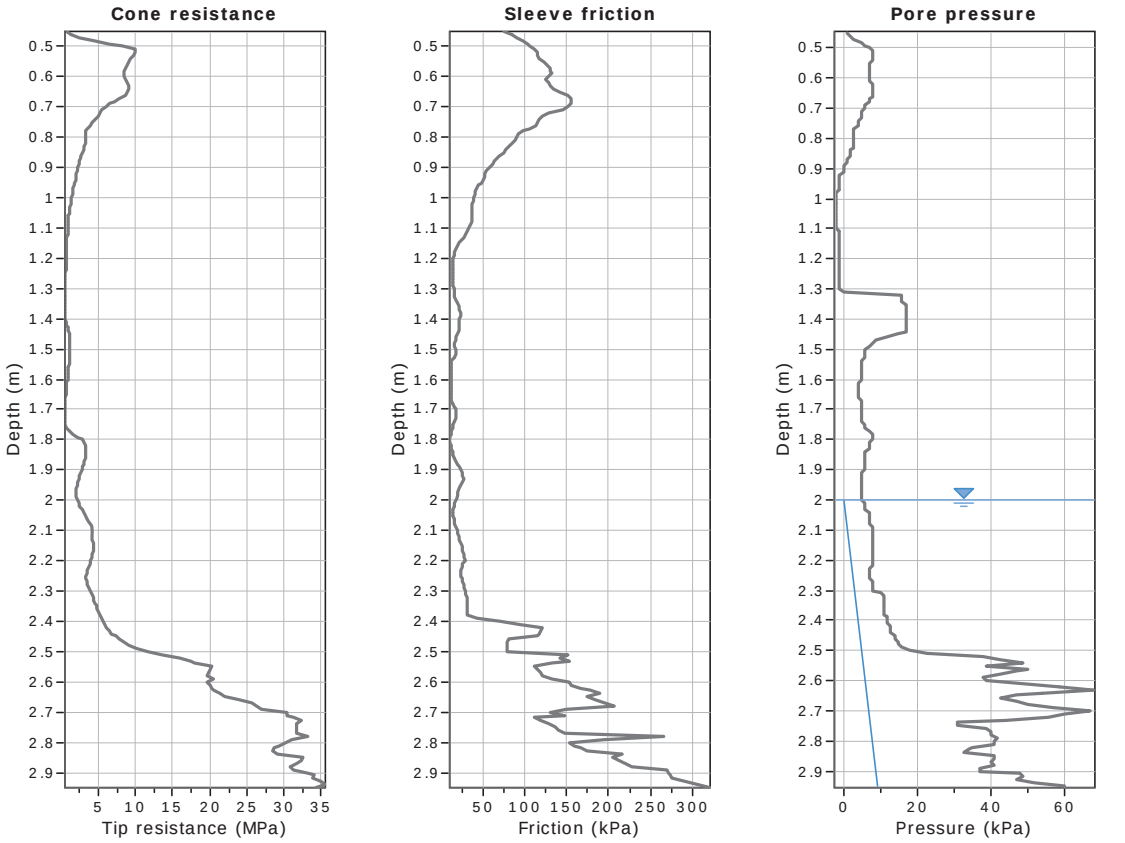

The plot below presents the cross correlation coeficient between the raw qc and fs values (as measured on the field). X axes presents the lag distance (one lag is the distance between two sucessive CPT measurements).

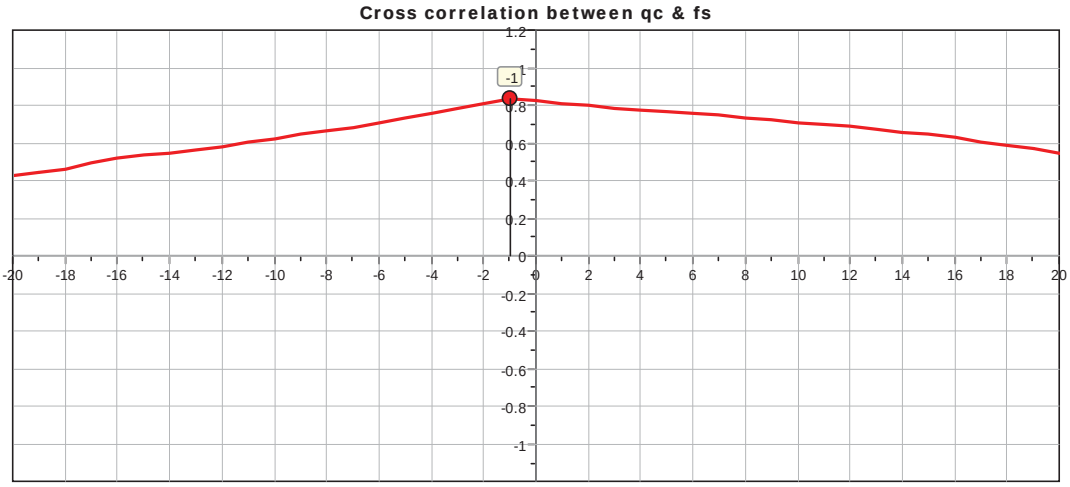

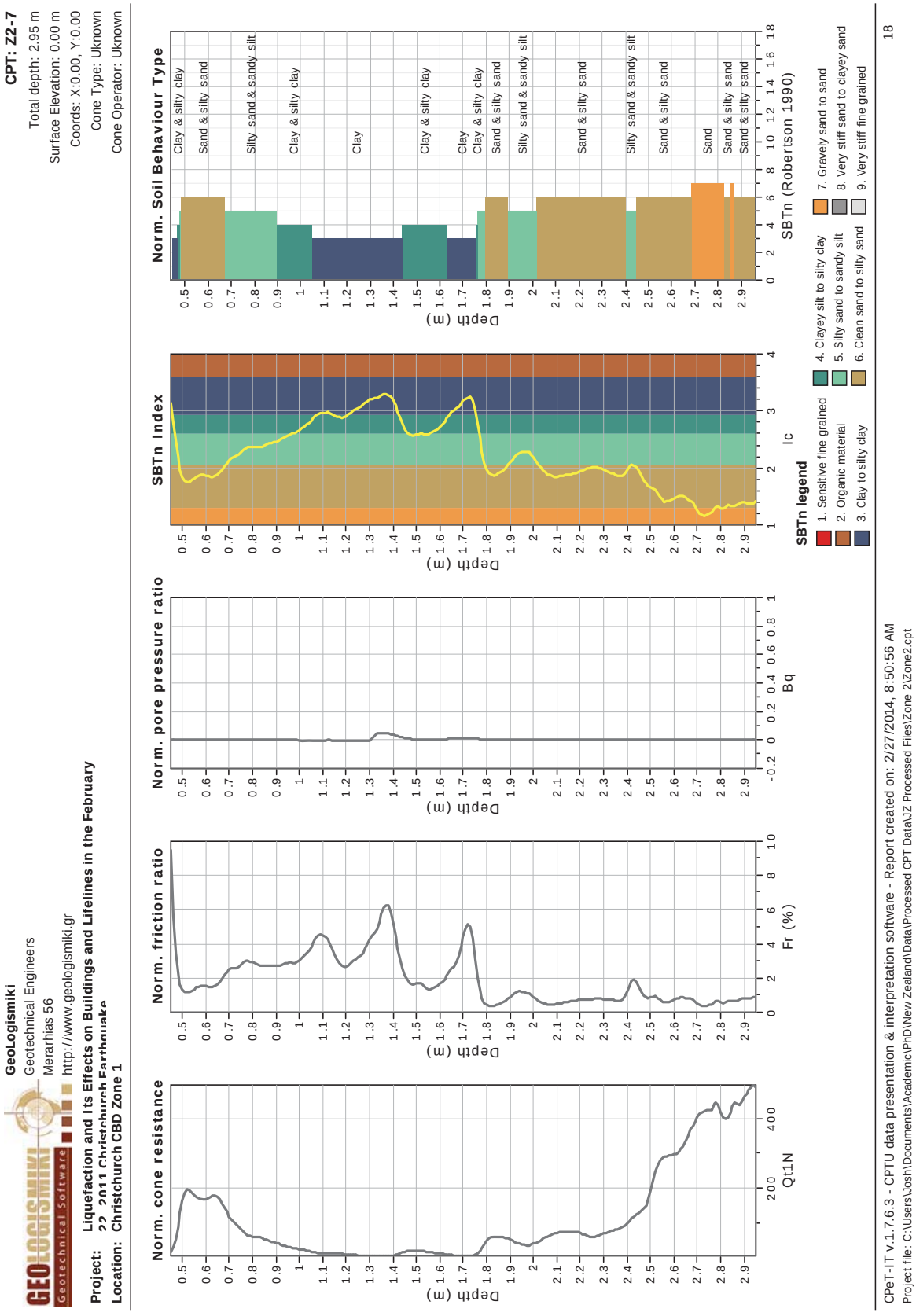
GeoLogismiki
Geotechnical Engineers
Merarchias 56
http://www.geologismiki.gr
Project: Liquefaction and Its Effects on Buildings and Lifelines in the February 22, 2011 Christchurch Earthquake
Location: Christchurch CBD Zone 1
CPT: Z2-7
Total depth: 2.95 m
Surface Elevation: 0.00 m
Coords: X:0.00, Y:0.00
Cone Type: Uknown
Cone Operator: Uknown
Norm. cone resistance
Norm. friction ratio
Norm. pore pressure ratio
SBTn Index
Norm. Soil Behaviour Type
Depth (m)
Qt1N
Fr (%)
Bq
Ic
SBTn (Robertson 1990)
Clay & silty clay
Sand & silty sand
Silty sand & sandy silt
Clay & silty clay
Clay
Clay & silty clay
Clay
Clay & silty clay
Sand & silty sand
Silty sand & sandy silt
Sand & silty sand
Silty sand & sandy silt
Sand & silty sand
Sand
Sand & silty sand
Sand & silty sand
SBTn legend
1. Sensitive fine grained
2. Organic material
3. Clay to silty clay
4. Clayey silt to silty clay
5. Silty sand to sandy silt
6. Clean sand to silty sand
7. Gravely sand to sand
8. Very stiff sand to clayey sand
9. Very stiff fine grained
CPeT-IT v.1.7.6.3 - CPTU data presentation & interpretation software - Report created on: 2/27/2014, 8:50:56 AM
Project file: C:\Users\Josh\Documents\Academic\PhD\New Zealand\Data\Processed CPT Data\JZ Processed Files\Zone 2\Zone2.cpt
18

GeoLogismiki
Geotechnical Engineers
Merarhias 56
http://www.geologismiki.gr

CPT: Z2-8
Total depth: 3.32 m
Surface Elevation: 0.00 m
Coords: X:0.00, Y:0.00
Cone Type: Uknown
Cone Operator: Uknown

Project: **Liquefaction and Its Effects on Buildings and Lifelines in the February 22, 2011 Christchurch Earthquake**
Location: **Christchurch CBD Zone 1**

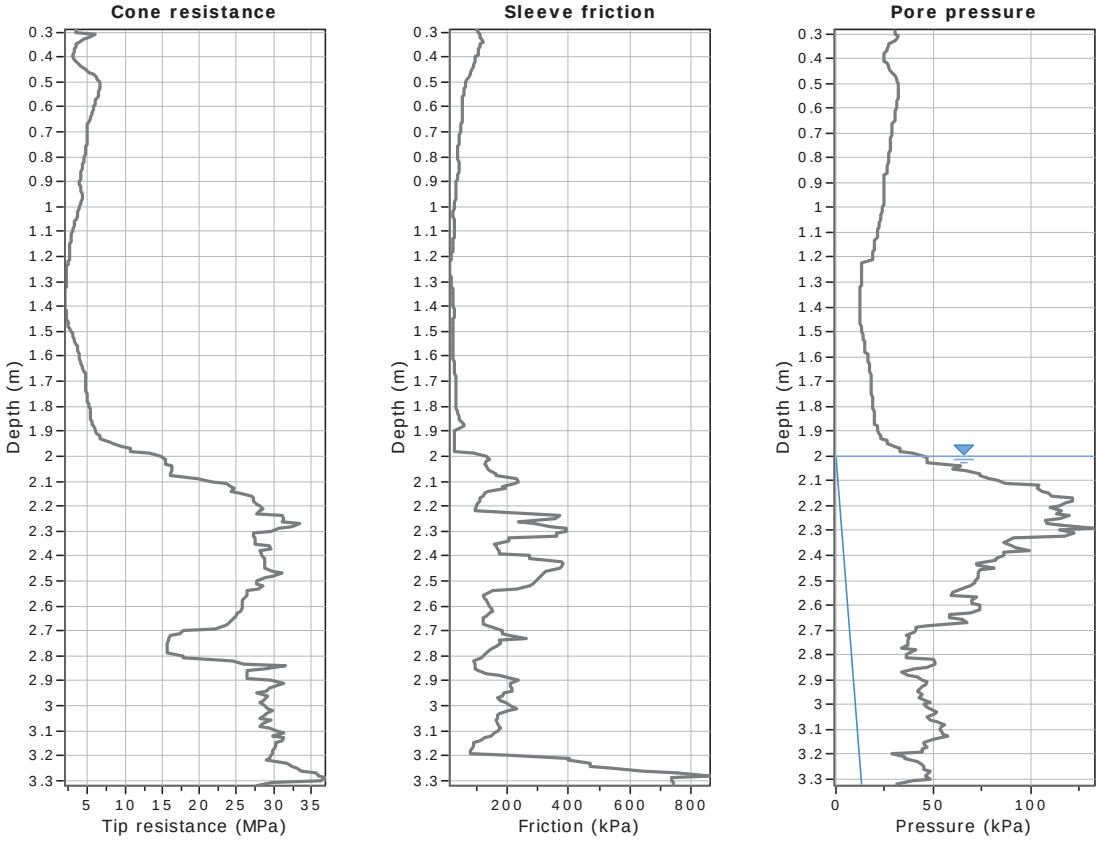

The plot below presents the cross correlation coeficient between the raw qc and fs values (as measured on the field). X axes presents the lag distance (one lag is the distance between two sucessive CPT measurements).

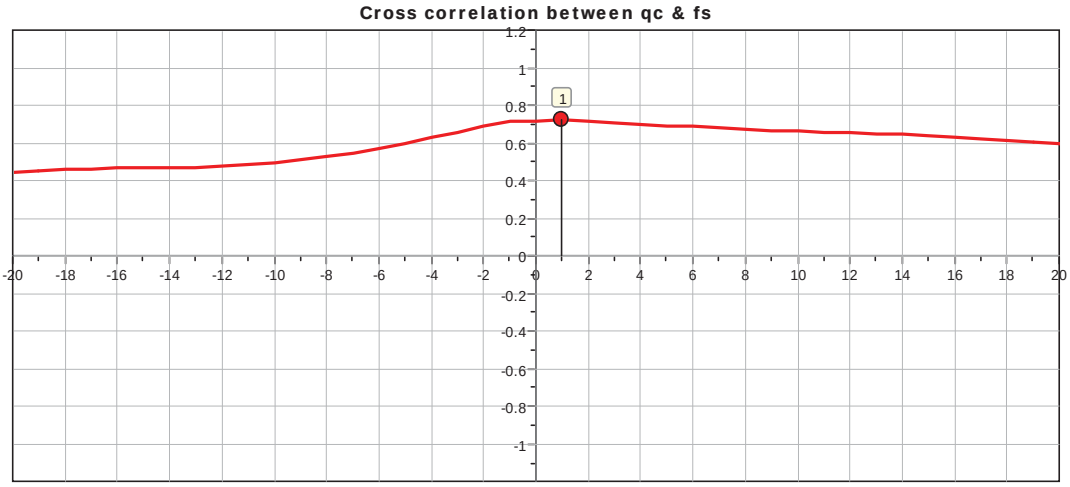

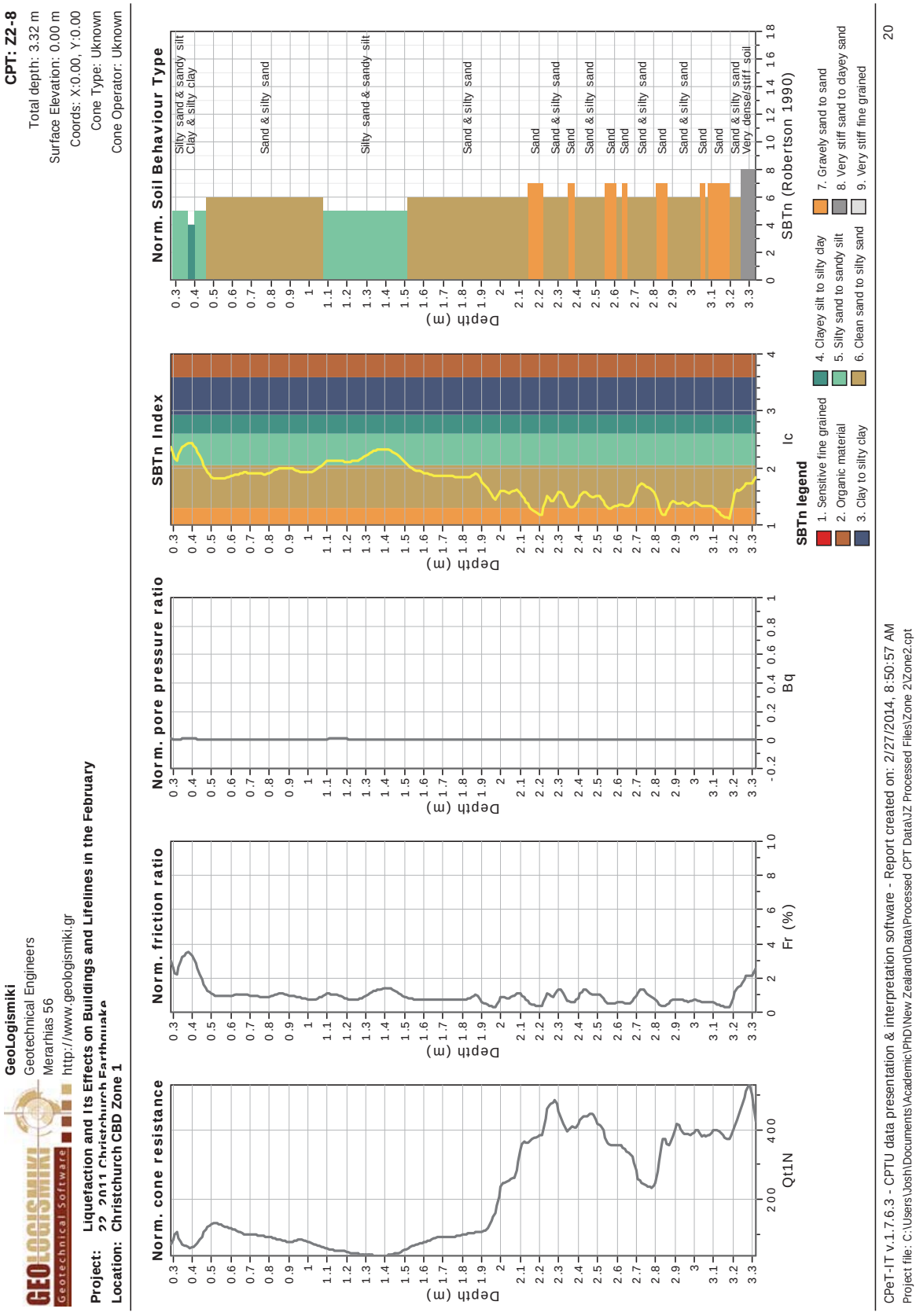
GeoLogismiki
Geotechnical Engineers
Merarhias 56
http://www.geologismiki.gr
Project: Liquefaction and Its Effects on Buildings and Lifelines in the February 22, 2011 Christchurch Earthquake
Location: Christchurch CBD Zone 1
CPT: Z2-8
Total depth: 3.32 m
Surface Elevation: 0.00 m
Coords: X:0.00, Y:0.00
Cone Type: Uknown
Cone Operator: Uknown
Norm. cone resistance
Norm. friction ratio
Norm. pore pressure ratio
SBTn Index
Norm. Soil Behaviour Type
Depth (m)
Qt1N
Fr (%)
Bq
Ic
SBTn (Robertson 1990)
Silty sand & sandy silt
Clay & silty clay
Sand & silty sand
Silty sand & sandy silt
Sand & silty sand
Sand
Very dense/stiff soil
SBTn legend
1. Sensitive fine grained
2. Organic material
3. Clay to silty clay
4. Clayey silt to silty clay
5. Silty sand to sandy silt
6. Clean sand to silty sand
7. Gravely sand to sand
8. Very stiff sand to clayey sand
9. Very stiff fine grained
CPeT-IT v.1.7.6.3 - CPTU data presentation & interpretation software - Report created on: 2/27/2014, 8:50:57 AM
Project file: C:\Users\Josh\Documents\Academic\PhD\New Zealand\Data\Processed CPT Data\JZ Processed Files\Zone 2\Zone2.cpt
20

GeoLogismiki
Geotechnical Engineers
Merarhias 56
http://www.geologismiki.gr

CPT: Z2-9
Total depth: 2.09 m
Surface Elevation: 0.00 m
Coords: X:0.00, Y:0.00
Cone Type: Uknown
Cone Operator: Uknown

Project: **Liquefaction and Its Effects on Buildings and Lifelines in the February 22, 2011 Christchurch Earthquake**
Location: **Christchurch CBD Zone 1**

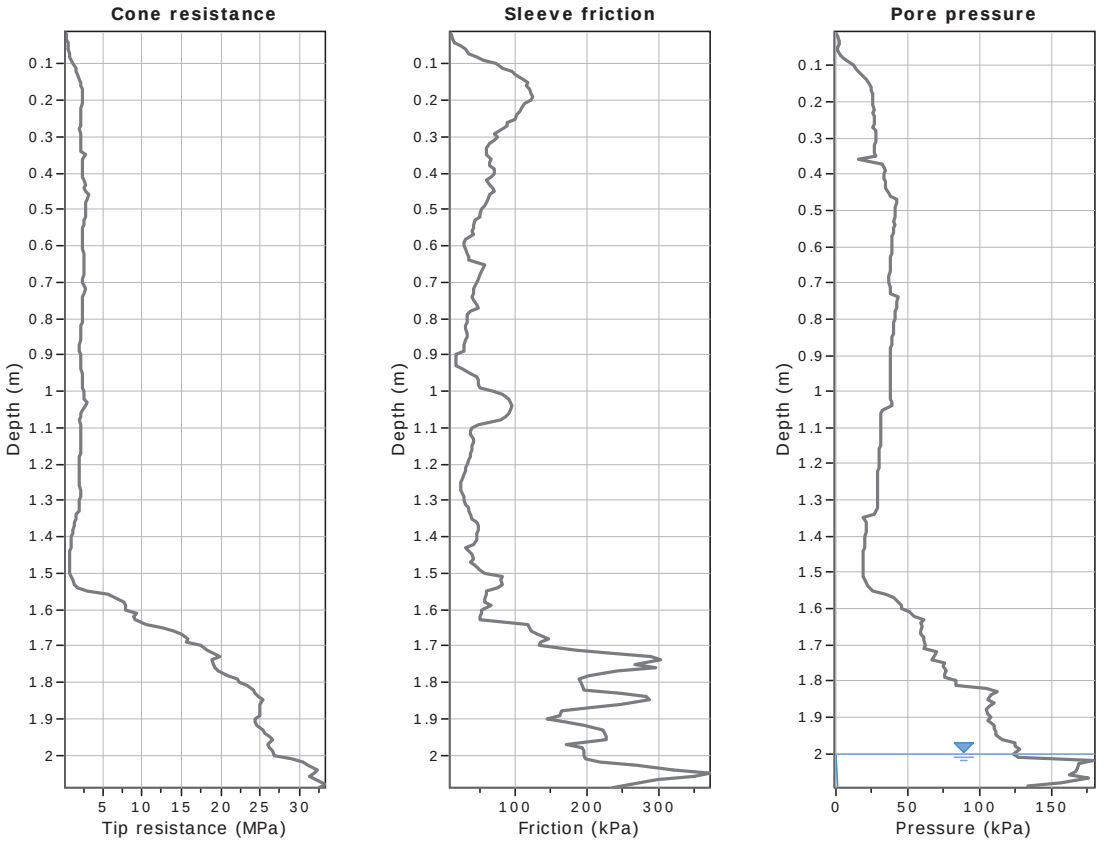

The plot below presents the cross correlation coeficient between the raw qc and fs values (as measured on the field). X axes presents the lag distance (one lag is the distance between two sucessive CPT measurements).

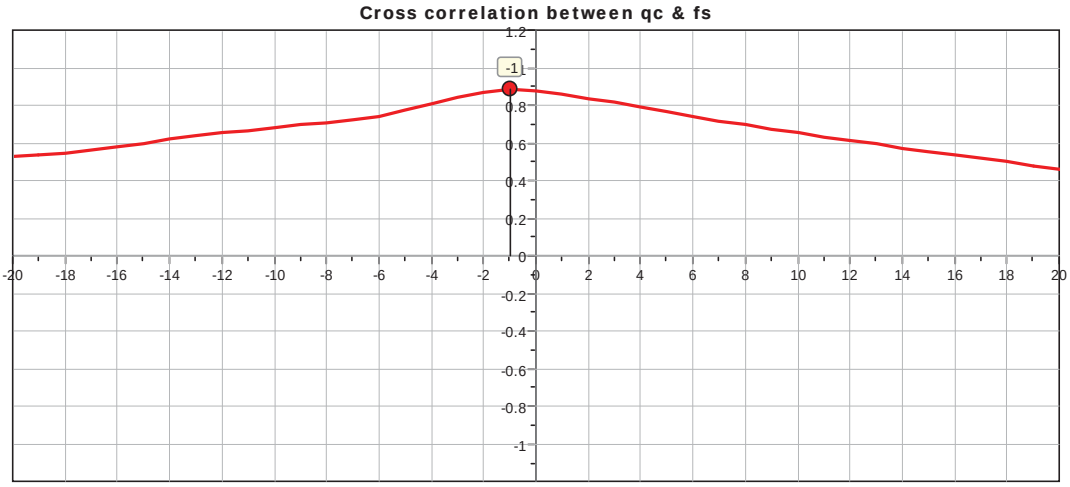

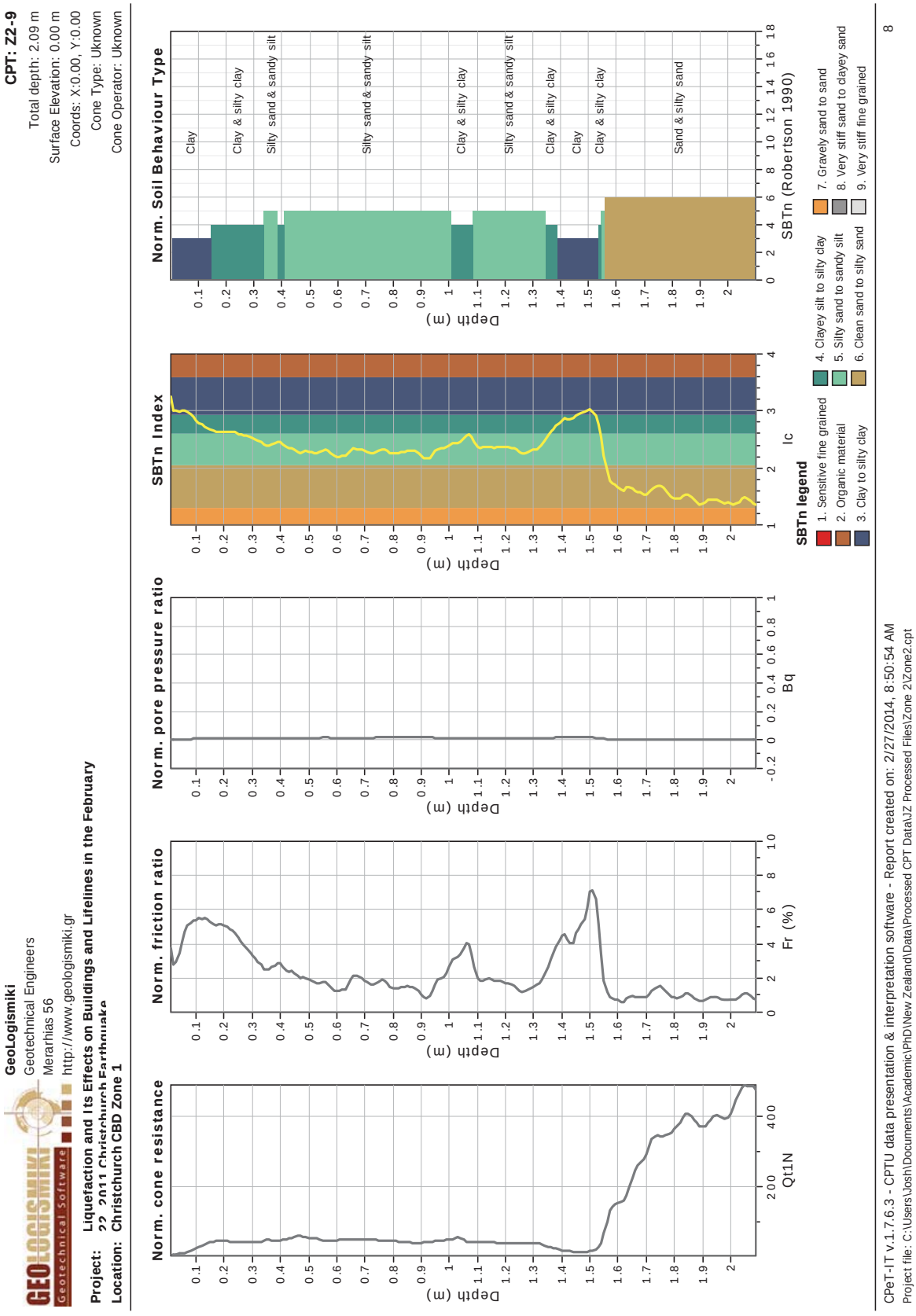
GeoLogismiki
Geotechnical Engineers
Merarhias 56
http://www.geologismiki.gr
Project: Liquefaction and Its Effects on Buildings and Lifelines in the February 22, 2011 Christchurch Earthquake
Location: Christchurch CBD Zone 1
CPT: Z2-9
Total depth: 2.09 m
Surface Elevation: 0.00 m
Coords: X:0.00, Y:0.00
Cone Type: Uknown
Cone Operator: Uknown
Norm. cone resistance
Norm. friction ratio
Norm. pore pressure ratio
SBTn Index
Norm. Soil Behaviour Type
Depth (m)
Qt1N
Fr (%)
Bq
Ic
SBTn (Robertson 1990)
Clay
Clay & silty clay
Silty sand & sandy silt
Clay & silty clay
Silty sand & sandy silt
Clay & silty clay
Clay
Clay & silty clay
Sand & silty sand
SBTn legend
1. Sensitive fine grained
2. Organic material
3. Clay to silty clay
4. Clayey silt to silty clay
5. Silty sand to sandy silt
6. Clean sand to silty sand
7. Gravely sand to sand
8. Very stiff sand to clayey sand
9. Very stiff fine grained
CPeT-IT v.1.7.6.3 - CPTU data presentation & interpretation software - Report created on: 2/27/2014, 8:50:54 AM
Project file: C:\Users\Josh\Documents\Academic\PhD\New Zealand\Data\Processed CPT Data\JZ Processed Files\Zone 2\Zone2.cpt
8

GeoLogismiki
Geotechnical Engineers
Merarhias 56
http://www.geologismiki.gr

CPT: Z2-10
Total depth: 2.31 m
Surface Elevation: 0.00 m
Coords: X:0.00, Y:0.00
Cone Type: Uknown
Cone Operator: Uknown

Project: **Liquefaction and Its Effects on Buildings and Lifelines in the February 22, 2011 Christchurch Earthquake**
Location: **Christchurch CBD Zone 1**

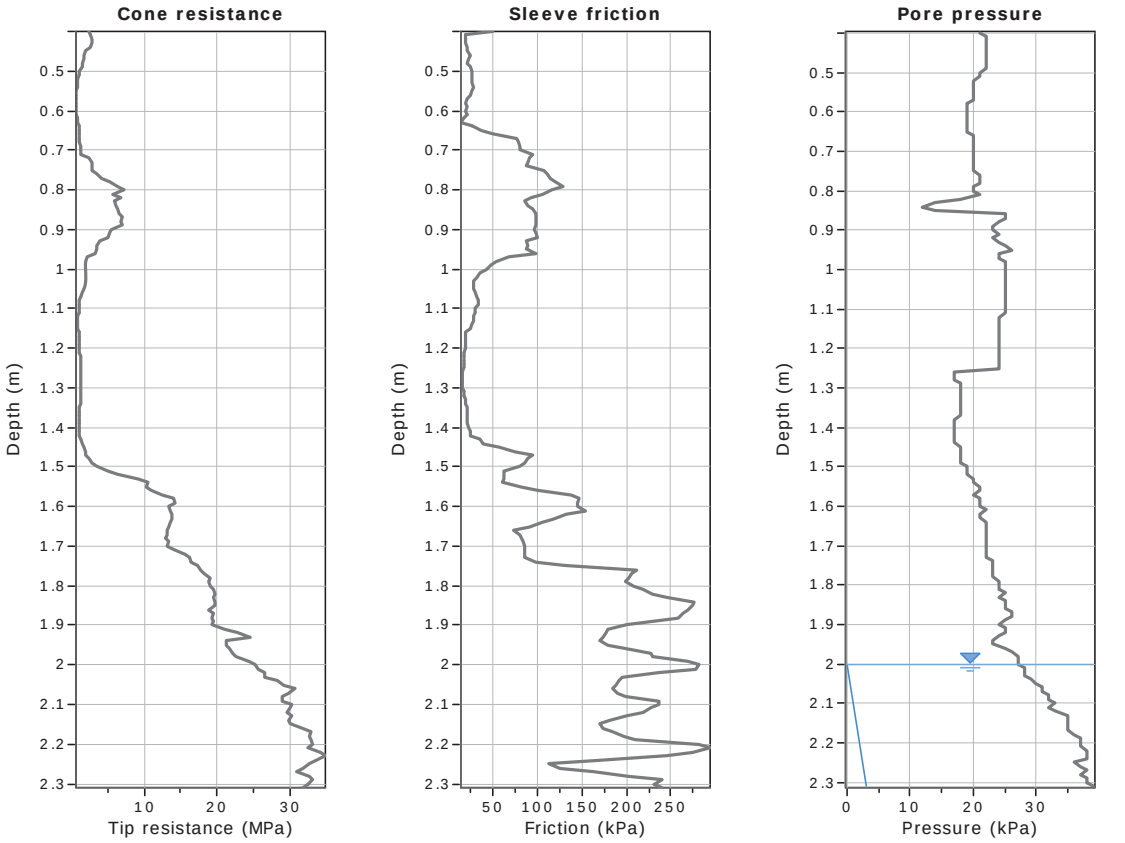

The plot below presents the cross correlation coeficient between the raw qc and fs values (as measured on the field). X axes presents the lag distance (one lag is the distance between two sucessive CPT measurements).

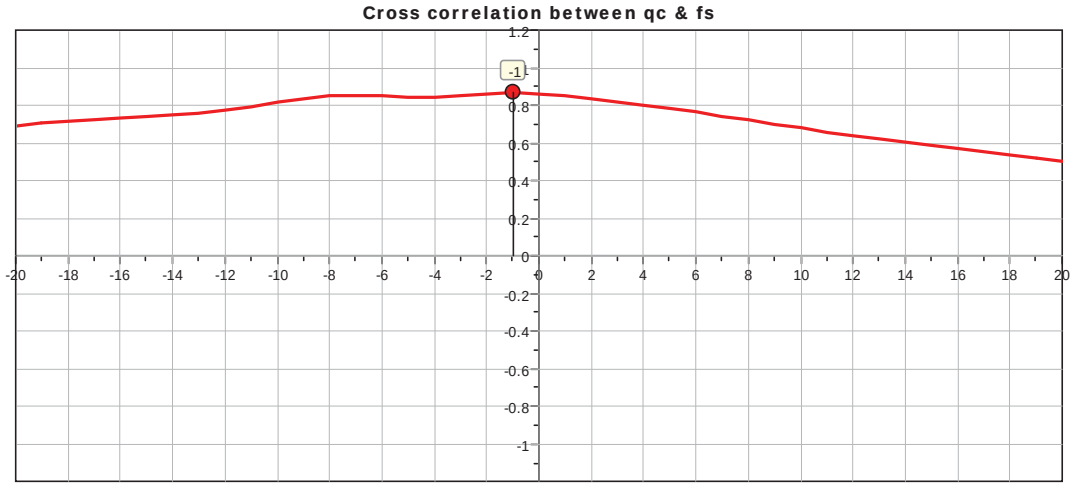

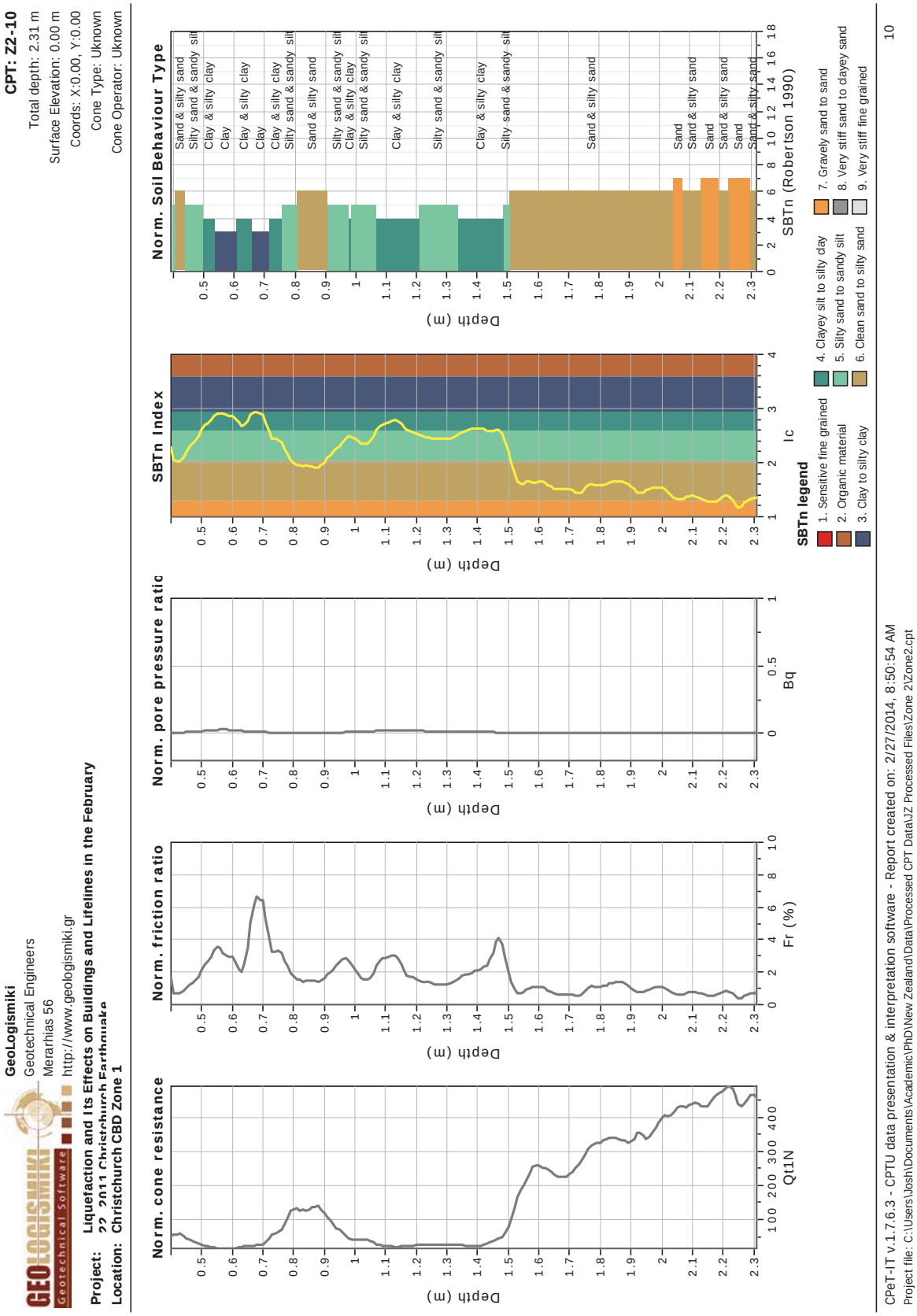
GeoLogismiki
Geotechnical Engineers
Merarchias 56
http://www.geologismiki.gr
Project: Liquefaction and Its Effects on Buildings and Lifelines in the February 22 2011 Christchurch Earthquake
Location: Christchurch CBD Zone 1
CPT: Z2-10
Total depth: 2.31 m
Surface Elevation: 0.00 m
Coords: X:0.00, Y:0.00
Cone Type: Uknown
Cone Operator: Uknown
Norm. cone resistance
Norm. friction ratio
Norm. pore pressure ratio
SBTn Index
Norm. Soil Behaviour Type
Depth (m)
Qt1N
Fr (%)
Bq
Ic
SBTn (Robertson 1990)
SBTn legend
1. Sensitive fine grained
2. Organic material
3. Clay to silty clay
4. Clayey silt to silty clay
5. Silty sand to sandy silt
6. Clean sand to silty sand
7. Gravely sand to sand
8. Very stiff sand to clayey sand
9. Very stiff fine grained
CPeT-IT v.1.7.6.3 - CPTU data presentation & interpretation software - Report created on: 2/27/2014, 8:50:54 AM
Project file: C:\Users\Josh\Documents\Academic\PhD\New Zealand\Data\Processed CPT Data\JZ Processed Files\Zone 2\Zone2.cpt
10

GeoLogismiki
Geotechnical Engineers
Merarhias 56
http://www.geologismiki.gr

CPT: Z2-11
Total depth: 5.88 m
Surface Elevation: 0.00 m
Coords: X:0.00, Y:0.00
Cone Type: Uknown
Cone Operator: Uknown

Project: **Liquefaction and Its Effects on Buildings and Lifelines in the February 22, 2011 Christchurch Earthquake**
Location: **Christchurch CBD Zone 1**

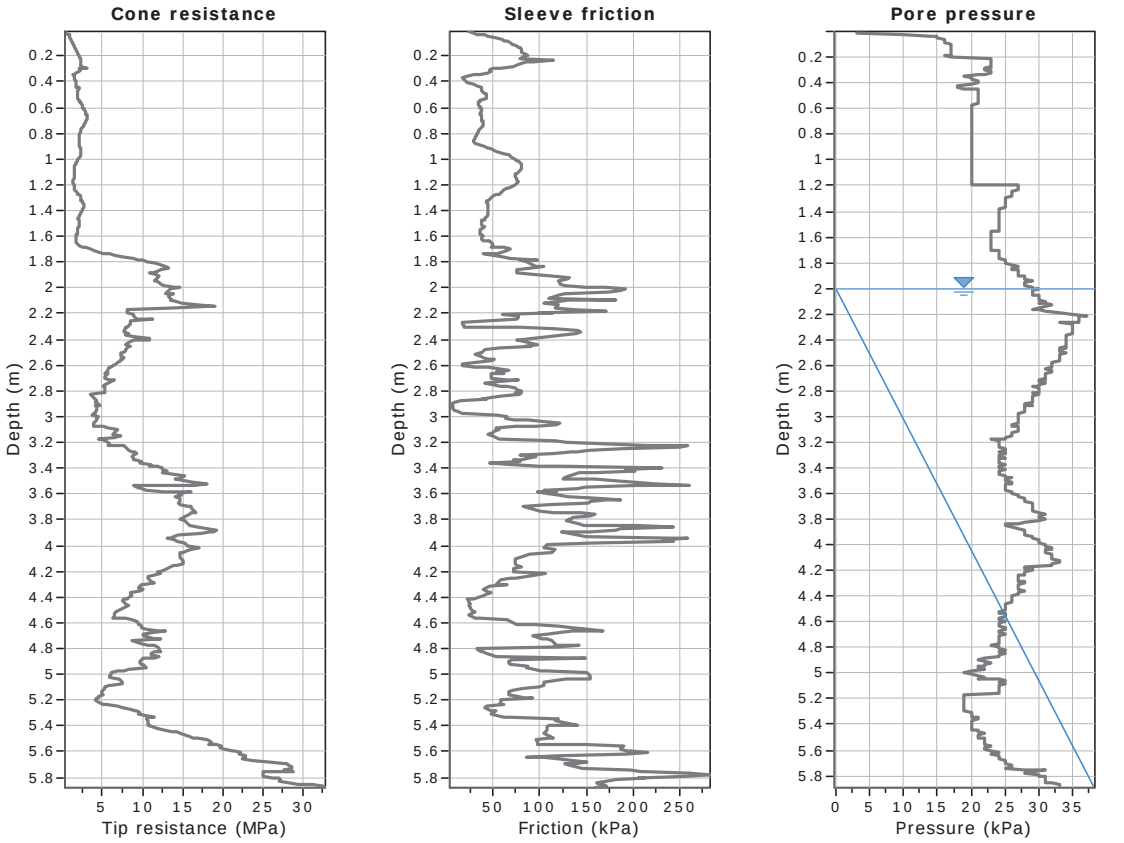

The plot below presents the cross correlation coeficient between the raw qc and fs values (as measured on the field). X axes presents the lag distance (one lag is the distance between two sucessive CPT measurements).

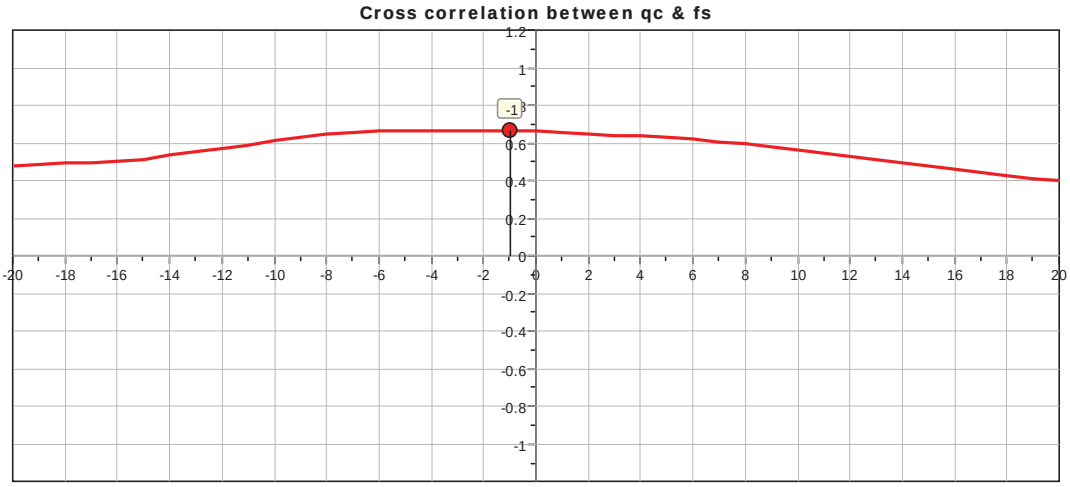

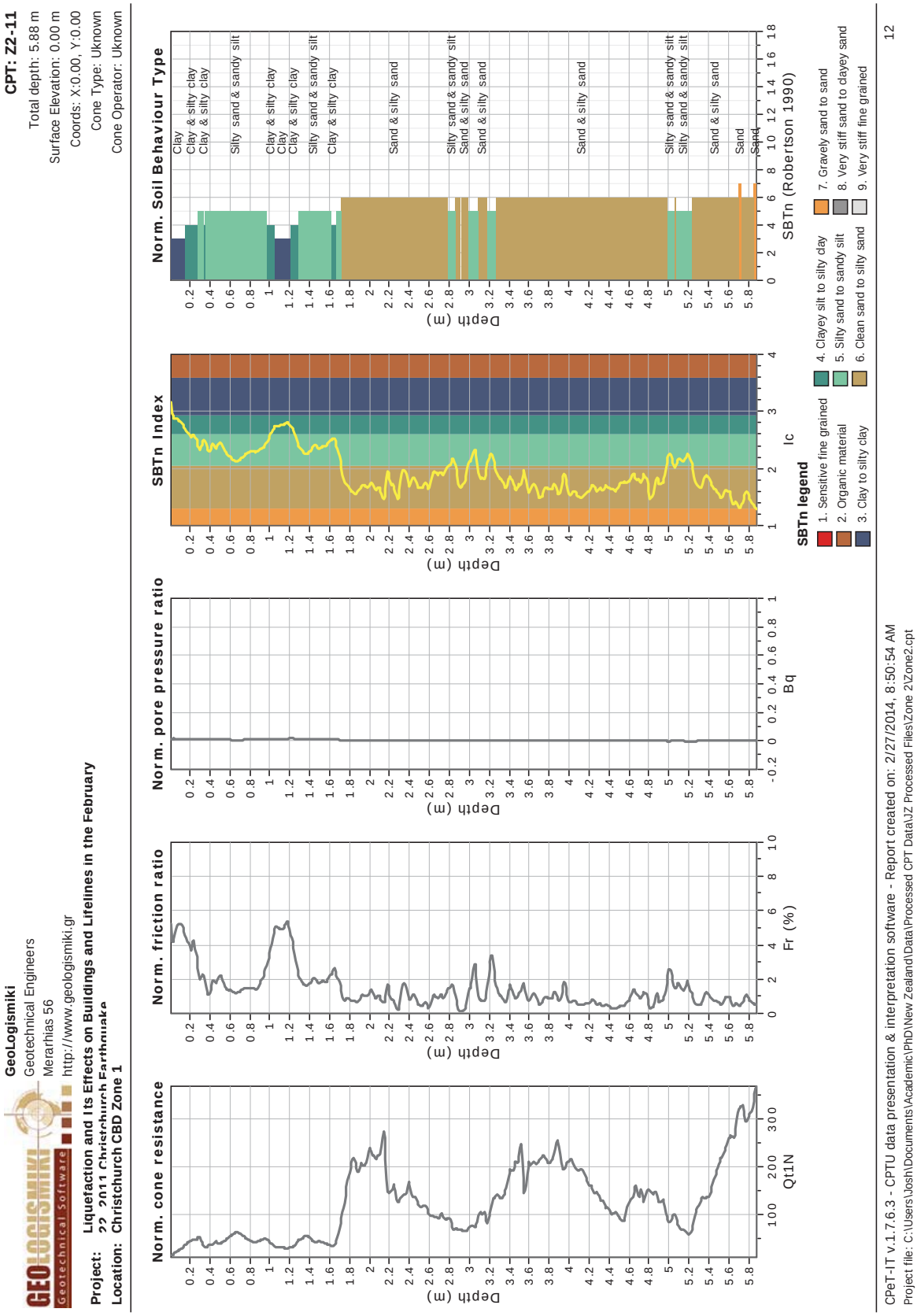
GeoLogismiki
Geotechnical Engineers
Merarhias 56
http://www.geologismiki.gr
Project: Liquefaction and Its Effects on Buildings and Lifelines in the February 22, 2011 Christchurch Earthquake
Location: Christchurch CBD Zone 1
CPT: Z2-11
Total depth: 5.88 m
Surface Elevation: 0.00 m
Coords: X:0.00, Y:0.00
Cone Type: Uknown
Cone Operator: Uknown
Norm. cone resistance
Norm. friction ratio
Norm. pore pressure ratio
SBTn Index
Norm. Soil Behaviour Type
Depth (m)
Qt1N
Fr (%)
Bq
Ic
SBTn (Robertson 1990)
SBTn legend
1. Sensitive fine grained
2. Organic material
3. Clay to silty clay
4. Clayey silt to silty clay
5. Silty sand to sandy silt
6. Clean sand to silty sand
7. Gravely sand to sand
8. Very stiff sand to clayey sand
9. Very stiff fine grained
CPeT-IT v.1.7.6.3 - CPTU data presentation & interpretation software - Report created on: 2/27/2014, 8:50:54 AM
Project file: C:\Users\Josh\Documents\Academic\PhD\New Zealand\Data\Processed CPT Data\JZ Processed Files\Zone 2\Zone2.cpt
12

GeoLogismiki
Geotechnical Engineers
Merarhias 56
http://www.geologismiki.gr

CPT: Z2-12
Total depth: 20.14 m
Surface Elevation: 0.00 m
Coords: X:0.00, Y:0.00
Cone Type: Uknown
Cone Operator: Uknown

Project:
Location:

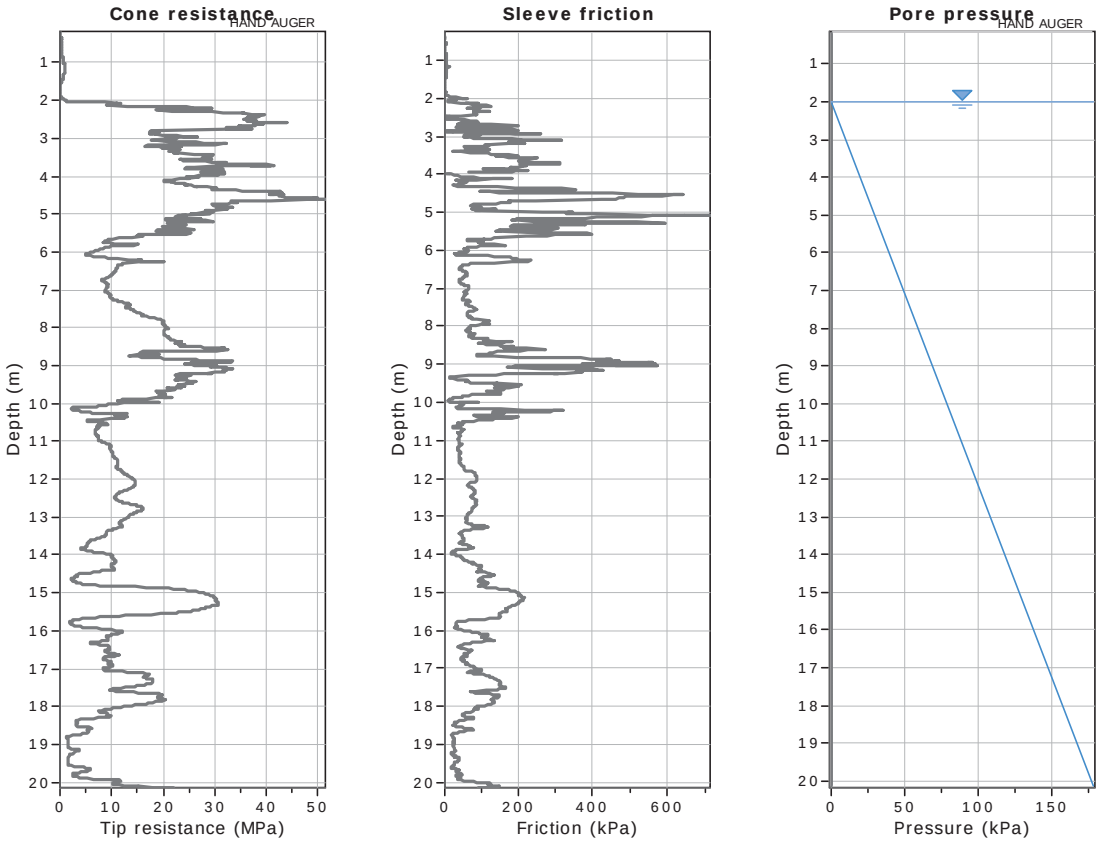

The plot below presents the cross correlation coeficient between the raw qc and fs values (as measured on the field). X axes presents the lag distance (one lag is the distance between two sucessive CPT measurements).

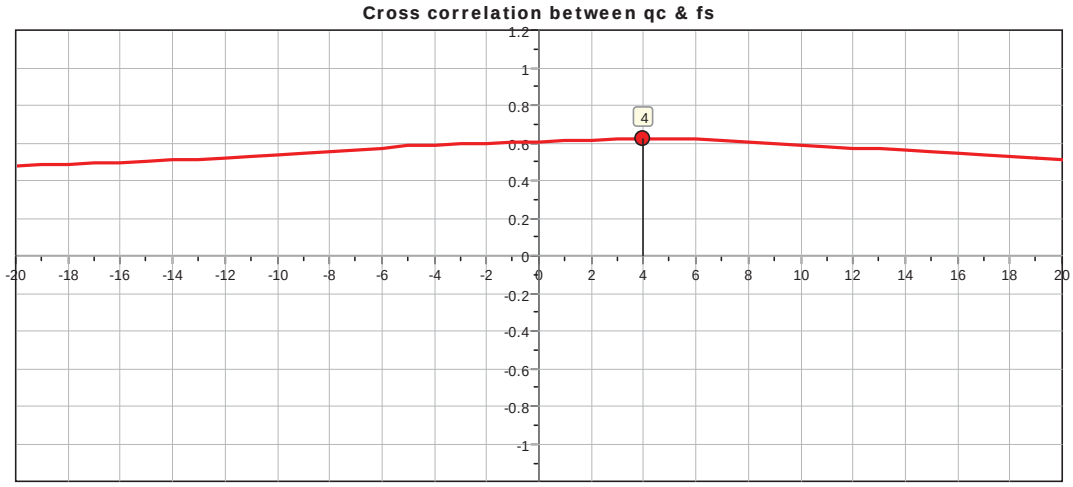

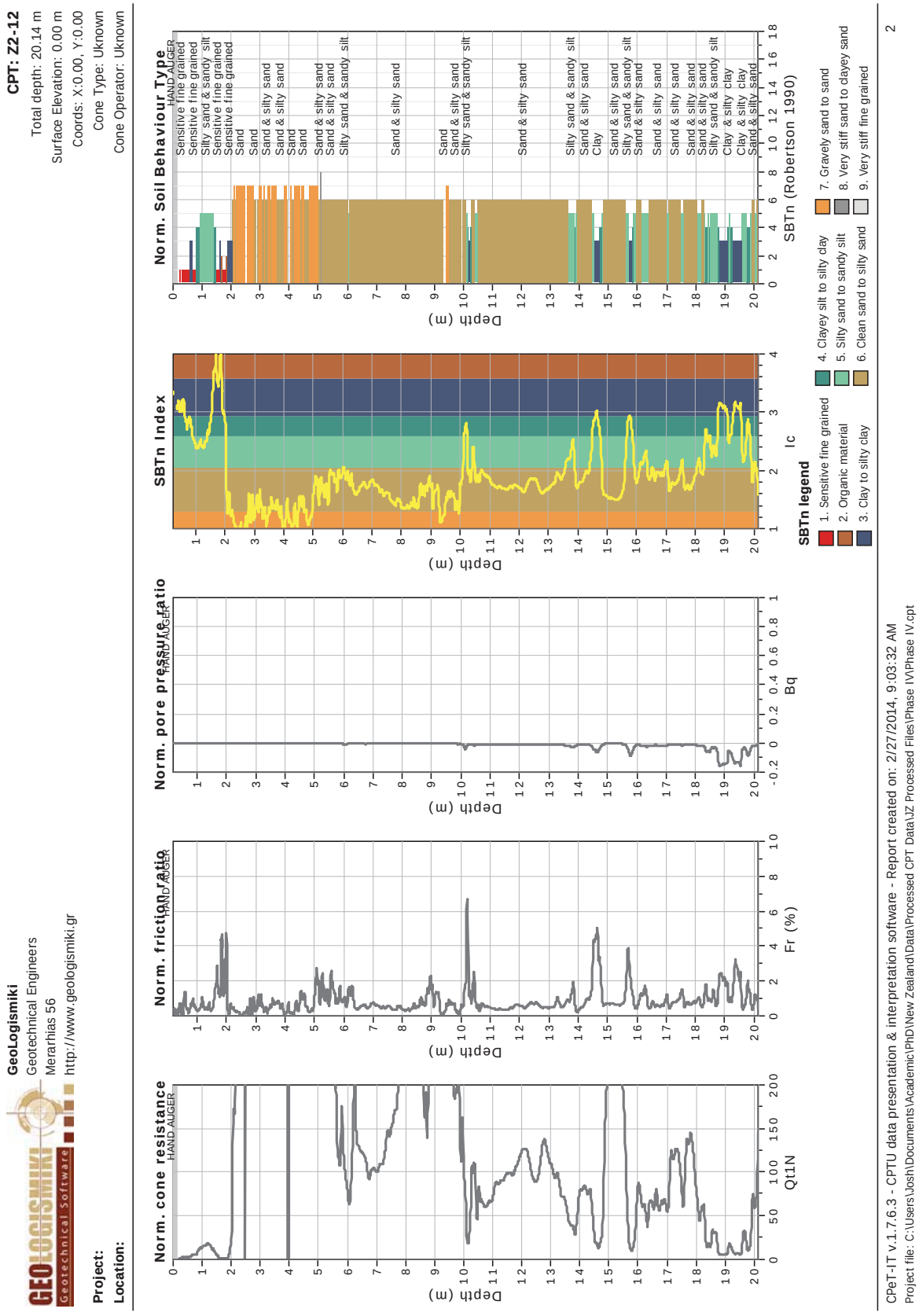
CPT: Z2-12
Total depth: 20.14 m
Surface Elevation: 0.00 m
Coords: X:0.00, Y:0.00
Cone Type: Uknown
Cone Operator: Uknown
GeoLogismiki
Geotechnical Engineers
Merarhias 56
http://www.geologismiki.gr
Project:
Location:
Norm. cone resistance
HAND AUGER
Qt1N
Norm. friction ratio
HAND AUGER
Fr (%)
Norm. pore pressure ratio
HAND AUGER
Bq
SBTn Index
Ic
Norm. Soil Behaviour Type
HAND AUGER
SBTn (Robertson 1990)
Depth (m)
SBTn legend
1. Sensitive fine grained
2. Organic material
3. Clay to silty clay
4. Clayey silt to silty clay
5. Silty sand to sandy silt
6. Clean sand to silty sand
7. Gravely sand to sand
8. Very stiff sand to clayey sand
9. Very stiff fine grained
CPeT-IT v.1.7.6.3 - CPTU data presentation & interpretation software - Report created on: 2/27/2014, 9:03:32 AM
Project file: C:\Users\Josh\Documents\Academic\PhD\New Zealand\Data\Processed CPT Data\JZ Processed Files\Phase IV\Phase IV.cpt
2

GeoLogismiki
Geotechnical Engineers
Merarhias 56
http://www.geologismiki.gr

CPT: Z2-13
Total depth: 20.35 m
Surface Elevation: 0.00 m
Coords: X:0.00, Y:0.00
Cone Type: Uknown
Cone Operator: Uknown

Project:
Location:

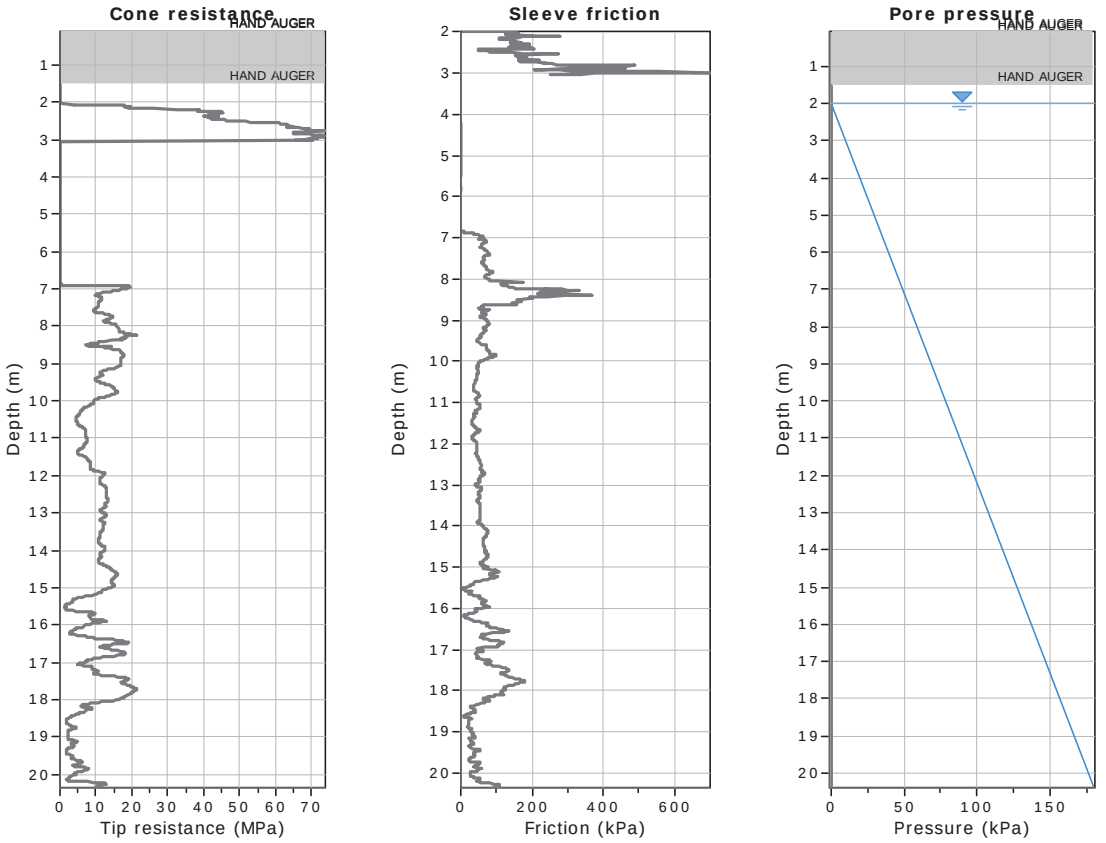

The plot below presents the cross correlation coeficient between the raw qc and fs values (as measured on the field). X axes presents the lag distance (one lag is the distance between two sucessive CPT measurements).

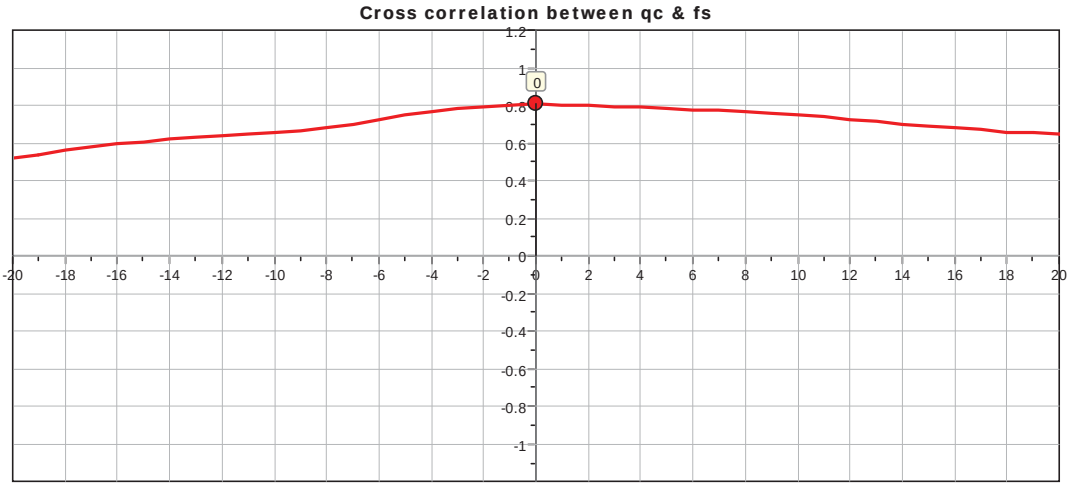

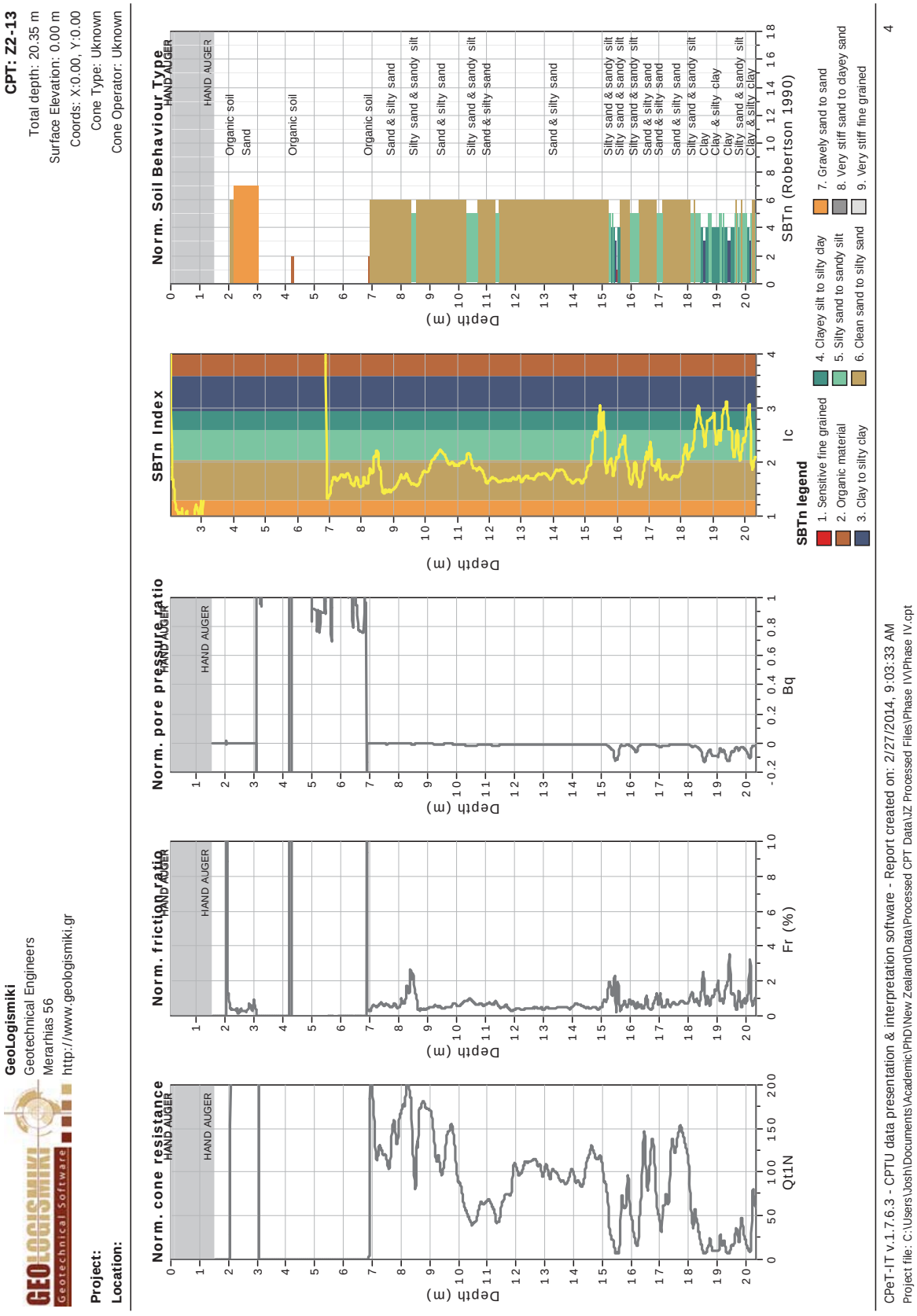
GeoLogismiki
Geotechnical Engineers
Merarchias 56
http://www.geologismiki.gr
Project:
Location:
CPT: Z2-13
Total depth: 20.35 m
Surface Elevation: 0.00 m
Coords: X:0.00, Y:0.00
Cone Type: Uknown
Cone Operator: Uknown
Norm. cone resistance
Norm. friction ratio
Norm. pore pressure ratio
SBTn Index
Norm. Soil Behaviour Type
HAND AUGER
Depth (m)
Qt1N
Fr (%)
Bq
Ic
SBTn (Robertson 1990)
Organic soil
Sand
Sand & silty sand
Silty sand & sandy silt
Clay & silty clay
Clay
Silty sand & sandy silty clay
SBTn legend
1. Sensitive fine grained
2. Organic material
3. Clay to silty clay
4. Clayey silt to silty clay
5. Silty sand to sandy silt
6. Clean sand to silty sand
7. Gravely sand to sand
8. Very stiff sand to clayey sand
9. Very stiff fine grained
CPeT-IT v.1.7.6.3 - CPTU data presentation & interpretation software - Report created on: 2/27/2014, 9:03:33 AM
Project file: C:\Users\Josh\Documents\Academic\PhD\New Zealand\Data\Processed CPT Data\JZ Processed Files\Phase IV\Phase IV.cpt
4

GeoLogismiki
Geotechnical Engineers
Merarhias 56
http://www.geologismiki.gr

CPT: Z2-14
Total depth: 19.68 m
Surface Elevation: 0.00 m
Coords: X:0.00, Y:0.00
Cone Type: Uknown
Cone Operator: Uknown

Project:
Location:

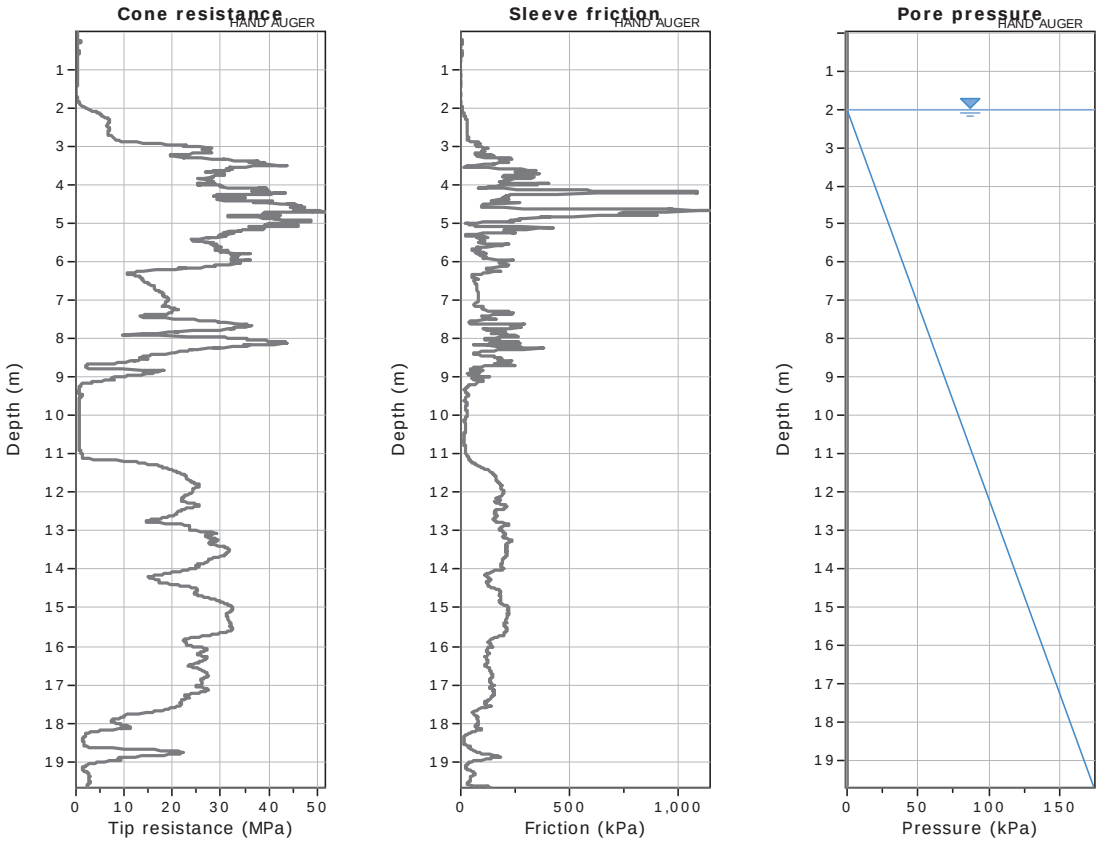

The plot below presents the cross correlation coeficient between the raw qc and fs values (as measured on the field). X axes presents the lag distance (one lag is the distance between two sucessive CPT measurements).

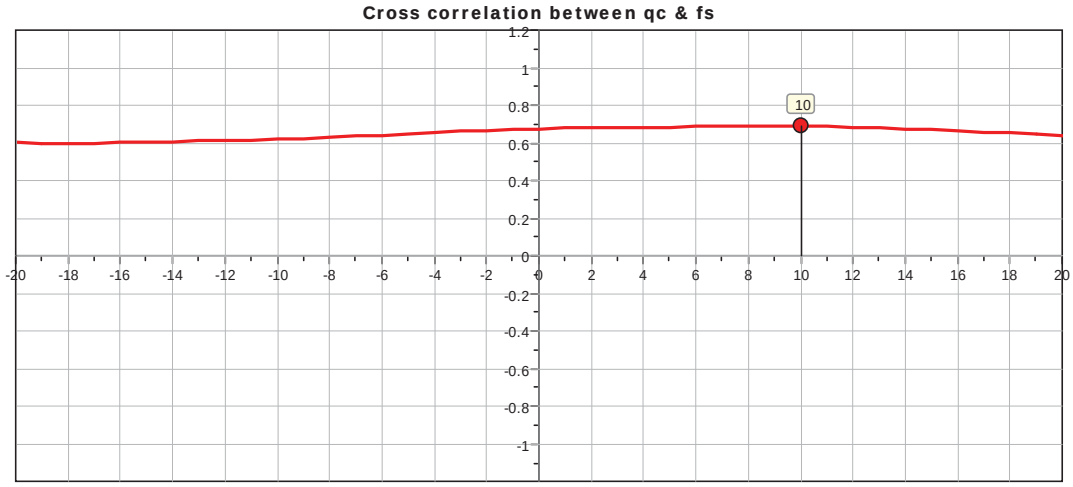

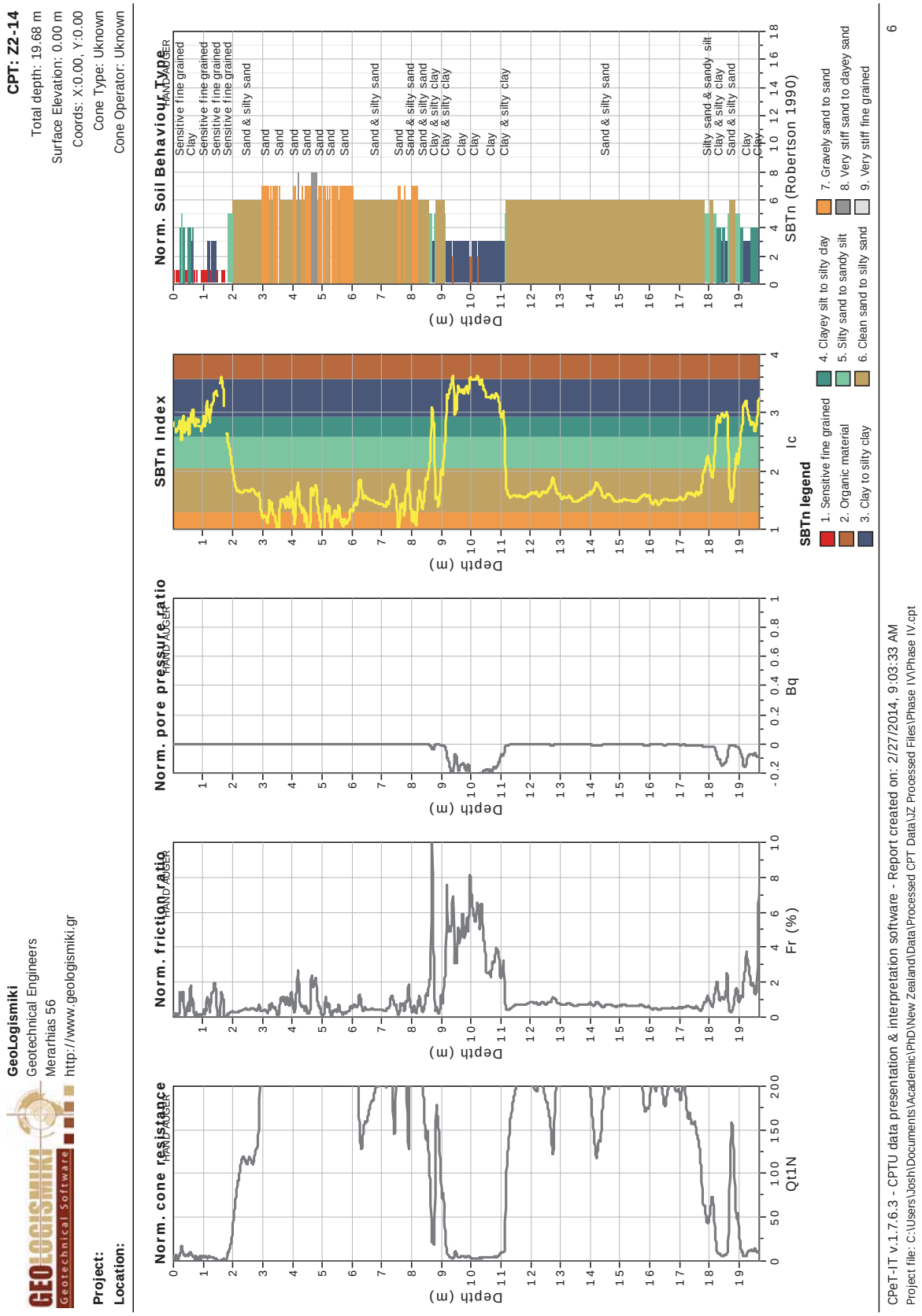
CPT: Z2-14
Total depth: 19.68 m
Surface Elevation: 0.00 m
Coords: X:0.00, Y:0.00
Cone Type: Uknown
Cone Operator: Uknown
GeoLogismiki
Geotechnical Engineers
Merarhias 56
http://www.geologismiki.gr
Project:
Location:
Norm. cone resistance
HAND AUGER
Qt1N
Norm. friction ratio
Fr (%)
Norm. pore pressure ratio
Bq
SBTn Index
Ic
Norm. Soil Behaviour Type
SBTn (Robertson 1990)
Depth (m)
SBTn legend
1. Sensitive fine grained
2. Organic material
3. Clay to silty clay
4. Clayey silt to silty clay
5. Silty sand to sandy silt
6. Clean sand to silty sand
7. Gravely sand to sand
8. Very stiff sand to clayey sand
9. Very stiff fine grained
CPeT-IT v.1.7.6.3 - CPTU data presentation & interpretation software - Report created on: 2/27/2014, 9:03:33 AM
Project file: C:\Users\Josh\Documents\Academic\PhD\New Zealand\Data\Processed CPT Data\JZ Processed Files\Phase IV\Phase IV.cpt
6

GeoLogismiki
Geotechnical Engineers
Merarhias 56
http://www.geologismiki.gr

CPT: Z2-15
Total depth: 3.24 m
Surface Elevation: 0.00 m
Coords: X:0.00, Y:0.00
Cone Type: Uknown
Cone Operator: Uknown

Project:
Location:

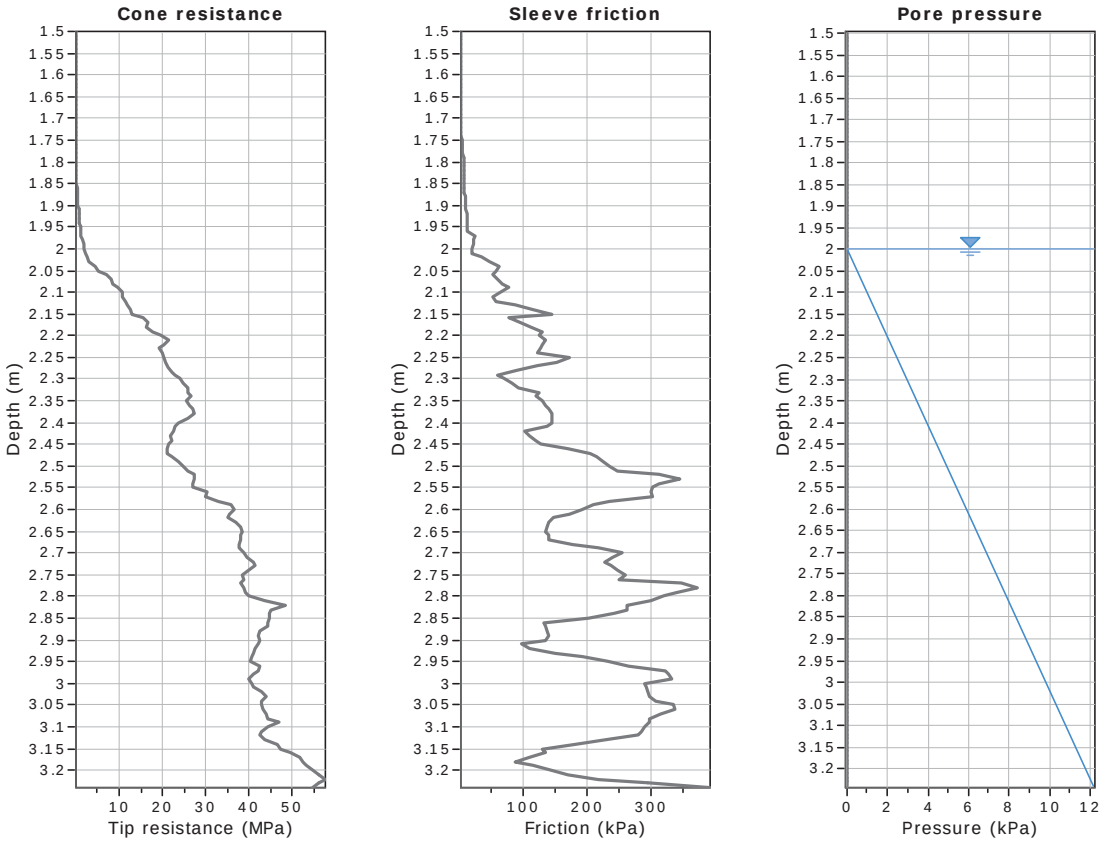

The plot below presents the cross correlation coeficient between the raw qc and fs values (as measured on the field). X axes presents the lag distance (one lag is the distance between two sucessive CPT measurements).

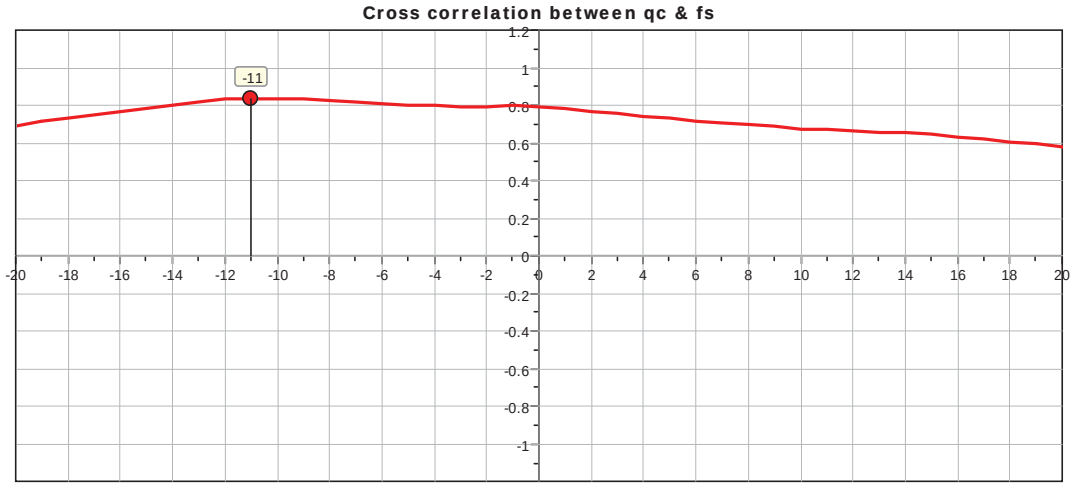

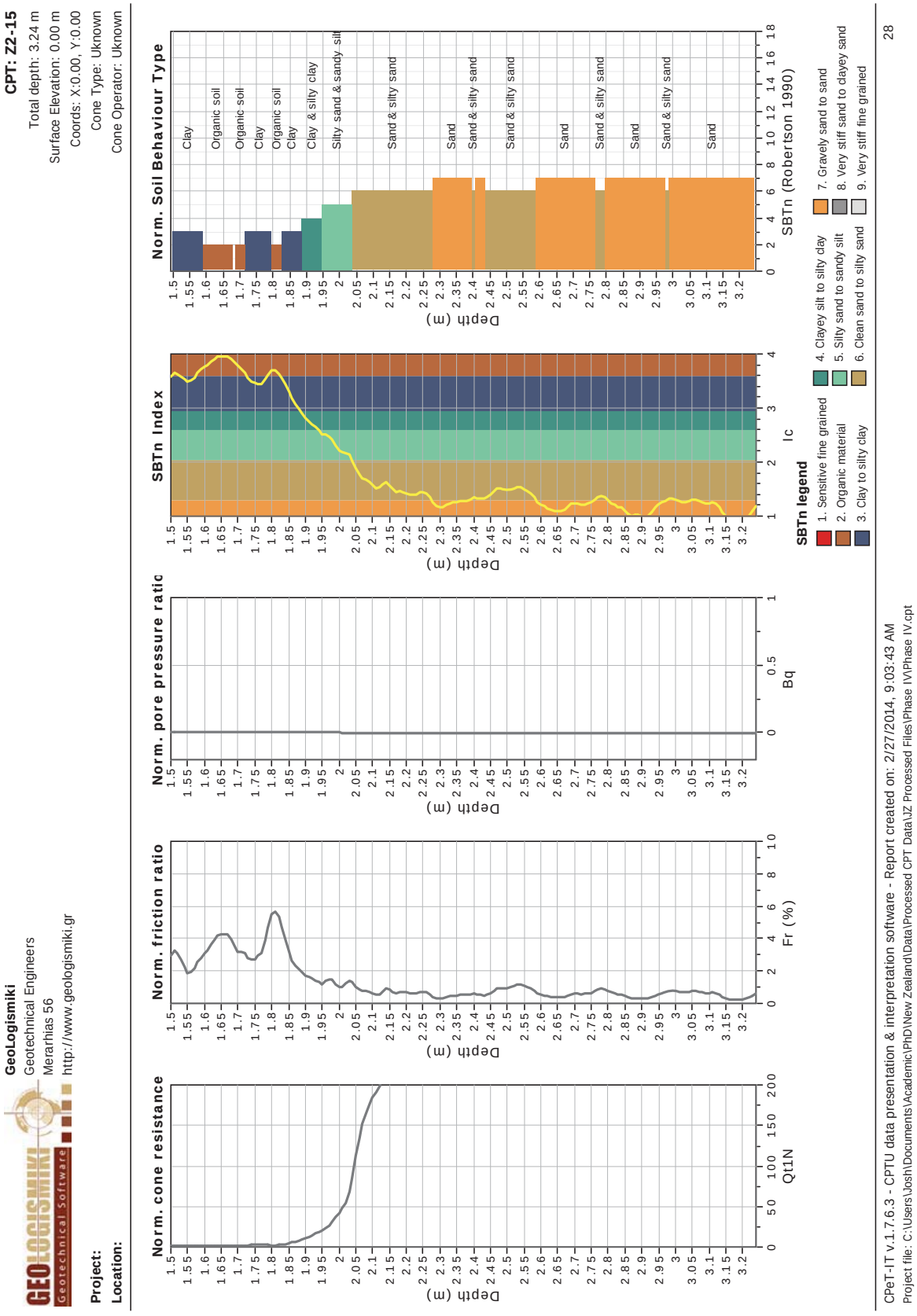
GeoLogismiki
Geotechnical Engineers
Merarchias 56
http://www.geologismiki.gr
Project:
Location:
CPT: Z2-15
Total depth: 3.24 m
Surface Elevation: 0.00 m
Coords: X:0.00, Y:0.00
Cone Type: Uknown
Cone Operator: Uknown
Norm. cone resistance
Norm. friction ratio
Norm. pore pressure ratio
SBTn Index
Norm. Soil Behaviour Type
Depth (m)
Qt1N
Fr (%)
Bq
Ic
SBTn (Robertson 1990)
Clay
Organic soil
Clay & silty clay
Silty sand & sandy silt
Sand & silty sand
Sand
SBTn legend
1. Sensitive fine grained
2. Organic material
3. Clay to silty clay
4. Clayey silt to silty clay
5. Silty sand to sandy silt
6. Clean sand to silty sand
7. Gravely sand to sand
8. Very stiff sand to clayey sand
9. Very stiff fine grained
CPeT-IT v.1.7.6.3 - CPTU data presentation & interpretation software - Report created on: 2/27/2014, 9:03:43 AM
Project file: C:\Users\Josh\Documents\Academic\PhD\New Zealand\Data\Processed CPT Data\JZ Processed Files\Phase IV\Phase IV.cpt
28

GeoLogismiki
Geotechnical Engineers
Merarhias 56
http://www.geologismiki.gr

CPT: Z2-16
Total depth: 18.95 m
Surface Elevation: 0.00 m
Coords: X:0.00, Y:0.00
Cone Type: Uknown
Cone Operator: Uknown

Project:
Location:

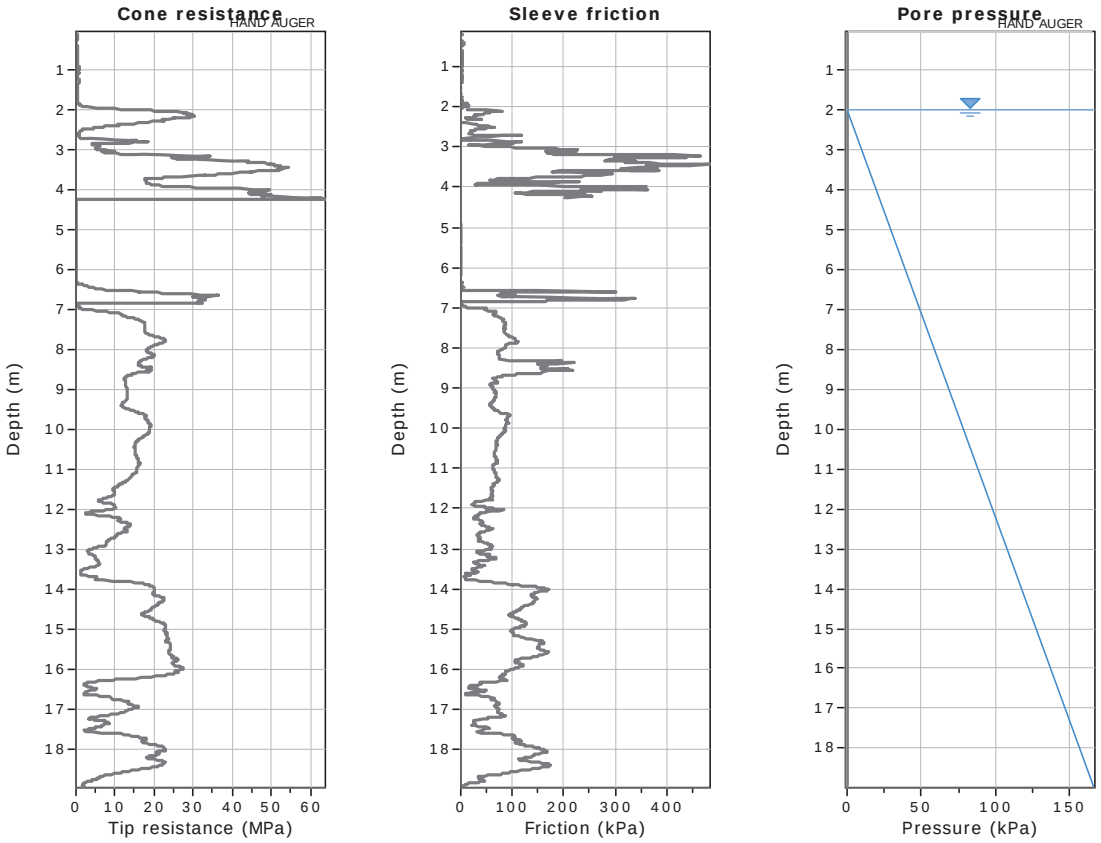

The plot below presents the cross correlation coeficient between the raw qc and fs values (as measured on the field). X axes presents the lag distance (one lag is the distance between two sucessive CPT measurements).

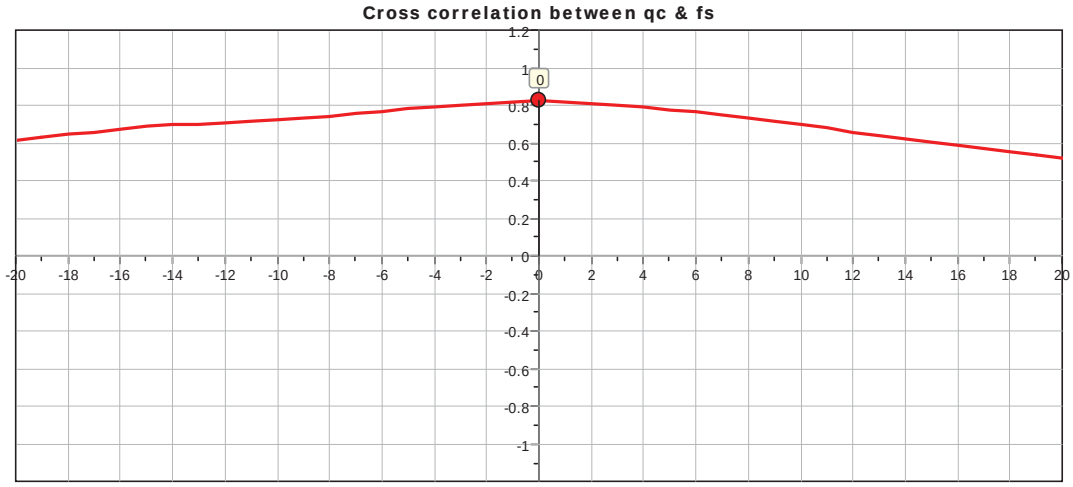

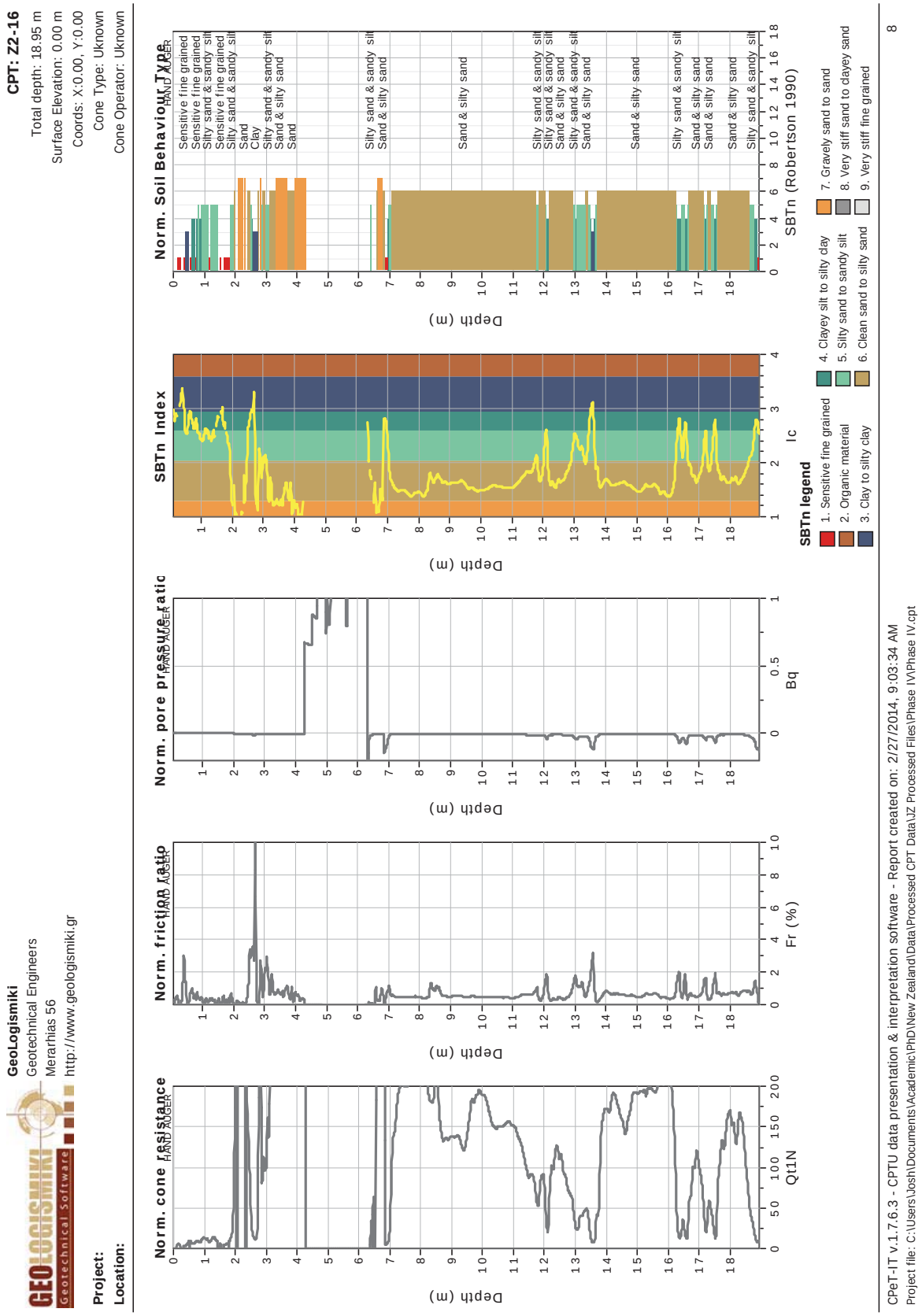
CPT: Z2-16
Total depth: 18.95 m
Surface Elevation: 0.00 m
Coords: X:0.00, Y:0.00
Cone Type: Uknown
Cone Operator: Uknown
Project:
Location:
GeoLogismiki
Geotechnical Engineers
Merarhias 56
http://www.geologismiki.gr
Norm. cone resistance
Norm. friction ratio
Norm. pore pressure ratio
SBTn Index
Norm. Soil Behaviour Type
SBTn (Robertson 1990)
Qt1N
Fr (%)
Bq
Ic
Depth (m)
SBTn legend
1. Sensitive fine grained
2. Organic material
3. Clay to silty clay
4. Clayey silt to silty clay
5. Silty sand to sandy silt
6. Clean sand to silty sand
7. Gravely sand to sand
8. Very stiff sand to clayey sand
9. Very stiff fine grained
CPeT-IT v.1.7.6.3 - CPTU data presentation & interpretation software - Report created on: 2/27/2014, 9:03:34 AM
Project file: C:\Users\Josh\Documents\Academic\PhD\New Zealand\Data\Processed CPT Data\JZ Processed Files\Phase IV\Phase IV.cpt
8

GeoLogismiki
Geotechnical Engineers
Merarhias 56
http://www.geologismiki.gr

CPT: Z2-17-Shallow
Total depth: 1.94 m
Surface Elevation: 0.00 m
Coords: X:0.00, Y:0.00
Cone Type: Uknown
Cone Operator: Uknown

Project: **Liquefaction and Its Effects on Buildings and Lifelines in the February 22, 2011 Christchurch Earthquake**
Location: **Christchurch CBD Zone 1**

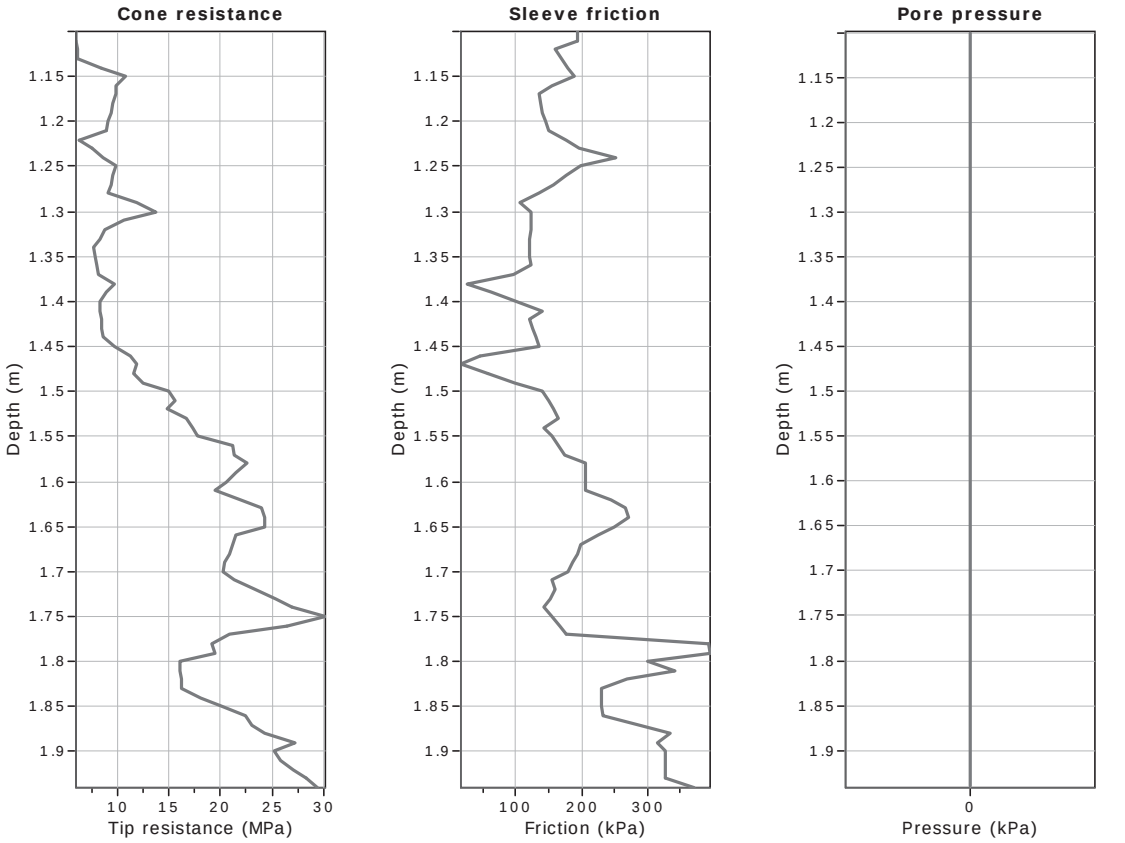

The plot below presents the cross correlation coeficient between the raw qc and fs values (as measured on the field). X axes presents the lag distance (one lag is the distance between two sucessive CPT measurements).

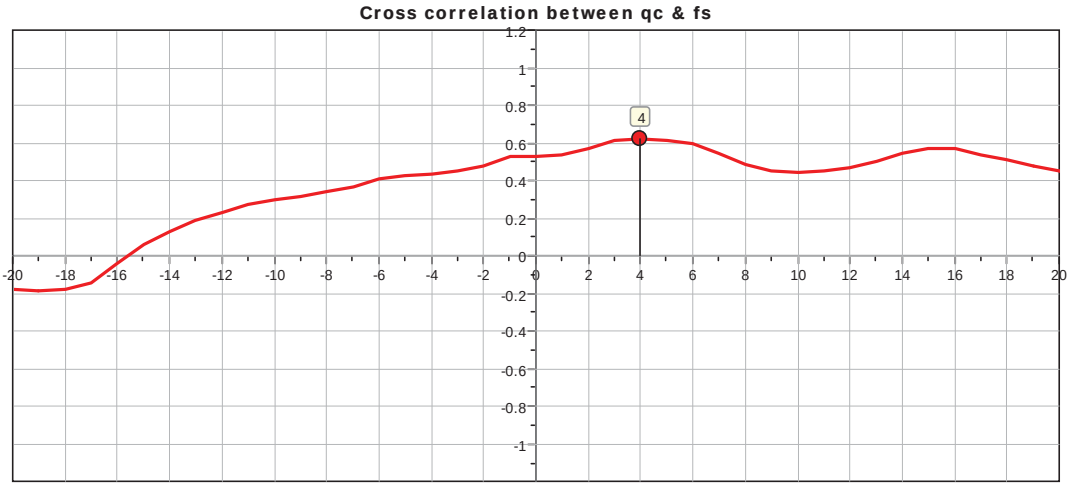

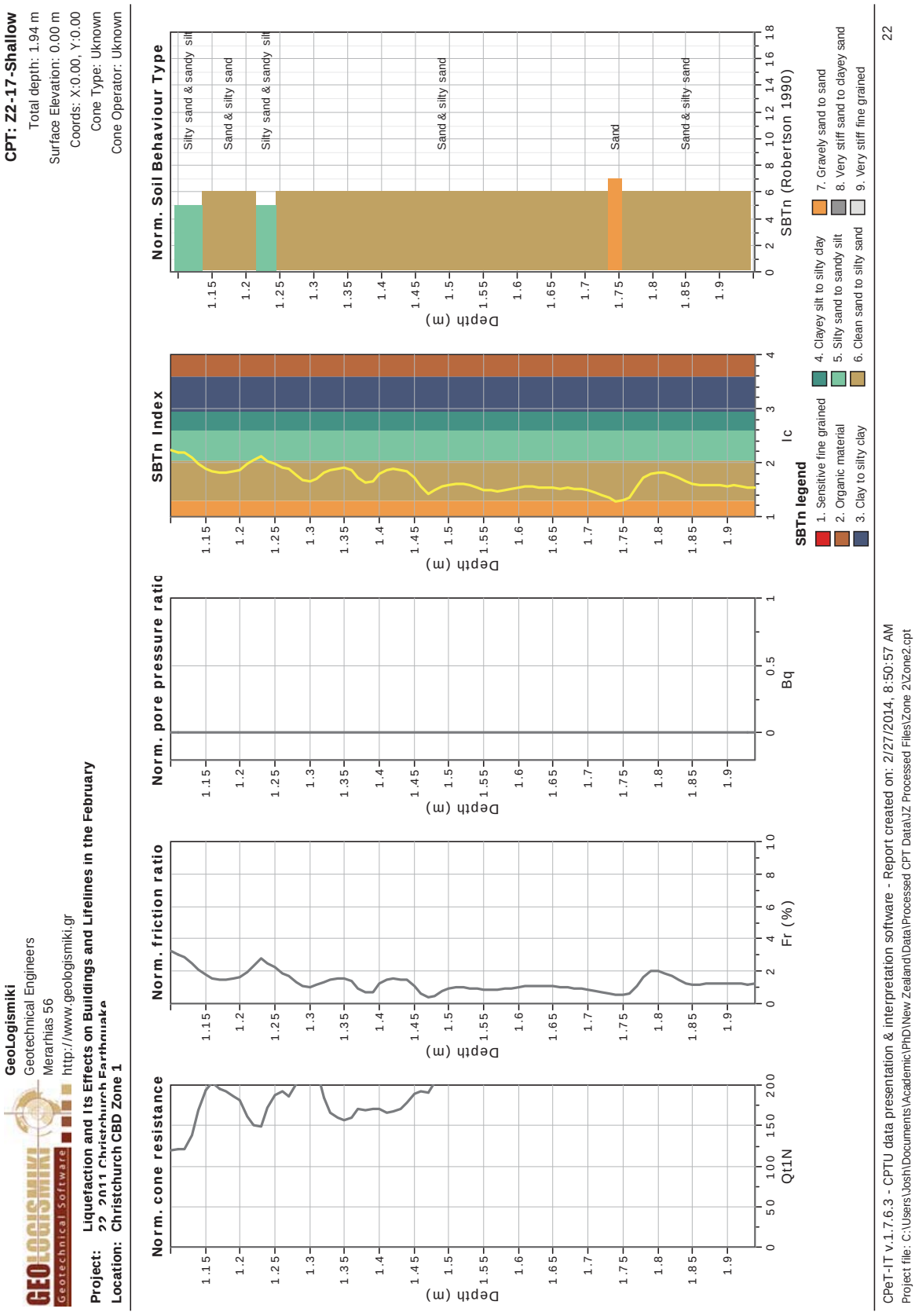
GeoLogismiki
Geotechnical Engineers
Merarchias 56
http://www.geologismiki.gr
Project: Liquefaction and Its Effects on Buildings and Lifelines in the February 22, 2011 Christchurch Earthquake
Location: Christchurch CBD Zone 1
CPT: Z2-17-Shallow
Total depth: 1.94 m
Surface Elevation: 0.00 m
Coords: X:0.00, Y:0.00
Cone Type: Uknown
Cone Operator: Uknown
Norm. cone resistance
Qt1N
Norm. friction ratio
Fr (%)
Norm. pore pressure ratio
Bq
SBTn Index
Ic
Norm. Soil Behaviour Type
SBTn (Robertson 1990)
Silty sand & sandy silt
Sand & silty sand
Silty sand & sandy silt
Sand & silty sand
Sand
Sand & silty sand
Depth (m)
SBTn legend
1. Sensitive fine grained
2. Organic material
3. Clay to silty clay
4. Clayey silt to silty clay
5. Silty sand to sandy silt
6. Clean sand to silty sand
7. Gravely sand to sand
8. Very stiff sand to clayey sand
9. Very stiff fine grained
CPeT-IT v.1.7.6.3 - CPTU data presentation & interpretation software - Report created on: 2/27/2014, 8:50:57 AM
Project file: C:\Users\Josh\Documents\Academic\PhD\New Zealand\Data\Processed CPT Data\JZ Processed Files\Zone 2\Zone2.cpt
22

GeoLogismiki
Geotechnical Engineers
Merarhias 56
http://www.geologismiki.gr

CPT: Z2-17-Deep
Total depth: 7.26 m
Surface Elevation: 0.00 m
Coords: X:0.00, Y:0.00
Cone Type: Uknown
Cone Operator: Uknown

Project: **Liquefaction and Its Effects on Buildings and Lifelines in the February 22, 2011 Christchurch Earthquake**
Location: **Christchurch CBD Zone 1**

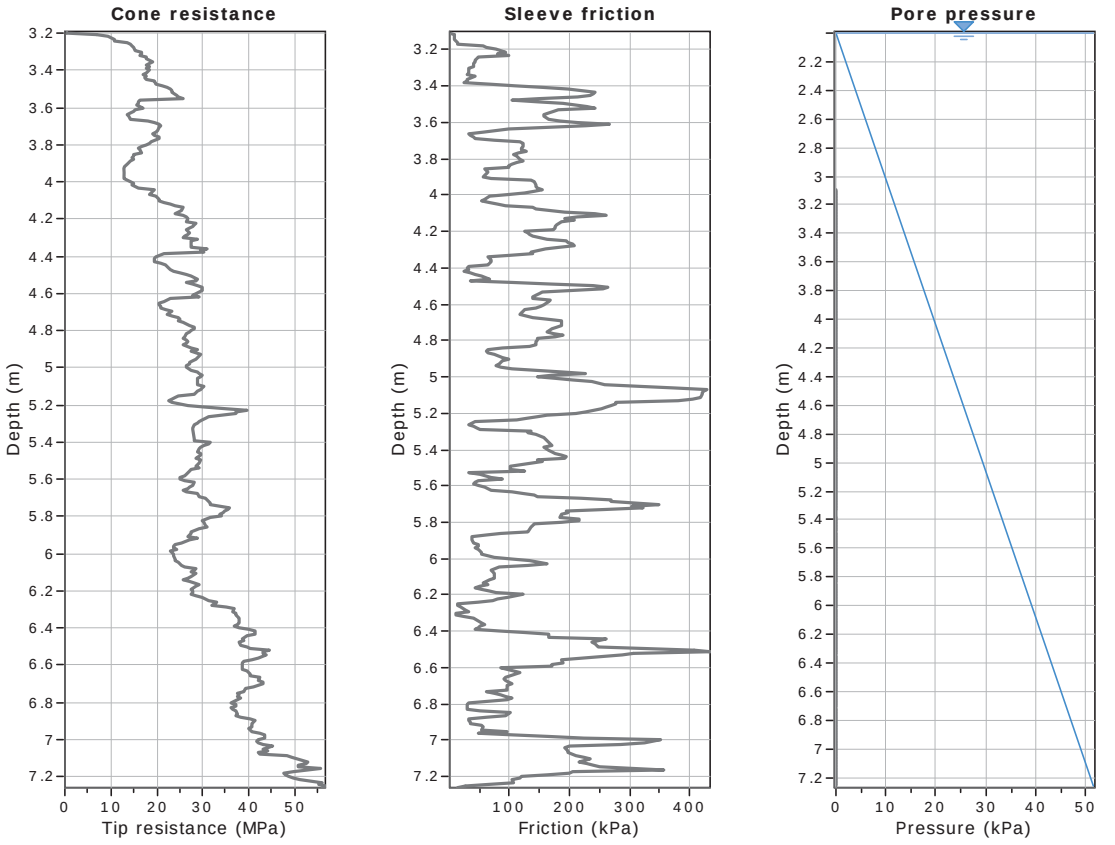

The plot below presents the cross correlation coeficient between the raw qc and fs values (as measured on the field). X axes presents the lag distance (one lag is the distance between two sucessive CPT measurements).

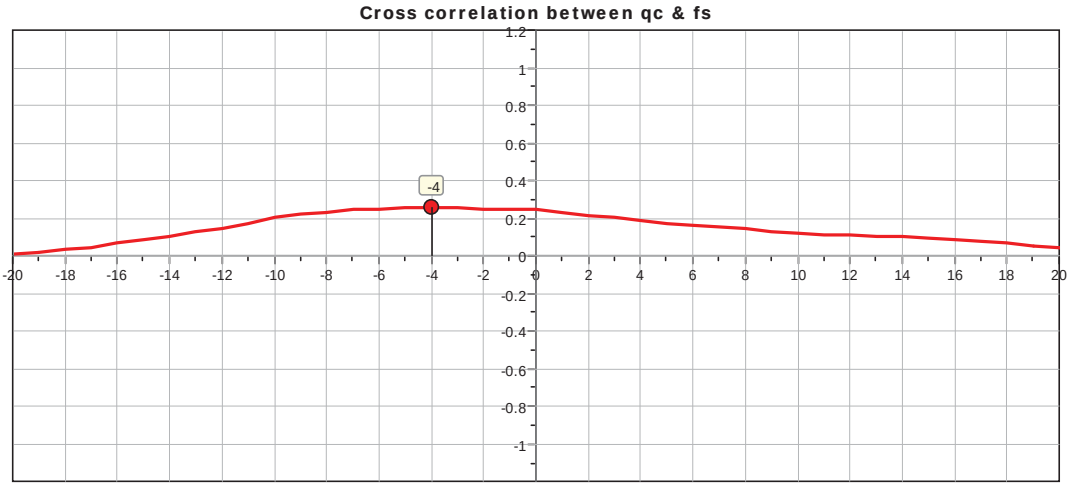

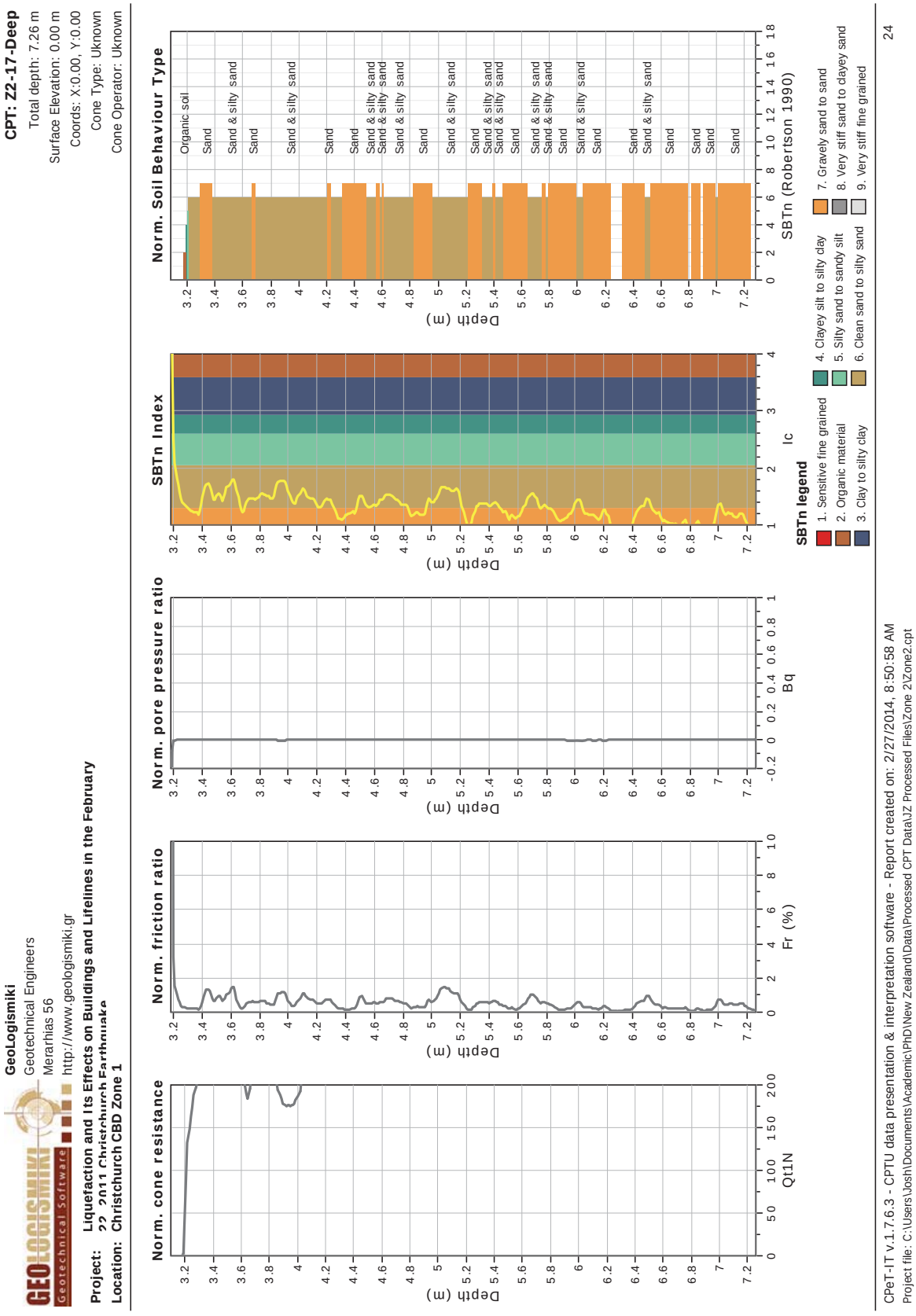
GeoLogismiki
Geotechnical Engineers
Merarchias 56
http://www.geologismiki.gr
Project: Liquefaction and Its Effects on Buildings and Lifelines in the February 22, 2011 Christchurch Earthquake
Location: Christchurch CBD Zone 1
CPT: Z2-17-Deep
Total depth: 7.26 m
Surface Elevation: 0.00 m
Coords: X:0.00, Y:0.00
Cone Type: Uknown
Cone Operator: Uknown
Norm. cone resistance
Norm. friction ratio
Norm. pore pressure ratio
SBTn Index
Norm. Soil Behaviour Type
Depth (m)
Qt1N
Fr (%)
Bq
Ic
SBTn (Robertson 1990)
Organic soil
Sand
Sand & silty sand
SBTn legend
1. Sensitive fine grained
2. Organic material
3. Clay to silty clay
4. Clayey silt to silty clay
5. Silty sand to sandy silt
6. Clean sand to silty sand
7. Gravely sand to sand
8. Very stiff sand to clayey sand
9. Very stiff fine grained
CPeT-IT v.1.7.6.3 - CPTU data presentation & interpretation software - Report created on: 2/27/2014, 8:50:58 AM
Project file: C:\Users\Josh\Documents\Academic\PhD\New Zealand\Data\Processed CPT Data\JZ Processed Files\Zone 2\Zone2.cpt
24

GeoLogismiki
Geotechnical Engineers
Merarhias 56
http://www.geologismiki.gr

CPT: Z2-18
Total depth: 20.60 m
Surface Elevation: 0.00 m
Coords: X:0.00, Y:0.00
Cone Type: Uknown
Cone Operator: Uknown

Project:
Location:

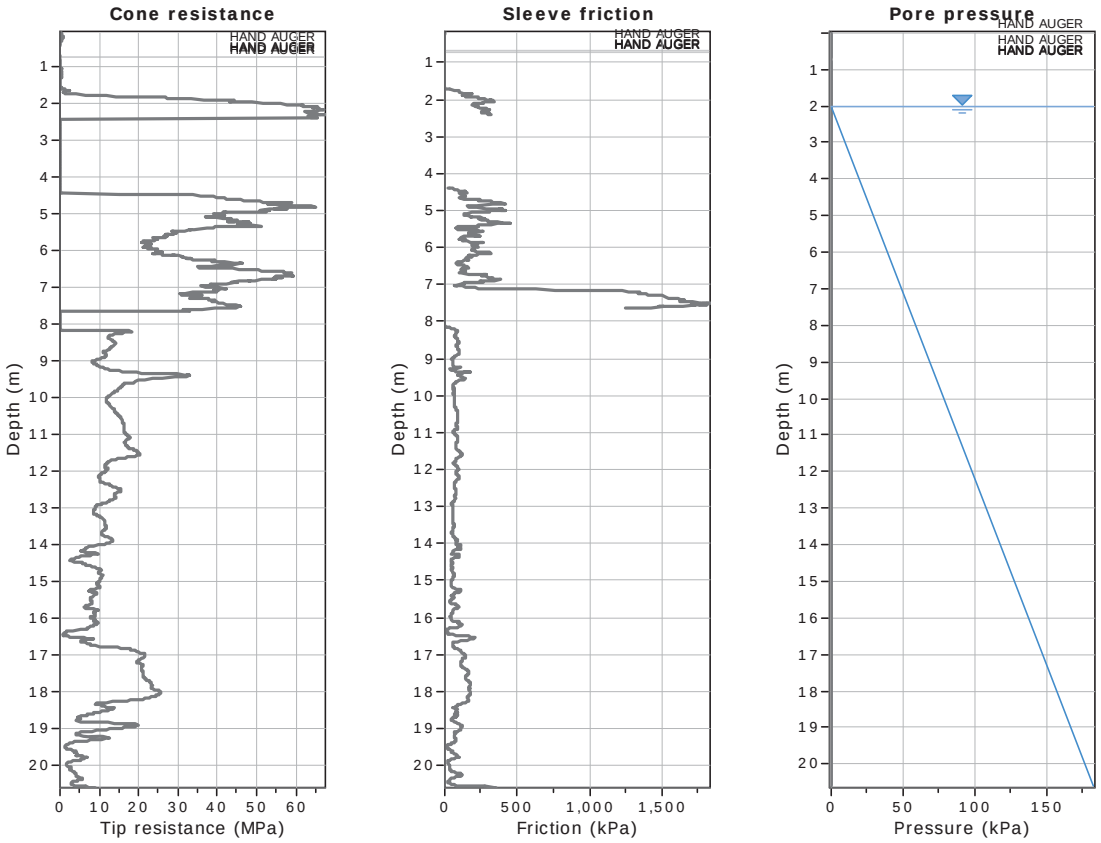

The plot below presents the cross correlation coeficient between the raw qc and fs values (as measured on the field). X axes presents the lag distance (one lag is the distance between two sucessive CPT measurements).

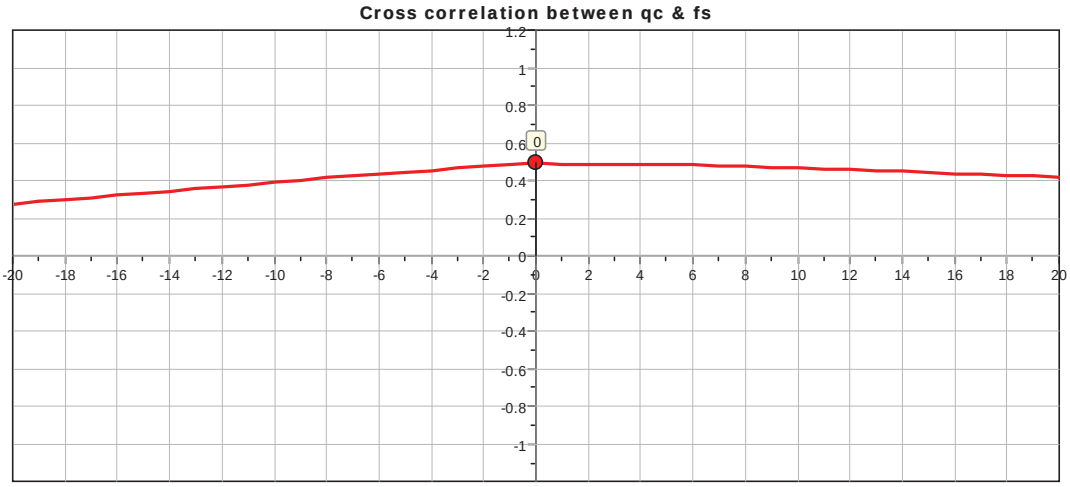

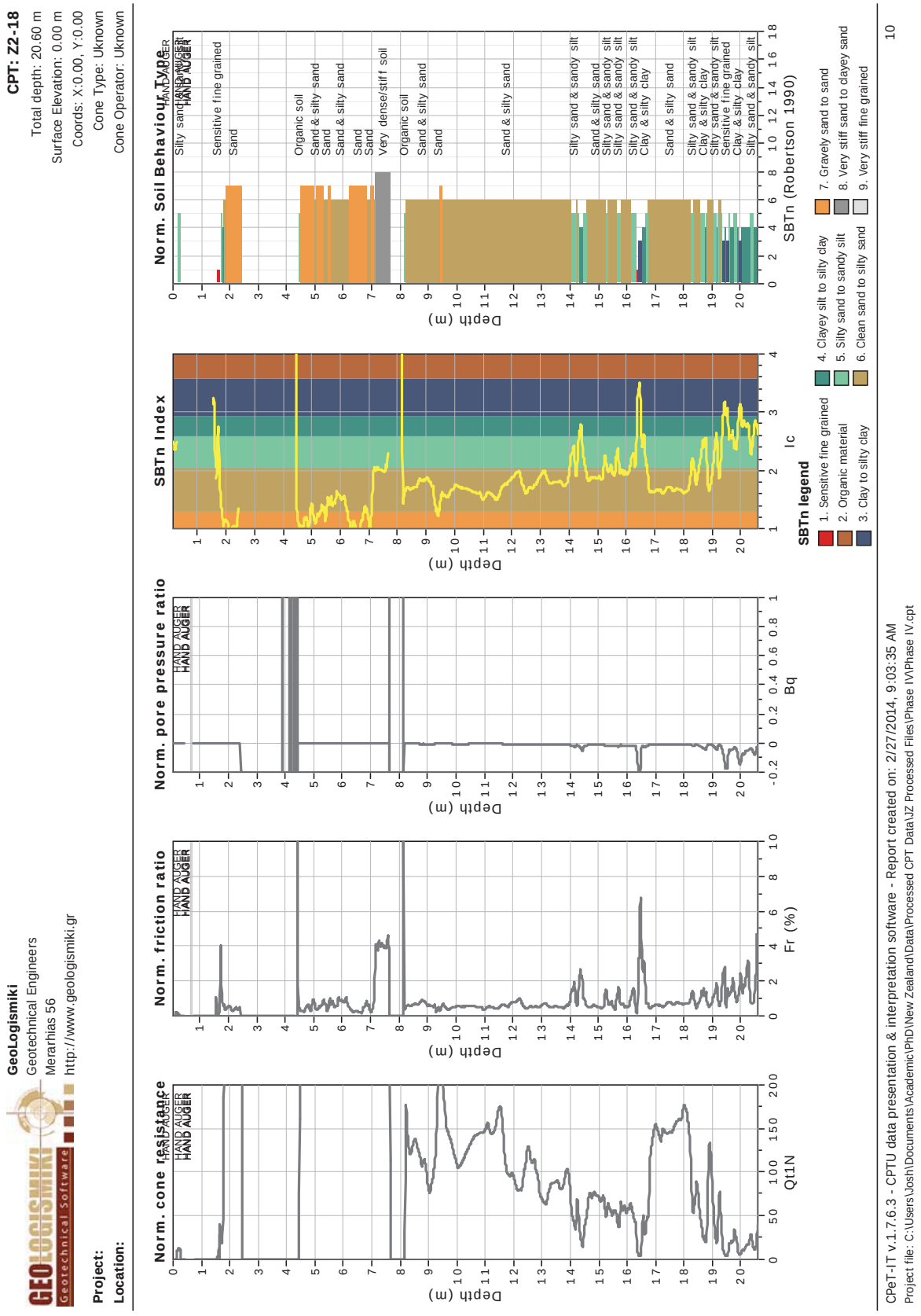
CPT: Z2-18
Total depth: 20.60 m
Surface Elevation: 0.00 m
Coords: X:0.00, Y:0.00
Cone Type: Uknown
Cone Operator: Uknown
GeoLogismiki
Geotechnical Engineers
Merarhias 56
http://www.geologismiki.gr
Project:
Location:
Norm. cone resistance
Norm. friction ratio
Norm. pore pressure ratio
SBTn Index
Norm. Soil Behaviour Type
SBTn (Robertson 1990)
SBTn legend
1. Sensitive fine grained
2. Organic material
3. Clay to silty clay
4. Clayey silt to silty clay
5. Silty sand to sandy silt
6. Clean sand to silty sand
7. Gravely sand to sand
8. Very stiff sand to clayey sand
9. Very stiff fine grained
HAND AUGER
Depth (m)
Qt1N
Fr (%)
Bq
Ic
CPeT-IT v.1.7.6.3 - CPTU data presentation & interpretation software - Report created on: 2/27/2014, 9:03:35 AM
Project file: C:\Users\Josh\Documents\Academic\PhD\New Zealand\Data\Processed CPT Data\JZ Processed Files\Phase IV\Phase IV.cpt

GeoLogismiki
Geotechnical Engineers
Merarhias 56
http://www.geologismiki.gr

CPT: Z2-18F
Total depth: 19.90 m
Surface Elevation: 0.00 m
Coords: X:0.00, Y:0.00
Cone Type: Uknown
Cone Operator: Uknown

Project:
Location:

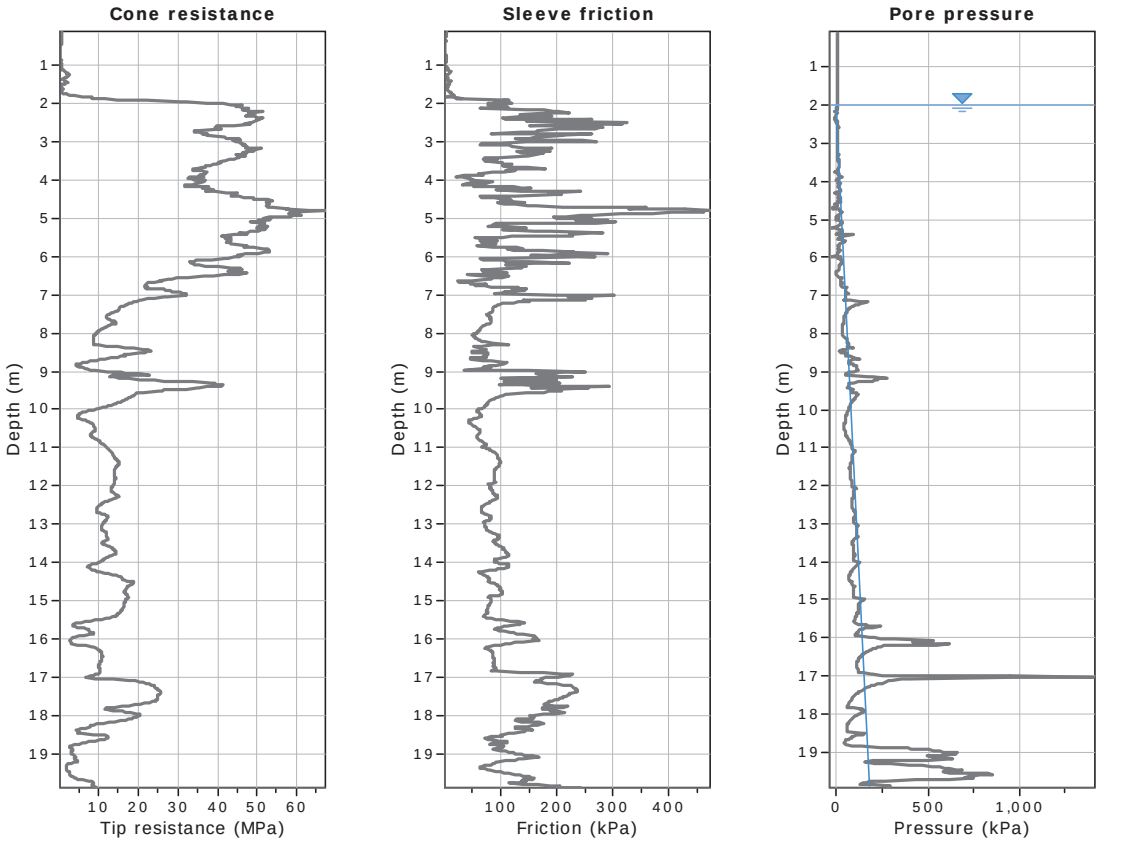

The plot below presents the cross correlation coeficient between the raw qc and fs values (as measured on the field). X axes presents the lag distance (one lag is the distance between two sucessive CPT measurements).

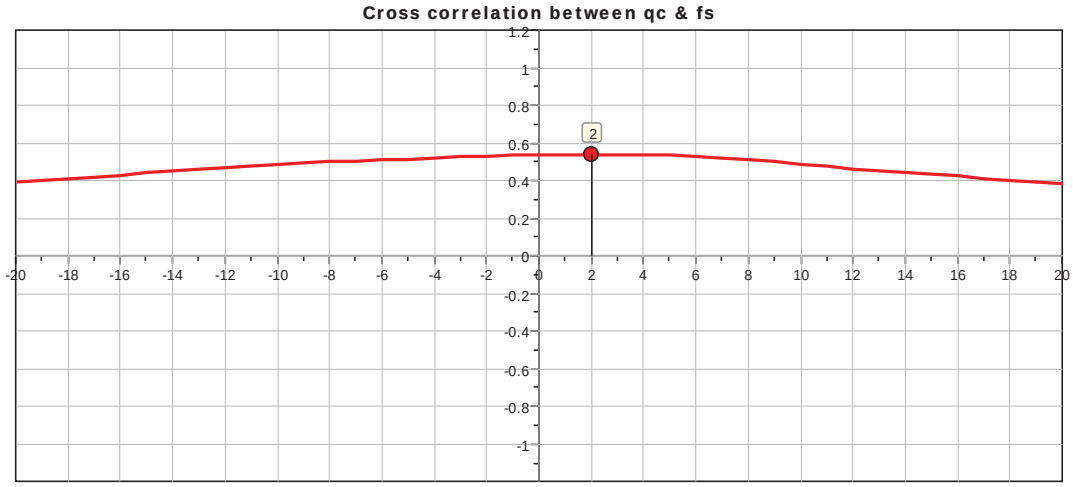

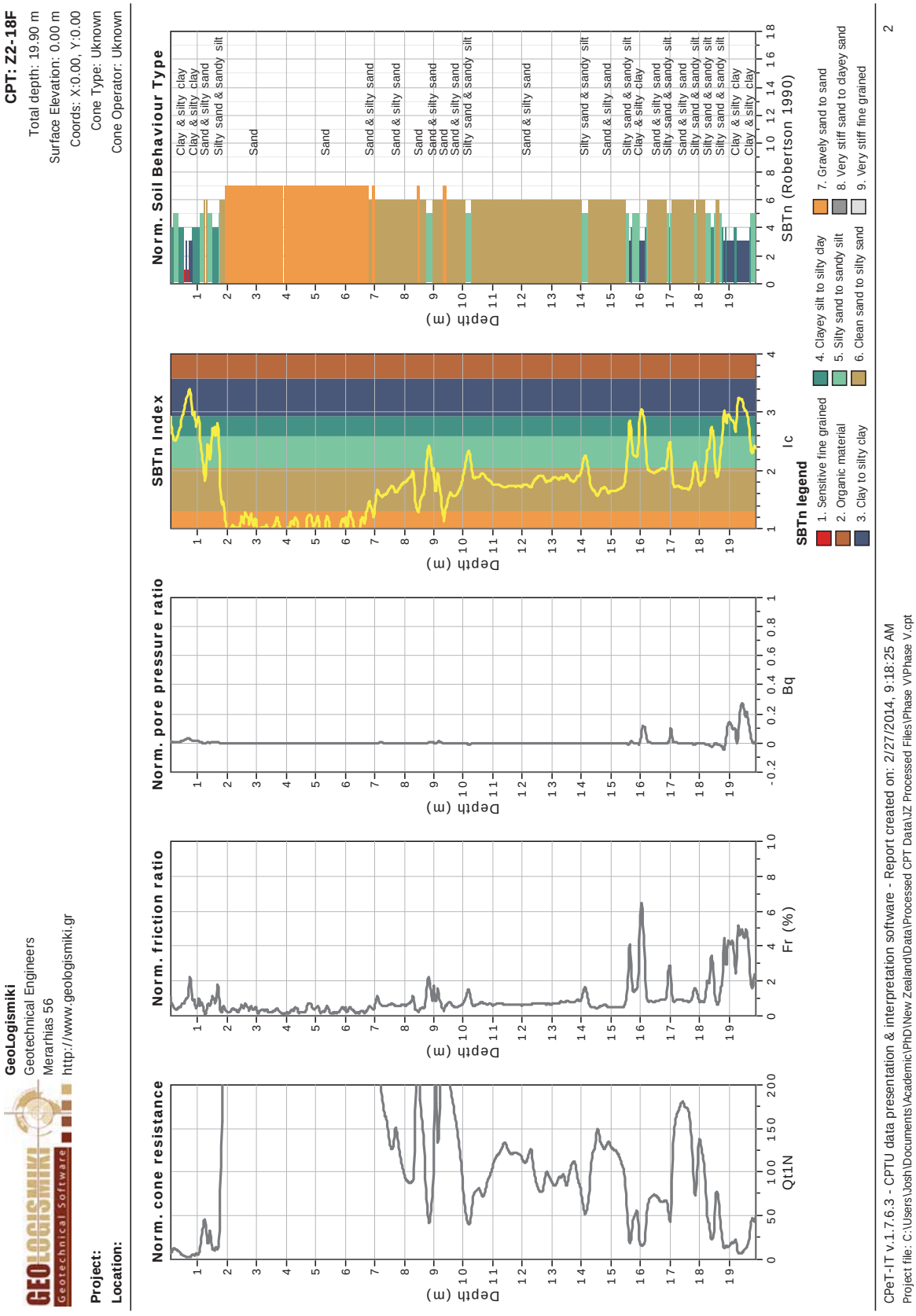
CPT: Z2-18F
Total depth: 19.90 m
Surface Elevation: 0.00 m
Coords: X:0.00, Y:0.00
Cone Type: Uknown
Cone Operator: Uknown
GeoLogismiki
Geotechnical Engineers
Merarhias 56
http://www.geologismiki.gr
Project:
Location:
Norm. cone resistance
Qt1N
Norm. friction ratio
Fr (%)
Norm. pore pressure ratio
Bq
SBTn Index
Ic
Norm. Soil Behaviour Type
SBTn (Robertson 1990)
Depth (m)
SBTn legend
1. Sensitive fine grained
2. Organic material
3. Clay to silty clay
4. Clayey silt to silty clay
5. Silty sand to sandy silt
6. Clean sand to silty sand
7. Gravely sand to sand
8. Very stiff sand to clayey sand
9. Very stiff fine grained
CPeT-IT v.1.7.6.3 - CPTU data presentation & interpretation software - Report created on: 2/27/2014, 9:18:25 AM
Project file: C:\Users\Josh\Documents\Academic\PhD\New Zealand\Data\Processed CPT Data\JZ Processed Files\Phase V\Phase V.cpt
2

GeoLogismiki
Geotechnical Engineers
Merarhias 56
http://www.geologismiki.gr

CPT: Z2-19
Total depth: 19.21 m
Surface Elevation: 0.00 m
Coords: X:0.00, Y:0.00
Cone Type: Uknown
Cone Operator: Uknown

Project:
Location:

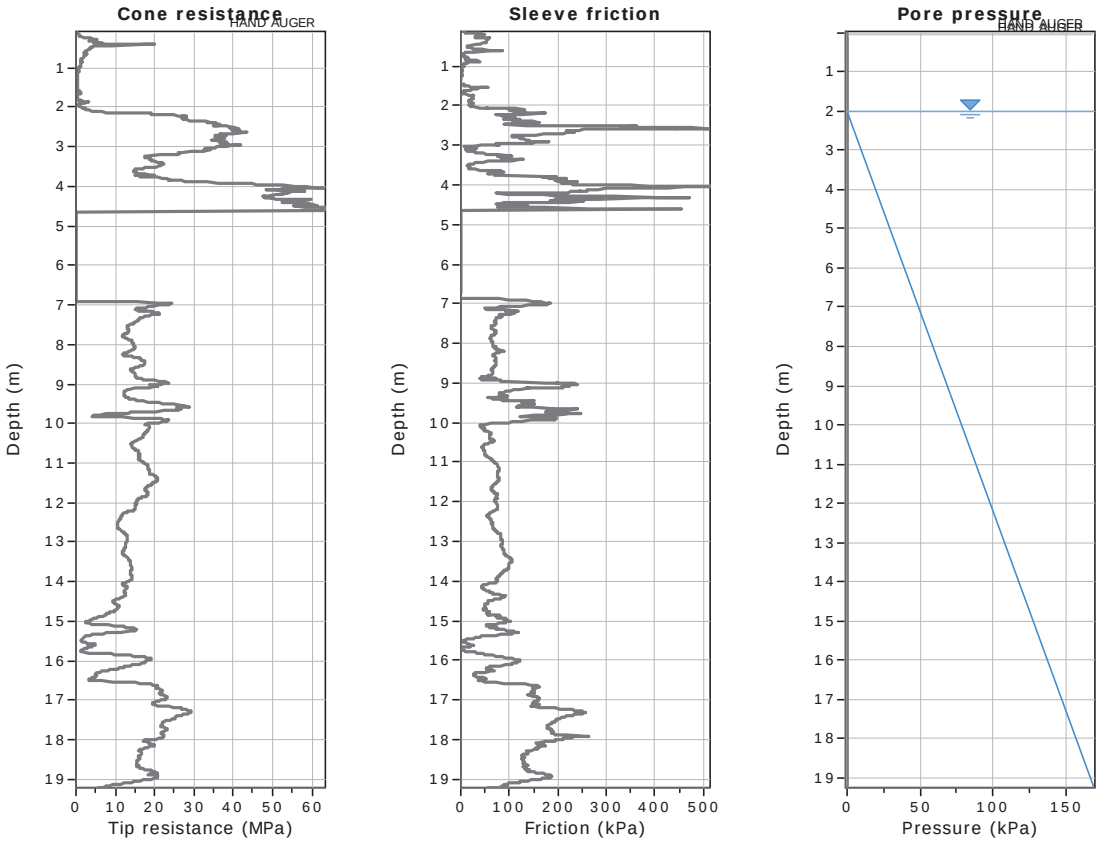

The plot below presents the cross correlation coeficient between the raw qc and fs values (as measured on the field). X axes presents the lag distance (one lag is the distance between two sucessive CPT measurements).

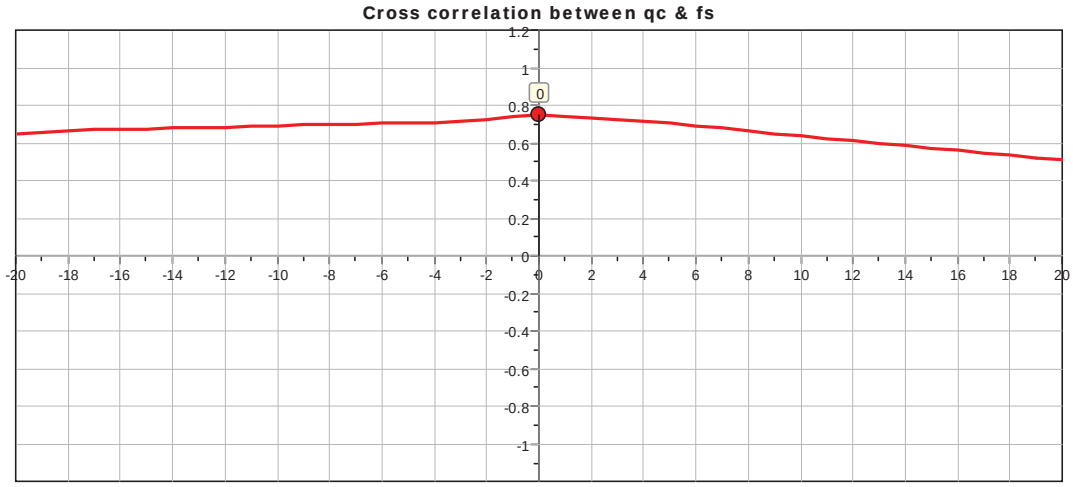

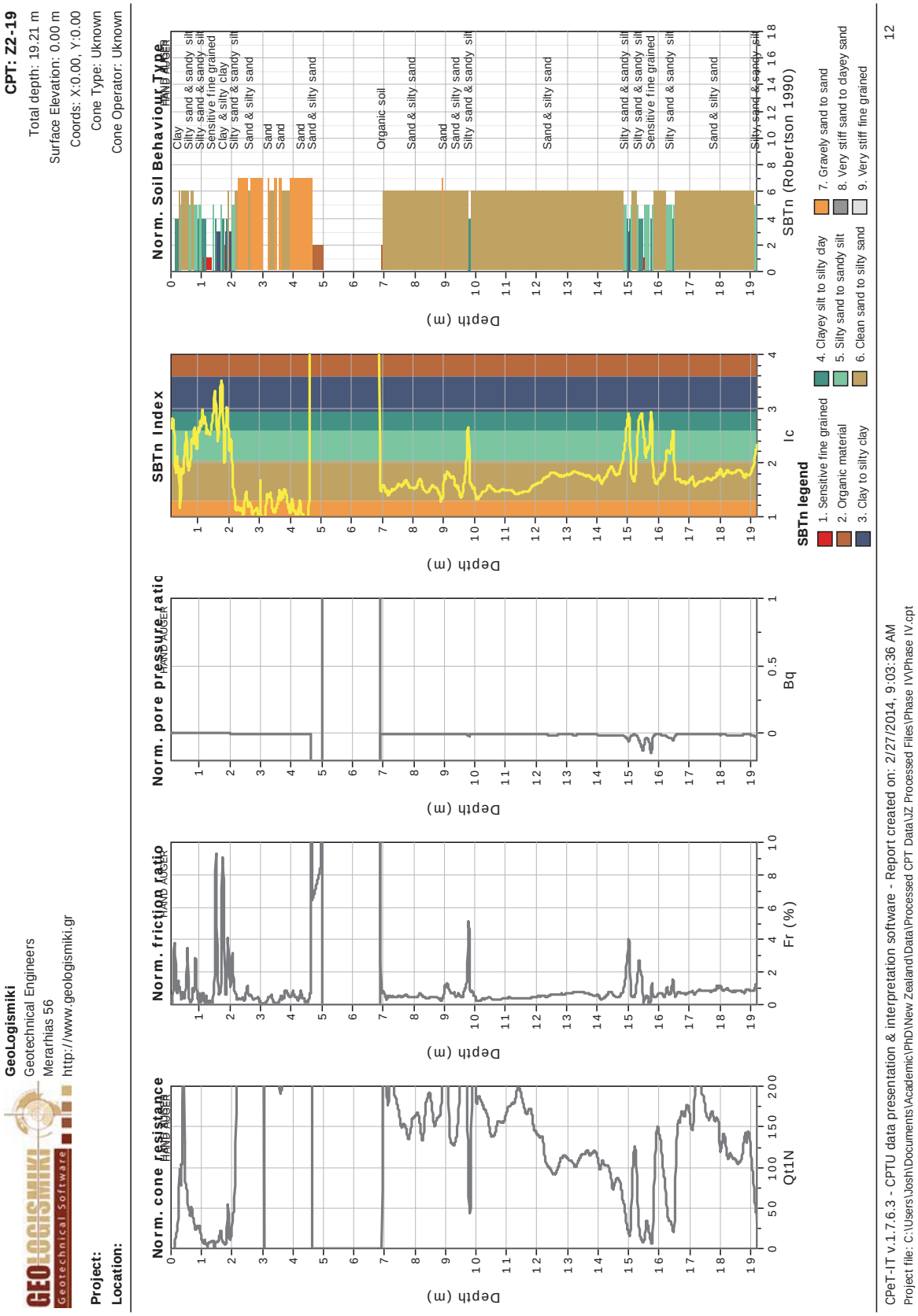
CPT: Z2-19
Total depth: 19.21 m
Surface Elevation: 0.00 m
Coords: X:0.00, Y:0.00
Cone Type: Uknown
Cone Operator: Uknown
GeoLogismiki
Geotechnical Engineers
Merarhias 56
http://www.geologismiki.gr
Project:
Location:
Norm. cone resistance
Norm. friction ratio
Norm. pore pressure ratio
SBTn Index
Norm. Soil Behaviour Type
HAND AUGER
Qt1N
Fr (%)
Bq
Ic
SBTn (Robertson 1990)
Depth (m)
Clay
Silty sand & sandy silt
Sensitive fine grained
Clay & silty clay
Sand & silty sand
Sand
Sand & silty sand
Organic soil
SBTn legend
1. Sensitive fine grained
2. Organic material
3. Clay to silty clay
4. Clayey silt to silty clay
5. Silty sand to sandy silt
6. Clean sand to silty sand
7. Gravely sand to sand
8. Very stiff sand to clayey sand
9. Very stiff fine grained
CPeT-IT v.1.7.6.3 - CPTU data presentation & interpretation software - Report created on: 2/27/2014, 9:03:36 AM
Project file: C:\Users\Josh\Documents\Academic\PhD\New Zealand\Data\Processed CPT Data\JZ Processed Files\Phase IV\Phase IV.cpt
12

GeoLogismiki
Geotechnical Engineers
Merarhias 56
http://www.geologismiki.gr

CPT: Z2-20
Total depth: 21.53 m
Surface Elevation: 0.00 m
Coords: X:0.00, Y:0.00
Cone Type: Uknown
Cone Operator: Uknown

Project:
Location:

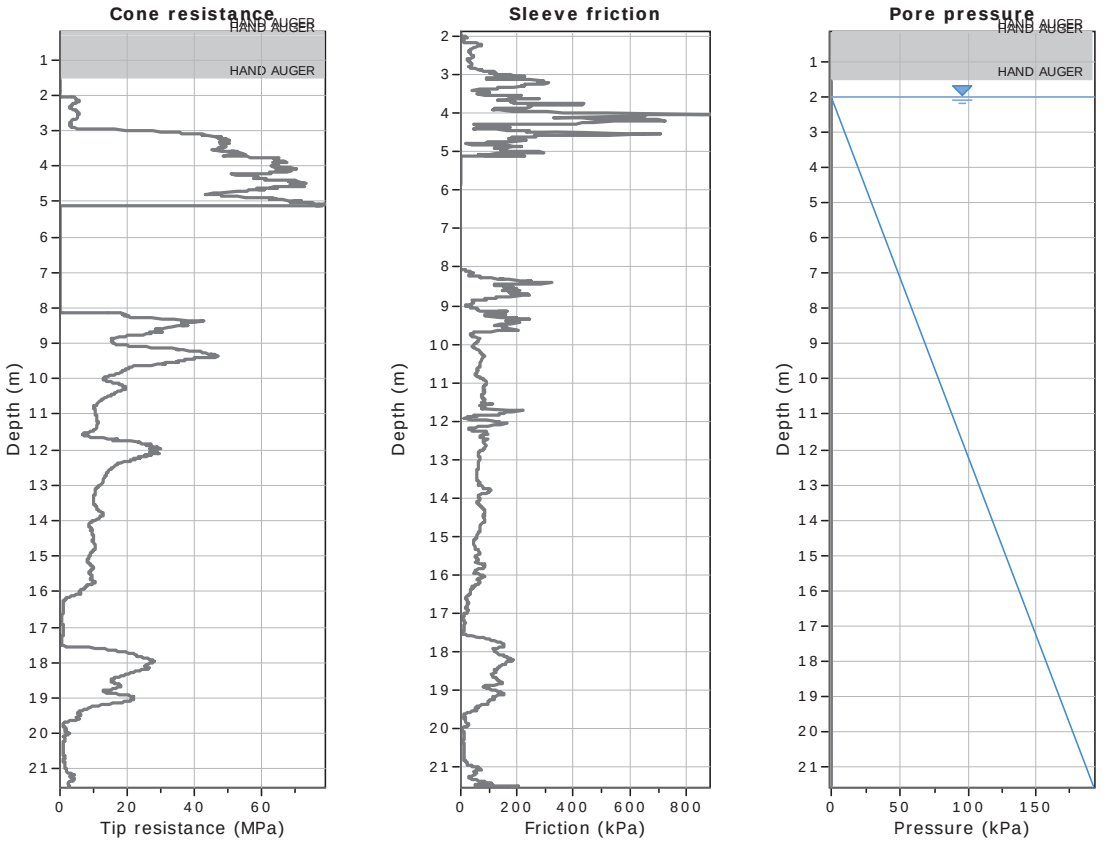

The plot below presents the cross correlation coeficient between the raw qc and fs values (as measured on the field). X axes presents the lag distance (one lag is the distance between two sucessive CPT measurements).

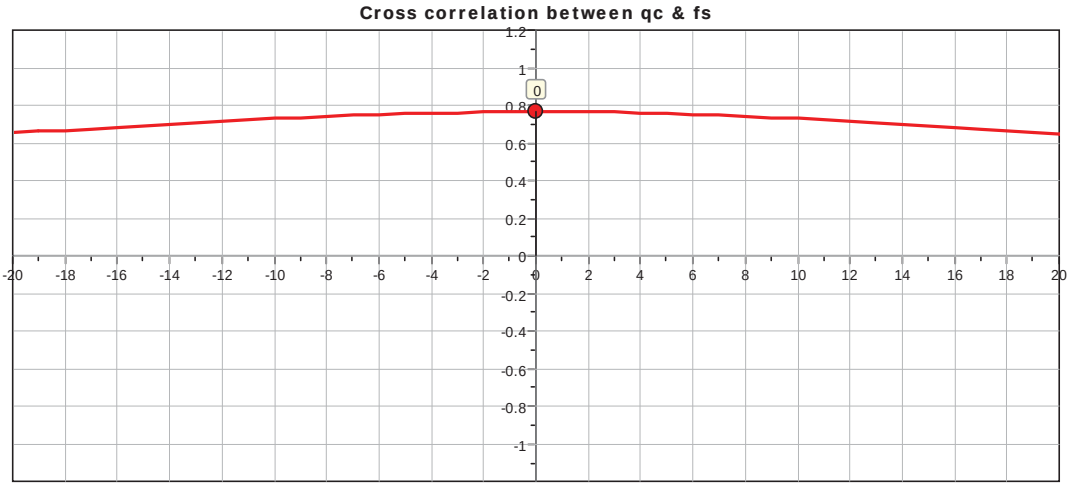

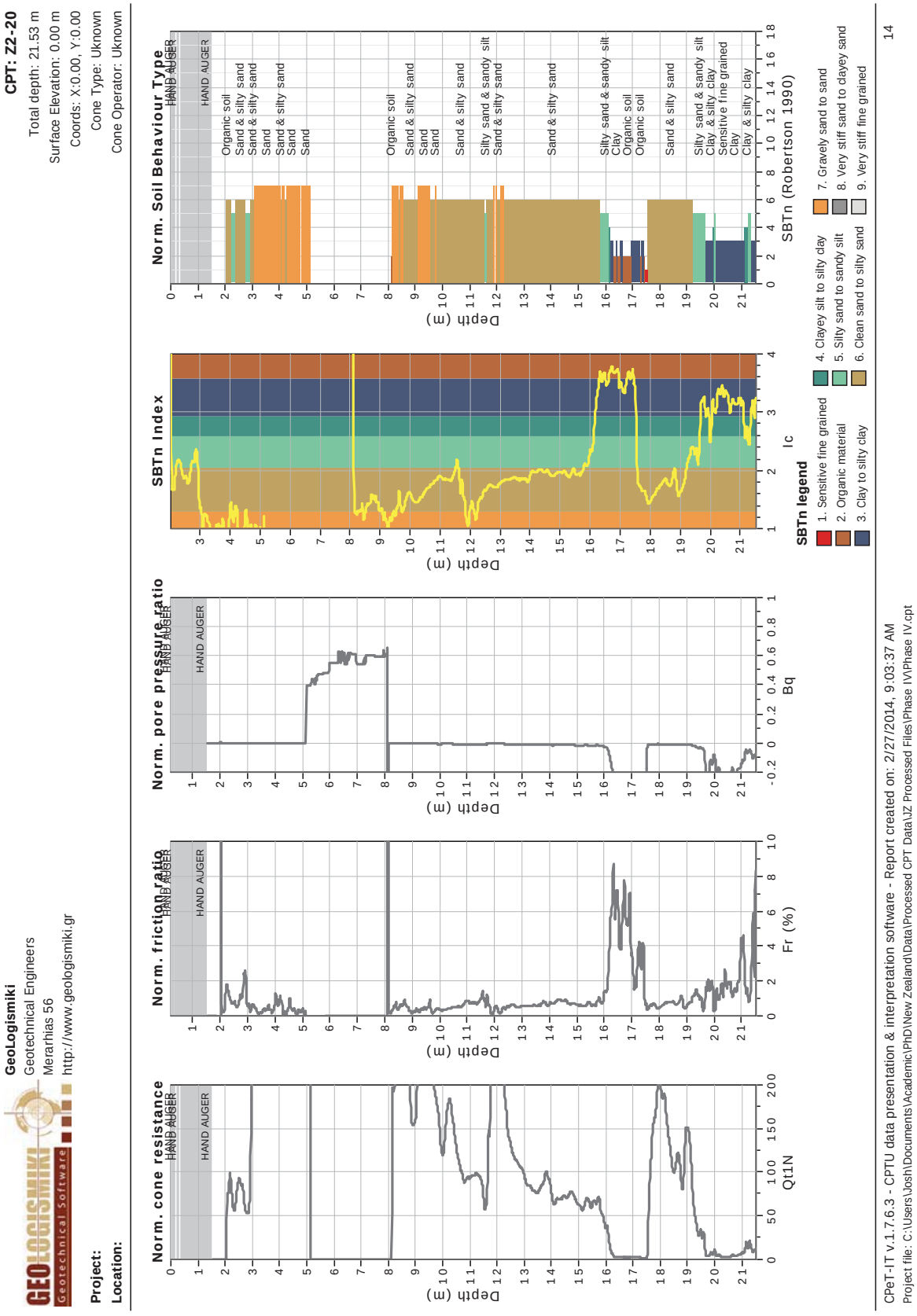
GeoLogismiki
Geotechnical Engineers
Merarchias 56
http://www.geologismiki.gr
Project:
Location:
CPT: Z2-20
Total depth: 21.53 m
Surface Elevation: 0.00 m
Coords: X:0.00, Y:0.00
Cone Type: Uknown
Cone Operator: Uknown
Norm. cone resistance
Norm. friction ratio
Norm. pore pressure ratio
SBTn Index
Norm. Soil Behaviour Type
HAND AUGER
Qt1N
Fr (%)
Bq
Ic
SBTn (Robertson 1990)
Depth (m)
SBTn legend
1. Sensitive fine grained
2. Organic material
3. Clay to silty clay
4. Clayey silt to silty clay
5. Silty sand to sandy silt
6. Clean sand to silty sand
7. Gravely sand to sand
8. Very stiff sand to clayey sand
9. Very stiff fine grained
Organic soil
Sand & silty sand
Sand
Silty sand & sandy silt
Clay & silty clay
Sensitive fine grained
Clay
Clay & silty clay
CPeT-IT v.1.7.6.3 - CPTU data presentation & interpretation software - Report created on: 2/27/2014, 9:03:37 AM
Project file: C:\Users\Josh\Documents\Academic\PhD\New Zealand\Data\Processed CPT Data\JZ Processed Files\Phase IV\Phase IV.cpt
14

GeoLogismiki
Geotechnical Engineers
Merarhias 56
http://www.geologismiki.gr

CPT: Z2-21
Total depth: 20.05 m
Surface Elevation: 0.00 m
Coords: X:0.00, Y:0.00
Cone Type: Uknown
Cone Operator: Uknown

Project:
Location:

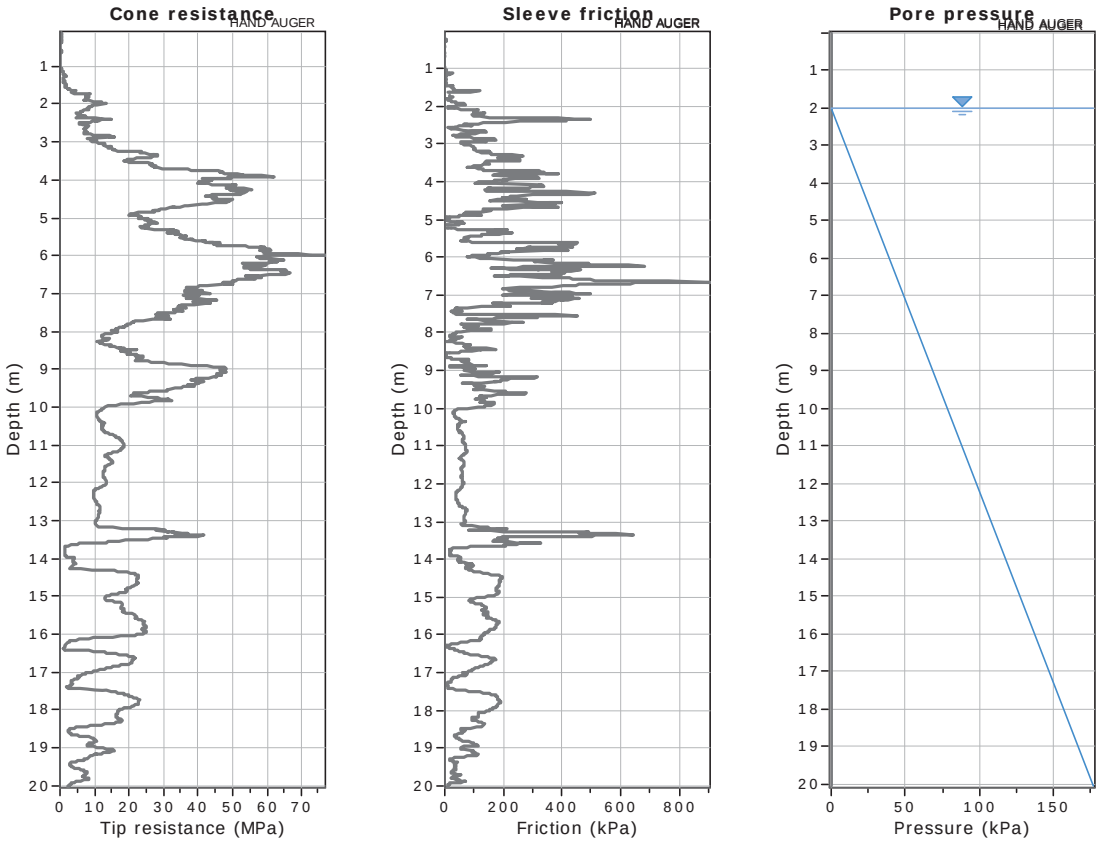

The plot below presents the cross correlation coeficient between the raw qc and fs values (as measured on the field). X axes presents the lag distance (one lag is the distance between two sucessive CPT measurements).

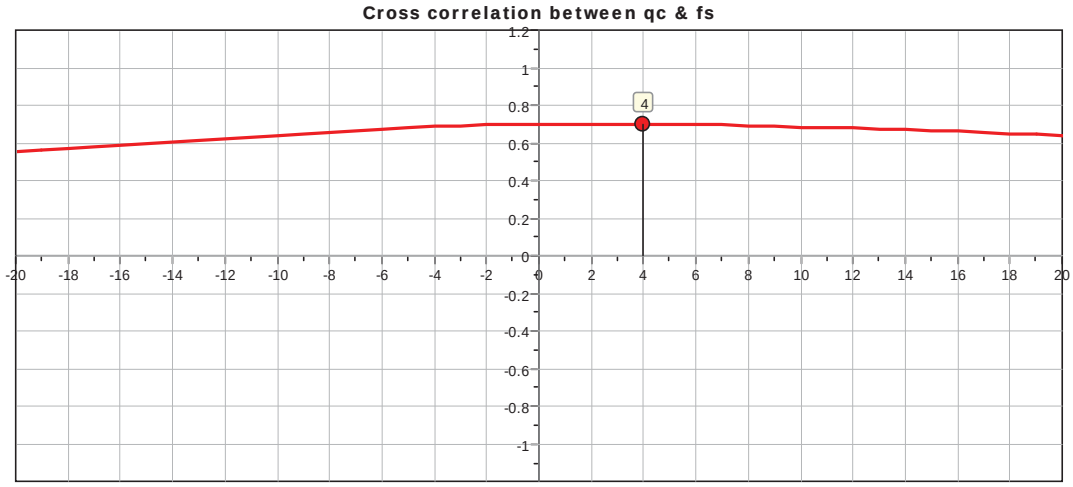

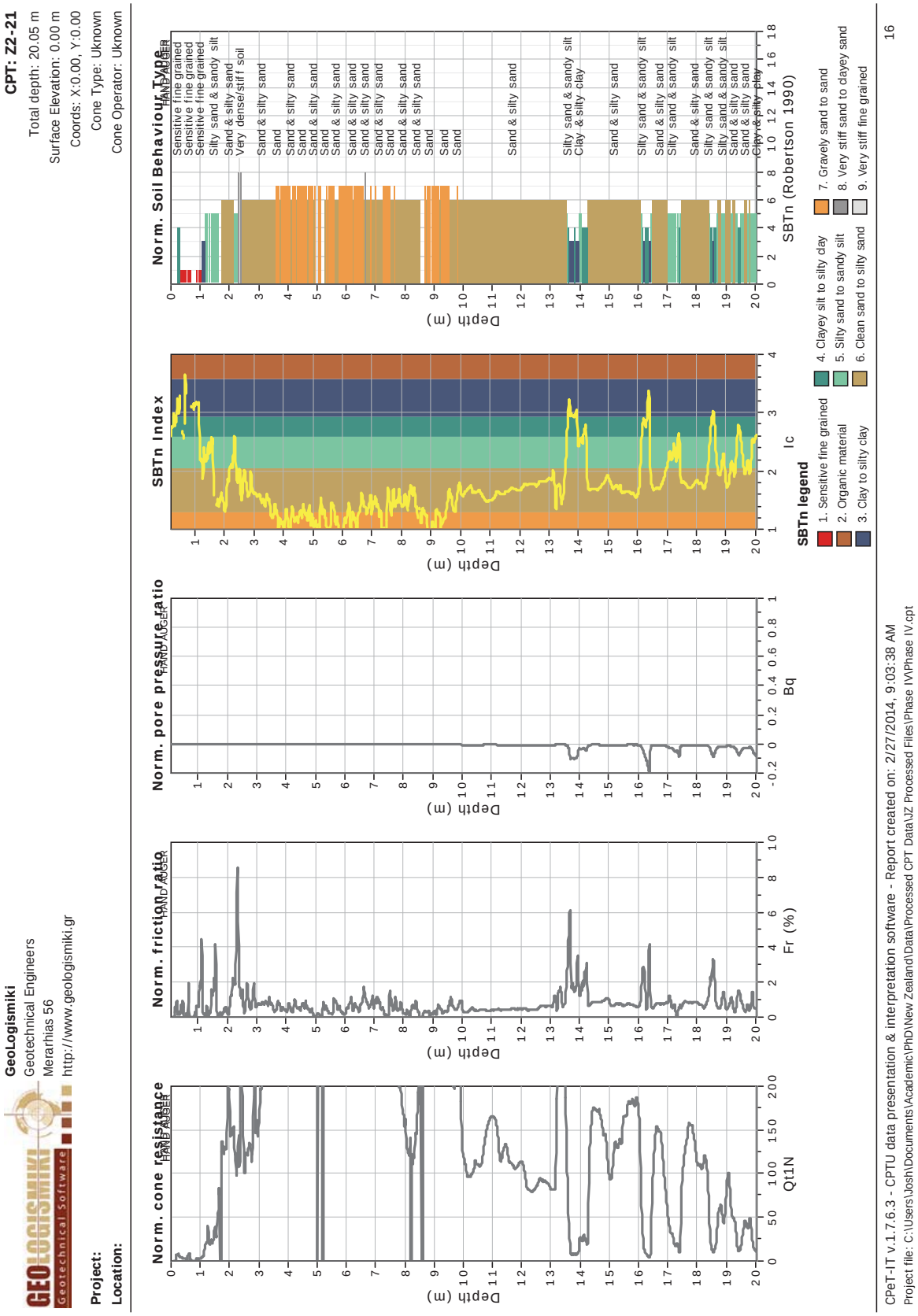
CPT: Z2-21
Total depth: 20.05 m
Surface Elevation: 0.00 m
Coords: X:0.00, Y:0.00
Cone Type: Uknown
Cone Operator: Uknown
GeoLogismiki
Geotechnical Engineers
Merarhias 56
http://www.geologismiki.gr
Project:
Location:
Norm. cone resistance
Norm. friction ratio
Norm. pore pressure ratio
SBTn Index
Norm. Soil Behaviour Type
SBTn (Robertson 1990)
SBTn legend
1. Sensitive fine grained
2. Organic material
3. Clay to silty clay
4. Clayey silt to silty clay
5. Silty sand to sandy silt
6. Clean sand to silty sand
7. Gravely sand to sand
8. Very stiff sand to clayey sand
9. Very stiff fine grained
CPeT-IT v.1.7.6.3 - CPTU data presentation & interpretation software - Report created on: 2/27/2014, 9:03:38 AM
Project file: C:\Users\Josh\Documents\Academic\PhD\New Zealand\Data\Processed CPT Data\JZ Processed Files\Phase IV\Phase IV.cpt
16

GeoLogismiki
Geotechnical Engineers
Merarhias 56
http://www.geologismiki.gr

CPT: Z2-22
Total depth: 13.43 m
Surface Elevation: 0.00 m
Coords: X:0.00, Y:0.00
Cone Type: Uknown
Cone Operator: Uknown

Project:
Location:

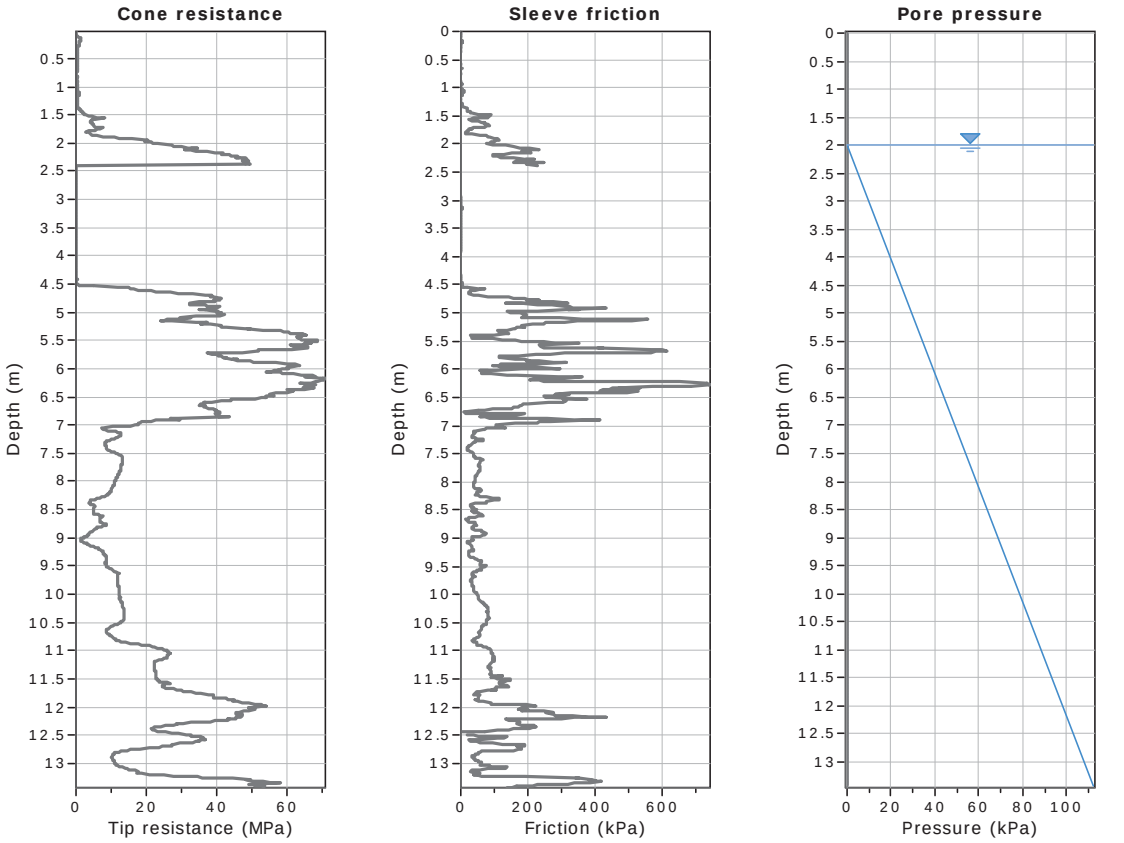

The plot below presents the cross correlation coeficient between the raw qc and fs values (as measured on the field). X axes presents the lag distance (one lag is the distance between two sucessive CPT measurements).

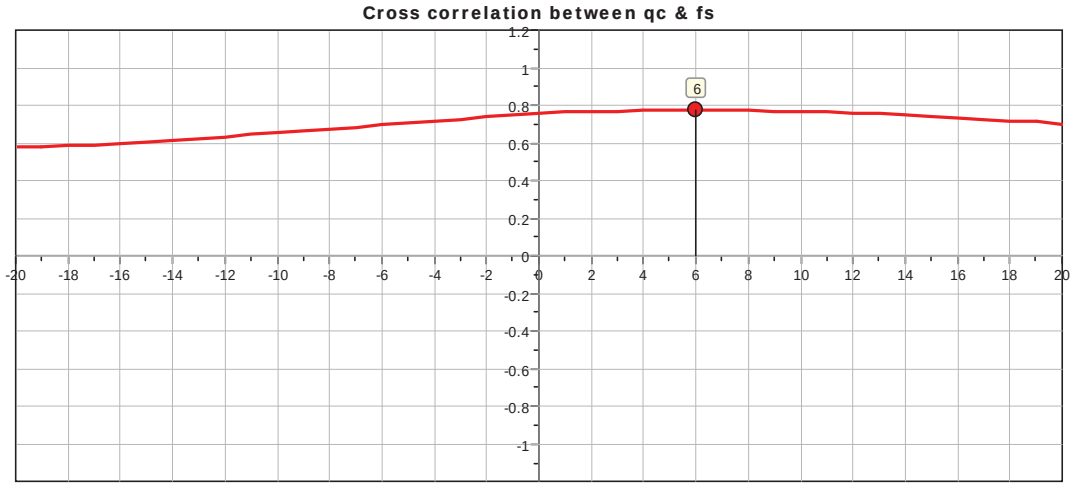

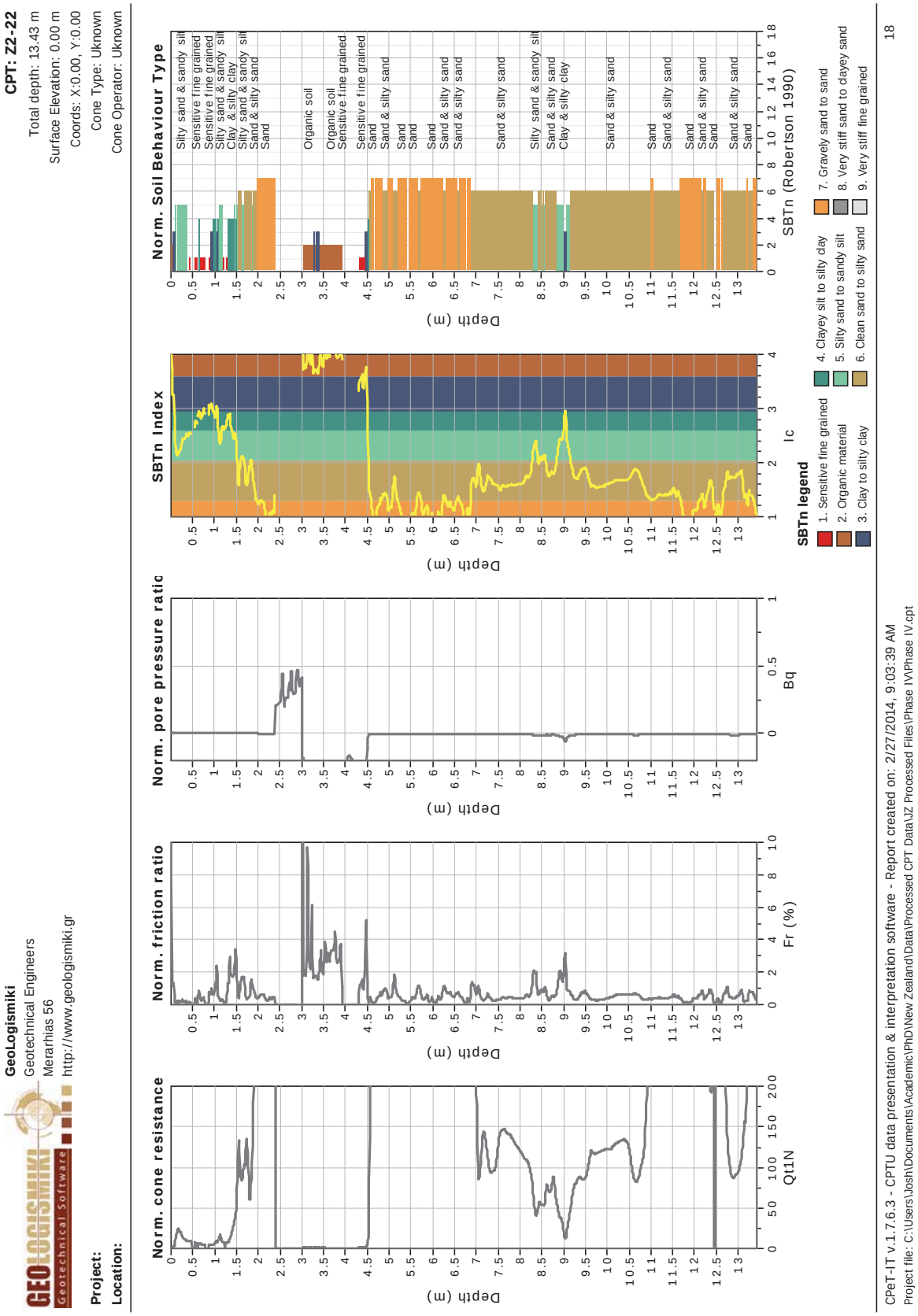
GeoLogismiki
Geotechnical Engineers
Merarchias 56
http://www.geologismiki.gr
Project:
Location:
CPT: Z2-22
Total depth: 13.43 m
Surface Elevation: 0.00 m
Coords: X:0.00, Y:0.00
Cone Type: Uknown
Cone Operator: Uknown
Norm. cone resistance
Qt1N
Norm. friction ratio
Fr (%)
Norm. pore pressure ratio
Bq
SBTn Index
Ic
Norm. Soil Behaviour Type
SBTn (Robertson 1990)
Depth (m)
SBTn legend
1. Sensitive fine grained
2. Organic material
3. Clay to silty clay
4. Clayey silt to silty clay
5. Silty sand to sandy silt
6. Clean sand to silty sand
7. Gravely sand to sand
8. Very stiff sand to clayey sand
9. Very stiff fine grained
CPeT-IT v.1.7.6.3 - CPTU data presentation & interpretation software - Report created on: 2/27/2014, 9:03:39 AM
Project file: C:\Users\Josh\Documents\Academic\PhD\New Zealand\Data\Processed CPT Data\JZ Processed Files\Phase IV\Phase IV.cpt
18

GeoLogismiki
Geotechnical Engineers
Merarhias 56
http://www.geologismiki.gr

CPT: Z2-23
Total depth: 13.29 m
Surface Elevation: 0.00 m
Coords: X:0.00, Y:0.00
Cone Type: Uknown
Cone Operator: Uknown

Project:
Location:

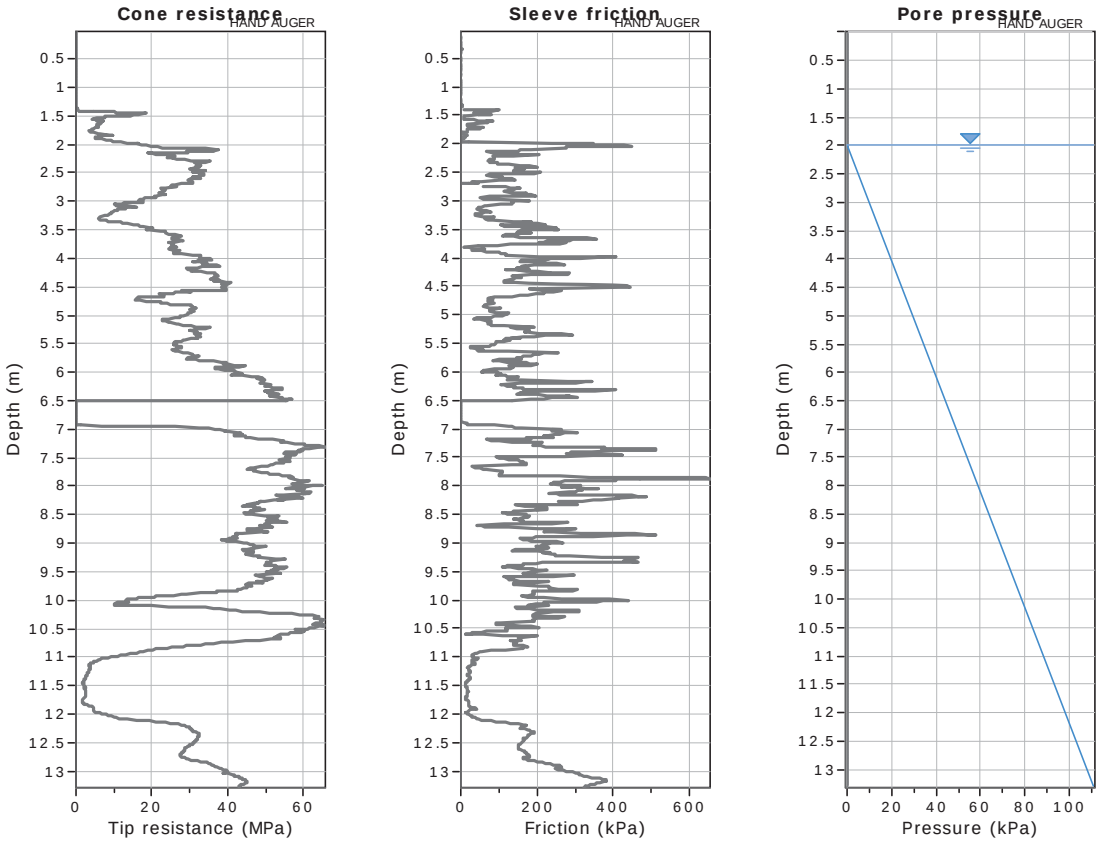

The plot below presents the cross correlation coeficient between the raw qc and fs values (as measured on the field). X axes presents the lag distance (one lag is the distance between two sucessive CPT measurements).

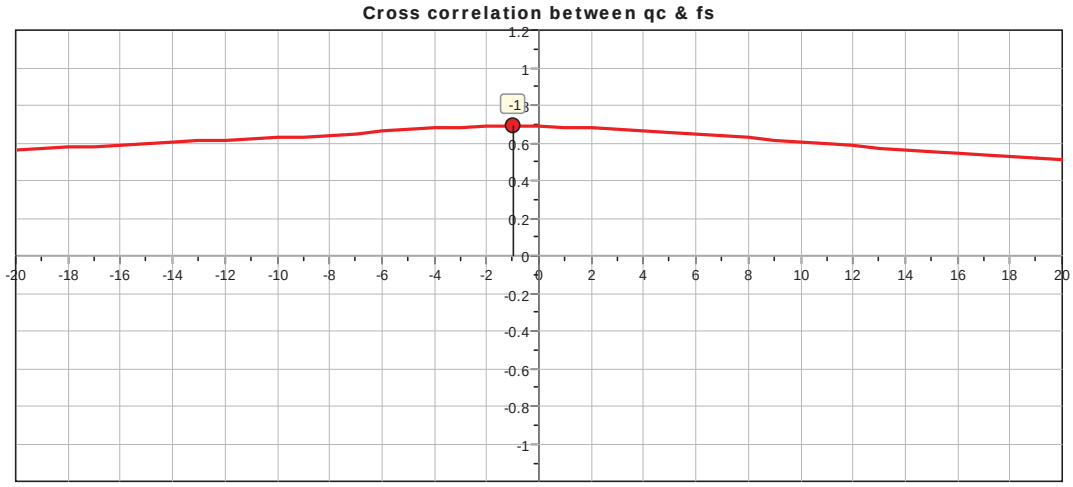

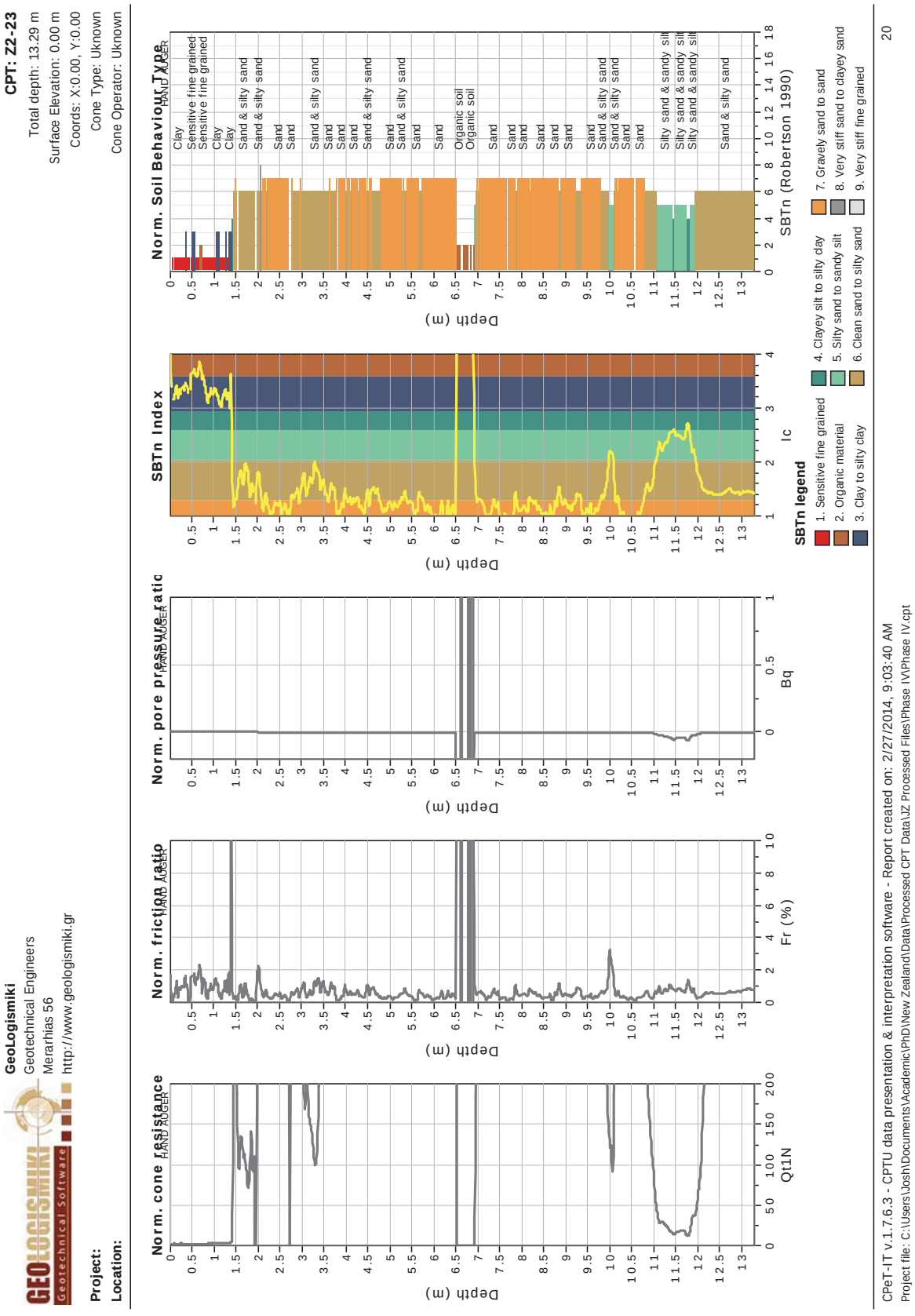
GeoLogismiki
Geotechnical Engineers
Merarhias 56
http://www.geologismiki.gr
Project:
Location:
CPT: Z2-23
Total depth: 13.29 m
Surface Elevation: 0.00 m
Coords: X:0.00, Y:0.00
Cone Type: Uknown
Cone Operator: Uknown
Norm. cone resistance
Norm. friction ratio
Norm. pore pressure ratio
SBTn Index
Norm. Soil Behaviour Type
HAND AUGER
Qt1N
Fr (%)
Bq
Ic
SBTn (Robertson 1990)
Depth (m)
SBTn legend
1. Sensitive fine grained
2. Organic material
3. Clay to silty clay
4. Clayey silt to silty clay
5. Silty sand to sandy silt
6. Clean sand to silty sand
7. Gravely sand to sand
8. Very stiff sand to clayey sand
9. Very stiff fine grained
CPeT-IT v.1.7.6.3 - CPTU data presentation & interpretation software - Report created on: 2/27/2014, 9:03:40 AM
Project file: C:\Users\Josh\Documents\Academic\PhD\New Zealand\Data\Processed CPT Data\JZ Processed Files\Phase IV\Phase IV.cpt
20

GeoLogismiki
Geotechnical Engineers
Merarhias 56
http://www.geologismiki.gr

CPT: Z2-24
Total depth: 19.80 m
Surface Elevation: 0.00 m
Coords: X:0.00, Y:0.00
Cone Type: Uknown
Cone Operator: Uknown

Project:
Location:

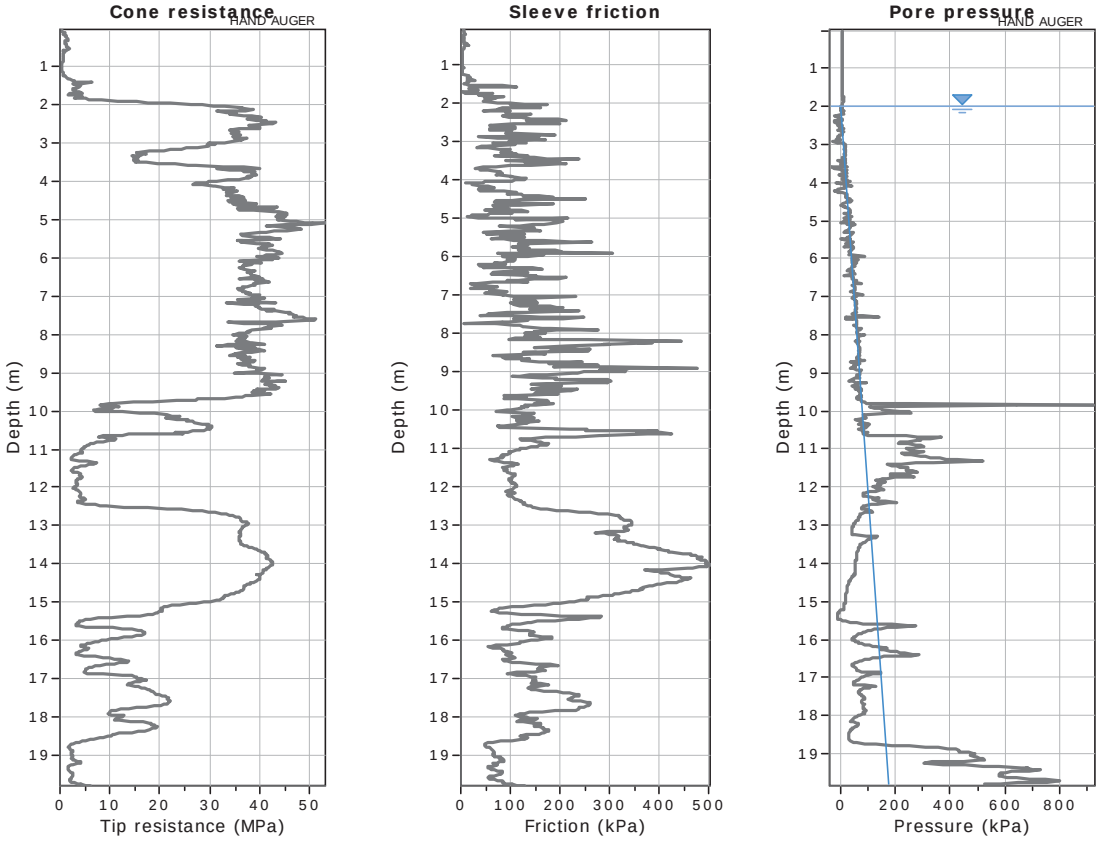

The plot below presents the cross correlation coeficient between the raw qc and fs values (as measured on the field). X axes presents the lag distance (one lag is the distance between two sucessive CPT measurements).

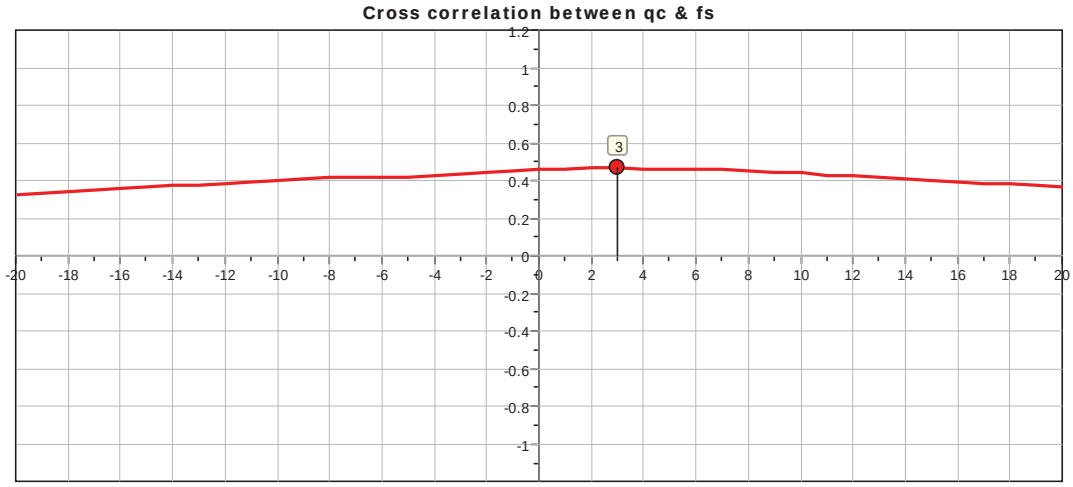

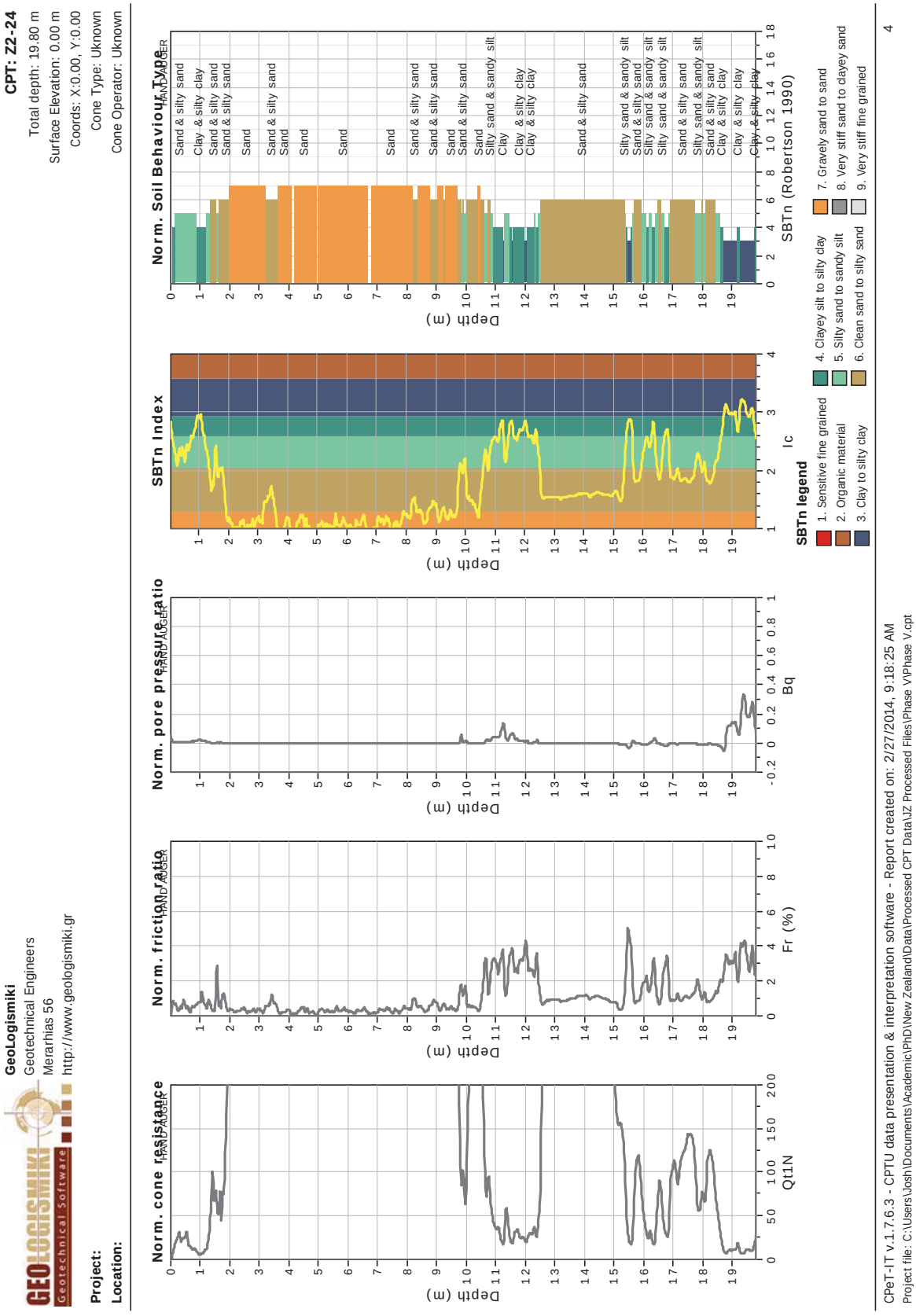
CPT: Z2-24
Total depth: 19.80 m
Surface Elevation: 0.00 m
Coords: X:0.00, Y:0.00
Cone Type: Uknown
Cone Operator: Uknown
GeoLogismiki
Geotechnical Engineers
Merarhias 56
http://www.geologismiki.gr
Project:
Location:
Norm. cone resistance
Norm. friction ratio
Norm. pore pressure ratio
SBTn Index
Norm. Soil Behaviour Type
HAND AUGER
Depth (m)
Qt1N
Fr (%)
Bq
Ic
SBTn (Robertson 1990)
SBTn legend
1. Sensitive fine grained
2. Organic material
3. Clay to silty clay
4. Clayey silt to silty clay
5. Silty sand to sandy silt
6. Clean sand to silty sand
7. Gravely sand to sand
8. Very stiff sand to clayey sand
9. Very stiff fine grained
CPeT-IT v.1.7.6.3 - CPTU data presentation & interpretation software - Report created on: 2/27/2014, 9:18:25 AM
Project file: C:\Users\Josh\Documents\Academic\PhD\New Zealand\Data\Processed CPT Data\JZ Processed Files\Phase V\Phase V.cpt
4

GeoLogismiki
Geotechnical Engineers
Merarhias 56
http://www.geologismiki.gr

CPT: Z2-25
Total depth: 20.38 m
Surface Elevation: 0.00 m
Coords: X:0.00, Y:0.00
Cone Type: Uknown
Cone Operator: Uknown

Project:
Location:

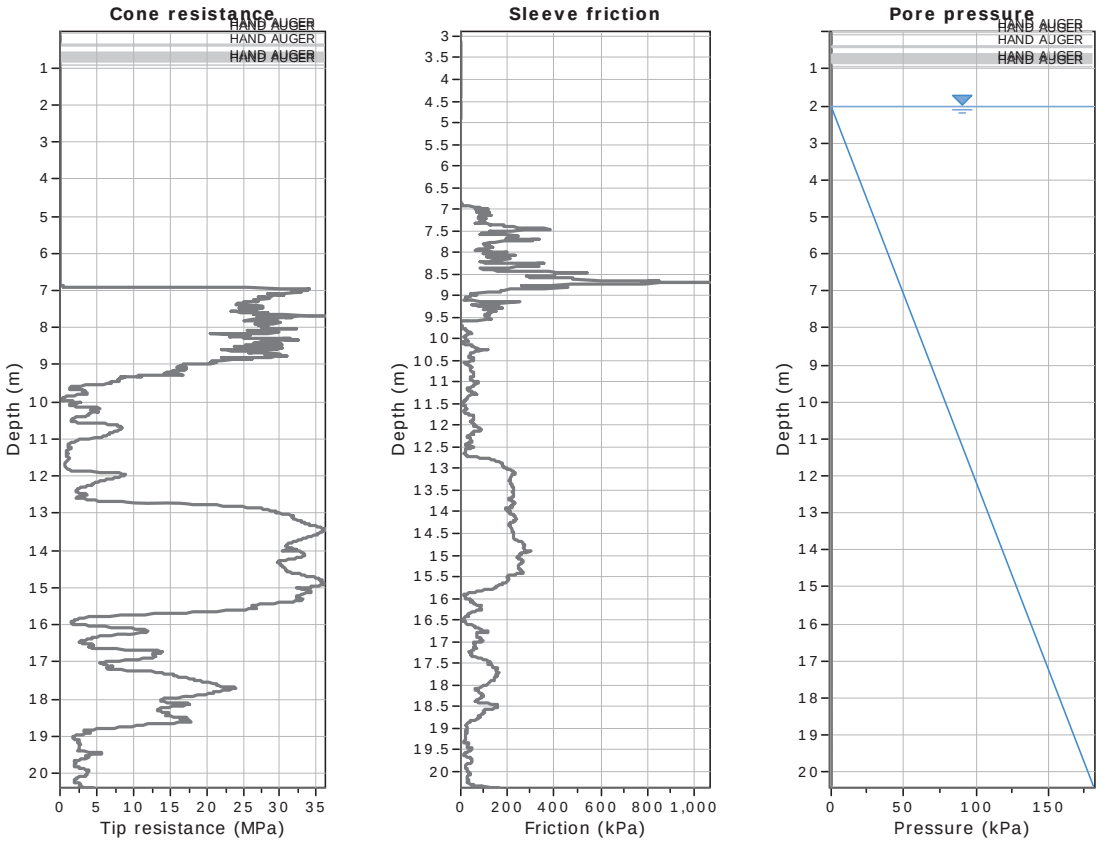

The plot below presents the cross correlation coeficient between the raw qc and fs values (as measured on the field). X axes presents the lag distance (one lag is the distance between two sucessive CPT measurements).

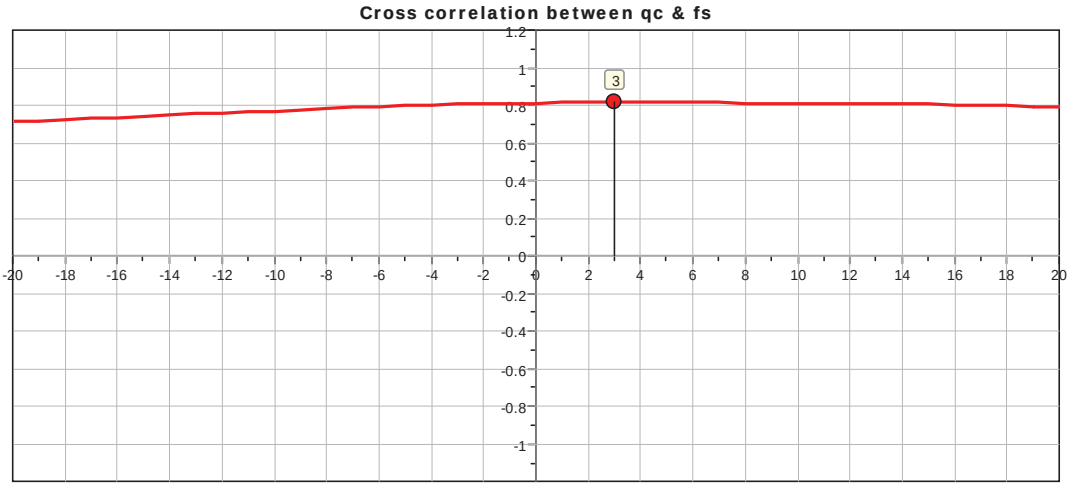

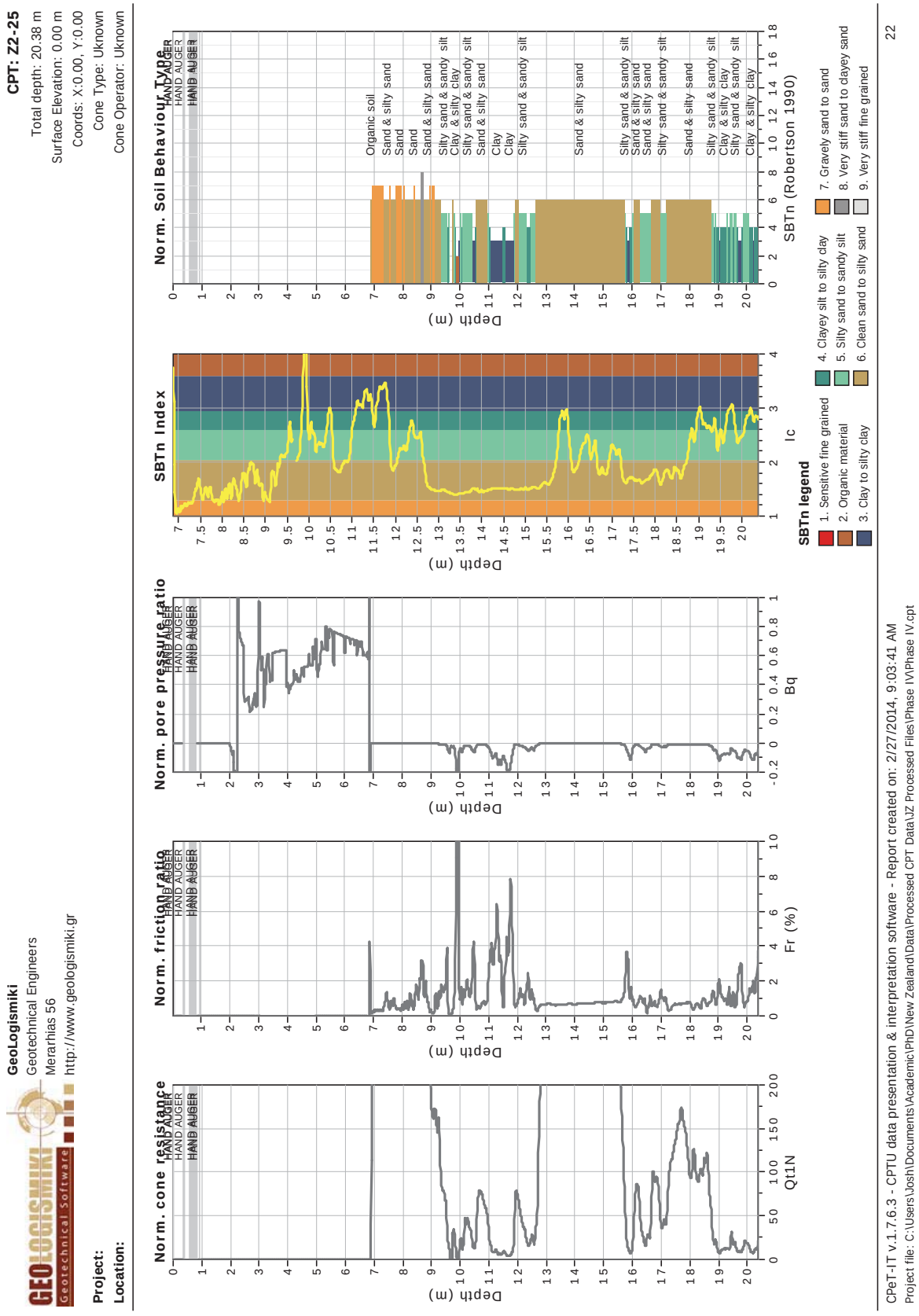
GeoLogismiki
Geotechnical Engineers
Merarhias 56
http://www.geologismiki.gr
Project:
Location:
CPT: Z2-25
Total depth: 20.38 m
Surface Elevation: 0.00 m
Coords: X:0.00, Y:0.00
Cone Type: Uknown
Cone Operator: Uknown
Norm. cone resistance
Qt1N
Norm. friction ratio
Fr (%)
Norm. pore pressure ratio
Bq
SBTn Index
Ic
Norm. Soil Behaviour Type
SBTn (Robertson 1990)
Depth (m)
HAND AUGER
Organic soil
Sand & silty sand
Sand
Sand & silty sand
Silty sand & sandy silt
Clay & silty clay
Silty sand & sandy silt
Sand & silty sand
Clay
Clay
Silty sand & sandy silt
Sand & silty sand
Silty sand & sandy silt
Sand & silty sand
Silty sand & sandy silt
Sand & silty sand
Silty sand & sandy silt
Clay & silty clay
Silty sand & sandy silt
Clay & silty clay
SBTn legend
1. Sensitive fine grained
2. Organic material
3. Clay to silty clay
4. Clayey silt to silty clay
5. Silty sand to sandy silt
6. Clean sand to silty sand
7. Gravely sand to sand
8. Very stiff sand to clayey sand
9. Very stiff fine grained
CPeT-IT v.1.7.6.3 - CPTU data presentation & interpretation software - Report created on: 2/27/2014, 9:03:41 AM
Project file: C:\Users\Josh\Documents\Academic\PhD\New Zealand\Data\Processed CPT Data\JZ Processed Files\Phase IV\Phase IV.cpt
22

GeoLogismiki
Geotechnical Engineers
Merarhias 56
http://www.geologismiki.gr

CPT: Z2-25F
Total depth: 19.80 m
Surface Elevation: 0.00 m
Coords: X:0.00, Y:0.00
Cone Type: Uknown
Cone Operator: Uknown

Project:
Location:

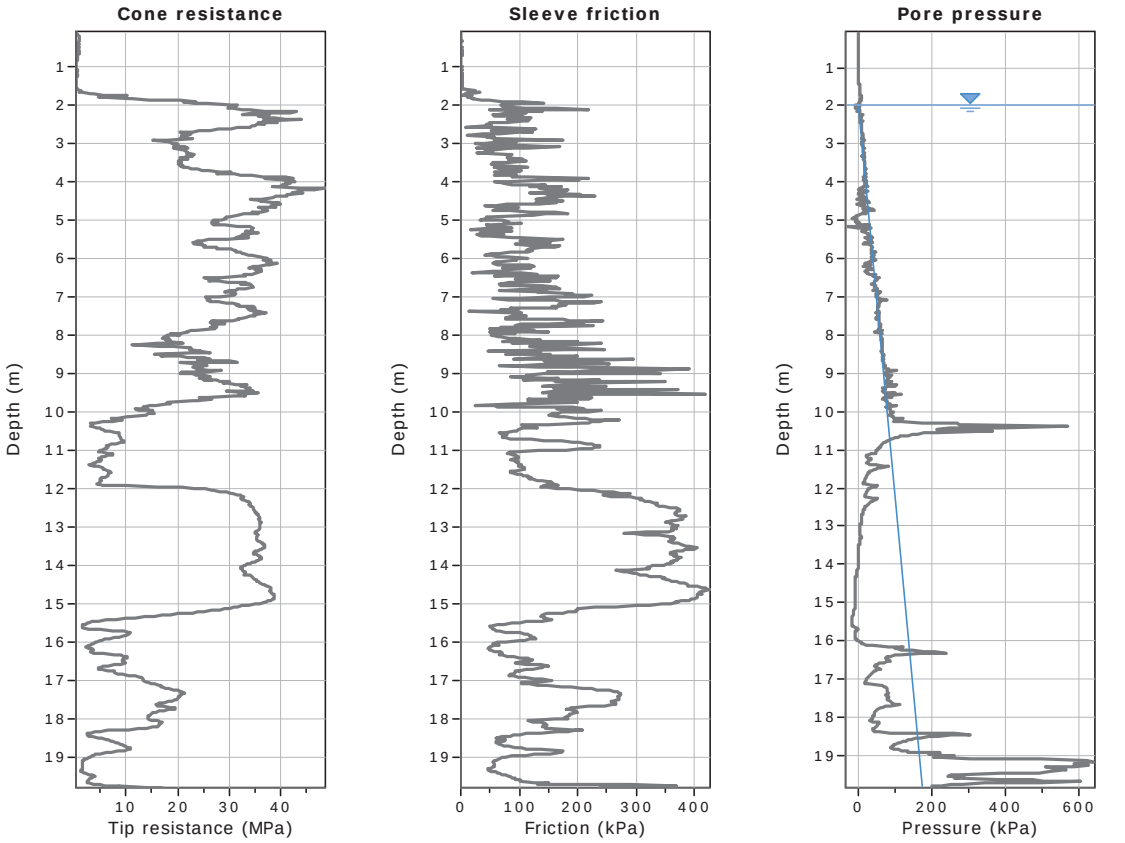

The plot below presents the cross correlation coeficient between the raw qc and fs values (as measured on the field). X axes presents the lag distance (one lag is the distance between two sucessive CPT measurements).

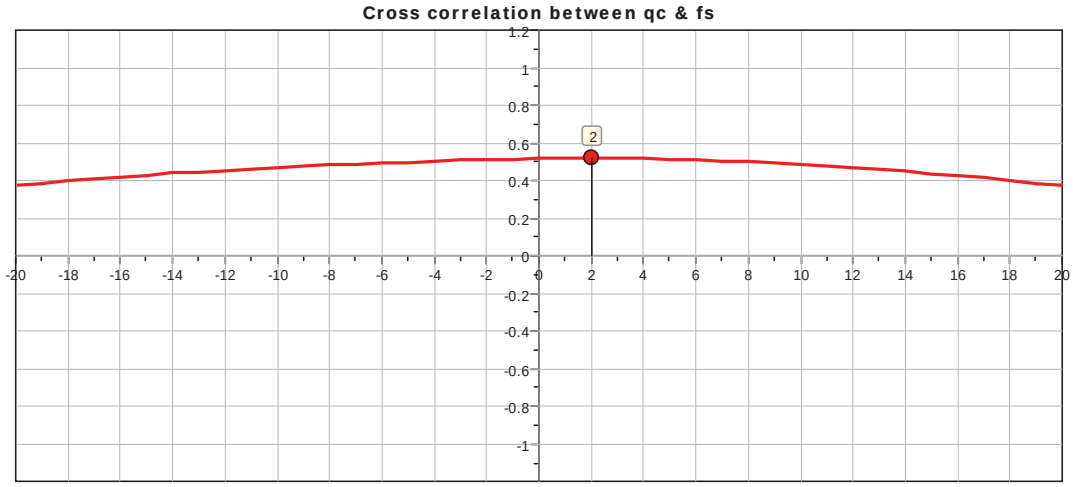

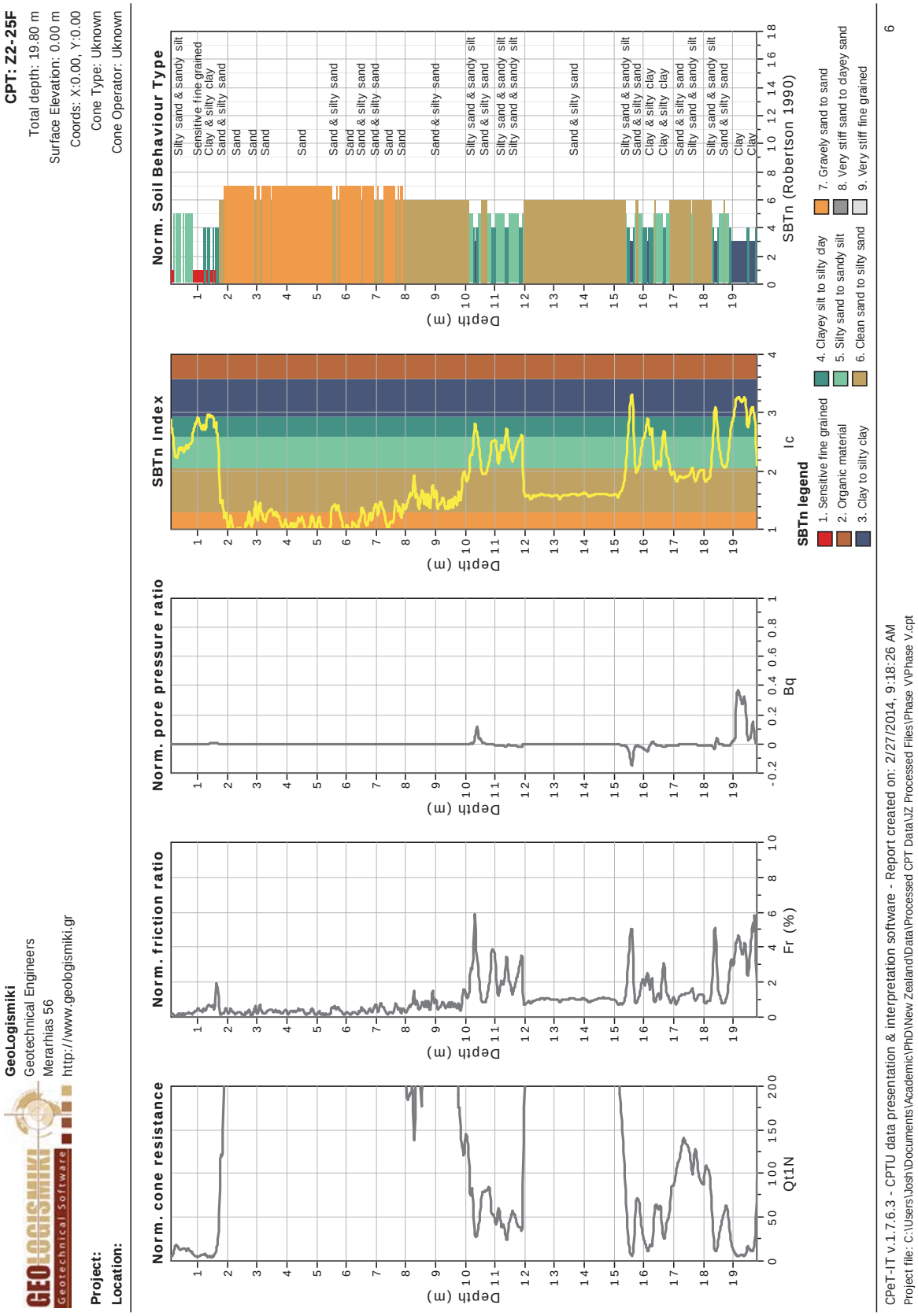
GeoLogismiki
Geotechnical Engineers
Merarhias 56
http://www.geologismiki.gr
Project:
Location:
CPT: Z2-25F
Total depth: 19.80 m
Surface Elevation: 0.00 m
Coords: X:0.00, Y:0.00
Cone Type: Uknown
Cone Operator: Uknown
Norm. cone resistance
Qt1N
Norm. friction ratio
Fr (%)
Norm. pore pressure ratio
Bq
SBTn Index
Ic
Norm. Soil Behaviour Type
SBTn (Robertson 1990)
Depth (m)
SBTn legend
1. Sensitive fine grained
2. Organic material
3. Clay to silty clay
4. Clayey silt to silty clay
5. Silty sand to sandy silt
6. Clean sand to silty sand
7. Gravely sand to sand
8. Very stiff sand to clayey sand
9. Very stiff fine grained
CPeT-IT v.1.7.6.3 - CPTU data presentation & interpretation software - Report created on: 2/27/2014, 9:18:26 AM
Project file: C:\Users\Josh\Documents\Academic\PhD\New Zealand\Data\Processed CPT Data\JZ Processed Files\Phase V\Phase V.cpt
6

GeoLogismiki
Geotechnical Engineers
Merarhias 56
http://www.geologismiki.gr

CPT: Z2-26
Total depth: 19.90 m
Surface Elevation: 0.00 m
Coords: X:0.00, Y:0.00
Cone Type: Uknown
Cone Operator: Uknown

Project:
Location:

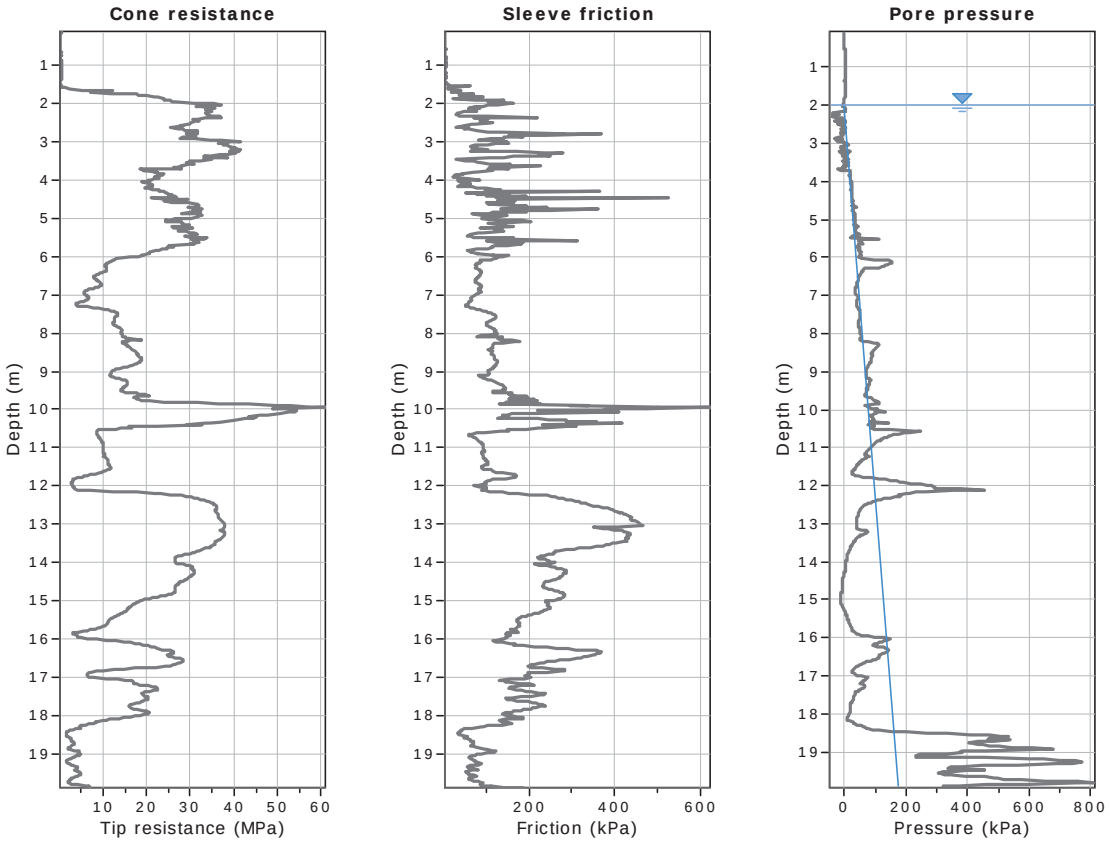

The plot below presents the cross correlation coeficient between the raw qc and fs values (as measured on the field). X axes presents the lag distance (one lag is the distance between two sucessive CPT measurements).

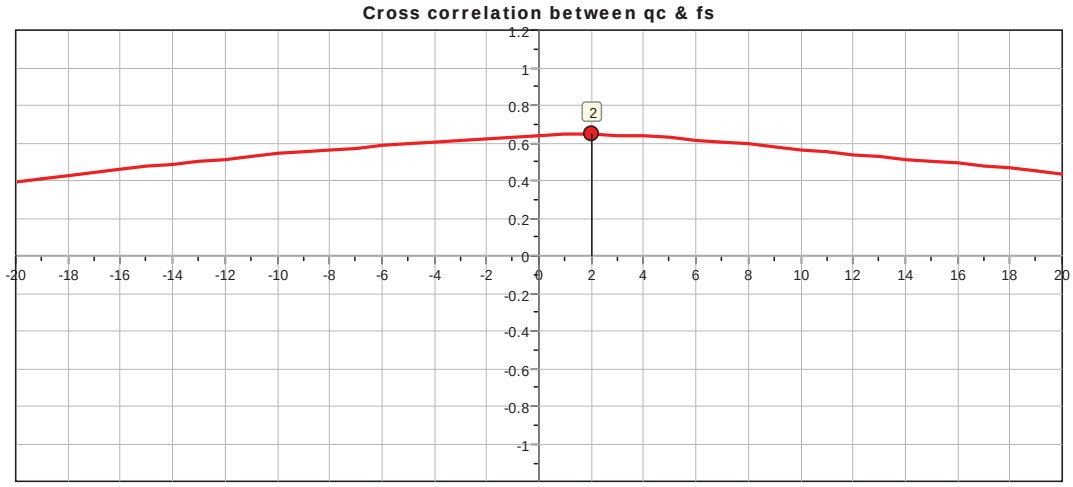

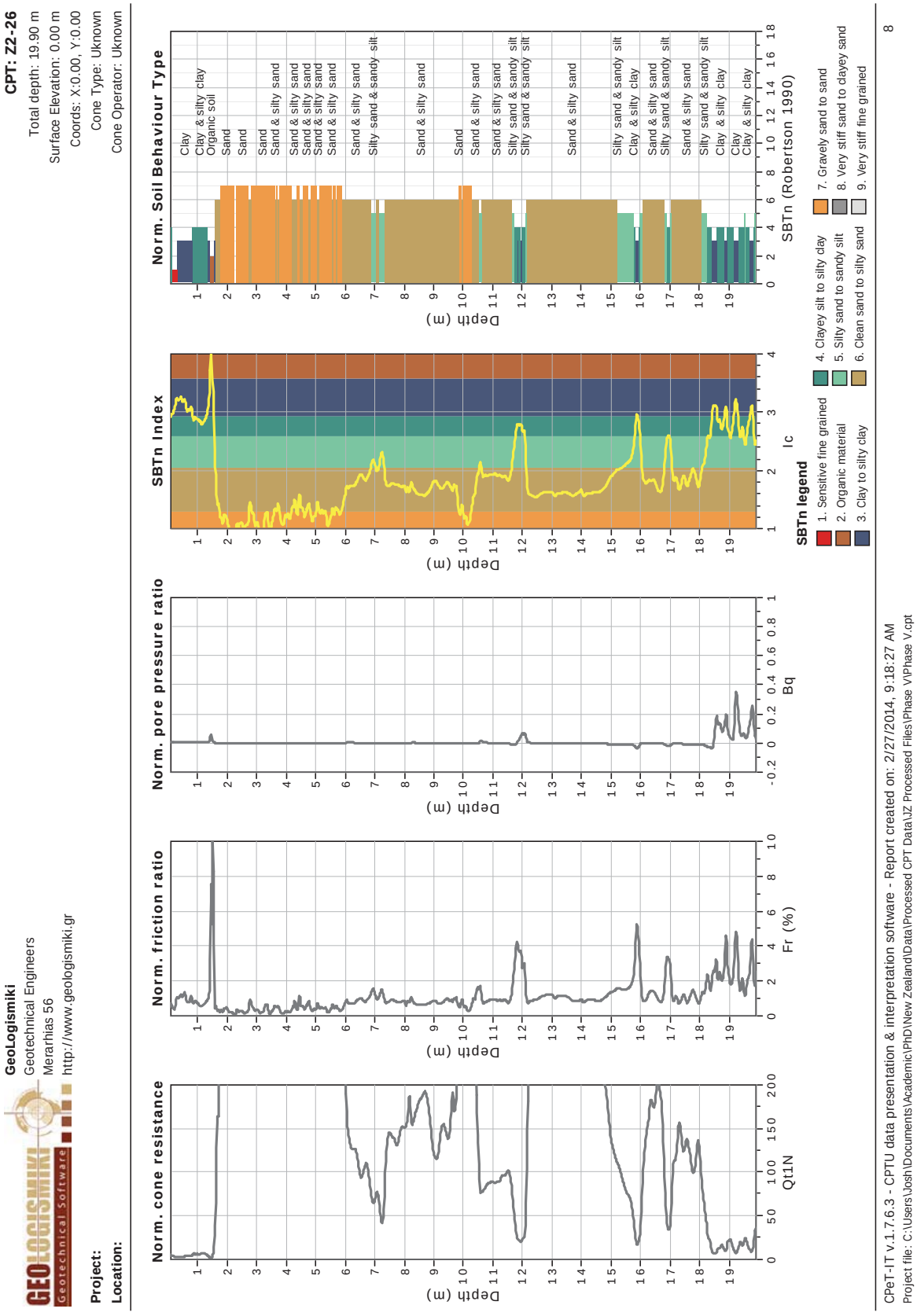
CPT: Z2-26
Total depth: 19.90 m
Surface Elevation: 0.00 m
Coords: X:0.00, Y:0.00
Cone Type: Uknown
Cone Operator: Uknown
GeoLogismiki
Geotechnical Engineers
Merarhias 56
http://www.geologismiki.gr
Project:
Location:
Norm. cone resistance
Qt1N
Norm. friction ratio
Fr (%)
Norm. pore pressure ratio
Bq
SBTn Index
Ic
Norm. Soil Behaviour Type
SBTn (Robertson 1990)
Depth (m)
SBTn legend
1. Sensitive fine grained
2. Organic material
3. Clay to silty clay
4. Clayey silt to silty clay
5. Silty sand to sandy silt
6. Clean sand to silty sand
7. Gravely sand to sand
8. Very stiff sand to clayey sand
9. Very stiff fine grained
CPeT-IT v.1.7.6.3 - CPTU data presentation & interpretation software - Report created on: 2/27/2014, 9:18:27 AM
Project file: C:\Users\Josh\Documents\Academic\PhD\New Zealand\Data\Processed CPT Data\JZ Processed Files\Phase V\Phase V.cpt
8

GeoLogismiki
Geotechnical Engineers
Merarhias 56
http://www.geologismiki.gr

CPT: Z2-27
Total depth: 3.10 m
Surface Elevation: 0.00 m
Coords: X:0.00, Y:0.00
Cone Type: Uknown
Cone Operator: Uknown

Project:
Location:

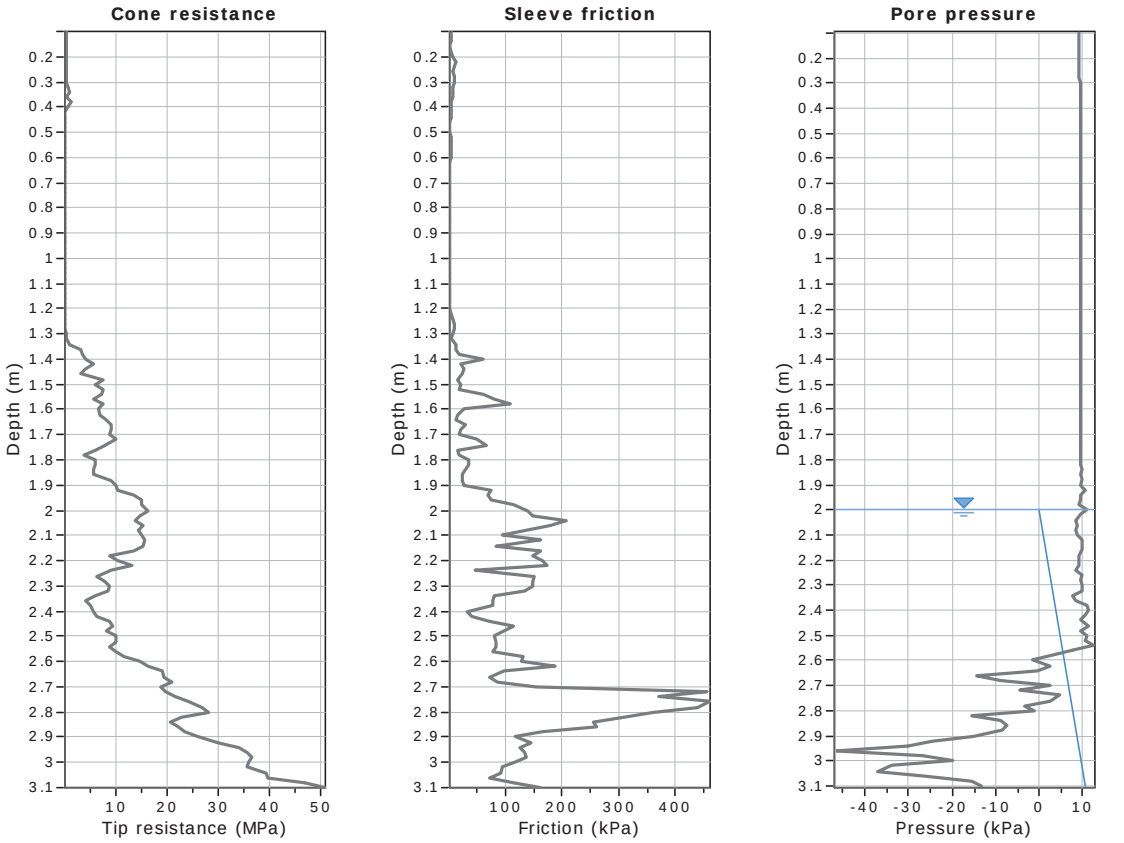

The plot below presents the cross correlation coeficient between the raw qc and fs values (as measured on the field). X axes presents the lag distance (one lag is the distance between two sucessive CPT measurements).

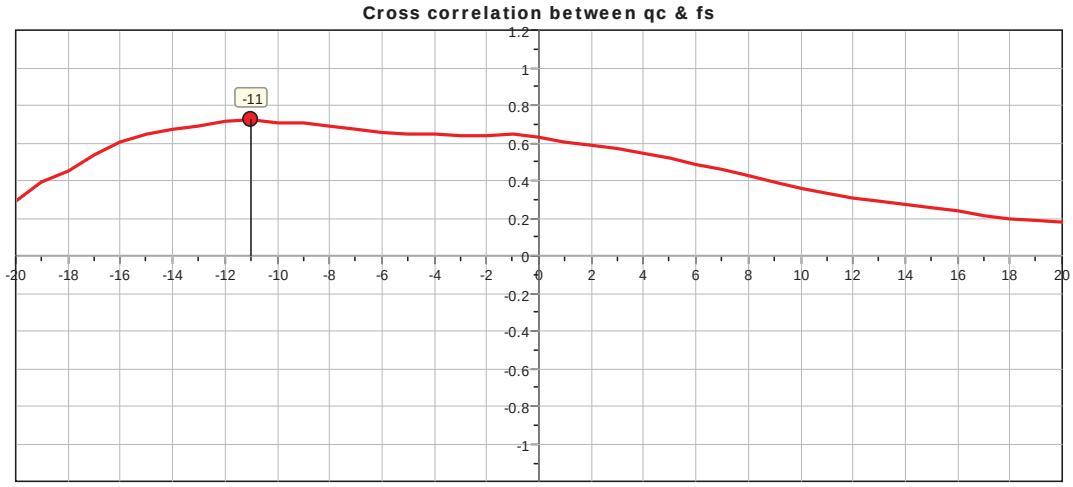

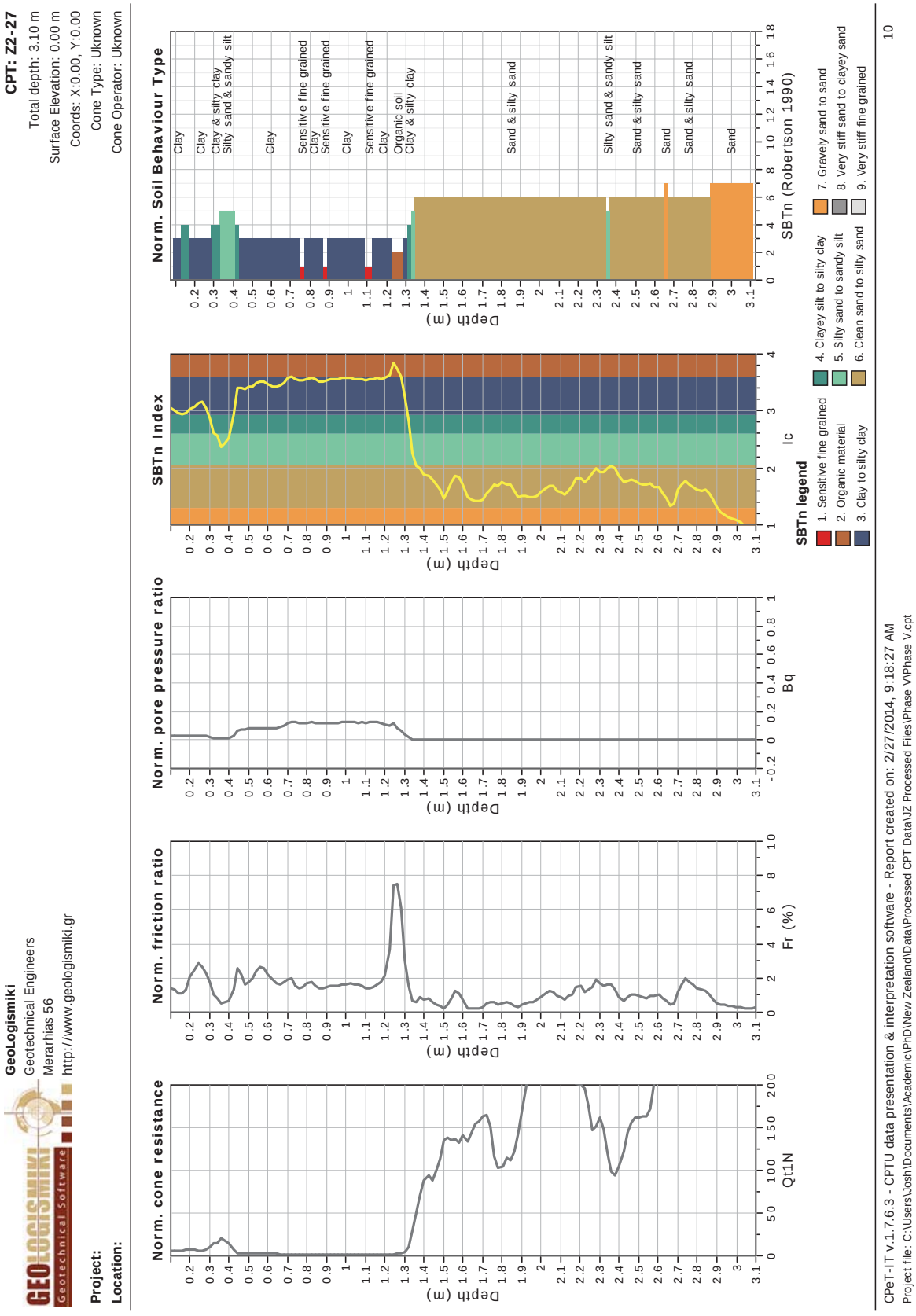
GeoLogismiki
Geotechnical Engineers
Merarchias 56
http://www.geologismiki.gr
Project:
Location:
CPT: Z2-27
Total depth: 3.10 m
Surface Elevation: 0.00 m
Coords: X:0.00, Y:0.00
Cone Type: Uknown
Cone Operator: Uknown
Norm. cone resistance
Qt1N
Norm. friction ratio
Fr (%)
Norm. pore pressure ratio
Bq
SBTn Index
Ic
Norm. Soil Behaviour Type
SBTn (Robertson 1990)
Depth (m)
SBTn legend
1. Sensitive fine grained
2. Organic material
3. Clay to silty clay
4. Clayey silt to silty clay
5. Silty sand to sandy silt
6. Clean sand to silty sand
7. Gravely sand to sand
8. Very stiff sand to clayey sand
9. Very stiff fine grained
CPeT-IT v.1.7.6.3 - CPTU data presentation & interpretation software - Report created on: 2/27/2014, 9:18:27 AM
Project file: C:\Users\Josh\Documents\Academic\PhD\New Zealand\Data\Processed CPT Data\JZ Processed Files\Phase V\Phase V.cpt
10

GeoLogismiki
Geotechnical Engineers
Merarhias 56
http://www.geologismiki.gr

CPT: Z2-28
Total depth: 21.06 m
Surface Elevation: 0.00 m
Coords: X:0.00, Y:0.00
Cone Type: Uknown
Cone Operator: Uknown

Project:
Location:

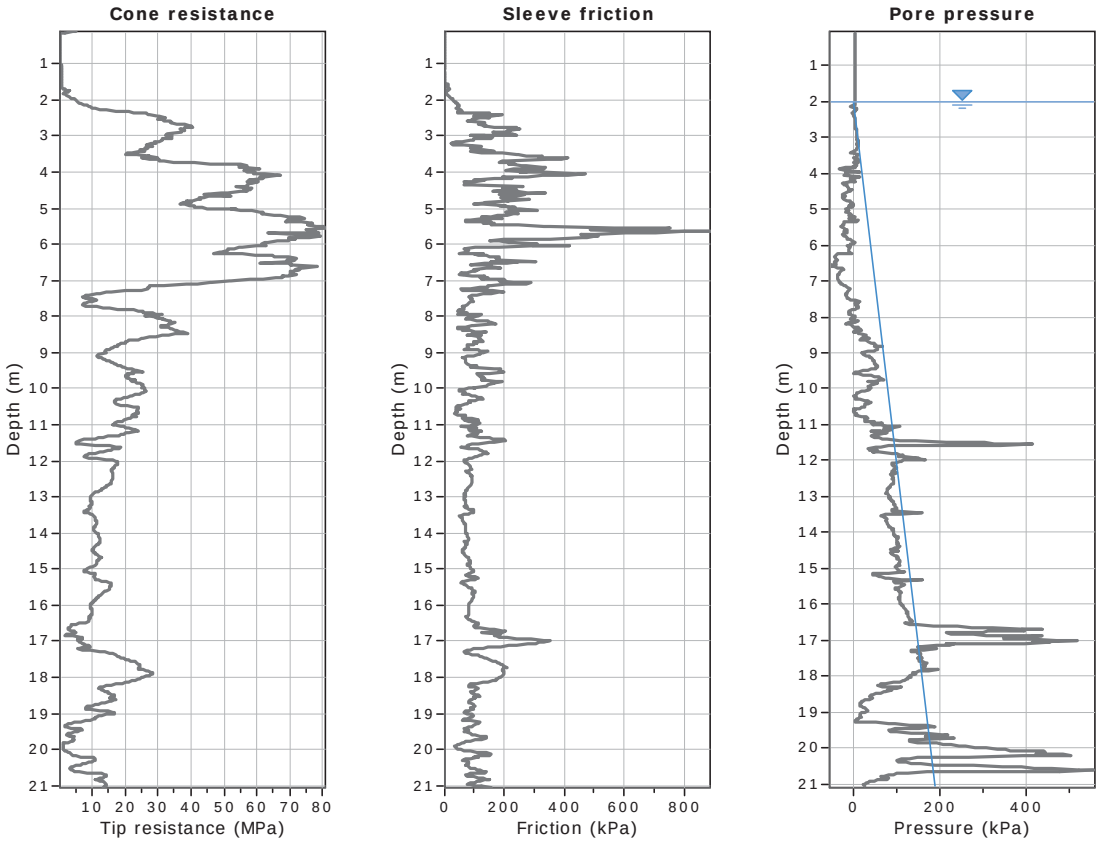

The plot below presents the cross correlation coeficient between the raw qc and fs values (as measured on the field). X axes presents the lag distance (one lag is the distance between two sucessive CPT measurements).

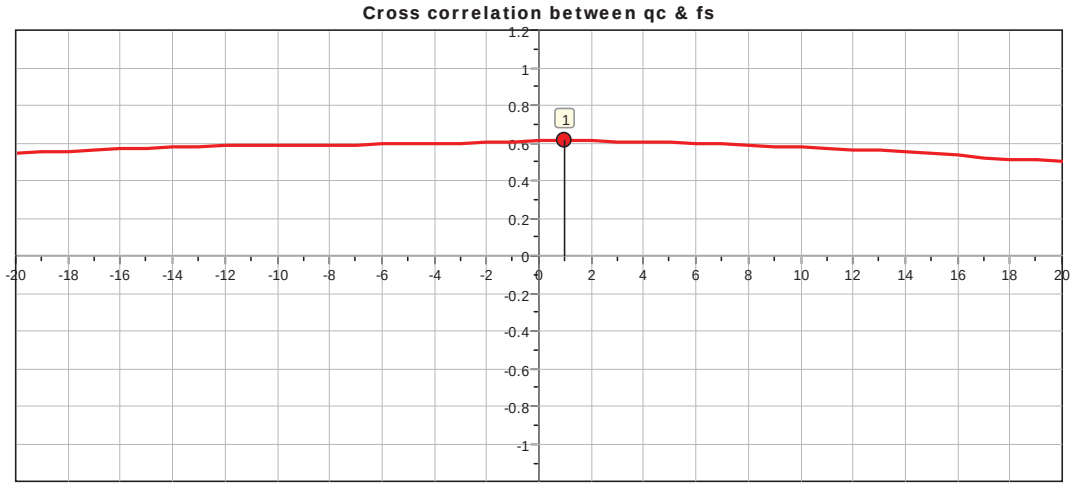

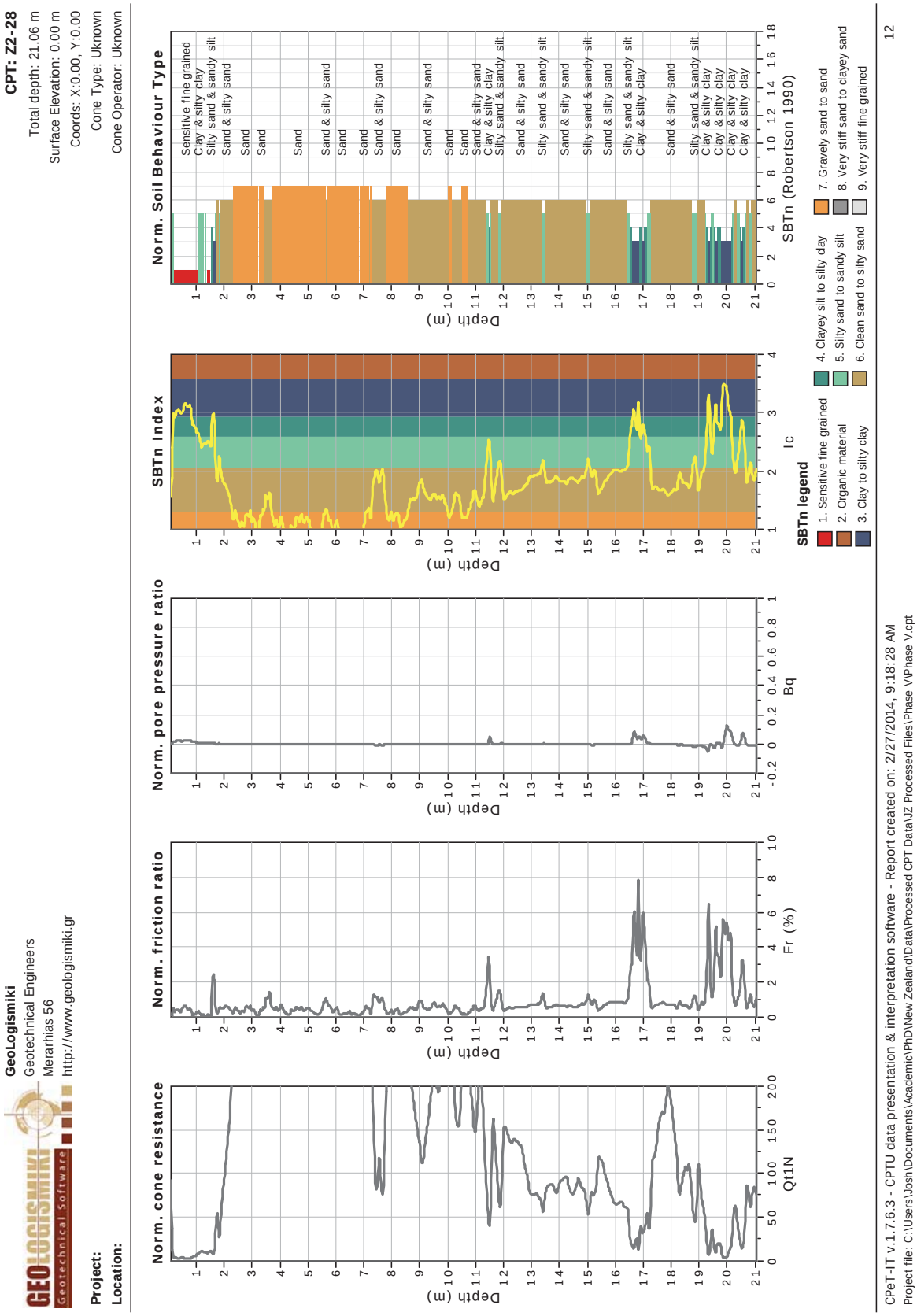
CPT: Z2-28
Total depth: 21.06 m
Surface Elevation: 0.00 m
Coords: X:0.00, Y:0.00
Cone Type: Uknown
Cone Operator: Uknown
GeoLogismiki
Geotechnical Engineers
Merarhias 56
http://www.geologismiki.gr
Project:
Location:
Norm. cone resistance
Qt1N
Norm. friction ratio
Fr (%)
Norm. pore pressure ratio
Bq
SBTn Index
Ic
Norm. Soil Behaviour Type
SBTn (Robertson 1990)
Depth (m)
SBTn legend
1. Sensitive fine grained
2. Organic material
3. Clay to silty clay
4. Clayey silt to silty clay
5. Silty sand to sandy silt
6. Clean sand to silty sand
7. Gravelly sand to sand
8. Very stiff sand to clayey sand
9. Very stiff fine grained
CPeT-IT v.1.7.6.3 - CPTU data presentation & interpretation software - Report created on: 2/27/2014, 9:18:28 AM
Project file: C:\Users\Josh\Documents\Academic\PhD\New Zealand\Data\Processed CPT Data\JZ Processed Files\Phase V\Phase V.cpt
12

GeoLogismiki
Geotechnical Engineers
Merarhias 56
http://www.geologismiki.gr

CPT: Z2-29
Total depth: 23.92 m
Surface Elevation: 0.00 m
Coords: X:0.00, Y:0.00
Cone Type: Uknown
Cone Operator: Uknown

Project:
Location:

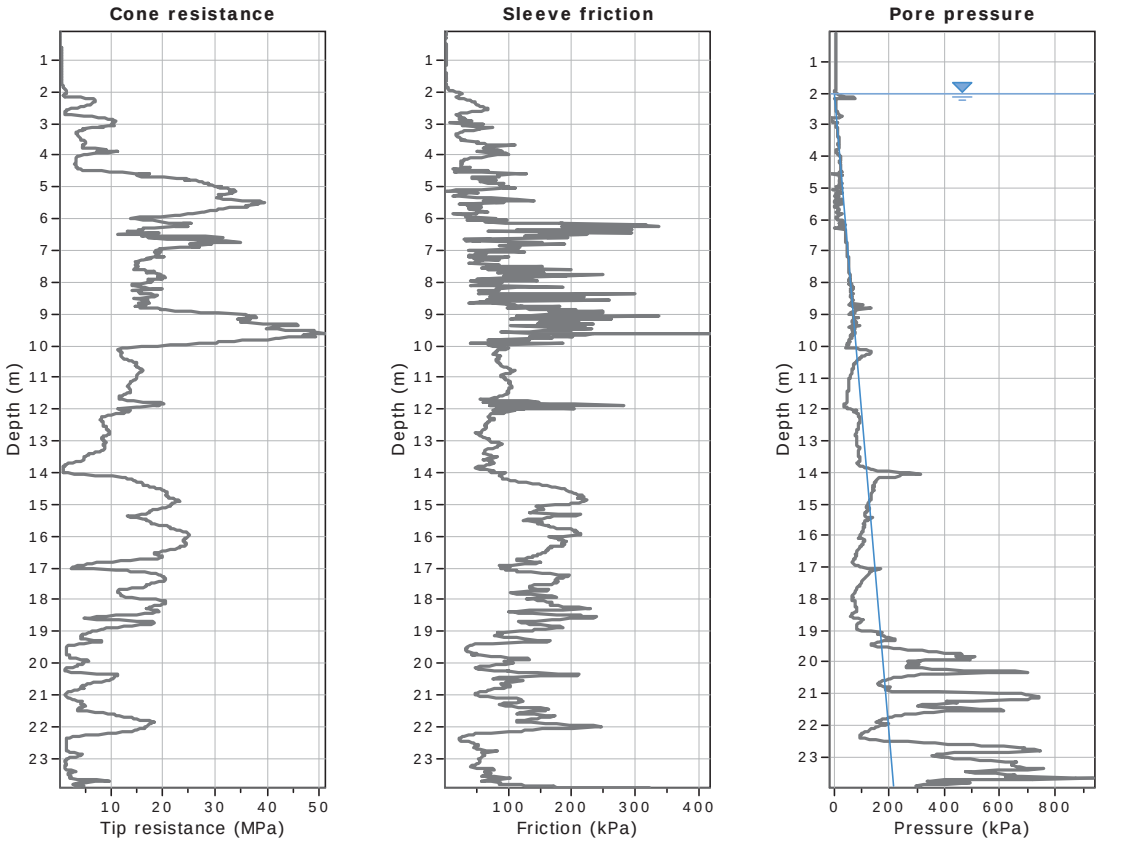

The plot below presents the cross correlation coeficient between the raw qc and fs values (as measured on the field). X axes presents the lag distance (one lag is the distance between two sucessive CPT measurements).

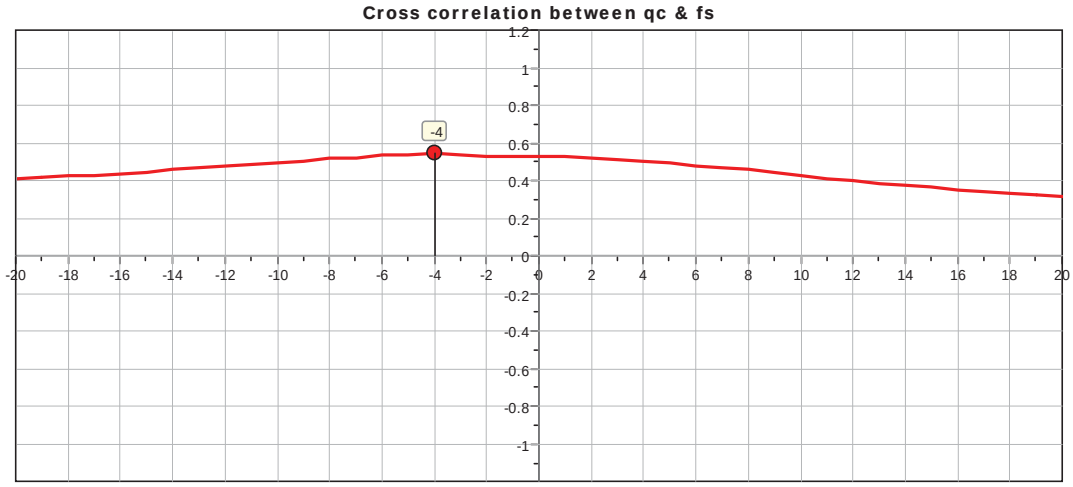

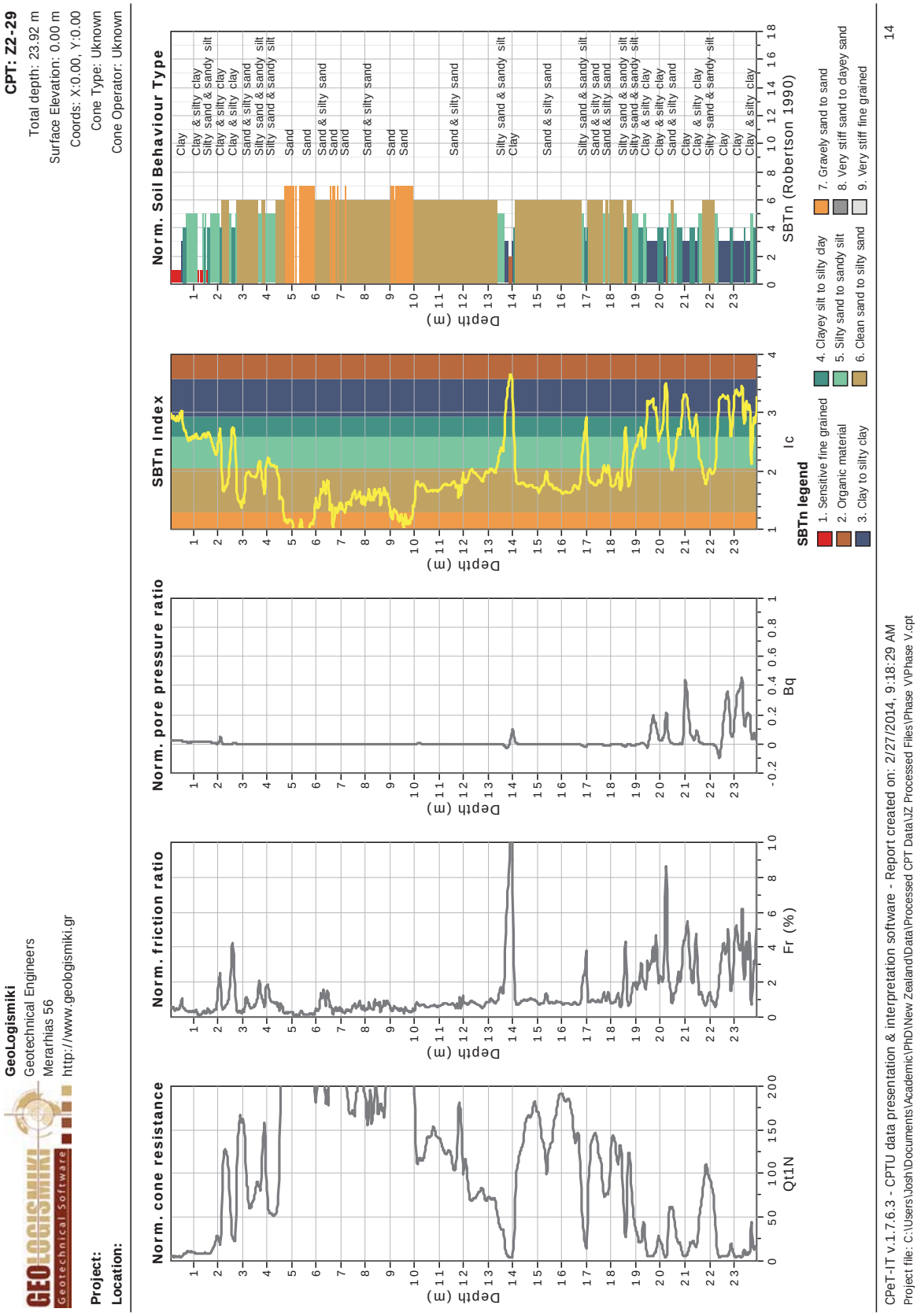
GeoLogismiki
Geotechnical Engineers
Merarhias 56
http://www.geologismiki.gr
Project:
Location:
CPT: Z2-29
Total depth: 23.92 m
Surface Elevation: 0.00 m
Coords: X:0.00, Y:0.00
Cone Type: Uknown
Cone Operator: Uknown
Norm. cone resistance
Norm. friction ratio
Norm. pore pressure ratio
SBTn Index
Norm. Soil Behaviour Type
Depth (m)
Qt1N
Fr (%)
Bq
Ic
SBTn (Robertson 1990)
SBTn legend
1. Sensitive fine grained
2. Organic material
3. Clay to silty clay
4. Clayey silt to silty clay
5. Silty sand to sandy silt
6. Clean sand to silty sand
7. Gravely sand to sand
8. Very stiff sand to clayey sand
9. Very stiff fine grained
CPeT-IT v.1.7.6.3 - CPTU data presentation & interpretation software - Report created on: 2/27/2014, 9:18:29 AM
Project file: C:\Users\Josh\Documents\Academic\PhD\New Zealand\Data\Processed CPT Data\JZ Processed Files\Phase V\Phase V.cpt
14

GeoLogismiki
Geotechnical Engineers
Merarhias 56
http://www.geologismiki.gr

CPT: Z2-30
Total depth: 20.36 m
Surface Elevation: 0.00 m
Coords: X:0.00, Y:0.00
Cone Type: Uknown
Cone Operator: Uknown

Project:
Location:

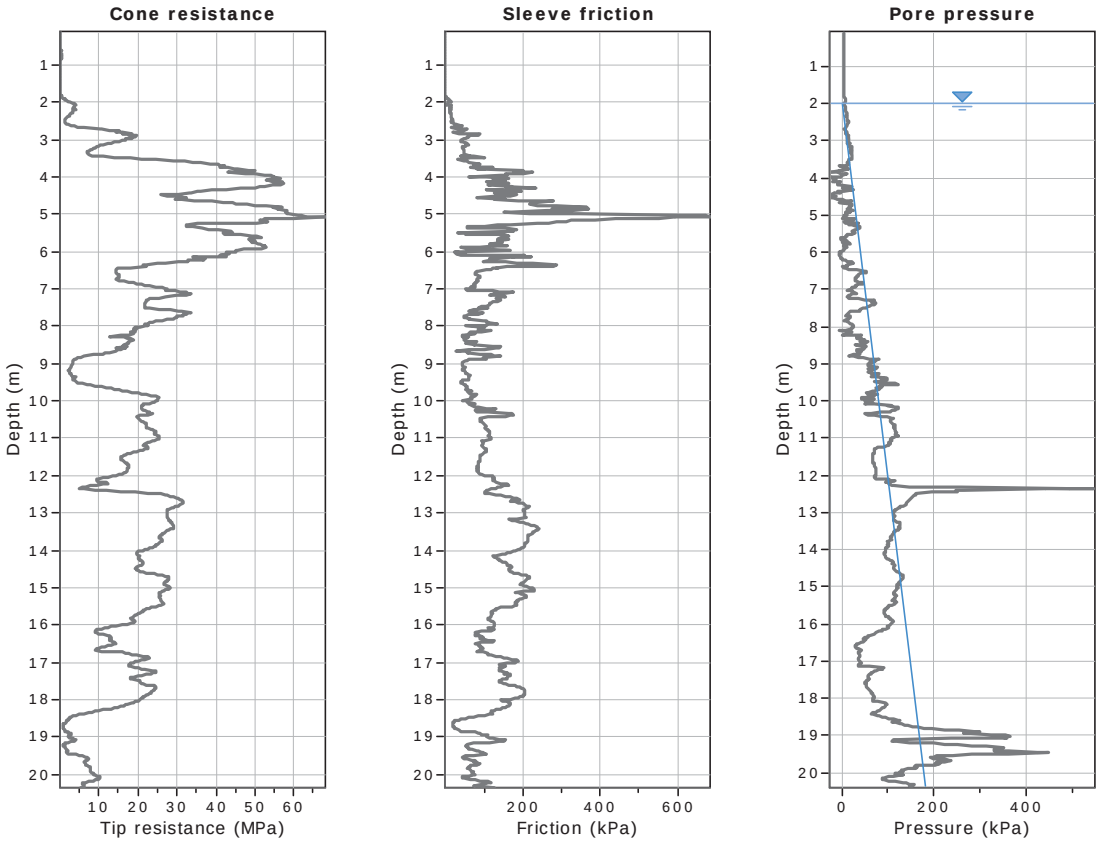

The plot below presents the cross correlation coeficient between the raw qc and fs values (as measured on the field). X axes presents the lag distance (one lag is the distance between two sucessive CPT measurements).

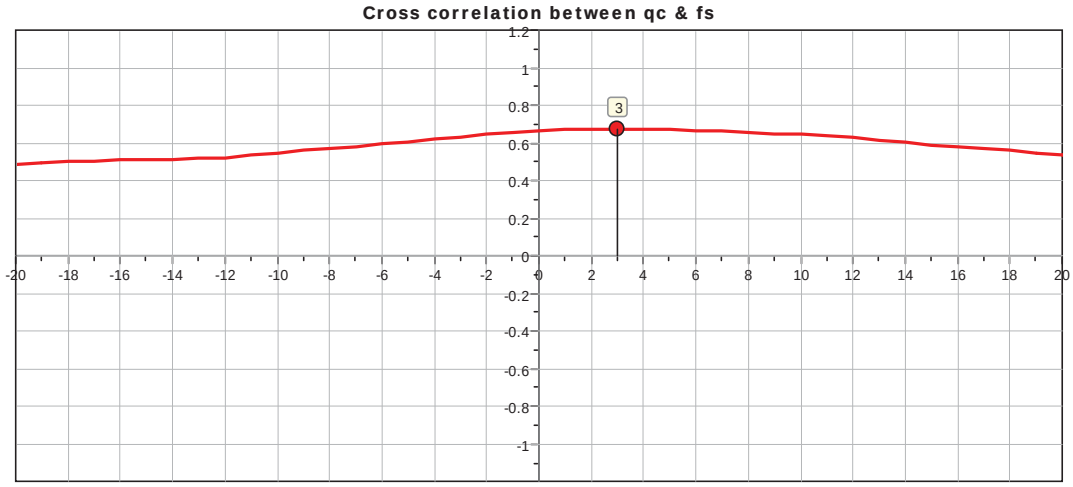

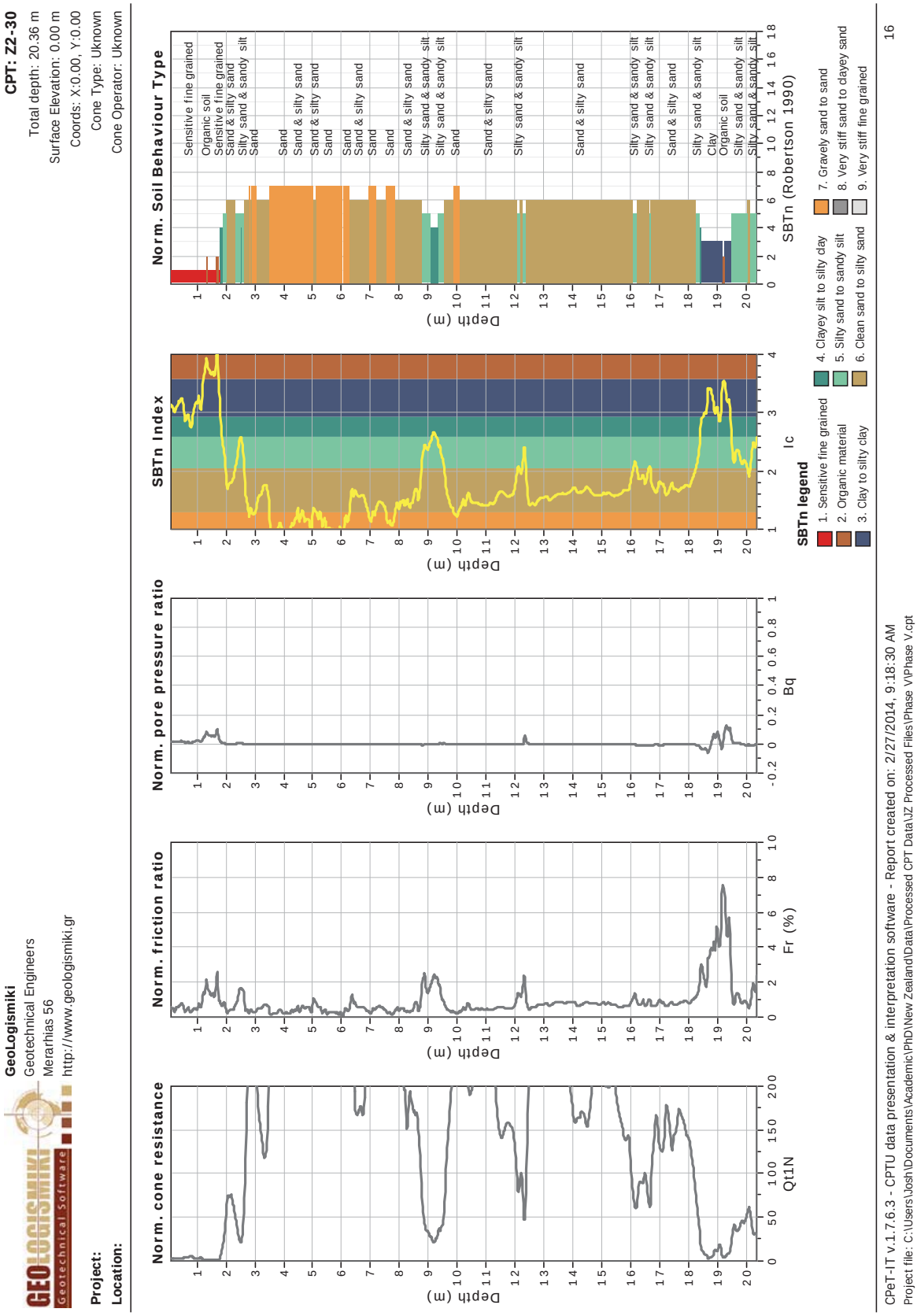
GeoLogismiki
Geotechnical Engineers
Merarhias 56
http://www.geologismiki.gr
Project:
Location:
CPT: Z2-30
Total depth: 20.36 m
Surface Elevation: 0.00 m
Coords: X:0.00, Y:0.00
Cone Type: Uknown
Cone Operator: Uknown
Norm. cone resistance
Qt1N
Norm. friction ratio
Fr (%)
Norm. pore pressure ratio
Bq
SBTn Index
Ic
Norm. Soil Behaviour Type
SBTn (Robertson 1990)
Depth (m)
SBTn legend
1. Sensitive fine grained
2. Organic material
3. Clay to silty clay
4. Clayey silt to silty clay
5. Silty sand to sandy silt
6. Clean sand to silty sand
7. Gravelly sand to sand
8. Very stiff sand to clayey sand
9. Very stiff fine grained
CPeT-IT v.1.7.6.3 - CPTU data presentation & interpretation software - Report created on: 2/27/2014, 9:18:30 AM
Project file: C:\Users\Josh\Documents\Academic\PhD\New Zealand\Data\Processed CPT Data\JZ Processed Files\Phase V\Phase V.cpt
16

GeoLogismiki
Geotechnical Engineers
Merarhias 56
http://www.geologismiki.gr

CPT: Z4-1
Total depth: 19.01 m
Surface Elevation: 0.00 m
Coords: X:0.00, Y:0.00
Cone Type: Uknown
Cone Operator: Uknown

Project:
Location:

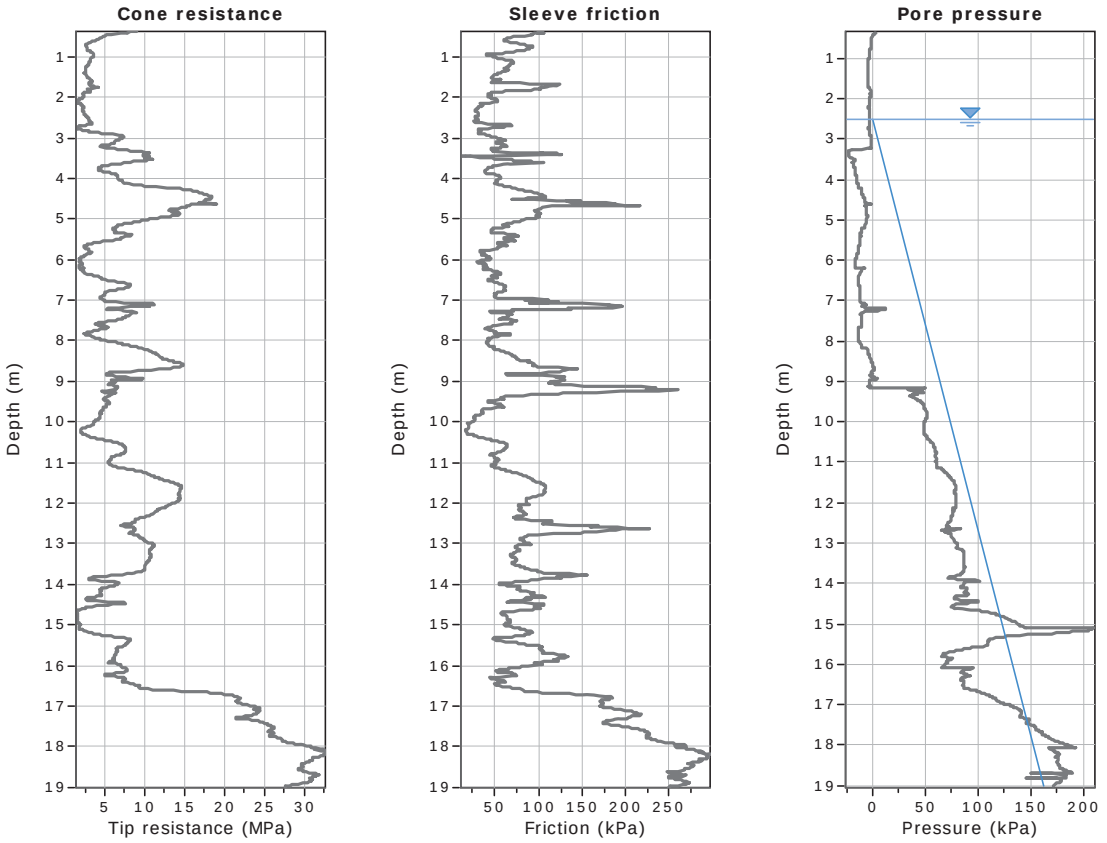

The plot below presents the cross correlation coeficient between the raw qc and fs values (as measured on the field). X axes presents the lag distance (one lag is the distance between two sucessive CPT measurements).

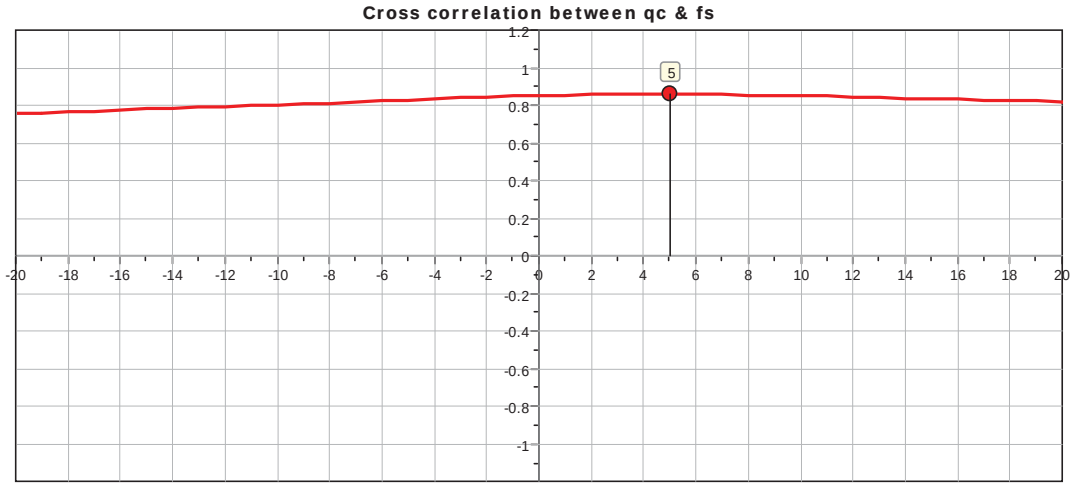

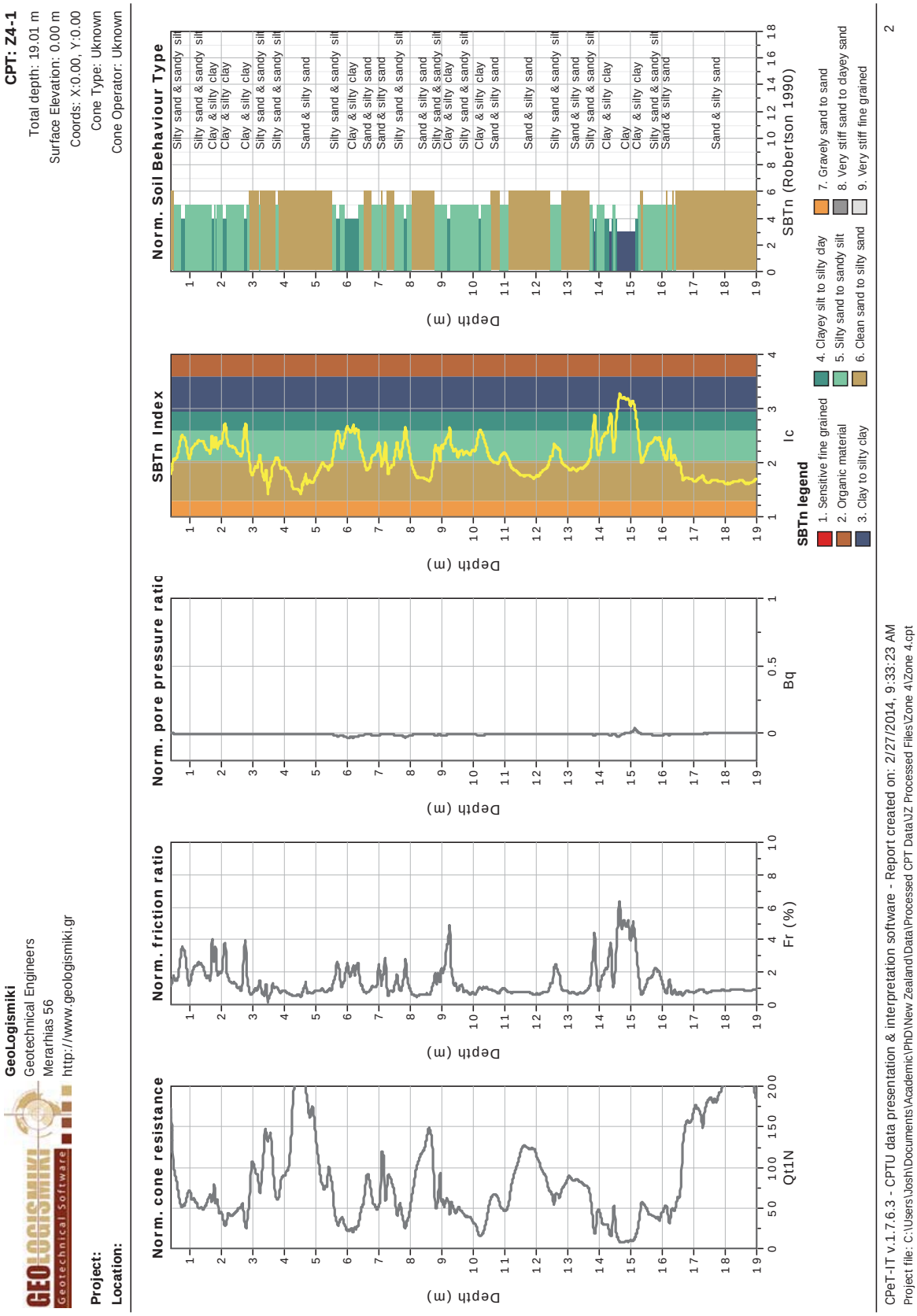
GeoLogismiki
Geotechnical Engineers
Merarchias 56
http://www.geologismiki.gr
Project:
Location:
CPT: Z4-1
Total depth: 19.01 m
Surface Elevation: 0.00 m
Coords: X:0.00, Y:0.00
Cone Type: Uknown
Cone Operator: Uknown
Norm. cone resistance
Qt1N
Norm. friction ratio
Fr (%)
Norm. pore pressure ratio
Bq
SBTn Index
Ic
Norm. Soil Behaviour Type
SBTn (Robertson 1990)
Depth (m)
SBTn legend
1. Sensitive fine grained
2. Organic material
3. Clay to silty clay
4. Clayey silt to silty clay
5. Silty sand to sandy silt
6. Clean sand to silty sand
7. Gravely sand to sand
8. Very stiff sand to clayey sand
9. Very stiff fine grained
CPeT-IT v.1.7.6.3 - CPTU data presentation & interpretation software - Report created on: 2/27/2014, 9:33:23 AM
Project file: C:\Users\Josh\Documents\Academic\PhD\New Zealand\Data\Processed CPT Data\JZ Processed Files\Zone 4\Zone 4.cpt
2

GeoLogismiki
Geotechnical Engineers
Merarhias 56
http://www.geologismiki.gr

CPT: Z4-2
Total depth: 14.04 m
Surface Elevation: 0.00 m
Coords: X:0.00, Y:0.00
Cone Type: Uknown
Cone Operator: Uknown

Project:
Location:

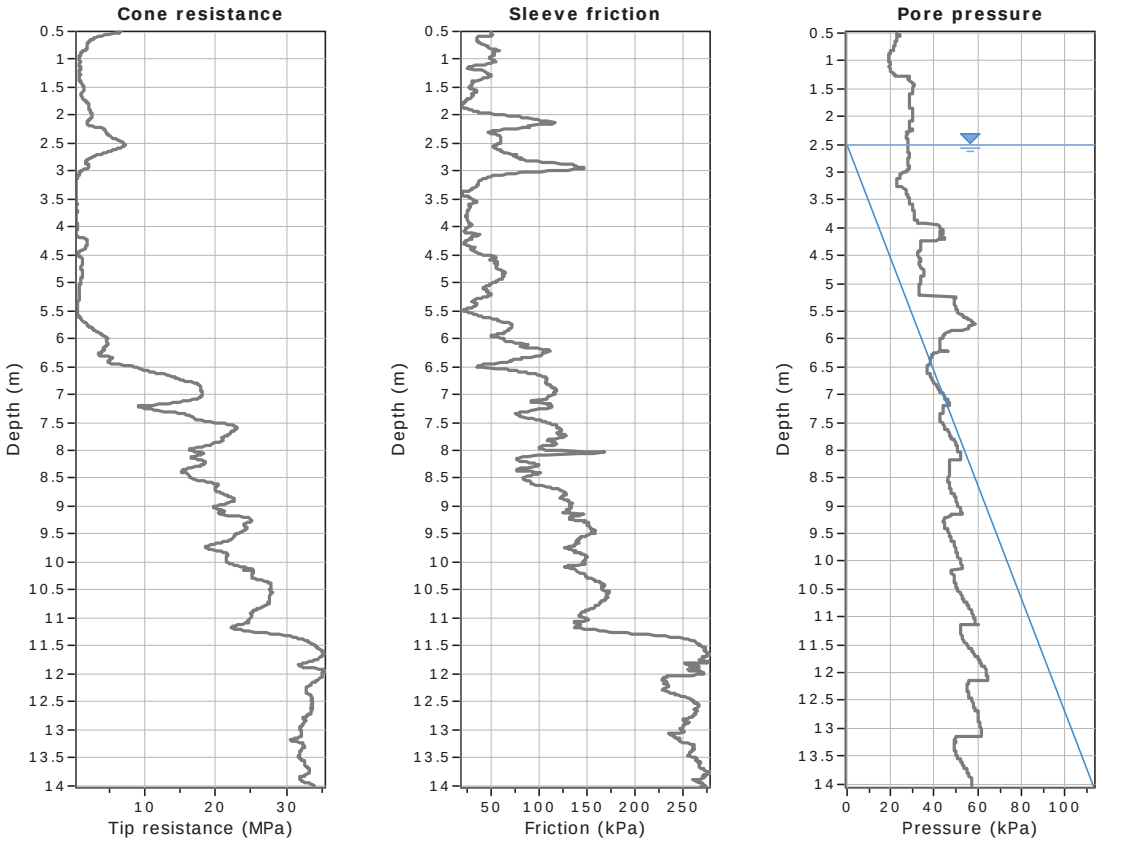

The plot below presents the cross correlation coeficient between the raw qc and fs values (as measured on the field). X axes presents the lag distance (one lag is the distance between two sucessive CPT measurements).

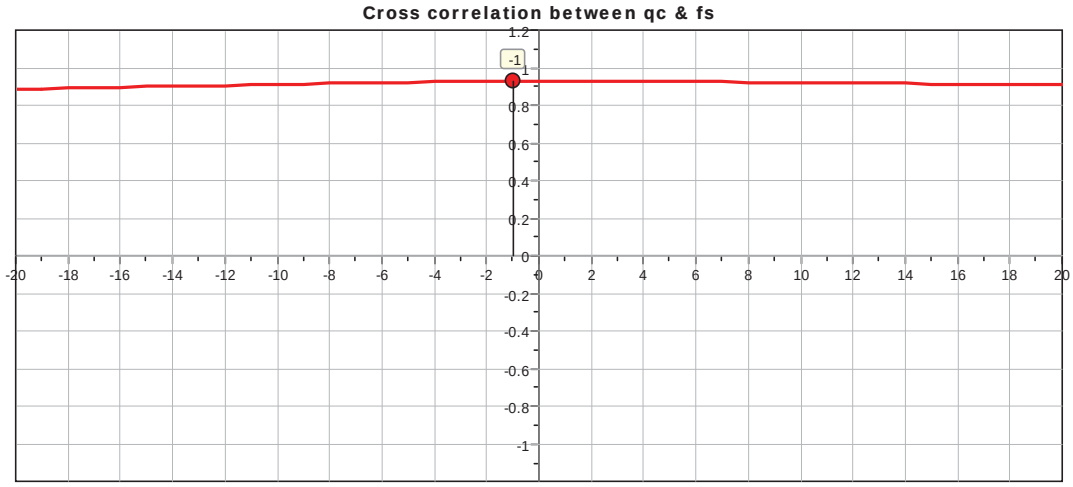

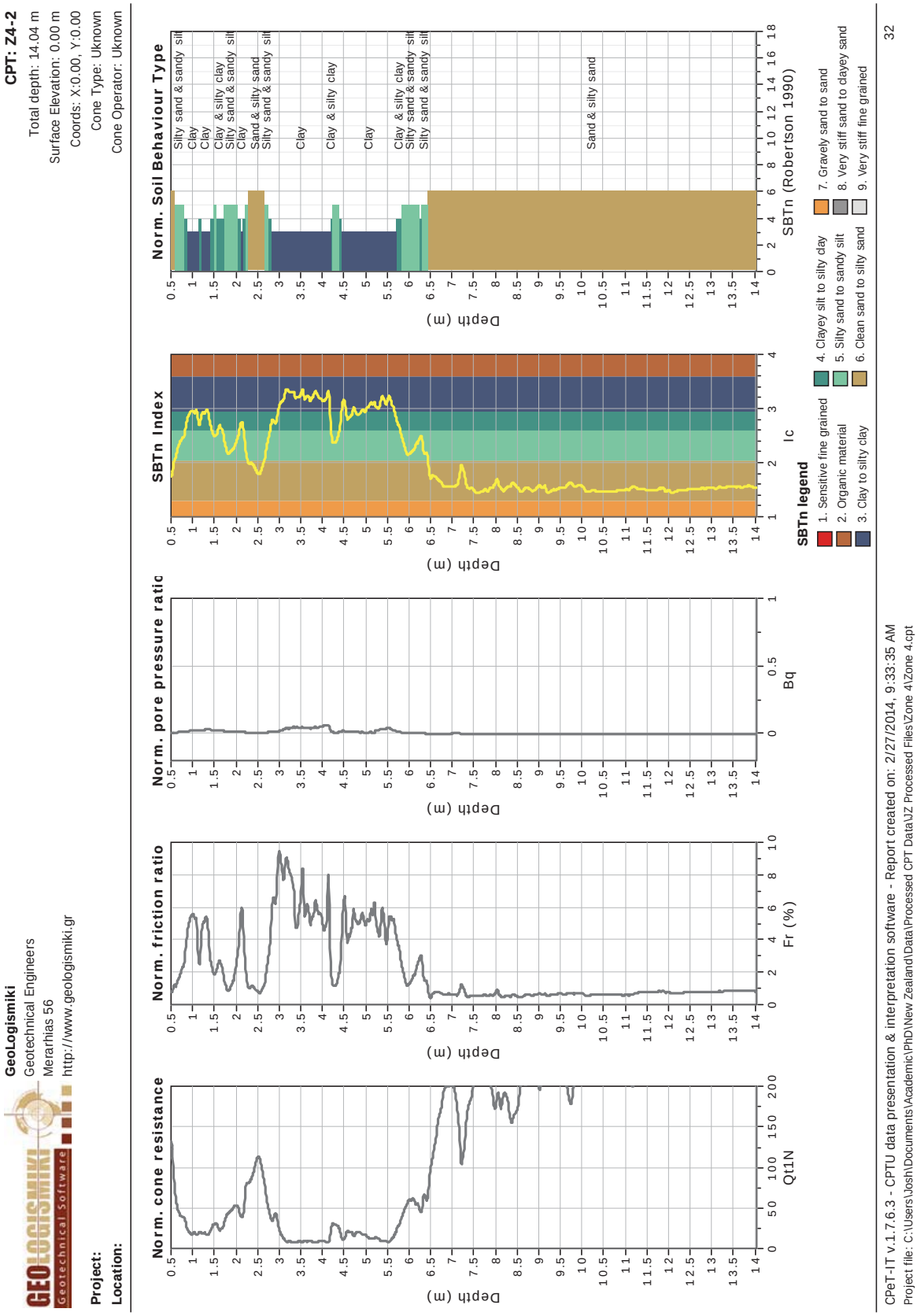
CPT: Z4-2
Total depth: 14.04 m
Surface Elevation: 0.00 m
Coords: X:0.00, Y:0.00
Cone Type: Uknown
Cone Operator: Uknown
GeoLogismiki
Geotechnical Engineers
Merarhias 56
http://www.geologismiki.gr
Project:
Location:
Norm. cone resistance
Qt1N
Norm. friction ratio
Fr (%)
Norm. pore pressure ratio
Bq
SBTn Index
Ic
Norm. Soil Behaviour Type
SBTn (Robertson 1990)
Depth (m)
SBTn legend
1. Sensitive fine grained
2. Organic material
3. Clay to silty clay
4. Clayey silt to silty clay
5. Silty sand to sandy silt
6. Clean sand to silty sand
7. Gravely sand to sand
8. Very stiff sand to clayey sand
9. Very stiff fine grained
CPeT-IT v.1.7.6.3 - CPTU data presentation & interpretation software - Report created on: 2/27/2014, 9:33:35 AM
Project file: C:\Users\Josh\Documents\Academic\PhD\New Zealand\Data\Processed CPT Data\JZ Processed Files\Zone 4\Zone 4.cpt
32

GeoLogismiki
Geotechnical Engineers
Merarhias 56
http://www.geologismiki.gr

CPT: Z4-3
Total depth: 13.39 m
Surface Elevation: 0.00 m
Coords: X:0.00, Y:0.00
Cone Type: Uknown
Cone Operator: Uknown

Project:
Location:

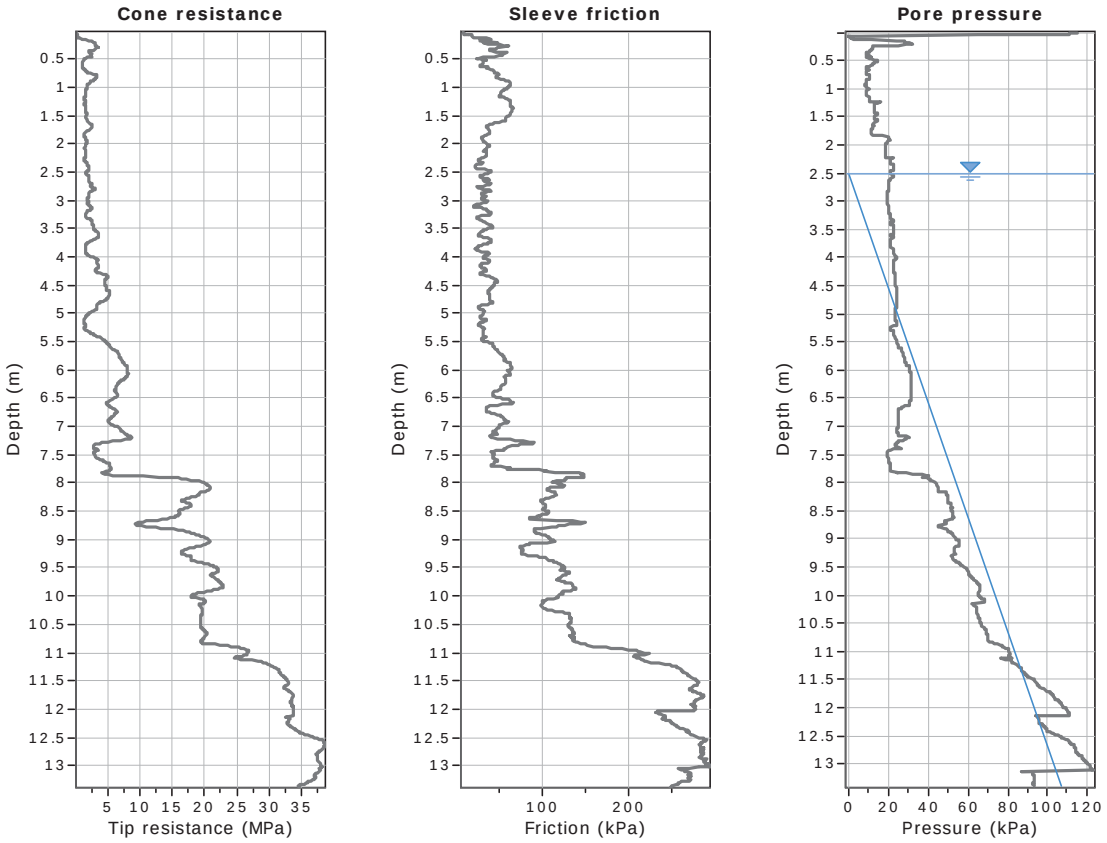

The plot below presents the cross correlation coeficient between the raw qc and fs values (as measured on the field). X axes presents the lag distance (one lag is the distance between two sucessive CPT measurements).

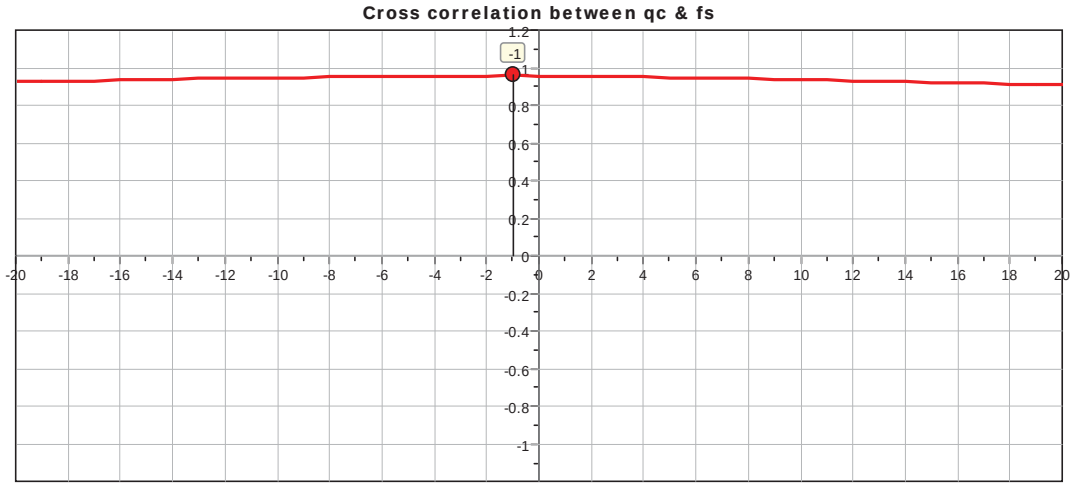

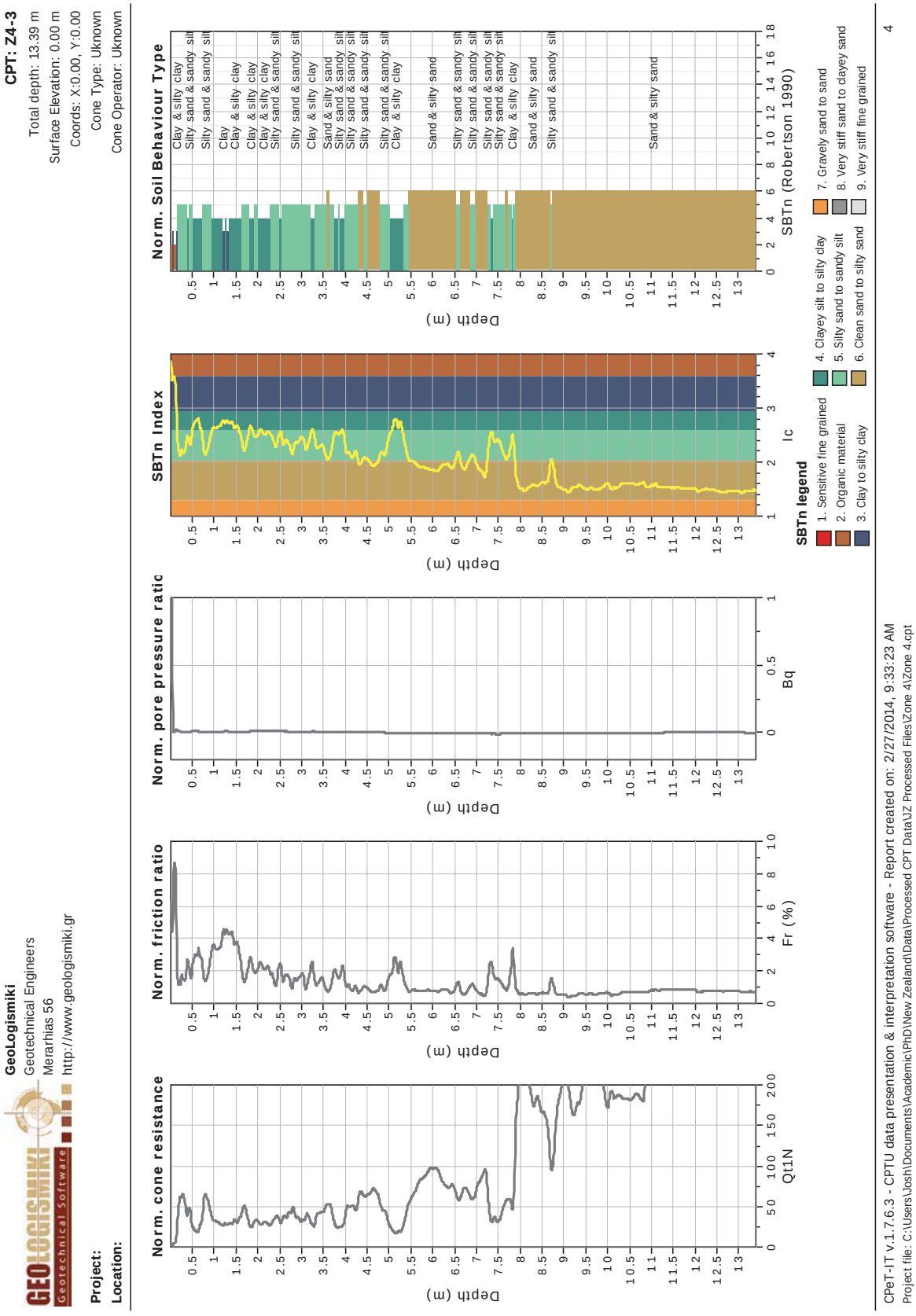
CPT: Z4-3
Total depth: 13.39 m
Surface Elevation: 0.00 m
Coords: X:0.00, Y:0.00
Cone Type: Uknown
Cone Operator: Uknown
Project:
Location:
GeoLogismiki
Geotechnical Engineers
Merarhias 56
http://www.geologismiki.gr
Norm. cone resistance
Norm. friction ratio
Norm. pore pressure ratio
SBTn Index
Norm. Soil Behaviour Type
Depth (m)
Qt1N
Fr (%)
Bq
Ic
SBTn (Robertson 1990)
SBTn legend
1. Sensitive fine grained
2. Organic material
3. Clay to silty clay
4. Clayey silt to silty clay
5. Silty sand to sandy silt
6. Clean sand to silty sand
7. Gravely sand to sand
8. Very stiff sand to clayey sand
9. Very stiff fine grained
CPeT-IT v.1.7.6.3 - CPTU data presentation & interpretation software - Report created on: 2/27/2014, 9:33:23 AM
Project file: C:\Users\Josh\Documents\Academic\PhD\New Zealand\Data\Processed CPT Data\JZ Processed Files\Zone 4\Zone 4.cpt
4

GeoLogismiki
Geotechnical Engineers
Merarhias 56
http://www.geologismiki.gr

CPT: Z4-4
Total depth: 13.88 m
Surface Elevation: 0.00 m
Coords: X:0.00, Y:0.00
Cone Type: Uknown
Cone Operator: Uknown

Project:
Location:

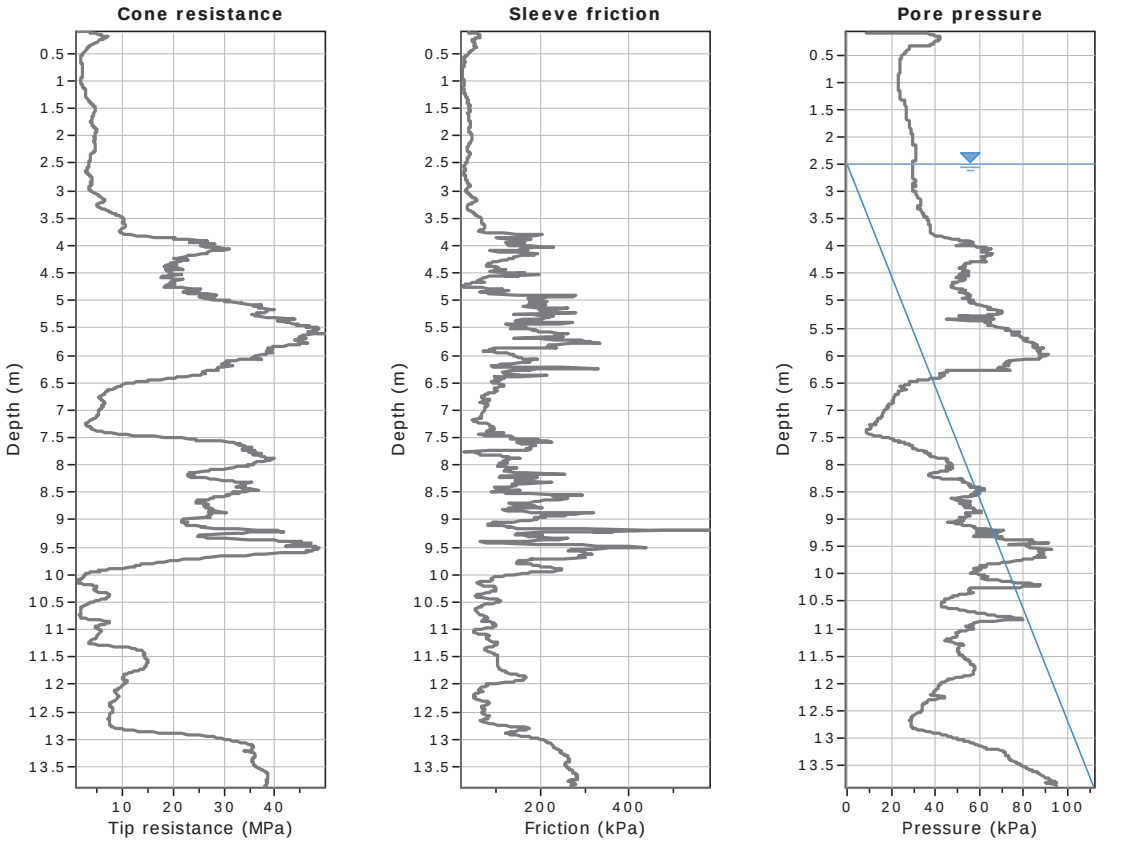

The plot below presents the cross correlation coeficient between the raw qc and fs values (as measured on the field). X axes presents the lag distance (one lag is the distance between two sucessive CPT measurements).

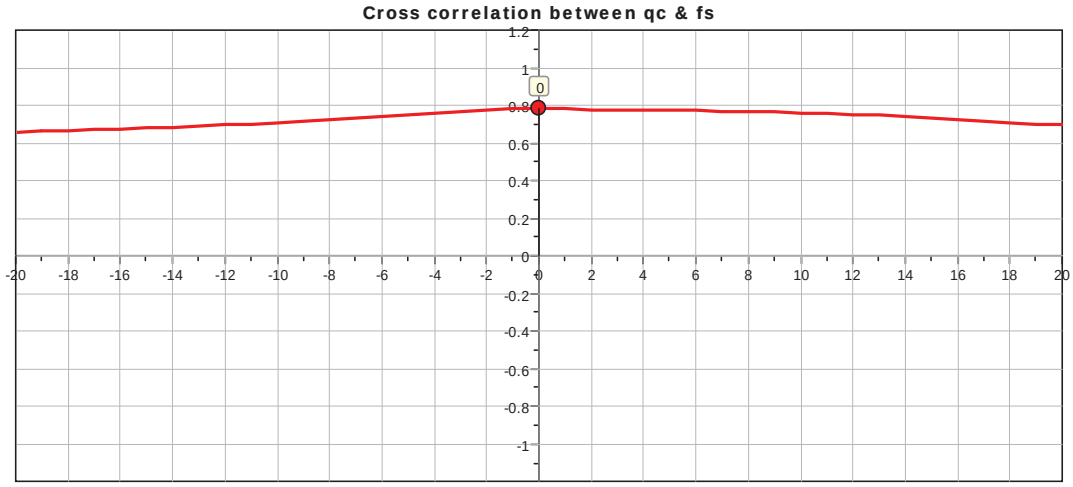

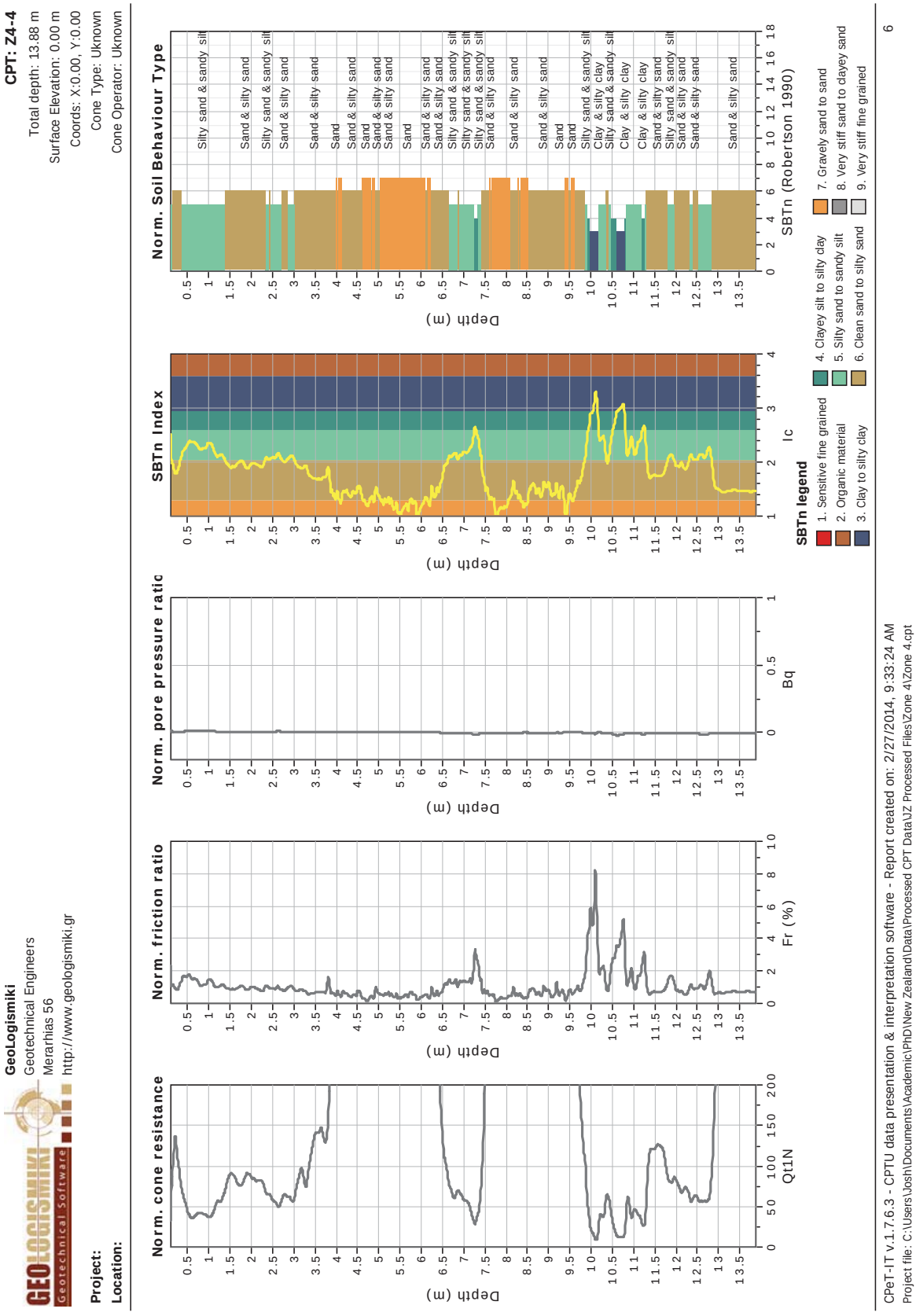
GeoLogismiki
Geotechnical Engineers
Merarchias 56
http://www.geologismiki.gr
Project:
Location:
CPT: Z4-4
Total depth: 13.88 m
Surface Elevation: 0.00 m
Coords: X:0.00, Y:0.00
Cone Type: Uknown
Cone Operator: Uknown
Norm. cone resistance
Qt1N
Norm. friction ratio
Fr (%)
Norm. pore pressure ratio
Bq
SBTn Index
Ic
Norm. Soil Behaviour Type
SBTn (Robertson 1990)
Depth (m)
SBTn legend
1. Sensitive fine grained
2. Organic material
3. Clay to silty clay
4. Clayey silt to silty clay
5. Silty sand to sandy silt
6. Clean sand to silty sand
7. Gravely sand to sand
8. Very stiff sand to clayey sand
9. Very stiff fine grained
CPeT-IT v.1.7.6.3 - CPTU data presentation & interpretation software - Report created on: 2/27/2014, 9:33:24 AM
Project file: C:\Users\Josh\Documents\Academic\PhD\New Zealand\Data\Processed CPT Data\JZ Processed Files\Zone 4\Zone 4.cpt
6

GeoLogismiki
Geotechnical Engineers
Merarhias 56
http://www.geologismiki.gr

CPT: Z4-5
Total depth: 24.82 m
Surface Elevation: 0.00 m
Coords: X:0.00, Y:0.00
Cone Type: Uknown
Cone Operator: Uknown

Project:
Location:

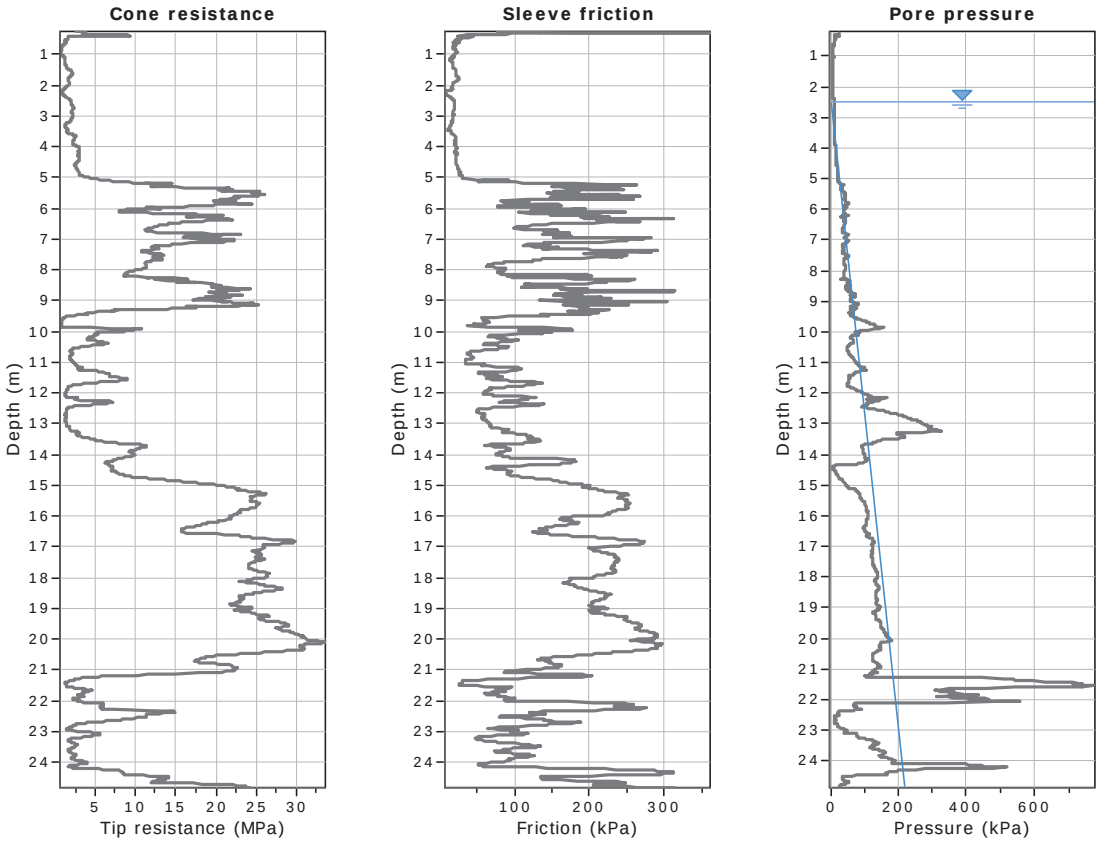

The plot below presents the cross correlation coeficient between the raw qc and fs values (as measured on the field). X axes presents the lag distance (one lag is the distance between two sucessive CPT measurements).

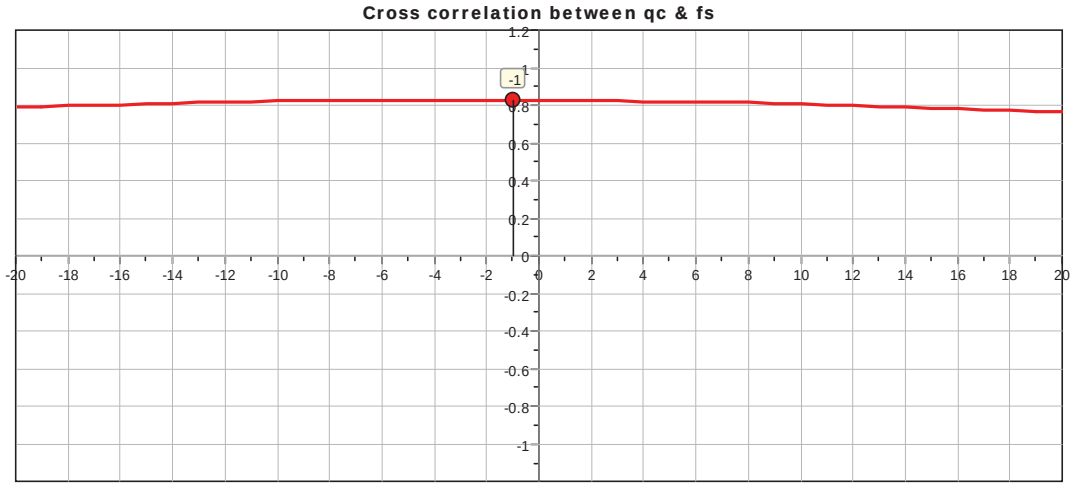

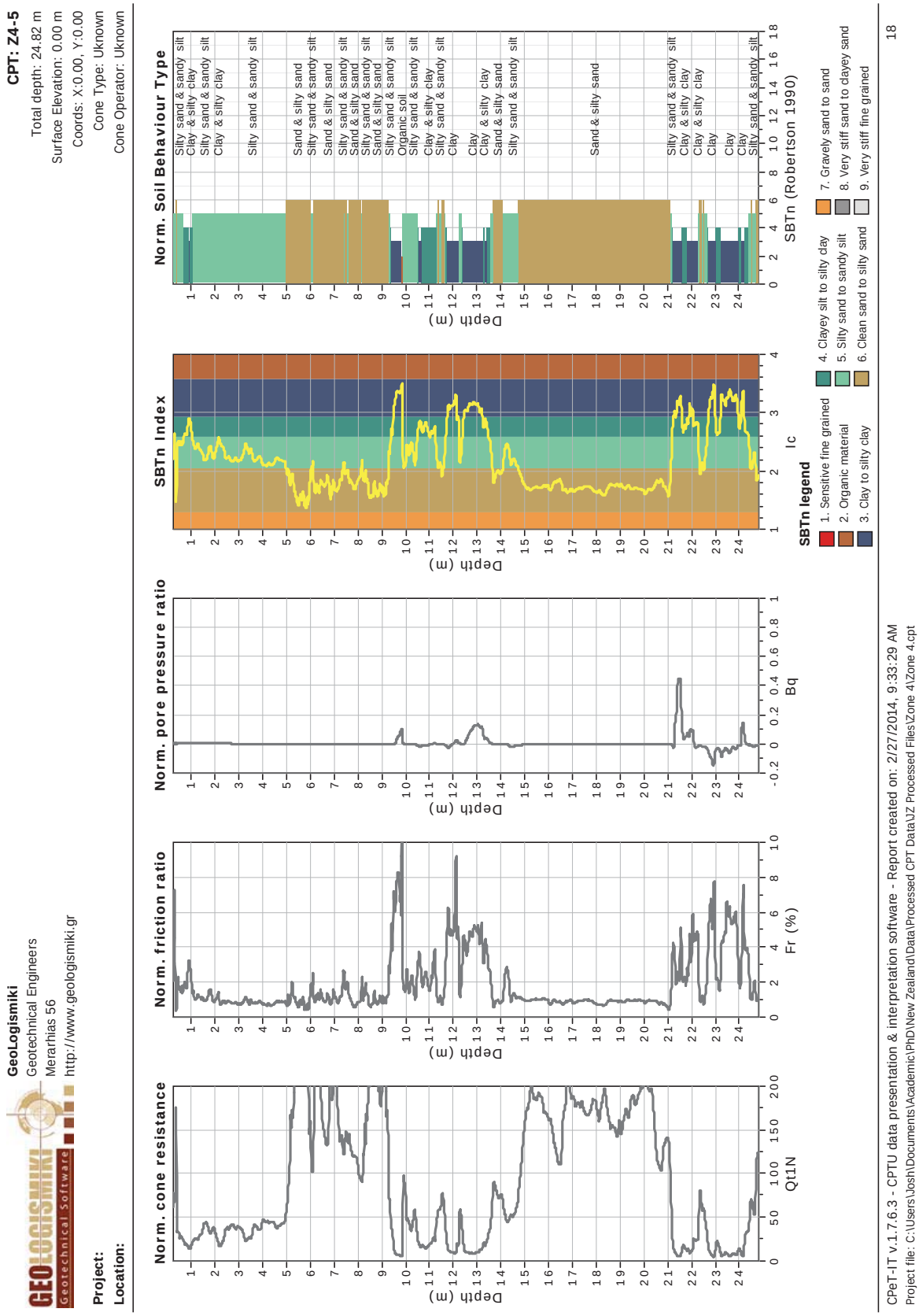
GeoLogismiki
Geotechnical Engineers
Merarhias 56
http://www.geologismiki.gr
Project:
Location:
CPT: Z4-5
Total depth: 24.82 m
Surface Elevation: 0.00 m
Coords: X:0.00, Y:0.00
Cone Type: Uknown
Cone Operator: Uknown
Norm. cone resistance
Qt1N
Norm. friction ratio
Fr (%)
Norm. pore pressure ratio
Bq
SBTn Index
Ic
Norm. Soil Behaviour Type
SBTn (Robertson 1990)
Depth (m)
SBTn legend
1. Sensitive fine grained
2. Organic material
3. Clay to silty clay
4. Clayey silt to silty clay
5. Silty sand to sandy silt
6. Clean sand to silty sand
7. Gravely sand to sand
8. Very stiff sand to clayey sand
9. Very stiff fine grained
CPeT-IT v.1.7.6.3 - CPTU data presentation & interpretation software - Report created on: 2/27/2014, 9:33:29 AM
Project file: C:\Users\Josh\Documents\Academic\PhD\New Zealand\Data\Processed CPT Data\JZ Processed Files\Zone 4\Zone 4.cpt
18

GeoLogismiki
Geotechnical Engineers
Merarhias 56
http://www.geologismiki.gr

CPT: Z4-6
Total depth: 14.20 m
Surface Elevation: 0.00 m
Coords: X:0.00, Y:0.00
Cone Type: Uknown
Cone Operator: Uknown

Project:
Location:

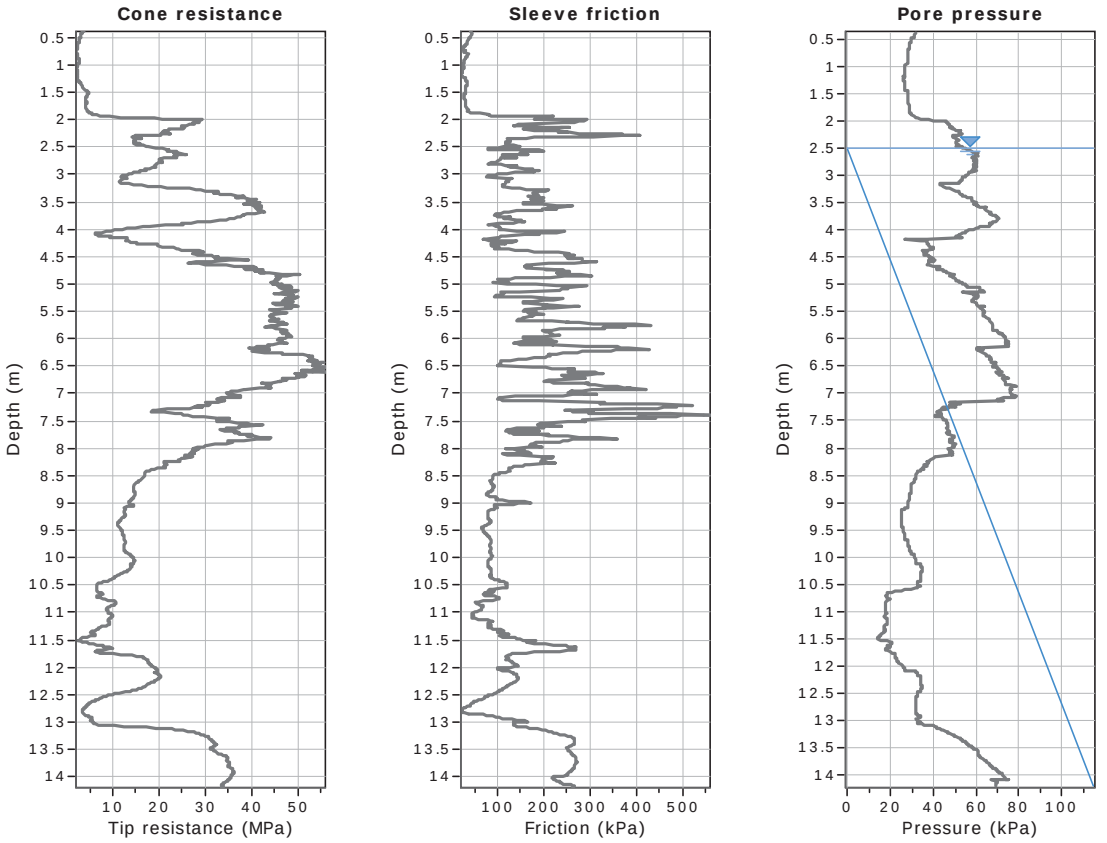

The plot below presents the cross correlation coeficient between the raw qc and fs values (as measured on the field). X axes presents the lag distance (one lag is the distance between two sucessive CPT measurements).

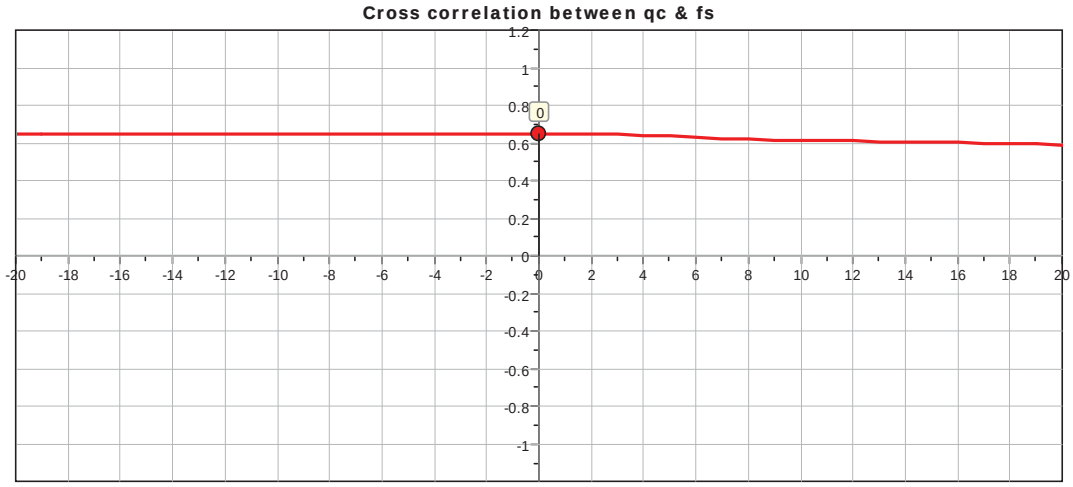

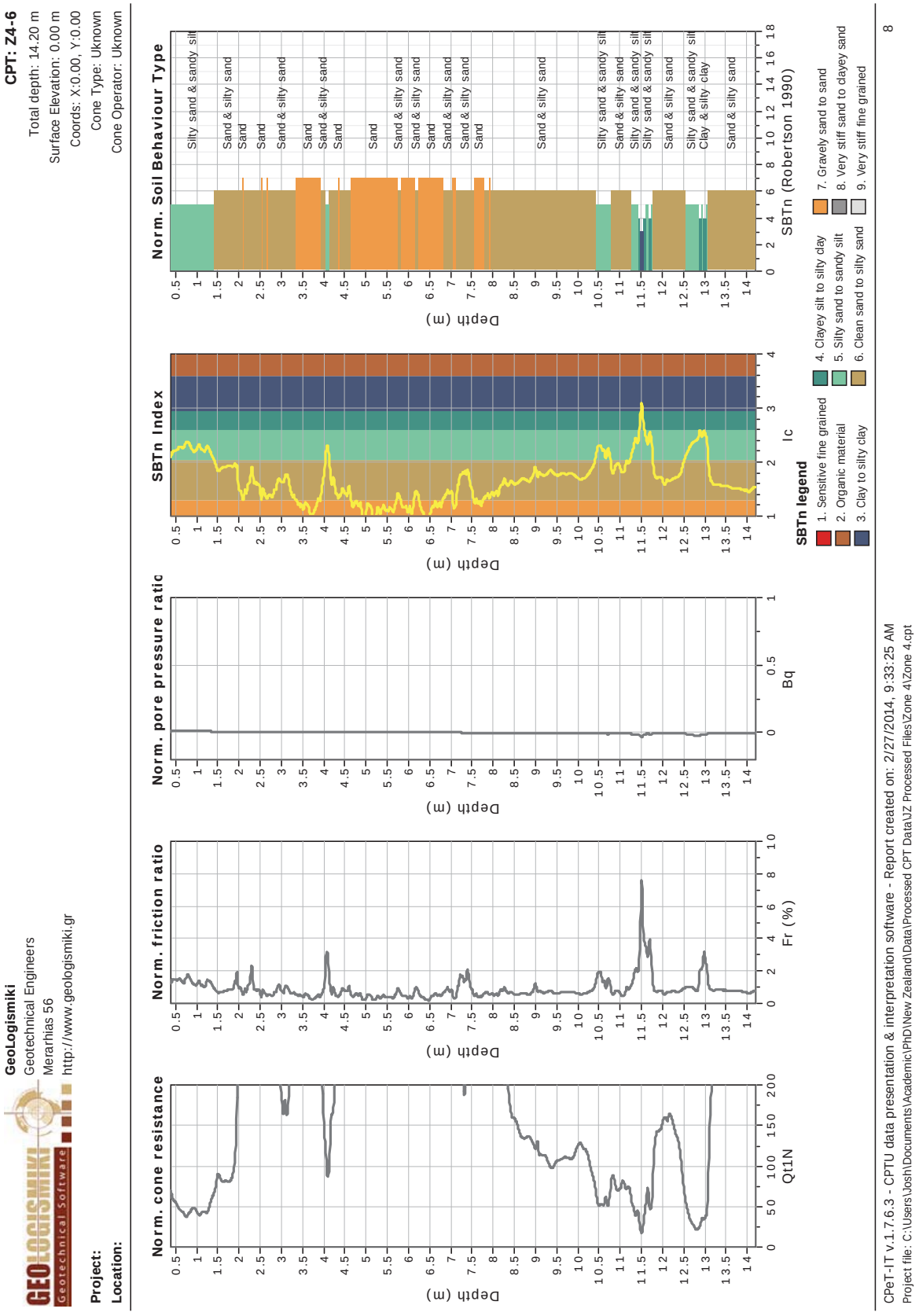
GeoLogismiki
Geotechnical Engineers
Merarhias 56
http://www.geologismiki.gr
Project:
Location:
CPT: Z4-6
Total depth: 14.20 m
Surface Elevation: 0.00 m
Coords: X:0.00, Y:0.00
Cone Type: Uknown
Cone Operator: Uknown
Norm. cone resistance
Qt1N
Norm. friction ratio
Fr (%)
Norm. pore pressure ratio
Bq
SBTn Index
Ic
Norm. Soil Behaviour Type
SBTn (Robertson 1990)
Depth (m)
SBTn legend
1. Sensitive fine grained
2. Organic material
3. Clay to silty clay
4. Clayey silt to silty clay
5. Silty sand to sandy silt
6. Clean sand to silty sand
7. Gravely sand to sand
8. Very stiff sand to clayey sand
9. Very stiff fine grained
CPeT-IT v.1.7.6.3 - CPTU data presentation & interpretation software - Report created on: 2/27/2014, 9:33:25 AM
Project file: C:\Users\Josh\Documents\Academic\PhD\New Zealand\Data\Processed CPT Data\JZ Processed Files\Zone 4\Zone 4.cpt
8

GeoLogismiki
Geotechnical Engineers
Merarhias 56
http://www.geologismiki.gr

CPT: Z4-7
Total depth: 18.18 m
Surface Elevation: 0.00 m
Coords: X:0.00, Y:0.00
Cone Type: Uknown
Cone Operator: Uknown

Project:
Location:

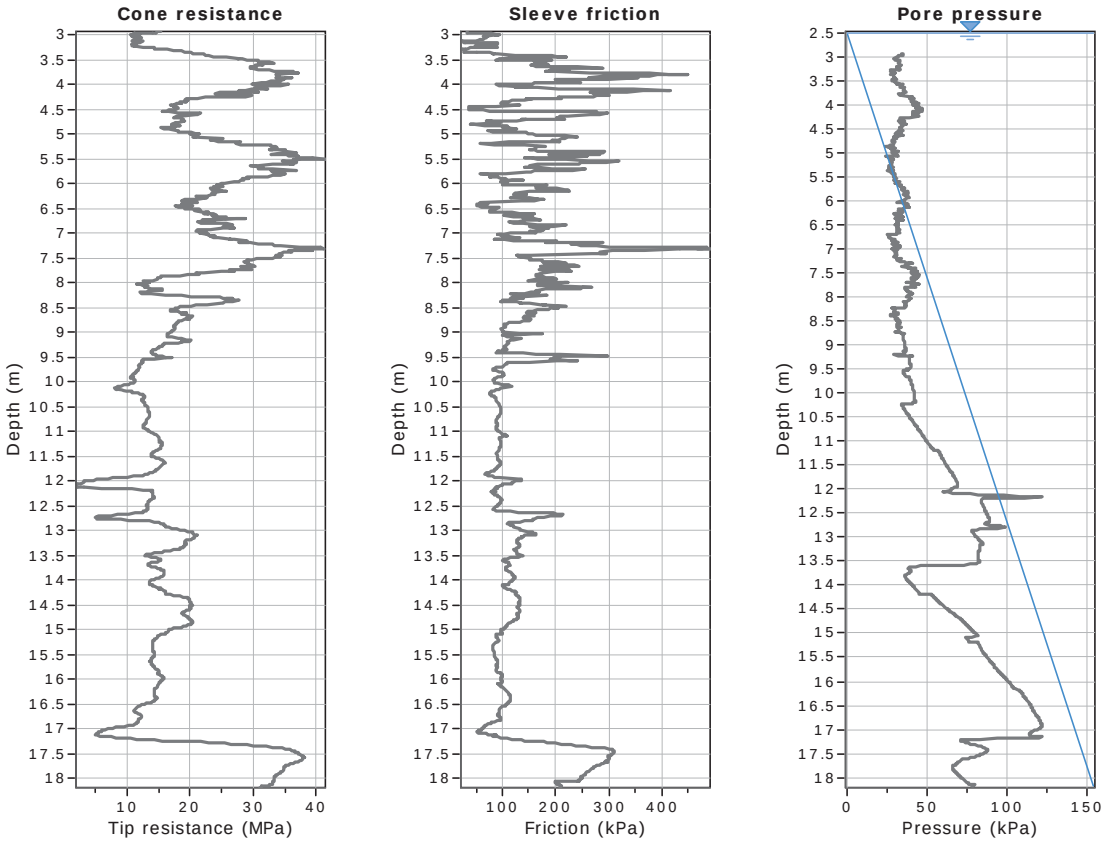

The plot below presents the cross correlation coeficient between the raw qc and fs values (as measured on the field). X axes presents the lag distance (one lag is the distance between two sucessive CPT measurements).

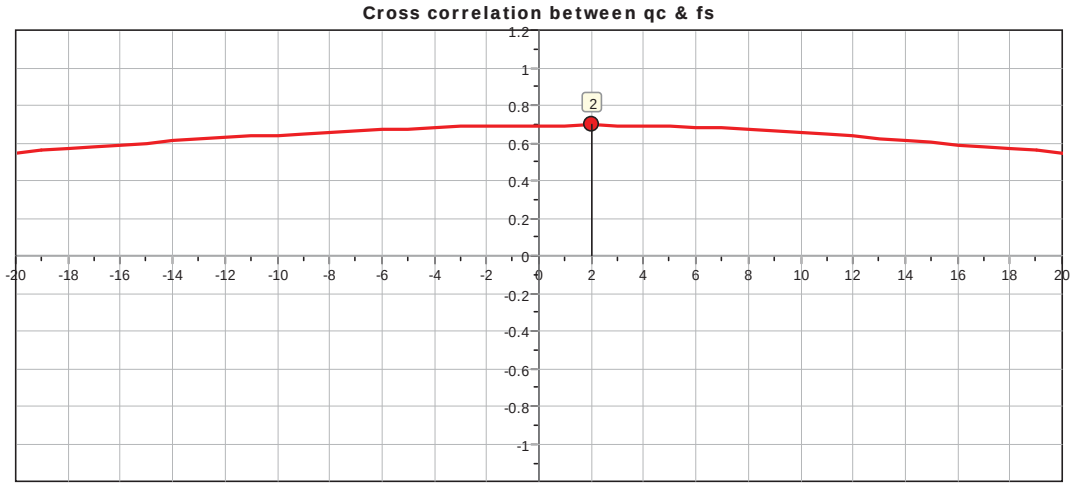

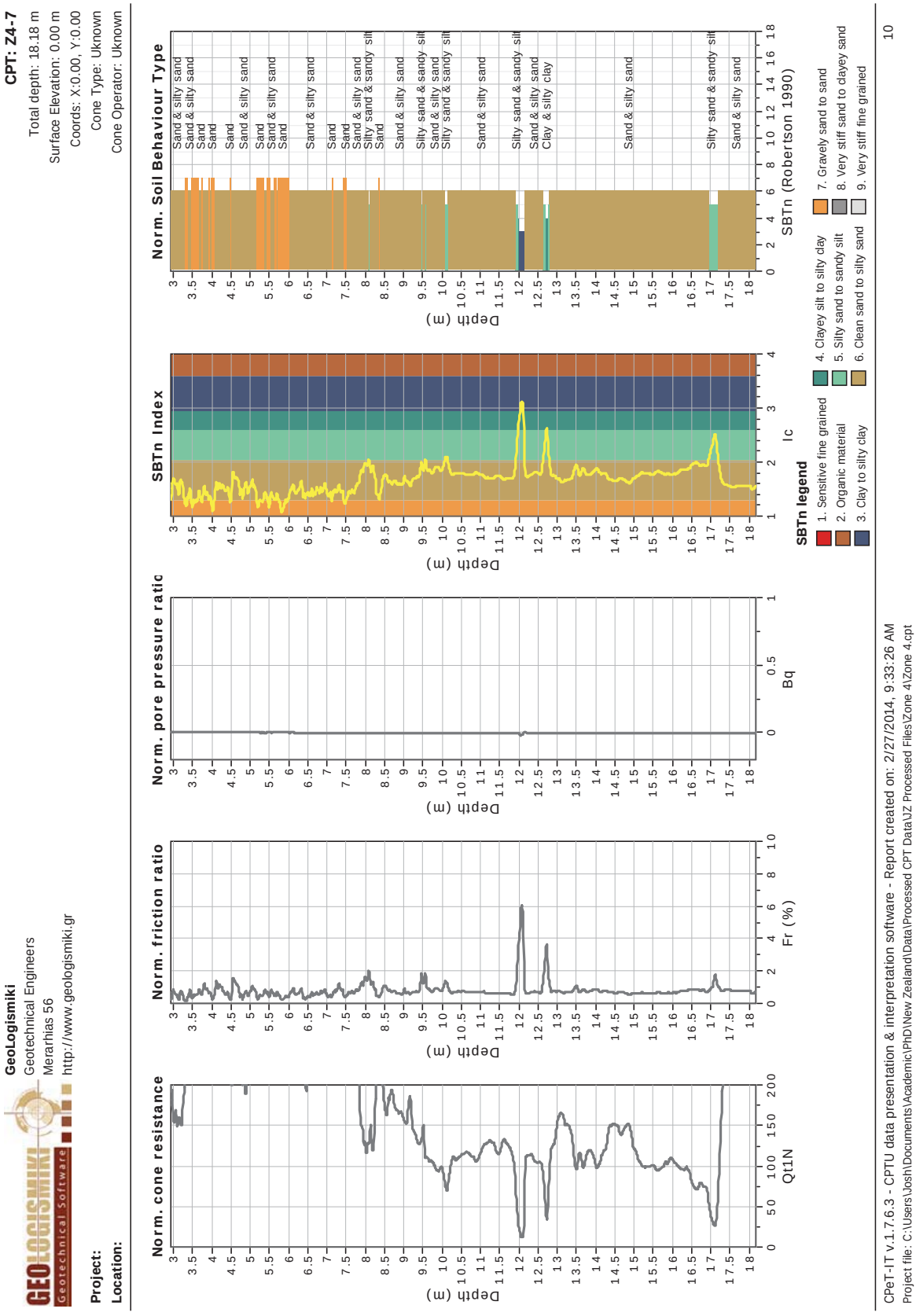
GeoLogismiki
Geotechnical Engineers
Merarhias 56
http://www.geologismiki.gr
Project:
Location:
CPT: Z4-7
Total depth: 18.18 m
Surface Elevation: 0.00 m
Coords: X:0.00, Y:0.00
Cone Type: Uknown
Cone Operator: Uknown
Norm. cone resistance
Qt1N
Norm. friction ratio
Fr (%)
Norm. pore pressure ratio
Bq
SBTn Index
Ic
Norm. Soil Behaviour Type
SBTn (Robertson 1990)
Depth (m)
SBTn legend
1. Sensitive fine grained
2. Organic material
3. Clay to silty clay
4. Clayey silt to silty clay
5. Silty sand to sandy silt
6. Clean sand to silty sand
7. Gravely sand to sand
8. Very stiff sand to clayey sand
9. Very stiff fine grained
CPeT-IT v.1.7.6.3 - CPTU data presentation & interpretation software - Report created on: 2/27/2014, 9:33:26 AM
Project file: C:\Users\Josh\Documents\Academic\PhD\New Zealand\Data\Processed CPT Data\JZ Processed Files\Zone 4\Zone 4.cpt
10

GeoLogismiki
Geotechnical Engineers
Merarhias 56
http://www.geologismiki.gr

CPT: Z4-8
Total depth: 15.02 m
Surface Elevation: 0.00 m
Coords: X:0.00, Y:0.00
Cone Type: Uknown
Cone Operator: Uknown

Project:
Location:

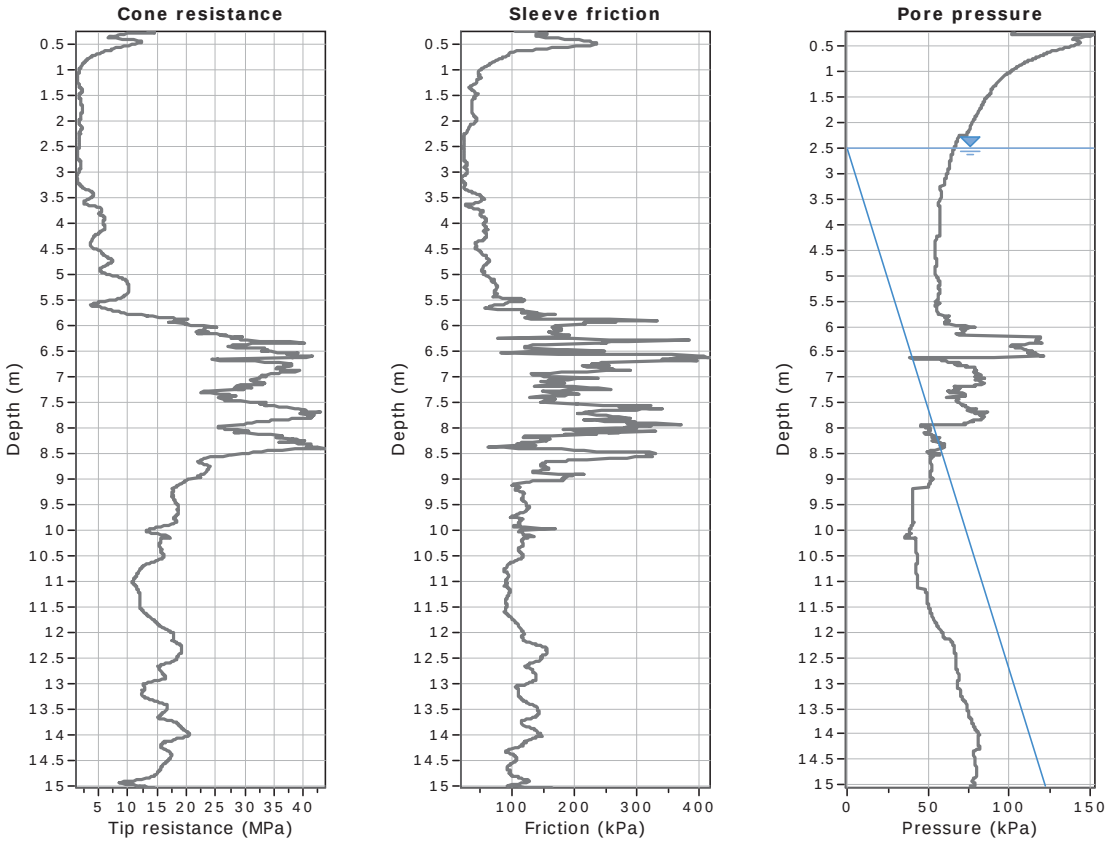

The plot below presents the cross correlation coeficient between the raw qc and fs values (as measured on the field). X axes presents the lag distance (one lag is the distance between two sucessive CPT measurements).

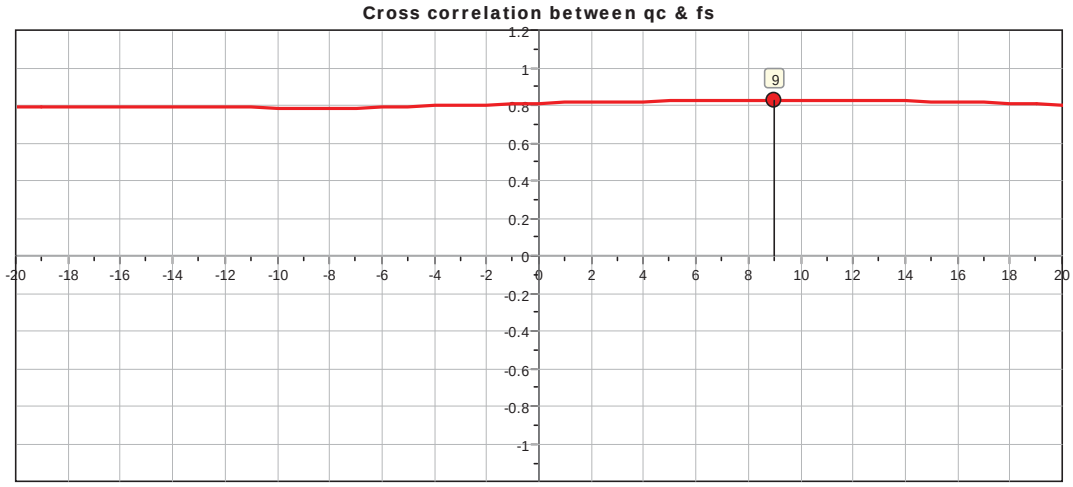

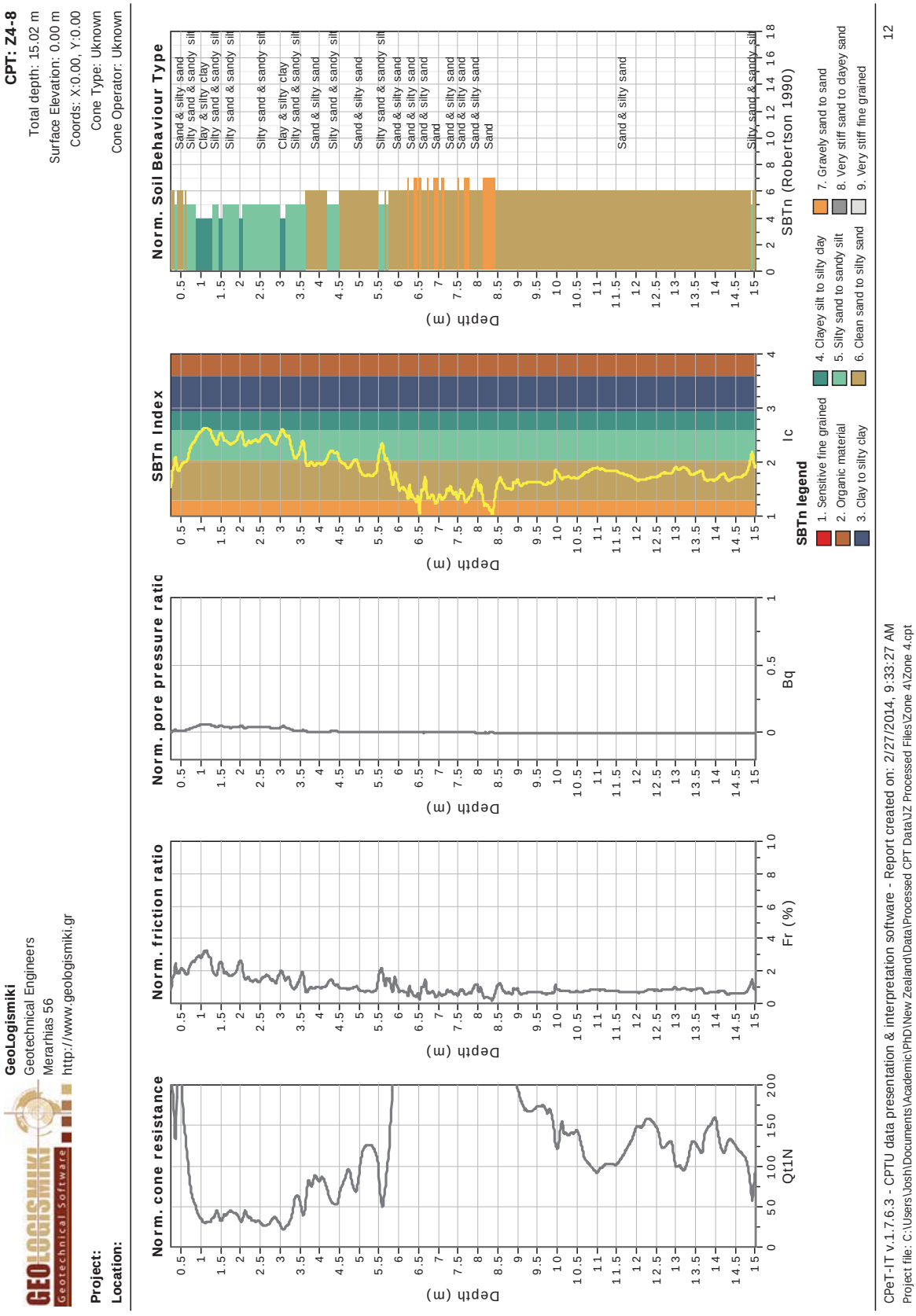
CPT: Z4-8
Total depth: 15.02 m
Surface Elevation: 0.00 m
Coords: X:0.00, Y:0.00
Cone Type: Uknown
Cone Operator: Uknown
GeoLogismiki
Geotechnical Engineers
Merarhias 56
http://www.geologismiki.gr
Project:
Location:
Norm. cone resistance
Qt1N
Norm. friction ratio
Fr (%)
Norm. pore pressure ratio
Bq
SBTn Index
Ic
Norm. Soil Behaviour Type
SBTn (Robertson 1990)
Depth (m)
SBTn legend
1. Sensitive fine grained
2. Organic material
3. Clay to silty clay
4. Clayey silt to silty clay
5. Silty sand to sandy silt
6. Clean sand to silty sand
7. Gravely sand to sand
8. Very stiff sand to clayey sand
9. Very stiff fine grained
CPeT-IT v.1.7.6.3 - CPTU data presentation & interpretation software - Report created on: 2/27/2014, 9:33:27 AM
Project file: C:\Users\Josh\Documents\Academic\PhD\New Zealand\Data\Processed CPT Data\JZ Processed Files\Zone 4\Zone 4.cpt
12

GeoLogismiki
Geotechnical Engineers
Merarhias 56
http://www.geologismiki.gr

CPT: Z4-9
Total depth: 5.43 m
Surface Elevation: 0.00 m
Coords: X:0.00, Y:0.00
Cone Type: Uknown
Cone Operator: Uknown

Project:
Location:

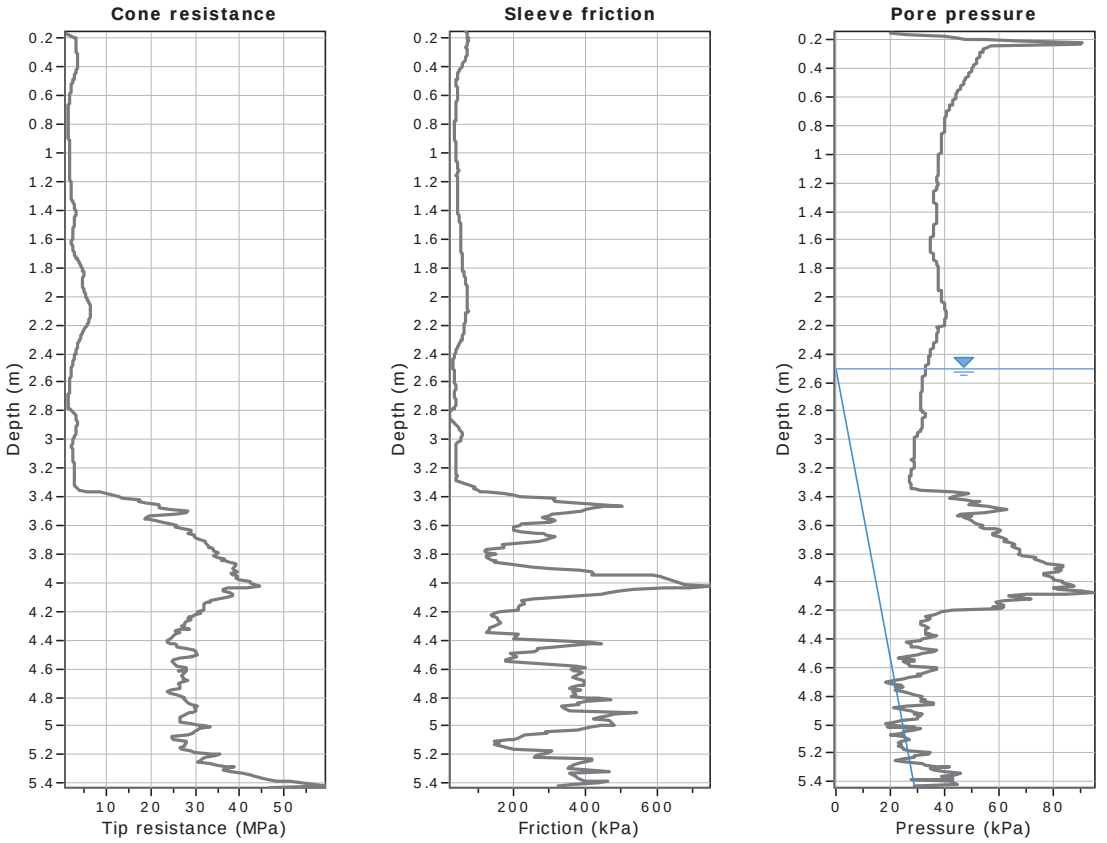

The plot below presents the cross correlation coeficient between the raw qc and fs values (as measured on the field). X axes presents the lag distance (one lag is the distance between two sucessive CPT measurements).

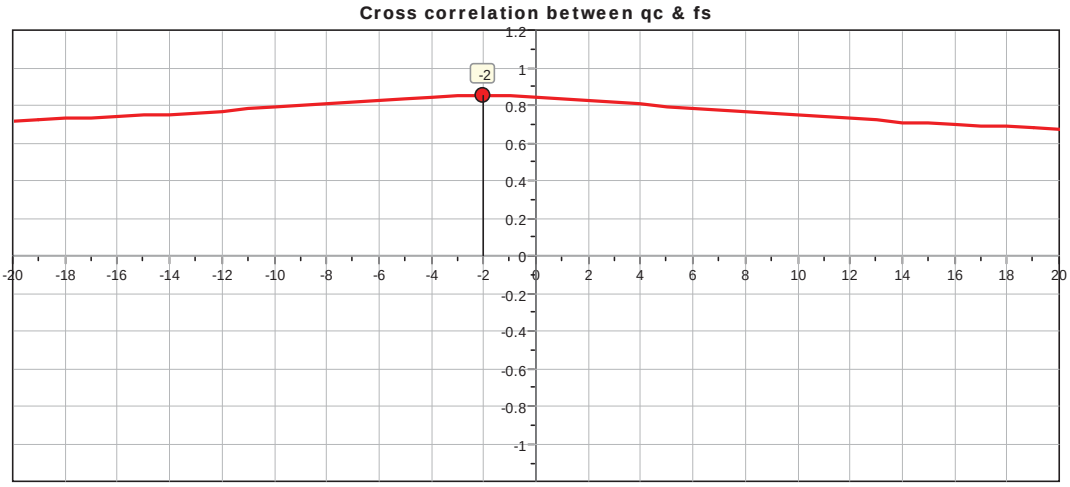

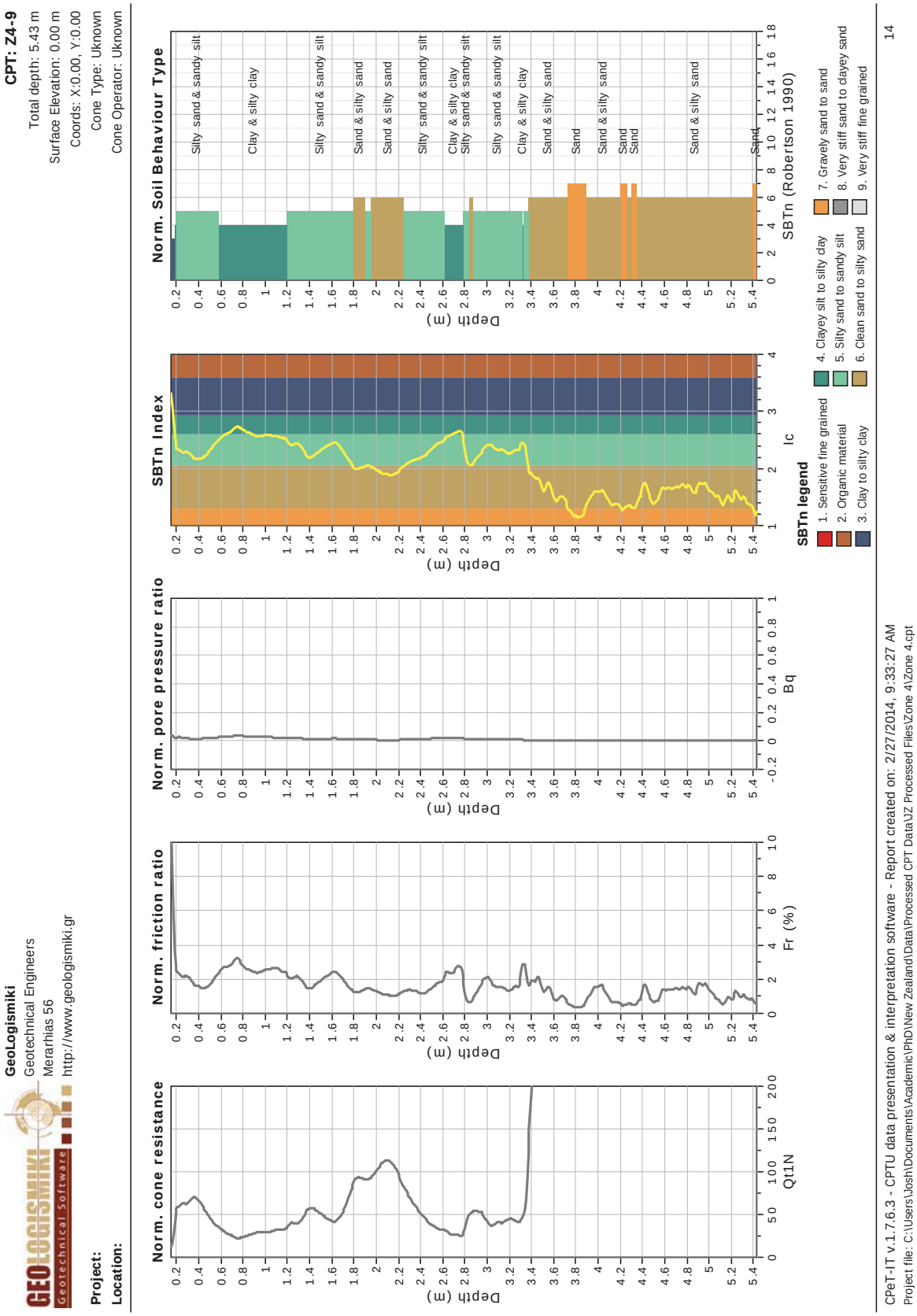
CPT: Z4-9
Total depth: 5.43 m
Surface Elevation: 0.00 m
Coords: X:0.00, Y:0.00
Cone Type: Uknown
Cone Operator: Uknown
GeoLogismiki
Geotechnical Engineers
Merarhias 56
http://www.geologismiki.gr
Project:
Location:
Norm. cone resistance
Norm. friction ratio
Norm. pore pressure ratio
SBTn Index
Norm. Soil Behaviour Type
SBTn (Robertson 1990)
SBTn legend
1. Sensitive fine grained
2. Organic material
3. Clay to silty clay
4. Clayey silt to silty clay
5. Silty sand to sandy silt
6. Clean sand to silty sand
7. Gravely sand to sand
8. Very stiff sand to clayey sand
9. Very stiff fine grained
CPeT-IT v.1.7.6.3 - CPTU data presentation & interpretation software - Report created on: 2/27/2014, 9:33:27 AM
Project file: C:\Users\Josh\Documents\Academic\PhD\New Zealand\Data\Processed CPT Data\JZ Processed Files\Zone 4\Zone 4.cpt
14

GeoLogismiki
Geotechnical Engineers
Merarhias 56
http://www.geologismiki.gr

CPT: Z4-10
Total depth: 17.18 m
Surface Elevation: 0.00 m
Coords: X:0.00, Y:0.00
Cone Type: Uknown
Cone Operator: Uknown

Project:
Location:

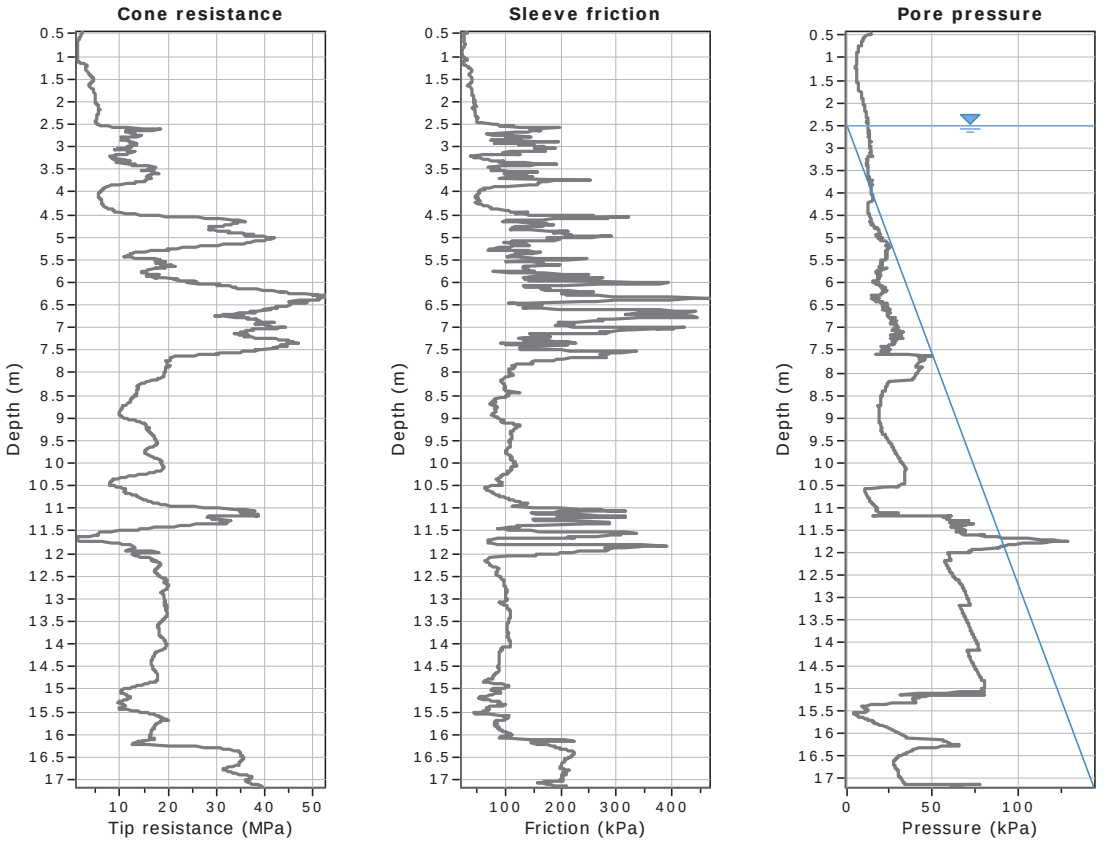

The plot below presents the cross correlation coeficient between the raw qc and fs values (as measured on the field). X axes presents the lag distance (one lag is the distance between two sucessive CPT measurements).

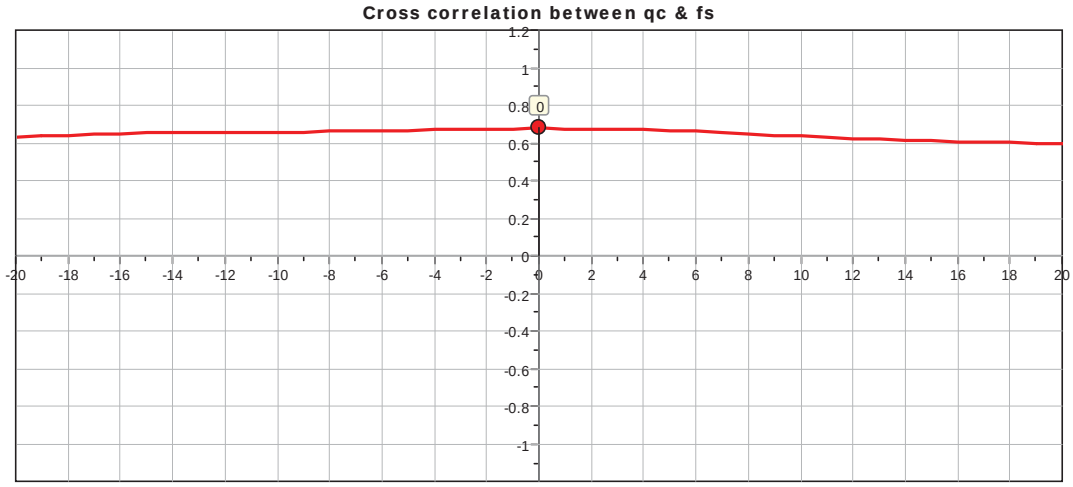

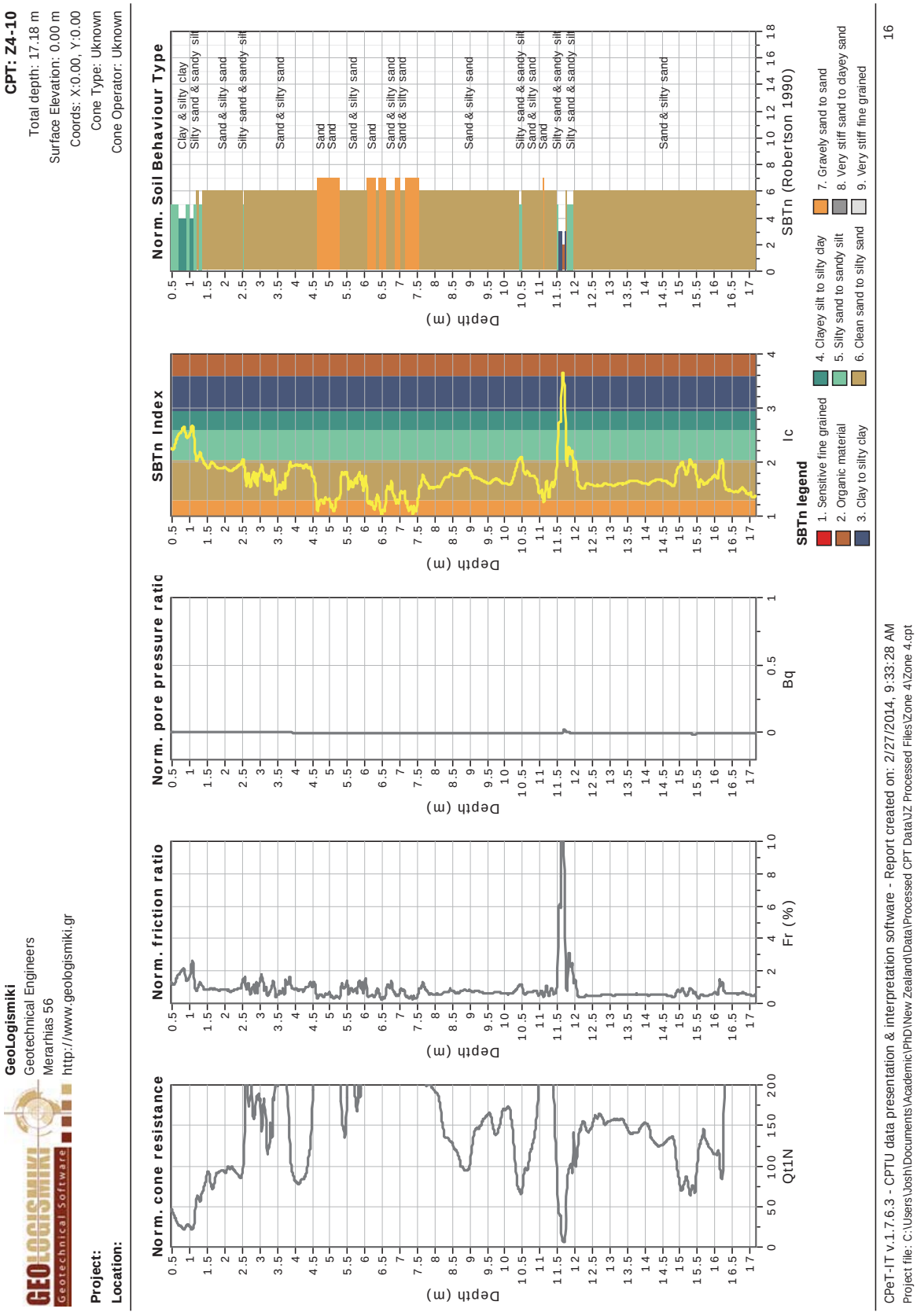
GeoLogismiki
Geotechnical Engineers
Merarhias 56
http://www.geologismiki.gr
Project:
Location:
CPT: Z4-10
Total depth: 17.18 m
Surface Elevation: 0.00 m
Coords: X:0.00, Y:0.00
Cone Type: Uknown
Cone Operator: Uknown
Norm. cone resistance
Qt1N
Norm. friction ratio
Fr (%)
Norm. pore pressure ratio
Bq
SBTn Index
Ic
Norm. Soil Behaviour Type
SBTn (Robertson 1990)
Depth (m)
SBTn legend
1. Sensitive fine grained
2. Organic material
3. Clay to silty clay
4. Clayey silt to silty clay
5. Silty sand to sandy silt
6. Clean sand to silty sand
7. Gravely sand to sand
8. Very stiff sand to clayey sand
9. Very stiff fine grained
CPeT-IT v.1.7.6.3 - CPTU data presentation & interpretation software - Report created on: 2/27/2014, 9:33:28 AM
Project file: C:\Users\Josh\Documents\Academic\PhD\New Zealand\Data\Processed CPT Data\JZ Processed Files\Zone 4\Zone 4.cpt
16

GeoLogismiki
Geotechnical Engineers
Merarhias 56
http://www.geologismiki.gr

CPT: Z4-11
Total depth: 11.50 m
Surface Elevation: 0.00 m
Coords: X:0.00, Y:0.00
Cone Type: Uknown
Cone Operator: Uknown

Project:
Location:

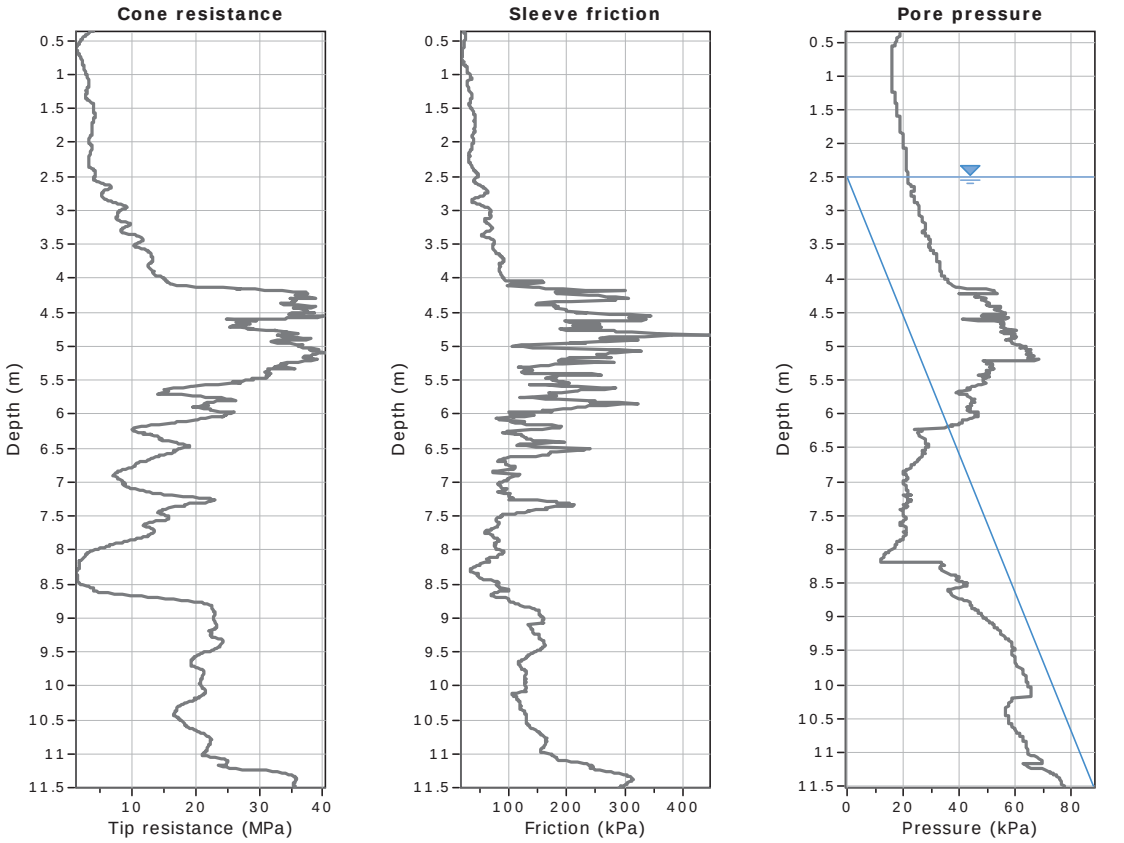

The plot below presents the cross correlation coeficient between the raw qc and fs values (as measured on the field). X axes presents the lag distance (one lag is the distance between two sucessive CPT measurements).

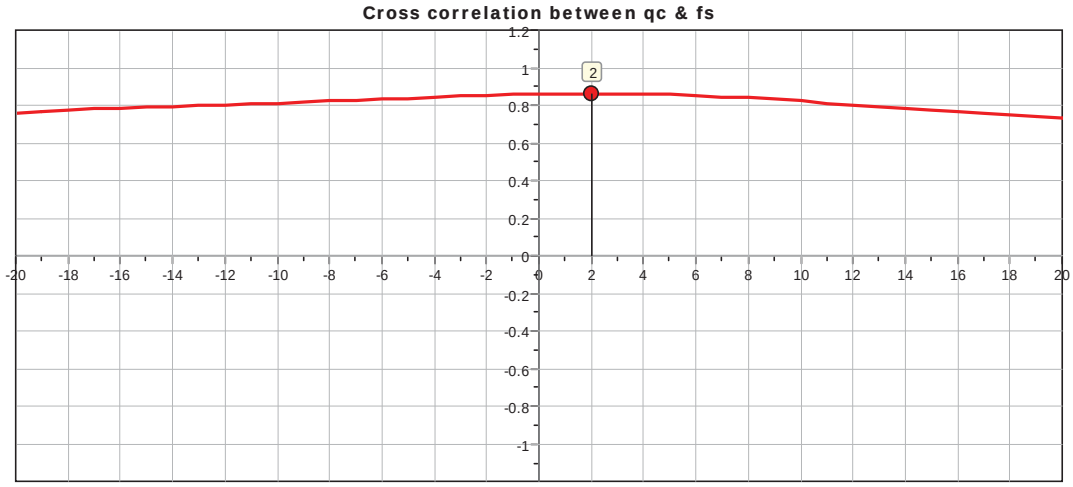

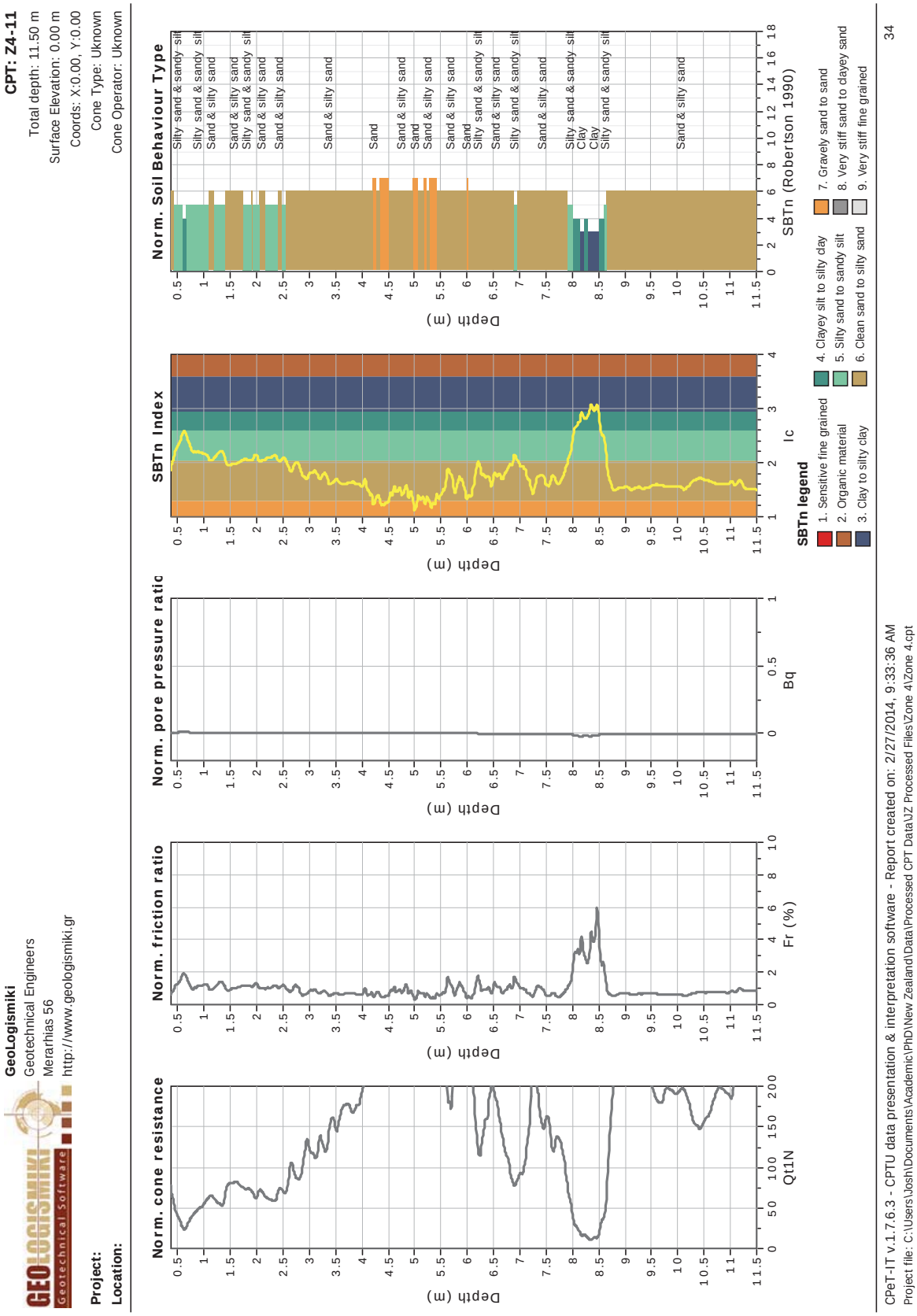
GeoLogismiki
Geotechnical Engineers
Merarchias 56
http://www.geologismiki.gr
Project:
Location:
CPT: Z4-11
Total depth: 11.50 m
Surface Elevation: 0.00 m
Coords: X:0.00, Y:0.00
Cone Type: Uknown
Cone Operator: Uknown
Norm. cone resistance
Qt1N
Norm. friction ratio
Fr (%)
Norm. pore pressure ratio
Bq
SBTn Index
Ic
Norm. Soil Behaviour Type
SBTn (Robertson 1990)
Depth (m)
SBTn legend
1. Sensitive fine grained
2. Organic material
3. Clay to silty clay
4. Clayey silt to silty clay
5. Silty sand to sandy silt
6. Clean sand to silty sand
7. Gravely sand to sand
8. Very stiff sand to clayey sand
9. Very stiff fine grained
CPeT-IT v.1.7.6.3 - CPTU data presentation & interpretation software - Report created on: 2/27/2014, 9:33:36 AM
Project file: C:\Users\Josh\Documents\Academic\PhD\New Zealand\Data\Processed CPT Data\JZ Processed Files\Zone 4\Zone 4.cpt
34

GeoLogismiki
Geotechnical Engineers
Merarhias 56
http://www.geologismiki.gr

CPT: Z4-12
Total depth: 12.07 m
Surface Elevation: 0.00 m
Coords: X:0.00, Y:0.00
Cone Type: Uknown
Cone Operator: Uknown

Project:
Location:

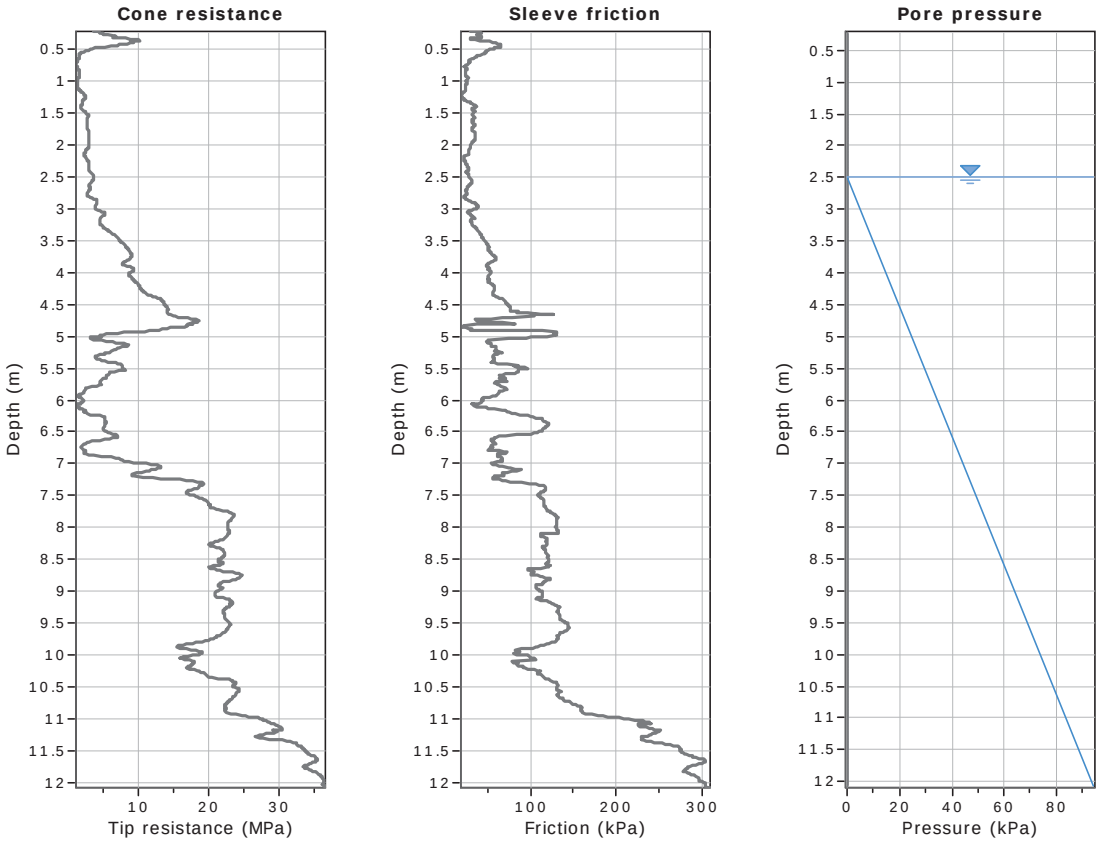

The plot below presents the cross correlation coeficient between the raw qc and fs values (as measured on the field). X axes presents the lag distance (one lag is the distance between two sucessive CPT measurements).

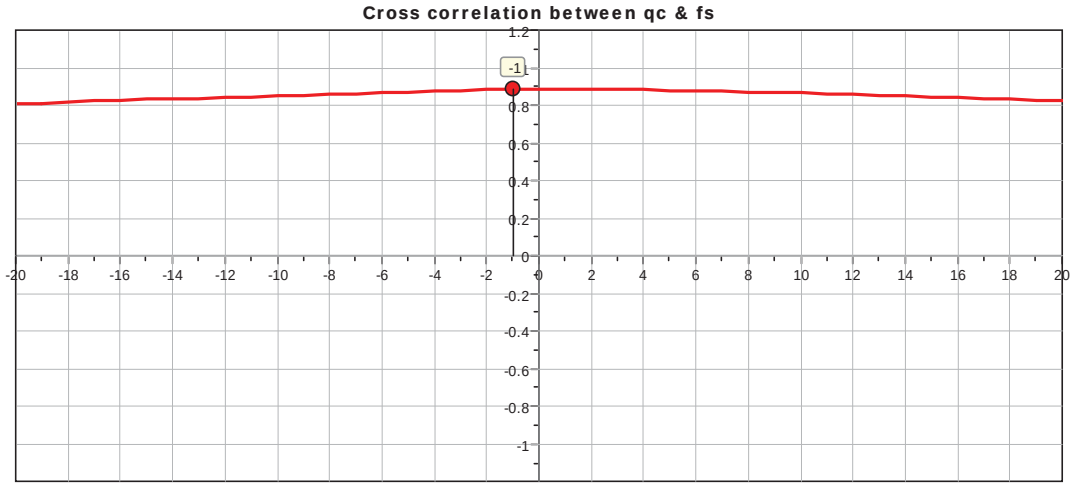

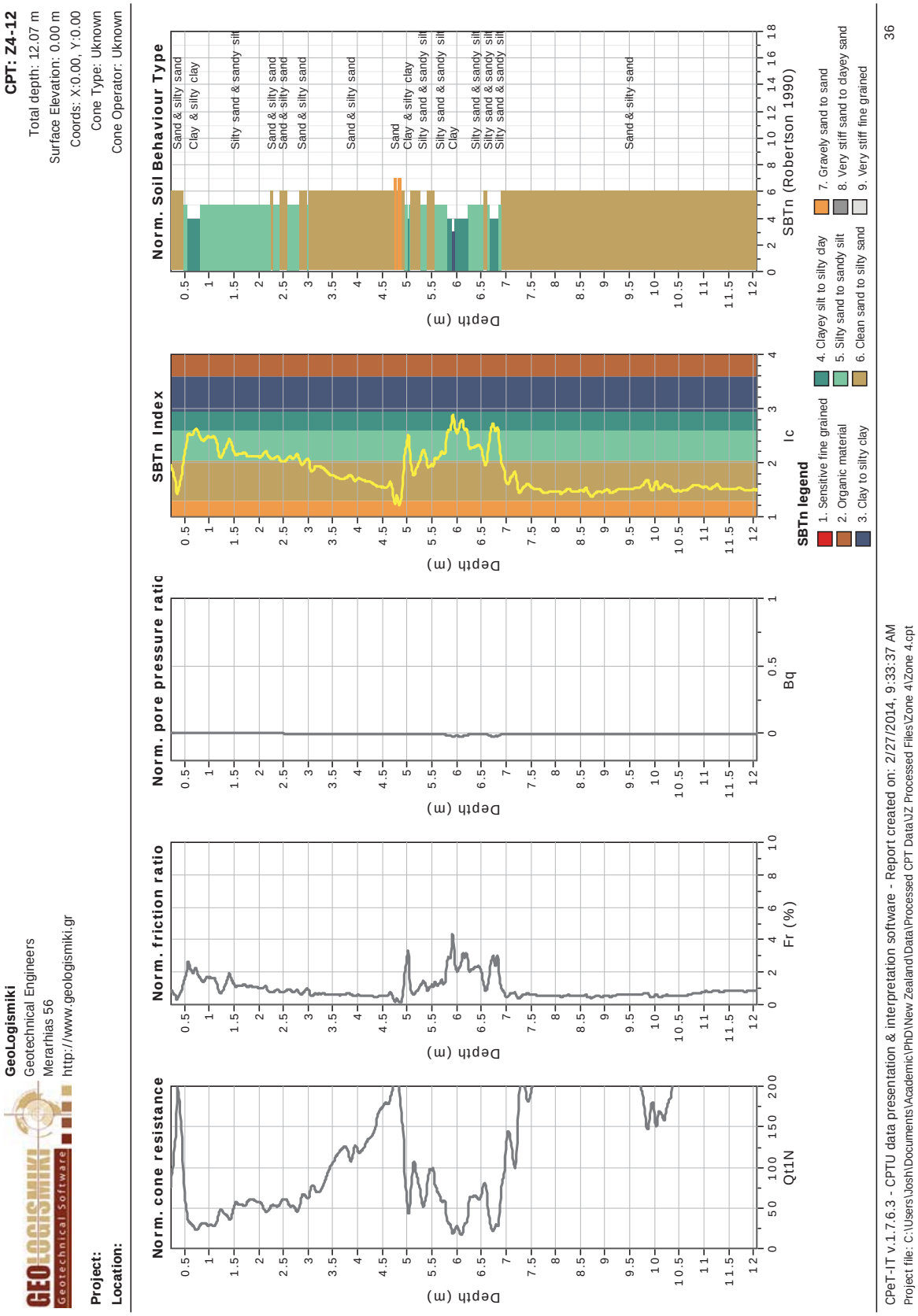
GeoLogismiki
Geotechnical Engineers
Merarhias 56
http://www.geologismiki.gr
Project:
Location:
CPT: Z4-12
Total depth: 12.07 m
Surface Elevation: 0.00 m
Coords: X:0.00, Y:0.00
Cone Type: Uknown
Cone Operator: Uknown
Norm. cone resistance
Qt1N
Norm. friction ratio
Fr (%)
Norm. pore pressure ratio
Bq
SBTn Index
Ic
Norm. Soil Behaviour Type
SBTn (Robertson 1990)
Depth (m)
SBTn legend
1. Sensitive fine grained
2. Organic material
3. Clay to silty clay
4. Clayey silt to silty clay
5. Silty sand to sandy silt
6. Clean sand to silty sand
7. Gravely sand to sand
8. Very stiff sand to clayey sand
9. Very stiff fine grained
CPeT-IT v.1.7.6.3 - CPTU data presentation & interpretation software - Report created on: 2/27/2014, 9:33:37 AM
Project file: C:\Users\Josh\Documents\Academic\PhD\New Zealand\Data\Processed CPT Data\JZ Processed Files\Zone 4\Zone 4.cpt
36

GeoLogismiki
Geotechnical Engineers
Merarhias 56
http://www.geologismiki.gr

CPT: Z4-13
Total depth: 17.61 m
Surface Elevation: 0.00 m
Coords: X:0.00, Y:0.00
Cone Type: Uknown
Cone Operator: Uknown

Project:
Location:

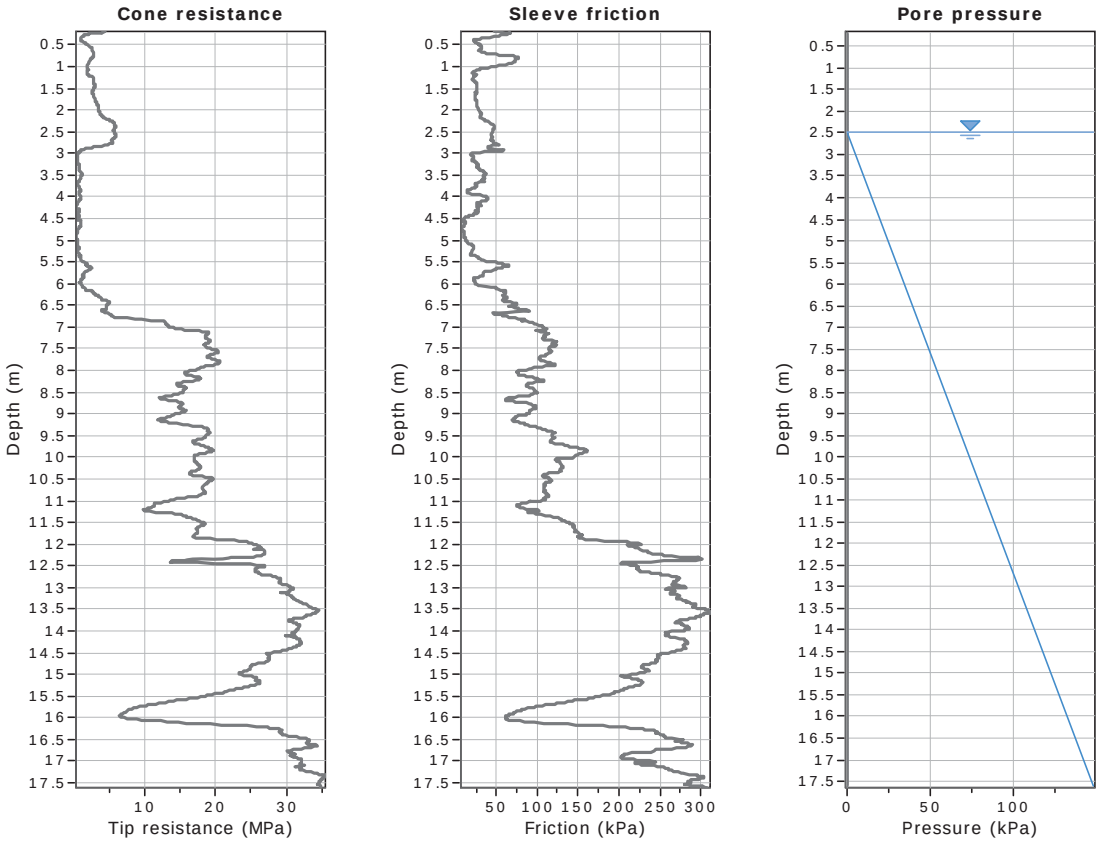

The plot below presents the cross correlation coeficient between the raw qc and fs values (as measured on the field). X axes presents the lag distance (one lag is the distance between two sucessive CPT measurements).

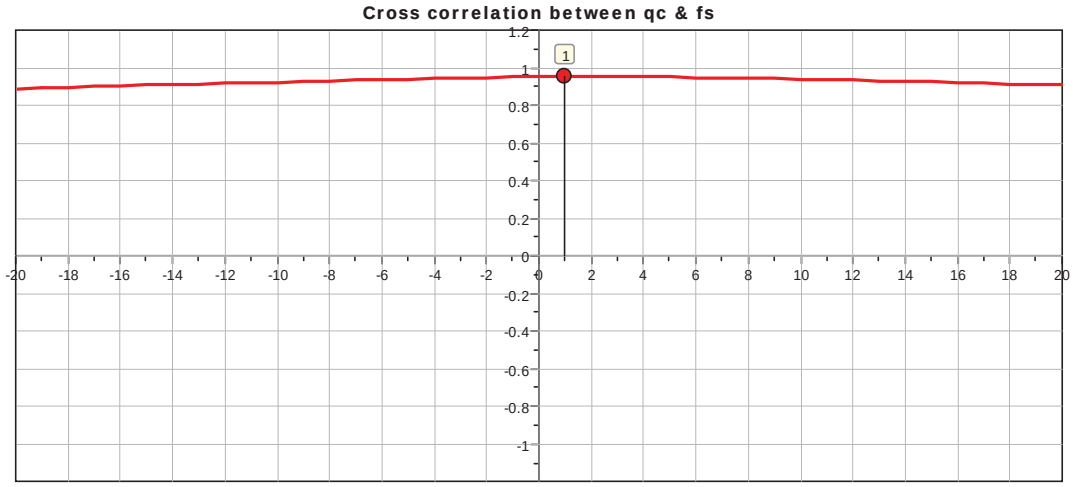

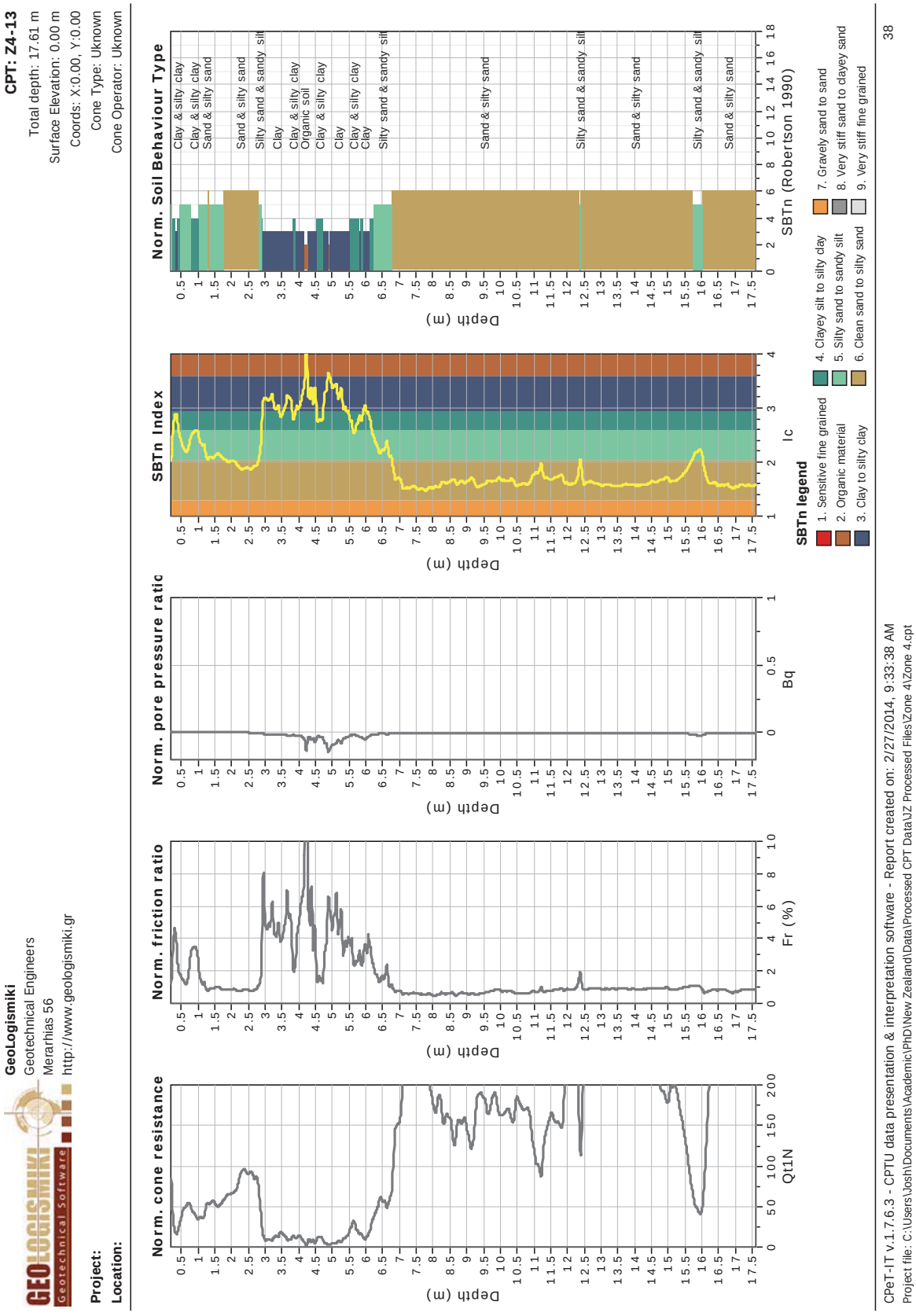
CPT: Z4-13
Total depth: 17.61 m
Surface Elevation: 0.00 m
Coords: X:0.00, Y:0.00
Cone Type: Uknown
Cone Operator: Uknown
GeoLogismiki
Geotechnical Engineers
Merarhias 56
http://www.geologismiki.gr
Project:
Location:
Norm. cone resistance
Qt1N
Norm. friction ratio
Fr (%)
Norm. pore pressure ratio
Bq
SBTn Index
Ic
Norm. Soil Behaviour Type
SBTn (Robertson 1990)
Depth (m)
SBTn legend
1. Sensitive fine grained
2. Organic material
3. Clay to silty clay
4. Clayey silt to silty clay
5. Silty sand to sandy silt
6. Clean sand to silty sand
7. Gravely sand to sand
8. Very stiff sand to clayey sand
9. Very stiff fine grained
CPeT-IT v.1.7.6.3 - CPTU data presentation & interpretation software - Report created on: 2/27/2014, 9:33:38 AM
Project file: C:\Users\Josh\Documents\Academic\PhD\New Zealand\Data\Processed CPT Data\JZ Processed Files\Zone 4\Zone 4.cpt
38

GeoLogismiki
Geotechnical Engineers
Merarhias 56
http://www.geologismiki.gr

CPT: Z4-14
Total depth: 6.78 m
Surface Elevation: 0.00 m
Coords: X:0.00, Y:0.00
Cone Type: Uknown
Cone Operator: Uknown

Project:
Location:

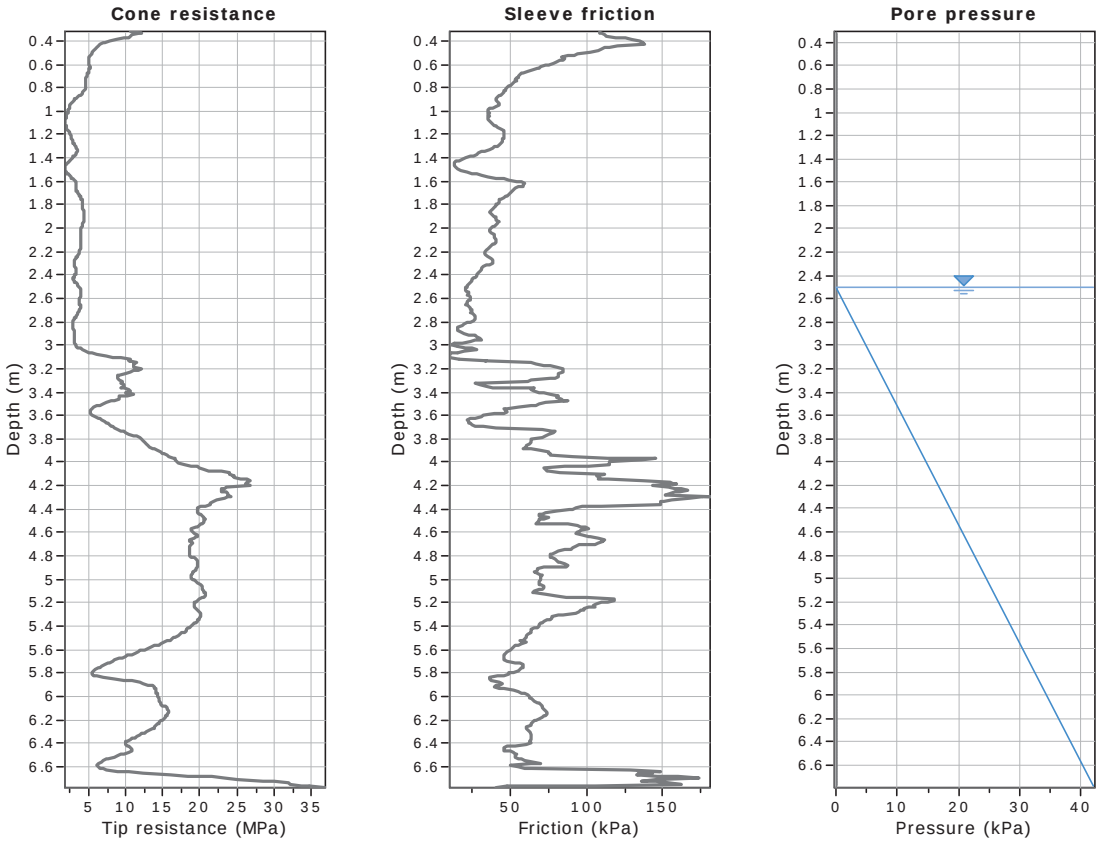

The plot below presents the cross correlation coeficient between the raw qc and fs values (as measured on the field). X axes presents the lag distance (one lag is the distance between two sucessive CPT measurements).

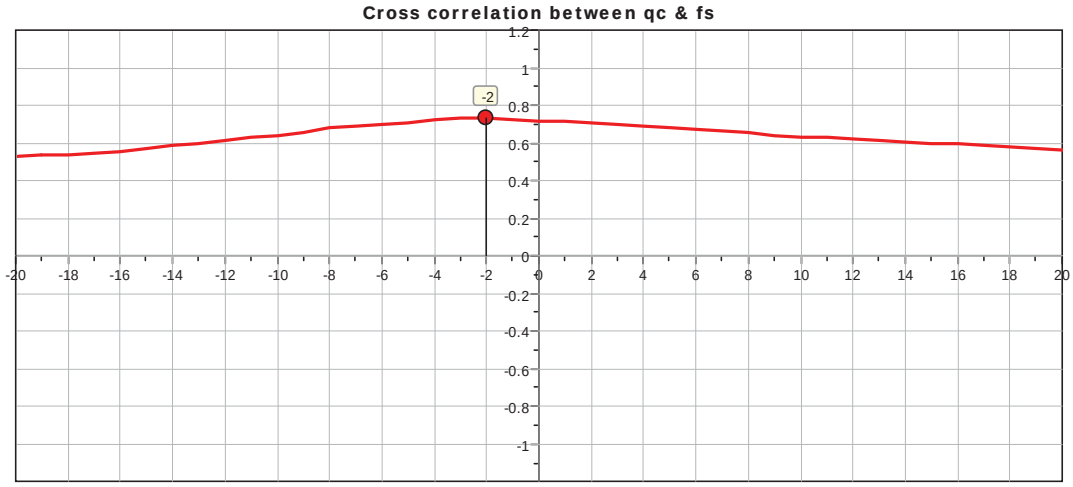

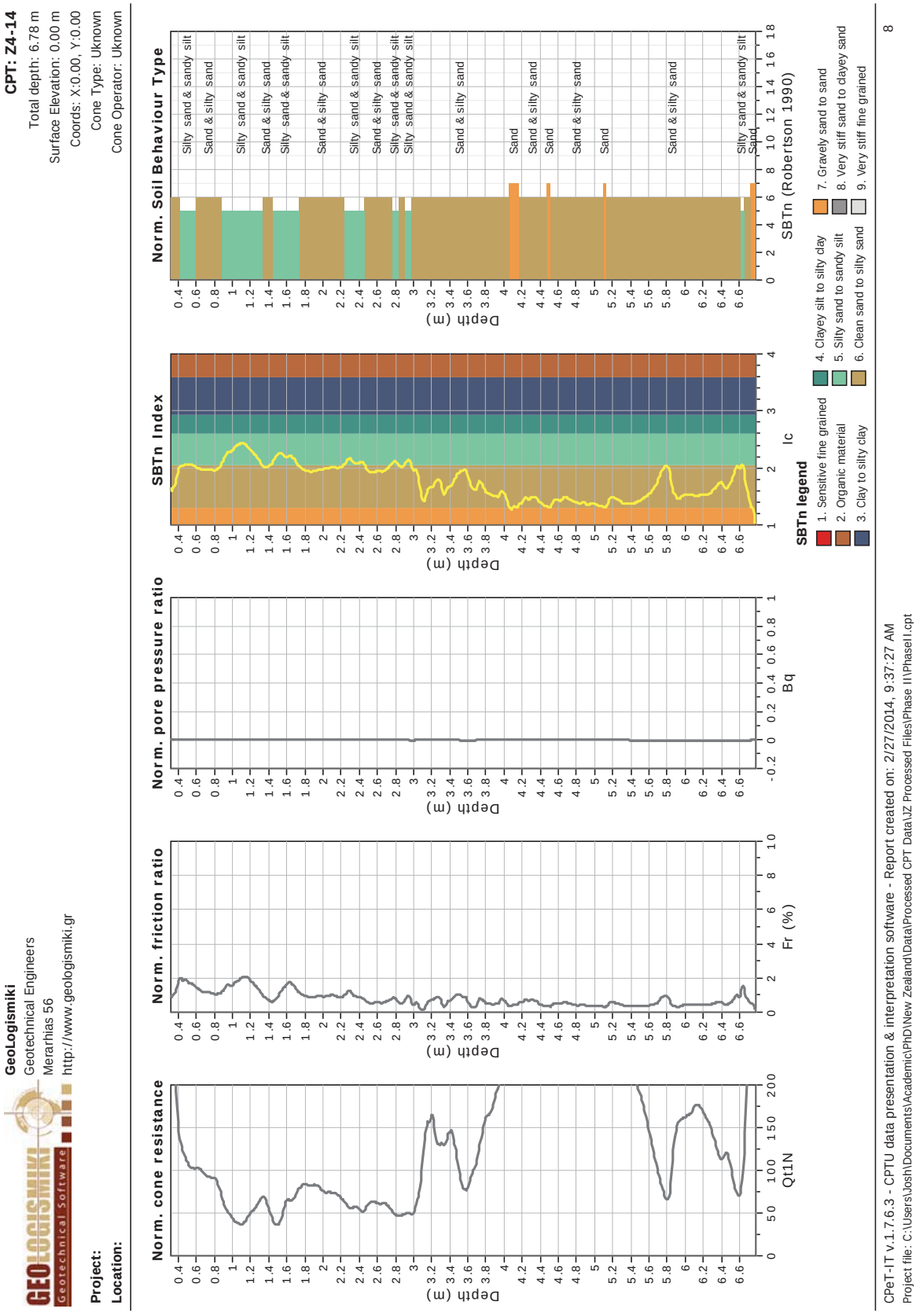
CPT: Z4-14
Total depth: 6.78 m
Surface Elevation: 0.00 m
Coords: X:0.00, Y:0.00
Cone Type: Uknown
Cone Operator: Uknown
GeoLogismiki
Geotechnical Engineers
Merarhias 56
http://www.geologismiki.gr
Project:
Location:
Norm. cone resistance
Qt1N
Norm. friction ratio
Fr (%)
Norm. pore pressure ratio
Bq
SBTn Index
Ic
Norm. Soil Behaviour Type
SBTn (Robertson 1990)
Depth (m)
SBTn legend
1. Sensitive fine grained
2. Organic material
3. Clay to silty clay
4. Clayey silt to silty clay
5. Silty sand to sandy silt
6. Clean sand to silty sand
7. Gravely sand to sand
8. Very stiff sand to clayey sand
9. Very stiff fine grained
CPeT-IT v.1.7.6.3 - CPTU data presentation & interpretation software - Report created on: 2/27/2014, 9:37:27 AM
Project file: C:\Users\Josh\Documents\Academic\PhD\New Zealand\Data\Processed CPT Data\JZ Processed Files\Phase II\PhaseII.cpt
8

GeoLogismiki
Geotechnical Engineers
Merarhias 56
http://www.geologismiki.gr

CPT: Z4-15
Total depth: 6.46 m
Surface Elevation: 0.00 m
Coords: X:0.00, Y:0.00
Cone Type: Uknown
Cone Operator: Uknown

Project:
Location:

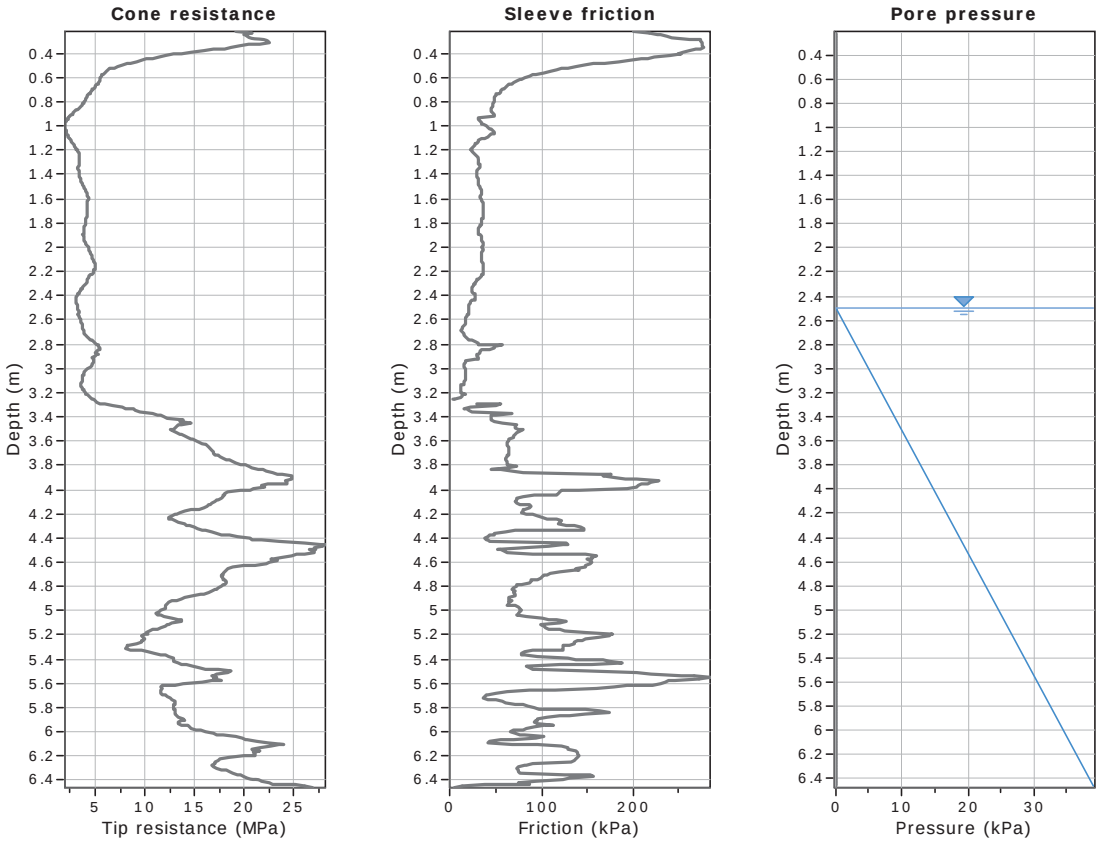

The plot below presents the cross correlation coeficient between the raw qc and fs values (as measured on the field). X axes presents the lag distance (one lag is the distance between two sucessive CPT measurements).

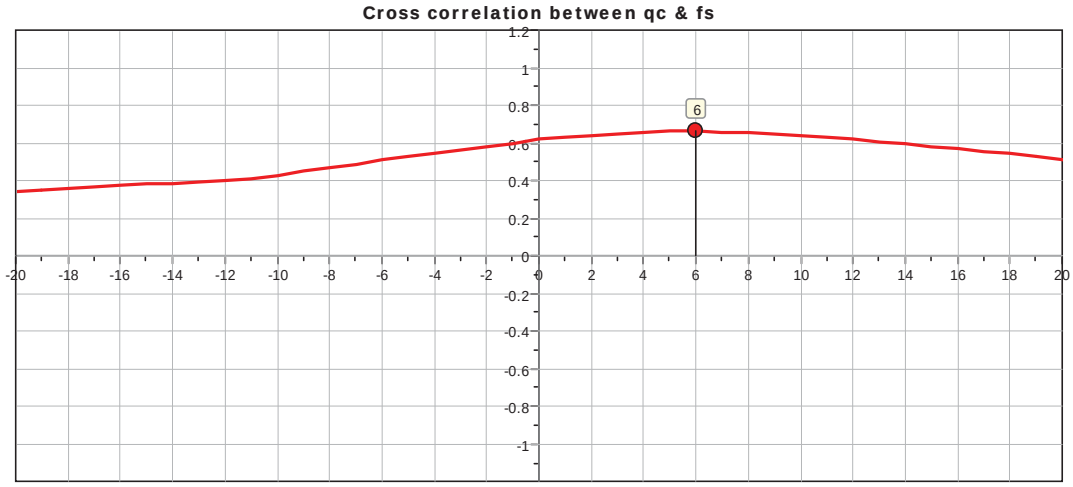

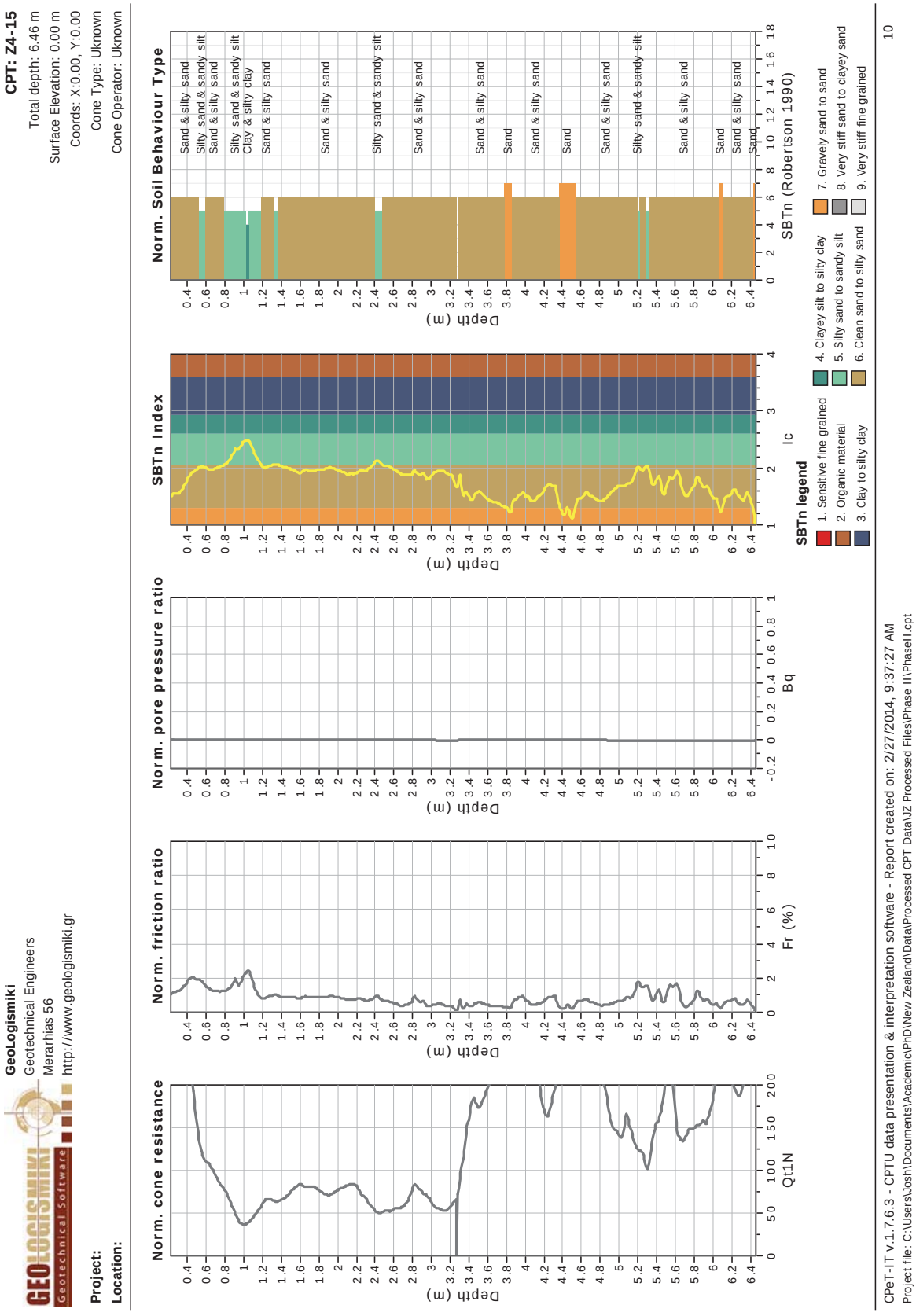
GeoLogismiki
Geotechnical Engineers
Merarhias 56
http://www.geologismiki.gr
Project:
Location:
CPT: Z4-15
Total depth: 6.46 m
Surface Elevation: 0.00 m
Coords: X:0.00, Y:0.00
Cone Type: Uknown
Cone Operator: Uknown
Norm. cone resistance
Qt1N
Norm. friction ratio
Fr (%)
Norm. pore pressure ratio
Bq
SBTn Index
Ic
Norm. Soil Behaviour Type
SBTn (Robertson 1990)
Depth (m)
SBTn legend
1. Sensitive fine grained
2. Organic material
3. Clay to silty clay
4. Clayey silt to silty clay
5. Silty sand to sandy silt
6. Clean sand to silty sand
7. Gravely sand to sand
8. Very stiff sand to clayey sand
9. Very stiff fine grained
CPeT-IT v.1.7.6.3 - CPTU data presentation & interpretation software - Report created on: 2/27/2014, 9:37:27 AM
Project file: C:\Users\Josh\Documents\Academic\PhD\New Zealand\Data\Processed CPT Data\JZ Processed Files\Phase II\PhaseII.cpt
10

GeoLogismiki
Geotechnical Engineers
Merarhias 56
http://www.geologismiki.gr

CPT: Z4-16
Total depth: 2.72 m
Surface Elevation: 0.00 m
Coords: X:0.00, Y:0.00
Cone Type: Uknown
Cone Operator: Uknown

Project:
Location:

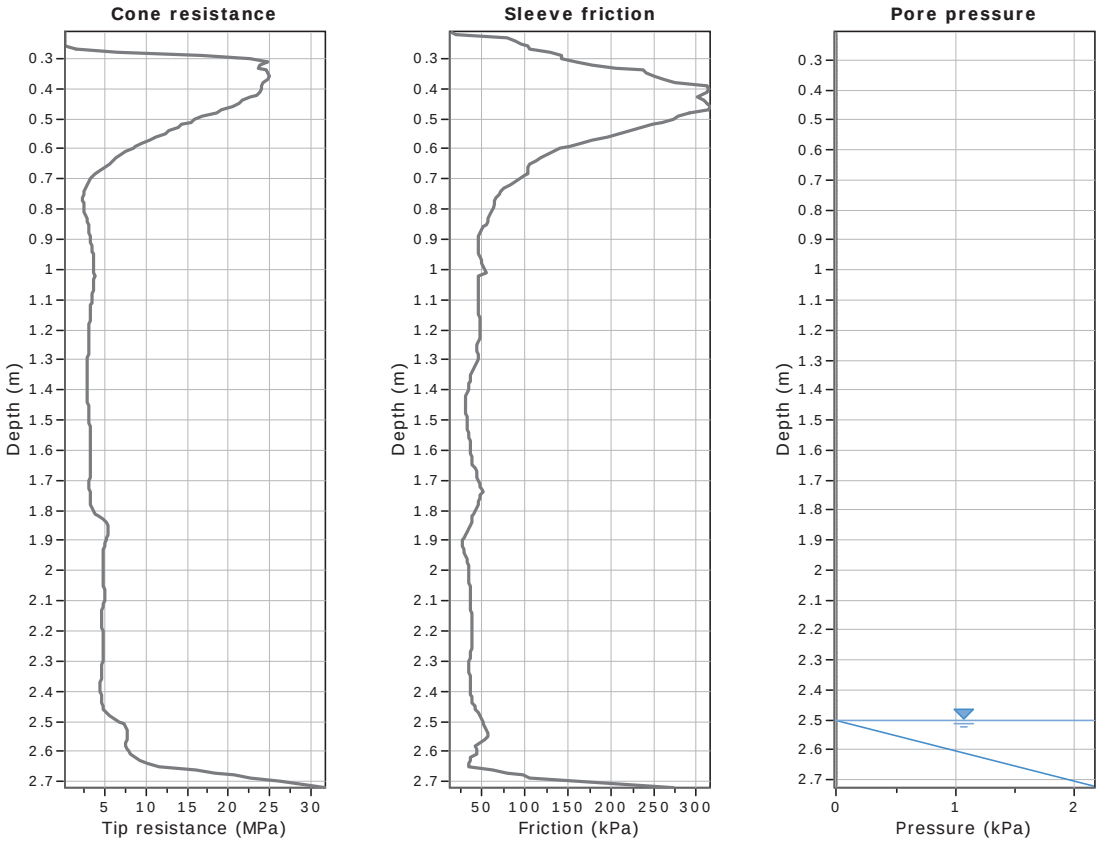

The plot below presents the cross correlation coeficient between the raw qc and fs values (as measured on the field). X axes presents the lag distance (one lag is the distance between two sucessive CPT measurements).

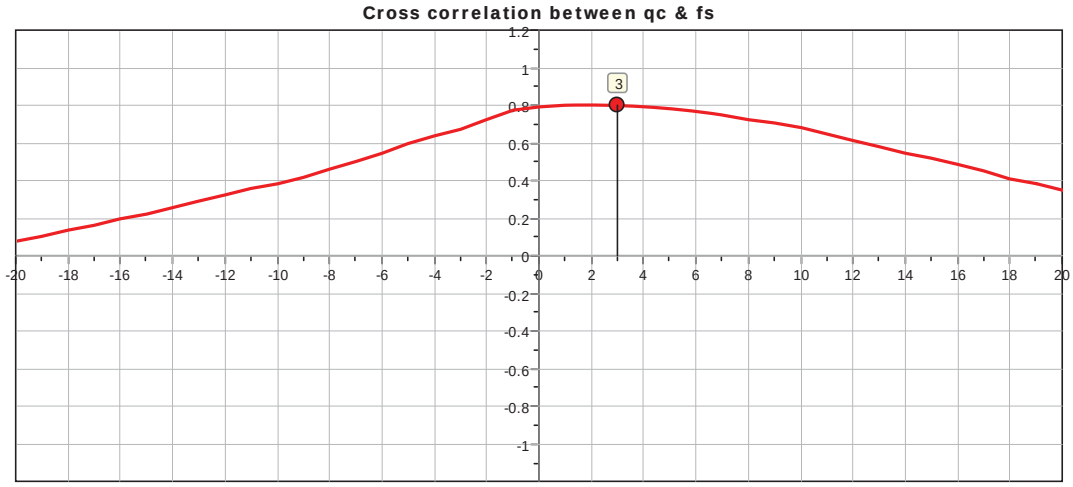

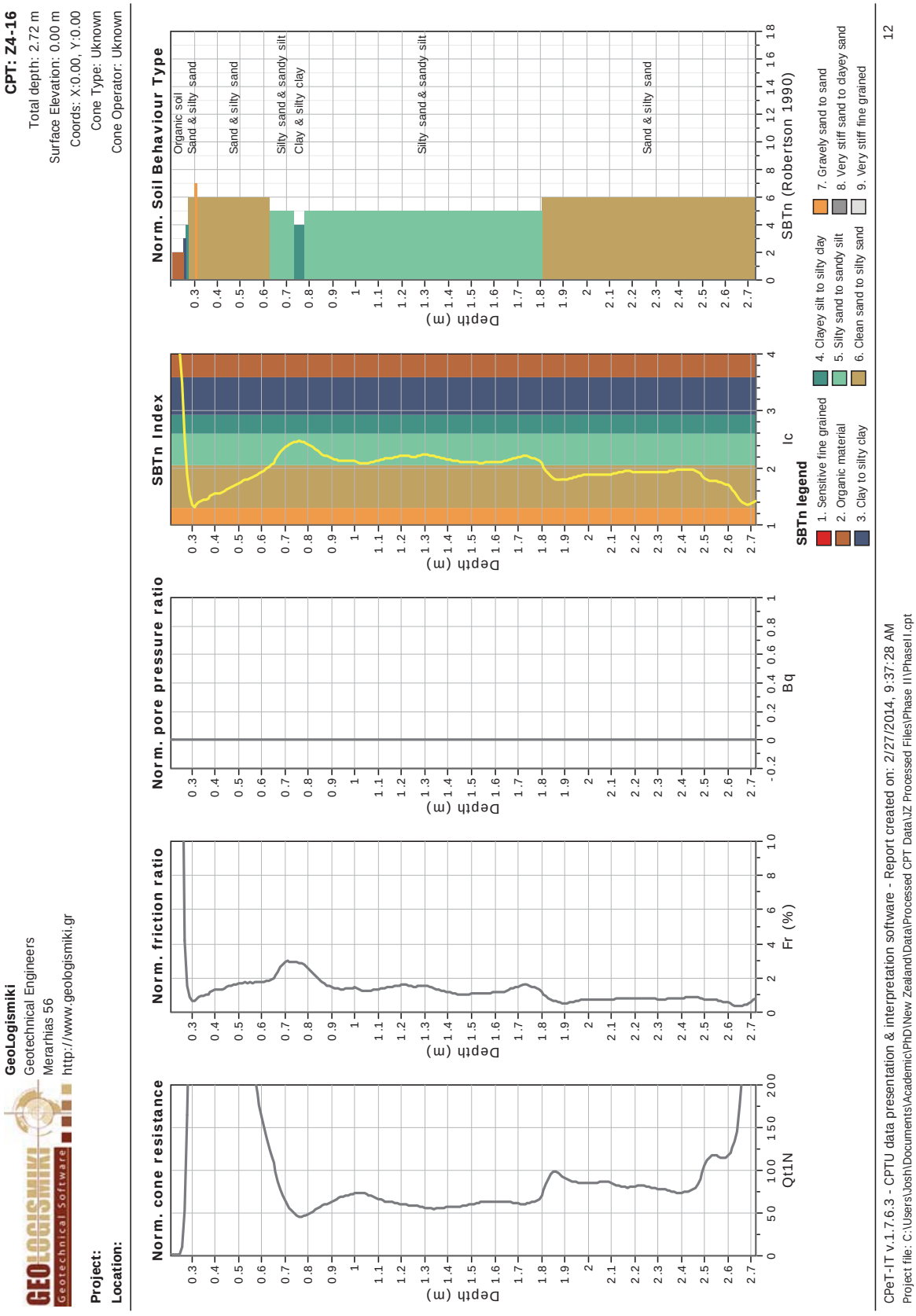
CPT: Z4-16
Total depth: 2.72 m
Surface Elevation: 0.00 m
Coords: X:0.00, Y:0.00
Cone Type: Uknown
Cone Operator: Uknown
GeoLogismiki
Geotechnical Engineers
Merarhias 56
http://www.geologismiki.gr
Project:
Location:
Norm. cone resistance
Qt1N
Norm. friction ratio
Fr (%)
Norm. pore pressure ratio
Bq
SBTn Index
Ic
Norm. Soil Behaviour Type
SBTn (Robertson 1990)
Organic soil
Sand & silty sand
Sand & silty sand
Silty sand & sandy silt
Clay & silty clay
Silty sand & sandy silt
Sand & silty sand
Depth (m)
SBTn legend
1. Sensitive fine grained
2. Organic material
3. Clay to silty clay
4. Clayey silt to silty clay
5. Silty sand to sandy silt
6. Clean sand to silty sand
7. Gravely sand to sand
8. Very stiff sand to clayey sand
9. Very stiff fine grained
CPeT-IT v.1.7.6.3 - CPTU data presentation & interpretation software - Report created on: 2/27/2014, 9:37:28 AM
Project file: C:\Users\Josh\Documents\Academic\PhD\New Zealand\Data\Processed CPT Data\JZ Processed Files\Phase II\PhaseII.cpt
12

GeoLogismiki
Geotechnical Engineers
Merarhias 56
http://www.geologismiki.gr

CPT: Z4-17
Total depth: 2.93 m
Surface Elevation: 0.00 m
Coords: X:0.00, Y:0.00
Cone Type: Uknown
Cone Operator: Uknown

Project:
Location:

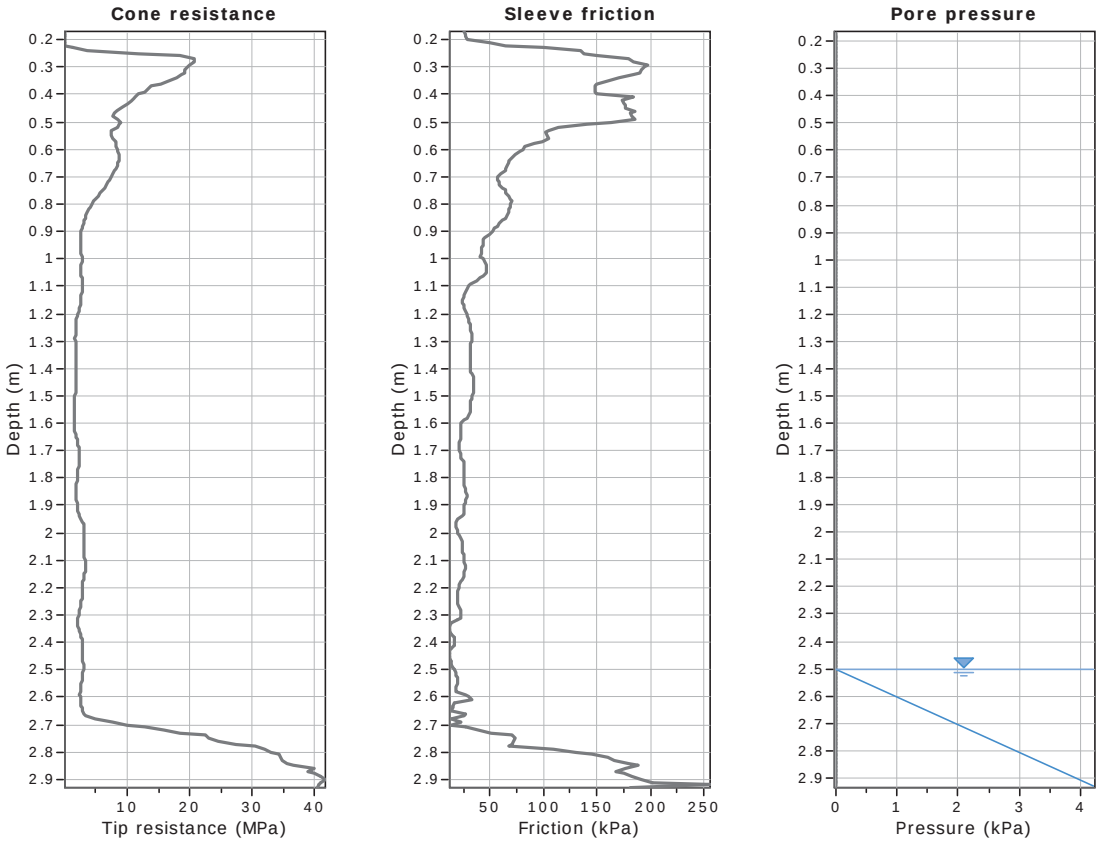

The plot below presents the cross correlation coeficient between the raw qc and fs values (as measured on the field). X axes presents the lag distance (one lag is the distance between two sucessive CPT measurements).

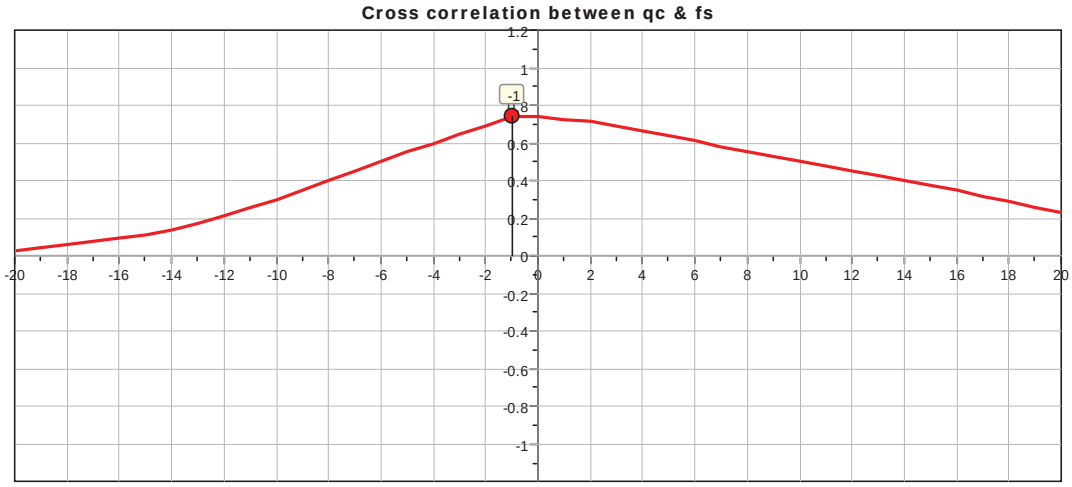

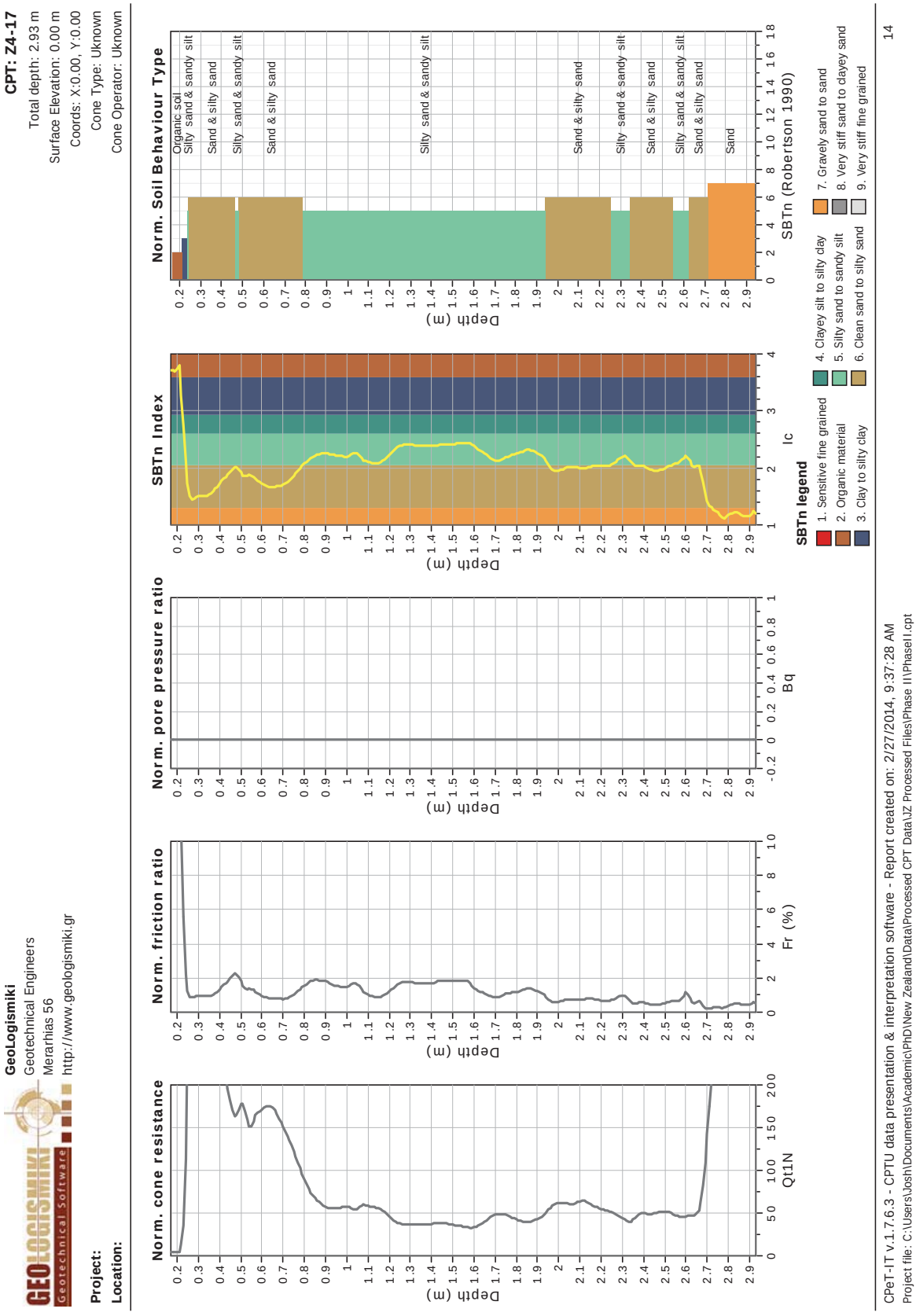
GeoLogismiki
Geotechnical Engineers
Merarhias 56
http://www.geologismiki.gr
Project:
Location:
CPT: Z4-17
Total depth: 2.93 m
Surface Elevation: 0.00 m
Coords: X:0.00, Y:0.00
Cone Type: Uknown
Cone Operator: Uknown
Norm. cone resistance
Norm. friction ratio
Norm. pore pressure ratio
SBTn Index
Norm. Soil Behaviour Type
Depth (m)
Qt1N
Fr (%)
Bq
Ic
SBTn (Robertson 1990)
Organic soil
Silty sand & sandy silt
Sand & silty sand
Silty sand & sandy silt
Sand & silty sand
Silty sand & sandy silt
Sand & silty sand
Silty sand & sandy silt
Sand & silty sand
Sand
SBTn legend
1. Sensitive fine grained
2. Organic material
3. Clay to silty clay
4. Clayey silt to silty clay
5. Silty sand to sandy silt
6. Clean sand to silty sand
7. Gravely sand to sand
8. Very stiff sand to clayey sand
9. Very stiff fine grained
CPeT-IT v.1.7.6.3 - CPTU data presentation & interpretation software - Report created on: 2/27/2014, 9:37:28 AM
Project file: C:\Users\Josh\Documents\Academic\PhD\New Zealand\Data\Processed CPT Data\JZ Processed Files\Phase II\PhaseII.cpt
14

GeoLogismiki
Geotechnical Engineers
Merarhias 56
http://www.geologismiki.gr

CPT: Z4-18
Total depth: 6.44 m
Surface Elevation: 0.00 m
Coords: X:0.00, Y:0.00
Cone Type: Uknown
Cone Operator: Uknown

Project:
Location:

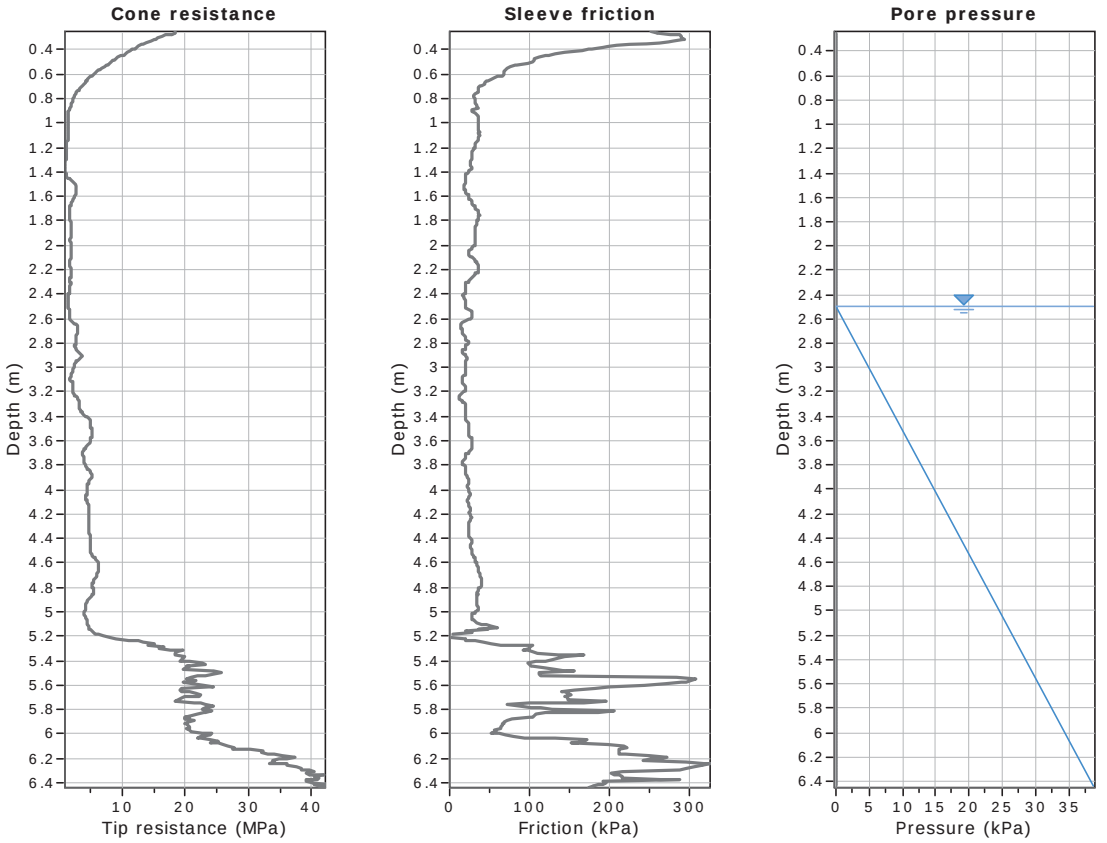

The plot below presents the cross correlation coeficient between the raw qc and fs values (as measured on the field). X axes presents the lag distance (one lag is the distance between two sucessive CPT measurements).

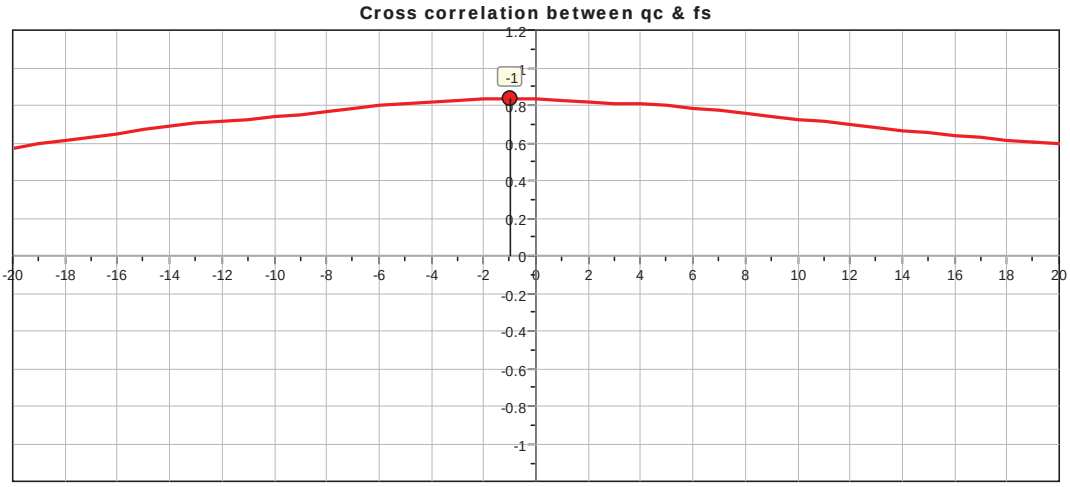

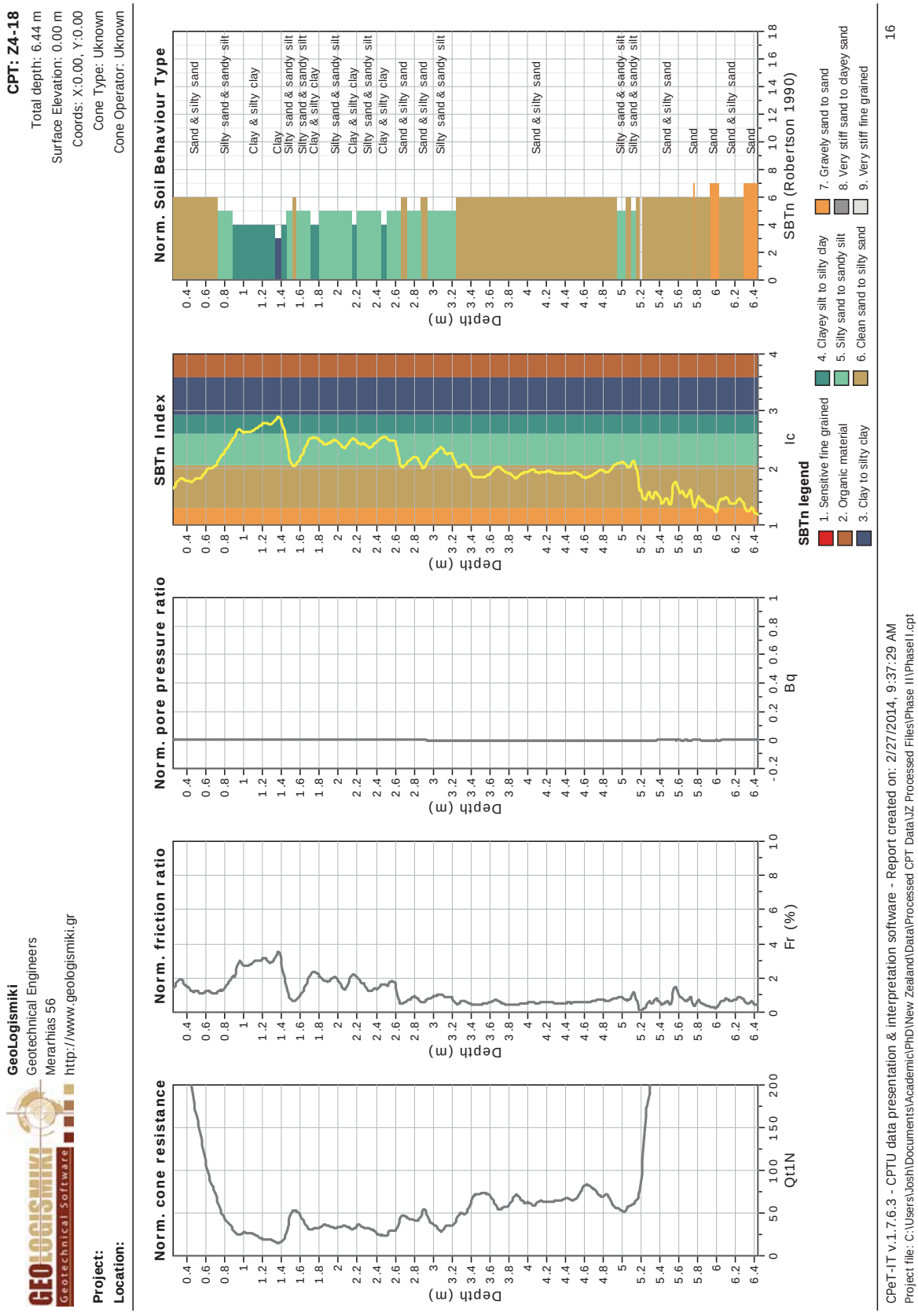
CPT: Z4-18
Total depth: 6.44 m
Surface Elevation: 0.00 m
Coords: X:0.00, Y:0.00
Cone Type: Uknown
Cone Operator: Uknown
GeoLogismiki
Geotechnical Engineers
Merarhias 56
http://www.geologismiki.gr
Project:
Location:
Norm. cone resistance
Norm. friction ratio
Norm. pore pressure ratio
SBTn Index
Norm. Soil Behaviour Type
Depth (m)
Qt1N
Fr (%)
Bq
Ic
SBTn (Robertson 1990)
SBTn legend
1. Sensitive fine grained
2. Organic material
3. Clay to silty clay
4. Clayey silt to silty clay
5. Silty sand to sandy silt
6. Clean sand to silty sand
7. Gravely sand to sand
8. Very stiff sand to clayey sand
9. Very stiff fine grained
Sand & silty sand
Silty sand & sandy silt
Clay & silty clay
Clay
Sand & silty sand
Sand
CPeT-IT v.1.7.6.3 - CPTU data presentation & interpretation software - Report created on: 2/27/2014, 9:37:29 AM
Project file: C:\Users\Josh\Documents\Academic\PhD\New Zealand\Data\Processed CPT Data\JZ Processed Files\Phase II\PhaseII.cpt
16

GeoLogismiki
Geotechnical Engineers
Merarhias 56
http://www.geologismiki.gr

CPT: Z4-19
Total depth: 5.60 m
Surface Elevation: 0.00 m
Coords: X:0.00, Y:0.00
Cone Type: Uknown
Cone Operator: Uknown

Project:
Location:

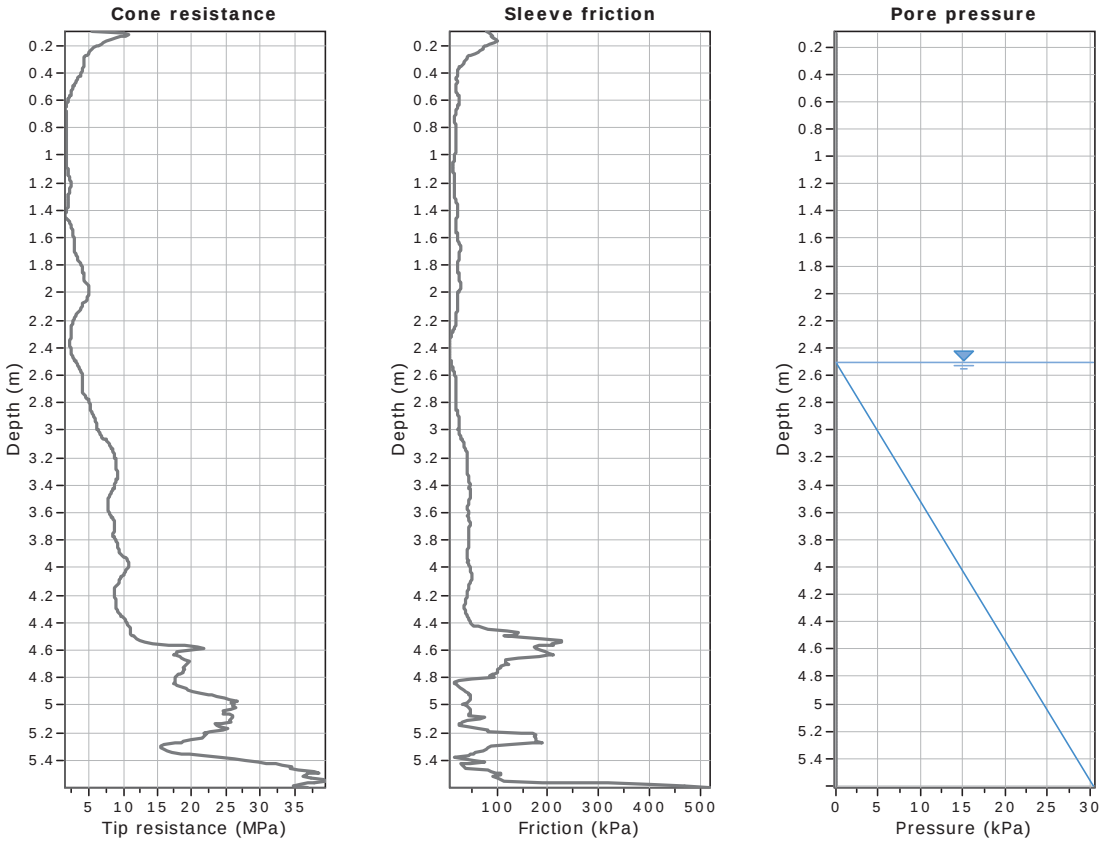

The plot below presents the cross correlation coeficient between the raw qc and fs values (as measured on the field). X axes presents the lag distance (one lag is the distance between two sucessive CPT measurements).

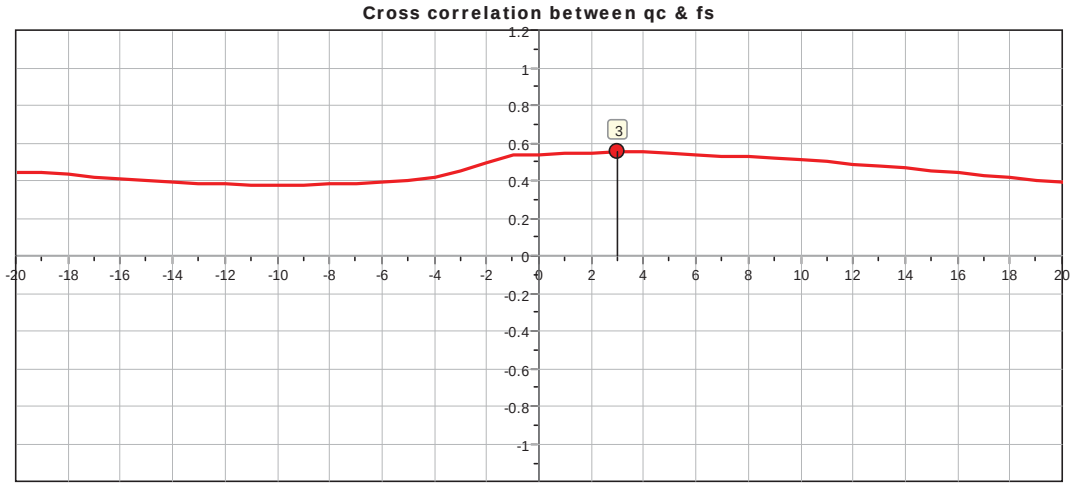

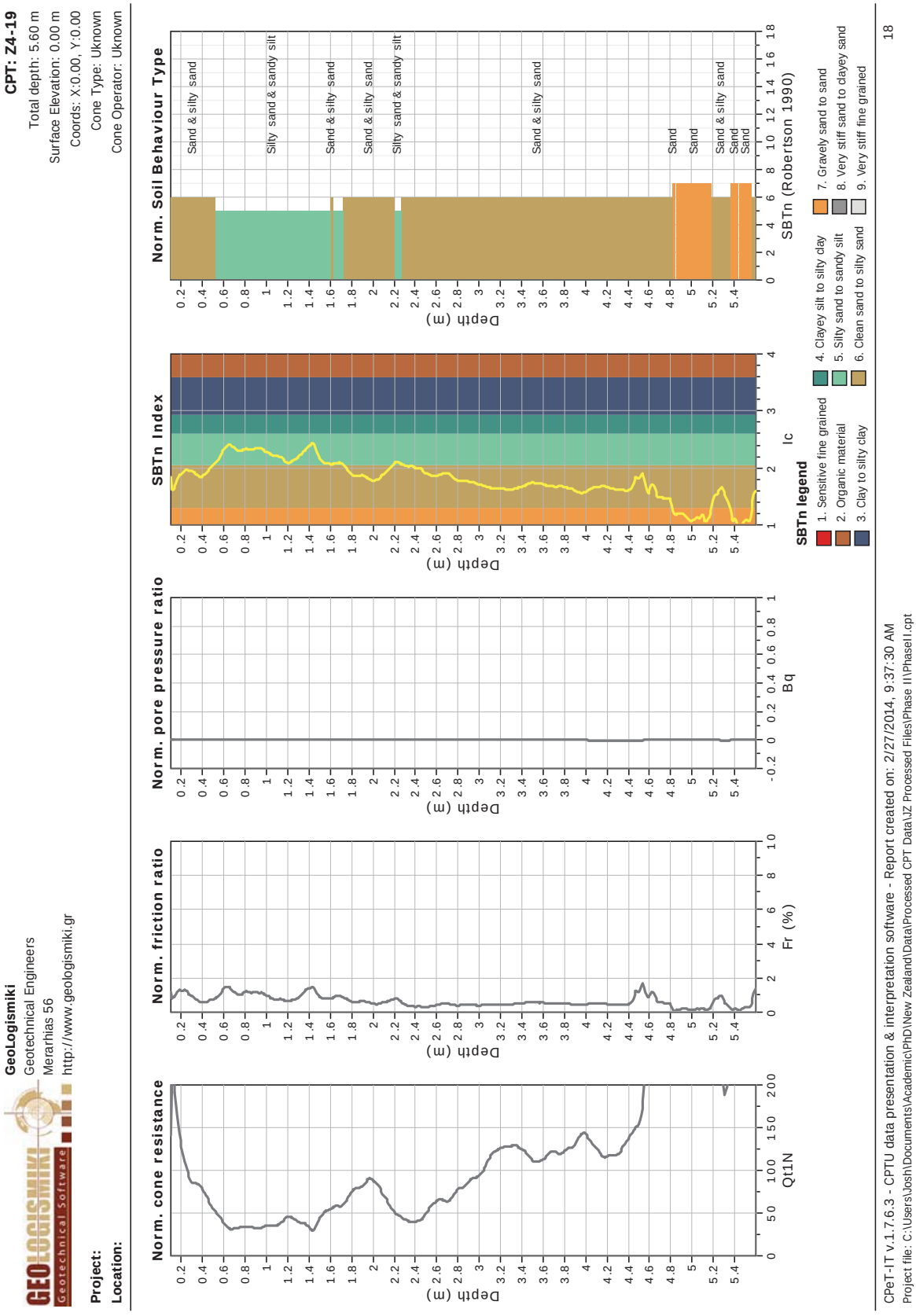
CPT: Z4-19
Total depth: 5.60 m
Surface Elevation: 0.00 m
Coords: X:0.00, Y:0.00
Cone Type: Uknown
Cone Operator: Uknown
GeoLogismiki
Geotechnical Engineers
Merarhias 56
http://www.geologismiki.gr
Project:
Location:
Norm. cone resistance
Qt1N
Norm. friction ratio
Fr (%)
Norm. pore pressure ratio
Bq
SBTn Index
Ic
Norm. Soil Behaviour Type
SBTn (Robertson 1990)
Depth (m)
Sand & silty sand
Silty sand & sandy silt
Sand & silty sand
Silty sand & sandy silt
Sand & silty sand
Sand
Sand
Sand & silty sand
Sand
Sand
SBTn legend
1. Sensitive fine grained
2. Organic material
3. Clay to silty clay
4. Clayey silt to silty clay
5. Silty sand to sandy silt
6. Clean sand to silty sand
7. Gravely sand to sand
8. Very stiff sand to clayey sand
9. Very stiff fine grained
CPeT-IT v.1.7.6.3 - CPTU data presentation & interpretation software - Report created on: 2/27/2014, 9:37:30 AM
Project file: C:\Users\Josh\Documents\Academic\PhD\New Zealand\Data\Processed CPT Data\JZ Processed Files\Phase II\PhaseII.cpt
18

GeoLogismiki
Geotechnical Engineers
Merarhias 56
http://www.geologismiki.gr

CPT: Z4-20
Total depth: 5.23 m
Surface Elevation: 0.00 m
Coords: X:0.00, Y:0.00
Cone Type: Uknown
Cone Operator: Uknown

Project:
Location:

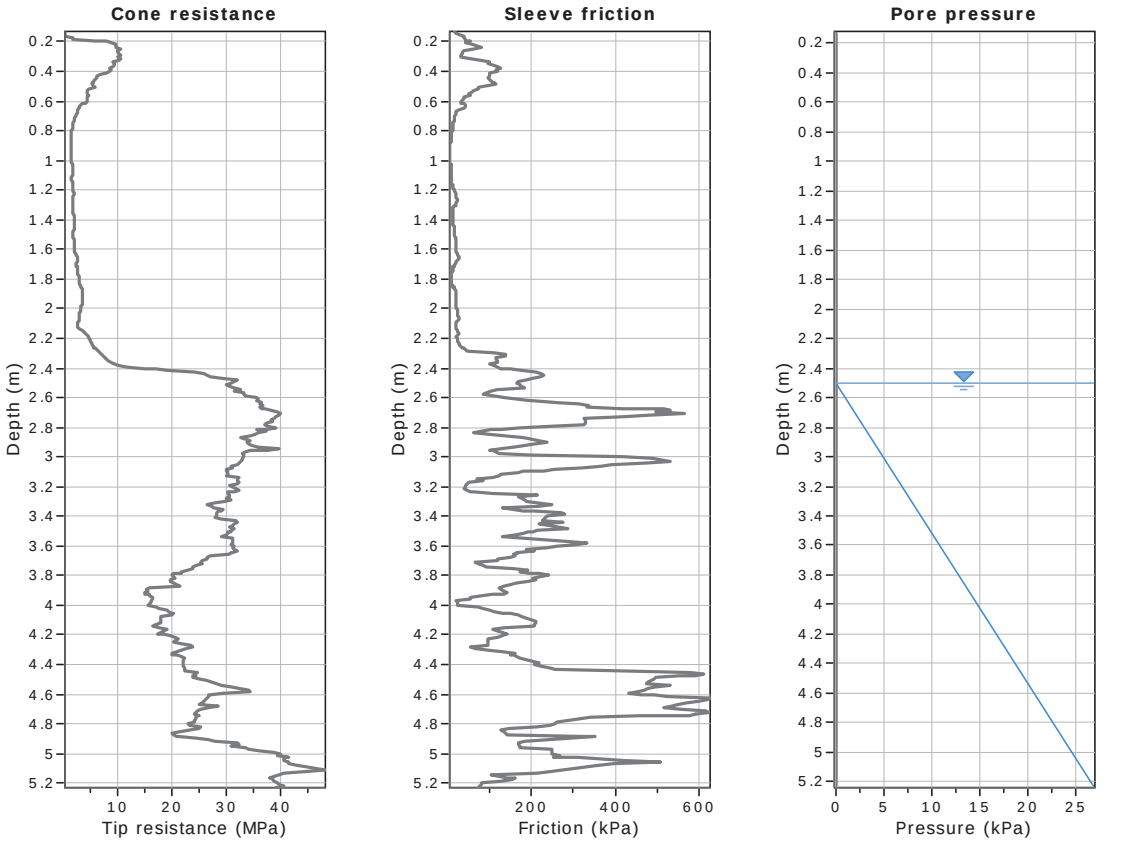

The plot below presents the cross correlation coeficient between the raw qc and fs values (as measured on the field). X axes presents the lag distance (one lag is the distance between two sucessive CPT measurements).

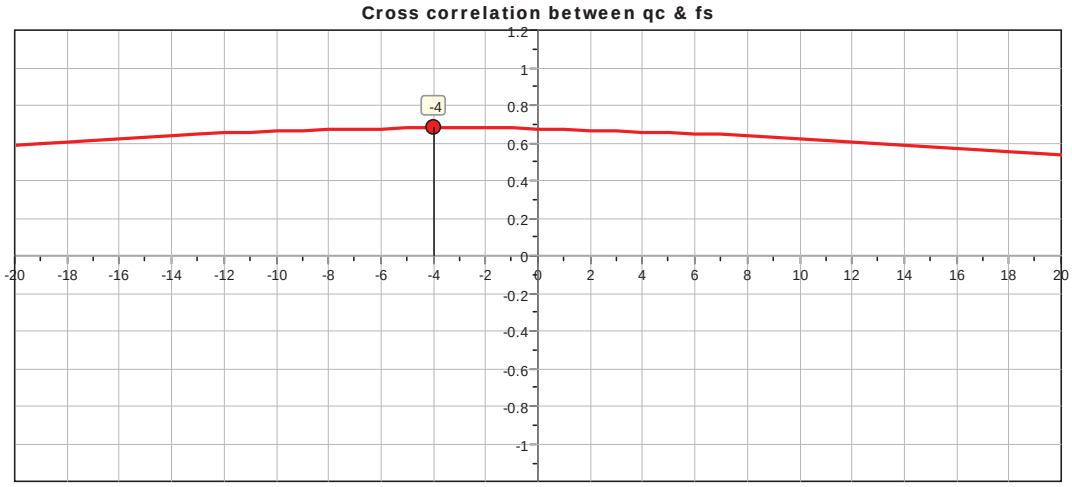

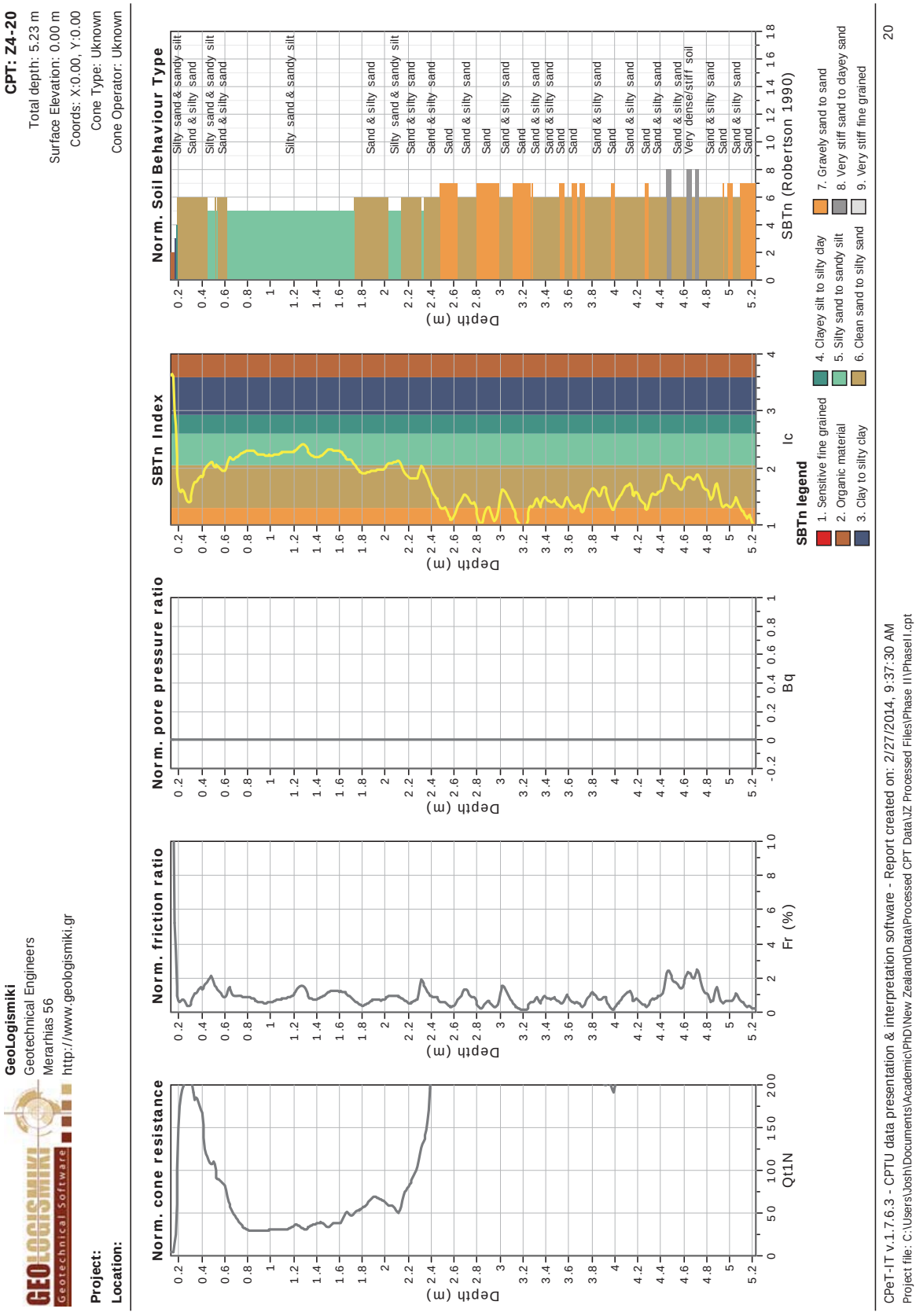
GeoLogismiki
Geotechnical Engineers
Merarhias 56
http://www.geologismiki.gr
Project:
Location:
CPT: Z4-20
Total depth: 5.23 m
Surface Elevation: 0.00 m
Coords: X:0.00, Y:0.00
Cone Type: Uknown
Cone Operator: Uknown
Norm. cone resistance
Norm. friction ratio
Norm. pore pressure ratio
SBTn Index
Norm. Soil Behaviour Type
Depth (m)
Qt1N
Fr (%)
Bq
Ic
SBTn (Robertson 1990)
SBTn legend
1. Sensitive fine grained
2. Organic material
3. Clay to silty clay
4. Clayey silt to silty clay
5. Silty sand to sandy silt
6. Clean sand to silty sand
7. Gravely sand to sand
8. Very stiff sand to clayey sand
9. Very stiff fine grained
CPeT-IT v.1.7.6.3 - CPTU data presentation & interpretation software - Report created on: 2/27/2014, 9:37:30 AM
Project file: C:\Users\Josh\Documents\Academic\PhD\New Zealand\Data\Processed CPT Data\JZ Processed Files\Phase II\PhaseII.cpt
20

GeoLogismiki
Geotechnical Engineers
Merarhias 56
http://www.geologismiki.gr

CPT: Z4-22
Total depth: 3.45 m
Surface Elevation: 0.00 m
Coords: X:0.00, Y:0.00
Cone Type: Uknown
Cone Operator: Uknown

Project:
Location:

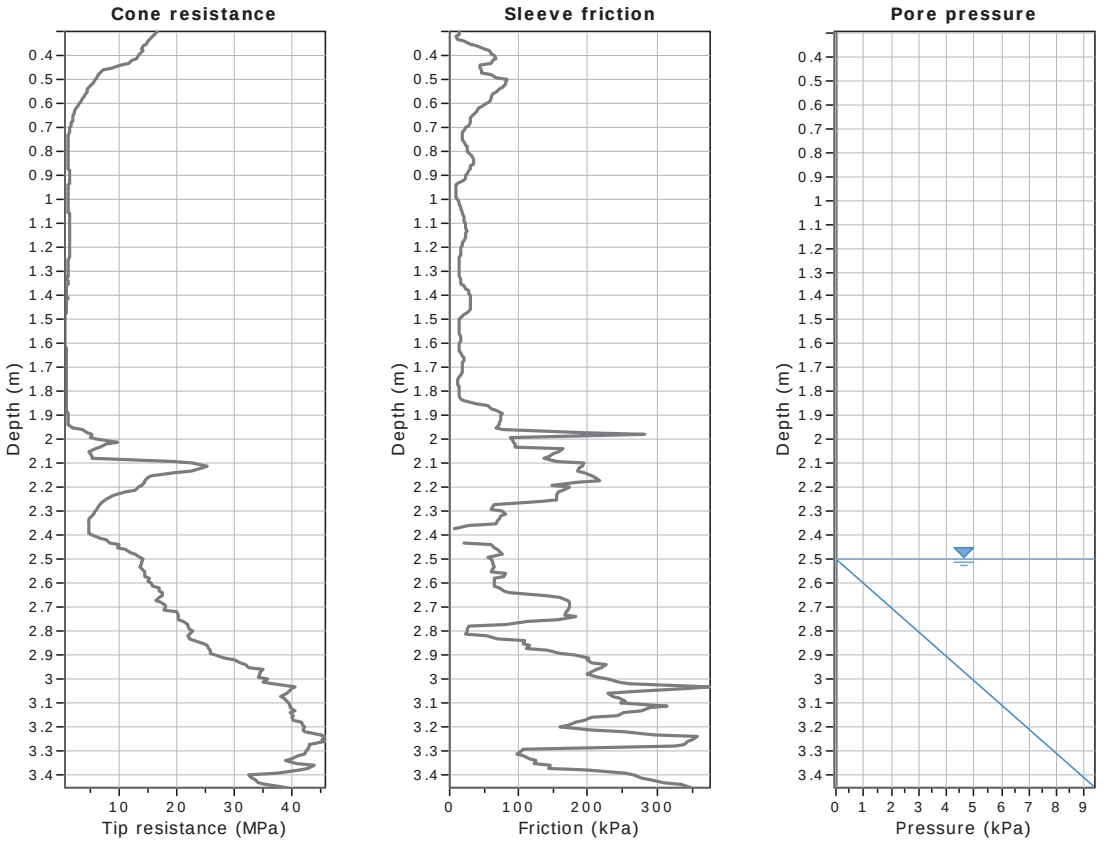

The plot below presents the cross correlation coeficient between the raw qc and fs values (as measured on the field). X axes presents the lag distance (one lag is the distance between two sucessive CPT measurements).

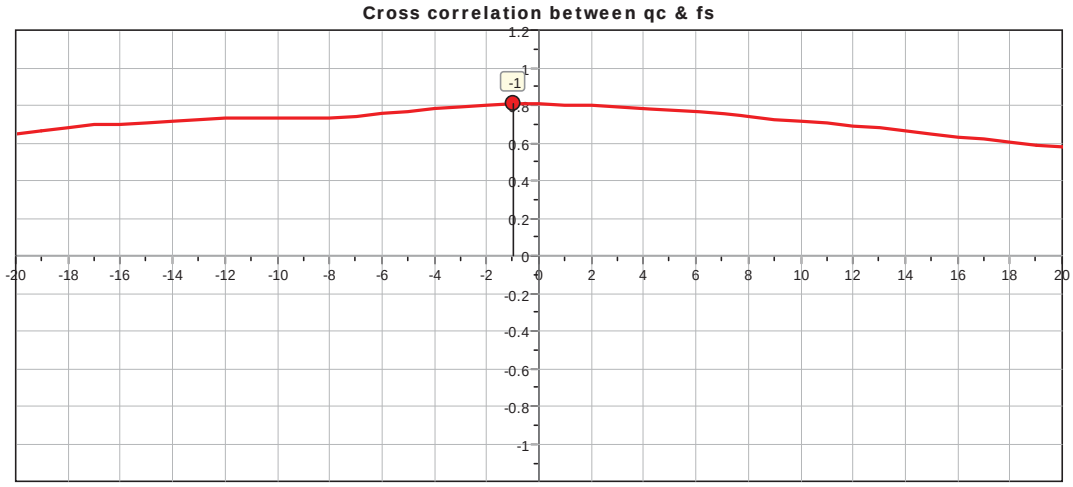

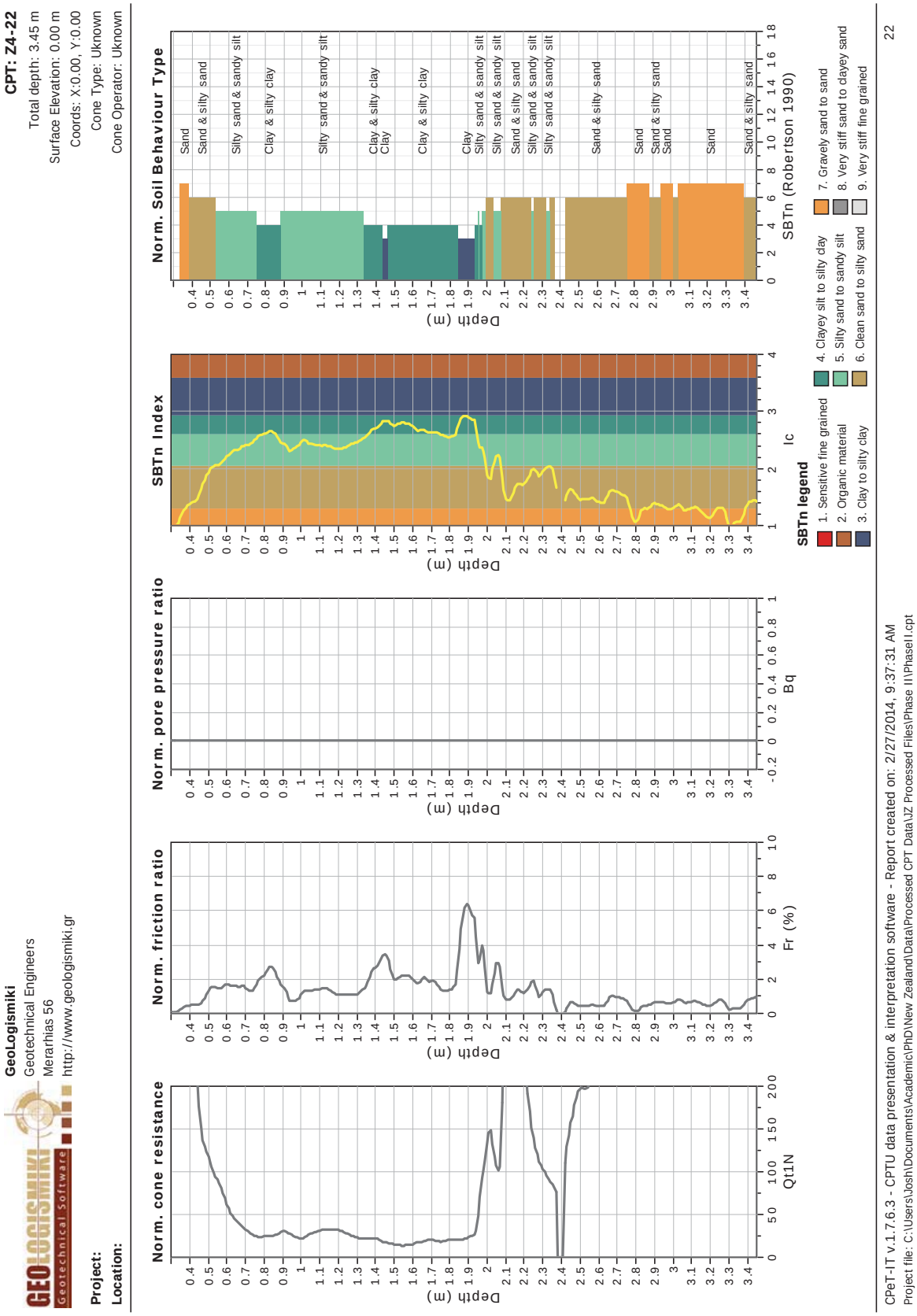
CPT: Z4-22
Total depth: 3.45 m
Surface Elevation: 0.00 m
Coords: X:0.00, Y:0.00
Cone Type: Uknown
Cone Operator: Uknown
GeoLogismiki
Geotechnical Engineers
Merarhias 56
http://www.geologismiki.gr
Project:
Location:
Norm. cone resistance
Norm. friction ratio
Norm. pore pressure ratio
SBTn Index
Norm. Soil Behaviour Type
SBTn (Robertson 1990)
SBTn legend
1. Sensitive fine grained
2. Organic material
3. Clay to silty clay
4. Clayey silt to silty clay
5. Silty sand to sandy silt
6. Clean sand to silty sand
7. Gravely sand to sand
8. Very stiff sand to clayey sand
9. Very stiff fine grained
CPeT-IT v.1.7.6.3 - CPTU data presentation & interpretation software - Report created on: 2/27/2014, 9:37:31 AM
Project file: C:\Users\Josh\Documents\Academic\PhD\New Zealand\Data\Processed CPT Data\JZ Processed Files\Phase II\PhaseII.cpt
22

GeoLogismiki
Geotechnical Engineers
Merarhias 56
http://www.geologismiki.gr

CPT: Z4-23
Total depth: 3.00 m
Surface Elevation: 0.00 m
Coords: X:0.00, Y:0.00
Cone Type: Uknown
Cone Operator: Uknown

Project:
Location:

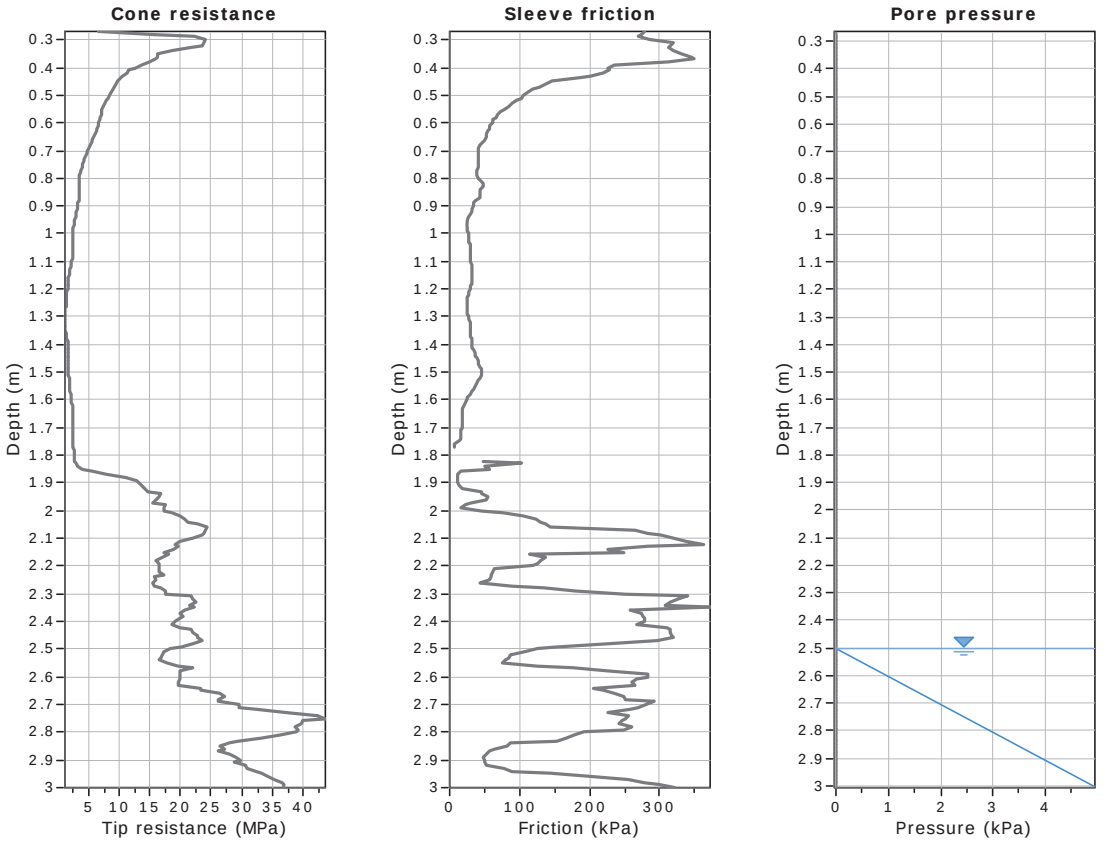

The plot below presents the cross correlation coeficient between the raw qc and fs values (as measured on the field). X axes presents the lag distance (one lag is the distance between two sucessive CPT measurements).

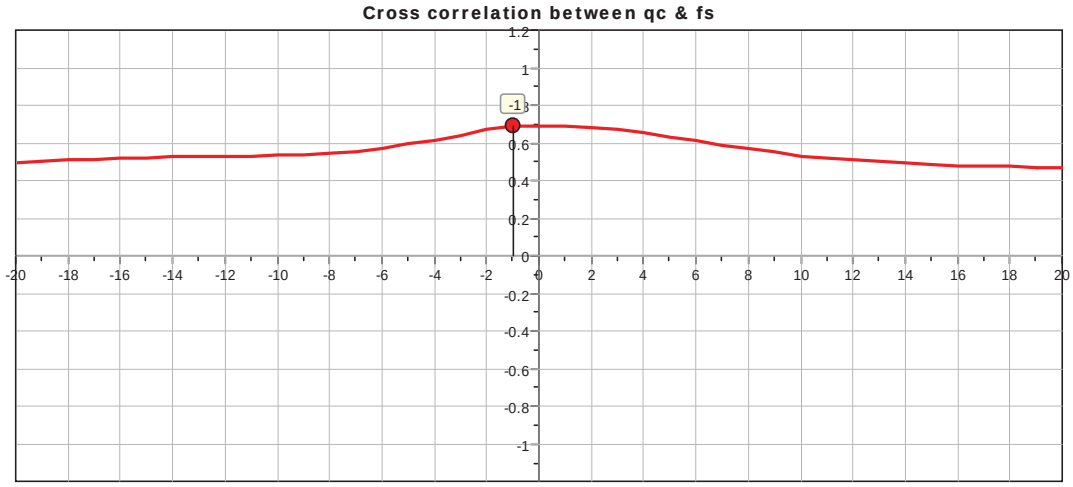

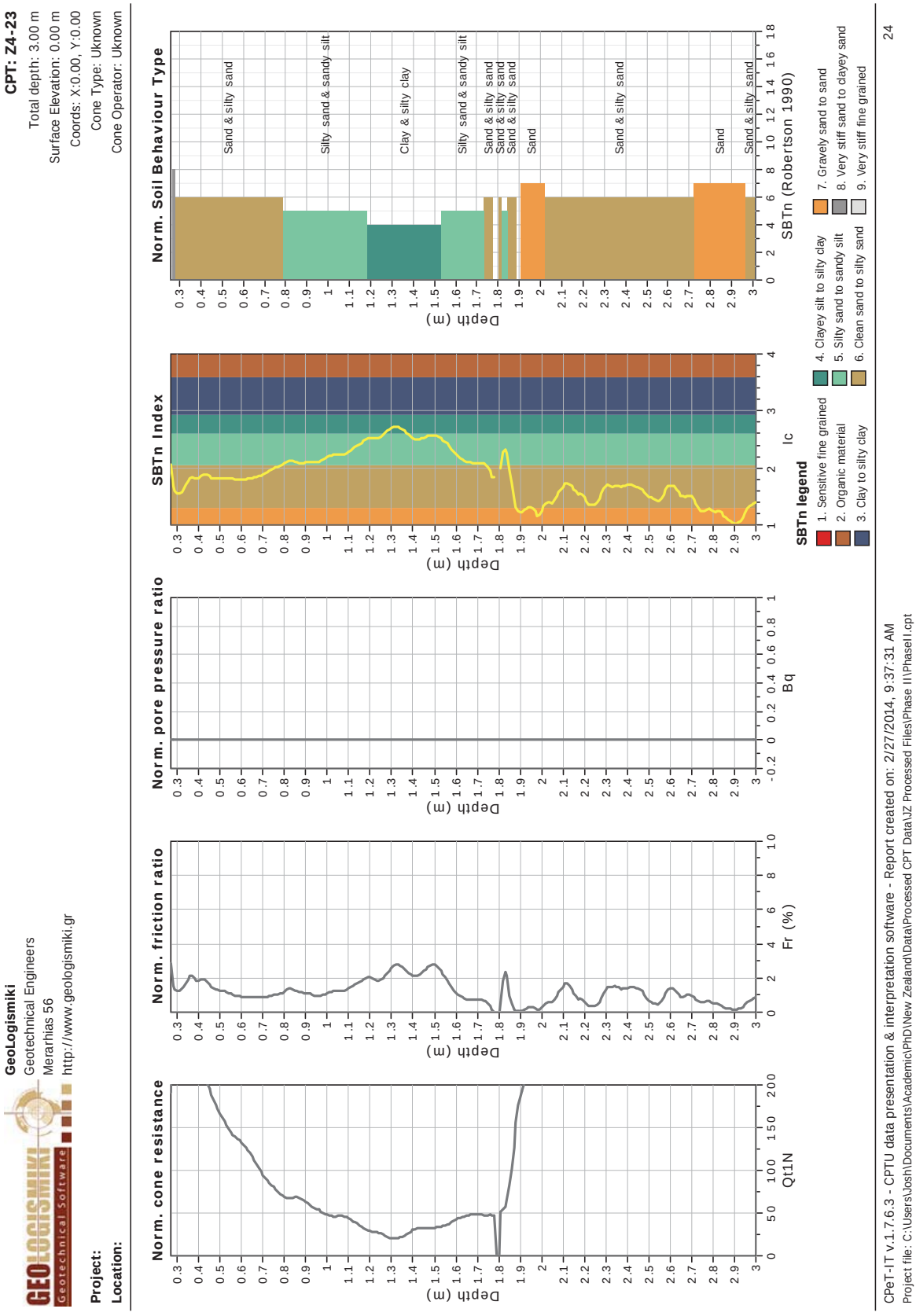
GeoLogismiki
Geotechnical Engineers
Merarhias 56
http://www.geologismiki.gr
Project:
Location:
CPT: Z4-23
Total depth: 3.00 m
Surface Elevation: 0.00 m
Coords: X:0.00, Y:0.00
Cone Type: Uknown
Cone Operator: Uknown
Norm. cone resistance
Norm. friction ratio
Norm. pore pressure ratio
SBTn Index
Norm. Soil Behaviour Type
Depth (m)
Qt1N
Fr (%)
Bq
Ic
SBTn (Robertson 1990)
Sand & silty sand
Silty sand & sandy silt
Clay & silty clay
Silty sand & sandy silt
Sand & silty sand
Sand & silty sand
Sand & silty sand
Sand
Sand & silty sand
Sand
Sand & silty sand
SBTn legend
1. Sensitive fine grained
2. Organic material
3. Clay to silty clay
4. Clayey silt to silty clay
5. Silty sand to sandy silt
6. Clean sand to silty sand
7. Gravely sand to sand
8. Very stiff sand to clayey sand
9. Very stiff fine grained
CPeT-IT v.1.7.6.3 - CPTU data presentation & interpretation software - Report created on: 2/27/2014, 9:37:31 AM
Project file: C:\Users\Josh\Documents\Academic\PhD\New Zealand\Data\Processed CPT Data\JZ Processed Files\Phase II\PhaseII.cpt
24

GeoLogismiki
Geotechnical Engineers
Merarhias 56
http://www.geologismiki.gr

CPT: Z4-24
Total depth: 13.30 m
Surface Elevation: 0.00 m
Coords: X:0.00, Y:0.00
Cone Type: Uknown
Cone Operator: Uknown

Project:
Location:

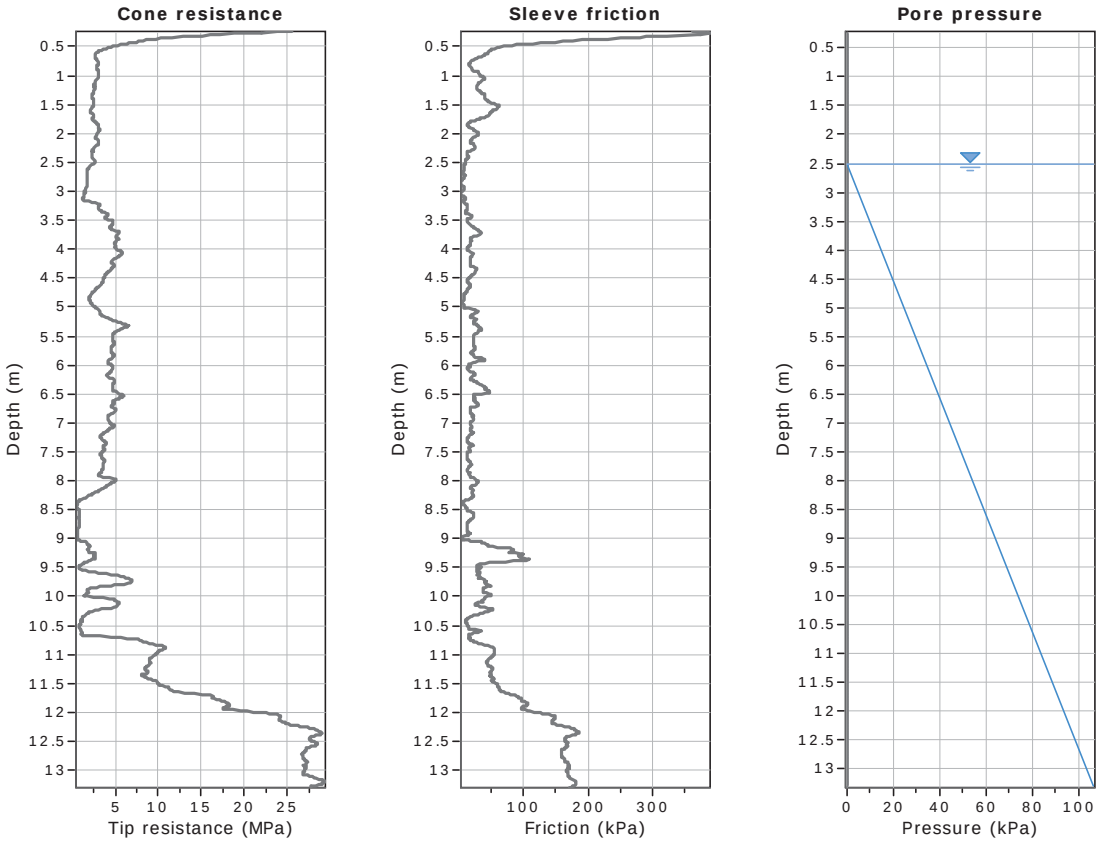

The plot below presents the cross correlation coeficient between the raw qc and fs values (as measured on the field). X axes presents the lag distance (one lag is the distance between two sucessive CPT measurements).

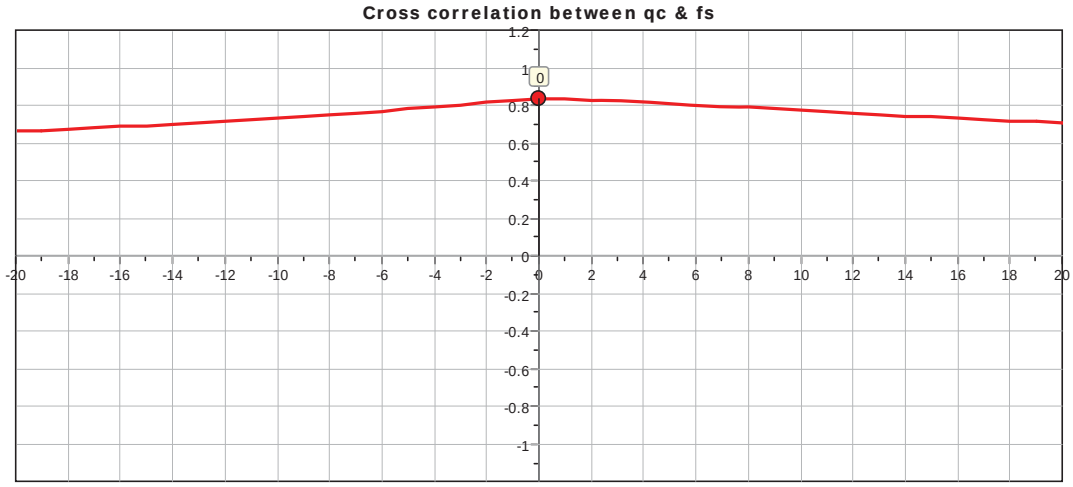

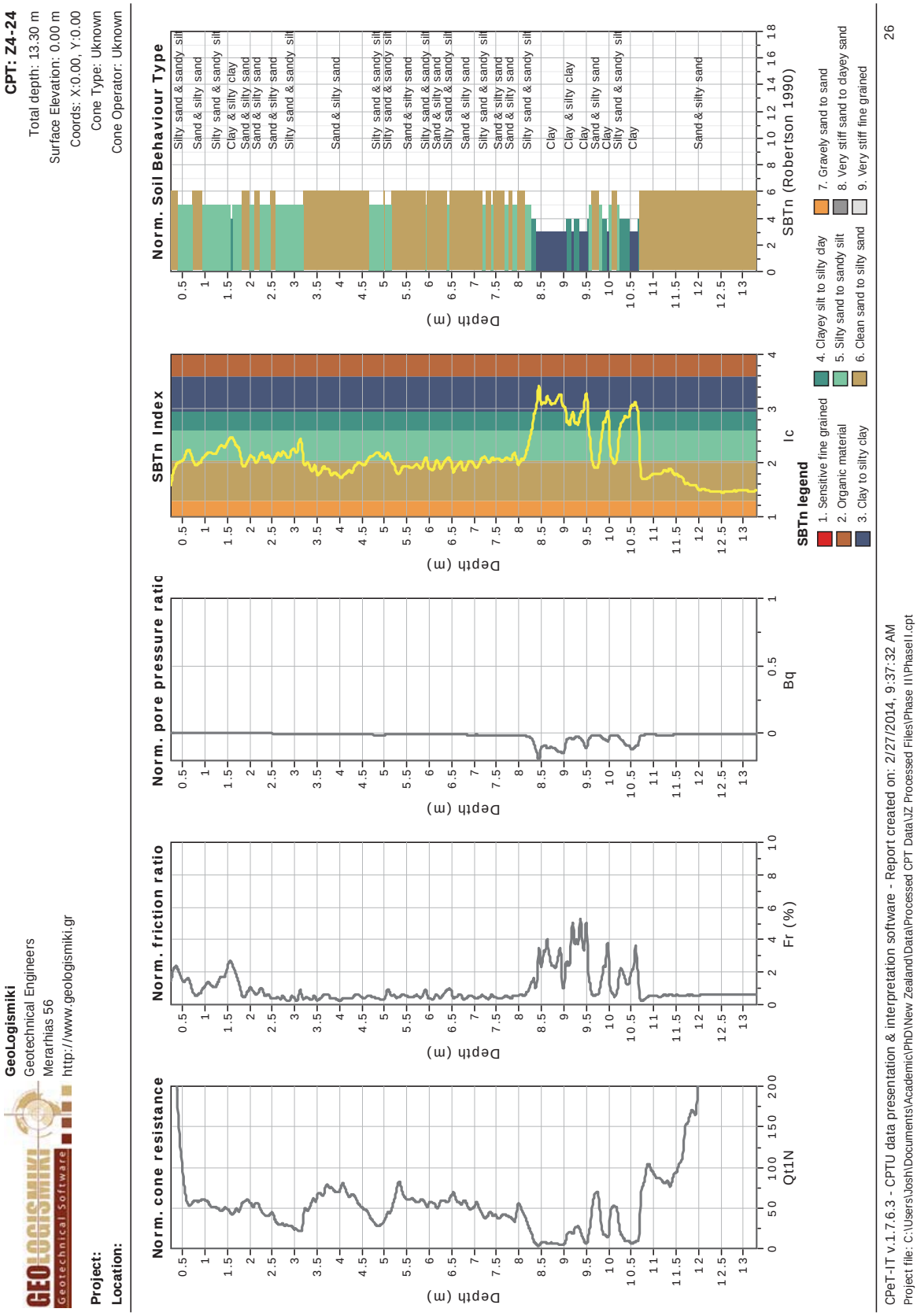
CPT: Z4-24
Total depth: 13.30 m
Surface Elevation: 0.00 m
Coords: X:0.00, Y:0.00
Cone Type: Uknown
Cone Operator: Uknown
Project:
Location:
GeoLogismiki
Geotechnical Engineers
Merarhias 56
http://www.geologismiki.gr
Norm. cone resistance
Qt1N
Norm. friction ratio
Fr (%)
Norm. pore pressure ratio
Bq
SBTn Index
Ic
Norm. Soil Behaviour Type
SBTn (Robertson 1990)
Depth (m)
SBTn legend
1. Sensitive fine grained
2. Organic material
3. Clay to silty clay
4. Clayey silt to silty clay
5. Silty sand to sandy silt
6. Clean sand to silty sand
7. Gravely sand to sand
8. Very stiff sand to clayey sand
9. Very stiff fine grained
CPeT-IT v.1.7.6.3 - CPTU data presentation & interpretation software - Report created on: 2/27/2014, 9:37:32 AM
Project file: C:\Users\Josh\Documents\Academic\PhD\New Zealand\Data\Processed CPT Data\JZ Processed Files\Phase II\PhaseII.cpt
26

GeoLogismiki
Geotechnical Engineers
Merarhias 56
http://www.geologismiki.gr

CPT: Z4-25
Total depth: 9.18 m
Surface Elevation: 0.00 m
Coords: X:0.00, Y:0.00
Cone Type: Uknown
Cone Operator: Uknown

Project:
Location:

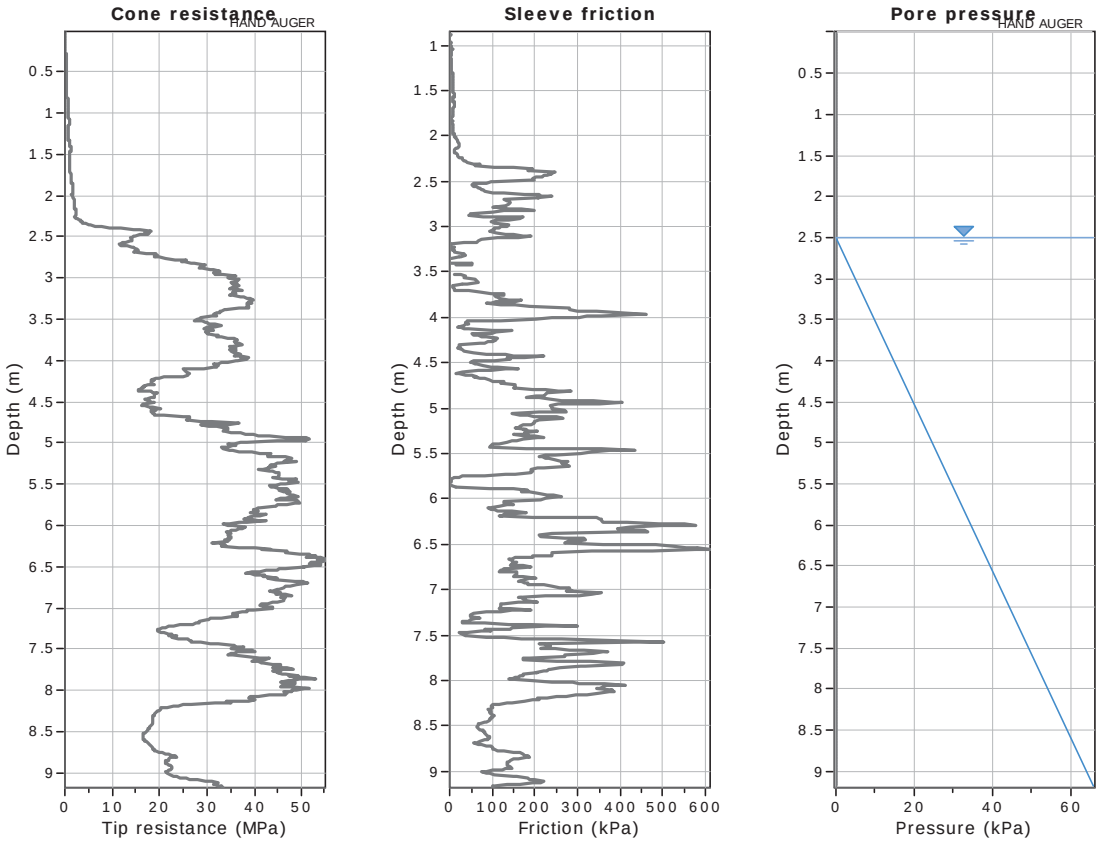

The plot below presents the cross correlation coeficient between the raw qc and fs values (as measured on the field). X axes presents the lag distance (one lag is the distance between two sucessive CPT measurements).

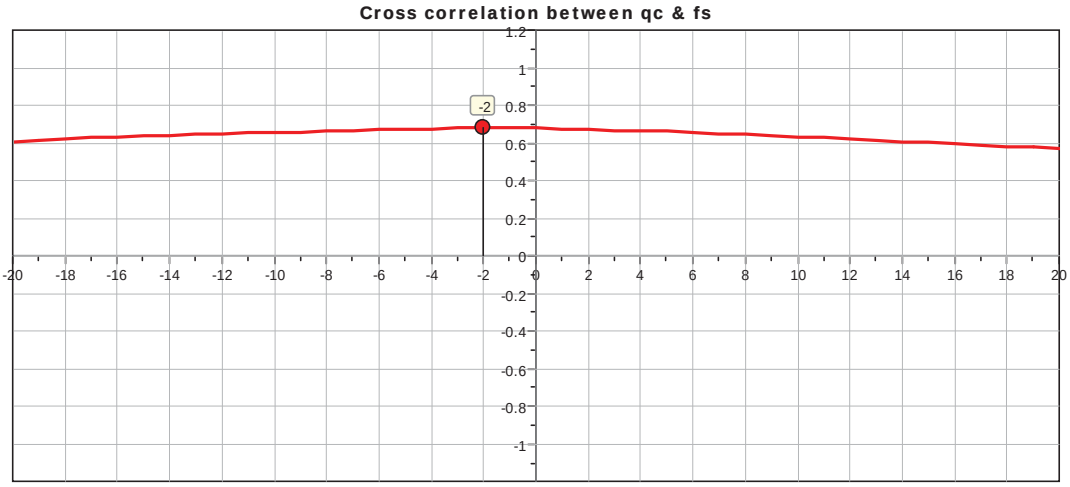

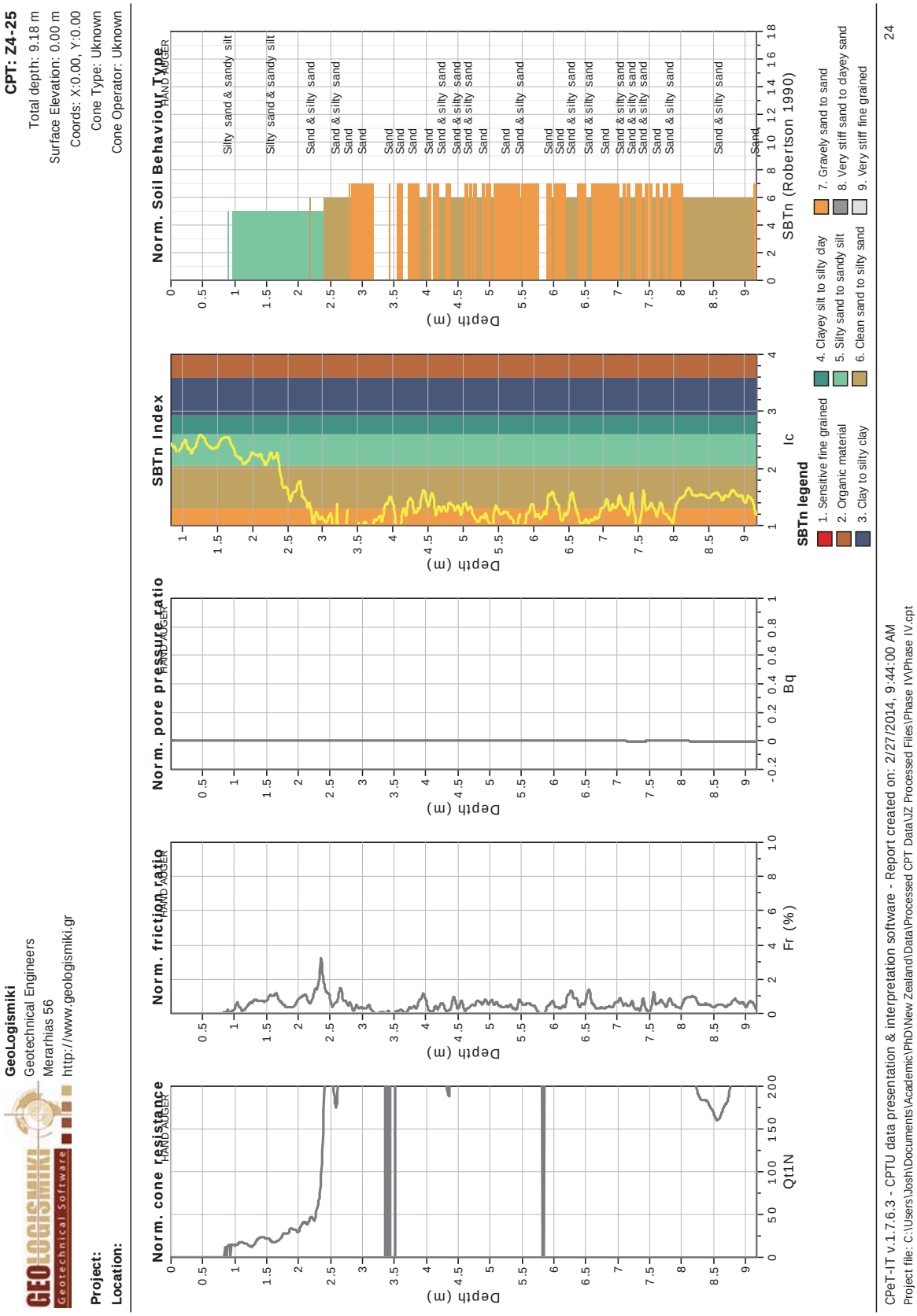
CPT: Z4-25
Total depth: 9.18 m
Surface Elevation: 0.00 m
Coords: X:0.00, Y:0.00
Cone Type: Uknown
Cone Operator: Uknown
Project:
Location:
GeoLogismiki
Geotechnical Engineers
Merarhias 56
http://www.geologismiki.gr
Norm. cone resistance
Norm. friction ratio
Norm. pore pressure ratio
SBTn Index
Norm. Soil Behaviour Type
SBTn (Robertson 1990)
SBTn legend
1. Sensitive fine grained
2. Organic material
3. Clay to silty clay
4. Clayey silt to silty clay
5. Silty sand to sandy silt
6. Clean sand to silty sand
7. Gravely sand to sand
8. Very stiff sand to clayey sand
9. Very stiff fine grained
CPeT-IT v.1.7.6.3 - CPTU data presentation & interpretation software - Report created on: 2/27/2014, 9:44:00 AM
Project file: C:\Users\Josh\Documents\Academic\PhD\New Zealand\Data\Processed CPT Data\JZ Processed Files\Phase IV\Phase IV.cpt
24

GeoLogismiki
Geotechnical Engineers
Merarhias 56
http://www.geologismiki.gr

CPT: Z4-26
Total depth: 18.85 m
Surface Elevation: 0.00 m
Coords: X:0.00, Y:0.00
Cone Type: Uknown
Cone Operator: Uknown

Project:
Location:

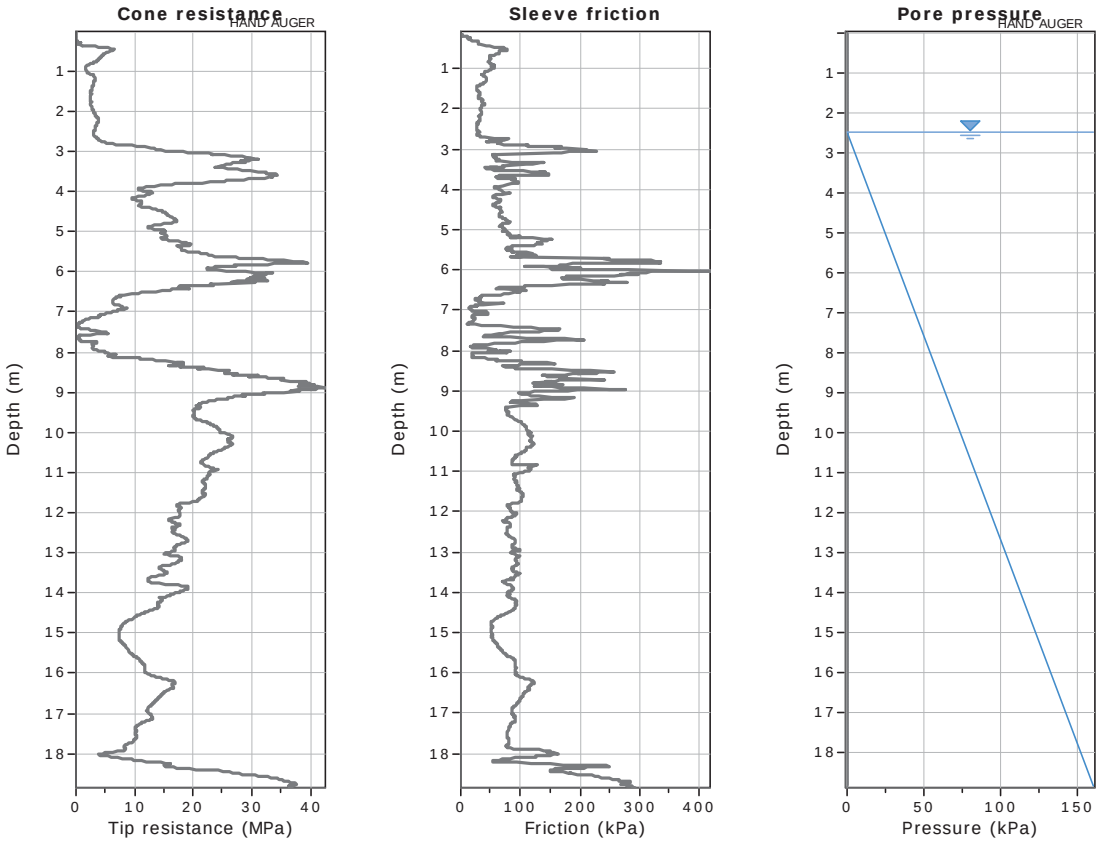

The plot below presents the cross correlation coeficient between the raw qc and fs values (as measured on the field). X axes presents the lag distance (one lag is the distance between two sucessive CPT measurements).

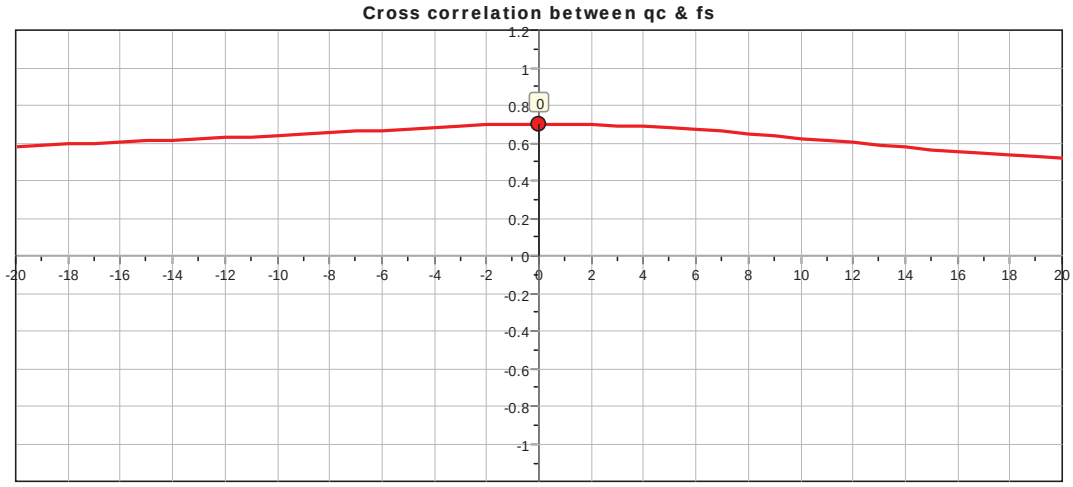

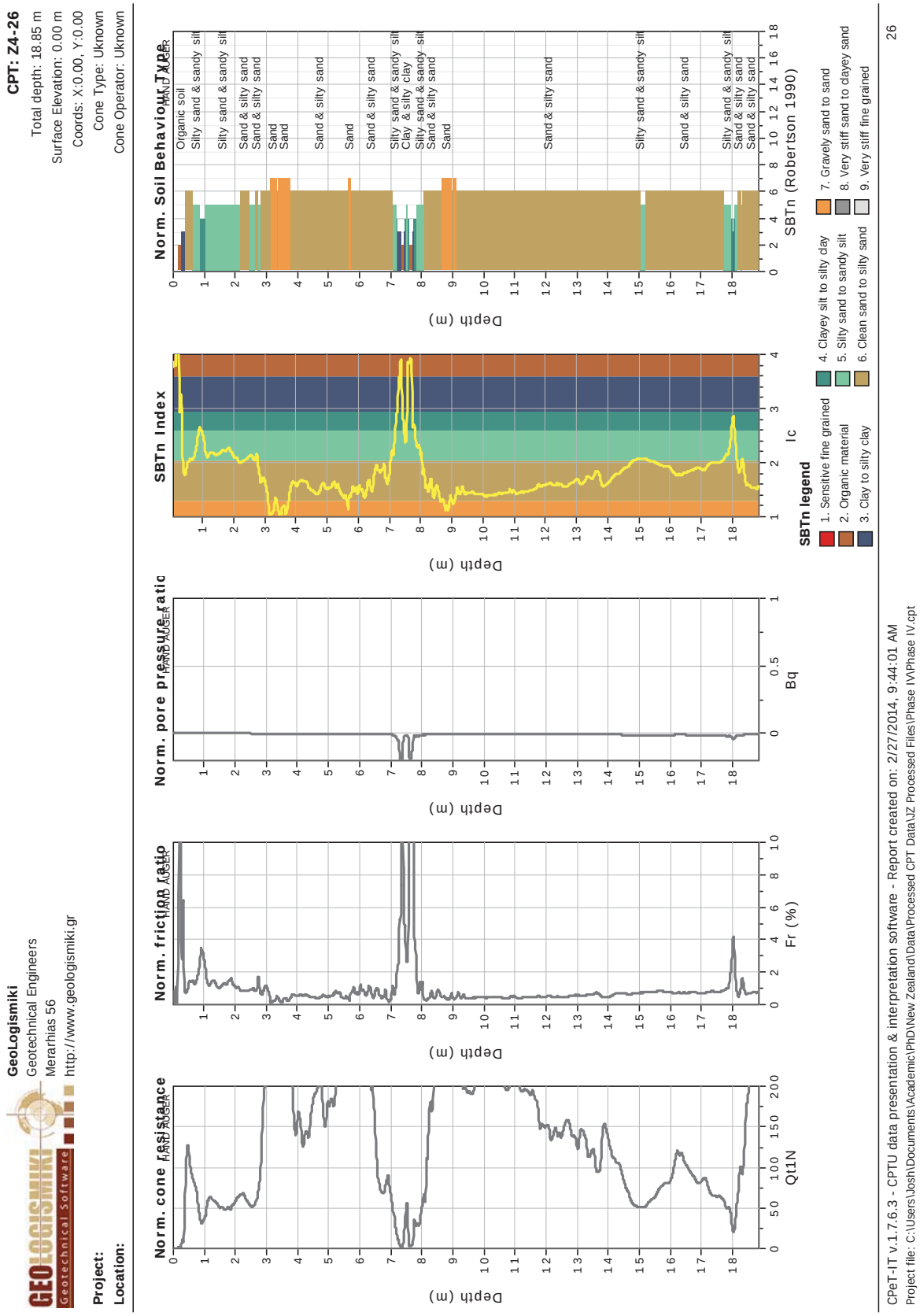
GeoLogismiki
Geotechnical Engineers
Merarhias 56
http://www.geologismiki.gr
Project:
Location:
CPT: Z4-26
Total depth: 18.85 m
Surface Elevation: 0.00 m
Coords: X:0.00, Y:0.00
Cone Type: Uknown
Cone Operator: Uknown
Norm. cone resistance
Norm. friction ratio
Norm. pore pressure ratio
SBTn Index
Norm. Soil Behaviour Type
HAND AUGER
Qt1N
Fr (%)
Bq
Ic
SBTn (Robertson 1990)
Depth (m)
Organic soil
Silty sand & sandy silt
Sand & silty sand
Sand
Clay & silty clay
SBTn legend
1. Sensitive fine grained
2. Organic material
3. Clay to silty clay
4. Clayey silt to silty clay
5. Silty sand to sandy silt
6. Clean sand to silty sand
7. Gravely sand to sand
8. Very stiff sand to clayey sand
9. Very stiff fine grained
CPeT-IT v.1.7.6.3 - CPTU data presentation & interpretation software - Report created on: 2/27/2014, 9:44:01 AM
Project file: C:\Users\Josh\Documents\Academic\PhD\New Zealand\Data\Processed CPT Data\JZ Processed Files\Phase IV\Phase IV.cpt
26

GeoLogismiki
Geotechnical Engineers
Merarhias 56
http://www.geologismiki.gr

CPT: Z4-27
Total depth: 25.02 m
Surface Elevation: 0.00 m
Coords: X:0.00, Y:0.00
Cone Type: Uknown
Cone Operator: Uknown

Project:
Location:

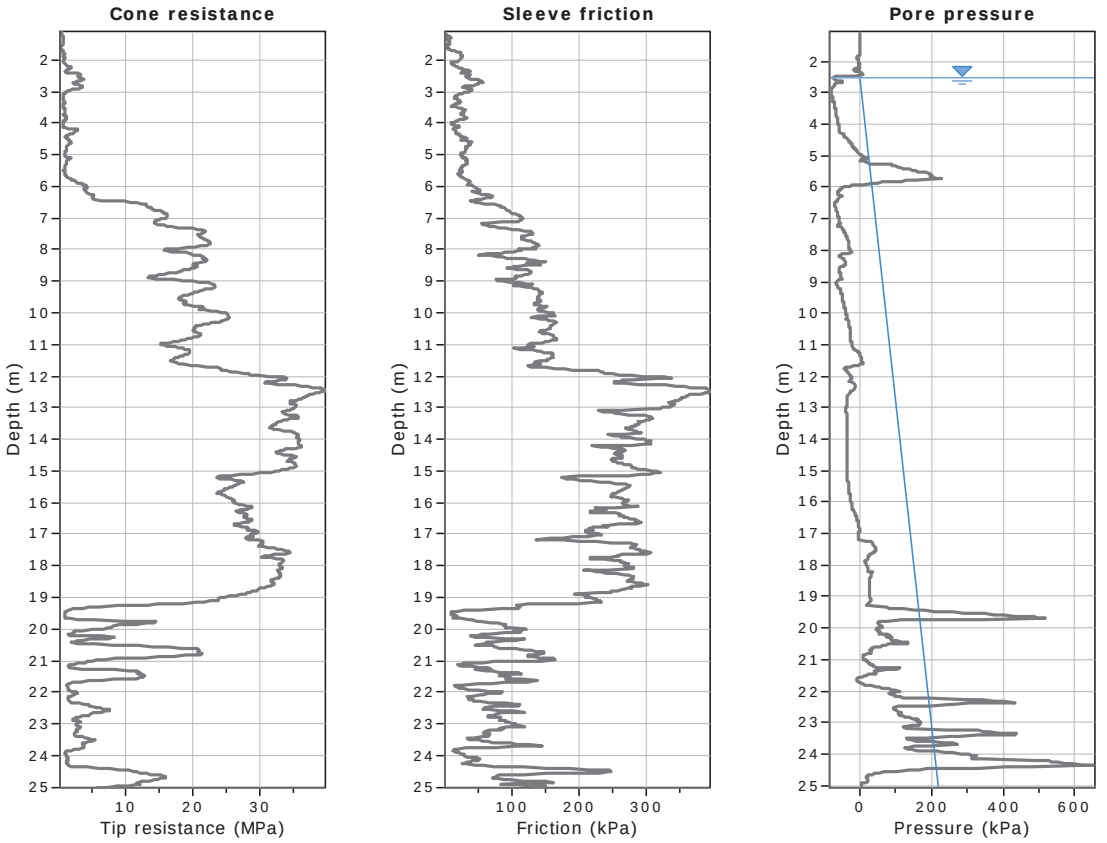

The plot below presents the cross correlation coeficient between the raw qc and fs values (as measured on the field). X axes presents the lag distance (one lag is the distance between two sucessive CPT measurements).

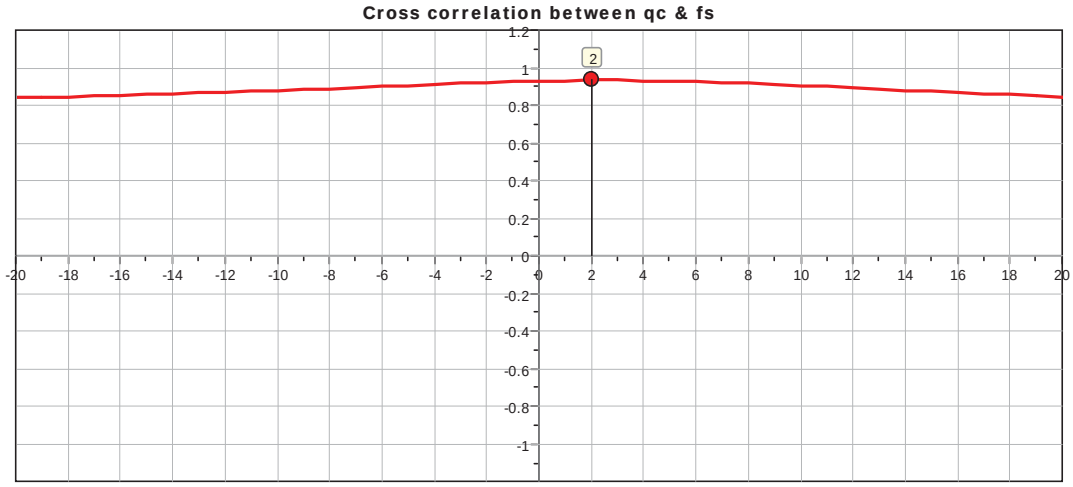

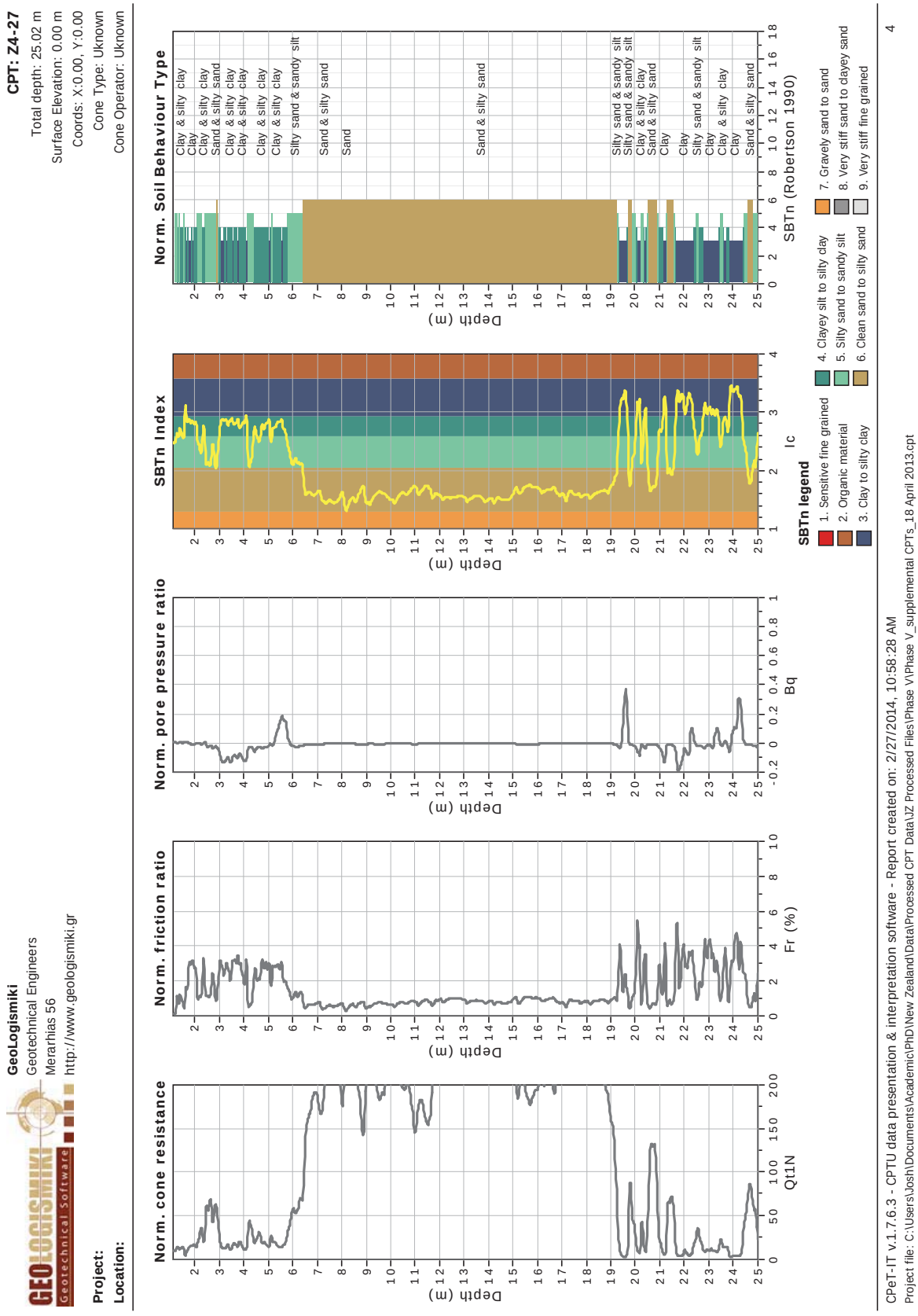
GeoLogismiki
Geotechnical Engineers
Merarhias 56
http://www.geologismiki.gr
Project:
Location:
CPT: Z4-27
Total depth: 25.02 m
Surface Elevation: 0.00 m
Coords: X:0.00, Y:0.00
Cone Type: Uknown
Cone Operator: Uknown
Norm. cone resistance
Qt1N
Norm. friction ratio
Fr (%)
Norm. pore pressure ratio
Bq
SBTn Index
Ic
Norm. Soil Behaviour Type
SBTn (Robertson 1990)
Depth (m)
SBTn legend
1. Sensitive fine grained
2. Organic material
3. Clay to silty clay
4. Clayey silt to silty clay
5. Silty sand to sandy silt
6. Clean sand to silty sand
7. Gravely sand to sand
8. Very stiff sand to clayey sand
9. Very stiff fine grained
CPeT-IT v.1.7.6.3 - CPTU data presentation & interpretation software - Report created on: 2/27/2014, 10:58:28 AM
Project file: C:\Users\Josh\Documents\Academic\PhD\New Zealand\Data\Processed CPT Data\JZ Processed Files\Phase V\Phase V_supplemental CPTs_18 April 2013.cpt
4

GeoLogismiki
Geotechnical Engineers
Merarhias 56
http://www.geologismiki.gr

CPT: Z4-28
Total depth: 24.50 m
Surface Elevation: 0.00 m
Coords: X:0.00, Y:0.00
Cone Type: Uknown
Cone Operator: Uknown

Project:
Location:

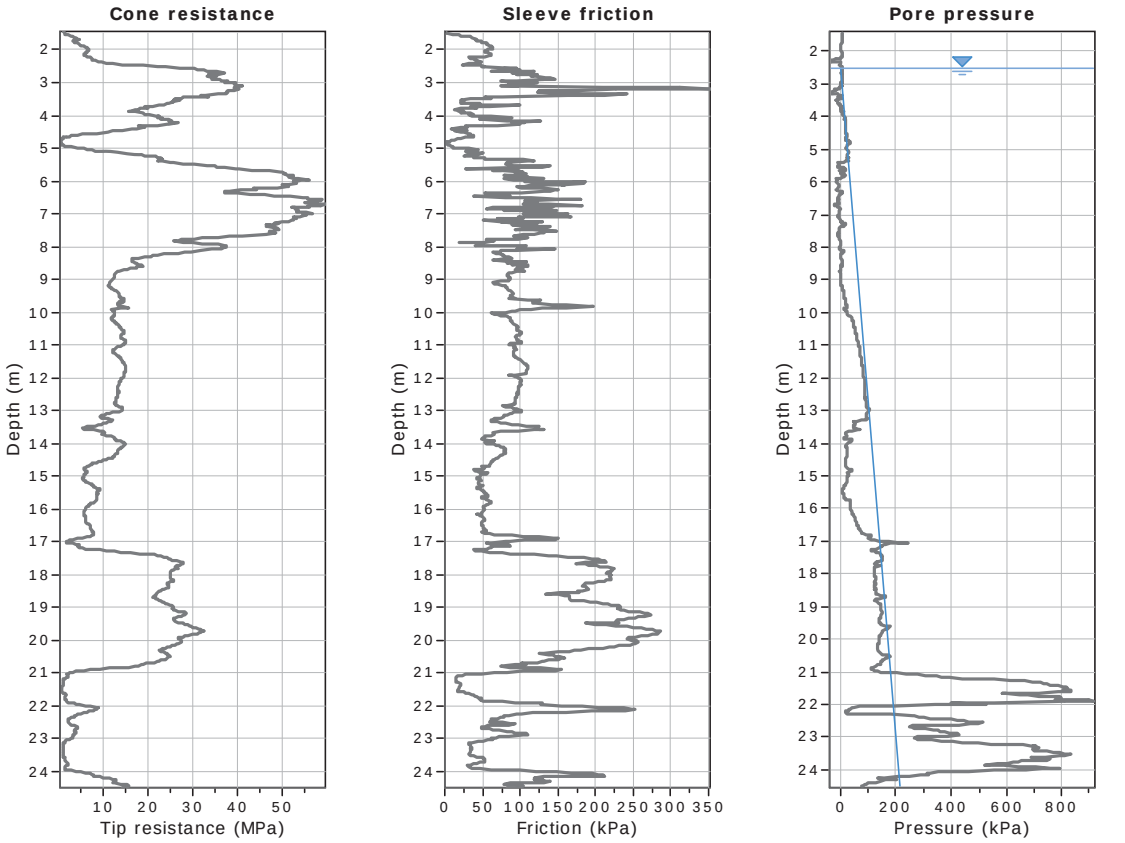

The plot below presents the cross correlation coeficient between the raw qc and fs values (as measured on the field). X axes presents the lag distance (one lag is the distance between two sucessive CPT measurements).

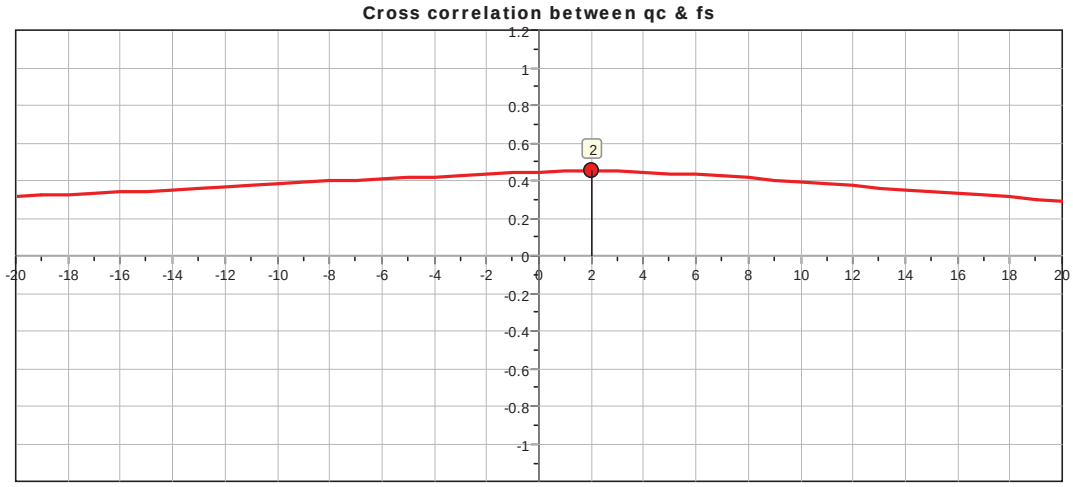

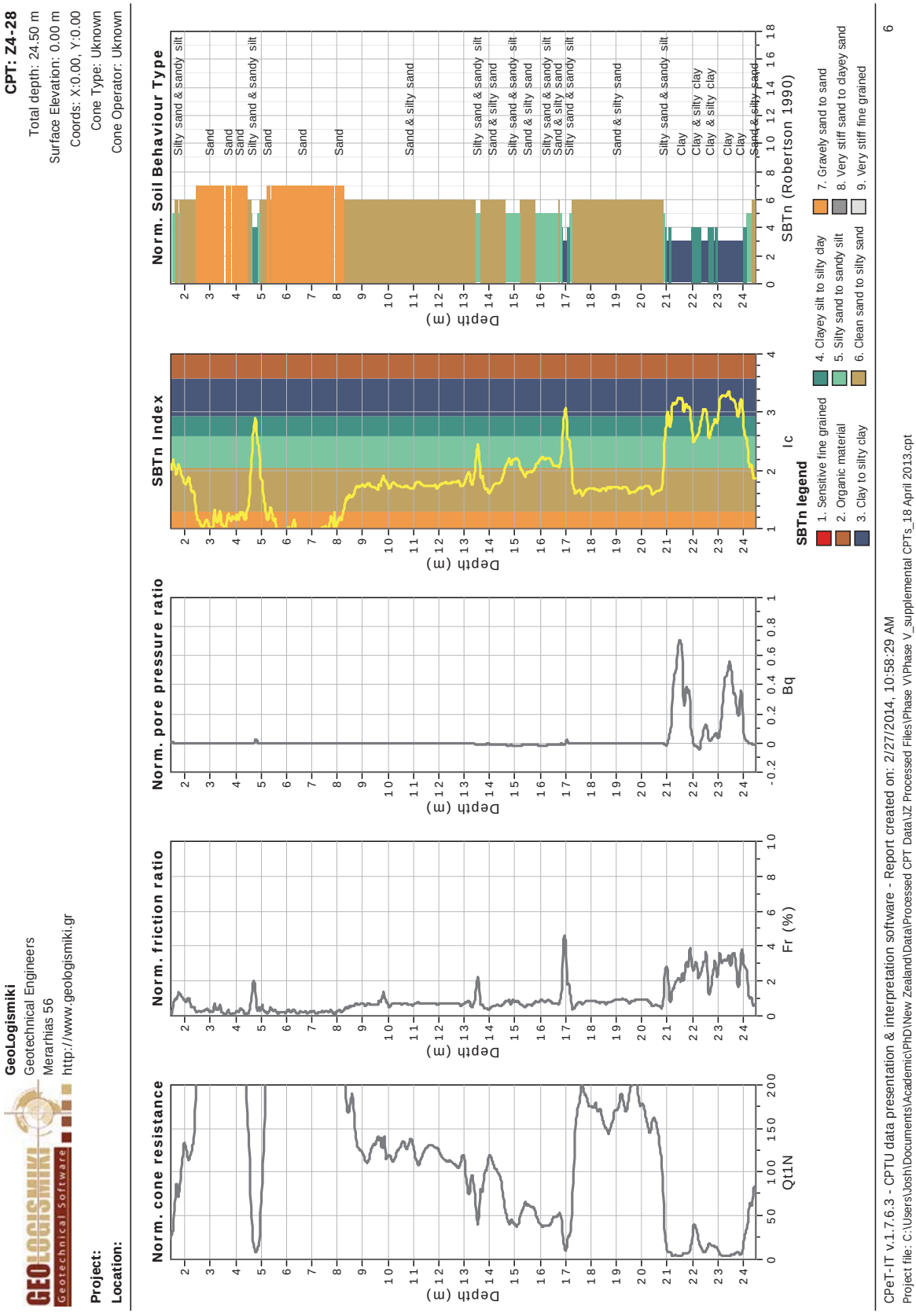
GeoLogismiki
Geotechnical Engineers
Merarhias 56
http://www.geologismiki.gr
Project:
Location:
CPT: Z4-28
Total depth: 24.50 m
Surface Elevation: 0.00 m
Coords: X:0.00, Y:0.00
Cone Type: Uknown
Cone Operator: Uknown
Norm. cone resistance
Qt1N
Norm. friction ratio
Fr (%)
Norm. pore pressure ratio
Bq
SBTn Index
Ic
Norm. Soil Behaviour Type
SBTn (Robertson 1990)
Depth (m)
SBTn legend
1. Sensitive fine grained
2. Organic material
3. Clay to silty clay
4. Clayey silt to silty clay
5. Silty sand to sandy silt
6. Clean sand to silty sand
7. Gravely sand to sand
8. Very stiff sand to clayey sand
9. Very stiff fine grained
CPeT-IT v.1.7.6.3 - CPTU data presentation & interpretation software - Report created on: 2/27/2014, 10:58:29 AM
Project file: C:\Users\Josh\Documents\Academic\PhD\New Zealand\Data\Processed CPT Data\JZ Processed Files\Phase V\Phase V_supplemental CPTs_18 April 2013.cpt
6

GeoLogismiki
Geotechnical Engineers
Merarhias 56
http://www.geologismiki.gr

CPT: Z5-1
Total depth: 15.39 m
Surface Elevation: 0.00 m
Coords: X:0.00, Y:0.00
Cone Type: Uknown
Cone Operator: Uknown

Project:
Location:

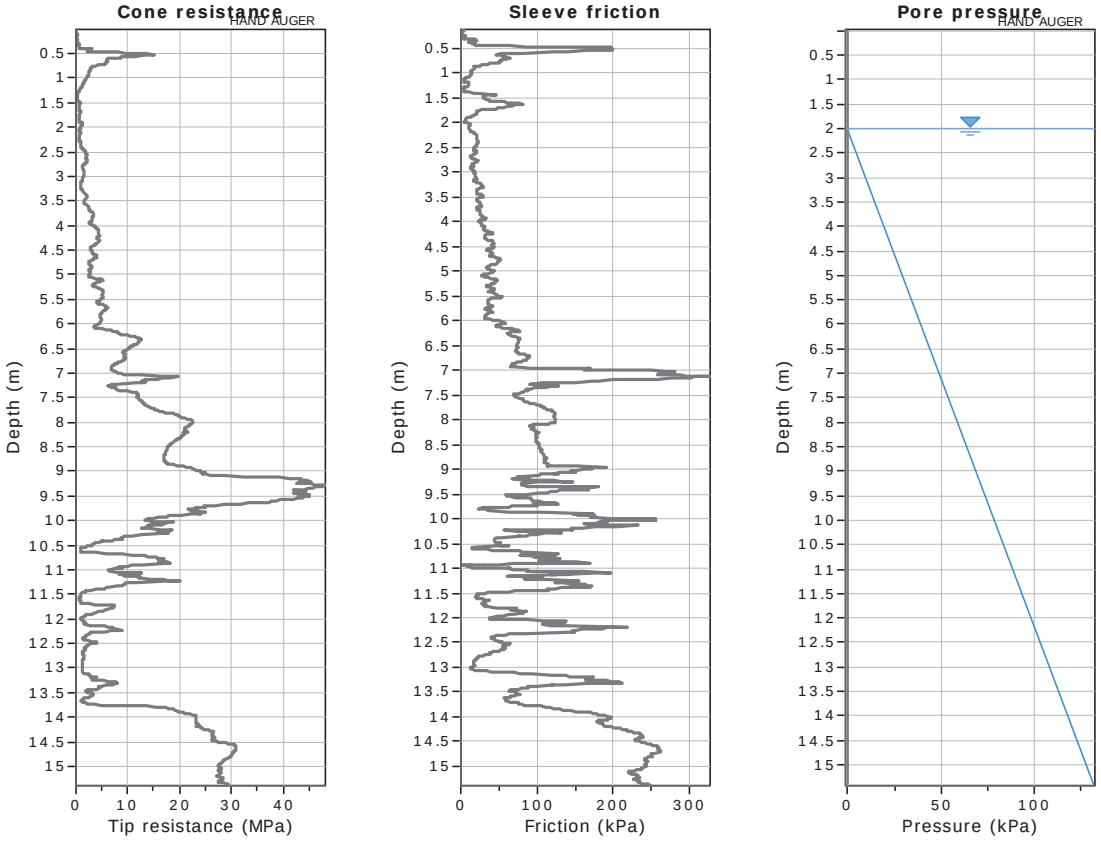

The plot below presents the cross correlation coeficient between the raw qc and fs values (as measured on the field). X axes presents the lag distance (one lag is the distance between two sucessive CPT measurements).

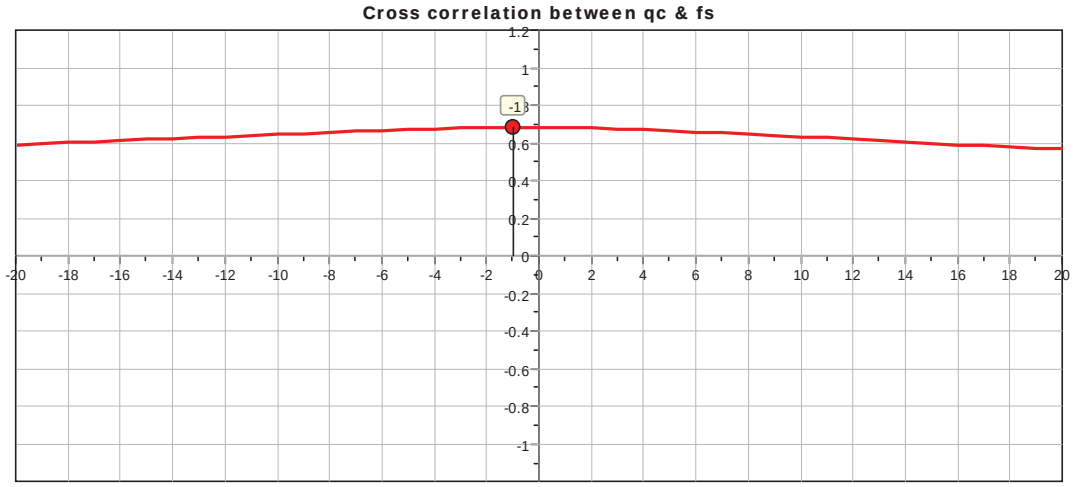

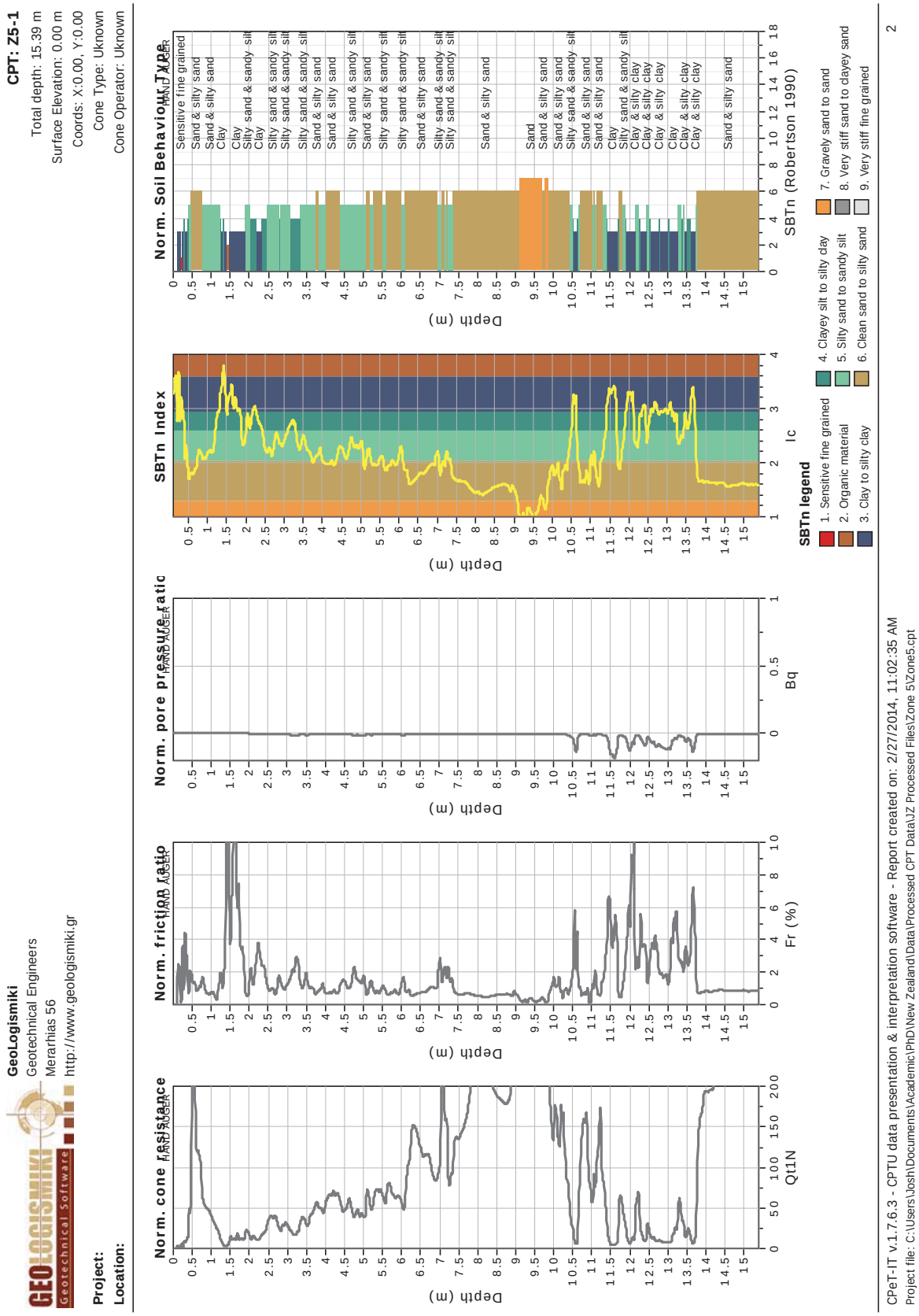
CPT: Z5-1
Total depth: 15.39 m
Surface Elevation: 0.00 m
Coords: X:0.00, Y:0.00
Cone Type: Uknown
Cone Operator: Uknown
GeoLogismiki
Geotechnical Engineers
Merarhias 56
http://www.geologismiki.gr
Project:
Location:
Norm. cone resistance
Norm. friction ratio
Norm. pore pressure ratio
SBTn Index
Norm. Soil Behaviour Type
HAND AUGER
Qt1N
Fr (%)
Bq
Ic
SBTn (Robertson 1990)
Depth (m)
SBTn legend
1. Sensitive fine grained
2. Organic material
3. Clay to silty clay
4. Clayey silt to silty clay
5. Silty sand to sandy silt
6. Clean sand to silty sand
7. Gravely sand to sand
8. Very stiff sand to clayey sand
9. Very stiff fine grained
Sensitive fine grained
Sand & silty sand
Clay
Silty sand & sandy silt
Sand & silty sand
Silty sand & sandy silt
Clay & silty clay
Sand
CPeT-IT v.1.7.6.3 - CPTU data presentation & interpretation software - Report created on: 2/27/2014, 11:02:35 AM
Project file: C:\Users\Josh\Documents\Academic\PhD\New Zealand\Data\Processed CPT Data\JZ Processed Files\Zone 5\Zone5.cpt
2

GeoLogismiki
Geotechnical Engineers
Merarhias 56
http://www.geologismiki.gr

CPT: Z5-2
Total depth: 6.79 m
Surface Elevation: 0.00 m
Coords: X:0.00, Y:0.00
Cone Type: Uknown
Cone Operator: Uknown

Project:
Location:

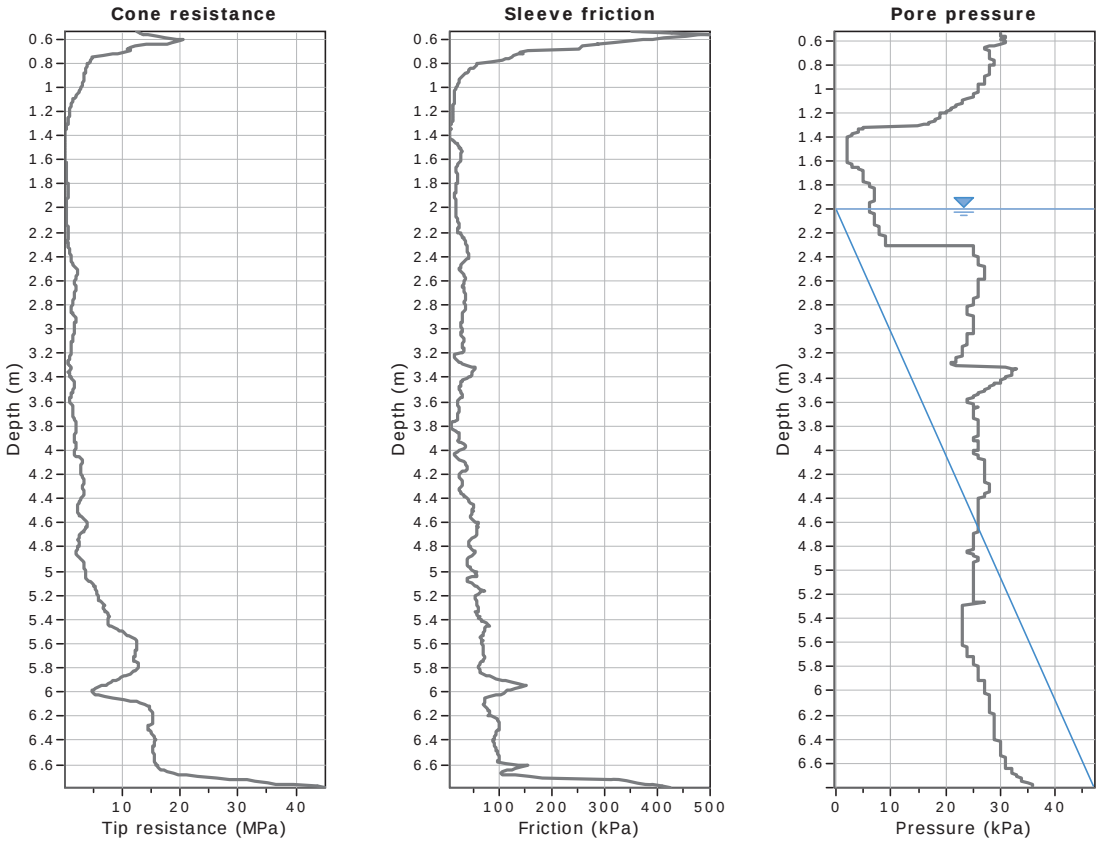

The plot below presents the cross correlation coeficient between the raw qc and fs values (as measured on the field). X axes presents the lag distance (one lag is the distance between two sucessive CPT measurements).

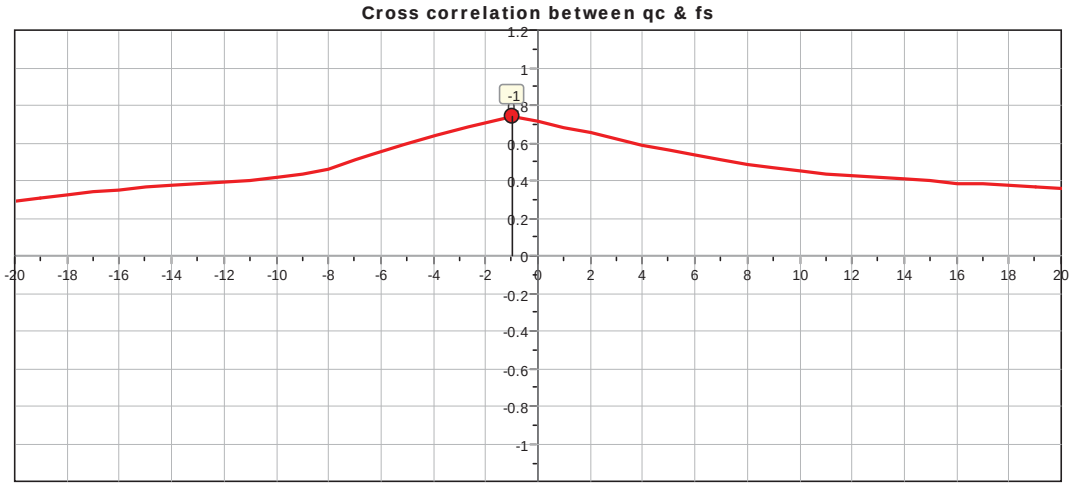

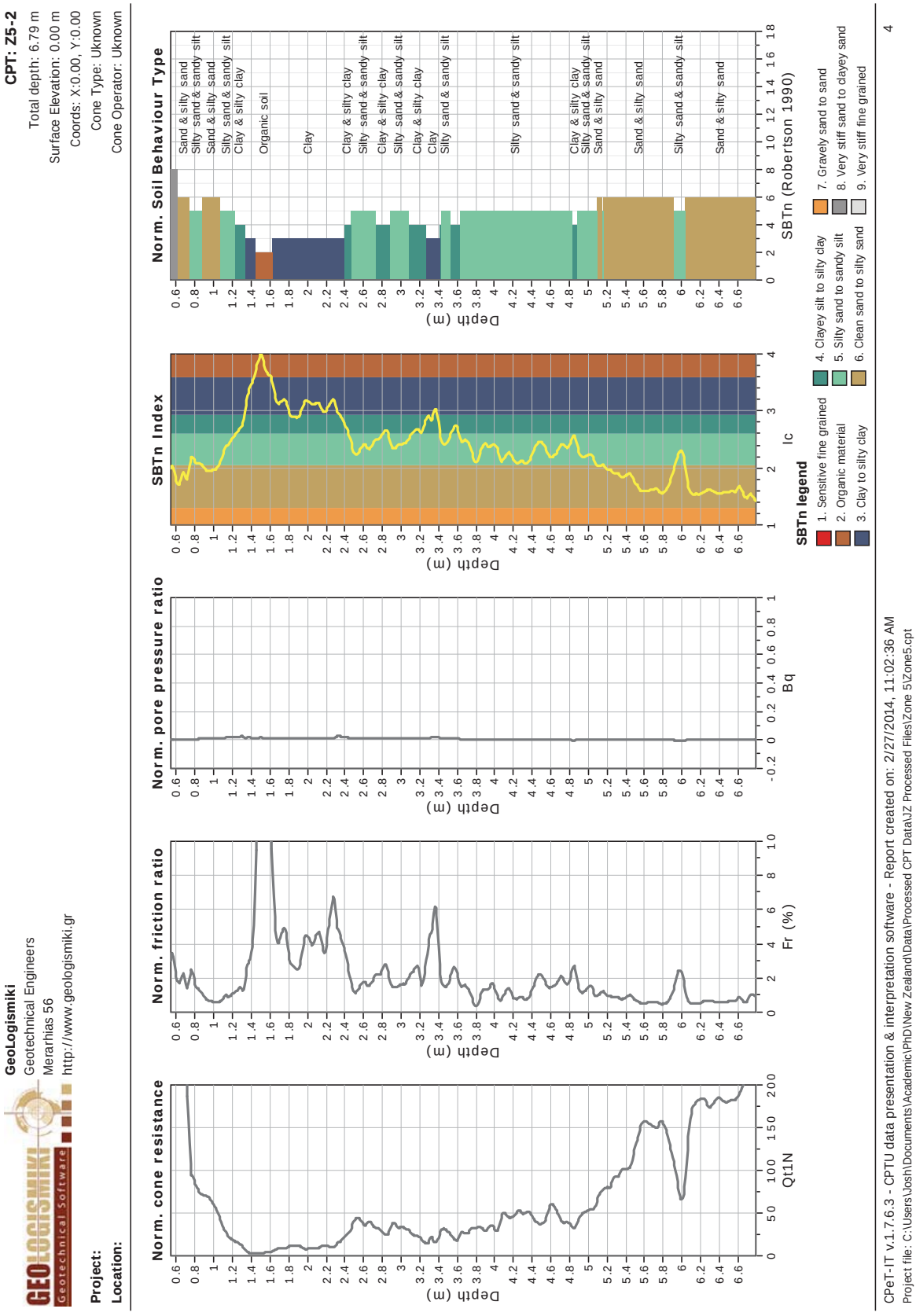
GeoLogismiki
Geotechnical Engineers
Merarhias 56
http://www.geologismiki.gr
Project:
Location:
CPT: Z5-2
Total depth: 6.79 m
Surface Elevation: 0.00 m
Coords: X:0.00, Y:0.00
Cone Type: Uknown
Cone Operator: Uknown
Norm. cone resistance
Qt1N
Norm. friction ratio
Fr (%)
Norm. pore pressure ratio
Bq
SBTn Index
Ic
Norm. Soil Behaviour Type
SBTn (Robertson 1990)
Depth (m)
SBTn legend
1. Sensitive fine grained
2. Organic material
3. Clay to silty clay
4. Clayey silt to silty clay
5. Silty sand to sandy silt
6. Clean sand to silty sand
7. Gravely sand to sand
8. Very stiff sand to clayey sand
9. Very stiff fine grained
CPeT-IT v.1.7.6.3 - CPTU data presentation & interpretation software - Report created on: 2/27/2014, 11:02:36 AM
Project file: C:\Users\Josh\Documents\Academic\PhD\New Zealand\Data\Processed CPT Data\JZ Processed Files\Zone 5\Zone5.cpt
4

GeoLogismiki
Geotechnical Engineers
Merarhias 56
http://www.geologismiki.gr

CPT: Z5-3
Total depth: 6.81 m
Surface Elevation: 0.00 m
Coords: X:0.00, Y:0.00
Cone Type: Uknown
Cone Operator: Uknown

Project:
Location:

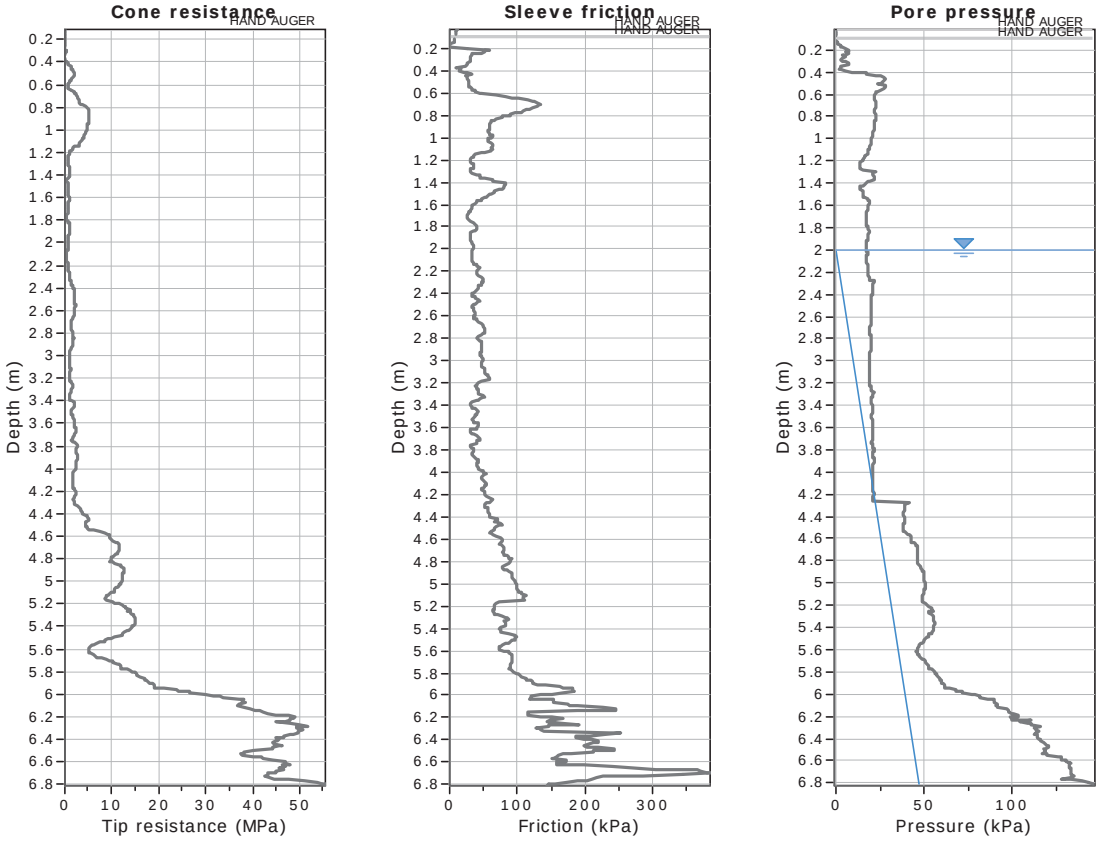

The plot below presents the cross correlation coeficient between the raw qc and fs values (as measured on the field). X axes presents the lag distance (one lag is the distance between two sucessive CPT measurements).

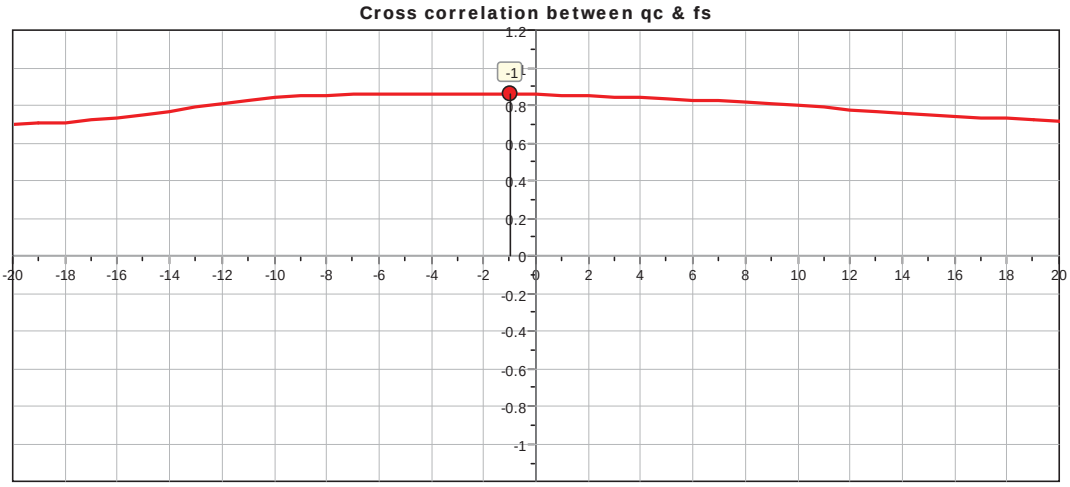

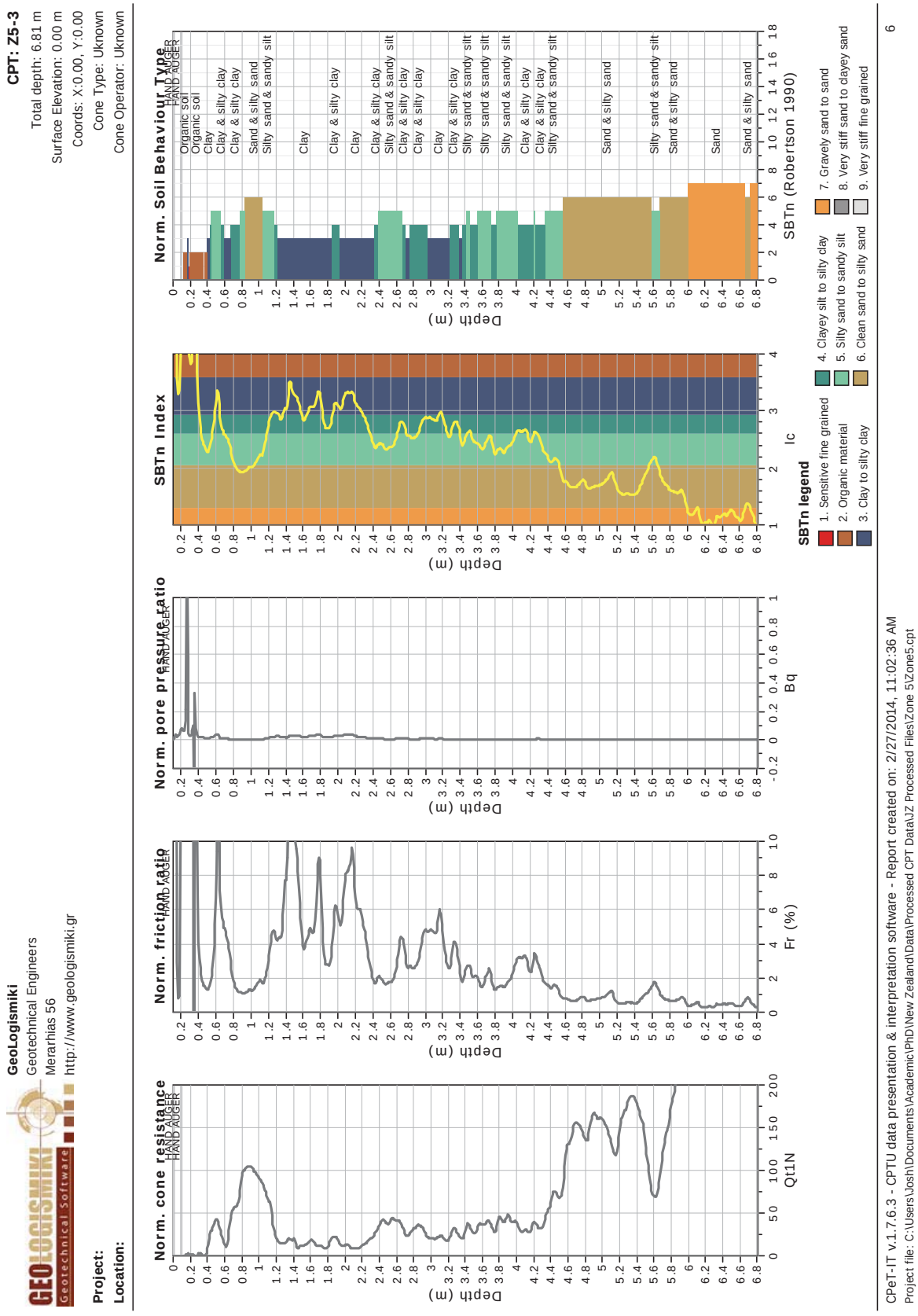
GeoLogismiki
Geotechnical Engineers
Merarchias 56
http://www.geologismiki.gr
Project:
Location:
CPT: Z5-3
Total depth: 6.81 m
Surface Elevation: 0.00 m
Coords: X:0.00, Y:0.00
Cone Type: Uknown
Cone Operator: Uknown
Norm. cone resistance
Norm. friction ratio
Norm. pore pressure ratio
SBTn Index
Norm. Soil Behaviour Type
Depth (m)
Qt1N
Fr (%)
Bq
Ic
SBTn (Robertson 1990)
HAND AUGER
Organic soil
Clay
Clay & silty clay
Sand & silty sand
Silty sand & sandy silt
SBTn legend
1. Sensitive fine grained
2. Organic material
3. Clay to silty clay
4. Clayey silt to silty clay
5. Silty sand to sandy silt
6. Clean sand to silty sand
7. Gravely sand to sand
8. Very stiff sand to clayey sand
9. Very stiff fine grained
CPeT-IT v.1.7.6.3 - CPTU data presentation & interpretation software - Report created on: 2/27/2014, 11:02:36 AM
Project file: C:\Users\Josh\Documents\Academic\PhD\New Zealand\Data\Processed CPT Data\JZ Processed Files\Zone 5\Zone5.cpt
6

GeoLogismiki
Geotechnical Engineers
Merarhias 56
http://www.geologismiki.gr

CPT: Z5-5
Total depth: 10.09 m
Surface Elevation: 0.00 m
Coords: X:0.00, Y:0.00
Cone Type: Uknown
Cone Operator: Uknown

Project:
Location:

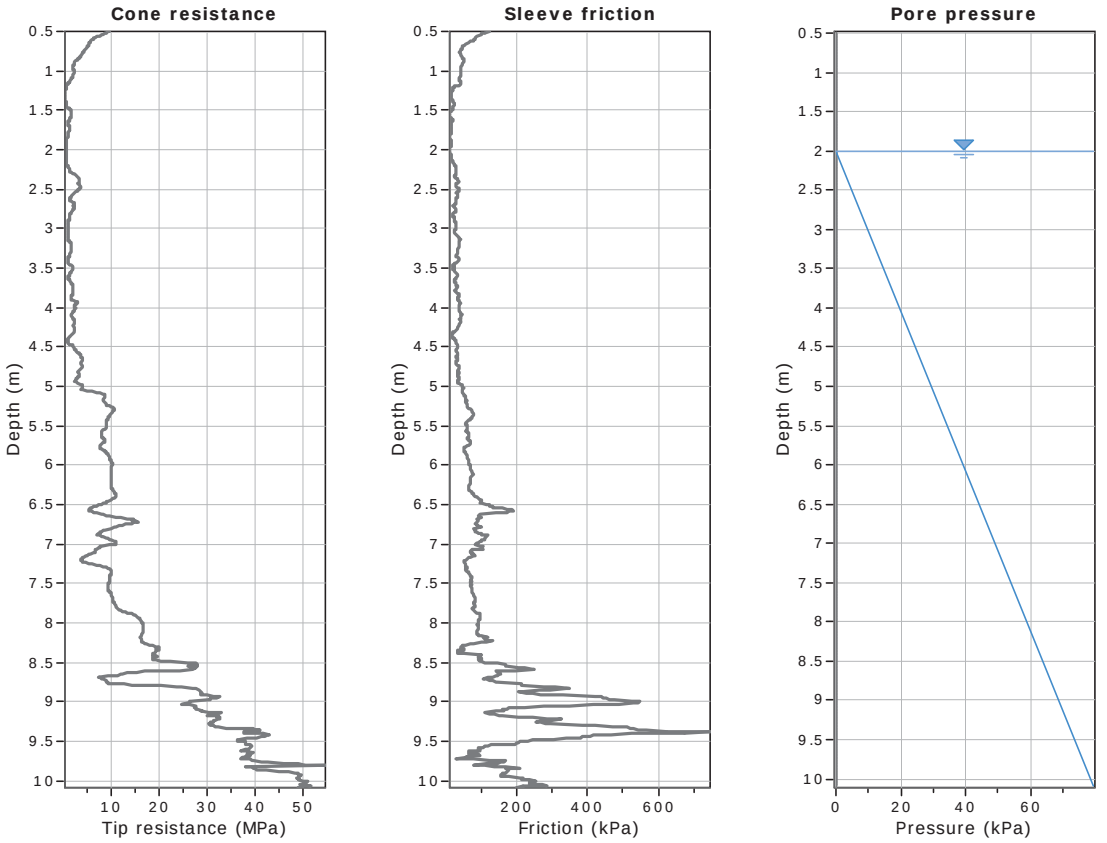

The plot below presents the cross correlation coeficient between the raw qc and fs values (as measured on the field). X axes presents the lag distance (one lag is the distance between two sucessive CPT measurements).

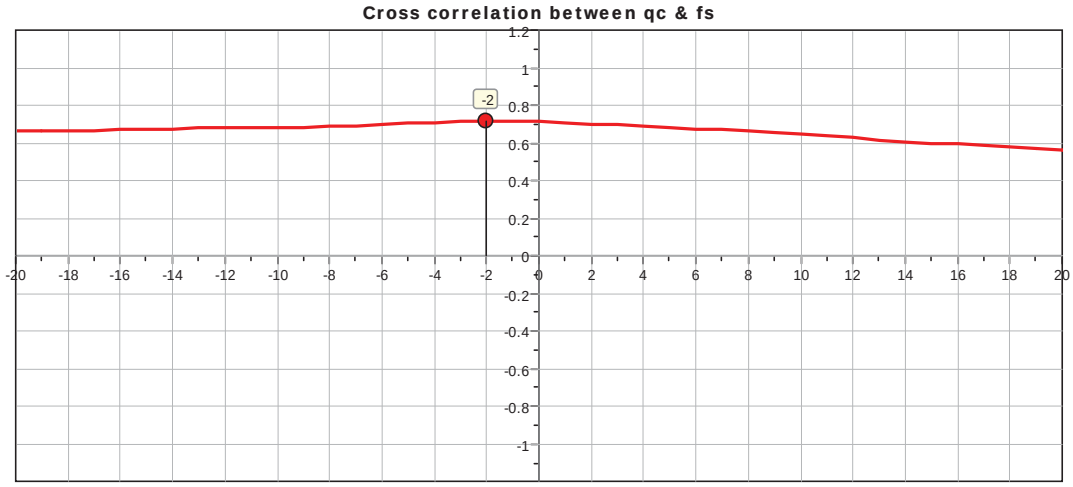

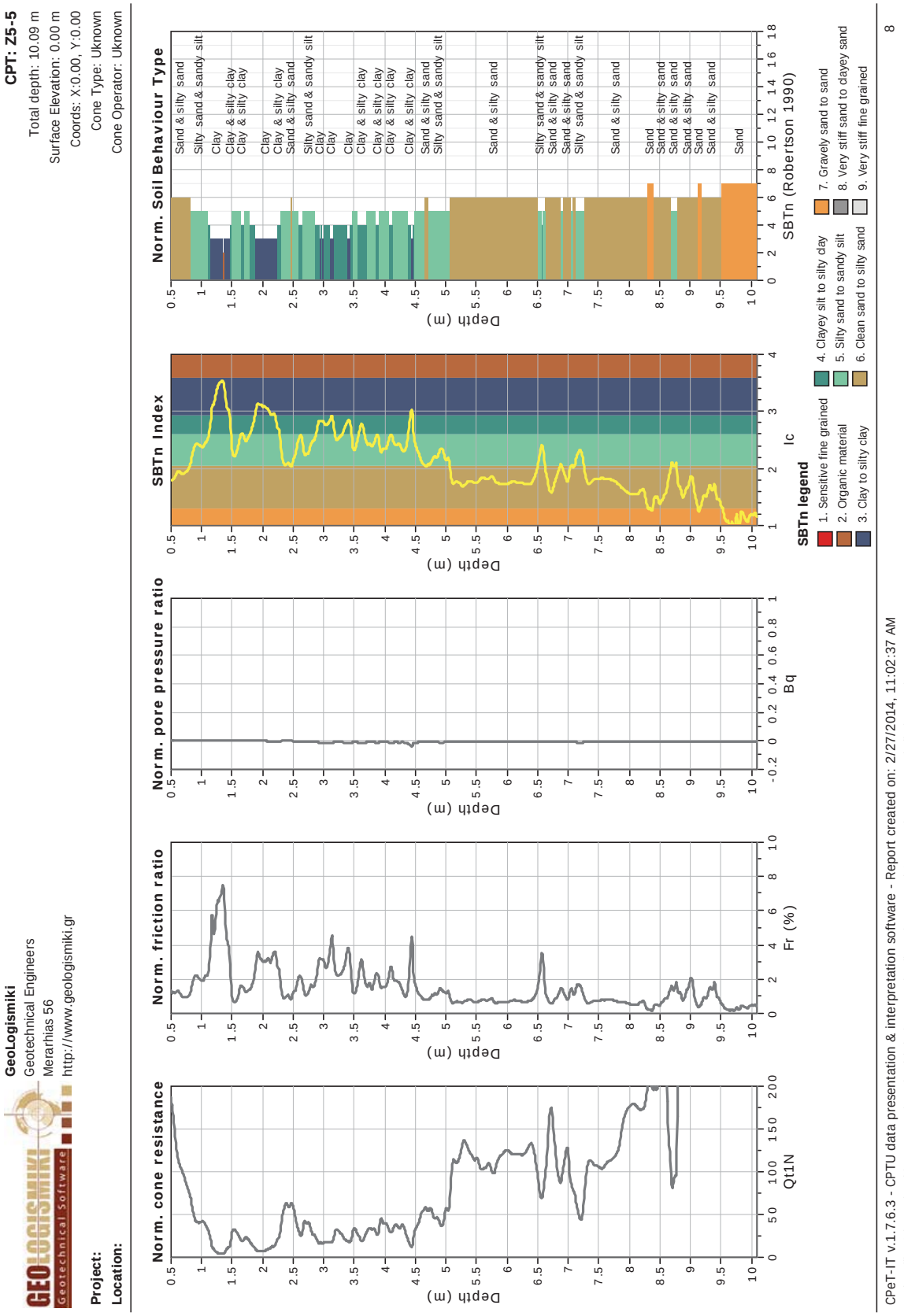
CPT: Z5-5
Total depth: 10.09 m
Surface Elevation: 0.00 m
Coords: X:0.00, Y:0.00
Cone Type: Uknown
Cone Operator: Uknown
GeoLogismiki
Geotechnical Engineers
Merarhias 56
http://www.geologismiki.gr
Project:
Location:
Norm. cone resistance
Qt1N
Norm. friction ratio
Fr (%)
Norm. pore pressure ratio
Bq
SBTn Index
Ic
Norm. Soil Behaviour Type
SBTn (Robertson 1990)
Depth (m)
SBTn legend
1. Sensitive fine grained
2. Organic material
3. Clay to silty clay
4. Clayey silt to silty clay
5. Silty sand to sandy silt
6. Clean sand to silty sand
7. Gravely sand to sand
8. Very stiff sand to clayey sand
9. Very stiff fine grained
CPeT-IT v.1.7.6.3 - CPTU data presentation & interpretation software - Report created on: 2/27/2014, 11:02:37 AM
Project file: C:\Users\Josh\Documents\Academic\PhD\New Zealand\Data\Processed CPT Data\JZ Processed Files\Zone 5\Zone5.cpt
8

GeoLogismiki
Geotechnical Engineers
Merarhias 56
http://www.geologismiki.gr

CPT: Z5-6
Total depth: 20.68 m
Surface Elevation: 0.00 m
Coords: X:0.00, Y:0.00
Cone Type: Uknown
Cone Operator: Uknown

Project:
Location:

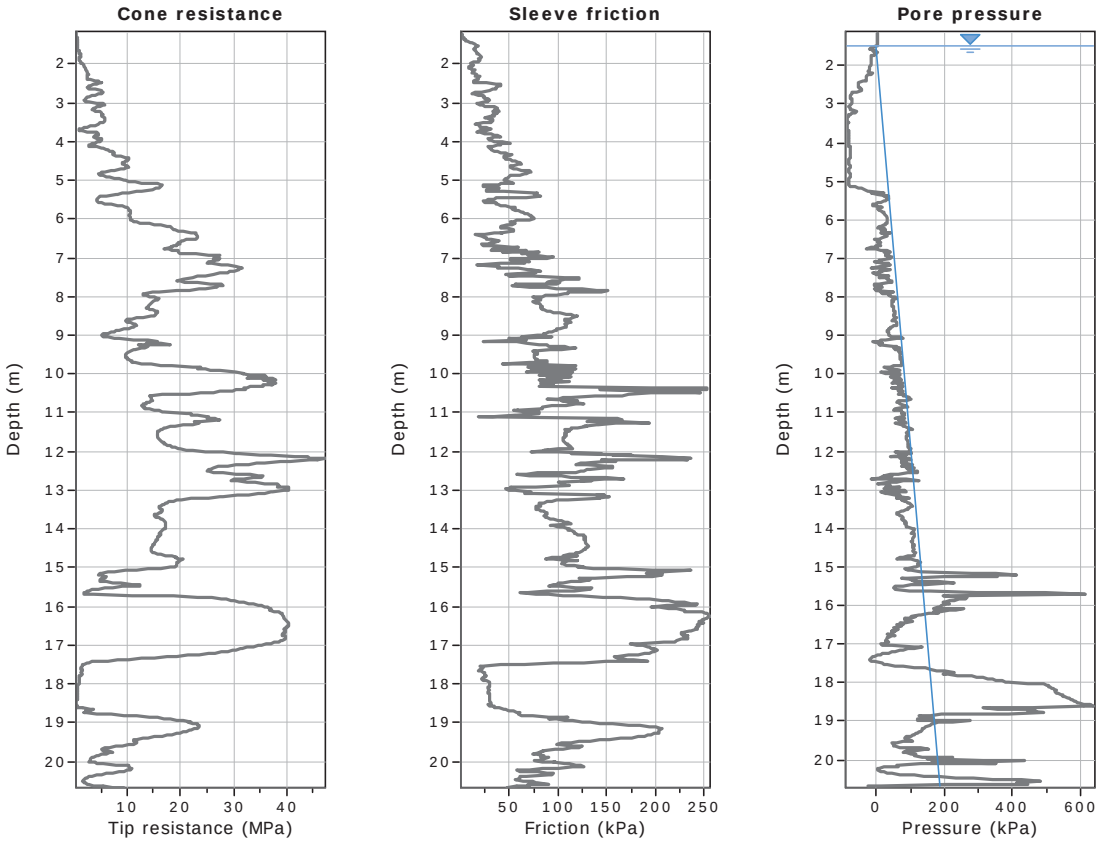

The plot below presents the cross correlation coeficient between the raw qc and fs values (as measured on the field). X axes presents the lag distance (one lag is the distance between two sucessive CPT measurements).

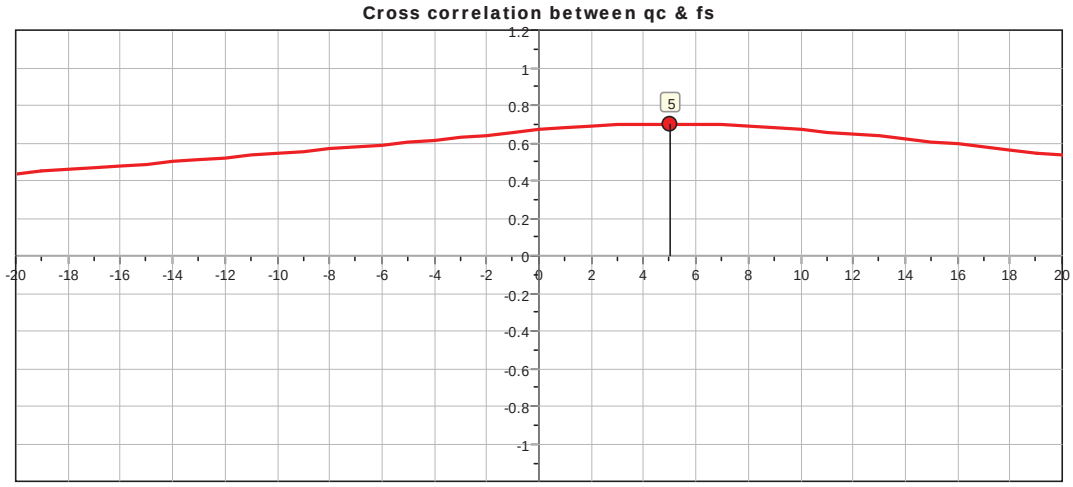

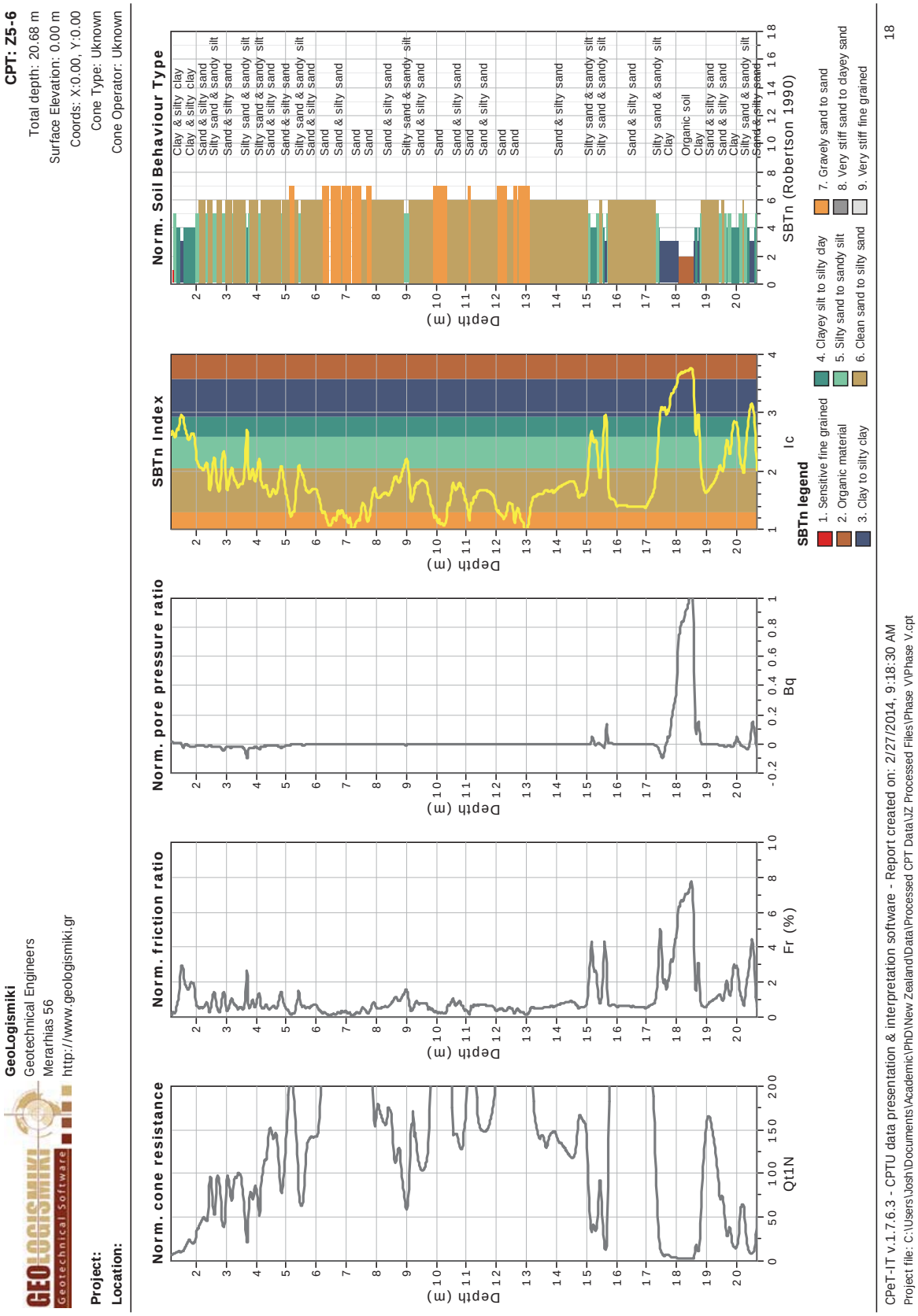
CPT: Z5-6
Total depth: 20.68 m
Surface Elevation: 0.00 m
Coords: X:0.00, Y:0.00
Cone Type: Uknown
Cone Operator: Uknown
GeoLogismiki
Geotechnical Engineers
Merarhias 56
http://www.geologismiki.gr
Project:
Location:
Norm. cone resistance
Qt1N
Norm. friction ratio
Fr (%)
Norm. pore pressure ratio
Bq
SBTn Index
Ic
Norm. Soil Behaviour Type
SBTn (Robertson 1990)
Depth (m)
SBTn legend
1. Sensitive fine grained
2. Organic material
3. Clay to silty clay
4. Clayey silt to silty clay
5. Silty sand to sandy silt
6. Clean sand to silty sand
7. Gravely sand to sand
8. Very stiff sand to clayey sand
9. Very stiff fine grained
CPeT-IT v.1.7.6.3 - CPTU data presentation & interpretation software - Report created on: 2/27/2014, 9:18:30 AM
Project file: C:\Users\Josh\Documents\Academic\PhD\New Zealand\Data\Processed CPT Data\JZ Processed Files\Phase V\Phase V.cpt
18

GeoLogismiki
Geotechnical Engineers
Merarhias 56
http://www.geologismiki.gr

CPT: Z5-7
Total depth: 21.06 m
Surface Elevation: 0.00 m
Coords: X:0.00, Y:0.00
Cone Type: Uknown
Cone Operator: Uknown

Project:
Location:

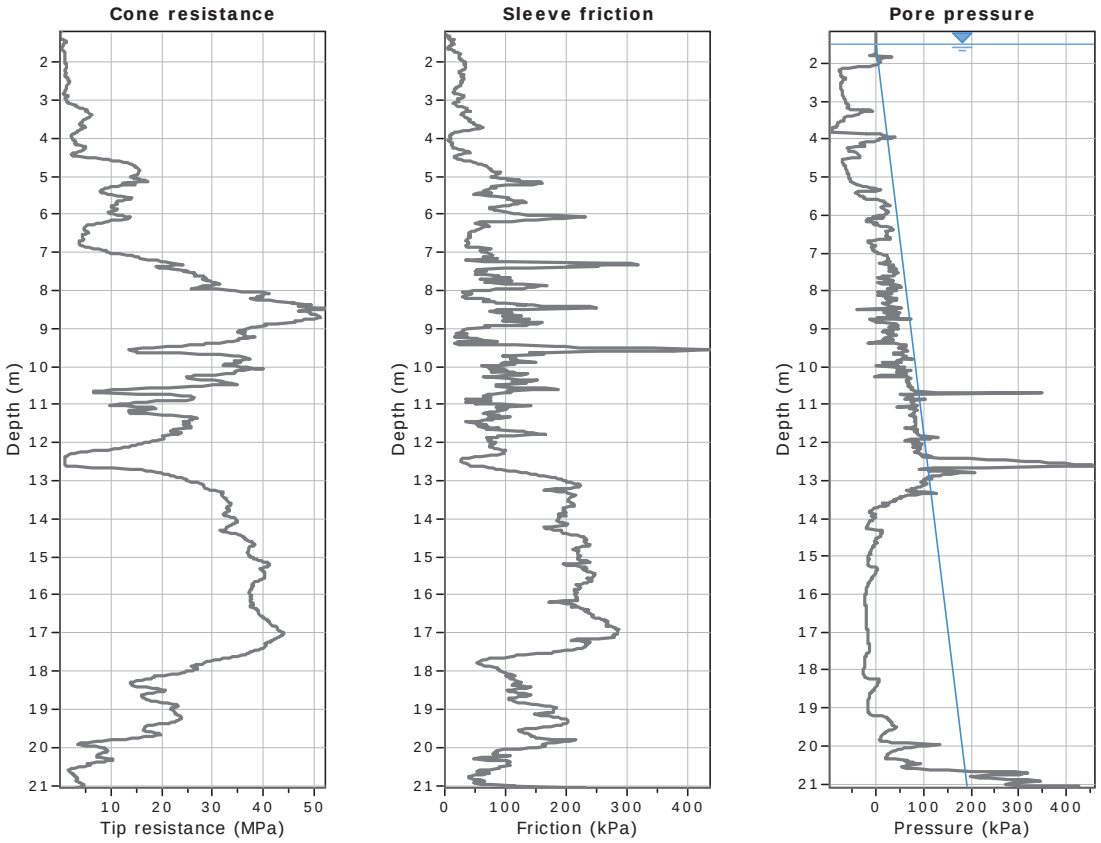

The plot below presents the cross correlation coeficient between the raw qc and fs values (as measured on the field). X axes presents the lag distance (one lag is the distance between two sucessive CPT measurements).

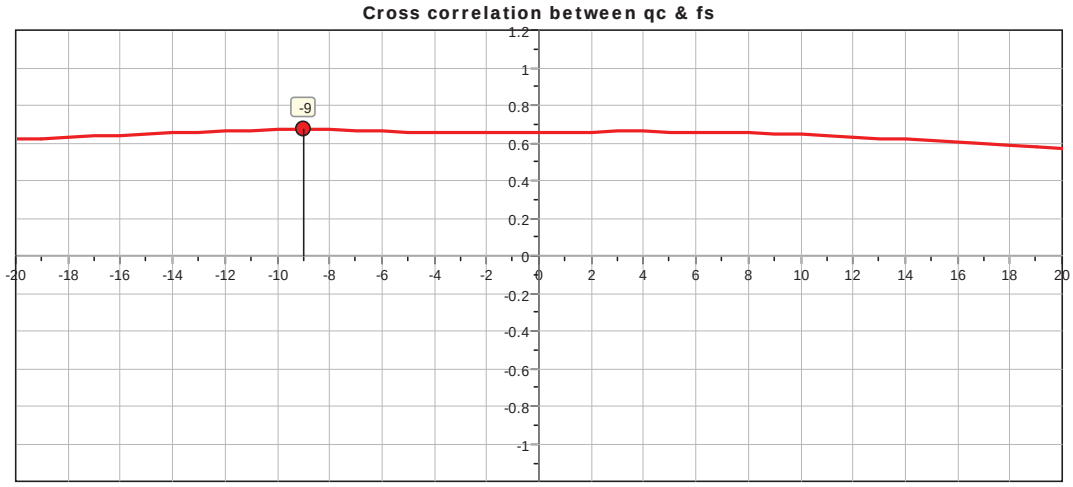

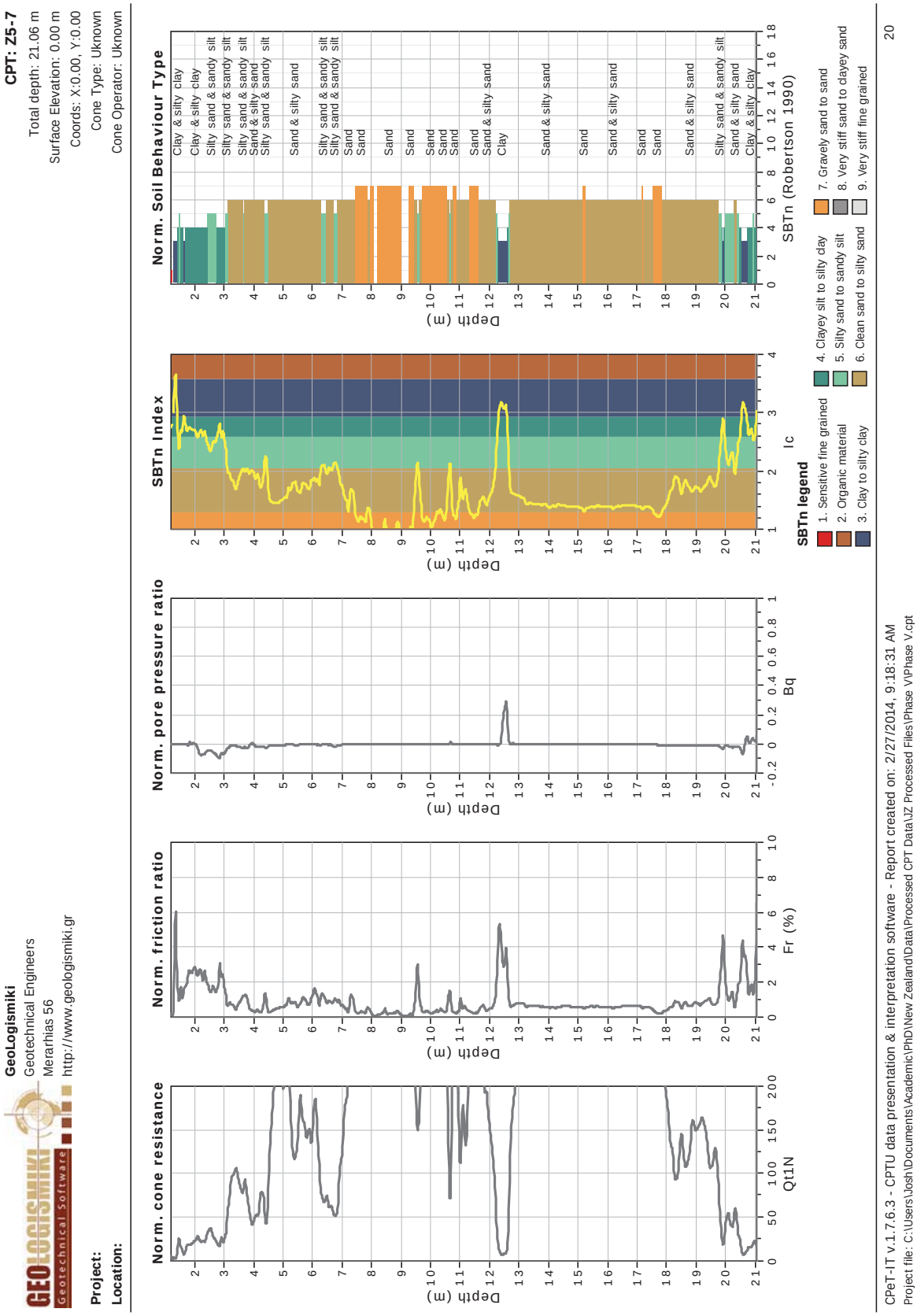
CPT: Z5-7
Total depth: 21.06 m
Surface Elevation: 0.00 m
Coords: X:0.00, Y:0.00
Cone Type: Uknown
Cone Operator: Uknown
GeoLogismiki
Geotechnical Engineers
Merarhias 56
http://www.geologismiki.gr
Project:
Location:
Norm. cone resistance
Qt1N
Norm. friction ratio
Fr (%)
Norm. pore pressure ratio
Bq
SBTn Index
Ic
Norm. Soil Behaviour Type
SBTn (Robertson 1990)
Depth (m)
SBTn legend
1. Sensitive fine grained
2. Organic material
3. Clay to silty clay
4. Clayey silt to silty clay
5. Silty sand to sandy silt
6. Clean sand to silty sand
7. Gravely sand to sand
8. Very stiff sand to clayey sand
9. Very stiff fine grained
CPeT-IT v.1.7.6.3 - CPTU data presentation & interpretation software - Report created on: 2/27/2014, 9:18:31 AM
Project file: C:\Users\Josh\Documents\Academic\PhD\New Zealand\Data\Processed CPT Data\JZ Processed Files\Phase V\Phase V.cpt
20

GeoLogismiki
Geotechnical Engineers
Merarhias 56
http://www.geologismiki.gr

CPT: Z5-8
Total depth: 20.56 m
Surface Elevation: 0.00 m
Coords: X:0.00, Y:0.00
Cone Type: Uknown
Cone Operator: Uknown

Project:
Location:

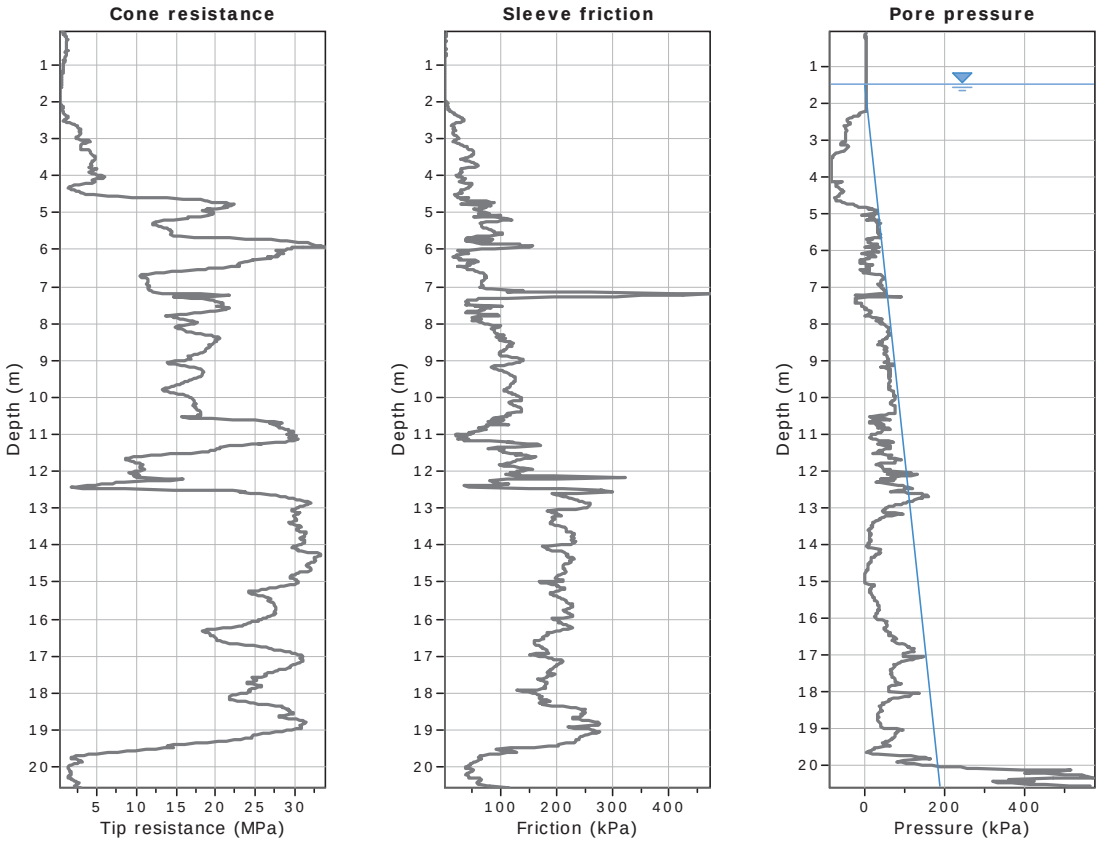

The plot below presents the cross correlation coeficient between the raw qc and fs values (as measured on the field). X axes presents the lag distance (one lag is the distance between two sucessive CPT measurements).

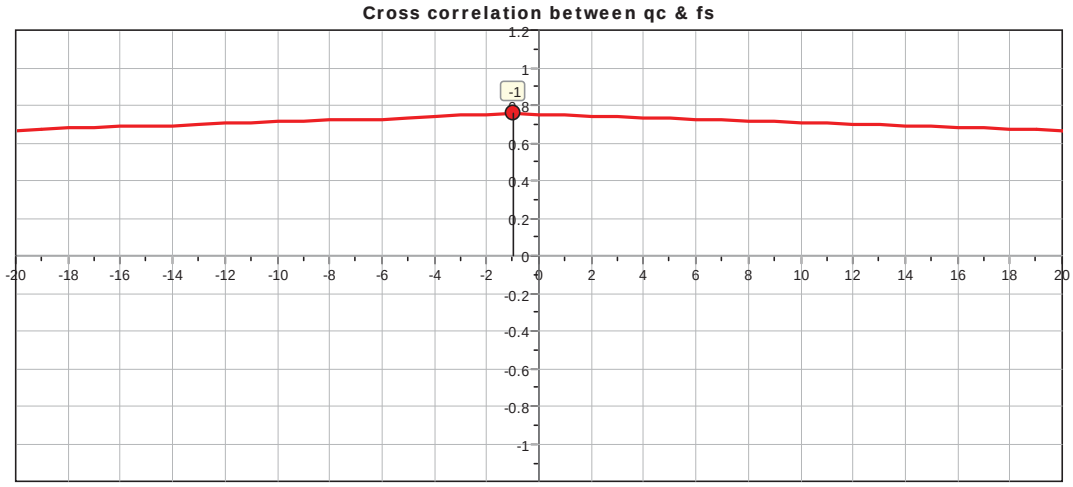

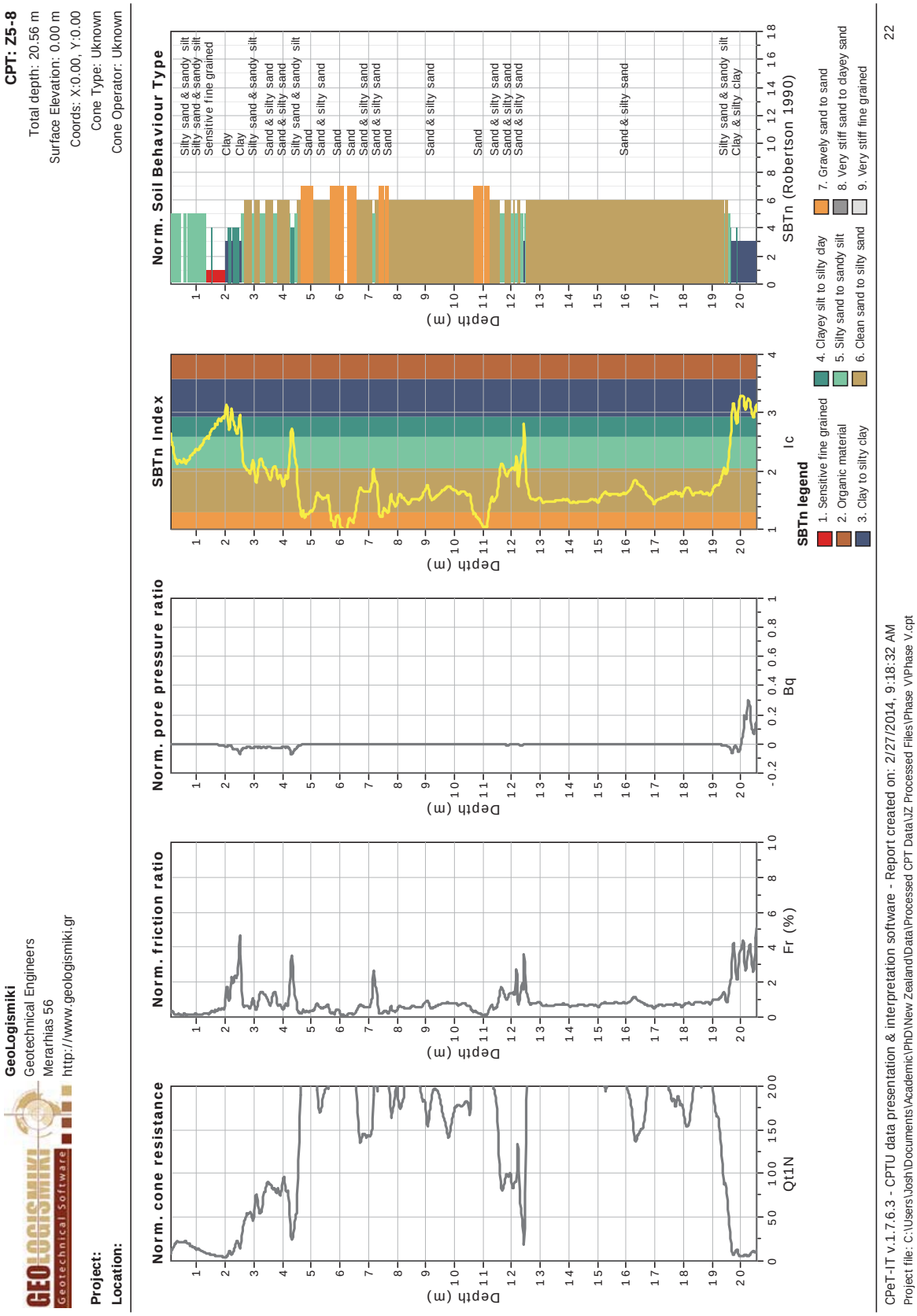
CPT: Z5-8
Total depth: 20.56 m
Surface Elevation: 0.00 m
Coords: X:0.00, Y:0.00
Cone Type: Uknown
Cone Operator: Uknown
GeoLogismiki
Geotechnical Engineers
Merarhias 56
http://www.geologismiki.gr
Project:
Location:
Norm. cone resistance
Qt1N
Norm. friction ratio
Fr (%)
Norm. pore pressure ratio
Bq
SBTn Index
Ic
Norm. Soil Behaviour Type
SBTn (Robertson 1990)
Depth (m)
SBTn legend
1. Sensitive fine grained
2. Organic material
3. Clay to silty clay
4. Clayey silt to silty clay
5. Silty sand to sandy silt
6. Clean sand to silty sand
7. Gravely sand to sand
8. Very stiff sand to clayey sand
9. Very stiff fine grained
CPeT-IT v.1.7.6.3 - CPTU data presentation & interpretation software - Report created on: 2/27/2014, 9:18:32 AM
Project file: C:\Users\Josh\Documents\Academic\PhD\New Zealand\Data\Processed CPT Data\JZ Processed Files\Phase V\Phase V.cpt
22

GeoLogismiki
Geotechnical Engineers
Merarhias 56
http://www.geologismiki.gr

CPT: Z5-9
Total depth: 20.38 m
Surface Elevation: 0.00 m
Coords: X:0.00, Y:0.00
Cone Type: Uknown
Cone Operator: Uknown

Project:
Location:

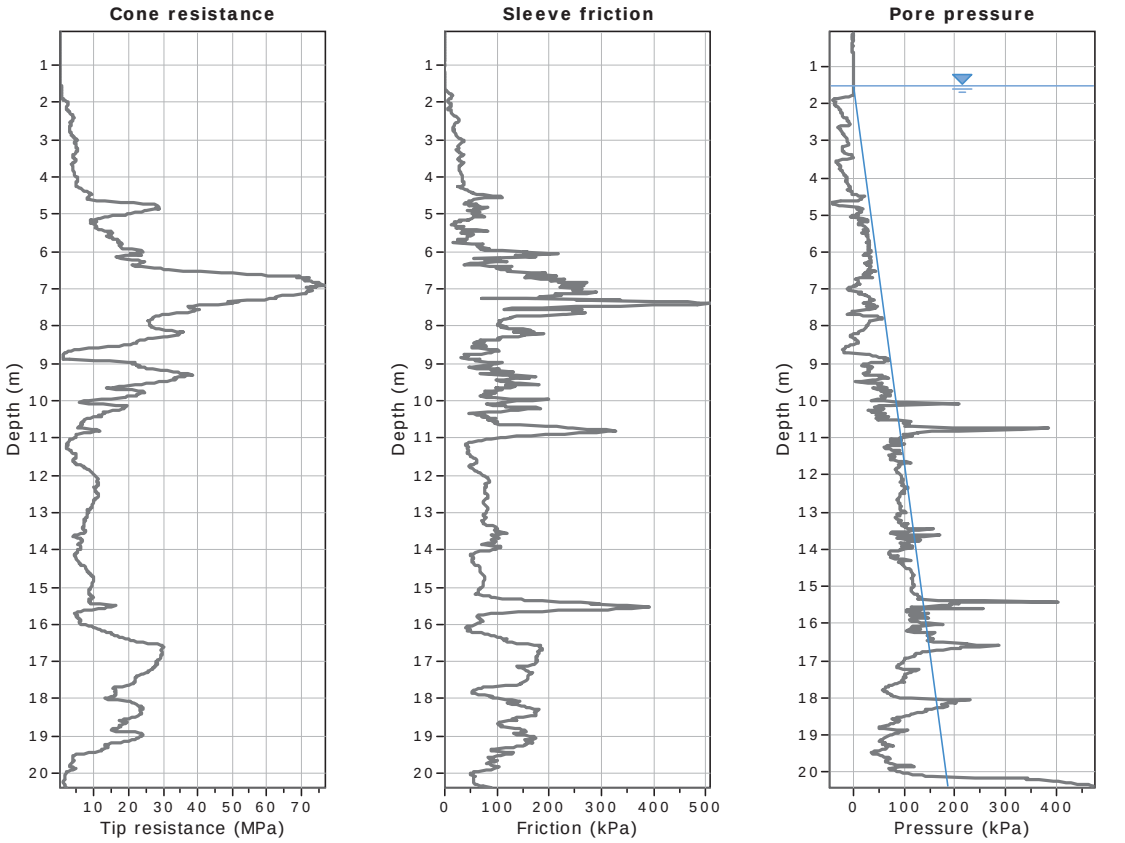

The plot below presents the cross correlation coeficient between the raw qc and fs values (as measured on the field). X axes presents the lag distance (one lag is the distance between two sucessive CPT measurements).

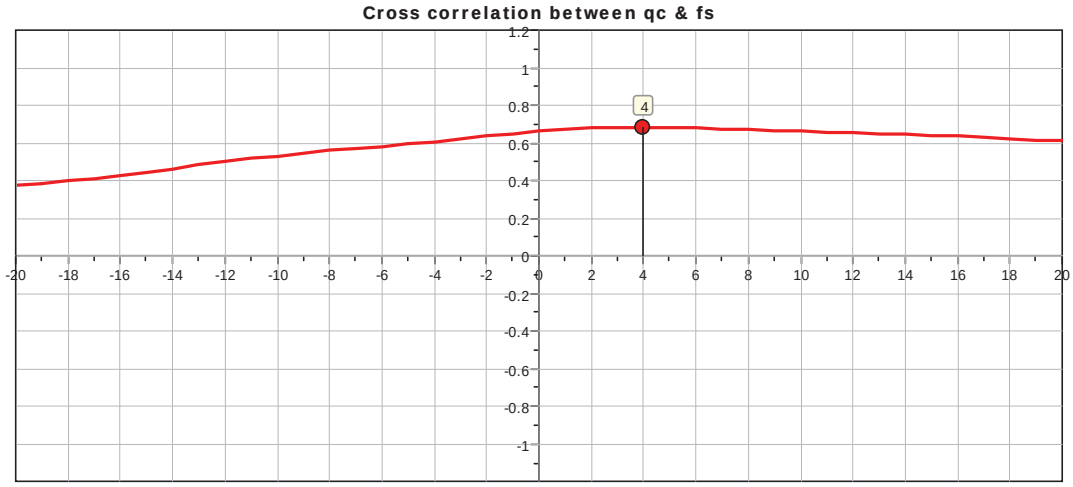

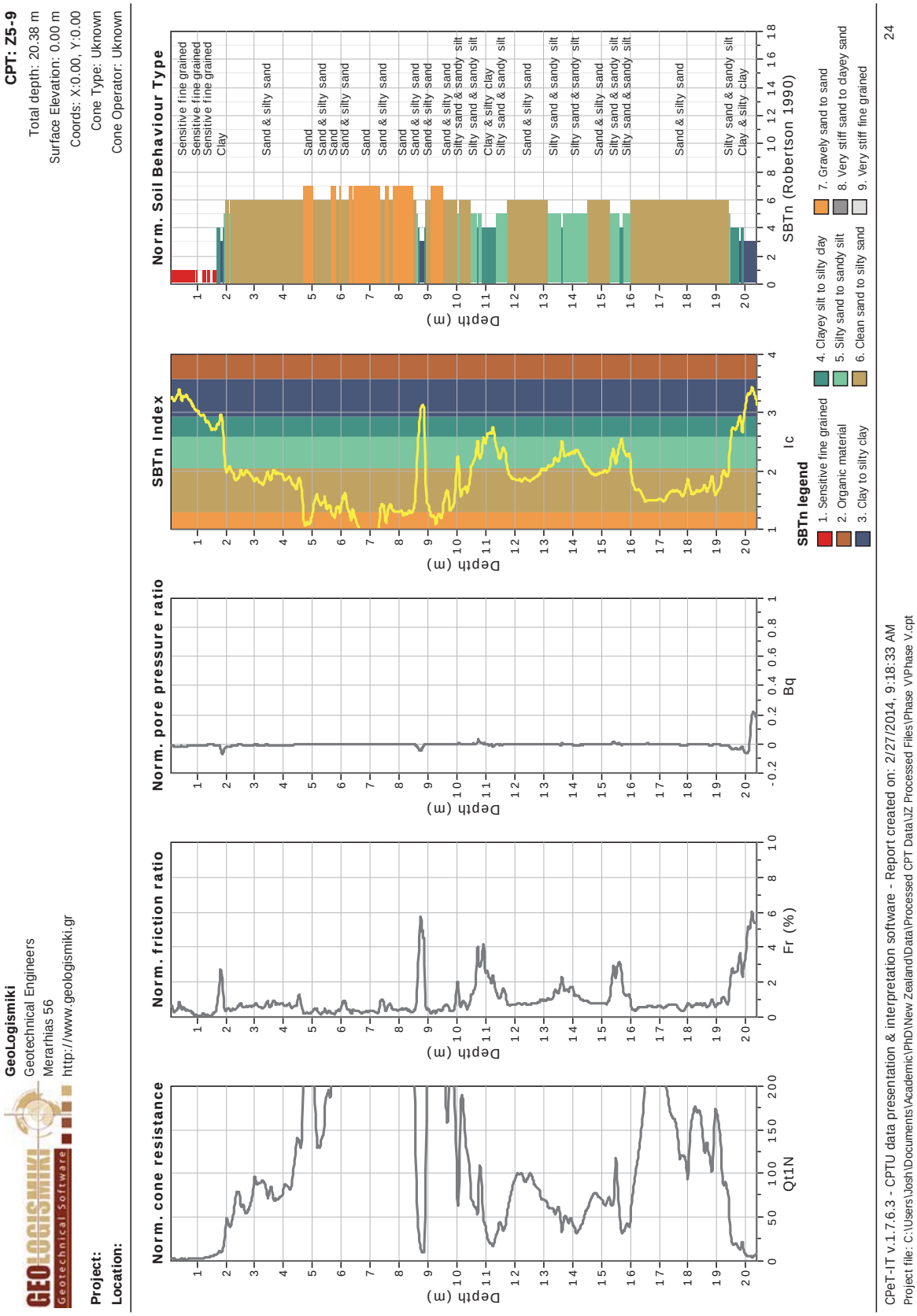
CPT: Z5-9
Total depth: 20.38 m
Surface Elevation: 0.00 m
Coords: X:0.00, Y:0.00
Cone Type: Uknown
Cone Operator: Uknown
GeoLogismiki
Geotechnical Engineers
Merarhias 56
http://www.geologismiki.gr
Project:
Location:
Norm. cone resistance
Qt1N
Norm. friction ratio
Fr (%)
Norm. pore pressure ratio
Bq
SBTn Index
Ic
Norm. Soil Behaviour Type
SBTn (Robertson 1990)
Depth (m)
SBTn legend
1. Sensitive fine grained
2. Organic material
3. Clay to silty clay
4. Clayey silt to silty clay
5. Silty sand to sandy silt
6. Clean sand to silty sand
7. Gravely sand to sand
8. Very stiff sand to clayey sand
9. Very stiff fine grained
CPeT-IT v.1.7.6.3 - CPTU data presentation & interpretation software - Report created on: 2/27/2014, 9:18:33 AM
Project file: C:\Users\Josh\Documents\Academic\PhD\New Zealand\Data\Processed CPT Data\JZ Processed Files\Phase V\Phase V.cpt
24

GeoLogismiki
Geotechnical Engineers
Merarhias 56
http://www.geologismiki.gr

CPT: Z5-10
Total depth: 21.00 m
Surface Elevation: 0.00 m
Coords: X:0.00, Y:0.00
Cone Type: Uknown
Cone Operator: Uknown

Project:
Location:

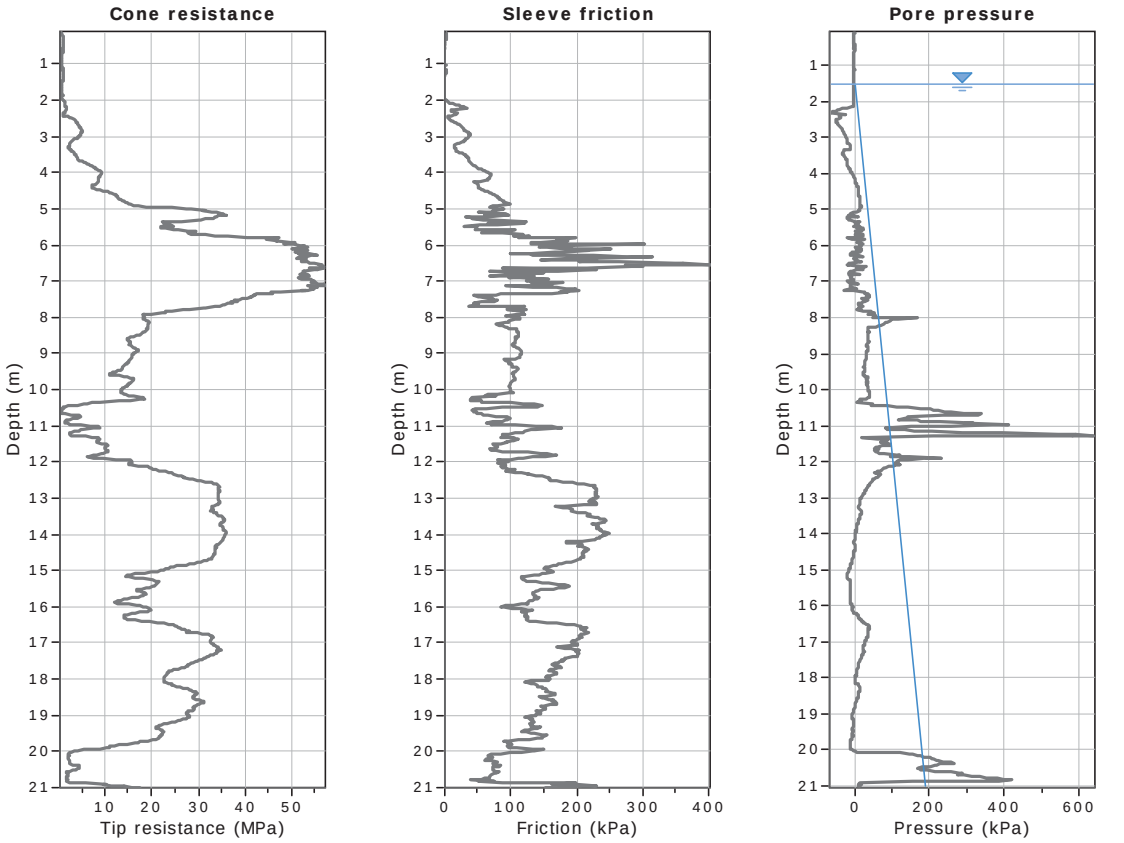

The plot below presents the cross correlation coeficient between the raw qc and fs values (as measured on the field). X axes presents the lag distance (one lag is the distance between two sucessive CPT measurements).

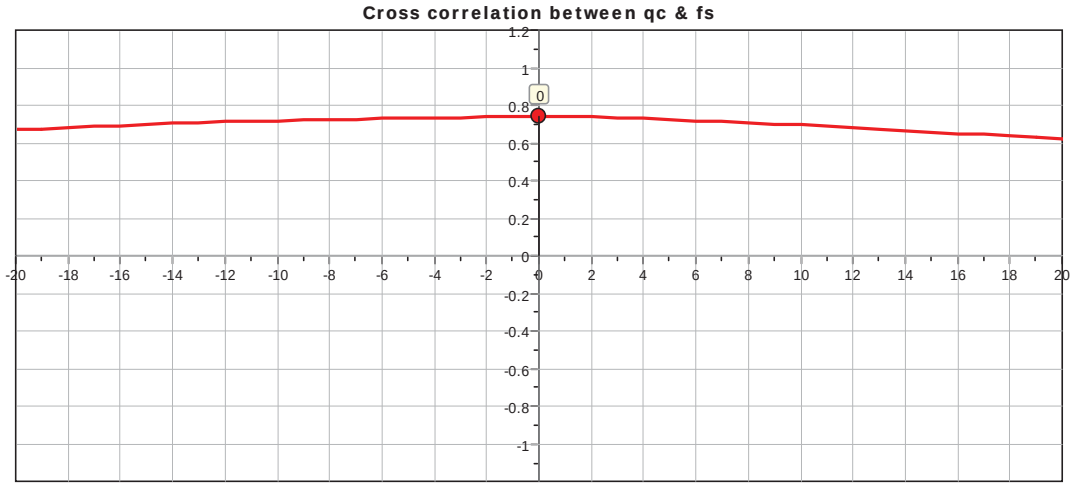

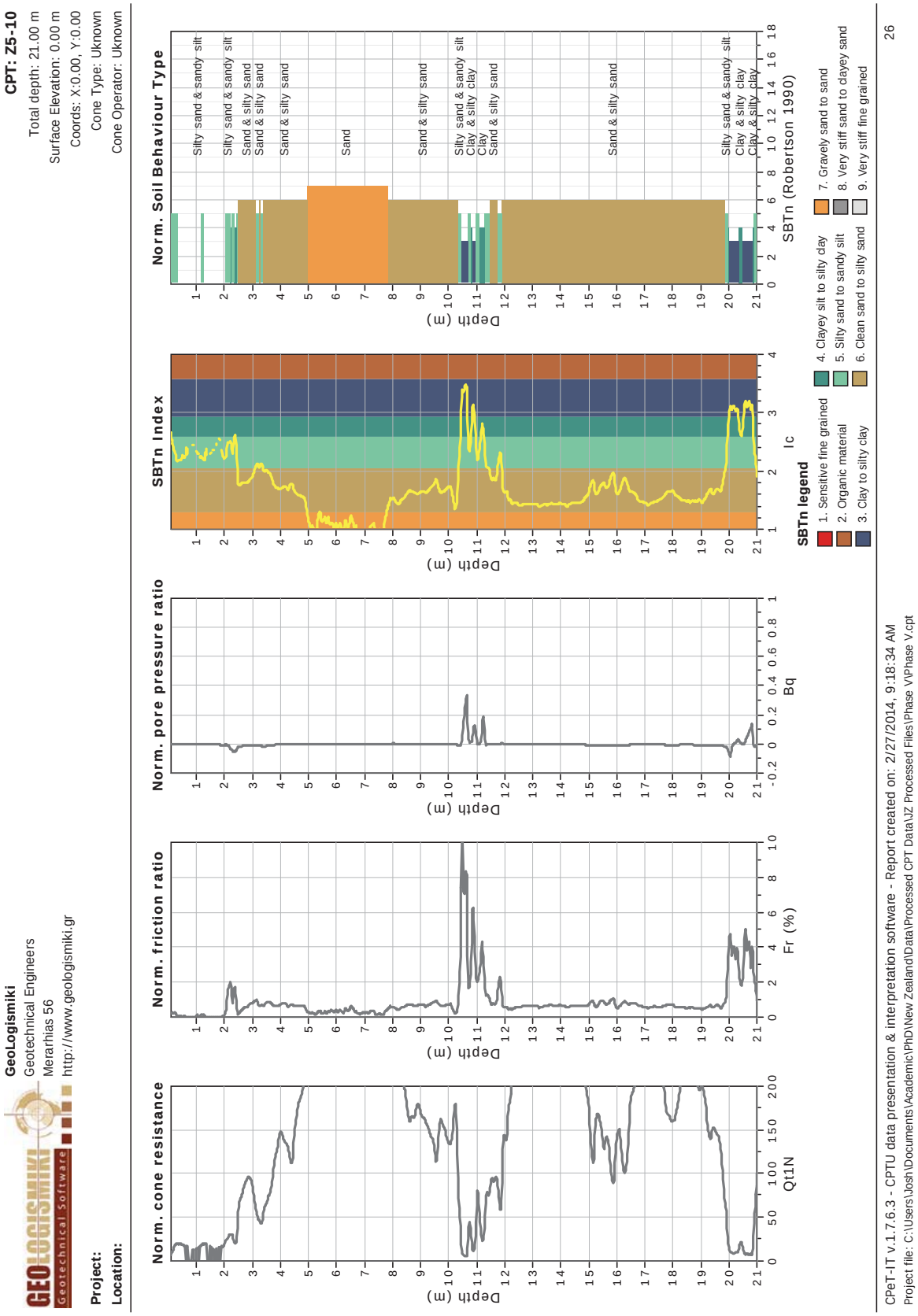
CPT: Z5-10
Total depth: 21.00 m
Surface Elevation: 0.00 m
Coords: X:0.00, Y:0.00
Cone Type: Uknown
Cone Operator: Uknown
GeoLogismiki
Geotechnical Engineers
Merarhias 56
http://www.geologismiki.gr
Project:
Location:
Norm. cone resistance
Qt1N
Norm. friction ratio
Fr (%)
Norm. pore pressure ratio
Bq
SBTn Index
Ic
Norm. Soil Behaviour Type
SBTn (Robertson 1990)
Depth (m)
Silty sand & sandy silt
Sand & silty sand
Sand
Silty sand & sandy silt
Clay & silty clay
Clay
Sand & silty sand
SBTn legend
1. Sensitive fine grained
2. Organic material
3. Clay to silty clay
4. Clayey silt to silty clay
5. Silty sand to sandy silt
6. Clean sand to silty sand
7. Gravely sand to sand
8. Very stiff sand to clayey sand
9. Very stiff fine grained
CPeT-IT v.1.7.6.3 - CPTU data presentation & interpretation software - Report created on: 2/27/2014, 9:18:34 AM
Project file: C:\Users\Josh\Documents\Academic\PhD\New Zealand\Data\Processed CPT Data\JZ Processed Files\Phase V\Phase V.cpt
26

GeoLogismiki
Geotechnical Engineers
Merarhias 56
http://www.geologismiki.gr

CPT: Z5-11
Total depth: 21.08 m
Surface Elevation: 0.00 m
Coords: X:0.00, Y:0.00
Cone Type: Uknown
Cone Operator: Uknown

Project:
Location:

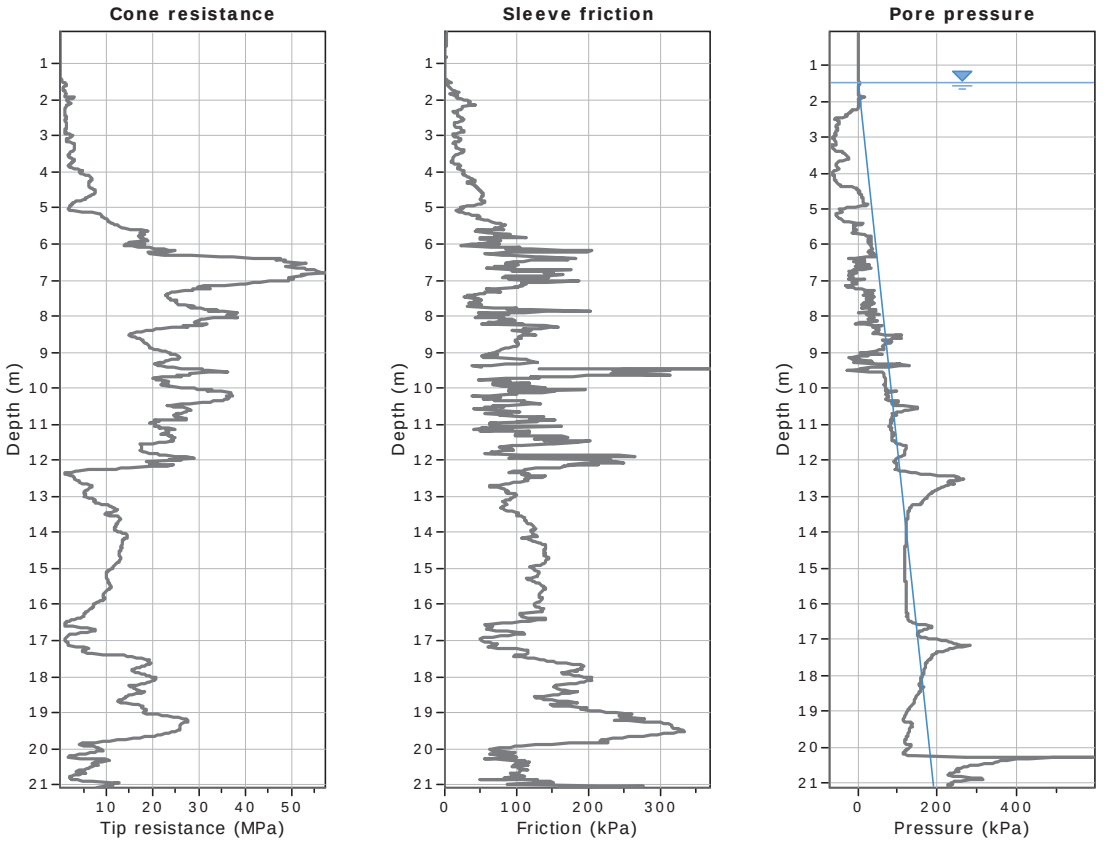

The plot below presents the cross correlation coeficient between the raw qc and fs values (as measured on the field). X axes presents the lag distance (one lag is the distance between two sucessive CPT measurements).

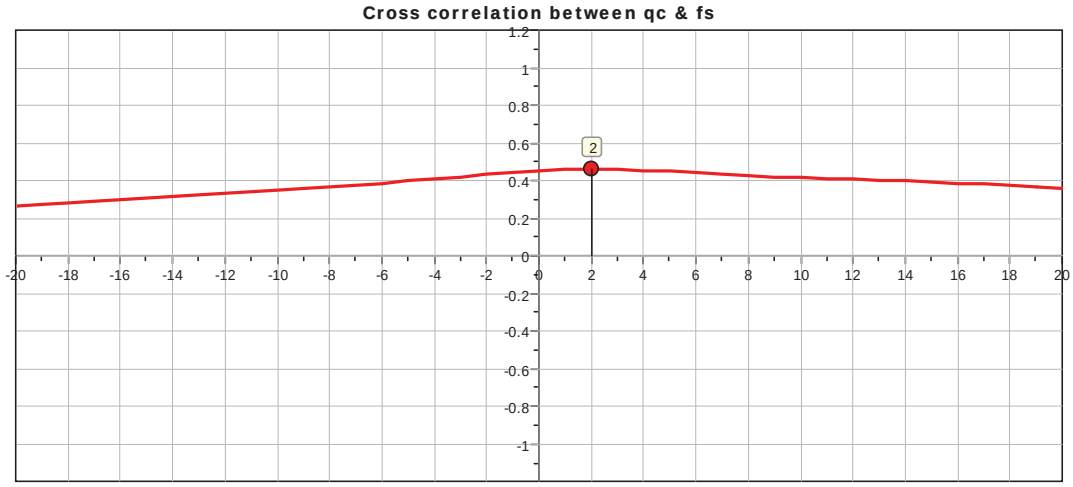

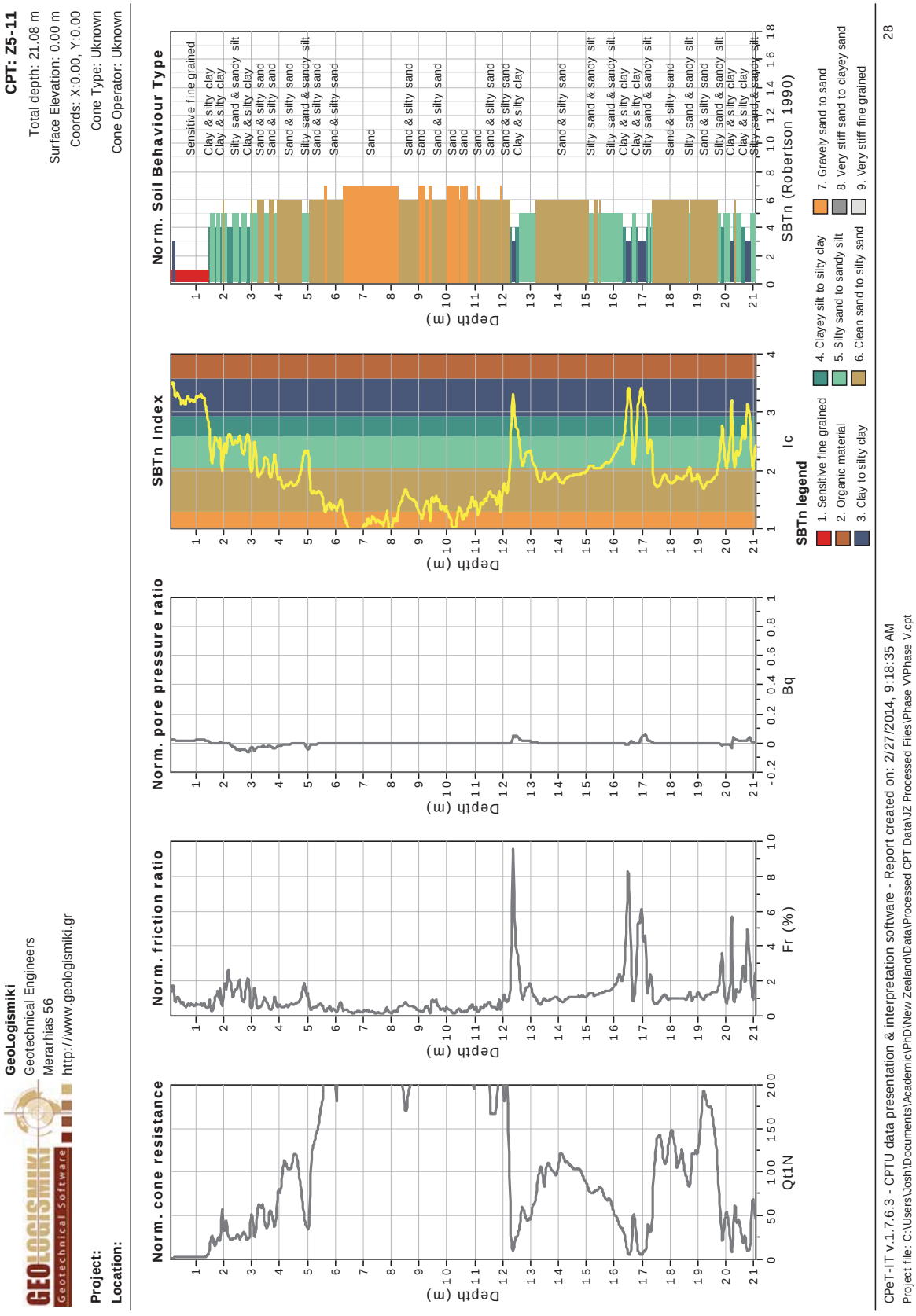
CPT: Z5-11
Total depth: 21.08 m
Surface Elevation: 0.00 m
Coords: X:0.00, Y:0.00
Cone Type: Uknown
Cone Operator: Uknown
GeoLogismiki
Geotechnical Engineers
Merarhias 56
http://www.geologismiki.gr
Project:
Location:
Norm. cone resistance
Qt1N
Norm. friction ratio
Fr (%)
Norm. pore pressure ratio
Bq
SBTn Index
Ic
Norm. Soil Behaviour Type
SBTn (Robertson 1990)
Depth (m)
SBTn legend
1. Sensitive fine grained
2. Organic material
3. Clay to silty clay
4. Clayey silt to silty clay
5. Silty sand to sandy silt
6. Clean sand to silty sand
7. Gravely sand to sand
8. Very stiff sand to clayey sand
9. Very stiff fine grained
CPeT-IT v.1.7.6.3 - CPTU data presentation & interpretation software - Report created on: 2/27/2014, 9:18:35 AM
Project file: C:\Users\Josh\Documents\Academic\PhD\New Zealand\Data\Processed CPT Data\JZ Processed Files\Phase V\Phase V.cpt
28

GeoLogismiki
Geotechnical Engineers
Merarhias 56
http://www.geologismiki.gr

CPT: Z5-12
Total depth: 20.08 m
Surface Elevation: 0.00 m
Coords: X:0.00, Y:0.00
Cone Type: Uknown
Cone Operator: Uknown

Project:
Location:

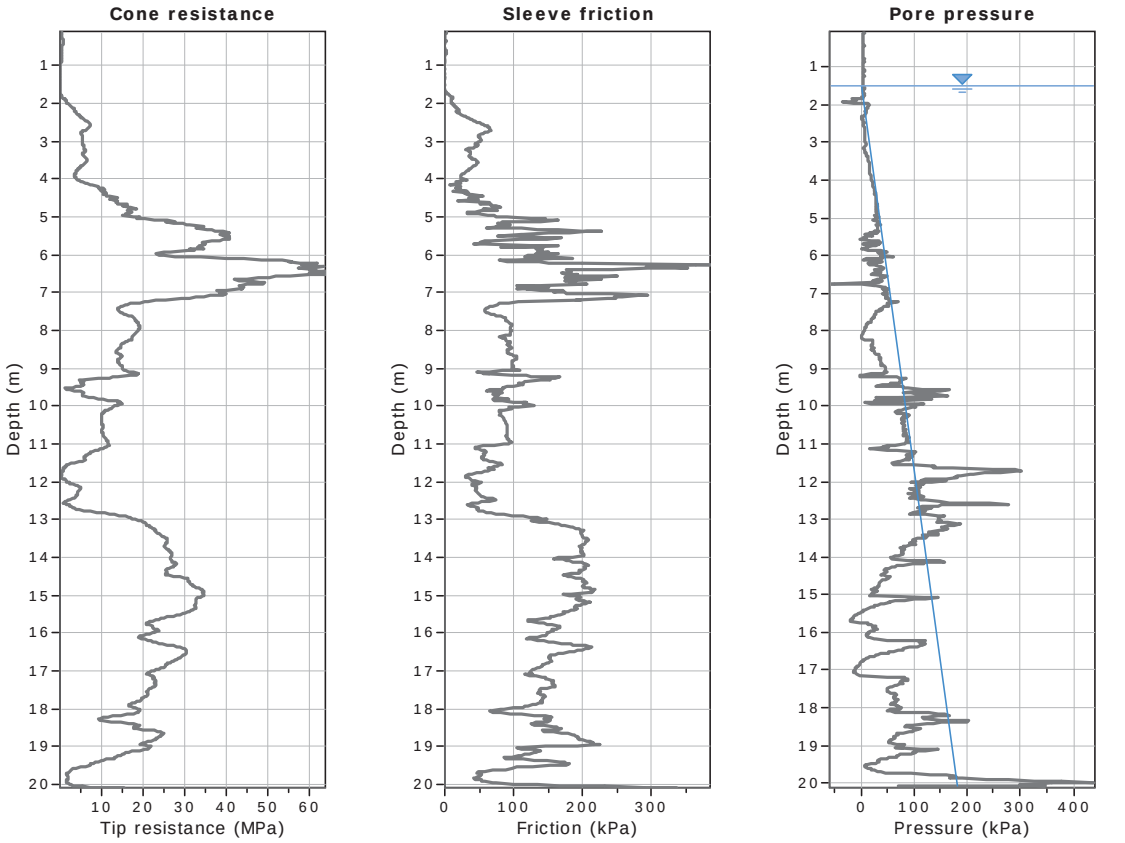

The plot below presents the cross correlation coeficient between the raw qc and fs values (as measured on the field). X axes presents the lag distance (one lag is the distance between two sucessive CPT measurements).

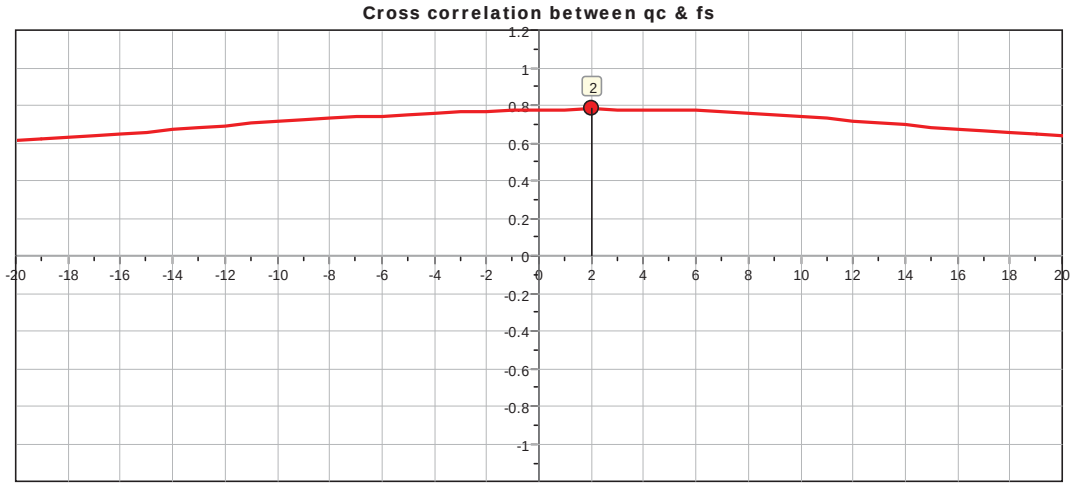

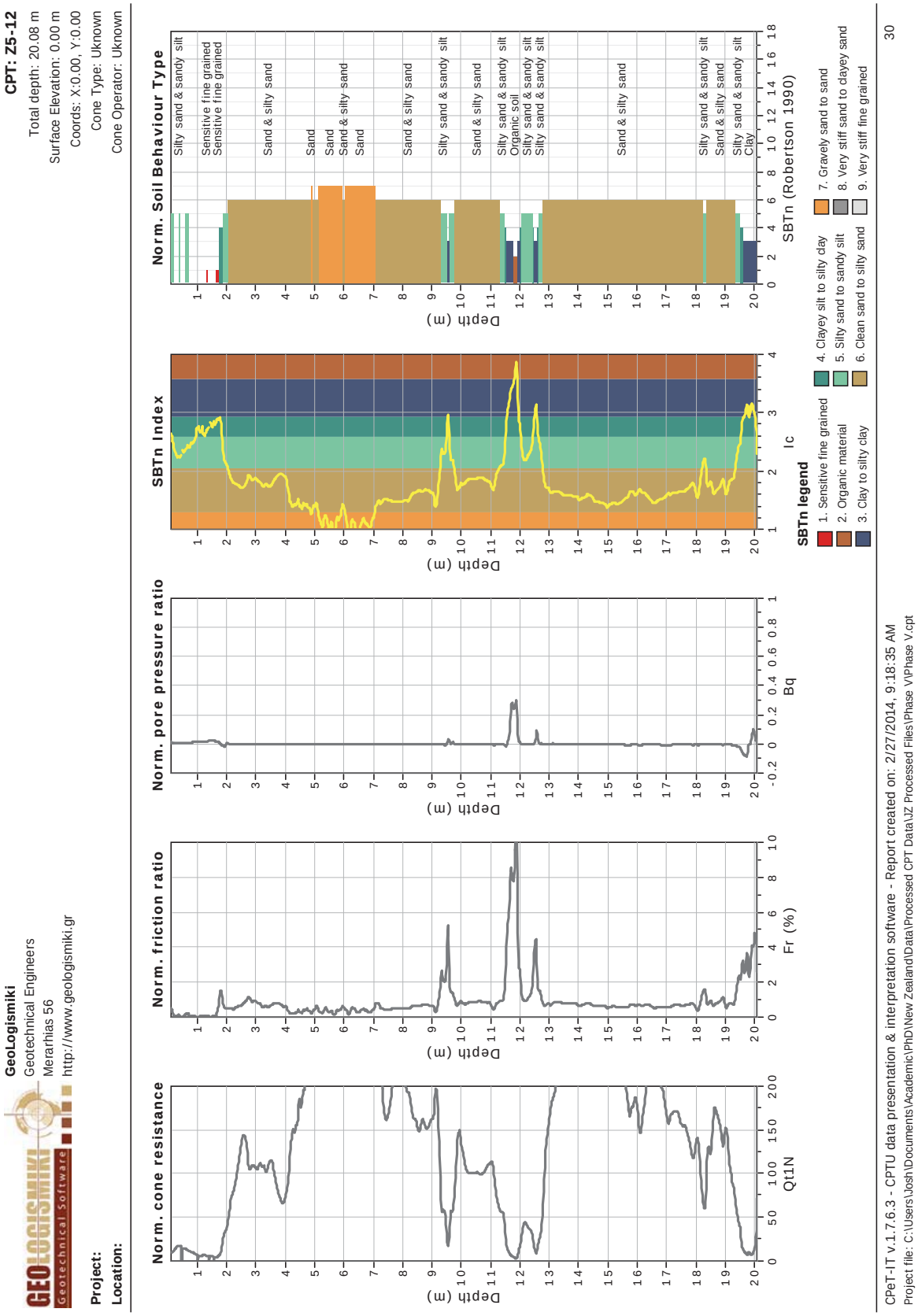
CPT: Z5-12
Total depth: 20.08 m
Surface Elevation: 0.00 m
Coords: X:0.00, Y:0.00
Cone Type: Uknown
Cone Operator: Uknown
GeoLogismiki
Geotechnical Engineers
Merarhias 56
http://www.geologismiki.gr
Project:
Location:
Norm. cone resistance
Qt1N
Norm. friction ratio
Fr (%)
Norm. pore pressure ratio
Bq
SBTn Index
Ic
Norm. Soil Behaviour Type
SBTn (Robertson 1990)
Depth (m)
SBTn legend
1. Sensitive fine grained
2. Organic material
3. Clay to silty clay
4. Clayey silt to silty clay
5. Silty sand to sandy silt
6. Clean sand to silty sand
7. Gravely sand to sand
8. Very stiff sand to clayey sand
9. Very stiff fine grained
CPeT-IT v.1.7.6.3 - CPTU data presentation & interpretation software - Report created on: 2/27/2014, 9:18:35 AM
Project file: C:\Users\Josh\Documents\Academic\PhD\New Zealand\Data\Processed CPT Data\JZ Processed Files\Phase V\Phase V.cpt
30

GeoLogismiki
Geotechnical Engineers
Merarhias 56
http://www.geologismiki.gr

CPT: Z8-1
Total depth: 7.03 m
Surface Elevation: 0.00 m
Coords: X:0.00, Y:0.00
Cone Type: Uknown
Cone Operator: Uknown

Project:
Location:

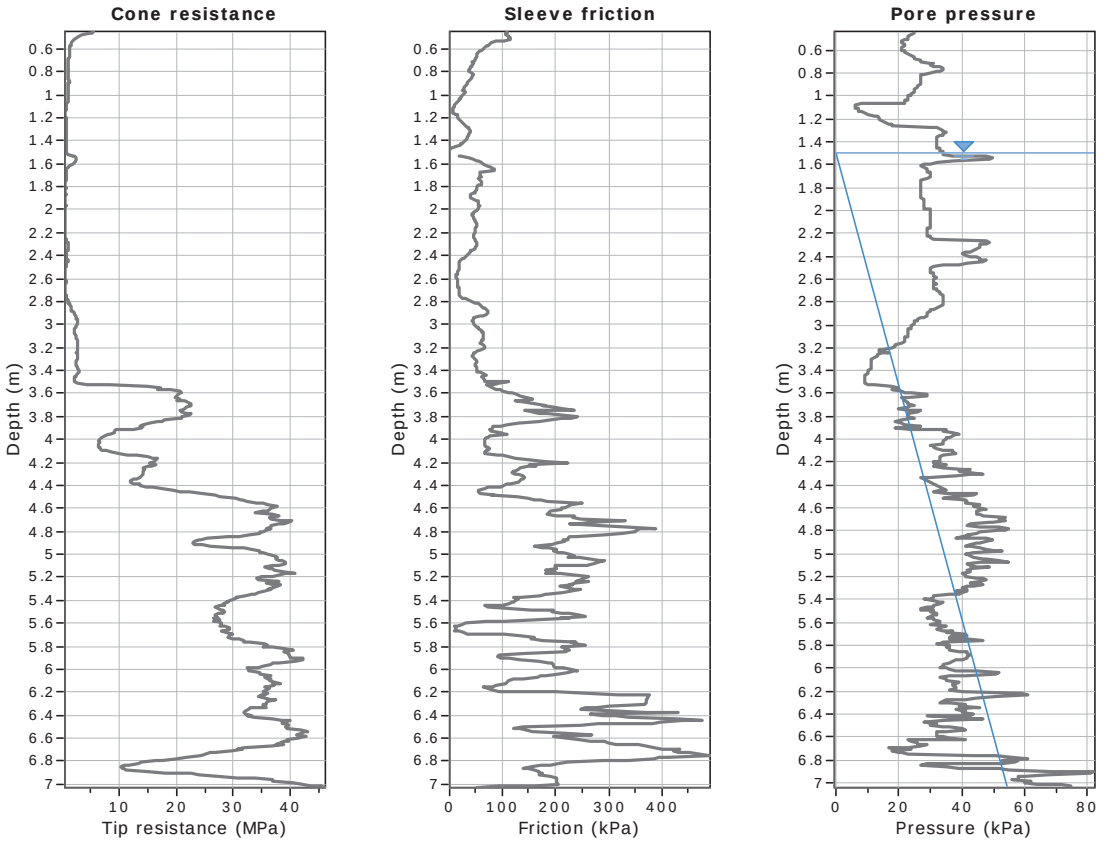

The plot below presents the cross correlation coeficient between the raw qc and fs values (as measured on the field). X axes presents the lag distance (one lag is the distance between two sucessive CPT measurements).

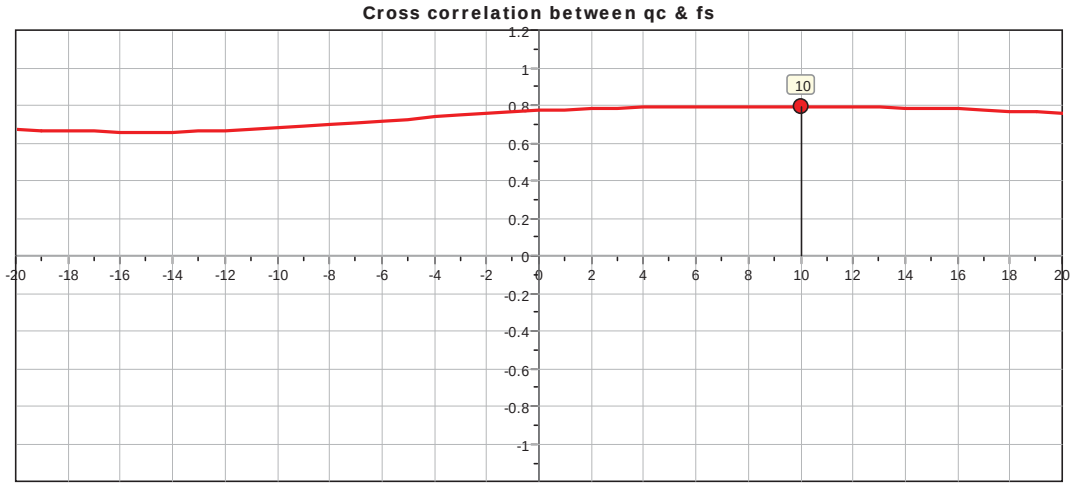

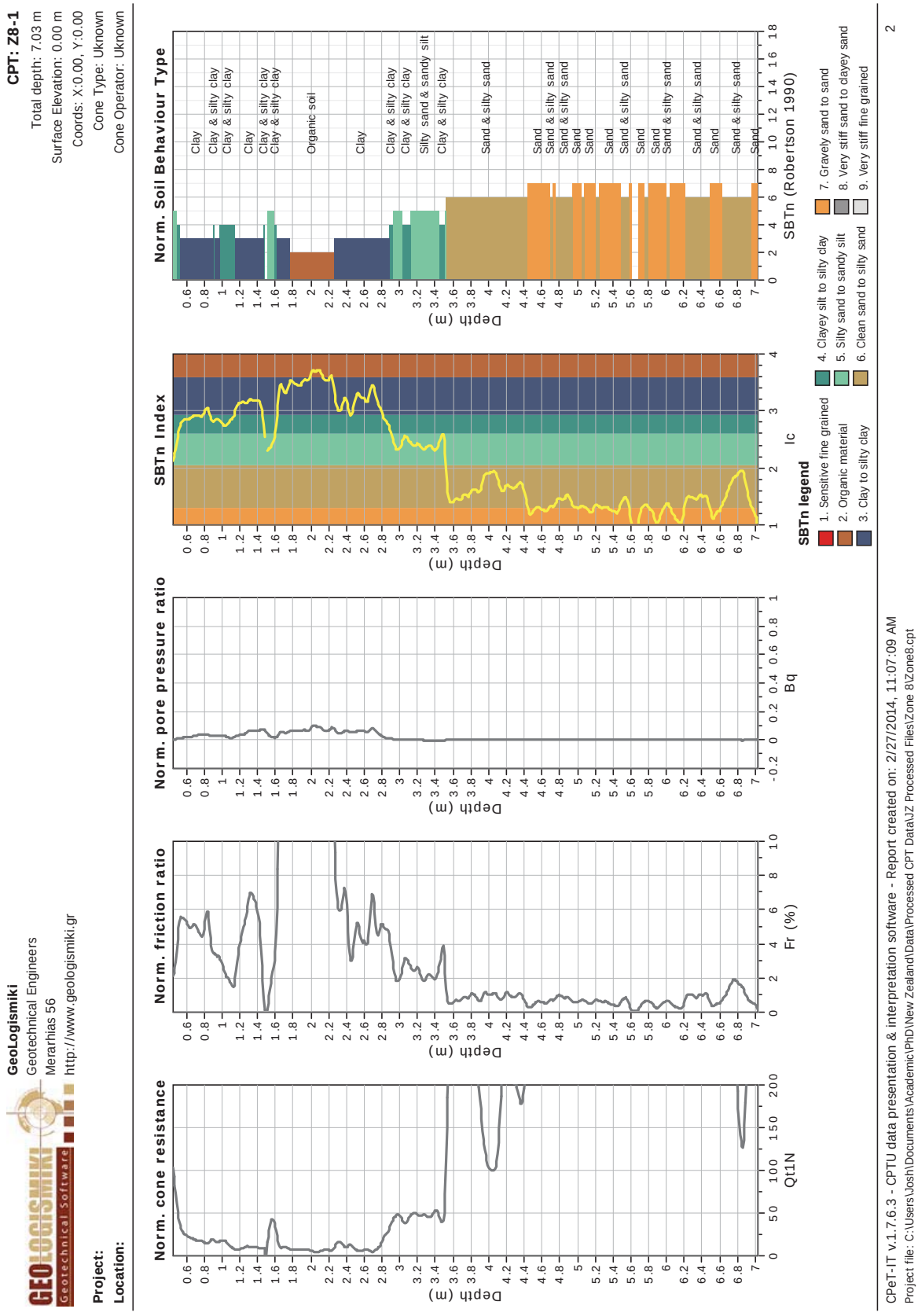
CPT: Z8-1
Total depth: 7.03 m
Surface Elevation: 0.00 m
Coords: X:0.00, Y:0.00
Cone Type: Uknown
Cone Operator: Uknown
GeoLogismiki
Geotechnical Engineers
Merarhias 56
http://www.geologismiki.gr
Project:
Location:
Norm. cone resistance
Norm. friction ratio
Norm. pore pressure ratio
SBTn Index
Norm. Soil Behaviour Type
SBTn legend
1. Sensitive fine grained
2. Organic material
3. Clay to silty clay
4. Clayey silt to silty clay
5. Silty sand to sandy silt
6. Clean sand to silty sand
7. Gravely sand to sand
8. Very stiff sand to clayey sand
9. Very stiff fine grained
CPeT-IT v.1.7.6.3 - CPTU data presentation & interpretation software - Report created on: 2/27/2014, 11:07:09 AM
Project file: C:\Users\Josh\Documents\Academic\PhD\New Zealand\Data\Processed CPT Data\JZ Processed Files\Zone 8\Zone8.cpt
2

GeoLogismiki
Geotechnical Engineers
Merarhias 56
http://www.geologismiki.gr

CPT: Z8-2
Total depth: 13.88 m
Surface Elevation: 0.00 m
Coords: X:0.00, Y:0.00
Cone Type: Uknown
Cone Operator: Uknown

Project:
Location:

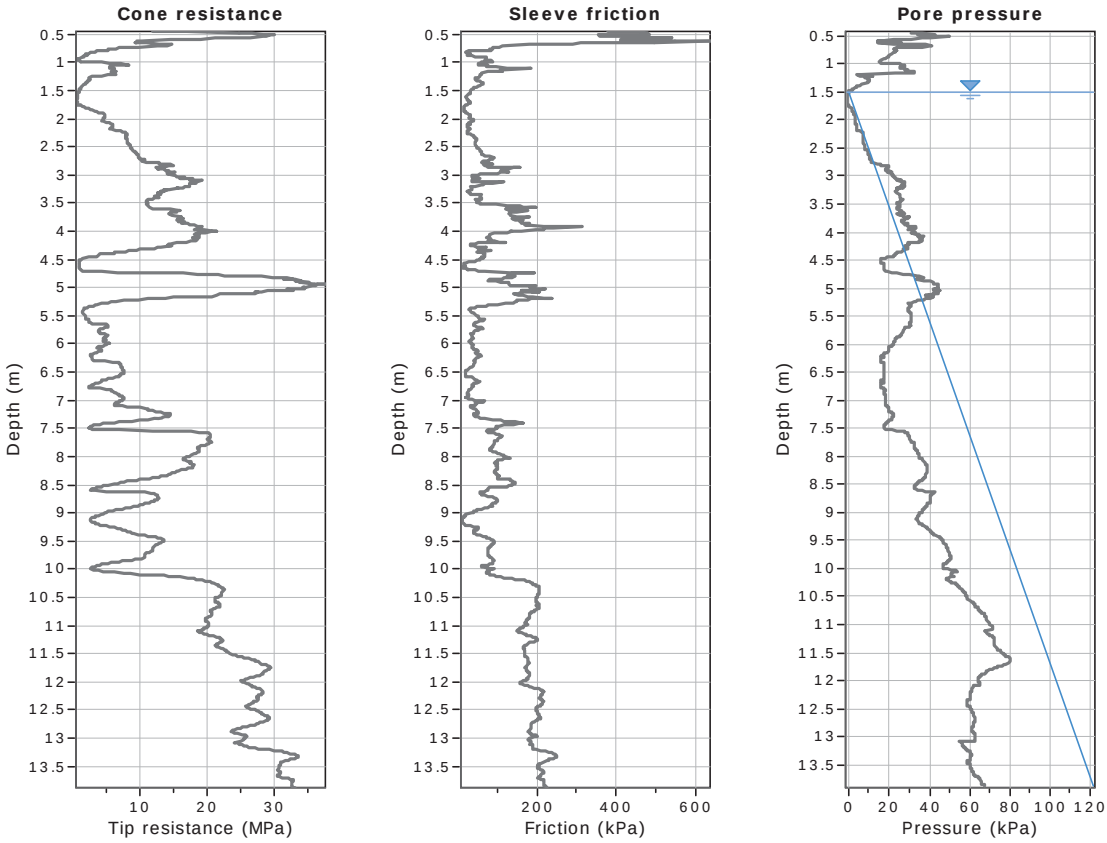

The plot below presents the cross correlation coeficient between the raw qc and fs values (as measured on the field). X axes presents the lag distance (one lag is the distance between two sucessive CPT measurements).

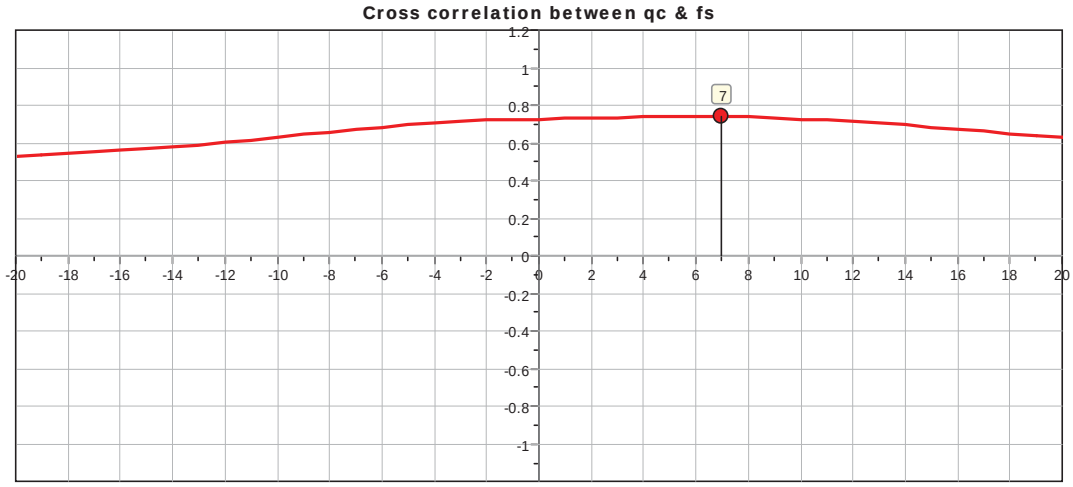

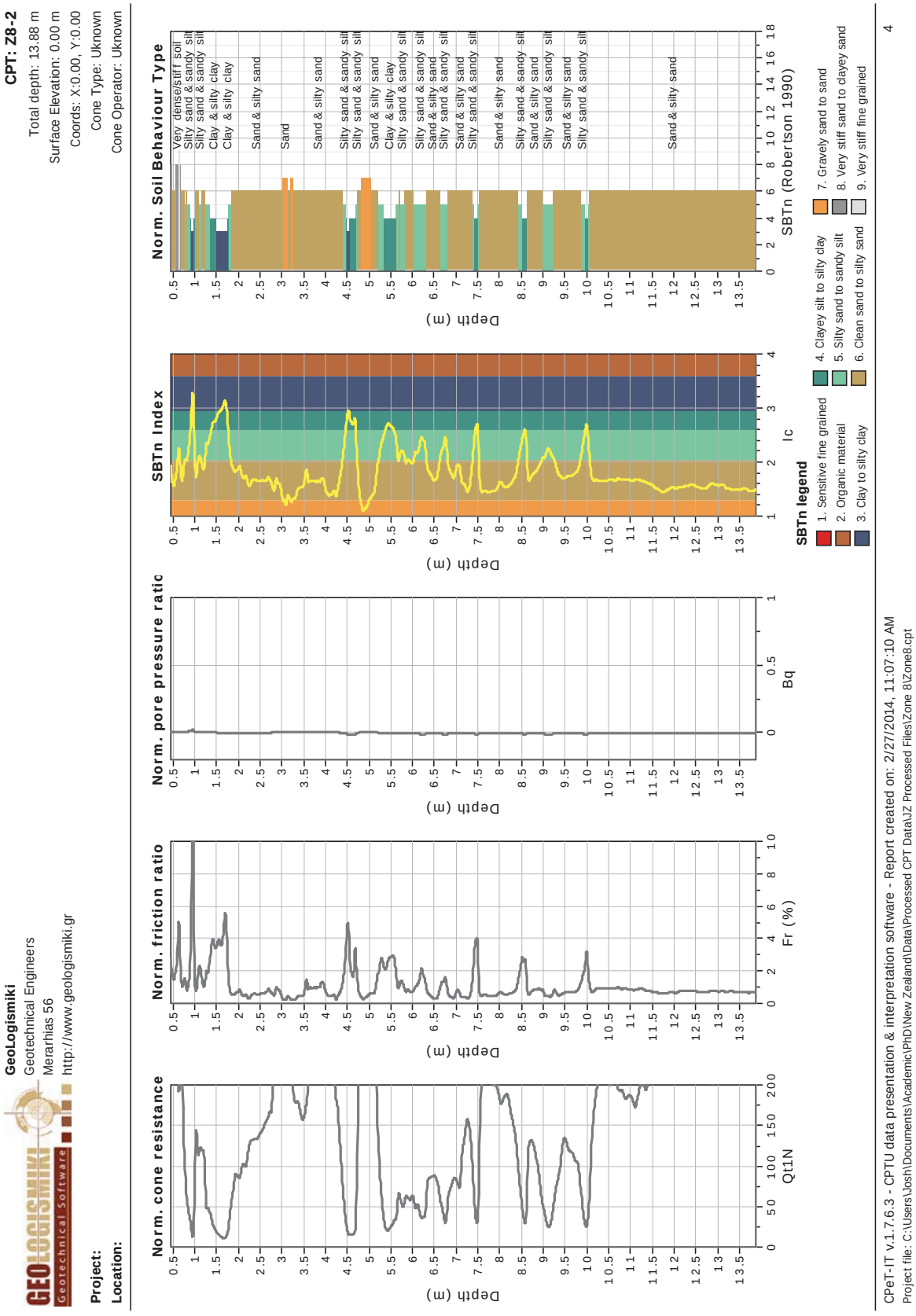
GeoLogismiki
Geotechnical Engineers
Merarchias 56
http://www.geologismiki.gr
Project:
Location:
CPT: Z8-2
Total depth: 13.88 m
Surface Elevation: 0.00 m
Coords: X:0.00, Y:0.00
Cone Type: Uknown
Cone Operator: Uknown
Norm. cone resistance
Qt1N
Norm. friction ratio
Fr (%)
Norm. pore pressure ratio
Bq
SBTn Index
Ic
Norm. Soil Behaviour Type
SBTn (Robertson 1990)
Depth (m)
SBTn legend
1. Sensitive fine grained
2. Organic material
3. Clay to silty clay
4. Clayey silt to silty clay
5. Silty sand to sandy silt
6. Clean sand to silty sand
7. Gravely sand to sand
8. Very stiff sand to clayey sand
9. Very stiff fine grained
CPeT-IT v.1.7.6.3 - CPTU data presentation & interpretation software - Report created on: 2/27/2014, 11:07:10 AM
Project file: C:\Users\Josh\Documents\Academic\PhD\New Zealand\Data\Processed CPT Data\JZ Processed Files\Zone 8\Zone8.cpt
4

GeoLogismiki
Geotechnical Engineers
Merarhias 56
http://www.geologismiki.gr

CPT: Z8-3
Total depth: 3.84 m
Surface Elevation: 0.00 m
Coords: X:0.00, Y:0.00
Cone Type: Uknown
Cone Operator: Uknown

Project:
Location:

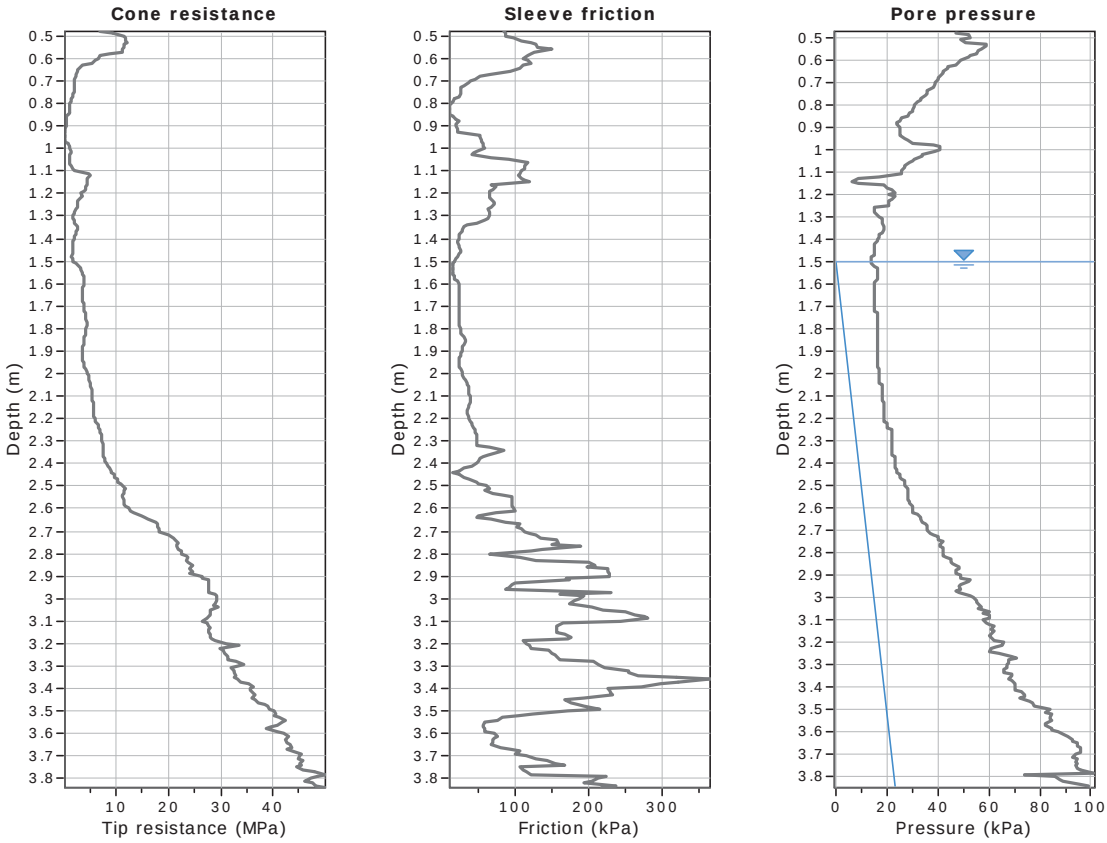

The plot below presents the cross correlation coeficient between the raw qc and fs values (as measured on the field). X axes presents the lag distance (one lag is the distance between two sucessive CPT measurements).

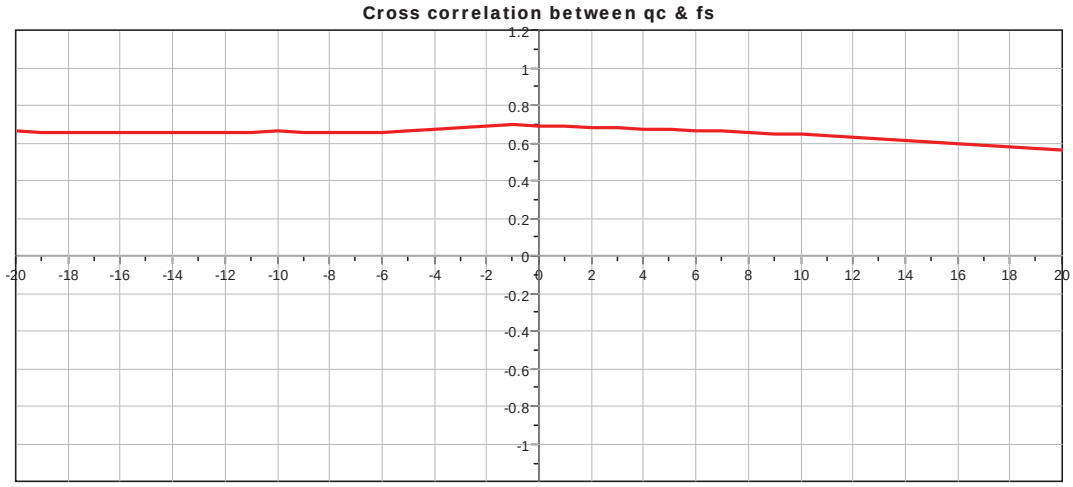

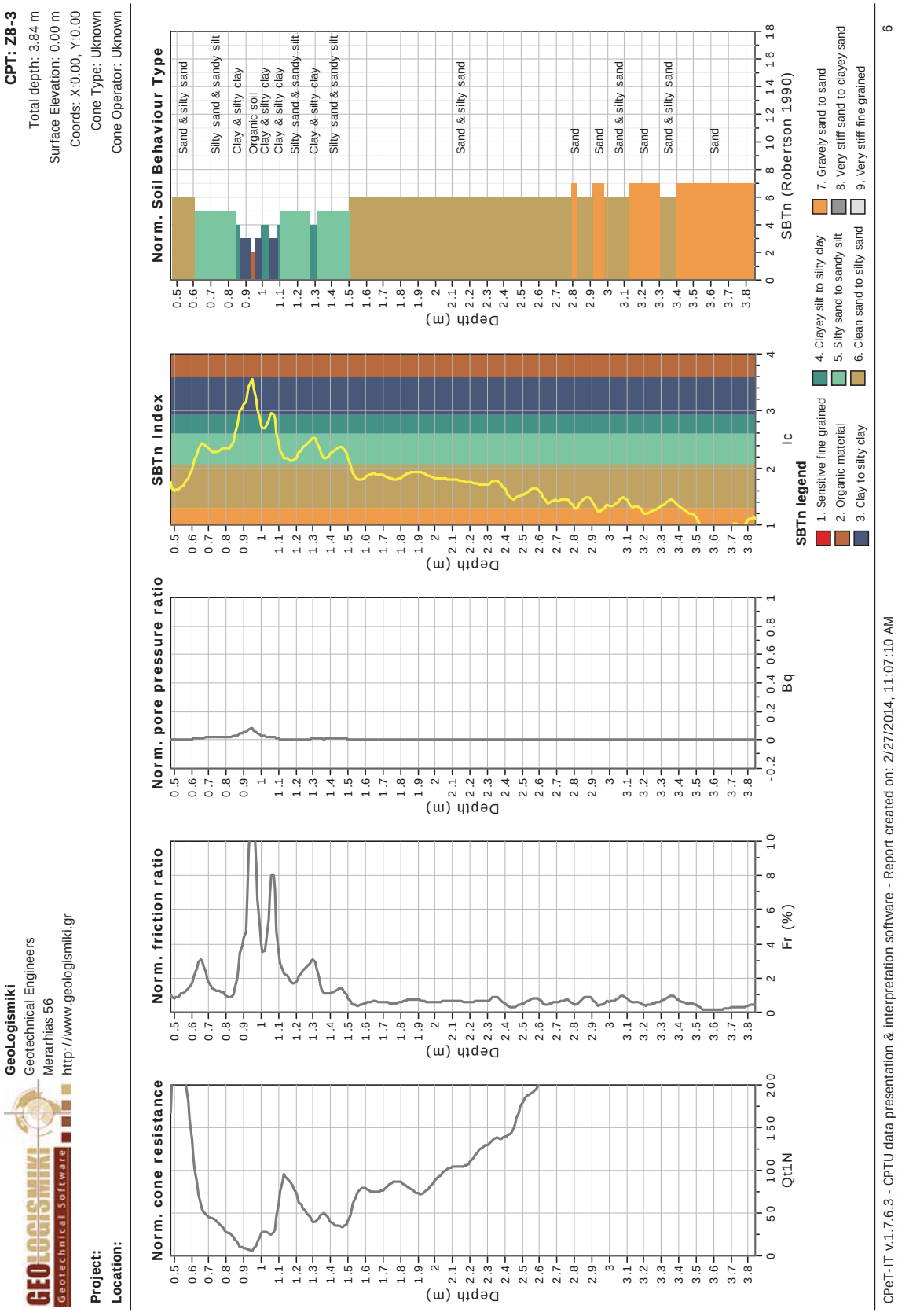
CPT: Z8-3
Total depth: 3.84 m
Surface Elevation: 0.00 m
Coords: X:0.00, Y:0.00
Cone Type: Uknown
Cone Operator: Uknown
GeoLogismiki
Geotechnical Engineers
Merarhias 56
http://www.geologismiki.gr
Project:
Location:
Norm. cone resistance
Norm. friction ratio
Norm. pore pressure ratio
SBTn Index
Norm. Soil Behaviour Type
Depth (m)
Qt1N
Fr (%)
Bq
Ic
SBTn (Robertson 1990)
Sand & silty sand
Silty sand & sandy silt
Clay & silty clay
Organic soil
Sand
SBTn legend
1. Sensitive fine grained
2. Organic material
3. Clay to silty clay
4. Clayey silt to silty clay
5. Silty sand to sandy silt
6. Clean sand to silty sand
7. Gravely sand to sand
8. Very stiff sand to clayey sand
9. Very stiff fine grained
CPeT-IT v.1.7.6.3 - CPTU data presentation & interpretation software - Report created on: 2/27/2014, 11:07:10 AM
Project file: C:\Users\Josh\Documents\Academic\PhD\New Zealand\Data\Processed CPT Data\JZ Processed Files\Zone 8\Zone8.cpt
6

GeoLogismiki
Geotechnical Engineers
Merarhias 56
http://www.geologismiki.gr

CPT: Z8-4
Total depth: 20.54 m
Surface Elevation: 0.00 m
Coords: X:0.00, Y:0.00
Cone Type: Uknown
Cone Operator: Uknown

Project:
Location:

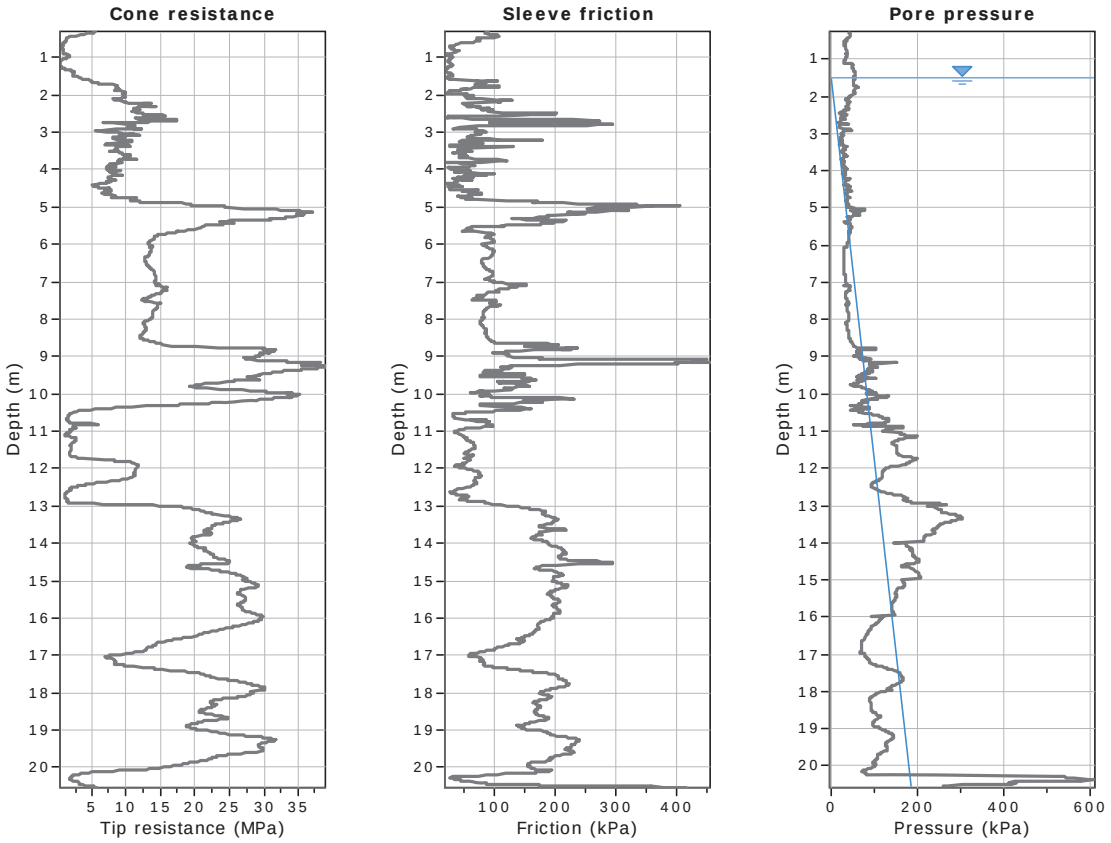

The plot below presents the cross correlation coeficient between the raw qc and fs values (as measured on the field). X axes presents the lag distance (one lag is the distance between two sucessive CPT measurements).

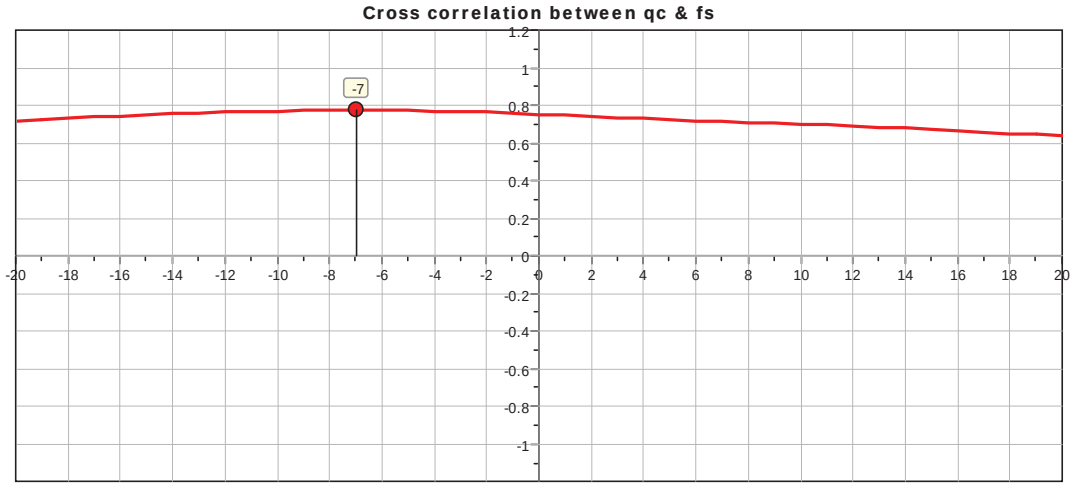

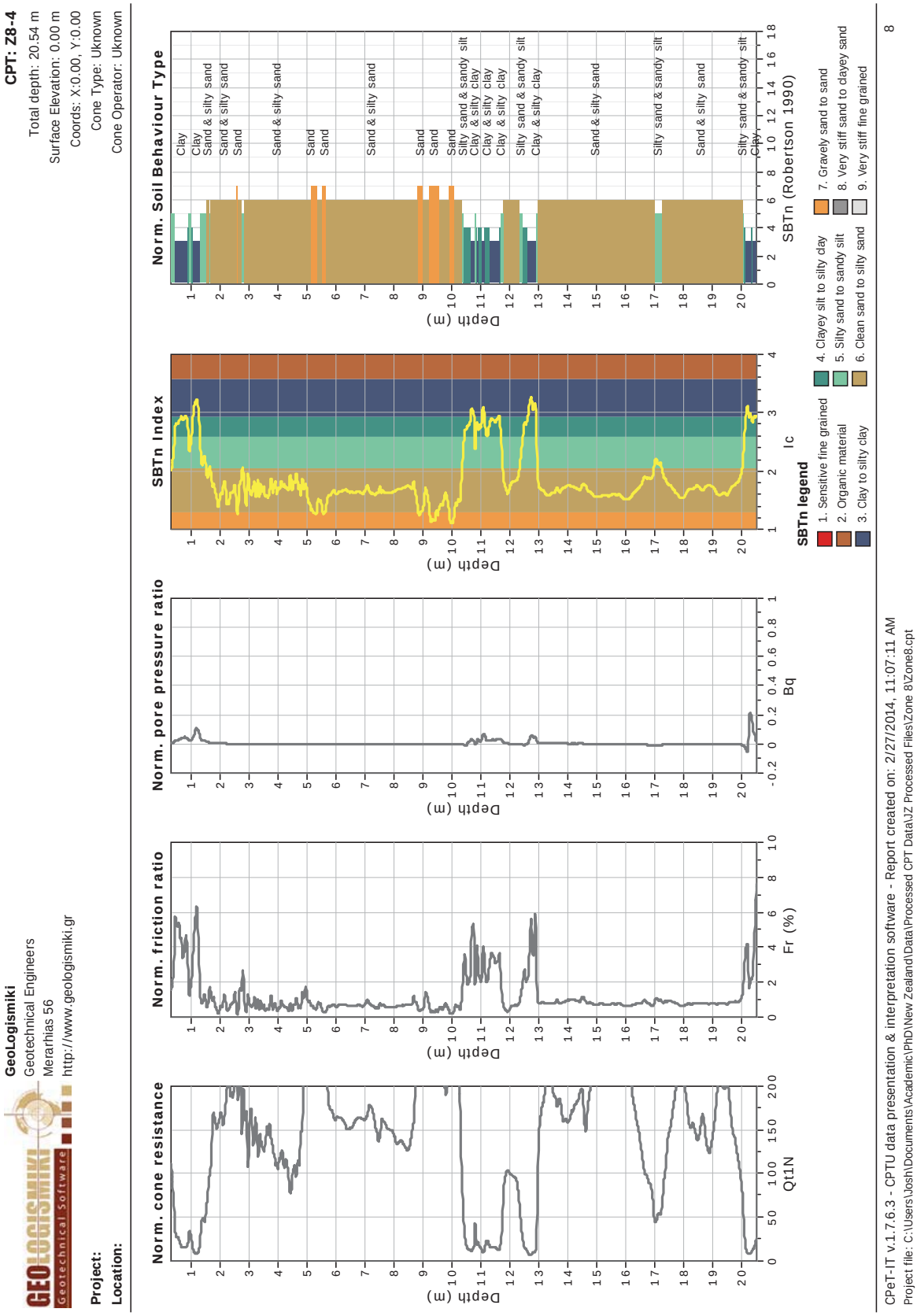
CPT: Z8-4
Total depth: 20.54 m
Surface Elevation: 0.00 m
Coords: X:0.00, Y:0.00
Cone Type: Uknown
Cone Operator: Uknown
GeoLogismiki
Geotechnical Engineers
Merarhias 56
http://www.geologismiki.gr
Project:
Location:
Norm. cone resistance
Qt1N
Norm. friction ratio
Fr (%)
Norm. pore pressure ratio
Bq
SBTn Index
Ic
Norm. Soil Behaviour Type
SBTn (Robertson 1990)
Depth (m)
SBTn legend
1. Sensitive fine grained
2. Organic material
3. Clay to silty clay
4. Clayey silt to silty clay
5. Silty sand to sandy silt
6. Clean sand to silty sand
7. Gravely sand to sand
8. Very stiff sand to clayey sand
9. Very stiff fine grained
CPeT-IT v.1.7.6.3 - CPTU data presentation & interpretation software - Report created on: 2/27/2014, 11:07:11 AM
Project file: C:\Users\Josh\Documents\Academic\PhD\New Zealand\Data\Processed CPT Data\JZ Processed Files\Zone 8\Zone8.cpt
8

GeoLogismiki
Geotechnical Engineers
Merarhias 56
http://www.geologismiki.gr

CPT: Z8-6
Total depth: 17.76 m
Surface Elevation: 0.00 m
Coords: X:0.00, Y:0.00
Cone Type: Uknown
Cone Operator: Uknown

Project:
Location:

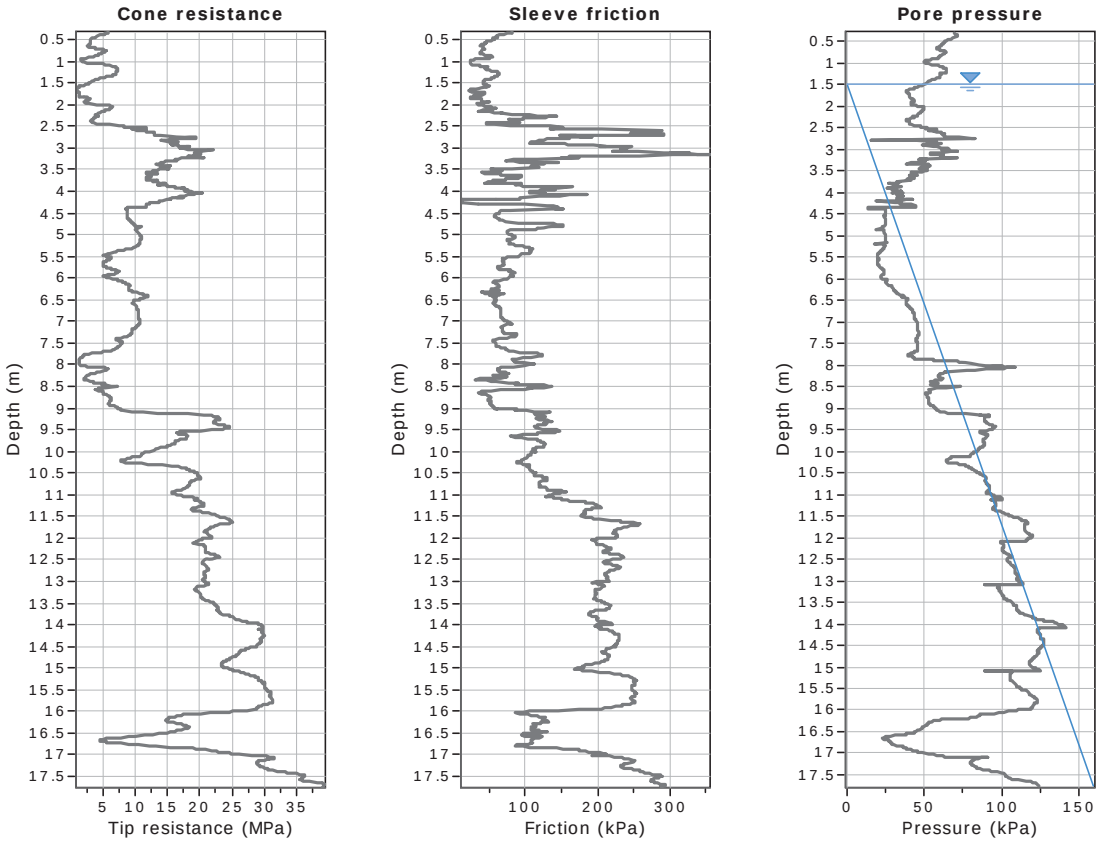

The plot below presents the cross correlation coeficient between the raw qc and fs values (as measured on the field). X axes presents the lag distance (one lag is the distance between two sucessive CPT measurements).

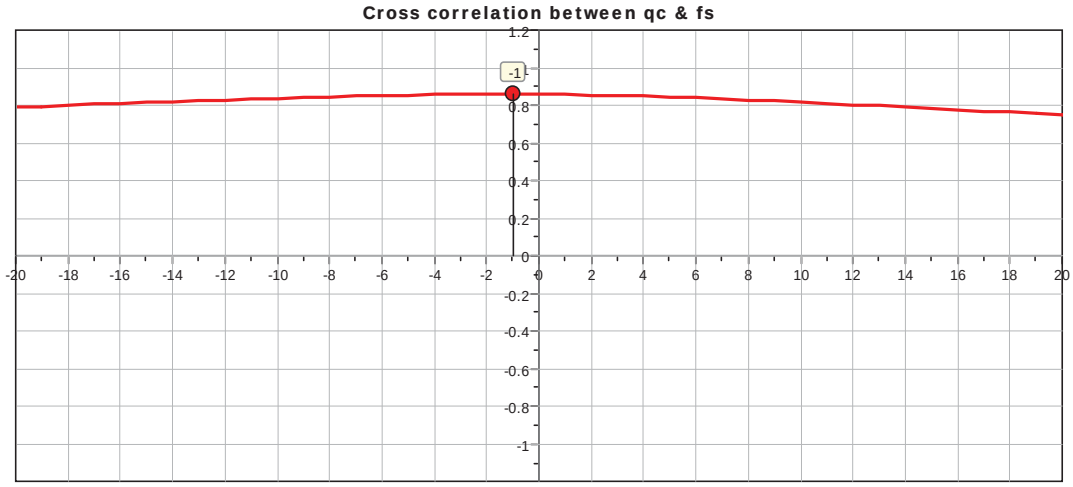

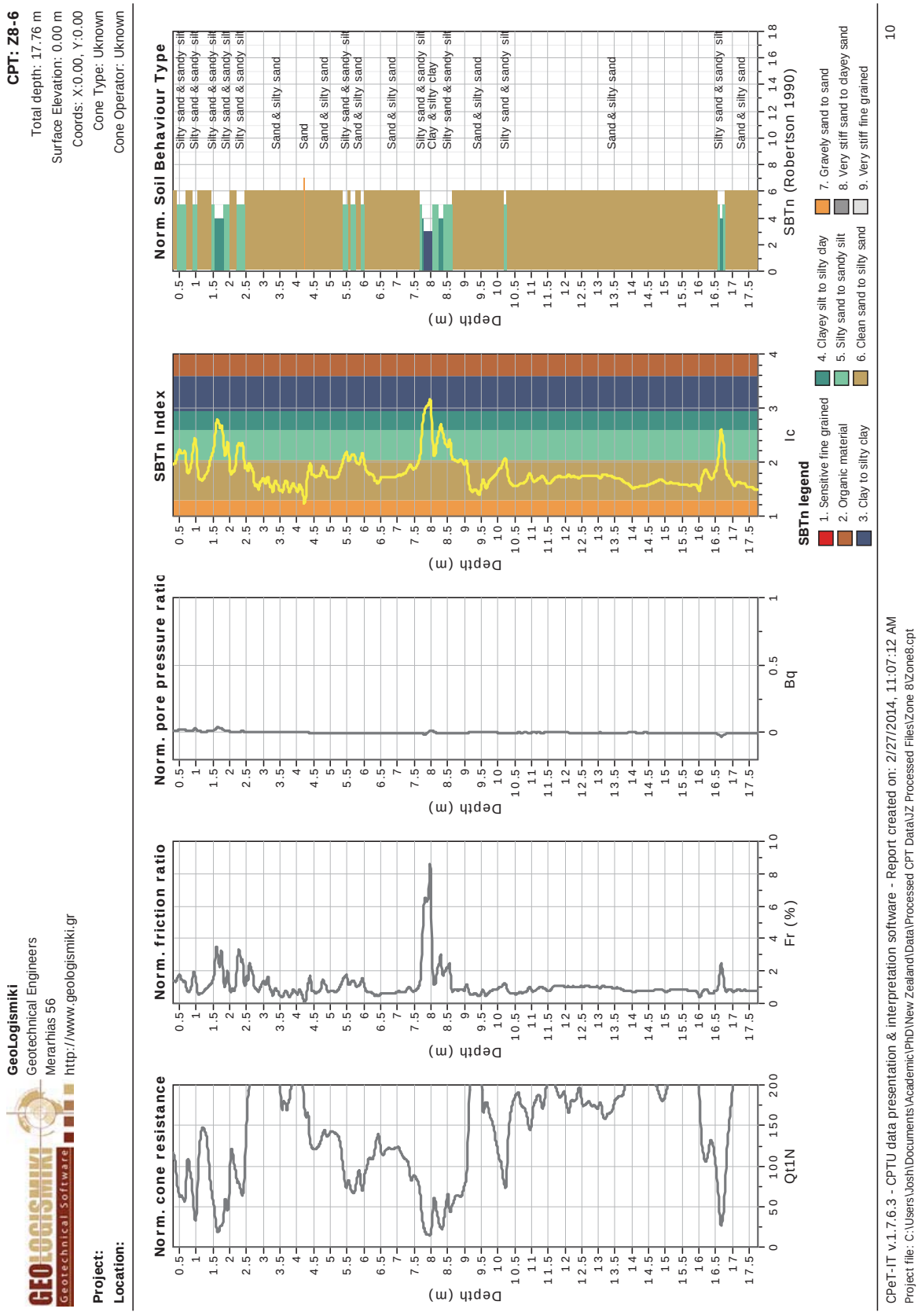
CPT: Z8-6
Total depth: 17.76 m
Surface Elevation: 0.00 m
Coords: X:0.00, Y:0.00
Cone Type: Uknown
Cone Operator: Uknown
GeoLogismiki
Geotechnical Engineers
Merarhias 56
http://www.geologismiki.gr
Project:
Location:
Norm. cone resistance
Qt1N
Norm. friction ratio
Fr (%)
Norm. pore pressure ratio
Bq
SBTn Index
Ic
Norm. Soil Behaviour Type
SBTn (Robertson 1990)
Depth (m)
SBTn legend
1. Sensitive fine grained
2. Organic material
3. Clay to silty clay
4. Clayey silt to silty clay
5. Silty sand to sandy silt
6. Clean sand to silty sand
7. Gravely sand to sand
8. Very stiff sand to clayey sand
9. Very stiff fine grained
CPeT-IT v.1.7.6.3 - CPTU data presentation & interpretation software - Report created on: 2/27/2014, 11:07:12 AM
Project file: C:\Users\Josh\Documents\Academic\PhD\New Zealand\Data\Processed CPT Data\JZ Processed Files\Zone 8\Zone8.cpt
10

GeoLogismiki
Geotechnical Engineers
Merarhias 56
http://www.geologismiki.gr

CPT: Z8-7
Total depth: 10.04 m
Surface Elevation: 0.00 m
Coords: X:0.00, Y:0.00
Cone Type: Uknown
Cone Operator: Uknown

Project:
Location:

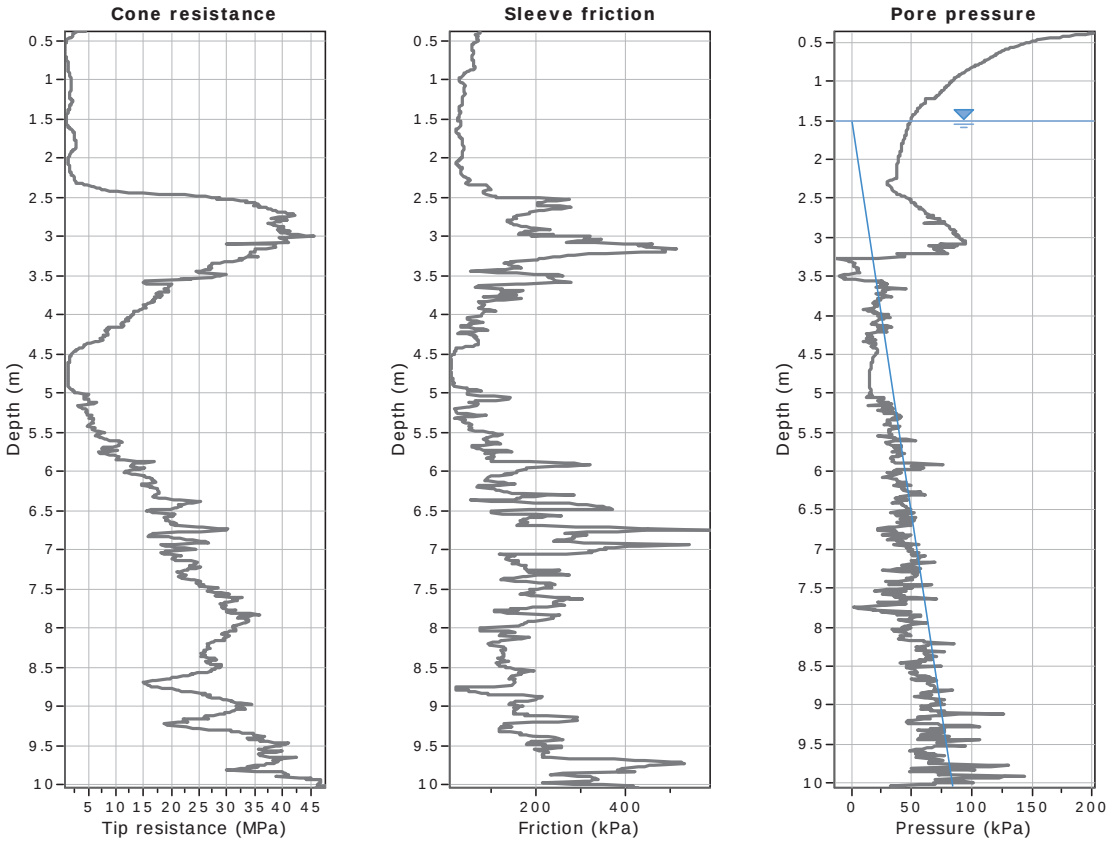

The plot below presents the cross correlation coeficient between the raw qc and fs values (as measured on the field). X axes presents the lag distance (one lag is the distance between two sucessive CPT measurements).

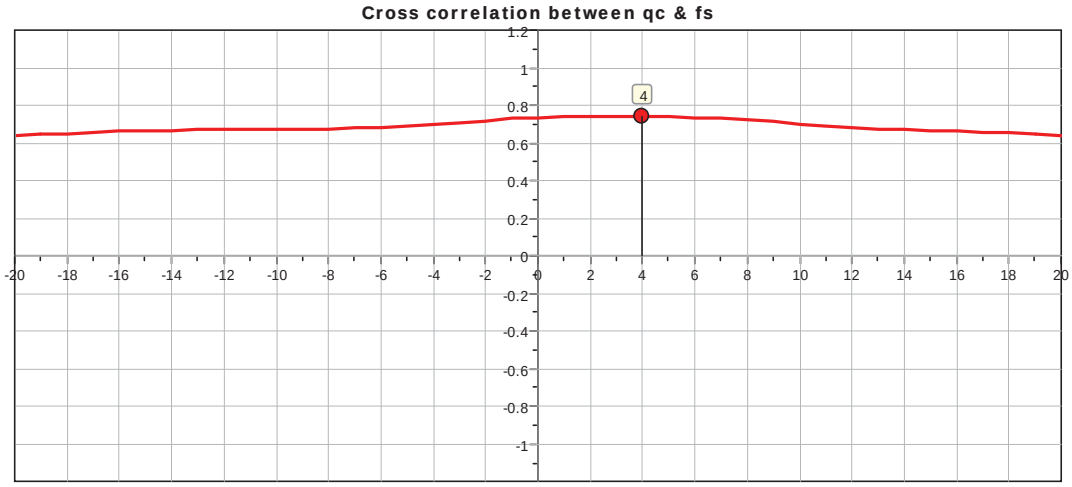

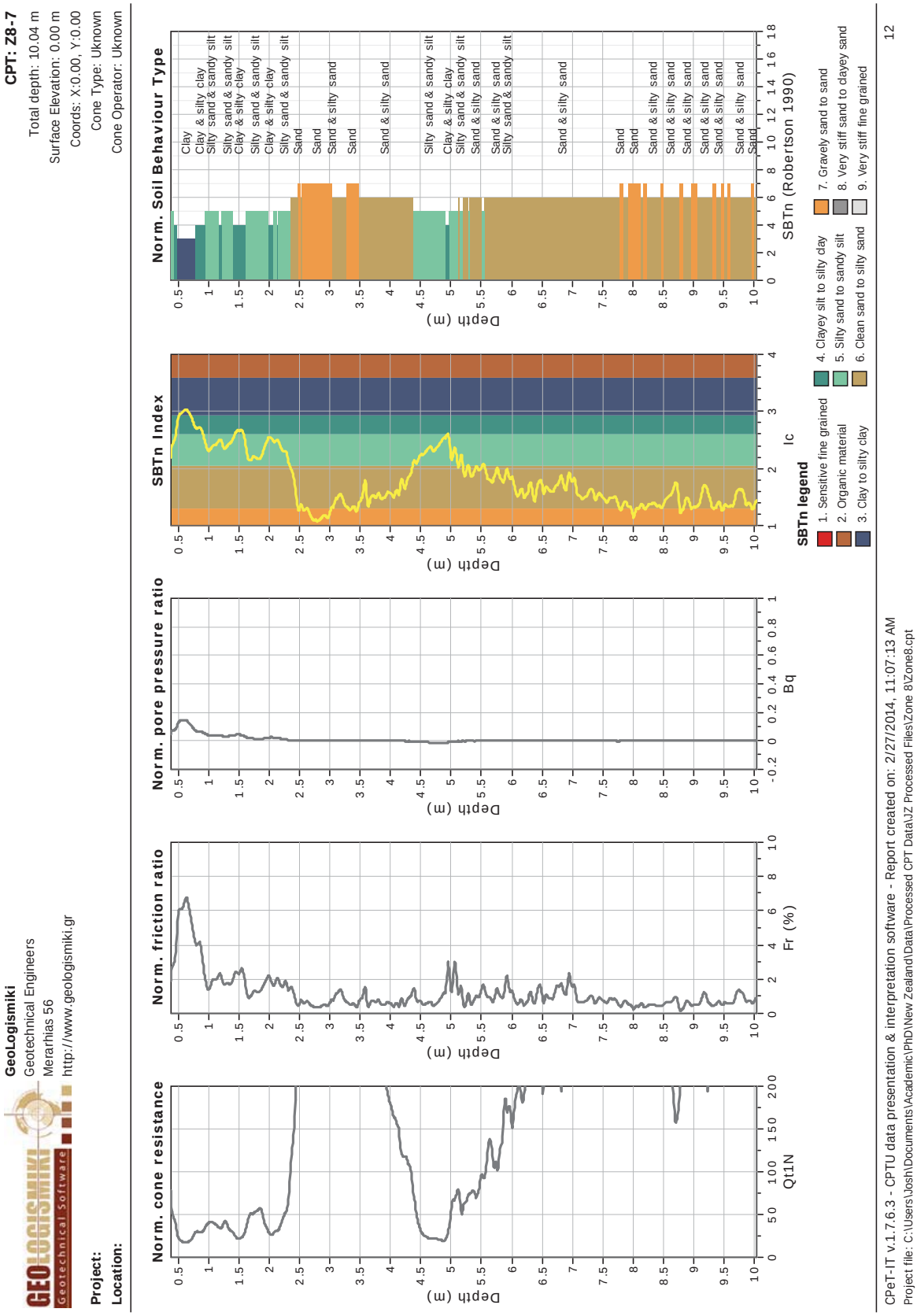
CPT: Z8-7
Total depth: 10.04 m
Surface Elevation: 0.00 m
Coords: X:0.00, Y:0.00
Cone Type: Uknown
Cone Operator: Uknown
GeoLogismiki
Geotechnical Engineers
Merarhias 56
http://www.geologismiki.gr
Project:
Location:
Norm. cone resistance
Norm. friction ratio
Norm. pore pressure ratio
SBTn Index
Norm. Soil Behaviour Type
SBTn legend
1. Sensitive fine grained
2. Organic material
3. Clay to silty clay
4. Clayey silt to silty clay
5. Silty sand to sandy silt
6. Clean sand to silty sand
7. Gravely sand to sand
8. Very stiff sand to clayey sand
9. Very stiff fine grained
CPeT-IT v.1.7.6.3 - CPTU data presentation & interpretation software - Report created on: 2/27/2014, 11:07:13 AM
Project file: C:\Users\Josh\Documents\Academic\PhD\New Zealand\Data\Processed CPT Data\JZ Processed Files\Zone 8\Zone8.cpt
12

GeoLogismiki
Geotechnical Engineers
Merarhias 56
http://www.geologismiki.gr

CPT: Z8-8
Total depth: 21.28 m
Surface Elevation: 0.00 m
Coords: X:0.00, Y:0.00
Cone Type: Uknown
Cone Operator: Uknown

Project:
Location:

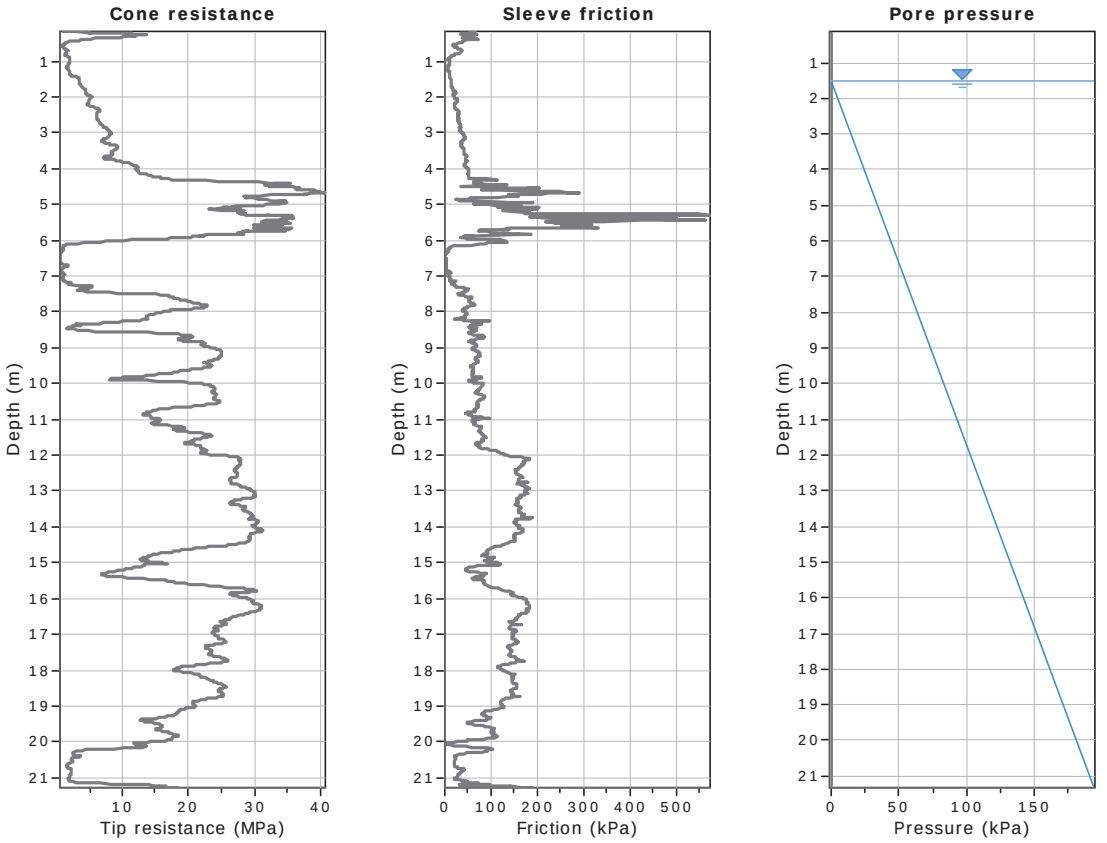

The plot below presents the cross correlation coeficient between the raw qc and fs values (as measured on the field). X axes presents the lag distance (one lag is the distance between two sucessive CPT measurements).

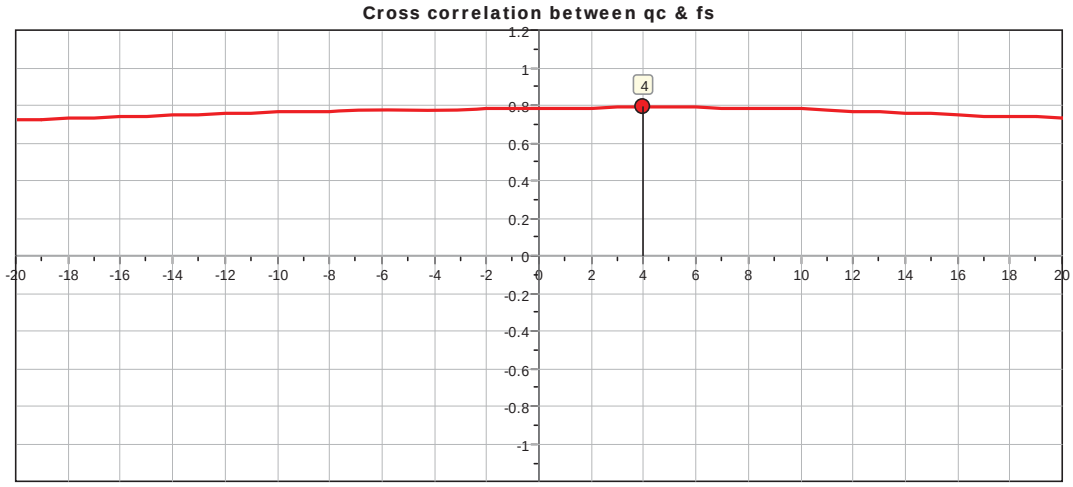

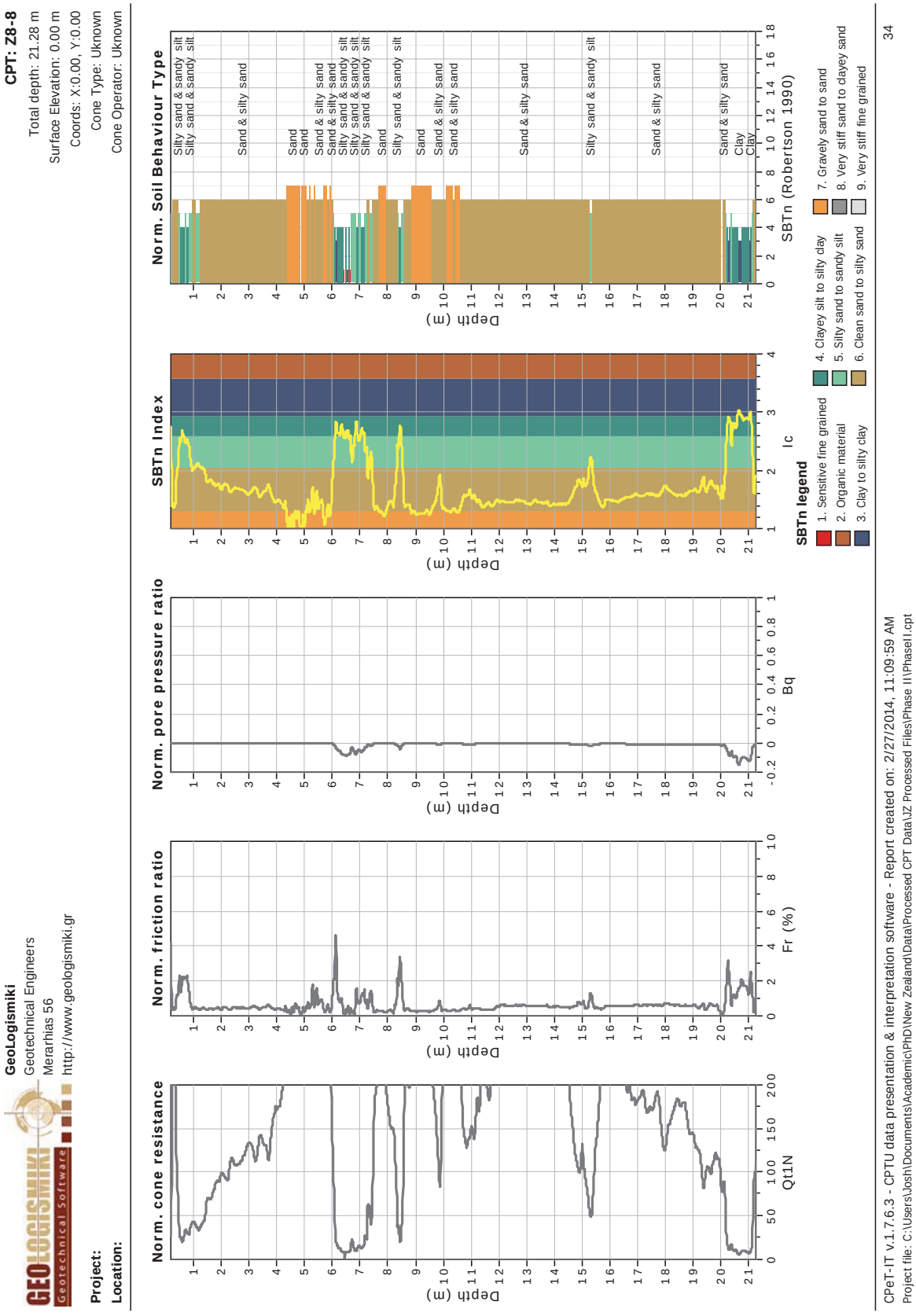
CPT: Z8-8
Total depth: 21.28 m
Surface Elevation: 0.00 m
Coords: X:0.00, Y:0.00
Cone Type: Uknown
Cone Operator: Uknown
GeoLogismiki
Geotechnical Engineers
Merarhias 56
http://www.geologismiki.gr
Project:
Location:
Norm. cone resistance
Qt1N
Norm. friction ratio
Fr (%)
Norm. pore pressure ratio
Bq
SBTn Index
Ic
Norm. Soil Behaviour Type
SBTn (Robertson 1990)
Depth (m)
SBTn legend
1. Sensitive fine grained
2. Organic material
3. Clay to silty clay
4. Clayey silt to silty clay
5. Silty sand to sandy silt
6. Clean sand to silty sand
7. Gravely sand to sand
8. Very stiff sand to clayey sand
9. Very stiff fine grained
CPeT-IT v.1.7.6.3 - CPTU data presentation & interpretation software - Report created on: 2/27/2014, 11:09:59 AM
Project file: C:\Users\Josh\Documents\Academic\PhD\New Zealand\Data\Processed CPT Data\JZ Processed Files\Phase II\PhaseII.cpt
34

GeoLogismiki
Geotechnical Engineers
Merarhias 56
http://www.geologismiki.gr

CPT: Z8-9
Total depth: 17.58 m
Surface Elevation: 0.00 m
Coords: X:0.00, Y:0.00
Cone Type: Uknown
Cone Operator: Uknown

Project:
Location:

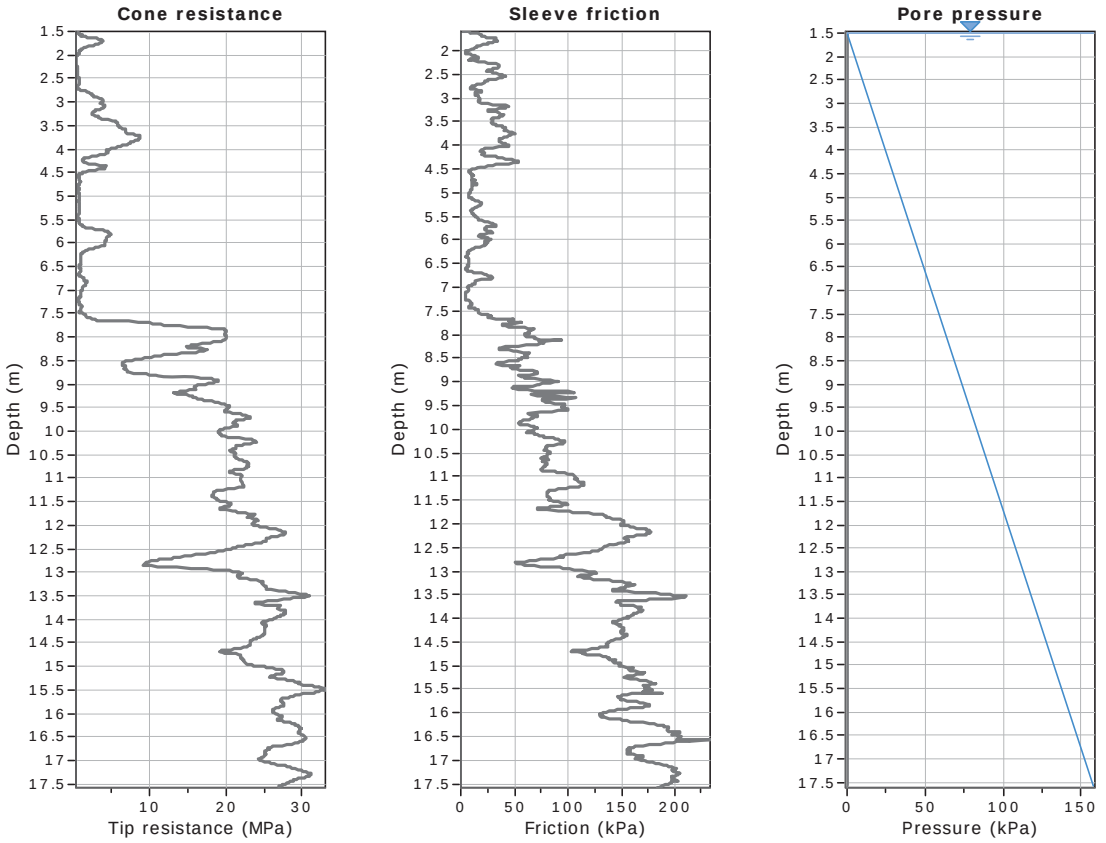

The plot below presents the cross correlation coeficient between the raw qc and fs values (as measured on the field). X axes presents the lag distance (one lag is the distance between two sucessive CPT measurements).

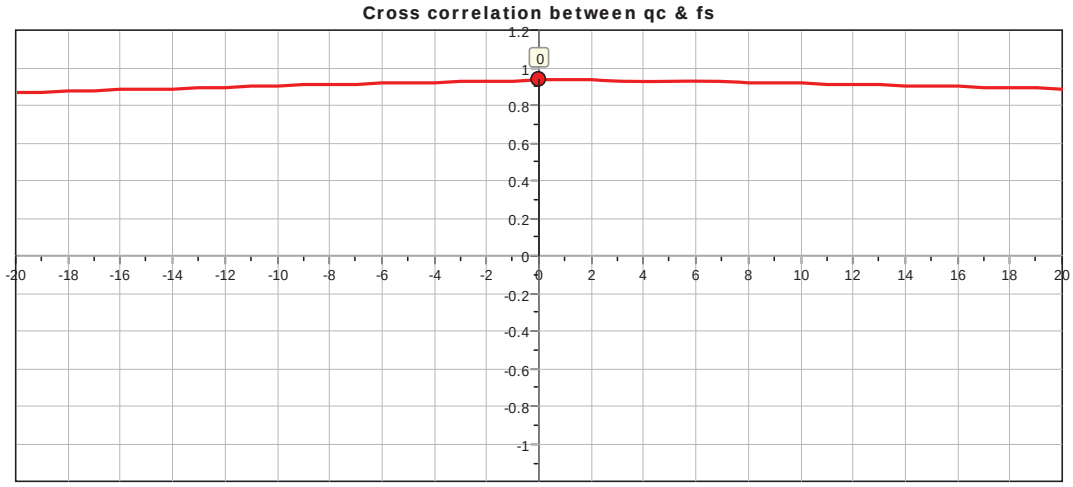

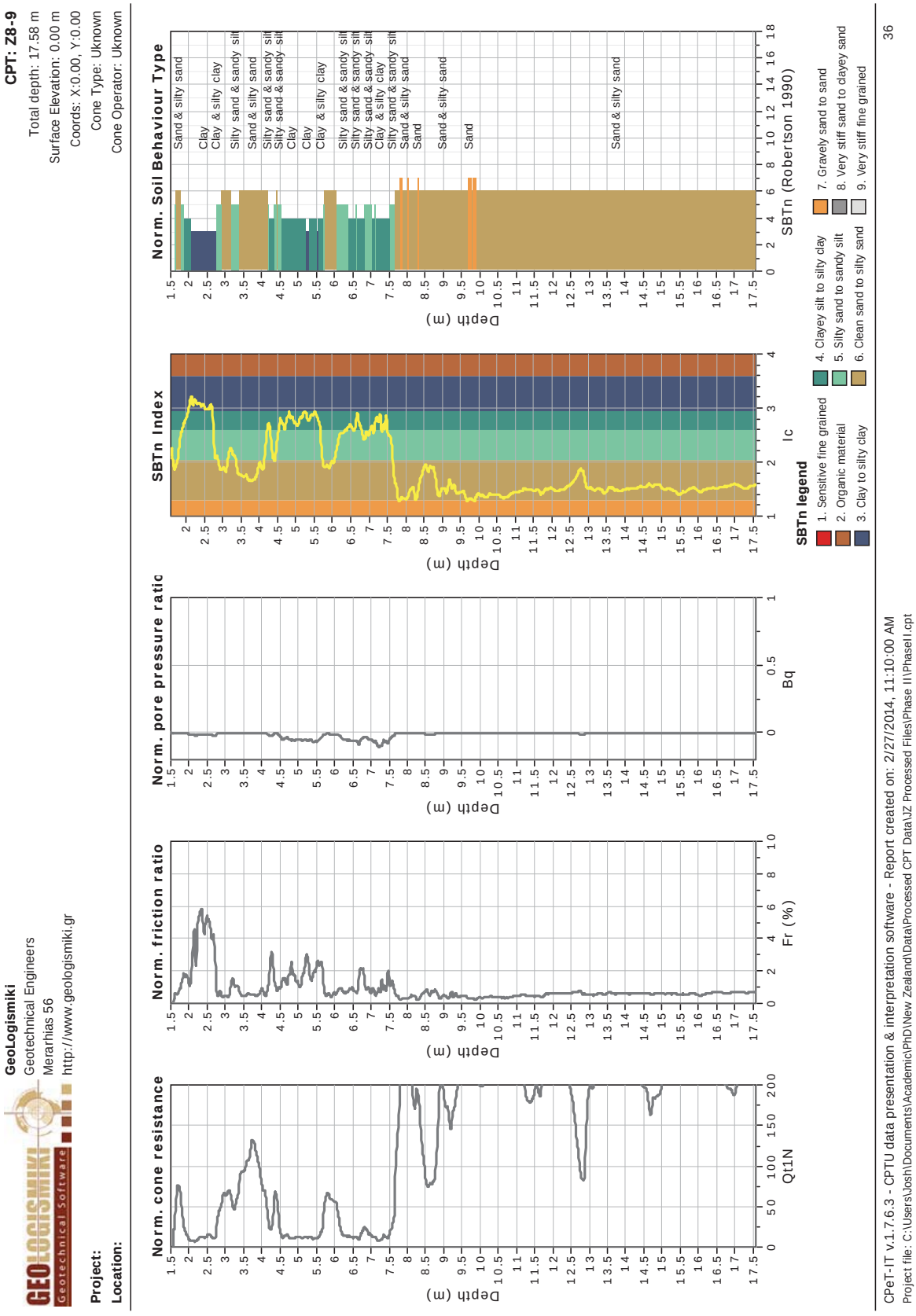
CPT: Z8-9
Total depth: 17.58 m
Surface Elevation: 0.00 m
Coords: X:0.00, Y:0.00
Cone Type: Uknown
Cone Operator: Uknown
GeoLogismiki
Geotechnical Engineers
Merarhias 56
http://www.geologismiki.gr
Project:
Location:
Norm. cone resistance
Norm. friction ratio
Norm. pore pressure ratio
SBTn Index
Norm. Soil Behaviour Type
SBTn legend
1. Sensitive fine grained
2. Organic material
3. Clay to silty clay
4. Clayey silt to silty clay
5. Silty sand to sandy silt
6. Clean sand to silty sand
7. Gravely sand to sand
8. Very stiff sand to clayey sand
9. Very stiff fine grained
SBTn (Robertson 1990)
CPeT-IT v.1.7.6.3 - CPTU data presentation & interpretation software - Report created on: 2/27/2014, 11:10:00 AM
Project file: C:\Users\Josh\Documents\Academic\PhD\New Zealand\Data\Processed CPT Data\JZ Processed Files\Phase II\PhaseII.cpt
36

GeoLogismiki
Geotechnical Engineers
Merarhias 56
http://www.geologismiki.gr

CPT: Z8-10
Total depth: 17.68 m
Surface Elevation: 0.00 m
Coords: X:0.00, Y:0.00
Cone Type: Uknown
Cone Operator: Uknown

Project:
Location:

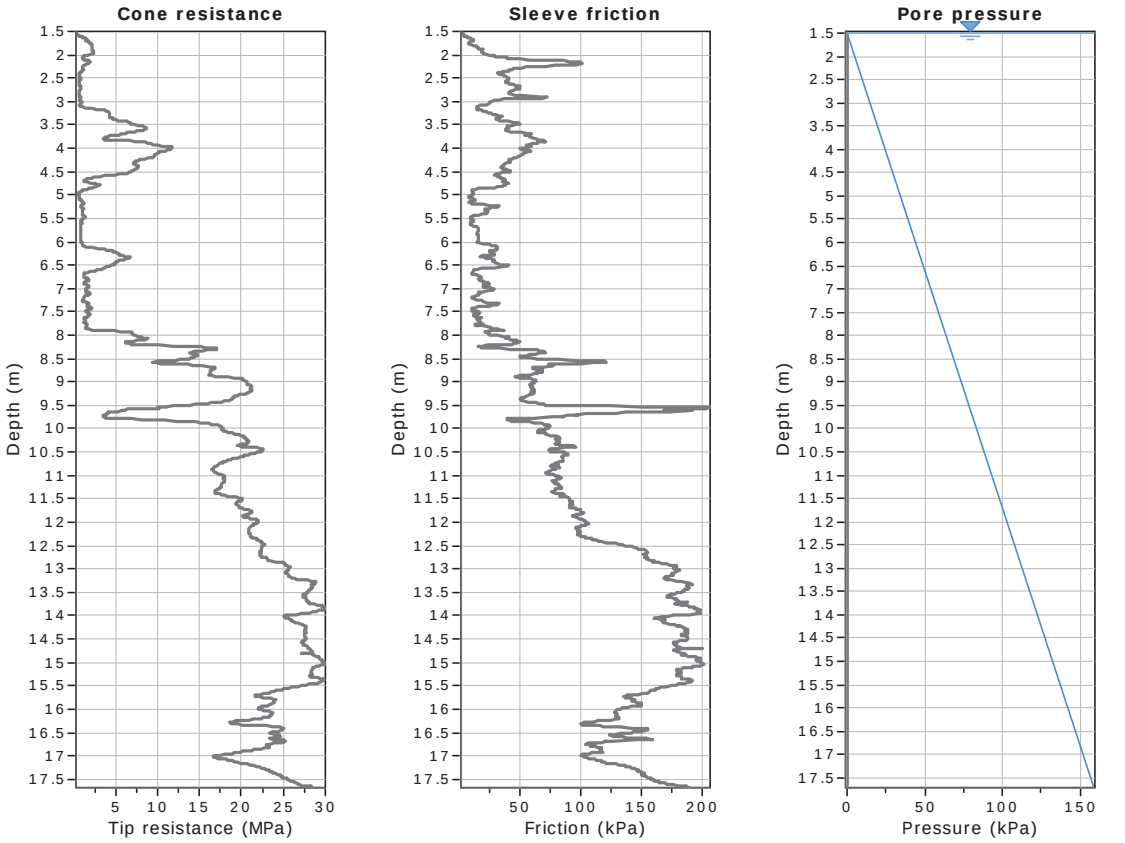

The plot below presents the cross correlation coeficient between the raw qc and fs values (as measured on the field). X axes presents the lag distance (one lag is the distance between two sucessive CPT measurements).

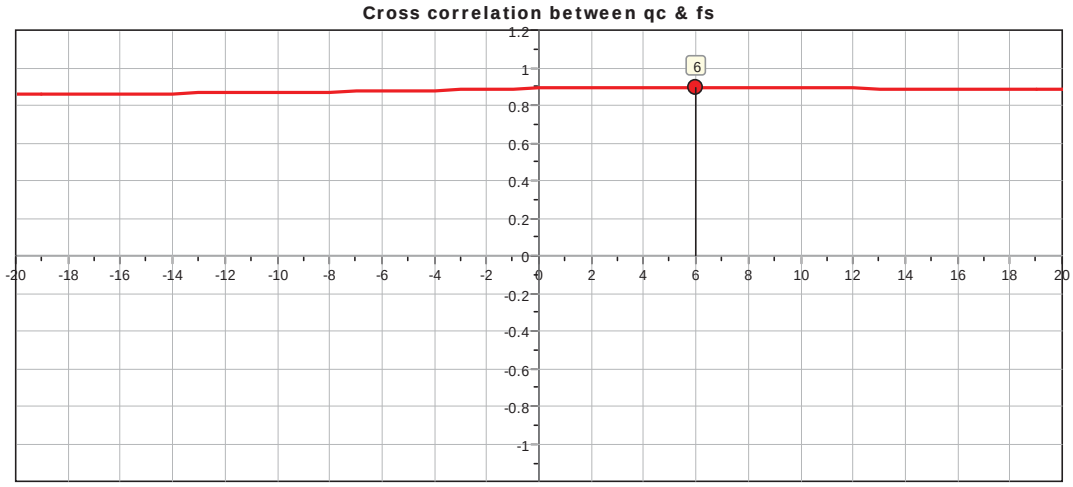

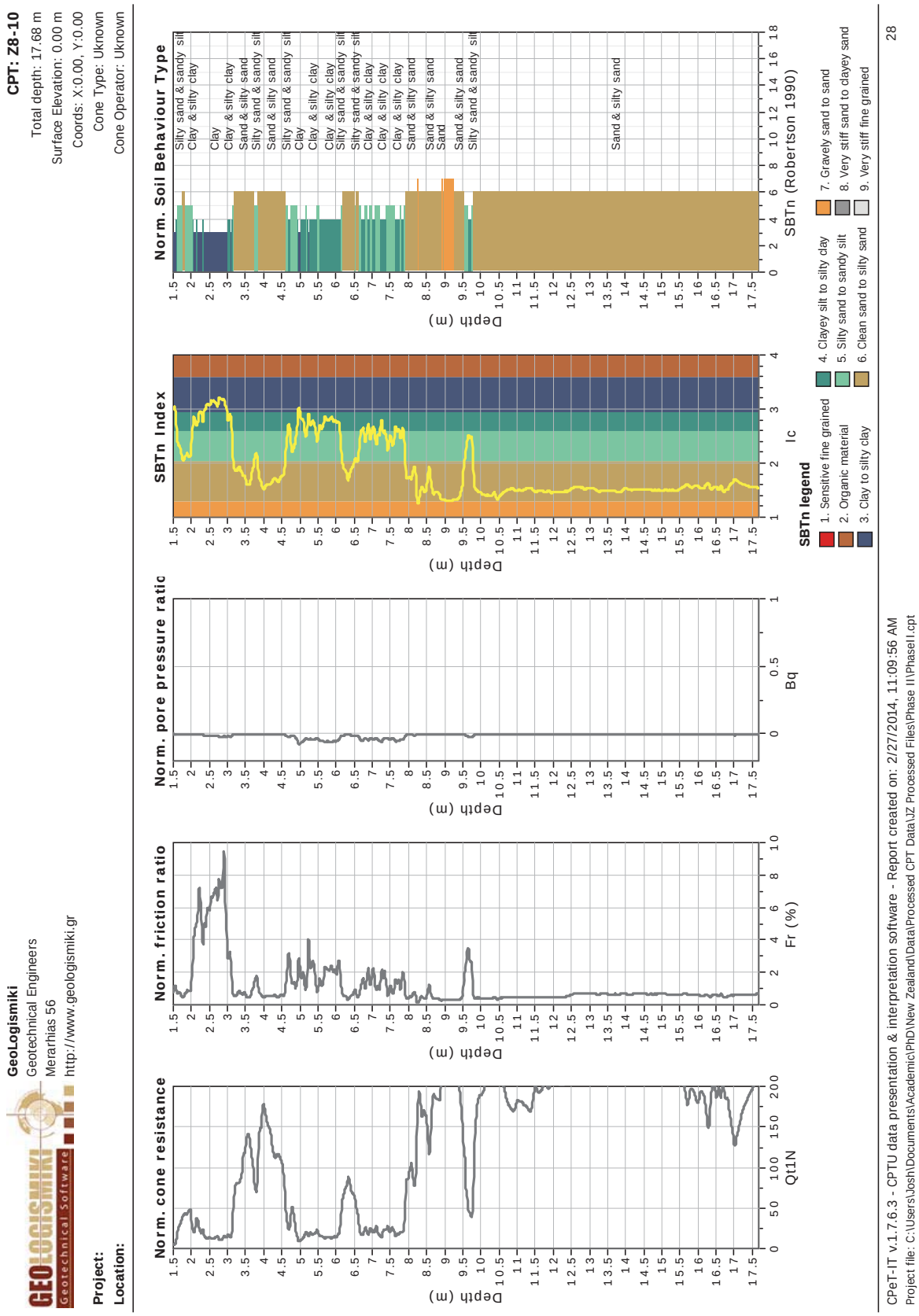
CPT: Z8-10
Total depth: 17.68 m
Surface Elevation: 0.00 m
Coords: X:0.00, Y:0.00
Cone Type: Uknown
Cone Operator: Uknown
GeoLogismiki
Geotechnical Engineers
Merarhias 56
http://www.geologismiki.gr
Project:
Location:
Norm. cone resistance
Qt1N
Norm. friction ratio
Fr (%)
Norm. pore pressure ratio
Bq
SBTn Index
Ic
Norm. Soil Behaviour Type
SBTn (Robertson 1990)
Depth (m)
SBTn legend
1. Sensitive fine grained
2. Organic material
3. Clay to silty clay
4. Clayey silt to silty clay
5. Silty sand to sandy silt
6. Clean sand to silty sand
7. Gravely sand to sand
8. Very stiff sand to clayey sand
9. Very stiff fine grained
CPeT-IT v.1.7.6.3 - CPTU data presentation & interpretation software - Report created on: 2/27/2014, 11:09:56 AM
Project file: C:\Users\Josh\Documents\Academic\PhD\New Zealand\Data\Processed CPT Data\JZ Processed Files\Phase II\PhaseII.cpt
28

GeoLogismiki
Geotechnical Engineers
Merarhias 56
http://www.geologismiki.gr

CPT: Z8-11
Total depth: 7.20 m
Surface Elevation: 0.00 m
Coords: X:0.00, Y:0.00
Cone Type: Uknown
Cone Operator: Uknown

Project:
Location:

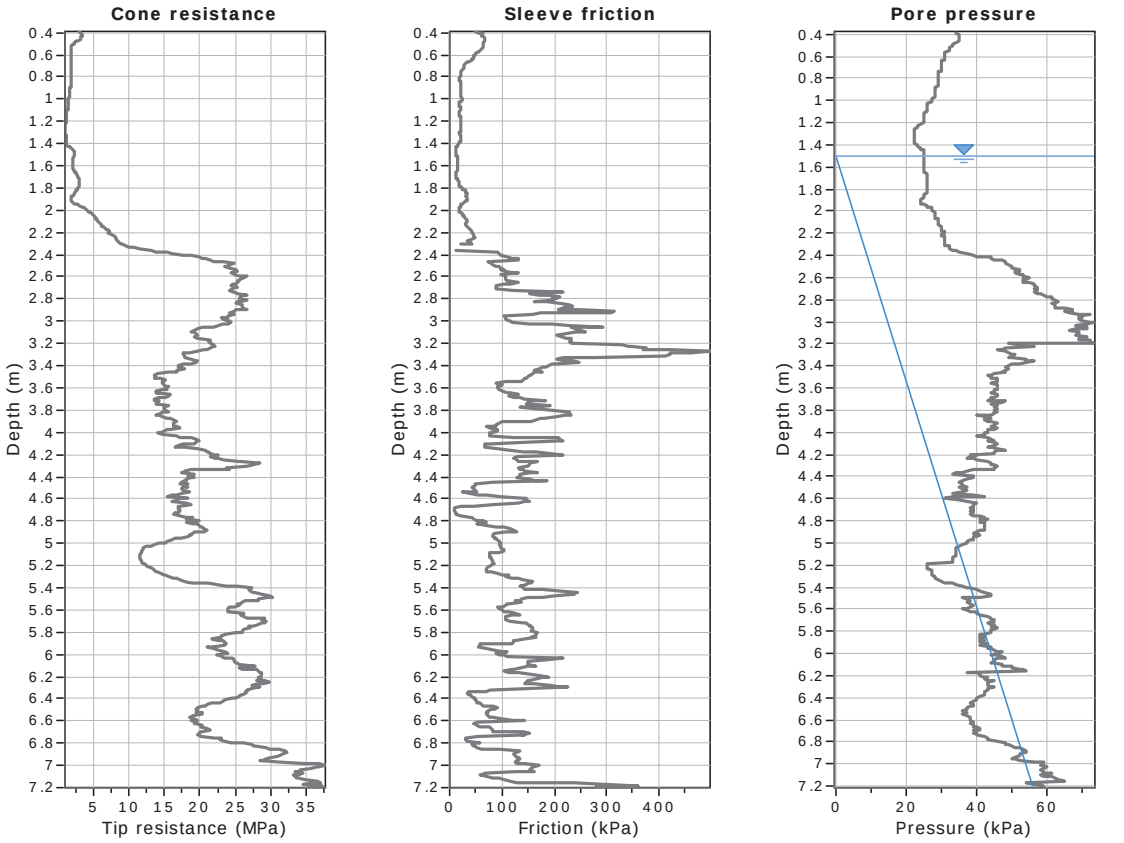

The plot below presents the cross correlation coeficient between the raw qc and fs values (as measured on the field). X axes presents the lag distance (one lag is the distance between two sucessive CPT measurements).

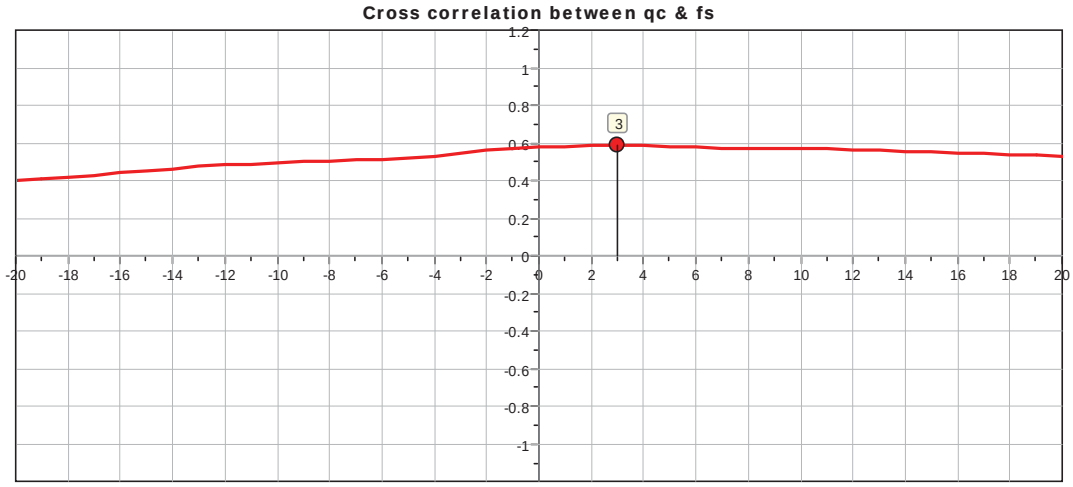

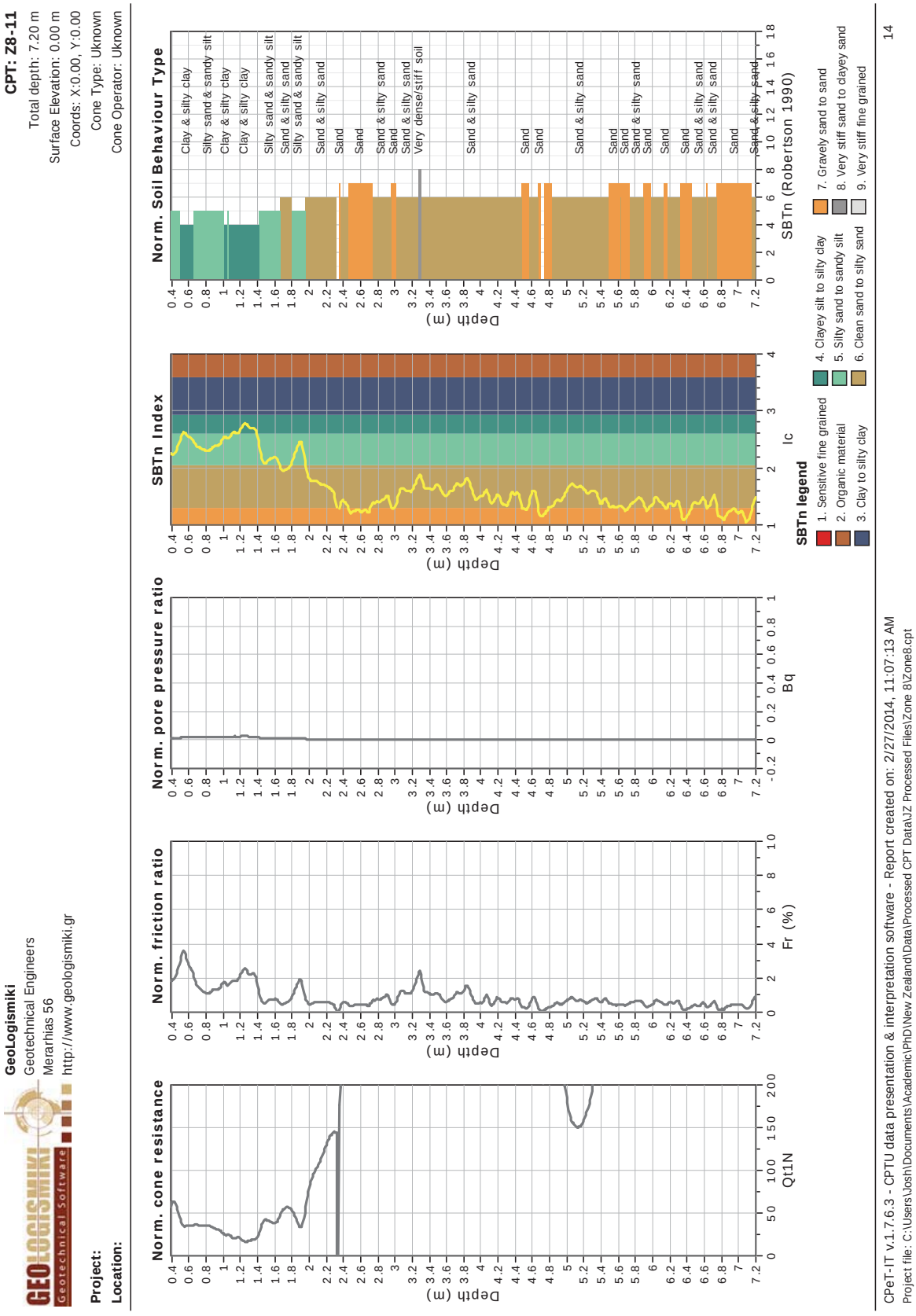
GeoLogismiki
Geotechnical Engineers
Merarhias 56
http://www.geologismiki.gr
Project:
Location:
CPT: Z8-11
Total depth: 7.20 m
Surface Elevation: 0.00 m
Coords: X:0.00, Y:0.00
Cone Type: Uknown
Cone Operator: Uknown
Norm. cone resistance
Norm. friction ratio
Norm. pore pressure ratio
SBTn Index
Norm. Soil Behaviour Type
Depth (m)
Qt1N
Fr (%)
Bq
Ic
SBTn (Robertson 1990)
SBTn legend
1. Sensitive fine grained
2. Organic material
3. Clay to silty clay
4. Clayey silt to silty clay
5. Silty sand to sandy silt
6. Clean sand to silty sand
7. Gravely sand to sand
8. Very stiff sand to clayey sand
9. Very stiff fine grained
CPeT-IT v.1.7.6.3 - CPTU data presentation & interpretation software - Report created on: 2/27/2014, 11:07:13 AM
Project file: C:\Users\Josh\Documents\Academic\PhD\New Zealand\Data\Processed CPT Data\JZ Processed Files\Zone 8\Zone8.cpt
14

GeoLogismiki
Geotechnical Engineers
Merarhias 56
http://www.geologismiki.gr

CPT: Z8-12R-1
Total depth: 15.81 m
Surface Elevation: 0.00 m
Coords: X:0.00, Y:0.00
Cone Type: Uknown
Cone Operator: Uknown

Project:
Location:

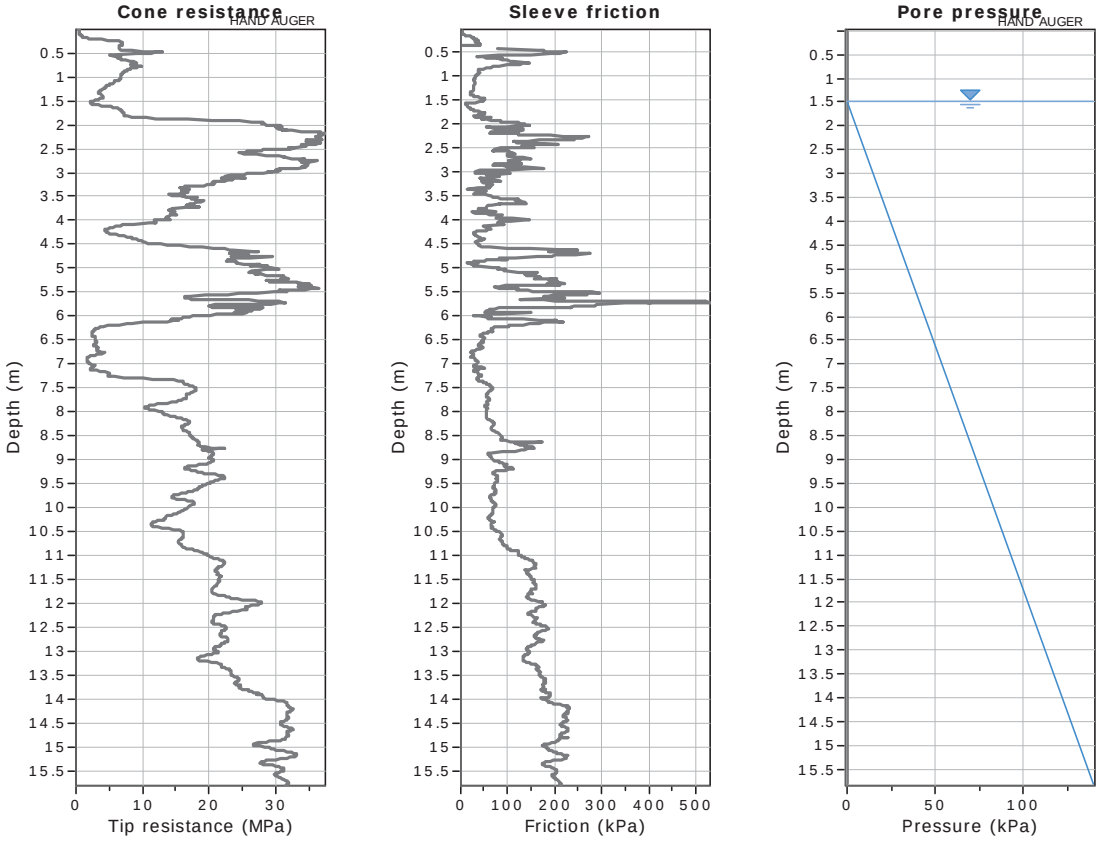

The plot below presents the cross correlation coeficient between the raw qc and fs values (as measured on the field). X axes presents the lag distance (one lag is the distance between two sucessive CPT measurements).

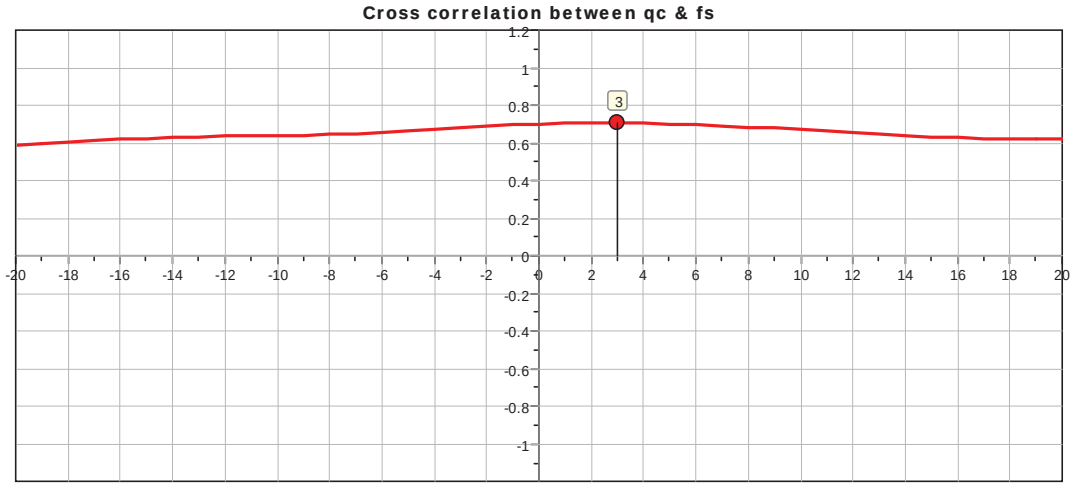

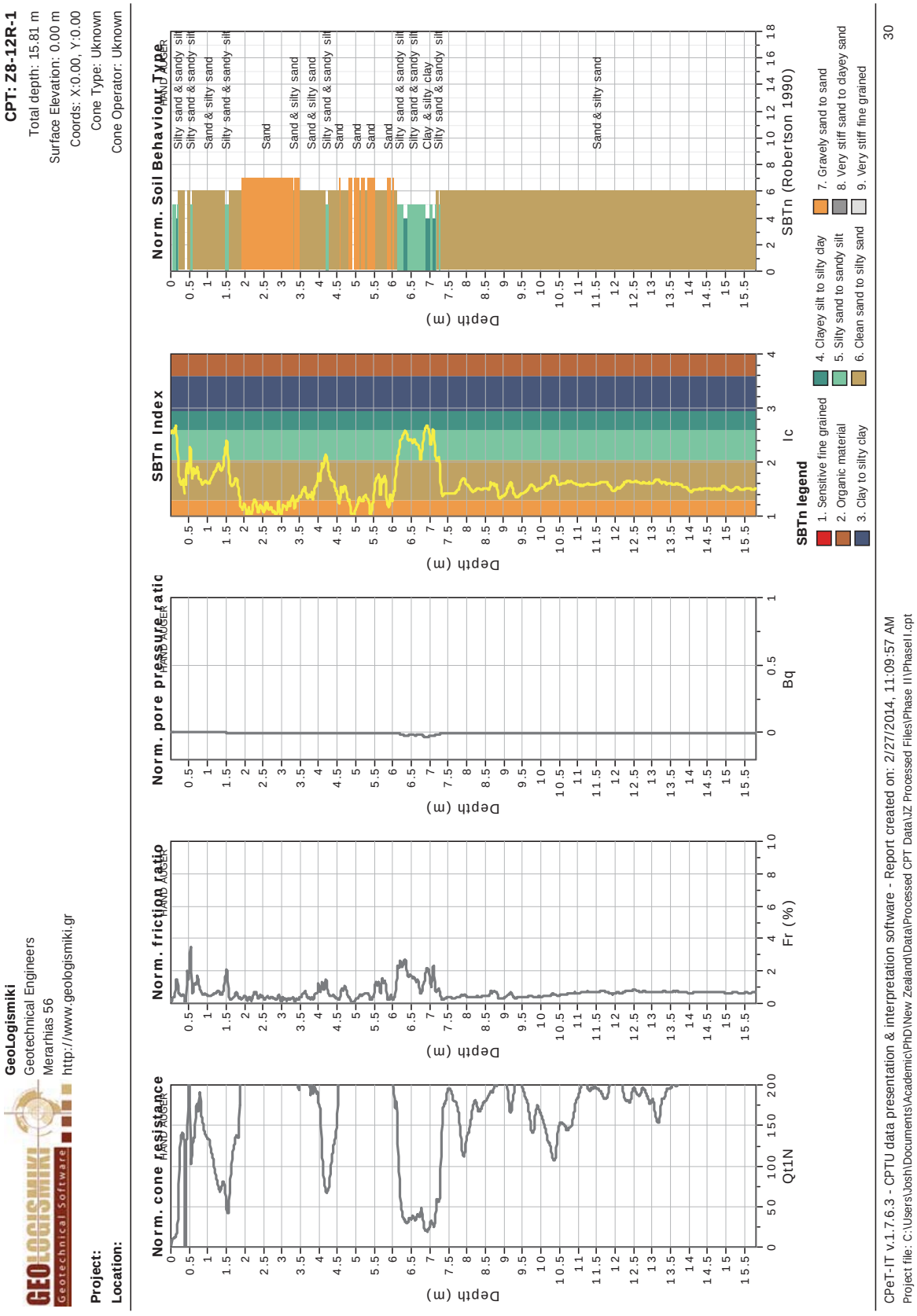
CPT: Z8-12R-1
Total depth: 15.81 m
Surface Elevation: 0.00 m
Coords: X:0.00, Y:0.00
Cone Type: Uknown
Cone Operator: Uknown
GeoLogismiki
Geotechnical Engineers
Merarhias 56
http://www.geologismiki.gr
Project:
Location:
Norm. cone resistance
Norm. friction ratio
Norm. pore pressure ratio
SBTn Index
Norm. Soil Behaviour Type
HAND AUGER
Qt1N
Fr (%)
Bq
Ic
SBTn (Robertson 1990)
Depth (m)
SBTn legend
1. Sensitive fine grained
2. Organic material
3. Clay to silty clay
4. Clayey silt to silty clay
5. Silty sand to sandy silt
6. Clean sand to silty sand
7. Gravely sand to sand
8. Very stiff sand to clayey sand
9. Very stiff fine grained
Silty sand & sandy silt
Sand & silty sand
Sand
Clay & silty clay
CPeT-IT v.1.7.6.3 - CPTU data presentation & interpretation software - Report created on: 2/27/2014, 11:09:57 AM
Project file: C:\Users\Josh\Documents\Academic\PhD\New Zealand\Data\Processed CPT Data\JZ Processed Files\Phase II\PhaseII.cpt
30

GeoLogismiki
Geotechnical Engineers
Merarhias 56
http://www.geologismiki.gr

CPT: Z8-13
Total depth: 16.57 m
Surface Elevation: 0.00 m
Coords: X:0.00, Y:0.00
Cone Type: Uknown
Cone Operator: Uknown

Project:
Location:

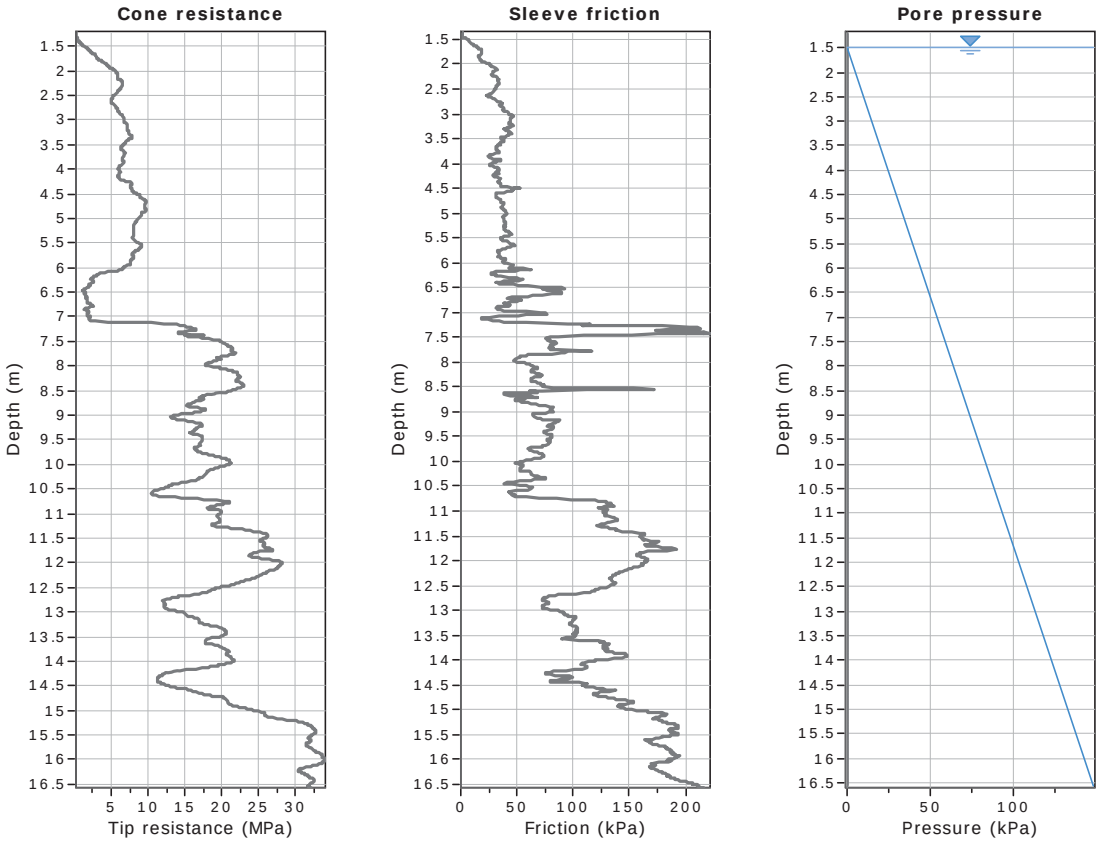

The plot below presents the cross correlation coeficient between the raw qc and fs values (as measured on the field). X axes presents the lag distance (one lag is the distance between two sucessive CPT measurements).

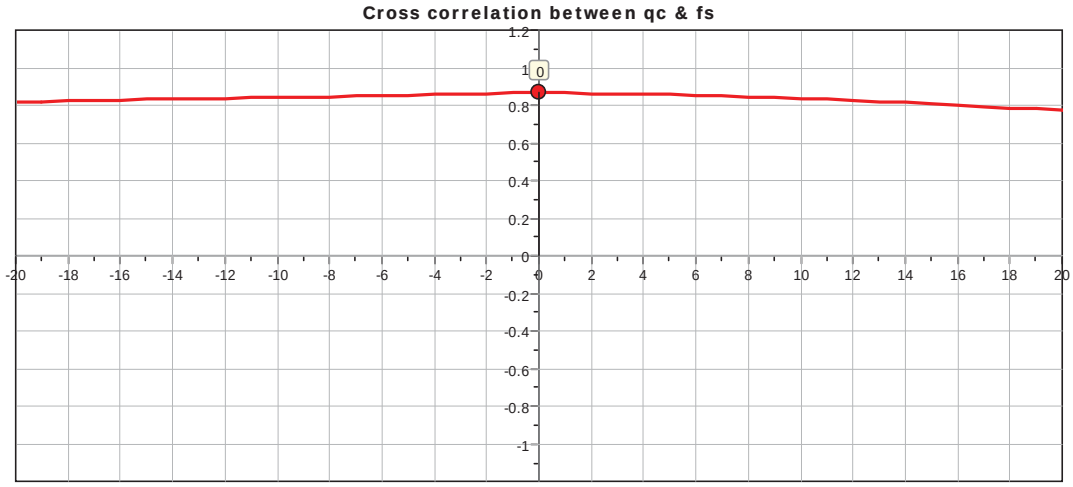

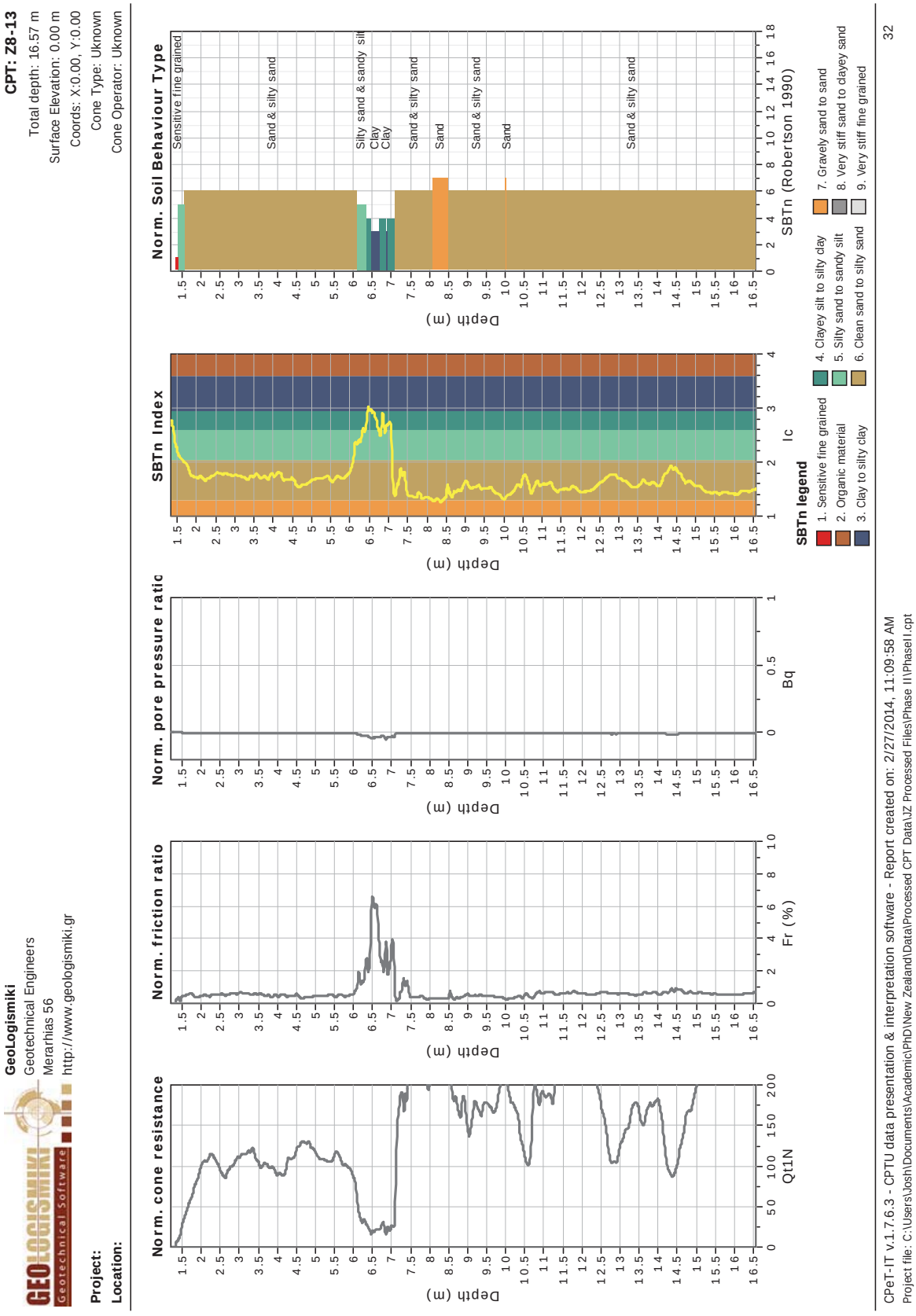
GeoLogismiki
Geotechnical Engineers
Merarhias 56
http://www.geologismiki.gr
Project:
Location:
CPT: Z8-13
Total depth: 16.57 m
Surface Elevation: 0.00 m
Coords: X:0.00, Y:0.00
Cone Type: Uknown
Cone Operator: Uknown
Norm. cone resistance
Qt1N
Norm. friction ratio
Fr (%)
Norm. pore pressure ratio
Bq
SBTn Index
Ic
Norm. Soil Behaviour Type
SBTn (Robertson 1990)
Depth (m)
Sensitive fine grained
Sand & silty sand
Silty sand & sandy silt
Clay
Clay
Sand & silty sand
Sand
Sand & silty sand
Sand
Sand & silty sand
SBTn legend
1. Sensitive fine grained
2. Organic material
3. Clay to silty clay
4. Clayey silt to silty clay
5. Silty sand to sandy silt
6. Clean sand to silty sand
7. Gravely sand to sand
8. Very stiff sand to clayey sand
9. Very stiff fine grained
CPeT-IT v.1.7.6.3 - CPTU data presentation & interpretation software - Report created on: 2/27/2014, 11:09:58 AM
Project file: C:\Users\Josh\Documents\Academic\PhD\New Zealand\Data\Processed CPT Data\JZ Processed Files\Phase II\PhaseII.cpt
32

GeoLogismiki
Geotechnical Engineers
Merarhias 56
http://www.geologismiki.gr

CPT: Z8-14
Total depth: 8.92 m
Surface Elevation: 0.00 m
Coords: X:0.00, Y:0.00
Cone Type: Uknown
Cone Operator: Uknown

Project:
Location:

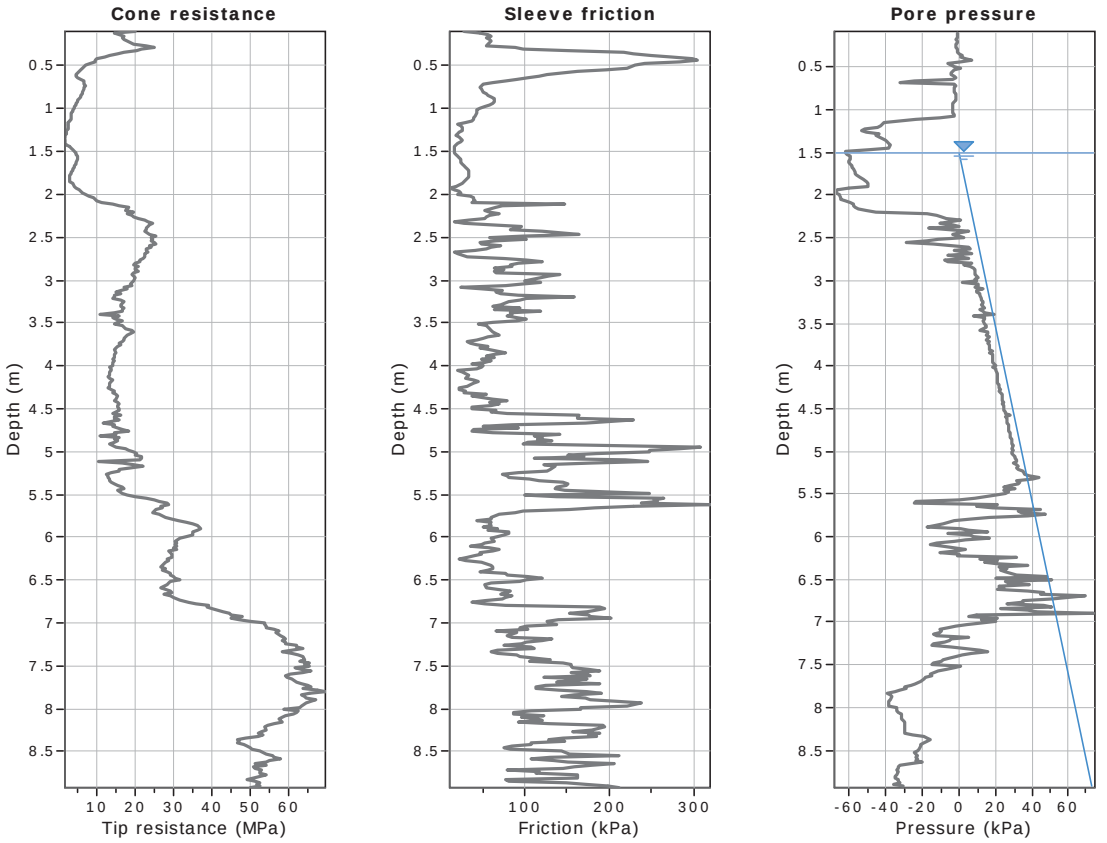

The plot below presents the cross correlation coeficient between the raw qc and fs values (as measured on the field). X axes presents the lag distance (one lag is the distance between two sucessive CPT measurements).

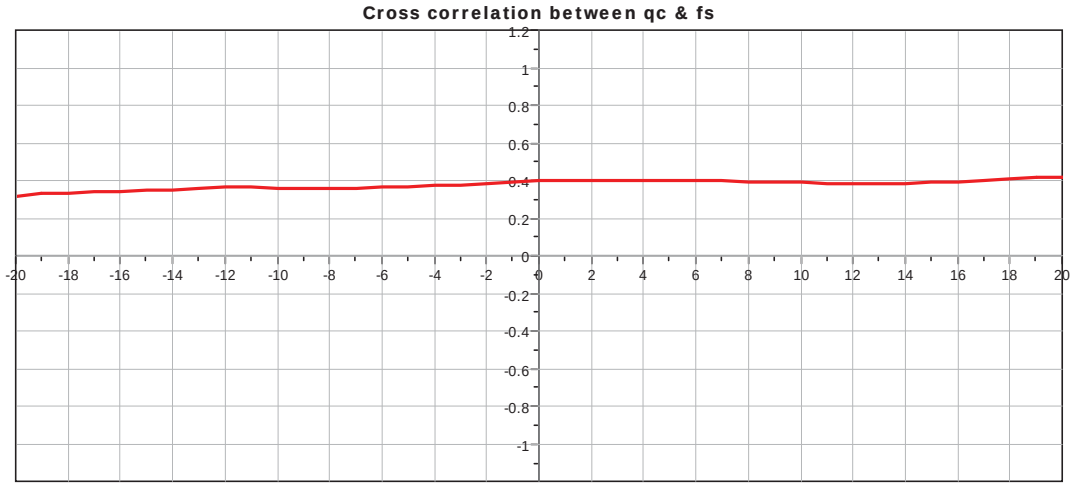

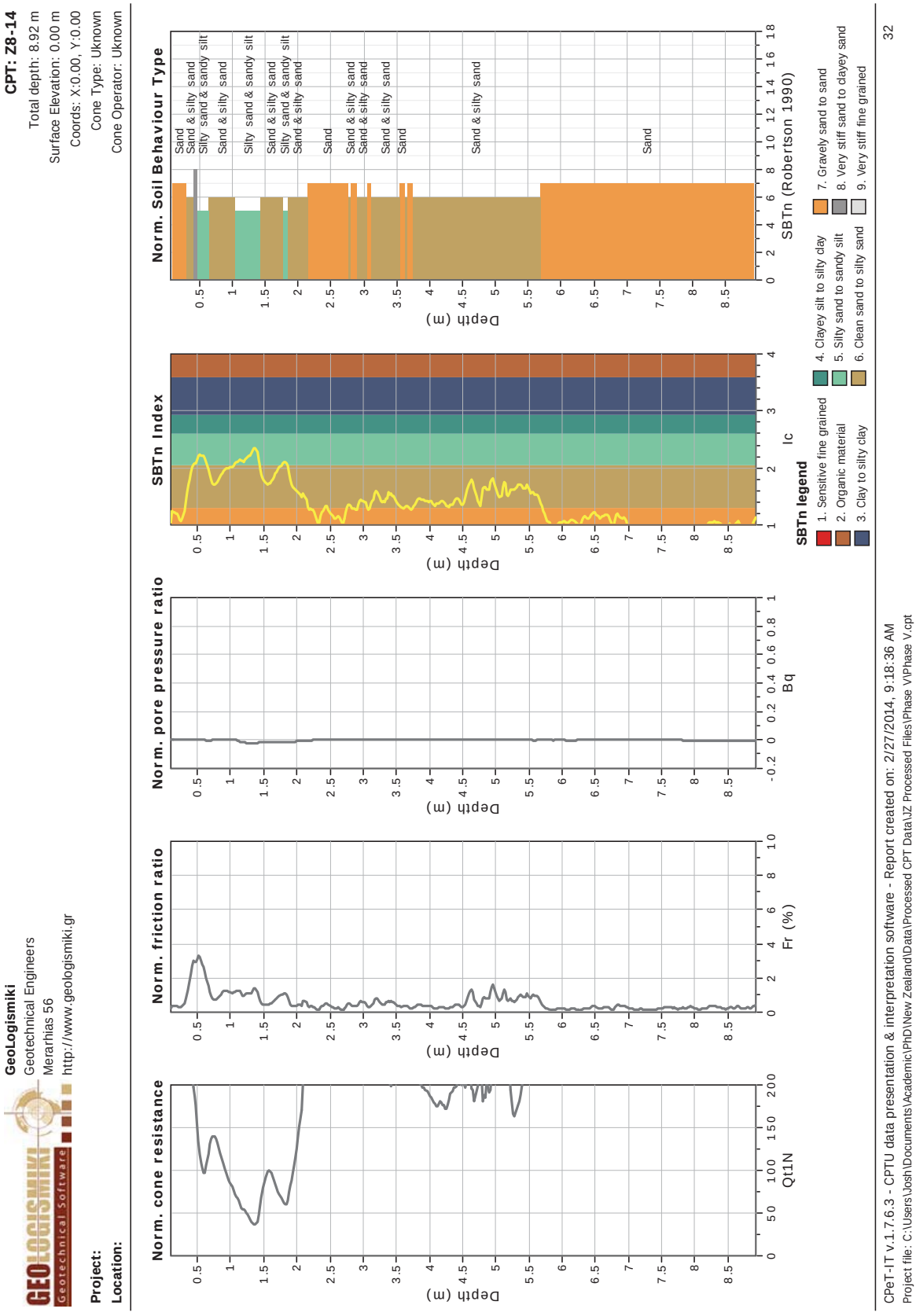
CPT: Z8-14
Total depth: 8.92 m
Surface Elevation: 0.00 m
Coords: X:0.00, Y:0.00
Cone Type: Uknown
Cone Operator: Uknown
GeoLogismiki
Geotechnical Engineers
Merarhias 56
http://www.geologismiki.gr
Project:
Location:
Norm. cone resistance
Qt1N
Norm. friction ratio
Fr (%)
Norm. pore pressure ratio
Bq
SBTn Index
Ic
Norm. Soil Behaviour Type
SBTn (Robertson 1990)
Depth (m)
SBTn legend
1. Sensitive fine grained
2. Organic material
3. Clay to silty clay
4. Clayey silt to silty clay
5. Silty sand to sandy silt
6. Clean sand to silty sand
7. Gravely sand to sand
8. Very stiff sand to clayey sand
9. Very stiff fine grained
CPeT-IT v.1.7.6.3 - CPTU data presentation & interpretation software - Report created on: 2/27/2014, 9:18:36 AM
Project file: C:\Users\Josh\Documents\Academic\PhD\New Zealand\Data\Processed CPT Data\JZ Processed Files\Phase V\Phase V.cpt
32

GeoLogismiki
Geotechnical Engineers
Merarhias 56
http://www.geologismiki.gr

CPT: Z8-15
Total depth: 21.12 m
Surface Elevation: 0.00 m
Coords: X:0.00, Y:0.00
Cone Type: Uknown
Cone Operator: Uknown

Project:
Location:

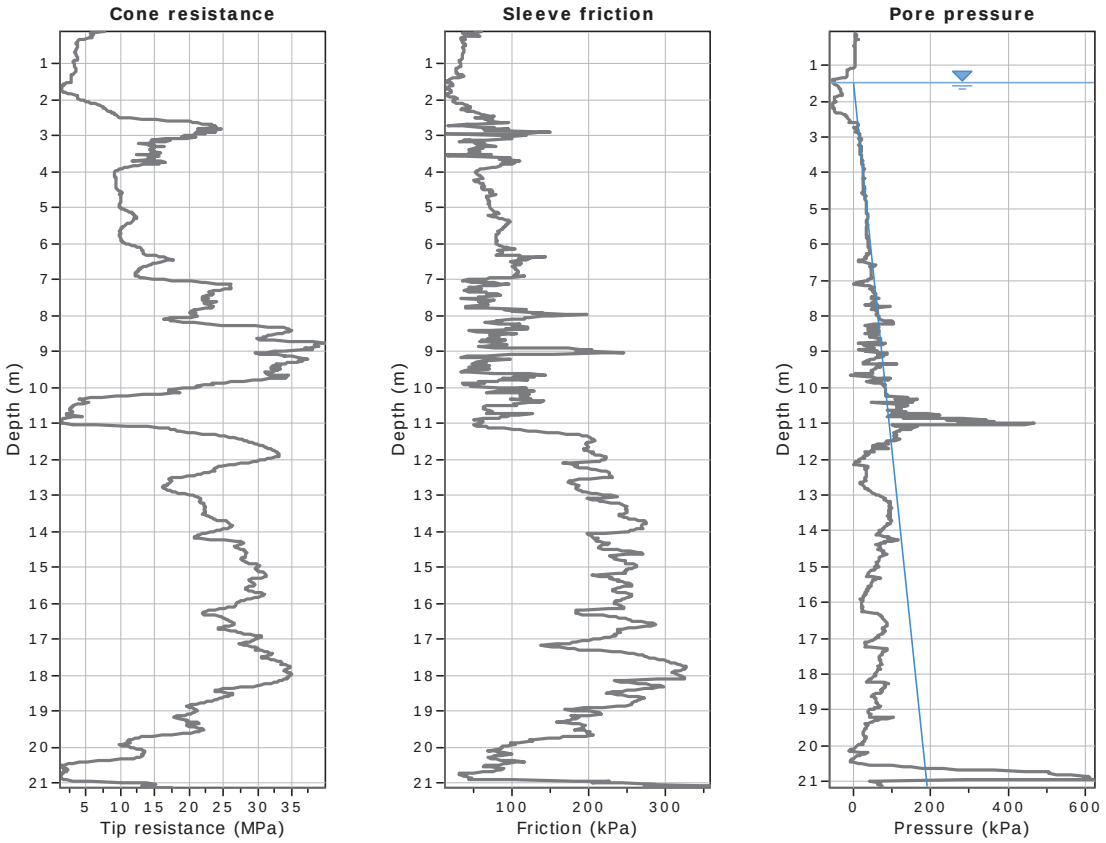

The plot below presents the cross correlation coeficient between the raw qc and fs values (as measured on the field). X axes presents the lag distance (one lag is the distance between two sucessive CPT measurements).

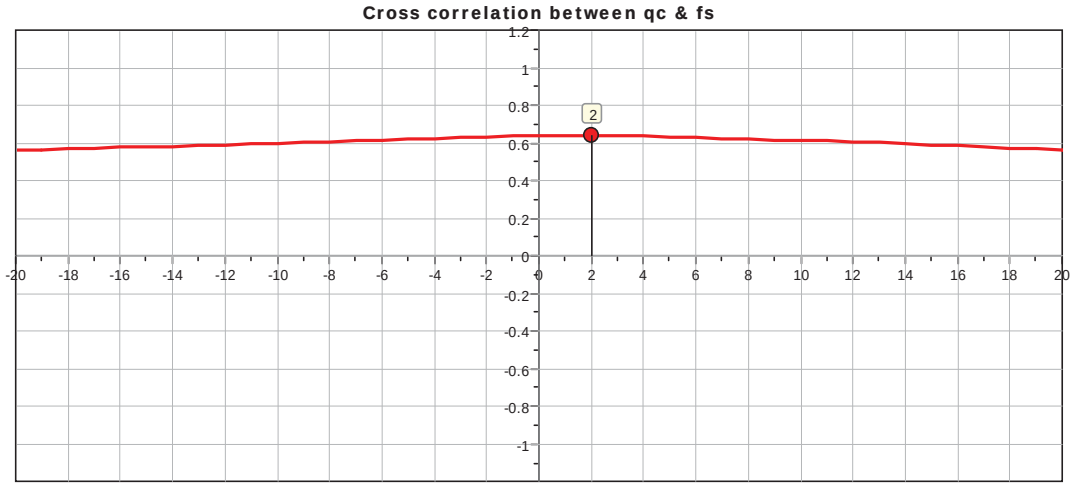

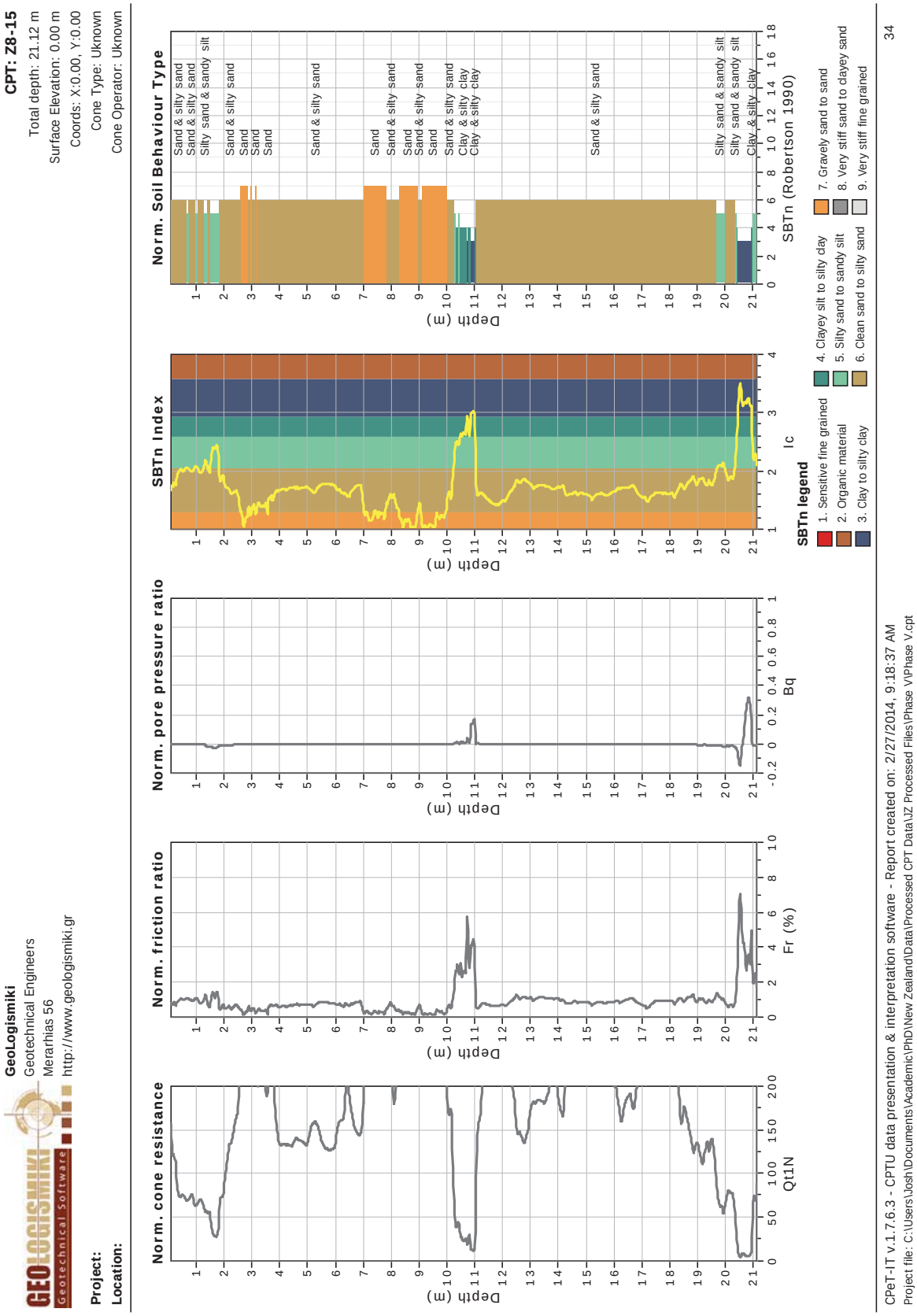
GeoLogismiki
Geotechnical Engineers
Merarhias 56
http://www.geologismiki.gr
Project:
Location:
CPT: Z8-15
Total depth: 21.12 m
Surface Elevation: 0.00 m
Coords: X:0.00, Y:0.00
Cone Type: Uknown
Cone Operator: Uknown
Norm. cone resistance
Qt1N
Norm. friction ratio
Fr (%)
Norm. pore pressure ratio
Bq
SBTn Index
Ic
Norm. Soil Behaviour Type
SBTn (Robertson 1990)
Depth (m)
SBTn legend
1. Sensitive fine grained
2. Organic material
3. Clay to silty clay
4. Clayey silt to silty clay
5. Silty sand to sandy silt
6. Clean sand to silty sand
7. Gravely sand to sand
8. Very stiff sand to clayey sand
9. Very stiff fine grained
CPeT-IT v.1.7.6.3 - CPTU data presentation & interpretation software - Report created on: 2/27/2014, 9:18:37 AM
Project file: C:\Users\Josh\Documents\Academic\PhD\New Zealand\Data\Processed CPT Data\JZ Processed Files\Phase V\Phase V.cpt
34

GeoLogismiki
Geotechnical Engineers
Merarhias 56
http://www.geologismiki.gr

CPT: Z8-16
Total depth: 21.14 m
Surface Elevation: 0.00 m
Coords: X:0.00, Y:0.00
Cone Type: Uknown
Cone Operator: Uknown

Project:
Location:

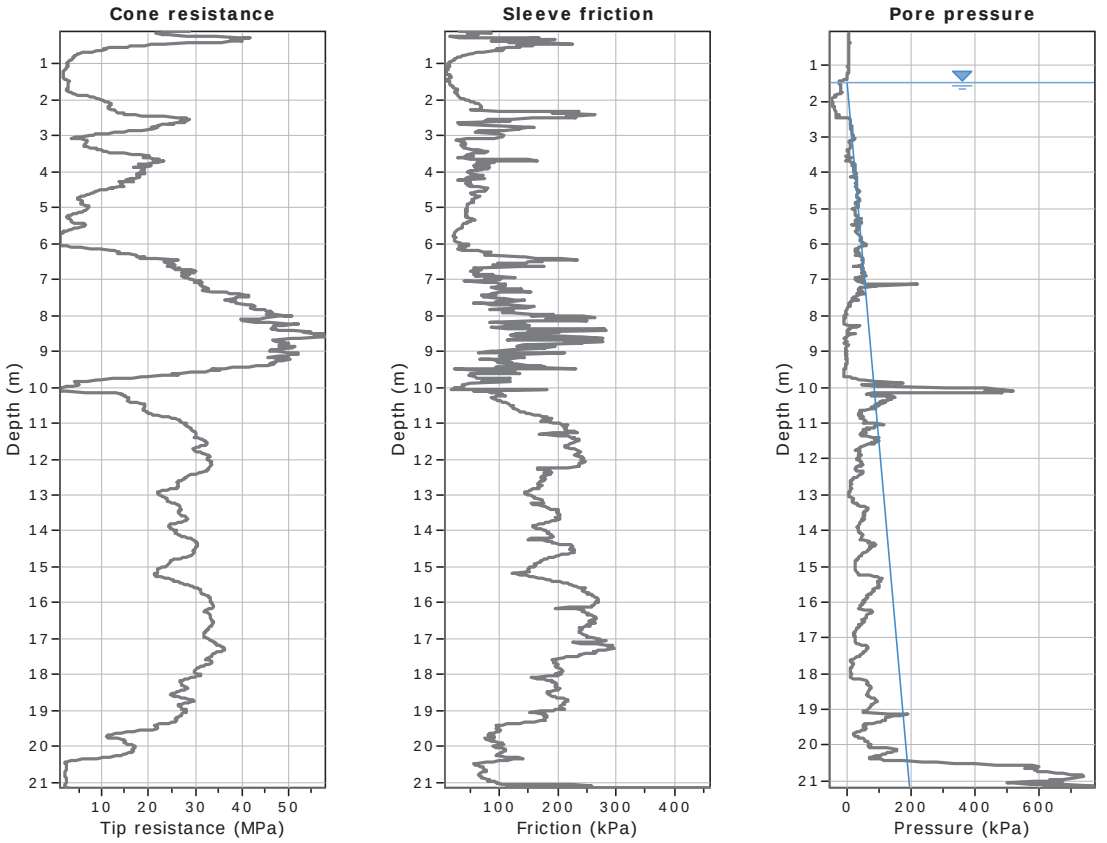

The plot below presents the cross correlation coeficient between the raw qc and fs values (as measured on the field). X axes presents the lag distance (one lag is the distance between two sucessive CPT measurements).

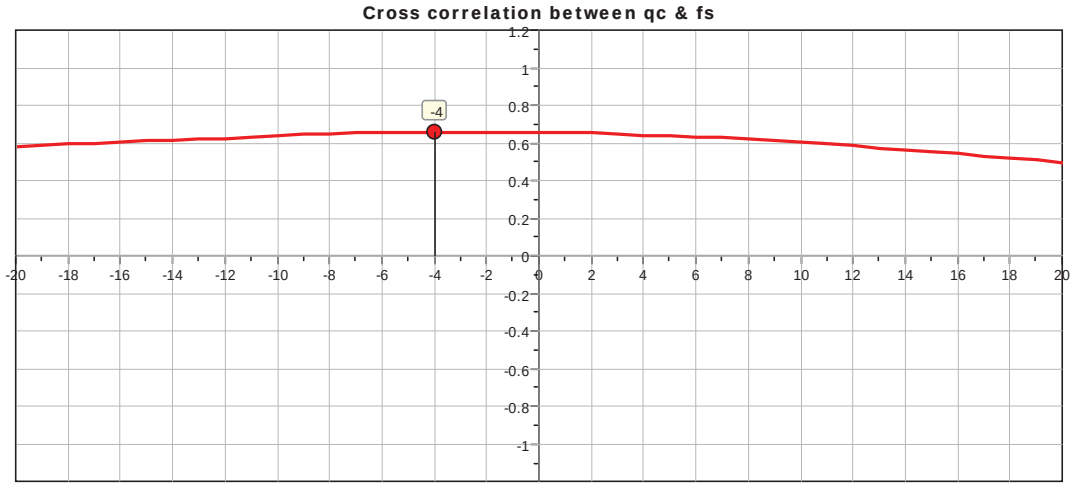

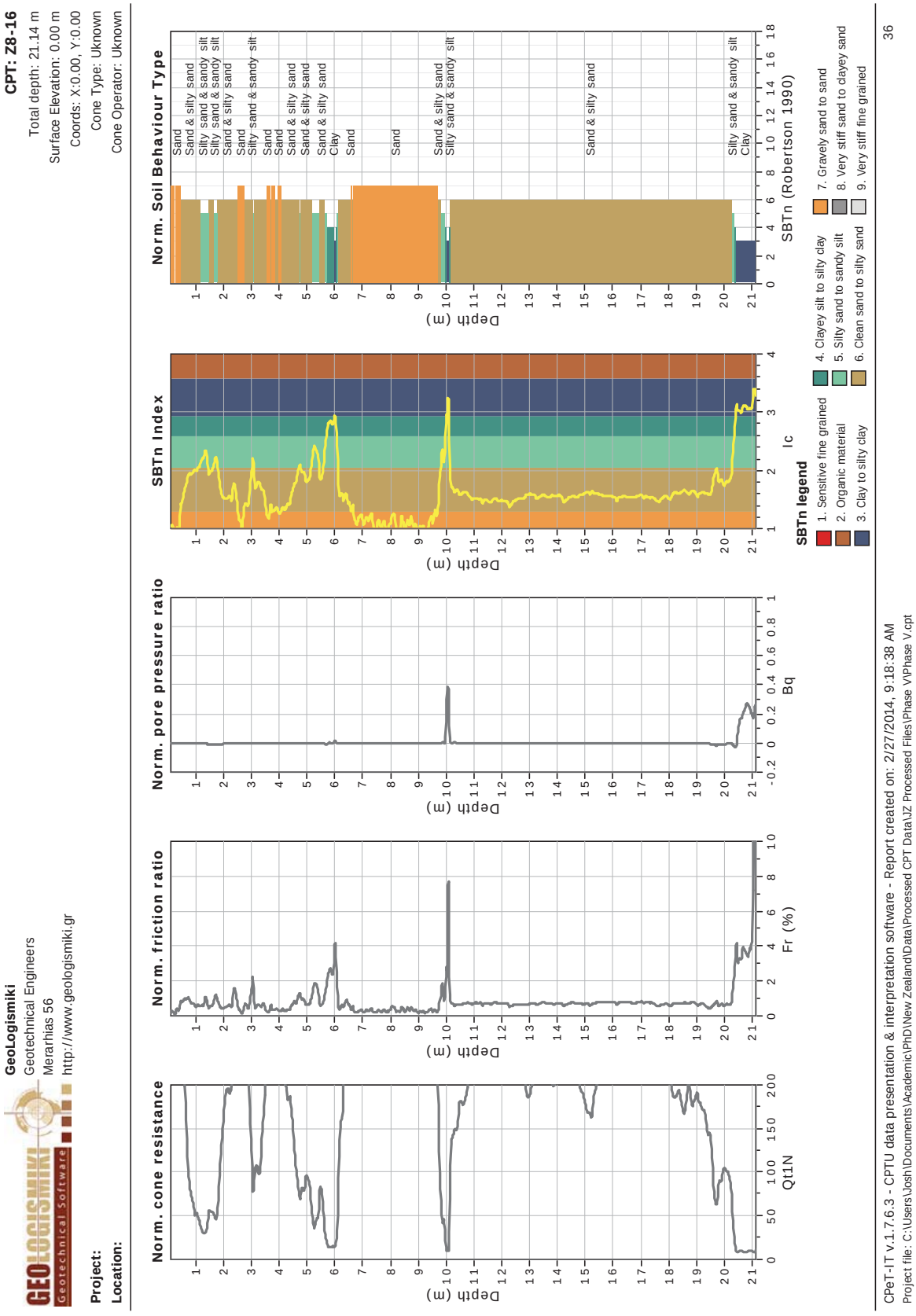
CPT: Z8-16
Total depth: 21.14 m
Surface Elevation: 0.00 m
Coords: X:0.00, Y:0.00
Cone Type: Uknown
Cone Operator: Uknown
GeoLogismiki
Geotechnical Engineers
Merarhias 56
http://www.geologismiki.gr
Project:
Location:
Norm. cone resistance
Qt1N
Norm. friction ratio
Fr (%)
Norm. pore pressure ratio
Bq
SBTn Index
Ic
Norm. Soil Behaviour Type
SBTn (Robertson 1990)
Depth (m)
SBTn legend
1. Sensitive fine grained
2. Organic material
3. Clay to silty clay
4. Clayey silt to silty clay
5. Silty sand to sandy silt
6. Clean sand to silty sand
7. Gravely sand to sand
8. Very stiff sand to clayey sand
9. Very stiff fine grained
CPeT-IT v.1.7.6.3 - CPTU data presentation & interpretation software - Report created on: 2/27/2014, 9:18:38 AM
Project file: C:\Users\Josh\Documents\Academic\PhD\New Zealand\Data\Processed CPT Data\JZ Processed Files\Phase V\Phase V.cpt
36

GeoLogismiki
Geotechnical Engineers
Merarhias 56
http://www.geologismiki.gr

CPT: Z8-17
Total depth: 21.94 m
Surface Elevation: 0.00 m
Coords: X:0.00, Y:0.00
Cone Type: Uknown
Cone Operator: Uknown

Project:
Location:

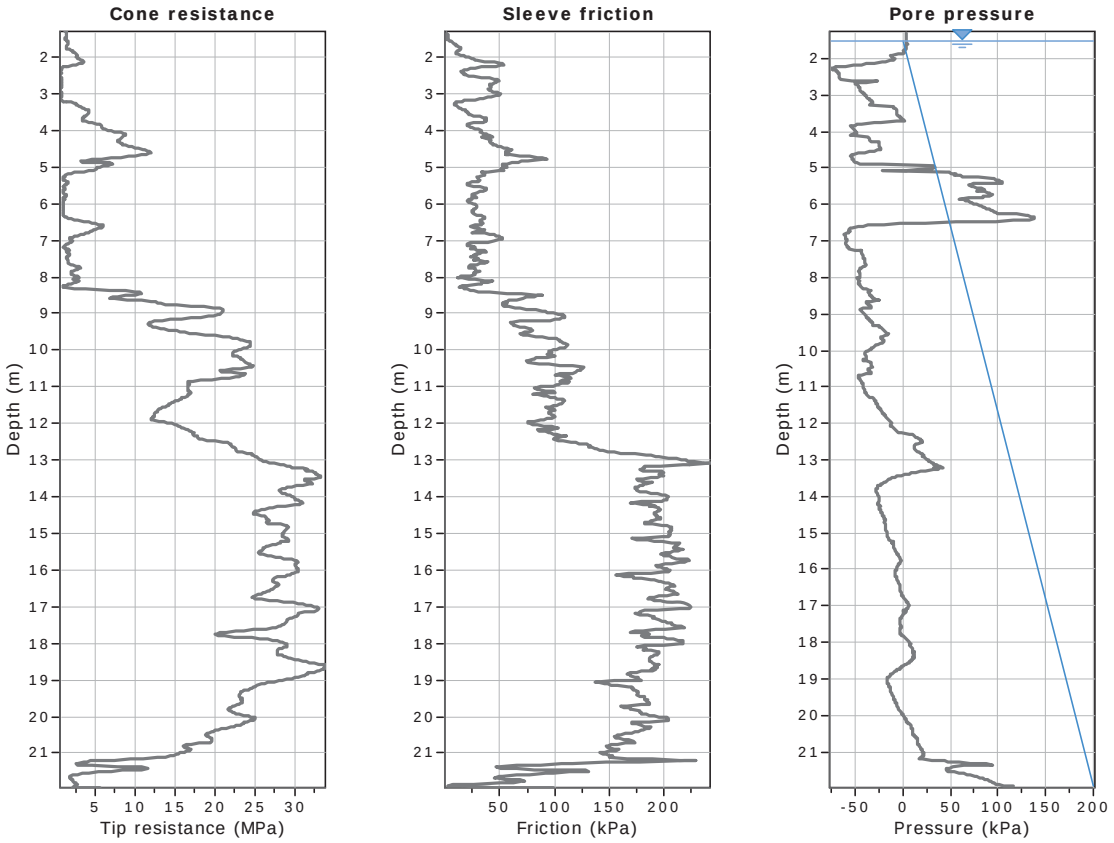

The plot below presents the cross correlation coeficient between the raw qc and fs values (as measured on the field). X axes presents the lag distance (one lag is the distance between two sucessive CPT measurements).

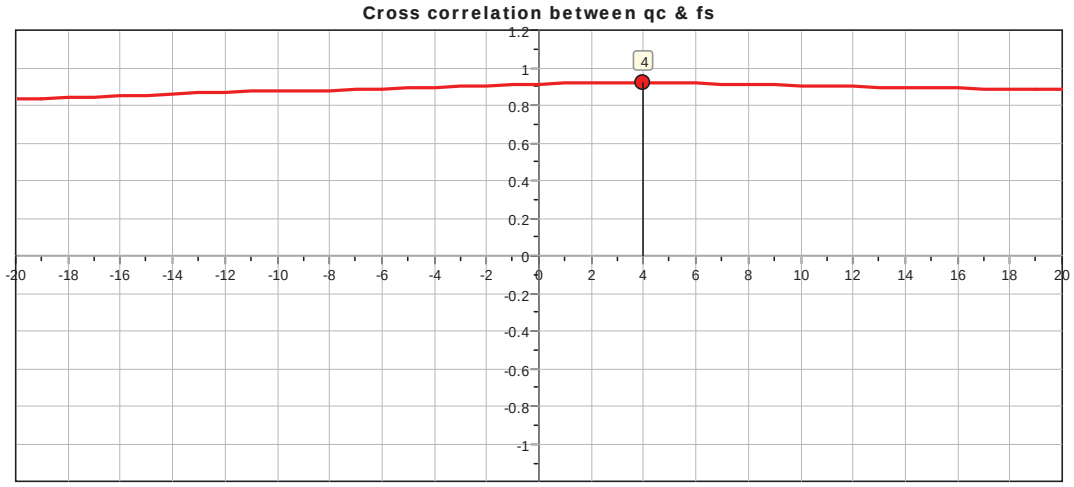

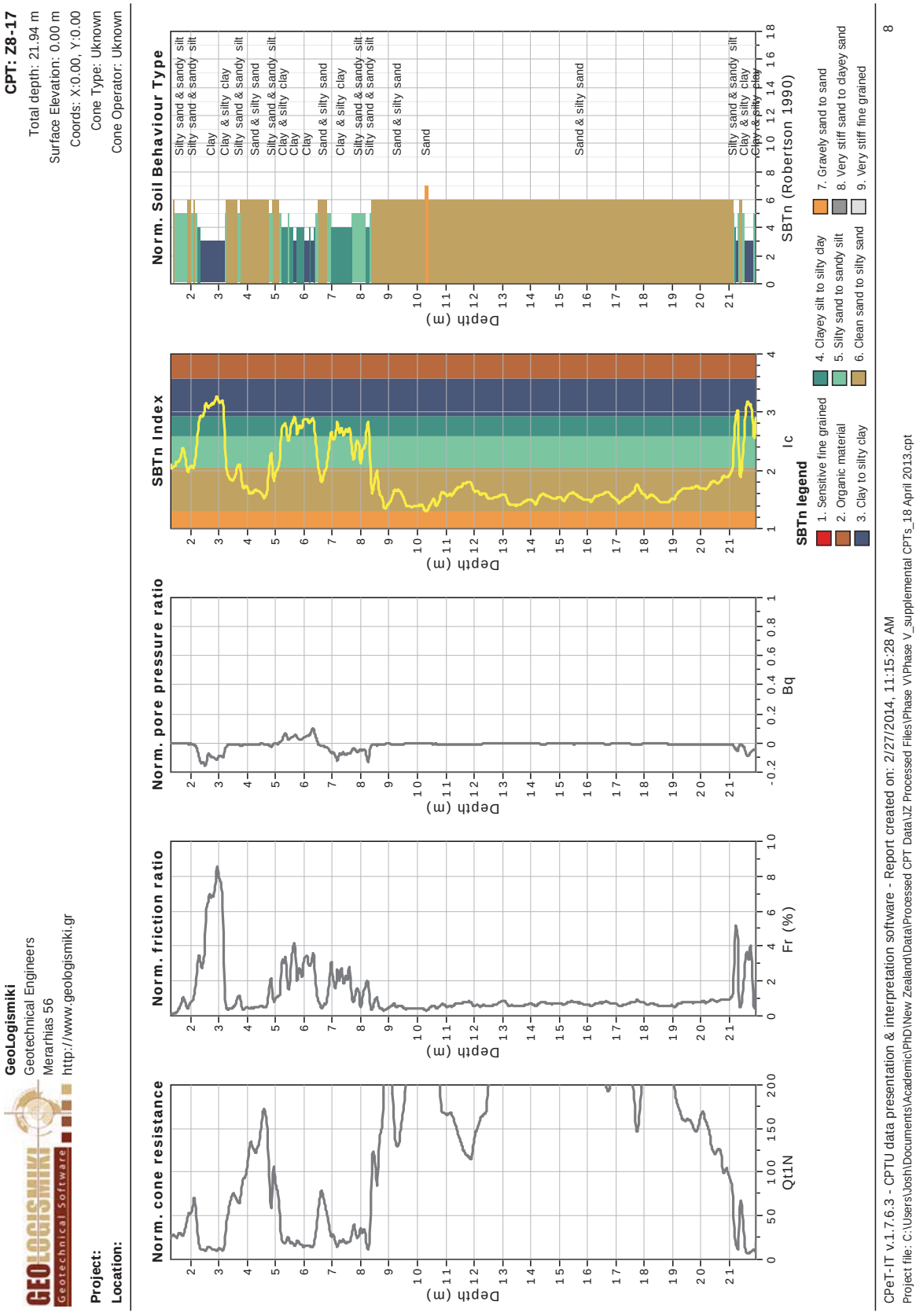
CPT: Z8-17
Total depth: 21.94 m
Surface Elevation: 0.00 m
Coords: X:0.00, Y:0.00
Cone Type: Uknown
Cone Operator: Uknown
GeoLogismiki
Geotechnical Engineers
Merarhias 56
http://www.geologismiki.gr
Project:
Location:
Norm. cone resistance
Qt1N
Norm. friction ratio
Fr (%)
Norm. pore pressure ratio
Bq
SBTn Index
Ic
Norm. Soil Behaviour Type
SBTn (Robertson 1990)
Depth (m)
SBTn legend
1. Sensitive fine grained
2. Organic material
3. Clay to silty clay
4. Clayey silt to silty clay
5. Silty sand to sandy silt
6. Clean sand to silty sand
7. Gravely sand to sand
8. Very stiff sand to clayey sand
9. Very stiff fine grained
CPeT-IT v.1.7.6.3 - CPTU data presentation & interpretation software - Report created on: 2/27/2014, 11:15:28 AM
Project file: C:\Users\Josh\Documents\Academic\PhD\New Zealand\Data\Processed CPT Data\JZ Processed Files\Phase V\Phase V_supplemental CPTs_18 April 2013.cpt
8

GeoLogismiki
Geotechnical Engineers
Merarhias 56
http://www.geologismiki.gr

CPT: Z8-18
Total depth: 22.02 m
Surface Elevation: 0.00 m
Coords: X:0.00, Y:0.00
Cone Type: Uknown
Cone Operator: Uknown

Project:
Location:

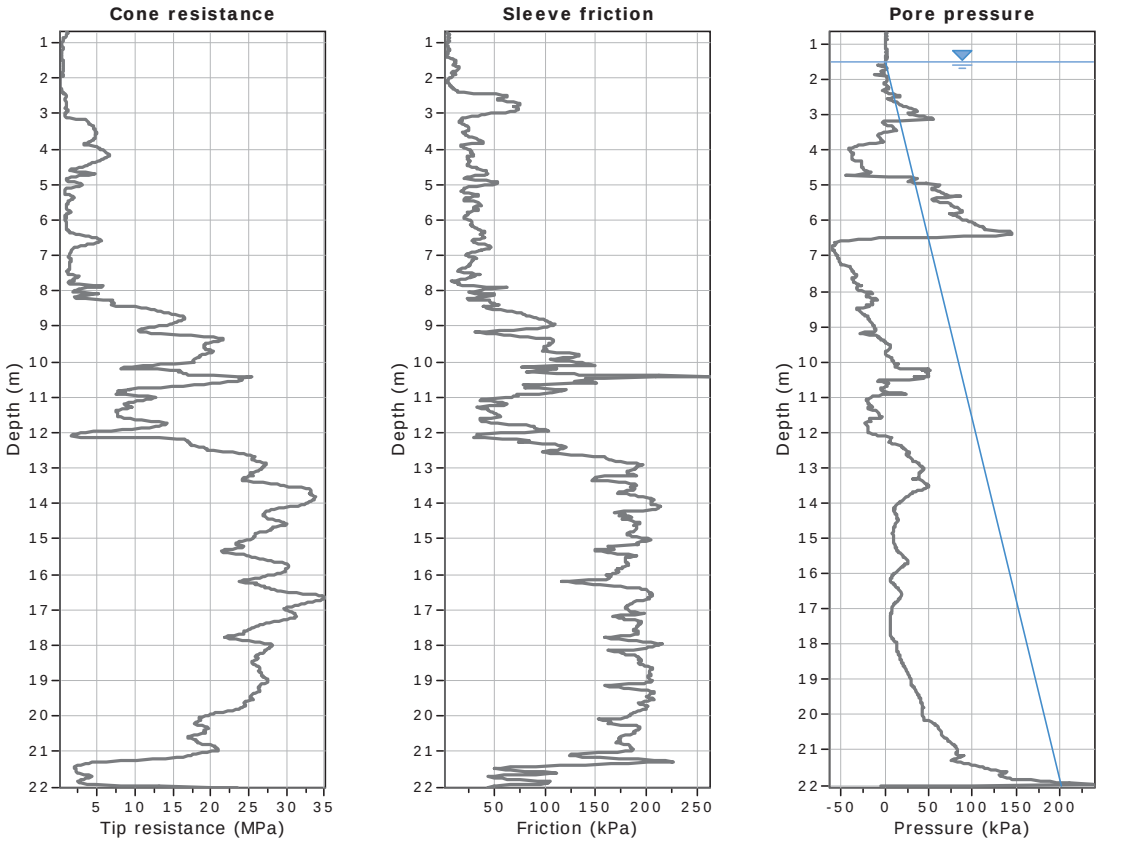

The plot below presents the cross correlation coeficient between the raw qc and fs values (as measured on the field). X axes presents the lag distance (one lag is the distance between two sucessive CPT measurements).

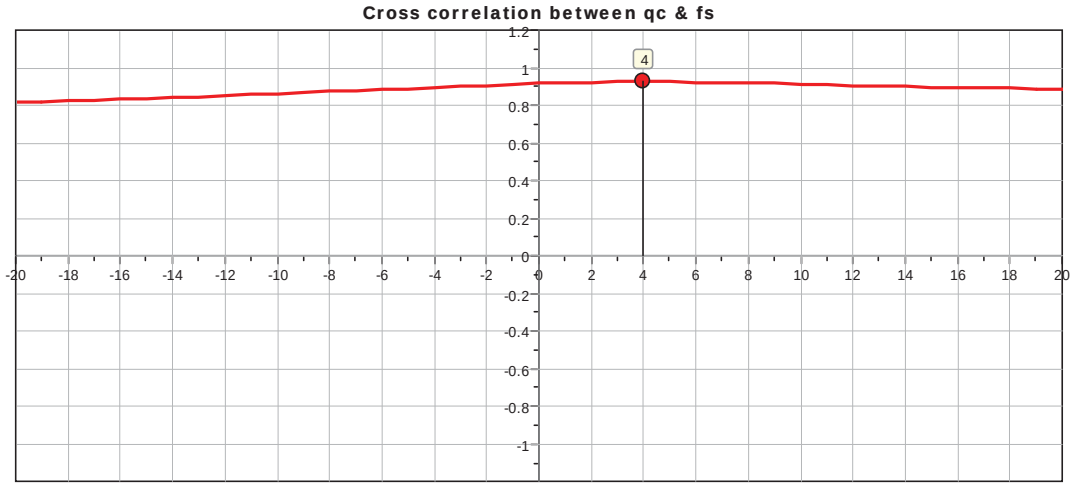

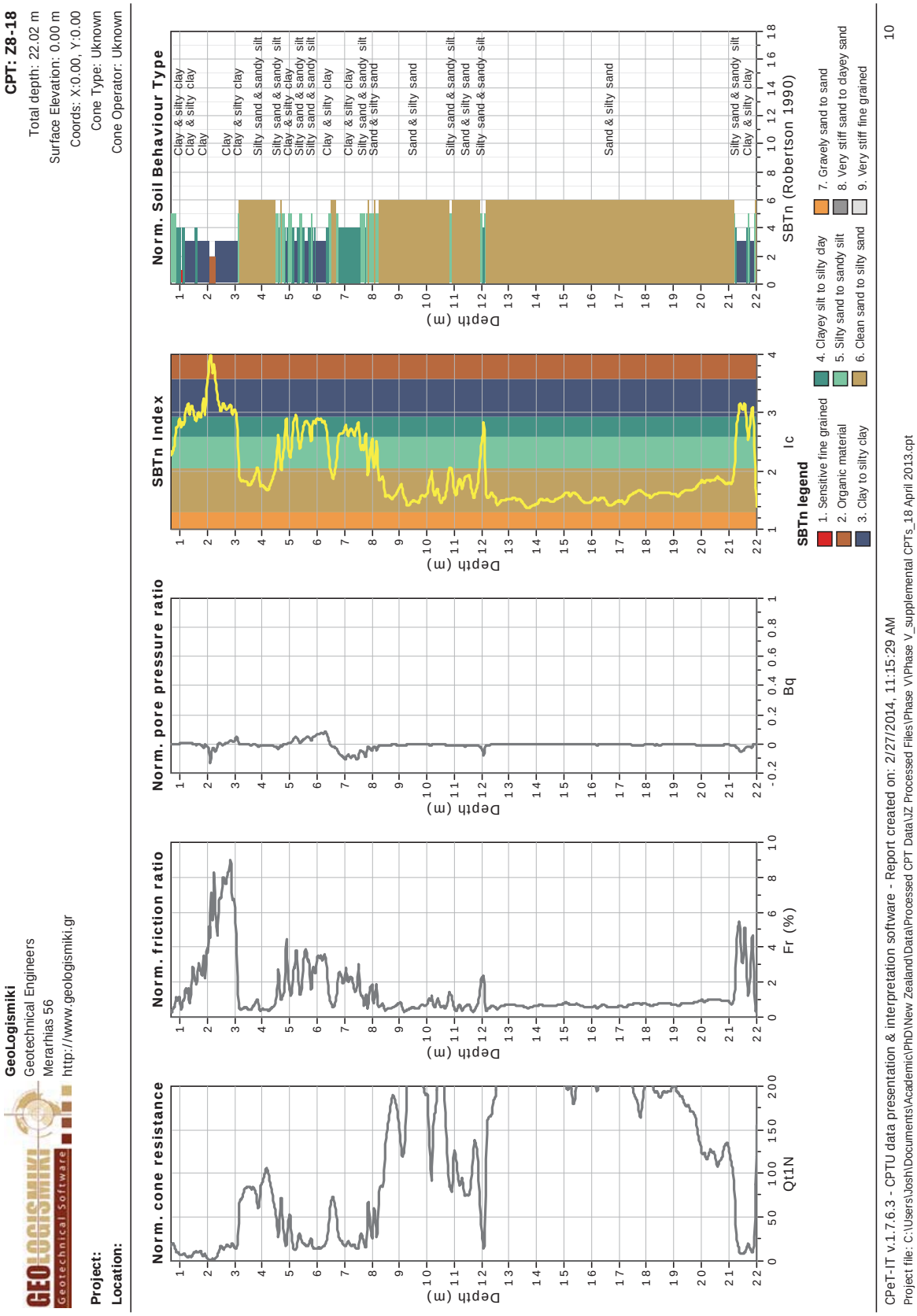
CPT: Z8-18
Total depth: 22.02 m
Surface Elevation: 0.00 m
Coords: X:0.00, Y:0.00
Cone Type: Uknown
Cone Operator: Uknown
GeoLogismiki
Geotechnical Engineers
Merarhias 56
http://www.geologismiki.gr
Project:
Location:
Norm. cone resistance
Qt1N
Norm. friction ratio
Fr (%)
Norm. pore pressure ratio
Bq
SBTn Index
Ic
Norm. Soil Behaviour Type
SBTn (Robertson 1990)
Depth (m)
SBTn legend
1. Sensitive fine grained
2. Organic material
3. Clay to silty clay
4. Clayey silt to silty clay
5. Silty sand to sandy silt
6. Clean sand to silty sand
7. Gravely sand to sand
8. Very stiff sand to clayey sand
9. Very stiff fine grained
CPeT-IT v.1.7.6.3 - CPTU data presentation & interpretation software - Report created on: 2/27/2014, 11:15:29 AM
Project file: C:\Users\Josh\Documents\Academic\PhD\New Zealand\Data\Processed CPT Data\JZ Processed Files\Phase V\Phase V_supplemental CPTs_18 April 2013.cpt
10

GeoLogismiki
Geotechnical Engineers
Merarhias 56
http://www.geologismiki.gr

CPT: Z9-1
Total depth: 19.90 m
Surface Elevation: 0.00 m
Coords: X:0.00, Y:0.00
Cone Type: Uknown
Cone Operator: Uknown

Project: **Liquefaction and Its Effects on Buildings and Lifelines in the February 22, 2011 Christchurch Earthquake**
Location: **Christchurch, New Zealand**

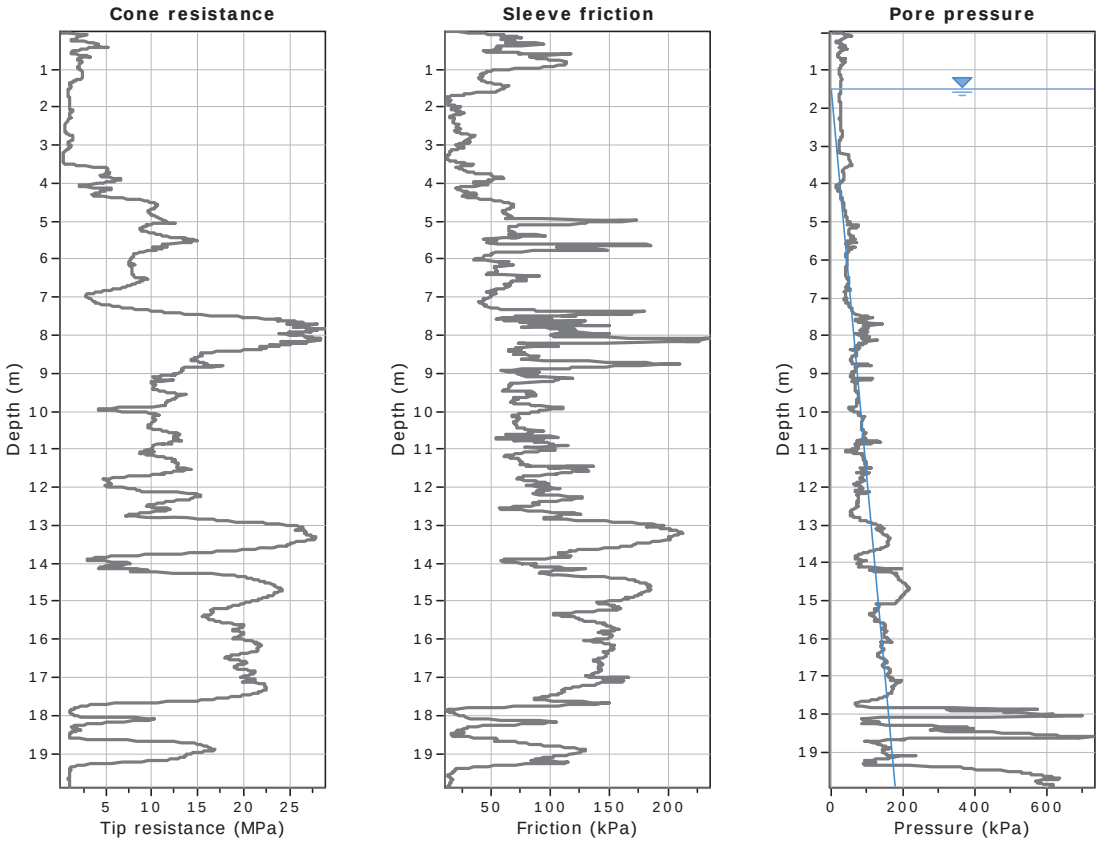

The plot below presents the cross correlation coeficient between the raw qc and fs values (as measured on the field). X axes presents the lag distance (one lag is the distance between two sucessive CPT measurements).

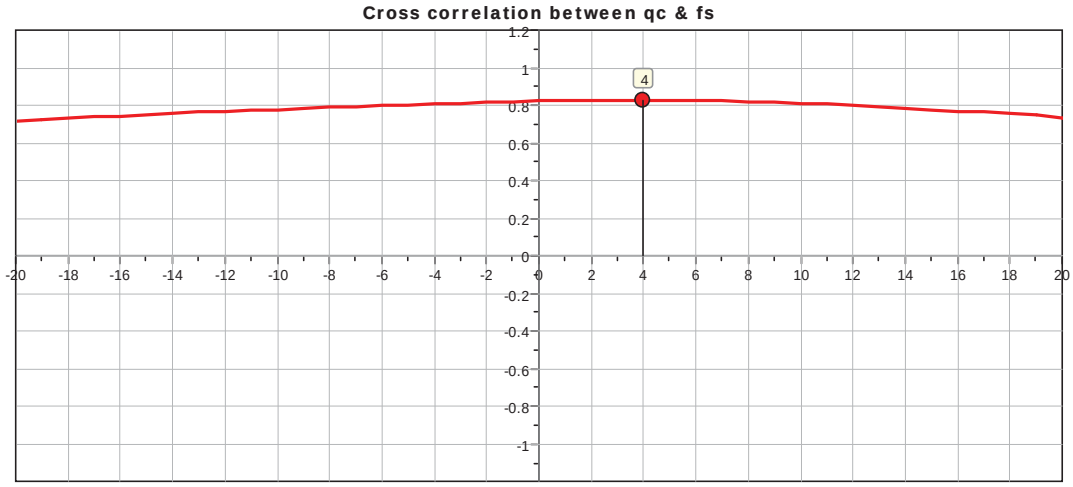

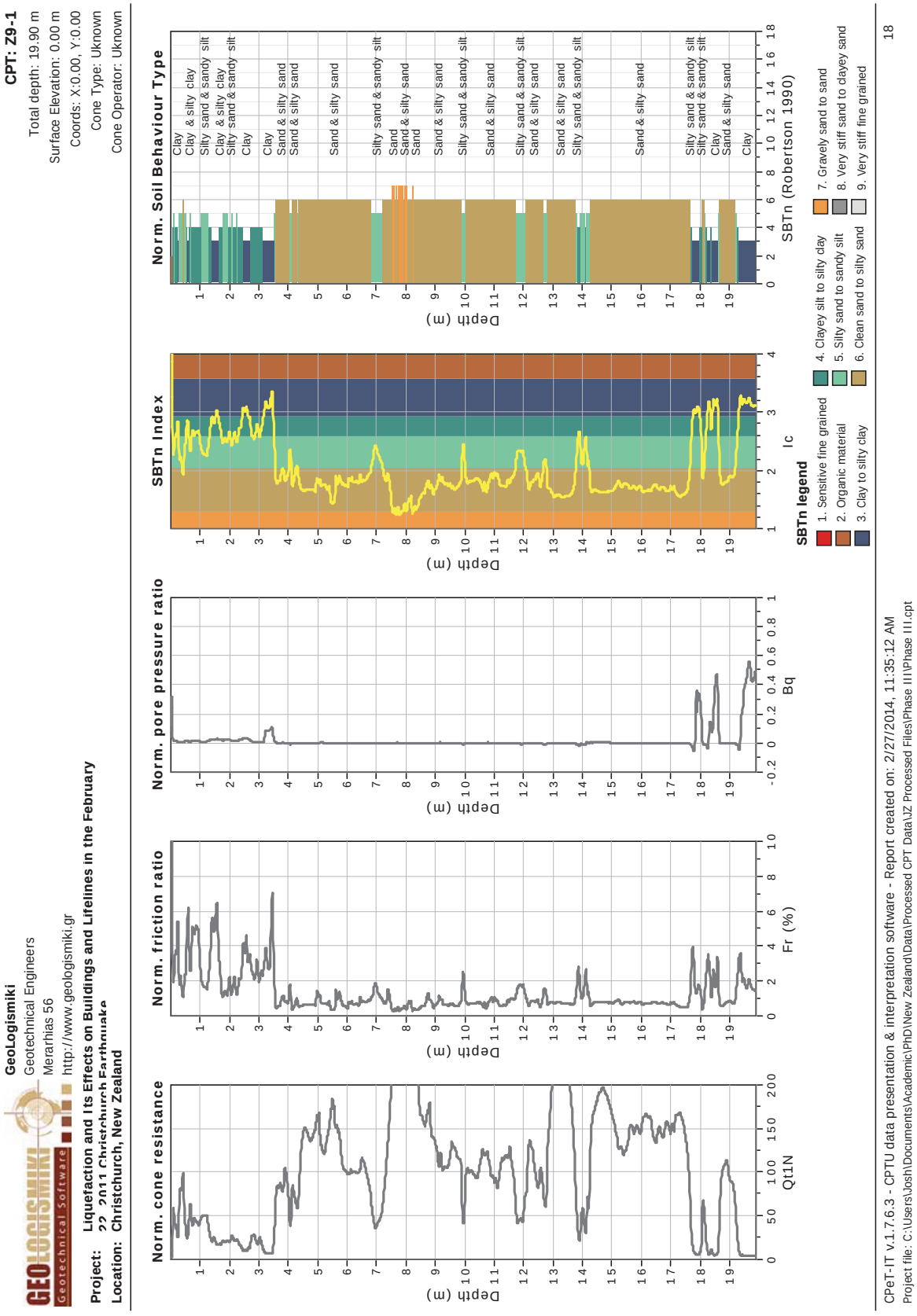
CPT: Z9-1
Total depth: 19.90 m
Surface Elevation: 0.00 m
Coords: X:0.00, Y:0.00
Cone Type: Uknown
Cone Operator: Uknown
GeoLogismiki
Geotechnical Engineers
Merarhias 56
http://www.geologismiki.gr
Project: Liquefaction and Its Effects on Buildings and Lifelines in the February 22, 2011 Christchurch Earthquake
Location: Christchurch, New Zealand
Norm. cone resistance
Qt1N
Norm. friction ratio
Fr (%)
Norm. pore pressure ratio
Bq
SBTn Index
Ic
Norm. Soil Behaviour Type
SBTn (Robertson 1990)
Depth (m)
SBTn legend
1. Sensitive fine grained
2. Organic material
3. Clay to silty clay
4. Clayey silt to silty clay
5. Silty sand to sandy silt
6. Clean sand to silty sand
7. Gravely sand to sand
8. Very stiff sand to clayey sand
9. Very stiff fine grained
CPeT-IT v.1.7.6.3 - CPTU data presentation & interpretation software - Report created on: 2/27/2014, 11:35:12 AM
Project file: C:\Users\Josh\Documents\Academic\PhD\New Zealand\Data\Processed CPT Data\JZ Processed Files\Phase III\Phase III.cpt
18

GeoLogismiki
Geotechnical Engineers
Merarhias 56
http://www.geologismiki.gr

CPT: Z9-2
Total depth: 7.22 m
Surface Elevation: 0.00 m
Coords: X:0.00, Y:0.00
Cone Type: Uknown
Cone Operator: Uknown

Project: **Liquefaction and Its Effects on Buildings and Lifelines in the February 22, 2011 Christchurch Earthquake**
Location: **Christchurch, New Zealand**

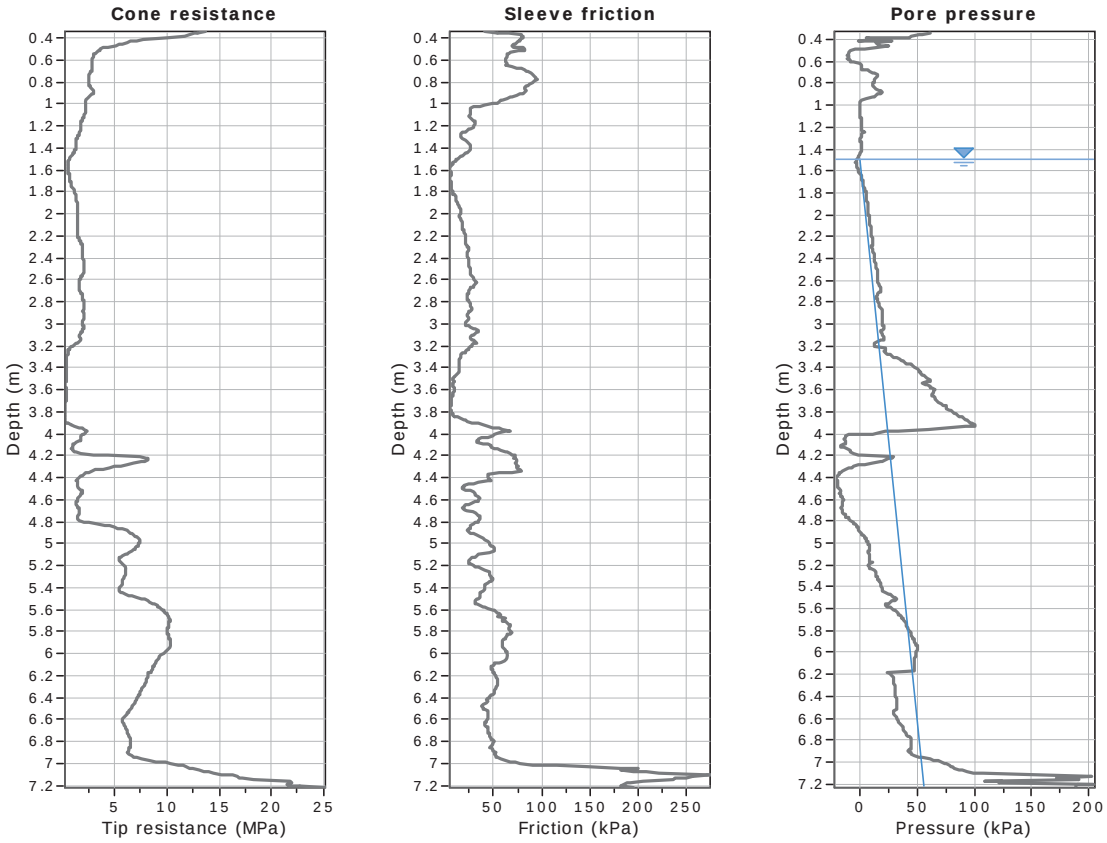

The plot below presents the cross correlation coeficient between the raw qc and fs values (as measured on the field). X axes presents the lag distance (one lag is the distance between two sucessive CPT measurements).

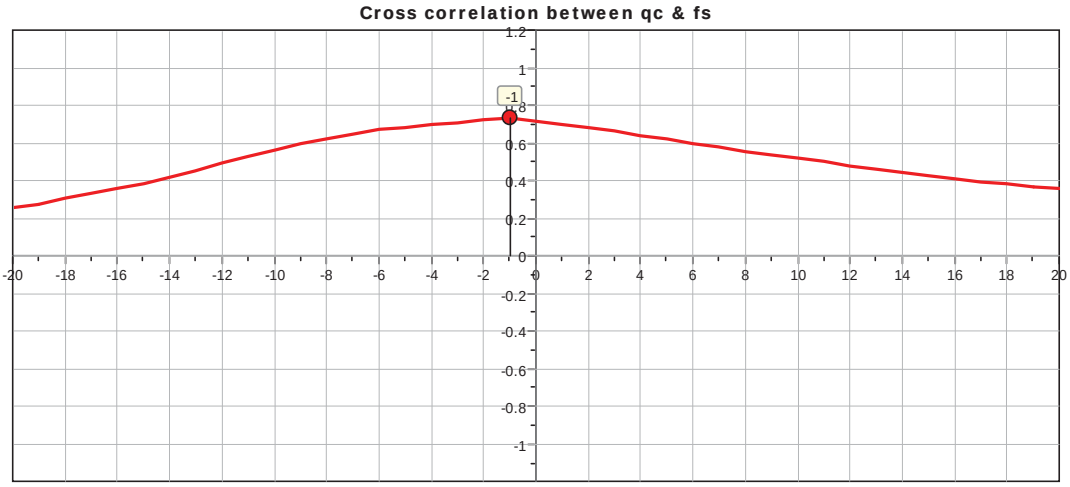

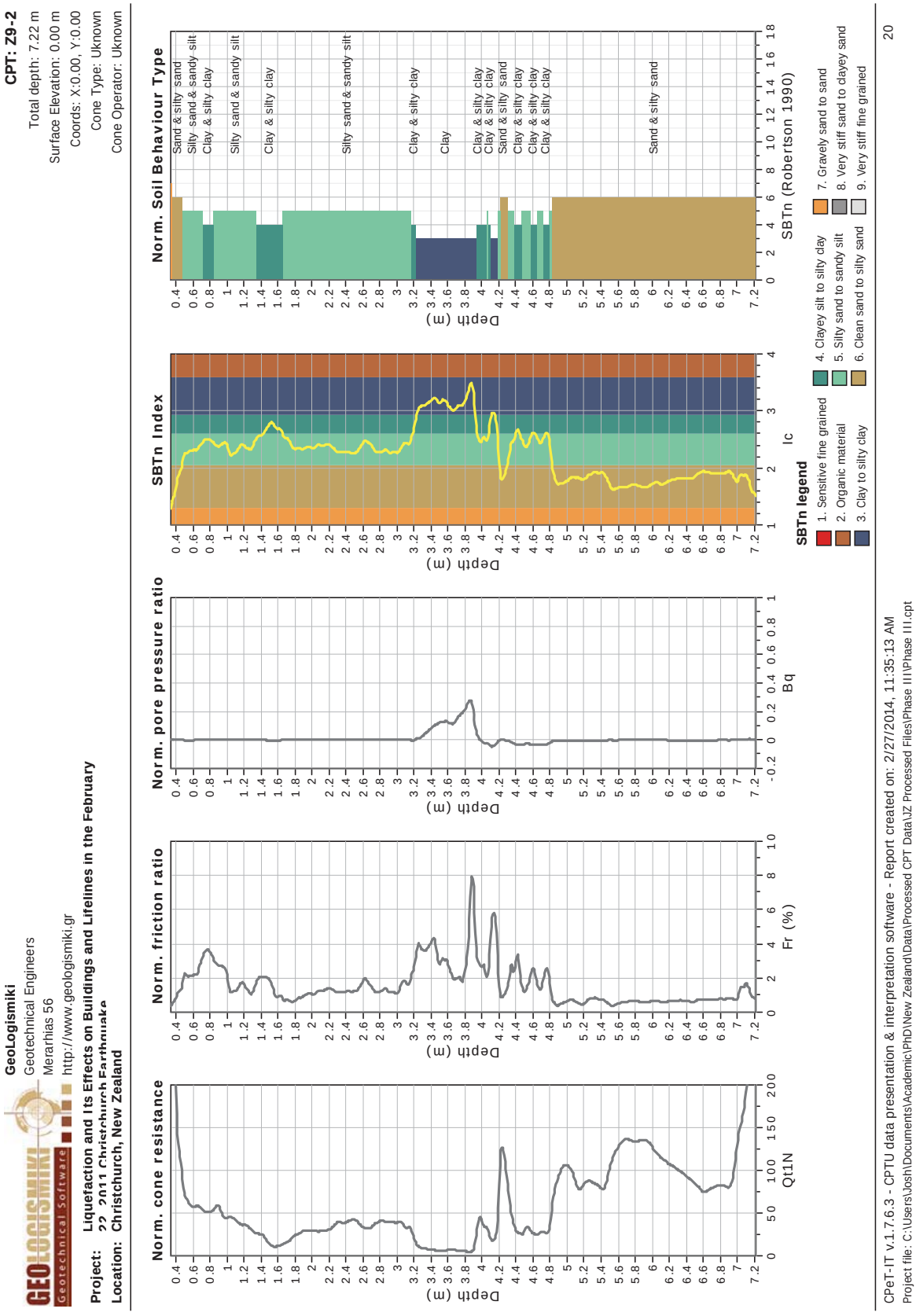
GeoLogismiki
Geotechnical Engineers
Merarhias 56
http://www.geologismiki.gr
Project: Liquefaction and Its Effects on Buildings and Lifelines in the February 22, 2011 Christchurch Earthquake
Location: Christchurch, New Zealand
CPT: Z9-2
Total depth: 7.22 m
Surface Elevation: 0.00 m
Coords: X:0.00, Y:0.00
Cone Type: Uknown
Cone Operator: Uknown
Norm. cone resistance
Norm. friction ratio
Norm. pore pressure ratio
SBTn Index
Norm. Soil Behaviour Type
Depth (m)
Qt1N
Fr (%)
Bq
Ic
SBTn (Robertson 1990)
Sand & silty sand
Silty sand & sandy silt
Clay & silty clay
Silty sand & sandy silt
Clay & silty clay
Silty sand & sandy silt
Clay & silty clay
Clay
Clay & silty clay
Clay & silty clay
Sand & silty sand
Clay & silty clay
Clay & silty clay
Clay & silty clay
Sand & silty sand
SBTn legend
1. Sensitive fine grained
2. Organic material
3. Clay to silty clay
4. Clayey silt to silty clay
5. Silty sand to sandy silt
6. Clean sand to silty sand
7. Gravely sand to sand
8. Very stiff sand to clayey sand
9. Very stiff fine grained
CPeT-IT v.1.7.6.3 - CPTU data presentation & interpretation software - Report created on: 2/27/2014, 11:35:13 AM
Project file: C:\Users\Josh\Documents\Academic\PhD\New Zealand\Data\Processed CPT Data\JZ Processed Files\Phase III\Phase III.cpt
20

GeoLogismiki
Geotechnical Engineers
Merarhias 56
http://www.geologismiki.gr

CPT: Z9-3
Total depth: 11.46 m
Surface Elevation: 0.00 m
Coords: X:0.00, Y:0.00
Cone Type: Uknown
Cone Operator: Uknown

Project: **Liquefaction and Its Effects on Buildings and Lifelines in the February 22, 2011 Christchurch Earthquake**
Location: **Christchurch, New Zealand**

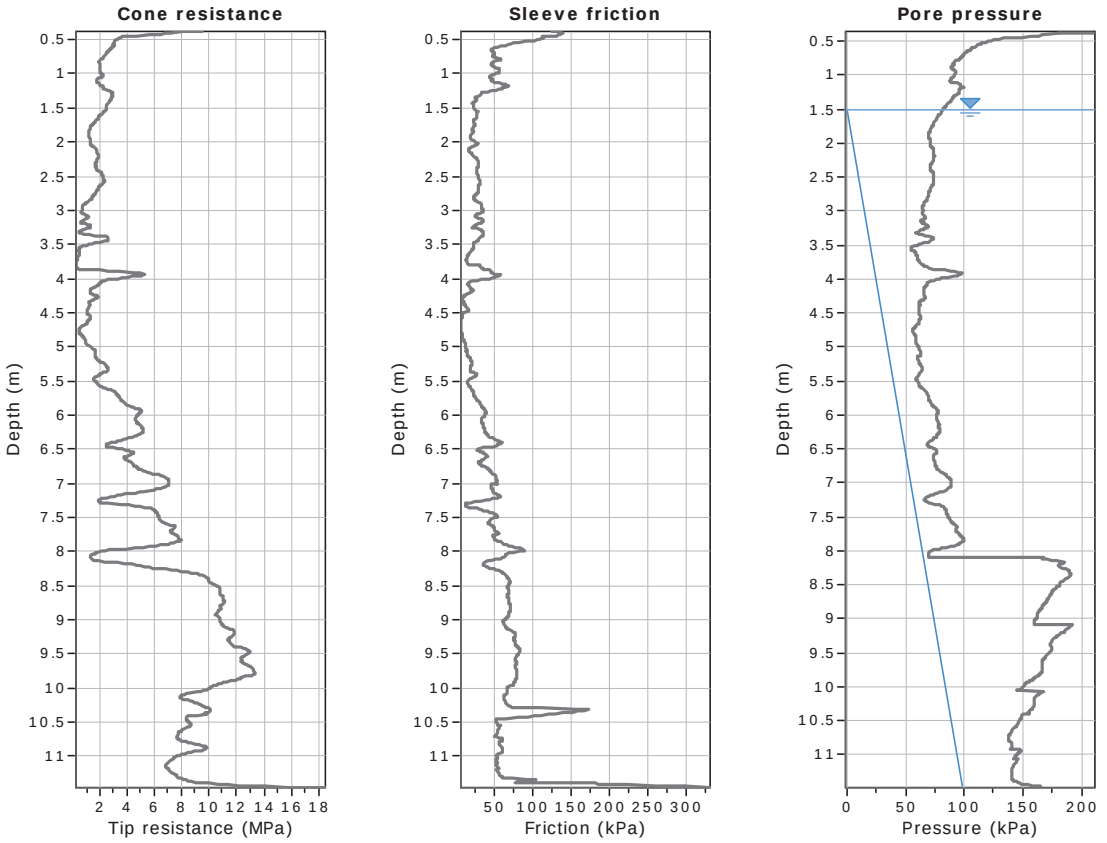

The plot below presents the cross correlation coeficient between the raw qc and fs values (as measured on the field). X axes presents the lag distance (one lag is the distance between two sucessive CPT measurements).

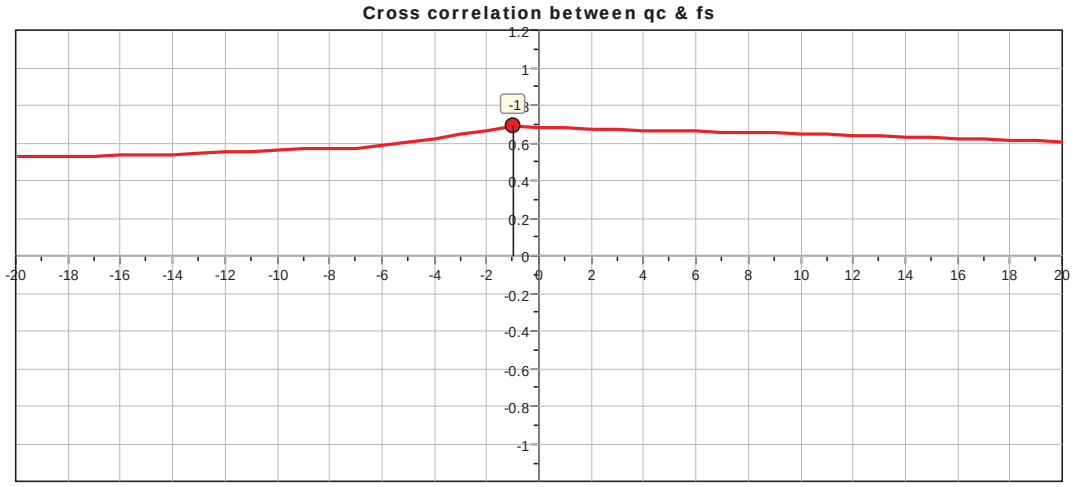

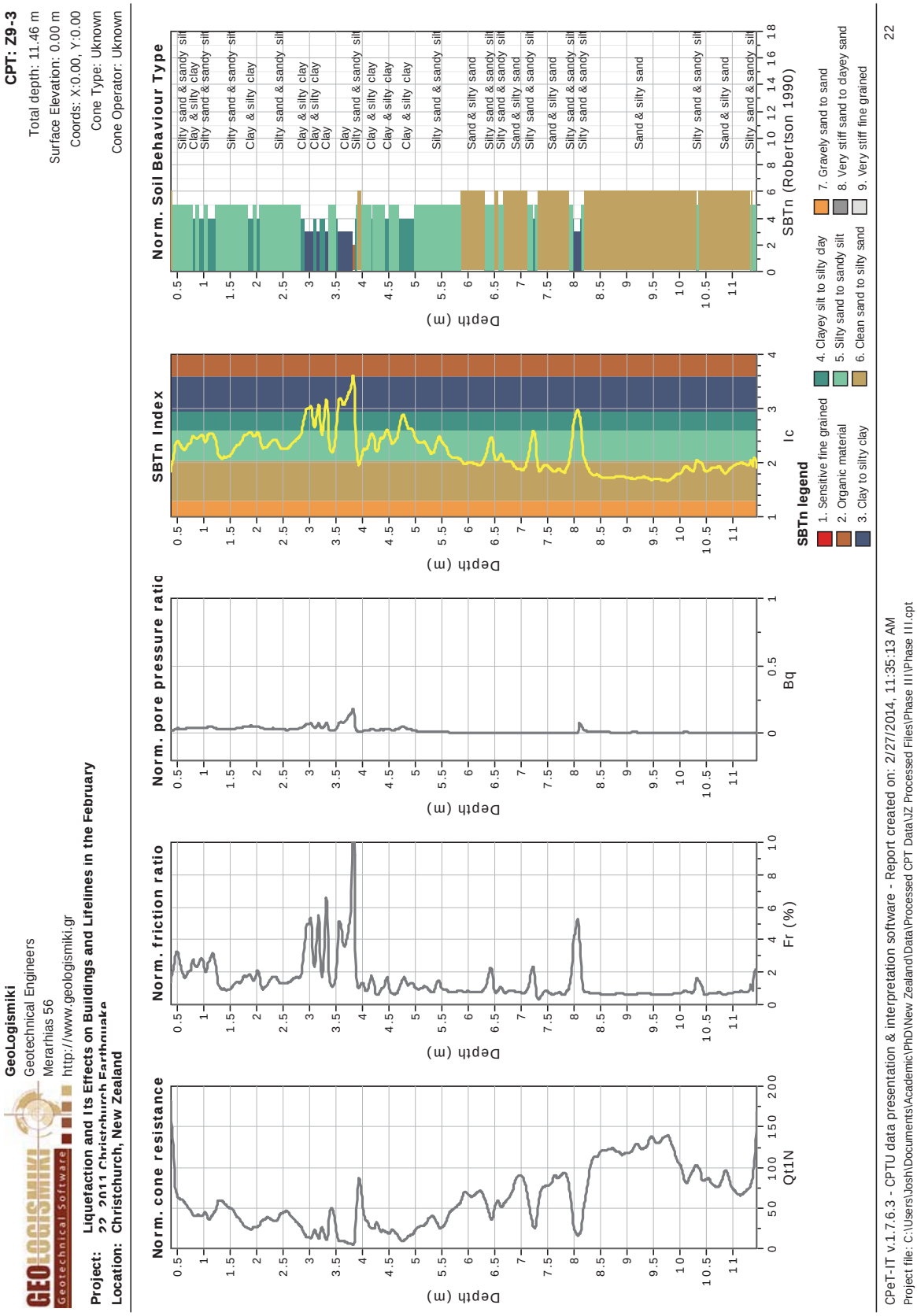
GeoLogismiki
Geotechnical Engineers
Merarchias 56
http://www.geologismiki.gr
Project: Liquefaction and Its Effects on Buildings and Lifelines in the February 22, 2011 Christchurch Earthquake
Location: Christchurch, New Zealand
CPT: Z9-3
Total depth: 11.46 m
Surface Elevation: 0.00 m
Coords: X:0.00, Y:0.00
Cone Type: Uknown
Cone Operator: Uknown
Norm. cone resistance
Qt1N
Norm. friction ratio
Fr (%)
Norm. pore pressure ratio
Bq
SBTn Index
Ic
Norm. Soil Behaviour Type
SBTn (Robertson 1990)
Depth (m)
SBTn legend
1. Sensitive fine grained
2. Organic material
3. Clay to silty clay
4. Clayey silt to silty clay
5. Silty sand to sandy silt
6. Clean sand to silty sand
7. Gravelly sand to sand
8. Very stiff sand to clayey sand
9. Very stiff fine grained
CPeT-IT v.1.7.6.3 - CPTU data presentation & interpretation software - Report created on: 2/27/2014, 11:35:13 AM
Project file: C:\Users\Josh\Documents\Academic\PhD\New Zealand\Data\Processed CPT Data\JZ Processed Files\Phase III\Phase III.cpt
22

GeoLogismiki
Geotechnical Engineers
Merarhias 56
http://www.geologismiki.gr

CPT: Z9-4
Total depth: 19.90 m
Surface Elevation: 0.00 m
Coords: X:0.00, Y:0.00
Cone Type: Uknown
Cone Operator: Uknown

Project: **Liquefaction and Its Effects on Buildings and Lifelines in the February 22, 2011 Christchurch Earthquake**
Location: **Christchurch, New Zealand**

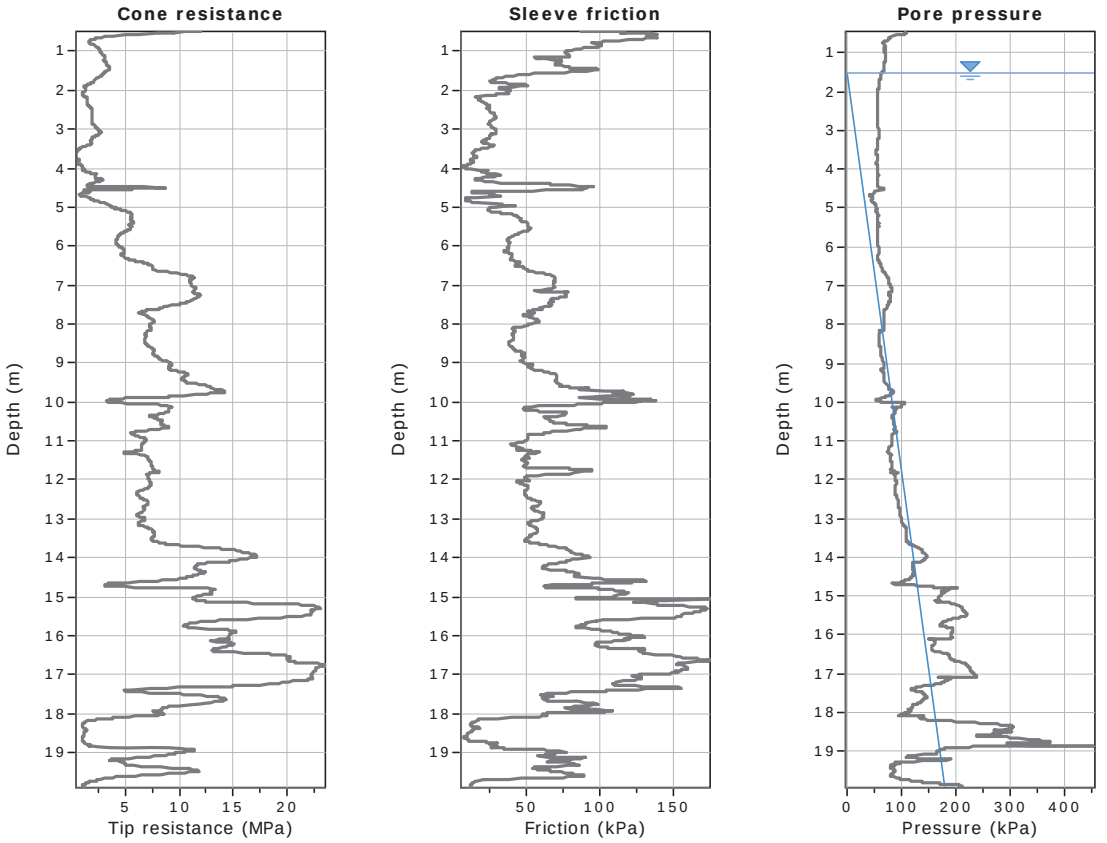

The plot below presents the cross correlation coeficient between the raw qc and fs values (as measured on the field). X axes presents the lag distance (one lag is the distance between two sucessive CPT measurements).

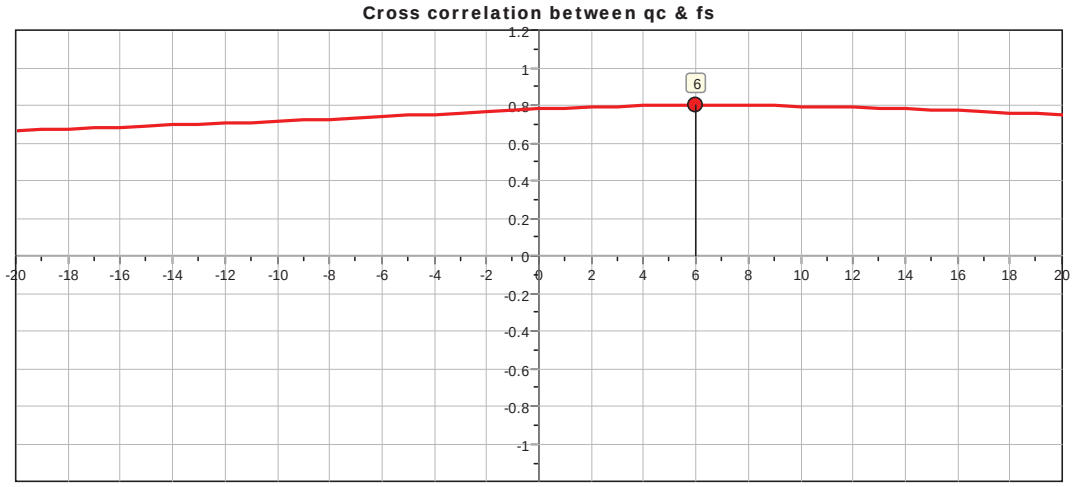

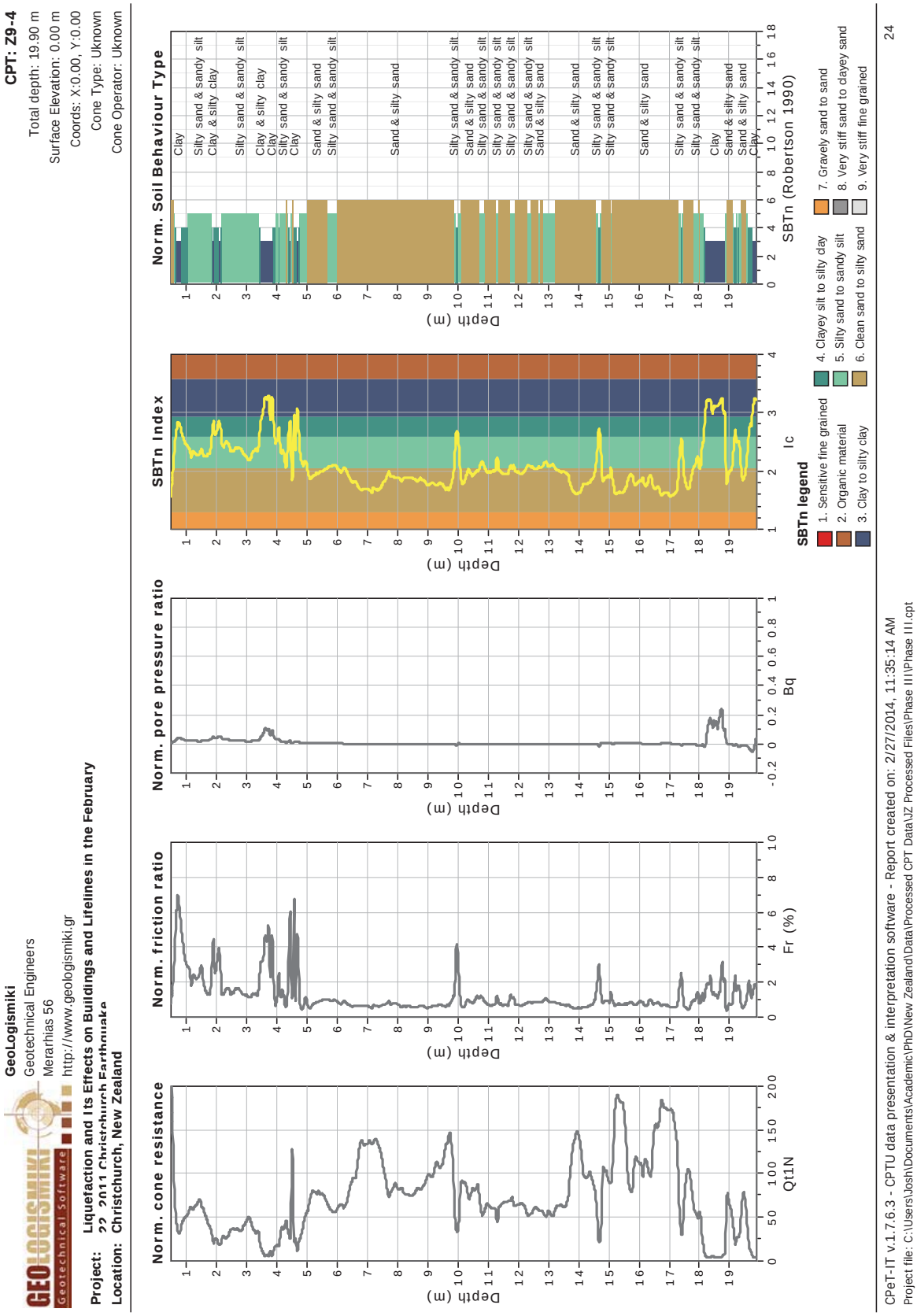
GeoLogismiki
Geotechnical Engineers
Merarhias 56
http://www.geologismiki.gr
Project: Liquefaction and Its Effects on Buildings and Lifelines in the February 22, 2011 Christchurch Earthquake
Location: Christchurch, New Zealand
CPT: Z9-4
Total depth: 19.90 m
Surface Elevation: 0.00 m
Coords: X:0.00, Y:0.00
Cone Type: Uknown
Cone Operator: Uknown
Norm. cone resistance
Qt1N
Norm. friction ratio
Fr (%)
Norm. pore pressure ratio
Bq
SBTn Index
Ic
Norm. Soil Behaviour Type
SBTn (Robertson 1990)
Depth (m)
SBTn legend
1. Sensitive fine grained
2. Organic material
3. Clay to silty clay
4. Clayey silt to silty clay
5. Silty sand to sandy silt
6. Clean sand to silty sand
7. Gravely sand to sand
8. Very stiff sand to clayey sand
9. Very stiff fine grained
CPeT-IT v.1.7.6.3 - CPTU data presentation & interpretation software - Report created on: 2/27/2014, 11:35:14 AM
Project file: C:\Users\Josh\Documents\Academic\PhD\New Zealand\Data\Processed CPT Data\JZ Processed Files\Phase III\Phase III.cpt
24

GeoLogismiki
Geotechnical Engineers
Merarhias 56
http://www.geologismiki.gr

CPT: Z9-5
Total depth: 19.90 m
Surface Elevation: 0.00 m
Coords: X:0.00, Y:0.00
Cone Type: Uknown
Cone Operator: Uknown

Project: **Liquefaction and Its Effects on Buildings and Lifelines in the February 22, 2011 Christchurch Earthquake**
Location: **Christchurch, New Zealand**

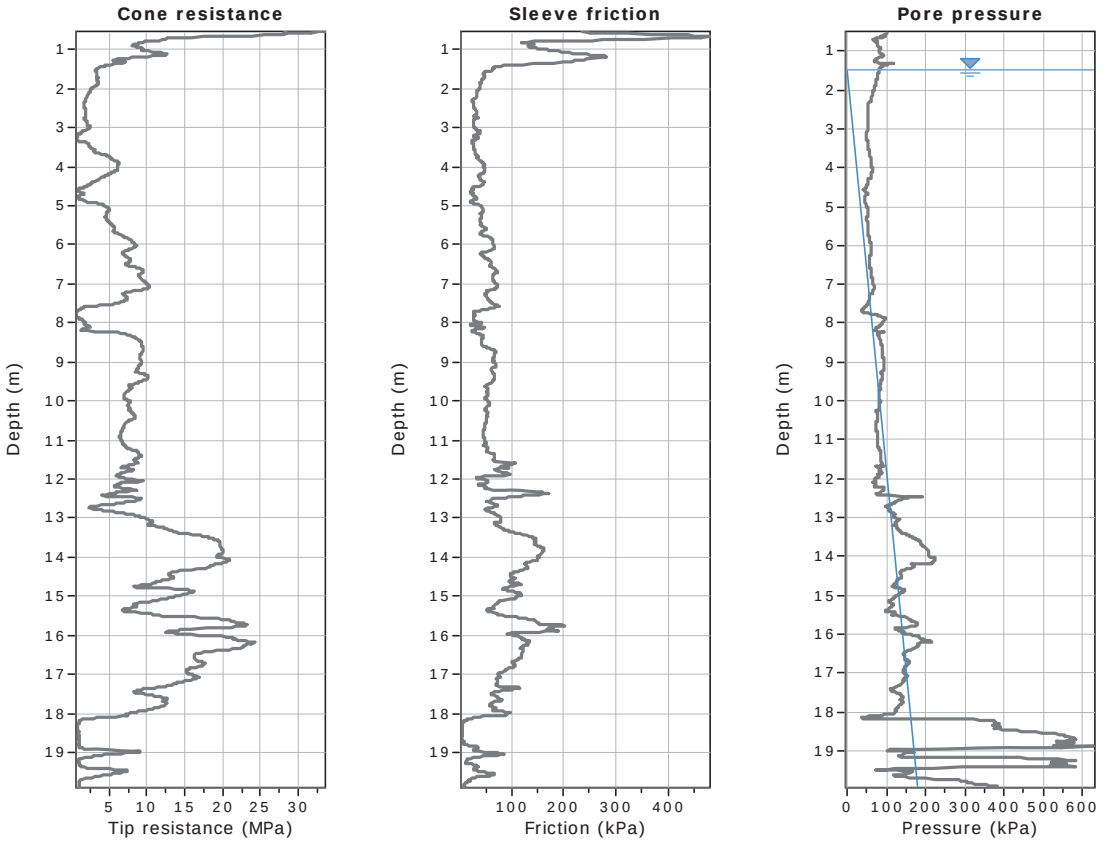

The plot below presents the cross correlation coeficient between the raw qc and fs values (as measured on the field). X axes presents the lag distance (one lag is the distance between two sucessive CPT measurements).

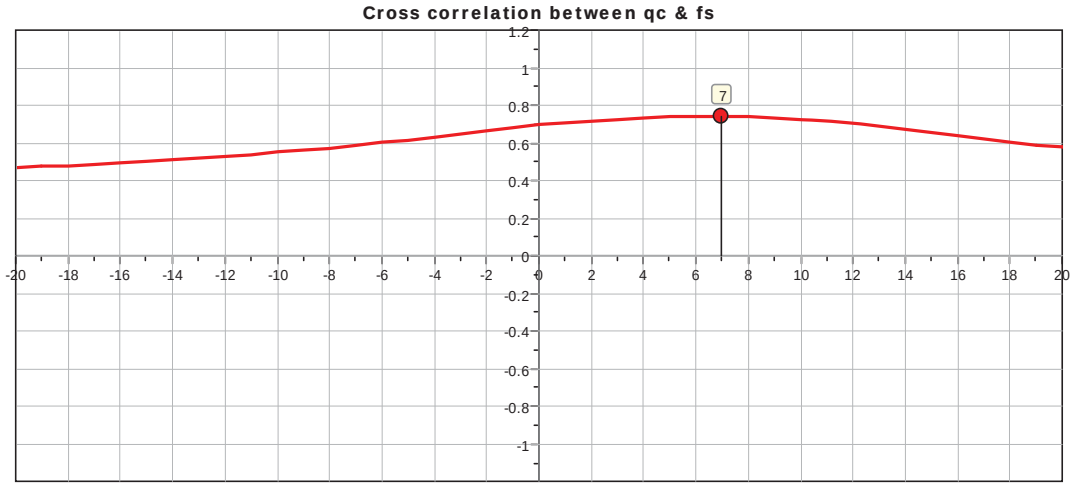

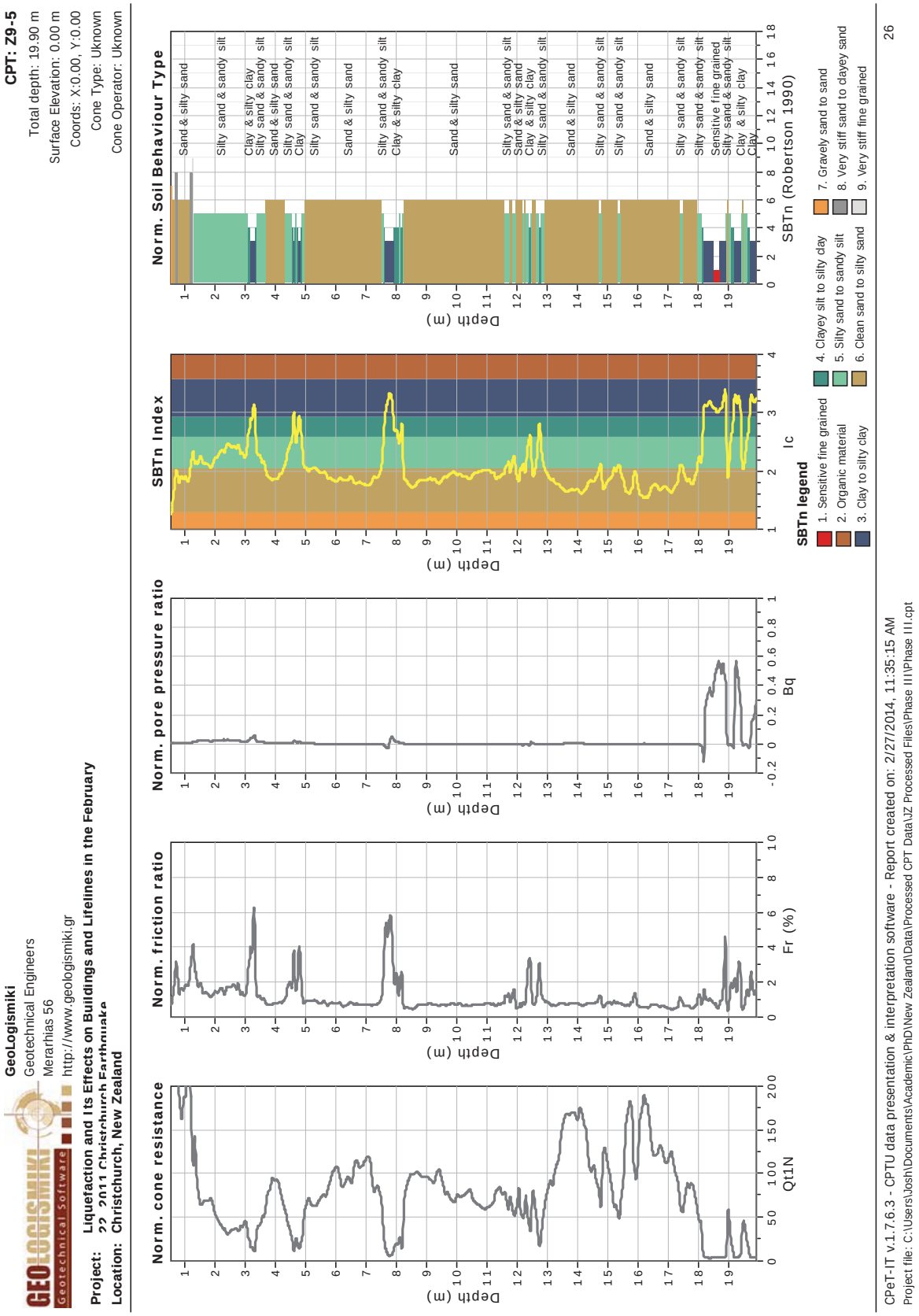
GeoLogismiki
Geotechnical Engineers
Merarhias 56
http://www.geologismiki.gr
Project: Liquefaction and Its Effects on Buildings and Lifelines in the February 22, 2011 Christchurch Earthquake
Location: Christchurch, New Zealand
CPT: Z9-5
Total depth: 19.90 m
Surface Elevation: 0.00 m
Coords: X:0.00, Y:0.00
Cone Type: Uknown
Cone Operator: Uknown
Norm. cone resistance
Qt1N
Norm. friction ratio
Fr (%)
Norm. pore pressure ratio
Bq
SBTn Index
Ic
Norm. Soil Behaviour Type
SBTn (Robertson 1990)
Depth (m)
SBTn legend
1. Sensitive fine grained
2. Organic material
3. Clay to silty clay
4. Clayey silt to silty clay
5. Silty sand to sandy silt
6. Clean sand to silty sand
7. Gravely sand to sand
8. Very stiff sand to clayey sand
9. Very stiff fine grained
CPeT-IT v.1.7.6.3 - CPTU data presentation & interpretation software - Report created on: 2/27/2014, 11:35:15 AM
Project file: C:\Users\Josh\Documents\Academic\PhD\New Zealand\Data\Processed CPT Data\JZ Processed Files\Phase III\Phase III.cpt
26

GeoLogismiki
Geotechnical Engineers
Merarhias 56
http://www.geologismiki.gr

CPT: Z9-7
Total depth: 24.60 m
Surface Elevation: 0.00 m
Coords: X:0.00, Y:0.00
Cone Type: Uknown
Cone Operator: Uknown

Project: **Liquefaction and Its Effects on Buildings and Lifelines in the February 22, 2011 Christchurch Earthquake**
Location: **Christchurch, New Zealand**

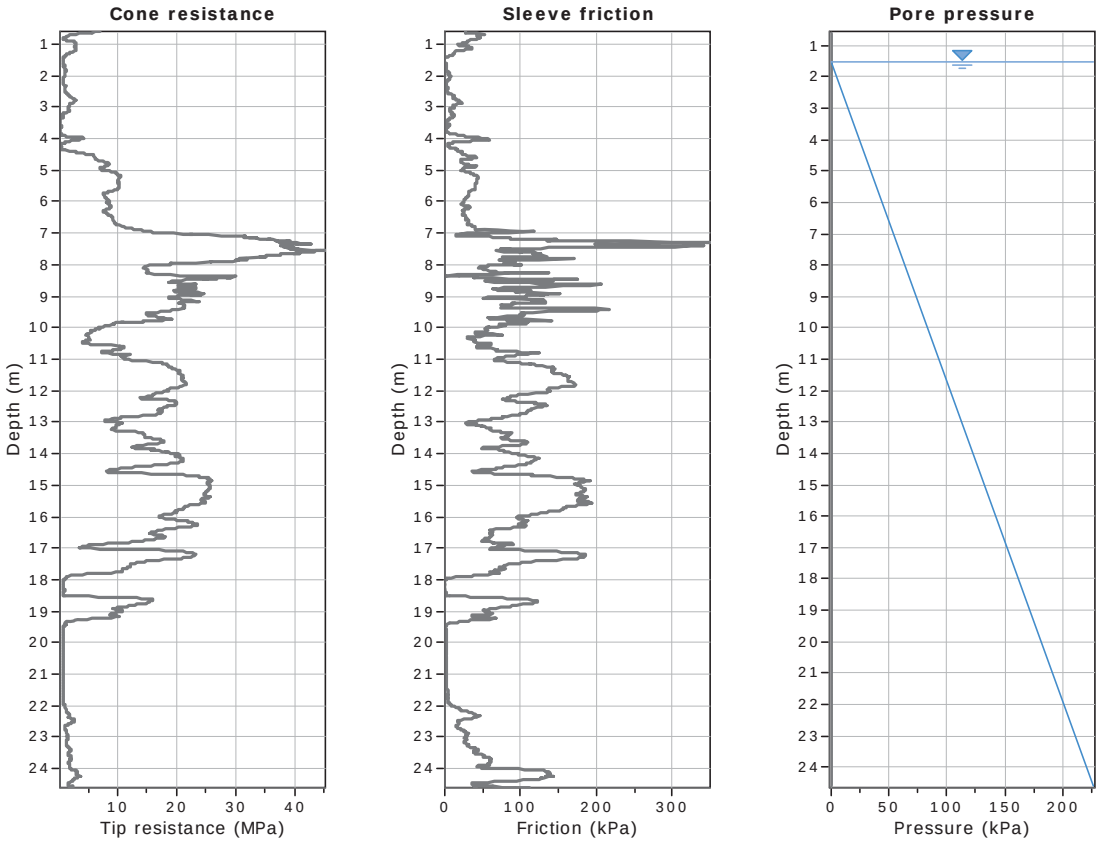

The plot below presents the cross correlation coeficient between the raw qc and fs values (as measured on the field). X axes presents the lag distance (one lag is the distance between two sucessive CPT measurements).

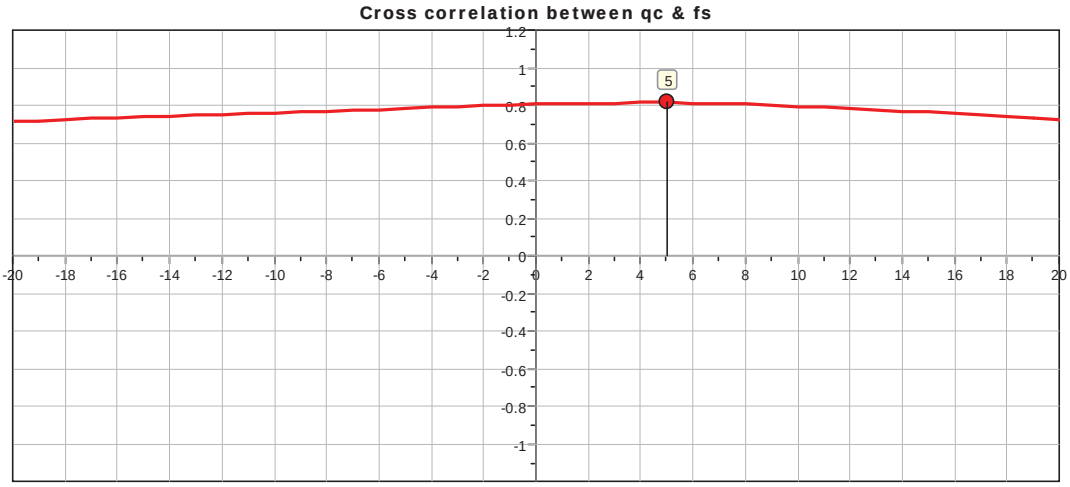

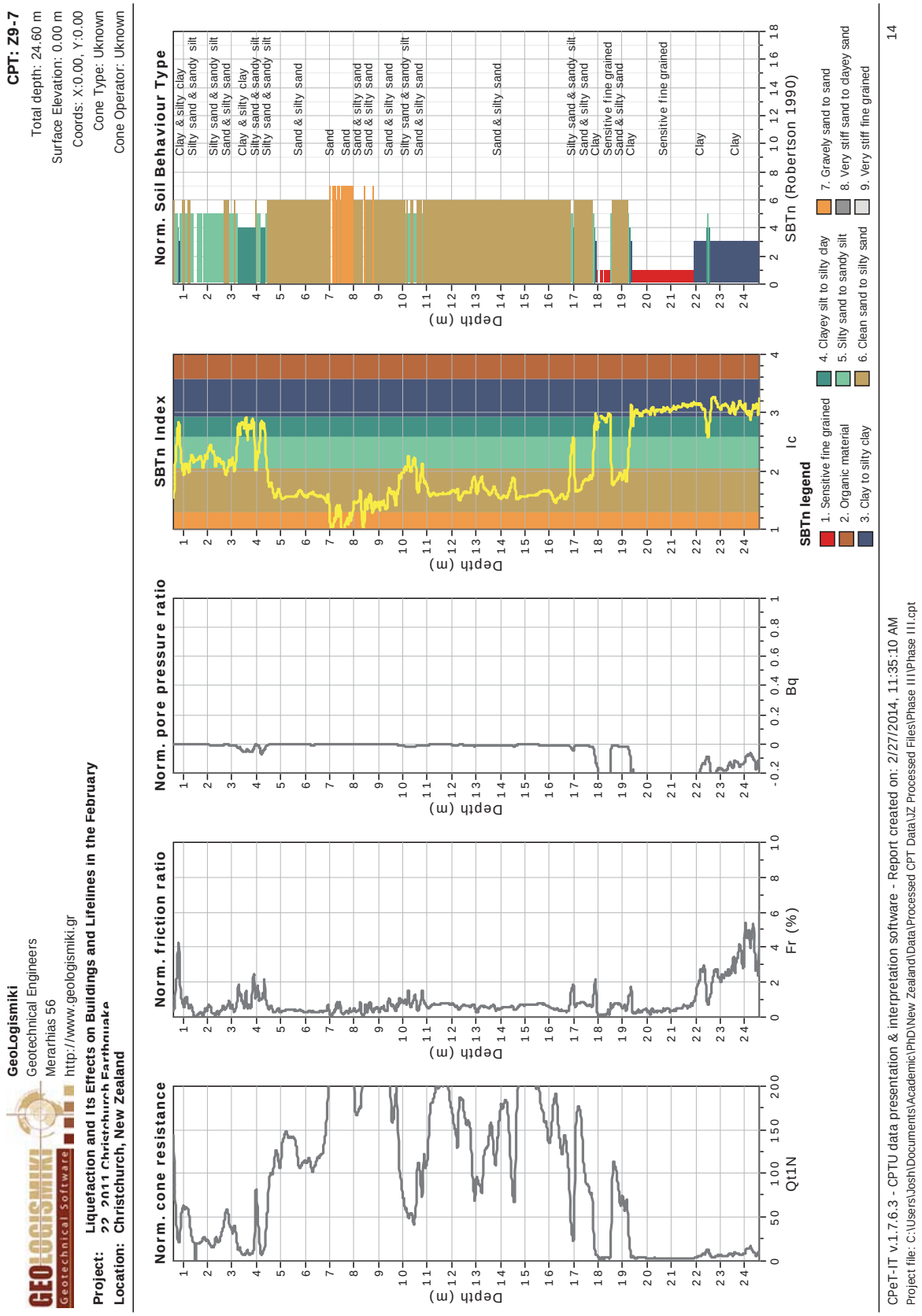
GeoLogismiki
Geotechnical Engineers
Merarhias 56
http://www.geologismiki.gr
Project: Liquefaction and Its Effects on Buildings and Lifelines in the February 22, 2011 Christchurch Earthquake
Location: Christchurch, New Zealand
CPT: Z9-7
Total depth: 24.60 m
Surface Elevation: 0.00 m
Coords: X:0.00, Y:0.00
Cone Type: Uknown
Cone Operator: Uknown
Norm. cone resistance
Qt1N
Norm. friction ratio
Fr (%)
Norm. pore pressure ratio
Bq
SBTn Index
Ic
Norm. Soil Behaviour Type
SBTn (Robertson 1990)
Depth (m)
SBTn legend
1. Sensitive fine grained
2. Organic material
3. Clay to silty clay
4. Clayey silt to silty clay
5. Silty sand to sandy silt
6. Clean sand to silty sand
7. Gravely sand to sand
8. Very stiff sand to clayey sand
9. Very stiff fine grained
CPeT-IT v.1.7.6.3 - CPTU data presentation & interpretation software - Report created on: 2/27/2014, 11:35:10 AM
Project file: C:\Users\Josh\Documents\Academic\PhD\New Zealand\Data\Processed CPT Data\JZ Processed Files\Phase III\Phase III.cpt
14

GeoLogismiki
Geotechnical Engineers
Merarhias 56
http://www.geologismiki.gr

CPT: Z9-8
Total depth: 6.75 m
Surface Elevation: 0.00 m
Coords: X:0.00, Y:0.00
Cone Type: Uknown
Cone Operator: Uknown

Project: **Liquefaction and Its Effects on Buildings and Lifelines in the February 22, 2011 Christchurch Earthquake**
Location: **Christchurch, New Zealand**

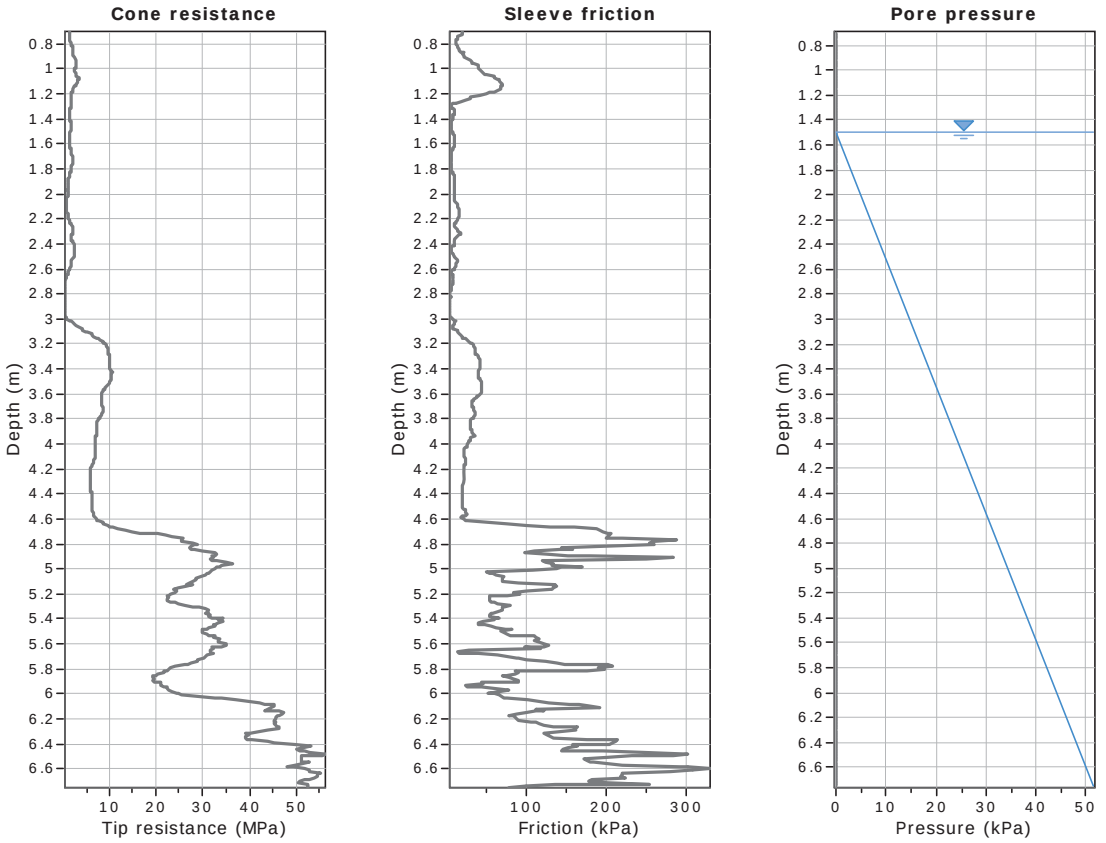

The plot below presents the cross correlation coeficient between the raw qc and fs values (as measured on the field). X axes presents the lag distance (one lag is the distance between two sucessive CPT measurements).

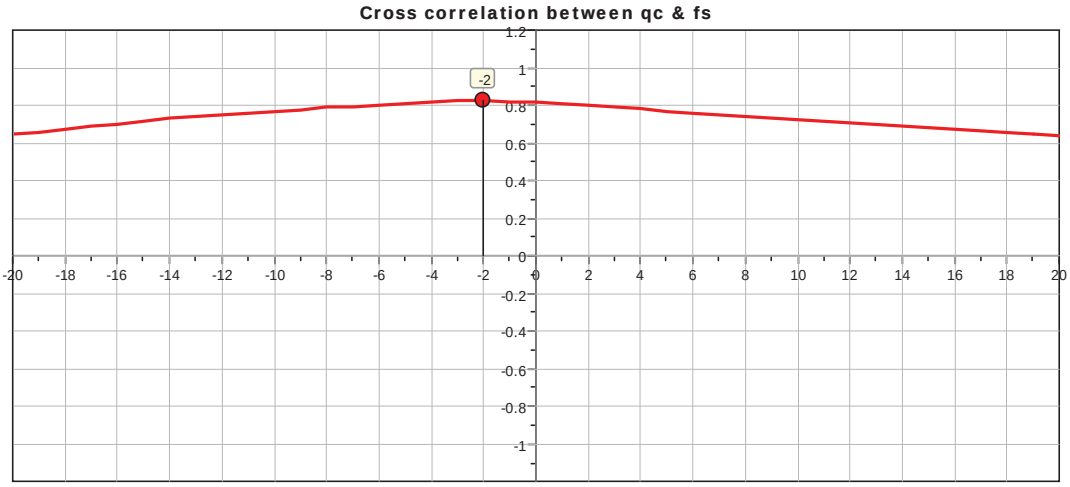

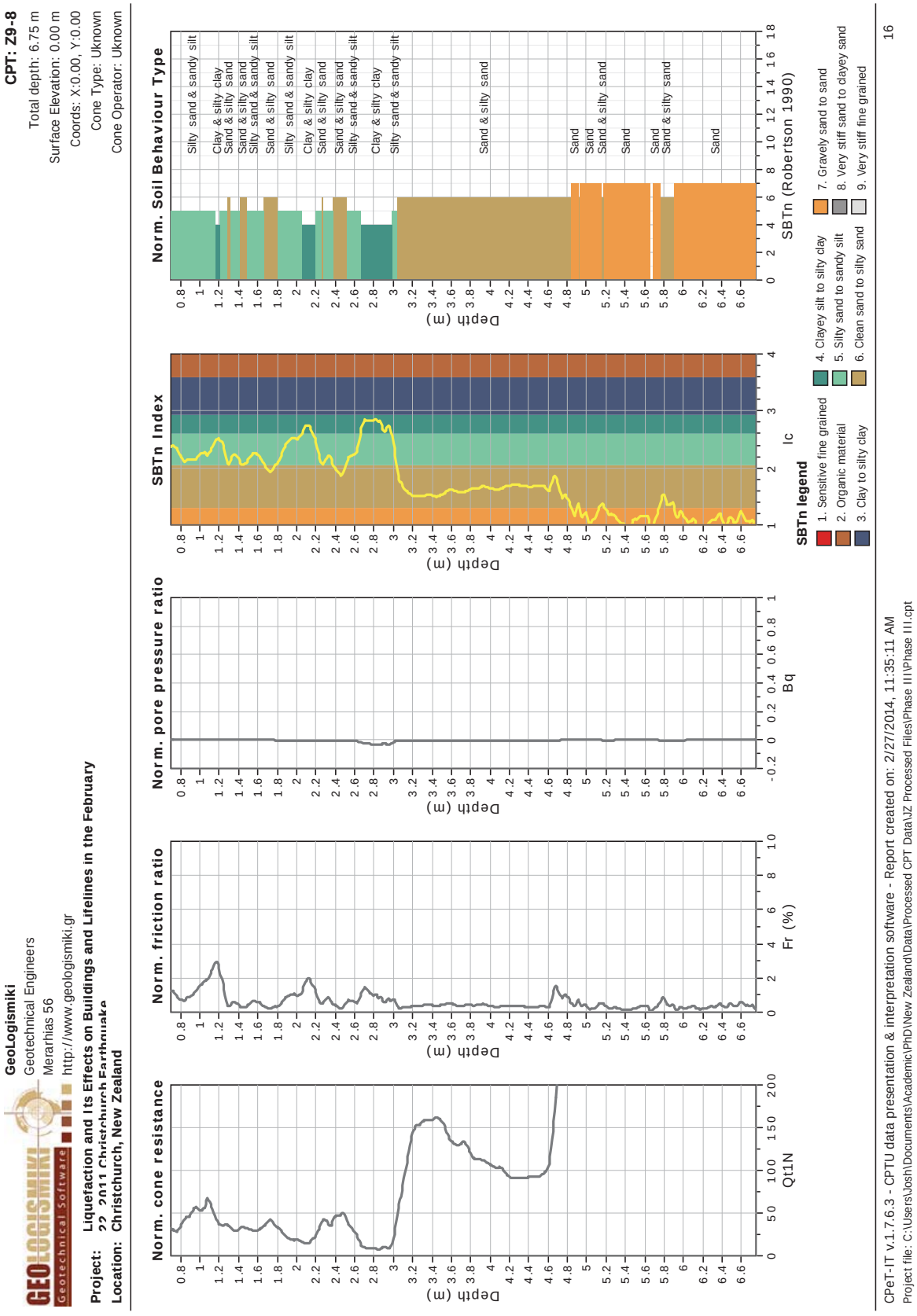
GeoLogismiki
Geotechnical Engineers
Merarchias 56
http://www.geologismiki.gr
Project: Liquefaction and Its Effects on Buildings and Lifelines in the February 22, 2011 Christchurch Earthquake
Location: Christchurch, New Zealand
CPT: Z9-8
Total depth: 6.75 m
Surface Elevation: 0.00 m
Coords: X:0.00, Y:0.00
Cone Type: Uknown
Cone Operator: Uknown
Norm. cone resistance
Norm. friction ratio
Norm. pore pressure ratio
SBTn Index
Norm. Soil Behaviour Type
Depth (m)
Qt1N
Fr (%)
Bq
Ic
SBTn (Robertson 1990)
SBTn legend
1. Sensitive fine grained
2. Organic material
3. Clay to silty clay
4. Clayey silt to silty clay
5. Silty sand to sandy silt
6. Clean sand to silty sand
7. Gravely sand to sand
8. Very stiff sand to clayey sand
9. Very stiff fine grained
Silty sand & sandy silt
Clay & silty clay
Sand & silty sand
Sand
Sand & silty sand
CPeT-IT v.1.7.6.3 - CPTU data presentation & interpretation software - Report created on: 2/27/2014, 11:35:11 AM
Project file: C:\Users\Josh\Documents\Academic\PhD\New Zealand\Data\Processed CPT Data\JZ Processed Files\Phase III\Phase III.cpt
16